# DIGGING DEEPER

VOLUME 1

PROCEEDINGS OF THE NINTH BIENNIAL MEETING OF THE SOCIETY FOR GEOLOGY APPLIED TO MINERAL DEPOSITS
DUBLIN, IRELAND 20TH-23RD AUGUST 2007

# DIGGING DEEPER

Edited by

Colin J. Andrew *et al*
*Cambridge Mineral Resources plc,*
*Navan, Ireland.*

VOLUME 1

The 9th Biennial SGA Meeting is organized by the Irish Association for Economic Geology with assistance from the Society of Economic Geologists

Cover Design: Woodcut showing methods of deepening mines in the 16th Century.

From Georgius Agricola (1556) "De Re Metallica"



Published and distributed by the Irish Association for Economic Geology

ISBN [0-950989-4-4] set of two volumes
ISBN [0-950989-4-4] Volume 1
ISBN [0-950-989-4-4] Volume 2

# Volume 1



# Volume 2

# Table of Contents

## Volume 1

# Preface

In 2003 the Council of the Society for Geology Applied to Mineral Deposits (SGA) decided to accept the offer from the Irish Association for Economic Geology (IAEG) to organize its' 9th Biennial Meeting. The title proposed was "Digging Deeper", not meant in the this literal sense (although this is partly true in some ore districts) but metaphorically in terms of using more scientific applications and methodologies to understand mineral deposits and also to use advanced techniques in mineral exploration. The IAEG believed that this would have a broad interest to industry which is presently booming and would, we believed, still be in the throws of this boom in 2007.

The IAEG is Ireland's most influential geological association and has been in existence since 1973 and has hosted several international conferences and published a number of major thematic volumes. However the 9th Biennial SGA Meeting will be the largest geological conference ever held in the country and an event that the IAEG is proud to be associated with.

Although the minerals industry has traditionally been "boom and bust", the current strong upsurge in metal prices (hitting historic record levels for several commodities), and the resultant boom for the exploration and mining industry has been coupled with a major problem in that limited experienced geological professionals are available for the industry's demands. This is an issue that must be addressed, and urgently.

Of particular interest has been the massive upsurge in recent times of exploration for uranium, coupled not only with the substantive price rise, but also with the world-wide demand to deal with perceived global-warning. Clearly in an energy driven world fossil fuels are not only now perceived as damaging but also are clearly finite and hence the newly perceived "green credentials" of nuclear power. This interest was underlined by the strong interest in the thematic session on uranium at the conference.

Closer to home the Irish minerals industry continues, and enjoys good profitability at last, and the zinc mines at Navan, Lisheen and Galmoy prosper and a new phase of exploration in the Irish midlands has began to flourish and Ireland's first gold mine achieved producer status in 2007.

Twenty two thematic sessions were agreed by the SGA and the call for presentations brought 409 extended abstracts for review from authors based in 49 different countries. The Society of Economic Geologists kindly organized a thematic session entitled *Compressional Tectonics, Expanding Resources: Exploration Advances in the Tethyan Belt*.

The team of 46 Conveners completed their tasks of review and the result of this effort is the volumes to which this note is the preface and which includes 394 presentations. The Editor would like to thank all of these individuals for the sterling effort they put in, not only as reviewers but also as solicitors for additional papers. The presentations were made over four days in four parallel oral sessions with additional poster display sessions.

Eight short courses were offered over the weekend prior to the conference - Orogenic Lode Gold Deposits, Granite related Gold Deposits, Sediment Hosted Base-Metal Deposits, Sediment Hosted Base Copper Deposits, Isotopes in Exploration, Exploration for Skarn Deposits, Applied Structural Geology for Economic Geologists, Advances in 3D Geological Modelling. In addition seven field trips to the Iberian Pyrite Belt, Parys Mountain/Avoca, Irish Zn/Pb Deposits, Lode Gold Deposits in Dalradian of Northern Ireland, Rehabilitation of Old Mine Sites in Ireland, Fennoscandinavia and to Poland were offered and run.

In addition an extensive social program for delegates and for accompanying persons was organized and attracted an extremely high level of interest.

Of course no conference such as this could be organized without you the delegates, the speakers the poster presenters, the conveners and the session chairmen. The IAEG thanks you for all of your efforts thus far and it behoves me, and behalf of the Organizing Committee, to wish you all a successful and scientifically fulfilling meeting and also to encourage you to enjoy the delights of Dublin and Ireland.

Colin J. Andrew
Chairman – Technical Sessions

Navan, Ireland
June 2007

# Meeting Committee

| | | |
|---|---|---|
| Gerry Stanley | Chairman | *Geological Survey of Ireland* |
| John Pyne | Deputy Chairman | *Exploration and Mining Division, Department of Communications, Marine and Natural Resources* |
| Colin Andrew | Technical Committee Chairman | *Cambridge Mineral Resources plc* |
| Eibhlin Doyle | Treasurer | *Geological Survey of Ireland* |
| Ed Slowey | Sponsorship | *CSA Ltd* |
| Kerr Anderson | Field Trips and Short Courses | *Ormonde Mining plc* |
| Wayne Cox | Marketing | *Exploration and Mining Division, Department of Communications, Marine and Natural Resources* |
| Sandy Archibald | IAEG | *Aurum Exploration Services Ltd.* |
| Catherine Ault | IAEG | *Aurum Exploration Services Ltd.* |
| John Graham | Trinity College liaison | *Trinity College Dublin* |
| | | |
| Hartwig Frimmel | SGA – President | *University of Würzburg* |
| David Leach | SGA – Treasurer | *United States Geological Survey* |
| Jan Pasava | SGA – Executive Secretary | *Czech Geological Survey* |
| Adrian Boyce | SGA – Councillor | *Scottish Universities Environmental Research Centre* |
| Anna Vyazalova | SGA – Student Representative | *Czech Geological Survey* |
| Rich Goldfarb | SGA – SEG President | *United States Geological Survey* |
| | | |
| Secretariat | Ms Nicky McGrane | *Conference Partners* |
| | Ms Leah Duxbury | *Conference Partners* |
| | Ms Lisa Collins | *Conference Partners* |
| | (Ms Sinead Marrinan) | *ex Conference Partners* |

# Editors

*(listed in alphabetical order)*


Colin Andrew
*Cambridge Mineral Resources plc, London, England*

Irvine Annesley
*Saskatchewan Research Council, Saskatoon, Canada*

Sandy Archibald
*Aurum Exploration Ltd. Navan, Ireland*

Georges Beaudoin
*Université Laval, Québec, Canada*

Frank P. Bierlein
*Centre for Exploration Targeting, University of Western Australia, Crawley, Australia*

Gregor Borg
*Petrology and Economic Geology Research Group, Martin-Luther-University Halle-Wittenberg, Germany*

Adrian Boyce
*Scottish Universities Environmental Research Centre, East Kilbride, Scotland*

Dave Broughton
*Department of Geology and Geological Engineering, Colorado School of Mines, Golden, USA*

Vertrees "Mac" Canby
*Phelps Dodge Exploration Corporation, Coham, United Kingdom*

James Cleverley
*Predictive Mineral Discovery CRC & Computational Geoscience for Predictive Discovery, Exploration & Mining, CSIRO, Bentley, Australia*

John Clifford
*Clifford Consultants, Athlone, Ireland.*

David Cooke
*CODES, the ARC Centre of Excellence in Ore Deposits, University of Tasmania, Hobart, Tasmania, Australia*

Michel Cuney
*UMR G2R-CNRS-CREGU, Henri Poincaré University, Vandoeuvre les Nancy, France*

Hartwig Frimmel
*Institute of Mineralogy, University of Würzburg, Würzburg, Germany*

Rich Goldfarb
*United States Geological Survey, Denver, Colorado, USA*

David Groves
*Centre for Exploration Targeting, University of Western Australia, Crawley, Australia*

Steffen Hageman
*Center for Exploration Targeting, School of Earth and Geographical Sciences, University of Western Australia, Australia*

Richard Herrington
*Department of Mineralogy, Natural History Museum, London, England*

Al Hofstra
*United States Geological Survey, Denver, Colorado, USA*

David Huston
*Geoscience Australia, Canberra, Australia*

Kate Johnson
*United States Geological Survey, Reston, USA*

Andy Kerr
*Geological Survey of Newfoundland and Labrador, Department of Natural Resources, St. John's, Newfoundland,, Canada,*

Kalin Kouzmanov
*Institute of Isotope Geochemistry and Mineral Resources, ETH Zürich, Switzerland*

Duncan Large
*Consultant, Braunschweig, Germany*

Ross Large
*Centre for Ore Deposit Research, University of Tasmania, Hobart, Tasmania, Australia*

David Leach
*U.S. Geological Survey, Denver, Colorado, USA*

Bernd Lehmann
*Institute of Mineralogy, University of Würzburg, Würzburg, Germany*

Dave Lentz
*Dept. of Geology, University of New Brunswick, Fredericton, Canada*

Alistair McCready
*Mining & Minerals Division, Saskatchewan Research Council, Saskatoon, Canada*

Laurie Meinert
*Department of Geology, Clark Science Center, Smith College, Northampton, Maine, USA*

Julian Misierwicz
*Gold Fields International Services Limited, Oxford, England*

Ferenc Molnár
*Department of Mineralogy, Eötvös Loránd University, Hungary.*

Robert Moritz
*Section des Sciences de la Terre, Université de Genève, Genève, Switzerland*

Jan Pasava
*Czech Geological Survey, Prague, Czech Republic*

Jan Peter
*Central Canada Division, Geological Survey of Canada, Ottawa, Ontario, Canada*

Irena Peytcheva
*Institute of Isotope Geochemistry and Mineral Resources, ETH Zürich, Switzerland*

Albecht von Quadt
*Institute of Isotope Geochemistry and Mineral Resources, ETH Zürich, Switzerland*

Patrick Redmond
*Teck Cominco Ireland, Dublin, Ireland*

Gordon Riddler
*Maghreb Minerals PLC, London, England*

Paul Roberts
*Predictive Mineral Discovery CRC and CSIRO Exploration & Mining, Bentley, Australia*

Steve Roberts
*School of Ocean and Earth Science, National Oceanography Centre, University of Southampton, Southampton, England*

Peter Scott
*Camborne School of Mines,*
*University of Exeter in Cornwall, Penryn,*
*Cornwall, England.*

Gerry Stanley
*Geological Survey of Ireland, Dublin, Ireland*

Holly Stein
*Department of Geosciences, Colorado State University, Fort Collins, Colorado, USA*

Dave Symons
*Dept. of Earth and Environmental Sciences, University of Windsor, Windsor, Ontairio, Canada*

Fernando Tornos
*Instituto Geológico y Minero de España. Salamanca, Spain*

Jamie Wilkinson
*Department of Earth Science and Engineering, Imperial College London, London, England*

Patrick Williams
*School of Earth Sciences, The University of Melbourne, Parkville. Australia.*

# ORE DEPOSITS THROUGHOUT SPACE AND TIME

EDITED BY:

NICK ARNDT

FRANK P. BIERLEIN

DAVID HUSTON

# Concentration of ore and industrial minerals in Central Europe: temporal, structural and sequence stratigraphic classification schemes

Dill, H.G.
*Federal Institute for Geosciences and Natural Resources, P.O. Box 510163 D-30631 Hannover, Germany*

Sachsenhofer, R.F.
*Department of Applied Geosciences and Geophysics, University of Leoben, Peter Tunner Strasse 5, A-8700 Leoben, Austria*

Grecula, P., Sasvári, T., Palinkaš, l. A., Borojević-Šoštarić S., Strmić-Palinkaš S., Prochaska, W., Garuti, G., Zaccarini, F., Arbouille, D., Schulz H.-M.
*Košice, Slovakia, Zagreb, Croatia, Modena, Italia, Geneva, Switzerland*

ABSTRACT: A classification of non-metallic and metallic deposits as well as energy resources has been performed for Central Europe. The Variscan metallogenesis in Central Europe outside the Alps with predominantly granitophile elements is denominated as an "ensialic metallogenesis", whereas the Alpine successor shows all the hallmarks of an "ensimatic metallogenesis". Part of the Variscan metallotect was re-activated during Alpine metallogenesis and incorporated into the Alpine metallotect. Classification schemes based on the age of formation, structure and sequence stratigraphic elements are discussed. Planar architectural elements in the various schemes such as unconformities, transgressive surfaces, flooding surfaces and sequence boundaries play a decisive role in siting ore traps and correlating mineral deposits.

KEYWORDS: ore minerals, industrial minerals, energy resources, Central Europe, classification, age of formation, structures, sequence stratigraphy

## 1. INTRODUCTION

Central Europe looks back on more than 2000 years of mining and on more than 500 Ma of ore mineralization and deposition of non-metallic and energy resources. The area hosts some of the most well-known deposits on earth, *e.g.* Rammelsberg (Germany), Kupferschiefer (Germany, Poland), Bleiberg (Austria), Jáchymov (Czech Republic). Many of these have significantly contributed to the understanding of the origin of similar deposits elsewhere in the world. Several attempts have been made to subdivide this metallotect and place its mineral deposits into a classification scheme (Petrascheck 1963, Bernard *et al*. 1976, Baumann 1979, Pouba & Ilavský 1986, Jaffé 1986, Dill 1989, 1994, Walther & Dill 1995).

Classification of mineral and energy resources may be performed in different ways, dependant upon the data base for the area under consideration and the audience for whom the paper is written. The traditional classification scheme in the mining industry is based on mineral commodities (*e.g.* monographs like "The Iron Ore Deposits of Europe"; Zitzmann 1997).

In the following sections, the mineralization processes and the resultant deposits are subdivided into various first- and second order categories.

## 2. TEMPORAL AND STRUCTURAL CLASSIFICATION SCHEMES

The Variscan and Alpine metallogenetic successions are not very much different as far as the types of deposits are concerned. A sequence of stratabound, thrust-bound and collision-/granite-related deposits developed during the Variscan and Alpine metallogenesis. The late Variscan/early Alpine and sub-Hercynian/Laramide/late Alpine uplift resulted in the formation of a set of unconformities or, in geomorphological terms, peneplains with which supergene and hypogene mineralizations are associated. The limit between the late and early Alpine epochs of unconformity-related mineralization coincides with the period of maximum spreading in the Alpine Tethys during mid-Jurassic times. Re-mobilization was

triggered along deep-seated fault zones during various periods of the Variscan and Alpine metallogenetic cycles.

## *2.1 Variscan Metallogeny*

### *2.1.1 Stratabound Deposits*

*Precambrian-Cambrian*: Graphite and semigraphite deposits, silicate-(and carbonate-) hosted base metal-iron sulphide deposits (VHMS-, SMS-, Kieslager-Type), carbonate-hosted Fe deposits, Sn-W-Au-Pb-Cu deposits, Cr-Ti-Ni-PGE and magnesite deposits.

*Ordovician-Silurian*: Ironstone deposits (Thuringite-/Wabana-Type), Au-bearing Cu-Zn-Fe sulphide deposits (VMS-Type), graphite-meta-anthracite and oil shale deposits, uraniferous polymetallic deposits (Black shale-Type)

*Devonian-(Lower) Carboniferous*: Fe-Mn deposits (Lahn Dill-Type/ SEDEX), base metal-Fe sulphide-barite deposits (Rammelsberg-Type/SMS-Type), W and magnesite deposits, Cu-Mo-W deposits (Porphyry-Type),

*Upper Carboniferous:* Graphite deposits in the Alpine realm, ironstone deposits in the Variscan basins (claybands and blackbands)

### *2.1.2 Thrustbound and fold-related metamorphogenic deposits*

Ag-bearing base metal vein-type deposits, Cu-bearing Fe-oxide vein-type deposits, Cu-Sb-siderite vein-type deposits (Siegerland-Type), Au-Sb-As vein-type deposits (mesothermal Au-Sb vein-type), Au-W vein deposits, thrustbound talc and asbestos deposits in (ultra)basic igneous rocks, feldspar-quartz pegmatoids and quartz lodes

### *2.1.3 Collision (granite)-related deposits*

Disseminated Ni-Cu deposits, Sn-W-Mo vein-type, greisen and skarn deposits, Pb-Cu-Zn-Ag vein deposits, polymetallic and monotonous U vein-type deposits, feldspar-quartz and polymetallic Li-Nb-Ta pegmatites, talc (soapstone) replacement deposits in carbonate rocks

## *2.2. Alpine Metallogeny*

### 2.2.1 *Early Alpine supergene and hypogene deposits related to the Post-Variscan* unconformity

*Supergene deposits*: Kaolin saprolite associated with the early Alpine unconformity, U vein-like deposits beneath the early Alpine unconformity

*Hypogene deposits*: Meso- to epithermal polymetallic Hg-precious metal vein-type deposits in volcano-sedimentary series, U-Mo-Cu vein-type and stratiform deposits in volcano-sedimentary series, fluorite-barite and base metal vein-type, impregnation and replacement deposits, Fe–(barite) vein-type deposits, Fe-base metal-barite vein-type and replacement deposits, polymetallic siderite and magnesite replacement deposits.

### *2.2.2 Stratabound deposits*

*Upper Carboniferous-Lower Permian*: U deposits in intermontane basins in the extra-Alpine realm (Coal- and Oil-Shale-Type), U deposits in intermontane basins in the Alpine realm (Volcanic-Type), Sn-Au-PGE/PGM paleoplacers

*Middle to Upper Permian:* Polymetallic Cu deposits in the epicontinental and Alpine basins (Red bed-Type/SHSCD-Type), U deposits in Alpine basins (Red bed-Type), U-Cu deposits in the Alpine basin (Red bed-Type), polymetallic Cu deposits in the epicontinental basin (Kupferschiefer-Type), Na-, K and bitter salt-bearing evaporite deposits in the epicontinental and Alpine basins (Zechstein- and Haselgebirge-Type), barite deposits in Alpine basins (Sabkha-Type), Ni-Cu-PGE and Fe sulphide deposits in the Alpine basin (Rift-related Type), polymetallic barite deposits in the Alpine basin (Initial Rift-SEDEX-Type)

*Triassic*: Polymetallic Cu deposits in the epicontinental and Alpine basins (Red bed-Type), U deposits in the epicontinental and Alpine basins (Red bed-Type), Na-earth alkaline-elements-bearing evaporite and Pb deposits in the epicontinental and Alpine basins (Sabkha-Type), Fe-Mn-Cu polymetallic deposits in the Alpine basin (Rift-related – Red Sea-Type), polymetallic barite deposits in the Alpine basin (Advanced Rift- SEDEX-Type), Hg deposits in the Alpine basin (Composite SEDEX-Type), Fe-Mn deposits in the Alpine basin (SEDEX-Type), Cu-Ni deposits in the Alpine basin (embryonic Ophiolite-Type), carbonate-hosted Pb-Zn deposits in the epicontinental basin (Silesian-Type/ MVT), Carbonate-hosted Pb-Zn deposits in the Alpine basin (Alpine-Type/MVT).

*Jurassic-Lower Cretaceous*: Na- and earth alkaline elements-bearing evaporite deposits in epicontinental basin, coal deposits and oil shales, ironstone deposits in the epicontinental basin (Minette-Type), Mn deposits in the Alpine basin, Cr-Cu-Fe and magnesite deposits in the Alpine basin (Ophiolite-Type)

*Cretaceous*: Fe-P deposits in the epicontinental basin (Pebble Iron Ore / Black River-Type), strontium deposits in epicontinental basin.

*Tertiary:* Ti-Zr placer deposits in epicontinental basins, amber deposits in epicontinental basins, Fe-Mn deposits in the foreland and flysch basins (Pelosiderite-Type), alkaline and earth alkaline elements-bearing evaporite deposits in rift- and intermontane basins, S deposits in foreland basins, smectite-attapulgite deposits in the Alpine foreland and flysch basins, arc-related Au-Ag-Cu-Mo-Pb-Zn-Sb-Hg porphyry and epithermal deposits, kaolinite-illite-smectite-mixed layer-alunite-silica deposits in intra- and backarc basins, zeolite deposits in backarc basins, perlite deposits in backarc basins, diatomite deposits in backarc, foreland and epicontinental basins, quartz sand deposits in epicontinental basins (glass sand).

*Quaternary*: Sn-Au-Ti and gemstone placer deposits (Type: modern placers), diatomite deposits.

### *2.2.3 Thrustbound and fold-related metamorphogenic deposits*

Polymetallic Cu deposits, thrustbound talc-nephrite-asbestos-leucophyllite deposits in (ultra)basic igneous rocks and in carbonates, quartz vein-type deposits (Alpine-type quartz veins), Au deposits (Alpine-type/mesothermal Au veins), Fe deposits, Sb deposits

### *2.2.4 Collision (granite)-related deposits*

W-Mo-Nb-Ta-Pb and fluorite vein and greisen deposits, polymetallic feldspar quartz pegmatite and greisen deposits, polymetallic Pb-Zn-Cu deposits, iron-Cu-As-Sb-Hg-Au skarn and vein deposits, Sb replacement and vein-type deposits

### *2.2.5 Late Alpine supergene and hypogene deposits related to the Subhercynian and Laramide unconformity*

*Supergene deposits*: Kaolinite saprolite on the Variscan basement and in Mesozoic to Cenozoic rocks**,** bauxite deposits on late Alpine unconformities, tripoli deposits on late Alpine unconformities, Fe-Mn-P deposits on the Variscan basement (Hunsrück-Type and Lahn-Type), manganiferous Pb deposits associated with the late Alpine unconformity, Ni-Cr–Co laterites on ultrabasic rocks, amorphous magnesite deposits

*Hypogene deposits:* Pb-Zn-Fe and fluorite-barite-calcite-quartz vein-type deposits, carbonate-hosted Pb-Zn deposits, U deposits

### *2.2.6 Deposits controlled by igneous activity along deep-seated faults and remobilization*

Bi-Co-Ni deposits, Fe-Pb-Zn and barite-fluorite deposits, polymetallic Nb deposits.

## 3. SEQUENCE STRATIGRAPHIC CLASSIFICATION SCHEME

Planar elements used in sequence stratigraphy, such as TS (transgressive surface), FS (flooding surface) and SB (sequence boundary) are the key elements in predicting the position of diagenetic and epigenetic mineral deposits of epicontinental basins and rift grabens. The effective accommodation space is decisive for non-metallic commodities such as evaporites, covering the whole spectrum from fluorite (HST: highstand systems tracts) through carnallite (LST: lowstand system tracts), and energy resources such as duricrust-bound uranium mineralization in regressive deposits (HST). The present observations indicate that system-tract-related mineralization, developed during early diagenesis in coastal sabkhas, (Zechstein salt) and inland playas (sandstone-hosted U deposits) with almost no time difference between formation of the host rocks and the deposit, proper. Minerals in salt seams may undergo a great variety of compositional and structural alteration; taken to the extreme, they may become self-intrusive on burial and pierced into the roof rocks. The ratio of thickness of evaporite sediments (effective accommodation) to total accommodation provided during basin subsidence, which is equivalent to the thickness of seam plus hanging wall rocks, is a measure for the intensity of halokinetic processes. The geological situations recorded for MVT deposits accommodated in a HST come close to what is well known from hydrocarbon plays in carbonate rocks, where hydrocarbons are expelled from overpressured basin deeps, an example of which is the Wiesloch Zn-Pb deposit. In systems-tract-related mineral deposits and in hydrocarbon deposits, the build-up of traps and the element mobilization have both a strong vertical component. Opposed to that, the majority of stratabound sediment-hosted mineral deposits are of moderate thickness and SB-controlled vein-type deposits die out very swiftly underneath the plane which they are related to in space.

For decades economic geology has been the battle ground between different schools, trying to convince each other that deposits are either epigenetic or syngenetic. As long as modern radiometric age dating of metal deposits was in the state of infancy, there was little room for compromise between the two. An ever-increasing number of age data collected from stratabound sediment-hosted deposits, *per ascensum* vein-type as well as *per descensum* vein-like deposits has led to the shrinkage of the gap between advocates of epigenetic and syngenetic deposits. In the Bohemian Massif, for example, radiometric age dating has furnished evidence that granite-related U mineralization was at full swing at depth, while hypogene vein mineralization with fluorite and pitchblende commenced at shallow depth underneath the early Alpine unconformity/SB. At the same a time a tropical climate sparked pervasive supergene alteration of basement rocks on the late Variscan/early Alpine peneplain truncating the uplifted Variscan basement blocks and ending up with kaolin deposits of commercial value. Base metal vein-type mineralization (called in German Rückenerze) controlled in their aerial distribution by the palaeogeography of the Kupferschiefer sea is contemporaneous with the epigenetic Kupferschiefer mineralization in the mining districts in Poland. Base metal mineralizations encountered in MVT deposits in Middle Triassic calcareous host rocks at Wiesloch (Germany), in Upper Silesia (Poland) and in Late Palaeozoic carbonates at La Calamine (Belgium), although being located far apart from each other, have a common bounding surface which delimits ore mineralization. It is a type-1 SB that forms the basis for *per descensum* kaolin deposits, the seal for *per ascensum* vein-type deposits and the transgressive surface for the Late Cretaceous sea to encroach upon the Variscan basement blocks from the Atlantic and the Tethyan oceans.

## 4. SUMMARY AND CONCLUSIONS

The Variscan metallogenesis in Central Europe outside the Alps with predominantly granitophile elements is denominated as an "ensialic metallogenesis", acting under more or less closed-system conditions, whereas the Alpine successor shows all the hallmarks of an "ensimatic metallogenesis", when for a period of time the system was open for elements to be introduced from subcrustal sources. The Variscan metallogenesis may largely be taken as a continuum, whereas the Alpine metallogenesis in the extra-Alpine region as well as in the Tethyan basin is either indirectly or directly affected by the formation of an oceanic crust in the Penninic, Meliata and Vardar zones.

The linkage between the classical temporal - structural classification scheme of deposits and the newly-introduced sequence stratigraphic scheme are planar structural elements such as unconformities and sequence boundaries. Even a few examples out of the wide range of deposits in Central Europe document that too much emphasis placed on the distinction of epigenetic vein-type and stratabound syn(dia) genetic deposits is not advisable and may be in practice sometimes unworkable. Finding common tie lines may provide predrill estimates of the geological parameters and rather help geologists siting the ore trap.

## REFERENCES


Baumann L (1979) Some aspects of mineral deposits formation and the Metallogeny of Central Europe. *Verhandlungen der Geologischen Bundesanstalt* pp 3: 205-220

Bernard JH, Cadek J, Klominsky J (1976) genetic problems of the Mesozoic fluorite-barite mineralization of the Bohemian Massif. *Geol. Inst. Warshaw* pp 1976: 217-226.

Dill H G (1989) Metallogenetic and geodynamic evolution in the Central European Varsicide – a prewell site study for the German Continental Deep Drilling Programme. *Ore Geology Review* pp 4: 279-304

Dill H G (1994) Facies variation and mineralization in Central Europe from the late Paleozoic through the Cenozoic. *Economic Geology* pp 89: 42-61

Jaffé F C (1986) Switzerland. In: Dunning, F.W. & Evans, A.M. (eds) Mineral deposits of Europe, vol. 3 Central Europe *IMM & Miner. Soc. London*,

Petrascheck WE (1978) Zur Altersbestimmung einiger ostalpiner Lagerstätten. *Mitteilungen der Österreichischen Geologischen Gesellschaft* pp 68: 79-87

Pouba Z, Ilavsky J (1986) Czechoslovakia. In: Dunning, F.W. & Evans, A.M. (eds) Mineral deposits of Europe, 3, Central Europe. *IMM & Miner. Soc. London,* 117-173

Walther HW (1986) Federal Republic of Germany. In: Dunning, F.W. & Evans, A.M. (eds) Mineral deposits of Europe vol. 3, Central Europe *IMM & Miner. Soc. London,* 175-301.

Walther HW, Dill HG (1995) Die Bodenschätze Mitteleuropas - Ein Überblick. In: Walter, R. (ed) *Die Geologie von Mitteleuropa,* Schweizerbart, Stuttgart, 526-542.

Zitzmann A (ed.) (1977) The iron ore deposits of Europe and adjacent areas. *Bundesanstalt für Geowissenschaften und Rohstoffe*, Hannover 418 pp.

# Derivation of Global Metallogenic and Resource Data from Ore-Deposit Age-Frequency Distributions

Stephen E. Kesler
*Department of Geological Sciences, University of Michigan, Ann Arbor, MI, USA - 48105*

Bruce H. Wilkinson
*Department of Earth Sciences, Syracuse University, Syracuse, NY, USA - 13244-1070*

ABSTRACT: We have shown that deposits that form deep in the crust have distinctly different age-frequency distributions from those that form at shallow depths and that this difference reflects the depths at which the deposits are formed. Confirmation that these age-frequency distributions are controlled by exhumation is seen in the fact that they can be used to calculate exhumation (erosion) rates that are identical to those estimated by other methods. A computational model constrained by the age-frequency distributions can be used to generate a deposit endowment for a steady-state Earth. Results of this model calculation provide information on the number and distribution of ore deposits throughout the crust thereby yielding the first quantitative estimate of the ore deposit endowment of Earth's entire crust. Comparison of steady-state model results to those of the real Earth provide a quantitative method for identification of metallogenic provinces and epochs. Example model calculations show that currently known deposits make up less than 2% of Earth's total copper endowment and confirm that Precambrian orogenic gold deposits constitute a highly anomalous metallogenic event.

KEYWORDS: metallogenic province, metallogenic epoch, age-frequency distribution, ore deposit

## 1 INTRODUCTION

We have shown that age-frequency distributions for ore deposits in convergent margin settings, are controlled largely by the combination of burial and uplift known collectively as exhumation (Kesler & Wilkinson, 2006). Here, we show that a model based on this generalization provides the first quantitative estimate of global crustal mineral endowments as well as the nature and distribution of metallogenic provinces and epochs through time.

## 2 CONTROLS ON AGE-FREQUENCY DISTRIBUTIONS OF ORE DEPOSITS

Exhumation controls age-frequency distributions for ore deposits because it takes time for deposits that form in the subsurface to reach the surface (and become part of the age-frequency distribution). The age of an ore deposit at the surface reflects primarily the depth at which it formed, with deposits that formed at shallow levels in the crust being exhumed more quickly (in geological terms) than deposits that formed at deep levels. As a result, age-frequency patterns for groups of deposits that form at shallow and deep levels in the same geological environment will differ.

Deposits that form at shallow levels will have age-frequency patterns characterized by numerous young deposits and a gradual decrease in number of deposits through time. Deposits that form at deep levels will have age-frequency patterns characterized by few or no young deposits, followed by an increase in the number of deposits to a maximum, and then a gradual decline in number of deposits of increasing age (Kesler & Wilkinson, 2006, Fig. 1).

The fact that some deposits are buried under younger rocks after they form whereas others are uplifted and eroded immediately does not change these generalizations because burial is an important part of the overall exhumation process. This fact is often forgotten, although it is the driving force behind mineral exploration, which seeks deposits that have remained in the subsurface because of just such burial.

## 3 MODEL SIMULATION OF AGE-FREQUENCY DISTRIBUTIONS

Age-frequency distributions derived from many individual deposits of a single type provide information on their distribution in space and time, including global resources and metallogenic provinces/epochs. The length of the time period used to bin data for age-frequency plots will control which of the two end-member curves noted above is generated. Bins with long time periods will generate age-frequency distributions typical of shallow deposits because the time required for a deposit to be exhumed is included in the first time period. Care must be taken to use a bin with a time period that captures the full structure of the age-frequency distribution. The ultimate loss of information would result from use of a single bin with duration equal to the age of Earth (4.5 Ga).

Age-frequency distributions for epithermal, porphyry copper, and orogenic gold deposits, which form at successively deeper crustal levels in convergent margins are shown in Figure 1. These distributions take the form predicted above, with a relatively abrupt increase in numbers of deposits to a maximum (modal) number, and then a gradual decrease in the number of increasingly older deposits.

Proof that these distributions are controlled by exhumation is provided by the fact that they can be used to calculate exhumation rates similar to those obtained for convergent margin terranes by other methods. Average exhumation rates can be calculated by dividing the modal age of each deposit type (*i.e*., the amount of time it took the age bin with the largest number of deposits to be exhumed) by the depth at which most deposits formed (modal depth, 0.5 km for epithermal, 1.9km for porphyry copper, 10 km for orogenic gold), as estimated from recent compilations by Simmons *et al*. (2005), Seedorf *et al*. (2005), Goldfarb *et al*. (2005) and Singer *et al*. (2005). Modal exhumation rates calculated using these parameters are 167, 158 and 63 m/m.y. for epithermal, porphyry copper and orogenic gold, respectively. Exhumation rates calculated for the youngest deposits in each group (0.3, 1.15, and 52 m.y.), using the same modal depths, are 1667, 1652 and 192 m./m.y., respectively.

These rates agree closely with rates estimated by other methods, including cosmic isotopes, apatite fission-track, and sediment fluxes. Estimates for continent-scale terranes and long time periods range from 20 to 50 m/m.y. (Bernet *et al*., 2002; Wilkinson, 2005). Estimates for smaller regions range from 100 to 500 (Kirchner *et al.*, 2001), with a few reaching values of 1000 to 5000 m/m.y. (Vance *et al.*, 2003; Willett *et al.*, 2003), which are similar to the large values calculated above from appearance of youngest deposits.

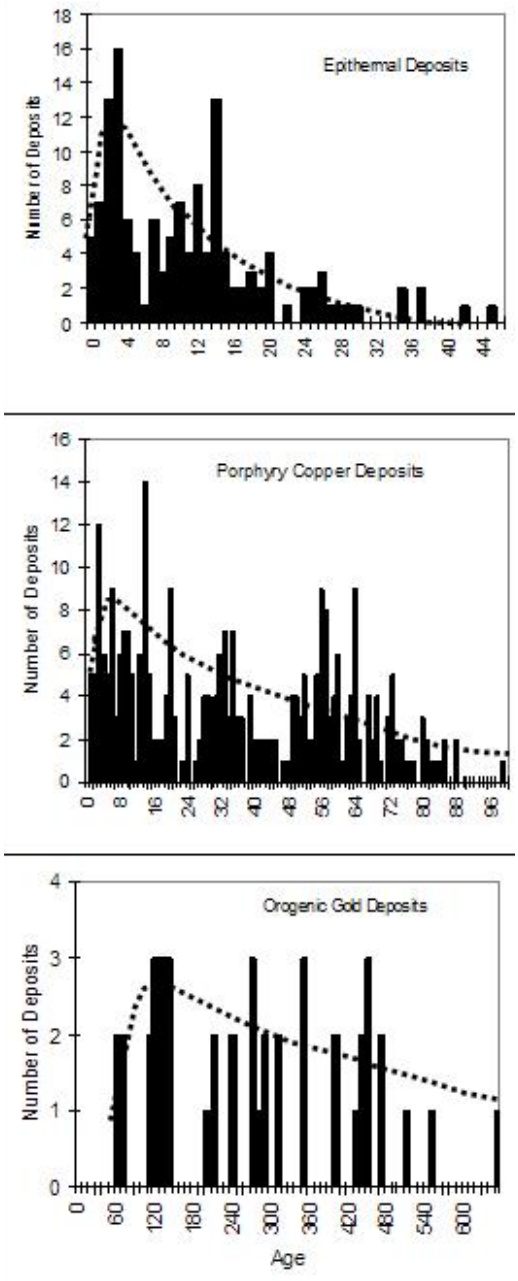


Figure 1. Age-frequency distributions for epithermal, porphyry copper and orogenic gold deposits. Dashed lines are best-fits to the data.

We have developed a computational model that reproduces the observed age-frequency distributions for ore deposits by simulating the movement of deposits through Earth's crust and

their appearance at the surface. Computationally, the model forms a series of deposits of a specific type and allows them to move upward or downward, or to remain at the same level (stasis) with the passage of each time interval such that individual deposits in the series follow many different paths through the crust. This process reflects the point made above that rocks and their contained deposits undergo both burial and uplift through time. The model evaluates numerous possible up-down-stasis combinations for a group of deposits until it yields a best fit to the number of individuals and their age-frequency distribution for the deposit type of interest (Fig. 2).

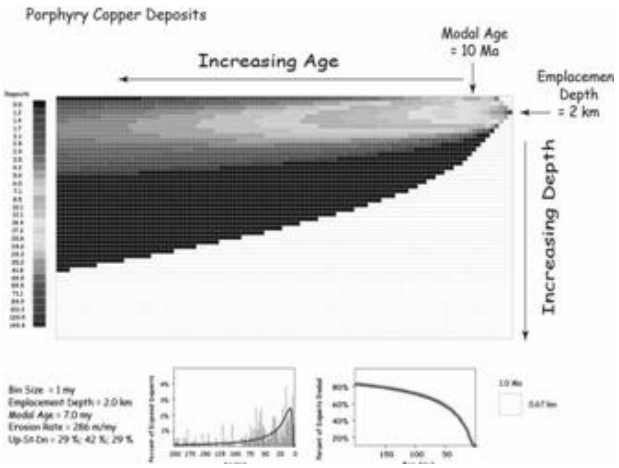


Figure 2. Example of model calculation for porphyry copper deposits emplaced at 2 km depth. Upper panel shows distribution of deposits in crust. Lower panels show (left) best-fit model for age-frequency distribution and (right) number of deposits removed by erosion through time.

## 4 QUANTITATIVE ASSESSMENT OF RESOURCES AND METALLOGENIC FEATURES FROM THE MODEL SIMULATIONS

The model simulations allow the first truly quantitative assessment of metal provinces/epochs and global resources. This is possible because the model estimates the number of ore deposits of a specific type that should be present in an Earth that have formed deposits continuously (that is, a steady-state Earth).

From the standpoint of global reserve estimates, the model provides direct, quantitative information on the number of deposits at all depths in the crust, including depths that are far below those constrained by reasonable extrapolations of surface and near-surface geologic data (Fig. 2). For instance, model simulation of the age-frequency distribution for porphyry copper deposits suggests that Earth has formed approximately 100,000 of these deposits through Phanerozoic time, and that about two-thirds of these have been removed by erosion. Known deposits (with the age-frequency that controls this model) make up about 1.6% of the ~33,000 deposits that remain in Earth's crust. Total copper endowment represented by these porphyry copper deposits is about $1.2 * 10^{11}$ tonnes. Assuming that other important copper deposit types have similar exhumation histories and that porphyry copper deposits make up about 57% of total copper deposits (Singer, 1995), total global copper resources of Phanerozoic age amount to approximately $2*10^{11}$ tonnes. There are no equivalent estimates to which this value can be compared, but the U.S. Geological Survey recently estimated that the copper endowment of the United States to a depth of 1 km is $\sim 10*10^{8}$ tonnes (Anonymous, 1998), which is almost the same as the $\sim 8*10^{8}$ indicated for that crustal slice by our model. Significantly, the US Geological Survey estimate was based on detailed geological data and involved a large number of professionals working from decades of field observation, whereas our model is based only on ages of known deposits.

From the standpoint of metallogenic features, by simulating a steady-state Earth, our model provides a quantitative basis for recognition of both provinces and epochs. Any deviation from this steady-state in quantity of deposits, whether positive or negative, reflects an anomalous event. One very good example of this is provided by the age-frequency distribution for orogenic gold deposits. Although the age-frequency distribution of Phanerozoic deposits follows the general form predicted above, Precambrian deposits are far more abundant than would be predicted by preservation alone. These older orogenic gold deposits formed at the same crustal depths, or possibly even shallower because of higher heat flow. Their presence at the present surface requires exhumation (erosion) rates of about 0.004 m/m.y., which are far less than rates of ~5 m/m.y. that have been estimated for Precambrian shield terranes from other methods (Bierman & Caffee, 2002). Unless these other rates or greatly in error, Precambrian orogenic gold deposits must have been formed in considerably greater abundance than their Phanerozoic counterparts.

## 5 CONCLUSIONS

Age-frequency distributions of ore deposits that form in the subsurface can be modeled computationally by simulating their up, down and stasis movement through the crust. These models confirm that the age-frequency distributions are controlled by exhumation and provide the first quantitative basis for estimation of global mineral resources and recognition of metallogenic provinces and epochs.

## REFERENCES


Anonymous (1998) 1998 Assessment of undiscovered deposits of gold, silver, copper, lead and zinc in the United States: *U.S. Geological Survey Circular* 1178, 21pp.

Bernet M, Reiners PW, Brandon M Garver JI (2002) Average erosion rate of the Colorado Plateau estimated from thermochronologic data [abs.]. *Geological Society of America Abstracts with Programs* 34: 322.

Bierman PR, Caffee M (2002) Cosmogenic exposure and erosion history of Australian bedrock landforms. *Geological Society of America Bulletin* 14: 787–803

Goldfarb RJ, Baker T, Dubé B, Groves DI, Hart CJR, Gosselin P (2005) Distribution, character and genesis of gold deposits in metamorphic terranes. In Hedenquist JW, Thompson JFH, Goldfarb RJ, Richards JP (eds) *Economic Geology - One Hundredth Anniversary Volume (1905-2005): Society of Economic Geologists*, pp 1069-1096.

Kesler SE, Wilkinson BH (2006) The Role of Exhumation in the Temporal Distribution of Ore Deposits. *Economic Geology* 101: 919-922.

Kirchner JW (2001) Mountain erosion over 10 yr, 10 k.y., and 10 m.y. time scales. *Geology* 29 591–594.

Seedorf E, Dilles JH, Proffett JM, Jr, Einaudi MR, Zurcher L, Stavast WJA, Johnson DA, Barton MD (2005) Porphyry copper deposits: characteristics and origin of hypogene features. In Hedenquist JW, Thompson JFH, Goldfarb RJ, Richards JP (eds) *Economic Geology - One Hundredth Anniversary Volume (1905-2005): Society of Economic Geologists,* pp 251-298.

Simmons SF, White NC, John DA (2005) Geological characteristics of epithermal precious and base metal deposits In Hedenquist JW, Thompson JFH, Goldfarb RJ, Richards JP (eds) *Economic Geology - One Hundredth Anniversary Volume (1905-2005): Society of Economic Geologists,* pp 485-522.

Singer, DA (1995) World Class Base and Precious Metal Deposits – A Quantitative Analysis. *Economic Geology* 90: 88-104

Singer DA, Berger VI, Moring BC (2005) Porphyry copper deposits of the world: database, maps, and preliminary analysis. *USGS Open-File Report* 2005-1060 (http://pubs.usgs.gov/of/2005/1060/).

Vance D, Bickle M, Ivy-Ochs S, Kubik PW (2003) Erosion and exhumation in the Himalaya from cosmogenic isotope inventories of river sediments. *Earth Planetary Science Letters* 206: 273-288.

Willett SD, Fisher D, Fuller C, Yeh E-C, Lu C-Y. (2003) Erosion rates and orogenic-wedge kinematics in Taiwan inferred from fission-track thermochronometry. *Geology 31:* 945-948.

Wilkinson BH (2005) Humans as geologic agents-a deep time perspective. *Geology* 33: 161-164.

# Gold Endowment of the Earth's Crust Over Time

Hartwig E. Frimmel
*Institute of Mineralogy, University of Würzburg, Am Hubland, D-97074 Würzburg, Germany*

ABSTRACT: The analysis of gold production data as well as reserve and resource estimates for different genetic types of gold deposits revealed that the Witwatersrand palaeoplacer and orogenic deposits account for almost 80% of all known gold. Most of the gold has been added to the continental crust as early as 3.0 Ga. About half of that gold has been recycled repeatedly on a lithospheric scale, predominantly by plate-tectonically induced magmatic and hydrothermal fluid circulation. The overall proportion of known gold bound in ore bodies corresponds to that of gold that is dissolved in modern crustal fluids.

KEYWORDS: gold, deposit types, lithospheric recycling, Archaean

## 1 INTRODUCTION

Total historic gold production is estimated (based on Gosselin & Dube 2005; updated) at approximately 183,000 tonnes (t). This gold has been mined from a variety of deposit types that range in age from Archaean to Recent. Economic gold concentrations in ore bodies are typically at a level that corresponds to an enrichment factor of about $10^4$ relative to average crustal background levels (*e.g.* Krauskopf & Bird 1995). The existence of these ore bodies implies transport and concentration of gold by magmatic, hydrothermal and sedimentary processes in spite of the very low reactivity of this noble metal. The relative significance of these processes remains unclear. The aim of this study is therefore to evaluate the principle mechanisms of gold distribution in Earth's crust as well as possible temporal variations of these mechanisms over geological time.

To that effect, data on past gold production, reserves and resources – largely based on the gold data base of the Geological Survey of Canada (Gosselin & Dube 2005), Raw Materials Data© (2006), and Handley (2004), and supplemented by numerous other, largely unpublished data - were analyzed for different genetic groups of gold deposits.

## 2 RELATIVE SIGNIFICANCE OF GOLD DEPOSIT TYPES

Economic gold concentrations occur in a series of different tectonic settings at different crustal levels, thus giving rise to numerous types of gold deposits. Here the emphasis is on the gold-transporting agents and the source of the gold. Therefore, notwithstanding several far more detailed classification schemes that have been proposed previously, gold deposits are grouped here, for the sake of simplicity, into only seven classes. These are: (i) epithermal Au deposits that form(ed) in the near-surface environment in oceanic and continental volcanic arcs along convergent plate margins; (ii) porphyry Cu-Au(-Mo) deposits, including intrusion-related and skarn deposits, at shallow crustal levels in the same plate tectonic position as the epithermal deposits; (iii) orogenic Au deposits at various crustal levels, which formed syn-tectonically synchronously, or shortly after, regional metamorphism and magmatism during lithosphere-scale accretionary and continental collision orogeny; (iv) Carlin-type Au deposits at shallow crustal levels, typically found as structurally controlled, epigenetic replacement in sedimentary rocks within continental extensional regimes (basin and range province) along a craton margin, with or without influence from shallow crustal intrusives; (v) volcanogenic,

polymetallic, Cu-dominated massive sulphide deposits that form(ed) near oceanic back-arc spreading centres; (vi) Au in magmatic PGE as well as Ni-Cu deposits in mafic to ultramafic intrusive complexes; (vii) syn-sedimentary Au deposits; and (vii) placer and palaeoplacer deposits, mainly found in foreland basins.

The relative significance of these various genetic deposit types is shown in terms of recent production (Fig. 1a) and total known gold, including past production, reserves and resources (Fig. 1b). It is obvious from these distributions that the two most important deposit types are orogenic and placer deposits. The latter class is dominated by the Archaean palaeoplacer deposits of the Witwatersrand (South Africa), which make up >90 % of all known placer deposits.

## 3 GOLD TRANSFER TO THE CRUST OVER TIME

There is strong evidence for a much greater proportion of gold having been added to the crust in the Archaean than anytime later. The distribution of gold over geological time (Fig. 2) shows a marked bimodal pattern with most of the gold being either Cenozoic or Mesoarchaean in age. The vast majority of gold deposits that formed at shallow crustal levels, such as epithermal, Carlin-type and porphyry-related deposits, are Cenozoic, which can be explained by the much higher preservation potential of younger shallow crustal rocks. Note that about 50% of all continental crust is Phanerozoic (Goodwin 1991). In contrast, deposits that formed at deeper crustal levels are more evenly distributed over time. The same argument as for the shallow crustal gold deposits should apply even more so to placer deposits, bearing in mind that they typically form on the surface and in environments that are particularly prone to subsequent erosion. Yet, more than 90% of all placer gold stems from the Archaean, with only 5.7% from the Cenozoic. This bias towards the Archaean is even more exacerbated if one considers that effectively all of that Archaean placer gold comes from the Witwatersrand Basin. The uniqueness of this supergiant amongst gold provinces has been explained by a combination of factors, which include an Au-rich hinterland (*i.e.* Palaeo- to Mesoarchaean granite-greenstone belts), a foreland basin setting that, combined with Archaean environmental conditions (no vegetation cover on land, intense chemical weathering), led to particularly vigorous sediment-reworking, and an exceptional preservation beneath a thick cover of Neoarchaean flood basalt and in the middle of one of the oldest and most stable cratons (Frimmel *et al*. 2005). Other Archaean placer deposits comparable to those of the Witwatersrand might have existed also on other Archaean continents but would have been eroded or recycled into the crust during subsequent plate tectonic processes. Consequently, the theoretical rate of Au transfer into the crust should have been even higher in the Archaean than is reflected in the strongly skewed distribution of known placer gold towards Archaean deposits shown in Figure 2.

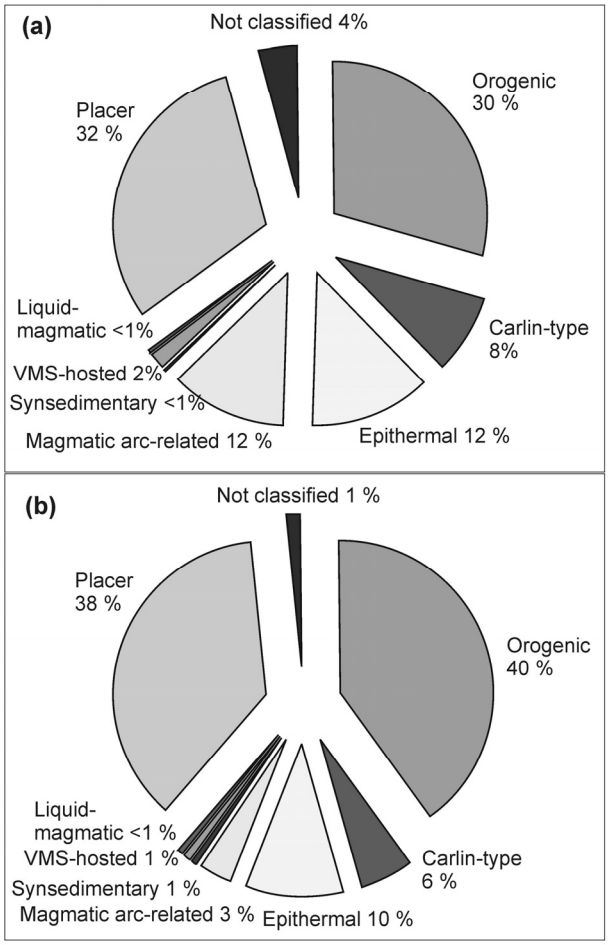


Figure 1. Relative significance of different gold deposit types in terms of (a) recent global production (1984-2005) and (b) total past production, reserves and resources combined.

A peculiar feature of the Witwatersrand gold is its extraordinarily high Re and Os contents (Kirk *et al*. 2002; Frimmel *et al*. 2005). The latter in particular is not compatible with gold precipitation from aqueous hydrothermal fluids, because of the very low solubility of Os in such fluids (Xiong & Wood 2000), but is best ex-

plained by derivation from a hot mantle that was characterized by a higher melt proportion. This is supported by the Re/Os ratio in the Witwatersrand gold, which is close to that of the mantle, and the initial $^{187}Os/^{188}Os$ ratio of 0.108, which corresponds to that estimated for the mantle at about 3.0 Ga (Kirk *et al*. 2002).

Since then gold deposits have formed largely by a combination of magmatic and hydrothermal (including metamorphic) processes. The majority of known gold deposits show evidence of gold precipitation from aqueous-carbonic, sulphur-bearing hydrothermal fluids (temperature >200 $^{o}$C) of relatively low salinity and a redox state that is more reducing than the haematite-magnetite buffer (Phillips & Evans 2004). Near-surface crustal fluids (meteoric, seawater) lack the amount of sulphur to carry significant amounts of Au-hydrosulphide complexes, which are the dominant species in most Au-mineralizing systems. Metamorphic fluids are typically not produced at rates that are sufficient to maintain fluid flow through a given structure to form an ore body, and formation waters tend to be too oxidizing.

Silicate melts are inefficient carriers of gold – Au concentrations in silicic igneous rocks do not exceed the crustal average - and liquid-magmatic gold forms only an insignificant portion of the overall gold budget (Fig. 1). Most of the Au that is being transported by a melt will be extracted into a fluid phase upon crystallization and degassing of the magma. Consequently, magmatic fluids, such as those involved in the formation of porphyry deposits, intrusion-related, IOCG or skarn deposits, volcanogenic epithermal deposits, and possibly even some orogenic gold deposits can have high Au concentrations.

The overall proportion of crustal gold that is concentrated into ore bodies is minute, calculated at 66‰. This proportion corresponds to the ratio between average Au concentration in crustal rocks and that in crustal fluids.

The extent of gold recycling in the crust by hydrothermal fluids may be assessed by the Os concentrations in the gold. That concentration should decrease with every remobilization event. In this context it is worth comparing Os contents in gold of different ages (Kirk *et al*. 2002; Frimmel *et al*. 2005). The Mesoarchaean Witwatersrand gold has Os concentrations on the order of $10^{0}$ to $10^{4}$ ppb. Mesoarchaean orogenic, undoubtedly hydrothermal, gold from the Barberton greenstone belt has an order of magnitude less Os than given by the lower end of the range for the Witwatersrand gold ($10^{-1}$ ppb), but still more than Proterozoic to Phanerozoic gold ($10^{-3}$ – $10^{-1}$ ppb). It is suggested, therefore, that this decrease in Os over time reflects progressive hydrothermal recycling of initially Os-rich gold, most of which has been added to the crust already by Mesoarchaean times.

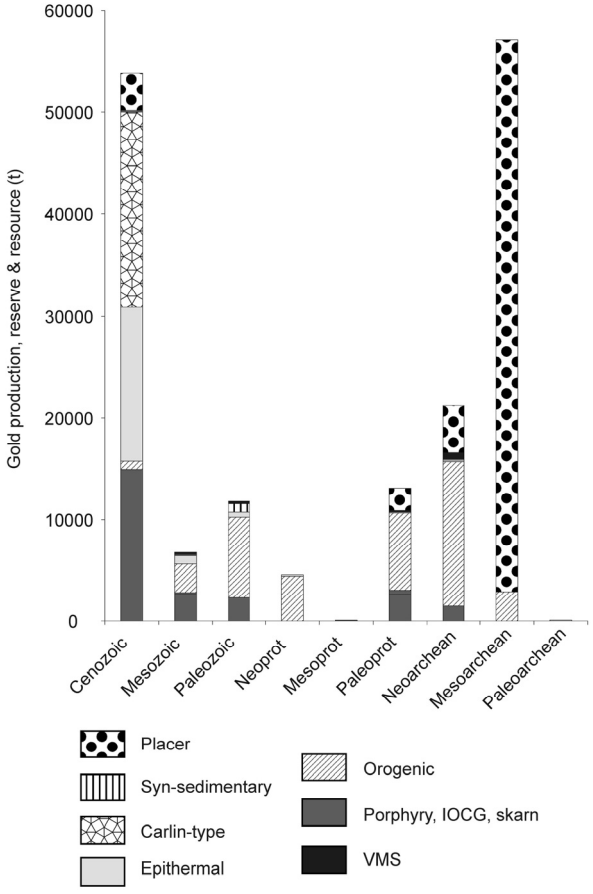


Figure 2. Distribution of known gold deposit types over geologic time.

## 4 CONCLUSIONS

The analysis of past production data as well as reserve and resource estimates for the principal genetic gold deposit types, combined with available data on the geochemical behaviour of gold, lead to the following conclusions:

(i) The Witwatersrand palaeoplacer and orogenic gold deposits are by far the two economically most important gold deposit types;

(ii) The Cenozoic and Mesoarchaean Eras are the most important times for the formation of gold deposits (32 and 34% of global gold, respectively);

(iii) As the large proportion of Cenozoic deposits is an artifact of the much higher preser-

vation potential of younger deposits rather than a reflection of particularly high rates of gold addition to the crust, the actual age distribution of gold deposits is strongly biased towards the Archaean. Most of the known gold was sequestered from the mantle to the crust by the Mesoarchaean, possibly by $H_2O$-rich melts as typically found in active plate margins. Subsequently, that gold was repeatedly recycled on a lithospheric scale, driven by plate tectonic processes.

(v) While magmatic fluids were probably the most effective agents for the redistribution of gold in the crust, the overall proportion of known gold that became concentrated into ore bodies over time is very small and corresponds to the proportion of gold that is dissolved in modern crustal fluids.

The actual cause for the very high rates of gold addition to the crust in Archaean times remains unresolved. It may be a question of juvenile crust formation rate – in itself a controversial issue. In that case, the conclusion reached here would support the model of most of the continental crust having formed already in the Archaean or earlier. The highest crustal gold concentrations should then be expected for the time after initial gold concentration into the core in the Hadean (Wood *et al*. 2006) and at the time when plate tectonic processes started to operate in a still relatively hot lithosphere. Alternatively, the extraordinary gold-enrichment noted here for the Mesoarchaean may be explained by major meteorite bombardement that has been suggested for the time at approximately 3.2 Ga (Glikson 2001).

## ACKNOWLEDGEMENTS

M. Tredoux kindly provided samples of Barberton gold. J. Kirk and J. Chesley are thanked for unpublished Re and Os data on those samples. Financial support from the Deutsche Forschungsgemeinschaft (grant FR2183/3-1) is gratefully acknowledged.

## REFERENCES

Frimmel HE, Groves DI, Kirk J, Ruiz J, Chesley J, Minter WEL (2005) The formation and preservation of the Witwatersrand goldfields, the largest gold province in the world In: Hedenquist JW, Thompson JFH, Goldfarb RJ, Richards JP (eds) *Economic Geology One Hundreth Anniversary Volume.* Society of Economic Geologists, Littleton, pp 769-797.

Glikson AY (2001) The astronomical connection of terrestrial evolution: crustal effects of post-3.8 Ga mega-impact clusters and evidence for major 3.2 ± 0.1 Ga bombardment of the Earth-Moon system. *J. Geodyn.* 32: 205-229.

Goodwin AM (1991) *Precambrian Geology: The Dynamic Evolution of the Continental Crust.* Academic Press, London.

Gosselin P, Dube B (2005) Gold deposits of the world: distribution, geological parameters and gold content *Geological Survey of Canada Open File* 4895. pp 221.

Handley JRF (2004) *Historic Overview of the Witwatersrand Goldfields*. Handley, Howick.

Kirk J, Ruiz J, Chesley J, Walshe J, England G (2002) A major Archean gold and crust-forming event in the Kaapvaal Craton, South Africa. *Science* 297: 1856-1858.

Krauskopf KB, Bird DK (1995) *Introduction to Geochemistry*. McGraw-Hill, New York.

Phillips GN, Evans KA (2004) Role of $CO_2$ in the formation of gold deposits. *Nature* 429: 860-863.

Raw Materials Data (2006) Digital data base August 2006, *Raw Materials Group, Stockholm*

Wood BJ, Walter MJ, Wade J (2006) Accretion of the Earth and segregation of its core. *Nature* 441: 825-833.

Xiong Y, Wood SA (2000) Experimental quantification of hydrothermal solubility of platinum-group elements with special reference to porphyry copper environments. *Mineral. Petrol*. 68: 1-28.

# Mesoarchaean basement of the Witwatersrand: a possible source of the gold?

Berit Lehrmann & Hartwig E. Frimmel
*Institute of Mineralogy, University of Würzburg, Am Hubland, D-97074 Würzburg, Germany*

ABSTRACT: First petrological and lithogeochemical data on mafic rocks, intersected in a borehole through pre-Witwatersrand basement, provide new insights into the petrogenesis of that basement, with implications on the possible source of the world's largest known accumulation of gold. The mafic rocks are hornblende gabbro and are overlain by granite. Both are considered cogenetic and a product of fractional crystallization due to crystal settling in a 3.08 Ga volcanic arc. Arc magmatism is suggested to have contributed significantly to the gold budget in the source area of the Witwatersrand sediments.

KEYWORDS: gold genesis, Archaean, volcanic arc, Witwatersrand

## 1 INTRODUCTION

For the past century, the genesis of the world's largest known gold deposits in the Mesoarchaean Witwatersrand Basin (South Africa) has been one of the most controversial topics in economic geology. Considering the proportion of gold in the fluvial conglomerates of the Witwatersrand relative to that in all other known types of gold deposits, *i.e.* 35 % of all known gold (Frimmel 2007), it becomes obvious that the understanding of the genesis of that gold is of first order importance for developing any meaningful strategy in future exploration attempts to find new gold deposits of this type. Almost any conceivable model has been suggested to explain this enormous geochemical anomaly in the Witwatersrand (for review see Frimmel *et al.* 2005), including the introduction of gold into its host rocks by magmatic, metamorphic or hydrothermal fluids, hydrothermal activity on the former seafloor, precipitation from seawater, microbially mediated gold deposition, and accumulation as placer gold. In the last two decades, essentially two schools of thought dominated the discussion: one has argued for the post-depositional introduction of gold via long-range hydrothermal transport (hydrothermal model – with a number of varieties; Phillips & Law 2000), whereas the other has argued for the introduction of detrital gold particles into the host sediments, with subsequent, post-depositional, local mobilization over only very short distances (modified palaeoplacer model; Pretorius 1981). All of the currently available data and observations can be explained by a modified palaeoplacer model, whereas some of them are incompatible with a hydrothermal model. The former model is therefore favoured (Frimmel *et al*. 2005). However, the question of the ultimate source of all the inferred detrital gold (in total at least 80,000 t of gold) remains unresolved.

In the past, those researchers who agreed with a palaeoplacer model assumed that typical Archaean greenstone-hosted gold-quartz veins (orogenic gold deposits), examples of which are being mined elsewhere on the Kaapvaal Craton and on many other cratons worldwide, served as prime source of the detrital gold (*e.g*., Robb & Meyer 1990; Loen 1992). Re-Os isotope data on the gold (Kirk *et al.* 2002) revealed a calculated Re-Os age for the gold of 3.03 Ga, which is older than the age of sedimentation, an initial $^{187}Os/^{188}Os$ ratio that corresponds to that of the mantle at 3.03 Ga, and furthermore Os concentrations in the Witwatersrand gold, which are orders of magnitude higher than those found in younger gold. High Os concentrations are not expected in hydrothermal systems because of the very low solubility of Os in aqueous fluids (Xiong & Wood 2000). Due to its strongly

siderophile character, Os is rather concentrated in magmatic phases and by analogy it is speculated that the Os-rich Witwatersrand gold is not derived from point sources of greenstone-hosted orogenic gold deposits, but from magmatic gold.

Numerous Palaeo- to Neoarchaean greenstone belts surround the 2.90 to 2.84 Ga Witwatersrand Basin, but they are the deeply eroded remnants of potential source areas at the time of Witwatersrand sedimentation. Information on the actual basement beneath the Witwatersrand Basin fill is limited, because of a lack of outcrop. Effectively all previous studies on the immediate basement rocks focused on granitoids as they dominate in these basement domains. Minor gold-sulphide mineralization associated with pervasive hydrothermal alteration of the granitoids is related to the same hydrothermal alteration that affected the Witwatersrand Basin fill (Klemd *et al*. 1994) and thus cannot be the source of the detrital gold.

This study focuses on mafic rocks in the immediate pre-Witwatersrand basement, which were drilled some 90km WSW of Johannesburg. Here we present first petrological and lithogeochemical results in order to assess the petrogenesis of these mafic rocks and their potential as source of some of the Witwatersrand gold. Preliminary U-Pb single zircon data indicate a crystallization age of 3077 ± 6 Ma (D. Hallbauer, *unpubl. data,* 2004).

## 2 PETROLOGY

The mafic rock in question is overlain by coarse-grained granite, whose composition borders that of granodiorite. No sharp intrusive contact exists, but intervening between the two rock types is a decimeter-thick transition zone that is characterized by the abundance of largely chloritized biotite and minor allanite. The granite consists of microcline, plagioclase, quartz and biotite, with accessory zircon, titanite, and apatite. The mafic rock is coarse-grained, relatively equigranular and is composed predominantly of randomly orientated amphibole and plagioclase with minor Ti-bearing biotite and microcline, and accessory titanite, zircon, apatite, and magnetite. The amphibole grains range in composition from actinolite to magnesio-hornblende. Plagioclase is entirely retrogressed to albite. No relics of clinopyroxene were found, and thus the magnesio-hornblende is interpreted as magmatic. This is supported by a lack of evidence of medium-grade metamorphic overprint in the associated granite in which not even quartz recrystallized.

All rock types show signs of variable pervasive hydrothermal alteration. This is manifest in the conversion of hornblende to actinolite, the albitization and saussuritization of plagioclase, the chloritization of biotite and the formation of white mica at the expense of microcline. In addition, a hydrothermal alteration along microfractures can be discerned, which led to the

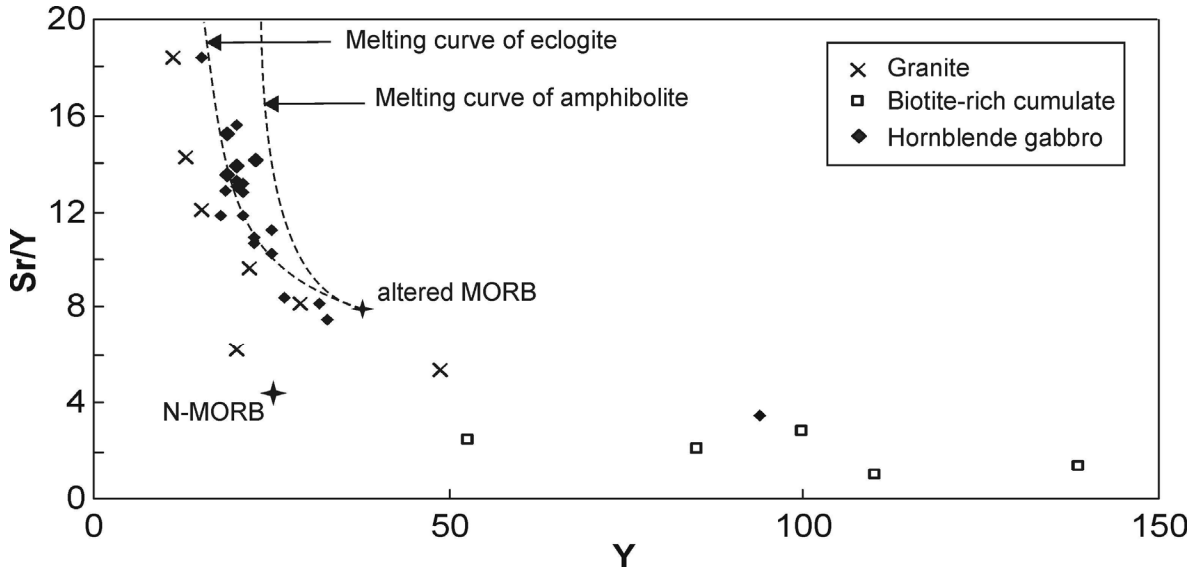


Figure 1. Sr/Y versus Y diagram for granite, underlying hornblende gabbro, and intervening biotite-rich cumulate. The trend approximates partial melting curves of altered mid-oceanic ridge (MORB, from Gill 1981) leaving behind an eclogitic residue.

formation of chlorite, calcite, quartz, pyrite, and chalcopyrite as veinlets.

Themobarometric calculations confirm lower greenschist-facies metamorphic conditions for the pervasive alteration, whereas sub-greenschist-facies temperatures are inferred for the later hydrothermal infiltration during brittle deformation.

## 3 GEOCHEMISTRY

A total of 33 whole rock analyses (XRF, ICP-MS) are used for lithogeochemical characterization and geotectonic interpretation. Based on the major element distribution, the samples can be classified as gabbro (or quartz diorite, according to Middlemost 1994) and granite, respectively. The trace element distribution of the granite conforms to that of volcanic arc granite. Similarly, most of the mafic samples plot in all traditional geotectonic discrimination diagrams in the fields for volcanic arc-related basites. An adakitic or TTG-affinity can be ruled out because of low Sr/Y ratios (<20 in all samples). These ratios match those of typical island arc andesite, dacite and rhyolite. For both the granitic and gabbroic samples they follow consistently a trend that can be explained by the partial melting of altered mid-oceanic ridge basalt leaving behind an eclogitic residue (Fig. 1). The originally biotite-rich transition zone follows the same trend towards higher Y contents and thus supports the interpretation by fractional crystallization from the same magma.

The analyses for Au by fire assay and ICP-MS techniques revealed concentrations of around 5 ppb, which is close to the lower limit of detection. Thus the studied rock compares well with typical Archaean greenstones elsewhere (Meyer & Saager 1985; Stone & Crocket 2003).

## 4 DISCUSSION AND CONLUSIONS

The retrograde, hydrothermal alteration that is apparent throughout the drilled basement rocks is ascribed to the regional, lower greenschist-facies metamorphism that affected the entire Witwatersrand Basin and is also comparable with the alteration described previously from other granitoids in pre-Witwatersrand basement.

Of interest here is the genesis of the igneous protoliths. The granite and the hornblende gabbro are interpreted as cogenetic for several reasons, including the lack of an intrusive contact, the presence of minor microcline throughout the hornblende gabbro, even tens of metres away from the contact, and similar geochemical characteristics. The separation into the two distinct rock types is explained by crystal settling in magma of intermediate composition, with the hornblende gabbro being a cumulate. Even the intervening biotite-rich zone might be the product of fractional crystallization. All geochemical indicators for specific geotectonic settings point to a volcanic arc along an active margin. The only exception is the Zr/Y ratio, which is too high for such an interpretation but most likely the result of zircon accumulation in the lower, gabbroic portion.

The new finding of calc-alkaline volcanic arc-related magmatism in the immediate basement of the Witwatersrand has important ramifications for our understanding of the tectonothermal evolution of the central Kaapvaal Craton and for the possible source of the Witwatersrand gold.

A 3077 Ma volcanic arc along the northern margin of the Witwatersrand Basin would be coeveal with bimodal, rift-related magmatism recorded in the 3086 – 3074 Ma Dominion Group. For the close proximity between the two coeval magmatic provinces, a back-arc position seems likely for the Dominion Group. Fluvial conglomerates in the Dominion Group contain abundant uraninite – analogous to the Witwatersrand conglomerates – but lacks gold. This important difference can be explained by the bulk of that gold having been added to the crust during volcanic arc formation, which would have involved the transfer of gold by wet melts from the lithospheric mantle into juvenile crust – similarly as in modern porphyry systems. This, by now largely eroded, volcanic arc would then present itself as prime candidate for the source of the bulk of Witwatersrand gold.

Around the same time, an extensive juvenile volcanic arc has been suggested to have developed along the northern and western margin of the Kaapvaal Craton, some 200km north of the Witwatersrand Basin ((Poujol *et al*. 2003). It contains numerous gold deposits, including a Witwatersrand-type palaeoplacer deposit (Uitkyk Formation in the Pietersburg Belt). Although it is just another example of the importance of Mesoarchaean volcanic arc formation for the transfer of gold into the continental crust, it was probably too far north to have contributed much to the Witwatersrand gold.

ACKNOWLEDGEMENTS

D. Hallbauer is thanked for providing the analyzed drill core. U. Schüβler and H. Bätz helped with EMPA and ICPMS analyses, respectively. Financial support from the Deutsche Forschungsgemeinschaft (grant FR 2183/3-1) is gratefully acknowledged.

REFERENCES

Frimmel HE (2007) Gold endowment of the Earth's crust over time In: *Andrew C (ed) 9th Biennial SGA Meeting. Dublin,* under review.

Frimmel HE, Groves DI, Kirk J, Ruiz J, Chesley J, Minter WEL (2005) The formation and preservation of the Witwatersrand goldfields, the largest gold province in the world In: Hedenquist JW, Thompson JFH, Goldfarb RJ, Richards JP (eds) *Economic Geology One Hundreth Anniversary Volume. Society of Economic Geologists,* Littleton, pp 769-797.

Gill J (1981) *Orogenic Andesite and Plate Tectonics*. Springer, Heidelberg.

Loen JS (1992) Mass balance constraints on gold placers: possible solutions to "source area problems". *Econ. Geol.* 87: 1624-1634.

Kirk J, Ruiz J, Chesley J, Walshe J, England G (2002) A major Archean gold and crust-forming event in the Kaapvaal Craton, South Africa. *Science* 297: 1856-1858.

Klemd R, Wülbers A, Hallbauer DK, Barton JM (1994) Evidence for the origin of hydrothermal alteration in granitoids after Witwatersrand Basin deposition. *Austral. J. Earth Sci.* 41: 131-140.

Meyer M, Saager R (1985) The gold content of some Archaean rocks and their possible relationship to epigenetic gold-quartz vein deposits. *Mineral. Deposita* 20: 284-289.

Middlemost EAK (1994) Naming materials in the magma/igneous rock system. *Earth-Science Reviews* 37: 215-223.

Phillips GN, Law JDM (2000) Witwatersrand gold fields: Geology, genesis and exploration. *SEG Reviews 13*: 439-500.

Poujol M, Robb LJ, Anhaeusser CR, Gericke B (2003) A review of geochronological constraints on the evolution of the Kaapvaal Craton, South Africa. *Precambr. Res.* 127: 181-213.

Pretorius DA (1981) Gold and uranium in quartz-pebble conglomerates. *Econ. Geol. 75th Anniversary Volume*: 117-138.

Robb LJ, Meyer FM (1990) The nature of the Witwatersrand hinterland: Conjectures on the source-area problem. *Econ. Geol*. 85: 511-536.

Stone WE, Crocket JH (2003) Platinum-group element contents of chromites from mafic-ultramafic layered flows, Abitibi greenstone belt, Ontario: implications for geochemical fractionation and mineral exploration. *Mineral. Petrol.* 78: 139-147.

Xiong Y, Wood SA (2000) Experimental quantification of hydrothermal solubility of platinum-group elements with special reference to porphyry copper environments. *Mineral. Petrol.* 68: 1-28.

# Spatial-temporal evolution of Au-U deposits in the Ukrainian, Baltic and Aldan shields and the Precambrian Baikal Fold Area

I.G. Mineeva & A.I. Makarov
*Institute of Mineral Resources (VIMS), Moscow, Russia*

ABSTRACT: Au-U, U and Au deposits have been studied in rift structures of different age on the Ukrainian, Baltic, Aldan shields, and in the Precambrian Baikal fold area**.** The Precambrian and Phanerozoic Au-U deposits are genetically related to greenstone-hosted iron formations and carbonaceous schists that developed within the ancient rift structures. Recurrent evolution of iron ore-carbon systems as caused by polyphase rifting led to spatio-temporal changes in the genetic association of the Au-U deposits.

KEYWORDS: shields, rift, greenstone belts, iron formations, Au-U deposits

## 1 INTRODUCTION

The Ukrainian and Baltic Precambrian shields of Eastern Europe host two economically important genetic types of U and Au-U deposits:

(1) Early Proterozoic U-bearing albitites and iron-alkaline metasomatites developed on the Baltic and particularly on the Ukrainian shield;

(2) Riphean unconformity-type deposits found on the Baltic shield only. These deposits formed in the Precambrian East European intracontinental protorift related to the unconformity surface between Archaean granite-greenstone basement and overlying Early Proterozoic volcanic-sedimentary rocks that include abundant ferruginous and carbonaceous units.

On the Aldan shield, the Precambrian Au-U, U and Au deposits were replaced by specific Mesozoic Au-U deposits related to potassic alkaline magmatism (*e.g*. Torgoi deposit) or potassic alkaline metasomatism (*e.g*. Elkon deposits). However all of these deposits are confined to high-grade iron formations.

The Mesozoic-Cenozoic rifting provided optimal conditions for the rejuvenation of Au-U mineralization at the expense of reworking of the ancient weathering crusts that are preserved within iron formations.

## 2 AU-U AND U DEPOSITS ON THE PRECAMBRIAN SHIELDS OF EASTERN EUROPE

The Au-U and U deposits on the Ukrainian and Baltic shields occur in different parts of the regional Precambrian Eastern European protorift, which extends in a NW direction from the Black Sea through Krivoy Rog - Kursk-Belgorod to Onega Lake - Kuusamo - Karasjok (Baltic shield). The protorift formed during the early stage of continental crust formation. It is characterised by granite-greenstone belts which hosting the world's richest iron formations (Krivoy Rog, Kursk - Belgorod, Karelia and Sweden) and numerous occurrences of sodium alkaline metasomatites. Rich iron deposits are developed in different blocks of the protorift in addition to Au-U and U deposits.

The U and Au-U deposits on the Ukrainian shield are located among iron-carbonate alkaline metasomatites at the flanks of iron ore deposits in the Krivoy Rog region (Pervomayskoe, Krasnogvardeyskoe). The iron formations are overlain by phyllites and carbonaceous - carbonate shales that underwent intense sodium metasomatism.

The economic-grade U deposits formed in albitites after granites, migmatites and gneisses in the Kirovograd ore region - an area of pervasive early Proterozoic granitization on the western part of the Krivoy Rog Rift. Small gold de-

posits in graphitic gneisses rim economic deposits of U-bearing albitites.

The Au-U deposits in the Karelian part of the rift (Baltic shield) are also related to the alkaline metasomatites. We note three provinces of U-bearing alkaline metasomatites: North Sweden (Arjeplog), Finland (Kuusamo) and Onega (Middle Padma). In the most subsided Onega block of the palaeorift, the Middle Padma PGE-Au-U-V deposit (1.8 Ga) developed in albitites and phlogopite metasomatites in a brecciation zone at the contact of shungite schists and dolomites (Mineeva 2001). The ore mineralization includes brannerite, pitchblende, coffinite, selenides of Au, PGE and Ag and association of V minerals. Gold and gold-iron occurrences are localized in the basal quartz conglomerates at the base of early Proterozoic sequence.

The Middle Riphean marks the start of a new stage of formation of branched graben-like rift structures on the Eastern European shields. The rejuvenated Ladoga rift (Baltic shield) developed at the western marginal part of the Karelia protorift block during this period. The Pashsko-Ladoga segment of the rift hosts the Karku unconformity-type U deposit. The U mineralization is localized in the upper part of the carbonaceous-sulphide schists developed in the base of the Riphean feldspar-quartz sandstones, gravel stones and conglomerates overlain by basaltic porphyrites. Rich ore lodes are stratabound within graphite-bearing schists. The ore assemblage is pitchblende, coffinite, sulphides, minor Ni and Co arsenides and secondary uranium minerals. The mineralization defines a wide range of age (from 1500-1400 to 180 Ma) indicating a prolonged evolution of U ore formation.

## 3 POLYCHRONOUS RIFTING ON THE ALDAN SHIELD AND PRECAMBRIAN BAIKAL FOLD AREA

The geological structure of the Aldan shield and Baikal fold area was influenced by the Precambrian and Phanerozoic rifting. The Precambrian rift system evolved in the western part of the shield at the boundary with the Baikal fold area. A system of submeridional Archaean and Archaean - early Proterozoic (3.1-3.0 Ga) greenstone belts forms a preserved fragment of the intracontinental Chara-Tokko protorift belt, which extends beneath the sedimentary cover throughout the entire Siberian platform to the Arctic Ocean. These ancient rifts were significantly rejuvenated in the early Proterozoic.

The sub-latitudinal Palaeoproterozoic Baikal-Vitim rift (1060-825 Ma) separates the Eastern Siberian Platform and the Precambrian Baikal fold area. The rift structure includes randomly oriented greenstone structures (Fedorovskiy 1985).

The Precambrian rift structures are characterized by linear-tectonic weathering crusts, which mostly developed in permeable zones along the unconformity surface at the contact of the alu

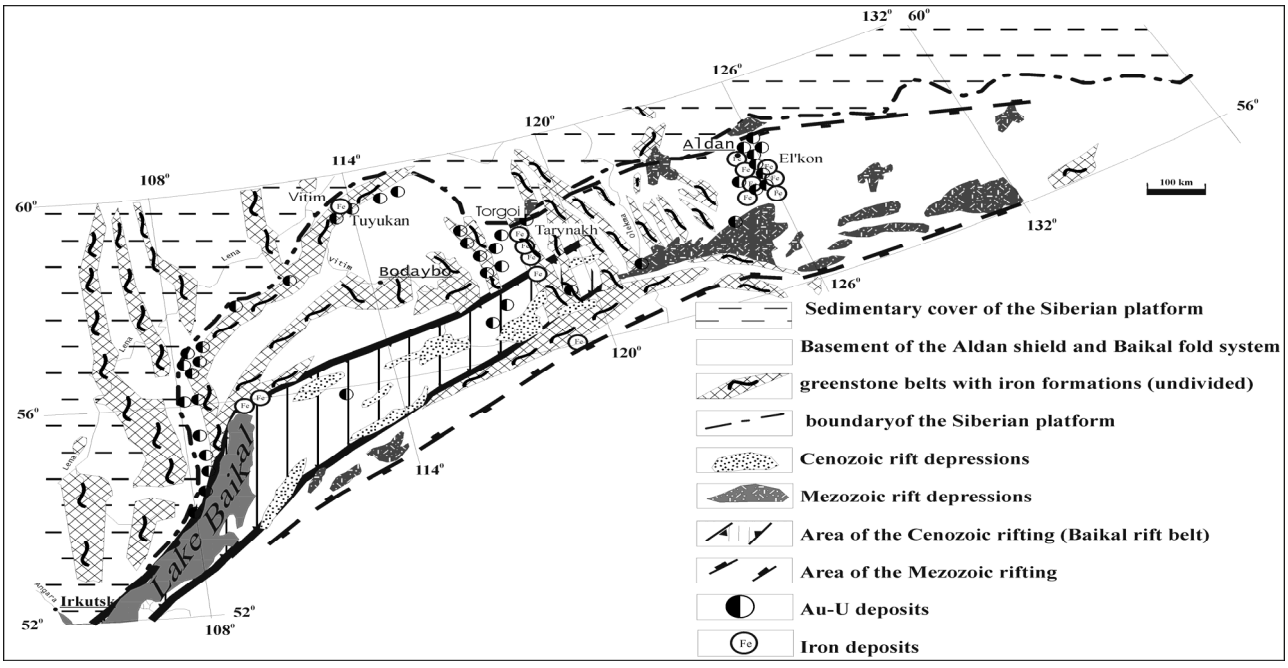


Figure 1. Distribution map of Au-U and Fe deposits on the Aldan shield and Baikal fold area

minosilicate (granite – greenstone) and carbonate-carbonaceous or carbonate–iron–carbonaceous formations.

The Mesozoic rift depressions of sublatitudinal and NE strike separate the Aldan shield from the platform in the north and from the Stanovoi shield in the south. The depressions extend eastward to the Pacific Ocean.

Cenozoic rifting led to the formation of the largest Baikal rift. Numerous young Eocene-Quaternary faults and rift depressions formed at this time; these cut across ancient rift zones and are traceable into the Aldan shield. In general, the Baikal rift opening occurred eastward along the Stanovoi shield and still continues, as evidenced by ongoing seismic activity

## 4 AU-U DEPOSITS ON THE ALDAN SHIELD AND BAIKAL FOLD AREA

### *4.1 Au-U deposits and iron formations on the Aldan shield*

Unlike other shields the Aldan shield lacks Precambrian-aged economic Au-U and U deposits. The formation of Au-U, U and Au deposits occurred during the Mesozoic (at around 145 Ma). The spatial relationship of the Mesozoic Au-U and Au deposits with ancient iron or carbonaceous formations is preserved. The iron formations of magnetite and magnetite-pyroxene banded quartzites formed in the Archaean - early Proterozoic greenstone belts within the submeridional Chara-Tokko proto-rift belt (Tarynakh iron deposit).

The Mesozoic Murun massif of ultrapotassic nepheline syenites (115-130 Ma) is located at the northern flank of this iron formation. The nepheline syenites (10.0-13.0% $K_2O$) and outer contact fenites enclose the Torgoi U-Th-REE (Au-PGE) deposit. The U, Th, Zr and REE ore mineral associations are typical for alkaline complexes (brannerite, pitchblende, coffinite, thorite, huttonite, monazite, loparite, and wadeite). The Au, PGE, Cu, Bi, Co and Ni minerals are inconsistent with K-alkaline rocks (sperrylite, froodite, sobolevskite, sudburyite, native gold, canfieldite, parkerite, djerfisherite, safflorite and others).

The Mesozoic high-grade Au-U deposits of the Aldan shield (145 Ma) formed on the El'-kon horst - the uplifted large block of Archaean - Proterozoic metamorphic rocks of the crystalline basement - in zones of rejuvenation of Precambrian rifting structures. Two differently aged iron formations can be recognized: Archaean magnetite quartzites (3000 Ma) and early Proterozoic phlogopite-magnetite skarns (2000-1800 Ma); these formed in the lower and upper parts of the Archaean Fedorov suite, respectively. Many Mesozoic Au-U deposits are situated at the flanks of Archaean and early Proterozoic iron formations located also in the Fedorov suite, which includes some large iron deposits (*e.g.* Taezhnoye, Pionerskoye). The Au-U deposits are hosted by brecciated potassic alkaline metasomatites. The ore-bearing metasomatites (10-12% $K_2O$; 0.1-0.2% $Na_2O$) consist almost entirely of adularia, phlogopite, sulphides and carbonates. Similar to other Precambrian shields, the main uranium mineral is brannerite. Gold occurs as fine disseminations in pyrite. The geochemical associations of siderophile and chalcophile elements (Ti, Fe, Zr, V, Mn, Nb, W, Ag, As, Mo, Tl, Sb and Cu) are typical for Mesozoic Au-U metasomatites of the Aldan shield.

### *4.2 Au-U deposits and iron formations in the Baikal fold area*

Early (1800 Ma) and late Proterozoic (1800-1300 Ma) phosphorous-iron-manganese-siliceous formations are abundant in the Palaeoproterozic system of the Baikal-Vitim greenstone belts in the Baikal fold area. Numerous small Au-U and Au deposits of variable ages occur at the flanks of iron formations.

The brecciated haematite quartzites, areas of apatite-microcline accumulation and zones of intense haematitization along the fault zones are favourable for the formation of ore mineralization.

The Au-U occurrences related to early Proterozoic iron formations contain horizons of Na-Fe metasomatism in aegirine-bearing albitites. This process is similar to but less intense than Na-Fe metasomatism on the Ukrainian shield (Krivoy Rog). Ore mineralization is represented by decomposed brannerite, uraninite, cyrtolite, allanite, monazitite, apatite, magnetite and haematite.

Small U-Au and Th-REE occurrences (1380-800-580-405 Ma) are confined to the flanks of Riphean iron deposits of the Vitim group (Fe-Au-U Touyukan deposit). Ore zones in iron formations occur over significant distances of 3km and more and consist of several en-echelon mineralized lodes.

## 5 DISCUSSION

The source of ore material in these deposits is the topic of heated discussions. The primary Au-U deposits formed in early Proterozoic rift structures with greenstone belts containing various iron and carbonaceous formations and products of submarine volcanism. Subsequent evolution of the early Proterozoic Au-U deposits was governed by sodium-carbonate metasomatism. During the Riphean stage, Au-U, U and Au mineralization developed in weathering crusts, leading to large unconformity-type ore deposits.

During each active rifting stage in the Phanerozoic, magmatism and volcanism led to a change in the genetic type of Au-U deposits with preservation of relict Precambrian rift structures and, particularly, modified iron formations. This process might have been exemplified on the Aldan shield, where Proterozoic iron formations of Precambrian rift structures contain unusual types of Au-U deposits related to potassic alkaline magmatism, volcanism and metasomatism. The deposits inherited some mineralogical and geochemical features of Precambrian mineralization. The Mesozoic age of the U mineralization corresponds to the age of rift structure activation.

We suggest that rich Au-U deposits in the breccciated K-metasomatites of the Aldan shield formed due to the complete transformation of ancient unconformity-related Au-U deposits during Mesozoic rifting.

## 6 CONCLUSIONS

1. Both Precambrian and Phanerozoic Au-U deposits on the Precambrian shields are genetically related to ancient iron formations and carbonaceous sequences developed in greenstone belts within the Precambrian rift systems.

2. Compositionally diverse Au-U deposits are commonly characterized by siderophile - chalcophile associations of Fe, Ti, Zr, PGE, Cr, Ni, Co, V, Pb, Zn, Ag, Cu, W and Nb, and formed in the uplifted blocks of rift structures due to decomposition of iron formations. In the subsided blocks, Au-U mineralization was mainly confined to the carbonaceous sequences overlying iron ore formations.

3. Post-granitization sodium alkaline metasomatism completed the early Proterozoic rifting in the greenstone belts, and developed along long-lived rift structures in major uplifted blocks of the Earth's crust. This is particularly typical for the shields of Eastern Europe and Precambrian fold system. This process was accompanied by the formation of Au-U deposits in sodium alkaline metasomatites.

4. Subsequent evolution of Au-U mineralization was related to the Riphean crusted formation, providing favourable conditions for the formation of ore-bearing weathering crusts in the rift structures after previously existing Au-U, U and Au deposits.

5. Each new stage of the Phanerozoic Au-U and U ore formation involves renewal of ancient rift systems, decomposition of ancient iron formations and subsequent accumulation of carbonaceous matter, which facilitated the rejuvenation of uranium and gold mineralization. Recurrent evolution of iron ore-carbon system generated by poly-phase rifting led to the spatial-temporal evolution of genetic types of Au-U deposits.

## REFERENCES


Fedorovskiy VS (1985) Early Proterozoic on the Baikal fold area Moscow: *Nauka* (in Russian)

Mineeva IG, Guseva NN (2001) Primary and transformed carbonaceous PGE-Au-U ores on Precambrian shields: role of petroleum. In A. Piestrzynsky et al. (eds), *Mineral Deposits at the Beginning of the 21st Century,* Lisse, Swets & Zeitlinger: p. 63-66.

# Change from plume to convergent tectonics in the early Archaean: metallogenic implications in the Pilbara Craton, Western Australia

David L. Huston
*Geoscience Australia, GPO Box378, Canberra, ACT 2601, Australia*

Martin J. Van Kranendonk, Arthur H. Hickman & Franco Pirajno
*Geological Survey of Western Australia, 100 Plain St, East Perth, WA 6004, Australia*

ABSTRACT: At ~3.2 Ga the driver of crustal growth in the 3.7-2.83 Ga Pilbara Craton changed from mantle plume to plate tectonic processes. Although volcanic-hosted massive sulfide and lode-gold deposits spanned this change, factors such as the development of arc-related volcanic basins and transpressional orogenic belts favor development of larger deposits after the initiation of plate tectonics. Development of passive margins after 3.2 Ga allowed deposition of Hamersley-type banded iron formations, the source of most of the world's iron. Porphyry Cu-Mo and epithermal deposits are present in rocks older than 3.2 Ga, suggesting that these deposits spanned most of geologic time and that porphyry Cu-Mo deposits form in settings other than convergent margins.

KEYWORDS: Pilbara Craton, metallogeny, mantle plumes, convergent tectonics, Archaean

## 1 INTRODUCTION

The history of the Pilbara Craton spans nearly 900 million years, from *ca*. 3.7 Ga to *ca*. 2.83 Ga. Hickman (2004) and Smithies *et al*. (2005a,b) suggested that the style of crustal growth in this craton changed at about 3.2 Ga from mantle plumes to plate-tectonic processes. Although not as well mineralized as some Neoarchaean cratons, the Pilbara Craton has a great diversity in deposit types. This diversity, along with the change in tectonic process at 3.2 Ga, provides insight into relationships between tectonic process and metallogeny.

## 2 GEOLOGICAL EVOLUTION OF THE PILBARA CRATON

Crustal growth in the >3.2 Ga East Pilbara Terrane (EPT) was caused by mantle plume events at 3.53-3.42 Ga (Warrawoona event), 3.35–3.29 Ga (Kelly event), and 3.27–3.24 Ga (Sulphur Springs event). Each event resulted in deposition of ultramafic–mafic and felsic volcanic rocks and intrusion of granites. Deformation associated with these plume events, along with density contrasts, initiated dome complexes that typify the EPT, and by 3.2 Ga the EPT was a stable, buoyant proto-continent that was a locus for later growth by plate tectonic processes.

The oldest rocks of the West Pilbara Superterrane (WPS), equate to the Sulphur Springs event. These rocks and ~3.12 Ga bimodal volcanics showing the first evidence of subduction related tectonics (Smithies *et al.* 2005b) were accreted onto the WPS during the 3.07 Ga Prinsep Orogeny (Van Kranendonk *et al*. 2006).

Between 3.02 Ga and 2.92 Ga, extension produced a major ENE-trending nested basin system, the DeGrey Superbasin. Development of the Mallina and Croydon Basins, which are part of this superbasin, was accompanied by granite and mafic-ultramafic intrusion. The superbasin closed between 2.92 Ga and 2.89 Ga.

The last major event to affect the Pilbara Craton was the emplacement of evolved granites and pegmatites at 2.89-2.83 Ga.

## 3 MINERAL DEPOSITS ASSOCIATED WITH MANTLE PLUME EVENTS

The EPT contains numerous mineral deposits with a large variety in metal content and origin. Excluding lode-gold and Sn-Ta deposits, these deposits can be related to mantle plume events.

### 3.1 *Warrawoona plume event (3.53-3.42 Ga)*

The Warrawoona Group, a product of the Warrawoona event, contains mafic-ultramafic volcanic rocks, with felsic volcanic rocks limited to the 3.47-3.46 Ga Duffer and 3.45-3.42 Ga Panorama Formations (Van Kranendonk *et al*. 2006). The Duffer and ~3.49 Ga Dresser Formations host VHMS and strataform barite deposits, whereas the Panorama Formation hosts polymetallic epithermal deposits.

The small VHMS and barite deposits occur in clusters, with the largest lens about 1.2Mt. Although deformation obscures the setting of the VHMS deposits, the Dresser barite deposits are hosted in shallow water rocks next to growth faults (Nijman *et al*. 1998). In contrast, epithermal deposits and advanced argillic alteration assemblages formed in subaereal or very shallow subaqueous environments. Although the most significant deposit, the ~3.45 Ga Miralga Creek deposit (Goellnicht *et al*. 1989), is hosted by the Panorama Formation, advanced argillic alteration (Van Kranendonk & Pirajno, 2004) and epithermal-like vein textures and possible sinters are associated with the shallow water Strelley Pool Chert.

### 3.2 *Lode-gold event (3.43-3.32 Ga)*

Small lode gold deposits are hosted by the Warrawoona Group along faults that ring domal granite complexes. Lead isotopes from Au-related galena yield model ages of 3.43-3.31 Ga (Zegers *et al.* 2002; Huston *et al.* 2002), consistent with geological age constraints of 3.47-3.32 Ga. Although mineralogical, textural and fluid inclusion characteristics (Zegers *et al*. 2002; T. Mernagh, *unpub. data*) are similar to lode-gold deposits in younger provinces, these deposits formed along normal faults (Zegers *et al.* 2002) and are not related to major through-going fault systems as in other, younger, lode-gold districts (Vearncombe *et al.* 1989).

### 3.3 *Kelly plume event (3.35-3.29 Ga)*

The most significant mineral deposit associated with the Kelly plume event is the 3.31 Ga Spinifex Ridge porphyry deposit with has a 500 Mt resource grading 0.06% Mo and 0.09% Cu. This is one of many porphyry and vein-style Cu±Mo±Au deposits associated with Kelly-aged plugs and stocks. Lead isotope model ages of ~3.29 Ga suggests Zn-Pb-Cu VHMS deposits formed near the end of the Kelly event.

### 3.4 *Sulphur Springs plume event (3.27-3.24 Ga)*

Although granites formed during the Sulphur Springs event are widespread, supracrustal rocks and mineral deposits are restricted to the western part of the EPT and include ~3.24 Ga VHMS deposits in the Panorama district (total resource of 12Mt; Brauhart *et al*., 1998). These deposits are temporally associated with the K-rich Strelley Monzogranite that contains minor contemporaneous greisen and Cu-Zn-Sn-Mo veins (Brauhart *et al*. 1998).

## 4 MINERAL DEPOSITS ASSOCIATED WITH CONVERGENT EVENTS

In contrast to the EPT, deposits in the WPS relate to processes typical of convergent margins.

### 4.1 *Whundo event (3.12 Ga)*

The ~3.12 Ga Whundo Group, the oldest intra-oceanic arc, contains small (to 2Mt) VHMS deposits. Based on metal content of the deposits and the primitive character of the hosts, this belt has similarities with the Neoarchaean, VHMS-rich Abitibi Subprovince.

### 4.2 *Extensional basins (3.02-2.92 Ga)*

After accretion of the WPS to the EPT at 3.07 Ga, 3.02-2.92 Ga extension formed the DeGrey Superbasin. The basal Gorge Creek Basin, along the EPT-WPS boundary, contains Algoma-type BIF with iron-ore deposits. To the west this basin is overlain by volcanic rocks of the Mallina Basin. These rocks host VHMS deposits with ages of 2.96-2.95 Ga (Huston *et al*. 2002). The Mallina and contemporaneous Mosquito Creek Basins are dominated by turbidites with 2.93-2.92 Ga epigenetic Zn-Pb-Cu deposits. Layered mafic-ultramafic bodies, which host orthomagmatic Ni-Cu-PGE and Ti-V deposits, intruded the Mallina Basin and underlying units at 2.95-2.92 Ga (Huston *et al.* 2002).

### 4.3 *Basin closure (2.92-2.89 Ga)*

Limited geochronological data (Neumayr *et al.* 1998; Huston *et al.* 2002) suggest a second, richer, lode-gold event in the Pilbara affected the Mallina and Mosquito Creek Basins at 2.92-2.89 Ma. Like most other lode-gold provinces (*e.g*., Vearncombe *et al.* 1989) but unlike the first Au event in the EPT, Au is associated with through-going crustal-scale shear zones that accompanied basin closure.

## 5 LATE GRANITES

Pegmatites associated with 2.89-2.83 Ga, high-K granites have been major sources of Sn and Ta, from both alluvial and hard rock mines.

## 6 METALLOGENESIS OF OTHER PALAEO- TO MESOARCHAEAN TERRAINS

The Kaapvaal Craton (southern Africa) contains stratiform barite deposits between 3.55 and 3.26 Ga, ~3.26 Ga VHMS deposits, epithermal Hg±Au deposits, iron ore associated with ~3.45 Ga and ~3.26 Ga Algoma-type BIFs, ~3.08 Ga lode-gold deposits that produced over 320 tonnes of gold, and the earliest (~2.99 Ga) Hamersley-type BIFs (de Ronde *et al.* 1989; Ward 1999; Huston & Logan 2004). The Dharwar Craton (India) contains ~3.30 Ga stratiform barite and BIFs, and the Singhbum-Orissa Craton (India) contains ~3.21 Ga BIFs. The Isua belt (Greenland) and Amazonia Craton (South America), contain Palaeoarchean BIFs of various ages, and the Aldan shield (Russia) contains stratiform barite (Huston & Logan 2004). The ~2.95 Ga Golden Grove district (Australia) is the oldest major VHMS district, with over 30 Mt of ore.

## 7 DISCUSSION AND CONCLUSIONS

Changes in crustal growth mechanisms at ~3.2 Ga have important implications to the type, setting and size of mineral deposits formed during the Palaeo- and Mesoarchaean. Modern geological features formed by mantle plumes, such as ocean islands and plateaux, tend to be either irregularly shaped or equidimensional, particularly in comparison with arcs and other features along convergent margins. Hence, linear features, including arcs and deformational belts would have only formed after 3.2 Ga.

Data from the Pilbara Craton suggest that the metallogeny of lode-gold, VHMS and iron ore deposits is affected by changes in tectonic processes. Lode-gold deposits are the most affected. Despite similarities in fluid composition and alteration assemblages, early lode-gold deposits in the Pilbara differ from younger deposits in that they are related to ring faults around granite complexes, and formed during normal shearing (Zegers *et al*. 2002). These relationships and age data indicate that these deposits formed during normal faulting during doming, although no consensus exists on if this was related to core complex formation or the rising of granites due to density contrasts. This environment contrasts with younger lode-gold deposits in the Pilbara and Kaapvaal Cratons and elsewhere, which formed during the late stages of orogenesis and are associated with crustal-scale, transpressional shear zones that allow tapping of a larger gold source, and lead to larger gold accumulations.

Although plume-related crustal growth could produce volcanic-dominated basins ideal for VHMS deposition, these basins would be small and compartmentalized, limiting potential for giant deposits. More extensive basins formed along convergent margins would be more favorable for large VHMS-forming systems.

Another consequence of changes in crustal growth processes is that passive margins would have been less abundant during plume-driven crustal growth. The earliest passive margin sequence, the 2.99 Ma Pongola Supergroup (Kaapvaal Craton) (Nelson *et al.* 1999), post-dates initiation of plate tectonics. As some models for the genesis of Hamersley-type BIFs infer iron deposition when deep, $Fe^{2+}$-rich oceanic waters upwell onto passive margins (*c.f.* Huston & Logan 2004 and references therein), the lack of passive margins prior to 3.2 Ga would preclude deposition of Hamersley-type BIFs, the world's major source of iron ore.

Porphyry-related Cu-Mo-Au deposits of the Kelly plume event, along with similar younger systems (*e.g.* Oslo graben, porphyry Mo in the Glitrevann ring-type volcano-plutonic complex; Climax type systems in Colorado), suggest that porphyry mineralization is not necessarily associated with subduction at convergent margins.

## ACKNOWLEDGEMENTS

This contribution is published with permission of the Chief Executive Officer of Geoscience Australia and the Director of the Geological Survey of Western Australia. It benefited from comments by David Cameron and Hugh Smithies.

## REFERENCES

Brauhart CW, Groves DI, Morant P (1998) Regional alteration systems associated with volcanogenic massive sulfide mineralization at Panorama, Pilbara, Western Australia. *Economic Geology* 93: 292-302.

de Ronde CEJ, Kamo S, Davis DW, de Wit, MJ, Spooner ETC (1991) Field, geochemical and U-Pb isotopic constraints from hypabyssal felsic intrusions within the Barberton greenstone belt, South Africa: implications for tectonics and the timing of gold mineralization. *Precambrian Research* 49: 261-280.

Goellnicht NM, Groves IM, Groves DI, Ho SE, McNaughton NJ (1988) A comparison between mesothermal gold deposits of the Yilgarn Block and gold mineralization at Telfer and Miralga Creek, Western Australia: indirect evidence for a non-magmatic origin for greenstone-hosted gold deposits. *Geology Department and Extension Service, University of Western Australia, Publication* 12: 23-40.

Hickman AH (2004) Two contrasting granite−greenstone terranes in the Pilbara Craton, Australia: evidence for vertical *and* horizontal tectonic regimes prior to 2900 Ma. *Precambrian Research* 131: 153-172.

Huston DL, Logan GA (2004) Barite, BIFs and bugs: evidence for the evolution of the Earth's early hydrosphere. *Earth and Planetary Science Letters* 220: 41-55.

Huston DL, Sun S-S, Blewett RS, Hickman AH, Van Kranendonk M, Phillips D, Baker D, Brauhart CW (2002) The timing of mineralization in the Archean Pilbara Craton, Western Australia. *Economic Geology* 97: 733-756.

Nelson DR, Trendall AF, Altermann W (1999) Chronological correlations between the Pilbara and Kaapvaal cratons. *Precambrian Research* 97: 165-189.

Neumayr P, Ridley JR, McNaughton NJ, Kinny PD, Barley ME, Groves DI (1998) Timing of gold mineralization in the Mt. York district, Pilgangoora greenstone belt, and implications for the tectonic and metamorphic evolution of an area linking the western and eastern Pilbara Craton. *Precambrian Research* 88: 249-265.

Nijman W, de Bruijne KCH, Valkering ME (1998) Growth fault control of early Archaean cherts, barite mounds and chert-barite veins, North Pole Dome, eastern Pilbara, Western Australia. *Precambrian Research* 88: 25-52.

Smithies RH, Van Kranendonk MJ, Champion, DC (2005a) It started with a plume – early Archaean basaltic proto-continental crust. *Earth and Planetary Science Letters* 238: 284-297.

Smithies RH, Champion DC, Van Kranendonk MJ, Howard HM, Hickman AH (2005b) Modern-style subduction processes in the Mesoarchaean: geochemical evidence from the 3.12 Ga Whundo intraoceanic arc. *Earth and Planetary Science Letters* 231: 221-237.

Van Kranendonk MJ, Hickman AH, Smithies RH, Williams IR, Bagas L, Farrell TR (2006) Revised lithostratigraphy of Archean supracrustal and intrusive rocks in the northern Pilbara Craton, Western Australia. *Western Australia Geological Survey Record* 2006/15, pp57.

Van Kranendonk MJ, Pirajno F (2004) Geochemistry of metabasalts and hydrothermal alteration zones associated with c. 3.45 Ga chert and barite deposits: implications for the geological setting of the Warrawoona Group, Pilbara Craton, Australia. *Geochemistry: exploration, environment, analysis* 4: 253-278.

Vearncombe JR, Barley ME, Eisenlohr BN, Groves DI, Houstoun SM, Skwarnecki MS, Grigson MW, Partington GA (1989) Structural controls on mesothermal gold mineralization: examples from the Archean terranes of southern Africa and Western Australia: *Economic Geology Monograph* 6: 124-134.

Ward JHW (1999) The Metallogeny of the Barberton greenstone belt, South Africa and Swaziland. *Geological Survey of South Africa* Memoir 86. pp116.

Zegers TE, Barley ME, Groves DI, McNaughton NJ, White SH (2002) Oldest Gold: Deformation and Hydrothermal Alteration in the Early Archean Shear Zone-Hosted Bamboo Creek Deposit, Pilbara, Western Australia. *Economic Geology* 97: 757-773.

# Proterozoic mineral systems in Australia and their genesis

Franco Pirajno[1] & Leon Bagas[1, 2]
[1]*Geological Survey of Western Australia, 100 Plain Street, East Perth, WA 6004, Australia*
[2]*Centre for Exploration Targeting, School of Earth and Geographical Sciences, The University of Western Australia, 35 Stirling Highway, Crawley, WA 6009, Australia*

ABSTRACT: Proterozoic mineral systems in Australia include: 1) iron formations or banded iron-formations (BIFs); 2) orogenic and intrusion-related; 3) orthomagmatic; 4) mineral systems associated with anorogenic magmatism; 5) rift-related stratiform and stratabound sedimentary-hosted; and 6) uranium ore systems. These mineral systems formed in intraplate, plate margin, back-arc rift and collisional tectonic settings.

KEYWORDS: Proterozoic, mineral systems, North Australian Craton, West Australian Craton, South Australian Craton

## 1 MINERAL SYSTEMS

In this paper we present a brief review of Australia's Proterozoic mineral systems, which host several world-class deposits. The main Proterozoic mineral systems in Australia are summarized below (Fig.1; Pirajno and Bagas, in press).

### 1.1 *Iron formations*

The early Palaeoproterozoic (*ca.* 2400 Ma) Hamersley Basin is endowed with the world's largest Fe resources, which are time equivalent of the Transvaal Group iron formations in South Africa. Three major ore types are recognised in the Hamersley Basin banded iron-formations (BIF): 1) Low-P, leached BIF; 2) high P, martite-geothite ore; and 3) low P, martite-microplaty hematite ore. The origin of BIF and of granular iron formation (GIF) remains a contentious issue in terms of both source of metals (Fe and Mn) and the tectonic setting and hydrothermal processes. Subaqueous hydrothermal discharges in lakes and/or ocean basins or in Red Sea type brine pools have been invoked. In all cases a density and oxic-anoxic stratified system is required to enable precipitation of $Fe^{3+}$. These deposits reflect the onset of continental shelf environments and the assembly of supercontinents, *ca*. 2400 and 1800 Ma.

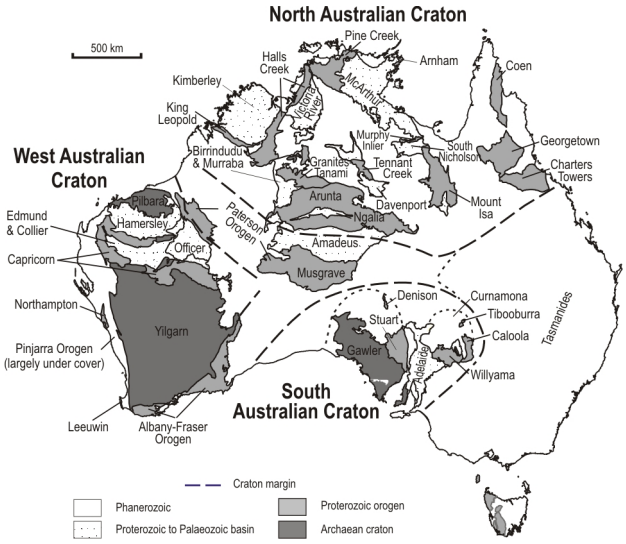


Fig. 1. Simplified map of Australia showing the location of Phanerozoic, Proterozoic and Archaean terranes in Australia.

### 1.2 *Orogenic and intrusion-related systems*

Orogenic and intrusion-related ore systems are very common in the Proterozoic rocks of Australia, with examples from the Pine Creek, Granites-Tanami, and Arunta orogens in the North Australian Craton (NAC) and Capricorn Orogen in the West Australian Craton (WAC; Fig.1).

### 1.3 *Orthomagmatic ore systems*

Orthomagmatic Ni-Cu-PGE and Fe-Ti-V ore deposits in mafic-ultramafic systems are present in the Halls Creek Orogen (NAC) and the *ca.* 1080 Ma Giles suite in the Musgrave Complex (Paterson Orogen).

### 1.4 *Mineral systems associated with anorogenic magmatism*

Mineral systems associated with anorogenic magmatism encompass a wide range of hydrothermal deposits of which the economically most important are the iron oxide-copper-gold (IOCG) ore systems, such as the *ca.* 1580 Ma world-class Olympic Dam in the SAC. To the same group may belong the Abra Pb-Cu-Ba (Capricorn Orogen) and the world-class Telfer Au-Cu (Paterson Orogen). Between 1100 and 800 Ma alkaline rocks, including carbonatites and diamondiferous lamproites, were emplaced in the NAC, South Australian Craton (SAC) and WAC. The 1180 Ma Argyle lamproite in the NAC is the world's largest diamond producer. Studies elsewhere suggest that these alkaline rocks are the distal expression of mantle plume events.

### 1.5 *Rift-related stratiform and stratabound sedimentary-hosted*

Stratiform and stratabound sedimentary-rock hosted giant and world-class massive sulphide deposits developed between *ca.* 1700 and 1500 Ma in the McArthur River-Mount Isa and Broken Hill rift systems. These deposits are all hosted in organic-rich shales and associated with clastic-evaporitic successions and bimodal igneous activity. Conceptual models of ore genesis posit discharge of hydrothermal fluids along major basin faults, synsedimentary exhalations of these fluids in oxygen deficient pools and bacterial sulphate reduction in order to produce $H_2S$ and precipitate sulphides. An unusual and large non-sulphide Pb carbonate ore deposit, Magellan, is hosted in clastic rocks of the *ca*. 1800 Ma Earaheedy Group. The lack of sulphides suggests that the deposit is related to palaeoweathering processes, which induced oxidation and mobilization of Pb.

### 1.6 *Uranium ore systems*

Apart from U contained in IOCG deposits, world-class unconformity stratabound deposits occur in the Pine Creek Orogen, with the Jabiluka as the main representative.

## 2 DISCUSSION

Australia's Proterozoic mineral systems are best understood within the framework of the geological and geodynamic factors that control the genesis and preservation of the deposits. Australia's Proterozoic terranes were formed in intracratonic, convergent plate margin, or collisional tectonic settings. Fig. 2 illustrates the main tectonic settings of Australia's Proterozoic mineral systems (Pirajno & Bagas, in press).

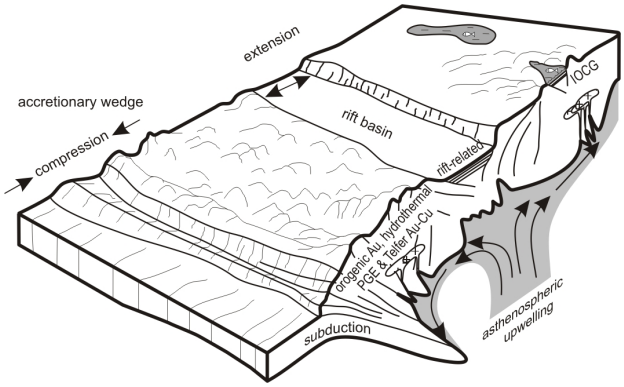


Fig. 2. Collision and back-arc rift settings of Proterozoic mineral systems in Australia. The figure is schematic, not to scale, and is only designed to provide a holistic view.

Iron formations of the Hamersley Basin probably constitute the largest endowment of Fe in the world. Barley *et al*. (1997) proposed to link flood basalt volcanism, with large input of $Fe^{2+}$ into the ocean and the origin of the banded iron-formations of the Hamersley Basin. Epsilon Nd signatures ($\varepsilon Nd = +1.0\pm0.5$) of BIF from the Hamersley Basin confirm volcanic and/or hydrothermal mantle sources (Alibert & McCulloch, 1993). Isley (1995), and Isley & Abbott (1999) also suggested a link between plume-related igneous activity and the deposition of iron-formations during the Archaean and Proterozoic. They used the geochronological record of plume activity between 3800 and 1600 Ma, as indicated by the presence in the geological record of komatiites, flood basalt, mafic dyke swarms, and mafic-ultramafic layered intrusions. Condie *et al*. (2000) proposed that the world-wide occurrence of passive margins, platform sediments and iron formations at around 1900 Ma could be indicative of a superplume event.

Intraplate tectonothermal events involve magmatic underplating and extensional tectonics, driven by mantle plumes or asthenospheric upwelling in rift settings associated with far field tectonic stresses. The predominance of bimodal magmatic systems in several of the Australia's Proterozoic terranes (Pine Creek; McArthur River-Mount Isa, Broken Hill) and the presence of dyke swarms and large igneous provinces support intracratonic tectonic scenarios (Fig. 2). Arc-terranes and their lateral accretion have been recognised in regions such as the Arunta Orogen and Musgrave Complex (Wade *et al.* 2006), the Gascoyne Complex (a remnant of an Andean-style arc terrane, which was extensively deformed and metamorphosed during the *ca*. 2000-1960 Ma Glenburgh Orogeny; Sheppard *et al.* 2005), and the Halls Creek Orogen in the Kimberley Craton (Griffin *et al.*, 2000). Widespread development of orogenic Au lodes in the NAC during *ca*. 1800 Ma appears to be related to the collision between the WAC and NAC (*e.g*. Bagas, 2004). Betts & Giles (2006) envisaged a north-dipping subduction system or zone on the southern margin of the NAC, with concomitant continental back-arc extension, which would have formed the McArthur-Mount Isa rift-system (Fig. 2).

The plate margin and subduction-related tectonics of Australia's Proterozoic are lacking in calc-alkaline volcano-plutonic rocks and related mineral systems (*e.g*. porphyry and epithermal deposits), which are typically found in these tectonic settings. It is possible such mineral systems may be absent due to erosion and/or metamorphism-deformation; the latter perhaps preventing recognition. In the Halls Creek Orogen, for which a subduction tectonic setting followed by collision is proposed by Griffin *et al*. (2000), low-sulphidation adularia-sericite epithermal Au has been recently discovered in the 1855 Ma Whitewater Volcanics (Pirajno & Bagas, in press).

The thermal impact of mantle plumes and associated magmatism cannot be underestimated. In addition to direct generation of magmas, thermal anomalies associated with mantle plumes constitute powerful heat sources in the crust. Plumes may be responsible for the inception of crustal-scale hydrothermal circulation and high-T and low-P metamorphism, which may result in a wide range of ore deposits in hotspot-related rift systems (Pirajno, 2004). Examples are the numerous hydrothermal veins present in the Capricorn Orogen, which are indicative of widespread crustal-scale hydrothermal circulation (Pirajno, 2004). High geothermal gradients linked to continental mafic magmatism may have favoured large-scale circulation of hydrothermal fluids, which would have been responsible not only for the emplacement of the vein and lode deposits but also in the modification and remobilisation of earlier syngenetic and/or epigenetic deposits into structurally prepared sites.

IOCG deposits appear to be linked to extensional settings with episodes of anorogenic bimodal and alkaline magmatism. In IOCG systems, the unifying factors are the enrichment in Fe–P–F and widespread alkali metasomatism in host rocks (Oreskes & Hitzman, 1993). Typically, IOCG hydrothermal systems form in shallow (4-6km deep) crustal environments and are the expression of volatile-rich, alkaline magmas. Several IOCG deposits cover the time span of *ca*. 1800 to 1100 Ma and they appear to be linked to planetary-scale rifting events and the assembly and breakup of supercontinents. The assembly of the Proterozoic supercontinent Rodinia, may have acted as a large insulation blanket on sublithospheric mantle flow, resulting in accumulation of heat, rise of mantle diapirs, melting, rifting of the continental crust, and finally the inception of regional-scale hydrothermal systems at shallow levels in the crust. Alternatively, IOCG-REE-U mineralization is common in both Proterozoic and Phanerozoic extensional environments where mineralised saline fluids were sourced from evaporites (Barton & Johnson 1996). Barton & Johnson (1996) cited examples of Holocene hydrothermal Fe-oxides formed from evaporitic sources and the correlation of the IOCG of Mesozoic age with zones of low-latitude as revealed by continental reconstructions. The evaporitic source model of Barton & Johnson (1996) suggests that circulation of hydrothermal fluids is caused by magmatic heat, that igneous rocks are the source of the metals, and that the metal transport is effected by chlorides supplied by evaporitic deposits. In addition, widespread Na-alteration associated with the deposits is also related to the evaporites, which supplied the large amounts of Na to the hydrothermal fluids.

The world-class stratiform massive sulphide deposits in the McArthur River-Mount Isa rift-system may ultimately owe their genesis to mantle-generated heat. Genetic models for the McArthur River-Mount Isa and Broken Hill

sedimentary-hosted stratiform and stratabound deposits have been discussed in detail by Large *et al*. (2005). The host rocks are metamorphosed evaporite-carbonate-clastic rocks and the sulphide mineralization is associated with organic-rich siltstone and shale. A generally accepted model posits the activity of hypersaline brines that discharge in a reduced environment (*e.g*. bottom of anoxic basin or lake; Large *et al.*, 2005). This model suggests bacterial mediation with biogenic sulphate reduction being a major contributor of $H_2S$ leading to sulfide precipitation. The range of $\delta^{34}S$ values from -13 to +30‰ in the ores (Large *et al.* 2005) support sulfate reduction. The alteration patterns are characterised by regional-scale Na- and K-metasomatism, phyllosilicate alteration, and silicification. Regional K-feldspar (microcline, adularia and albite) metasomatism is associated with major fault zones along which the giant base metal deposits are situated. Hydrothermal fluids and heated basinal brines were driven by the emplacement of mafic intrusions in the rift basins with metals sourced from mafic and felsic volcanic rocks (Large *et al*. 2005).

Australia's Proterozoic mineral endowment is probably one of the most varied and richest in the world. Major advances in understanding these mineral systems have been made in the last 30 years, in terms of tectonic settings and mechanisms of ore genesis, largely due to precise age dating using the U-Pb, K-Ar and Ar-Ar systems. Nevertheless much remains to be done, especially in view of the ever increasing demand of metals provided by Australia's vast mineral resources.

## ACKNOWLEDGEMENTS

This contribution is published with permission of the Director of the Geological Survey of Western Australia.

## REFERENCES

Alibert C, McCulloch MT (1993) Rare earth element and neodymium composition of the banded iron-formations and associated shales from Hamersley, Western Australia. *Geochim Cosmochim Acta* 57: pp. 187–204

Bagas L (2004) Proterozoic evolution and tectonic setting of the northwest Paterson Orogen, Western Australia. *Precambrian Res* 128: pp. 475–496

Barley, ME, Pickard AL, Sylvester PJ (1997) Emplacement of a large igneous province as a possible cause of banded iron formation 2.45 billion years ago. *Nature* 385: pp. 55–58

Barton, MD, Johnson DA (1996) Evaporitic source model for igneous-related Fe oxide-(REE-Cu-Au-U) mineralization. *Geology* 24: pp. 259–262

Betts, P.G., Giles, D. (2006) The 1800-1100 Ma tectonic evolution of Australia. *Precambrian Res* 144: pp. 92–125

Condie KC, Des Marais DJ, Abbott D (2000) Geologic evidence for a mantle superplume event at 1.9 Ga. *Geochem Geophys Geosys* 1, Pap No. 2000GC000095

Griffin TJ, Page RW, Sheppard S, Tyler IM (2000) Tectonic implications of Palaeoproterozoic post-collisional, high-K felsic igneous rocks from the Kimberley region of nortwestern Australia. *Precambrian Res* 101: pp. 1–23

Isley AE (1995) Hydrothermal plumes and the delivery of iron to banded iron formation. *Journal of Geology* 103: pp. 169–185

Isley AE, Abbott DH (1999) Plume-related mafic volcanism and the deposition of banded iron formation. *Geophys Res* 104: pp. 15461–15477

Large R, Bull S, McGoldrick PJ, Waters S, Derrick GM, Carr GR (2005) Stratiform and stratabound Zn-Pb-Ag deposits in Proterozoic sedimentary basins, northern Australia. *Economic Geology* 100: pp. 931–963

Oreskes N, Hitzman MW ,(1993) A model for the origin of Olympic Dam-type deposits. *Geol Assoc Can Spec Pap* 40:pp. 615–633

Pirajno F (2004) Hotspots and mantle plumes: global intraplate tectonics, magmatism and ore deposits. *Mineral Petr* 82: pp. 183–216

Pirajno F, Bagas L (in press) A review of Australia's Proterozoic mineral systems and genetic models. *Precambr Res*

Sheppard S, Occhipinti SA, Nelson DR (2005) Intracontinental reworking in the Capricorn Orogen, Western Australia: the 1680-1620 Ma Mangaroon Orogeny. *Aust J Earth Sci* 52: pp. 443–460

Wade BP, Barovic KM, Hand M, Scrimgeour IR, Close DF (2006) Evidence for early Mesoproterozoic arc magmatism in the Musgrave Block, central Australia: implications for Proterozoic crustal growth and tectonic reconstructions of Australia. *Geology* 114: pp. 43–63

# Causative links between thermal history, deformation mode and hydrothermal mineralization in continental lithosphere of the Australian Proterozoic

Klaus Gessner
*pmd*CRC, Centre for Exploration Targeting, The University of Western Australia, Crawley WA 6008, Australia*
*pmd*CRC, Computational Geoscience for Predictive Discovery, CSIRO Exploration and Mining, Kensington, WA 6102, Australia*

ABSTRACT: The Mount Isa Inlier is a deformed and metamorphosed Proterozoic rift system in Queensland, Australia, which is extraordinary rich in base metals, and has considerable gold and uranium resources. Here it is suggested that the metal prospectivity of the Mt Isa Inlier is closely related to the preferential formation of vertical permeability, which formed as a consequence of the deformation of hot and mechanically decoupled lithosphere in a sequence of extensional and contractional events. Enrichment of heat-producing elements in pre-rift basement resulted in an upper crust geothermal gradient of up to 50 °C/km, leading to strong vertical partitioning of mechanical behaviour in extension and shortening of the continental lithosphere. During the structural evolution of the Mount Isa Inlier, vertical permeability was enhanced significantly parallel to steepened fold limbs, reactivated foliation, and damage zones along high-angle fault systems. Vertical permeability generates short fluid pathways across gradients of pressure, temperature, and chemical composition; favoring the formation of high grade and high tonnage hydrothermal deposits. The link between thermally weakened crust, steep tectonic grain and mineral prospectivity is likely to play a key role in many other mineral provinces.

KEYWORDS: Mount Isa, Continental lithosphere, Proterozoic metal provinces

## 1 INTRODUCTION

Two of the outstanding characteristics of the Australian Proterozoic are its numerous large sulphide and oxide ore deposits, and its extraordinary tectono-thermal evolution. The Mount Isa Inlier in northwest Queensland represents the largest outcrop area of the Australian Proterozoic, and hosts a number of very large mineral deposits such as shale hosted massive sulphide Pb-Zn-Ag, structurally controlled Fe-sulphide Cu, Fe-oxide Cu-Au, and Broken Hill-type Pb-Zn-Ag. The thermal history of the Mount Isa Inlier is controlled by intraplate extension and contraction events spanning about 300 million years of the Palaeo- to Mid-Proterozoic. A further characteristic of the Proterozoic lithosphere in Mt Isa, and elsewhere in Australia, is the relatively high geothermal gradient due to an extraordinary enrichment of radiogenic elements in basement rocks.

## 2 THERMAL MODELING

A series of thermal models have been carried out to better understand the impact of radiogenic heat production and of the depth of burial of radioactive basement. For this purpose a model of a layered lithosphere (base of the lithosphere: ~200 km at 1250 ºC; surface at 25 ºC) was generated, based on the seismic velocity model of Drummond et al., 1998. Typical U, Th and K contents of crustal rocks in Mt Isa (McLaren, 1999) were used to calculate current heat production rates for various layers in the lithosphere. The objective has been to match the current surface heat flow of 80 $mW \cdot m^{-2}$ (Hyndman & Sass, 1966) to then calculate the thermal structure for the Proterozoic at 1.5 Ga.

## 3 RESULTS

The current thermal structure of the crust at Mt Isa is most likely related to a mid-crustal layer enriched with felsic intrusives underlain by mafic lower crust to ~ 55km. Assuming a

sedimentary cover of up to 7.5km, this gradient would have been substantially higher in the Proterozoic. Due to the higher heat production at 1.5 Ga melting temperatures of granite and peridotite would have been reached at 13 and 32km respectively (Figure 1).

## 4 THERMAL-MECHANICAL MODEL

This means that as long as the hot basement in Mt Isa was buried under a thick insulating overburden (such as tectonic slices or sedimentary basins), there has been a potential for crustal melting, due to elevated geotherms of up to 50 ºC $km^{-1}$ (Figure 1). A further important implication of a high geothermal gradient is thermal weakening. The lack of shear strength in the thermally weakened lower crust and upper mantle prevented localization of plastic shear zones (Ord & Hobbs, 1989), favouring metamorphic core complexes over distributed rifts in extension, and suppressing the formation of alpine-type orogenic nappe-stack in contraction. As a consequence, contractional orogenesis resulted in low-pressure metamorphism and steep folding of a thin, decoupled upper crust. This mechanical decoupling of steeply folded upper crust and lateral flow of the middle and lower crust has been demonstrated by a number of scaled physical analog modeling studies (Cruden *et al*., 2004; Cagnard *et al*., 2006). Furthermore, the steep structural grain in the upper crust leads to a high degree of mechanical anisotropy at high angles to the tectonic shortening direction, which tends to favour orogen-parallel elongation. There is also a strong tendency for reverse-sense shear zones to turn into strike slip fault zones, as oblique components of convergence will become dominant once the shear zones have steepened.

## 5 IMPLICATION FOR MINERAL PROSPECTIVITY

Hydrothermal mineralization requires metal-bearing fluids to flow across gradients of pressure, temperature, chemical concentration, or a combination of these gradients (Phillips 1991). The existence of vertical or steeply dipping aquifers within the architecture of a mineralizing system can be of great significance, because they provide a higher potential for fluid to flow across gradients of temperature and pressure than horizontal, or shallowly dipping aquifers.

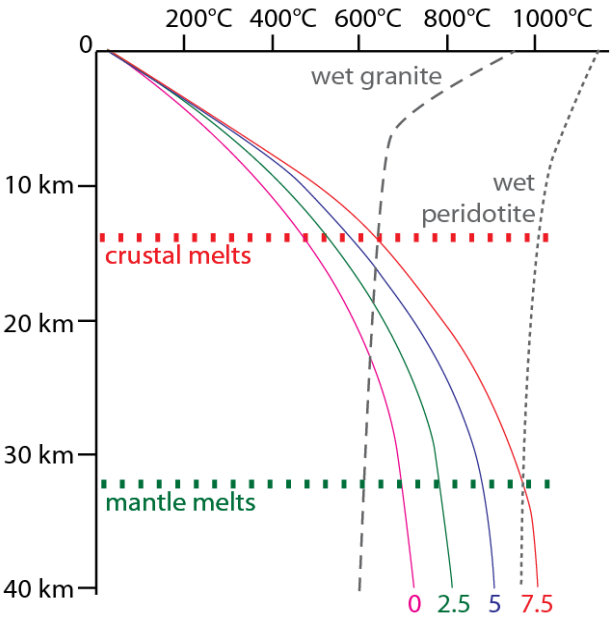


Figure1: Geothermal gradients modeled for lithosphere at Mt Isa. Curves in color show resulting Proterozoic geotherms for variable depths of burial below sedimentary basins, from exposed basement (0 km overburden) to 7.5 km burial depth. Notice intersection of wet granite and peridotite solidi at ~13 and ~32 km depth in 7.5 km overburden case.

A steep aquifer is also more likely to favour free thermal convection, which is a highly effective fluid flow driving process in hydrothermal systems. In addition to the presence of inclined and steeply dipping aquifers, the overall high thermal gradient in the Proterozoic of Mount Isa would have favored free thermal convection over conductive heat transfer in areas with high permeability. The likelihood of free thermal convection to occur is therefore significantly increased by the steepening of stratigraphy and deformation fabrics in the upper crust. These steepened fabrics favoured the formation of deep-rooted strike slip fault zones, which provided pathways for surface fluids, metamorphic fluids from different lithospheric domains, and fluids from the mantle, thus leading to an increased likelihood of mineral precipitation.

## ACKNOWLEDGEMENTS

Xstrata Copper Australia are thanked for supporting this research, which was carried out as part of the predictive mineral discovery Co-operative Research Centre, pmd*CRC.

## REFERENCES


Cagnard, F., Durrieu, N., Gapais, D., Brun, J.-P., and Ehlers, C., 2006, Crustal thickening and lateral flow during compression of hot lithospheres, with particular reference to Precambrian times: *Terra Nova*, v. 18, p. 72-78.

Cruden, A.R., Nasseri, M.B., and Pysklywec, R.N., 2004, Three-dimensional strain partitioning in analogue versus numerical models of convergent orogens: *Bolletino di Geofisica teorica et applicata*, v. 45, p. 70-73.

Hyndman, R.D., and Sass, J.H., 1966, Geothermal Measurements at Mount Isa, Queensland: *Journal of Geophysical Research*, v. 71, p. 587-601.

McLaren, S., Neumann, N., Sandiford, M., and Wyborn, L., 1999, Post-intrusion heating associated with high-heat-producing Proterozoic granites; implications for mineralisation? : *AGSO Research Newsletter* v. 30, p. 23-26.

Ord, A., and Hobbs, B.E., 1989, The strengt of the continental crust, detachment zones and the development of plastic instabilities: *Tectonophysics*, v. 158, p. 269-289.

Phillips, O.M., 1991, *Flow and reactions in permeable rocks:* Cambridge, UK, Cambridge University Press, 285 p.

# Quadrilátero Ferrífero and Hamersley Province: so far apart and yet so close to each other.

C.A. Rosière[1], M.E. Barley[2], S.G. Hagemann[2] & V.E. Suckau[3]

*1Instituto de Geociências, Univ. Fed. de Minas Gerais, Brazil*
*2Centre for Exploration Targeting, University of Western Australia, WA, Australia*
*3Minerações Brasileiras Reunidas, Minas Gerais, Brazil*

ABSTRACT: The stratigraphic and tectonic evolution of the Minas and Hamersley Basins were similar, particularly during the late Archaean/Palaeoproterozoic time period, with the extensive sedimentation and formation of banded iron formations in shallow to deep platformal environment and associated with volcanic centers. Both present similar tectonic architectures of a fold belt, formed at relative shallow crustal conditions, followed by the development of domal structures of still uncertain origin and formation mechanism. The deformation created new and activated older discontinuities, that conducted mineralizing fluids. to localized low strain (strain shadows), thereby producing haematite veins, mullion-shaped and concordant high-grade ore bodies.

KEYWORDS: Quadrilátero Ferrífero, Hamersley Province, BIF, Iron Mineralization

## 1 INTRODUCTION

Although located in distinct Archaean palaeocontinents (Atlantica and Ur, respectively), the Minas (Quadrilátero Ferífero) and Hamersley (Western Australia) Basins present several similarities during their stratigraphic and tectonic evolution from opening to closure. Deformational features during the Palaeoproterozoic Transamazonian/Mineiro and Ophtalmian orogenies, have also contributed in similar manners to the flow patterns of fluids responsible for the iron mineralization.

This paper discusses these similarities as well as focusing on the mineralization processes involved in the development of high-grade iron ore deposits and its relation to the associated thermal-tectonic events.

## 2 THE BIF-BEARING MINAS BASIN IN THE QUADRILÁTERO FERRÍFERO.

### 2.1 *Lithostratigraphic Units*

The Minas Supergroup (MSG) (Dorr, 1969) is a Palaeoproterozoic iron formation-bearing sequence outcropping in the Quadrilátero Ferrífero Mineral District (QF), located at the south-eastern extremity of the São Francisco Craton. The sedimentary rocks of the MSG unconformably overlie the Archaean Rio das Velhas greenstone belts (2.6–2.7 Ga, Machado *et al*. 1992) with surrounding Late Archaean granitic and gneiss/migmatite blocks. The Rio das Velhas Supergroup comprise a volcanic-rocks bearing unit, (the Nova Lima Group) and a sandstone-conglomerate unit (the Maquiné Group)

The MSG comprises a basal unit consisting of alluvial to deltaic-marine sandstones and conglomerates covered by pelagic carbonaceous shales, and locally volcaniclastic rocks. These sequences are formally integrated in the Caraça Group which underlies the iron formations and dolomites of the Itabira Group subdivided in the Cauê (BIFs) and Gandarela Formations (2.42 Ga, Babinski *et al*. 1995). Following an apparent apparent gradual uplift , the continuous deposition of these units was interrupted by the development of an erosional unconformity and the local development of supergene Fe-mineralization. A new cycle starts with the sedimentation of the Piracicaba Group which comprises Fe-rich sandstone and BIF- and Hm pebbles conglomerates intercalated with pelitic layers (shallow-water deltaic environment), carbonaceous shales (Barreiro Fm), chert, carbonates and banded iron formations (Taboões Fm), reflecting a recurrent deepening of the Minas Basin.

The Sabará Group (2.12 Ga, Machado *et a*l.

1992) is defined by volcanogenic rocks and turbidites deposited after a long hiatus in sedimentation. The Itacolomi Group is the youngest sedimentary sequence in the QF with sandstones, arkoses and BIF (Hm?) – pebble conglomerates.

## 2.2 *Critical stratigraphic questions*

The interpretation of the evolution of the Minas Basin, particularly in the upper sequences, is made difficult due to two main reasons: the relative lack of systematic studies of the Piracicaba Group stratigraphy and the complex tectonic style dominant in the eastern domain of the QF. In this area. Palaeoproterozoic Transamazonian/Mineiro and Neoproterozoic Brasiliano/Aracuaí orogenies have interfered with and reoriented older structures, and imposed a westward vergence, resulting in the development of complex interference patterns and several allochthonous slices and blocks**.**

On the other hand, the stratigraphy of the western domain is more readily interpreted. The structural scenario is dominated by flexural folds and a domal structure setting of uplifted granite-gneissic bodies probably triggered by younger granites (2.08 Ga, Noce, 1995), producing structures related to the collapse phase of Transamazonian/Mineiro Orogeny. (Alkmim & Marshak, 1998)

Ill-defined clastic sequences such as the Tamanduá quartzite occur also as allochthonous blocks in the eastern part of the QF. Another point that deserves a reinterpretion is the origin of the pelitic rocks of the Batatal Formation, whose lithological complexity has so far been overlooked due to the deep weathering mantle. This formation is described as composed by "sericite and graphite phyllites". It is actually comprised of layers of chert, carbonates, volcanoclastic and other volcanic-related rocks and probably turbiditic sequences that grade upward and laterally into iron formations. The Batatal Formation, represents the basal part of the shale-iron formation pair, deposited in the deeper environment of the Minas platform

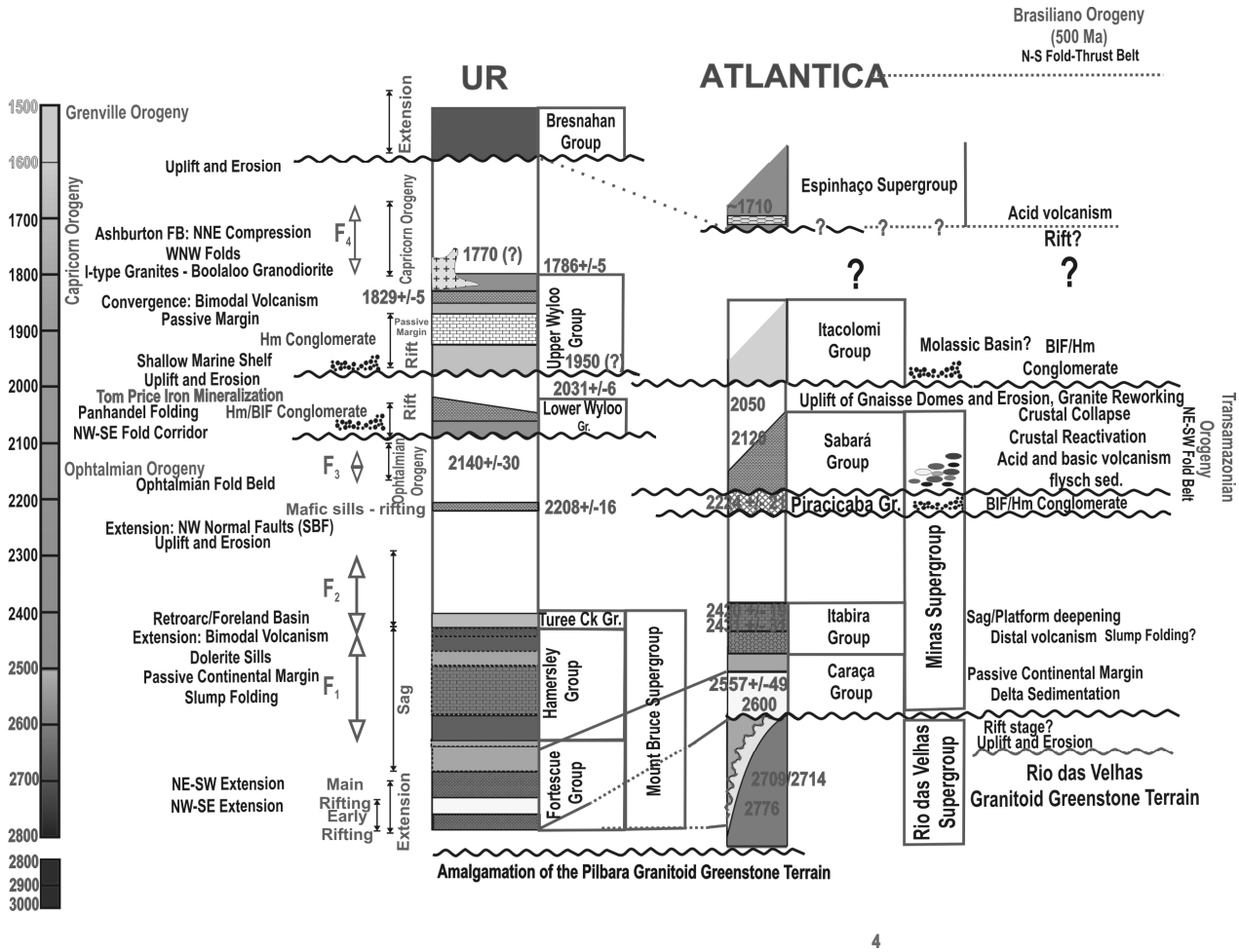


Fig. 1 Comparative table between the geologic evolution of the Minas and Hamersley Basins On the left, stratigraphic column of the Hamersley Basin with main geologic events. On the right, equivalent information for the Minas Basin

similar to the BIF-sequences analyzed by Krapez *et al*, (2003).

## 3 THE MINAS AND HAMERSLEY BASINS: COMPARATIVE ANALYSIS AND DISCUSSION

### 3.1 *Stratigraphy and tectonic evolution*

The iron formations of the Itabira Group were deposited on a shallow to deep platformal environment distal to the volcanic centers, source of the Fe-rich hydrothermal exhalations as evidenced by the lack of extensive volcanic units and by the presence of fluvio-deltaic sediments of the Moeda Formation on the base of sequence. Apparently no remains of the proximal, volcanic source can be found due to the intensive deformation undergone by the Minas Supergroup during the Brasiliano/Araçuaí Orogeny, although some volcanoclastic sediments are still encountered in the Batatal Formation. This is distinctively different from the Hamersley Basin (HB), where several different environments are registered in the geological record along the border of the Pilbara Craton (Barley et al. 1999). In the case of the Minas Supergroup, several allochthonous blocks may be interpreted as part of its basal sequence that are now lost in the stratigraphic and tectonic complexity of the Province, in the east from the QF, or even in units that are presently considered as belonging to the Rio das Velhas Supergroup, such as the Casa Forte Fm/Maquiné Group.

Although available geochronology does not allow precise correlation there are tectonic and stratigraphic similarities between the Sabará Group and the Lower Wyloo Group and the Itacolomi and the Upper Wyloo Group.

The sedimentation of the Piracicaba Group appears pene-contemporaneous with the pre-Ophtalmian rifting deposition of the Lower Wyloo Group with the development Fe-rich sandstones and BIF-pebbles conglomerate (Cercadinho Fm) that is co-relatable with the Beasley River Quartzite/Three Corner Conglomerate. The Sabará volcanism is also coincident with the eruption of the Cheela Spring Basalts fissure volcanoes (Fig 1).

The opening of the Ashburton Basin and onset of sedimentation of the Upper Wyloo Group BIF-bearing conglomerates (Mt McGrath) in Western Australia is contemporaneous with the deposition of the silicilastic sediments of the Itacolomi Group (Fig 1).

### 3.2 *Implications for iron mineralization*

The similar tectonic histories of the two provinces, at least up to the Mesoproterozoic, has provided the structural architecture for both hypogene and supergene hydrothermal processes. Both the massive, hard iron ore bodies of the Hamersley Province (*e.g.*, the Mt Tom Price deposit) and the Quadrilátero Ferrífero (*e.g.*, the Águas Claras, Mutuca, Feijão deposits) are situated within regional synclines and associated with the uplift of the granite-gneiss domes and the related hydrothermal fluid flux. Geological, geochemical and numerical simulation all show that the regional synclines, both in the QF and in the HP, especially in the closure of flexural folds that acted as traps for focused fluid flow by fault zones and their associated fracture networks. (Fig. 2).

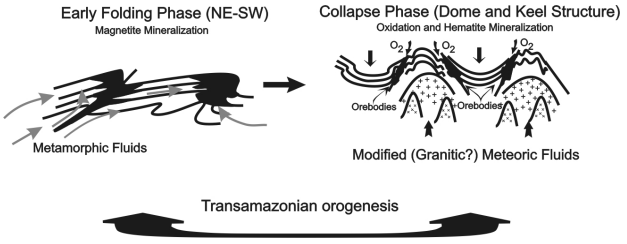


Fig. 2 Schematic representation of fluid path for the formation of the massive high-grade (>63% Fe) iron ore bodies from the Quadrilátero Ferrífero. Mineralization developed in two stages during the Transamazonian/Mineiro event: 1- Synmetamorphic magnetite mineralization in the early stages of the first folding phase. 2. Haematite mineralization by modified meteoric fluids during the collapse stage, coincident with the development of dome-and-keel structures and partial uplift of the sequence (after Rosière & Rios, 2004)

Large faults, such as the Mutuca Fault and reactivated basin border faults, were probably important fluid pathways for fluids and controlled the concentration of large deposits in certain areas of the Quadrilátero Ferrífero, such as along the Serra do Curral Range representing the northernmost border of the Minas Basin (Fig. 3). Previous work in the QF (Rosière & Rios, 2004) has indicated that mineralization first occurred under the influence of metamorphic fluids expelled during the Transamazonian/Mineiro Orogeny, and was later oxidized by modified surface waters, during the collapse phase of this tectonic event, with uplift of gneiss domes, probably triggered by granite-genesis in deeper, presently unexposed crustal levels (Fig. 2). In the Hamersley Province,

hydrothermal Fe-mineralization developed similarly to the QF, under progressively oxidising conditions (Taylor *et al*, 2001; Thorne *et al.*, 2004) related to the evolution of the penecontemporaneous Ophtalmian orogeny, Panhandle folding and Lower Wyloo Group. A further controlling condition is the permeability of bounding strata, in particular shales and dolerites, which may have acted as an aquitard to fluid flow (Mt Tom Price, HP; Tamanduá and Capitão do Mato Mines, QF)

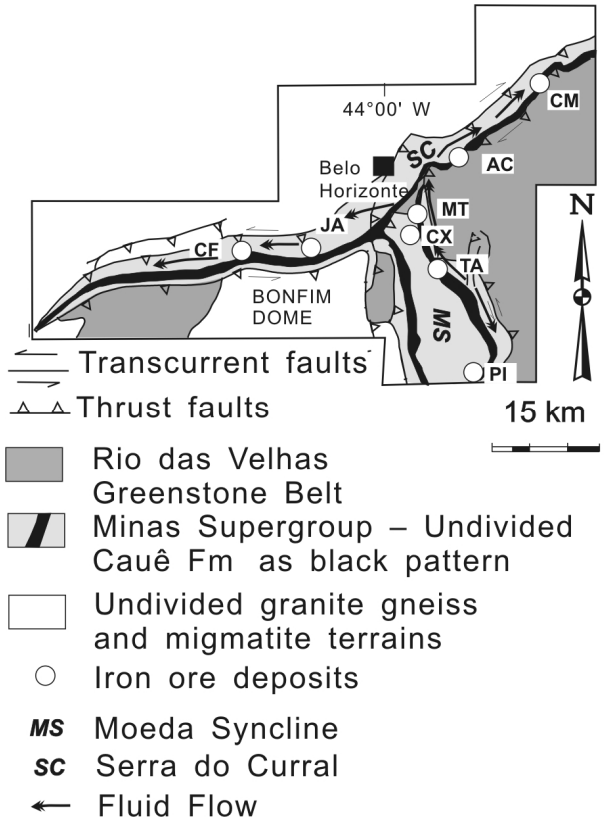


Fig. 3 Schematic geologic map displaying the confluence between the Serra do Curral (SC) and Moeda Syncline (MS) with representation of metamorphic fluid flow, which is interpreted to be the fluid source that formed high-grade iron deposits. Iron deposits: PI – Pico; TA – Tamanduá, MT – Mutuca; CX – Capão Xavier, AC – Águas Claras; JÁ – Jangada, CF – Córrego do Feijão, CM – Córrego do Meio.

## ACKNOWLEDGEMENTS

The authors thank the CNPq, UWA and MBR for the support. CAR particularly thanks H. Quade and J.H.Grossi Sad for the inspiring ideas that were partially recovered in the conception of this paper. C. Spier and G. Mendes are also thanked for the discussions, sharing valuable information and presenting important outcrops in the field. L. Lobato and F. Braars have generously reviewed the text.

## REFERENCES

Alkmim, F F and Marshak, S, (1998) Transamazonian orogeny in the southern São Francisco craton, Minas Gerais, Brazil: evidence for paleoproterozoic collision and collapse in the Quadrilátero Ferrífero, *Precambrian Research* 90:29-58

Babinski, M., Chemale, F., Jr., and Van Schmus, W. R., (1995) The Pb/Pb age of Minas Supergroup carbonate rocks, Quadrilátero Ferrífero, Brazil, and its implications to the correlation with BIFs from South Africa and Australia: *Precambrian Research* 72: 235-245.

Barley ME, Pickard AL, Hagemann SG, Folkert SL (1999) Hydrothermal origin for the 2 billion year old giant iron ore deposit, Hamersley Province, Western Australia. *Mineralium Deposita* 34:784–789

Dorr, J V N 2nd, (1969) Physiographic, stratigraphic and structural development of the Quadrilátero Ferrífero, Minas Gerais, *U. S. Geological Survey Professional Paper* 641-A:110p.

Krapež, B, Barley ME, Pickard AE (2003)Hydrothermal and resedimented origins of the precursor sediments to banded iron formation: sedimentological evidence from the Early Palaeoproterozoic Brockman Supersequence of Western Australia, *Sedimentology* 50,5: 979 – 1011.

Machado, N., Noce, C. M., Ladeira, E. A., and Belo de Oliveira, O. A., 1992, U-Pb Geochronology of Archean magmatism and Proterozoic metamorphism in the Quadrilátero Ferrífero, southern São Francisco craton, Brazil: *Geological Society of America Bulletin* 104: 1221-1227

Noce, C.M. 1995. Geocronologia dos eventos magmáticos, sedimentares e metamórficos na região do Quadrilátero Ferrífero, Minas Gerais. *Inst. de Geociência*s, São Paulo, PhD Thesis: 128 p.

Rosière, C.A. & Rios, F. J., (2004) The origin of haematite in high grade iron ores based on infrared microscopy and fluid inclusion studies: the example of the Conceição mine, Quadrilátero Ferrífero, Brazil, *Economic Geology* 99: 611-624.

Taylor D, Dalstra HJ, Harding AE, Broadbent GC, Barley ME (2001) Genesis of high-grade haematite orebodies of the Hamersley Province, Western Australia. *Economic Geology* 96:837–873

Thorne WS, Hagemann SG, Barley ME (2004) Petrographic and geochemical evidence for the hydrothermal evolution of the North Deposit, Mt Tom Price, Western Australia. *Mineralium Deposita* 39: 766-783.

# Polyphase Metallogenesis in the Carajás Cu-Au Belt, Brazil

K.M. Volp
*Universidade Federal do Pará, Belém, Brasil*

ABSTRACT: Polyphase Cu-Au metallogenesis in the Carajás Cu-Au Belt, Brazil is considered to have occurred in three distinct epochs, *ca*. 2.76, *ca*. 2.55 Ga and a *ca.* 1.88 Ga. The 2.76 Ga event coincides with formation of the Itacaiúnas Supergroup host rocks and emplacement of the Estrela granite complex. An intrusion-related genesis for 2.55 Ga IOCG mineralization has been accepted at the Salobo deposit, however, contradictory data and models persist for the Igarapé Bahia-Alemão, Serra Pelada, Cento e Dezoito and Igarapé Cinzento deposits. Ore genesis models and age determinations at the Serra Verde and Igarapé Bahia-Alemão deposits may be consistent with a primary syngenetic model. REE mineral age dating has been interpreted to indicate a ca. 1.88 Ga intrusion-related Cu (IR-Cu) class, at the Breves deposit, however contradictory age dating and/ or ore genesis interpretations exist for the Estrela, Águas Claras and Gameleira deposits. Ore genesis models for IR-Cu deposits, are indeed complex as these Cu-dominant systems are associated with variable amounts of Au, Ag, W, Mo, Sn, Bi, enrichments in As, Ni, Co, Zn and Pb, and the common association of B, F and or Li in their gangue mineralogy.

KEYWORDS: Carajás, IOCG deposit, intrusion-related Cu, geochronology

## 1 POLYPHASE CU-AU METALLOGENESIS IN CARAJÁS

Geochronological work in the Carajás Cu-Au Belt indicates that there are several distinct ages for granite emplacement at 2.76 Ga, 2.63-2.64 Ga, 2.55-2.53 and *ca*.1.88 Ga (Machado *et al.* 1991). Cu-Au mineralization in Carajás has often been described in terms of two metallogenic epochs, a 2.7 - 2.5 Ga event associated with deposits of the Fe-oxide Cu-Au (IOCG) class and a *ca*. 1.88 Ga intrusion-related Cu association and the link between magmatism and Cu-Au mineralization has often been made as the basis for ore genesis models in Carajás. Regional geology, deposit geology and lithostratigraphic geochronology for the Carajás region have been discussed previously and the reader is referred to Tallarico *et al*. (2004), Villas & Santos (2001) and Porter (2000).

Deposits considered to belong to the IOCG class include the majority of Cu-bearing deposits in the region, several, world-class, *i.e*. the Salobo, Serra Verde, Cristalino, Igarapé Bahia-Alemão, Sossego-Sequerinho, 118 and Igarapé Cinzento deposits. Deposits which have been considered to belong to a 1.88 Ga intrusion-related Cu (IR-Cu) association include Breves, Estrela, Gameleira and Águas Claras. However, considering the geochronological data available, the classification of Carajás Cu-Au deposits as belong to either the 2.7-2.5 Ga IOCG or *ca* 1.88 Ga IR-Cu class is not necessarily that simple and this paper presents the current state of this debate.

## 2 ORE GENESIS MODELS FOR CU-AU DEPOSITS IN CARAJÁS

Genetic models for Cu-Au deposits in Carajás have varied with time, beginning with the early and significant Salobo deposit and applied to other deposits, in turn, as they were discovered. Syngenetic volcanic-exhalative models were initially popular, and followed, in the early 1990's, by mixed syngenetic-epithermal models which linked *ca*. 1.88 or 2.55 Ga granites to ore genesis for Salobo, Pojuca and Igarapé Bahia. It was Huhn (1996), on the basis of

large-scale sodic-potassic alteration and alteration-mineralization mineral associations at Salobo, who first proposed that Salobo, Pojuca and Igarapé Bahia, and by inference other copper-gold occurrences in Carajás, belonged to the iron oxide copper-gold group of deposits. The subsequent discoveries of Sossego-Sequerinho and Cristalino were quickly characterised as belonging to the IOCG class of deposits and have age determinations *ca*. 2.5 to 2.7 Ga.

Geochronological data and descriptions for the 118 (Cento e Dezoito) and Igarapé Cinzento deposits may suggest a Proterozoic IOCG class of deposits. An unpublished *ca*. 1.88 Ga Ar-Ar age determination on a Cu-bearing biotite vein from 118 (DOCEGEO 2001, unpublished data), however, no detailed work has been published for this deposit. Age determinations on Cu-bearing biotite veins (Ar-Ar) and Cu-ore (Sm-Nd) for Igarapé Cinzento are *ca.* 1.85 and 1.81, and 1.75 Ga, respectively, however, this deposit also has Archaean Re-Os molybdenite ages *ca*. 2.55, 2.6 and 2.71 Ga (Silva *et al.* 2006).

At the as yet undated Serra Pelada deposit models for an IOCG genesis and an epithermal deposit overprinted by supergene processes have been presented by Groves *et al.* (2000) and Cabral *et al.* (2002), respectively, and Cabral *et al*. considered that Serra Pelada was possibly the result of 1.88 Ga granitic fluids.

Tallarico *et al.* (2004), on the basis of their work at the Breves deposit, considered that the Águas Claras, Breves and Gameleira deposits may belong to a Cu-Au-(W-Bi-Sn) association related to *ca*. 1.88 Ga Carajás suite granites (IR-Cu). A similar interpretation was also suggested for the Estrela deposit (Volp 2005; Lindenmayer *et al.* 2006). The orthomagmatic genesis of these deposits, having a Cu-rich system with variable amounts of Au, Ag, W, Mo, Sn, Bi and enrichments F, B, As, Ni, Co, Zn and Pb, is hotly debated and geochronological data (discussed below) may only be conclusive for the Breves deposit.

## 3 IS SERRA VERDE AN IOCG DEPOSIT?

Uniquely, an IOCG classification has not been proposed for the Serra Verde deposit. At Serra Verde a model of syngenetic submarine volcanogenic model overprinted by contact metamorphism from the Estrela granite complex (2.76 Ga) was presented by Reis and Villas (2002). A later *ca.* 2.6 Ga Re-Os molybdenite age by Marschik *et al*. (2005) was interpreted to suggest a genetic relationship with 2.56–2.76 Ga alkaline granitoids or 2.6–2.7 Ga magmatism, and these authors made no mention of an IOCG classification.

## 4 A MAGMATIC SOURCE FOR CARAJÁS ARCHAEAN IOCG DEPOSITS?

The majority of age determinations for IOCG deposits in Carajás can be loosely grouped as *ca.* 2.7-2.5 Ga and temporally coincide with the formation of Itacaiúnas Supergroup (primary host rocks for these deposits), *ca.* 2.76, 2.63 and 2.55 Ga alkaline magmatism, and development of the Carajás strike slip system. An intrusion-related genesis for Cu–Au mineralization in IOCG provinces, including Carajás, has been presented by Pollard (2006) largely based on the work of Réquia *et al.* (2003) and Tallarico *et al.* (2005) who may have established a magmatic IOCG mineralization association for the Salobo and Igarapé Bahia deposits. Age determinations by Réquia *et al.* (2003) for mineralization at the Salobo deposit indicated two temporally separated pulses of molybdenite deposition at 2.58 Ga and 2.56 Ga. The former coincides with a published U–Pb age for the Old Salobo Granite and was interpreted to suggest that main stage bornite-chalcopyrite-magnetite ore formation (2.58 Ma; Pb-Pb) may have been contemporaneous with granite magmatism. At the Igarapé-Bahia-Alemão deposit a 2.58 Ga SHRIMP age for hydrothermal monazite from the matrix of ore-bearing magnetite breccias, being similar to published Pb-Pb zircon ages for Archaean A-type Carajás granites, was interpreted to indicate that IOCG mineralization at Igarapé Bahia was temporally related to magmatism (Tallarico *et al.* 2005). This is in contrast, however, to previously published ca. 2.74 to 2.76 Ga Pb-Pb age determinations for chalcopyrite (Galarza 2002) which are similar to ages obtained for host rocks at the deposit, and consistent with the syngenetic ore genesis model presented by Dreher *et al*. (2006).

Pollard (2006) also considered that the 2.76 Ga Estrela granite complex (Barros *et al*. 2001) was closely associated spatially with known Cu-Au mineralization and of an age similar to that for sulphides from the Cristalino deposit (Pb-Pb age of 2.72 Ga, Soares *et al.* 2001). It is noted, however, that the Cristalino deposit is located over 15km to the south of the Estrela granite complex and no Archaean granites have

been documented in the area.

## 5 PROTEROZOIC INTRUSION-RELATED CU DEPOSITS

Age determinations for magmatism and mineralization at the Breves deposit are consistent with the interpretation that the deposit formed *ca*. 1.88 Ga and is genetically associated with Cu-mineralization (Tallarico *et al*. 2004; Botelho *et al.* 2006). Tallarico *et al.* (2004) considered it noticeable, that the Águas Claras and Gameleira deposits show a spatial relationship between *ca.* 1.88 Ga granites and have a metalliferous character similar to that of Breves. Previous 2.36 Ga Pb-Pb age determinations for chalcopyrite and cobaltite at the Águas Claras deposit, however, are inconsistent with a 1.88 Ga genesis and hydrothermal sericite alteration of host arenite at 2.13 Ga (Rb-Sr whole rock) was considered to prove that the nearby Carajás granite had no genetic relation to the deposit (Silva *et al*. 2001).

Geochronological and paragenetic investigations from Gameleira, are also inconclusive with age determinations on Cu-bearing veins at *ca*. 1.88, and 1.84 and 2.4 Ga, by Ar-Ar and Sm-Nd, respectively (DOCEGEO 2001, unpublished data; Galarza 2002, unpublished PhD thesis), and Re-Os dating of molybdenite at ca. 2.4 and 2.6 Ga, from which Marschik *et al*. (2005) concluded that the formation of Cu-Au-Mo mineralization at Gameleira was unrelated to 1.8 - 1.9 Ga anorogenic granites.

Age determinations at the Estrela deposit include *ca*.1.88 and 1.85 ages for Cu-bearing veins (Ar-Ar on biotite, DOCEGEO 2001, unpublished data; and Sm-Nd, Lindenmayer *et al.* 2006, respectively) and EPMA monazite ages, from Cu-bearing veins and aplites for monazite growth at *ca*. 1886 Ma (magmatic) and 1.85-1.83 Ga (hydrothermal). These EPMA ages were interpreted to suggest that Cu-mineralization took place after two stages of monazite growth and may preclude a *ca.* 1.88 Ga genesis for copper (Volp *et al.* 2006). These data were considered to indicate that Cu-mineralization at Estrela is a related to a younger event, possibly the hydrothermal fluid system of a hidden intrusion. In contrast to these Cu ages, a single *ca.* 2.7 Ga Re-Os molybdenite age at Estrela led Lindenmayer *et al*. (2006) to propose two generations of molybdenite mineralization at *ca*. 2.7 and 1.88 Ga.

Ore genesis models for deposits interpreted to belong to the *ca.* 1.88 Ga Cu-Au-(W-Bi-Sn) association are varied and no one model satisfactorily explains the complex metal-gangue association of a Cu-rich system with variable amounts of Au, Ag, W, Mo, Sn, Bi and enrichments F, B, As, Ni, Co, Zn and Pb (Villas & Santos 2001; Pimentel *et al*. 2003; Tallarico *et al*. 2004; Volp 2005; Botelho *et al*. 2006, Lindenmayer *et al*. 2006). Tallarico *et al.* (2004) suggested that Breves is similar to major mineralization associated with Sn-specialised granites in the Carajás region and intrusion-related gold deposits. Botelho *et al.* (2006) considered that Breves has mineralogical and geochemical signatures similar to those of Cu-Au porphyries, IOCG deposits and Sn-W mineralization hosted by granitic cupolas. They presented a granite-related model for ore-genesis at Breves whereby a reduced Cu-Au ore body was derived from the interaction of mixed magmatic-meteoric fluids with oxidised country rocks. It was considered that Cu, Au, Mo, As and Co may have been derived from country rocks enriched in these metals as they are characteristic of older Carajás deposits. Work by Lindenmayer *et al*. (2006) presented a mixed model for the genesis of the Estrela deposit illustrating the interaction of metamorphic fluids with both mafic host rocks and meteoric fluids and the precipitation of Cu-rich ores, from a magmatic sulphur source, to account for enrichment in Ni and Co. This mixed genesis was considered to produce a hybrid deposit similar to both IOCG and Cu-Au porphyry deposits.

## ACKNOWLEDGEMENTS

The author wishes to thank Companhia Vale do Rio Doce (CVRD) for access to the Estrela deposit and support during fieldwork for the author's doctoral research. Patrick Williams and Netuno Villas provided helpful comments on an earlier version of the manuscript.

## REFERENCES

Botelho NF, Moura MA, Texeira LM, Olivo GR, Cunha LM, Santana MU (2006) In Queiroz ET, Marini OJ, Ramos BW (2006) eds. Caracterização de depósitos minerais em distritos mineiros da Amazônia, *ADIMB, Ouro Preto* 2006.

Cabral AR, Lehmann B, Kwitko R, Cravo CHC (2002) The Serra Pelada Au–Pd–Pt deposit, Carajás mineral province, northern Brazil; reconnaissance mineralogy and chemistry of very high grade palladian gold mineralization. *Economic Geology* 97:1127–1138

Dreher AM, Xavier RP, Martini SL (2006) Fragmental rocks of the Igarapéd Bahia Cu-Au deposit, Carajás mineral province, Brazil. *Revista Brasileira de Geociências* 35(3):359-368

Galarza MAT, Macambira MJB, Villas RNN (2002). Geocronologia e geoquímica isotópica (Pb,S,C e O) do depósito de Cu-Au do Igarapé Bahia, Província Mineral de Carajás (PA), Brasil. *41º Congresso Brasileiro de Geologia, João Pessoa, Brasil.*

Groves DI, Grainger CJ, Vielreicher NM (2000) Palabora Cu and Serra Pelada Au-PGE: End members of the Fe-oxide Cu-Au deposit group. *In SGA Annual Meeting, November 5-8, 2001.*

Huhn SRB (1996) Sao os depósitos cupríferos de Carajás do tipo Cu-Au-U-ETR? *V Simpósio de Geologia da Amazônia, Belém, Brasil*, pp. 140-143

Lancaster Oliveira J, Fanton J, Almeida AJ, Leveille RA, Vieira S (2000) Discovery and geology of the Sossego copper–gold deposit, Carajás District, Pará State, Brazil. In: I*UGS, Intern Geol Congr,* 31, [CD-ROM]

Lindenmayer ZG, Fleck A, Gomes CH, Santos ABS, Paula FC, Laux JH, Pimentel MM<, Sardinha AS (2006) Caracterização geológia do Alvo Estrela (Cu-A), Serra dos Carajás, Pará. In Queiroz ET, Marini OJ, Ramos BW (2006) eds. Caracterização de depósitos minerais em distritos mineiros da Amazônia, *ADIMB, Ouro Preto*, 2006.

Marschik R, Mathur R, Ruiz J, Leveille RA, Almeida AJ (2005) Late Archaean Cu-Au-Mo mineralization at Gameleira and Serra Verde, Carajás Mineral Province, Brazil: constraints from Re-Os molybdenite ages. *Mineralium Deposita* (2005) 39: 983–991

Pimentel MM, Lindenmayer ZG, Laux JH, Armstrong R, Araújo JC (2003) Geochronology and Nd geochemistry of the Gameleira Cu–Au deposit, Serra dos Carajás, Brazil: 1.8–1.7 Ga hydrothermal alteration and mineralization. *J South American Earth Sciences*, 15:803–813

Pollard (2006) An intrusion-related origin for Cu–Au mineralization in iron oxide–copper–gold (IOCG) provinces *Mineralium Deposita* (2006) 41: 179–187

Porter TM (2000) *ed.* Hydrothermal iron oxide copper-gold and related deposits: a global perspective, *Australian Mineral Foundation, Adelaide.*

Reis FN, Villas RN (2002) Mineralização e alteração hidrothermal no depósito cuproaurífero de Serra Verde, Província mineral de Carajás. *Revista Brasileira de Geociências* 32(1):69-86

Réquia K, Stein H, Fontboté L, Chiaradia M (2003) Re–Os and Pb–Pb geochronology of the Archaean Salobo iron oxide copper–gold deposit, Carajás mineral province, northern Brazil. *Mineralium Deposita* 38:727–738

Silva CMG, Macambira MJB, Villas RN (2001) Depósito de Cu-Au de Águas Claras: Resultados Geocronológicos Pb-Pb e Rb-Sr, Serra dos

Carajás, Pará. *VII Simpósio de Geologia da Amazônia, Bélem, extended abstracts* [CD-ROM]

Silva AG, Texeira JBG, Pimentel MM, Vasconcelos PM, Arielo A, Rocha WJSF (2006) Geologia e mineralizaçãoes de Fe-Cu-Au do Alvo GT46 (Igarapé Cinzneto), Carajás. In Queiroz ET, Marini OJ, Ramos BW (2006) eds. Caracterização de depósitos minerais em distritos mineiros da Amazônia, *ADIMB, Ouro Preto*, 2006.

Soares ADV, Macambira MJB, Santos MGS, Vieira EAP, Massoti FS, Souza CIJ, Padilha JL, Magni MCV (2001) Depósito Cu (Au) Cristalino, Serra dos Carajás, PA: Idade da mineralização com base em análises Pb–Pb em sulfetos (dados preliminares). *VII Simpósio de Geologia da Amazônia, Bélem, extended abstracts* [CD-ROM]

Tallarico FHB, McNaughton NJ, Groves DI, Fletcher IR, Figueiredo BR, Carvalho JB, Rego JL, Nunes AR (2004) Geological and SHRIMP II U-Pb constraints on the age and origin of the Breves Cu-Au-(W-Bi-Sn) deposit, Carajás, Brazil. *Mineralium Deposita (*2004) 39: 68–86

Tallarico FHB, Figueiredo BR, Groves DI, Kositcin N, McNauhton NJ, Fletcher IR (2005) Geology and SHRIMP U-Pb Geochronology of the Igarapé Bahia Deposit, Carajás Copper-Gold Belt, Brazil: An Archaean (2.57 Ga) Example of Iron-Oxide Cu-Au-(U-REE) Mineralization. *Economic Geology,* v. 100, pp. 7–28

Villas RN, Santos MD (2001) Gold deposits of the Carajás mineral province: deposit type and metallogenesis. *Mineralium Deposita* 36:300-331

Volp KM (2005) The Estrela Copper deposit, Carajás, Brazil: Geology and Implications of a Proterozoic Copper Stockwork. *8th SGA, Beijing China, abstracts.*

Volp KM, Evins, P, Meffre S (2006) EPMA and LA-ICPMS dating of hydrothermal REE-minerals from the Estrela Copper Deposit, Carajás, Brazil. *16th Goldschmidt conference, Melbourne, Australia, abstracts*

# Origin of the Talvivaara Ni-Cu-Zn deposit in Finland, and indications for ore potential of 2.1-1.9 Ga black shale formations in the world

K. Loukola-Ruskeeniemi
*Helsinki University of Technology*

M.-L. Airo
*Geological Survey of Finland*

ABSTRACT: The Talvivaara Ni-Cu-Zn deposit is hosted by metamorphosed black shale and contains 338 Mt of low-grade ore averaging 0.27% Ni, 0.14% Cu, and 0.55% Zn. The geochemistry was comprehensively studied with 1,960 samples. The high graphitic C contents (average 7-8%) and average thickness of 120m in drill cores in rift-related 1.9-2.1 Ga black shale formations in eastern and northern Finland point to vigorous organic productivity and preservation of organic material in anoxic conditions. Black shale formations are more abundant also in other parts of the world during 2.1-1.9 Ga than during other time periods which may record the breakup of supercontinents resulting in closed marine basins and increased hydrothermal activity in ocean ridges. Black shale of this age is potential in exploration for massive sulphide ores. Black shale is easily located with the aid of geophysical measurements also in sparsely outcropped or deeply weathered terrains. Preliminary characterization of ore-potential black shale is even possible with interpretation of airborne magnetic and gamma-ray responses.

KEYWORDS: black shale, sulphide deposits, nickel, Precambrian, Talvivaara, Finland

## 1 INTRODUCTION

Black shale is encountered in the vicinity of most Palaeoproterozoic sulphide deposits in the Fennoscandian Shield. This relationship is common in other parts of the world and in formations of other geological eras. However, the thickness of the black shale formations and the concentrations of organic carbon and sulphur are higher in the 2.1-1.9 Ga formations in Finland than in most other occurrences in the world. In eastern Finland, also black shale - hosted sulphide deposits and occurrences are encountered. The largest is the Talvivaara Ni-Cu-Zn deposit (Loukola-Ruskeeniemi & Heino, 1996).

In addition to the Fennoscandian Shield, black shale formations 2.1-1.9 Ga in age are encountered, for example, in South Africa, Western and Northern Australia, Ontario, and Zimbabwe.

## 2 TALVIVAARA NICKEL DEPOSIT

The Talvivaara deposit is located in eastern Finland. It is hosted by metamorphosed black shale and contains 338 Mt of low-grade ore averaging 0.27% Ni, 0.14% Cu, and 0.55% Zn (Reino, *personal communication*). The dimensions of the metamorphosed black shale formation are 20 km in N-S direction and one km in W-E direction. The Ni-Cu-Zn ore bodies are enveloped by black shale. The deposit contains two ore bodies: the Kuusilampi ore body and the Kolmisoppi ore body. Black calc-silicate rocks (also called graphite-rich meta-carbonate rocks) with calcium content exceeding 3.5% are encountered as intercalations 10cm to 3m thick within the metamorphosed black shale, with an average thickness of 0.9m. Metamorphosed black shale with fine-grained sulphide-rich lamination cut by quartz-sulphide veins is shown in Figure 1.

## 3 SULPHIDE MINERALS

Pyrite and pyrrhotite are the dominant sulphide minerals in the Talvivaara deposit. Pyrite, pyrrhotite, chalcopyrite, sphalerite, alabandite, and pentlandite occur both as fine-grained disseminations (<0.01mm) and as coarser grains in quartz sulphide veins. Fine-grained (<0.01 mm)

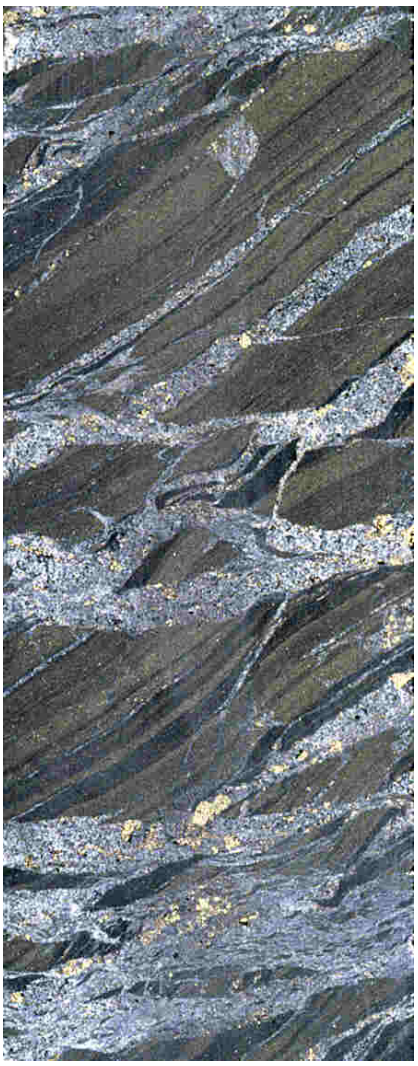

Figure 1. Metamorphosed black shale from the Talvivaara Ni-Cu-Zn deposit, Kolmisoppi ore body. Drill core section. Width of the core is 3 cm. Photo by Jari Väätäinen, Geological Survey of Finland.

spheroidal pyrite has gradually coalesced and recrystallized into coarser grains. In the Ni-rich black shale, spheroidal fine-grained (<0.01mm) pyrite contains more Ni and less Co than coarse-grained pyrite. During recrystallization and remobilization processes, part of the Ni in the fine-grained pyrite became incorporated into pyrrhotite and pentlandite

## 4 GEOCHEMISTRY

The geochemistry of the Talvivaara black shale was studied using 1,960 samples selected from cores drilled by the Geological Survey of Finland. Different sample sizes were compared: 10m, 3m, 0.5m, 0.1m in drill core. Even the 10m long drill core sections gave fairly good picture of the geochemistry of the deposit.

The median graphitic C value is 7.5% and median sulphur value 9.2%. Sulphur to carbon ratios typically vary between 0.3 and 2.0 in the Talvivaara black shale. The Talvivaara values are comparable with those in black shale along the whole ancient rift zone in the Kainuu-Outokumpu area (Fig. 2).

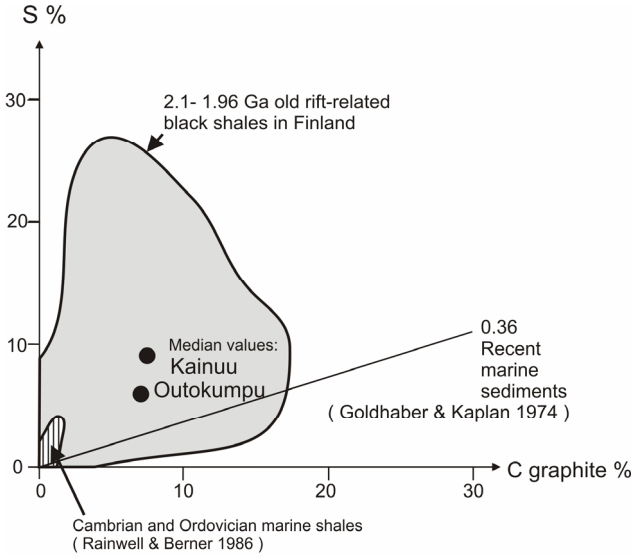


Figure 2. Concentrations of graphitic carbon and sulphur are high in the 2.1-1.9 Ga rift-related metamorphosed black shale in eastern Finland, in the Kainuu and Outokumpu areas. Talvivaara deposit is situated in Kainuu. Recent marine sediments contain much less sulphur in average.

Also manganese content is fairly high at Talvivaara. Especially black calc-silicate rocks contain abundant Mn, with a median value of 0.85%. The black shale layers with ≥0.8% of Mn contain more Ag, Au, Hg, S, Li, Ca and Mg and exhibit higher S/C, Co/Ni, Cu/Zn and S/Se ratio than black shale with Mn<0.8%.

Maximum gold content in 50cm long drill core sections is 150 ppb and maximum silver content 49 ppm. Platinum group element concentrations are not high either. Maximum values encountered in 10cm long drill core sections were 0.42 ppb Ir, 27 ppb Pt, and 73 ppb Pd.

New data analyzed by the Talvivaara mining company of a large, 3000 tonne sample give the average Ag concentration of 1 g/t, Au 0.009-0.012 g/t, and Pd 0.023-0.074 g/t for the Kuusilampi ore body (Reino, personal communication).

## 5 ISOTOPE GEOCHEMISTRY

Carbon isotope $\delta^{13}C$ (PDB) values of organic C from 15 black shale samples range

from -24 to -27 per mil, whereas organic C from two black calc-silicate rock samples exhibit values from-23 to -24 per mil.

Sulphur isotope $\delta^{34}S$ values were determined for pyrite, pyrrhotite, alabandite and sphalerite. A more or less constant value of -5 per mil was obtained for the black shale containing less than 0.1% Ni and less than 0.8% Mn (Loukola-Ruskeeniemi, 1995). Median value for both pyrrhotite and pyrite in the black shale with Ni ≥0.1% is 3 per mil. Black calc-silicate rocks exhibit heavy S isotope values, from -3.8 to +20.8 per mil for pyrrhotite and from -7.1 to +20.8 per mil for pyrite. Black calc-silicate rock intercalations in drill core 3344:329 are shown as stars in Figure 3.

## 6 ORIGIN OF THE TALVIVAARA DEPOSIT

The precursor of the Talvivaara black shale was organic-rich mud deposited on the sea floor in anoxic conditions, because concentrations of organic C and S are high, carbon isotope $\delta^{13}C$ (PDB) values indicate organic origin and Ce depletion in rare earth element patterns suggests seawater (Loukola-Ruskeeniemi & Heino, 1996).

The deposit is in part syngenetic in origin, as evidenced by uniform distribution of Ni in the horizon with Ni≥0.1% and the size of the deposit; S isotope $\delta^{34}S$ compositions (Fig. 3); and occurrence of pentlandite, chalcopyrite, and sphalerite in the fine-grained (<0.01 mm) sulphide material.

The elevated concentrations of Ni, Cu, and Zn have their origin in hydrothermal processes, because the S isotope $\delta^{34}S$ composition is comparable to that of sulphides in polymetallic sulphide deposits in the Red Sea deeps and the Guyamas basin.

Black calc-silicate rock intercalations probably precipitated from hydrothermal solutions, because they have elevated Ca, Mg, F, P, and Ag concentrations as do solutions found in recent Galapagos mounds hydrothermal field reported by Maris *et al.* (1984); exhibit rare earth element values typical of Mn-rich seawater near recent hydrothermal sites; and exhibit heavy S isotope values.

The black shale horizon containing 0.8 or more percent Ni+Cu+Zn probably contained primarily syngenetic concentrations of Ni, Cu, and Zn (Ni<0.1%), which were deposited from seawater contaminated with hydrothermal fluids, and was introduced by hydrothermal upwelling solutions resulting in increased Ni, Cu, and Zn concentrations and precipitation of the precursor of black calc-silicate rock intercalations, as supported by Na depletion (Fig. 3), which indicates hydrothermal alteration.

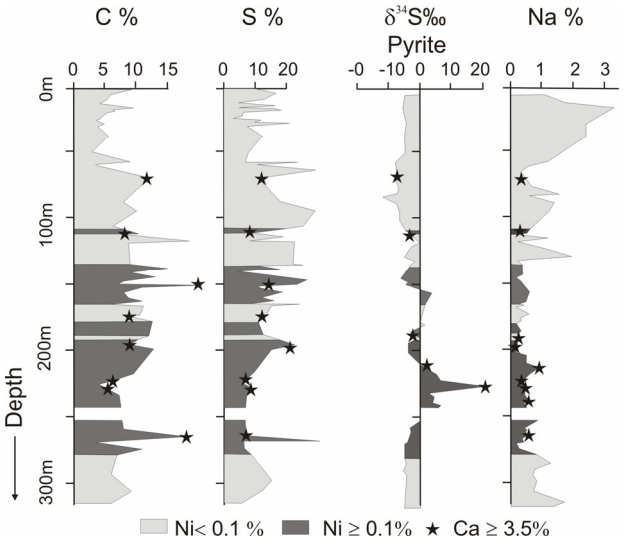


Figure 3. Concentrations of graphitic carbon and sulphur, S-isotope $\delta^{34}S$ values of pyrite and sodium content in metamorphosed black shale in the Kuusilampi ore body, drill core 3344:329, from depth 0 to 300m. Dark-colored horizons represent black shale with Ni≥0.1%, light-coloured horizons black shale with Ni<0.1%, and stars indicate black calc-silicate rock intercalations. Quartz vein is located in the depth of 250m.

## 7 BLACK SHALE FORMATIONS 2.1-1.9 BILLION YEARS IN AGE

Thick black shale formations (>120m in drill core) with high average graphitic C contents (7-8%) are encountered not only at Talvivaara but all the way for hundreds of kilometers in the Proterozoic formations in eastern Finland (Loukola-Ruskeeniemi, 1998). This ancient rift zone hosts also the Outokumpu Cu-Co-Zn sulphide deposits. Comparable thickness and graphitic carbon content is encountered also in many locations in northern Finland. Huge masses of carbon, sulphur and heavy metals have deposited on sea bottom for some 2 billion years ago indicating vigorous organic productivity and preservation of organic material on sea bottom in anoxic conditions, maybe in a 'stratified ocean'.

Around modern and ancient vents, bacteria, the basic producer organisms, are engaged in symbiotic relationships with worms and other higher life forms. These life forms may con-

tribute to some extent to the organic load of Precambrian rift-related black shale in addition to primitive algae and bacteria.

The amount of atmospheric oxygen was evidently much lower in the Precambrian than today, and anoxic conditions may have prevailed over large parts of the ocean. A theory claims that in the shallow water environment of some restricted basins, stromatolites periodically produced so much oxygen that some of the primitive life forms could not adjust to the environmental change and their population dramatically decreased resulting in deposition of large masses of organic material (Loukola-Ruskeeniemi, 2000).

## 8 INDICATIONS FOR EXPLORATION

Black shale formations are more abundant in the world during 2.1-1.9 Ga than during other time periods. Condie *et al.* (2001) suggested that this may record the breakup of supercontinents resulting in closed marine basins and increased hydrothermal activity in ocean ridges. Therefore, black shale of this age may serve as a potential exploration tool for massive sulphide ores.

Characterization of black shale provides us exploration tool since black shale affected by hydrothermal fluids can be recognized, for example, with a geochemical study.

Black shale is easily located with the aid of geophysical measurements also in glaciated or deeply weathered terrains. Preliminary characterization of ore-potential black shale is even possible with interpretation of airborne magnetic and gamma-ray responses (Airo & Loukola-Ruskeeniemi, 2004).

A black shale map of Finland was compiled by Arkimaa *et al*. (2000) where geophysical anomalies were divided into two categories: red lines indicate black shale formations with known outcrops or drill cores and blue lines indicate potential black shale formations with similar geophysical indications but no drilled data or outcrops to prove the indication. This map and database provide assistance for exploration in Finland.

## ACKNOWLEDGEMENTS

We thank chief geologist Jouni Reino from the Talvivaara mining company for new information and valuable comments on the manuscript and 6FP EU project BIOSHALE for travel funding.

## REFERENCES

Airo ML, Loukola-Ruskeeniemi K (2004) Characterization of sulphide deposits by airborne magnetic and gamma-ray responses in eastern Finland. *Ore Geology Reviews* 24: 67-84.

Arkimaa H., Hyvönen E, Lerssi, J, Loukola-Ruskeeniemi K, Vanne, J (2000) Proterozoic black shale formations and aeromagnetic anomalies in Finland. Map 1:1 000 000. Geological Survey of Finland, Espoo: *Geologian tutkimuskeskus*.

Condie KC, Des Marais DJ, Abbott D (2001) Precambrian superblumes and supercontinents: a record in black shales, carbon isotopes, and paleoclimates? *Precambrian Research* 106: 239-260.

Goldhaber MB, Kaplan IR (1974) The sulfur cycle, in Goldhaber MB (ed) *The sea,* v. 5, Marine chemistry: New York, Wiley, p. 569-655.

Loukola-Ruskeeniemi K (1995) Origin of the Talvivaara black-shale-hosted Ni-Cu-Zn deposit, eastern Finland. In: Autio, S. (ed.) Geological Survey of Finland, Current Research 1993-1994. *Geological Survey of Finland. Spec. Paper* 20: 31-46.

Loukola-Ruskeeniemi K (1999) Origin of black shales and the serpentinite-associated Cu-Zn-Co ores at Outokumpu in Finland. *Economic Geology* 94: 1007-1028.

Loukola-Ruskeeniemi K (2000) Mass extinction of primitive life forms for two billion years ago? The *112th annual meeting of the Geological Society of America. November 13-16, 2000, Reno, Nevada. Abstracts with programs* A-5

Loukola-Ruskeeniemi K, Heino T (1996) Geochemistry and genesis of the black shale-hosted Ni-Cu-Zn deposit at Talvivaara, Finland. *Economic Geology* 91: 80-110.

Maris CRP, Bender ML, Froelich PN, Barnes R, Luedtke, NA (1984) Chemical evidence for advection of hydrothermal solutions in the sediments of the Galapagos mounds hydrothermal field. *Geochim. Cosmochim. Acta* 48: 2331-2346.

# FUTURE DIRECTIONS IN ECONOMIC GEOLOGY – RESEARCH & TEACHING

EDITED BY:

ADRIAN BOYCE

RICH GOLDFARB

ROSS LARGE

# Exploring for Oil and Minerals

Andrew Mackenzie
*Rio Tinto, 6 St James's Square, London, SW1Y 4LD*

ABSTRACT: Future forecasts of oil, gas, metal and mineral supplies are hopelessly unreliable and usually pessimistic, partly because they take insufficient account of likely future technical advances. However there is a geological basis for asserting a finite life for oil and gas: almost all likely places where oil and gas can form, accumulate and persist can now be accessed and imaged by the latest drilling and seismic technology. Conversely, most minerals and metals occur in many geological settings where technology has not yet advanced to the point where they can be recovered economically: there is no real ceiling on likely reserves and hence they can be regarded as near-infinite. The biggest technical breakthroughs needed to extend oil and gas reserves are for enhanced recovery, especially from tighter reservoirs; while minerals and metal reserves would be best served by breakthroughs in the commercial and in-situ extraction of deeper deposits.

KEYWORDS: Oil, Gas, Metals, Minerals, Exploration, Reserves

## 1 INTRODUCTION

The materiality of life depends critically on the science of geology. Everything we can touch has been dug-up or pumped from the Earth, pulled out of the air, or grown. Yet there are significant differences – driven by economic and geological perceptions – between industries based on materials that exist as fluids in the earth, like oil and gas, and those based on solids, like minerals and metals.

## 2 DEMAND

It is claimed by some that oil and gas production could fail to keep up with demand within a century or less. These perceptions are based on current estimates of oil and gas resources that, while somewhat pessimistic, are nonetheless reasonably compelling. First because the geological conditions for commercial deposits seem to be well understood with oil and gas rarely existing deeper than 5km below the surface or seabed. Second because advances in technologies, like 3-D seismic, deep-water and high-angle drilling, expandable tubing, hydraulic fracturing and multi-lateral wells connected to a single bore, now permit most deposits to be imaged with some precision and extracted at reasonable cost, albeit in many cases with less than 50 per cent recovery. The greatest upsides in oil and gas supply lie in future technologies which could increase oil recoveries by up to a factor of two using methods such as the injection of miscible gases or other solvents, and in-place alteration of oil-water interfacial tensions; and which reduce the cost of transporting gas to its major markets.

It is believed that most useful minerals and metals will last for much longer than oil and gas. Economic concentrations of useful minerals and metals are formed by a vast array of geological processes that span the full range of an Earth scientist's knowledge; and most minerals and metals can be substituted by other lower cost minerals and metals when their prices are too high. Such mineral and metal concentrations often persist over much wider ranges of pressure, temperature, and deformational histories than oil and gas deposits. Yet most of these metal and mineral concentrations in the Earth are not accessible with current mining techniques, many of which cannot reach much deeper than 1km, and would be unacceptable near centres of population, in areas of natural beauty or environmentally fragile re-

gions. Technology advances that increase depth and accessibility safely and economically with a negligible environmental footprint could yield unbounded increases in reserves, probably by orders of magnitude.

## 3 PERCEIVED TRENDS

These perceived trends in supply-demand balances between oil and gas and minerals and metals, along with environmental concerns - like oil, gas and coal's inferred contribution to global climate change - drive relative long-run pricing, which then reinforces the trends. The consistently high margins for oil and gas production over much of the last decade have fostered huge technological advances denied the mining and minerals industry. However current high oil and gas prices are forcing the search for alternative energy sources - all of which are dependent on mining techniques like those employed to collect coal, tar sands and uranium. Even the hardware for renewable energy sources like solar and wind requires specialist metals and minerals. These new developments, combined with the search for new geological materials to save energy, low-energy approaches to mining, and current high prices for minerals and metals, are heralding new mining technologies that will make it much more practical to access deeper deposits with high recovery and negligible environmental footprints. These technologies include advanced environmental rehabilitation, long wall underground mining, block caving, high-pressure grinding, solution mining, and in-place leaching.

Scientists need to acquire an even more fundamental understanding of earth processes, the physics and chemistry of vapour-liquid-solid interactions, and the properties of geological materials, if the quest for dramatically increased oil and gas recovery, lower environmental impact, and much deeper mining are to succeed.

Perhaps the most exciting area is the opportunity to extract more and more minerals and metals in-situ and remotely through fracturing and then leaching. Target mineralization should be deep so that there is a chance of extracting them without any significant surface expression. Hence, they can and should be near large centres of population to guarantee us access to the high level of technical skills that we need to run such operations. As there is essentially no environmental footprint, the closeness to areas of outstanding natural beauty, fragile areas, large cities, etc is a non event. The whole concept is that one extracts only the metal of value and leaves the rest.

The process is to first remove non mineralised material from underneath the mineralisation. This has to be carted to the surface, preferably by hydraulic transport as it is cheaper than lifting, and of course will have a ready market near a large city as road fill, aggregate for concrete, etc. Whilst we could never compete competitively with the quarrying business at this step we can at least cover our haulage to the surface costs.

The next step is to fracture the material because in place leaching does require some permeability. We have undertaken a lot of research modelling the flow and leaching progress in heaps and are in the process of extending this to heaps of large broken material in place. Then is the placement of a barrier. We have successfully demonstrated barrier technology for certain circumstances and are moving to see this in a commercial rather than in a demonstration phase.

Finally comes in-place leaching. Understanding in-place leaching still has a long way to go but we are confident that what we can do in the laboratory we can ultimately do in place.

# The Changing Face of Mineral Exploration — A People Story

John F.H. Thompson
*Teck Cominco Limited, Vancouver, British Columbia, Canada*

ABSTRACT: Exploration has seen vast changes over the last twenty years following a period of low metal prices and more recently high metal prices. The net result is a shortage of qualified people and the expectation that many more will retire in the next ten years. While there have been a number of technical advances in exploration, qualified and motivated people with a wide range of skills and interests are more important than ever. The people challenge will be the defining issue for the industry and educators over the next ten or more years.

KEYWORDS: Geoscientists, exploration, discovery, field skills

## 1 EXPLORATION CYCLES

In the last twenty years the exploration business has seen enormous changes. Following an extended period of very low metal prices we have seen unprecedented, uniformly high prices across all major commodities. Regardless of expected corrections, global demand from developing countries and long term restrictions in supply may influence metal prices positively for several years to come.

Both the low and the high cycle drove consolidation initially for survival and more recently to increase market share and reserves. The bulging coffers that many companies have amassed provide further incentives for merger and acquisition activity. Consolidation has been complex and exciting – at least to those with the upper hand – and has touched all parts of the business from majors to juniors, and from explorers to analytical, drilling and other service companies.

Low metal prices and consolidation had a disastrous effect on exploration budgets and more importantly on people. Many left the industry and few new graduates were hired. Since the resurgence, the budgets of those companies that remain have increased and new exploration companies have appeared in significant numbers. Budgets are well up and significant hiring is in progress. The negative effect of the previous downturn, however, more or less removed a generation of explorers and the full impact of this loss will become increasingly apparent when the current group of senior explorers ("baby boomers") retire.

The extreme nature of the recent cycles has had an enormous knock-on effect on universities. The low accelerated the demise of many departments that provided education and research relevant to the mining industry – including earth science, mining engineering, metallurgy and mineral processing. While the industry has seen a rapid recovery, universities do not find it as easy to respond in short order and the imminent retirement of many senior faculty will happen just as industry desperately needs people. The prognosis is not good!

There have been other changes over the last ten years. Following the reduction of east-west animosity, many new jurisdictions became acceptable to explorers. In the late nineties, there were few limits to the places that people would go in the search for new deposits. Since then however the industry has had to adjust to heightened Middle East conflicts and terrorism, and a political shift in some countries that is less favorable to international mining companies. Environmental and social concerns have become increasingly important and while most companies work diligently on these issues, there are areas where mining simply will not be allowed. Companies have had to reassess the jurisdictions where they can realistically work

and are now careful to balance both technical and non-technical risks. All of these factors influence the jobs of explorers and put new demands on social, cultural and related people skills.

Economic and political pressures have changed the business of exploration. Increasing emphasis is placed on risk and portfolio management and measurable success is demanded. Gone are the days of a celebrated "technical success". Joint ventures and strategic alliances have become more common. Technical methods are assessed, used and ranked more rigorously, particularly when viewed as a means of developing targets more effectively. There is perhaps less reliance on simplistic panaceas and more recognition of a toolbox of methods to be applied as and when appropriate. Improved business and technical focus sounds good, but it is only as successful as the people who apply it. And of course, capable people with a solid range of experience are in short supply.

## 2 PEOPLE IN EXPLORATION

Technical sophistication in the exploration business continues to increase (Kelley *et al*, 2006; Sillitoe & Thompson, 2006). Driven largely by computer power, new geophysical and spectral techniques can collect vast amounts of data which can be processed almost immediately. Similarly multi-element geochemistry with low detection limits on a wide range of media (streams, soils, partial or selective leaches, gases *etc*.) is the industry standard. The result in all cases is an enormous amount of data, which can be combined in databases and GIS for interrogation, inversion and analysis. The results are used to generate targets by a combination of techniques that include simplistic anomaly recognition, selected data combinations, and use of artificial intelligence or neural networks. The toolbox is full of ways to generate and handle data and one could conclude that exploration is therefore becoming less dependent on people.

People are however more important than ever and the range of skills required for exploration is increasing. The following summarizes some of the people contributions for success.

### *2.1 Field work*

While there are many tools to assist field exploration including various hand-held devices, the fundamental ability to recognize minerals, textures, rock associations, structures and three dimensional configurations cannot be artificially duplicated. This is partly an inherent attribute, but to do it really well requires training and experience. Field skills are obviously critical for making maps, but the recognition skills honed during mapping are also a prerequisite to effective drill core logging, albeit augmented by physical and chemical data. In covered terrain, the targets may be generated by remote techniques, but drill chip or core logging is critical to evaluating the results and determining the need for follow-up.

Furthermore as subsurface geological and other data are accumulated, interpretation is greatly influenced by the ability to understand primary lithological and secondary alteration patterns. There is no substitute for having mapped these relationships and hence having a personal experiential database.

Unfortunately field work is in general decline. Few university courses devote significant time to field training. State geological surveys have minimal budgets, have limited field programmes, and at least by comparison to the past, employ few students. And companies are short staffed relative to their rapidly expanding budgets and have little time to provide sufficient training and mentorship to generate the next cadre of field explorationists.

### *2.2 Exploration programmes*

Every exploration programme starts with an idea whether based on a target type, a regional concept or the potential use of a new technique. The idea must be turned into a realistic programme through the accumulation of public data, proof of concept work, evaluation of logistics (including consideration of personal safety), budgeting and some estimation of risk and reward. The latter will typically consider issues related to the jurisdiction, if the company is not already established there – ultimately to answer the question: if we find something can we mine it?

Generative exploration requires a specific approach and relatively few explorers are really good at it. In addition to being able to navigate through various types of data, the quality of which varies enormously among jurisdictions, the generative explorer must be able to synthesize the information and present it in a coherent fashion. Presentation involves an element of salesmanship. While quantitative ranking techniques are applied by some companies, an ef-

fective presentation may win the day when the choice is among similar technical options.

Once established, a programme requires people with skills focused at a scale that requires attention to detail. Selection of appropriate techniques, targeting and data analysis are crucial. The programme also needs technical management based on teams with multiple specialties. Many programmes will have several decision points, each requiring careful evaluation. The goal is to reach the drill test as efficiently as possible. Drill results may form the basis for further work or potentially an exit strategy. While there are ways to increase confidence in the decision making process, the final call will be made by people.

Many discoveries involve several separate programmes/companies and therefore we know that incorrect decisions have been made. Similarly, there is abundant evidence that companies stay too long on some projects when the chance of a serious discovery has long since passed. Decisions are made for many reasons and the technical merits of the data are not always paramount – this is part of the exploration process. The fact is that people drive exploration programmes and some are better at it than others.

### *2.3 Exploration business*

Exploration is only one part of the mining business. In major companies, operations and the cash flow are the life blood of the company. Exploration is one way to replace dwindling resources but companies have alternatives – acquiring deposits, or acquiring and merging with other companies to provide an enhanced asset base. Explorers in major companies have to understand all of these options and be able to place projects in an appropriate corporate context. Since decisions on programmes will be made by senior management and boards with many concerns and limited technical knowledge, the ability to explain a complex technical programme will determine the exploration budget.

Although the junior sector is quite different, selling programmes to raise money is the key to success. Junior companies are frequently run by geologists with technical ideas and considerable entrepreneurial spirit. Converting enthusiasm to clearly defined concepts while resisting the temptation to over promote is the key to success. This is all about people skills – judgment, presentation, persuasion and negotiation.

### *2.4 Discovery*

Whatever the business approach and the size of the company, and whatever the target types, technical methods and management philosophy, there is only one measure of success – the discovery of an economic orebody. Some companies, some teams, and some individuals have a better discovery track record than others, but the reasons for disproportionate success are poorly understood. What is clear is that there is something distinctive about the nature of the people involved in multiple successes – whether these people are pounding rocks, leading teams, or defining the overall strategy that puts the programme in place. It is about people.

## 3 THE CHALLENGE

The challenge for the mining industry in general and exploration in particular is to find the right people to sustain the business. Since a significant number of geoscientists will retire within the next ten years, this is likely to be the defining issue for the exploration industry. Failure will result in a lack of discovery and since there will be a similar shortage of mining engineers and mineral processors, there will also be many challenges in turning the few discoveries that are made to mines. Those who join our business in the next few years will enjoy unprecedented opportunities and in all likelihood unprecedented salaries. Similarly, universities that choose to meet the challenge and provide superior students are likely to enjoy excellent support from the industry.

Geoscientists are particularly suited to operating in the complex multicultural world of modern mineral exploration. The very breadth of geoscience – encompassing all of the basic sciences both qualitatively and quantitatively while simultaneously introducing the major issues that face our world – resources, the global economy, the environment, and social awareness, is an incredible training ground. Geoscientists can go on to do many things completely unrelated to their primary training, but for those who also acquire field skills, have a love of adventure, and live for discovery, there is a fantastic future ahead.

## REFERENCES

Kelley, D.L., Kelley, K.D., Coker, W.B., Caughlin, B., and Doherty, M.E., 2006, Beyond the obvious limits of ore deposits: the use of mineralogical, geochemical, and biological features for the remote detection of mineralization: *Economic Geology,* v. 101, p. 729-752.

Sillitoe, R.H., and Thompson, J.F.H., 2006, Changes in Mineral Exploration Practice: Consequences for Discovery: *SEG Special Publication* no. 12, pp. 193-219.

# New Integrated Geometallurgical Research Initiatives and Implications for the Future of Economic Geology

S.G. Walters
*CODES ARC Centre of Excellence in Ore Deposits, University of Tasmania and Julius Kruttschnitt Mineral Research Centre, University of Queensland.*

R.R. Large
*CODES ARC Centre of Excellence in Ore Deposits, University of Tasmania*

B. Adair
*Julius Kruttschnitt Mineral Research Centre, University of Queensland.*

ABSTRACT: The emerging area of geometallurgy represents a cross-discipline challenge that requires more effective communication, shared methodologies and a common technical language between the range of professional disciplines that support major mining operations – in particular economic geologists, mining engineers and mineral processors. This challenge also requires major new research and education initiatives that will provide the next generation of practitioners. A new collaborative research initiative is underway, strongly supported by the global mining industry. The project includes technology development drivers in the areas of automated core logging, automated microscopy, new approaches to textural analysis and small-scale physical testing. Many of these have spin-off implications for other areas of economic geology.

KEYWORDS: Geometallurgy, ore characterisation, mineral deposits.

## 1 GEOMETALLURGICAL CHALLENGE

The emerging area of geometallurgy is part of the ongoing commercial and cultural trend towards more effective mine site integration and optimization (Williams & Richardson, 2004). This involves a quantified and spatially constrained understanding of ore characterisation in terms of relationships to critical processing performance behaviors.

For base and precious metal mining operations these behaviors include blasting, crushing, grinding, liberation and recovery. Related issues include tracking deportment of deleterious elements and minerals; providing inputs into environmental waste rock management; and increasing comminution energy efficiency. A key outcome is enhanced economic optimization of mining *i.e.* a manufacturing process typically involving ore production, product extraction and product refinement.

Geometallurgy is a cross-discipline challenge that requires more effective communication, shared methodologies and a common technical language between the wide range of professional disciplines that support major mining operations – in particular economic geologists, mining engineers and mineral processors.

Significant disjoints can occur across this shared challenge, which are often exacerbated by separate tertiary education pathways. Divisional organizational structures on many mine sites can also dilute the 'one-mine' strategy required for successful geometallurgical implementation.

The historical impediments to geometallurgical integration require major new education and teaching initiatives backed by new technology developments and coordinated research.

## 2 NEW RESEARCH INITIATIVES

The need for large-scale, coordinated geometallurgical research has been recognised by the minerals industry, resulting in commencement of a major new initiative in mid-2005. The AMIRA International P843 'GeM$^{III}$' project (**Ge**ometallurgical **M**apping and **M**ine **M**odelling) is a cross discipline collaboration that brings together three major Australian research groups for the first time; CODES the ARC Centre of Excellence in Ore Deposits at the University of Tasmania, a world-leader in economic geology-related research; the Julius Kruttschnitt Mineral Research Centre (JKMRC) at the University of Queensland, a world-leader in mining and mineral processing research; and the WH Bryan Mining Geology

Research Centre (BRC) at the University of Queensland, which aims to be a world leader in mining geostatistics, operations research and optimisation in mine design and planning.

The four-year project is supported by 15 sponsors, including most of the world's largest resource companies and will receive over A$8 million in funding from industry and the Australian Research Council. This is supporting a team of over 20 researchers. A feature of the project is access to a portfolio of world-class mining operations in Australia and North America. The main current research focus is related to aspects of base and precious metal hard rock mining.

The project aims to deliver fundamental knowledge, tools and methods for more effective approaches to geometallurgical definition of mineralogy, element deportment and texture that can be linked to mineral processing performance and efficiency at a range of scales. Outcomes will be improved indices of processing performance that can be embedded in resource block models to define processing domains, which can be exploited in mine planning and optimization. To achieve these aims the project is involved in a range of technology developments that although focused on geometallurgical applications, have relevance to other areas of economic geology. These include more automated core logging technologies, new applications of automated microscopy, and development of software-based texture analysis and categorization techniques, all linked to new small-scale physical testing (Walters & Kojovic, 2006).

The underlying link to other areas of economic geology is a more rigorous and systematic approach to the measurement of mineralogy and texture attributes at a wide range of scales. Once defined, these attributes can be variably exploited from the perspective of processing behaviors (mineralogy and texture destruction), mineral exploration (mineralogy and texture pathfinders) or ore genesis (mineralogy and texture associations).

## 3 AUTOMATED CORE LOGGING

'Traditional' visual logging techniques produce outputs that are generally not designed to correlate with mineral processing attributes. In addition visual logging has poor QA/QC compared to other data types and is often carried out by junior staff, a situation exacerbated by current trends to deskilling. The project is employing a novel approach designed to help overcome these problems based on automated bench-scale logging instrumentation for petrophysical and mineralogical measurement.

Two automated logging systems are currently being used. The GEOTEK Multi Sensor Core Logger (MSCL) is a bench scale system based on automated linear feed of drill core past a sensor array. Within the current project this array is dominated by petrophysical sensors that include gamma attenuation density, P-wave velocity, resistivity and magnetic susceptibility. The approach is a logical derivate of down-hole geophysical logging that involves bringing rock to the sensor rather than placing the sensor into the rock. It allows use of the extensive archived core available at most sites, which is typically associated with historical processing performance information.

The majority of petrophysical attributes can provide proxies for potential mineral processing performance such as derivates of P-wave velocity and density to strength and elastic moduli. Detailed deposit-based petrophysical characterisation also has implications for exploration applications such as constrained geophysical inversion modelling.

Over 80 GEOTEK systems are in use primarily for ocean drilling and petroleum applications (Schultheiss et al., 2004). Although based on mature technology this is the first system adapted to the needs of the metalliferous mining industry. The logger is fully containerized and has been deployed at sponsor sites. The GEOTEK logger is also equipped with a high resolution digital imaging system. Sophisticated image analysis techniques are being used to provide meso-textural classification and categorization.

More direct core-based mineralogical information is provided through technology collaboration involving the CSIRO HyLogger™ (Huntington *et al,* 2006). HyLogger™ is an automated spectral analysis and imaging system that collects systematic short wave length infrared (SWIR) reflectance spectra. These can be classified into dominant SWIR-responsive mineral species and their compositional variations (chlorites, white micas, clays, *etc.*). Distribution of 'soft' SWIR-responsive phases show relationships to comminution behavior related to decrease of bulk strength. Detailed deposit-based characterisation of ore-related SWIR-assemblages has implications for the use of

SWIR-based exploration techniques typically related to detection of deposit alteration halos.

## 4 INTEGRATED MICRO-ANALYTICAL MINERAL MAPPING

In the last decade there have been major ongoing advances in the field of automated micro-analytical mineral mapping mainly related to the development of automated SEM-based X-ray microscopy such as the JKTech MLA and Intellection QEMSCAN$^{TM}$ systems.

The mineral identification and mapping capabilities provided by these systems result in quantified digital imaging of classified mineral maps amenable to software-based image analysis of mineralogy and texture (Gu, 2003). The techniques have proven highly effective for the quantified analysis and interpretation of liberation in comminuted products such as concentrates and tailings. The majority of major mineral companies now operate in-house facilities.

Applications of automated SEM-based microscopy in GeM$^{III}$ are being extended to mapping intact textures. This is supported by a dedicated MLA facility at the University of Tasmania based on an FEI Quanta 600 SEM and access to extensive MLA facilities and development at JKMRC.

The lessons of automated SEM-based microscopy are being used to develop complimentary optical microscopy systems. Significant advances have occurred in automated optical microscopy mainly driven by the needs of other sectors such as pathology. Two Leica DM600M computer-controlled optical microscopy systems are being used within the project. In combination with application of sophisticated image analysis software, this provides routine texture-based digital image capture and classification.

The integrated combination of more automated MLA and optical microscopy provides new capabilities for handling large volumes of mineral mapping and texture analysis. A resurgent emphasis on microscopy linked to new hardware and advanced software has implications for all areas of economic geology.

## 5 TEXTURAL CLASSIFICATION AND MODELLING

The traditional textural classification and categorization schemes used by geologists are poorly correlated with processing performance. At the hand specimen or core scale traditional geological classification schemes are largely based on visual observation that can be subjective and experience based. The advent of automated digital microscopy, presents new opportunities for a more systematic and reproducible approach to textural classification and categorization based on quantified, statistical methods. However, automated microscopy techniques generate large volumes of increasingly complex measurements.

The aim is to provide more effective software-based methods for textural analysis, feature extraction and categorization with relevance to processing performance. Typical parameters include systematic grain size, grain shape and association from analysis of automated microscopy products. Much of this work involves in-house software development. Significant advances are being made in the application of wavelet functions to texture-based image analysis and automated feature extraction (Leigh, *in press*).

Another aspect is the use of classified mineral maps of intact texture to simulate and predict potential processing performance. This involves use of sophisticated finite element modelling techniques to simulate fundamental mineral-based fracturing and liberation. The work is providing important insights into how rock textures behave and interact under processing conditions.

## 6 SMALL SCALE PHYSICAL TESTING

A wide variety of physical tests are currently employed to assess processing performance. These include strength (UCS, Point Load), hardness (Bond Work Index) and comminution (JK Drop Weight and Sag Mill Comminution) together with bench-scale flotation or leaching.

The majority of physical testing is conducted during feasibility using drill core. Incomplete knowledge or non-representative results can have a major negative effect on achieving design capacity and economic performance particularly during start up.

Many current physical tests are based on large sample volumes that require large-scale compositing of core samples. Combined with high cost, this limits sampling density and often results in inappropriate compositing and blending. The 'noise' related to poorly constrained compositing typically generates poor comparative statistics based on small sample sets that disguise natural geological variability. The aim

is to create a new approach to geometallurgical characterization that enables highly constrained samples with defined textural and mineralogical attributes to be tested for processing performance. This has required development of a suite of new and modified physical testing methods capable of providing meaningful processing parameters based on large numbers of small sample volumes (Walters & Kojovic, 2006).

This approach allows fundamental relationships to be determined based on geologically constrained inputs. The aim is to enable prediction of processing performance through application of integrated modelling based on textural and mineralogical attributes.

## 7 CONCLUSIONS

The emerging area of geometallurgy represents a cross-discipline challenge that requires new research initiatives. The AMIRA P843 GeM$^{III}$ project represents a response to these challenges that is strongly supported by the minerals industry. There are a range of technology drivers within the project that have direct relevance to the future of economic geology.

## ACKNOWLEDGEMENTS

The authors wish to acknowledge financial support and permission to publish from sponsors of the AMIRA International P843 Project - Anglo Gold Ashanti, Anglo Platinum, Barrick, BHP Billiton, CVRD, Datamine, Inco, Golder Associates, GEOTEK, Metso Minerals, Newcrest, Newmont, Rio Tinto, Teck Cominco, Xstrata Copper, and Zinifex.

## REFERENCES

Williams SR, Richardson JM, (2004) Geometallurgical Mapping: A New Approach That Reduces Technical Risk. *Proceedings 36th Annual Meeting Canadian Mineral Processors*, 241-268

Huntington J, Quigley M, Yang K, Roache T, Young C, Roberts I, Whitbourn IL, Mason P (2006) A Geological Overview of HyLogging 18,000m of Core from the Eastern Goldfields of Western Australia, *Proc. 6th International Mining Geology Conference, Darwin, NT, Australia*, 21–23 August 2006, 45-50.

Leigh G (in press) Automatic Extraction of Objects Using the Skeleton of the Continuous Wavelet Transform with Application to Mineral Textures. submitted to *IEEE International Conference on Image Processing (ICIP) in San Antonio, Texas, September 16–19.*

Schultheiss PJ, Holland, ME, Francis, TJ, Roberts JA, Carter RM (2004) Fulfilling the Promise of the DSDP/ODP Legacy with Multiparameter Logging of Archive Cores, *Eos Trans. Am. Geophys. Union, 85* (47).

Walters S, Kojovic, T (2006) Geometallurgical Mapping and Mine Modelling (GeM$^{III}$) – The Way of the Future. *Proc. SAG2006 Conference, Vancouver*, Vol IV, 411-425.

Gu Y (2003) Automated Scanning Electron Microscope Based Mineral Liberation Analysis - An Introduction to the JKMRC/FEI Mineral Liberation Analyser. *Jl. Minerals Materials Characterization and Engineering*, 2, (1), 33-41.

# Future directions in exploration geophysics research and education

Howard Golden
*Western Metals Ltd, 31 Malcolm St., West Perth WA 6005, Australia*

ABSTRACT: The future of research with respect to mineral exploration will be driven not by computing power or large bandwidth data acquisition systems. It will most likely not be technologically driven at all, although technical advancements will certainly be featured in research projects. Rather it will be focused by necessity on problems in search of solution. The challenge facing the prognosticator is not to predict what technologies or software will be the focus of future research, but rather the issues on which researchers will be focusing. These issues will attract funding, public interest, and consequently the imagination and efforts of researchers. The targeted research challenges will include, but not be limited to, deeper exploration for a wider range of minerals, time lapse monitoring of petroleum and mineral deposits, and the search for water resources. Further, research and where the research is carried out, will be driven by the vibrant nature, or lack of it, of the educational system in any jurisdiction. This is an area where much of the Western world would seem to be in decline, whereas other counties continue to improve. In the global economy is this a problem, or just a redistribution of expertise to less traditional sources? Only time will tell.

KEYWORDS: geophysical exploration; research; education

## 1 INTRODUCTION

The most effective avenues of research have always been in response to a pressing need in society or industry. Certainly serendipity is often a key component in major discoveries, but even accidental discoveries don't achieve widespread application unless a need for them is clearly present. In geophysics in particular, it has been tempting for many workers to take advantage of technological breakthroughs in electronics or computing power and apply these to a solution that is either not applicable to existing challenges or is not applied in a way that addresses the issues at hand. Consequently, to attempt to address the future of geophysical research, the most effective approach is to try to predict the areas of exploration that will be most important and preset the biggest challenges in the future. Having done this, the solutions will take care of themselves. The other challenge, once one had defined the problems to be solved, is who will solve them? The people in academic institutions and industry who be looking at these problems need to be trained. This is proving to be one of the biggest challenges of our industry. Fewer courses, fewer students and graduates, and arguably lower standards are impeding the ability of Western tertiary educational institutions to produce and to provide the talent to push forward basic exploration and research. At the same time, other countries are producing significant numbers of graduate geophysicists. It is conventional wisdom among geoscientists in the West that it is critical to remediate this state of affairs. If that is the case, the challenge is formidable. On the other hand, perhaps Western governments, universities, and industry will have to get used to employing foreign-born scientists.

## 2 WHICH CAME FIRST: THE PROBLEM OR THE SOLUTION?

Research in exploration geophysics must address the issues at hand to be effective. The most illustrative example of this is the application in the 1950s of new airborne electromagnetic technology to nickel exploration in Canada. The result was the very rapid discovery of more than 80 deposits, with a gross value of more than $100 billion (Witherly 2000).

On the other side of the coin are technologies for which the jury is still out on as to whether the solution was really in response to a problem or vice versa. The Lockheed Martin gravity gradiometer, subsequently adapted for airborne geophysics by BHP Billiton, Bell Geospace, and ARKeX Geophysics, was nothing short of a brilliant piece of R&D taking advantage of state-of-the-art technology. Since its implementation in 1997, no major greenfield discoveries as a result of its application have been publicly reported. Whereas this doesn't in any way diminish the technology or those who developed it, it does perhaps point to the fact that, while most would agree that fast acquisition of large areas of gravity data is a good thing, the application of the technology has not solved a stated problem in any way that is visible..

## 3 THE CHALLENGE FOR GEOPHYSICAL RESEARCH

So, what will be the challenges going forward that will inspire geophysical researchers to go beyond themselves and produce new and exciting results? As ore deposits become harder and harder to find, and deeper covered exploration is becoming the norm, looking deeper will rise as a predominant issue. Already the focus of technologies such as the Titan, MIMDAS, Phoenix V-8, and Geoferret array- based geophysical systems, deeply penetrating geophysical technologies will continue to attract research funding.

The issue of detecting very high-grade nickel and copper orebodies, or "perfect conductors", will also continue to draw attention from researchers. The "flying laboratory" concept of multiple measurements, such as EM, IP, Magnetics, radiometrics, gravity and hyperspecral imaging all taken simultaneously on one aircraft is a topic of conversation, but may once again be a case of technology for technology's sake with no specific problem in mind.

High impact geophysical research has also historically come from incremental improvements on established technologies. Rystrom et. al. (2000) describe in elegant detail the advances in acquisition, processing, and interpretation of airborne magnetic data during the decades since it was first introduced. These kinds of incremental improvements to established technologies will continue to add value to the research chain.

Water "mining" will rise to the top of the agenda, as it not only is a key component of mining operations, but will be a prominent issue in the media as climate change and demands on finite water resources gain real and emotional value in the world. Because research dollars go to areas of perceived crises, water-related geophysics will become a hot topic in the twenty-first century.

Regarding mineral deposit exploration issues, one of the biggest challenges to explorationists is the gap that exists between the district and project scales. Very broad-scale techniques are improving regularly, with understanding of deep crustal and global phenomena, and the techniques such as seismic tomography to measure them, being the subjects of serious research worldwide. At the district- or province-scale, exploration targets are regularly defined in academic and industry circles using an ever more available array of regional data sets gathered for decades by airplanes and on the ground. Also direct detection of certain types of targets on a detailed project-scale perhaps may be the best honed of the exploration geophysicist's tools. This leaves that critical level of scale existing between the district- and project-scale as a major challenge for researchers.

Some current research efforts are being aimed at this scale gap. Magnetotellurics (MT) is often cited as a potential tool for bridging this gap, and advances are being made in data acquisition and processing of MT data. MT and other data sets can be more effective if used in concert, and various joint inversion, display, and analysis schemes are under development. These include projects such as GOCAD, the UBC-Geophysical Inversion Facility, and BHP Billiton's SolidEarth software.

Various other advances, relating to both the non-mining and exploration environments, will certainly impact the direction of research efforts in geophysics. These include time-lapse deposit and reservoir depletion monitoring, unexploded ordnance detection, and void detection for defense and engineering.

## 4 THE CHALLENGE FOR GEOPHYSICS EDUCATION

Two fundamental issues regarding geophysics education must be addressed. The first is the incontrovertible need to teach and engender multi-disciplinary exploration. As the targets get more difficult to find, a broader and inte-

grated view of exploration and geoscience is needed to go forward and be successful. This is a complex issue and needs to be a cooperative effort between academia and industry. This is as true for the way in which exploration departments in companies are organized, as well as for an emphasis on interdisciplinary education in universities. There is also a historic, but abandoned paradigm in major mining companies of employing teams of geoscientists, and providing in-house mentoring and formal and informal training of new graduates. It would be beneficial to see that re-introduced.

The second issue involves where researchers will come from. There seems to be a conventional wisdom in the industry and among Western academics that it is critical for future Western-based geoscientists to be native Western individuals who graduate from Western universities.

No less an august body than the British Geophysical Association (BGA) in 2006 concluded that "action is needed now to address a simultaneous increase in demand for qualified geophysicists and a rapid decline in recruitment to geophysics programmes. Our strongest recommendation is that geophysics must be included into the physics A-level syllabus to add to the interest and encourage more students to read physics, as well as to increase awareness of geophysics as a career."

Ray Cas, Director of the Australian Crustal Research Centre at Monash University, spoke eloquently to the attendees as Chairman of the 2006 ASEG Conference in Melbourne of the problem in Australian universities in attracting and keeping geoscience students. He pointed out with despair the situation in which students are being snatched up by industry, often after a three-year degree, depleting the ranks of honours and post-graduated candidates.

These Western educational woes are illustrated *ad infinitum* by charts such as the one below from the BGA report.

If one puts all the emotion, patriotism, self interest, and perhaps xenophobia aside, the obvious way to view this dearth of geoscience graduates from Western universities is to adopt a more global approach and ask where are the geoscientists going to come from?

The answer may be an international one. Christopher Scinta, in his 2006 Wall Street Journal article, wrote that "in 2004, Chinese schools awarded 351,000 bachelor degrees in engineering, computer science and information technology, while the U.S. awarded only 137,000 similar degrees, according to a Duke University study. India was close behind with 112,000".

More to the point, the Society of Exploration Geophysicists (SEG) has been told that there are 30,000 geophysicists in China, with 1,000 new graduates in geophysics each year (Fleming 2007). Another SEG report by Dennis Yanchak estimates the number of geophysicists working in Russia at 50,000, with more than 300 geophysicists graduating each year from Russian universities. The SEG report on India by B. S. Bora estimates much lower numbers with 1200 working geophysicists and 160 annual graduates, but India produces only 1% of the world's petroleum.

In the new global economy, perhaps the thinking in the geophysical community needs to shift. There is a case to be made for the efforts

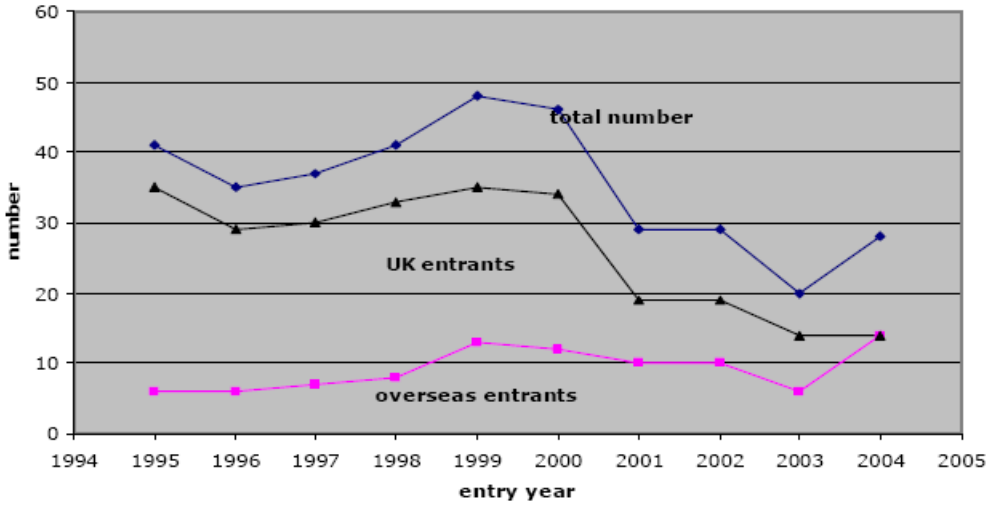


Figure 1: Single subject Geophysics MSc by numbers

in geoscience education to be shifted to ensuring that graduates worldwide, wherever they are, receive a high quality education. Instead of desperately shoring up withering departments in Australia, USA, and the UK, maybe working to improve programs in India, China, and Russia makes more sense.

Clearly the fewer geoscience departments still thriving in the Western countries are performing their jobs admirably if their graduates are snapped up by the industry. They should be patting themselves on the back. And every country should continue to improve their education systems and encourage their citizens to study all manner of important pursuits including geophysics. But in the end, if the Western world is happy to import fruit, shoes, and iPods, why shouldn't it import geophysicists?

## 5 CONCLUSIONS

Wherever the future of prediction and detection of mineral deposits leads, research into improvements in geophysical techniques and interpretation will continue to break new ground. The direction of these efforts must be guided primarily by the real and perceived needs of explorers.

The human resources to lead the innovative enterprises will of necessity be derived from the locations where adequate numbers of geoscientists are being trained.

## REFERENCES


British Geophysical Association, A Joint Association of The Royal Astronomical Society and the Geological Society, 2006.

Rystrom,V. L., Finn C. A. and Descsz-Pan, M., High Resolution, Low Altitude Aeromagnetic and Electromagnetic Survey of Mt Rainier, *Open-File-Report* 00-027, 2000.

Fleming, M. Executive director, Society of Exploration Geophysics, *Pers. Comm*, 2007.

Scinta , C., U.S. Firms Search for Technical Talent,, *Wall Street Journal,* July 26, 2006.

Witherly, K, The quest for the Holy Grail in mining geophysics: A review of the development and application of airborne EM systems over the last 50 years, *The Leading Edge,* Volume 19, Issue 3, pp. 270-274 (March 2000).

# Future directions in exploration geochemistry research: Pursuit of the far-field features of mineral deposits

Karen D. Kelley
*U.S. Geological Survey, MS964, Denver, CO 80225 USA*

David L. Kelley
*Newmont Mining Corporation, Malozemoff Technical Facility, 10101 E. Dry Creek Rd, Englewood, CO 80112 USA*

ABSTRACT: Future research in exploration geochemistry should focus on developing and further documenting unconventional methods for the detection of concealed mineral deposits. Geochemical attributes that can be recognized beyond the obvious limits of the deposits may be considered far-field features of ore deposits. They can be primary, if formed during mineralization, or secondary, if formed after the mineralizing process, as a result of weathering. Research should focus on understanding the formation, consistency, and the scale of far-field features. Three specific avenues of research are suggested: (a) determining a genetic link between primary far-field features and ore deposits, (b) understanding the processes that lead to secondary far-field features, and (c) documenting the scale and footprint of primary and secondary features. Incorporation of methods for detecting far-field features into field-based exploration programs may increase the probability of success, especially in covered terrains.

KEYWORDS: concealed deposits; geochemical exploration

## 1 INTRODUCTION

In recent years, increased attention has been focused on geochemical exploration methods that are designed for concealed terrains. Conventional geochemical exploration methods, such as stream sediment, soil, and lithogeochemical surveys are effective methods when deposits are exposed. However, unexposed deposits or those that are concealed by younger rocks commonly require unconventional detection methods.

The primary physiochemical signatures of hydrothermal systems can extend far beyond the limit of any associated mineralization. A variety of mineralogical and geochemical phenomena related to mineralization have been recognized (summarized in Kelley *et al*., 2006) that should increase our ability to detect mineralization in the far-field or in deeply covered areas. Far-field geochemical features include both primary, if formed in association with mineralization or alteration processes, or secondary if formed from the interaction of ore deposits with the hydrosphere and biosphere. Primary far-field features include mineral, isotopic, or element halos, as well as thermal anomalies in host rock sequences (Fig. 1A). A number of newly investigated secondary far-field features include the development of reduced columns by electrochemical processes in transported overburden, geochemical dispersion related to the expulsion of ground water from tectonic and seismic compression, dispersion of vapor above ore deposits, and geochemical dispersion related to biological processes (Fig. 1B).

Future research with respect to far-field geochemical features can be divided into three main themes: (1) determining a genetic link between primary far-field features and ore deposits, (2) understanding processes that lead to secondary far-field features, and (3) documenting the scale and footprint of primary and secondary features.

## 2 GENETIC LINK BETWEEN PRIMARY FAR-FIELD FEATURES AND ORE DEPOSITS

Many ore deposits have a thermal, geochemical, mineralogical, or isotopic aureole

that extends beyond the physical expression of the orebody or alteration zone (Fig. 1A). Methods that can detect these changes are potentially important aspects of exploration strategies. However, many of these features have been documented in only a few case studies and a genetic link to mineralization processes is commonly only empirical. For example, studies using conodont alteration indices (CAI), vitrinite reflectance data, or illite crystallinity indices have documented an increasing temperature gradient towards ore (Kelley *et al*., 2006). This has been observed for MVT deposits (Goebel, 1996; Sangster *et al*., 1994) and sedimentary exhalative deposits (Maynard *et al*., 2001). A few examples also exist for porphyry deposits (Meuzelaar, 1995; Cunningham *et al*., 2004). In nearly all of these cases, documentation of a temporal or genetic link to mineralization is lacking.

Similarly, geochemical, mineralogical, or isotopic signatures in zones adjacent to but distal from an orebody (*e.g.*, alteration halos) are commonly assumed to be genetically related to the mineralizing event. However, owing to the fact that ore deposits typically mark sites of focused, prolonged, and repeated hydrothermal fluid flow, geochemical or isotopic anomalies can be produced during pre- or post-mineralizing events.

The key to confirming a definitive genetic link is establishing the timing of different fluid or hydrothermal events and comparing these to known ages for the deposits. Apatite fission track (AFT) thermochronology is a method that can establish the thermal history of rocks and also define the spatial extent of the thermal footprint associated with hydrothermal systems at shallow levels in the crust (<3-5 km). For example, one recent AFT study around Carlin-type gold deposits in Nevada (Hickey, 2007) shows ages that are coincident with two thermal events, including a regional cooling period and a younger event associated with mineralization. The U-Th/He radiometric technique is also ideal for constraining the temperature and timing of palaeofluid flux. This method has recently been developed for primary or secondary minerals such as apatite, rutile, fluorite, titanite, or zircon (McInnes *et al*., 2004; Evans *et al*., 2005; Reiners *et al*., 2004). These minerals are common accessory phases in many different mineral deposit types, both within the orebody or in adjacent alteration zones. Therefore, methods that can utilize these minerals to document the timing of fluid flow events will greatly expand our understanding of genetic links between far-field geochemical or mineralogical features and ore deposits.

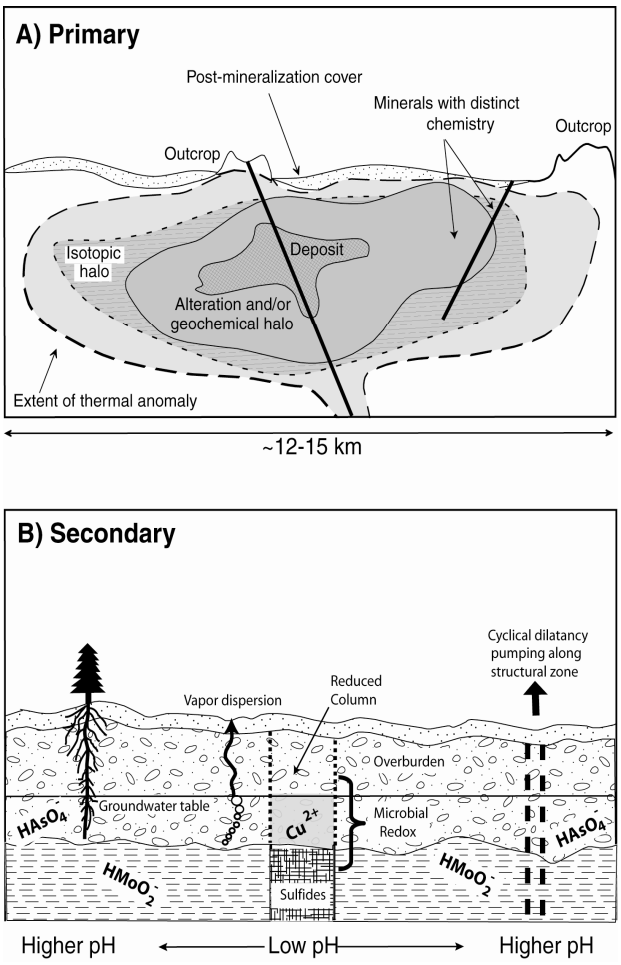


Figure 1A. Schematic diagram illustrating some primary far-field features. B. Close-up of deposit area showing possible secondary far-field features. Modified from Kelley *et al.* (2006).

## 3 PROCESSES THAT CONTROL SECONDARY FAR-FIELD FEATURES

When ore deposits interact with the hydrosphere and biosphere, the processes can create far-field features of secondary origin (Fig. 1B). Self-potential currents associated with oxidizing sulfide deposits are the basis for electrochemical dispersion models. The model developed by Hamilton (2000) proposes that the upward propagation of reduced species to the water table forms a reduced column over the mineralized zone and geochemical anomalies are developed in the overlying overburden (Fig. 1B), suggesting that direct detection of sulphide-bearing mineral deposits concealed by

transported glacial overburden is possible (Hamilton, 2000; Cameron *et al*., 2004). Whether or not reduced columns form in different environments is unknown and should be investigated. For example, such columns may form in arid environments at the base of the vadose zone. If so, this may serve as the site for additional dispersion processes, such as cyclical dilatancy pumping , hydromorphic dispersion, or vapor dispersion. Establishing a link to mineralization at depth through isotopic studies in overburden (*see* Hall *et al.*, 2004) will also improve our understanding of secondary dispersion processes. The role of biological processes in reduced chimney environments needs to be further investigated to determine if they play a dominant or subordinate role. Causes of any elevated groundwater temperature and piezometric highs, such as reported in Hamilton *et al.* (2003, 2004) should be fully investigated.

The formation of geochemical anomalies related to buried ore deposits by cyclical dilatancy pumping is controversial. It is clear that seismic activity causes redistribution of crustal fluids and meteoric groundwater, and to the extent that such waters can carry a geochemical signature of buried mineral deposits (especially those that are oxidizing), it is logical to expect that surface geochemical anomalies can form. Detailed studies of discharging groundwater and soil geochemical anomalies over known porphyry deposits in the hyper-arid Atacama desert have been interpreted to have formed by the surface expulsion of groundwater following earthquakes (*e.g*., Cameron *et al*. 2002). Isotopic studies that can demonstrate a genetic link between the mineral deposit and the surface geochemical enrichment can help resolve this controversy. Additional studies that address the extent that cyclical dilatancy pumping occurs in nature would provide increased incentive for developing exploration methods that target this process.

Surprisingly little research has been done over the past decade to understand processes that lead to vapour dispersion, despite the fact that impressive examples from mineral exploration case studies have been previously published (Klusman, 1993). Understanding the processes that lead to the formation of specific vapor phases, the stability of these compounds in overburden settings, and sampling and analytical protocols required to measure them are all fundamental to establishing the utility of soil gas methods in mineral exploration.

The role of biological processes in the formation of geochemical anomalies in overburden environments is largely unknown. Recent work has shown that bacteria are important catalysts in promoting the breakdown of sulfides at kinetic rates much higher than previously thought (Enders *et. al*., 2006). Although a close relationship between microbial populations and reduced columns is suspected, an understanding of their role in controlling the chemical environment and the transport and fixation of elements is essential. The recognition of sulphate-reducing bacteria in 8,000 year old glacial sediments overlying a VMS deposit at Cross Lake, Ontario, Canada suggests that they may be essential to maintaining the reduced column and for concentrating elements in the near surface (Goodhue & Southam, 2005)

## 4 SCALE AND FOOTPRINT OF FAR-FIELD FEATURES

The scale of far-field features is highly variable and poorly understood. In the case of secondary features, the scale is likely controlled by the efficiency of the process responsible for producing it, rather than the size of the deposit. For example, in many cases, a small deposit can display a broad anomaly (and vice versa), if the secondary dispersion process is efficient. On the other hand, there are many examples where the size or intensity of fluid flow and thermal anomalies correlates with the size (or grade) of the deposit or district. For example, the footprint of some of the most important sedimentary rock-hosted uranium or zinc districts can be hundreds of kilometers. In some cases, it has been possible to document the spatial and temporal movements of fluids (mapping of palaeo-aquifers) through detailed mineralogical, geochemical, and isotopic studies (*e.g.*, Kotzer & Kyser, 1995). Recent work by Tosdal *et al*. (2003) suggests that there could be a correlation between the size of the thermal footprint of Carlin-type gold systems and gold endowment of the area.

Owing to the fact that the scale of many features is documented in only a few cases, future applied studies to test the scale of features within and between deposit types is the logical first step. Such studies should address optimal sampling parameters and density for the feature to be clearly defined.

## 5 CONCLUSIONS

Future research in exploration geochemistry should focus on determining a genetic link between primary far-field features and ore deposits, a better understanding of the processes that lead to secondary far-field features, and documenting the scale and footprint of primary and secondary features. Inherent in such research is a better understanding of the processes responsible for producing far-field features and of the interrelationship of geological, geochemical, and hydrological processes. For example, it is likely that reduced columns, biological dispersion and vapor dispersion are complexly linked. The success of such research requires multidisciplinary research teams and expertise outside of the field of economic geology.

## REFERENCES


Cameron, E.M., Leybourne, M.I., and Kelley, D.L., 2002, Exploring for deeply-covered mineral deposits: formation of geochemical anomalies in northern Chile by earthquake-induced surface flooding of mineralized groundwaters: *Geology,* v. 30, p. 1007-1010.

Cameron E.M., Hamilton, S.M., Leybourne, M.I., Hall, G.E.M., and McClenaghan, M.B., 2004, Finding deeply buried deposits using geochemistry: *Geochemistry: Exploration, Environment, Analysis,* v. 4, p. 7-32.

Cunningham, C.G., Austin, G.W., Naeser, C.W., Rye, R.O., Ballantyne, C.H., Stamm, R.G., Barker, C.E., 2004, Formation of a paleothermal anomaly and disseminated gold deposits associated with the Bingham Canyon porphyry Cu-Au-Mo system, Utah: *Economic Geology,* v. 99, p. 789-806.

Enders, M. S., Knickerbocker, C., Titley, S. R. and Southam, G., 2006, The role of bacteria in supergene environment of the Morenci porphyry copper deposit, Greenlee County, Arizona; *Economic Geology*, v. 101, p. 59-70.

Evans, N.J., Wilson, N.S.F., Cline, J.S., McInnes, B.I.A., and Byrne, J., 2005, Fluorite (U-Th)/He thermochronology: Constraints on the low temperature history of Yucca Mountain, Nevada: *Applied Geochemistry*, v. 20, p. 1099-1105.

Goebel, E.D., 1996, The pathway for MVT hydrothermal fluids within the tri-state mining district from stratigraphic plotting of conodont alteration indices, *in* Sangster, D.F., ed., *Carbonate-hosted lead-zinc deposits: Society of Economic Geologists Special Publication* No. 4, p. 413-418.

Goodhue, L., and Southam, G., 2005, *unpublished report for Canadian Mining Industry Research Organization,* 15p.

Hall, G.E.M., Hamilton, S.M., McClenaghan, M.B. and Cameron, E.M., 2004, Secondary geochemical signatures in glaciated terrain: SEG 2004, Perth, Extended Abstracts Volume, p 79-84.

Hamilton, S.M., 2000, Spontaneous potentials and electrochemical cells, *in*,Hale, M. & Govett, G.J.S, eds, Geochemical remote sensing of the sub-surface: *Handbook of Exploration Geochemistry*, Elsevier, Amsterdam, v. 7, p. 81-119.

Hamilton, S.M., Hall, G.E.M., McClenaghan, M.B., Cameron, E.M., 2003, Rapid mass-transport of elements through clay and the possible role of redox gradients, *in Proceedings to the 6th International Symposium on Environmental Geochemistry, Edinburgh, Scotland,* September 8.

Hamilton, S.M., Cameron, E.M., McClenaghan, M.B. and Hall, G.E.M., 2004, Redox, pH and SP variation over mineralization in thick glacial overburden, Part II: field investigation at Cross lake VMS property: *Geochemistry: Exploration, Environment, Analysis*, v. 4, p. 45-58.

Hickey, K., 2007, Thermal footprints – dating the far-field extent of hydrothermal flow using low-temperature thermochronology: *Mineral Exploration Roundup07 Abstract Volume, Jan. 29-Feb. 1, 2007, Vancouver, BC,* p. 42-43.

Kelley, D.L., Kelley, K.D., Coker, W.B., Caughlin, B., and Dohery, M.E., 2006, Beyond the obvious limits of ore deposits: Mineralogical, geochemical and biological features for the remote detection of mineralization: *Economic Geology*, v. 101, p. 729-752.

Klusman, R.W., 1993, *Soil gas and related methods for natural resource exploration,* John Wiley & Sons, Chichester, UK, 483 p.

Kotzer, T.G., and Kyser, T.K., 1995, Petrogenesis of the Proterozoic Athabasca Basin, northern Saskatchewan, Canada, and its relation to diagenesis, hydrothermal uranium mineralization and paleohydrology: *Chemical Geology*, v. 120, p. 45-89.

Maynard, B.J., Elswick, E.R., Hower, J.C., 2001, Reflectance of dispersed vitrinite in shales hosting Pb-Zn-Cu ore deposits in western Cuba: comparison with clay crystallinity: *International Journal of Coal Geology*, v. 47, p. 161-170.

McInnes, B.I.A., Evans, N.J., Sukarna, D., Permanadewi, S., Garwin, S., Belousova, E., Griffin, W.L., and Fu, F., 2004, Thermal histories of Indonesian porphyry copper-gold deposits determined by U-Th-He, U-Pb, Re-Os, K-Ar and Ar-Ar methods: SEG 2004 *Predictive mineral discovery under cover: Extended abstracts*, p. 343-346.

Meuzelaar, T., 1995, Metasomatism and oxygen isotope exchange within hydrothermally altered sedimentary rocks, Rico, Colorado: *Unpublished M.Sc. thesis, Pullman, Washington, Washington State University,* 194 p.

Reiners, P.W., Spell, T.L., Nicolescu, S., and Zanetti, K.A., 2004, Zircon (U-Th)/He thermochronology : He diffusion and comparisons with 40Ar/39Ar dating : *Geochimica et Cosmochimica Acta*, v. 68, p. 1857-1887.

Sangster, D.F., Nowlan, G.S., and McCracken, A.D., 1994, Thermal comparison of Mississippi Valley-Type lead-zinc deposits and their host rocks using fluid inclusion and conodont color alteration index data: *Economic Geology*, v. 89, p. 493-514.

Tosdal, R.M., Hickey, K.A., Donelick, R.A., Arehart, G.B., and Chakurian, A.M., 2003, Distinguishing hydrothermal events using apatite fission-track thermochronology; implications for Au-mineralization in the Carlin-Jerritt Canyon region, northern Nevada: *Geological Society of America.*

# The Future of University-Industry Collaboration in Ore Deposit Research — A Personal View

Richard M. Tosdal
*Mineral Deposit Research Unit, University of British Columbia, Vancouver, British Columbia, Canada*

ABSTRACT: Geological research, whether completed by industry- or university-based geoscientists, plays a role in the discovery, development, and exploitation of major ore deposits. Such research defines the regional and local metallogenic setting of mineralization and generates ore-genetic models that interrelate the parts of a deposit within the wider footprint of the ore-forming system. Despite the success, there are challenges to the sustainability of collaborative research. Of particular note are understanding the culture of the collaborators, communicating results in a timely manner, managing the impact of the commodity cycles, understanding of the ownership of intellectual property resulting from the research, and attracting talented geoscientists.

KEYWORDS: Research, Appreciation, Culture, Intellectual property, Communication

## 1 ROLE OF RESEARCH

Geological research plays a critical role in the discovery, development, and exploitation of major ore deposits. Such research defines the regional metallogenic setting, constrains ore forming processes, and generates ore-genetic models that interrelate the parts of a deposit within the wider footprint of the ore-forming system. These models, based on rigorous academic research, are inherently predictive, leading to very practical outcomes. As the search for new mineral resources becomes increasingly more challenging, research can take on an increasingly more important role in the future of the mineral industry. However, research implies different activities to different parts of the greater economic geology community. Understanding and appreciating the range of views of what constitutes research is critical for a vibrant community, and underpins any collaborative industry-university research partnership.

Research from the perspective of the mineral industry is conducted along two avenues. One research activity is through exploration by industry for a particular deposit type of interest. Much is learned about a geologic terrane, deposit type, or exploration technology through these efforts. Unfortunately, much of this information or data is also not made public because of the nature of competitive business activities, and because companies are not in the business of publishing results. Additional research focused on technology development, such as geophysical and geochemical techniques, augments results from corporate research and development activities. Financial support for these activities is derived from corporate budgets. The second avenue is through funding university-based researcher(s) to address specific questions of interest that will not be addressed by an individual company as a part of the normal course of business. These questions have very practical outcomes, develop new technology for exploration, or develop new concepts and understanding of the ore environment. It is this second research avenue that is the subject here.

Research from the academic perspective seeks to understand the setting and genesis of a particular ore deposit or process involved in its formation. The activities do not necessarily contribute information immediately applicable to either exploration or mining. Nonetheless, the cumulative effect of this information leads to models or techniques that are predictive and applicable to mining and exploration activity. Financial support for this research is traditionally obtained from government and (or) industry sources. With the exception of a couple of countries who encourage collaborative industry-university research through competitive

government grant programs that match industry financial contributions, funding from government funding agencies to support economic geology has been increasingly difficult to secure, as the financial resources have shrunk and the competition for those funds increased.

## 2 CURRENT STATE OF UNIVERSITY-INDUSTRY RESEARCH

University-based research is derived from the efforts of a single researcher to those of large research groups created and sponsored by consortia of industry, government, and industry. Several factors impact the university – industry research environment. Of foremost importance is the declining number of economic geology faculty in university departments around the world due to (1) shifting priorities within universities, (2) decreased direct economic impact of the minerals industry on the economies in developed countries and the consequent perception of a "sunset" industry, and (3) a decrease in involvement of mining companies with universities. In addition, new research directions within universities have created increased competition for university and human resources.

In parallel with the university changes is an evolution in the relationship between mineral companies and universities. Companies have become considerably larger and most now operate internationally. Two challenges are the consequence of the globalization. One is the increased demand on industry-sponsored research efforts to be broadly applicable across the range of corporate activities. The second is a "decentralization" of research activities by either spreading the sponsored projects around the world and thus competing with research funding on a global basis, or funding more local research results that are themselves more applicable around the world.

### *2.1 Industry-university collaborative groups*

To meet some of the challenges, university-based research groups that represent a joint venture between a university, a consortium of mining companies, and in some cases government, have been established. Examples include the Mineral Deposit Research Unit (MDRU) at the University of British Columbia, Mineral Exploration Research Centre (MERC) at Laurentian University, Centre for Ore Deposit Research (CODES) at the University of Tasmania, Center for Mineral Resources (CMR) at the University of Arizona, Centre for Exploration Targeting (CET) at the University of Western Australia, and the Economic Geology Research Unit (EGRU) at James Cook University. These groups focus principally on exploration related questions. Other research groups emphasize mining- or environment-related issues.

Many but not all of the exploration focused consortia were established in part by financial resources provided by government programs and university initiative. Some consortia continue (2007) to receive significant funding from government via direct supporting grants or from the university through direct funding of research positions. Others are now largely self-funded, building upon the previous investment by industry, university, and government.

The collaborative research consortia around the world are predicated on providing an environment where a range of research skills, expertise, and knowledge can be marshaled to address research questions. Critical to these efforts is involvement of university faculty, postdoctoral level researchers, and graduate students. Of equal importance is their access to research facilities available at the university. Each group also depends on the direct input from the mineral industry into the research projects. This linkage is accomplished through many routes, the most common of which is establishing industry-dominated advisory groups to help chart future directions.

### *2.2 Research brokers*

Decades ago, industry-sponsored research brokers were created to facilitate communication and to establish collaborative research. Two examples are AMIRA International in Australia and CAMIRO in Canada. These organizations broker research, either originating from university researchers or directly from industry sponsors. Prior to the advent of internet-based communication, the brokers provided an invaluable service of facilitating university-industry research, and a means for a single university researcher to access a range of potential industry sponsors for their research program.

There are now challenges to the sustainability of the brokers. (1) The growth of integrated research groups creates competition, as the research consortia organize, fund, and complete research projects in-house. This step limits the need for a third party as a broker. (2) Rapid web-based communication provides a means for any researcher or research consortium to es-

tablish communications with potential industry sponsors. (3) Mining companies now have exploration offices located around the world, thereby facilitating access to industry sponsors for research providers.

### *2.3 Individual researchers*

Single economic geology faculty members within university departments are diminishing around the world. At the same time, research opportunities for those still active are becoming more and more difficult to secure because of competition from the larger research providers, as well as from the challenge presented to the single researcher by their environment. It remains unclear whether these individuals can survive without linking their activities with others or with larger research groups.

## 3 CHALLENGES FOR THE FUTURE

Successful university-industry collaborative research faces many challenges. Five are of particular note as they affect the ability of research groups to meet future research and for the mineral industry to continue to function and participate in collaborative activities.

### *3.1 Appreciation of the collaborators culture*

Successful research depends upon several factors beyond the scope of the project itself. Of paramount importance is an understanding of the culture of the collaborators, be they at a university or with the industry. It is not uncommon for a university researcher to lament that they cannot secure funding from industry to undertake a research project, or that a project is of such interest that the industry should just fund it. Conversely, it is equally common to hear the complaint from industry that a university researcher is not proposing or undertaking research of any interest, impact on, or application to their activities. Each complaint reflects the lack of appreciation of the culture of the other as well as a lack of willingness, or an opportunity, to communicate in a language understood by the other. For example, industry is composed of many different corporate units, each with different goals, directions, and philosophies. Industry is not a monolithic entity. Instead it is governed by business principles and driven by the profit motive. The industry cannot be confused with a government grant agency that reviews good ideas and then provides funds to undertake the research program. Industry funds research projects that have the potential to provide a result that may help them in their activities on the short- or long-term. They are consumers of information and research results, and not an altruistic funding organism. Conversely, university researchers are not contractors or consultants, or a cheap source of labor. The researchers are driven by a willingness and interest to investigate a range of topics, usually for modest financial support. Their career pressures stem from a public recognition of their research through the publication of their research in peer-reviewed journals or at professional conferences. Effective communication and appreciation of the other's culture is the basis for rewarding collaborative research programs.

### *3.2 Intellectual property*

Intellectual property and publication of research results derived from a research project is a growing challenge to the future of collaborative research. Ownership of intellectual property is becoming increasingly important to universities, as they search for additional sources of financial support. In many fields, the ownership of the intellectual property can provide significant future income to the university and to the researchers involved in the project. The universities, as a result, are becoming increasingly more aggressive in claiming ownership of the intellectual property. Companies are becoming equally aggressive in asserting their ability to use the results of the research project they fund in any way that benefits them. The net results can be failed research opportunities or months of delay during negotiations.

In most, but certainly not all exploration-related research, it is difficult to envision a situation wherein the results of a research project result in definable economic gain. Nonetheless, the issue is significant, as it also has an implication for the ability of the researchers to communicate their results to the larger community in a timely manner. If the companies own the intellectual property, then will the researcher have the opportunity to publish the results in a timely manner that impacts their career? Conversely, if the universities own the intellectual property, can the results of a research project utilizing an economically significant exploration project be a basis to assert a partial ownership to that corporate asset? Although this scenario is certainly unlikely, the need to understand the long-term implication and develop a coherent view and legal defini-

tion of intellectual property is a critical challenge, regardless of the discipline.

### *3.3 Long term versus short term*

Commodity prices fluctuations are a well-known economic reality and one that drives the strategic planning of mining companies. Currently, with the developing economies of east Asia, commodity prices are at an all time high. How long into the future these prices will continue is unknown. Nonetheless, exploration expenditure is now also at all time high, which translates into increased opportunities for collaborative exploration-related research. It is a time of riches, with more opportunity than talent to tackle them. Conversely, five years ago commodity prices were low. As a consequence, obtaining research funding to establish collaborative research projects was extremely difficult, even for the most well connected research consortia around the world. The net effect was the shrinking of research activities, disappearance of faculty, and the consequent diminished capacity to train the next generation of practicing geoscientists to meet industry demands.

Alleviating the impact of commodity price cycles is a major challenge to industry and universities. The university community must appreciate that commodity prices and business principals drive industry activities. Conversely, the industry as a whole must appreciate that the university community cannot turn on research and training activities whenever commodity prices are high. Once a university program is gone, it will not be replaced. A collaborative vision to sustain research and training programs is required. Whether or not the current trend toward sustaining large collaborative university-industry research groups is the solution is unknown. It is a topic worthy of debate and undoubtedly will be viewed differently depending upon the culture.

### *3.4 Communication and delivery*

Communication is crucial to any project. It is also an activity that implies different actions to different parts of the larger community. To the university researcher, communication is derived around presenting his or her work at professional meetings and in scientific journals. To the industry, it is understanding and receiving the research results in a timely manner, and in a form that is easily translated and usable to assist in corporate activities. These cultural differences must be appreciated to ensure successful collaborative industry-university research.

### *3.5 Human resources*

There is a critical shortage of qualified and experienced geoscientists in the industry. Likewise, many graduate programs are suffering from a shortage of talented graduates to undertake the unprecedented research opportunities. Some of the graduate student shortages reflect the enhanced opportunities for employment by the industry. Perhaps more importantly, however, is the overall shrinking of ore deposit programs in university geoscience departments around the world, and thus the numbers of young geoscientists who might enter the research or industrial worlds.

Globally, there are increases in undergraduate enrollments in universities due to the range of job possibilities. But these increases are not universal. One can wonder what the opportunities will be for these young scientists, once they complete the four to nine years required to become a thinking and creative geoscientist. They are not created overnight.

## 4 A PERSONAL VIEW ON THE FUTURE

There is a strong, but not universal recognition, appreciation, or even agreement of the importance of university-based research and advanced education of geoscientists to the future of the mineral industry. The role of research in developing concepts, models, and techniques is, however, well recognized and the need for this information to ensure a vibrant industry is appreciated. What is underappreciated is the need for tangible support by the university community from the mineral industry. Ore deposit research within the university competes with other disciplines, and during recent years has generally been losing status to emerging industries such as biotechnology or computer sciences. Departments and whole programs have been closed, and others have been merged into new mega-departments, thereby diluting geoscience activities with other disciplines.

With the current commodity price boom, the opportunities are there to build the long-term relationships that carry a researcher or research group through a price low. On the larger scale, universities and the industry wishing a flow of research recognition and perhaps, more importantly, trained scientists, must think in longer terms and not driven simply by short-term business needs.

# Geological Surveys – where do they fit in the 21st Century?

Garth Earls
*Geological Survey of Northern Ireland, Colby House, Stranmillis Court, Belfast BT9 6BS, Northern Ireland.*

ABSTRACT: Geological surveys grew out of the need for natural resources, driven initially by the Industrial Revolution, and have been in existence since 1835. Although originally tasked with geological mapping, they have evolved into wider spheres. The relationship between geologically driven industry, consultancy and academia has continued to develop, but with an increasing blurring of historical boundaries. The strategic development of geoscience research may be better served if each sector maintains its core 'national' capabilities of wealth creation (industry), education (academia) and the collection, archiving, interpretation and dissemination of Earth science data (geological surveys). Research agendas can then be strategically aligned with key drivers and involve the geoscience community. The need to better inform politicians, decision makers and the general public is fundamental to ensuring long term success for the geoscience community.

KEYWORDS: geological survey, geoscience research, outreach

## 1 INTRODUCTION

The role of geological surveys has evolved considerably over the past three decades. Most were established to advance the understanding of the natural resources of a country, and in many cases this remains their primary function. However, in some mature mining countries and in nations less well endowed with exploitable natural resources, the focus of geological surveys has been changing to adapt to the wider environmental and political agendas. The origin of geological surveys can be traced back to the Industrial Revolution and it is no surprise the British Geological Survey (BGS), dating from 1835, was the first geological survey in the world (Allen, 2003). The Geological Survey of Ireland (GSI) was formed as part of the BGS in 1845 (Herries Davies, 1995) and the Geological Survey of Northern Ireland (GSNI) was established in 1947.

In geological sciences, the roles of academia, industry and consultancy have always existed in parallel with geological surveys. In the past, these roles have been well defined. However, in the early 21st century the fundamental role of some of these sectors is being questioned and reevaluated.

## 2 HISTORICAL CONTEXT

The initial brief of any geological survey is to map the geology of the country and assess the natural resources. For example, within Great Britain and Ireland this has been completed at reconnaissance scale (1 inch to the mile) and largely completed at more detailed scales (6 inches to the mile or 1:10,000). The initial plan was to complete a systematic survey working from the south to the north. This is essentially what happened in Ireland. However, in Great Britain political pressures dictated that systematic surveying was to be superseded by reactive surveying when the increasing need for coal resulted in the prioritization of work programmes into areas of Carboniferous rocks.

Many geological surveys, and the BGS is perhaps the classic example, maintained colonial offices and mapped frontier areas up until relatively recent times. This type of approach provided excellent skills, training and discipline in geological mapping and reporting.

## 3 THE MODERN GEOLOGICAL SURVEY

Geological surveys now undertake a leading

role in, and offer an integrated solution to, aspects of economic and environmental issues. Geoscience has always contributed to a nation's wealth creation, and increased environmental awareness has recognized the role geoscience can play in the mitigation of a wide range of green issues. Modern geological surveys have evolved into truly multidisciplinary organizations through increased involvement in geophysics, geochemistry and information technology.

The fundamental role of a modern geological survey is to provide impartial geoscientific information to support and facilitate the development and/or protection of the nation's natural resources and environment. One of the key issues is the nature of information that a geological survey should collect and provide. Historically, the activities of a geological survey focused on geological field mapping, and the production of maps and memoirs representing the essential record of the geology of the nation.

However, as geological surveys have expanded their sphere of work into other disciplines, some of the bedrock mapping skills developed over decades are in decline. This increasing shortage is further exacerbated by the 'skill sets' now being taught in universities that are becoming more classroom oriented. Consequently there is a real shortage of quality geological fieldwork skills. To this end the BGS has introduced specialist courses to develop and upgrade geological mapping skills.

A modern geological survey operates in a global environment that encompasses geoscientists practicing in industry, consultancy and academia. In the past, the roles and responsibilities for each sector were relatively well defined. However, over the past three decades, the increased need for geological information, the direction from some governments to recover costs, and grant-based incentives to promote interdisciplinary research have resulted in the blurring of the boundaries of historical responsibility.

## 4 RELATIONSHIPS

In seeking to define the respective roles of the geological fraternity in the 21st century, there is need to understand where each sector originated and it's evolution over the previous decades.

Industry. The corporate sector of geoscience has been a fundamental driver for discovery, innovation and economic growth in many countries. Although the gold rushes tend to dominate in the public perception of wealth and geology, it is the basic commodities that in the past have driven and underpinned economies – hydrocarbons, metals and aggregates. Industry understands the exploration and development of these resources better than any other geological sector.

Industry responds to key drivers – commodity price and new discoveries being high up the list. One of the challenges for industry has been planning the human resource issue throughout the boom and bust commodity rollercoaster. At the height of a boom geological surveys will select from a much reduced and more inexperienced field to fill a vacancy compared with the bottom of the commodity cycle.

Consultancy. In the past decades, changes in employment patterns have spawned the relatively new breed of geological consultant. Historically, most geologists were part of a company, but as with industry in general, the pattern of outsourcing work has resulted in a diverse selection of small consultancy operations. Of course there are many well staffed geological consultancies, especially in the hydrocarbons sector. However, in the minerals sector, smaller consultancies tend to be more specialized when compared with the global consultancy industry. However, through the use of specialist consultants organizations can improve performance through analysis of existing problems and the identification and cross-fertilization of best practice.

Academia. Of all the geological sectors, academic geology has perhaps been under more threat than any other. In the 1980s-90s numerous university geology departments were amalgamated or closed. Almost all of these closures were cited as 'for budgetary reasons' but the reality is that some closures were 'political' decisions while other departments of similar size and expenditure were allowed to survive.

The speed and regularity of these closures approached a feeding frenzy as universities sought to offload departments with arguably irrational haste. In some instances geology departments did not appreciate the seriousness of the threat, and assumed that because they had been in existence for decades that they were safe.

Geology departments should not be proud of boasting that 90%+ of graduates end up with a job in geology. The more science graduates that are employed in decision making roles outside scientific disciplines, the better the future is for science. This is especially true of geoscience, where all aspects of the subject find themselves having to continually appraise management and government of the necessity of geological input and expertise. Geoscience has never been more relevant, yet many governments still appear ignorant to the fact that geoscience provides solutions to many 21st century problems.

The reduction in geology departments, resulted in making the surviving departments less secure, and changes in grant funding methodologies has steered universities towards the formation of campus companies and greater collaboration with the remaining geoscience sectors: "Knowledge Transfer" is one of today's buzzwords. This in turn has resulted in the blurring of boundaries with the traditional roles of the geological surveys and universities.

Geological surveys. There can be little doubt that geology in general and perhaps geological surveys in particular attract a certain type of individual. The nature of the early years of geological mapping often involved long periods in the field and consequently management issues could only be dealt with on an infrequent basis. There was often a less rigorous monitoring role from government and although budgets would have to be fought for, the development of mapping programmes and scientific output were generally not well audited. Stories of a geologist continuing to map in the same area throughout their career are not uncommon.

The 1980s introduced the concept of privatization to many organizations and the presumed need for a national capability to be maintained through a central government system was questioned. Indeed the question of whether geological surveys should be out with government and/or operating on a completely commercial basis is still on the agenda today.

There are different financial models for geological surveys. Some surveys are funded by central government and provide all their services to their stakeholder community at zero or low cost (*e.g.* GSI). Some surveys, such as the BGS, are part funded by government and are mandated to recover full economic cost through working for other parts of government and the private sector. Both models can work well, but require astute leadership and political acumen to read the changing winds of government policy and funding to ensure successful long term development. As in all geological sectors, complacency is not an option.

Fundamentally, geological surveys are about national capability – the collection, archiving, interpretation and delivery of strategic geoscience data. This information needs to be provided to the ever increasing user community to support and facilitate economic development, ensure environmental protection, provide research opportunities and contribute to policy and decision making. Increasing the awareness of the value of geoscience among the general public is also a major role.

## 5 THE WAY FORWARD

There is no doubt that there is increased cooperation between all sectors of geoscience and that this will continue at greater pace. Although there are genuine long term advantages in cooperative research there are some boundaries which should remain in place. For example, geology departments are the home of education and geological surveys represent a national capability and archive. Collaboration, especially between academia and geological surveys will increase. This is primarily driven from government and is to be commended and will foster closer symbiotic relationships.

There always have been areas of mutual benefit where co-operation has flourished. Field mapping in particular has benefited from geological survey funded academic research. However, as mapping skills in academia are in decline, surveys need to find different ways of undertaking regional and local mapping.

Historically, university departments have had a shorter term agenda than the longer term view maintained by a geological survey through systematic surveying and archived data. The realignment of temporal perspective by both sectors will blur another boundary.

Strategic geoscience data and knowledge will play a fundamental role in providing answers to many of the big scientific, technological and environmental issues of the 21st Century. It is imperative that geoscience in general and geological surveys in particular become close to the centre of government.

To this end the need to increase the profile of geoscience among politicians, decision makers and the general public is becoming ever more important. This type of approach is not something that can be implemented once and then forgotten about. The world is continually changing – news stories are ephemeral, and are soon forgotten by most of the audience.

Geological surveys, often through government press offices, have the opportunity to continually elevate the profile of geoscience in the community. Too often in the past, geology as a discipline has failed to communicate the excitement and relevance of the science.

As the degree of multi-disciplinarity continues to increase, at the centre of increasing levels of cooperation will be closer liaisons with social scientists and economists in relation to future societal and quality of life issues.

So, is the present commodity boom a godsend? For those working in it, it certainly is – but what about the future? Historically there has always been a time lag between high commodity prices and an increase in student numbers studying geoscience. In the UK the evidence suggests that even five years into the present boom there has been a gradual decline in the numbers applying to study geology at university.

If this trend is repeated elsewhere, it has serious implications for major issues facing Planet Earth in years to come. The geologists of today may be even more employable in retirement than they are at present.

ACKNOWLEDGEMENTS

The text has been improved through discussions with colleagues in GSNI and BGS.

REFERENCES

Allen, PM. (2003) A geological survey in transition. *British Geological Survey Occasional Publication* No. 1. pp220

Herries Davies, GL (1995) *North from the Hook 150 years of the Geological Survey of Ireland.* Criterion Press Dublin. pp342

# Economic Geology Research and Teaching in Asia – What is needed? What can we do?

Noel C. White
*Asia Now Resources Corporation, Toronto, Canada*

ABSTRACT: Asia is the powerhouse driving the vibrant economic conditions now enjoyed in many parts of the world, and demand for resources from the region is the key factor in the current health of the global mining industry. Asia has a large share of the world's geoscientific population, but they are mostly not engaged with geoscientists in the rest of the world. There are major problems in training, access to international literature, opportunities for mine visits, and in publication of research results and deposit descriptions. It is important that geoscientists in this region be encouraged to participate in the global geoscientific community. There are many ways that societies, companies, universities and individuals can encourage this.

KEYWORDS: economic geology, research, training, Asia

## 1 INTRODUCTION

Asia is the powerhouse of the vibrant economic conditions now enjoyed in many parts of the world. Demand for resources from China and India, on top of the normal demand from Europe, Japan and the USA, has driven commodity prices to levels that are compensating mining companies for the preceding difficult years.

The phenomenal expansion of Asian economies over the past few decades creates the paradoxical situation where, in China for example, the economy is about to become the world's third largest, yet this first class economy is still dependent on a third world domestic mining industry. The high demand for resources in Asia naturally poses the question, "Can these resources be sourced locally?" "How well explored are the countries of Asia?" "Are there human resources there to sustain active and expanded exploration and mining?"

Before the current boom in Asian economies, a review of the potential for mining investment in east and central Asia carried out for The World Bank (Clark *et al.*, 2003) included a study of exploration potential. In a forum presenting the conclusions of this study, it was stated: "Overall, Asia is a net importer of metals. However, its known endowment and abundance of prospective settings indicate that Asia is capable of meeting all its mineral needs…Most of the region is either unexplored, ineffectively explored, or, at best, under explored…There are no geological reasons why Asia cannot make substantial contributions to world trade in most major mineral commodities" (White, 2002).

Since publication of that report, demand for resources in Asia has expanded dramatically. There has been a substantial, though less dramatic increase in exploration activity by western companies in the region. For exploration and mining to continue to grow in Asia it is essential that most of the technical personnel required to sustain that growth must come from within the region. That is dictated both by them being unavailable from other regions, and the need for personnel who speak Asian languages, so able to communicate with local people.

In the long term, the availability of adequately trained geoscientists depends on the quality of teaching and research carried out in institutes of higher education throughout the region. Interested western learned societies, companies, aid agencies and individuals all have a role to play in encouraging a healthy research and teaching environment in the region. What is the current situation for geoscientific research and teaching in the region, and what can we do to address problems?

## 2 BACKGROUND

I address this issue, not as someone who has studied it deeply, but as someone who has plenty of opportunity to observe the situation in many parts of the region. I have worked extensively throughout Asia for more than 20 years, and have spent a large proportion of my time in China over the past three years. I have frequent contact with academic, government and industry geologists, and correspond with others. In preparing this paper I obtained answers to a questionnaire from key contacts in China, India, Mongolia and South Korea, to supplement my own experience and observations.

## 3 KEY ISSUES FOR GEOSCIENCES IN ASIA

### 3.1 *Numbers of Geoscientists*

"How many geologists are there in the country" seems like a very simple question, however in the absence of official figures it is difficult to assess, and as several respondents pointed out, it depends on definitions. In China, there are at least five kinds of geologists: in universities doing teaching and research; in institutes doing research; in regional surveys in Beijing doing management; in provincial departments doing management; and in exploration companies (state-owned and private) doing exploration. Estimates for the number of geologists vary widely (from 100,000 to 2 million), depending on who is included; the Geological Society of China has 50,000 members, of whom probably 12,000 are economic geologists. The great majority of geoscientists work in industry, with relatively few in universities.

In India the estimated numbers are much smaller, despite the similar total national population. The highest estimate (5500) is probably overly conservative, but highlights that people trained in geology in India mostly work in other fields. Most work in state and central government surveys, with only a small number employed in industry, though this number is rising as foreign companies become more involved in exploration there.

Compared to China, all other countries in Asia have relatively small numbers of geoscientists, with Vietnam probably having the second-largest population after China. Indonesia and the Philippines also have substantial numbers, reflecting the importance of mining and exploration in those countries. Mongolia is an interesting contrast to other Asian countries, as about 80% of all geoscientists (~1500) work in industry. This reflects the small total population, and the strong emphasis on exploration and mining.

### 3.2 *Quality of Training*

Based on comments from respondents and consistent with my observations, basic geological training in Asian countries is generally sound, but training in economic geology is generally poor. This results largely from curricula being outdated and a lack of up to date information about ore deposit models, and new scientific technology or exploration techniques. It is also because undergraduates generally rely on local literature which is outdated or not of international standard. There is a marked difference in quality of training between students from undistinguished local universities and those from larger universities where teaching is done by a leading researcher. Some respondents report a decline in the quality of geological education in recent years, with less emphasis on field training.

A lack of field training for geologists after they complete their basic education creates a serious situation in China, and probably other countries of the region. Very often, field geologists work on projects for decades without further training, and without updated exploration models, totally dependent on what they learned from text books decades before. Senior level geologists or managers have to make decisions based on what inexperienced field geologists present to them. Senior technical experts and academicians base their genetic interpretations and theories on the same inadequate sources, and these experts then provide the basis for decisions at levels ranging from the central government to exploration projects. Consequently, large or potentially large ore deposits are not recognized or explored properly, and an industry that is a key foundation of the national economy continues to stagnate.

### 3.3 *Access to Literature and Deposits*

Leading universities and research institutes in the region have good library facilities, giving graduate students and researchers access to international literature. Smaller regional universities do not have such access, nor do professional geologists working in exploration teams. In general undergraduate students use text books in their national language; these are typi-

cally outdated and of poor quality. Few teachers have good familiarity with recent developments in economic geology, and this is often apparent in misinterpretation of deposits. An unfortunate consequence of the high status of older academics and researchers is that their interpretations may become enshrined as facts because of their source, not because their conclusions have stood up to rigorous examination.

The explosion in access to the internet in the Asian regions suggests a possible solution to the limited access to geoscientific literature. There is a need for suitable materials that are accessible through the internet, including workshop and shortcourse notes as well as technical papers. While materials in the local language would be of great benefit, especially at undergraduate level, internet access to English-language materials would still have a significant impact.

Apart from the lack of up to date literature, an equally significant problem is lack of opportunity for all but the few leading researchers to visit key deposits. Lack of funds makes it difficult for working explorers to visit examples of the deposits they are exploring for, even when examples occur nearby. Travel to visit deposits in other countries is unheard of for all but a tiny minority. Hierarchical structures also mean that such opportunities, if they occur at all, go to senior managers, not to the practitioners on the ground who have to make critical judgments based on what they see.

### 3.4 *Publication of Research Results*

Throughout the region, most researchers published in local or national journals, not international ones, though notably in India and South Korea there is increasing emphasis on international publication. While leading national journals maintain good standards, the quality of publications drops rapidly in smaller local journals. In China it is common to pay for publication, and there may be little reviewing prior to publication (one 'researcher' boasts of publishing over 40 papers in one year!). Papers assert conclusions without giving comprehensive descriptions and justifications.

Authors used to working in this environment have difficulty dealing with the demands of western journals, both technically and linguistically.

### 3.5 *Key Needs*

My own experience in China is that there is a voracious appetite for lectures and training, so it is no surprise that all respondents from all countries mentioned a need for exposure to international lecturers, workshops, short courses and conferences. Getting large numbers of Asian geologists to international meetings is impossible, so the need is clearly for more visits to Asia by lecturers from other parts of the world. Such visits would impact on researchers and practitioners, and both directly and through them, on students. It would increase technical knowledge and increase enthusiasm and participation. Emphasis should be placed on training field exploration geologists in practical skills, and updated exploration models.

Materials that could have an impact on undergraduate teaching are needed to improve both the standard and interest in economic geology. Workshop notes from courses held elsewhere were specifically mentioned as valuable. Inviting Asian researchers to collaborate with western researchers would be a useful way to bring more of them into the mainstream of research, with mutual benefits as opportunities abound for research in Asia. Research facilities in China are generally good, but in most other parts of the region are limited; access and support for Asian researchers to work in western laboratories would enhance their research impact, as well as encouraging them to publish their results internationally.

## 4 WHAT CAN WE DO?

Asia has a large share of the world's geoscientific population, but they are mostly not engaged with geoscientists in the rest of the world. Does that matter? Yes it does!

- If Asia continues to be a large part of global resource demand, it is inevitable that it will become a larger part of resource supply, especially considering that most of the region is unexplored or, at best, under-explored. Western geoscientists and exploration companies are needed and want to participate in the exploration and resulting discoveries (and resulting rewards).
- Asia is a unique part of global geology, and as such it provides opportunities for research into new deposits, new styles of deposits, new variants of deposits, and new deposit settings. It should be of great interest to economic researchers.

- If learned societies such as SGA and SEG are to achieve their goal of representing economic geologists internationally, they need to focus attention on the Asian region and encourage participation of Asian geologists.

There are things that the societies, companies, universities and individuals can do to increase participation of Asian geologists in international economic geology, and in doing so enhance their own activities in the region.

### 4.1 *Societies*

Build membership by advertising (translate!), by inviting membership by influential individuals, particularly leading academics, and by encouraging those members to recruit their students and others; explain the benefits you already provide (translate!) – most people simply do not know; develop associations with leading national societies to increase access to potential members; encourage companies to make membership a normal part of educating their staff; support lectures and short courses; make short course notes and other up to date training materials available to teachers in the region, and through the internet; adjust dues to reflect what potential members can afford to pay; encourage researchers to publish in your journals by providing assistance to deal with language and technical problems; offer advice to governments and ministries, and encourage greater participation in and support for educational and training initiatives.

### 4.2 *Companies*

Take an active role in training your local staff by providing them with society memberships; encourage the societies to provide lectures, short courses and workshops, not only for your own staff; sponsor lecturers and workshops and make them available to other groups (universities, students, surveys, other companies); provide field visits and field training for your own staff, and make them available to other groups; sponsor students and local academics to attend conferences – promote your own good citizenship and their participation in the global geoscientific community.

### 4.3 *Universities*

Encourage collaboration between Asian researchers and your own staff; provide access to research facilities (and the support required to use them); reward international participation by staff, and encourage and reward involvement in joint projects and joint supervision of students not enrolled at your university; invite international students to spend time with you; cultivate opportunities to develop relationships that will last for decades; find ways to fund collaboration, either yourself, through companies, or through Government agencies.

### 4.4 *Individuals*

Develop contacts and relationships in the region; volunteer to give lectures, workshops, whatever you can do; support these activities through your societies, and encourage and support their activities in the region; when travelling in the region, take some students with you and share your experience and knowledge with them (it's fun!); help someone prepare a paper for publication in a western journal; lobby your company, your society, your university, your government, for more activity in the region.

## ACKNOWLEDGEMENTS

I am grateful to the following individuals for their frank discussion of the issues dealt with in this paper: Kaihui Yang, Zengqian Hou, Taofa Zhou, Zhaoshan Chang, Guochen Dong; Guojian Xu, Zhiming Yang, Sereenen Jargalan, Kyu-youl Sung, MK Panigrahi, and Biswajit Mishra.

## REFERENCES

Clark A, Naito K, Stevens N, van der Veen P, Williams J (2003) *The potential for mining investment in transition economy countries of east and central Asia.* The World Bank Group Mining Department, Mining Journal Books, London: 103 pp + CD.

White NC (2002) *Introduction to the metallogeny and ore deposits of Asia. Mineral Potential of Asia,* MMAJ Mineral Resources Centre Tokyo: 5-6.

# Future education trends--what does industry want

M.S. Enders, R.P. Highsmith & G. Simon
*Newmont Mining Corporation, Denver, CO, USA*

ABSTRACT: Faced with a continuing decline in geoscience and economic geology education, industry will have to develop their own internal training programs similar to what has happened in the oil business. To be effective, industry will have to rely on universities to produce quality graduates with a strong fundamental background in science or engineering and geology regardless of whether this background includes classic economic geology training. Industry will select students for employment with a broad background and a potential to excel in a variety of areas, and who are critical thinkers with ability to integrate, interpret, and predict in 3D and 4D from multiple datasets.

KEYWORDS: economic geology, geoscience education, future

## 1 INTRODUCTION

The future of classical economic geology education is at risk of declining to a point of unsustainability. In general, enrollment in undergraduate geosciences programs has been declining at the same time graduate level programs in economic geology continue to be eliminated or reduced. The aging demographics of teaching and research faculty in economic geology point to a potential crisis in economic geology education as older faculty retire within the next 5 to 10 years. Except for the several top universities that have minerals-focused curricula, current geoscience and economic geology education often suffer from limited field and data intensive study, hands-on experience with ore bodies, and cross disciplinary exposure to mining engineering, metallurgy and mineral economics. This looming education crisis could not be more ill-timed given the current global "super cycle" bull market across all mineral commodities.

Furthermore, there appears to be an over emphasis on exploration at the expense of the geoscience role in the broader mining value chain - mining, processing and environmental. The mining business is changing rapidly these days and Laznicka (2006) asserts that *"…the need for resources-related geosciences will diminish in relation to extractive technologies, environmental and socio-political aspects."* This conclusion is directly related to the big challenges currently facing the mining industry.

These challenges are related to four key issues. First, due to the globalization of the economy and stunning growth in places like China and India, there is a huge demand for metals and other natural resources at a time when new deposits are more difficult and certainly more expensive to discover. Supply to these markets is further restricted because it takes longer than ever to get them permitted, developed and into production. Second, all elements of the mining value chain have been hit by escalating operating and capital costs, which have risen faster that metals prices on a percentage basis. Third, there is a dire need for talent and labor to support a vibrant workforce in the mining industry. This is further exacerbated by the ugly demographics of an aging mining workforce in the developed countries, half of whom will retire in 10 years; and the lack of in-country capacity to educate first–rate geoscientists in the developing world. Fourth, economic development associated with new and existing mining operations is seriously challenged by the new paradigms of social and environmental responsibility. This will drive us to focus on new approaches to mining, processing, and environmental management with the goal of minimizing costs and maximizing metal

recovery from the world's giant and world-class ore bodies while continuing to explore for new orebodies.

So, it is within this context that we examine the needs of the mining industry for undergraduate geoscience and classic graduate-level economic geology education.

## 2 SCENARIO PLANNING

Below, we offer three scenarios of the future and describe their features and implications for undergraduate geosciences and graduate-level economic geology education.

### *2.1 Wishful thinking*

This scenario is based on the widely held view that the trend of reducing or eliminating economic geology programs is unsustainable and that there are compelling reasons to rebuild these programs. Some would say that market forces will significantly increase the demand for and salaries of geoscientists. This increased demand will bolster enrollment in undergraduate geoscience education and restore the lost luster of classic economic geology education and research.

In this scenario, it is assumed that governmental support for geosciences education will grow with time. Alternatively, there are those who believe that industry or alumni will have to step up with endowments or other sustainable fund raising initiatives to support the geoscience departments. Furthermore, we assume that the aging baby boomer generation of geoscientists and economic geologists will want to retire early and take up teaching positions as non-tenured, adjunct, part-time or even full-time faculty positions. It would be even better if faculty and industry professionals could do sabbaticals or exchanges.

The implication of this scenario is that the new "super cycle" will last long enough to sustain a generation of robust education, research and jobs in the mining industry and academic community. Based on this implication, we name this scenario "Wishful Thinking".

### *2.2 Steady state*

This scenario is based on the assumption that the remaining graduate-level economic geology programs remain more or less intact and that we can continue to source good undergraduate programs from a variety of universities around the world. This would depend on several top universities with minerals-focused curricula located principally in the developed world, as well as a number of smaller programs with limited resources that focus on specific research topics and/or produce motivated mining-focused graduates.

In this scenario, we assume that governmental support for public education continues its steady decline, particularly in the geosciences and mineral resource education. Industry, on the other hand, will continue to provide significant support through endowments, sustainable funding, internships for students and research support. The top programs, mostly in Canada, Australia, United States and Western Europe, will offer quality training for high-potential foreign national geoscientists through special masters programs or classic M.Sc. or Ph.D. degrees. These top schools would also provide significant outreach services to industry and other universities through collaborative workshops, field trips and short courses. Resident nationals would have the opportunity to pursue classic graduate studies in economic geology that could lead to careers in industry or academia. Those graduates with strong industry experience would be in high demand in either career track.

The implication of this scenario is that the new "super cycle" is just another of the many cycles in the mineral industry and will not last long enough to develop critical mass in support of education, research and jobs before the next downturn. At which time, we would expect a flood of geoscientists returning to graduate schools and as potential replacement faculty for retiring professors. We name this scenario "Steady State" because this is the way it has always been.

### *2.3 Stealing with pride*

This scenario is based on the assumption that Laznicka (2006) is correct, and that the remaining graduate-level economic geology programs continue to diminish or become irrelevant. We further assume that it will remain possible to recruit quality students from a variety of geoscience programs around the world that will call themselves Departments of "Earth and Planetary Science" or "Earth and Environmental Science". These recruits will be selected for employment based more on who they are, than on what they know; although, they still must have a fundamental background in the sciences or engineering. Preference will likely

be given to holders of advanced degrees, particularly Ph.D.'s in a related field even if it is not economic geology.

In this scenario we assume that the current university programs cannot keep pace with demand for graduates nor provide the type of education industry requires. In this case, industry will adopt the oil company approach of providing intensive in-house education and training for new employees and continuing education and development for existing employees. This will be supplemented by collaborative training programs such as those offered by the American Association of Petroleum Geologists (AAPG). Employers will require at least 6 months of solid training in the first year and from 2 to 4 weeks of continuing education per year thereafter. This training will be in the form of further education in depth about a technical discipline, in breadth about other technical areas, or in the areas of business, finance or management. As in the steady state scenario, we anticipate that much of this training will come from current industry geoscientists augmented by remaining faculty or adjunct faculty associated with industry or a collaborative education program like AAPG's.

The implications of this scenario are that industry will provide for itself and offer the amount and type of education and training that is required appropriate for their needs and the global economic cycles. Furthermore, this approach strengthens both undergraduate and graduate programs in general geosciences as it does not rely on variable and cyclical support for specialty economic geology education. On the other hand, industry will expect that graduates have a strong background in the basic sciences including geology, and that they will possess good interpersonal and team skills along with the ability to think critically and to integrate, interpret and predict outcomes from broad multi-disciplinary datasets. Based on these implications, we name this scenario "Stealing with Pride" because the mining business must adapt the best practices from the oil companies which have so successfully implemented this approach.

## 3 EXPECTATIONS OF EDUCATORS

Industry will need robust academic programs that provide quality fundamental education and training in the geosciences. The focus should be on broad exposure rather than narrow specialization, field and data based rather than theoretical or lab based experiences, and on developing team skills rather than individual efforts. It will be more important that an undergraduate have a solid basis of understanding of physics, math, chemistry and geology rather than specific class room exposure to mineral deposits or exploration methods without the fundamentals. It will be more critical that graduates have the ability to integrate, interpret and predict in 3D and 4D from diverse data sets than to have a specific background in economic geology or mineral exploration methods.

We support Etheridge's (2004) assertion that

*"...our educational and research institutions have become compartmentalized along sub-discipline lines, and narrow specialist skills have been favored over integrative skills, both in teaching and in research. In addition, there has been a shift away from field-based geological teaching to lab-based teaching of sub-disciplines in isolation. As a result, geoscience graduates have acquired a somewhat partitioned set of skills, and have been encouraged to specialize before they have a sound, integrated set of geological skills and knowledge."*

Arguably, a very specific set of skills is appropriate for academic research into the plethora of economic geology problems described by Hedenquist et al. (2004), but these only go so far to support the requirements of industry.

Industry is looking for well rounded geoscientists that are intelligent, enthusiastic and have passion for discovery. That discovery may take many forms: what lies over the hill in the next outcrop, how to most effectively derisk an exploration play, using mineralogy to optimize metal recovery, using soil science to facilitate rapid re-vegetation, or how to best handle a local community's concerns about our activities in the nearby hills, for examples.

Educational programs of the future should produce intelligent graduates for employment in the mining business with a broad background. We are looking for people who have a track record, even in school, of significant achievements not only in their chosen field but across disciplines whether technical, social or cultural. We will train a chemist to be a geochemist, a physicist to be a geophysicist, a geologist to be an explorer, a mineralogist to be a metallurgist or an anthropologist to be a project manager. Interests and experiences outside of classic geology will be valued, as will out-of-the-box thinkers, and those who bring diversity in perspective and background. Finally, we

will value interpersonal and communication skills perhaps the most, because it is rare indeed these days to find an individual who has made a significant contribution without collaboration with others in a team setting, formal or informal.

## 4 CONCLUSIONS

So, we conclude that it is unlikely that any one of the three scenarios outlined will play out exactly as we describe. Nonetheless, we believe that there is an inevitable evolution taking place today that will most likely tend towards the Stealing with Pride scenario adapted to the mining industry. This will be further driven by consolidation of the industry during the next down cycle where majors will turn into super majors, who can afford to invest in the full value chain of mining geosciences, including education and training of its workforce. The junior and mid-tier sector will contract, and its geoscientists with good experience, background and values will re-join the majors, return to graduate school or re-supply the retiring faculty lines at the remaining economic geology programs and geoscience departments.

## ACKNOWLEDGEMENTS

The authors would like the reader to know that the views expressed herein reflect our personal opinions and are not the official views of Newmont Mining Corporation. However, we do acknowledge Newmont's support to express these views and participate in the SGA Dublin conference.

## REFERENCES

Etheridge, M.A., 2004, Research, exploration and predictive mineral discovery, *in proceedings of the Soc. Econ. Geol. 2004 Predictive Mineral Discovery Under Cover Symposium*, p. 31-34.

Hedenquist, J.W., Goldfarb, R.J., Goode, A.D.T., Hall, G.C., Hannington, M.D., Hitzman, M.W., Kesler, S.E., Lipson, R.D., Meinert, L.W., Sillitoe, R.H., and Thompson, J.F.H., Are there cutting-edge developments in research that can be applied to mineral exploration?, *in proceedings of the Soc. Econ. Geol. 2004 Predictive Mineral Discovery Under Cover Symposium*, p. 181-188.

Laznicka, P., 2006, Pre-, syn-, and post-geoscientific sources of industrial metals, in proceedings of the 12th Quadrennial *IAGOD Symposium, Moscow, August 21-24, 2006,* 4 p.

# Challenges and opportunities for teaching, research and employment in Economic Geology – A UK Higher Education Perspective.

Stephen Roberts
*School of Ocean and Earth Science, National Oceanography Centre, University of Southampton, Southampton,SO14 3ZH UK.*

ABSTRACT: Each year in the region of ~1100 students in the UK enter undergraduate degree programs within the broad field of Geoscience including Geology and Geophysics. The best graduates from UK Geoscience departments hold core geological skills, informed and accredited by Professional Societies and Agencies and a range of key skills, which significantly promote their employability. They take up careers within the mineral exploration, hydrocarbon, geotechnical and environmental sectors, education and non-geological graduate jobs. Whilst the UK graduate pool is but one of many available to the global mineral exploration industry, the high caliber and skills of many of these graduates appears to remain attractive. Although Geoscience is well represented in the courses offered by Research Intensive Universities in the UK, the situation is less rosy when a similar audit of researchers in the area of Economic Geology is considered. The lack of investment in Economic Geology Research presents a challenge for UK researchers to unite and increase the profile of their science. The challenge for Mineral Exploration companies is to nurture leading academics and ensure they are valued by their institutions and governmental organizations, a side effect of this support will be a continued supply of highly qualified Geoscientist wishing to enter careers in the mineral exploration industry.

KEYWORDS: Economic Geology, Education, Research

## 1 INTRODUCTION

Each year in the region of ~1100 students in the UK enter undergraduate degree programs within the broad field of Geoscience; this includes Geology and Geophysics. A significant proportion of these graduates eventually gain employment in the Mineral Resources sector. This paper investigates the numbers of students entering and graduating with Geoscience degrees in the UK, the skills these graduates possess and the employment opportunities available to them. Attention is then focused on Economic Geology research within the UK Higher Education (HE) sector, commenting on the current situation and recognizing some potential opportunities and pitfalls which may lie ahead. Finally the paper explores the linkages between research led teaching in Economic Geology and the future career aspirations of Geoscience undergraduates.

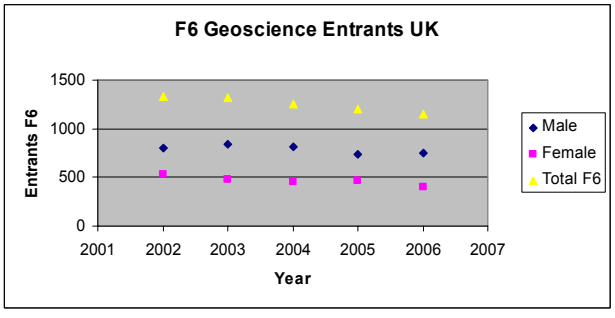


Figure 1. Entrants to UK Geoscience Courses. Source UCAS.

## 2 GEOSCIENCE IN THE UK

Successful applications to Geoscience (F6) Degree programs in the UK are typically in the region of 1100 candidates per year for the past 5 years, with the numbers declining by around 5% per year over the period 2001-2005 (Table 1; Figure 1). In overall UK terms this represents less than 0.5% of all candidates entering UK HE in a given year (336,938 in 2006; Table 1). The entrants, of which in the region of 60% are male, enroll in degree programs within one of the ~33 HE institutions in the UK which offer degrees in Geosciences. The Universities and

| Year | Male | Female | Total | Total UK |
|---|---|---|---|---|
| 2006 | 751 | 403 | 1154 | 336938 |
| 2005 | 740 | 467 | 1207 | 348848 |
| 2004 | 813 | 447 | 1260 | 320537 |
| 2003 | 835 | 484 | 1319 | 316242 |
| 2002 | 803 | 532 | 1335 | 309460 |

Table 1. UK Entrants. Source UCAS

ognized as traditional Geology and Geophysics programs but with one or two institutions now offering some less traditional pathways including Geology with Theatre Studies and Geology with Neuroscience. Importantly, Geology and Geophysics are offered by the majority of the UK Russell Group Universities, which is an association of 20 major research-intensive universities of the United Kingdom. In 2004/5, Russell Group Universities accounted for 65% (over £1.8billion) of UK Universities' research grant and contract income, 56% of all doctorates awarded in the United Kingdom, and over 30% of all students studying in the United Kingdom from outside the EU; it is these institutes that tend to attract the majority of the most highly qualified applicants.

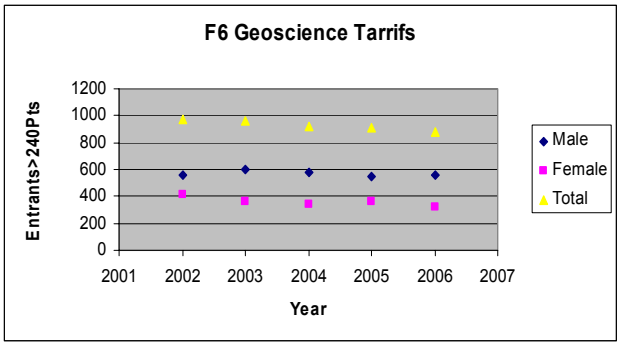


Figure 2. Number of candidates to UK Geoscience Courses with more than 240 UCAS Tariff Points

Although the total numbers of applicants to Geoscience courses has been in decline, this fall in numbers is less pronounced if the actual entry qualifications offered by candidates are taken into account. For example, by examining the number of candidates offering 240pts UCAS Tariff Points (CCC at A'level) and candidates offering >360 UCAS tariff points (AAA at A'level) the decline is typically only 1-2 % per year (Figure 2). This discrepancy may reflect that many UK HE Geoscience departments have been increasing their entrance grades over the past 5 years, removing a "tail" of less well qualified candidates. Nevertheless given a low drop-out rate, the UK can expect to graduate around 1000 Geoscientists in any given year.

## 3 SKILLS OF UK GEOSCIENCE STUDENTS

Whilst UK Universities and Geoscience departments seek to maintain their academic autonomy, subject and institutional academic review by the Quality Assurance Agency (QAA), an independent body funded by subscriptions from UK universities and colleges of higher education, Geological Society of London Degree accreditation and QAA subject centre "benchmark" statements, provide guiding principles as to the core cognitive and key skills expected of a UK geoscientist. For example, the Geological Society seek to accredit degrees which ensure that the qualifications achieved meet the academic requirements for election of Fellows and for validation of Fellows as Chartered Geologists by the Council of the Geological Society. In turn the QAA, through subject benchmark statements, expect Earth Science departments to produce well-rounded, flexible graduates capable of demonstrating proficiency not only in discipline-specific knowledge but also in the Graduate Key Skills. Furthermore in both QAA and Geological Society Accreditation fieldwork achieves a high priority with an expectation of in the region of 80 days fieldwork in a 3 year degree program. A major focus of Higher Education Strategy in the last 5 years has been in the development of graduates "Employability Skills" such as communication, teamworking, adaptability and flexibility, problem-solving, planning, organization, initiative and self awareness. Consequently, the best graduates form UK Geoscience departments should hold core geological skills, informed by the Geological Society and QAA, and a range

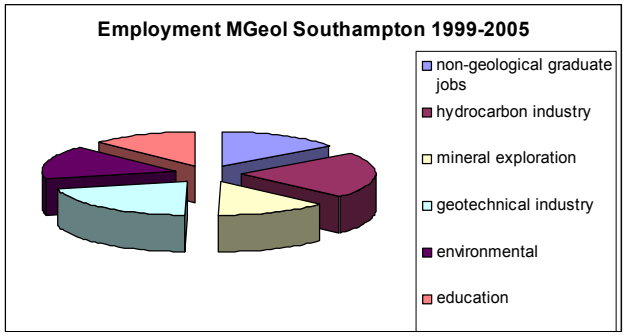


Figure 3. Employment destinations of Southampton Geosciences Graduates. Source SOES Programme Review 2006.

of key skills, which significantly promote their employability.

## 4 DESTINATIONS OF UK GEOSCIENCE GRADUATES

Employment of UK graduates overall is high ~96% and evidence suggests that this is reflected in a typical Geoscience cohort. Data for the Southampton MGeol program for the past 5 years shows a ~98% graduate employment rate and a high uptake of Geoscience careers with the predominant destinations including hydrocarbon, geotechnical and environmental sectors, education and non-geological graduate jobs and mineral exploration (Figure 3). There is little reason to suspect that these data are not typical of UK Geoscience employment trends. Recent surveys (2004) suggest that average starting salaries are typically in the region of £19,533 which is in line with average salaries of other subjects in Physical Sciences (Table 2); Southampton Geoscience graduates on average tending to earn more than other Russell club and non-Russell club universities.

Whilst the UK graduate pool is but one of many available to the global mineral exploration industry, the high caliber and skills of many of these graduates appears to remain attractive. However, a key challenge for the Mineral Exploration sector is to attract these high caliber students in a highly competitive market place. For example, the environmental and geotechnical companies have been a healthy recruiter of graduates for the past 10-15 years, at a time when the mineral exploration sector in particular was a moribund place for graduate employment. Nevertheless, it is now evident that many major companies are taking graduate recruitment seriously, with some established well developed and increasingly popular summer placement programs *e.g.* Rio Tinto and Anglo American.

| | Soton | Russell | Others |
|---|---|---|---|
| Subject | Average Salary | Average Salary | Average Salary |
| (F6) Geology | £19,533 | £16,298 | £17,005 |
| (F3) Physics | £19,380 | £20,840 | £17,493 |
| (F8) Physical Geog. | £15,034 | £16,598 | £15,481 |
| (G1) Mathematics | £20,800 | £20,688 | £18,482 |
| (G4) Computer Sci. | £23,409 | £22,034 | £18,194 |
| (H2) Civil engineering | £19,755 | £20,416 | £20,488 |
| (H3) Mechanical Eng. | £21,406 | £21,509 | £20,524 |
| (H4) Aerospace Eng | £22,197 | £21,081 | £19,554 |
| (H6) Electronic Eng | £22,965 | £20,301 | £18,689 |

Table 2. Average salaries UK Graduates 2004. Source HESA

## 5 ECONOMIC GEOLOGY RESEARCH, UK

Although the Russell group of Universities is well represented in a list of universities offering Geoscience Higher degrees, the situation is less rosy when a similar audit of earth science departments actively researching in the area of economic geology is concerned. Presently only 5 "Russell departments" are actively involved in mineral deposit studies meetings and economic geology research. There is also little evidence of a substantive recruitment of researchers in economic geology. In part the explanation for this lack of investment can be found in the impact factor of economic geology Journals.

Impact factors for *Mineralium Deposita* and *Economic Geology* are 1.45 and 1.17 respectively. These languish well below other Earth Science Journals such as *Geochimica et Cosmochmica Acta, EPSL* and *Geology* (See Table 3). Consequently, although a snapshot of publication in *Mineralium Deposita* for the year 2006, shows that the UK makes a significant contribution to the first author contributions, it is also noteworthy that significant research findings in mineral deposits research are to be found in other higher impact journals.

| Journal Title | Total Cites | Impact Factor | Articles |
|---|---|---|---|
| ECON GEOL | 4182 | 1.172 | 61 |
| MINER DEPOSITA | 1059 | 1.454 | 48 |
| ORE GEOL REV | 533 | 0.981 | 45 |
| GEOCHIM COSMOCHIM | 28126 | 3.897 | 413 |
| GEOLOGY | 14954 | 2.982 | 249 |
| EARTH PLANET SC LETT | 20325 | 3.434 | 436 |
| J STRUCT GEOL | 5095 | 2.109 | 144 |

Table 3. Journal Impact Factors. Source: Thompson ISI

Threats to the remaining active economic geology research centers in the UK arise in a variety of forms. Within the Research Assessment Exercise (RAE), to which all departments are subject, individual publication and research income are key metrics. Due to a variety of reasons, including the applied and industrial up-

take of material, the low citation and impact factor of economic geology articles and journals, the general perception of economic geology by senior mangers in the Higher education sector is poor.

Evolution of the RAE process offers even more profound challenges to economic geology research in the UK. Under the present RAE model, subject specialists are employed to review submitted manuscripts and comment on the impact in the field, this serves to negate the low impact and ciation of the submitted article. However, the new evaluation system will move to "metrics" where the impact factor of the journal, citations, research income and PhD students, will become major drivers. Given two candidates of similar caliber in the present research and funding environment and the perceived challenge of climate change, heads of department will invariably appoint a climate change researcher over an economic geologist especially given the former has the opportunity to publish in a higher impact journal gaining higher citation and with the opportunity for greater Research Council income.

Consequently, the challenge for UK academics is to unite and increase the profile of their science. The challenge for Mineral Exploration companies is to nurture leading academics and ensure they are valued by their institutions and governmental organizations; in the UK that is the Natural Environment Research Council.

## 6 RESEARCH LED TEACHING IN ECONOMIC GEOLOGY

Given the Global nature of Geoscience research and recruitment, an obvious strategy is to allow Economic Geology research to whither in the UK. However, the link between research-led teaching and the desire of high quality undergraduates to pursue careers in the mineral exploration industry should not be underestimated. Similarly, where UK Higher Education policy goes, other nations tend to follow and the threats recognized above could quickly materialize, if they have not already, in other parts of the academic world.

## ACKNOWLEDGEMENTS

Jim Andrews and Martin Palmer are thanked for reviews and feedback on this work.

## 8 REFERENCES

UCAS - http://www.ucas.com/

HESA - http://www.hesa.ac.uk/

Thompson…ISI
http://scientific.thomson.com/products/wos/

# Implications of electron backscatter diffraction study for interpretation of common sulphide mineral textures.

Alan P. Boyle, Craig D. Barrie & David J. Prior
*Department of Earth & Ocean Sciences, University of Liverpool, Liverpool L69 3GP, U.K.*

ABSTRACT: Interpretation of mineral textures is an important part of understanding any ore deposit. Currently, this mostly involves viewing polished surfaces using a reflected light microscope (sometimes with etching) coupled sometimes with collecting backscatter electron images in a scanning electron microscope and chemical maps using an electron microprobe and rarely with transmission electron microscopy. It is now possible, routinely, to collect crystallographic information at the sub-micron scale to an accuracy typically better than 1º using electron backscatter diffraction (EBSD). Crystallographic data acquired by EBSD help to constrain the interpretation of textures (primary and secondary), commonly providing solutions not contemplated using other analytical methods.

KEYWORDS: electron backscatter diffraction, sulphide, pyrite, texture

## 1 INTRODUCTION

Mineral textures provide the key information required for relating micro-chemical and microstructural-scale data to field scale data when attempting to understand the formation and evolution of an ore body. However, while the concept of textural interpretation is simple in theory, it is fraught with difficulty in practice. The opaque nature and cubic (or near cubic) crystallography of most of the commonly occurring sulphides make them difficult to study using traditional light-microscopy and scanning electron microscopy (SEM) methods, certainly compared to studying transparent, non-cubic, minerals like quartz or calcite. On top of this, many common sulphide minerals (*e.g*. galena, chalcopyrite, and sphalerite) are rheologically weak and easily modified. Their history is easily erased by recrystallisation, even at only slightly elevated temperatures. On the other hand, pyrite is relatively strong and refractory. It can preserve evidence from its primary formation right through to its near destruction in some orogenic environments; it is also the world's most abundant and probably most studied sulphide mineral. However, because pyrite is opaque and cubic, its inner secrets are not easily given up.

Around 10 years ago, the use of SEM-based electron backscatter diffraction (EBSD) and orientation contrast (OC) imaging was introduced to the ore deposits community at the Frank Vokes birthday celebration meeting in Trondheim (Craig 1998), with the paper on material from Sulitjelma, Norway, being published the next year (Boyle *et al*. 1998) Since then, the Liverpool Microstructural Group has advertised this technique at a range of meetings and recently published two more papers on pyrite textures (Freitag *et al.* 2004; Ohfuji *et al.* 2005), which demonstrate the utility of EBSD-derived crystallographic information for understanding problems of pyrite formation and modification. Steve Reddy has described a case study linking pyrite microstructure and trace element composition (Reddy 2005). The technique has now become mainstream in other areas of mineralogy, petrology, materials science and even palaeontology, but steadfastly refuses to be taken up by mainstream ore geologists; over 20 papers were published in 2006 by *Mineralium Deposita* alone in which petrographic interpretations of opaque mineral textures relied on just reflected light and/or SEM back-scattered electron imaging, sometimes with chemical element maps.

The purpose of this presentation is, there-

fore, to continue raising awareness of EBSD among the ore deposits community and to recommend caution in over interpreting textures in the absence of crystallographic information.

## 2 THE EBSD TECHNIQUE

In the mid-1990s, new developments allowed routine electron backscatter diffraction analysis to be completed on standard SEMs (though much of this work was completed in an SEM built specifically for EBSD, Fig. 1). The only requirement was the ability to tilt the polished specimen surface to an angle of 20º to the electron beam and to place a low low-light camera with a phosphor screen forward of the sample as shown in Fig. 1. The camera collects an electron backscatter pattern from a submicron spot, which software interprets in terms of crystallographic orientation generally to better than 1º. For pyrite, around 6 points per second can be analysed, allowing crystallographic maps to be built up quickly by automatically analysing an array of grid points. Solid state detectors placed above and below the camera collect atomic number contrast and orientation contrast images, respectively.

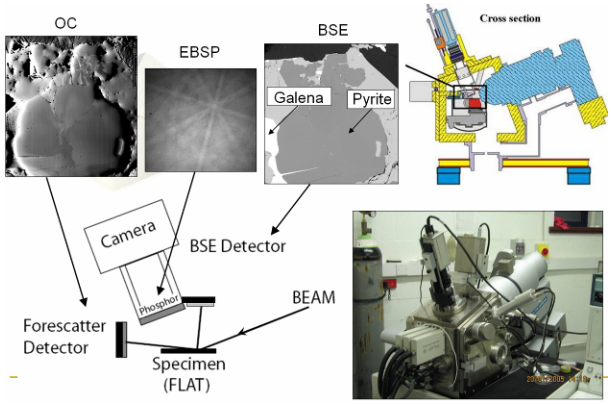


Fig. 1. Schematic for EBSD setup in CamScan X500 CrystalProbe. BSE detector obtains a standard atomic number contrast (BSE) image. Forescatter detector acquires an orientation contrast (OC) image. Phosphor screen collects an electron backscatter pattern (EBSP) imaged by the camera.

## 3 CASE STUDIES

Three example case studies are discussed. It has been generally accepted following the studies of Cox *et al.* (1981) and McClay and Ellis (1983; 1984) that during deformation, pyrite behaviour changes from more or less brittle to plastic at about 425ºC. Many authors have been guided by this when interpreting pyrite textures in rocks of known metamorphic grade (including one of the current authors: Cook *et al.* 1993), and some have even used it to determine metamorphic grade (*e.g.* Kuşcu & Erler 2002).

### *3.1 Case study 1 – annealing textures*

It is commonly assumed (*e.g.* Brown & McClay 1993; Tiwary e*t al.* 1998; Kuşcu & Erler 2002) that, in the absence of deformation, pyrite will anneal at temperatures above about 425ºC, leading to foam textures with 120º triple junctions as dislocations are swept out of the pyrite lattice and grain boundary migration occurs (*e.g.* RL image in Fig. 2). The OC image in Fig. 2 of a Sulitjelma massive pyrite ore, which experienced at least 520ºC metamorphism, demonstrates that while 120º triple junctions have developed, the pyrite grains have not annealed by removal of internal dislocations. They preserve internal strains involving up to 15º of <100> lattice rotation (see pole figures in Fig. 2). The grey scale variations shown in the OC image of Fig. 2 are analogous to wavy extinction in quartz; they are just invisible in reflected light and SEM/BSE imaging.

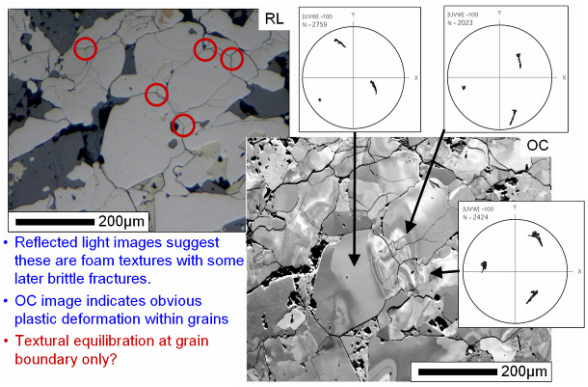


Fig. 2. Reflected light (RL) and orientation contrast (OC) images of massive pyrite ore, Sulitjelma, Norway. RL image shows pyrite grains with well-developed 120º triple junctions (circled). OC image of the same area has grey-scale variations indicating substantial intra-pyrite grain deformation, confirmed by <100> rotation girdles in pole figures.

### *3.2 Case study 2 – replacement textures*

Replacement or pseudomorphing of sulphide minerals by other sulphide or oxide minerals is commonly reported. The reflected light image in Fig. 3 shows small grains of pyrite in the cores of larger magnetite grains which in turn are enclosed in massive pyrite ore of grain size

similar to the magnetite grains. The simplest interpretation is, perhaps, that some of the massive pyrite ore grains have been replaced by magnetites and some relics of the original pyrite grain being preserved in the cores of the magnetites. The problem with this interpretation is that the inclusions within a particular magnetite host should all have the same (or at least very similar) crystallographic orientation. The three histograms in Fig. 3 summarise the minimum misorientation angles between adjacent pyrite inclusions (this means the minimum rotation required to make the two grains the same crystallographic orientation). The histogram distributions shown are close to theoretical random for cubes (Mackenzie 1958). Clearly the texture in Fig. 3 has not formed by a simple replacement process of three of the massive pyrite ore grains. Possible alternative explanations include:

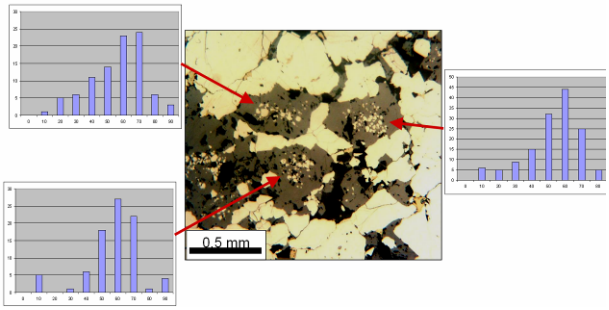


Fig. 3. Reflected light image of three magnetite grains hosting core regions of small pyrite grains, Sulitjelma, Norway. Histograms represent misorientation distributions between adjacent pyrite inclusions.

- Magnetite overgrows and partly replaces a fine grained massive pyrite ore, and then pyrite outside the magnetite continues to grow during annealing (*e.g.* Gu & McClay 1992).
- Massive pyrite ore is hydraulically fractured by an oxidising fluid resulting in local grain size reduction associated with oxidation of shattered pyrite to form magnetite.

Other evidence for amphibolite facies brittle and plastic deformation in the Sulitjelma ores favours the second explanation (Boyle *et al.* 1998).

### 3.3 *Case Study 3 – Low temperature plastic deformation of pyrite*

As mentioned above, it is commonly accepted that pyrite behaves in a brittle/cataclastic fashion below about 425ºC. Freitag *et al* (2004) have documented plastic deformation in pyrite from the Green's Creek, Alaska, deposit at about 350ºC. The Gjersvik deposit, Norway, experienced about 420ºC (Cook & Hoefs 1997) during metamorphism, but preserves thoroughly plastically deformed massive sulphide ores rather than the expected brittle-ductile transition type textures (Fig. 4).

## 4 CONCLUSIONS

The three case studies are representative of much wider studies being undertaken by the authors, and demonstrate the very real likelihood that pyrite and other sulphide textures may be systematically misinterpreted in the absence of information about the crystallography of the minerals. This information can now be obtained in a routine way in a suitably equipped SEM, and should become more widely used by the ore deposits community.

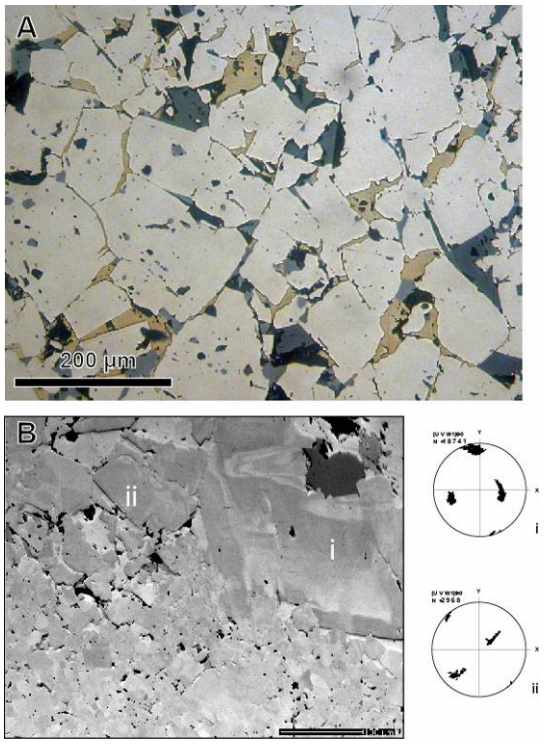


Fig. 4. A. Reflected light image of massive sulphide ore with subhedral pyrite blasts (Gjervik, Norway). B. Orientation contrast view of Gjersvik massive sulphide ore illustrating grey scale variation within large pyrite blasts (scale bar is 100 µm). <100> pole figures demonstrate plastic lattice rotation deformation in grains i and ii in B.

## REFERENCES


Boyle AP, Prior DJ, Banham MH, and Timms NE (1998) Plastic deformation of metamorphic pyrite: new evidence from electron-backscatter diffraction and forescatter orientation-contrast imaging. *Mineralium Deposita* 34: 71-81

Brown D, and McClay KR (1993) Deformation textures in pyrite from the Vangorda Pb-Zn-Ag deposit, Yukon, Canada. *Mineralogical Magazine* 57: 55-66

Cook NJ, Halls C, and Boyle AP (1993) Deformation and metamorphism of massive sulphides at Sulitjelma, Norway. *Mineralogical Magazine* 57: 67-81

Cook NJ, and Hoefs J (1997) Sulphur isotope characteristics of metamorphosed Cu---(Zn) volcanogenic massive sulphide deposits in the Norwegian Caledonides. *Chemical Geology* 135: 307-324

Cox SF, Etheridge MA, and Hobbs BE (1981) The experimental ductile deformation of polycrystalline and single- crystal pyrite. *Economic Geology* 76: 2105-2117

Craig JR (1998) Frank M. Vokes Symposium. *Mineralium Deposita* V34: 3

Freitag K, Boyle AP, Nelson E, Hitzman M, Churchill J, and Lopez-Pedrosa M (2004) The use of electron backscatter diffraction and orientation contrast imaging as tools for sulphide textural studies: example from the Greens Creek deposit (Alaska). *Mineralium Deposita* 39: 103-113

Gu L, and McClay KR (1992) Pyrite deformation in stratiform lead-zinc deposits of the Canadian Cordillera. *Mineralium Deposita* 27: 169-181

Kuşcu İ, and Erler A (2002) Pyrite deformation textures in the deposit of Küre mining district (Kastamonu-Turkey). *Turkish Journal of Earth Sciences* 11: 205-215

Mackenzie JK (1958) Second paper on statistics associated with the random disorientation of cubes. *Biometrika* 45: 229-240

McClay KR, and Ellis PG (1983) Deformation and recrystallization of pyrite. *Mineralogical Magazine* 47: 527-538

McClay KR, and Ellis PG (1984) Deformation of pyrite. *Economic Geology* 79: 400-403

Ohfuji H, Boyle AP, Prior DJ, and Rickard D (2005) Structure of framboidal pyrite: an electron backscatter diffraction study. *American Mineralogist* 90: 1693-1704

Reddy S (2005) *Microstructural controls on trace element variability in ore minerals* Oxford Instruments, p. 6.

Tiwary A, Deb M, and Cook NJ (1998) Use of pyrite microfabric as a key to tectono-thermal evolution of massive sulphide deposits - an example from Deri, southern Rajasthan, India. Mineralogical Magazine 62: 197-212

# COMPRESSIONAL TECTONICS, EXPANDING RESOURCES: EXPLORATION ADVANCES IN THE TETHYAN BELT

EDITED BY:

VERTREES "MAC" CANBY

DUNCAN LARGE

FERENC MOLNÁR

ROBERT MORITZ

# Geodynamic causes of copper and gold concentrations in the Tethys belt

Andor L.W. Lips
*BRGM - Mineral Resources Division; 3, avenue C. Guillemin, BP36009, 45060 Orléans cedex 2, France;*

ABSTRACT: A review of the spatial and temporal distribution of different styles of mineralization along the 5,000 km long Cretaceous-Tertiary Tethys belt highlights the heterogeneous appearance of copper and gold in space and time. It can be estimated that the Alpine-Tethys Belt has been hosting over eighty million tonnes of copper metal and nearly seven thousand tonnes of gold metal. Many different styles of copper- and gold-bearing ore deposits have formed during three dominant periods of the overall northward motion of Africa and Arabia during the last 100 Ma. Progressive closure of the Tethys oceanic basins occurred through multistage subduction, obduction, accretion, and syn- to post-orogenic extension processes along the active margin of southern Eurasia. The geodynamic evolution has produced different characteristic frequencies and amplitudes in the distribution of copper and of gold concentrations along the Tethys belt.

KEYWORDS: Tethys belt, copper, gold, ore deposit, geodynamics

## 1 INTRODUCTION

It appears that ore deposits form at times of a destabilized orogen, an uncomfortable orogen, in which changing plate motions, plate reorganisation, slab roll-back, slab break-off, orogenic collapse, and/or other lithosphere-scale effects are contributing to a transient state of its thermal configuration and its stress distribution (Lips 2002). As it appears that ore deposits have formed in these transient geodynamic settings how well do we know what happened exactly? How to track down the chain of processes translating initial cause of continent-scale geodynamic processes to the final consequence of ore deposit formation? The transient settings are often poorly recorded in the regional tectonic memory and processes pre- and post-dating the "true" event may become misidentified as the deposit's controlling process.

This paper provides an overview on copper and gold concentrations in the Tethys convergent margin setting at a plate-scale resolution. The discussion focuses on the 100 Ma to Recent development of the Tethys belt with some comparison to similar scale convergent margin settings like the southwest Pacific or the Andes. Earliest studies with similar objectives (Dixon & Perreira, 1974; Jankovic, 1977) already showed that the location of a variety of mineral deposits in specific tectonic settings could be related to the development of the Tethyan region.

## 2 A COMPARISON OF THE TETHYS, ANDES, AND SOUTHWEST PACIFIC

The Tethys belt, Andes and Southwest Pacific clearly differ in size, in duration of subduction, in inherited tectonic geometry, in exploration history, and in metal potential.

The Andes, over 4 million km$^2$, developed during long-lasting subduction along the western margin of the South America continent (and the margin of Gondwana) and hosts a dozen world class deposits of Au (>300 tonnes), and of Cu (> 10 Mt).

The development of the Southwest Pacific, circa 18 million km$^2$ (including seas), dominantly involved Tertiary ocean arc subduction, has not yet achieved the stage of continent-continent collision, and hosts 5-10 world class and large deposits of Au (100-400 tonnes and Grasberg > 1000 tonnes), and of Cu (> 0.5 Mt).

The Tethys belt (figure 1), over 5 million km$^2$, developed during late Cretaceous-Tertiary

subduction along the southern margin of the Eurasian plate, subsequent continent-microplate interaction, minimal present-day subduction and syn- to post-collision extension, and hosts a dozen large deposits of Au (> 200 tonnes), and of Cu (1-8 Mt).

In summary the three belts show remarkable differences for total copper contents, and remarkable similarities in total gold metal contents (Table 1).

| | Total Copper | Total Gold |
|---|---|---|
| Andes | > 580 Mt | > 6 kt |
| SW Pacific | > 25 Mt | > 4 kt |
| Tethys | > 80 Mt | > 6.5 kt |

Table 1. Copper and gold metal contents in the Andes, SW Pacific and Tethys belts (based on available public company and literature data).

What is the relation between the observed copper and gold metal volumes and the duration of subduction, the inherited tectonic setting (*e.g*. presence, absence of continental fragments in the overriding plate), the different exploration histories and cultural heritage, or the secondary processes related to the primary process of subduction ?

## 3 IDENTIFICATION OF PRESENT AND PAST GEODYNAMIC SETTINGS

Information about the present-day situation in relation to ore deposit formation is dominantly obtained from: (i) seismic epicentre distribution and seismic tomography, revealing processes currently acting in the lithosphere, (ii) outcrop patterns, giving insight in the erosion level, and (iii) space-geodetic measurement campaigns concerning the present-day crustal motions. Information about the past is obtained from: (i) the establishment and evolution of magmatic arc systems from the late Mesozoic to the Pliocene, (ii) subduction processes giving insight in the relative direction and rate of plate motions, (iii) traces of large-scale fault structures, and (iv) the distribution and characteristics of the ore deposits.

Geophysical observation tools (seismics, seismic tomography, gravimetry *etc.*) allow us to investigate the present day geometry of the lithosphere. The application of seismic tomography may allow to estimate the age of the subduction system at the present active margin and to back-track secondary processes (*e.g*. roll-back, slab break-off) related to the subduction history in the last 10 to 20 million years. Such observation techniques are highly appreciated in the assessment of a region with young mineral deposits (*e.g*. SW Pacific). In older systems, the elucidated processes often remain speculative as the related crustal reflection of these lithosphere-scale processes are not significantly recovered.

Slab break-off has been proposed as a major factor in the generation of magmas and mineralization in the Balkan, but a true link between slab break-off and mineralization has not been significantly established yet (Lips, 2002). Slab break-off has been proposed by independent geophysical, tectonic and geochemical studies for the Miocene-Quaternary Carpathian volcanic belt, host to significant mineral deposits. Integration of the geochronology data reconfirms the NW to SE progression of volcanism along the belt during gradual detachment of the subducting slab. In contrast, the main timing of the mineral deposits does not follow this trend (Neubauer *et al.* 2005).

Characterization of the magmatic history (by integrating geochemical, geophysical, and geological observations) appears to remain the better approach to examine the intermediate steps between the lithosphere-asthenosphere interaction and ore deposit formation. Magmatic and hydrothermal histories potentially resolving differences in subduction related signatures, mantle contributions and/or crustal contaminations remain a crucial link in the identification of the geodynamic control on ore deposit formation.

## 4 GEODYNAMICS AND ORE DEPOSIT EVOLUTION IN THE TETHYS BELT

A review of the spatial and temporal distribution of different styles of mineralization along the 5,000 km long Cretaceous-Tertiary Tethys belt highlights the heterogeneous appearance of copper and gold in space and time. Based on available information regarding past production, reserves, and resources of the main known mining districts, it can be estimated that the Alpine-Tethys Belt has been hosting over 80 million tonnes of copper metal and approximately 7 thousand tonnes of gold metal.

Copper- and gold-bearing ore types include VHMS, Cu-(Au) porphyry, skarn, mesothermal vein and replacement base metal and gold de-

posits, sediment-hosted gold, diatreme-hosted gold, IOCG, and high- and low-sulphidation type epithermal deposits. The deposits have formed during different stages of the overall northward motion of Africa and Arabia during the last 100 My resulting in the progressive closure of the Tethys oceanic basins through multistage subduction, obduction, accretion, and syn- to post-orogenic extension processes along the active margin of southern Eurasia.

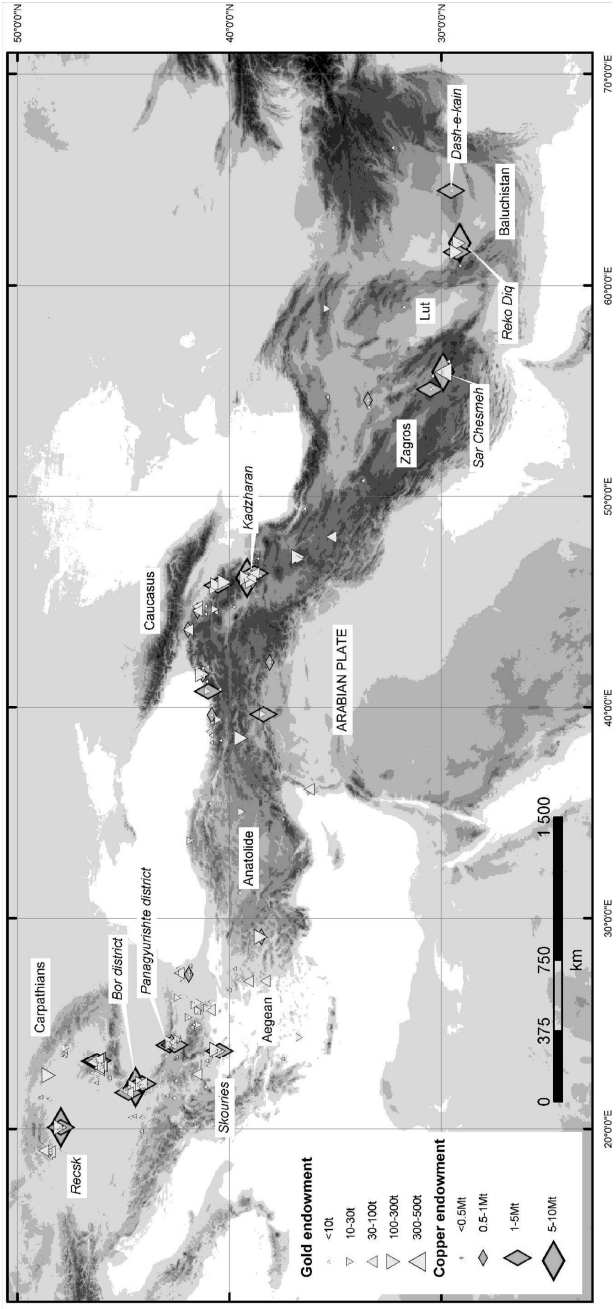


Figure 1. Overview of main copper and gold bearing deposits in the Tethys belt.

Compared to the Andes and SW Pacific, subduction rates along the Tethys margin have always been very low at about 10 to 20km per million years, 10 to 20 % of Pacific subduction rates. As a consequence less oceanic lithosphere has been consumed at the convergent margin and less internal friction was present in the orogenic wedge.

The most fertile successive periods can be assigned to characteristic tectono-magmatic stages in the overall convergent setting:

i) Late Cretaceous: development of a subcontinuous, diachronous volcanic island arc stretching from Romania to Iran, characterised by both submarine (VHMS deposits) and subaerial hydrothermal activity (magmatic-hydrothermal mineralization);

ii) Palaeogene: extensive post-collisional calc-alkaline and shoshonitic magmatism from Central Europe to Eastern Iran, the end of this period (late Eocene-Oligocene) being marked by epithermal to mesothermal gold and porphyry mineralization, with the main mineralized domains locally controlled but aligned according to the overall architecture of the entire belt; and,

iii) Neogene: discontinuous magmatic activity with some subduction affinity in the stages of collapse of the orogenic wedge in the overriding plate, and related epithermal gold and Cu-(Au) porphyry mineralization. (Carpathians, Aegean region, Baluchistan), and Carlin-type gold (NW Iran; Lescuyer *et al.*, 2003).

The superposition of mineralization associated with the above three periods has resulted in the appearance of gold and copper mining district distributions with different characteristic frequencies and amplitudes:

i) Late Cretaceous records 35% Cu and 20% Au. Gold and copper concentration associated with Cu-(Au) porphyry and epithermal gold deposits or VHMS deposits in Serbia (Bor district), Bulgaria (Panagyurishte and, less, east Bulgaria), and northeast Turkey, associated with Andean-style subduction, initiated by N-S Europe-Africa convergence since 100 Ma.

ii) Palaeogene records 16% Cu and 22% Au in many different ore deposit types mostly dominated by gold and some with minor copper all across the Tethys belt. Moderate convergence rates, post

collision volcanism after first collage of blocks with continental lithosphere, and reorganization of the orogenic wedges on the convergent margin characterize settings of these deposits.

iii) Neogene records 50% Cu and 58% Au, in Cu-(Au) porphyry and epithermal gold deposits, more rich in gold than the Cretaceous deposits (dominantly in Romania, Iran, Armenia, Aegean region). Stagnant to absent convergence in collapse of orogenic wedges. Most dominant collapse areas determined by free tectonic boundaries (Aegean and Carpathian arcs, south Lut in Iran) or accommodated by large transfer systems (eastern margin of Arabia block).

ACKNOWLEDGEMENTS

The author acknowledges contributions from Jean-Luc Lescuyer (now at Areva) to previous investigations. Encouragement by Antonio Arribas to submit the manuscript have been much appreciated. Editorial comments from Ferenc Molnár have helped to improve the document.

REFERENCES

Dixon, C. J. and J Pereira (1974) Plate tectonics and mineralization in the Tethyan region. *Mineralium Deposita*, 9, 185-198.

Jankovic, S. (1977) The copper deposits and geotectonic setting of the Tethyan Eurasian metallogenic belt. *Mineralium Deposita,* 12, 37-47.

Lescuyer J.L., A. Hushmand Zadeh, F. Deliran (2003) Gold metallogeny in Iran: a preliminary review. *Mineral Exploration and Sustainable Development* (Eliopoulis et al., eds.), Millpress Rotterdam, pp 1185-1188.

Lips, A.L.W. (2002) Cross-correlating geodynamic processes and magmatic-hydrothermal ore deposit formation over time; a review on southeast Europe. In: Blundell D, Neubauer F, von Quadt A (eds) *The timing and location of major ore deposits in an evolving orogen.* Geological Society, London, Special Publications, 204, pp 69-79.

Neubauer, F, A.L.W Lips, K. Kouzmanov, J. Lexa, P. Ivascanu (2005) Subduction, slab detachment and mineralization: The Neogene in the Apuseni Mountains and Carpathians. *Ore Geology Reviews,* 27, 13-44.

# A brief review of metal discoveries in the Tethyan belt since 1992

Vertrees M. "Mac" Canby
*Phelps Dodge Exploration Corporation, Cobham, United Kingdom*

ABSTRACT: Since 1992, copper and gold deposits overwhelmingly dominated both value and number of new discoveries, or resource expansions, in the Tethyan metallogenic belt. Nearly all of the raw, in-ground value of deposits with resources, and those considered likely to generate resources in the near future (representing an aggregate of roughly $78 billion at $2200/t Cu, $10,000/t Ni, $500/oz Au, $10/oz Ag and $1100/t Zn), is contributed by magmatic-related systems, namely porphyry CuAu deposits, and porphyry- and diatreme-related low-sulphidation epithermal (LSE) or transitional porphyry-low-sulphidation AuAg deposits. The dominance of gold deposits both in number and to a lesser extent in value reflects the application of bulk-minable gold deposit models, long-term price increases, and heap-leach process technology, while the dominance of Cu is attributable to the large tonnages of porphyry systems and the presence of one giant deposit cluster (Reko Diq). Notably absent are significant additions to PbZn(Ag) resources due a hiatus in price and unstable regional politics; absent are large Ag-dominant epithermal systems; and, in particular contrast to discovery history in the Pacific rim, absent are new giant high-sulphidation epithermal (HSE) systems. While the frequency of discovery of porphyry deposits continues, individual deposit size has so far not exceeded ~300Mt since the discovery of Reko Diq cluster in 1993-1998.

KEYWORDS: Tethyan, metal, discoveries, review

## 1 INTRODUCTION

Tethyan metallogeny has historically been well-rounded, including a spectrum of metal deposits associated with both diverging and converging plate boundaries. Historic production and early discoveries spanned the range of large PbZn(Ag) metasomatic and vein deposits associated with both Tertiary magmatism and regional metamorphism in the Balkan peninsula, as well as 'Irish-type' sediment-hosted PbZn deposits in central Iran, representing tensional Tethyan tectonism. Also historically mined were low-grade, supergene-upgraded Fe deposits likely related to early rifting (extension) stages such as at Kremikovtzi (other examples may be Ljubija in Bosnia, Rudabánya in Hungary), Bulgaria, as well as the giant Hg deposits of Triassic age at Idrija, Slovenia. Significant historic copper production came from oceanic spreading-related deposits in Jurassic ophiolites in Cyprus. In contrast, exploration success since 1992 has been dominated by gold and copper discoveries largely related to compressional tectonics, dominantly of Tertiary age

Data from seventy-seven metal deposits and prospects explored during 1992-2007 include all of the largest deposits discovered (or expanded) throughout the period, as well as information from numerous minor deposits and prospects. For this study, where official resource calculations are not yet available, rough estimates of potentially-economic contained metal are made based on drilling and other geologic data largely taken from company press releases or other public sources. The exploration projects considered range from genuine new discoveries, to resource expansions in previously-known resources or mines. Discovery of 'new' Au and Cu prospects and deposits ranges from many where ancient mining had occurred but where state-run economies delayed the flood of discoveries made in exploration booms elsewhere (Ada Tepe, Bulgaria) to those where other

commodities were previously recognized (alunite at Kisladag, Turkey; antimony at Sary Gunay, Iran; Richards *et al.*, 2007) to those where no significant pre-discovery occurrences were documented (Perama Hill, Greece). Notably, 65% of the projects explored were new targets, and they contributed roughly 80% of the discovery-added value, in contrast to ~20% contributed by deposit extensions. Discovery data are strongly influenced by access to published material released by explorers, often junior exploration companies whose reporting requirements and incentives contrasts with those of major companies or government institutions. The influence of metal price trends and favorable exploration and mining environments is evident in the discovery timing, discovery rate, and metal affinity of the explored prospects. Turkey, with its combination of complex geology and relatively favorable and stable business climate, accordingly accounts for roughly 40% of the total number of explored projects, although the related metal value contribution is about 16%.

## 2 METAL AFFINITIES OF THE NEW DISCOVERIES

Total gross in-ground value of the contained, discovered metal is nearly equally distributed between Cu (accounting for 48% of value) and Au (49%), with Ni, Zn+Pb and Ag making up about 1% each. Roughly 65% of the targets were explored dominantly as AuAg targets.

| Deposit type | Explored targets, % of total explored | % value in deposit class | Largest in class; % of total new Tethyan metal value |
|---|---|---|---|
| Porphyry | 25 (32%) | 75% | Reko Diq (48%), Skouries (~6%), Xietongmen (~6%), Colnic-Rovina?(~4%), Kizilviran?(~4%), Kisladag (~3%) |
| LSE/ISE | 23 (30%) | 14% | Rosia Montana (9.5%); Sary Gunay (~2%) |
| HSE | 16 (21%) | 2% | Perama Hill (~1%) |
| VMS | 5 (~5%) | 1% | Çayeli (<1%) |
| Other Au | 6 (~6%) | | |
| Laterite | 1 (~1%) | | Çaldag |
| Other | 1 (~1%) | | |

Table 1: Summary characteristics of 77 exploration projects from the Tethyan metallogenic belt during 1992-2007

## 3. DEPOSIT TYPES DISCOVERED, 1992-2007

Porphyry deposits dominate the contained discovered metal during the time period, accounting for 75% of the contained value. Of these, the Reko Diq deposit cluster, at ~2.5Bt of 0.51%Cu 0.27g Au, contains roughly 48% of the metal value, and is by far the largest metal accumulation in the metallogenic belt. LSE deposits contain 14% of the metal value, while HSE deposits contain only 2%, and only 1% resides in both VMS or lateritic Ni discoveries. Ag occurs entirely as a by-product of low-sulphidation Au deposits, porphyries, and VMS deposits. Notably, despite their large size and often distinctive alteration zoning, new porphyry occurrences of both CuAuMo (Xietongmen, Tibet; Halilaga, AS, Kizilviran, Turkey; Ilovitza, Macedonia) and Au-only affinity (Byeli Vrch, Slovakia) continue to be found with frequency in the Tethyan belt, although the cumulative metal content of these new discoveries still lags that of Reko Diq. Although the Yulong deposit has been known since at least the 1980s, discovery history and timing of other Tertiary porphyry systems of the Gangdese and Yulong CuAuMo(PbZn) belts of the eastern Tethys in Tibet is not clear. Recent discovery of the significant Xietongmen deposit indicates that more porphyry discoveries are likely.

Four large bulk-minable, magmatic-related gold deposits, of low-sulphidation (Rosia Montana, Romania; Sary Gunay, Iran), porphyry (Kisladag) and porphyry-centered carbonate-hosted affinity (Çopler, Turkey) contribute most of the Au-specific mineralization of the region. Numerous smaller low-sulphidation deposits, dominantly vein stockworks, account for a large number of AuAg occurrences, frequently of high grade but typically containing $\leq$1Moz. These comprise both magmatic-related systems (*e.g.* deposits of western Turkey), as well as deposits lacking clear magmatic origins and possibly related to formation of metamorphic core complexes as in the Rhodopes Mountains of Bulgaria (Ada Tepe; Dimitrov, 2007). In common with evolution of other low-sulphidation epithermal districts (Esquel, Argentina; Midas, Nevada; El Penon, Chile), further determined exploration in these districts will likely result in discovery of blind bonanza ore shoots. High-sulphidation epithermal deposits are numerous (comprising

~21% of the projects explored), but despite their historic significance at the Bor and Chelopech CuAu deposits, they contributed little metal during recent exploration. Nonetheless, exploration histories in the Tethyan belt and elsewhere show that, in common with the Maricunga belt of Chile, even weakly-mineralized remnants of HSE lithocaps may be proxies for adjacent porphyry CuAu or Au systems as at Kisladag (Turkey), Halilaga (Turkey), Recsk (Hungary) and Ilovitza (Macedonia).

Combined high nickel prices, and development of heap-leaching technology as at Çaldag, Turkey, will encourage exploration and re-evaluation of known laterite deposits throughout the numerous ophiolite belts of various ages within the Tethyan belt. Confinement of these deposits to areas which have uneroded (and by their nature, relatively thin) laterite horizons suggests that future resource additions will be relatively small.

## 4 CONCLUSIONS AND FUTURE TRENDS

The current trend of Cu and Au dominance in Tethyan-related metal discoveries is likely to continue, but will likely see expansion as exploration resumes for both metasomatic carbonate-replacement ZnPbAg deposits related to Tertiary magmatism, as well as Irish- and MVT-type deposits in Mesozoic basins.

Bonanza-grade, blind LSE vein AuAg discoveries will likely be made in new districts as well as established LSE districts. New HSE AuAg(Cu) deposits may be recognized within the relatively immature eastern Tethyan belt, where significant CuAu(Mo) porphyry deposits have already been discovered.

## ACKNOWLEDGEMENTS

The author gratefully acknowledges Dr. Feri Molnar for comments on the manuscript, and the useful input of Dr. Ozcan Yigit on Turkish discoveries.

## REFERENCES

Corser, P.G., Gossage, B.L., Lattanzi, C.R., Marek, J.M., Smith, S. (2006) Technical Report on the Rosia Montana Gold Project, Transylvania, Romania. Gabriel Resources website www.gabrielresources.com

Dimitrov, D. (2007, this volume) Low-sulphidation 'non-magmatic epithermal AuAg deposits of the eastern Rhodopes mountains, Bulgaria.

Janković S (1990) The Ore Deposits of Serbia: Regional metallogenic settings, environments of deposition and types. *Mining and Geology Faculty Belgrade.* 760

Richards, J.P., Wilkinson, D., Ulrich, T. (2007) Geology of the Sari Gunay Epithermal Gold Deposit, Northwest Iran; *Economic Geology*: 101, 1455-1497.

# The Atlas zinc-lead province and analogies within the Tethyan zinc belt

Neal A. Reynolds & Wallace Mackay
*CSA Australia*

The Atlas district from Morocco through Algeria to Tunisia hosts very extensive zinc-lead mineralization, mainly in carbonate rocks, though few large deposits are known to date. Mineralization is related to fluid flow accompanying Miocene deformation and uplift, with deposits hosted in rocks from Triassic to late Miocene age. The Atlas province forms part of the Tethyan zinc belt which encompasses several large and globally significant zinc provinces from the Mediterranean to China. The belt includes atypical carbonate-hosted deposits, including deposits with likely input from magmatic systems formed within foreland thrust belts. The Atlas is no exception, and Miocene zinc-lead mineralization was approximately synchronous with alkaline bimodal volcanism and associated gold-polymetallic mineralization. Despite a long mining history, the Atlas district like much of the Tethyan belt has had limited exploration and still holds high potential for new world-class discoveries.

KEYWORDS: zinc, Atlas, Tethys, carbonate-hosted

## 1 THE ATLAS ZINC PROVINCE

Extensive carbonate-hosted zinc-lead mineralization in the Atlas orogen from Morocco through Algeria to Tunisia has been exploited since Phoenician and Roman times. The Tertiary Atlas orogeny resulted from collision of the passive African margin with a northerly-derived arc terrain, driven by subduction roll-back (Rosenbaum *et al,* 2002), culminating in thin-skinned thrust imbrication and emplacement of deep-water flysch nappes over the carbonate platform in the mid- to late-Miocene. The arc terrain encompasses the Kabylie in Algeria, the Rif in Morocco and the Betic in southern Spain.

Most known deposits in the Atlas province are small, the largest being Touissit – Bou Beker – El Abed on the Morocco-Algeria border (Fig. 1), with an estimated global resource of *c.* 67 Mt at 7% Pb and 3% Zn. The Bou Grine deposit in Tunisia with an estimated global resource of 7.3 Mt at 9.7 % Zn and 2.4 % Pb was the most significant modern discovery. The mine was put into production by Metall Mining Corp in 1992 and was subsequently operated by Breakwater Resources from 1997 until closure in 2005.

Much of the zinc-lead mineralization in the Atlas district is hosted in Jurassic-Cretaceous platform carbonate rocks deposited on the southern passive margin of Tethys, overlying rift- to sag- phase sediments including Permian red-beds and Triassic evaporites. Triassic halites were mobilised as fault-controlled diapers by successive extensional and compressional loading events in the Cretaceous and Tertiary. Significant mineralization also occurs in syn- to post collisional Tertiary sediments, including lacustrine carbonates and calcareous sandstones deposited in pull-apart basins within the thrust belt, as well as in Tertiary volcanics.

Relationships between Miocene- and Cretaceous-hosted mineralization in northern Tunisia clearly demonstrate that a major zinc-lead mineralizing event occurred in the mid- to late-Miocene. There is no compelling evidence for an earlier Cretaceous mineralizing event. Neogene zinc-lead mineralization was synchronous with post-collisional alkaline volcanism along the northern margin of the Atlas orogen, within and south of the northerly derived arc terrain.

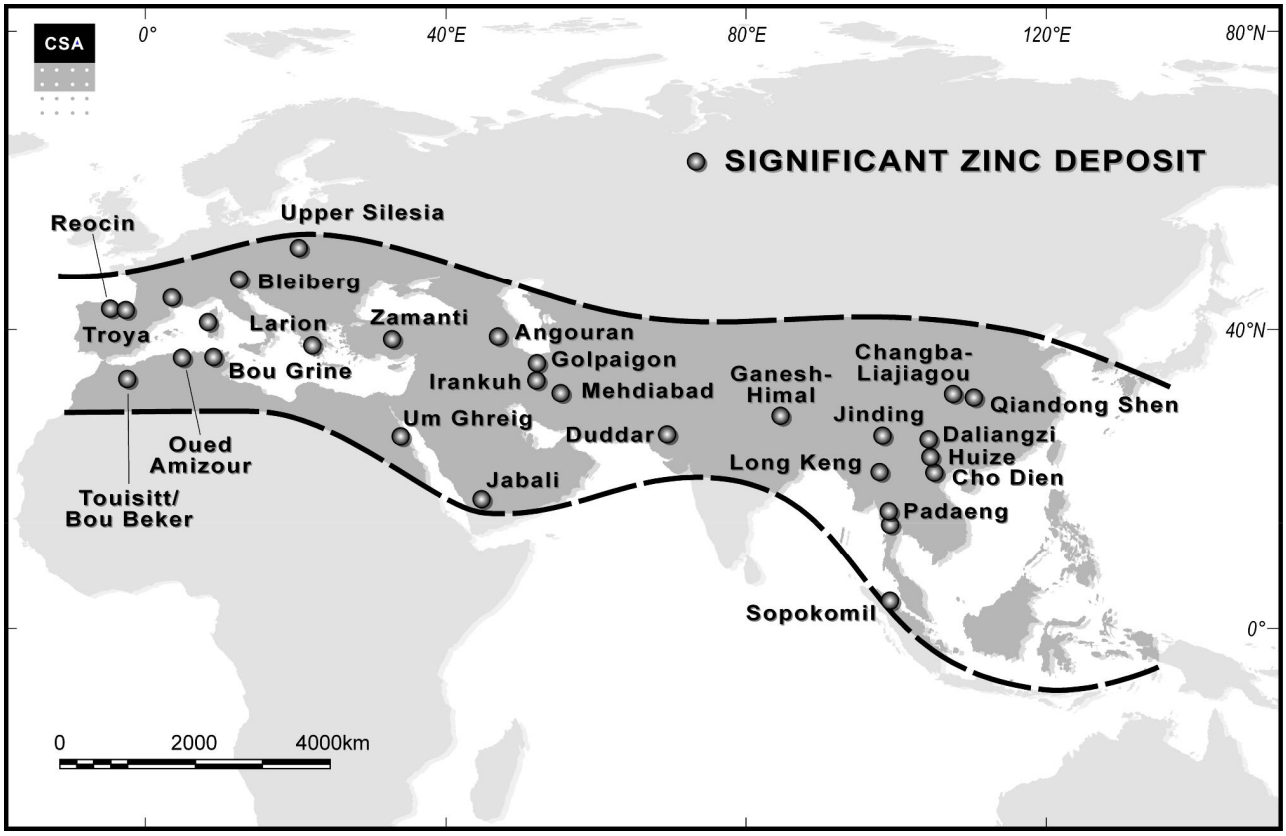


Figure 1. Significant zinc deposits within the Tethyan zinc belt

Gold-copper-polymetallic mineralization occurs within the volcanic terrain, and at Oued Amizour in Algeria a substantial zinc-lead deposit (*c.* 30 Mt at 5.5% Zn, 1.4% Pb) is hosted by mid-Miocene rhyo-dacitic volcanics.

Miocene zinc-lead mineralization across the Atlas belt can be related to large-scale mobilisation of basinal brines driven by tectonic compression, loading, and uplift. Fluid systems were variably influenced by synchronous magmatism, and fluid chemistry was variably influenced by interaction with Permian red-beds and Triassic evaporites, leading to a range of hybrid deposit chemistry and styles.

Zinc-lead deposit style was influenced by host rocks, with stratabound-replacement deposits forming in reactive, permeable Neogene sediments, and more typical dissolution- and structurally controlled styles occurring in well-lithified Jurassic-Cretaceous carbonates.

## 2 THE TETHYAN ZINC BELT

The Atlas forms a small part of the Tethyan zinc belt (Fig. 1) which encompasses several large and globally significant zinc provinces from the Mediterranean to China, including the Basque-Cantabrian basin (Réocin), Silesia, Iran (Angouran, Mehdiabad), Western Thailand (Padaeng) and Southwest China (Jinding, Daliangzi).

The Tethyan belt is an important repository for zinc-lead deposits as a result of its evolutionary history. Successive rifting events on the northern margin of Gondwana from the Devonian to the Cretaceous resulted in a succession of Tethyan 'oceans' in a broadly circum-equatorial setting, which closed through northward drift and collision of the rifted terranes with Laurussia and Laurasia.

Early Permian rifting in northern Gondwana marks the commencement of the most significant zinc metallogenic cycle, and initiated the break-up of Pangea. Rifting migrated eastward and broad Jurassic to Cretaceous carbonate shelf and marginal-basin sequences were deposited. The thick carbonate sequences provided ideal trap settings when zinc-lead mineralizing hydrothermal fluid flow was initiated by Tertiary inversion, collision, and uplift on the Tethyan margins.

While many of the Tethyan zinc-lead districts slot into the MVT basket, such as Silesia, the belt also includes atypical carbonate-hosted deposits, as is seen in the Atlas. High-level Miocene mineralization at Angouran affects a

basement core-complex and Oligocene-Miocene sedimentary-volcanic cover and straddles a transition from sulphide to hypogene oxide mineralization with evidence of magmatic input (Gilg *et al,* 2003). Angouran occurs within a belt of Miocene compression related mineralization in the central Zagros belt which also includes Irankuh and Mehdiabad. Jinding in Yunnan occurs in a similar thrust-belt setting, hosted in lacustrine carbonates and carbonate-cemented fanglomerates in a syn-orogenic basin in the Himalayan foreland (Kyle & Li, 2002).

The Padaeng deposit in Thailand and the deposits of the Yunnan-Sichuan-Guizhou triangle in SW China (*e.g*. Daliangzi, Huize) are high-grade deposits controlled by major Tertiary strike-slip faults in the distal Himalayan foreland.

The relationship of MVT mineralization to tectonic evolution of orogenic foreland settings has been described by Bradley & Leach (2003). The Tertiary-hosted Atlas and Tethyan deposits illustrate a variation on this theme, with deposits occurring within foreland thrust belts during extensional collapse.

## 3 CONCLUSIONS

The Neogene-hosted deposits of the Atlas belt show close similarities in style and setting to the world-class Iranian deposits and Jinding stratabound-replacement carbonate-hosted zinc-lead deposits within Tertiary thrust belts.

Much of the Tethyan zinc province has had limited exploration and still holds potential for new world-class discoveries. This is certainly the case within the Atlas, where despite the long mining history there has been very limited modern exploration in most of the belt, for a variety of (mainly political) reasons. The close similarity in metallogenic setting with other world-class Tethyan districts supports the potential for large deposits in Neogene host rocks that have not been a focus for previous exploration.

## ACKNOWLEDGEMENTS

Thanks are due to many geologists with whom we have worked on some of these deposits, and to Cam Allen and Duncan Large for constructive discussions on Atlas and Tethyan zinc-lead metallogeny and exploration potential. Thanks also to Zinifex Ltd and Albidon Ltd for support and permission to present this paper.

## REFERENCES

Bradley DC and Leach DL (2003) Tectonic controls of Mississippi-valley type lead-zinc mineralization in orogenic forelands. *Mineralium Deposita* 38:652-667.

Gilg HA, Allen C, Balassone G, Boni M, and Moore F (003)The 3-stage evolution of the Angouran Zn "oxide"-sulphide deposit, Iran. In *Mineral Exploration and Sustainable Development,* Eliopoulos et al. (ed.s), Millpress: 77-80

Kyle JR and Li N (2002) Jinding: A giant Tertiary sandstone-hosted Zn-Pb deposit, Yunnan, China: *Society of Economic Geologists Newsletter* 50: 1, 9-16.

Rosenbaum G, Lister GS and Duboz C (2002) Reconstruction of the tectonic evolution of the western Mediterranean since the Oligocene. In: Rosenbaum, G. and Lister, G. S. 2002. Reconstruction of the evolution of the Alpine-Himalayan orogeny. *Journal of the Virtual Explorer,* 8: 107-130.

# Fossil Nickel Laterites in the Ophiolite Belts of the Alpine-Himalayan System: Case Studies of the Balkan Region

Christian Masurenko
*European Nickel PLC, Belgrade, Serbia*

Dusan Tanaskovic
*European Nickel d.o.o. in Serbia, Belgrade, Serbia*

ABSTRACT: The Alpine-Himalayan System, which stretches from NW Serbia through Albania, Macedonia and Greece into Turkey and further to Iran, hosts some significant nickel bearing soils and sediments that could only occur under severe tropical weathering conditions. Ultramafic rocks such as dunite, harzburgite and more importantly serpentinite are the protoliths of lateritic zones, and play an important role in the development of Ni-bearing sediments or Ni-laterite. Serpentinite is a common product of hydrothermal alteration of olivine in the presence of water at temperatures between 200–500$^{o}$ C.

KEYWORDS: ophiolites, serpentinite, nickel laterite

## 1 CHARACTERISTICS AND GENESIS OF NICKEL LATERITES

Fossil laterites are those protected from erosion by a cover of silicified or ferruginous crust. To develop these, certain factors must act together:

a) A soil mantle of appropriate thickness, containing high water concentrations
b) circulating ground and meteoric water on a base barrier (clay horizon)
c) Tropical weathering conditions
d) Vertical pH gradients, to precipitate elements variably over a profile
e) Soils enriched in Fe and Al.

'Fossil laterites' are generally remnants of the Tethyan closure and the Alpine orogeny during Upper Cretaceous. The ophiolitic Melange unit sits on a basement of metamorphic series and has been covered by Neogene sediment formations. However, laterites of some deposits in Serbia belong to the "oolitic sedimentary" type.

Tropical weathering conditions dominated during Lower Cretaceous and also Palaeogene age. These conditions led to the separation of nickel from silicon and other associated elements. The relatively mobile elements such as Ni, Co, and Mn were leached and re- deposited lower in the profile whilst more stable elements such as Fe and to a lesser extent Al were concentrated as oxides and hydroxides

| Minerals | Description | Grade % |
|---|---|---|
| Goethite | (Fe,Al)OOH x H2O | Up to 1.7 % Ni, 0.2 % Co |
| Mn Oxides | (Co, Ni)O2MnO2xH2O | Up to 8 % Ni, 2 % Co |
| Nontronite | (Fe, Ca, Na, Mg, Al) clay | Up to 4 % Ni |
| Ni Serpentine | (Mg, Fe) hydrated silicate | Up to 12 % Ni |
| "Garnierite" | Hydrated Mg silicate | Up to 30 % Ni |
| Chlorite | (Mg, Fe, Al) hydrated silicate | Up to 15 % Ni |

Table 1. Minerals containing high nickel contents

in the upper part of the profile. Together with the very immobile silicon, these minerals formed the "silicified crust" that protected the fossil laterite from further erosion.

Ni-laterites in the Balkans, compared to those of western Turkey, vary in their chemical and mineralogical composition. The formation of oolitic sedimentary Ni ores took place in the Upper Cretaceous. Some of the significant lateritic nickel deposits belong to the "pellet later-

ites," which are generally fine-grained, loosely-cemented sediments of oolitic texture.

The dominant ultramafic rocks in ophiolite complexes represent remnants of sub-oceanic mantle. The Tethyan Ophiolite Belt, being part of the Alpine-Himalayan system, is one of the longest ophiolite belts in the world. The collision process comprising closure of the Palaeotethys started in the middle Triassic and continued to the Cretaceous. By end of the Jurassic, the ophiolites were obducted onto continental crust. The ages of the ophiolites as reported in the literature are: mid-Jurassic in the belt of former Yugoslavia, Albania and Greece, and late-Cretaceous in Turkey, Cyprus, Syria and Iran.

## 2 BALKAN REGION

The ophiolite belt of former Yugoslavia has been divided in three zones: the Zagreb–Tuzla domain which is in close contact with the Vardar-Zone; the Tuzla–Brezovica–Radusa zone and further to the south the Mirdita zone.


Figure 2. Alpine-Himalayan Belt

All ophiolite complexes in these belts demonstrate the same general features, consisting of layered gabbros, sheeted dykes, sills and pillow lavas which are often covered by thick sequences of calcareous, clastic and flysch sediments. The ultramafic cumulate rocks are mostly represented by dunite and harzburgite which play an important role as source in forming Ni bearing laterites – chromitite, websterite and wehrlite.

### 2.1 *The Vardar and Mirdita Zones*

The Vardar Zone stretches from northern Serbia approximately 1,000 km through Macedonia to northern Greece. It is 60-80 km wide and occurs between the Serbia-Macedonia Massive to the east and the Dinarides in the west. This zone was initiated as a fracture during the early Palaeozoic Vendian.

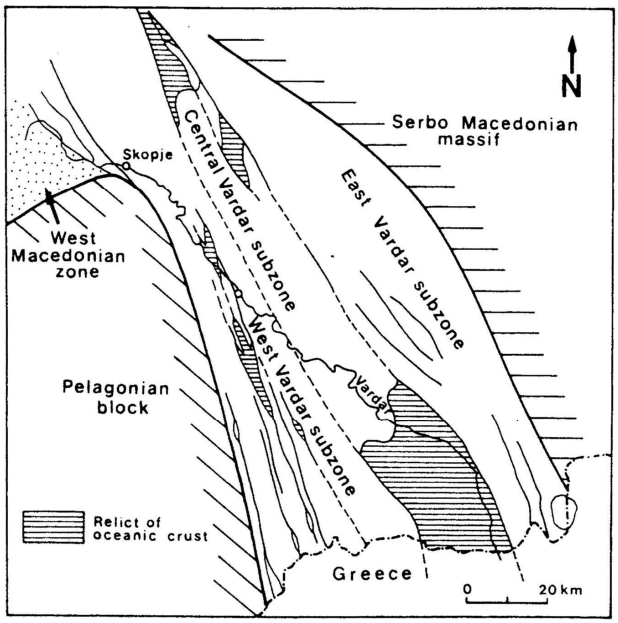


Figure 1. The Vardar Zone and its principal tectonic units (after Boev-Jancovic, 1996)

During Alpine deformation, the Vardar Zone was differentiated into 3 subzones, with the various ophiolite complexes occurring in the central subzone. Major fractures and thrust faults mainly trend NNW-SSE.The ophiolite complexes of the Vardar Zone developed when oceanic lithosphere was thrust onto continental crust during Upper Jurassic/Lower Cretaceous.

In case of the Ni laterite deposits in Albania and Serbia, laterization started during middle and upper Cretaceous. Peridotites and serpentinites were uplifted and exposed at the surface during the Middle Jurassic. Tropical conditions formed the so-called weathering crust, and Ni-laterite deposits in Serbia and Albania are a result of the erosion of these Cretaceous fossil laterites. During the Palaeogene this duricrust material was transported into lacustrine environments as pisolitic-oolitic sedimentary iron-nickel deposits such as Mokra Gora in Serbia and Bitincka in Albania.

The Vardar Zone extends to the southeast and east, and grades into the Izmir-Ankara-Erzincan Suture Zone.

### 2.2 *The Izmir-Ankara-Erzincan (IAE) Suture Zone*

The IAE Suture Zone, which developed during the closure of the Neotethys, extending roughly 3000km east to west through Turkey. It is divided into two main zones: the North Anatolian Thrust Zone, an imbricated thrust zone of

ophiolites and cover sediments; and the Sakardag-Cavusdagi Thrust Zone which consists of metamorphic rocks and deformed basin sediments. Recent studies indicate that most of the ophiolites in Turkey, especially in the south of the IAE Zone, were formed in supra-subduction zones that are enriched in chromium, iron, nickel and platinum. Tropical laterization occurred especially during the Miocene-Pliocene.

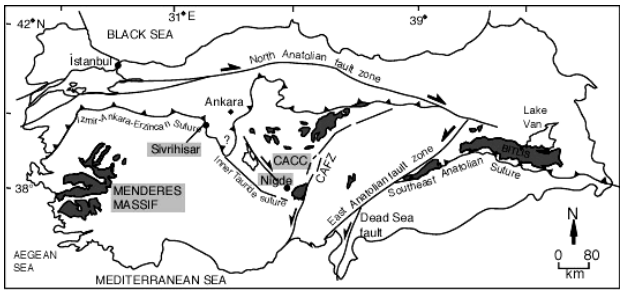


Figure 3. Izmir-Ankara-Erzincan Suture Zone

## 2.3 *The Caldag Nickel Laterite Deposit in western Turkey*

Lateritic weathering prevailed during tropical-subtropical climate conditions that dominated in the area during the Eocene-Miocene. This type of weathering led to the separation of Ni from silicon and associated elements. During this process, the relatively mobile elements such as Ni, Co and Mn were leached and redeposited at depth in the profile, whilst stable elements such as Fe and lesser Al were concentrated in the forms of oxides and hydrated oxides in the upper part of the profile. This upper part formed a duricrust protecting the laterite from erosion.

Nickel, iron, cobalt and manganese remain within the lateritic profile in solution as bicarbonates due to the excess $CO_2$. The ore zones, and related mineralogy of Caldag Laterite Sequence, are summarized as follows:

*Serpentinite Zone***:** Moderately weathered serpentinite contains background values of 0.2 - 0.3% Ni and 0.02% Co. With increased weathering, Fe is removed while Si and Al increase sharply At the same time, Mn is enriched together with Ni and Co, which reflects the association of asbolane with Ni and Co. Mg is relatively stable.

*Weathered Serpentine Zone:* Clays including montmorillonite, nontronite and minor illite, and quartz (chalcedony), as boxworks and fillings; talc, magnesite, garnierite and asbolane. Ni is contained, in order of importance, in: asbolane, garnierite and smectite.

*Yellow Limonite Zone:* Goethite, haematite, smectite, chlorite, asbolane, calcite, chromites and quartz. Nickel is contained, in order of importance, in: goethite, asbolane and smectite. Ni mainly reports to fines in the limonitic ore. Hence, such ores are amenable to upgrading by crushing and screening.

*Red Limonite Zone:* Haematite predominates, but otherwise contains the same mineral assemblage as that observed in the limonite horizon.

European Nickel's deposit at Çaldag comprises a JORC reserve of 33Mt at 1.14% Ni and 0.07% Co, containing 0.38Mt Ni and 0.022Mt Co.

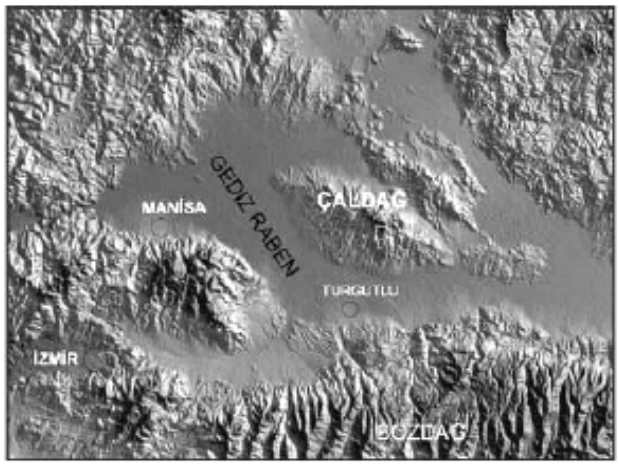


Figure 4. SAT Image - Colour coded SRTM shaded topographical image of the Gediz Graben and Caldag mountain (after Kaymacki, 2005)

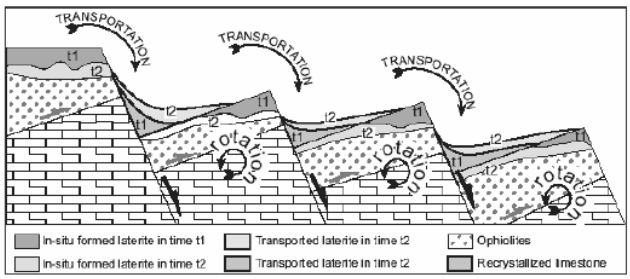


Figure 5. Conceptual model for development of laterites of different origin (after Kaymakci, 2005)

## 3 PROCESSING OF NICKEL LATERITE ORES

European Nickel PLC (ENickel) developed a unique process of recovering the nickel from lower-grade laterite, and in 2004 leaching is

started constructing a pilot plant at the Caldag deposit 70km east of Izmir. Though acid common in the copper industry it had not yet

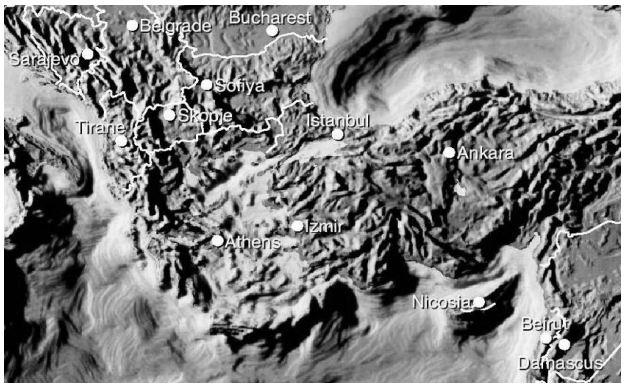


Figure 4. Location of Ni laterites in the SE European Ophiolite Belt (stars = ENickel licences)

yet been applied to Ni laterites. The nickel at Caldag is present in the goethitic phase and is soluble in dilute sulphuric acid. In three trial heaps ENickel irrigated ore over 18 months, recovering ~78 % of Ni and 82 % of Co into solution. Leach liquor is treated on a continuous basis in a downstream precipitation plant, pro-

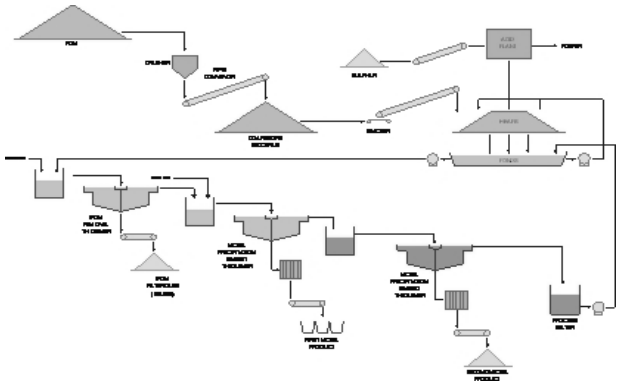

Figure 7. Acid leach process

ducing an intermediate product with Ni-Co content of up to 36 %.

## 4 CONCLUSION

- Compared to other nickel laterite deposits in Africa and South America, nickel laterites in SE Europe are all 'fossil' laterites
- The ophiolites in the Alpine Himalayan System have a great potential for nickel-bearing laterites, due to their exposure to tropical conditions during the Cretaceous
- The sequences were preserved by a siliceous duricrust, or thick sedimentary cover
- Highest nickel values are found in the contact zone of weathered saprolitic serpentinite and limonite horizon
- Laterization process needs more attention to understand genesis of mineral zones, potentially helping the mining industry develop hydrometallurgical treatment of such ores and more environmentally-friendly processing

Caldag is one 'pearl' in the ophiolite belts, and using a new leaching process, relatively low-grade ores have generated interest recently.

## REFERENCES

M. Zeki Billor & F. Gibb (2004), *The Mineralogy and Chemistry of the Chromite Deposits of Southern and Tauric Belt, Turkey*

R.G. Coleman (1977), *Ophiolites*, Springer Verlag, Heidelberg

B. Boev & S. Jankovic (1996), Nickel and Nickeliferous Iron Deposits of the Vardar Zone (SE Europe) with particular Reference to the Rzanovo-Studena Voda Ore-Bearing Series, Stip

Journal of Conference Abstract (1999), Symposium F04 – East Mediterranean Ophiolites – *Magmatic Processes and Geodynamic Implications, Strasbourg*

N. Kaymakci (2005), *Structural Analysis of Caldag Nickel Occurrence: field observations and Quickbird Image interpretation, Turkey*

European Nickel PLC (2002), Geological Report of Caldag Nickel Laterite Deposit, unpublished, Turkey

N. Skarpelis (1999), *Lateritic Weathering Crusts as a Source of Ferruginous Spheroidal Particles of Sedimentary Nickelferous Iron Ores,* Greece

D.G. Eliopoulos & M. Economou-Eliopoulos (1999), Geochemical and Mineralogical Characteristics of Fe-Ni and Bauxite-Laterite Deposits of Greece, Ore Geology Reviews, Greece *European Nickel, Web Page* (2006), www.enickel.co.uk

# Recent Discoveries and Exploration Trends in Turkey

Ozcan Yigit
*Department of Geological Engineering, Canakkale Onsekiz Mart University, Canakkale 17020, Turkey*

ABSTRACT: Modern exploration programs, mainly by multinational exploration and mining companies, in the last two decades have revealed the mineral potential of the ancient land of Turkey. The country became a gold producer in 2001, previously the only gold produced in Turkey was a by-product from base-metal mines. Currently the country has two active gold mines, Ovacik and Kisladag and more metal mines in development, such as Copler, Efemcukuru, Mastra, Cerattepe, Caldag and Madenkoy. In terms of industrial minerals Kazan and Beypazari mines will begin production of trona soon. Buoyant metal prices, amendment of the mining law in 2004 as well as economic stability have attracted more major and junior exploration and mining companies into Turkey. The main exploration and development focus has been precious- and base-metals, especially gold and copper, though industrial minerals attracted some mining giants. Porphyry copper-gold, epithermal gold and volcanic-associated massive sulphide deposits are the main exploration interests while carbonate-hosted lead-zinc deposits, especially non-sulphide zinc, are other targets. Recent advancements in mining technology have attracted companies' attention to low-grade lateritic nickel deposits of the country.

KEYWORDS: Turkey, Tethyan Metallogeny, Gold, Copper, Mineral Exploration

## 1 INTRODUCTION

Turkey is an emerging country for mineral exploration and mining on the doorstep of Europe. The country has relatively underexplored prospective land area of *ca*. 780,000 km$^2$, the largest in Europe and approximately 1.5 times larger than France. Most of the exploration effort is still concentrated on outcrop geology and surface geochemistry with less emphasis on buried conceptual targets.

Gold is the major target commodity of Turkish mineral exploration. Thus, most of the recent discoveries as well as mining developments are of gold deposits, though base metal potential of the country has attracted some major companies.

A new approach to old prospects and districts in the brown fields has been the main exploration trend with relatively less emphasis on green field exploration.

Most of the metallogeny of Turkey is linked to the development of Tethyan Eurasian Metallogenic Belt (TEMB) (Jankovic, 1977) within the Alpine-Himalayan orogenic system that formed from Jurassic-Cretaceous to present. Turkish segment of the TEMB contains many different types of mineral deposits related to subduction, collision, post-collision and rifting processes (Yigit, 2006).

Recent discoveries as well as exploration trends and mining have been addressed in the order of economic and/or geologic importance in this paper, based on the author's comprehensive GIS database of mineral deposits and prospects of Turkey. The paper also evaluates mineral exploration potential and future exploration trends of Turkey.

## 2 RECENT DISCOVERIES

Changes in the Turkish mining law in 1985 have stepped up mineral exploration activities and resulted in many discoveries, though some of these new discoveries resulted from reinvestigation of long-known prospects. Furthermore, amendment of the mining law in 2004 almost tripled the exploration licenses assigned by

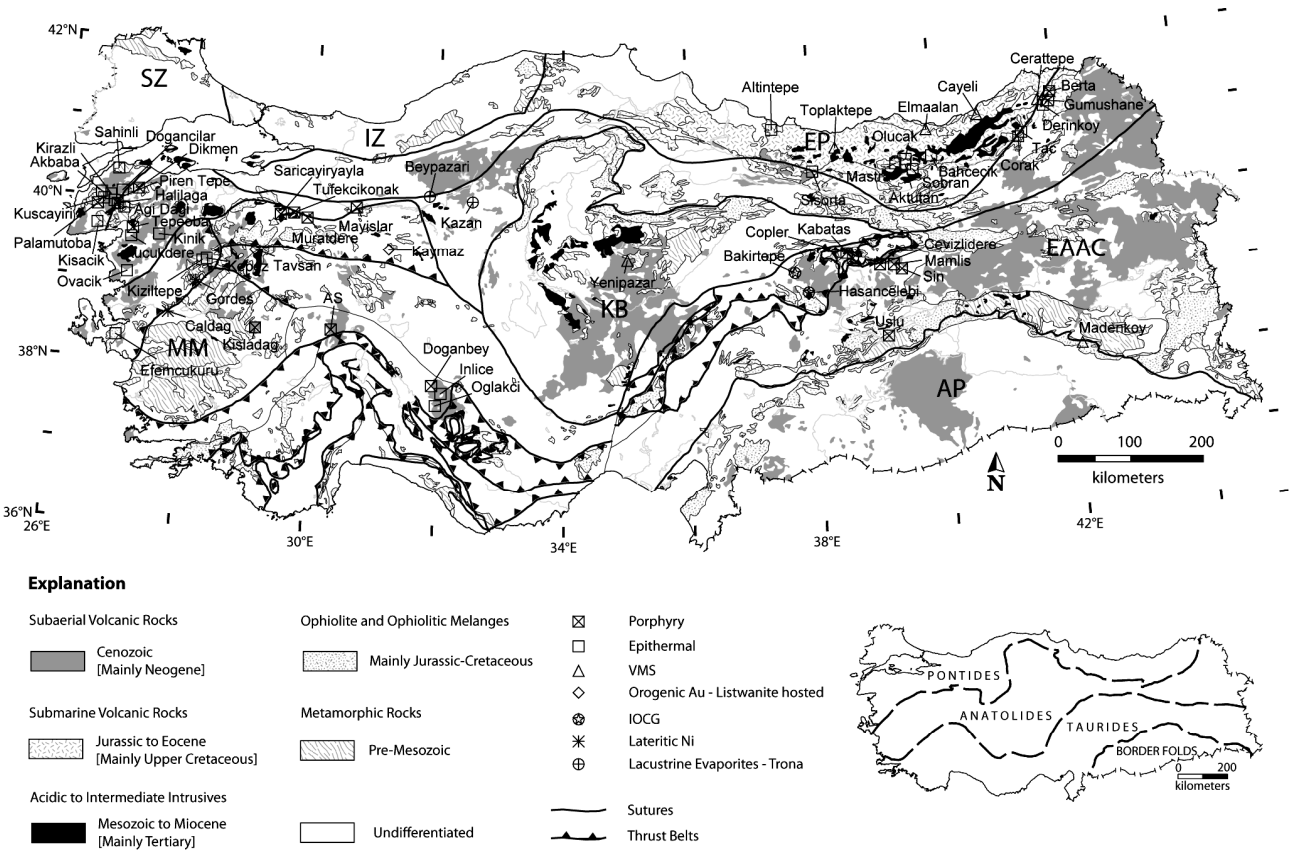


Figure 1. Distribution and types of mineral deposits and prospects mentioned in the paper with geology and major tectonic units of Turkey, emphasis on the host-rock lithologies. Geology modified from MTA (1989). Inset shows major tectonic units (after Ketin, 1966). AP: Arabian Platform, EAAC: East Anatolian Accretionary Complex, EP: Eastern Pontides, IZ: Istanbul Zone, KB: Kirsehir Block, MM: Menderes Massif, SZ: Strandja Zone. Lambert Conformal Conic Projection for Turkey, scale accurate for the location's latitude.

mining bureau. Figure 1 shows distribution and types of the mineral deposits mentioned in the paper in relation to geologic and tectonic setting.

Ovacik Au-Ag deposit, the first Au mine in Turkey, was one of these discoveries and opened in 2001. Kisladag Au deposit, the biggest gold mine in Turkey, began commercial production in July 2006. Copler Au-Ag and Efemcukuru Au deposits are being developed and will be in production next year. Mastra Au, Cerattepe Cu-Au-Ag and Madenkoy Cu-Zn-Au-Ag deposits are undergoing development work and will be in production soon. There are ongoing feasibility studies in Agidagi Au-Ag, Kirazli Au and Yenipazar Cu-Pb-Zn-Au-Ag deposits. Cevizlidere Cu-Au-Mo prospect, formerly known as Kizilviran, is another advanced stage prospect. Caldag Ni-Co deposit, though not a new discovery, will be in full production by the end of this year and first Ni concentrate will be produced in the first quarter of 2008.

In terms of industrial minerals, the recent discovery of Kazan deposit with >600 Mt @ 31 % trona reserves north of Ankara, associated with Eocene lacustrine environment, will be in production this year using solution mining technology. Beypazari trona deposit with 236 Mt @ 70-90 % $Na_2CO_3$ reserves, second largest reserves after Wyoming, USA, is located approximately 60km ENE of Kazan and is intended to be in production this year.

## 3 DEPOSIT TYPES OF CURRENT INTEREST

Despite Turkey possessing a wide spectrum of mineral deposits, recent mineral exploration programs are concentrated on mainly Au only or Au-Cu systems including porphyry Au (Cu-Mo) and epithermal Au (Ag) including both high- and low-sulphidation (HS and LS) styles. Polymetallic (Cu-Pb-Zn-Au-Ag) volcanic-associated massive sulphide (VMS) deposits and carbonate-hosted Pb-Zn deposits including Mississippi Valley type (MVT) and carbonate replacement (CR) deposits with non-sulphide zinc are the main interest to base-metal compa-

nies. Lateritic Ni deposits are also currently being explored for. Deposit types relatively less explored for, with known or potential examples, are orogenic Au systems including listwanite hosted deposits such as Kaymaz and Tavsan and iron oxide Cu-Au (IOCG) systems such as Bakirtepe prospect and Hasancelebi district, the largest Fe resource in Turkey, containing 685Mt ore at 19 % Fe, plus $TiO_2$.

### 3.1 *Porphyry Cu-Au (Mo)*

Porphyry deposits and prospects of Turkey are mainly associated with Late Cretaceous to Miocene age granitoids related to both island-arc and continental-arc settings, forming three roughly E-trending belts, Pontides, Anatolides and Border Folds (Yigit, 2006). Kisladag with 5.06 Moz Au reserves (135Mt @ 1.16 g/t) and 8.29 Moz Au resources, Copler with 2.8 Moz Au reserves (52Mt @ 1.66 g/t) and 3.53 Moz resources, Gumushane (30Mt @ 0.3 % Cu and 0.3 g/t Au resources) and Tepeoba (44Mt @ 0.43 % Cu and Mo resources) are examples of porphyry systems.

Newly discovered prospects such as Cevizlidere (118m @ 0.63 % Cu, 0.2 g/t Au and alteration zones with many known HS epithermal systems, such as Agi Dagi (1.26 Moz Au resources), Kirazli (0.80 Moz Au resources) and recently discovered Piren Tepe prospect (over 46.90m @ 1.79 g/t Au in one drill hole). Sahinli, Dogancilar, Kisacik, Kepez, Kiziltepe, Kinik and Kuscayiri are other recently discovered prospects in the area.

In NE Turkey, Tac (11.8 Mt @ 1.80 g/t Au and 0.13 % Cu resources), Mastra (1.09 Mt @ 12.34 g/t Au resources), Altintepe, Corak, Olucak, Bahcecik, Sobran, Derinkoy and Sisorta are examples of recent epithermal discoveries.

Newly discovered Inlice HS epithermal prospect in S central Turkey has significant drill hole intercepts, i.e. up to 37.70m @ 4.7 g/t Au. Other prospects such as Doganbey and Oglakci in the area may together form a new exploration district.

### 3.3 *Polymetallic VMS*

VMS deposits in Turkey can be evaluated in two categories, Kuroko and Cyprus types. Kuroko-type deposits in Turkey are limited to Late Cretaceous bimodal volcanic rocks of the eastern Pontides, NE Turkey while Cyprus-type deposits are associated with ophiolitic rocks of the Kure district in N Turkey and Ergani district in SE Turkey.

63 g/t Mo in one drill hole), Halilaga (298.2m @ 0.50 g/t Au and 0.53 % Cu in one drill hole), "AS" (115m @ 0.8 g/t Au and 0.82 % Cu in one drill hole), Uslu, Muratdere, Saricayiryayla, Tufekcikonak, Mayislar, Dikmen, Palamutoba, Kabatas, Mamlis, Sin and Berta are being explored for their economic potential.

### 3.2 *Epithermal Au-Ag*

Epithermal deposits in Turkey are mainly associated with subaerial volcanic rocks of calc-alkaline affinity and are mainly clustered in two distinct regions, NE and W Turkey. Most of the current epithermal Au exploration focuses on Biga Peninsula in NW Turkey and W Turkey. Konya volcanic complex is a promising area in S central Turkey.

Ovacik LS epithermal Au-Ag mine contains 0.52 Moz Au total reserves (1.24Mt @ 13.1 g/t). Efemcukuru with 0.78 Moz Au reserves (1.86 @ 13.14 g/t) is an epithermal system in development. Other LS systems such as Kucukdere and Akbaba contain small gold resources, 0.29 Moz and 0.32 Moz respectively.

Volcano-plutonic complex of the Biga Peninsula in NW Turkey exhibits world-class Cayeli deposit (11.60 Mt @ 3.65 % Cu, 5.87 % Zn, 0.34 % Pb, 0.56 g/t Au and 49 g/t Ag reserves) is a typical example of a Kuroko-type system with gold. Cerattepe deposit (oxide: 3 Mt @ 4.2 g/t Au and 151 g/t Ag; sulphide: 3.7 Mt @ 5.2 % Cu, 1.2 g/t Au and 25 g/t Ag reserves) has some characteristics of epithermal systems in submarine environment as does Toplaktepe prospect, which has a barite-Au-Ag association with minor base-metals. Elmaalan is another recently evaluated prospect in NE Turkey. Madenkoy Cyprus-type VMS deposit (25.8 Mt @ 2.06 % Cu, 0.93 % Zn and 31.49 % S, plus Au and Ag) in SE Turkey is another development project and is intended to be in production soon.

Yenipazar deposit (4.7 Mt @ 0.45 % Cu, 1.44 % Pb, 1.64 % Zn, 1.66 g/t Au and 35.6 g/t Ag resources) in central Turkey is undergoing feasibility studies. Hosted in Palaeozoic schist, it is the only reported metamorphosed VMS deposit in Turkey known to the author.

### 3.4 *Lateritic Ni*

Lateritic Ni deposits of Turkey are associated with ophiolitic assemblages of mainly Jurassic to Cretaceous age, running through Balkans, Greece and Turkey to Iran. Ophiolite formation is related to subtropical to tropical

conditions in mainly Eocene to Miocene times.

Sulphuric acid heap leaching, a common technique for processing copper ores, has not been used for nickel ores. However, low clay content of some lateritic Ni deposits such as Caldag (33.5 Mt @ 1.14 % Ni, plus Co reserves) and Gordes assists the heap leach process and makes economical Ni and Co recoveries possible. Therefore, new production technology for low grade lateritic Ni deposits makes Turkey an attractive locus for lateritic Ni exploration and mining.

## 4 FUTURE TRENDS

Exploration efforts in the last two decades proved that Turkey is a new frontier of mineral exploration and mining, particularly as a prime gold country. Base-metal deposits, especially precious metal-rich systems, have long been appreciated and continue to hold exploration interest. Porphyry Au-Cu, epithermal Au and polymetallic VMS systems are major deposit types for exploration. Lateritic Ni potential of the country will attract more players into the exploration arena. Turkey is also one of the strongest players in industrial minerals, especially boron and trona.

To date most of the exploration efforts concentrated on relatively big and easy targets in shallow depth without much emphasis on geologic setting of the ore forming systems. Due to lack of deep drillings (>250m) in exploration programs in Turkey, the porphyry potential of many epithermal districts has never been fully tested. Therefore, future exploration programs should incorporate geological background of the ore forming system as well as surface geochemistry and geophysical studies.

Many areas of Turkey lack known mineral occurrences not because of unfavorable geologic setting but due to insufficient studies, therefore, reconnaissance exploration should focus in these areas rather than known districts. Exploration companies should go back to the old prospects with new ideas and should try to test not only surface geochemical and geophysical anomalies but also geological anomalies!

## ACKNOWLEDGEMENTS

Many thanks are given to Mac Canby for his kind invitation to write this paper. Catherine Yigit is gratefully acknowledged for editing.

## REFERENCES

Jankovic S (1977) The copper deposits and geotectonic setting of the Tethyan Eurasian metallogenic belt. *Mineralium Deposita* 12: 37–47.

Ketin I (1966) Tectonic units of Anatolia (Asia Minor). *MTA Bulletin* 66: 23– 34.

MTA (1989) Geologic map of Turkey. Scale 1:2000000, MTA, Ankara.

Yigit O (2006) Gold in Turkey — a missing link in Tethyan metallogeny. *Ore Geology Reviews* 28: 147–179.

# The Inlice High-sulphidation Epithermal Gold Discovery: Defining a Potential New Gold Belt in Turkey

D.J. Hall, R.P. Foster & B. Yildiz
*Stratex International plc, London, U.K.*

S.D. Redwood
*Independent Consultant, Panama*

ABSTRACT: Inlice is a new high-sulphidation epithermal gold prospect in the Erenler Dağı Volcanic Belt in western Anatolia, Turkey, in an area with no previously known gold. Mineralization is associated with vuggy and sugary quartz in steeply dipping, structurally controlled silica ledges which cut an andesitic volcanic dome. The main Ana Ledge has an average grade of 2.94 g/t gold over a length of 600 meters and width of 18.0 meters, based on drilling. Following the Inlice discovery, Aster imagery was used to identify at least six other major advanced argillic lithocaps in the Erenler Dağı belt with potential for epithermal and porphyry mineralization, including the Doğanbey prospect where porphyry gold-molybdenum mineralization outcrops beneath the lithocap. The Erenler Dağı belt is similar to the Maricunga belt of Chile which contains over 40 Moz gold, yet twenty years ago had no discoveries.

KEYWORDS: Turkey; Inlice; Gold; High-sulphidation Epithermal; Lithocap; Maricunga

## 1 INTRODUCTION

The Inlice prospect in the Erenler Dağı Volcanic Belt (or Konya Volcanic Belt) of western Anatolia, Turkey is a new high-sulphidation epithermal gold system discovered by Stratex International Plc. The Erenler Da-ğı Volcanic Belt is located 245km south of Ankara and 35 to 60km west of the city of Konya at an altitude of 1,000m to 2,334m. The area is well networked with three paved highways.The area had no known occurrences of gold and had not been considered a gold target despite many years of exploration by MTA and foreign companies in Turkey prior to the Inlice discovery in 2003. Stratex was led to the area by its general manager Bahri Yildiz, who had sampled roadside outcrops. Subsequent visits identified the mineralization as being high-sulphidation epithermal associated with vuggy quartz and with encouraging gold values (including 13.0m @ 4.1 g/t and 7.0m @ 4.1 g/t). Stratex rapidly advanced the project by mapping and rock chip sampling to drilling, with intersection of economic grades and widths of gold in the first drill hole. The early recognition of the style of mineralization, the association with Miocene volcanism, use of Aster imagery, and securing of open ground in the 60km by 30km volcanic belt has led to the definition of several major lithocaps in the district with considerable potential for the discovery of additional high-sulphidation epithermal gold systems and porphyry gold +/- copper systems.

## 2 REGIONAL GEOLOGICAL SETTING

Four tectonic subdivisions in Turkey consist of: the Pontides, the Anatolides, the Taurides, and the Border Fold Zone. The Erenler Dağı Volcanic Belt is positioned geographically and geologically between the Tauride and Anatolide units and was erupted in response to the northward subduction of the African Plate beneath Anatolia along the Cyprean Arc from Jurassic to Miocene times.

The Erenler Dağı Volcanic Belt comprises four volcanic centres of the high-K calc-alkaline andesitic-dacitic volcanic suite with an area of 60km x 40km. The volcanic belt is elongated north-south, being bounded by graben faults on the north-east and south-east margins. These centers (Tocak, Erenkilit, Bostandağ, and Alacadağ) are of Upper Miocene to Pliocene age (11.9 – 3.2 Ma;

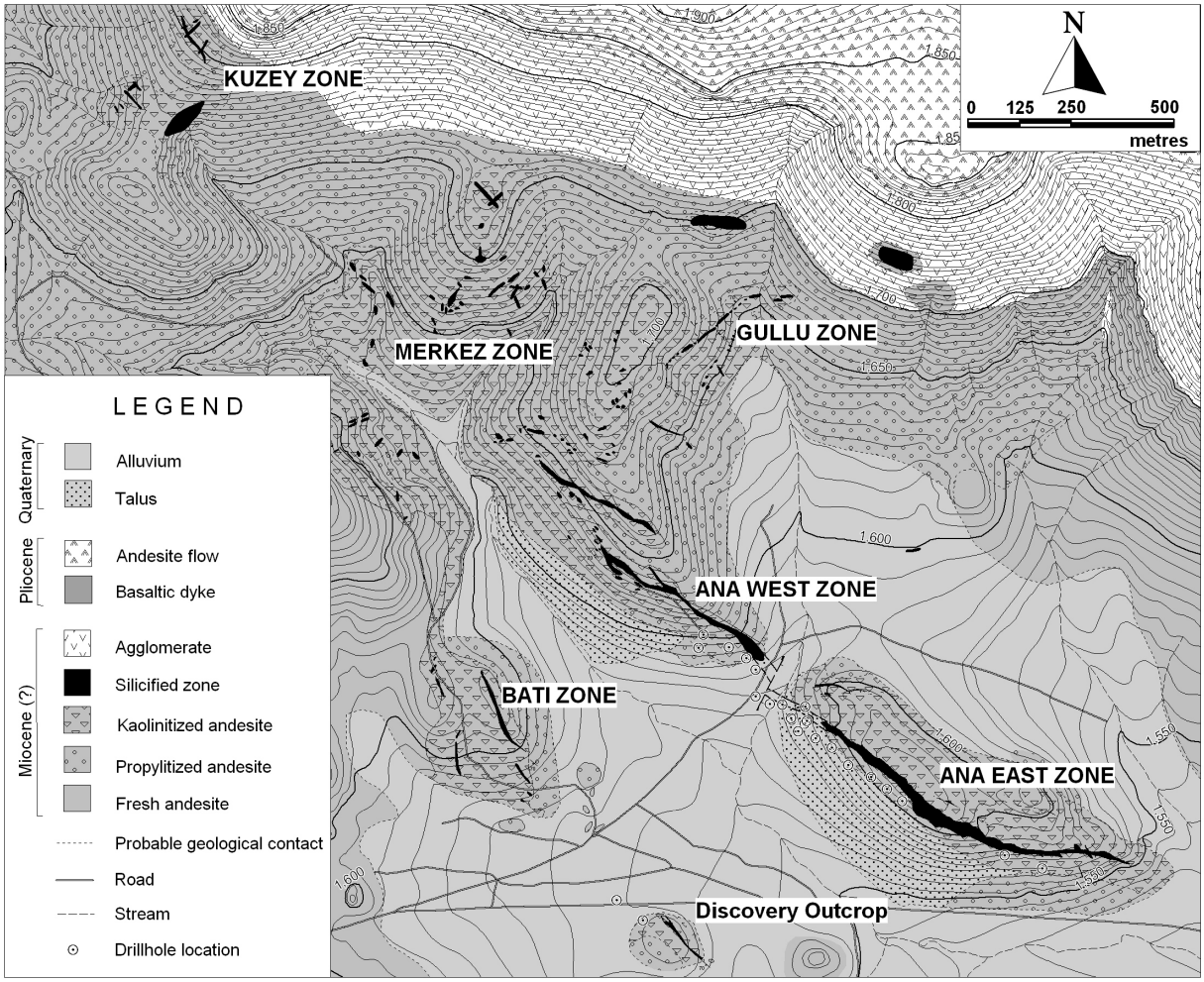


Fig. 1. Geology of the Inlice prospect illustrating key silica ledges

Besang *et al.,* 1977) and are dominated by ignimbrites and lava domes interbedded with fluvial-lacustrine limestone, marl and shales (Keller *et al.*, 1977; Temel *et al*., 1998; Karakaya *et al*., 2001). The petrochemistry and isotope signatures are similar to those of the young volcanic rocks of the Central Andes.

Volcanic-related hydrothermal activity in the volcanic rocks is clearly exhibited in the form of multiple clay-dominated alteration zones containing kaolinite, halloysite, alunite, illite, montmorillonite and zeolites together with cristobalite and quartz (Karakaya *et al*., 2001)

## 3 GEOLOGY AND MINERALIZATION

Inlice comprises a number of steeply dipping silica ledges hosted by homogenous andesitic forming what is interpreted to be a dome. This is overlain by agglomerates and, locally, ignimbrites and lithic tuffs, followed by andesitic lava flows and intercalated fluvio-lacustrine sediments of Pliocene age. The silicification and extensive clay alteration are confined to the Miocene rocks. The silica ledges are tabular bodies of residual and replacement silica which renders them resistant to erosion and hence they are topographically prominent over much of their length. The ledges are controlled by a dextral oblique-slip normal fault system that cuts the dome.

The dominant trend of the most prominent silica ledges is WNW to NW (Fig. 1). The longest and widest ledge is the Ana Zone (Ana East and Ana West), which strikes N50° - 80° W and dips 60°-70° SW. The Batı and Discovery Zones (probably the same ledge) strike N20° - 40° W and dips 70°- 80° SW. The Ana Zone comprises mostly vuggy and sacchoroidal (sugary) quartz, the residual products of extreme acid-leaching of the host andesite. Eastwards along the Ana East section of the ledge, the vuggy and sugary quartz give way to chalcedony, which, on the basis of its texture, is believed to have inverted from original opal. Chalcedonic silica is also the

main silica type within the Discovery Zone and southern part of the Batı Zone.

The alteration haloes enveloping the silica ledges grade outwards from quartz-alunite and quartz-kaolinite to illite-chlorite and smectite-chlorite assemblages, reflecting in-creasing fluid pH and decreasing temperatures (Sillitoe, 2006). Hypogene alunite is present and locally can be mapped as discrete zones, especially in the immediate footwall of the central part of the Ana Zone.

The highest and most consistent gold values identified to date are associated with vuggy and sugary quartz in the Ana Zone. Outcrop sampling with values up to 7.58 g/t gold over 8.2m; 2,000m of exploration drilling indicate a higher-grade zone with an average width of 18.0 m and average grade of 2.94 g/t gold over a strike of about 600m.

The zone remains open to further drilling. Significantly, the Ana ledge persists without any surface expression beneath the shallow valley that divides the East and West zones (Fig. 1). Drilling has confirmed the presence of faulting but no significant loss of mineralization, and the low relief is probably due to a greater proportion of friable sugary quartz.

Supergene oxidation is shallow, generally less than 40 metres in the Ana Zone, and is characterized by jarosite after pyrite. The dominant sulphide mineral is fine grained pyrite, which ranges in content from 1-3 volume %, unusually low for vuggy quartz, to semi-massive accumulations of up to 30 volume %. The pyrite is accompanied by minor amounts of enargite and subordinate luzonite, but copper contents rarely exceed 0.3%. The main late-stage mineral in the ledges is kaolinite, which partially lines cavities in vuggy quartz. This kaolinite is believed to have precipitated from acidic fluid drawn down from the formerly overlying steam-heated horizon above the palaeo-water table. Native sulphur is also commonly observed as vuggy fillings. In a few instances crystalline barite also lines fractures in vuggy quartz, where it appears to pre-date the late kaolinite (Sillitoe, 2006).

Geochemically the gold-rich silica ledges are characterized by a very close association between gold and As, Cu, Hg, Te, Tl, and Sb and slightly less so with Mo and Pb. Both Ba and P contents are very low. The gold distribution is remarkably homogenous, rarely exceeding 10 g/t and with a maximum of 14 g/t recorded to date. Silver-gold ratios are less than 1.

The chalcedonic eastern portion of the Ana Zone is characterized by low gold values (10-100 ppb Au) both at surface and at depth; As-Hg-Te-Tl signature is much weaker. Ba, P, Pb and, to a lesser extent Zn, tend to be enriched, and Ag-Au ratios are considerably higher, commonly between 10 and 100. Preliminary investigations of the Discovery-Batı Zone indicate similar geochemical characteristics.

## 4 ERENLER DAĞI VOLCANIC BELT

Following the discovery at Inlice, Stratex employed Aster satellite imagery to define other areas of silica and clay alteration in the Erenler Dağı Volcanic Belt. Follow-up led to identification of at least six substantial lithocap areas with potential for porphyry gold +/- copper and epithermal gold mineralization (Redwood 2005a, b).

Doğanbey, currently the company's priority exploration target outside Inlice, is situated near the topographic rim of an eroded stratavolcano (Redwood, 2006). In the lowest exposed parts of the alteration zone a prominent gold-molybdenum geochemical rock anomaly extending over an area of 1,000m x 800m has been identified. This coincides with the presence of 1-3mm wide quartz veinlets that are translucent and may have dark borders. The veinlets pre-date the advanced argillic alteration. Such quartz veinlets are characteristic of porphyry gold deposits where they form in potassic alteration which, at Doğanbey, appear to have been overprinted by illite and then, in part, by advanced argillic alteration (Sillitoe, 2006).

The discovery of the Doğanbey porphyry gold centre is conceptually important for the exploration of the other major areas of alteration in the Erenler Dağı Volcanic Belt including Çukurağıl, Oğlakçı, Gavur Gölü, Mesudiye, and Orta Karaören. Importantly this type of porphyry-gold mineralization is currently being exploited at Eldorado Gold's 4.5 Moz (reserve) Kısladağ gold deposit that is also hosted by a Miocene-age volcanic complex in western Turkey.

The Erenler Dağı Volcanic Belt is remarkably similar to the Maricunga belt of Chile in terms of both geology and exploration history (Sillitoe, 2006). Maricunga comprises a series of little-eroded stratovolcanoes and dome

complexes of Miocene age with high-sulphidation epithermal gold and/or silver (La Coipa, Purén, Esperanza) to porphyry gold (Refugio, Marte-Lobo) and gold-copper deposits (Cerro Casale). Intriguingly, like Ereneler Dağı in 2004, no gold had been discovered in the Maricunga belt before the early 1980's and yet today it boasts discoveries totaling in excess of 40 Moz Au. This highlights the considerable exploration potential of not only the Ereneler Dağı Volcanic Belt, but also of Tertiary volcanic belts throughout the Tethyan Eurasian Metallogenic Belt.

## ACKNOWLEDGEMENTS

The professional input of remote sensing consultant Dr Tony Starling to the Konya exploration program is warmly acknowledged. The authors thank Stratex for allowing publication of this contribution.

## REFERENCES

Besang C, Eckhardt F, Harre W, Kreuzer, H. & Müller P. (1977) Radiometrische Altersbe-stimmungen an neogenen Eruptivgesteinen der Türkei. *Geologisches Jahrbuch* B25: 3-36.

Karakaya, M, Karakaya N. & Temel A. (2001) Kaolin Occurrences in the Erenler Dagi Volcanics, Southwest Konya Province, Turkey. *International Geology Review* 43:711-721.

Keller J., Jung D., Burgath K. & F. Wolf (1977) Geologie und petrologie des Neoge-nen kalkalkali-vulkanismus von Konya (Erenler Dag-Alaca Dag Massiv, Zentral-Anatolien). *Geologisches Jahrbuch* B25: 37-117.

Tobey E., Schneider A., Alegria A, Olcay L, Perantonis G, Quiroga J. 1998.Skouries porphyry copper/gold deposit, Chalkidiki, Greece - Setting, mineralization and resources, in Porter, T.M. (Ed), 1998 - *Porphyry and Hyd-rothermal Copper and Gold Deposits - A Global Perspective;* PGC Publishing, Ade-laide: 175-184.

Redwood, S. D. (2005a) Konya Recce –Preliminary Report (Turkey). *Report for Stratex Exploration Ltd., London,* 10 September 2005, 4 p.

Redwood, S. D. (2005b) Exploration of the Konya and Inlice Projects, Western Anatolia, Turkey. *Report for Stratex Exploration Ltd., London,* October 2005, 47 p.

Redwood, S. D. (2006) Exploration of the Doğanbey Project, Konya, Turkey. *Report for Stratex International plc, London,* April 2006, 26 p.

Sillitoe, R.H. (2006) Geological Features and Exploration Potential of the Inlice and Doğanbey gold prospects, Konya Volcanic Belt, Turkey. *A report prepared for Stratex International plc*, 6 November 2006, 13 pp.

Temel A, Gündogdu M. N. & Gourg A. (1998) Petrological and geochemical characteristics of Cenozoic high-K calc-alkaline volcanism in Konya, Central Anatolia, Turkey. *Journal of Volcanology and Geothermal Research* 85: 327-354.

# Rare metals in the ores of Armenia

Hayk P. Aloyan
*Lydian Resource Company Ltd*

ABSTRACT: State and formational-technological development extent of mineral raw material of rare metals are reviewed and assessed. To develop the multipurpose utilization of polymetallic raw material, the top-priority targets and preponderant metals are proposed to establish local centers of rare-metal industry at the large-scale mining enterprises.

KEYWORDS: scandium, platinoids, rhenium, cadmium, Alpine folded zone.

## 1 INTRODUCTION

Armenia is one of the ancient centers of mining industry. Nowadays, a reliable raw material basis for long-term development of mining and metallurgical industry is established. Armenia is located in the South Caucasus and plays an important role in the metallogenic structures of the Alpine folded zone. Pre-Alpine basis of Armenian upland has heterogenic structure. Alpine geodynamics have sharply contrasting and asymmetric features. Ophiolite belt of Lesser Caucasus is regarded as a zone of marginal-continental riftogenesis which has founded one of branches of meso-Tethys oceanic basin (Fig. 1). On the territory of Armenia, meso-Tethys existed during Jurassic and Cretaceous periods and interrupted in the early Senonian at the beginning of collision. Orogenic epoch of region development has begun since Oligocene. Neo-Tethys suture appeared in Cenozoic as a result of collision of Arabian and Eurasian plates.

The metallogeny of Armenia is stipulated by the complexity of geodynamic features. It is characterizing by the absence of particular metallogenic zones for definite metals, as well as by multicomponent and multistage ore clusters. Rare metals do not form any separate deposits on the territory Armenia. They mainly occur in porphyry Cu-Mo ore associations with stockwork type of mineralization, as well as in copper-ore and gold-polymetallic ore associations with vein type of mineralization. These associations are characterized by the overall presence of Cd, Se, Te and Bi, while platinoids, Re, Sc and V occur in porphyry Cu-

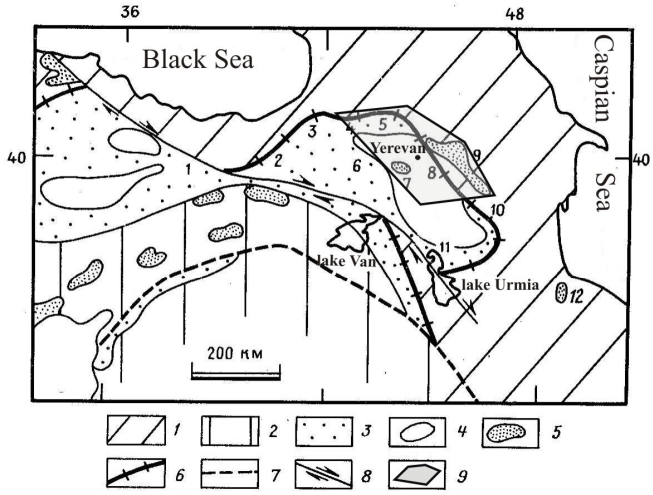


Figure 1. Suture of meso-Tethys within the limits of Armenian upland (Bazhenov *et al.*, 1991. Edited by Hayk Aloyan)

*Legend:* 1 – Caucasus margin of Eurasian plate of Hercynian consolidation; 2 – Iranian-Armenian active margin of Arabian plate of Baikal consolidation; 3 – ophiolites development regions; 4 – pre-Alpine land masses; 5 – ophiolite allochthons; 6 – meso-Tethys suture; 7 – neo-Tethys suture; 8 – shears; 9 – territory of Armenia.
*Numbers on the figure:* ophiolites of Turkey – r.Kilkit valley (1), Chorokh-Karasu interfluve (2), r.Chorokh basin (3), Karakios (6); ophiolites of Armenia – Amasia (4), Shirak and Basum mountain ranges (5), l.Sevan basin (8-9), Vedi (7); ophiolites of Iran – Karadag (10), Khoi (11), c.Reshta (12).

Mo deposits, and Ga, Ge, In and Tl – in gold-polymetallic deposits.

## 2 RHENIUM, RADIOGENIC OSMIUM, PLATINOIDS

*Rhenium (Re)* minerals occur in porphyry Cu-Mo ore deposits. The average Re grades vary in molybdenum concentrates of developed deposits between 260 ppm (Kajaran) to 524 ppm (Agarak) and in concentrates from those deposits which were explored in detail and prepared for commercial development, between 340 ppm (Lichk) and 740 ppm (Teghout). The average Re concentration in ores from these deposits is 0.1-0.3 ppm. High Re concentration was recorded in ores from the Vaiotsdzor group of deposits, *i.e.*, an average of 4,000-18,800g Re in a tonne of molybdenum concentrate. However, these deposits have not been explored in detail and their reserves have not been calculated or assessed and this calls for a first-priority exploration of these deposits.

The total rhenium reserves in Armenian ores, taking into account both the proven and geological reserves make up approximately 10-12% of the World reserves.

*Platinum group elements (PGE.* An analysis of ore associations for platinum potential has revealed that it is traditionally associated with Alpine-type ultramafic rocks of Sevan ophiolites association. The average content of platinum group elements (PGE) in ores of the porphyry Cu-Mo association varies between 0.016 ppm (Kajaran) to 0.024 ppm (Agarak) and this varies from 0.156-0.211 (Kajaran) to 0.371 ppm (Agarak) in the molybdenum concentrate and from 0.131-0.166 (Kajaran) to 0.151 ppm (Agarak) in the copper concentrate. The highest PGE abundance is associated with ores of the early high-temperature molybdenum stage of mineralization, which is characterized by preponderance of platinum (Pt) over palladium (Pd) contrary to the general ratio Pd:Pt>1. As the ore-formation temperature declines, the PGE concentrations drop, and the Pd:Pt ratio changes with a sharp decline in the absolute values and with an insignificant preponderance of platinum. Keeping in mind the achieved technologic advances regarding the principal commercial components (Cu, Mo, Re) vs. the total PGE concentration in the summary concentrate (approximately 0.35-0.40 ppm), 30-35% of these elements are accumulated in copper concentrates and 60-65%, in molybdenum ones, while their losses in the tailings are insignificant.

The aggregate forms of PGE in the ore associations in Armenia still have not been revealed. These elements are irregularly distributed in the ores. PGE are present in ores as isomorphic impurities in ore minerals. Taking into consideration the earlier established correlation relationships between rhenium and radiogenic osmium, and between molybdenum and rhenium, the contours of ores enriched in elements of the three-member paragenesis, *i.e.* molybdenum-rhenium-osmium, have been outlined (Fig. 2).

Processing of the whole collected data obtained from exploration of the Kajaran deposit has allowed calculating, based on the data of group analyses and technological tests, over 130 tonnes of PGE resources. The most promising development reserves are concentrated within the central part of the Kajaran stockwork at horizons of 1980-1850m MSL within an area of 500x800m. It is notable that the porphyry deposits in USA (Climax and others) enclose approximately 150 tonnes of PGE, which allows approximately 1 t Pt and Pd annual production from the primary material at a ratio Pt:Pd = 35:65.

The copper-molybdenum ore association is more promising in Armenia than the traditional chromite association (dunite-harzburgite) both in terms of element concentrations and in terms of the element reserves and the technical feasibility of simultaneous recovering commercial elements. This is a fundamentally new approach. These data form a basis for initiating purposeful mineralogical-geochemical and technological studies aiming to assess the prospects of rock associations in the country with respect to their platinum and radioactive-element potential. Such a giant deposit as the Kajaran may become the first-priority target.

Studies performed by the author revealed that all known large brown coal and oil shale deposits in Armenia were metalliferous, much the same as black-shale successions in the World, and contained commercial concentrations of Au, Ag, Pt and Pd. Total PGE concentrations vary within wide limits: from 0.5-1 to 8-10 ppm. Mo abundance with higher PGE concentrations in some targets (Jajur, Jermanis, Nor-Arevik, *etc.*) reaches a value of 0.2%, which is many times higher than the commercial concentrations in currently worked copper-molybdenum deposits (Kajaran, Agarak).

## 3 CADMIUM, SELENIUM, TELLURIUM, BISMUTH.

*Cadmium (Cd)* reserves have been included in the State Ore-Reserve Register of the Republic for three deposits: Shahumyan, Akhtala and Armanis containing vein type copper-pyrite ores. Cadmium is generally present as an impurity in sphalerite and rarely forms an independent mineral pribramite [(ZnCd)S] with an average Cd concentration up to 5%. The average Cd abundance in ores of the Sahumyan deposit (up to 60% of all registered reserves are concentrated here) is 270ppm, whereas its content is 1.5-4.8 kg/tonne in concentrates.

Analysis of available data on the cadmium-bearing potential of polymetallic ores has shown that cadmium enrichment in certain sphalerite varieties is associated with the temperature of ore-forming solutions and with Cd concentration in them. Dark-colored varieties of sphalerite (marmatite) in the Sotk epithermal gold deposit are richer in cadmium than light-colored varieties from the Margahovit, Azatek and Kakavasar mesothermal-epithermal gold deposit: this is possibly caused by replacement of zinc with cadmium at a relatively high temperature. The total expected Cd reserves in Armenia may exceed many times the reserves included into the State Register and reach percent of the World total reserves, which would mean a considerable strategic commodity potential.

*Selenium (Se)* and *tellurium (Te)*. Reserves, which are included into the State Register, have been calculated in the mined porphyry Cu-Mo deposits such as the Kajaran, Agarak, and vein copper deposits such as Kapan and Shahumyan. The highest selenium concentrations were recorded in molybdenite from the Kajaran deposit and in galena from the Shahumyan deposit. Se and Te are extracted in the highest degree from the copper concentrate during processsing copper-molybdenum and copper ores from the Kajaran deposit and from lead concentrate from the polymetallic ore at the Shahumyan deposit. Of great interest are vein copper-pyrite deposits in Northern Armenia at the western flank of the Alaverdi ore cluster (Alaverdi, Agvi, Alvard, *etc.*) that are regarded as targets for bacterial and sulphuric-acid leaching. The Se abundance in mono-minerallic ores is 235-328 ppm. Se is present in the ores of polymetallic ore association (Gazmi, Azatek, Kakavasar deposits) as isomorphic admixture in crystal lattices of sulphides and sulphosalts, whereas Te forms lead, bismuth, silver and gold tellurides. Tellurides in the Meghradzor gold deposit are of a particular importance, since they pass in the process of ore flotation into the auriferous concentrate. The total industrial reserves exceed 15 tonnes.

The Hankavan porphyry copper deposit in Central Armenia and its individual sites are the first-priority targets for supplementary explora-

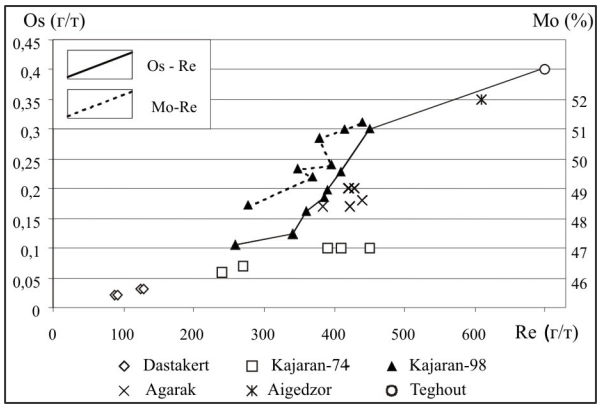


Figure 2. Plot of Mo-Re-Os paragenetic triad in the Armenian copper-molybdenum deposits.

tion (for Se, Te and Bi). Lately, Armenian technologists have scored cardinal successes in the technology of through extraction of Se and Te: up to 70-80% from concentrates and up to 98% from solutions.

*Bismuth (Bi)* is typical for the porphyry copper-molybdenum, gold and polymetallic ore associations in Armenia. The State Register includes reserves of seven deposits: porphyry copper-molybdenum – Kajaran, Agarak; porphyry copper – Lichk; copper-sulphur-pyrite Alaverdi; vein gold-polymetallic - Lichkvaz-Tei, Terterasar and Armanis. 95% of all Bi reserves are contained in copper-molybdenum ore of the Kajaran deposit. The principal concentrators of Bi in ores of the copper-molybdenum ore association are chalcopyrite (0.006-0.043%), galena (0.042-0.067%), pyrite (0.002-0.034%) and molybdenite (from 0.001-0.003 to 0.023%). Those reserves, which are not included into the Register, are vein gold-polymetallic ores in the Gladzor, Azatek (Kayadir site), Kakavasar, and Privol'noe deposits. Bismuth concentrations in these ores are 0.01-0.1 % in galena and 0.2-1% in lead concentrate. Bismuth abundance in polymetallic ore (galena) of the Marjan-Mazmazak ore cluster exceeds 1.0%. Bi reserves in these deposits have not been calculated and the targets have not been

evaluated. Lead, copper and tin concentrates are the principal sources for Bi production. The technology of ore dressing and metallurgical processing of the concentrates for producing metallic Bi is well worked out in the world practice, and Armenian technologists worked out the technology of processing converter dust for producing aggregate cadmium-bismuth cement material. Metallurgical recovery for Bi is very high in all stages of treatment. The marketable product is very pure Bi (99.999%).

## 4 VANADIUM AND SCANDIUM

*Vanadium (V).* The average V concentration in the ore of the Kajaran porphyry Cu-Mo deposit is 200 ppm. Approximately 80-85% of V are contained in magnetite, and the average abundance of magnetite in the ore is approximately 1%. From calculations, performed by the author, the V reserves within the contour of commercial Cu-Mo reserves are 350,000t. The Yerevan Mining-Metallurgical Institute worked out and tested a technology for producing vanadium-containing magnetite concentrate from ore-dressing tailings of the Kajaran copper-molybdenum deposit according to a flowsheet including magnetite separation with additional magnetic cleaning of the crushed product. As a result, high-quality magnetite concentrate containing 60-65% iron, was produced from dumped tailings; magnetite recovery into the concentrate reached 75%. Abundance of V in the magnetite concentrate varied from 0.25 to 0.56%. Both V and Ti in the Agarak deposit are also common in the host rocks. Deposits of the copper-molybdenum ore association such as the Kajaran and Agarak deposits, may be regarded as those of a new, type of ores promising for vanadium with the element concentrations being not inferior to those in well-known ores of titanomagnetite deposits. The present author views ore-dressing tailings as raw material for V production. Simultaneously, magnetite concentrates can be utilized as substitute of high-grade iron ores for ferromolybdenum production, which dictates the necessity of setting such alloy production in the area of the Artsvanik tailings dump. Production of the scarce ferrovanadium can be organized by providing sufficient technological and mineralogical-geochemical substantiation.

*Scandium (Sc).* Presence of scandium in ores of the Sotk gold deposit and in the Kajaran porphyry copper-molybdenum and Lichk porphyry copper deposits was established by the authors. For instance, Sc concentrations in sulphide ores of the Sotk deposit are 5-6 ppm, and those in oxidized ores are 15-20 ppm. In the process of ore dressing approximately 75-80% Sc passes into slime. The Sc concentrations in ore of the Kajaran deposit may vary between 6 and 20 ppm, and approximately 50-85% of Sc concentrates in tailings. In the Lichk deposit, Sc is concentrated predominantly in molybdenite (5-6 ppm).

Scandium production from iron-bearing ore-dressing tailings at the Kajaran copper-molybdenum deposit is appear to be the most promising. Sc reserves in the registered ores of the Kajaran deposit are over 30,000 t at average grade of 15 ppm. At that, hundreds of million of tonnes of old tailings have not been taken into account. The commercial value of these reserves is supported by the ore-association affinity of these ores with the copper-porphyry type, by the Sc concentration in iron-bearing ore-dressing tailings, by the production capacities of the integrated works, and, finally, by the high price and the strategic importance of the metal. However, a set of mineralogical-geochemical and metallurgical studies has to be undertaken for the final solution of this problem. This problem is stated for the first time taking into consideration the very high recovered Sc value, as well as the technological and production capacities of the Zangezur copper-molybdenum integrated works.

## 5 CONCLUSIONS

1. There are rhenium, selenium, tellurium, bismuth, cadmium, vanadium, platinoids, scandium, radiogenic osmium *etc*. in the copper, copper-molybdenum, auriferous and polymetallic concentrates of Armenia.
2. Copper-molybdenum formation of porphyry ores is more perspective by its content, scales and technical possibilities of platinum group elements extraction as by-products than the chromite formation. Iron-bearing dressing tailings from copper-molybdenum formation deposits can serve as raw material for scandium, vanadium, titanium and iron extraction.
3. By their noble-metal and rare-metal features, the coal-bearing associations of Armenia are comparable with the gold-ore and polymetallic deposits by the and favourable geological mining conditions.

# Geodynamics of the Neo-Tethys arc and associated porphyry copper mineralization in Iran

H. Asadi Haroni
*Mining Department, Isfahan University of Technology, Isfahan, Iran*

F. Aiaty
*Geology Department, Isfahan University, Isfahan, Iran*

ABSTRACT: The Zagros Orogenic Belt (ZOB) is part of the Alpine-Himalayan orogenic and metallogenic belt and extends in a NW-SE direction throughout Iran. The ZOB is divided into three parallel geological subdivisions of the Urumieh-Dokhtar Magmatic Arc (UDMA), the Sanandaj-Sirjan Zone and the Zagros Folded Belt. The evidence from country-scale integration of aeromagnetic, geological and mineral occurrence data and trace element analysis of the UDMA rocks supports a subduction model, associated with the closure of the Neo-Tethys ocean, for the origin of the ZOB. Two types of Cu-Mo and Cu-Au porphyry mineralizations are found along the UDMA. The Cu-Mo porphyry type is very common and mostly found in the SE and NW of the UDMA. Whereas, the Cu-Au porphyry type is quite rare and only one prospect (Dalli) has been recently discovered in the central UDMA. The magmatic rocks at the vicinity of the Dalli prospect shows a calk-alkaline affinity.

KEYWORDS: Neo-Tethys, Iran, Porphyry Copper, Data Integration

## 1 INTRODUCTION

The Zagros Orogenic Belt (ZOB) in Iran is part of the Alpine-Himalayan metallogenic and orogenic belt and extends over 2000km in a NW-SE direction from the Eastern Anatolian Fault of eastern Turkey to the Oman Line in southern Iran (Alavi, 1994). Such environments, across the Alpine arc, from Italy through the Balkans and Turkey and to Iran, favour the occurrence of porphyry copper, massive sulphide and chromite deposits, hydrothermal Pb, Zn and Ba deposits, and numerous occurrences of Au, Ag, As, Sb, Hg deposits related to epithermal systems connected to the ophiolites and arc volcanism. Based on geological and petrological evidences, both subduction model and less favorable continental rifting model have been proposed for the origin of the ZOB. Among those who support the subduction model, however, there is disagreement, in terms of magmatic affinity and certain spatial features and elements typical of a subduction setting such as the precise location of the suture zone-with ophiolites and the volcanic arc (Alavi, 1994).

A rift model for the origin of the volcanic rocks and their geodynamic situation along the ZOB was proposed by Sabzehei (1974). He argued that the volcanic rocks belong to the Central Iran Mass and are mainly alkaline in origin.

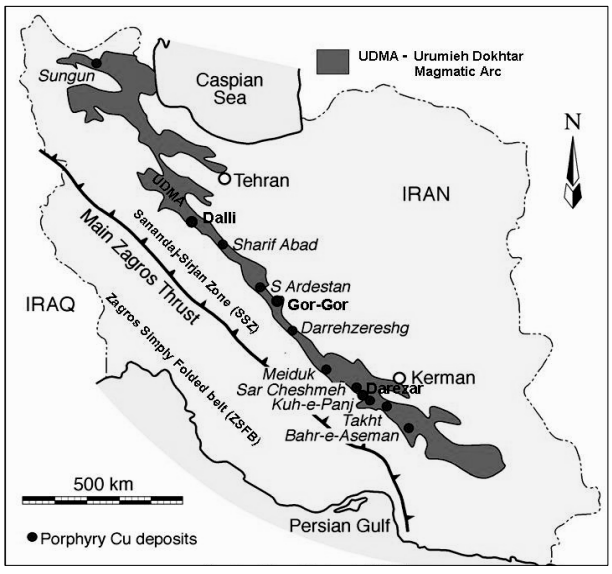


Fig. 1. Approximate boundaries of geological subdivisions of the ZOB and associated porphyry copper deposits in Iran

In this paper, a review of the known models for the origin of the ZOB is followed by integrated analysis of aeromagnetic, geological and mineral occurrence data of the ZOB as well as petrological studies of the magmatism to define

the best geodynamic model. Particular emphasis is made on the characteristics and magmatic association of two different types of Cu-Mo porphyry and Cu-Au porphyry mineralizations associated with the volcanic arc of the ZOB.

## 2 ORIGIN OF THE ZOB

The subduction-related settings in different parts of the ZOB are believed to be associated with the closure of the Neo-Tethys ocean, between the Afro-Arabian Plate and the Iranian Plate. The generally-accepted way in which Alavi (1994) sub-divides the ZOB distinguishes three elongated parallel zones from NW to SE *viz.*, the Urumieh-Dokhtar Magmatic Arc (UDMA), the Sanandaj-Sirjan Zone (SSZ) and the Zagros Simply Folded Belt (ZSFB), (Fig. 1). He postulates that the boundary between the UDMA and SSZ is formed by the Zagros Suture (ZS), characterized by some elongated, mylonitized and sheared ophiolites. The boundary between the SSZ and ZSFB is formed by the so-called Main Zagros Thrust (MZT), and many researchers propose it as the main suture zone along the ZOB (Berberian & King, 1981). The MZT grades into the lesser-deformed ZSFB and eventually into the undeformed sediments of the Mesopotamian-Persian Gulf Basin.

The UDMA, characterizing Neo-Tethys magmatism in Central Iran, comprises a linear magmatic arc which extends along the entire length of the ZOB. It is said to be an Andean-type magmatic arc formed by NE subduction along the active continental margin of the Central Iran Block during the Alpine orogeny (Sengor, 1990). Alavi (1994) suggested that it is an Andean-type magmatic arc resulting from NE subduction along the eastern margin of the SSZ. Its formation has also been interpreted as post-collision magmatism (related to orogenic collapse), rather than subduction. An alternative hypothesis is that the volcanism of the UDMA was originated in a continental rift setting (Sabzehei, 1974).

Miocene plutonic rocks are well-represented in the UDMA and mostly include diorite, granodiorite and granitoids. Oligo-Miocene volcanic rocks are widespread as flows of andesite, dacite and pyroclastics. Granitoid rocks of the UDMA are tentatively classified as calc-alkaline I-type Cordilleran-type products (Alavi, 1994). Richards (2003) argued that Cenozoic volcanic rocks of UDMA range from calc-alkaline to alkaline composition, nevertheless, the bulk of Eocene-Miocene magmatism is medium to high calc-alkaline in character. On the basis of the trace element compositions of Cenozoic magmatism, he explained a subduction origin for these suits.

Subvolcanic rocks were analysed for oxides and trace elements by ICP-MS in Amdel laboratory in Australia, to define the magmatic affinity of the central UDMA, surrounding the recently discovered Dalli Cu-Au porphyry prospect (Fig. 1). On the basis of the $K_2O+Na_2O/SiO_2$ diagram of Le Bas *et al* (1986), the rocks at Dalli area clearly shows a sub-alkaline affinity (Fig. 2). Plotting $SiO_2$–FeO/MgO diagram shows that the sub-alkaline rocks have calk-alkaline affinity rather than tholeiite.

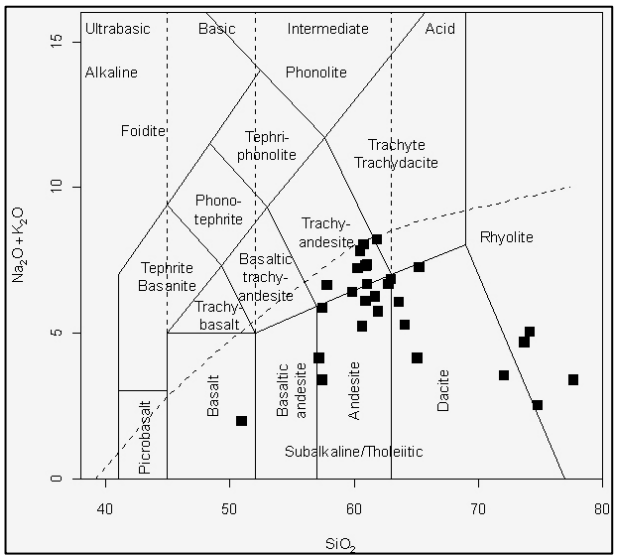


Fig 2. Chemical classification of the of UDMA rocks, using Na2O+K2O/SiO2 diagram of Le Bas *et al* (1986)

Plotting trace element results of ICP-MS analysis at Dalli area on the Spider diagram of Weaver & Tarney (1984), normalized by the lower crust, shows a high concentrations of U and Th and relatively low concentrations of Nb, Ti and P. This evidence characterizes a subduction setting for the UDMA rocks, located at the proximity of the Dalli Cu-Au porphyry prospect (Fig. 3).

In addition, to test the hypothesis of the subduction model and define more precisely its related geological features, in a country-scale GIS framework, geology (lithological and structural attributes) and mineral occurrences were digitized from three 1:1000 000-scale map sheets covering the ZOB. Magnetic data of the nation-

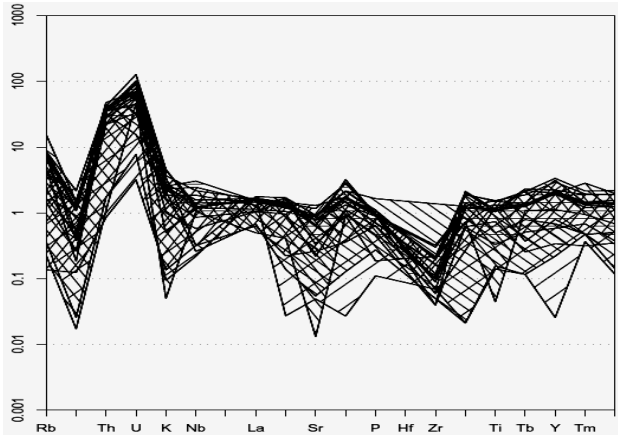


Fig. 3. Spider diagram of trace element analytical results of the magmatic rocks at Dalli area

wide airborne reconnaissance survey (7.5-km line spacing), conducted in 1976, was digitized from total magnetic field contour maps. State of the art visualization and enhancement techniques have been applied to the aeromagnetic data set for interpretation. Finally, all data sets were re-formatted to a uniform map projection (Lat-Long coordinates) and combined to create a database and GIS covering the whole of the ZOB. Most rock types have specific magnetic susceptibilities and therefore aeromagnetic measurements, when suitably processed, can distinguish different rock types. Shaded-relief total intensity magnetic field map of Iran clearly shows the geological subdivisions of Zagros. The strongest anomalies on this map, which appears in purple/red, extend in a NW-SE direction and coincide with the UDMA. The analytic signal of the total magnetic field was used to map anomalies associated with rocks of high magnetic susceptibility, both outcropping and at depth. Paterson and Reeves (1985) point out that the analytic signal is independent of the inclination of the geomagnetic field and magnetic information is displayed in a more interpretable manner than total magnetic intensity. Therefore, the color-scale shaded-relief analytic signal map of Iran was used to map outcropping and sub-surface igneous rocks and define more precisely the boundaries of the UDMA, SSZ and ZSFB.

Inverted gray-scale shaded-relief image of the total magnetic field map of Iran was used for subsurface structural mapping along the ZOB (Fig. 4). On this map, high-amplitude magnetic anomalies appear in black. This map was used to identify NW-SE, NE-SW and N-S structures. The boundary of the SSZ and UDMA is clearly marked by these structures. The NE-SW and N-S faults appear to postdate the NW-SE structures. By overlaying the known igneous rocks of the UDMA on the analytic signal map of Iran, it is possible to map other zones of surface and subsurface igneous rocks along the UDMA. The magnetic signatures characterizing the exposed ophiolites of the ZOB were used to infer that certain elongated features, represented unrecognized ophiolite bodies at surface and at depth. The newly mapped ophiolites are located in the SSZ,

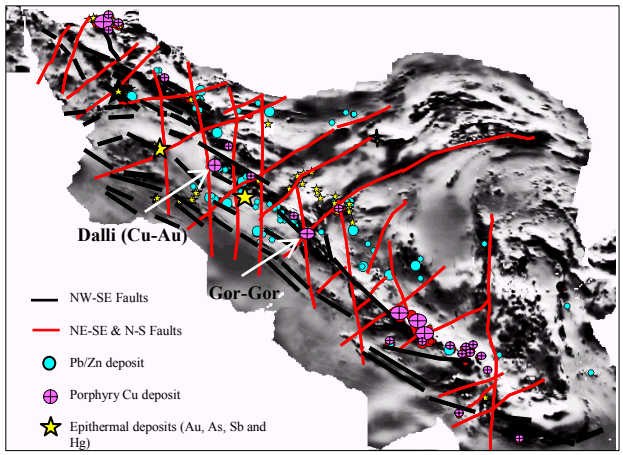


Fig. 4. Inverted grey scale total magnetic field intensity map of Iran with the overlaying mineral deposits and the main linear structures along the ZOB

which could characterize the ZOB suture zone at the contact of the SSZ and the UDMA, as initially proposed by Alavi (1994).

Combining published ideas with the new interpretations described above, the following geodynamic history is proposed for the ZOB. The ZOB formed by an early Mesozoic separation of the Central Iranian continental block from the Gondwana landmass and then a NE-dipping subduction of the newly generated Neo-Tethyan oceanic crust below the Iranian microcontinent, during Eocene. Anatexis of the subducted material led to the formation of a magmatic arc (the UDMA) with calk-alkaline affinity and associated porphyry copper mineralization. Subsequent collision of the Afro-Arabian and Iranian Plates resulted in south-westward thrusting and stacking of passive margin rocks forming an accretion wedge with suture materials (*e.g.*, ophiolite in the SSZ).

## 3- METALLOGENY OF THE ZOB

Calc-alkaline volcano-plutonic rocks of the UDMA host several manto, porphyry deposits

and in places disseminated/vein type base metal and precious metal deposits (Fig. 5). The active mines and most of the large porphyry deposits are located in the SE and NW of the UDMA. The very large Sarcheshmeh mine (~1200 Mt at 0.64% Cu, 0.03% Mo and 0.02 g/t Au) and Songun deposit (~900 Mt at 0.76% Cu and 0.06% Mo) are located in the SE and NW corner of the UDMA, respectively. These and several other porphyry deposits are associated with Miocene granodiorite to quartz-monzonite stocks. In these deposits, mineralization is basically associated with potassic and quartz-sericite alterations.

In the central UDMA, although there are no known porphyry copper deposits, three porphyry prospects of Dalli (Cu-Au), Gor-Gor (Cu-Mo) and South Ardestan (Cu) have been discovered (Figs. 1&5) over the past two years. Dalli (~1.2 g/t Au and ~0.75% Cu) is so far the only reported Cu-Au porphyry prospect in the ZOB and lies on the western margin of central UDMA near its contact with SSZ. Three mineralized porphyry centers at Dalli lie within a NE trending corridor of altered Oligo-Miocene intrusives ranging from diorite to tonalite to granodiorite intruding Paleogene andesitic volcanics. The mineralized intrusive rocks at Dalli are affected by intense potassic alteration (quartz-secondary biotite-magnetite) with overprinted phyllic alteration (quartz-sericite-specularite±chlorite), strong silisification and surrounded by extensive propylitic alteration. Gor-Gor and South Ardestan prospects are mostly similar to those porphyry deposits, located in NW and SE of the UDMA.

The contact of UDMA and SSZ is potentially important for epithermal Au, Ag, As, Sb, Hg mineralizations of epithermal and Carlin type in character. Two disseminated/vein type Carlin like gold deposits of Zarshuran (~11 Mt@ ~6 g/t Au) and Aghdarreh (~5 Mt @ ~4 g/t Au) are the second and the third largest gold deposits in Iran. These deposits are hosted by silicified carbonate and black shale which are usually found a short distance from volcano-plutonic rocks of UDMA.

## REFERENCES


Alavi, M (1994) Tectonic of the Zagros orogenic belt of Iran, new data and interpretations. *Tectonophysics* pp 229: 211-238.

Le Bas, MJ, Lemaitre, RW, Streckeisen, A Zanettin B (1986) A chemical classification of volcanic rocks based on the total alkali silica diagram. *Jour. Pet* pp 27:745-750.

Richards, JP (2003) Metallogeny of the Neo-Thetys Arc in Central Iran. *7th Biennial SGA Meeting, Athens* pp 1237-1239.

Sabzehie, M (1974) Les melanges ophiolitique de la region d'E Sphandagheh. *These Doctorat Etat, Grenoble, France,* pp 121-132.

Sengor, AMC (1990) A new modle for the Late Palaeozoic-Mesozoic tectonic evolution of Iran and implication for Oman. *Geological Society of London Special Publication* pp 49:797-831.

Weaver, B and Tarney J (1984) Empirical approach to estimating the composition of the continental crust. *Nature* pp 310:575-579.

# Porphyry copper gold deposits at Reko Diq Complex, Chagai Hills Pakistan

A. Razique & G. Lo Grasso
*Tethyan Copper Company Pyt. Limited, Pakistan*

T. Livesey
*Barrick Gold Corporation, UK*

ABSTRACT: Reko Diq volcano-magmatic igneous complex is developed in the Western Chagai Belt associated with continental margin subduction tectonics. It lies in a multiphase intrusion complex within the inner rim of a major eroded strato-volcano. Several multiphase porphyry copper - gold systems of dioritic to tonalitic composition were emplaced in a volcano-sedimentary sequence during the Oligocene - Miocene. Porphyry deposits in Reko Diq exhibit concentric patterns of alteration from potassic cores extending outward to intermediate argillic silica-sericite-chlorite, phyllic and propylitic zones. Both hypogene chalcopyrite-bornite and supergene chalcocite style mineralization is developed in Reko Diq porphyry complex. A global copper-gold resource of 2.4 billion tonnes @ 0.51% Cu and 0.27g/t Au has been calculated to date.

KEYWORDS: porphyry, alteration, mineralization, sulphides

## INTRODUCTION

Reko Diq Porphyry copper-gold complex is located in the Western Chagai District of Pak istan, lying between 29°05' latitude and 62°00' longitude nearly 45 kilometres north of the main RCD highway leading from Quetta to Iran (Fig1)

Porphyry copper gold deposits developed within Reko Diq consist of large volumetrically cylindrical ore bodies emplaced vertically with coaxially distributed zones of alteration and mineralization. The intrusions are composed of diorite, and or tonalites cutting across the Paleocene sediments and Oligocene andesitic and pyroclastic volcanics. A total of fifteen significant porphyry systems have been discovered within Reko Diq complex out of which four are drilled to resource category. Supergene copper enrichment is developed in the older central Reko Diq Tanjeel deposit whereas the rest of all porphyry deposits are associated with hypogene copper gold mineralization.

## 1 REGIONAL GEOTECTONICS

Chagai magmatic Arc extends north-south for 150 km and east-west for 400 km in northwestern Balochistan and neighboring Afghanistan and Iran. In regional geo-tectonic context, this arc is part of the several thousand kilometers long Tethyan belt developed on the southern margins of Gondwanic Lut block in Iran and Afghan micro continental block (Stocklin, 1977, Lawrence *et al.*, 1981). Chagai arc terrain dominantly consists of subduction related magmatism of calc-alkaline association initi ated in the late Cretaceous. Therefore, it is considered to have developed due to the northward subduction of Arabian oceanic plate (Stonely 1974) or Neo-Tethyan under the southern margin of Dasht-e-Margo basement block as continental margin of Andean type (Sillitoe & Khan, 1977).

## 2 GEOLOGY

Reko Diq volcano-magmatic igneous complex lies in a multiphase intrusion complex within the inner rim of a major eroded strato-volcano. The mineralized intrusions are composed of diorite - tonalite suit porphyries hosted by late Eocene-Oligocene andesitic volcanics, pyroclastics and Palaeocene sediments. K-Ar age dating revealed that the oldest porphyry, associated with the Tangeel supergene copper deposit, was emplaced 26.7 Ma; whereas all the younger diorite and tonalite

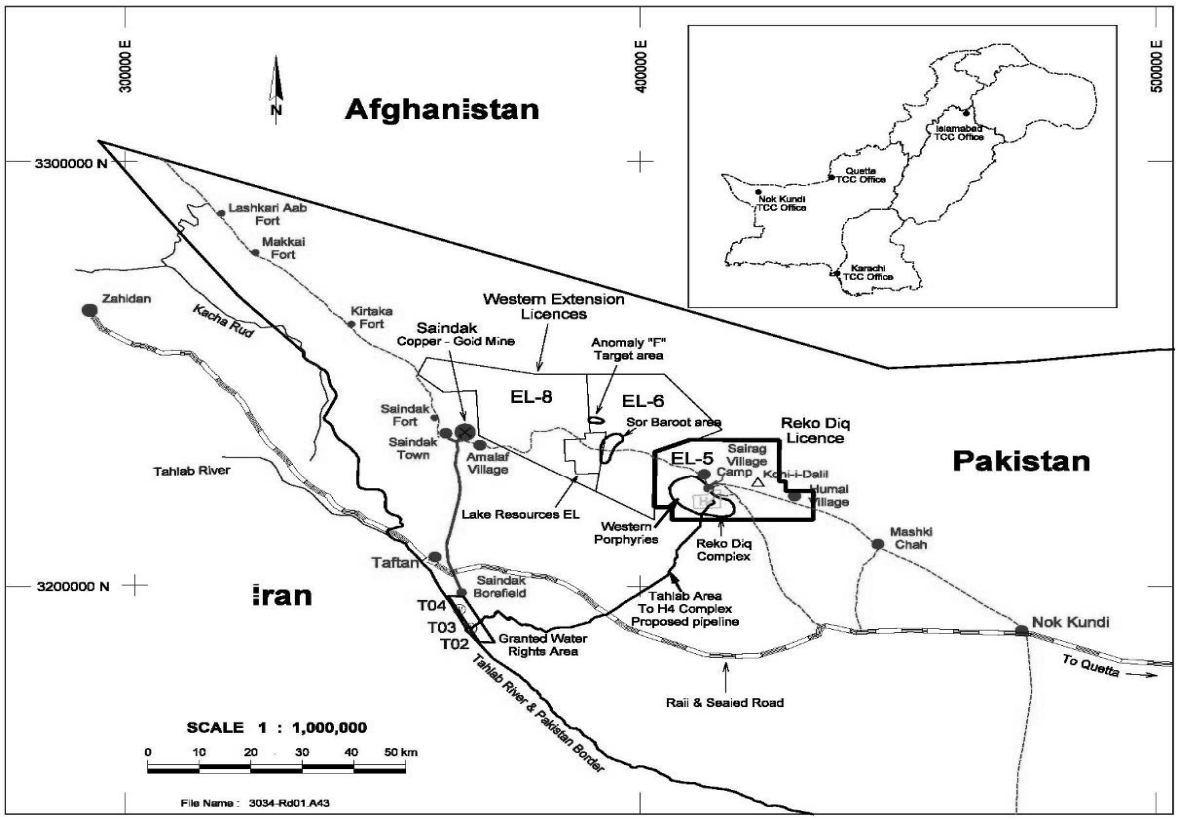


Figure 1. Location and accessibility map of Reko Diq porphyry complex, District Chagai Pakistan

porphyries associated with hypogene mineralization are dated as 10-12 Ma.

The sedimentary sequence underlying Reko Diq volcanic edifice is mainly composed of fluviatile or deltaic sandstone, siltstone and discontinuous poorly sorted inter-beds of conglomerates correlated to the Palaeocene Juzzak formation (Fatmi, 1977). Late stage, weakly mineralized inter-mineral feldspar-biotite porphyry stocks locally cut across parts of the western porphyries. Young mafic volcanics and dykes are exposed peripheral to the porphyries and around the Reko Diq igneous complex.

## 3 ALTERATION

Hydrothermal alteration Reko Diq porphyry complex is developed with coaxial concentric zonation pattern around the porphyry system similar to the alteration model proposed by Lowell & Guilbert, 1970. Early potassic alteration is associated with central part of the main porphyry intrusion followed by a discontinuous transitional zone of intermediate argillic alteration of retrograde phase. This is surrounded outward by phyllic, argillic and propylitic alteration zones. The alteration terminology have been adopted from literature (Burnham, 1962; Creasey, 1966 & Meyer & Hemley, 1968)

### *3.1 Potassic Alteration*

Potassic alteration of biotite-K-feldspars-magnetite assemblage is strongly developed within the central well mineralized diorite-tonalite porphyries, country volcanics and sediments. The primary mineralogy, mafics and plagioclase are largely recrystallized by hydrothermal alteration of pale brown specks of secondary biotite and K-feldspar flooding (Fig 2-B). Ground magnetics has provided the primary tool in identification of these porphyry systems due to the strong secondary magnetite development in the potassic core. Sericite-chlorite overprinting is common in potassic centers developed as a result of the late stage hydrothermal phases destroying the early potassic alteration.

### *3.2 Intermediate argillic alteration*

This is a discontinuous transition zone of alteration with sericite-clay chlorite (SCC) assemblage developed outwards from potassic centre. The associated magnetite tends to oxidize to specular haematite. It is mainly associ-

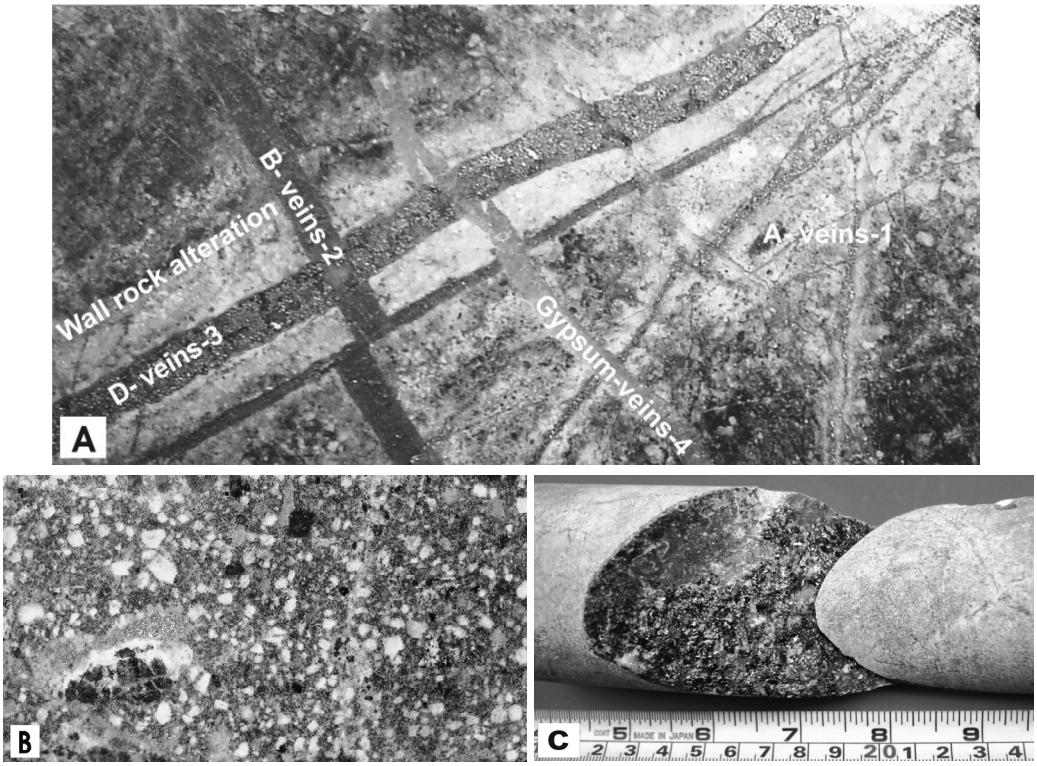


Figure 2 Diamond core photographs showing cross cutting veining relationships (A), feldspar-biotite porphyry with K-silicate alteration (B) and disseminated and veinlet chalcopyrite – bornite mineralization (C)

ated with host volcanics and contact breccia zones in almost all porphyry centers in Reko Diq.

### *3.3 Phyllic Alteration*

Phyllic alteration zone of quartz-sericite-clay mineral assemblage is extensively developed in Reko Diq porphyry complex. Hydrothermal quartz-sericite mosaics have destroyed the original rock textures and have totally replaced the primary mineralogy except phenocrysts of magmatic quartz. Hydrothermal quartz is ultra fine and is flooded in the surrounding volcanic rocks as silicification; Clay minerals (Kaolin) are also associated with phyllic alteration especially outwards along the contact with argillic alteration zones. According to Lowell & Guilbert (1970), Phyllic alteration generally includes part of the ore zone and all the marginally mineralized zones are rich in pyrite mineralization as in Reko Diq western porphyries.

### *3.4 Propylitic Alteration*

Propylitic alteration of chlorite-epidote assemblages extensively developed at the peripheries of all Reko Diq porphyry system. To the west a dyke swarm complex is represented by strong epidotization.

### *3.5 Hydrothermal Veining Phases*

Quartz stock working and magnetite-K feldspar veining have a significant positive correlation with higher copper grades >0.6% Cu intersected in Reko Diq western porphyries. Several hydrothermal phases resulted in the deposition of multiple crosscutting veins overgrown each other. At least five phases of crosscutting veins have been identified in the diamond core drilling samples. The intense early stage AB veining is confined to the main porphyry stock and potassic core of the system. The late stage sulphides D veins generally appear as coarse pyrite and chalcopyrite veins with well defined wall rock alteration selvages (Gustafson & Hunt, 1975). Gypsum veining cross cuts all the earlier phases particularly in western porphyris (Fig 2-A).

## 4 MINERALIZATION

### *4.1 Hypogene Copper Sulphides*

Hypogene copper-gold mineralization is developed below an oxide zone of 15-20 metres in the Reko Diq western porphyries. Copper sulphides pyrite-chalcopyrite-bornite is generally disseminated and veinlet with a total sulphide content of 2.5% (Fig 2-C). There is a very

strong positive correlation of potassic alteration and copper sulphides. The copper gold grades and chalcopyrite-bornite ratio increases the intensity of K-silicate alteration. Contact breccia zones and sediments, particularly sandstone and conglomerates are also well mineralized grading up to 0.8% Cu and 0.4g/t Au. Coarse grained pyrite, chalcopyrite D-veins and traces of molybdenum are common in SCC alteration zones.

### *4.2 Supergene Copper Enrichment*

Supergene copper mineralization at Reko Diq central Tanjeel copper deposit is developed in the form of a well defined chalcocite enrichment blanket below a leach cap of 40-50m. The leach cap is represented by strong leaching, Fe-oxidation, relict sulphides and pervasive sericite-clay alteration. Supergene alunite veining is common and dated as 3.8 Ma. The chalcocite blanket represents disseminated and veinlet pyrite and chalcocite (~5%) with a ratio of 7:3 respectively. Minor covellite, molybdenum and traces of cuprite also exist in the system.

## CONCLUSIONS

Porphyry Cu-Au deposits in Reko Diq complex are associated with calc-alkaline magmatism of Miocene age linked to rapid uplift, driven by the collision of the Arabian and Eurasian plates. Uplift had reduced substantially by the Pliocene, preserving a supergene Cu enrichment blanket at Tangeel.

Alteration paragenesis and distribution is typical of other porphyry Cu deposits (Gustafson & Hunt, 1975). Strongly potassically altered centers of the main tonalite porphyry stocks carry the highest copper-gold grades with up to 1.0% Cu and 0.8g/t Au. The porphyry carapaces are strongly stockworked and permeable volcano-sedimentary horizons have provided important traps for mineralizing fluids to migrate laterally form the mineralizing porphyries.

The delineation to date of 2.4 billion tonnes @ 0.51% Cu and 0.27 g/t Au places the Reko Diq porphyries in the top 5 of similar undeveloped projects worldwide.

## ACKNOWLEDGEMENTS

Special thanks go to John Schloderer and Pepe Perello for their valuable input in the understanding of the Reko Diq porphyry model. The study is funded by Barrick Gold Corporation.

## REFERENCES

Burnham, C.W., 1962, Facies and types of hydrothermal alteration. *Econ. Geol*., v.57, p.768 – 784

Fatmi, A.N., 1977, Mesozoic. In: Ibrahim Shah, S.M., (ed.) Stratigraphy of Pakistan. *Geol. Sur. Pak. Mem*. 12: 29-56

Gustafson, L.B., & Hunt, J.P 1975, The porphyry copper deposits at El Salvador, Chile. *Econ. Geol*.70, 1975, p.857 – 912.

Lowel J. D., & Guilbert J. M., 1970, Lateral and vertical Alteration-Mineralization zoning in porphyry ore deposits. (*Bull. Soc. Econ. Geol.* 4,V.65, p373-405.

Sillitoe, R. H., & Khan, S.N., 1977, Geology of Saindak porphyry copper deposit, Pakistan (*Paper submitted to Institute of Mining and Metallurgy*).

Sillitoe, R. H., 1977, Characteristics and controls of the largest porphyry copper – gold and epithermal gold deposits in the Circum-Pacific region. *Australian Jr. of earth sciences* (1997) 44, 373 – 388).

Siddiqui, R. H., 1996, Magmatic evolution of Chagai – Raskoh Arc terrene and its implication for porphyry copper mineralization. A Geosciences Laboratory project 1996 Islamabad ,Pakistan, *GEOLOGICA*, v.2, p.87 – 120.

Stocklin, J., 1977, Structural correlation of Alpine ranges between Iran and Central Asia. *Mem. H. Ser. Geol. Fr.,* 18: 333-353.

Stonely, R., 1974, Evolution of Continental margins bounding a former southern Tethys. In:Burk, C.A., & Drake, C.L., (eds) *The geology of continental margins.* Springer-Verlag, New York, 889-903.

# Porphyry Copper Potential of Tethyan Magmatic Arcs of Afghanistan

J.L. Doebrich, S. Ludington, S.G. Peters, C.A. Finn, J.C. Mars, L.C. Rowan, D.B. Stoeser, T.M. King & R.G. Eppinger
*U.S. Geological Survey, Reston, VA, Menlo Park, CA, & Denver, CO, USA*

A. Wasy, & M.O. Younusi
*Afghan Geological Survey, Kabul, Afghanistan*

ABSTRACT: Triassic, Cretaceous, and Palaeogene to Miocene intrusive and volcanic rocks represent areas where porphyry copper deposits may exist in Tethyan magmatic arcs in Afghanistan. A synthesis of geologic, mineral deposit, aerogeophysical, remote sensing, and geochemical data delineates regions permissive for undiscovered porphyry copper deposits. The Makran arc, Zarkashan, and Kundaylan regions have the greatest potential for undiscovered porphyry copper deposits. Concealed segments of magmatic arcs in southern Afghanistan, defined from aeromagnetic data, also represent prospective targets for exploration.

KEYWORDS: Porphyry copper, Afghanistan, Tethys, magmatic arc

## 1 INTRODUCTION

The findings presented here are an outgrowth of a mineral resource assessment of Afghanistan (Ludington *et al.* 2007) that is being conducted by a multidisciplinary team of U.S Geological Survey (USGS) and Afghan Geological Survey (AGS) scientists, and represent a preliminary look at porphyry copper potential of Afghanistan based on interpretation of existing and newly acquired data. Geologic, mineral resource, geophysical, and lithogeochemical data were compiled from a variety of data depositories (Doebrich & Wahl 2006; Sweeney *et al*. 2006a; b) and limited field verification has been conducted by the authors. New aerogeophysical and hyperspectral data were acquired by the USGS from surveys flown in 2006. The airborne geophysical data help delineate magmatic arc complexes and airborne hyperspectral and ASTER data are used to outline and characterize areas of hydrothermal alteration.

## 2 TETHYAN ARC MAGMATISM IN AFGHANISTAN

The geotectonic history of Afghanistan is one of Tethysides evolution. During the Late Palaeozoic to Triassic the southern margin of the Eurasia craton (Laurasia) extended to the Central Asia suture zone (Fig. 1). Beyond the craton margin lay the Palaeo-Tethys and Neo-Tethys oceans which separated Laurasia and Gondwana and which themselves were separated by a belt of continental blocks that had rifted from the northern margin of Gondwana beginning in the Triassic. At closure of the Palaeo-Tethys, these continental blocks collided with the Eurasian craton along the Central Asia suture to form the Cimmerides (Şengör 1984). Subsequent closure of the Neo-Tethys Ocean superimposed Cretaceous to Neogene structures and magmatic arcs on the Cimmeride belt and ultimately formed the Makran arc complex that extends from the Zagros Mountains of Iran through southern Afghanistan and into Pakistan (Fig. 1). Closure of the Neo-Tethys culminated with the Himalayan orogeny and collision of the Indian subcontinent with the newly expanded Eurasian continental margin to form the Alpides (Şengör 1984; Şengör & Natal'in 1996). Magmatic arcs identified in Afghanistan as having potential for porphyry copper deposits appear to range in age from Triassic to Mio cene. However, age designations are strictly from older data sources (Abdullah & Chmyriov 1977; Debon *et al.* 1987) and require verification by modern techniques. The oldest arc is associated with Triassic intrusions north of the Central Asia suture (Fig. 1) and thus represents a continental margin arc superimposed on the

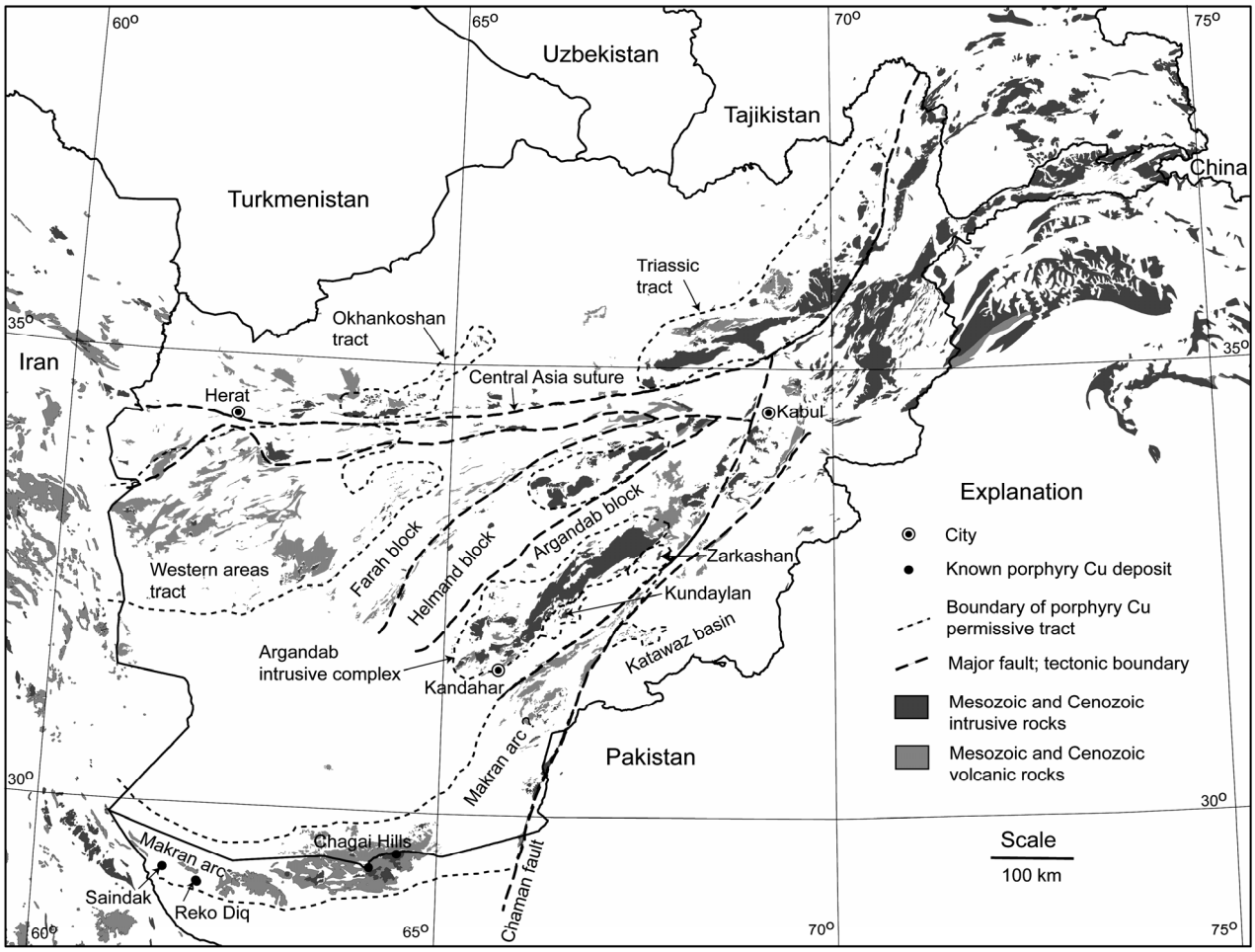


Figure 1. Map of Afghanistan and surrounding region showing features mentioned in the text.

Eurasian craton margin during closure of the Palaeo-Tethys. Magmatic arcs and provinces hosted in the Farah, Helmand, and Argandab Cimmeride blocks (Fig. 1) are associated with Cretaceous to Miocene intrusive complexes and batholiths. The Makran magmatic arc (Fig. 1) is the youngest of the arcs in Afghanistan and consists of Palaeogene to Miocene volcanic and intrusive rocks that are intermittently exposed from southeast Iran, through the Chagai Hills, and abruptly terminate at the Chaman fault (Fig. 1).

### 2.1 *Aerogeophysical anomalies*

The aerogeophysical coverage of Afghanistan allows for characterization of regions south of 35˚N excluding the higher elevations of the Hindu Kush in the central part of the country. A combination of newly compiled older aeromagnetic data (Sweeney *et al.* 2006a; b) and newly acquired aeromagnetic data delineate linear belts of circular to oval anomalies. The extent of the rocks of the Makran arc in the vicinity of the Chagai Hills is well displayed in the subsurface when expressed as magnetic gradients. Both total field anomaly and gradient maps document the very abrupt termination of magmatic arc rocks against the NE-trending Chaman fault. Several E-NE-trending subparallel linear anomalies are delineated beneath Neogene and Quaternary cover rocks and alluvium in western and southern Afghanistan. These appear to represent continuations of exposed magmatic arc complexes (*e.g.*, a continuation of the Argandab batholithic complex) as well as completely concealed arc segments. Further processing of the aeromagnetic and aerogravity data will be used to determine depth to basement in the covered regions of western and southern Afghanistan.

## 3 EVIDENCE OF PORPHYRY MINERALIZING SYSTEMS

### 3.1 *Known deposits and mineral localities*

There are no verified porphyry copper deposits in Afghanistan. However, porphyry-related deposits (Cu-Au skarns, Zn-Pb skarns,

Fe skarns, and polymetallic veins) are found throughout Afghanistan and help define regions permissive for undiscovered porphyry copper deposits.

The Makran magmatic arc in southern and southeastern Afghanistan hosts world-class porphyry copper-gold systems in Iran (Sar Cheshmeh, 12-10 Ma, 1,200Mt @ 0.7% Cu, 0.27 g/t Au) and Pakistan (Saindak, 23-19 Ma, 440Mt @ 0.41% Cu, 0.5 g/t Au; Reko Diq, 17 Ma, 807Mt @ 0.645 % Cu, 0.35 g/t Au) (Fig. 1) (Singer *et al.* 2005). In addition to Saindak and Reko Diq, the Dasht-e-Kain (21 Ma), Ziarat Pir Sultan, and Koh-i-Dalil porphyry copper deposits are present in this arc immediately to the south of the Afghanistan-Pakistan border (Fig. 1). Much of this arc is covered by Quaternary alluvium and aeolian deposits but concealed segments are clearly delineated by linear positive aeromagnetic anomalies.

The largest clustering of porphyry-related deposits in Afghanistan is in and proximal to the Oligocene Argandab intrusive complex (Fig. 1), a composite batholith of high-K metaluminous calc-alkaline granodiorite, granosyenite, and granite (Debon *et al.* 1987). The intrusive complex contains numerous gold-bearing and polymetallic veins, as well as copper and tungsten skarn prospects. However, the widespread exposure of mesozonal (?) batholithic rocks suggests that the area is relatively deeply eroded to below the conventional porphyry environment.

Gold-bearing copper skarns are concentrated in two areas (Zarkashan & Kundaylan; Fig. 1) proximal to late Cretaceous alkaline and oxidized granodiorite that crop out along the eastern margin of the Argandab intrusive complex. The evolved and K-rich nature of these intrusions and the Argandab intrusions (Debon *et al*. 1987) indicate that they were emplaced in a continental margin arc setting. Exploration of these two areas in the 1970's included trenching, tunneling, and drilling and small past production of gold and base-metals is reported (Abdullah *et al*. 1977). The skarns at Zarkashan have generated gold placers. In both areas, the intrusive body is well defined by a strong positive magnetic anomaly.

In western Afghanistan sparse occurrences of copper skarns, magnetite-haematite and epidote-garnet-magnetite skarns, and Cu-Au-Mo-bearing stockwork (Okhankoshan) are found associated with Oligocene and Miocene granitic rocks and coeval volcanic rocks.

### 3.2 *Hydrothermal alteration mapping using ASTER and airborne hyperspectral data*

ASTER data and logical operator algorithms were used to map areas of phyllic (sericite-bearing) and argillic (kalonite-bearing) altered rocks in the Chagai Hills, the Argandab intrusive complex, and in areas of the Katawaz basin (Fig. 1) (Mars & Rowan 2007). Mapped alteration varies in both geometry and intensity. Both elliptical and linear alteration patterns are documented in the Chagai Hills and Katawaz basin areas whereas linear patterns of alteration characterize the Argandab intrusive complex. Alteration intensity is greatest in the Katawaz basin area, where pervasive phyllic and argillic altered rocks are associated with Miocene diorite intrusions in Palaeogene sedimentary rock. Alteration is least extensive in the Chagai Hills.

Similar patterns and spectral characteristics have been documented in the Zagros magmatic arc of Iran (Mars & Rowan 2006) and in the Reko Diq area of Pakistan (Rowan *et al.* 2006). Elliptical argillic and phyllic alteration patterns as seen in the Katawaz basin are indicative of alteration related to shallowly eroded porphyry systems. Linear phyllic alteration patterns, as seen in the Argandab intrusive complex, are indicative of fault controlled vein systems, and consistent with the prevalence of polymetallic veins within the intrusive complex.

Airborne hyperspectral data were acquired from a WB-57 aircraft during a high-altitude survey of the Chagai Hills, Argandab intrusive complex, and the Katawaz basin area in 2006. Data processing and interpretation are in progress and will be used to calibrate the ASTER data and to further discriminate alteration mineralogy.

## 4 CONCLUSIONS

Triassic, Cretaceous, and Palaeogene to Miocene intrusive and volcanic rocks represent areas of porphyry copper potential (permissive tracts) in Tethyan magmatic arcs in Afghanistan. The Makran arc, Zarkashan, and Kundaylan tracts have the greatest potential for undiscovered porphyry copper deposits. Covered segments of magmatic arcs in southern Afghanistan also represent prospective targets. Furthermore, erosion levels suggest that undiscovered porphyry systems may be concealed beneath the volcanic-rock covered regions of western Afghanistan.

## ACKNOWLEDGEMENTS

This work is being supported through cooperative agreements with the U.S. Agency for International Development (USAID) and the Government of Afghanistan. Airborne geophysical and hyperspectral surveys were conducted in collaboration with the U.S. Department of Defense and NASA.

## REFERENCES

Abdullah S, Chmyriov VM, (eds) (1977) Map of mineral resources of Afghanistan. Kabul, Afghanistan: Democratic Republic of Afghanistan, Ministry of Mines and Industries, *Department of Geological and Mineral Survey,* V/O Technoexport USSR: scale 1:500,000

Abdullah S, Chmyriov VM, Stazhilo-Alekseev KF, Dronov VI, Gannan PJ, Rossovskiy LN, Kafarskiy AK, Malyarov EP (1977) Mineral resources of Afghanistan (2nd edition). Kabul, Afghanistan: *Republic of Afghanistan Geological and Mineral Survey*. pp419

Debon F, Afzali NH, Le Fort P, Sonet J (1987) Major intrusive stages in Afghanistan: typology, age, and geodynamic setting. *Geologische Rundschau* 76/1: 245-264

Doebrich JL, Wahl RR (2006) Geologic and mineral resource map of Afghanistan. *U.S. Geological Survey Open-File Report* 2006-1038: scale 1:850,000 [http://pubs.usgs.gov/of/2006/1038/]

Mars JC, Rowan LC (2006) Regional mapping of phyllic- and argillic-altered rocks in the Zagros magmatic arc, Iran, using Advanced

Spaceborne Thermal Emission and Reflection Radiometer (ASTER) data and logical operator algorithms. *Geosphere* 2: 161-186

Mars JC, Rowan LC (2007) Mapping phyllic and argillic-altered rocks in southeastern Afghanistan using advanced spaceborne thermal emission and reflection radiometer (ASTER) data: *U.S. Geological Survey Open-File Report* 2007-1006 [http://pubs.usgs.gov/of/2007/1006/]

Ludington SD, Orris GJ, Bolm KS Peters SG, et al. (2007), Preliminary mineral resource assessment of Afghanistan: *U.S. Geological Survey Open-File Report* 2007-1055 [http://pubs.usgs.gov/of/2007/1005/]

Rowan LC, Schmidt RG, Mars JC (2006) Distribution of hydrothermally altered rocks in the Reko Diq, Pakistan mineralized area based on spectral analysis of ASTER data. *Remote Sensing of Environment* 104: 74-87

Şengör AMC (1984) The Cimmeride orogenic system and the tectonics of Eurasia. *Geological Society of America Special Paper* 195. pp82

Şengör AMC, Natal'in BA (1996) Paleotectonics of Asia: fragments and synthesis. In: Yin A, Harrison M (eds) *The tectonic evolution of Asia.* Cambridge University Press, pp 486-640

Singer DA, Berger VI, Moring BC (2005) Porphyry copper deposits of the world: database, maps, and preliminary analysis. *U.S. Geological Survey Open-File Report* 02-268 [http://geopubs.wr.usgs.gov/Open–File/of02-268]

Sweeney RE, Kucks RP, Hill PL, Finn CA (2006a) Aeromagnetic and gravity surveys in Afghanistan: A web site for distribution of data. *U.S. Geological Survey Open-File Report* 2006-1204 [http://pubs.usgs.gov/of/2006/1204/]

Sweeney RE, Kucks RP, Hill PL, Finn CA (2006b) Aeromagnetic survey in western Afghanistan: A web site for distribution of data. *U.S. Geological Survey Open-File Report* 2006-1325 [http://pubs.usgs.gov/of/2006/1325/]

# Low-sulphidation, 'non-magmatic' epithermal Au-Ag deposits of the eastern Rhodopes mountains, Bulgaria

Dimitar L. Dimitrov
*Euromax Resources Inc*

ABSTRACT: The eastern part of Bulgaria's Rhodope mountains host at least 10 documented low-sulphidation epithermal Au-Ag occurrences and deposits, most of which were unrecognized by modern exploration until the 1990's, though many were worked in Thracian and later times. The deposits display a wide range of morphology, host rocks and variable geochemical signatures including Au:Ag ratios and relative enrichments or deficiencies in typical epithermal elements As, Sb, Hg, but show no enrichment in base metals. Many deposits occur at or immediately below the unconformity of basal Tertiary conglomerates and underlying metamorphic rocks, and are demonstrably older than most Tertiary volcanism in the region. Notably, none of the low-sulphidation systems appear to be related to magmatic rocks, and most appear to be older than the numerous adjacent Tertiary magmatic-related Pb-Zn systems, some of which have economic Au-Ag grades in their upper and peripheral portions.

KEYWORDS: Gold-silver, low-sulphidation, epithermal, Bulgaria

## 1. INTRODUCTION

Bulgaria's most recently discovered economic gold deposit is Ada Tepe, perhaps a "classic" low-sulphidation vein/stockwork system, developed at the contact of lower Tertiary sedimentary rocks, and underlying metamorphic rocks. Ada Tepe is one of many low-sulphidation Au-Ag occurrences throughout the adjacent Rhodopes Mountains that have been identified and explored within the last fifteen years. However unlike most low-sulphidation Au-Ag epithermal deposits worldwide, which are either hosted in, or clearly connected to contemporaneous volcanic/intrusive rocks, most of the Rhodopes occurrences have no such direct spatial or genetic tie to magmatic rocks. This paper summarizes basic geologic and geochemical information on several of these deposits, their spatial distribution, and their morphology. It is hoped that further study will use this basis as a stepping stone toward clarifying their genesis and spatial distribution.

## 2. GEOLOGIC SETTING

The low-sulphidation Au-Ag deposits occur over an area of approximately 2000km² (Figure 2). Roughly half are hosted in conglomerate-breccias, conglomerates and sandstones, presumed to be of Palaeocene - Eocene age. The remainder are hosted in gneisses, calc-schists, amphibolites and marbles of ages ranging from Proterozoic to Mesozoic age, which form the underlying basement to the lower Tertiary sediments. Although Ada Tepe and Makedontzi occur in sediments directly at the Terti-


Fig. 1 Location of E. Rhodopes low-sulphidation AuAg province

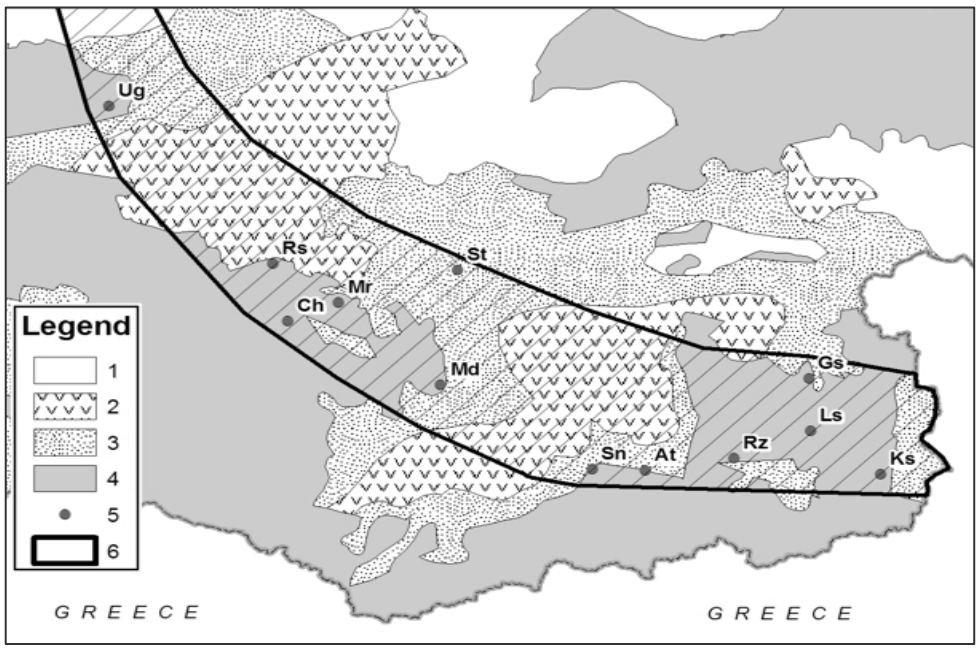


**Ug** - Ugovo**;**
**Rs** - Rusalsko;
**Ch** - Chernigovo;
**Mr** - Mirovetz;
**St** - Stremtsi;
**Md** - Makedontsi;
**Sn** - Surnak;
**At** - Ada Tepe;
**Rz** - Rozino;
**Gs** - Gornoseltsi;
**Ls** - Lensko;
**Ks** - Kostillkovo.

Fig. 2 Generalized map of E Rhodopes low- sulphidation Au-Ag province: **1** Pliocene-Quaternary sediments; **2** Upper Eocene-Miocene volcanic areas; **3** Palaeocene-Eocene sediments; **4** Metamorphic basement; **5** Low-sulphidation Au-Ag deposits and occurrences; **6** Eocene low-sulphidation Au-Ag belt.

ary/basement unconformity, at Stremtsi, the mineralization is hosted in sandstone-conglomerate at least 300m above metamorphic basement rocks. At many occurrences, Tertiary sediments are often removed by erosion or were never present. The age of mineralization has not been directly dated but at Surnak is well-constrained by the age of overlying post-ore limestones, of Priabonian age. In places, there is suggestion that early ore-related structures which controlled early Tertiary low-sulphidation Au mineralization, which is itself devoid of base-metals, may have been reactivated during Tertiary magmatic-related Pb-Zn-Ag systems of Oligocene age. At Rozino, localized Pb-Zn veinlets were intersected in basement rocks but do not appear to represent a continuous zoning pattern from adjacent Au mineralization. At Stremtsi, a silicified limestone unit which occurs at least 150m stratigraphically above the ore-hosting sandstone-conglomerate, and which may be younger than the Stremtsi Au mineralization itself, contains very high Ag values and is virtually devoid of Au.

## 3. ALTERATION, GEOCHEMISTRY AND DEPOSIT MORPHOLOGY

The deposits have textural and alteration features typical of low-sulphidation AuAg systems, including banded veins, cavernous carbonate-replacement textures, local adularia, massive silicification, and silica-white mica-chlorite alteration. Morphologies of the mineralized zones vary from roughly stratiform bodies of disseminations and strata-confined vein stockworks in sandstone-conglomerate (Stremtsi), to slab-like low-angle veins and adjacent overlying vein stockworks in basal sandstone-conglomerate (Ada Tepe), steeply-dipping wide stockworks/breccias (Spoluka-Mirovetz), to discreet, wide banded to massive quartz veins (Spoluka-Chernigovo).

The deposits are characterized by varying Ag:Au ratios and concentrations of As, Sb, Hg, locally Co and Ni, where ophiolitic lithologies are presented in the underlying basement.

## 4. CONCLUSIONS

The epithermal low-sulphidation hydrothermal systems of the east Rhodopes are emplaced along tectonic boundaries of early Palaeogene post-collision grabens and are hosted in the Precambrian metamorphic basement, and in the basal conglomerate-sandstone levels of lower Tertiary sedimentary units. These basic geologic data suggest that the early Tertiary Au(Ag) deposits and occurrences are more likely connected to the metamorphic core complexes than Eocene-Oligocene magmatic ac-

| Occurrence | Hostrock | Morphology | Ag:Au etc | Old workings |
|---|---|---|---|---|
| Ada Tepe | Tertiary conglomerates | Stratiform replacement; steep veins | 1:1 | Large |
| Surnak-Kuklitza | Gneiss/schist; marble | Breccia-sockwork and carbonate replacement | 10:1 (As, Co, Ni) | None |
| Stremtsi | Tertiary conglomerates. | Dissem. and stratabound veinlets | 5:1 (Mo, Sb) | Large |
| Lensko-Kostilkovo | Marble; schist | Veins parallel schistosity and carbonate replacement | 2:1 (As,Sb) | Large |
| Rozino | Tertiary conglomerates; granite; gneiss | Disseminated and stockwork | 2:1 (As,Sb,Mo) | Limited |
| Spoluka: Mirovetz | Gneiss | Breccia-stockwork | >10:1 | None |
| Spoluka: Chernigovo | Gneiss | Large vein | 1:1 | None |
| Makedontzi | Tertiary conglomerates. | Breccia, disseminated, steep veins | 5:1 (As,Ba) | None |
| SpolukaRusalsko | Gneiss | Breccia, stockwork; veins, | 5:1 (As,Sb) | None |
| Gornoseltsi/Dolnoseltsi | Tertiary conglomerates | Disseminated, veins parallel | 5:1 (Sb,As) | Limited |

Table 1: Summary characteristics of eastern Rhodopes low-sulphidation epithermal Au(Ag) systems

tivity. The Upper Cretaceous collision-related metamorphism is a possible heat source for the widespread low-sulphidation epithermal systems, developed in post-collision extension environments together with the extension of the early Tertiary graben depressions.

## ACKNOWLEDGEMENTS

Phelps Dodge Exploration is gratefully acknowledged for support, in particular that provided by Vertrees M. Canby and Dr. Leon Naftali. The author gratefully acknowledges the support of Dr. Don Baker, the field work of Kamen Ivanov and technical assistance of Ivan Alexiev.

## REFERENCES

Dimitrov, D., Pluschev, E. and Petrova, K. (1996): Comparison and modelling of the epithermal deposits in the Eastern Rhodopes. *Abstracts of ann. meet.-Sofia, Unesco-IGCP* Project No 356, vol. 2, pp.87-93, 1996.

Ivanhoe Balkans Ltd., (2005): *Presentation in Proceedings of SE Europe Geoscience Foundation, Sofia, Bulgaria, May 7-10 2005.*

Marchev, P., Singer, B., Jelev, D., Hasson, S., Moritz, R. and Bonev, N. (2004): The Ada Tepe deposit: a sediment-hosted, detachment fault-controlled, low-sulphidation gold deposit in the Eastern Rhodopes, SE Bulgaria. *Schweiz. Mineral.Petrogr.Ges.* 84,XXI-XX20, 2004.

# Regional to local ore controls on the formation of sedimentary rock-hosted gold deposits from the Eastern Rhodopes, Bulgaria

I. Márton & R. Moritz
*Dept. of Mineralogy, University of Geneva, Switzerland*

N. Bonev
*Dept. of Mineralogy, "St. Kliment Ohridski" University, Sofia, Bulgaria*

P. Marchev
*Bulgarian Academy of Sciences, Geological Institute, Sofia, Bulgaria*

ABSTRACT: The factors controlling the formation of sedimentary rock-hosted gold deposits from the Eastern Rhodopes, Bulgaria, vary from lithosphere scale (regional tectonics) to deposit scale (detachment and listric faults, host rock lithology). These controls are likely responsible for the different gold depositional processes in the various prospects. Sulphide deposition in iron-rich host rocks by very dilute fluids suggests sulphidation with subsequent cooling as a general and important depositional process in all the deposits. At some prospects (Ada Tepe, Kuklitza, Stremtzi) the decompression of hydrothermal system allows local concentration and deposition in high ore grades. The adularia recognised from these prospects reveals that it has a relatively disordered (sanidine-like) Al/Si distribution, reflecting rapidly changing crystallisation conditions. It is likely to have formed when the fluids moved up to a more permeable environment and started boiling.

KEYWORDS: Eastern Rhodopes, gold ore, depositional controls, sulphidation, boiling

## 1 INTRODUCTION

Sedimentary rock-hosted gold deposits with low sulphidation characteristics have been recently discovered in the Eastern Rhodopes, Bulgaria (Marchev *et al.* 2004; Marinova 2006; Márton *et al*. 2006). Such deposits are well known in western North America (*e.g*., detachment-hosted gold deposits, Carlin-type deposits, distal disseminated gold deposits, low sulphidation gold deposits). These opportunities open up new exploration and scientific interest in the Aegean region.

The objective of this paper is to take a broad view incorporating the tectonic setting, local geological and geochemical features in order to find an explanation for the significant gold endowment in the region and to understand more about the possible scale of ore-depositional systems. These factors are controlling also the specific gold depositional mechanism (*e.g*., sulphidation, boiling) at the different prospects.

Petrographic, stable isotope, XRD and microraman investigations were carried out to better characterize these depositional processes which are responsible for the local concentration of ore grades.

## 2 REGIONAL TECTONICS AS A KEY CONTROL ON ORE FORMATION

One of the main geological features of the Eastern Rhodopes is the abundant exposure of metamorphic complexes, separated by tectonic contacts related to the extensional history of the Rhodopes. Since the Cretaceous, the geological evolution of the Eastern Rhodopes is controlled by the convergent setting along the Eurasian plate margin (within the Aegean region, Fig. 1), experiencing a series of continental collision events (late Cretaceous to Eocene), followed by syn- and post-orogenic extension in a back-arc region (Bonev *et al.* 2006). The Aegean region is one of the most active, present-day continental extensional settings in the world, and is expressed by rapid stretching of the upper crust and by exhumation of the lower crust, exposed in metamorphic core complexes, during successive rifting phases with different styles of extension. The metamorphic terrains in the region include the Rhodope, Menderes and Kazdag Massifs, the Cyclades and Crete (Fig. 1) and are characterized by exposures of high-grade metamorphic rocks and associated granitic intrusions unroofed during extension that typi-

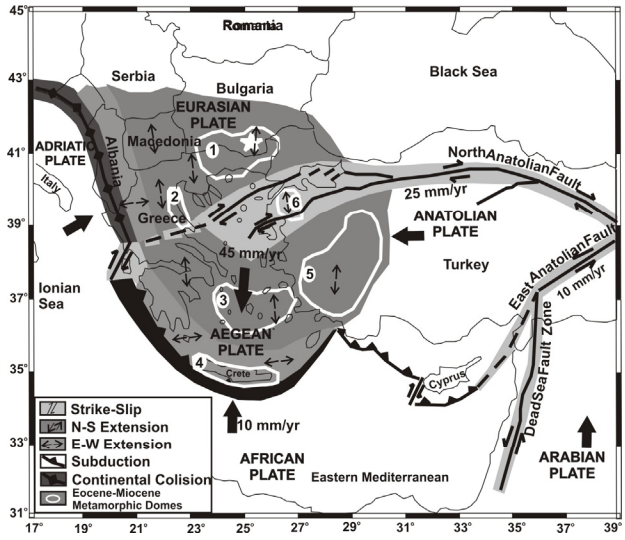


Figure 1. Plate tectonic configuration of the area around the Aegean with the southward migrating thrust front. The metamorphic domes are summarized after Lips *et al*. (2001): (1) Rhodope Massif, (2) Olympos-Peilon Region, (3) Cyclades-Arhipelago, (4) Crete, (5) Menderes Massif and (6) Kazdag Massif. The locus of the studied gold deposits is marked by a star in the Rhodope Massif.

cally follows crustal thickening (Lips *et al.* 2001). The roles of various processes, including erosion, buoyant rise, tectonic extension - brittle faulting and ductile flow, for exhuming high-grade metamorphic rocks from lower-middle crust to Earth's surface are not fully understood. There are still subjects of ongoing debate, such as (i) timing of core complex formation/extension, magmatism with respect to extension, and regional metamorphism, (ii) fundamental driving force(s) of extension, (iii) intimate relationship, both in space and time, between magmatism, hydrothermal mineralization and metamorphic core complex formation, (iv) the initial geometry of presently low-angle normal faults, and (v) the relationship between exhumation processes and graben formation.

An analogue example of the metamorphic core complex mode of extension is the Basin and Range Province of the western United States, where the extensional back-arc tectonic setting is considered to be the first order control for the world-class Carlin gold province (Cline *et al.* 2005, Emsbo *et al.* 2006). Therefore, the objective to consider the factors that operate at the orogen and lithosphere scales is important.

## 3 MAJOR LOCAL FACTORS CONTROLLING THE MINERALIZATION

The studied gold deposits in the Eastern Rhodopes are dominantly hosted by syn-detachment sedimentary rocks of Maastrichtian-Palaeocene age (Bonev *et al*. 2006; Marchev *et al*. 2004; Márton *et al.* 2006). A low angle normal fault between the metamorphic basement and the sedimentary rocks constitutes the major ore-controlling associated structure. The host rocks are (1) tectonically affected coarse grained conglomerates, generally with huge blocks of marbles; (2) fine grained sandstones, intercalated by organic rich layers; and, (3) very rarely, amphibolites.

The geometry of the ore bodies reveals the structural and lithological controls on the mineralization. They include: (a) strongly faulted rocks of the highly permeable sedimentary unit that offered a favourable channel-way for fluid circulation generating open space filling bonanza type mineralization in veins with a general E-W direction; (b) the deformed metamorphic rocks with a ductile fabric and the cataclasticly deformed detachment zone were the loci of focused fluid flow, toward lower pressure areas, where a massive, tabular ore body was formed immediately above the de-

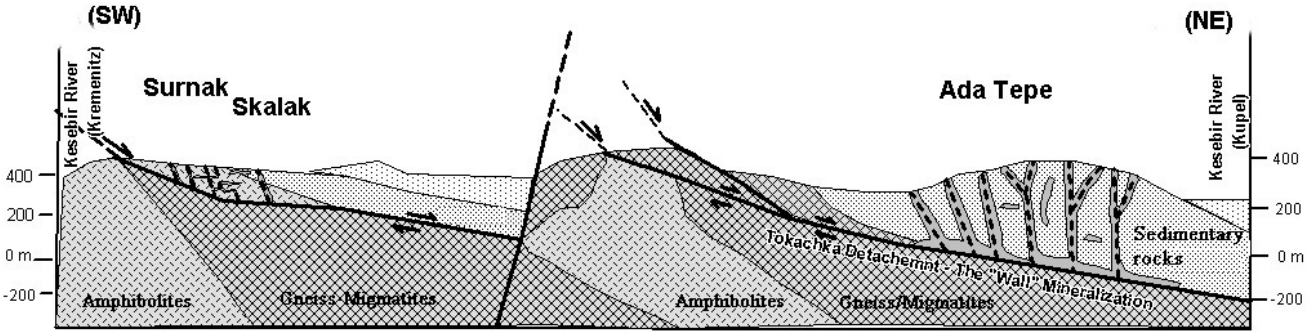


Figure 2. Typical cross section through the Krumovgrad area in the Eastern Rhodopes (Ada Tepe deposit and Skalak, Surnak, Kuklitza, and Kupel prospects). At Ada Tepe the main gold ore body is located above the detachment fault in the sedimentary cover. The alteration (predominantly silicification) and gold mineralization are controlled by steep normal faults. In addition, a tabular ore body (called the "Wall") lies directly along the detachment.

tachment fault. These zones consist of strongly altered rocks, replaced by silica, adularia, sericite, pyrite and carbonate minerals. Metamorphic basement rocks are generally barren, but at one prospect (Surnak) the increased permeability of connected observable structures along listric faults favours the ore deposition also within the metamorphic basement rocks.

## 4 ALTERATION AND MINERALOGY

Alteration consists of decarbonatization (silica replacement textures), silicification (chalcedony formation), sericitization, adularia formation and carbonate alteration, which are arranged both spatially and temporally in that order. The ore mineralogy is simple and consists of electrum (~75% Au), pyrite and traces of galena and telluride. The gangue of the veins comprises typically fine-grained quartz, adularia, and carbonates with typical colloform and banded textures. The evolution of the intensity of silica alteration can be observed in many places, starting with an initial network of small quartz veins along fractures, followed by either total silica replacement of the host rock or leaching of the host rock, resulting in extreme cases of leaching, in a network of small quartz veins with no host rock left between them.

## 5 DEPOSITIONAL PROCESSES

On the basis of the alteration mineralogy and textural relationships, it is possible that gold may have been deposited as a consequence of different physico-chemical processes in the various prospects. The abundant bladed quartz pseudomorphs replacing platy calcite and the presence of adularia suggest boiling in different prospects, including Ada Tepe, Kuklitsa, Kupel and Stremtsi (Noverraz, 2006). However, in cases of other prospects, such as Rosino, Surnak, Kremenitz and Skalak, boiling textures are scarce to absent, and intense fluid-rock interaction may be responsible for gold mineralization, where reduction of fluids may have been favoured by organic matter and ferrous-bearing minerals. This is based also on the fact that pyrite generally replaces amphiboles along cleavages and fractures.

The importance of sulphidation and gold transport as a bisulphide complex in the case of the studied deposits are indicated by (Márton *et al*. 2006): 1) petrographic evidence which suggest that sulphidation of iron-rich minerals in the host rock was an important process; 2) mass transfer studies which show that sulphur was one of the most abundant elements introduced by the hydrothermal fluids, whereas iron contents remained nearly constant; 3) the very low salinity of fluid inclusions and 4) high Au/Ag ratios in electrum. These observations are consistent with chemical reaction path modelling, which shows that sulphidation can result in the ore grades observed in the sedimentary-rock hosted gold deposits (Shenberger & Barnes 1989). Sulphur isotopic studies on pyrite (Márton *et al*. 2006) also may help to discriminate between the various processes and fluid sources proposed for the deposits.

The examination of high grade ore vein samples from Ada Tepe typically contains significant amounts of rhombic adularia (Fig.3). Studies from low sulphidation deposits (Nagayama 1993; Dong & Morrison 1995) show that there are some distinct differences in the crystal morphology and Al/Si ordering of adularia aggregates, and that only some types of

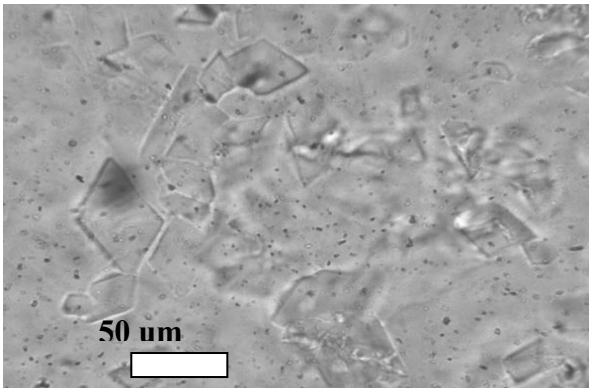


Figure 3. Rhombic crystals of adularia from the Ada Tepe prospect

adularia are associated with boiling and high grade gold mineralization. XRD and microraman studies show that adularia from Ada Tepe has a relatively disordered (sanidine-like) Al/Si distribution. A high rate of nucleation and crystal growth under low temperatures is the most accepted explanation for the generation of a metastable/highly disordered adularia. Decompression in hydrothermal systems is usually accompanied by boiling. The chemical changes the fluid undergoes during boiling include a raise in pH caused by the partitioning of volatiles preferentially into the steam phase and an increase in concentration of nonvolatile constituents that remain in the liquid phase as a result of the separation of steam. These factors promote supersaturation, which results in the sudden precipitation of silica, along with me-

tastable potassium-rich feldspar, sulphides and ore. The disordered adularia is also indicating the absence of an important thermal overprint after its crystallization, and therefore the absence of any late-stage fluid circulation postdating ore formation.

## 5 CONCLUSIONS

Regional (tectonic evolution) and local (host rock lithology, emplacement of extensional structures) ore controls were identified on the formation of sedimentary rock-hosted gold deposits from the Eastern Rhodopes. These are responsible for the different gold depositional processes at the various prospects. Carbonate rich sedimentary rocks have great pH buffering capacity (decarbonitization, silica replacement textures), but a low capacity for desulphidising the $H_2S$-rich hydrothermal fluids which optimizes gold enrichment and extensive metal transport. When fluids reach Fe-bearing rocks (conglomerates rich in gneiss and amphibolite clasts) gold precipitation (locally in solid solution with arsenous pyrite) is driven by desulphidation processes. Localized drops in gold solubility and precipitation of high grades ore is controlled by decompression of hydrothermal system, accompanied by boiling and sudden $H_2S$ loss.

## ACKNOWLEDGEMENTS

This study is part of I.M. Ph. D. project at the University of Geneva, financed by the Swiss National Science Foundation (Grants 200020-101853, 200020-113510 and SCOPES IB7320-111046). The geologic staff of *Balkan Mineral and Mining (Dundee Precious Metals)*, and *Cambridge Minerals Plc.* are thanked for their support during field work and for the thoughtful discussions.

## REFERENCES

Bonev N., Marchev P., Singer B. (2006) $^{40}Ar/^{39}Ar$ geochronology constraints on the Middle Tertiary basement extensional exhumation, and its relation to ore-forming and magmatic processes in the Eastern Rhodope. *Geodin. Acta* 19: 267-282.

Cline JS, Hofstra AH, Muntean JL, Tosdal RM, Hickey K.A. (2005) Carlin-type gold deposits in Nevada: critical geologic characteristics and viable models, *SEG 100th Anniversary Vol.:* 451-484.

Dong G, Morrison GW (1995) Adularia in epithermal veins, Queensland: morphology, structural state and origin. *Mineral. Deposita*, 30: 11-19.

Embso P, Groves DI, Hofstra AH, Bierlein FP (2006) The giant Carlin gold province: a protracted interplay of orogenic, basinal, and hydrothermal processes above a lithospheric boundary. *Miner. Deposita,* 41: 517-525.

Lips ALW, Cassard D, Sozbilir H, Yilmaz H, Wijbrans JR (2001) Multistage exhumation of the Menderes Massif, Western Anatolia (Turkey). *Int. J. Earth Science,* 89: 781-792.

Marchev P, Singer B, Jelev D, Hasson H, Moritz R, Bonev N (2004) The Ada Tepe deposit: a sediment-hosted, detachment fault-controlled, low-sulphidation gold deposit in the Eastern Rhodopes, SE Bulgaria, *Swiss Bull Mineral Petrol*, 84: 59-78.

Marinova I (2006) Open-space filling textures from the electrum-bearing, layer-like pervasive silicification in the low sulphidation Khan Krum gold deposit, SE Bulgaria, *Comp rend de l'Acad Bulgare des Sc.* 59:1027-1030.

Márton I, Moritz R, Marchev P, Vennemann T, Spangenberg, J (2006) Fluid evolution within Eastern Rhodopian sedimentary rock-hosted low-sulphidation epithermal gold deposits, Bulgaria. *Proceedings of the 2006 IGCP-486 Field Workshop, Izmir-Turkey,* 116-123.

Nagayama T (1993) Precipitation sequence of veins at the Hishikari deposits, Kyushu, Japan. *Resource Mineralogy Special Issue,* 14: 13-27.

Noverraz C (2006) The Stremtsi gold prospect, a sedimentary rock-hosted, low sulphidation epithermal system in the Tertiary Eastern Rhodopes, Bulgaria. *MSc thesis, Univ. of Geneva,* p. 97.

Shenberger DM, Barnes HL (1989) Solubility of gold in aqueous sulphide solutions from 150 to 350 ºC, *Geoch. and Cosmoch. Acta* 53:269-278

# The Stremtsi gold prospect: a sedimentary rock-hosted, low-sulphidation epithermal system in the Tertiary Eastern Rhodopes, Bulgaria

Cécile Noverraz*, Robert Moritz & Denis Fontignie
*Institute of Earth Sciences, University of Geneva, Geneva, Switzerland*
** Present address: Dept of Earth and Planetary Sciences, McGill University, Montreal, Canada*

Peter Marchev
*Geological Institute, Bulgarian Academy of Sciences, Sofia, Bulgaria*

Torsten Vennemann & Jorge Spangenberg
*Institute of Mineralogy and Geochemistry, University of Lausanne, Lausanne, Switzerland*

Kolio Kolev
*Balkan Mineral and Mining AD, Dundee Precious, Kardjali, Bulgaria*

ABSTRACT: The Stremtsi prospect belongs to a group of low-sulphidation, sedimentary rock-hosted deposits in south-eastern Bulgaria. The eastern part of the prospect shows strong silicification with high gold grades, whereas the western part consists of a barite, sphalerite and galena mineralization. Combined field, microscopic, fluid inclusion and stable isotope data support boiling as the main gold depositional process in the silicified zone. Whereas fluid inclusion and stable and strontium isotope data reveal fluid mixing in the barite and base metal part of the system. Sulphides have $\delta^{34}S$ values mainly between–5 and +5‰, which reveals a common ore fluid type throughout the Eastern Rhodopes during sedimentary rock-hosted gold ore formation.

KEYWORDS: low-sulphidation epithermal gold, sedimentary rock-hosted, Stremtsi, Eastern Rhodopes

## 1 INTRODUCTION

Low-sulphidation, sedimentary rock-hosted prospects are a new class of deposits recently described in the Eastern Rhodopes, Bulgaria. The most important of these are the Ada Tepe and Rosino prospects (Fig. 1; Marchev *et al.*, 2004a; Marton *et al*., 2006). The smaller Stremtsi prospect, described in this contribution, is located near the town of Kardajli, to the north-west of the main cluster of sedimentary rock-hosted epithermal gold prospects (Fig. 1). Its northern location is significant from an economic point of view, because it considerably expands the prospective area for such type of mineralization away from the main Ada Tepe and Rosino cluster (Fig.1). In this study we present new observations, fluid inclusion, stable and radiogenic isotope data from the Stremtsi prospect to understand its relationship with Ada Tepe, Rosino and neighbouring prospects.regional geology

The Eastern Rhodope massif is an accretionary orogen, where Cretaceous nappe tectonics and crustal thickening was followed by late

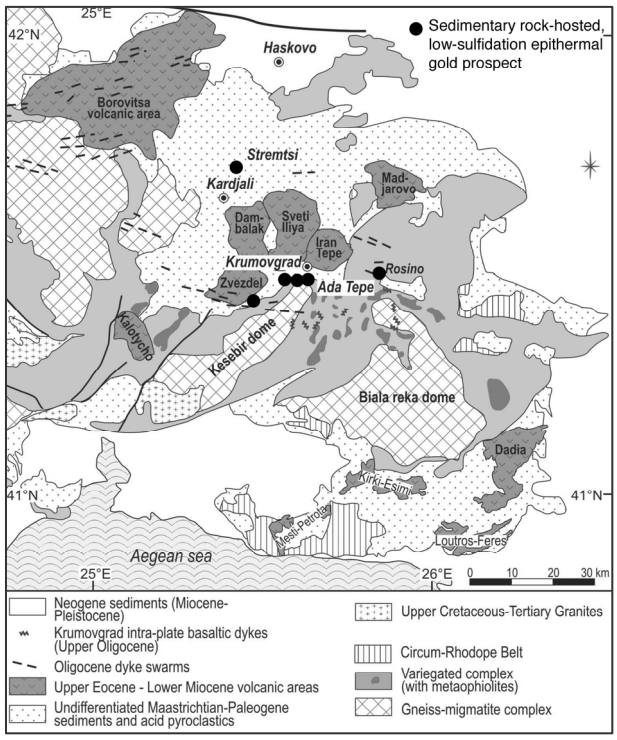


Figure 1: Regional geological setting and location of low-sulphidation, sedimentary rock-hosted epithermal gold prospect in the Eastern Rhodopes (after Marchev *et al).*

Cretaceous and Tertiary extension, with the formation of low-angle detachment faults, exhumation of metamorphic core complexes and sedimentary basins (Fig. 1; Marchev *et al*., 2005; Bonev *et al*., 2006a). Magmatism in the Eastern Rhodopes is late Cretaceous to Eocene (Marchev *et al.*, 2004b).

The Ada Tepe and Rosino gold prospects (Fig.1) have been dated at 34.99 and 35.94 Ma, respectively, by the $^{40}Ar/^{39}Ar$ technique (Marchev *et al*., 2004a, 2005). Ore formation is younger by ~2-3 Ma than the cooling ages of metamorphic micas (38.13 and 37.73 Ma, Bonev *et al*., 2006b), and older by ~3 Ma than the nearest magmatic rocks (Marchev *et al*., 2004a). Marchev *et al*. (2004a) linked the sedimentary rock-hosted gold mineralization to metamorphic core-complex formation, and recently Marchev *et al*. (2005) proposed a link with deep mantle magmas.

## 2 LOCAL GEOLOGICAL SETTING

The Stremtsi prospect is hosted by Priabonian conglomerate and sandstone, overlaying metamorphic basement rocks (exposed to the southwest, Fig.1). The principal mineral components of the clastic sedimentary rocks are feldspar, quartz and muscovite, with local occurrences of organic matter and coal, locally enriched in layers dominated by clay minerals. Framboidal pyrite is present, and is especially abundant in coal layers. The clastic sedimentary host rocks are stratigraphically overlain by, and younging upwards, a coal-bearing sandstone formation, a marl and limestone formation, latite-andesite flows and breccias, and finally a sequence consisting of tuff, sandstone, siltstone and mudstone. The latite-andesite volcanic rocks are the closest outcropping magmatic rocks, and have been dated by the K-Ar technique at 29.2 ± 1.1 and 33.1 ± 1.3 Ma (Marchev *et al*, 2004b). The main structural elements are subvertical ENE-WSW- and NE-SW-trending faults.

## 3 MINERALIZATION

The Stremtsi prospect presents many features typical for low-sulphidation epithermal deposits. It covers a 1km by 3km EW-oriented area, and it is subdivided in two zones. The eastern part coincides with the highest elevation of the prospect (Hissar tepe, 576m asl), and consists of a shallow, intensely silicified zone. This part is the location of old, underground mining, probably dating back to the Middle Age, or even Thracian times (Anatasov, 2000). It contains the highest gold grades of the prospect, as high as 23g/t. The western part consists of a disseminated and vein mineralization with barite, galena and sphalerite, and abundant carbonates. The two zones are underlain by small, quartz and carbonate veins, with ubiquitous, hydrothermal pyrite, generally with euhedral shapes. Gold grades are significantly lower than in the silicified zone, and reach a maximum of 6.5 g/t.

Hydrothermal alteration consists of (1) silicification, especially in the eastern zone, which coincides with the old workings, but also along the deeper veins, (2) argillic alteration with illite and dickite-kaolinite, and (3) late carbonatization, consisting mostly of dolomite in the western barite zone and along the deeper vein system. The mineralization consists mostly of quartz, carbonate and pyrite veins, with additional barite, sphalerite and galena in the western zone. The highest gold contents coincide with intense silicification in the old mining area, where adularia and silicified platy calcite replacement boiling textures are abundant. Hydrothermal brecciation, and low-temperature colloidal silica are present in the higher gold grade zones. Quartz veining occurred first, simultaneously with the deposition of gold and euhedral pyrite. The carbonate veins are generally considered as a later event, with the deposition of barite, sphalerite and galena as open space-filling textures.

## 4 FLUID INCLUSION INVESTIGATION

Fluid inclusion microthermometry was undertaken on dolomite and barite. Inclusions in dolomite follow growth zones and are interpreted as primaries. Inclusion trails in barite crosscut mineral boundaries, therefore they are interpreted as secondaries, although some intragrain clusters might be primaries. The homogenization temperatures in both minerals vary widely (106 to 247°C), even within the same fluid inclusion assemblage. Therefore, they are considered as unreliable. By contrast, ice-melting temperatures are consistent within fluid inclusion assemblages, thus it is concluded that compositions remained unchanged since trapping. Inclusions in dolomite are more saline than in later stage barite (3.6 to 5.1 and < 3.1 NaCl wt% equivalent, respectively; Fig. 2).

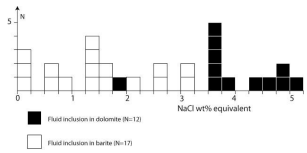


Figure 2. Salinity of fluid inclusions in barite and dolomite.

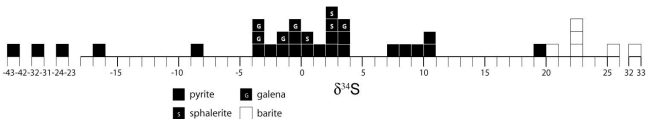


Figure 3. $\delta^{34}S$ (‰, CDT) values of pyrite, barite, sphalerite and galena

## 5 SULPHUR ISOTOPES

Sulphur isotopes have been measured on pyrite, barite, galena and sphalerite. The results can be divided in 4 groups (Fig. 3). The first group has $\delta^{34}S$ values between -5 and +5‰, and comprises pyrite, sphalerite and galena. The second group, composed of barite, shows $\delta^{34}S$ values between +20.5 and +32.7‰. These two groups are thought to be representative of the hydrothermal mineralizing fluid, as these are typical values for hydrothermal sulphur and correlated sulphates.

The third group shows a range of $\delta^{34}S$ values between +8 and +11‰, and is composed entirely of pyrite. It is interpreted as being the result of thermochemical $SO_4$ reduction. The fourth group has very light $\delta^{34}S$ values between -43 and -8‰. The later group is almost entirely composed of framboidal pyrite associated with coal. These very low $\delta^{34}S$ values are attributed to bacterial sulphate reduction. The processes affecting the third and fourth group are low-temperature processes, and probably diagenetic in origin.

## 6 ISOTOPIC COMPOSITIONS (O, C, Sr) OF CARBONATES

Carbon, oxygen and strontium isotopes were analysed in carbonate samples from the surface at the western barite-rich zone, and sampled in drill cores from veins underneath the western barite-rich zone and the eastern silicified zone.

Samples from the deep vein system display a positive correlation of stable isotopic compositions between –2.8 and +1.5 ‰ V-PDB for $\delta^{13}C$ values, and between 12.7 and 19.7 ‰ V-SMOW for $\delta^{18}O$ values (drill core samples in Fig. 4A), whereas those of the carbonates sampled in the western barite-rich zone show a negative correlation, with stable isotopic compositions between -0.6 and -3.9 ‰ V-PDB for $\delta^{13}C$ values, and between 13.4 and 23.3 ‰ V-SMOW for $\delta^{18}O$ values (surface samples in Fig. 4A).

The combined strontium and oxygen isotopic compositions of the deep vein samples fall in a cluster of values between 0.70937 and 0.71010,

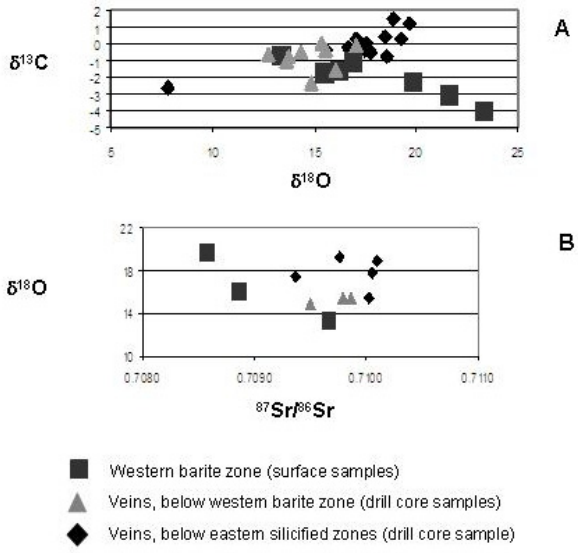


Figure 4. A: $\delta^{18}O$ and $\delta^{13}C$ values of carbonates. B: $^{87}Sr/^{86}Sr$ ratios and $\delta^{18}O$ values of carbonates.

and 14.8 and 19.2 ‰ V-SMOW (Fig. 4B), whereas carbonates from the western barite zone display a different tendency with a negative correlation of $\delta^{18}O$ values ranging between 13.4 and 19.7 ‰ V-SMOW, and $^{87}Sr/^{86}Sr$ ratios between 0.70857 and 0.70965 (Fig. 4B).

## 7 DISCUSSION AND CONCLUSIONS

The positive co-variation of the stable isotopic composition shown by carbonate samples from the deep veins (drill core samples in Fig. 4A) is attributed to cooling and boiling of the hydrothermal fluid, which is in line with the boiling evidence based on the presence of adularia and pseudomorphed, platy calcite in the high grade gold zone. The deeper vein system is probably the remnant of the channel-ways allowing the upward migration of the ore-forming fluid into the gold-rich silicified zone, where gold precipitation was mainly caused by boiling. The inclusion data show that the fluid was moderately saline (3.6-5.1 wt% NaCl eq.

Fig. 2).

The carbonates from the western barite zone display co-variations of the isotopic compositions, that are distinctly different from the carbonates of the deeper vein system (Fig. 4). This is explained as being a consequence of fluid mixing of an external fluid and the same deep fluid transporting and precipitating gold in the silicified zone. The external fluid explains one of the end-member composition of the trend displayed by the carbonate from the western barite zone (see end-member X in Fig. 4), that is low radiogenic strontium and carbon isotopic compositions ($^{87}Sr/^{86}Sr < 0.70857$ and $\delta^{13}C$ of –3.9‰, respectively) and high oxygen isotopic composition ($\delta^{18}O$ of 23.3 ‰). A fluid with such an isotopic composition could be a fluid that could have circulated through the rock units stratigraphically overlying the immediate host rocks of the Stremtsi prospect, since fluid equilibration with carbonate and organic-rich rocks yield fluids with, respectively, high $\delta^{18}O$ and low $\delta^{13}C$ values. The low $^{87}Sr/^{86}Sr$ ratios of the fluid are compatible with a fluid-interaction with Eocene limestones, which have $^{87}Sr/^{86}Sr$ ratios between 0.70765 and 0.70785 (Koepnick *et al.*, 1985), or even with the nearby latite-andesite volcanic rocks dated at 29.2 ± 1.1 and 33.1 ± 1.3 Ma, which have $^{87}Sr/^{86}Sr$ ratios between 0.7069 and 0.7076 (Marchev *et al*, 2004b). The variable salinities between 0 and 3.1 wt% NaCl equivalent of the fluid inclusions studied in barite (Fig. 2) support such a mixing scenario, whereby the external fluid would be the diluted counterpart (*i.e*. nil salinity), either a sedimentary fluid or a largely isotopically modified meteoric water.

Marton *et al*. (2006) report that gold depositional processes were variable among the different low-sulphidation sedimentary rock-hosted gold prospects in the Eastern Rhodopes. Stremtsi is a case, where boiling and fluid mixing were the dominant processes, with the highest gold grades associated to boiling. The dominant sulphur isotopic compositions of sulphides between -5 and +5‰ at Stremtsi is common to all low-sulphidation sedimentary rock-hosted gold prospects in the Eastern Rhodopes (Marton *et al*., 2006). This suggests that there is likely a common ore fluid present throughout the Eastern Rhodopes during epithermal ore formation in the sedimentary rocks. However, the distinctly higher salinities of 3.6 to 5.1 wt% NaCl eq. at Stremtsi, compared to the Ada Tepe prospect (~0 wt% NaCl eq., Marton *et al.*, 2006), and other sedimentary rock-hosted prospects in the Eastern Rhodopes (mostly < 2.2 wt% NaCl eq. except Sedefche, Marchev *et al*., 2005) suggests that local controls or processes modified the fluid compositions.

## ACKNOWLEDGEMENTS

This study is part of C.N. M..Sc. project at the University of Geneva, financed by the Swiss National Science Foundation (Grants 200020-101853, and 200020-113510), SCOPES (Grant IB7320-111046) and a grant from the Society of Economic Geology (Hugh E. McKinstry Fund).

## REFERENCES

Atanasov A (1996) The ancient gold mine Perperikon near the village of Stremtsi, Kurdzhali region. *Annual of the University of Mining and Geology "St. Ivan Rilski*": 45, part I Geology, 89-96

Bonev, N, Burg, J-P, ,Ivanov, Z (2006a) Moseozoic-Tertiary structural evolution of an extensional gneiss dome: The Kesebir-Kardamos Dome, Eastern Rhodopes (Bulgaria-Greece). *International Journal of Earth Sciences:* 95, 318-340

Bonev, N, Marchev, P, Singer, B (2006b) $^{40}Ar/^{39}Ar$ geochronology constraints on the Middle Tertiay basment extensional exhumation, and its relation to ore-forming and magmatic processes in the Eastern Rhodopes. *Geodinamica Acta:* 19, 267-282

Koepnick, RB, Burke, WH, Denison, RE, Hetherington, EA, Nelson, HF, Otto, JB, Waite, LE (1985) Cosntruction of the seawater 87Sr/86Sr curve for the Cenozoic and Cretaceous: supporting data. *Chemical Geology (Isotope Geoscience)*, 58: 55-81

Marchev P, Singer B, Jelev D, Hasson S, Moritz R, Bonev N (2004a) The Ada Tepe deposit: a sediment-hosted, detachment fault-controlled, low-sulfidation gold deposit in the Eastern Rhodopes, SE Bulgaria. *Schweizeriche Mineralogische und Petrographische Mitteilungen*: 84, 59-78

Marchev P, Raicheva, R, Downes, H, Vaselli, O, Vchiaradia, M, Moritz, R (2004b) Compositional diversity of Eocene-Oligocene basaltic magmatism in the eastern Rhodopes, SE Bulgaria: Implications for genesis and tectonic setting. *Tectonophysics:* 393, 301-328

Marchev P, Kaiser-Rohrmeier M, Heinrich C, Ovcharova M, Von Quadt A, Raicheva R (2005) Hydrothermal ore deposits related to post-orogenic extentional magmatism and core complex formation: The Rhodope Massif of Bulgaria and Greece. *Ore Geology Reviews:* 27, 53-89

Marton I, Moritz R, Marchev P, Vennemann T, Spangenberg J (2006) Fluid evolution within Eastern Rhodopian sedimentary rock-hosted low-sulfidation epithermal gold deposits, Bulgaria, *IGCP 486 Field Workshop 2006- Turkey, extended abstract*: 116-123

# The Geology and Metallogenesis of the Kassandra Mines Deposits, Northern Greece

Patrick Forward
*General Manager, Exploration at European Goldfields*

ABSTRACT: The region of the Kassandra Mines deposits can be subdivided into a series of NW-trending zones including the Serbo-Macedonian massif which hosts the deposits and comprises schists that are often mineralised. The Kassandra mining area comprises the Skouries Au-Cu porphyry and the Stratoni and Olympias massive sulphide deposits. The Skouries deposit is a typical Tertiary sub-alkaline Cu-porphyry deposit, forming a near-vertical pipe intruded into amphibolite and biotite schist country rock. The alteration zones at Skouries are restricted in extent in contrast to well developed concentric zones typical of high level porphyries. The Olympias mineralization is a massive sulphide stratabound poly-metallic (gold-lead-zinc-silver) replacement deposit hosted at a marble-gneiss contact with pyrite, arsenopyrite, sphalerite, galena as the main ore minerals. The deposit occurs within an uplifted block which has been subjected to footwall collapse with the bounding faults acting as conduits to mineralising fluids, interpreted to be a Tertiary sub-alkaline intrusive in origin. The Stratoni mines mineralization is classed as lead-zinc-silver carbonate replacement type mineralization, with pyrite, galena and sphalerite as the main ore minerals. The ore zones are often irregular, forming high-grade bodies. The deposits occur adjacent to the Stratoni Fault which has acted as a feeder to the same magmatic mineralizing fluids that resulted in the Olympias deposit. The structural architecture is key to understanding the development of these deposits both in terms of the distribution of mineralization and the formation of the traps that hold them.

KEYWORDS: Greece, subduction, porphyry, massive sulphide, copper, gold, lead, zinc, silver, replacement, footwall collapse.

## 1. GENERAL GEOLOGY AND METALLOGENIC BELTS

The Kassandra Mines deposits are located in the Chalkidiki peninsula, Northern Greece. The region comprises remnant fragments of the Aegeis land-mass that can be subdivided into a series of north-west-trending, linear zones representing successive south-southwestward migrating subduction episodes of the African plate in the Jurassic to Eocene period (Figure 1). The Serbo-Macedonian massif, which hosts the Kassandra deposits, represents a backland beneath which the African plate was sub-ducted. Successive subduction events were accompanied by volcanism and arc-type plutonic igneous intrusions. The massif comprises schists that are often mineralized and intruded by Variscan granites.

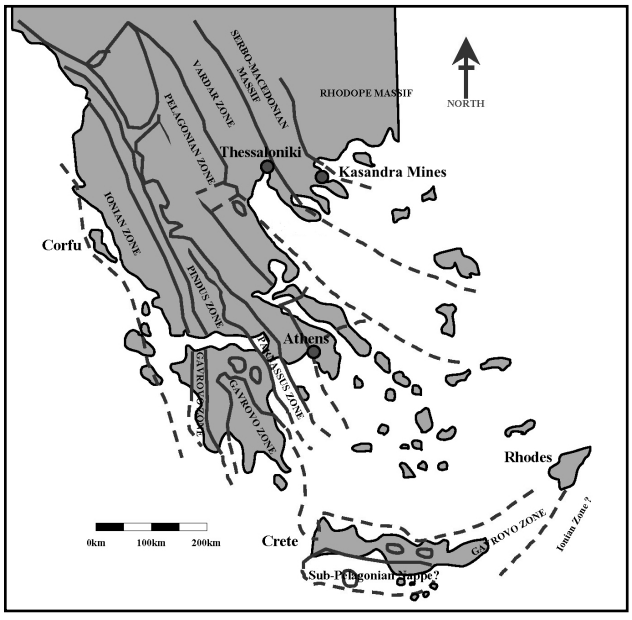


Figure 1. Tectonic subdivisions in Greece and location of the Kassandra Mines

The Balkan peninsular is subdivided into three major metallogenic provinces (Jankovic 1978): the Serbo-Macedonian and Anatolian metallogenic province (Pb-Zn-Ag ± As-Au, Cu-Mo ± Au), the late Cretaceous Neogene subduction zone (Pb, Zn, Cu, Au, Sb, Ag, Hg) and Triassic intracontinental rifting (Fe, Mn, Pb-Zn, ± Cu, Hg, Ba, Sb) related to late Cretaceous to Tertiary volcanic intrusive complexes. The Kassandra Mines Deposits are hosted within the Serbo-Macedonian province, a generally NE-SW trending belt comprising Pb-Zn-Ag ± Au replacement, fracture controlled Sb veining, Cu-Mo ±Au porphyry and stratiform volcano-sedimentary deposits. The Serbo-Macedonian province is contiguous with the Anatolian belt and also shows similarities to the mineral occurrences of the Rhodope Massif (Fig. 2).

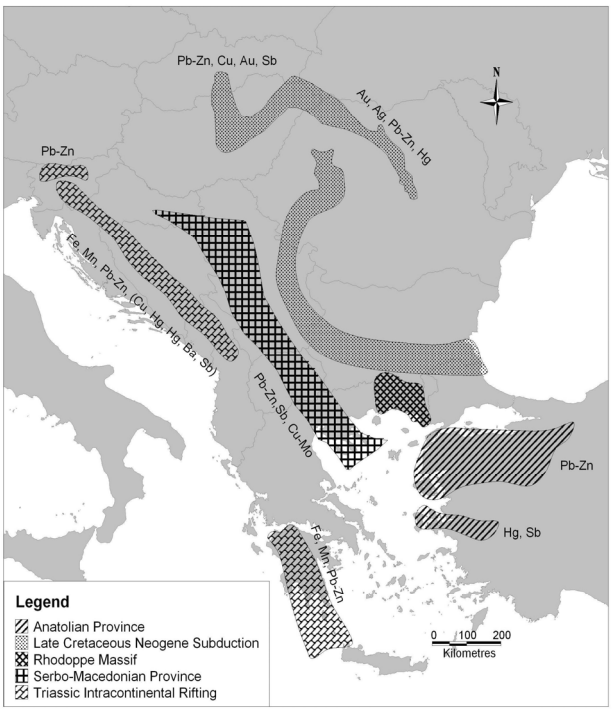


Figure 2. Metallogenic provinces of the Balkan Peninsular

## 2. LOCAL GEOLOGY

Within the area of the mines the Serbo-Macedonian belt comprises the Kerdilia and the Vertiskos formations.The two are separated by the Stratoni fault, an E-W to NW-SW, southerly dipping structure which is still active (Fig. 3). Recent movement along the fault is normal though it is thought that this could have been originally a reverse movement fault that placed the Vertiskos on top of the Kerdilia. Recent zircon dating (Himmerkus *et al*. 2006, 2003) has established that the Vertiskos Formation is Silurian in age and is thus older than the Upper Jurassic to Lower Cretaceous Kerdilia Formation, which is consistent with its origin as a major thrust fault bounding separate geologic terrains. This reverse movement is also supported by kinematic indicators in the rock (Cameron, 2007). The Kerdilia formation comprises a series of biotite, biotite hornblende and leucocratic gneisses, amphibolites and marbles. A

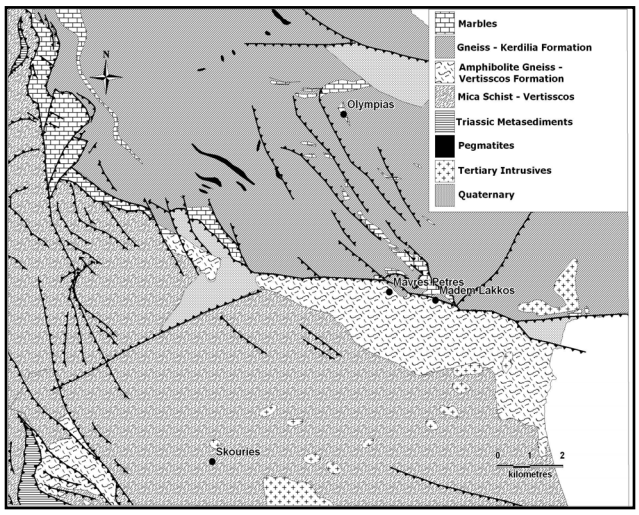


Figure 3. Geology of the Kasandra Mines Area

greywacke parent is suggested for some of the biotite gneisses and an igneous origin for the remaining biotite, biotite hornblende and leucocratic gneisses and also for the amphibolites. The Vertiskos formation comprises various biotite gneisses. Retrograde mineral assemblages in these gneisses and schist indicate a post metamorphic thermal event. The lower part of the sequence is dominated by olive green biotite and biotite-amphibole as indicated by diamond drill core intercepts at depth and by xenoliths in the border zone of the porphyry. Gray biotite gneisses and biotite-muscovite gneisses prevail nearer surface.

Based on isotopic ages and additional geological information (Kalogeropoulos *et al* 1989) the eastern part of the Serbo-Macedonian massif was affected by amphibolite facies regional metamorphism and deformation in the late Jurrasic and early Cretaceous. Tertiary ages of some amphibolites and pegmatites based K/Ar and Rb/Sr radiometric data in muscovites relates to delayed uplift in the Kerdilia formation (Kalogeropoulos & Theodoroudis 1988). The uplift is characterised by light isoclinal folding and thrusting which resulted in thickening of

the marble units. The metamorphic formations were intruded during the late and post deformational period at pressures of 5kbar and 350 to 550°C by pegmatite and aplite dikes, the Stratoni granodiorite (30Ma) and calc-alkaline lamprophyres (Papadakis 1971, Altherr *et al* 1976). The chemistry of the granodiorite is compatible with formation from a calc-alkaline magma of mainly mantle but also crust derived components (Kalogeropoulos *et al* 1989). The Skouries syenite porphyry (20Ma) is also representative of this Tertiary magmatism which relates to arc-type plutonic igneous associated with successive subduction events.

## 3. MINERAL DEPOSITS

The Kassandra mining area comprises the Skouries gold-copper porphyry and the Stratoni and Olympias massive sulphide deposits (Figure 5). The Olympias mineralization is a massive sulphide stratabound polymetallic (gold-lead-zinc-silver) replacement deposit hosted at a marble-gneiss con-tact with pyrite, arsenopyrite, sphalerite, galena as the main ore minerals. The Stratoni mines mineralization is also classed as lead-zinc-silver carbonate replacement type mineralization, with pyrite, galena and sphalerite as the main ore minerals.

In the case of both Stratoni and Olympias the ore is generally stratabound within the marble units or, more rarely fault controlled. At Stratoni the mineralization is developed within the antiformal axis zone of a lower marble horizon at the Madem Lakkos mine and within an upper marble horizon adjacent to the and within an upper marble horizon adjacent to the Stratoni Fault. (Fig. 4).

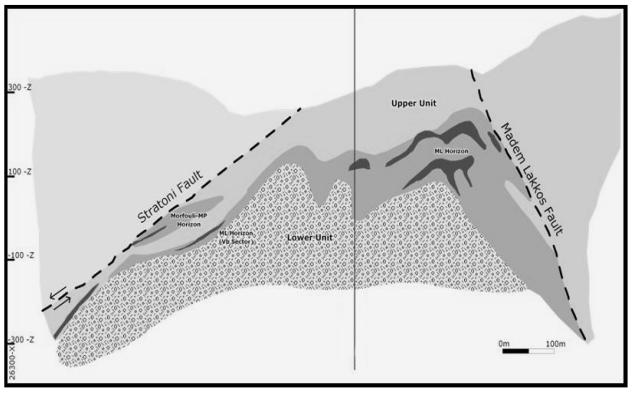


Figure 4. Projected cross section of the Madem Lakkos and Mavres Petres Deposits

In all cases the sulphide ore comprises both un-deformed massive sulphides and deformed sulphide ore with the latter characterised by brecciation, mylonitisation, folding and shearing. The most abundant ore minerals are pyrite, sphalerite, galena, arsenopyrite and chalcopyrite. Similar chemistry and fine zoning of sphalerite in both deformed and undeformed ore suggest that they come from the same system and were deposited after the onset of regional metamorphism. In addition copper-lead-zinc and copper – lead+zinc – silver bulk ore chemistry and lead silver relations irrespective of deformation indicate similarity to recognised skarn – replacement type deposits (Kalogeropoulos *et al* 1989).

Fluid inclusion work indicates that both deformed and undeformed sulphide ore were formed from $H_2O$ rich $CO_2$ bearing fluids with medium to low salinities of 2.5 to 6.5 wt.% NaCl eq. at fluctuating pressures of less than 500 bar and temperatures of 300 to 400°C at Olympias (Kilias *et al* 1996). Madem Lakkos is more proximal and therefore higher temperature with fluid inclusions indicating 480°C and also having complex salt contents.

The narrow range of sulphur isotopes and the rare occurrence of sulphates at the more proximal of the deposits suggests high ratios of reduced/oxidised sulphur species ratios, high temperature whilst low $\delta^{34}S_{initial}$ to $\delta^{34}S$ values indicate an igneous origin for the sulphur. (Kalogeropoulos *et al* 1989). It is therefore interpreted that a primarily magmatic fluid source for both the deformed and undeformed sulphide ores at both Stratoni and Olympias and the source of these fluids is thought to be a Tertiary sub-alkaline intrusive and is most likely the Stratoni granodiorite. These fluids have migrated along the Stratoni fault and through axial planar axes relating to earlier deformation and then into the marble horizons at Mavres Petres and Madem Lakkos. The earlier deformation has also resulted in a structural thickening and preparation of the marble units. The Olympias deposit occurs within an uplifted block which has been subjected to footwall collapse with the bounding faults acting as conduits to the mineralising fluids.

The Skouries syenite porphyry's final emplace-ment was controlled by northeast trending, steep dipping structures that provided the upper level conduits for the deep seated magma to be emplaced at shallower levels. This is demonstrated by the overall northeast trend of the known Tertiary intrusives which include the Stratoni granodiorite and the Skouries intrusion. The intrusion comprises a main porphyry

syenite stock with a series of branches on the southwest side (Fig. 5). After emplacement the porphyritic syenite was subject to polyphase alteration commencing with a pervasive alteration at 590°-640°C. The majority of the copper mineralization was emplaced during two later propylitic veining stages at temperatures of around 480°C and 380°C respectively, as indicated by isotope analyses (Frei, 1995), brought in most of the Cu, which was deposited in the form of chalcopyrite within quartz sul-

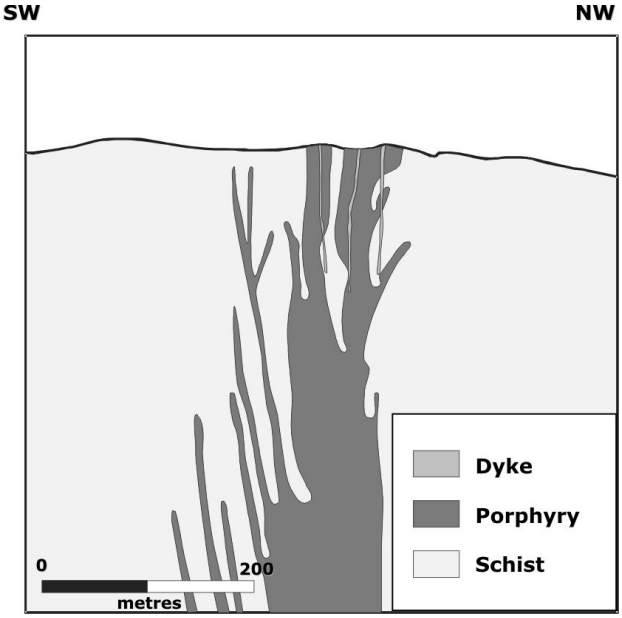


Figure 5. Cross section through the Skouries Syenite Porphyry Stock

phide veins through and around the stock. The range of $\delta^{18}O$ values for the fluids in equilibrium with vein quartz is within the typical range of early ore-forming magmatic fluids associated with porphyry mineralization with some phreatic mixing. Late propylitic alteration was more localised and affected the country rocks as well as the main stock and led to more disseminated sulphide. The $\delta^{34}S$ values from sulphides indicate a magmatic origin for the sulphur.

## 4. CONCLUSIONS

The mineralization of the Kassandra mines district is closely tied to Tertiary intrusions. Mineralising fluids are predominantly magmatic in origin. The igneous activity relates to successive subduction events. Controls on the emplacement of the intrusives and the conduits which have allowed fluid mígration into receptive host rocks as well as the preparation of those host rocks in terms of structural thickening and brecciation relate closely to the regional structure which is in turn related to the deformation history of this accretionary terrain.

## ACKNOWLEDGEMENTS

The above summary of the geology and metallogenesis of the Kassandra Mines deposits is a compilation of research carried out over the last twenty to thirty years as referenced below and I am grateful to the authors of these and other papers for their research. Hard work is also being carried out by all the Hellas Gold geological Staff and I am particularly grateful to Mr George Perantonis for his guidance over the last two years in the geology of the district and to Dr Greg Cameron for his recent work and the interesting discussions that have contribute to my understanding of the deposits.

## REFERENCES

Altherr R, Keller J, Harre W, Moehndore A, Kreu-zer H, Lenz H, Rashka H, Wendt J.(1976) Geochronology data on granitic rocks in the Aegean Sea, *Proc. of the Internat. Symp. on the History of the Mediterranean Basin, Yugoslavia:* 317-318

Cameron G (2007) A Report on the Geology and Exploration Potential of the Piavitza Polymetallic Sulphide Deposit Stratoni Area - Chalkidiki District, *Unpublished report for Hellas Gold*

Frei R (1995) Evolution of Mineralising Fluid in the Porphyry Copper Syatem of the Skouries Deposit, Northeast Chalkidiki (Greece): Evidence from Combined Pb-Sr and Stable Isotope Data, *Economic Geology* 90: 746-762

Himmerkus F, Reischmann T, and Kostopoulos D (2006) Permo-Carboniferous and Upper Jurassic Basement ages in the Kerdilion Unit, eastern Serbo-Macedonian Massif, Northern Greece, *Geophysical Research Abstracts.* 8, 05758

Kalogeropoulos S, Kilias S, Bitzios D, Nicolaou M, Both R (1989) Genesis of the Olympias Carbonate Hosted Pb-Zn Deposit, Eastern Chalkidiki Peninsula, Northern Greece. *Economic Geology* 84: 1210-1234

Kalogeropoulos S, Theodoroudis A (1988) K/Ar and Rb/Sr of the Minerals Biotite, Muscovite and Amphibolite from Rocks of the Serbo-Macedonian Massif, N Greece, *Unpub report IGME Athens Greece*

Kilias A, Falalakis G, Mountrakis D (1999) Cretaceous-Tertiary Structures and Kinematics of the Serbomacedonian Metamorphic Rocks and Their Relation to the Exumation of the Hellenic Hinterland (Macedonia Greece), *Internat. Journal of Earth Sciences* 88: 513-531

Papadakis A (1971) On the Age of Granitic Intrusion, Chalkidiki, Greece, *Annales Geol Pays Hellenic* 23: 297-300

# Alpine Metallogeny of the North-western and Central Dinarides

L. A. Palinkaš, S. Borojević Šoštarić & S. Strmić Palinkaš
*University of Zagreb, Faculty of Sciences, Department of Geology, Horvatovac bb, Zagreb*

ABSTRACT: The subject of the presentation is a review of Alpine Wilson cycle of the NW and Central Dinarides and its metallogenic characteristics. The Dinarides as an orogenic belt, between the Apulian microplate on the southwest and the Tisia ensialic block on the north, is a part of a long suture of the Tethyan ocean, squeezed between the Gondwana and Euroasian continents. It has well developed geotectonic units of the Alpine Wilson cycle, in contrast to the Alps, where the original geometry of tectonostratigraphic units was severely obliterated. Understanding the metallogeny of the Dinarides gives a clue to a more complex area along the whole Tethyan realm elsewhere. Ore deposits in the Dinarides are affiliated to particular Wilson cycle phases: early intracontinental rifting, advanced rifting, oceanization, subduction and collision.

KEYWORDS: Dinarides, metallogeny, Alpine Wilson cycle

## 1 NORTH-WESTERN AND CENTRAL DINARIDES

The Dinarides are an orogenic belt stretching 700 km along the north-eastern margin of the Apulia microplates (Dercourt *et al.* 1993). In the north this highly complex folded, thrusted, and imbricated belt merges with the Southern Alps and in the southeast with the Hellenides (Pamić & Balen, 2001). The main tectonostratigraphic units of the Central Dinarides display a regular zonal pattern from the Apulia plate to the Tisia block.

The tectonostratigraphic units are products of the Tethyan opening and closure during successive phases of the Alpine Wilson cycle, and are as follows: 1. Adriatic-Dinaridic carbonate platform (ADCP) – External Dinarides; 2. Carbonate-clastic formations of the passive continental margin (Bosnian flysch), 3. Dinaridic ophiolites, 4. Units of the active continental margin, olistostrom mélange, Sava-Vardar zone. The Internal Dinarides comprise units 2, 3 and 4. The Dinarides, as a whole, were thrust onto the units of the South Tisia block during the Pliocene.

The north-westernmost part of the Dinarides does not exhibit the same regular patterns as the Central Dinarides. The Dinarides deflects NE-SW, as the Zagorje-Mid-Transdanubian Zone (ZMTZ) between the Zagreb-Zemplin Line (ZZL) and the Periadriatic-Balaton Line (PBL), (Pamić & Tomljenović 1998), largely covered by the Sava nappe composed of Upper Palaeozoic and Triassic formations. ZMTZ, which is also named the Sava composite mega-unit, after Haas & Kovács (2001), bears elements of the External and Internal Dinarides and Southern Alps as well. It was squeezed between ZZL and PBL and extruded eastward by Tertiary indentation of the Adria (Apulia) microplate during formation of the Alps.

## 2 ALPINE GEODYNAMICS AND METALLOGENY OF THE NW AND CENTRAL DINARIDES

The possible boundary between Variscan and post-Variscan metallogenic events could be arbitrarily accommodated at the unconformity defined by Lower Carboniferous, deformed metamorphic basement and Lower-Middle Carboniferous flysch-type deposits, followed by the Upper Carboniferous-Permian molasse-type sedimentary rocks. The two Wilson cycles, Variscan (Post-Variscan) and Alpine could be separated by the beginning of Middle-Upper Permian red bed-type clastic sedimentation.

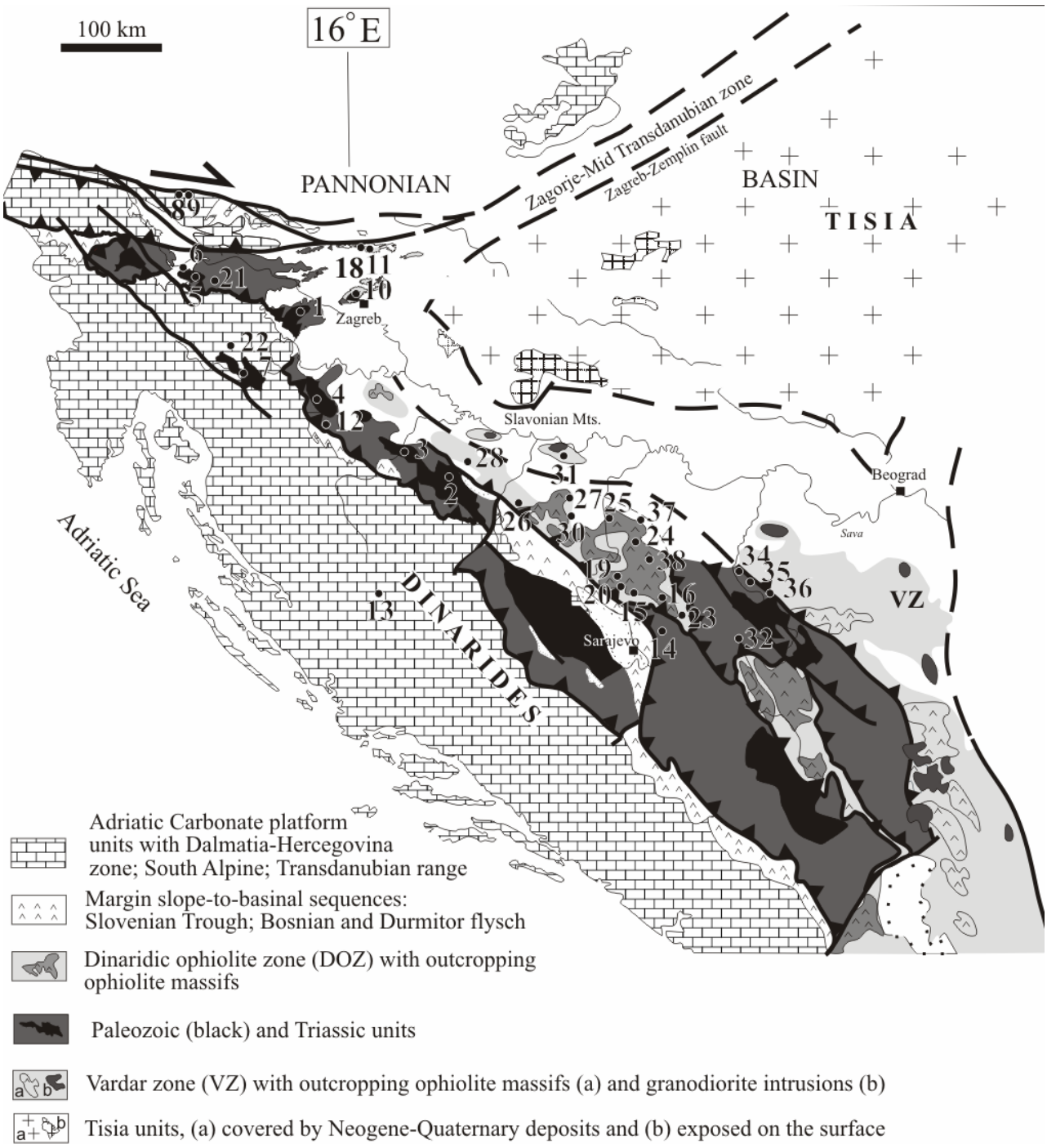


Fig.1 Metallogeny map of the North-western and Central Dinarides.

## 3. ALPINE WILSON CYCLE

The generation of the main tectono-stratigraphic units of the Dinarides, with characteristic lithologies is the result of a long-lasting evolution of the Dinaridic part of the Tethys. The stages of the Wilson cycle are recognized by specific magmatic formations responsible for the formation of a wide spectrum of mineral deposits and occurrences. In the NW and Central Dinarides one can recognize the following tectono-magmatic phases: 1. Early intracontinental rifting (Middle-Late Permian, thermal doming, incipient magmatism) 2. Advanced rifting (Middle Triassic, extensive submarine and subaerial volcanism and plutonism, basalts, spilites, keratophyres, gabbros, andesite-diorites,) 3. Oceanization, generation of

oceanic crust, (Jurassic-Early Cretaceous), 4. Subduction (Late Cretaceous-Palaeogene, emplacement of ophiolites in the accretionary wedge formations, ophiolitic mélange, basalt-rhyolites), 5. Collision (Palaeogene granitoids), and 6. Post-collision (Oligocene-Neogene andesite-dacites, granodiorites). From a metallogenic point of view the most productive were phases 1, 2 and 6. The mineral deposits related to each tectono-magmatic phase are:

***1)*** *The Permian Early intra-continental rifting (EIR);*

Deposits related to the incipient thermal events of the rifting; siderite-barite-polysulphide deposits (*1* Rude; *2* Ljubija; *3* Trgovska Gora Mountain.; *4* Petrova Gora Mountain., Palinkaš *et al.*, 2003).

Early intracontinental rifting took place on the Variscan basement of the Pangea. Incipient magmatism, caused by thermal doming and thinning of the continental crust, generated numerous hydrothermal cells in the thick piles of the post-Variscan non-metamorphosed sequences. The most widespread deposits, associated with the EIR, are siderite (± ankerite), deposits with minable lead and zinc sulphides. The stratabound ore occurs as lenticular, irregular, replacing bodies within limestone and dolostone, or vein-like intercalations in dark Carboniferous shale and siltite. The siderite-ankerite mineralization is accompanied by numerous monomineral or sulphide-bearing epigenetic, barite (±fluorite) deposits.

Deposits related to the dry-land and peritidal environments are represented by epigenetic, sedimentary uranium deposit, red bed type (*5* Žirovski Vrh); diagenetic, sedimentary copper deposit, Kupferschiefer-type (*6* Škofje); and early-diagenetic, Sabkha-type barite deposits (*7* Gorski Kotar).

***2)*** *Advanced Tethyan rifting (ATR);*

Carbonate hosted, low-temperature, lead-zinc deposits within the carbonate platform, MVT-Bleiberg-Mežica type (*8* Topla; *9* Mežica; *10* Sv. Jakob; *11* Ivanščica Mountain.; *12* Svinica; *13* Srb; *14* Olovo).

Sedimentary-exhalative (SEDEX) Fe, Mn, Ba, polysulphide (*15* Vareš; *16* Čevljanovići; *17* Bužim; *18* Mt. Ivanščica), Pb-Zn-Ba deposits (*19* Srednje-Borovica-Rupice; *20* Veovača); Hg deposits (*21* Idrija; *22* Tršće; *23* Draževići) (Palinkaš *et al.*, 2004).

***3)*** *Jurassic-Early Cretaceous oceanization;*

The Dinaride ophiolites are a part of the suture zone of the Tethyan ocean closure. They are characterized by a lherzolite belt, confined to the Dinarides, (the Dinaride Ophiolite Zone, DOZ, *sensu stricto*), and harzburgite-dunite belt placed mostly within the Vardar zone (Vardar Ophiolite Zone ,VOZ). The Dinaridic ophiolites are commonly dismembered or partially preserved as blocks of basalts, diabases, gabbros, serpentinites and peridotites. As a rule, one can state, however, that the number and size of the ore deposits related to the ophiolites diminish from the Hellenides-Albanides toward the Alps.

Ophiolite related deposits (Ozren, Čavka, Ljubić and Borja mountains) are characterized by the podiform chromite bodies linked with dunites (*24* Krivaja-Konjuh; *25* Bosanko Petrovo Selo; *26* Banja Luka; *27* Prnjavor; *28* Kozara-Pastirevo; *29* Zlatibor-Varda); magnesite and chrysotile asbestos deposits (*30* Čavka Mountain.); and copper mineralization, Cyprus vein and massive sulphide-type.

***4)*** *Cretaceous-Palaeogene subduction;*

Subduction phase in NW Dinarides must have started by the end of Late Jurassic as indicated by the first ophiolite emplacement. Gradual reduction of the Dinaridic part of the Tethys, accompanied by generation of a magmatic arc along the active continental margin, introduced a new sedimentary style in the fore-arc and back-arc basins. The subduction trench and slopes were filled with Cretaceous-Palaeogene flysch sedimentary rocks, followed by magmatic arc granitic plutonism and basalt-rhyolite volcanism. Their products are present in the Požeška Gora Mountain. as large masses of rhyolites and basalts, north of the Sava Neogene depression. Subduction ceased by the end of the Eocene, with the final emplacement of ophiolites, tectonization of the olistostrome mélange, followed by Alpine metamorphism and granite plutonism.

From a metallogenic point of view, the Alpine and Dinaridic subduction processes were barren in comparison to those in the Carpathians. The Eocene and Miocene syncollisional and post-collisional granite, andesite and dacite were, however, highly producing with numerous Pb-Zn-Ag, and Sb, hydrothermal and skarn deposits along the northern margin of the Dinarides, in the area of eastern Bosnia and western Serbia.

*5) Eocene-Oligocene syn-collision*;

Deposits related to the Eocene syncollisional granites (*31* Motajica Mountain), are represented by the pegmatites, aplites and greisens; hydrothermal ore occurrences and kaolin deposits.

*6) Early Oligocene post-collision;*

Deposits related to Early Oligocene post-collisional shoshonites and high-K calc-alkaline volcanic rocks are represented by the Pb-Zn-polysulphide hydrothermal deposits (*32* Srebrenica); kaolin deposits (*33* Bratunac); and antimony deposits (*34* Zajača; *35* Stolice; *36* Krupanj).

*7) Deposits related to subaerial weathering;*

*Bauxite deposits;* Bauxite deposits in the Dinarides occur in the vast region extending from Western and Central Slovenia to Croatia (Istria, Lika, Kordun, Adriatic islands, Dalmatia), and continuous to Western Bosnia and ends in Herzegovina and Montenegro. Bauxites were formed from Middle Triassic to Miocene time. The bauxites of each stratigraphic horizon have clear relationships to the hanging- and footwall layers, a definite geotectonic position and a wide geographic extention. Ten stratigraphic horizons with bauxite deposits were recognized in the Dinarides (Sokač & Šinkovec 1991): 1. Upper Triassic, 2. Malm, 3. Lower Cretaceous, 4. late Lower Cretaceous, 5. early Upper Cretaceous, 6. Senonian, 7. Early Palaeogene, 8. Late Palaeogene, 9. Oligocene and 10. Miocene.

*Nickeliferous laterites;* Weathering of ultramafic rocks produced Ni-laterites **(***37* Ozren Mt.; *38* Brazik-Tadići) in a short episodes of aerial exposure of the olistostrome mélange in the Lower Cretaceous time. Ni-laterite crust is thick between 0.3 and 12m and beside Ni contains Fe, Mn, and Co.

*Evaporites;* The Upper Permian evaporites were formed in the peritidal facies. The $\delta^{34}S$ value of the evaporites are mostly between +9‰ and+12.5‰.

*Salt (halite);* In contrast to the numerous Permian gypsum-anhydrite deposits in the Dinarides, the only rock-salt deposit *39* Tuzla is of Miocene age.

*Bentonites;* Bentonites in the Dinarides and South Tisia are related to Miocene pyroclastic rocks.

REFERENCES


Dercourt J, Ricou LE & Vrielynck B (1993) Atlas Tethys Palaeoenviromental Maps. *Gauthiers-Villars,* Paris, 307 pp.

Haas J, & Kovács S (2001) The Dinaridic-Alpine connection – as seen from Hungary. *Acta Geologica Hungarica* 44/2-3: 345-362.

Palinkaš AL, Borojević S, Strmić S, Prochaska W, & Spangenberg J (2003) Siderite-hematite-barite-polysulfide mineral deposits, related to the early intra-continental Tethyan rifting, Inner Dinarides. *In: Eliopoulos DG (Ed): Mineral Exploration and Sustainable Development,* Millpress, Rotterdam: 1225-1228.

Palinkaš LA, Strmić S, Spangenberg JE, Prochaska W, & Herlec U (2004) Ore-forming fluids in the Grübler orebody, Idrija mercury deposit, Slovenia. *Schweizerische Mineralogische und Petrographische Mitteilungen* 84: 173-188.

Pamić J, & Tomljenović B (1998) Basic geological data from the Croatian part of the Zagreb-Mid-Transdanubian Zone. *Acta Geologica Hungarica* 41: 389-400.

Pamić J, & Balen D (2001) Tertiary magmatism of the adjoining South Pannonian Basin. *Acta Volcanologica* 13 (1/2): 9-24.

Sokač K & Šinkovec B (1991) The bauxite of the Dinarides. *Travaux* 20-21: 1-13.

# The Cu-Au-Ag-Zn-Pb ore complex at Recsk, Hungary: a uniquely preserved and explored porphyry-skarn-epithermal system in the Palaeogene magmatic belt of the Alp-Carpathian-Dinaride system

Ferenc Molnár
*Department of Mineralogy, Eötvös Loránd University.*

ABSTRACT: The Palaeogene Volcanic Arc of Hungary is a part of the subduction-collision related magmatic belt of the Alps and its shallow erosion level is the consequence of northeastward lateral escapement of crustal fragments from the collision zone. Continous exploration during the past 40 years revealed that HS type ore with LS type overprint is laterally located in relation to a diorite intrusion whereas LS type ores are developed above one of the apexes of the intrusive body at Recsk. HS type alteration was formed by high temperature dilute fluids presumably originated from the low density portion of boiling magmatic fluids at depth. HS type ore with enargite-luzonite formed on a relatively low temperature from fluids with elevated salinities and it is suggested that their formation is related to the emergence, dilution and lateral flow of saline magmatic brines. The exceptional data base about the whole intrusive-volcanic system down to 1.2 km depth may support establishment of geologic models for other less explored areas in the Alp-Carpathian-Dinaride system.

KEYWORDS: metallogeny, intrusive-volcanic complex, Cu-porphyry deposit, epithermal gold

## 1 EXPLORATION HISTORY

The ore complex at Recsk consists of Cu(-Mo-Au)-porphyry, Cu-Zn-skarn and metasomatic Pb-Zn ores at depth, as well as high sulphidation ("HS") and low sulphidation ("LS") type epithermal Cu-Au and Au-Ag-Pb-Zn ores in the shallow zones of the volcanic cover. Exploitation of Ag-rich base metal ores from the LS type epithermal zones has begun in the 19$^{th}$ century followed by mining of massive enargite-luzonite in the HS type epithermal zones up to 1979. A drilling program started to follow mineralization towards depths led to the discovery of the porphyry system in 1967. In total 132, 1200 m deep drill holes were completed until 1984 and results initiated development of a mine with two 1200m deep shafts and adits with total length of 8456m from the -500 to -900m levels. Detailed mine exploration included 90,316m of underground drilling. Resources are summarized in the Table 1. After unsuccessful privatization attempts during the 90's, mine maintenance was terminated in 1999, and nowadays the well constructed shafts and adits are filled up by groundwater.

| Ore type | Resource Mt | Grade |
|---|---|---|
| Cu-porphyry | 109.4 | 0.96% Cu (at 0.8% cutoff) |
| Cu-skarn | 36 | 2.19% Cu (at 1.5% cutoff) |
| Zn-skarn | 11.5 | 4.98% Zn |
| Pb-Zn metasomatic orezones | 36.6 | 3.15-3.56% Zn 1.19-2.15 % Pb |

Table 1: reserves of the intrusion related ores at Recsk deep (after Fodor *et al.*, 1998)

In 1991, the epithermal gold potential of the shallow zones has been recognized by the Enargit Ltd. of Hungary and joint venturing with the Australia based Rhodes Mining Ltd. resulted in completing of 71 diamond drilling and determination of 36.5Mt resource of HS type gold mineralization (1.47 g/t @ 0.5 g/t; Földessy *et al*., 2002). Exploration of shallow epithermal zones has been revitalized by the Magyar Mining Plc. in 2003. Recent works has been focused on re-interpretation of drillcores,

assays, geophysical data etc. supported by academic research for better establishment an ore deposit model and for understanding the regional metallogenetic aspects of the ore complex at Recsk.

## 2 REGIONAL METALLOGENY

The Palaeogene Volcanic Arc of Hungary (PVAH) containing the intrusive-volcanic complex at Recsk is an approximately 300km long and 30-50km wide NE-SW trending belt along the northern margin of the Pannonian Basin and is located along the Periadriatic-Balaton-Darnó Line (PBDL; Fig.1).

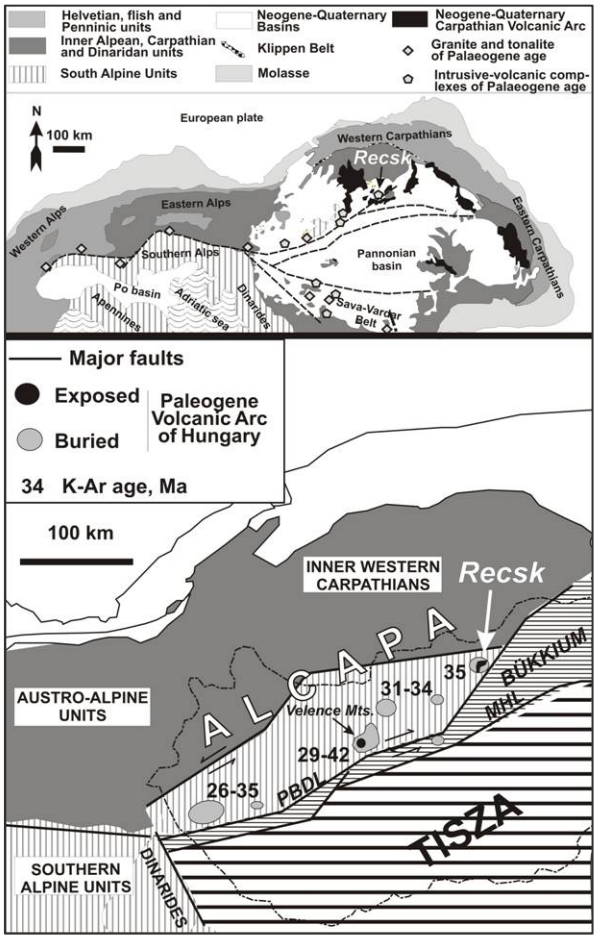


Figure 1: Palaeogene magmatic units in the Alp-Carpathian-N-Dinaride system and distribution of intrusive-volcanic complexes in the PVAH along the Periadriatic-Balaton-Darnó Line (PBDL).

The medium- to high K calc-alkaline intermediate intrusive and volcanic units of PVAH can be correlated with other post-syncollisional Palaeogene igneous belts along the Periadriatic Lineament in the Alps and in the northwestern part of the Sava-Vardar belt of the Dinarides (Benedek 2002, Pamic *et al.*, 2002). Oblique collision between the Adria microplate and the European Plate in the Alps generated north-eastward migration in extent of about 300km and rotation of crustal units (ALCAPA) during the late Oligocene- early Miocene. Thus the PVAH is an 'escaped' portion of the Periadriatic syn- and post-syncollisional magmatic belt which formed between the Adriatic microplate and the European Plate (Fig 1).

Intrusive-volcanic complexes of PVAH crop out near Recsk and in the Velence Mts., but they are totally covered by younger sediments in other parts of the arc (Fig 1). Metallogeny of PVAH is characterised by magmatic-hydrothermal systems producing Cu-porphyry and related epithermal mineralization during elongated igneous activities at Recsk and in the Velence Mts. These ore formations are absent further west along the Periadriatic Lineament, due to deeper erosion of magmatic complexes during emergence of Alps.

## 3 LOCAL GEOLOGY AND MINERALIZATION

The stratovolcanic sequence consists of four major units at Recsk (Földessy, 1975). Early stage pyroxene-amphibole andesite with peperite, agglomerate and lava flows is intercalated with shallow marine carbonate and marl of Upper Eocene age. Peripherial zones of superimposing volcanic sequences are also subaqueous, but their central, thickest zones (up to 700m thickness) were accumulated under subaerial conditions. These latter units are hydrothermally altered and consist of biotite amphibole andesite lava, agglomerate and crystal tuff-ditrema breccia in the northern part of the area (Lahóca Hill) and dacite dome-flow complexes to the south (Fig.2). The youngest volcanic unit without hydrothermal alteration consists of biotite amphibole andesite lava and agglomerate covering the eastern part of the Lahóca Hill (Fig.2). The stratovolcanic sequence is underlain by limestone, dolomite, chert and shale of Triassic age which are intruded by diorite porphyry. One apex of the subvolcanic intrusion is located under the northern part of the stratovolcanic sequence and another apex is under the dacite dome-flow compex to the south (Fig.2). The depth of these apexes is about 250-400m below the present surface.

The diorite intrusion hosts to Cu(Mo-Au) porphyry mineralization concentrated in the

phyllic (sericite, biotite, illite, chlorite) alteration mantle of the northern apex (Fig. 3). The average Mo and Au content is 0.009% and 0.13 g/t, respectively (Zelenka & Szebényi, 2002). Garnet-epidote-diopside-amphibole-serpentine-anhydrite endo-, and exoskarns host Cu and Zn ores. Metasomatic-replacement-vein type Pb-

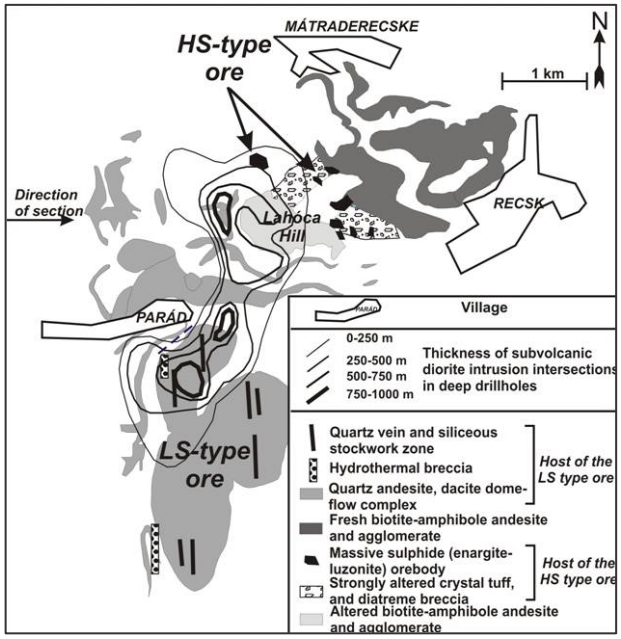


Figure 2: Outcrops of volcanic units and epithermal mineralization at Recsk with thickness contours of the subvolcanic intrusive bodies cut in 1200 deep drillholes under the stratovolcanic cover.

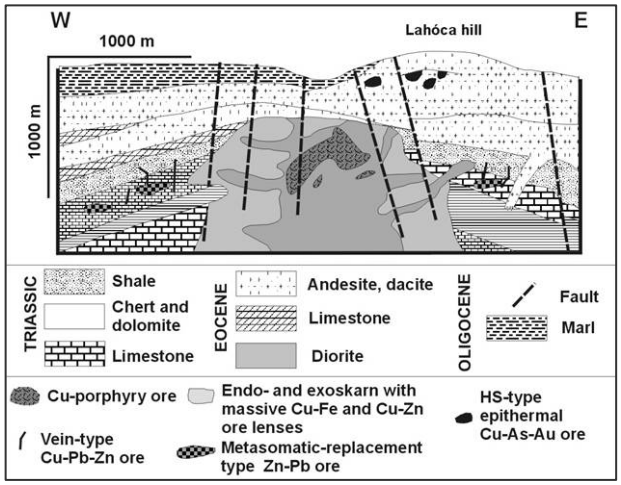


Figure 3: Section across the northern apex of the intrusion with location of ore types at Recsk.

Zn orebodies in carbonate units occur further away from the intrusion.

HS type epithermal mineralization occurs in the crystal tuff-ditrema breccia unit of the biotite-amphibole andesite stratovolcanic sequence of the Lahóca Hill (Fig 2), in lateral position to the northern apex of the subvolcanic intrusion. The tuff-diatreme breccia unit is underlain by andesitic lava flows with propylitic-argillic alteration and is covered by unaltered biotite-amphibole andesite in the eastern part of the Lahóca Hill (Fig. 2). Gold mineralization within the tuff-diatreme breccia unit is confined to massive enargite-luzonite lenses, pods of vuggy silica, stockwork of black chalcedony-like microcrystalline silica and polymict hydrothermal breccias with black siliceous-argillic matrix often showing fluidization flow textures. Polymict and monomict hydrothermal breccias with light grey microcrystalline silica and argillic matrix cut earlier formed ore-controlling structures and locally may also carry gold enrichments. Major gold concentrations are related to free gold grains in enargite-luzonite lenses and in vuggy silica and black microcrystalline silica as well as to framboidal to gel-like fine pyrite in black silica (Seres-Hartai & Földessy, 2001). The host rock shows advanced argillic alteration with dickite and silicification around ore controlling structures. The HS type ore is underlain and truncated by a zone in which banded quartz-carbonate veinlets with sphalerite, galena and grey ore minerals are enveloped by illite alteration. Thus the HS type ore formation was overprinted by a less acidic LS type hydrothermal event.

The LS type epithermal zones south of Parád village are located above the southern apex of the diorite porphyry intrusion (Fig. 2). Dacite and pyroclastic deposits host to banded and brecciated silica veins, stockworks and polymict matrix- to clast-supported breccia bodies with low contents of sphalerite, galena, grey ore, acanthite, pyrargyrite and rare Au-Ag-Bi-Te minerals. Host rocks are characterised by argillic alteration with predominance of illite and illite-smectite. Occurrences of silicified pods, alunite-kaolinite zones at various elevations and barite enrichments in silicified zones of the highest elevations are interpreted to be results of steam-heated alteration. Boiling of hydrothermal fluids is indicated by occurrences of quartz pseudomorphs after bladed calcite in banded quartz veins as well as by the presence of adularia in the matrix of hydrothermal breccia dikes. In breccia dikes, gold enrichment (up to 1.2g/t) is connected to adularia-bearing zones.

IR-microscopy supported microthermometry of enargite indicates that Cu-Au-As mineraliza-

tion of the HS type epithermal zone on the Lahóca Hill was formed from relatively low temperature (150-250°C) fluids with elevated salinities (4-13 wt% NaCl eq. Fig. 4). Textural evidences indicate that enargite precipitation was preceded by circulation of higher temperature (250-350°C) less saline (0-7 wt% NaCl eq.) fluids trapped in quartz in vugs within vuggy silica. In the deep porphyry copper ore zones, similar less saline fluids were developed as a consequence of boiling of magmatic fluids (Fig. 4). Upraising of these low density-high temperature fluids into the stratovolcanic sequence may have caused the high temperature acidic alteration preceding sulphide deposition in the HS type zones. The high salinity portion of boiling magmatic fluids underwent cooling and dilution (due to mixing with meteoric fluids?) and mobilization of these diluted magmatic fluids could have been responsible for transportation of heavy metals to the volcanic levels. The location of massive enargite-luzonite orebodies in relation to the apex of intrusion (Fig. 2) indicates lateral flow of these diluted saline fluids. Similar palaeohydrologic system for formation of the HS type ore was suggested at Lepanto, Philippines (Hedenquist *et al*., 1998).

Zones with LS type mineralization south of Parád are characterized by dilute (<4.5 wt% NaCl eq.) boiling hydrothermal fluids with temperatures between 140-280°C (Fig.4).

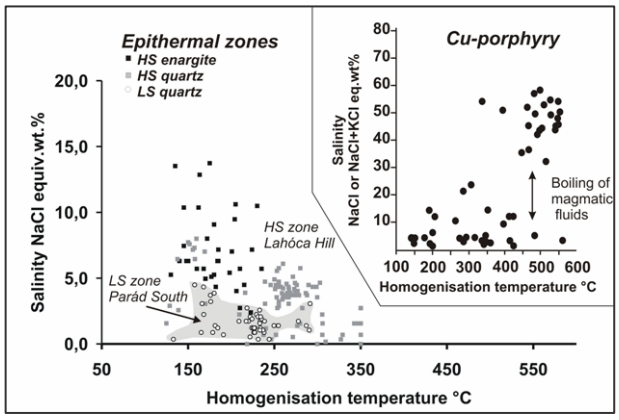


Figure 4: Fluid inclusion data for the porphyry and epithermal zones at Recsk.

## 4 CONCLUSIONS

The PVAH avoided deep erosion due to its northeastward escape from the Alpine collision zone during late Oligocene-early Miocene therefore intrusive-volcanic levels and related Cu-porphyry and epithermal mineralization are uniquely preserved. The ore complex at Recsk has been explored for 40 years and spatial relationships between the buried porphyry and shallow epithermal zones are well documented and may provide geologic model for exploration of deeper zones under outcrops of shallow epithermal systems in other areas of the Alp-Carpathian-Dinaride system. Refinement of ore deposit model at Recsk supports further drilling program for determination mineable epithermal gold reserves.

## ACKNOWLEDGEMENTS

Magyar Mining Plc. provided logistic support to this work. Company geologists N. Mound, K. Szentpéteri and J. Sweeney are thanked for discussions. V. Hurai is thanked for the access to the IR microscope at the Comenius U., Bratislava. This work was supported by the OTKA (HNSF) grant T 49633.

## REFERENCES

Benedek K (2002) Paleogene igneous activity along the easternmost segment of the Periadriatic-Balaton Lineament. *Acta Geologica Hungarica* 45:359-371

Fodor B, Forgács-Gombár G, Káli Z et al. (1998) Mineral resources and reserves of Hungary. *Annual Report of the Hungarian Geological Survey* 1998: 261p (in Hungarian)

Földessy J, Baksa CS, Szebényi G, Polgár I. (2002) History of exploration of the Lahóca Hill at Recsk. I*n: Szakáll S, Morvai G (Eds), Mineral exploration in Hungary during the XXth century. Miskolc-Rudabánya,* 155-168. (in Hungarian)

Hedenquist JW, Arribas A, Reynolds TJ (1998) Evolution of an intrusion-centered hydrothermal system: Far Southeast-Lepanto porphyry and epithermal Cu-Au deposits, Philippines. *Economic Geology* 93, 373-404.

Pamic J, Balen D, Herak M (2002) Origin and geodynamic evolution of Late Paleogene magmatic associations along the Periadriatic-Sava-Vardar magmatic belt. *Geodinamica Acta* 15: 209-231

Seres-Hartai É, Földessy J (2001) Native gold in the epithermal HS mineralization of the Recsk Ore Complex. *Acta Geologica Hungarica* 44: 463-473.

Zelenka T, Szebényi G. (2002) Exploration history of the base metal deposit at Recsk deep levels. In: *Szakáll S, Morvai G (Eds), Mineral exploration in Hungary during the XXth century. Miskolc-Rudabánya,* 169-198. (in Hungarian)

# Rudnitsa: New porphyry copper-gold occurrence in the Tertiary metallogenic belt, Serbia

Dejan Kozelj, Vetrees M. "Mac" Canby & Leon Naftali
*Phelps Dodge Exploration Corporation, Phoenix, Arizona, USA*

ABSTRACT: Rudnitsa porphyry copper-gold prospect is located in Central Serbia within Rashka ore field and Kopaonik metallogenic district (KMD) as part of Vardar zone in Serbo-Macedonian metallogenic province. It was discovered in 2004 after brief reconnaissance, magnetic surveys, and exploratory drilling. At surface, quartz-magnetite (martite) stockwork is surrounded by quartz-sericite-pyrite which grades outward into propylitic alteration. Magnetic surveys delineated well-developed magnetite alteration that is formed at depth above highly magnetic gabbro-serpentinite basement. After seven drillholes the porphyry copper-gold system still remains undefined because drilling was concentrated in and immediately around outcropping quartz magnetite alteration. New conceptual model is prepared in order to test potential for larger porphyry at depth and along strike of geochemical and magnetic anomalies to the north.

KEYWORDS: Porphyry, Copper, Gold, Kopaonik

## 1 INTRODUCTION

Serbia's two main base metal belts are the Upper Cretaceous Cu-Au±Mo, and Tertiary Pb-Zn-Ag ± Cu, Fe belts. At present, significant copper production in Serbia is from the Upper Cretaceous Cu-Au±Mo (Bor district) only, where a smelter is located. It treats copper concentrate from Bor, Veliki Krivelj, Majdanpek and small amounts from a Pb-Zn deposit at Rudnik. Rudnik and Rudnitsa belong to Tertiary belt where historic exploration focused on polymetallic lead-zinc-silver deposits related to Tertiary magmatic activity.

One of the main characteristics for the most of polymetallic deposits is strong structural and/or lithology control of mineralization. In most cases, deposits were formed at contact of quartz latite-diorite intrusions and Upper Cretaceous sedimentary series, or Jurassic serpentinite. However the most significant deposits formed in Triassic limestone (Trepca, Belo Brdo, Ajvalija, Kishnica).

Little historic exploration was dedicated to porphyry copper deposits. RTB Bor financed copper exploration of Tertiary belt from 1970-75 but discovered no economic deposits and made only one porphyry copper discovery at Kiseljak, containing 150 Mt of 0.27% Cu and 0.25g/t Au (Jankovic 1990). Accordingly, the Tertiary belt is under-explored for porphyry Cu-Au-Mo, which was the driving force beginning for additional exploration. Rudnitsa license (Fig.1) is located in the Rashka ore field, which extends from Plana on the north to Lipovica on the south, a total area of 500 km². Past exploration discovered several polymetallic deposits, some of economic interest (Kizevak, Karadak). Most of polymetallic de-


Figure 1. Position of Rudnitsa exploration license

posits are located in the far NE (Karadak) or SW (Lipovica) part of ore field. Advanced argillic alteration and associated Au mineralization reported at Bukovik, immediately south of Rudnitsa (Jankovic, 1990), is, speculatively, the shallow expression of another buried CuAu center along a roughly north-south to northeast structural belt which passes through Rudnitsa.

## 2 GEOLOGIC SETTING

Geology of Rashka ore field is complex. Basement is represented by upper Palaeozoic to lower Mesozoic amphibolite schist, limestone and dolomite; ortho-gabbros are present as result of dynamic metamorphism. According to determination of fauna from Trepca and Belo Brdo, calc-schists are Lower Triassic in age (Radulovic, Savich 1995).

Multiphase Tertiary volcanic activity was effusive and related to deep structures. Lower Miocene-Oligocene andesite-dacite volcaniclastics and lesser quartz-latite of a first phase are followed by second phase, sub-volcanic quartz latite; third phase is comprised of rare basalt flows and may extend to late Pliocene. Andesite thickness varies significantly as a result of the palaeorelief, number and length of pulses, character of volcano, vicinity of feeder, etc. Drillholes in the Kizevak PbZn deposit (5 km north of Rudnitsa) terminate in andesite breccia, whereas two drillholes at Karadak (0.5 km north of Rudnitsa) terminate in gabbros and serpentinite at 180m, while the deepest drillhole at Rudnitsa (550m) is suspended in aphanitic andesite-basalt. At Lipovica, the southwest end of volcanic complex, the deepest drillhole 500m remained in andesite-dacite

## 3 EXPLORATION HISTORY

Rudnica exploration dates back in Middle Ages and perhaps earlier, when intensive mining activity and smelting, as supported by slag found around Borovik hill, likely exploited oxidized Ag-bearing PbZn veins which cut the porphyry system. More than 130 pits and several adits are excavated in altered andesites. The presence of persistent anomalous Au grades in one large pit, in an area known locally as 'Zlatna Glava', suggests that some of the workings may have been for Au.

### 3.1 *Geological exploration before 2004*

Significant historic exploration for polymetallic mineralization was committed to the Rudnitsa area. Soil geochemistry at 200x100 m grid showed a copper anomaly (>100 ppm) on the west slope of Borovik hill, and detailed mapping (1:2500) defined 'strong silicification' at the summit but did not note porphyry copper characteristics. Historic drilling for PbZn targets thus began on the north slope of the hill and the closest drillhole to outcropping porphyry, RB-3, intersected 75m of 0.12% Cu, including 5m of 0.54% Cu immediately below the redox boundary; no Au assays were done except in PbZn veins, which subsequent work has shown to have notably lower Au grades than adjacent porphyry-type Cu-Au mineralization. After 3rd drillhole, the Karadak vein PbZn deposit was discovered about 1km north of Rudnitza, and the drillrig was moved for detailed exploration (Radulovic 1992).

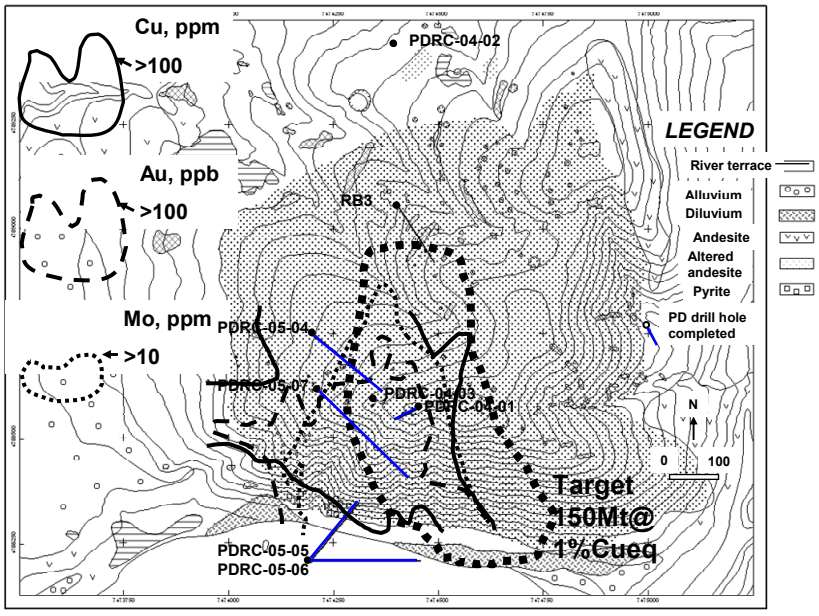


Figure 2. Rudnica soil geochemistry on geology map

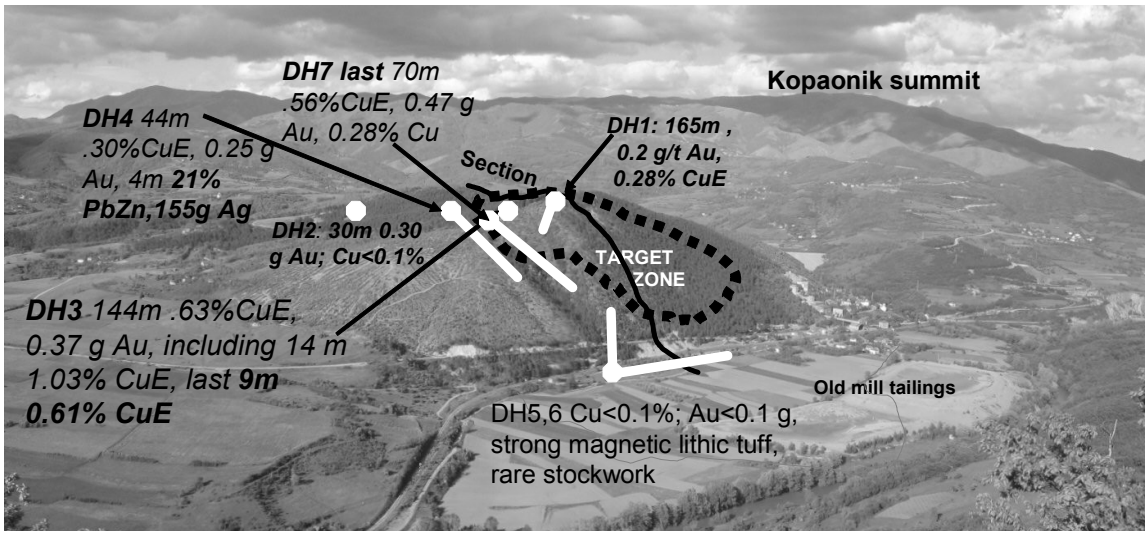


Figure 3: Overview on Rudnitsa with drillholes summary

### 3.2 *Recent geological exploration*

Literature study and a brief prospect visit verified Rudnitsa as an outcropping, unrecognized porphyry system. A brief rock chip campaign showed moderately anomalous Cu, Au on central Borovik hill, open to the south and with Au (>100 ppb) defining a N-S trending line. After license was issued, soil geochemistry at 100x50m grid defined anomalous Cu (>200 ppm), Mo (>20 ppm) and Au (> 20 ppb), concentrated in and around outcropping quartz-FeOx stockwork and secondary biotite at depth. Copper and gold anomaly is related to porphyry center (or outcropping parasitic centre), surrounded by anomalous Mo (Fig.2). Apart from Cu, Mo and Au were also open to the south (Kozelj 2005). Considering the abrupt termination of both stockwork to the south, as well as the presence of a major E-W striking structure, it was interpreted that the southern block could be downthrown by a post-mineral fault. To test this possible buried extension, two drillholes were drilled, which failed to intersect porphyry but did intersect andesite and basaltic tuff with intense magnetite alteration and anomalous Au and Cu values (to 0.1g/t and ~0.2% respectively).

### 3.3 *Geophysical survey*

A ground magnetic survey on 100mx10m grid was carried out at area 2x2 km centered on the outcropping porphyry stockwork.

3D magnetic models suggest that the resulting magnetic high is probably generated by two different sources: 1) a long wavelength component, interpreted as relatively deep high magnetic basement rocks (elevated block of serpentinite and gabbro); 2) a superimposed short-wavelength component interpreted as zones of secondary magnetite introduction, above the basement. The models are constrained using the information from drillholes where the depth to the basement is known.

Zones of hydrothermal magnetite enrichment are interpreted as a series of N-S trending bodies structure about 250 m width and more than 800 m long. The most intensive anomalies are interpreted as steeply dipping narrow structures (Lydia Nikova, 2005 - *unpublished data*).

### 3.4 *Exploration drilling and modeling*

Seven drillholes were completed to define quartz magnetite alteration and stockwork extension at depth. Drillholes 1, 3, 4 and 7 are collared within quartz-FeOx stockwork alteration, drillhole 2 in phyllic alteration some 900m north of the outcropping stockwork zone, and drillholes 5 and 6 tested the southern magnetic high possibly representing the downfaulted southern extension of the porphyry (Fig.4).

Drillhole 2 is located in outcropping phyllic alteration and rock chip values of 581 ppm Cu and Au 0.1 ppm Au; it remained in phyllic alteration with very thin secondary enrichment.

Drillholes in central part of porphyry center intersect an oxidized and leached zone up to 170m thick, a thin zone of secondary enrichment up to 70m thick, and a primary sulphide zone with variable alteration and stockwork intensity. Drillhole 3 was terminated early at 244m in an altered gabbro block averaging 0.38% Cu and 0.39 g/t Au. The most mineralized parts of all drillholes in central part are al-

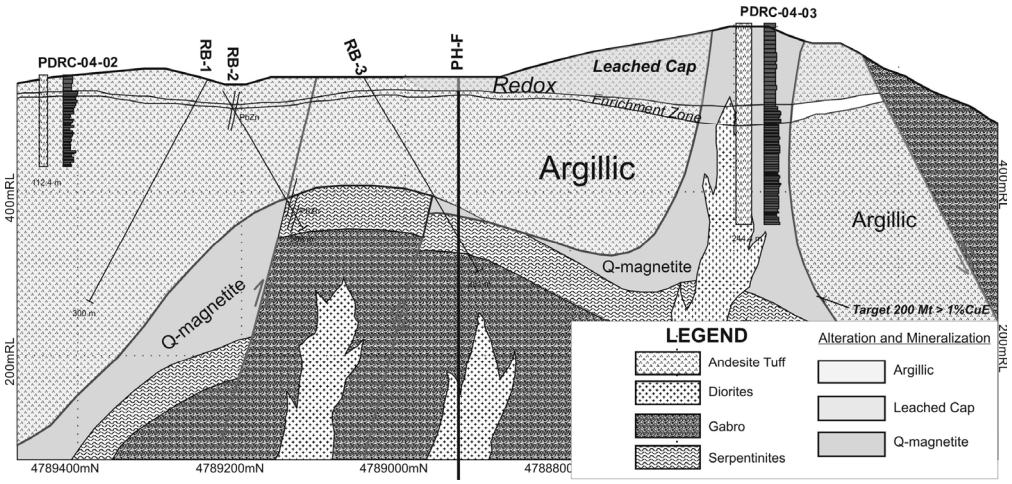


Figure 4: Conceptual N-S cross section

tered diorite dykes with intense stockwork quartz veining. The best interval was in the third hole, containing 144m (100-244m) of 0.403% Cu, 0.37 g/t Au, including 14m 0.85% Cu, 0.38 g/t Au. Angled drillhole 4 tested the depth extension of mineralization encountered in vertical drillhole 3. It returned weaker mineralization, (0.2-0.3% Cu and 0.1-0.3g/t Au), in addition to several Pb-Zn veins, some with high grades, including 2m of 21.16% Pb + Zn and 229g/t Ag in colloform-banded carbonate-galena-sphalerite mineralization. Drillhole 7 was drilled near drillhole 3 to test area immediately below 3. Neither drillhole 4 nor 7 confirmed vertical extension of the porphyry stockwork below drillhole 3, suggesting this mineralization either weakens at depth, or plunges parallel and away from these drill holes.

## 4 CONCEPTUAL MODEL

Several approaches were tested at Rudnitsa Cu-Au porphyry. The largest and most intense quartz-FeOx stockwork is detected at surface. So far this mineralization has not been traceable into a larger volume at depth. Magnetics, mapped structures, and geochemical patterns suggest a dominant N-S structural pattern. Accordingly, best potential for expansion is north from center of the exposed system. It is proposed that area with exposed and explored porphyry Cu-Au mineralization is parasitic centre of a larger body located at depth and to the north. Alternatively, the main part of porphyry style could be much deeper or slightly east.

## 5 CONCLUSIONS

Rudnitsa porphyry Cu-Au mineralization was discovered in 2004 after limited reconnaissance and rock chip sampling. Dense magnetite stockwork (>30 veins/m) is developed in quartz-magnetite alteration containing secondary biotite at depth. Results from seven drill holes indicate a grade of 0.2-0.3% Cu and 0.3-0.4 g/t Au with no significant molybdenum. Potential for a larger discovery remains, particularly to the north of the drilled system and at depth.

## ACKNOWLEDGEMENTS

We are very thankful to one of the great explorers in this area Bude “Lika” Radulovich, who discovered several of the polymetallic deposits. We appreciate his field support and geologic knowledge for the area.

## REFERENCES

Janković S (1990) THE ORE DEPOSITS OF SERBIA, Regional metallogenic settings, environments of deposition and types. *Mining and Geology Faculty Belgrade.* pp760

Janković S (1995) The principal metallogenic features of the Kopaonik district.- *Geology and Metallogeny of the Kopaonik Mountain*, 1995: 79-102

Koželj D (2005) Elaborat o izvršenim geološkim istraživanjima Rudnice u rudnom polju Raška za 2004-5. godinu. pp22

Radulović B (1992) Ležište cinka i olova Karadak.- Radovi *Geoinstituta, Beograd, knjiga* 27: 169-180

Radulovich B, Savich R (1995) Deposits and potential for base and precious metals in the ore field Raska. *Geology and Metallogeny of the Kopaonik Mountain*: 284-298

# The origin and evolution of the Belo Brdo Pb-Zn deposit, northern Kosovo: a preliminary field based interpretation

Milica Veselinovic-Williams, Peter J. Treloar & Andrew H. Rankin.
*Centre for Earth and Environmental Science Research, Faculty of Science, Kingston University, Penrhyn Road, Kingston upon Thames, Surrey, KT1 2EE, UK.*

ABSTRACT: The Belo Brdo deposit is one of the largest Pb-Zn deposits of the Kopaonik metallogenic district in the Vardar Zone. Several styles of sulphide mineralization and associated alteration are present. Three main ore bodies of hydrothermal replacement-type are hosted by Cretaceous carbonate rocks. An additional hydrothermal vein deposit is located within Tertiary andesites. Preliminary geological data suggest that the Belo Brdo deposit could represent epigenetic peripheral mineralized bodies linked to much larger, porphyry-style systems similar to those found elsewhere in supra-subduction zone settings.

KEYWORDS: Belo Brdo, Kopaonik, Vardar Zone, Pb-Zn mineralization

## 1 INTRODUCTION

The Kopaonik metallogenic district (Fig. 1) belongs to the NNW-SSE trending Vardar Zone, regarded as the easternmost tectonic unit of the Dinaride-Hellenide Belt (Marroni *et al.,* 2004). The Vardar Zone is a composite terrain consisting of both continental- and oceanic-derived slices (Robertson & Karamata, 1994; Dimitrijevic, 2001). Besides the occurrence of MOR-type ophiolites, the Vardar Zone is also characterized by ophiolites originating in a supra-subduction zone setting (Marroni *et al.*, 2004). Numerous economically significant deposits of lead-zinc, antimony, bismuth and molybdenum, as well as smaller copper, iron, tin, tungsten and gold deposits are present within the Vardar tectonic zone (Jankovic, 1990). The Pb-Zn mineral deposits extend northward from Kosovo, southern Serbia (Trepca, Crnac, Belo Brdo and Koporic) through western Serbia (Kizevak, Sastavci, Rudnik and Veliki Majdan) to easternmost Bosnia (Srebrenica). The deposits are likely related to Neogene calc-alkaline magmatic complexes (Jankovic, 1990). The Kopaonik metallogenic district (Fig.1) also known as the Trepca mineral belt hosts several skarn, hydrothermal replacement and vein type Pb-Zn (Ag) deposits (Jankovic, 1995). The replacement lead-zinc deposits are mainly irregular bodies, containing between several thousand and several million tonnes of ore in limestone and siliceous rocks.

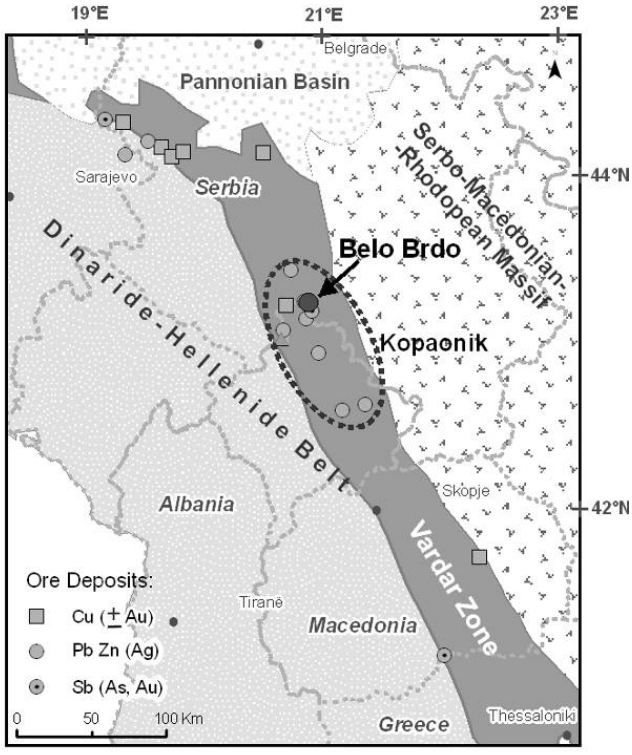


Figure 1. Location map of the Belo Brdo mine, Kopaonik metallogenic district, Serbia and disttribution of more important mineral deposits within the Vardar Zone of the Dinaride-Hellenide Belt (Modified after Marroni *et al*., 2004)

The Belo Brdo Mine works an underground lead, zinc and silver deposit located in northern

Kosovo. The mine was explored by Trepca Mines Ltd in 1927 and high-grade Pb-Zn-ore exploited on five levels until 1941. By 1990 a main shaft, drifts and production stopes had been established with 13 levels, from the lowest haulage level at an elevation of 1000m to the highest at 1425m above sea level. Total mineable reserves currently stand at 1.4 Mt at 5.99% Pb, 5.26% Zn and 86 g/t Ag.

The present study was initiated with the aim of improving understanding of the conditions of formation of the Pb-Zn (Ag) deposits in the Kopaonik metallogenic district of the Vardar Zone and to refine exploration models for similar deposits in the region.

## 2 GEOLOGY

Various lithostratigraphic and structural units of Triassic to Tertiary age have been recognized in the Belo Brdo region (Fig. 2). The tectonic stack includes, from bottom to top: Triassic metamorphic complex; an Ophiolite mélange Unit; a Jurassic Ophiolite Unit; and an Upper Cretaceous Flysch Unit. During the Early Oligocene, the tectonic nappe pile was intruded by the I-type Kopaonik intrusive complex (Dimitrijevic, 2001). The oldest rocks belong to the Suvo Rudiste Formation of Triassic age (Sudar, 1986). These metamorphic rocks are composed of argillic phyllite, phyllite, meta-sandstone, crystalline limestone and marble, as well as chlorite-mica-schist. The limestones occur either as the middle horizon with interlayers of phyllitic rocks, or as thick interlayers within the uppermost horizon of the series. At the contact with the Oligocene granodiorite, the limestones are metamorphosed to skarns and marbles and the pelites to hornfels.

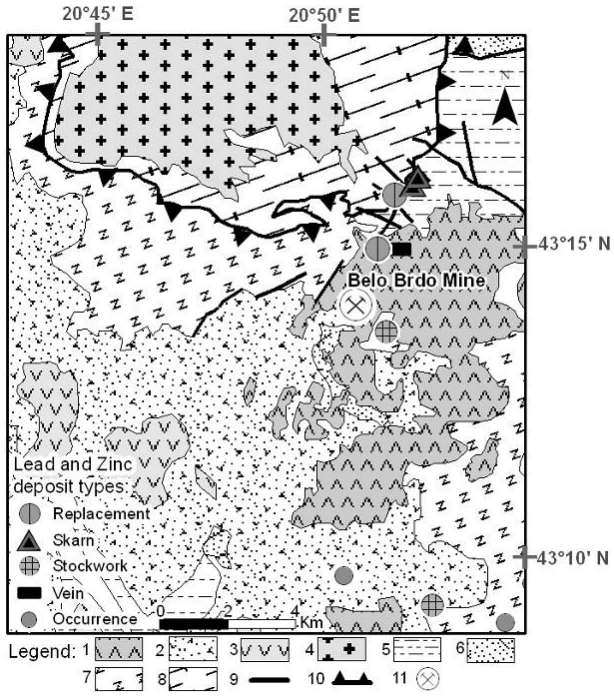


Figure 2. Simplified geological map of the Belo Brdo area. Tertiary: 1= Quartz-latite; 2 = Volcanoclastics of andesitic composition; 3 = Andesite-Dacite; 4 = Granodiorite. 5 = Upper Cretaceous sediments. Jurassic: 6 = Ophiolite olistostrome mélange; 7 = Ultramafic and mafic rocks. 8 = Triassic metamorphic rocks. 9 = Faults; 10 = Thrusts; 11 = Active mine (Modified after Jankovic, 1990)

Serpentinized ultrabasic rocks, known as the Ibar Massif, gabbros, diabases, basalts and sediments of the ophiolite association characterize the Jurassic ophiolite unit. They are thrust onto an ophiolite olistostrome mélange represented by meta-sandstones, phyllites and epidote-actinolite schists (Dimitrijevic, 1995).

The relationship between the serpentinites and the younger rocks is mostly of tectonic origin.

The serpentinite is strongly brecciated and tectonised and its protolith was a clinopyroxenebearing harzburgite. Basalts are developed as pillow lavas with pillows up to 2m in size.

In the northern part of the Belo Brdo deposit, transgressive Upper Cretaceous rocks unconformably overlie Triassic schists. The Upper Cretaceous sediments include, from bottom to top: reef limestone; marly limestone; and flysch. All the economic mineralization and high-grade ore bodies occur within the reef limestone (Miletic & Mladenovic, 1995).

During the Oligocene, the Kopaonik district was the location of considerable volcanic activity characterized by lava flows and volcanoclastic rocks (Fig. 2). The volcanic rocks are several hundreds of metres in thickness. Mineralogy and geochemistry reveal a range from andesitic through latitic to quartz-latitic composition (Cvetkovic, 1995). There is evidence of I-type *within plate* magmas that originated in an extensional regime that post-dates closure of the Vardar ocean (Karamata, 1995). Two phases of volcanic activity have been recognized (Jankovic, 1990). The first volcanic phase produced rocks of mainly andesitic composition and represents the largest part of the Belo Brdo volcanic complex. The andesites occur as lava flows, dykes and large masses of volcanoclastic material. Significant Pb-Zn mineralization often occurs adjacent to the dykes. Thick flows often have massive interiors with columnar jointing.

Andesites are mainly light to medium grey in colour and porphyritic in texture. They are composed of plagioclase, hornblende, biotite, augite and bronzite (Cvetkovic, 1995). The second volcanic phase is quartz-latite in composition and occurs as lava flows and dykes. The quartz-latite dykes, like the andesites, follow pre-existing structural trends and have also acted as ore traps for mineralizing fluids. They are hard and massive, light grey to dark grey in colour and with porphyry texture. They are composed of plagioclase, possible sanidine, quartz, hornblende, and rare augite.

## 3 MINERALIZATION

*Hydrothermal replacement mineralization* is the predominant and economically most important. It occurs, at, or close to, the tectonic contacts of the Cretaceous carbonates (rarely Triassic marbles) with Tertiary volcanoclastic rocks and/or Jurassic serpentinites. The GII ore body (Fig. 3) is irregularly shaped and plunges to the SE at 20° - 30°. Massive sulphide ore is dominated by pyrite, sphalerite and galena, together with variable amounts of arsenopyrite, chalcopyrite and a number of sulphosalts. Quartz and (Mn-Fe) calcite are the main hydrothermal gangue minerals. The degree of replacement of the carbonate rocks varies from local replacement in marginal parts of ore body, to complete in the ore body when only minor relicts of carbonate hosts are preserved.

*Vein-type mineralization* is hosted by Tertiary andesitic rocks. It consists of a quartz-carbonate-sulphide vein 1-2 m thick, with a strike length of 400 m. The essential ore mineral assemblage consists of galena, sphalerite and pyrite, accompanied by minor chalcopyrite, and antimonite.

*Skarn-type mineralization* was well developed in the GI ore body, which has now been completely mined out. Skarn mineralization is of limited appearance in the GII ore body and mineralization resembling a skarn assemblage was observed on only one level. Pyrite, amphibole and Fe-Mn carbonates occur in silicified limestones near the contact with volcanic rocks.

*Stockwork and veinlet-type mineralization* is sub-economic and occur peripheral to the main ore bodies. Stockwork structures consisting of quartz-carbonate veins have been recognised at the contact of serpentinites with limestones.

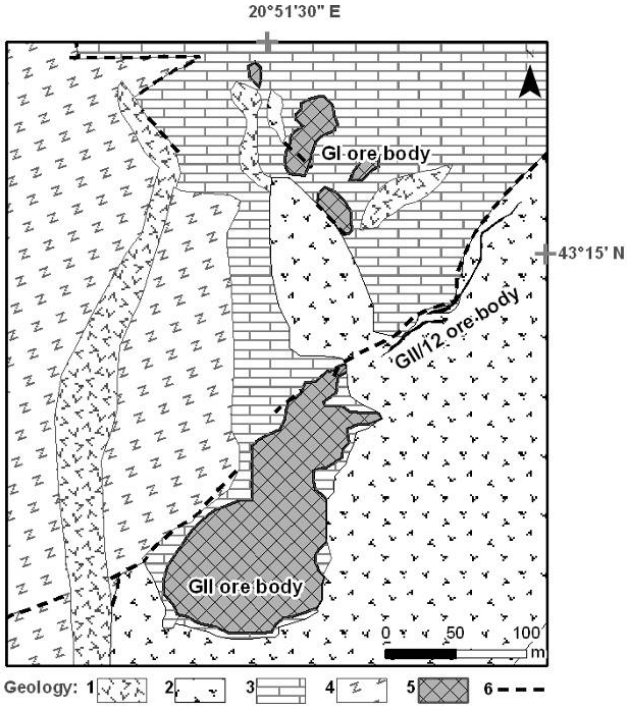


Figure 3. Simplified geological map of the underground level 1105 m, Belo Brdo deposit. 1 = Quartz-latite; 2 = Andesite; 3 = Reef limestones; 4 = Serpentinite; 5 = Ore body; 6 = Faults. (Modified after Miletic and Mladenovic, 1995).

Elsewhere pyrite and galena veinlets cut kaolinised and sericitised andesites and epithermal-style quartz-carbonate veins in chloritised andesites.

Zones of intense hydrothermal alteration are controlled by syn-deformational faults. Silicification, kaolinisation, listvanisation (also known as listvenitic alteration), chloritisation and sericitization are the major types of alteration. The hydrothermal alteration is most intense at the contact of the serpentinites and/or volcanics with carbonate rocks. On one sub-level at least two hydrothermal phases can be distinguished: listvanisation, a type of silicification combined with carbonatisation along the tectonic contact between serpentinite and carbonate, followed by a hydrothermal phase with deposition of pyrite and lead and zinc sulphides.

There is also local evidence for hydrothermal brecciation. Much of the ore in these areas appears as mineralised fragments cemented by later sulphide. Previously deposited sulphides are broken, rotated and transported as mineralised clasts that may be cemented by younger sulphides.

A wide variety of ore textures have been recognised including: replacement, open-space filling of fractures and vugs, dissemination in quartz veins, and banded, all of which are

mixed with varying amounts of quartz and carbonate gangue. Additionally, comb-quartz layer textures have been identified.

Massive sulphides are found in replacement zones of the carbonate host rocks. Galena, sphalerite and pyrite are the most abundant sulphides. Galena and sphalerite often form massive aggregates of coarse-grained crystals and can reach up to 4cm in diameter. Sphalerite is usually black in colour, probably due to increased amount of Fe. It has been observed that fine-grained pyrite and galena gradually progress into coarse-grained ore.

## 4 CONCLUSIONS

The Belo Brdo Pb-Zn deposit of the Kopaonik metallogenic district is located within the Vardar Zone, which consists of both continental- and oceanic-derived fragments. Several styles of mineralization were distinguished: hydrothermal replacement; vein; skarn; stockwork and veinlets. The ore bodies are associated with zones of intense silicification, sericitisation, argillisation, chloritisation, epidotisation displaying a clear structural control. Deep-seated structures of the Vardar Zone are likely to have provided a regional structural control along which calc-alkaline volcanic-intrusive complexes were emplaced. The Kopaonik district is situated in a tectonic setting similar to that of a continental island-arc collisional zone of Indonesia. Our hypothesis that the Belo Brdo deposit could represent epigenetic peripheral mineralized bodies linked to much larger, perhaps porphyry-style systems will be tested.

## ACKNOWLEDGEMENTS

Special thanks for organizing the access to the mine and supervision go to: Professor L. Palinkas, University of Zagreb, Croatia and Mr. I. Forjan, Development Officer of Trepca Mines Complex (under UNMIK). This research is funded by The Crustal Processes and Geodynamics Research group of the Centre for Earth and Environmental Science Research at Kingston University.

## REFERENCES

Cvetkovic V., Karamata S. and Knezevic V., (1995) Volcanic rocks of the Kopaonik district. *Geology and Metallogeny of the Kopaonik Mt. Symposium,* Belgrade, 185-194.

Dimitrijevic M. (1995) Ophiolitic melange of the Kopaonik Area. *Geology and Metallogeny of the Kopaonik Mt. Symposium,* Belgrade, 105-110.

Dimitrijevic M.D. (2001) Dinarides and the Vardar zone: a short review of the geology. *Acta Vulcanologica,* 13 (1-2): 1-8.

Jankovic S. (1990) The Ore Deposits of Serbia (Yugoslavia): Regional metallogenic settings, environments of deposition and types (In Serbian). *Rep. Drust. Fond za geol. Istraz.,* Econ. Geol. Fakultet Beograd, 760p.

Jankovic S. (1995) The principal metallogenic features of the Kopaonik District. Geology and *Metallogeny of the Kopaonik Mt. Symposium,* Belgrade, 79-101.

Karamata S. (1995) The Kopaonik Block, its position and genesis. *Geology and Metallogeny of the Kopaonik Mt. Symposium,* Belgrade, 41-45.

Marroni M., Pandolfi L., Saccani E. and Zelic, M. (2004) Boninites from the Kopaonik area (Southern Serbia): New evidences for suprasubduction ophiolites in the Vardar Zone. *Ofioliti* 29 (2): 251-254

Miletic G. and M. Mladenovic (1995) Promising areas lead and zinc deposit Belo Brdo. - *Geology and Metallogeny of the Kopaonik Mt. Symposium,* Belgrade, 275-283.

Robertson A.H.F. and Karamata S. (1994) The role of subduction-accretion processes in the tectonic evolution of the Mesozoic Tethys in Serbia. *Tectonophysics,* 234: 73-94

Sudar M., (1986) Mikrofosili i biostratigrafija trijasa unutrashnjih Dinarida Jugoslavije izmedju Gucheva i Ljubishnje. *Geoloshki Anali Balkanskoga Poluostrva,* 50: 151-394

# Basic research in service of successful exploitation in Pb-Zn-Ag Stari Trg mine, Trepča, Kosovo

S. Strmić Palinkaš & L. Palinkaš
*Institute of Mineralogy and Petrography, Faculty of Science, University of Zagreb, Croatia*

F. Molnar
*Department of Mineralogy, Eötvös Loránd University, Budapest, Hungary*

M. Diehl
*Trepča Under Unmik Administration, Zvečan, Kosovo*

ABSTRACT: Stari Trg/Trepča Pb-Zn-Ag deposit on Kosovo is a hydrothermal, metasomatic deposit. It is in operation by modern mining more than a century. The presented data are preliminary results of an extensive geochemical research undertaken in the underground mine by systematic sampling of ore and gangue minerals. Sampling took place along the vertical profile of the mining shaft from the surface to the depth (790m vertical elevation, eleven mining levels). Research is focused on the spatial P-T-X characteristics of the ore forming fluids. Use of variety of geothermometers, isotopes of S, O, C and H, together with fluid inclusion studies will constrain the Trepča genetic model, and determine termal gradient. Basic research will be prerequisite for more efficient prediction of the hidden ore reserves, and assessment of the area potential.

KEYWORDS: Geochemistry, hydrothermal metasomatism, low-sulphidation Pb-Zn-Ag deposit, Stari Trg, Trepča, Kosovo

## 1 INTRODUCTION

Stari Trg mine (42.9°N, 20.9°E), Trepca, is located 35 km NW from Pristina, Kosovo, within the Vardar zone of the Dinaride Alpine Belt (Fig. 1).

The geological formations consist of schist, phyllite, quartzite and marmorized limestones of Ordovician-Silurian age (Stari Trg Series). The principal mineralized stratum is limestone with developed palaeokarst (Mazic Limestone). The Stari Trg Series is unconformably overlain and partly obscured by andesite flows and tuffs of Miocene age. The older rocks of the region are strongly folded. An anticlinal structure, along which mine is developed, plunges about 40°NW. A nearly circular dacite and breccia pipe ransects the limestone-schist contact along the crest of the anticline (Fig. 1). At the surface and in the upper levels of the mine, the pipe contains a core of dacite surrounded by a mantle of breccia. The pipe terminates at depth and is absent in the lower levels of the mine. In the upper levels breccia is composed of subangular fragments of the country rocks and rounded fragments of dacites. In the deeper levels breccia cuts limestones and has characteristics of fluidized breccias with milled matrix (Forgan, 1949; Schumacher, 1954).

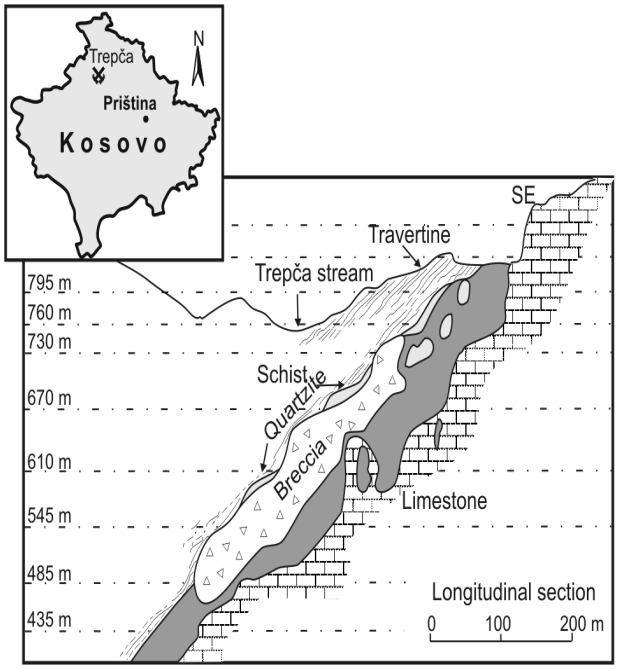


Figure 1. Geographical setting and longitudinal section of Stari Trg/Trepča mine.

Mineralization is represented by hydrothermal and skarn parageneses. Hydrothermal parageneses are composed of wide spectrum of sulphides (pyrite, pyrrhotite, arsenopyrite, silver bearing galena, sphalerite, jamesonite, bournonite), gangue carbonates and minor quartz. Skarn paragenesis, beside the above listed minerals, contains silicates (ilvaite, hedenbergite, garnet).

Stari Trg mine has 120,340 t of proven reserves (5.14% Pb, 5.13% Zn, 88.0 g/t Ag) and 311,660 t of probable reserves (5.10% Pb, 3.17% Zn, 80.5 g/t Ag). In the past 70 years ore production was 32 million tonnes with average annual production of 580,000 t.

At this moment under the temporary administration of UNMIK (United Nation Mission in Kosovo), the mine is being prepared for production and privatization. The main goal of the on-going studies is a detailed geochemical investigation, using various geothermometers to elucidate a genetic model and to construct a thermal profile of the deposit.

Breccia pipe within a palaeokarst hydrothermal system is formed by phreatomagmatic extrusion, during emplacement of dacitic magma. It served as a conduit for mineralizing fluids, but the ore is deposited in the host limestones.

The result should improve understanding of the architecture of this unique deposit and to improve prediction of potential ore reserves at the deeper levels, or laterally, where there has been much less intense erosion.

## 2 SAMPLING AND METHODS

Barren and mineralized samples were collected from the eleven levels of mine and on the surface (total vertical distance 790m). Barren samples are represented by limestones free of mineralization and volcanic rocks. Mineralized samples are hydrothermal and skarn paragenesis and their host limestones.

A fluid inclusion study was carried out to estimate the P-T-X conditions during mineralization.

Microthermometric measurements were performed on primary fluid inclusions on doubly polished, ~0.5 mm thick, wafers of quartz, calcite and dolomite from different mine levels.

Ore microscopy and electron microprobe analyses were done on well-polished ~0.5 mm thick polished thin sections of samples collected from the 10$^{th}$ level.

## 3 RESULTS

Reflected light microscopy shed light on the sequence of mineralization. The early quartz is overgrown by base metal sulphides which comprise pyrite followed by galena and sphalerite. Exsolution of chalcopyrite within sphalerite is frequent. Carbonates occur as a late phase with well developed crystals or in the crustiform bands locally alternating with quartz-rich bands. In skarn paragenesis silicates (ilvaite, hedenbergite, garnet) pre-date early quartz and arsenopyrite pre-dates pyrite. Electron microprobe data point to high Fe content of the sphalerite (11.9±0.9 and 10.4±0.4 wt % in hydrothermal and skarn paragenesis). The formation pressure of 1.2 and 2.5 kbar for hydrothermal and skarn paragenesis, respectively, were determined on the basis of sphalerite composition in equilibrium with pyrite and pyrrhotite (Hutchison & Scott, 1981).

Sphalerite and pyrite from skarn paragenesis are enriched in As comparing with hydrothermal minerals. Arsenopyrite (38 atomic % Fe, 34 atomic % As, 28 atomic % S) is found only in skarn parageneses. Chemical composition of arsenopyrite, co-existing with pyrite (Kretschmar & Scott, 1976), has constrained formation temperature for skarn paragenesis at 360°C.

Fluid inclusions (FIs) data suggest Na-Ca-chlorides as the main dissolved salts. FIs related to skarn paragenesis contain KCl as well. FIs in the early quartz from hydrothermal parageneses have salinity from 5.7 to 8.5 wt. % NaCl eq.. and homogenize ($T_h$) within an interval between 270 and 330°C. There is a gradual change of characteristics between samples from different levels. Boiling effects has been noticed in the carbonates from 7$^{th}$ level (liquid-rich FIs: 9.2-10.0 wt. % NaCl equ. and $T_h$=294-315°C, vapor-rich FIs: $T_h$=290-318°C). Salinity decreases with depth (3.4 to 4.9 wt. % NaCl eq.) while $T_h$ (270-330°C) does not show a steep gradient.

FIs in the early quartz from skarn paragenesis homogenize at high temperature (Th=310-355°C) and show moderate salinity (8.6-10.7 wt. % NaCl eq.). Salinity of the late carbonates are in the same range but $T_h$ has not been recorded due to massive decrepitation.

## 4 DISCUSSION

Geological setting and on-going geochemi-

cal investigations characterize the Stari Trg mineral deposit as a low sulphidation system (Corbett & Leach). The prevalence of carbonate host rocks differentiates this deposit from the other contemporaneous deposits in the region, and metasomatism is the dominant ore forming process. Local geology and lithology suggest a maar-type phreato-magmatic volcanism, which probably pre-dated ore formation. The palaeo-karst phenomena, however, controls ore formation spatially and mineralogically. This geochemical study should be considered as preliminary, and subsequent data will constrain the genetic model more strictly, and will be important for the prediction of hidden ore reserves and assessment of the area potential.

## REFERENCES


Corbett, G.J., & Leach, T.M. (1998): Southwest Pacific rim gold-copper systems: Structure, alteration and mineralisation: *Economic Geology, Special Publication* 6, 238 p.

Forgan C.B. (1948): Ore deposits at the Stari Trg lead-zinc mine. In: Dunham K.C. (ed): *18th International Geological Congress, London, Part VII, Symposium of Section F*, p. 290-307.

Hutchison M.N. & Scott S.D. (1981): Sphalerite geobarometry in the Cu-Fe-Zn-S system. *Economic Geology* 76: 143-153.

Kretschmar, U. & Scott, S.D. (1976): Phase relations involving arsenopyrite in the system Fe-As-S and their application. *Canadian Mineralogist,* 14: 364-386.

Schumacher F. (1954): The ore deposits of Yugoslavia and the development of its mining industry. *Economic Geology* 49: 451-492.

# Porphyry CuAu(Mo) mineralization and related advanced argillic alteration at Ilovitza, southeastern Macedonia

Vertrees M. "Mac" Canby
*Phelps Dodge Exploration Corporation, Cobham, United Kingdom*

Marin Alexandrov
*Professor, Faculty of Mining and Geology, Shtip, Macedonia*

Leon Naftali
*Phelps Dodge Exploration Corporation, Sofia, Bulgaria*

ABSTRACT: Porphyry-type CuAu(Mo) mineralization at Ilovitza, southeastern Macedonia, is closely linked with adjacent advanced argillic alteration hosting minor Au and base-metal occurrences. At Ilovitza, advanced argillic alteration is variably developed in both Tertiary volcanic rocks and Palaeozoic basement rocks, over a vertical range of at least 550 meters; adjacent porphyry-type stockwork alteration and CuAu(Mo) mineralization occurs over a vertical range of at least 500m, and is defined by a strong coincident magnetic high. Supergene leaching effectively removed all near-surface Cu. Peripheral advanced argillic alteration is relatively poor in metals considering its proximity to a large CuAu accumulation.

KEYWORDS: Porphyry, copper-gold, advanced argillic, Macedonia

## 1 INTRODUCTION

Since 2000, re-evaluation of historically-documented high-sulphidation alteration zones and major Pb-Zn metal deposits of eastern Macedonia demonstrates that nearly all such occurrences and districts are linked to low-grade Tertiary CuMo and CuAu porphyry systems (Fig. 1). Effective supergene leaching combined with low primary grades largely prevented historic recognition of both Cu content, and the porphyry affinity, of most of these systems. Subsequent exploration has identified Cu(Mo) porphyry systems at Kadiica and Osogovo, weakly-developed porphyry-type Cu(Au) mineralization at Dvorishte, and most recently, a CuAu(Mo) system at Ilovitza which likely contains several hundred million tonnes of low-grade CuAu mineralization, adjacent to widespread advanced argillic alteration containing weak Au-base metal mineralization.

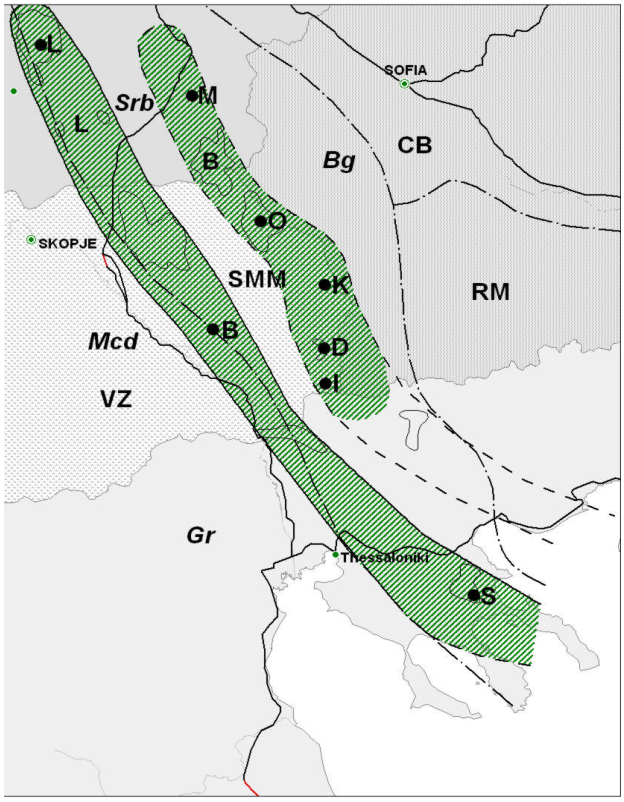


Fig. 1 Location: Tectonic units: *VZ*-Vardar zone; *SMM* -Serbo-Macedonian massif; *RM*-Rhodope massif; *CB*-Carpatho-Balkanides; Metallogenic zones: *L*-Lece-Chalkidiki; *B*-Besna Kobila-Osogovo; Prospects and targets: *L* - Lece, *B* - Buchim , *S* - Skouries, *M* - Machkatitza, *O* -Osogovo, *K* - Kadiica, *D* - Dvorishte, *I* – Ilovitza; Countries: *Srb*- Serbia, *Mcd*- Macedonia,*Bg*-Bulgaria, *Gr*- Greece

## 2 GEOLOGIC SETTING

Ilovitza is located between north-northwest-striking Tertiary magmatic-related mineral belts of the Lece-Chalkidiki zone, and the southward projection of the parallel Besna Kobila belt located immediately east (Figure 1). Although Pb and Zn are abundant in both belts, deposits of the Lece-Chalkidiki zone are notably

enriched in Au and Cu, whereas those of the Besna Kobila zone lack significant Au and are Mo-dominant, having been worked for primary Mo at Machkatitza, Serbia. Distinct Au enrichment in porphyry mineralization at Ilovitza may represent a departure from interpretations which relate Au enrichment to the presence of 'Vardar zone' ophiolitic rocks in the immediate basement of ore deposits.

Ilovitza is one of several porphyry systems of eastern Macedonia and northern Greece associated with volumetrically-minor exposed magmatic complexes (Red Ridge/Osogovo, Kadiica, Dvorishte, Macedonia; Skouries, Greece), as distinct from both Tertiary porphyry-related mineral systems within larger volcanic fields (Lece, Serbia; Plavitza, Macedonia), or large, altered volcanic fields which lack significant mineral occurrences (Petroshnitza, northern Macedonia).

Alteration and mineralization at Ilovitza are hosted in a roughly circular altered intrusion and intrusive breccia complex of probable Tertiary age, emplaced in lower Palaeozoic granite (Fig.2). The lower Palaeozoic granite is locally weakly foliated, contains coarse orthoclase megacrysts, and forms a roughly northwest-elongate body some 4km by 12km in size intruding Precambrian (?) mica schists and gneisses of the 'Serbo-Macedonian Massif.'

At surface, the Ilovitza Tertiary intrusive complex consists of a central, composite dacitic diatreme breccia body approximately 1.3km in diameter, cut by numerous dacite-granodiorite porphyry bodies and pods, and minor fine-grained andesite. This complex is centered on a hill of more than 400m absolute relief, surrounded at lower elevations by numerous small dikes and irregular bodies of dacitic tuff/breccia as well as non-brecciated intermediate volcanic rocks, cutting the basement granite and metamorphic rocks. Near-contact portions of the main dacitic diatreme, and these smaller peripheral bodies, locally contain abundant basement clasts. The contacts, and precise shape, of a dacite-granodiorite porphyry body mapped at surface within the main intrusive complex are obscured by poor exposure and intense hydrothermal alteration. Numerous isolated outcrops of dacitic porphyry elsewhere within the diatreme breccia commonly have vertical flow laminations and are too small to show as mapable units. Drilling demonstrates that dacite/ granodiorite porphyry expands at shallow depths into a fairly continuous body (Fig. 3), which is itself locally intruded by andesite porphyry and a late-mineral biotite latite-andesite porphyry, containing notably lower Au:Cu ratios than surrounding mineralized granodiorite porphyry.

## 3 ALTERATION

Alteration related to Tertiary magmatic activity at Ilovitza is variably present over an area of about 8km². Pervasive alteration is largely confined to a roughly 1.5km² area in and adjacent to the main intrusive complex. Smaller areas of pervasive and structurally-controlled alteration extend somewhat asymmetrically to the south and west of this intrusive complex. Alteration has not been

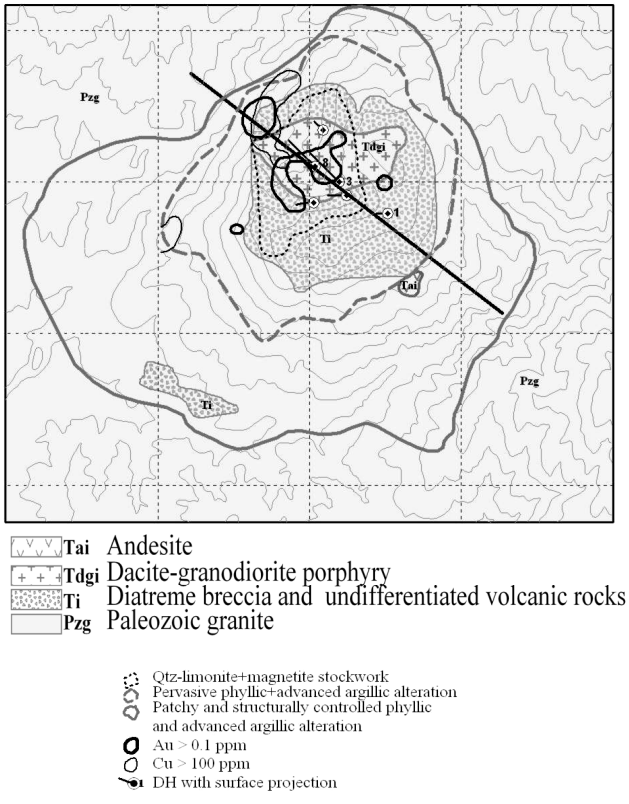


Fig.2 Generalized geology and alteration; grid is 1000x1000m; Fig. 3 cross-section shown as dark line

studied in detail, but visual observations document the following zones:

1) distal, structurally-controlled silicification, and silica- or silica-alunite-sulphide/FeOx altered rocks ('advanced argillic'), surrounded by narrow zones of clay alteration and bleaching, hosted in both fractured zones within basement granite, or within dikes/pods of Tertiary tuff-breccia. Such occurrences are present in zones a few

meters up to ~100m in maximum dimension, throughout the entire 8km² altered area.

2) proximal, pervasive quartz-sericite-clay-FeOx ('phyllic') alteration, which contains larger bodies of quartz-alunite alteration, hosted in both basement granite and Tertiary magmatic rocks;

3) proximal stockwork quartz-pyrite(FeOx) alteration and intense clay-sericite alteration largely confined to Tertiary dacitic breccia and dacite-granodiorite intrusive rocks;

4) central quartz-magnetite-sulphide (FeOx) stockwork and dissemination, with matrix alteration of illite-sericite(?), chlorite ('intermediate argillic alteration) containing patches of residual secondary biotite and K-feldspar, hosted in dacite-granodiorite porphyry, and minor andesite and latite-andesite porphyry dikes.

5) supergene sulphide oxidation, leaching, and argillization, locally extending as much as 150m below surface.

Distinct propylitic alteration is absent at Ilovitza. Alunite is typically sugary to coarsely crystalline in texture and locally occurs as mono-minerallic, coarsely-crystalline fibrous veins, breccia cement, and phenocryst replacement in pervasive silica-alunite altered dacite breccia. It appears hypogene in origin.

A single drill hole (#1, Fig. 3) collared in 'proximal' silica-alunite and phyllic alteration locally intersected low-density porphyry-type quartz-FeOx stockwork veining starting at less than 100m depth. The rapid transition within this hole from advanced argillic alteration, to distal porphyry-type stockwork, suggests that other zones of advanced argillic alteration may conceal mineralized stockworks at moderate depth, potentially expanding the target volume beyond that defined by outcropping stockwork. Notably, much of the broad area of 'distal,' largely structurally-controlled advanced argillic alteration lies well below the absolute elevation of exposed CuAu-bearing quartz-magnetite stockwork at Ilovitza.

## 4 MINERALIZATION

Ilovitza was known historically for minor PbZn(Cu) and Au occurrences, confined to distal and peripheral silica-FeOx and silica-alunite bodies outside of the pervasively-altered intrusive complex. Deep oxidation and leaching of the topographically-elevated intrusive complex obscured its sulphide content, whereas fresh sulphides at surface in peripherally alteration at lower elevations were more easily recognized historically. A short adit excavated in the early 1900s on a 1 to 2m, Au-bearing peripheral vein located south of the intrusive complex encountered pyrite-silica rock containing ~0.3% Pb, 0.3% Cu and 1-2ppm Au. Similar silica-FeOx and silica-alunite ledges and bodies at Kremen Chuka and other occurrences locally contain sparse disseminated galena, or yellowish oxidized Pb minerals, and commonly contain 0.05-0.5ppm Au, typically with elevated Pb but low (<500ppm) Cu values. Small dumps associated with shallow pits excavated both in bedrock as well as colluvium in the area of proximal quartz-alunite-iron oxide alteration, may represent Au workings or, alternatively, may have exploited alunite. Such occurrences contain erratic and weak Au, typically 0.1-0.5ppm Au over 2-4m widths. The only visible evidence of Cu mineralization at surface includes traces of enargite found in one siliceous ledge, very rare green copper oxides, and thin chalcocite coatings on sparse unoxidized pyrite exposed in a creek drainage on the northwest flank at the base of the leached cap.

Subsurface porphyry CuAu(Mo) mineralization is expressed at surface by a poorly-exposed, limonitic, leached stockwork zone approximately 900m by 600m in size, containing 0.08-0.7 ppm Au, 50-450 ppm Cu and 10-128 ppm Mo. At highest elevations, central portions of this leached cap contain up to 50-100 quartz and limonite-quartz veins per meter, comprising up to 25% of rock volume, within a sericitized and intensely (supergene?) clay-altered matrix. Quartz-dominant veinlets are largely devoid of sulphide cavities and have texture of both discontinuous 'A' veins as well as linear, center-line 'B' veins. Small exposures at lowest (550m) elevations on the western side of the stockwork zone contain 3-7% veinlet and disseminated magnetite, ~1% goethitic limonite, and lesser quartz-magnetite veinlets, within a silicified, chloritized matrix, likely representing intermediate argillic overprint of former K-silicate alteration. Although magnetite is present at surface only in isolated outcrops, ground magnetic surveys clearly define subsurface magnetite alteration as a roughly NNE-elongated, 80-1600nT magnetic high roughly 800m long and up to 300m wide, which appears to expand or plunge to the east and south. Peripheral portions of the

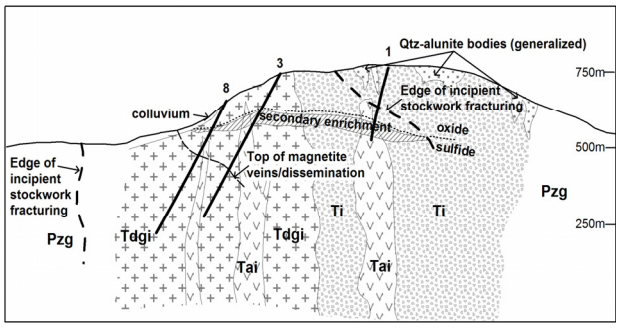


Fig.3. Cross section, view northeast. See Fig.2 for legend and section location

overall stockwork zone are characterized by sparse, hairline pyrite fractures with quartz-sericite(?) halos, likely corresponding to D-type veins. Surface rock chip sampling, limited drilling, and to a lesser extent soil sampling, define a large body containing 0.1-1ppm Au coinciding with the zone of stockwork veining. Hypogene Cu grades >0.15% occur largely as disseminated chalcopyrite, which appears largely confined to the western two-thirds of the stockwork body, which is characterized by the presence of magnetite(+martite), chlorite and relict biotite-K feldspar as groundmass alteration, and pyrite:chalcopyrite ratios generally $\leq$1:1. Stockwork veining in the eastern and higher-elevation part of the zone is characterized by higher py:cp ratio, more intense phyllic/argillic alteration, and the absence of magnetite. A supergene-enriched zone ranging from 9-70m thick containing 0.25-0.69% Cu as chalcocite and covellite represents enrichment of about 1.5x to 3x the hypogene grades; overlying leached cap contains about 150 ppm Cu. Molybdenum averages 20-80ppm throughout the CuAu mineralized zone and is present largely as molybdenite in quartz veinlets, which lack regular distribution. Soil sampling defines a classic, low-level Cu anomaly displaced laterally and down-slope from the topographically-high leached cap. Soil Au values >0.1ppm only partially delineate the mineralized stockwork, due to dilution and masking by relatively barren silica-alunite talus over much of the subcropping stockwork zone.

## CONCLUSIONS

Ilovitza is a further example of porphyry CuAu(Mo) mineralization and closely related advanced argillic alteration, in which overall metal content of the porphyry system greatly overshadows that of the surrounding high-sulphidation ledges, breccias and veins, to the extent the latter have been preserved by erosion. Deep supergene oxidation and leaching has removed nearly all surface evidence of Cu mineralization. The relatively large volume of CuAu mineralization at Ilovitza, compared to the small related volume of exposed Tertiary magmatic rocks, is perhaps analogous to the Buchim and Skouries deposits. Potential for expansion of the defined mineralization hinges upon its extension at depth and beneath widespread but relatively barren advanced argillic alteration elsewhere in the district.

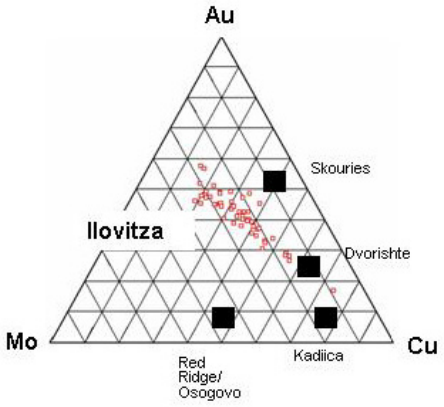


Fig. 4 Estimated relative Cu-Mo-Au contents of hypogene mineralization at Ilovitza (points) and other Tertiary porphyry systems in the southern Balkan Tertiary magmatic belt.

## ACKNOWLEDGEMENTS

We gratefully acknowledge Phelps Dodge Exploration for support, particularly the Macedonian staff Daniella Bombol, Annetta Donkova, Mitko Ligovski, Goran Kamchev, as well as expert technical assistance of Nelly Popova in Sofia, Bulgaria. Borche Hadji-Petrushev, Gerhard Westra and Lydia Nikova are also thanked for their contributions. We also thank Dr. Todor Serafimovski for his introduction to, and continued interest in, Macedonian metallogeny.

## REFERENCES

Tobey, E., Schneider, A., Alegria, A., Olcay, L., Perantonis, G., Quiroga, J. (1998) Skouries porphyry copper/gold deposit, Chalkidiki, Greece - Setting, mineralisation and resources, in Porter, T.M. (Ed) - *Porphyry and Hydrothermal Copper and Gold Deposits - A Global Perspective; PGC Publishing, Adelaide*

# The Kremnica Au-Ag epithermal deposit: an example of laterally outflowing hydrothermal system?

P. Koděra & V. Šucha
*Comenius University, Faculty of Natural Sciences, Department of Geology of Mineral Deposits, Mlynská dolina, 842 15 Bratislava, Slovakia*

J. Lexa
*Geological Institute, Slovak Academy of Sciences, Dúbravská cesta 9, 840 05 Bratislava, Slovakia*

A.E. Fallick
*Scottish Universities Environmental Research Centre, East Kilbride, Glasgow, UK*

ABSTRACT: The Neogene Kremnica low-sulphidation deposit is situated on marginal faults of a resurgent horst, associated with rhyolite magmatism. Wallrock alteration includes adularia, illite or I/S and kaolinite. South of the vein system extensive alteration continues with zones dominated by kaolinite, I/S and smectite replacing rhyolite. Fluid inclusion and stable isotope data indicate lateral outflow of fluids from N to S, with major boiling and Au deposition in central part of the vein system. Large areas of steam-heated waters probably accompanied the veins at subsurface level, while their outflow to S could be responsible for the extensive alteration of rhyolites, sporadic low-grade quartz/chalcedony veinlets with stibnite and silicite deposits in local limnic/lacustrine basins.

KEYWORDS: low-sulphidation, fluid inclusion, stable isotope, alteration, palaeohydrology

## 1 INTRODUCTION

Palaeohydrology of epithermal systems is one of the critical conditions determining the location of zones of alteration, boiling and precipitation of metals. Distribution of outflow zones largely depends upon structural setting and topographically controlled hydraulic gradients. As the low-sulphidation systems usually occur in low-relief terrain, vertical rather than lateral outflow of fluids is considered to be important for ore deposition. However, in terrains with higher relief the alteration pattern and mineral zoning can be displaced laterally and thus the classic model can be misleading in exploration.

Preliminary results from the Kremnica low-sulphidation Au deposit, hosted by moderate-relief terrain, demonstrate the essential role of reconstruction of palaeohydrology for exploration of this type of deposit. Kremnica has experienced considerable historical production (46 t Au, 208 t Ag), while recent exploration still confirmed significant resources on the 1st vein system. (18.8 Mt @ 1.6 g/t Au, 12.8 g/t Ag; *www.tournigan.com*).

Tournigan Gold currently explores license areas S and N of the known deposit to enlarge resources.

## 2 GEOLOGICAL SETTING

The Kremnica deposit is situated on marginal faults at the eastern side of the Kremnica resurgent horst (Fig. 1) in the central part of the N-S trending Kremnica volcanotectonic graben in Central Slovakia Volcanic Field (W Carpathians). The uplifted horst is build of the pre-graben andesite complex with sub-volcanic intrusions (16.2 - 15.0 Ma), representing central zone of a large andesite stratovolcano (Lexa *et al*. 1998). The resurgent horst is surrounded by andesitic rocks of graben fill (15.0 - 13.5 Ma).

The structure of the horst is dominated by N-S and NE-SW trending normal faults, corresponding to the regional stress field with a strong NW-SE extension during 13.5 - 9 Ma. Uplift of the horst was contemporaneous with epithermal mineralization (11.1 - 10.1 Ma; Kraus *et al.* 1999) and emplacement of rhyolite dykes (12.9 - 10.7 Ma), with corresponding granite porphyry subvolcanic intrusions at depth. Contemporary rhyolite domes, flows and volcanoclastic rocks occur S of the horst.

The system of epithermal veins is dominated by major transtensional fault that gradually opens towards the surface (up to the 80m thick vein in the central part - Šturec). The fault dipping 50°-60° is accompanied by low angle sec-

ond order vein structures close to the surface and complementary antithetic veins ("1st system"). In addition, in the hanging wall of the listric fault there is large complementary vein system ("2nd system"), underneath Kremnica town.

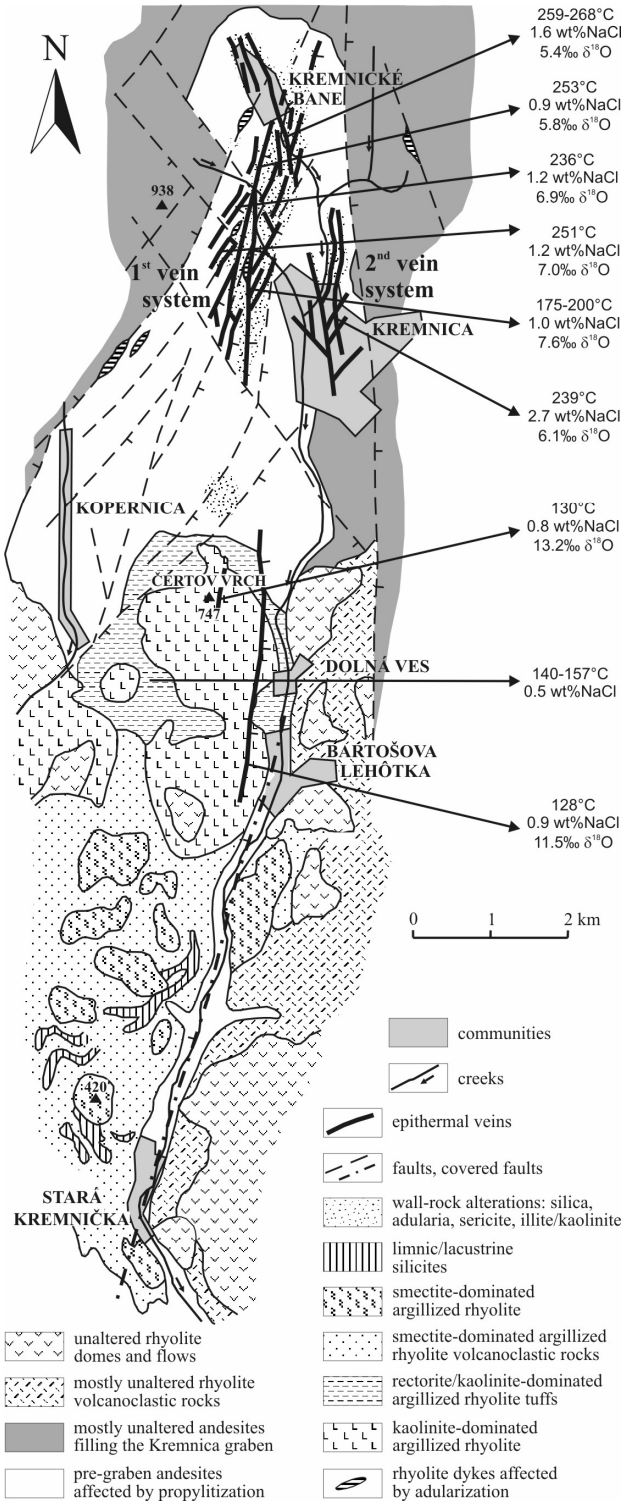


Figure 1. Structural scheme of the Kremnica hydrothermal system (after Kraus *et al*. 1994), with average Th or boiling temperatures, salinities and oxygen isotope composition of quartz from individual parts of the system.

## 3 MINERALIZATION AND ALTERATION

Vein filling of the 1st system is represented by banded and cavernous quartz, sometimes with carbonates. Microscopic Au is present as electrum in pyrite and quartz in dark quartz-chalcedony bands with fine dispersed pyrite/marcasite. Au and Ag contents decrease with depth, but simultaneously base-metals content, represented by sulphides, Ag sulphosalts, and tellurides, increase (Bohmer 1966, Veľký *et al*. 1998). Extensive wallrock alteration includes adularia, quartz, I/S, kaolinite, passing outwards into chlorite, smectite, variably with disseminated pyrite and carbonate (Kraus *et al.* 1994). Common presence of quartz pseudomorphs after bladed carbonate, adularia and hydrothermal breccias indicate boiling of fluids. Footwall structures are mineralized by stibnite.

Vertical extent of veins exceeds 1200m in the N part of the system and continue with some breaks at least 5km S from Šturec down to Bartošova Lehôtka in the form of mineralized quartz/chalcedony veins (1 - 4 g/t Au). At the Čertov Vrch hill ~3km S from Šturec hydrothermal breccias cemented by quartz/ chalcedony with cinnabar, minor Au and kaolinite are present, interpreted as a hot spring type mineralization (Veľký 1999). Surrounding rhyolite and rhyolite tuffs contain kaolinite, while south of the hill a deposit of I/S mineral rectorite occurs (Kraus *et al.* 1994). Smectite-dominated alterations extend further S, associated with limnic/lacustrine silicites near Stará Kremnička with increased Sb, As, Hg contents.

Veins of the 2nd system have gold present as visible aggregates in cavernous quartz-carbonate gangue (bonanza type Au), but average grades were ~4 g/t Au and 30 g/t Ag. Minor Ag-sulphosalts, tetrahedrite and base metal sulphides were also present. Wallrock alteration includes illite, kaolinite, passing outwards into I/S + kaolinite and smectite (Böhmer 1969).

## 4 FLUID INCLUSIONS

Microthermometry has been performed on fluid inclusions (FI) in quartz, sphalerite and carbonate. Systematic decrease in homogenisation temperatures (Th) was determined in direction from N to S on the 1st vein system (Fig. 1). Northernmost parts (Kremnické Bane) samples showed Th range ~259-268°C, while the higher temperatures apply to a deep sample (800m be-

low surface). In direction to S the vein system segments Schindler-Teich, Volle-Henne, Katarína showed a slight decrease in Th values (means ~253°, 236°, 251°C). Samples from the central part (Šturec) showed evidence about boiling of fluids at 175° or 200°C. Southernmost parts (B. Lehôtka, Čertov Vrch) showed evidence of boiling or condensation at 128° and 130°C, respectively, but the quartz host belongs to late stages of mineralization. Similar values (140-157°C) were obtained earlier from the I/S deposit Dolná Ves, located north from B. Lehôtka (Uhlík & Majzlan 2004). All along the 1st vein system average salinities are very low (~0.5 – 1.6 wt% NaCl eq.), with slight decrease towards S. This decrease can be related to mixing with fresh groundwater or it results from loss of dissolved $CO_2$ due to boiling.

Preliminary results from the 2nd vein system showed boiling at 239°, increased salinity ~0.7-5.9 wt% NaCl eq. and evidence about $CO_2$ presence.

Evidence of boiling indicates palaeodepth 89 or 164m in the central, and 25 to 50m in S part of the system. Boiling in 2nd vein system results in minimum palaeodepth 370m, but probably more due to the effect of dissolved $CO_2$.

## 5 STABLE ISOTOPES

Oxygen isotope data from quartz showed systematic decrease of $\delta^{18}O$ values from N (~5.5 ‰) to S (~12 ‰), which corresponds to decreasing Th values in this direction (Fig. 1). Calculated $\delta^{18}O_{fluid}$ ranges from -1 to -5.4 ‰, while the lightest values correspond to southernmost samples. Hydrogen isotope data from FIs (~-50 to -125 ‰) exhibit no apparent correlation with position within the vein system.

Fluid in equilibrium with illite and I/S show a relatively narrow range of O and H isotope compositions (Fig. 2), interpreted as meteoric fluid, largely affected by reequilibration with country rocks (O-shift), with some minor admixture of magmatic fluid. Kaolinite mineral data lay outside the kaolinite line, which excludes supergene origin. In order to question the genesis of kaolinite, $\delta^{18}O_{fluid}$ $\delta D_{fluid}$ were calculated at both 200°C (typical for high sulphidation systems) and 130°C (typical for descending steam-heated fluids). Clear overlap of the 130°C data with composition of fluids in equilibrium with illite, I/S strongly indicates the later environment for kaolinite deposition. Thus, kaolinite is thought to result from a collapse of acid sub-surface waters down into the system during final stages of mineralization, overprinting earlier alteration patterns with illite, I/S.

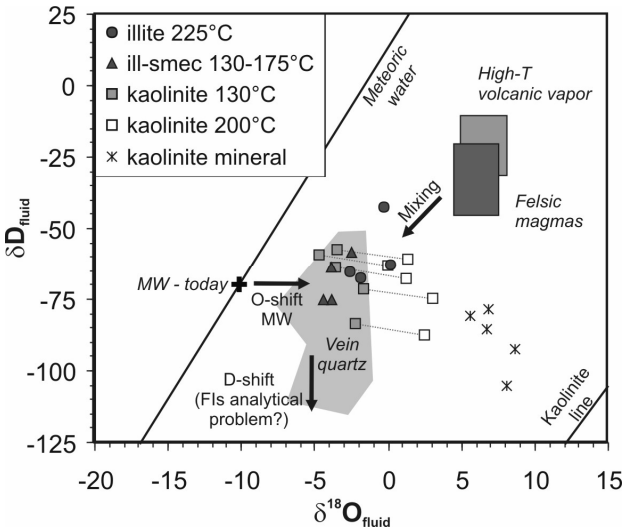


Figure 2. Isotopic composition of fluids in equilibrium with vein quartz (grey polygon), minerals from wallrock (kaolinite, illite) and regional alteration (I/S), calculated at estimated crystallization temperatures. Kaolinite is shown at two alternative temperatures, depending on genesis. Raw kaolinite data are shown for comparison with kaolinite line. O-shift indicates the effect of $\delta^{18}O$ re-equilibration by wallrock interaction. Low $\delta D_{fluid}$ values from quartz can result from analytical problems of extraction of water from fluid inclusions (Faure *et al* 2001).

## 6 DISCUSSION AND CONCLUSIONS

Continuous decrease of fluid temperatures from N to S indicates lateral outflow of fluids along N-S trending master fault hosting the mineralization of the 1st vein system. Lexa & Bartalský (1999) predicted the source area of fluids in N part of the system, corresponding to the centre of rhyolite magmatism, including granite porphyries. The lateral outflow was probably driven by hydraulic head of at least 100 m between N and S ends of the 1st vein system taking into account the present topography. However, FI data indicate increasing erosion towards N, thus the difference in palaeoaltitude could be larger. Prevalence of lateral outflow over vertical is further indicated by vertical zoning. In N part of the system Au associates with Fe-oxides and hydroxides, while base metals dominate at depth. The central part contains Au mostly in quartz and does not contain base metals at depth (Veľký *et al.* 1998).

Central part of the 1st vein system with evidence for extensive boiling, strongest K-metasomatism and brecciation, probably repre-

sent the area where major fluid flow has reached the level of boiling due to pressure decrease resulting from changing topography and wide opening of the host fault. The precipitation of adularia and Au was due to substantial decrease of their solubility with continuous boiling (Hedenquist *et al.* 2000). Some of the fluids continued to flow further S along the major fault, representing here the fluid source for veins and hot springs.

The 2nd vein system seems to have a slightly different position outside the major fault system with a different mineralization and increased palaeofluid temperatures and salinities. This difference can be partially related to deeper erosion level in this area (valley), however, bonanza-type Au may indicate sharp cooling and abrupt boiling in more vertically, rapidly ascending fluid compared to the 1st vein system.

The widespread presence of kaolinite in the wallrock alteration within the deposit suggests the presence of large area of steam-heated waters that must have accompanied the vein system at subsurface level (now eroded). These acid waters are known to result from condensation and dissolution of $H_2S$- and $CO_2$-bearing vapors released by boiling further in depth (Hedenquist *et al.* 2000). Taking into account the assumed palaeotopography, these acid fluids were collected by the water table and their subsurface flow towards S resulted in extensive alteration of rhyolite and deposition of lacustrine silicites. A relict of a hot spring system at Čertov Vrch probably represents a local discharge of these fluids at the palaeosurface. Stable isotopes indicate that during later stages these fluids also managed to penetrate downward into the veins, overprinting earlier alteration patterns. A similar example for this scenario is the Golden Cross LS Au-Ag deposit in New Zealand, where late-stage acid fluids penetrated up to 300 m into veins (Simpson *et al.* 2001).

Mineralized veins in S part of the system are similar to the late-stage Sb-bearing veins in the central part of the system in terms of structural position and mineral characteristics (Veľký *et al.* 1998). Considering the consequences of lateral outflow of fluids, Au potential at S of the area is limited to the mineralization related to deep-circulating, probably late-stage fluids that avoided boiling and Au-deposition when bypassing the central part of the 1st vein system.

## ACKNOWLEDGEMENTS

This study has been carried out as a a part of the project 0503 “Source of ore-bearing fluids in the metallogeny of Western Carpathians” financed by the Ministry of Environment of the Slovak Republic. Ľuboslav Maťo kindly provided majority of historical samples.

## REFERENCES

Böhmer M (1966) Geology and mineral associations of gold-bearing veins in the central part of the Kremnica ore field. Acta Geol Geogr Univ Comenianea, Bratislava, *Geologica* 11, 5 – 123 (in Slovak).

Böhmer M, Gerthofferová H, Kraus I (1969) To the problem of alterations of Central Slovakian neovolcanites. *Geol Zbor Geol Carpath* 20: 47-68.

Faure K, Brathwaite RL, Matsuhisa Y (2001) Do hydrogen isotope values of fluid inclusion water in vein quartz accurately reflect water of deposition? In: Cidu R (ed) *Water-rock interaction WRI-10 Lisse*, A.A. Balkema, pp 1517-1520.

Hedenquist JW, Arribas AR, Gonzales-Urien E (2000) Exploration for epithermal gold deposits. In: Hagemann G, Brown PE (eds) Gold in 2000. *Reviews in Econ Geol* 13, pp 245-277.

Kraus I, Šamajová E, Šucha V, Lexa J, Hroncová Z (1994) Diagenetic and hydrothermal alterations of volcanic rocks into clay minerals and zeolites (Kremnické Vrchy Mts., the Western Carpathians): *Geol Carpath* 45: 151-158.

Kraus I, Chernishev IV, Šucha V, Kovalenker VA, Lebedev VA, Šamajová E (1999) Use of illite for K/Ar dating of hydrothermal precious and base metal mineralization in central slovak Neogene volcanic rocks. *Geol Carpath* 50: 353-364.

Lexa J, Bartalský B (1999) Low-sulfidation epithermal gold deposit at Kremnica. In: Molnár F, Lexa J, Hedenquist JW (eds) Epithermal mineralization of the Western Carpathians. *Guidebook series Soc Econ Geol* 31: pp 265-273.

Lexa J, Halouzka R, Havrila M, Hanzel V, Kubeš P, Liščák P, Hojstričová V (1998) Explanation to the geological map of the Kremnické vrchy Mts. 1 : 50 000. *Geol Surv Slovak Rep, Bratislava*, 308 p.

Simpson MP, Mauk JL, Simmons SF (2001) Hydrothermal alteration and hydrologic evolution of the Golden Cross epithermal Au-Ag deposit, New Zealand. *Econ Geol* 96: 773-796.

Uhlík P, Majzlan J (2004) Conditions of mixed-layer illite-smectite formation at the deposit Dolná Ves on the southwest margin of Kremnica stratovolcano. *Mineralia Slovaca* 36: 331-338. (in Slovak)

Veľký P (1999) Results of exploration for Au-Ag ores in the southern part of the Kremnica ore field. *Mineralia Slovaca* 31: 269-274. (in Slovak)

Veľký P, Böhmer M, Korim M, Maťo, Ľ, Pitoňák P, Oroszlány J, Padúch M, Dimoš I, Verseghy R (1998) Complex evaluation of the Kremnica precious metal ore deposit. *Geol Surv Slovak Rep Open File Report,* 202 p (in Slovak).

# Mineralization and Recent Exploration in the Chelopech Cu-Au deposit, Bulgaria

Terry Briggs
*Technical Services Manager, Chelopech Mining EAD*

Plamen Doychev
*Chief Geologist, Chelopech Mining EAD*

Strahil Teriyski, Jordan Angelov & Petya Kuzmanova
*Senior Geologists, Chelopech Mining EAD*

ABSTRACT: The Chelopech Cu-Au deposit located within the Tethyan Metallogenic Belt, an elongated structure of Cretaceous-Tertiary magmatic activity. Chelopech is an active operation in west-central Bulgaria 70km east of the capital Sofia on the southern flank of the Balkan Range. It forms part of the Panagyurishte mining district where a number of cupriferous massive sulphide and porphyry copper deposits exist. Considerable work has been undertaken recently on modernisation of not only production related aspects of the operation, but also the technical related functions that support the operation in terms of geological planning, interpretation and modelling. Chelopech is about to enter an exciting phase of its history with plans to increase current production as well as production of copper and gold metal on-site. Future exploration success will be crucial to supporting this investment in capital.

KEYWORDS: Chelopech, Copper, Gold, Modelling

## 1 INTRODUCTION

The Tethyan belt is host to a series of world-class mineral deposits within Eastern Europe. Dundee Precious Metals is currently operating the Chelopech deposit in western Bulgaria as well as looking to develop the advanced Krumovgrad low sulphidation epithermal Au deposit in the south east of the country, and is exploring within the Bor District in Serbia (Fig. 1).

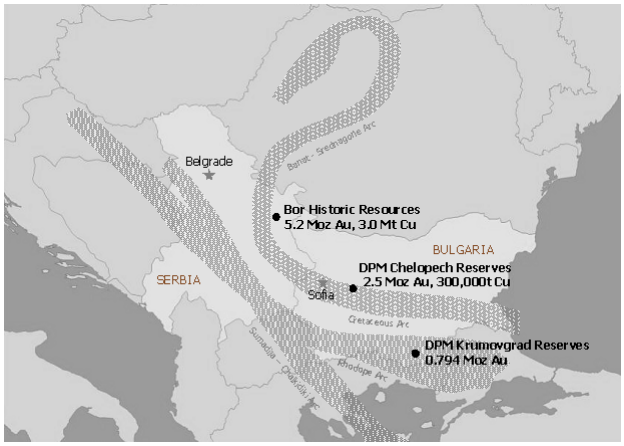


Figure 1. Map showing the Tethyan Arc through the Balkans and the position of the Chelopech Cu-Au deposit, Krumovgrad Au deposit and the Bor area.

Mining commenced at Chelopech in 1956, and to the end of 2006 a total of 16Mt @ 1.2% Cu has been extracted. The remaining resource at this time was 30Mt @ 1.5% Cu, 4.1g/t Au and 11g/t Ag. Dundee Precious Metals took over operating the Chelopech Cu-Au mine in late 2003 and since then has embarked on a significant campaign to modernise the equipment, mining methods, processing and technical aspects of the operation..

Geological practices have also had to change during this time as international standards have been applied from all aspects of information gathering to interpretation and reporting in the mine production environment.

## 2 REGIONAL GEOLOGICAL SETTING

The Chelopech deposit is located within the Panagyurishte metallogenic district on the northern margin of the Srednogorie tectonostratigraphic zone. The Panagyurishte mineral district is defined by a NNW alignment of porphyry-copper (Elatsite, Assarel, Medet, Vlaikov Vruh and others) and high sulphidation epithermal Cu-Au deposits (Chelopech, Radka, Krassen and others), which is oblique to the east-west orientation of the Srednogorie zone in

Bulgaria (Chambefort, 2005).

Mineralization in the Panagyurishte district is intimately related to late Cretaceous northerly directed subduction. In general terms the high sulphidation type epithermal Cu-Au deposits are associated with Sennonian volcanics and sub-volcanic intrusives of andesitic and rhyo-dacitic affinity whilst the porphyry deposits are generally associated with plugs and stocks of monzodiorites and quartz-syenodiorites. The geology of the Panagyurishte mining district comprises of a basement of Pre-Cambrian granitoid gneisses intruded by Palaeozoic and Cretaceous granites. The overlying Upper Cretaceous magmatic and sedimentary sequences are restricted to contemporaneous grabens orientated in a NW-SE direction

## 3 DEPOSIT SCALE GEOLOGY

The basement in the vicinity of the Chelopech deposit is comprised of granite gneisses, crystalline mica schists, quartzites and amphibolites. This basement is unconformably overlain by Permian terrigenous volcanics and in turn by a terrigenous and transgressive marginal marine sequences of Triassic, Jurassic and Upper Cretaceous ages. The Upper Cretaceous Chelopech Volcanic Formation attains thicknesses of up to 2000m. The Lower Chelopech Formation, which hosts the mineralization, is overlain via a non sequence, by an unmineralized volcanic sequence and ultimately by volcaniclastic and siliciclastic flyshoid sediments

## 4 MINERALIZATION

The Chelopech deposit is of classic "gold-enargite" high sulphidation epithermal style and is currently defined as a series of discrete ore bodies ranging in size from tens of metres to hundreds of metres in diameter with a general plunge to the southeast. Early faulting has controlled the location of silica envelopes which host the major sulphide mineralization. Further investigation is being undertaken as to the role of regional structures in the orientation and control of the mineralization.

The current mine is separated into "Central" and "Western" mining areas. The Central area is characterized by massive sub-volcanic andesitic intrusive. This unit is affected by advanced argillic alteration with widespread development of vuggy silica which hosts the sulphide mineralization. This is locally overprinted by several post-ore hydrothermal breccia pipes. The western region is dominated by volcano-sedimentary rocks, including tuffs and ashes, The vuggy silica ore envelopes vary from 150m to 300m in length, are 30m to 120m wide, and can extend at least 350m down dip..

Orebodies occur in a range of different morphologies, including lens-like, pipe-like and columnar bodies that typically dip steeply towards the south. These different types of geometries occur as a result of the different host rocks, the origin and nature of the mineralization fluid and the presence or absence of tectonic processes.

The mineralization (within economically mineable orebodies occurs as anastomosing veins, mineralized breccias, sub-horizontal massive sulphide bodies and disseminations.

The ore mineralogy is dominated by the iron sulphides pyrite and marcasite, which form on average about 50 vol.% of the ore bodies. The principal base-metal minerals comprise tennantite, enargite - luzonite and bornite - chalcopyrite together with subordinate famatinite, sphalerite and galena. A large number of sulphosalts have also been microscopically identified in the ores.

Pyrite is the earliest sulphide and occurs in a number of forms; as single well formed cubic metacrysts 0.1–2mm in diameter; as grains and granules formed by the partial or complete replacement of mafic minerals of host volcanics; as collomorphic or "cockscomb texture" radial forms of non-stoichiometric iron sulphide (melnikovite) up to 10cm in diameter with each layer up to 2–3mm in thickness; as dense massive pyrite aggregates of irregular form and comprising all of the other forms described herein.

Native gold is generally combined with small amounts of silver and copper and is found in different stages of the paragenetic sequence. Microscopic gold accompanies the first mineralized veins (chalcedony and tennantite). The main depositional phase of gold is associated with the tennantite-chalcopyrite-bornite paragenesis. The gold is generally fine grained and associated with pyrite, thus rendering the ores effectively refractory and this reduces recovery in the mill to *c.* 65%.

A late phase of deposition of gold is also associated with kaolinite/dickite, and barite and quartz veining. This phase of gold mineralization is more easily liberated during milling. (Fig. 2).

Gold – copper ratios vary from 1:3 in the large western orebodies to 1:4 in the main central orebodies.

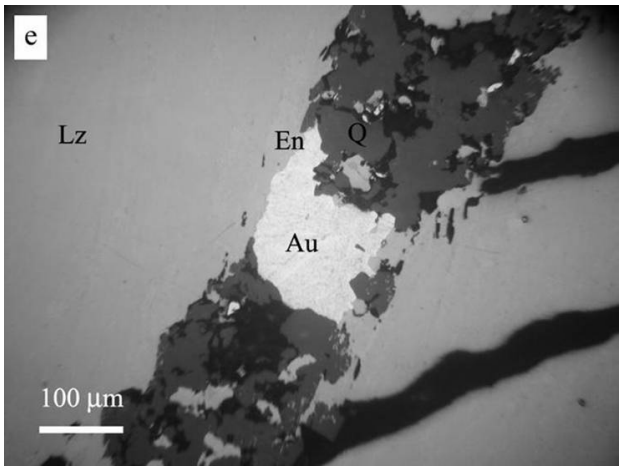


Figure 2. Free gold associated with quartz veining within luzonite (Lz) and enargite (En).

## 5 GEOLOGICAL METHODS OF MINERAL EXPLORATION

Since modernization began in 1994, Chelopech mine has become a fully mechanised trackless operation. This has been possible by the staged introduction of a fleet of trackless equipment ranging from production and development drill rigs to 40-50t capacity truck and LHD units Supporting this equipment was a progressive change in mining method from sub-level caving to long hole open stoping. The confidence to change mining methods can only come about from a confidence in the geological resource.

A considerable amount of geological knowledge has been obtained at Chelopech over the past 50 years through surface drilling (over 264,000m of surface drilling and in excess of 45,000m of underground drilling) and the subsequent development of the deposit The challenge with this large volume of data is ensuring that it is able to be verified. It is just as important to ensure that the data collected now is valid, as it is crucial in the estimation of the reserves and resources to an internationally recognised standard

Diamond drilling is currently undertaken from drill cubbies in areas of underground mine development to minimise drilling through the overburden from the surface. All drill core is logged on-site using hand-held data devices which can be digitally connected to the geological database to improve data efficiency.

Quality Control / Quality Assurance (QAQC) program has also been developed. Chelopech is fortunate to have an internationally accredited chemical laboratory run on-site where samples are assayed for a common suite of both economic and deleterious elements (Cu-Au-Ag-S-As). A series of blanks – repeats – duplicates and standards are included in every batch.

The development of the Chelopech geological database was undertaken using AcQuire©. This has in place a variety of mechanisms to ensure that the data entered from drilling and underground sampling passes a series of validation tests. Current geological interpretation makes use of historical and current information to generate alteration and mineralization models of the different lodes. Information gathered from geological mapping, including major structures – offsets – chemical and lithological boundaries is all used to assist with the generation of a 3-D model. The 3-D model is used to populate a grade control model using Gemcom©. Considerable improvement has been undertaken recently to equip the on-site geologists in the knowledge of resource estimation. This has brought about fundamental improvements in the site-based model, not least of which is the method of domaining the different orebodies which all have individual mineralization properties, this is best demonstrated in Figure 3 which shows the search ellipse applied to the entire deposit, and the individual search ellipses used now for selecting drill holes for estimation. The creation of variography can be used to directly compare with observations made underground. The ability to reiteratively create and validate the grade models on-site is a large step forward.

Conflicts still exist in the classification of reserves and resources in the formal reporting required by the Bulgarian Government and the internationally recognised systems such as JORC, Samrec and NI43-101. This makes the formal reporting of reserves and resources challenging.

A valid geological model is the most important first step in trying to understand the controls on mineralization.

Future programs will continue to validate this including further geological, geochemical and geophysical surveys along with ongoing mine extraction.

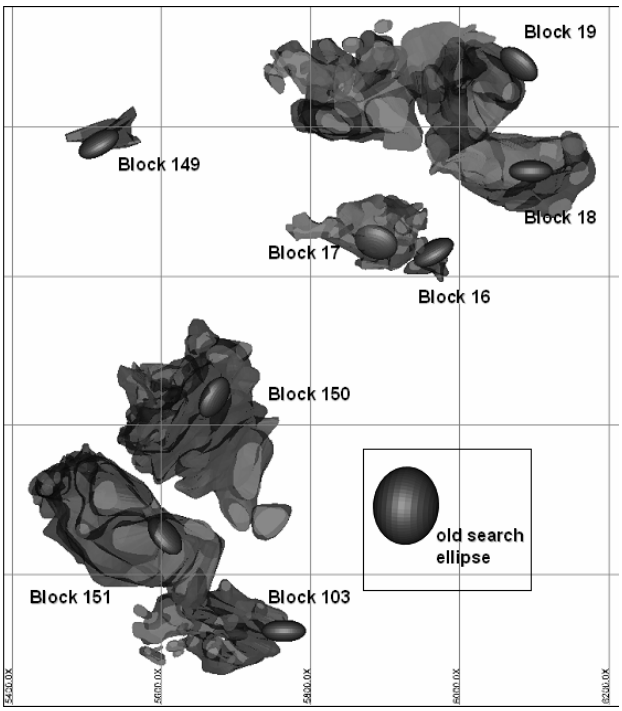


Figure 3. Deposit *vs* Orebody search ellipses.

## 6 CONCLUSION

Chelopech represents a large scale epithermal copper-gold deposit that is still being explored and uncovering new knowledge after 50 years of operation. With a remaining *in situ* resource twice what has been exploited in this time frame remaining it is hoped that exploration will continue to present a long life economic deposit that assists in uncovering more information on these systems.

## ACKNOWLEDGEMENTS

The authors would like to thank the management of DPM and Chelopech Mining EAD for permission to publish these results. Thanks are also extended to past and present staff of both these organisations and the exploration division of BMM.

## REFERENCE

Chambefort, I. 2005, The Cu-Au Chelopech Deposit, Panagyurishte District, Bulgaria: Volcanic setting, hydrothermal evolution and tectonic overprint of a Late Cretaceous high-sulphidation epithermal deposit. *Terre and Environment,* Volume 52, Universite de Geneve.

# Ore forming fluids in the Allchar Au-Sb-As-Tl deposit, FYR Macedonia.

S. Strmić Palinkaš, S. Borojević Šoštarić, L. Palinkaš & V. Bermanec
*Institute of Mineralogy and Petrography, Faculty of Science, University of Zagreb, Croatia*

B. Boev
*Faculty of Mining and Geology, Štip, Macedonia*

ABSTRACT: The Allchar Au-Sb-As-Tl mineral deposit is a Carlin-type mineralization with a zonal distribution of mineral parageneses and alterations. The zonation is a result of a spatial distribution of ore-forming fluids with different thermal and chemical characteristics as proven by a fluid inclusion study. Three zones are distinguished: 1. a southern Au-Sb-As zone, 2. a central zone, which hosts a Au-Sb-As-Tl-Hg mineralization, and 3. a northern As-Tl zone. Homogenization temperature and salinity decrease steadily from the southern to the northern zone of the deposit due to cooling and dilution of the fluids.

KEYWORDS: Carlin, Gold, Thallium, Arsenic, Antimony, Fluid inclusions

## 1 INTRODUCTION

The Allchar Au-Sb-As-Tl-Hg mineral deposit (41.1° N, 22.0° E) is located at the southern margin of the Vardar zone, 110km SE from Skopje, FYR Macedonia (Fig. 1).

The Allchar deposit is associated with a Pliocene calc-alkaline volcano-intrusive complex. It intrudes and overlies a Palaeozoic-Mesozoic basement along a major regional fault zone, between the rigid Pellagonian block on the west and the labile Vardar zone on the east (Janković & Jelenković, 1994). Volcanic activity lasted between 7.0 and 1.8 Ma (Boev, 1988). Its products are extrusive rocks, ranging in composition from andesite, quartz-latite to dacite, occasionally trachyte and latite, generally enriched in K and Rb (Karamata *et al*., 1994), and pyroclastic equivalents.

The mineralization displays characteristics typical for Carlin-type deposits such as (1) structural controls of mineralization by faults and folds; (2) calcareous sedimentary host rocks of diverse facies ± igneous rocks; (3) alterations including decarbonization, silicification, argillization and sulphidation; (4) submicron gold in association with pyrite, arsenian pyrite and arsenopyrite and (5) a Au, As, Hg, Sb and Tl geochemical signature (Radtke, 1985; Hofstra & Cline, 2000; Zhou & Wang, 2003). The deposit consists of three distinctive ore zones (Fig. 1): the southern high-temperature Zone I, which is the major centre of the Au mineralization, and is accompanied by variable amount of Sb and As minerals; the central Zone II contains significant amounts of

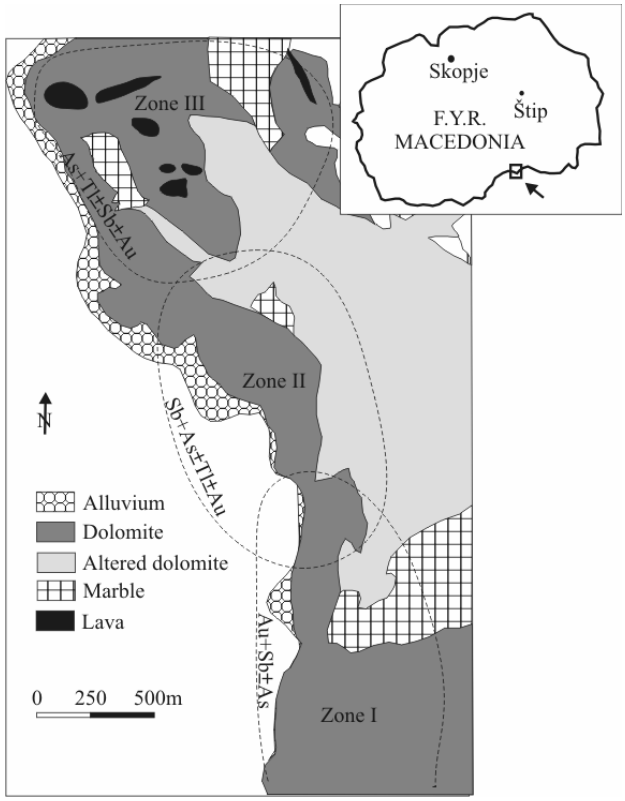


Figure 1. Geographical and geological setting of the Allchar mineral deposit.

Tl minerals beside Au, Sb and As mineralization, minor amounts of Ba, Hg and traces of Pb; and the northern low-temperature Zone III, which contains As and Tl mineralization, accompanied by minor Sb and traces of Hg and Au (Janković & Jelenković, 1994).

Mineralization is spatially related to a zoned hydrothermal alteration pattern, mainly silicification and argillization. The silicification in the southern part of the mineral deposit varies in intensity from partial to total replacement (jasperoid) (Percival & Radtke, 1994). In the northern part of the deposit argillization prevails and silicification occurs as chalcedony and opal (Boev, 1993).

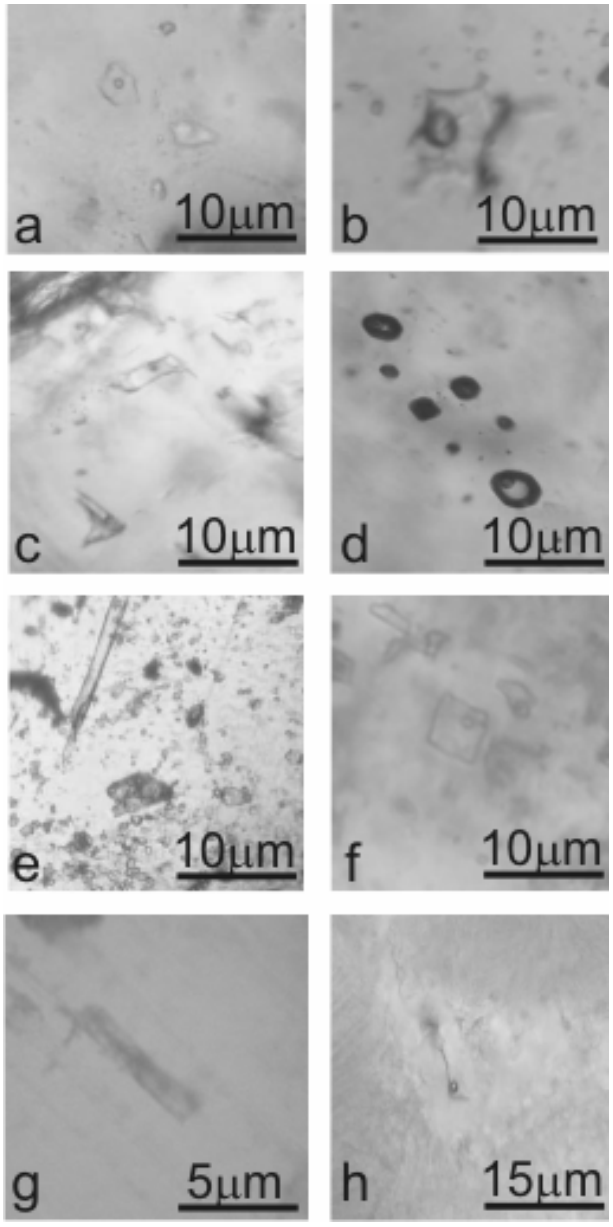


Figure 2. Fluid inclusions within a) quartz (Zone I); b) quartz (Zone II); c)calcite (Zone II); d) realgar (Zone III); e) orpiment (Zone III), f) dolomite (Zone III); g) lorandite (Zone III); h) opal (Zone III).

In Zone I, intensive silicification is represented by stibnite-bearing jasperoids and is accommodated within the centre of the hydrothermal activity. The jasperoids are composed of black, fine-grained, mosaic-textured microcrystalline quartz with irregular masses of white to gray quartz. The most abundant sulfides are pyrite, arsenopyrite, marcasite, stibnite and late stage realgar. They contain up to 20 g/t of gold. Weak to moderate silicification affected sedimentary rocks and tuffs by introduction of microcrystalline quartz. Sulphide mineralization consists of pyrite, stibnite and minor amounts of marcasite. Realgar is less abundant than in the jasperoids, while gold grades from 0.5 to 10 g/t.

In Zone II, arsenian ore occurs in the central part of deposit within argillized tuffs, Tertiary dolomite and sporadically within Triassic carbonate rocks. Sulphide mineralization is characterized by the presence of pyrite, realgar, orpiment, stibnite, finely disseminated marcasite and minor thallium-bearing sulphosalt minerals. The gold grades from <1 to 3 g/t.

Zone III is characterized by moderate to strong argillic alterations, which are wide spread and pervasive. Weak silicification is present locally, while dolomitization is intensive. Tl and As mineralization is represented by lorandite, rare Tl-bearing sulphosalts, like vrbaite, picopaulite, rebulite, simonite, bernardite, raguinite and parapierrotite (Percival & Radtke, 1994).

The aim of this study is to constrain the chemical and P-T evolution of the ore-bearing fluids based on an analysis of fluid inclusions.

## 2 SAMPLES AND METHODS

Microthermometric measurements were performed on primary fluid inclusions within doubly polished, ~0.5 mm thick, wafers of: (1) quartz associated with high temperature sulphide mineralization (Zone I, Fig. 1), (2) quartz and calcite from the central part of the deposit (zone II, Fig. 1), (3) realgar, orpiment, lorandite and dolomite associated with sulphide mineralization without Sb and enriched in As and Tl (Zone III, Fig. 1), and (4) opal associated with a low temperature mineralization, located in the northernmost part of Zone III (Fig. 1).

Analyses of evaporate mounds by scanning electron microscope equipped with EDX (SEM/EDX) were performed on realgar and or-

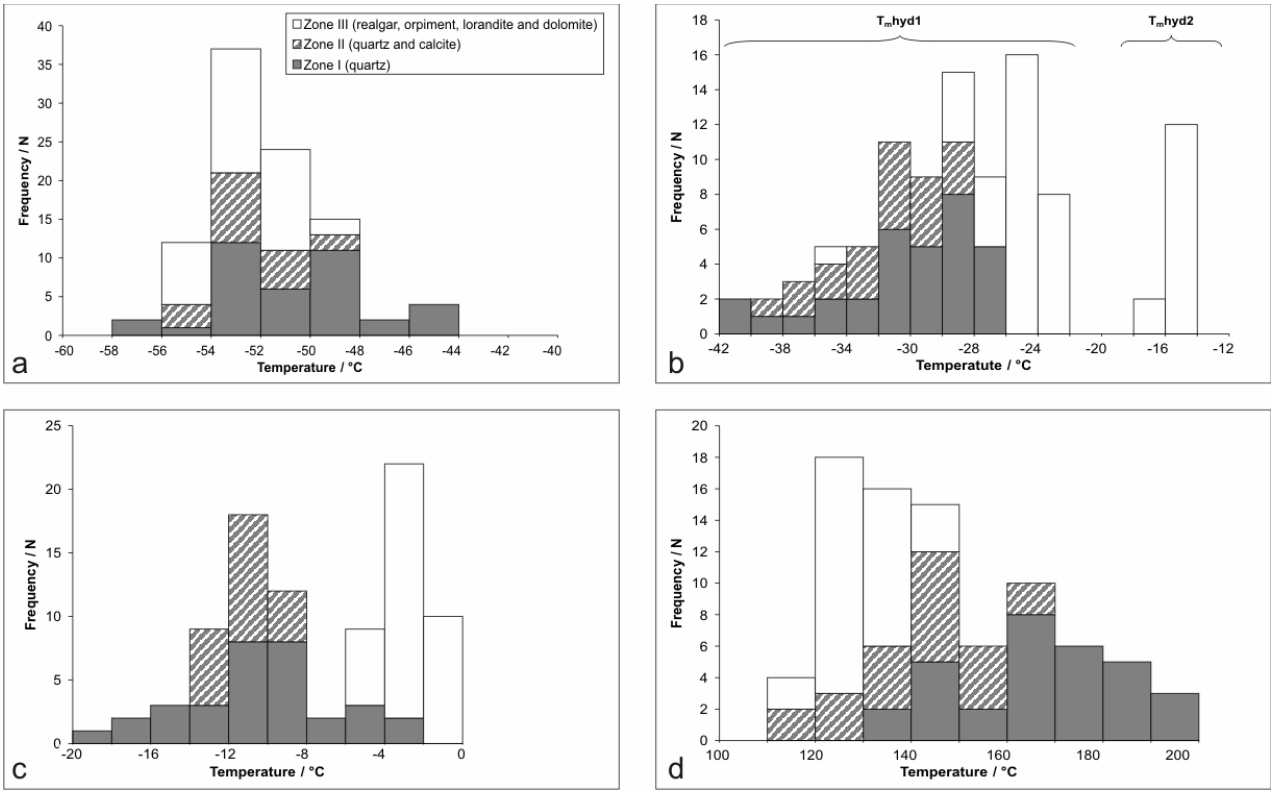


Figure 3. Frequency distribution of a) the eutectic temperature; b) melting temperatures of hydrates; c) the last melting temperature of ice; d) homogenization temperature within vapour phase.

piment samples studied by microthermometry as well. Evaporate mounds were prepared accordingly to the procedure described by Kontak (2004).

## 3 RESULTS

Zone I - Quartz associated with high temperature sulphide mineralization (Fig. 2): first melting (eutectic temperature, $T_e$) was obtained in an interval between -44.0 and -58.0°C (Fig. 3) and indicates the presence of bivalent cations. Final melting of hydrate ($T_m$hyd1) was recorded in a temperature range between -24.2 and -42.0°C (Fig. 3). Ice melting temperatures ($T_m$ice) in an interval from -2.4 to -18.1°C (Fig. 3) indicate a salinity from 4 to 21.3 wt.% NaCl eq. Homogenization ($T_h$) by vapour disappearance occurred in a temperature range from 131 to 200°C (Fig. 3). One fluid inclusion nucleated a recognizable clathrate phase, which melted at a temperature of -0.5°C ($T_m$chl), suggesting the presence of $CO_2$ and a salinity of 16 wt.% NaCl equ. $T_h$ was recorded at 201°C.

Zone II - Quartz and calcite from the central part of the deposit (Fig. 2): $T_e$ is in the range between -50.0 and -56.0°C (Fig. 3). $T_m$hyd1 was noticed between -27.2 and -39.0°C (Fig. 3). $T_m$ice in an interval from -10.5 to -13.1°C (Fig. 3) is in concordance with a salinity between 14.5 and 17.1 wt.% NaCl eq. Homogenization into the liquid phase occurred in a range from 120.0 to 165.5°C (Fig. 3).

Zone III - Realgar, orpiment, lorandite and dolomite associated with sulphide Sb-As-Tl-mineralization (Fig. 2): $T_e$ is in an interval between -49.3 and -54.2°C (Fig. 3). Melting occurs in a temperature range between -35 and 0°C, and showed the presence of two hydrates. Melting of the first hydrate ($T_m$hyd1) was recorded in a temperature interval between -22.0 and -24.5°C (Fig. 3). The temperature interval of the final melting of the second hydrate ($T_m$hyd2) was observed between -11.0 and -15.4°C (Fig. 3). The ice melting temperature ($T_m$ice) within the interval between -1.5 and -4.1°C (Fig. 3) corresponds to a salinity of 2.6 to 6.9 wt.% NaCl eq. Analyses of evaporate mounds by SEM/EDX confirmed the presence of NaCl and KCl as major dissolved salts. Homogenization within quartz and dolomite into the liquid phase was recorded between 120 and 152°C (Fig. 3). The temperature of total homogenization within orpiment and lorandite was not recorded due to massive decrepitation.

Zone III - Opal associated with the low temperature mineralization (Fig. 2): Microthermometric measurements were performed on

aqueous inclusions containing $CO_2$ and hydrocarbons and multiphase hydrocarbon inclusions. Within aqueous inclusions containing $CO_2$ and hydrocarbons first homogenization occurred in a temperature range from +31.0 to +33.0°C within the vapour bubble (liquid to vapor transition), while $T_h$ to the liquid phase was between 102 and 125°C (Fig. 3). $T_m$chl ranged from 2.4 to 7.0°C, and corresponds to a salinity from 6.0 to 13.5 wt.% NaCl eq. Complex hydrocarbon-bearing inclusions remained unfrozen at the minimum stage temperature of -180°C.

## 4 DISSCUSION

The Allchar deposit is characterized by a zonal distribution of mineral assemblages and alterations.

The fluid inclusion study reveals a change in temperature and composition of the mineralizing fluid across the different zones of the deposit. Homogenization temperatures and salinities decrease from the southern toward the northern part of the deposit interpreted as a result of cooling and dilution. Dilution is especially emphasized in Zone I with a high variability of salinities, Na/Ca molar ratios and $T_h$. The main dissolved salts in the southern zone are Ca-Na-chlorides with a Na/Ca molar ratio between 0.2 and 19.3. In the central part of the deposit, the Na/Ca molar ratio varies in a narrow range between 0.3 and 1.3. In the northern part of the deposit, fluids are enriched in potassium.

The presence of $CO_2$ is related to Sb-bearing jasperoids (Zone I) and to the opal, associated with the low temperature mineralization (Zone III).

The ore fluids transported gold, arsenic, antimony, thallium, mercury and iron. The dominance of marcasite over pyrite in Zone I suggests a pH below 5. The mineralization consisting mainly of sulphides suggests that the ore forming fluids were enriched in reduced sulphur. Under such conditions thallium is a very mobile element (Vink, 1993). Chemical analyses of country rocks within the Allchar deposit suggest volcanic and tuffaceous rocks as a possible source of thallium (Percival & Radtke, 1994). Reaction of the ore fluids with the host carbonates resulted in an increase of pH in the northern part of the deposit. Thallium sulphides show a small stability field under alkaline and reducing conditions (Vink, 1993).

Beran *et al*. (1990) reported hydrocarbon bearing fluid inclusions within realgar from Zone III. Also fluid inclusions within opal show involvement of organic matter, but its role in this type of mineralization is still unknown. Thallium mineralization is generally very rare and associated with the Carlin type of deposits. Carlin Au deposits are, on the other hand, spatially affiliated to organic rich carbonate host rocks. It gives another possibility in explaining the genesis of thallium mineralization. Thallium species in alkaline-reducing carbonate environments were remobilized by hydrothermal fluids and actively engaged in the mineralizing process, as a part of the volcanic activity in the region.

## 5 REFERENCES


Beran, A., Götzinger, M.A. & Rieck, B. (1990): Fluid inclusions in realgar from Allchar. *Neues Jahrbuch fur Mineralogie-Abhandlungen* 167: 345-348.

Boev, B. (1988): Petrological, geochemical and volcanic features of volcanic rocks of the Kozuf Mountain. *–Doct. Dissert., Faculty of Mining and Geology, Stip,* 195 pp. (in Macedonian).

Hofstra, A.H. & Cline, J.S. (2000): Characteristics and models for Carlin-type gold deposits. –In: HAGEMANN, S.G., & BROWN, P.E. (eds.): Gold 2000, *SEG Reviews in Economic Geology* 13: 163-220.

Janković, S. & Jelenković, R. (1994): Thallium mineralization in the Allchar Sb-As-Tl-Au deposit. *Neues Jahrbuch fur Mineralogie-Abhandlungen* 167: 283-297.

Karamata, S., Pavičevič, M.K., Korikovkij, S.B., Boronikhun, V.A. & Amthauer, G. (1994): Petrology and mineralogy of Neogene volcanic rocks from the Allchar area, the EY Republic of Macedonia. *Neues Jahrbuch fur Mineralogie-Abhandlungen* 167: 317-328.

Kontak, D.J. (2004): Analysis of evaporate mounds as a complement to fluid-inclusion thermometric data: case studies from granitic environments in Nova Scotia and Peru. *Canadian Mineralogist* 42: 1315-1329.

Percival, T.J. & Radtke, A.S. (1994): Sedimentary-rock-hosted disseminated gold mineralization in the Alšar district, Macedonia. *Canadian Mineralogist* 32: 649-665.

Radtke, A.S. (1985): Geology of the Carlin gold deposit, Nevada. *–US Geological Survey Professional Paper* 1267, 124 p.

Vink, B.W. (1993): The behaviour of thallium in the (sub)surface environment in terms of Eh and pH. *Chemical Geology* 109: 119-123.

Zhou, Y. & Wang, K. (2003): Gold in the Jinya Carlin-type deposit: characterization and implications. *Journal of Minerals and Materials Characterization and Engineering* 2: 83-100.

# The Talkheh Epithermal Copper Deposit, Central Iran

Abdolmajid Yaghubpur & Masoud Motallebi
*Department of Geology, Tarbiat Moalem University, 49 Mofateh Avenue, Tehran 15614, Iran.*

ABSTRACT: Mineral deposits of the Anarak area in central Iran, have been explored and mined since ancient times. The host rock, texture of the ore, temperature and salinity of the fluid inclusions, geochemistry, the role of the faults and fractures in the field, and the location of the deposit relative to volcanic activities in the area were investigated in detail. Based on the measured temperature of the fluid inclusion; the fissure and void filling type of deposition; irregular veins and veinlets; replacement and some colloidal texture as well as the lack of high temperature alteration minerals the Talkheh deposit is postulated to be an epithermal type.

KEYWORDS: copper, epithermal, Iran, Anarak, fluid inclusions

## 1 INTRODUCTION

Mineral deposits of the Anarak area in central Iran, (Fig. 1) have been explored and mined since ancient times. Many old working mines and slags are present in the area and some of the mining dates back to about 5000years B.C. (Bazin & ubner, 1969). The extracted metals in the old working mines were copper, lead, nickel, cobalt, gold, antimony, and the processed minerals were gypsum, sulphur, magnesite and turquoise. The Talkheh copper deposit, located 21 km northwest of the city of Anarak, is one of the copper occurrences of the Anarak area (Fig. 1).

The geology of the Anarak area was first studied by Stahl (1911) and the first report on the mineralization of the area mentioning the Talkheh deposit in his report was published by Ladame (1945). Ophiolite terranes in the Anarak area was studied and reported by Gansser (1955).

The metallogenic map of Anarak area, st 1:250,000 scale was published by Bariand (1963), Nickolas (1969), Sjerpt *et al.* (1969) and some mining companies such as Cofimines (1971) were subsequently involved in evaluation of the economic importance of the mineral potential of the area. In 1983, Walter and Momenzadeh (1983) studied the genesis of some of the mines in the Anarak area.

In 1975 a Russian group (Technoexpert) based on a formal contract with Geological Survey of Iran started detailed geochemical studies in the Anarak area and the results of their 17 volumes of geochemical reports were published by Mir publishing company in 1984, entitled "Outline of Metallogeny of Anarak area, central Iran", (Romanko *et al*., 1984).

## 2 GEOLOGY

The study area is located in the Anarak-Khur subzone that is part of the central Iran zone. The Morghab metamorphic complex (M) crops out to the south and north of the Talkheh copper deposit. The age of this metamorphic complex is postulated to be late Proterozoic (Romanko, 1984). The Morghab complex includes muscovite-schist, chlorite-schist and sericite- schist.

Another rock type covering the Morghab metamorphic rocks is the Lakh marble (Pz), which forms the topographic highs of the deposit area. The age of the rocks is postulated to be early Cambrian, and according to Romanko (1984) the age of Lakh marble is Batonian-Atdabanian. Lakh marble is the host rock of the Talkheh copper deposit.

Oligocene age conglomerate, sandstone and clayey sandstone (O) comprise part of the southern area of the Talkheh deposit. Recent

in

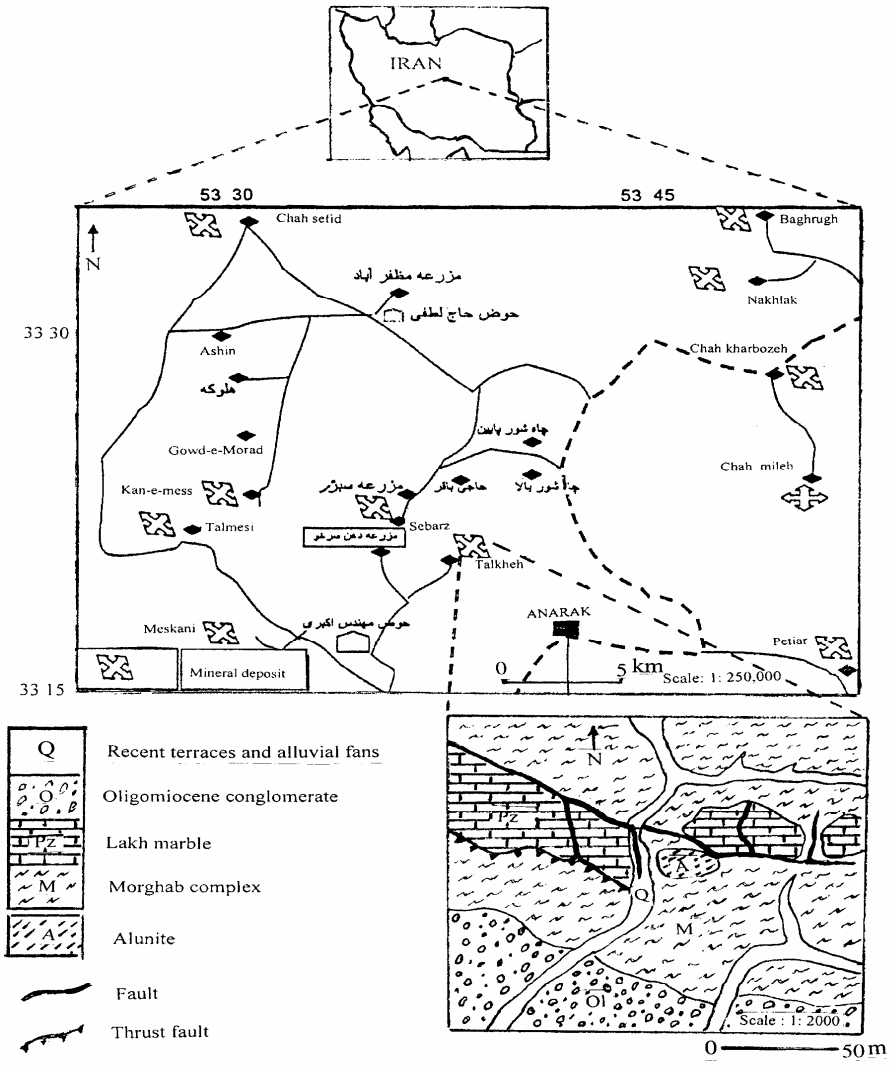


Figure 1: Location of the study area and geological map of the Talkeh copper deposit (after Motallebi, 2002)

terraces and alluvial fans (Q) are also present in the study area.

Structural influences are the main mineralizing control, and mineralization occurs mostly along northeast southwest striking faults. In addition to these major structures, mineralization also includes open space filling, replacement and stockwork textures.

## 3 MINERALOGY

Alteration of the deposit include: carbonization, alunitization, and silicification. Several quartz veins ranging in thickness from a few millimeters to 40cm cut the metamorphic rock, and abundant euhedral pyrite grains occur in these rocks. In the deposit area alunitization is extensive, and abundant jarocite and natrojarocite occurs in different parts of the deposit.

Several copper minerals have been identified the Talkheh copper deposit. Chalcocite veins and veinlets are present and in some parts covellite is more abundant relative to other copper minerals. Orthorhombic and isotropic chalcocite identified by XRD with needle shaped covellite on the margins of chalcocite are common.

Other minerals include tenurite, malachite, azurite and some iron-oxide minerals. Djurlite, digenite, atacamite and brochantite are the minerals newly identified and introduced in this paper. Electron microprobe analyses proved the existence of gold in several samples.

Fluid inclusions have been studied on calcite crystals with two or more daughter minerals. The temperature of homogenization and the salinity of the fluid were measured by a Linkam model THM600 with heating control TMS-94 and cooling control LNP. The salinity range of the fluids is 0.5 to 9.5 wt. percent NaCl equiva-

lent, and mainly between 2.5 to 3.5 wt. percent. The homogenization temperature ranges from 105 to 230°C, averaging between 135 and 155 °C.

## 4 GEOCHEMISTRY

Detailed studies on the correlation coefficient of geochemical data using the Spirman correlation coefficient method have indicated the positive but weak correlation between copper and zinc (0.33), barium (0.33), arsenic (0.22), cobalt (0.18), lead (0.17) and sulphur (0.16). Copper has a weak negative correlation coefficient with molybdenum (-0.1), vanadium (-0.15), chromium (-0.15), strontium (-0.2) and nickel (0.36).

## 5 CONCLUSIONS

In order to find the genesis and the model of formation of the Talkheh copper deposit, the host rock, texture of the ore, temperature and salinity of the fluid inclusions, geochemistry, the role of the faults and fractures in the field, and the location of the deposit relative to volcanic activities in the area were investigated in detail. Based on the measured temperature of the fluid inclusion; the fissure and void filling type of deposition; irregular veins and veinlets; replacement and some colloidal texture as well as the lack of high temperature alteration minerals the Talkheh deposit is postulated to be an epithermal type. The microscopic presence of gold in several samples suggests that prospecting for gold in this deposit may be promising.

## REFERENCES


Bariand, P., 1963, Contribution ala mineralogy de l'Iran , *Bull. Soc. France, Miner. Crist*., v. 76,p.17-64.

Bazin D,. and Hubner , H., 1969, Copper Deposits in Iran, *Geological Survey of Iran,* Report No. 13, 195 p.

Cofimines, (1971), Miscellaneous Survey ( August 1970 to July 1971), Semnan, Anarak, G*eological Survvey of Iran,* Internal Report.230 p.

Gansser, A., 1955, New Aspects of the Geology in Central Iran,*4th World Petroleum Conference, Section L/A/S, Rome, Italy*, p.280-300

Ladame, G., 1945, Les Resources Metalliferes de l'Iran. *Schweiz. Miner. Petr. Mitt.*.Vol.25, No. 1.,p.165-303.

Motallebi, M., 2004, Genesis of Talkheh and Kan-e-Mes deposits using geochemical and fluid inclusion studies, *M.Sc. Thesis, Tarbiat Moalem University, Tehran, Iran.,* 213p.

Nickolas, W., 1969, Report on the electric and radiometric survey of Meskani and Talmesi copper deposits, *Geological Survey of Iran*, Report No.25-G.65p.

Romanko, E. ed., 1984, Outline of metallogeny of Anarak area (Central Iran), Geologial Survvey of Iran, Report No. TE/NO, 21, *Mir. Pub. Company, Moscow,*136p.

Sjerp, N., Momenzadeh, M. and Mallakpour, M., (1969), Re evaluation of Meskani copper mine (Anarak area), *Geological Survey of Iran,* Internal Report. 40p.

Stahl, A. F., 1911, Persian, in *Hanlbuch der Regionalen Geologie*, Heidelberg, Hft. 8 v. 5, Pt. 6, 46p.

Walter, H. V. and Momenzadeh, M., 1983, Mineral deposits and metallogenic epochs in the area of geotraverse in Iran, in Geodynamic project (Geotraverse) of Iran, *Geological Survey of Iran,* Report No. 51.p. 489-499.

# Genetic constraints from REE geochemistry of the Koru lead-zinc deposits - Biga Peninsula, northwesten Turkey

F. Suner, A. Gedikoglu, M. Maral, D. Kiran, D .Maral, C. Altinay, A. Kepekli & Z. Aktuna
*İstanbul Technical Uninersity, Faculty of Mines, Dept. of Geology, Turkey*

ABSTRACT: The Koru lead-zinc deposits are located in the Biga Peninsula which is a very rich zone in terms of both metallic ores and industrial minerals. This high abundance of metallic and industrial minerals of the region is related to the volcanic and tectonic activities that have developed during different geological periods. Barite accompanies the lead-zinc mineralization of the Koru deposits, associated with Tertiary volcanic rocks. Pyrite, chalcopyrite, bornite, chalcocite, quartz and carbonate minerals are also present. This research focused on geochemical ways of investigation of depositional properties of $BaSO_4$-Pb-Zn formations.

KEYWORDS: Biga Peninsula, lead-zinc deposits, REE, geochemistry

## 1 INTRODUCTION

The Koru lead-zinc deposits are located in the Biga Peninsula, NW Turkey, which is a very rich zone in terms of both metallic ores and industrial minerals. Most of the metallic deposits and industrial occurrences in the region have been known and mined throughout the history. This richness of the region is related to the volcanic and tectonic activities that have developed during different geological periods.

Recent investigations in the Biga peninsula include geology, tectonics, rock and ore petrography, economic geology, and geochemistry, which have also been undertaken at the Koru lead-zinc deposits (Bozkaya, 2001; Bozkaya & Gokce, 2001, 2002; Besir, 2003; Maral, 2006)

The Koru lead – zinc deposits are located south of town of Umurbey, Biga Peninsula. The Tahtalikuyu and Eskikısla deposits are still mined for lead and zinc. Lead-zinc formations in the region are associated with Tertiary aged volcanic rocks. Barite accompanies the mineralization, as well as pyrite, chalcopyrite, bornite, chalcocite, quartz and carbonate.

There are two main ore types: massive veins and breccia. The breccia ore type hosted by the volcanic rocks while the massive vein ore type are related to tectonic openings.

The main focus of this research is to investigate $BaSO_4$-Pb-Zn formations in the Koru region in terms of geochemical aspects. For this purpose, major, minor, trace and rare element analyses were performed. These elements were also looked for in wall rocks.

The samples were collected from outcrops and the underground mines. They were collected in the main ore zones, but also within the host rocks in order to correlate the compositions of ore minerals and to get information on the development of ore formation. The underground mine samples were taken from ore veins and breccias wherever available. After the samples were pulverized and sieved, there were analyzed at ACMELAB, Canada for major, minor, trace and rare earth elements.

## 2 GEOLOGY

The mine area is surrounded by Tertiary volcanic rocks. These are distinguished as Baliklicesme and Can volcanic rocks. The first group consists of Eocene andesitic, basaltic andesitic, rarely rhyodacitic and dacitic rocks. The Can volcanic rocks are comprised of Oligocene-Miocene trachytic, latitic, dacitic and rhyolitic tuffs and agglomerates, andesitic and dacitic lavas. Quaternary alluvium covers large areas

Outcrops of Eocene Baliklicesme volcanic rocks are located in between the Biga and Laps-

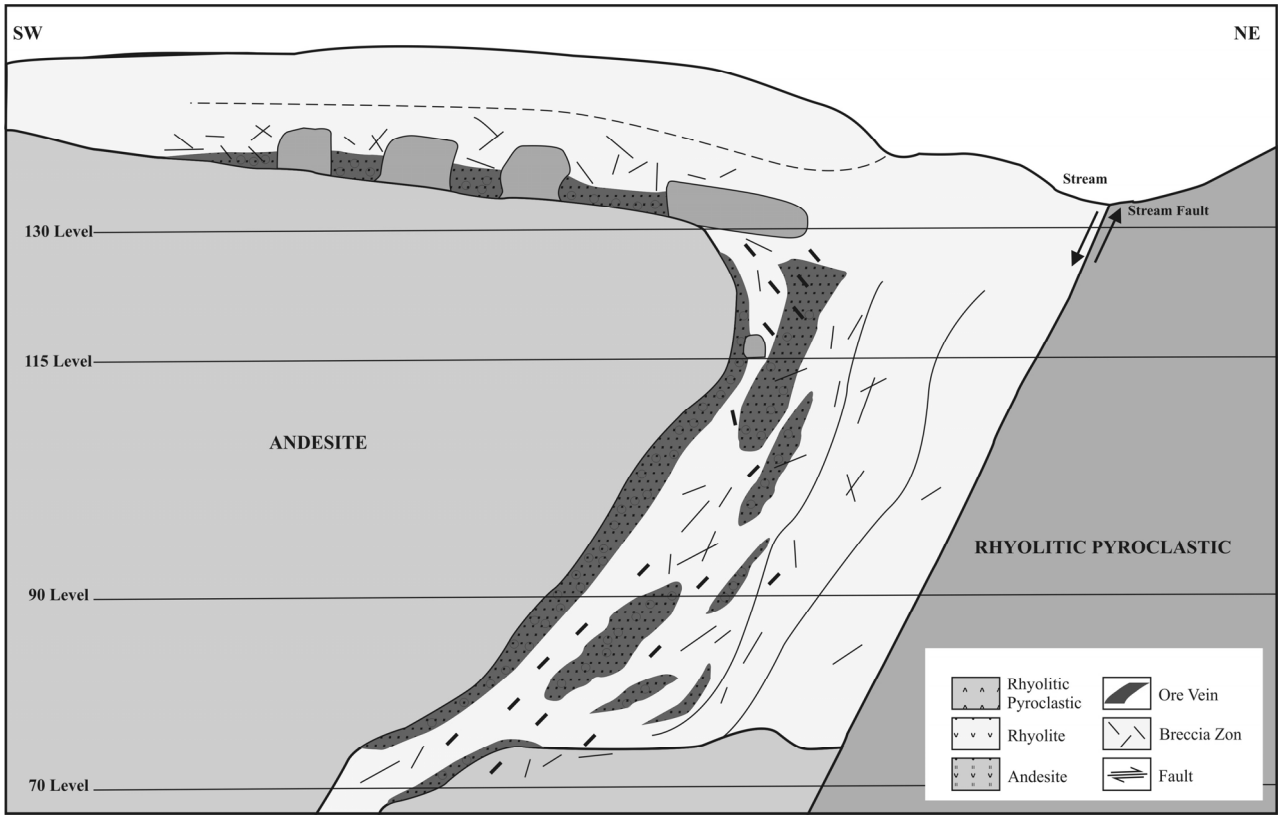


Fig.1. General structure of the Eskikisla deposit (Beşir, 2003)

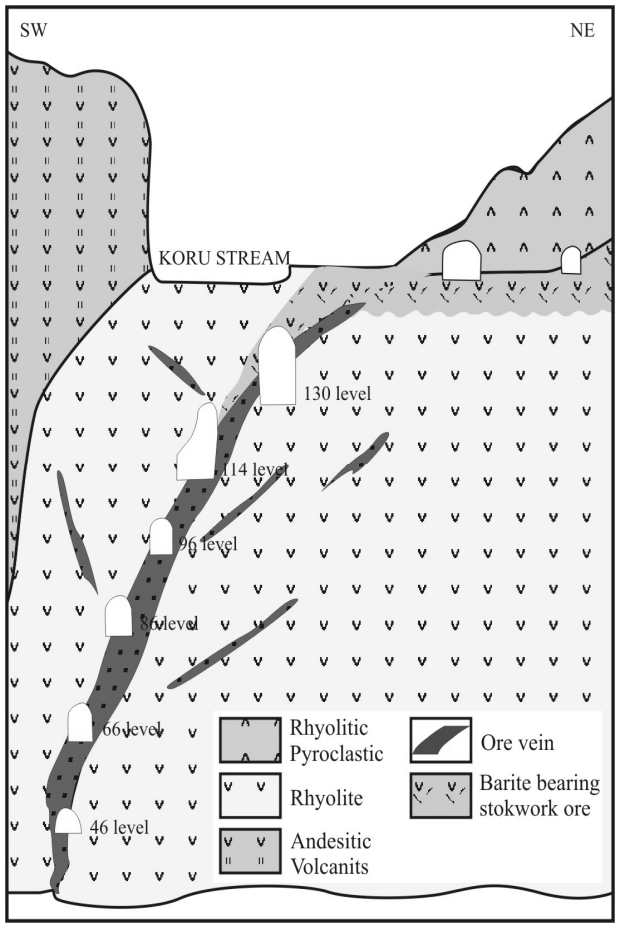


Fig.2. General structure of Tahtalikuyu deposit (Yildiz *et al.*, 2005)

eki county centers (Ercan *et al.*, 1995), and around the Koru deposits. Petrographic investigations show that andesitic lavas have porphyric texture and detected alteration minerals are chlorite and clay minerals. Generally, the tuffs exhibit a lithic character.

The Can volcanic rocks, are terrestrial volcanic products. The volcanic activity started in Oligocene and continued until the end of Miocene (Ercan *et al*., 1995; Siyako *et al*., 1989). Weathering and alteration affected the volcanic rocks with most of the lavas affected by silicic and argillic alteration. Tuffs were getting alteration and forming richness kaolin deposits. The volcanic rocks are particularly important because of their association with metallic ore deposits in North Western Anatolia. Hydrothermal alteration is intense and contains Ag, As, Au, Mo, Hg and Cu besides Pb and Zn.

The Can volcanic rocks appear in the center of the field and host the Koru barite bearing lead-zinc deposits (Figs 1 and 2). The mineralization is hosted by rhyolite, partly at the contact with andesite.

## 3 MINERALIZATION & GEOCHEMISTRY

The deposition field is hosted by the Can volcanic rocks and it exhibits two different

mineral formation types such as ore veinlets in the upper parts and ore veins along fault zones within the lower parts (Bozkaya *et al.*, 2002). Both ore types have mineralogic similarities. The main ore minerals are sphalerite and galena, with barite. Slight amounts of pyrite, chalcopyrite, marcasite, chalcocite, covellite, bornite and quartz accompany them.

Bozkaya & Gokce (2002) studied fluid inclusions and revealed the presence of CaCl and $MgCl_2$ in the mineralizing hydrothermal solutions. The salinity of the hydrothermal solutions is rather relatively high (in average 8.55% in a range 11.09 – 6.02%) during barite crystallization in the early stage of mineralization, while it decreased (in average 6.8%, in a range 9.99 – 2.07%) during the later sulphide episode of the mineralization. The presence of CaCl and $MgCl_2$ indicates that the mineralizing hydrothermal solutions are either seawater or fluids that have circulated through sedimentary rocks deposited in a marine environment (Bozkaya & Gokce 2002).

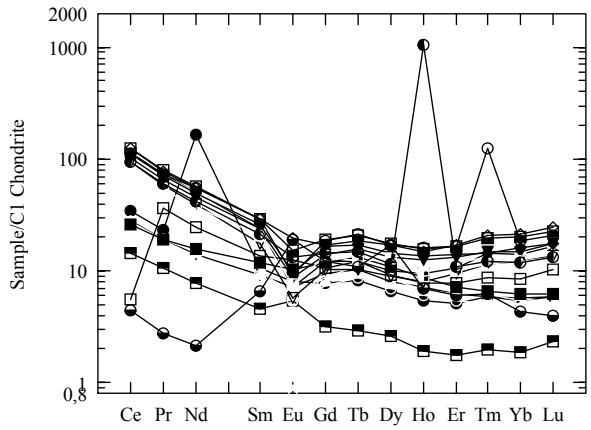


Fig.3. Chondrite-normalized whole rock REE patterns of ore-bearing volcanic rocks.

REE studies of both volcanics and sulphides and barites (Bozkaya & Gokce, 2002) show that the normalized REE values of barites show effect of seawater on formation conditions. Both the patterns of the galena, sphalerite and barite and the CeNd/YbNd-YbNd diagram have lead to the conclusion that these paragenesis had been formed within the volcanic rocks under the effect of deeply circulated seawater. which were enriched with respect to ore forming elements derived from volcanic rocks.

## 4 CONCLUSION

The results have reveal that seawater was an important component during the ore forming process. The lead-zinc-barite and other metallic occurrences have been formed under the control of both ore-bearing thermal solutions and sea water in a multiperiodic phase within the Oligo-Miocene volcanic rocks.

## REFERENCES


Beşir D (2003), Investigation of Koru Koyu (Lapseki - Çanakkale) Pb-Zn-Ag Deposits, *M.Sc.Thesis, D.E.U. Institute of Sciences*

Bozkaya, G., 2001. Geology of Koru (Çanakkale) Barite,Lead-Zinc Deposits, *Ph.D. Thesis, Cumhuriyet University* (Unpublished).

Bozkaya G. & Gökçe A., 2001. Ore Microscopy of Koru (Çanakkale) Barite – Lead - Zinc Deposits and Fluid Inclusion Values. *Cumhuriyet Universitesy Journal, Serie A- Earthsciences* 18 (1), 55-70.

Bozkaya G. ve Gokce A., (2002), Major, Trace and REE Geochemistry of of Koru (Çanakkale) Barite – Lead - Zinc Deposits *Bulletin of Turkey Geology*, 45:1-18

Ercan, T., Satır, M., Steinitz, G., Dora, A., Sarıfakıoğlu, E., Adis, C, Walter, H. Ve Yıldırım, T., 1995. The Properties of Tertiary Volcanism on Biga Penunsila and Gökçeada, Bozcaada and Tavşan Islands *M.T.A. Journal,* 117,55-86.

Maral D ( 2006), Investigation od Precious Metal Related to Sulfur Mineralisation on Biga Penunsila *M.Sc. Thesis, İ.T.U. Institute of Sciences*

Okay, A.Î., Siyako, M. ve Burkan, K.A., 1990. Geology and Tectonic Evolution of Biga Peninsula *Bulletin of T.P.J.D.* 2/1, 83-121.

Önem, S., 1974. Geology of Gelibolu Penunsila and Çanakkale *T.P.A.O. Research Group Report*, No: 877.

Siyako, M, Burkan, K.A. ve Okay, AX, 1989. Tertiary Geolgy of Biga ve Gelibolu Penunsilas and Hydrocarbon Reserve Estimation Studies, *Bulletin of T.P.J.D.* (3), 183-199.

Yildiz B, Unal N, Kilic S, Keskinler SY (2005) Preliminary Report on Koru Pb-Zn-Ag Deposits. *Canakkale Mining Group*

# The Breznik gold prospect, late Cretaceous Srednegorie belt, Bulgaria: evidence for an epithermal system telescoping a porphyry environment

Robert Moritz
*Institute of Earth Sciences, University of Geneva, Geneva, Switzerland*

Rumen Petrunov
*Geological Institute, Bulgarian Academy of Sciences, Sofia, Bulgaria*

Stanislav Stoykov, Jivko Todorov* & Strashimir Strashimirov
*Department of Economic Geology, University of Mining and Geology St Ivan Rilski, Sofia, Bulgaria*
** Euromax, Resources Ltd, Sofia, Bulgaria*

ABSTRACT: The Breznik epithermal gold prospect, late Cretaceous Western Srednogorie zone, consists of juxtaposed high- and low-sulphidation epithermal styles of mineralization. Drilling also indicates the presence of a porphyry-style stockwork at depth. A preliminary fluid inclusion study has revealed a hydrothermal evolution starting with high-temperature (~400°C) brine-vapour separation, followed by a sudden pressure drop with intense boiling, and final deposition of carbonates from a low-temperature, moderately saline fluid. Quartz associated with a pyrite-enargite assemblage records the trapping of diluted high-temperature brine and contracted vapour. The fluid inclusion data and the close proximity of different alteration and mineralization styles are likely the result of a porphyry system telescoped by epithermal mineralization.

KEYWORDS: fluid inclusions, epithermal gold, porphyry to epithermal transition, Breznik, Srednogorie belt

## 1 INTRODUCTION

The Breznik epithermal gold prospect is located in the late Cretaceous Banat-Timok-Srednogorie belt, a major copper and gold metallogenic province in Eastern Europe. The latter is characterized by clusters of porphyry-Cu and Au-Cu epithermal deposits in major mining districts, such as Bor-Madjanpek, Serbia and Panagyurishte, Bulgaria, separated from each other by segments devoid of major ore deposit/prospect districts (Ciobanu *et al*., 2002; von Quadt *et al*., 2005). The Breznik prospect is located in such a poorly endowed segment, in the Western Srednogorie tectonic zone, approximately 35km west of Sofia, in-between the Bor-Madjanpek and Panagyurishte districts.

Crummy *et al*. (2001) interpreted the Breznik occurrence as an anomalous epithermal deposit with both high-sulphidation and low-sulphidation characteristics. They recognized that the sulphidation characteristics document an evolution over time of the mineralizing hydrothermal system. Panayotov *et al*. (1982) mentioned the potential for porphyry-style mineralization at Breznik. Recent drilling supports the existence of such porphyry-style mineralization directly beneath the epithermal occurrence.

In this contribution, we present new fluid inclusion data, which document that a deep magmatic environment was overprinted by an epithermal system at Breznik.

## 2 LOCAL GEOLOGICAL SETTING

The Breznik prospect is hosted by late Cretaceous volcanic and volcanoclastic rocks of andesitic, trachyandesitic and trachybasaltic composition, intruded by porphyry stocks and dikes of gabbrodioritic composition belonging to the Western Srednogorie belt. Basement rocks in the Breznik area consist of Precambrian gneiss and schists, Cambrian-Devonian mafic volcanic rocks, Palaeozoic granitic intrusions, Permian-Triassic clastic sedimentary rocks, and Jurassic-Cretaceous limestone, shale and sandstone.

## 3 ALTERATION AND MINERALIZATION

The hydrothermal alteration and details about the mineralization have been described by Velinov (1967), Velinov & Kanazirski (1990) and Crummy *et al*. (2001). The altered and mineralized area is EW-oriented and covers an area of approximately 2.5 by 1.5 km. The prospect is subdivided into one northern and one southern mineralized area with distinct types of alteration and metal enrichments.

The northern part displays an advanced argillic alteration with small and shallow zones consisting of quartz, kaolinite and alunite surrounded by an alteration halo with kaolinite and sericite. This part of the prospect shows local anomalies of Mo, Te, and Au (locally over 2 g/t). The main opaque minerals recognized during drilling are pyrite, enargite, luzonite and tellurides.

The southern part of the prospect consists of a phyllic zone, immediately adjacent to the advanced argillic zone described above. The mineralization is linked to EW-oriented Mn-, Mg-, Fe-carbonates, chalcedony, quartz and pyrite veins. The intense carbonate, sericite and quartz alteration and EW trending veins overprint the advanced argillic alteration (Crummy *et al*., 2001). Trenching and drilling has revealed anomalous gold areas, with 4.1 g/t over an interval of 13m in one drill core. Pyrite is the predominant opaque phase, accompanied by tennantite, tetrahedrite, enargite, luzonite, goldfieldite, galena, sphalerite, chalcopyrite, and arsenopyrite. There is a preferential enrichment of gold in areas with Mn carbonates (Crummy *et al*., 2001).

Gravity geophysics and drilling show that the epithermal mineralization is underlain by a massive, EW-oriented porphyric body. Drill core samples contain stockworks of quartz - pyrite veins (Fig.1A), and anhydrite/gypsum ±pyrite veins.

## 4 FLUID INCLUSION PETROGRAPHY AND MICROTHERMOMETRY

Fluid inclusion micothermometry was carried out on drillcore material. Preliminary results were collected on four samples (Fig. 2). Except for one sample, all inclusions are primaries.

Sample BR-1-36 (Fig. 1B) was collected at a depth of 36m at the transition from the northern to the southern parts of the prospect. It comes from a breccia with altered granodioritic fragments in a matrix displaying cockade crustification, consisting of magmatic quartz in the innermost bands, surrounded by intergrown fine-grained silica, chalcedony, and euhedral quartz, and finally dolomite in the outermost zone. The innermost magmatic quartz is separated from the hydrothermal quartz by a zone of fine-grained silica (Fig. 1C). Sulphide deposition occurred during the transition to hydrothermal quartz (Fig. 1C).

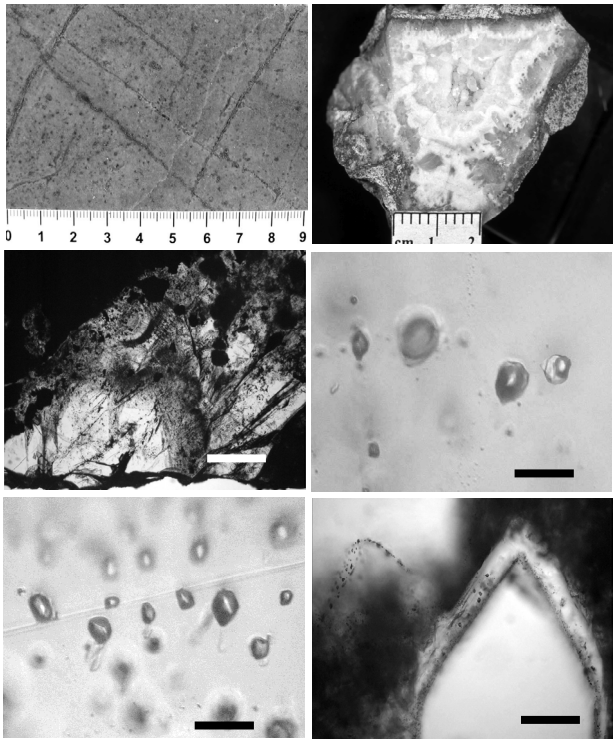

Figure 1. A: Quartz-pyrite stockwork in altered granodiorite, depth of 183m, scale in cm. B: Sample BR 1-36 with a matrix consisting of magmatic quartz (I) rimming granodiorite, surrounded by an intergrowth of hydrothermal chalcedony and euhedral quartz (II), and finally late stage dolomite (III). Scale in cm. C: Transition of fine-grained silica (X), recording a pressure drop between the early magmatic quartz (I) and the younger hydrothermal quartz (II) events. Black: sulphides. (Scale Bar 400μm) D: coexisting vapour and brine inclusions trapped by magmatic quartz (I in B) (Scale Bar 20μm). E: single phase, vapour-filled inclusions in hydrothermal quartz (II in B). (Scale Bar 20μm) F: growth zones with single phase, vapour-filled inclusions in euhedral, hydrothermal quartz (II in B). (Scale Bar 100μm)

The innermost magmatic quartz has trapped coexisting assemblages of vapour-rich and liquid-rich inclusions (Fig. 1D). The salinity of the liquid-rich inclusions is between 20.7 and 26.6 wt% NaCl equivalent, and the one of the vapour-rich inclusions is between 0.5 and 3.2 wt% NaCl equivalent. Homogenization temperatures are about 400°C for both the liquid- and vapour-rich inclusions (Fig. 2). The

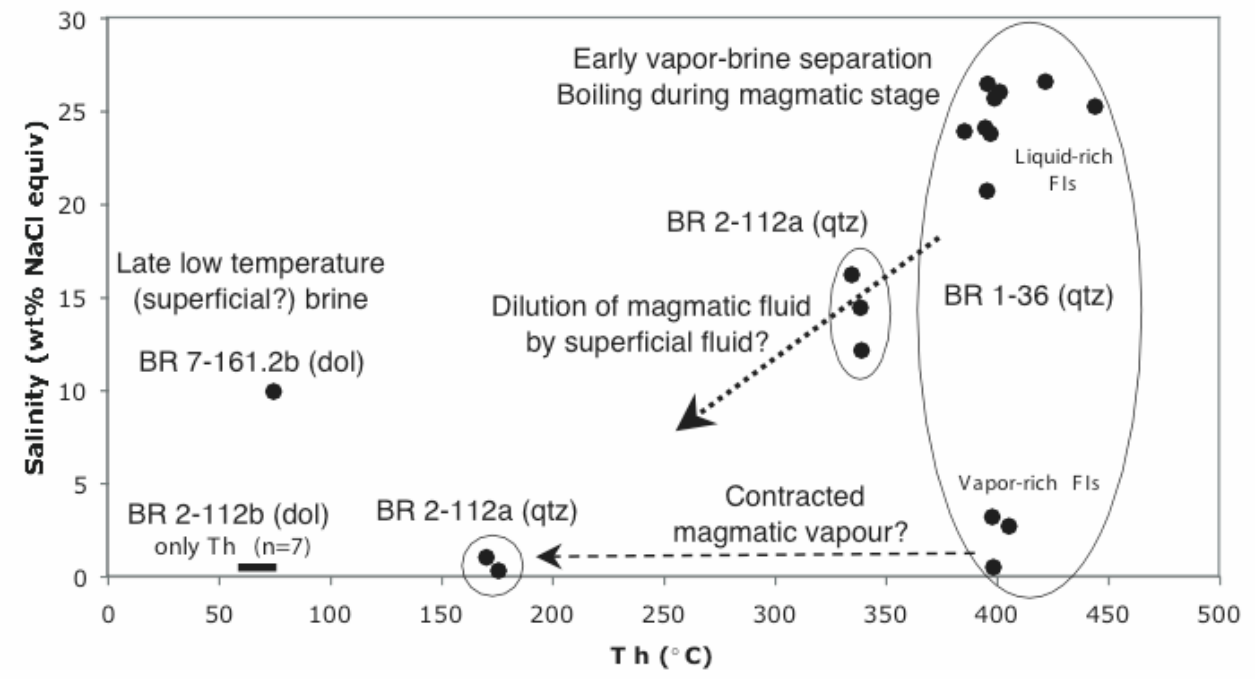


Figure 2. Microthermometric fluid inclusion data showing a fluid evolution from a magmatic stage with brine-vapour separation at about 400°C (BR 1-36) to hydrothermal conditions, with data (BR 2-112a) that are consistent with dilution of the saline magmatic fluid and contraction of the magmatic vapour. The end of the fluid evolution is marked by a low-temperature, brine depositing carbonates (BR 7-161.2b and BR 2-112b). Fis: fluid inclusions, qtz: quartz, dol: dolomite, Th: homogenization temperature.

younger hydrothermal quartz post-dating the fine-grained, silica gel event (Fig. 1C) only contains single phase, vapour-rich inclusions (Fig. 1D), with traces of $CO_2$, as detected by Raman spectroscopy, occurring typically along growth zones (Fig. 1E). Small inclusions of platy calcite are present in the euhedral hydrothermal quartz.

Late stage fluids were recognized in paragenetically late dolomite in samples BR-2-112b (depth of 112m) and BR-7-161.2b (depth of 161.2m) collected, respectively, in drill cores from the northern and southern parts of the prospect. Inclusions occur along well-defined growth zones and have a high liquid to vapour ratio at room temperature. The inclusions only yielded homogenization temperatures between 58 and 76°C, except one inclusion, which also yielded a salinity of 10 wt% NaCl equivalent (Fig. 2).

Sample BR-2-112a from the northern part of the prospect contains an assemblage of pyrite, enargite, tennantite/tetrahedrite and quartz. Quartz in this sample predates carbonate deposition, and contains two distinct groups of two-phase (at room temperature) fluid inclusions. In contrast to the other fluid inclusions of this study, there is no textural evidence, which may allow classifying them as primary inclusions. One group of inclusions has salinities between 12.2 and 16.2 wt% NaCl equivalent and homogenization temperatures between 334 and 339°C, and the second group of inclusions contains a dilute fluid with salinities of 0.5 to 1.1 wt% NaCl equivalent and homogenization temperatures at 170-176°C (Fig. 2).

## 5 DISCUSSION AND CONCLUSIONS

The fluid inclusion data record a sequence from high- to low-temperature conditions, partly linked to sudden pressure drops. Early brine-vapour separation occurred at about 400°C as a result of boiling during an initial, deep magmatic stage (Fig. 2). This was followed by a sudden pressure drop as documented by the fine-grained silica, deposited as a gel (*e.g.* Muntean & Einaudi, 2000), at the magmatic-hydrothermal quartz transition (Fig. 1C). During this abrupt pressure drop, the fluid was flashed to steam as recorded by the abundant vapour-rich inclusions in hydrothermal quartz (Figs 1E-F). Such boiling conditions are also documented by the platy calcite inclusions in hydrothermal quartz. The vapour-dominated environment of the hydrothermal system was followed by late carbonate deposition from a low-temperature, saline fluid (Fig. 2). The latter

could be a basinal brine, or its salinity could be due to condensation of a magmatic fluid in groundwater.

At this stage of the study it is not clear how the fluid with salinities of 12.2 to 16.2 wt% NaCl equivalent and homogenization temperatures of 334 to 339°C, and the dilute fluid with 0.5 to 1.1 wt% NaCl equivalent salinities and homogenization temperatures of 170-176°C (Fig. 2, both trapped in quartz associated with the pyrite-enargite assemblage) are related to the magmatic-hydrothermal evolution described above. They possibly record dilution of the early stage brine and trapping of contracted magmatic vapour.

The magmatic-hydrothermal transition documented by the fluid inclusion data, and the close spatial association of epithermal mineralization and alteration, and porphyry mineralization immediately underneath Breznik is reminiscent of other examples, where porphyry systems were telescoped by epithermal mineralization (*e.g*. Petrunov *et al*., 1991; Brathwaite *et al.*, 2001; Milu *et al*., 2004). As discussed by Sillitoe (1994), such telescoped mineralizing environments can be attractive economic targets, and the cause of the sudden magmatic-epithermal transition could be attributed to sector collapse in a volcanic environment. Such a sudden change of the local setting could also explain the juxtaposition of high- and low-sulphidation epithermal characteristics at Breznik, as the deep magmatic-hydrothermal system was suddenly exposed to and diluted by surficial fluids.

## ACKNOWLEDGEMENTS

This study was supported by the Swiss National Science Foundation (200020-101853 and 200020-113510), SCOPES (7BUPJ062276 and IB7320-111046) and the Bulgarian National Science Foundation (Grant NZ-1412). Balkan Mineral and Mining, and Euromax Resources are thanked for providing help during fieldwork and drill core sampling, and sharing information and data.

## REFERENCES

Brathwaite RL, Simpson MP, Faure K, Skinner DNB (2001) Telescoped porphyry Cu-Mo-Au mineralisation, advanced argillic alteration and quartz-sulphide-gold-anhydrite veins in the Thames district, New Zealand. *Mineralium Deposita*: 36, 623-640

Ciobanu, CL. Cook, NJ, Stein, H (2002) Regional setting and geochronology of the Late Cretaceous Banatitic magmatic and metallogenic belt. *Mineralium Deposita*: 37, 541-567

Crummy, J, Mutafchiev, I, Velinov, I, Petrunov, R (2001) The Breznik epithermal Au occurrence, Western Srednegorie – Bulgaria: an "atypical"(?) low-sulphidation hydrothermal system. In: Piestrzynski, A. et al. (eds), Balkema, Lisse, *Proceedings 6th biennial SGA meeting, Cracow, Poland*: 723-726

Milu, V, Milesi, J-P, Leroy, JL (2004) Rosia Poieni copper deposit, Apuseni Mountains, Romania: advanced argillic overprint of a porphyry system. *Mineralium Deposita:* 39, 173-188

Muntean, JL, Einaudi, MT (2000) Porphyry gold deposits of the Refugio district, Maricunga belt, Northern Chile. *Economic Geology*: 95, 1445-1472

Panayotov, A, Tsvetkov, K, Sapundjiev, K, Stoyanov, I (1982) Complex investigation and prospecting of minerals in western Srednogorie in accordance with Bardoto, Breznishko. *Ann. Commission Geology*: 22, 103-111 (in Bulgarian with English abstract)

Petrunov, R, Dragov, P, Neykov, H (1991) Polyelemental (with As, Sn, V, Bi, Ag, Te,Ge, Se, Etc.) mineralization in Assarel porphyry-copper deposit. *Reviews of the Bulgarian Geological Society*: 52, 1-7 (in Bulgarian with English abstract)

Sillitoe, RH (1994) Erosion and collapse of volcanoes; causes of telescoping in intrusion-centered ore deposits. *Geology*: 22, 945-948

Velinov, I (1967) Propylites and alunite quartzites in the region of Breznik. *Review of the Geological Institute, Bulgarian Academy of Sciences, Geochemistry, Mineralogy and Petrology* 16: 205-220 (in Bulgarian with English abstract)

Velinov, I, Kanazirski, M (1990) Formation nature and physico-chemical analysis of mineral parageneses in the metasomatic zones of acid leaching in the Western Srednogorie. *Geologica Balkanica*: 20, 59-71

Von Quadt, A, Moritz, R, Peytcheva, I, Heinrich, CA (2005) Geochronology and geodynamics and Cu-Au mineralization in the Panagyurishte region of the Apuseni-Banat-Timok-Srdnogorie belt, Bulgaria. Ore Geology Reviews: 27, 95-126

# 'Blind' porphyry CuAu (Mo) mineralization of Romania and its variable peripheral expressions as veins and skarns

Serban Vlad
*Bucharest, Romania*

ABSTRACT: Romania has a genuine accumulation of "blind" porphyry CuAuMo systems associated with Cu skarns or AuAg (PbZn) epithermal vein sets. Many such hidden structures were discovered inadvertently during State exploration as a consequence of exploration of Romanian's Carpathians being rich in vein/skarn ore types. Notable dichotomy between porphyries associated with peripheral skarns, versus epithermal ores, is expressed by age (Mesozoic versus Tertiary), precious metal content, alteration types and zoning, shape/size and extent of ore bodies. Preliminary conclusions on metallic/alteration assemblages around porphyries promote potential exploration vectors for what will be an increasingly important deposit type in the future.

KEYWORDS: Porphyry, copper, gold, Romania

## 1 GEOLOGICAL SETTING

The porphyry environment of Romania is related to late Jurassic-Lower Cretaceous, late Cretaceous and Neogene calc-alkaline magmatism (Fig.1) that acted during subduction-collision episodes of the Alpine orogenic cycle in the Carpathians (Vlad, 2005).

The late Jurassic-Lower Cretaceous event is associated with volcano-plutonic settings in the South Apuseni Mts, including extrusive marine volcanic rocks, intermediate to felsic, and deep-seated felsic plutons, yielding a composite system with well-expressed "epithermal" massive sulfide-stockwork Pb-Zn(Au) and inferred, but as yet undiscovered, subjacent porphyry CuAu (Vorta-Dealu Mare).

Late Cretaceous events are related to the well-known transcontinental Banatitic Magmatic-Metallogenetic Belt (BMMB). Porphyry systems with distal expressions are confined to Banat (South Carpathians), where the monzodiorite-diorite evolution line is porphyry productive whereas the granodiorite–granite trend is a non-porphyry metallogenic unit. Late Cretaceous systems can be divided into plutonic settings with wall-rock carbonate-skarn-porphyry CuMoWAu (Oravita-Ciclova), and plutonic-subvolcanic settings, with wall-rock carbonate: skarn-porphyry CuMoAu systems (Sasca-Moldova Noua, Sopot) or metamorphic wall-rock hosted porphyry CuMo systems with pyrite haloes (Bozovici).

The Neogene event stems from the transcontinental Tertiary-Quaternary volcanic arc developed from the Eastern Alps to the West and East Carpathians. Its metallogenesis is represented by ore clusters coincidental with fracture systems centered on volcanic-subvolcanic structures with inferred deep-seated plutons. Porphyry mineralization and peripheral vein/stockwork suites occur in the South Apuseni Mts, including the famous Golden Quadrilateral ('GC') with one of the world's highest gold endowments at 0.69t/km² (Vlad & Orlandea 2004), and Caliman-Gurghiu-Harghita Mt. (East Carpathians; (Borcos *et al.*, 1998). Calc-alkaline andesitic magmatis is porphyry-productive in these regions, whereas the sub-alkaline rhyodacitic magmatism that occurs in the GC yielded exclusively non-porphyry mineralization.

Volcano-plutonic settings can be divided into andesite volcanic-subvolcanic level, with porphyry CuAuMo and associated weakly-expressed related veins of LS/HS epithermal AuAg type (Deva, Rosia Poieni, Bolcana in the South Apuseni Mts and Fancele-Lapusna, Mermezeu-Zebrac, Ostoros, Sumuleu in the Caliman-Gurghiu-Harghita Mts); and andesite

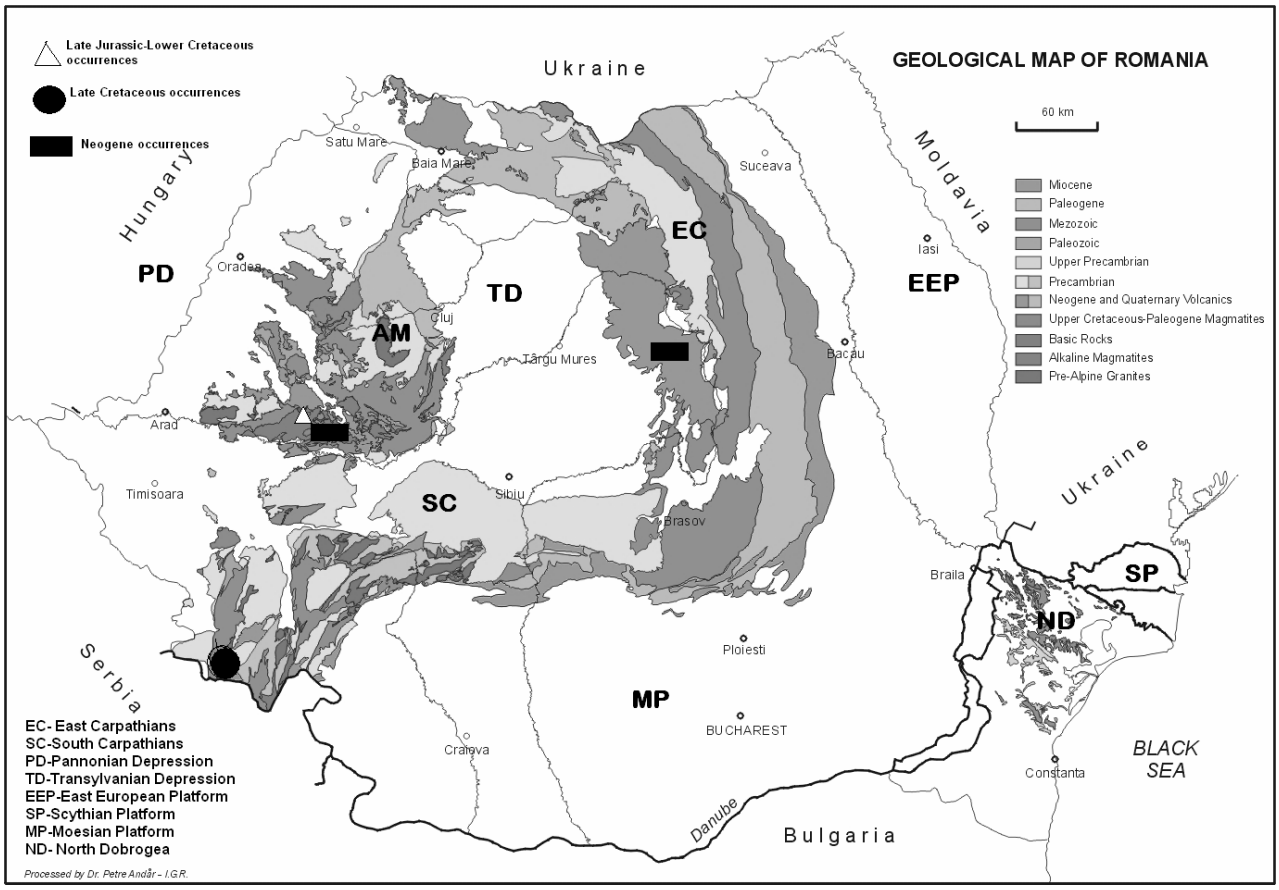


Figure 1: Porphyry environment of Romania

volcanic-subvolcanic levels with mineralization extending into adjacent clastic rocks, forming composite systems including porphyry CuAu with well expressed apical/lateral LS and HS epithermal AuAgPbZn proximal veins to AuAg distal veins (Tarnita, Trampoiele, Hanes-Larga, Muncaceasca_Stanija, Valea Tisei-Runculet, Remetea-Colnic, Musariu, Valea Morii, Magura-Faerag, Talagiu-Bratosin, Voia-Paraul lui Avram in the South Apuseni Mts) mineralization.

## 2 HISTORY

The two genetic couples, porphyry-skarn and porphyry-veins, require different exploration approaches, adjusting traditional exploration practices to varying degrees of erosion. Generally speaking, the historical mining industry focused on gold, while copper/base metals triggered largely scientific interest, allowing description of deposits/districts that became classic models for Alpine metallogeny. Skarns and veins were priority targets, and mining operations concentrated on wide zones with lower grade or on narrow mineralized zones of moderate grade. Much less attention was paid to low grade mineralization in stockworks or disseminations between vein zones. Near-surface gold and copper zones were often ignored. Consequently very few mines met market-economic standards. Numerous blind porphyry coppers were discovered inadvertently during state exploration aimed at extension of veins. The porphyry concept was largely ignored for a long period and exploration during the 1950s and 1960s concentrated on preconceived targets consisting of surface extensions of Cu skarns or AuAg (PbZn) veins.

In term of porphyry-skarn couple, skarns at Suvorov–Moldova Noua were exploited inefficiently by underground methods until the early 1970s when porphyries became to be recognized as a significant ore type (Ianovici *et al.*, 1977). After this, the system porphyry and related veins emerged as a recognized target, resulting in the bulk of blind occurrences of rather low grade but interesting Cu-Au systems.

## 3 CHARACTERISTICS

### *3.a. Late Jurassic-Lower Cretaceous metallogeny*

Vorta district (South Apuseni Mts) base-metal (Au?) discordant massive pods/stockworks are tectonically controlled bodies in silica-adularia- and argillically-altered dacite-andesite rocks. The deposit and associated minor occurrences represent the shallow expression of a deeper-seated felsic pluton. Surface indications and geochemical features provide evidence for a composite system with distal massive sulphide ores and proximal porphyry copper (with Au) along a 1km vertical column. A similar style of massive high-grade mineralization, although of high-sulphidation type, has been demonstrated at Choka Marin, in the Timok complex of Serbia.

*3.b. Late Cretaceous(Banatitic) metallogeny*

Skarn-porphyry systems of Banat represent the northern extension of the Timok Massif. Southern Banat occurrences have been uneconomically exploited, *e.g.* Suvorov-Moldova Noua (the open pit operation and subjacent areas still encloses circa 400Mt @ ~0.3% Cu) or those so far inconclusively explored, *e.g.* Sopot. Both areas contain blind porphyries capped by skarns with Cu-Mo low potential and undetermined Au potential. Garina–Varad area, south of Suvorov, displays a 1km high column with complete metasomatic zoning, from distal propylitic-argillic alteration on skarns/exoskarns, and central phyllic-potassic alteration associated with low grade CuMoPy mineralization. The argillic zone has a larger extent compared to the northern portions of the district. Sopot area hosts small igneous apophyses with restricted alteration aureoles characterized by propylitized-argillized skarns and central phyllic alteration hosting low-grade CuMoPy mineralization. The deeper part of the system is not yet investigated for blind porphyries.

*3.c. Neogene metallogeny- East Carpathians*

The 160 km long volcanic chain Căliman–Gurghiu–Harghita Mts consists of volcano-plutonic complexes composed of basaltic andesites to andesites and dacites, with restricted shoshonite occurrences in the south. Scarcity of mineralization to date is interpreted as a result of minimal erosion or simply non-productive magmatism.

High-sulphidation (?) epithermal–porphyry systems related to central-type volcano-plutonic structures are developed along 1.5km vertical columns in Neogene systems. The zoned alteration from sub-surface to exposures consists of inner potassic zone associated with propylitisation and outer siliceous, argillic and advanced argillic alteration. Metal zoning is represented by Cu(AuMo) at deep porphyry levels, followed upward by CuPbZn→ Au PbZn (including tellurides)→py Au→Hg (cinnabar) → (native sulphur) zones as veins, stockwork/breccia pipes, and impregnations in argillic and siliceous alteration. Such occurrences are related to the major volcano-plutonic edifices, *e.g*. Căliman caldera, Fâncel–Lăpuşna caldera, Zebrac–Mermezeu, Jirca, Şumuleu, Ostoroş, and Vârghiş. They represent a suitable target for regional modeling of young volcanic arc setting and related metallogenesis.

*3.d. Neogene metallogeny-South Apuseni Mts*

Magmatism here is calc-alkaline, multiphase, andesitic to dioritic, and centered on apophyses of deep-seated plutons (volcano-plutonic complexes) coeval with Miocene molasse in adjacent extensional basins. Plutons inferred from geophysics (mainly gravity) occur at 3-4km depth. Subcrustal parental magma is inferred as remelted, assimilated Mesozoic igneous rocks.

Metallogeny consists of low-sulfidation and high-sulfidation epithermal base metal/precious metal deposits proximally/distally associated with porphyry CuAu(Mo) systems. Alteration consists of potassic±phyllic which commonly encloses mineralization, to argillic, to propylitic marginal and/or pervasive regional; key proximal alteration of related veins is phyllic (sericite>smectite).

Vein-porphyry relations in the southern Apuseni can be divided into consanguineous sequences of porphyry-vein assemblages where migration of magmatic porphyry-related fluids toward shallower levels is reflected by zoned veins showing differentiated mobility of Cu and Au; and overprinting systems, where epithermal veins younger than the porphyry systems cross-cut the upper part of porphyries. These are derived from porphyry related fluids mixing with meteoric waters. Vertical extent of mineralized columns are up to 2km, consisting of base-metal/precious metal vein mineralization in the uppermost 300-400m or 'volcanic' levels, followed by 1000-1500m of porphyry mineralization in subvolcanic setting. Large scale zoning from the outside in, consists of pyrite halo with AuAg±Te and/or Pb Zn±Cu

veins and lenses, to stockworks with CuAu(Mo) porphyry mineralization.

Porphyries where apical portions cropped out include Deva and Rosia Poieni; those where apical parts either cropped out or were developed at shallow depth include Valea Morii, Tarnita, and Bolcana.

Romania has at least three documented genuinely 'blind' porphyry deposits, with mineralization starting at 300-800m depths. Musariu (~12Mt with 0.2% Cu and 0.3g/t Au) is related to the most extensive vein set in the Brad district and was mined down to >300m depth where the top of the porphyry system was encountered. The Muncaceasca West–Podul Ionului porphyry is capped by a silicified pyritic plate, and exploration on one level has defined ~9Mt @ 0.25% Cu; the mineralized column extends over 1.5km, and the Au-rich Corabia vein in upper parts was historically exploited. Talagiu has inferred resources of ~100-150Mt @ 0.3-0.4% Cu and 0.4-0.8g/t Au in porphyry, as well as ~3-4Mt with 1-10g/t Au and 5% PbZnCu in veins; blind mineralization starts at 400m beneath the surface and proceeds discontinuously for about 1000m; surface expression consisted of the Bratosin fracture with veins, breccias and disseminations in argillized, pyritised volcanics. The mineralized column is demonstrated over 1.5km vertically.

Systems in which porphyry deposits have only been inferred include Voia, where 500-700m of high-sulphidation epithermal alteration suggests a porphyry at depth. At Magura-Faerag, epithermal-mesothermal quartz-adularia AuAgTe veins and Au-bearing argillic alteration zones with ~2g/t Au suggest a porphyry at depth at around 300-400m. At the Popa-Stanija sector in the Muncaceasca field, PbZn/AuAg veins/stockworks in potassic>phyllic alteration with marginal argillic suggest a porphyry at depth based on alteration intensity as well as IP.

## 4 EXPLORATION POTENTIAL

Further study of mineralization-alteration zoning around Romania's blind porphyries in both skarn-porphyry and epithermal veins-porphyry 'couples' offers potential exploration vectors for what will become an increasingly important deposit style in the future. Application of such concepts to highly metal-endowed regions such as the Golden Quadrilateral, the richest precious metal unit in Europe, may eventually stimulate mining of such targets. In addition, challenges come from the southern East Carpathian volcano-plutonic edifices whose blind porphyry potential is much more speculative. A wealth of useful historic data is available to modern interpretations, creating a fertile field for international collaboration of research institutions as well as private domestic and foreign companies.

## ACKNOWLEDGEMENTS

The author is grateful to Mac Canby for suggesting this topic and discussions during the preparation of this article.

## REFERENCES

Borcos M, Vlad S, Udubasa G, Gabudeanu, B (1998) Qualitative and quantitative metallogenetic analysis of the ore genetic units in Romania *Inst Geol Rom, Bucharest, Rom Journal Min Dep, Special Issue*, 78, 158p

Ianovici V, Vlad S, Borcos M, Bostinescu, S. (1977) Alpine porphyry copper mineralizations of West Romania *Mineralium Deposita,* 12: 307-317.

Vlad SN (2005) Typology and management of metallic mineral resources Ed Casa *Cartii de Stiinta Cluj-Napoca*, 204p (in Romanian)

Vlad, S, Orlandea, E (2004) Metallogeny of the golden quadrilateral: style and characteristics of epithermal-subvolcanic mineralized structures, South Apuseni Mts, Romania *Studia Univ Babes-Bolyai, Cluj-Napoca, Geologia,* XLIX,1,: 15-31.

# SEDIMENTARY ROCK-HOSTED COPPER DEPOSITS

EDITED BY:

DAVE BROUGHTON

ROD KIRKHAM

JAN PASAVA

# Geology and Ore Deposits of the Zambian Copperbelt

David Broughton & Murray Hitzman
*Department of Geology and Geological Engineering, Colorado School of Mines, Golden, CO, 80401, USA*

David Selley, Robert Scott, Stuart Bull, Ross Large, Peter McGoldrick, Mawson Croaker & Nicky Pollington
*Centre for Ore Deposit Research, University of Tasmania, Hobart, Tasmania 7001, AUSTRALIA*

ABSTRACT: Sediment-hosted stratiform Cu-(Co) deposits of the Zambian Copperbelt occur at multiple stratigraphic levels of the Neoproterozoic Katangan Supergroup. Deposits show a consistent spatial relationship to basin architecture, a complex and multistage history of mineralization spanning early diagenetic replacement through to post-peak metamorphic vein emplacement, and associated basin-scale metasomatism. Both *in situ* and inferred mobile reductants were critical in ore deposition.

KEYWORDS: Zambian Copperbelt, sediment-hosted stratiform copper, Neoproterozoic

## 1 INTRODUCTION

The Central African Copperbelt is the world's largest and highest-grade sediment-hosted stratiform copper province, and includes both the Zambian Copperbelt (ZCB) and the Congolese Copperbelt to the northeast. The ZCB contains seven giant (>2Mt Cu) deposits and at least 18 smaller deposits, in total containing approximately 88Mt Cu (Fig. 1; Selley *et al.* 2005).

ZCB deposits have many elements common to the sediment-hosted stratiform copper deposit class (Gustafson & Williams 1980; Kirkham 1989; Hitzman *et al.* 2005), but also have important differences, including differences among individual deposits, and between Zambian and Congolese deposits (Cailteux *et al.* 1995). The ZCB has been and remains a critical metallogenic province in debating and understanding the genesis of major sediment-hosted copper deposits.

## 2. STRATIGRAPHY

Deposits in the ZCB are hosted by the Neoproterozoic Katangan Supergroup, a relatively thin (≤ 5km, commonly ≤ 2km) succession of predominantly marginal marine and terrestrial metasedimentary rocks deposited on Meso and Palaeoproterozoic basement granites, schists, metaigneous and metasedimentary rocks. Mafic igneous rocks, predominantly gabbroic-dioritic sills, occur in the Katangan sequence in the western part of the ZCB above the level of mineralization.

The basal portion of the sequence (Lower Roan Group) contains continental sandstones and conglomerates deposited in a series of restricted sub-basins controlled by extensional normal faults. These largely terrestrial sediments are abruptly overlain by a regionally extensive, variably organic-rich marginal marine siltstone/shale (Copperbelt Orebody Member or COM, *i.e.* the "Ore Shale") that contains the majority of ore deposits. This horizon is overlain by laterally extensive marine carbonates and finer grained clastic rocks which evolved into a platformal sequence of mixed carbonate and clastic (Upper Roan Group) rocks with abundant evaporitic textures, including widespread breccias thought to record the former presence of salt, now dissolved.

The overlying Mwashia Group contains shallow marine carbonate rocks at its base, which typically pass upwards into deeper marine siltstones and carbonaceous shales. The Grand Conglomerate, a diamictite of Sturtian age, marks the base of the Nguba Group of marine carbonates and clastic rocks. A similar diamictite-mixed carbonate-clastic sequence forms the Kundelungu Group, but is rarely preserved in the ZCB.

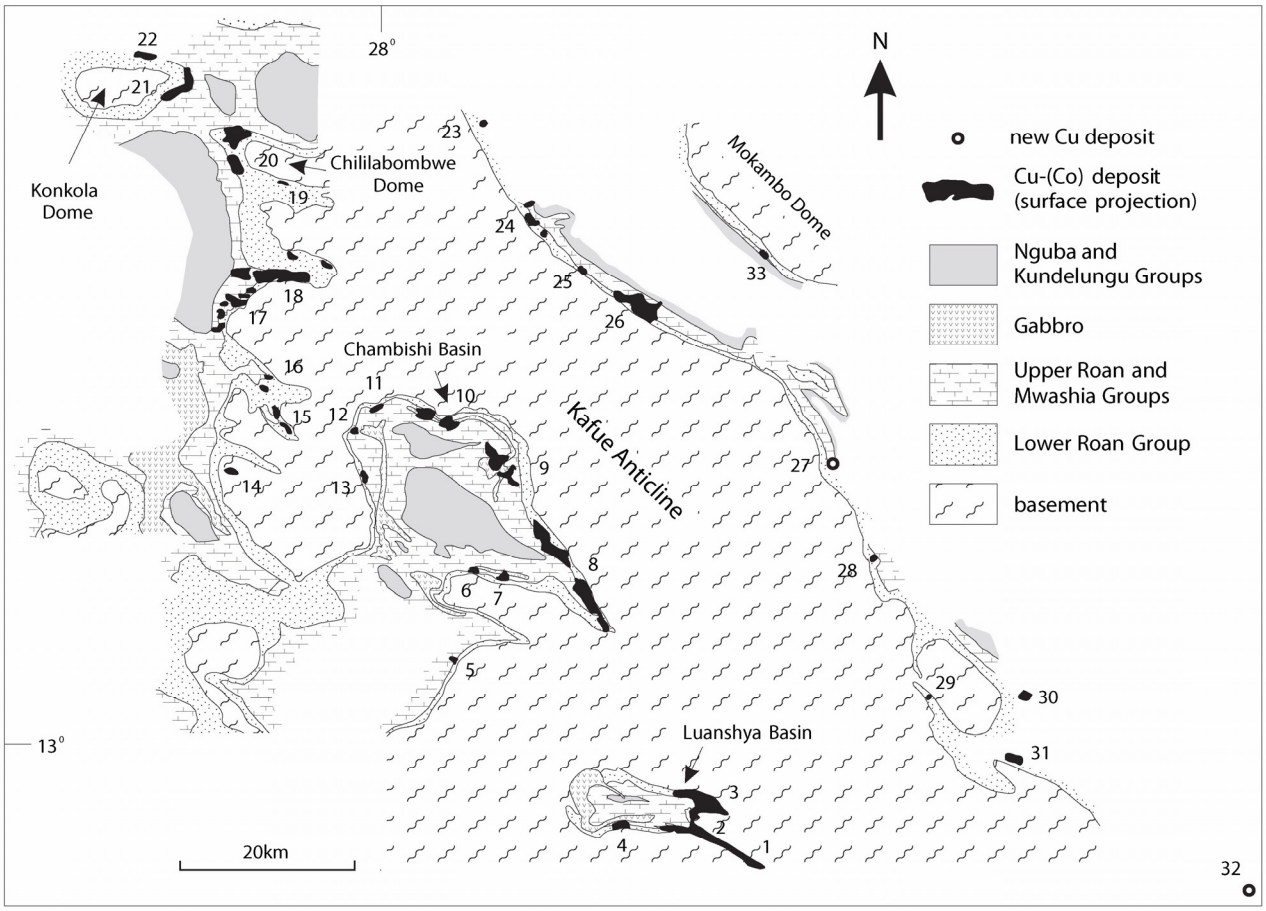


Fig. 1. Geology and ore deposits of the Zambian Copperbelt.1=Luanshya, 2=Roan Extension, 3=Baluba, 4=Lufubu S., 5=Chibuluma S., 6=Chibuluma W., 7=Chibuluma, 8=Nkana, 9=Chambishi SE, 10=Chambishi, 11=Pitanda, 12=Mwambashi A, 13=Mwambashi B, 14=Samba, 15=Fitula, 16=Mimbula, 17=Chingola A-F, 18=Nchanga, 19=Fitwaola, 20=Konkola, 21=Konkola N., 22=Musoshi, 23=Lubembe, 24=Luansobe, 25=Kasaria, 26=Mufulira, 27=Frontier, 28=Mwekera, 29=Ndola W., 30=Itawa, 31=Bwana Mkubwa, 32=Mokambo. Modified from Selley *et al.* 2005.

## 2 TECTONICS

The stratigraphic architecture of the Katangan Supergroup in the ZCB compares to that of Phanerozoic rift systems, and was affected by three significant tectonic events. Early Katangan rifting led to the development of isolated fault-controlled basins containing continental clastics (Lower Roan Group). Marked lateral thickness and facies changes are typical of this syn-rift stage. Subsequent linkage of these basins along master faults at a rift-climax stage resulted in widespread deposition of the COM (Ore Shale), and the first evaporitic deposits within the Katangan sequence (Selley *et al.* 2005). The mixed carbonate-clastic-evaporitic deposits of the uppermost Lower Roan Group and overlying Upper Roan Group represent post-rift and thermal-sag phases of relative tectonic quiescence.

A second period of extension occurred during late Mwashia to early Kundelungu time (~765-735 Ma, *i.e.* Sturtian) and was characterized by localized mafic igneous activity. Lateral facies and thickness changes also occur during this stage.

During the Pan-African Lufilian orogeny (~595-490 Ma), the ZCB underwent basin inversion and later compressive deformation which culminated in upper greenschist-grade metamorphism (~530 Ma).

## 3 DEPOSIT TYPES AND CONTROLS

Unlike many other sediment-hosted stratiform copper provinces, including the Congolese Copperbelt, orebodies in the ZCB occur at numerous stratigraphic levels (Fig. 2). Basement granites and schists commonly host mineralization subjacent to overlying deposits in the basal Katangan, and a historically subeconomic deposit, Samba, occurs in an erosional window of basement schists. “Arenite-hosted” deposits of the Lower Roan Group oc-

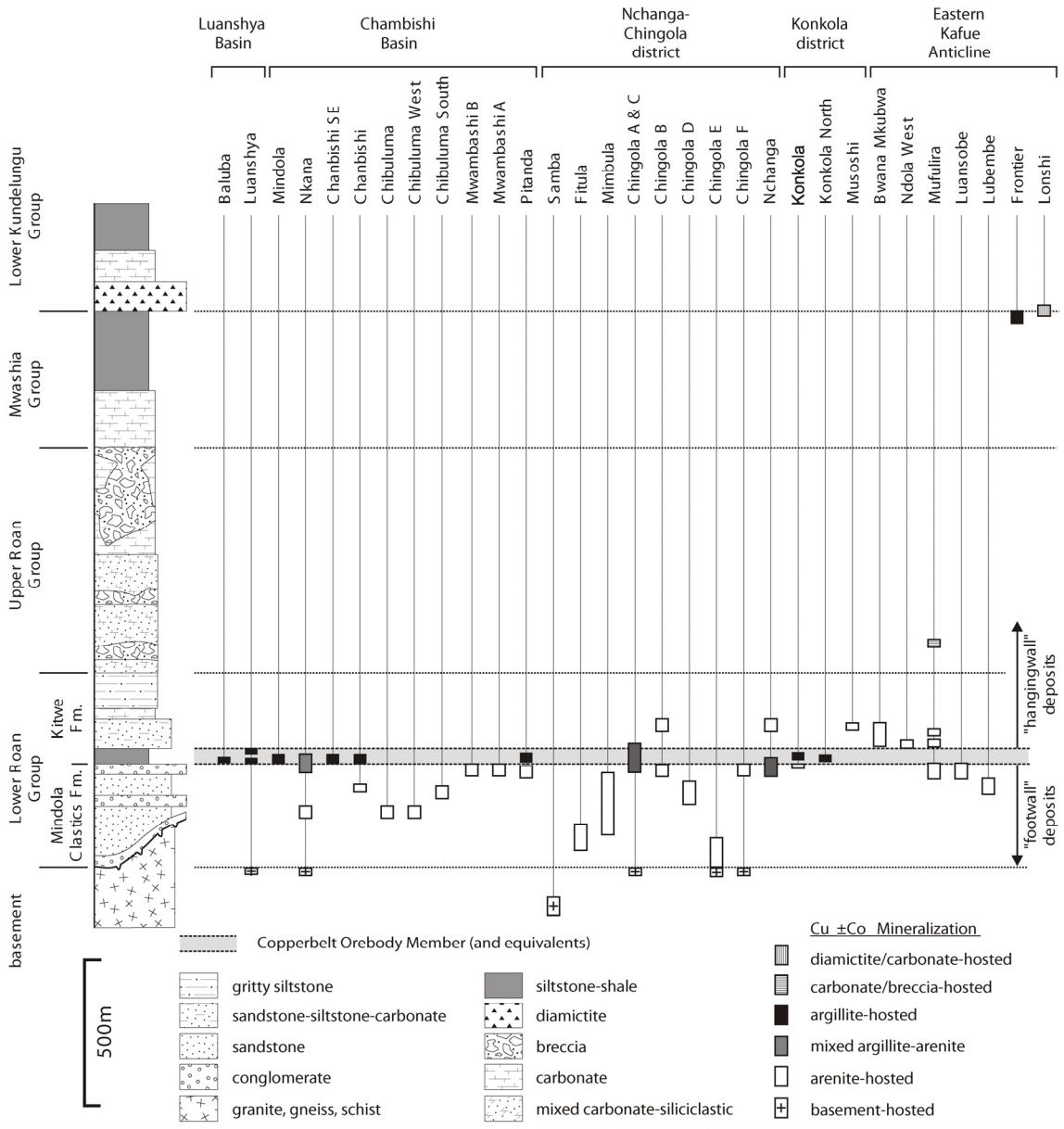


Fig. 2. Stratigraphy of the Katanga Supergroup, and stratigraphic distribution of ore deposits, in the Zambian Copperbelt. Modified from Selley *et al*. 2005.

cur both below and above the level of the COM (Ore Shale), and comprise approximately 30% of known ore. "Argillite-hosted" deposits of the COM account for almost 70% of ore. Newly delineated economic deposits at Frontier and Lonshi contribute about 2% to the ZCB copper inventory, and are particularly significant because they occur in carbonaceous siltstones-shales and diamictite of the uppermost Mwashia and lowermost Nguba Groups, rather than at classical positions within the Lower Roan.

The distribution, geometry, and size of deposits at all levels of the Katangan are fundamentally controlled by basin fault architecture (Annels, 1989; Selley *et al.* 2005) and the availability of both in situ and mobile reductants, the distribution of which are linked to basin structures (Fig. 3). Argillite-hosted deposits of both the COM and the upper Mwashia Group occur within relatively dark and locally carbonaceous siltstones, suggesting the former presence of an *in situ* organic reductant. The black carbonaceous shale facies of the COM hosts ore at Nchanga and Nkana, but also forms a barren, pyritic hangingwall to arenite-hosted deposits at Chingola and in the western Chambishi basin. Deposition of laterally continuous reduced host rocks at the rift climax stage provided a favourable environment for subsequent

deposit formation over substantial strike lengths of up to 17km. Arenite-hosted deposits occur in both the footwall and hangingwall of the COM and have more limited maximum strike lengths of 5 km. They occur at sites that were geometrically favourable for mobile hydrocarbon or sour gas accumulation, and in some instances (Mufulira) relict organic matter is present in intergranular pore space (Annels 1979). Both argillite- and arenite-hosted deposits contain so-called barren gaps of poorly mineralized strata that are typically associated with the fault-bounded shoulders of early sub-basins.

## 4 MINERALIZATION

Two hypogene mineralization assemblages occur in the ZCB. The volumetrically dominant type consists of pre-folding disseminated and lesser vein-hosted Cu-Co sulphides. The most typical sulphide assemblage in the deposits is chalcopyrite-bornite with subsidiary chalcocite and pyrite. The Central African Copperbelt is unusual among sediment-hosted stratiform copper districts in having Co (as carrolite) as an economically significant phase in some deposits, and low to negligible Ag, Zn, and Pb. The second type of hypogene mineralization is common but volumetrically minor, and consists of Cu-U-Mo-(Au) bearing phases in post-folding veins. Oxidized and supergene mineralization assemblages are common in many deposits and are known at depths of up to 1.5 kilometres.

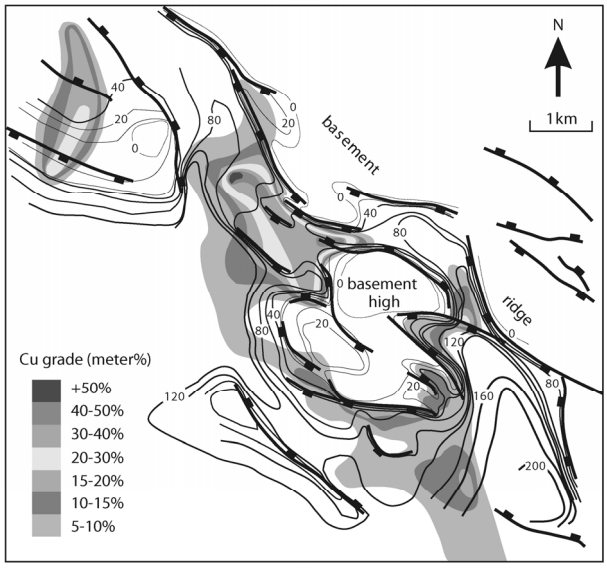


Fig. 3. Spatial relationships between argillite-hosted ore distribution and basin geometry at the Chambishi SE deposit. Modified from Selley *et al*. 2005.

Pre-folding Cu-Co sulphides display complex textural relationships that are best explained by multi-stage ore formation. Diagenetic to late diagenetic mineralization is indicated by the typically non-fracture controlled distribution of both sulphide and gangue phases, replacive textures of Cu-Co sulphides after diagenetic cements and pyrite, and an approximate 815Ma Re-Os isochron age for sulphide precipitation at the Konkola deposit. Brines capable of mobilizing metals were most likely generated during development of evaporitic environments in units of the Upper Roan Group, and/or subsequent dissolution of these evaporites to form the Upper Roan Group breccias.

Late diagenetic to early orogenic mineralization is recorded by pre-folding bedding-parallel fibre veinlets and texturally and compositionally comparable disseminated Cu-Co sulphides. Cu-Co sulphide deposition post-dated diagenetic emplacement of organic matter into arenites at Mufulira. A Re-Os isochron age on Cu-Co sulphides from two arenite- and one argillite-hosted deposits of 576±41 Ma is consistent with early orogenic hydrocarbon or sour gas production (Barra *et al* 2004).

Late to post-peak metamorphic Cu-U-Mo-(Au) mineralization recorded in post-folding veins shows a range of ages between approximately 500 and 530 Ma (Richards *et al* 1988; Torrealday *et al* 2000).

## 5 METASOMATISM

The ZCB is characterized by stratigraphically and laterally widespread metasomatism that records a protracted history of basinal brine migration. Although the alteration history is complex, it can be broadly categorized into an early Ca-Mg-$SO_4^-$, anhydrite- and dolomite-dominant stage involving brine reflux below the level of Upper Roan Group evaporites; a second, K-dominant stage characterized by widespread and commonly intense development of K-feldspar and locally sericite, best developed in rocks of the Lower Roan Group and associated with ore; and a third, Na-dominant stage characterized by development of albite, commonly at the expense of earlier-formed K-feldspar and locally at the expense of earlier-formed Cu-Co sulphide mineralization. Albite dominates in Upper Roan Group breccias and Mwashia-Lower Kundelungu strata. It is also locally associated with post-peak metamorphic

Cu-U-Mo-(Au) vein mineralization. Because of their lateral and stratigraphic extent, none of these alteration types are direct guides to ore, however their presence in an unexplored basin would demonstrate widespread brine circulation potentially favourable for ore deposition.

## REFERENCES


Annels AE (1979) Mufulira greywackes and their associated sulphides: *Institute of Mining and Metallurgy Transactions*, v. 88, p. B15-23.

Annels A.E. (1989) Ore genesis in the Zambian Copperbelt, with particular reference to the northern sector of the Chambishi Basin. In: Boyle RW, Brown AC, Jefferson CW, Jowett EC, Kirkham RV (eds) Sediment-hosted stratiform copper deposits. *Geological Association of Canada Special Paper* 36, pp 427-452.

Barra F, Broughton D, Ruiz J, Hitzman M (2004) Multistage mineralization in the Zambian Copperbelt based on Re-Os isotope constraints. *Geological Society of America Abstracts with Program*, vol 36 p516.

Cailteux J, Binda PL, Katekesha WM, Kampunzu AB, Intiomale MM, Kapenda D, Kaunda C, Ngongo K, Tshiauka T, Wendorff M (1995) Lithostratigraphical correlation of the Neoproterozoic Roan Supergroup from Shaba (Zaire) and Zambia, in the central African copper-cobalt metallogenic province; in: *Journal of African Earth Sciences,* vol. 19: 265-278.

Gustafson LB, Williams N (1981) Sediment-hosted stratiform deposits of copper, lead, and zinc: *Economic Geology 75th Anniversary Volume*, p. 139-178.

Hitzman M, Kirkham R, Broughton D, Thorson J, Selley D (2005) The sediment-hosted stratiform copper ore system: *Economic Geology 100th Anniversary Volume*, p. 609-642.

Kirkham RV (1989) Distribution, settings, and genesis of sediment-hosted stratiform copper deposits: *in* Boyle RW, Brown AC, Jefferson CW, Jowett EC, Kirkham RV (eds.), *Sediment-hosted Stratiform Copper Deposits,* Geological Association of Canada, Special Paper 36, p. 3–38.

Richards JP, Krogh TE, Spooner ETC (1988) Fluid inclusion characteristics and U-Pb rutile age of late hydrothermal alteration and veining at the Musoshi stratiform copper deposit, Central African Copper Belt, Zaire. *Economic Geology* 83, p.118-139.

Selley D, Broughton D, Scott R, Hitzman M, Bull S, Large R, McGoldrick P, Croaker M, Pollington N, Barra F (2005) A new look at the geology of the Zambian Copperbelt. *Economic Geology 100th Anniversary Volume,* p. 965-1000.

Torrealday HI, Hitzman MW, Stein HJ, Markley RJ, Armstrong R, Broughton D (2000) Re-Os and U-Pb dating of the vein-hosted mineralization at the Kansanshi copper deposit, Northern Zambia. *Economic Geology* 95, p. 1165-1170.

# Base metal ore deposit evolution and geodynamics in the Central African Copperbelt

Ph. Muchez, D. Brems, H. El Desouky, M. Haest & P. Vanderhaeghen
*Geodynamics & Geofluids Research Group, K.U.Leuven, Celestijnenlaan 200E, B-3001 Leuven, Belgium*

S. Dewaele
*Department of Geology and Mineralogy, Royal Museum for Central Africa, Leuvensesteenweg13, B-3080 Tervuren, Belgium*

W. Heijlen
*School of Earth and Environment, University of Leeds, Leeds, United Kingdom*

W. Mukumba
*Mopani Copper Mines Plc, Kitwe, Zambia*

ABSTRACT: Ore deposits in the Central African Copperbelt formed during several stages of the evolution of the Katanga sedimentary basin. The first mineralization phase occurred during diagenesis, either early or late depending on the ore district. A second major mineralization phase occurred during late Proterozoic metamorphism associated with the Lufilian orogeny (*e.g*. Nchanga deposit, Zambia). Several syn- to post-orogenic polymetallic and Cu-Ag deposits also occur in the Lufilian orogen (*e.g*. Kipushi and Dikulushi, DRC).

KEYWORDS: Copperbelt, geodynamics, sediment-hosted deposits

## 1 STRATIGRAPHY AND TECTONICS

The Katanga Supergroup is divided into the Roan, Nguba and Kundelungu Groups (Cailteux *et al.* 2005). Deposition of Roan sediments began following intrusion, uplift and erosion of the ~880Ma Nchanga granite, and ended around 750 Ma with deposition of the "Grand Conglomérat" glacial diamictite, which marks the base of the Nguba Group. The overlying Kundelungu Group is also marked by a basal diamictite ("Petit Conglomérat", ~620 Ma) and ends with the Plateaux Subgroup at ~500 Ma.

Early Katangan rifting led to the formation of a passive continental margin (Porada and Berhorst 2000). The Roan Group is made up of siliciclastic and carbonate sedimentary rocks and volcanic and plutonic mafic rocks emplaced in a continental rift. Gabbros, mafic lavas and pyroclastics present in the overlying Upper Roan and lower Mwashya Formations belong to a single syn-early Mwashya igneous event (Kampunzu *et al.* 2000). Key *et al.* (2001) date this magmatic period at 760 ± 5 Ma (U-Pb SHRIMP). During the Mwashya, rapid and differential subsidence occurred in the Roan platform (Porada & Berhorst 2000). The siliciclastics, carbonates and mafic igneous rocks of the Nguba are characteristic for a transition from a continental to a proto-oceanic rift system, comparable to the Red Sea (Kampunzu *et al*. 1991). Finally, the Kundelungu sedimentary rocks represent syn- to post-orogenic sedimentary deposits (Kampunzu & Cailteux 1999).

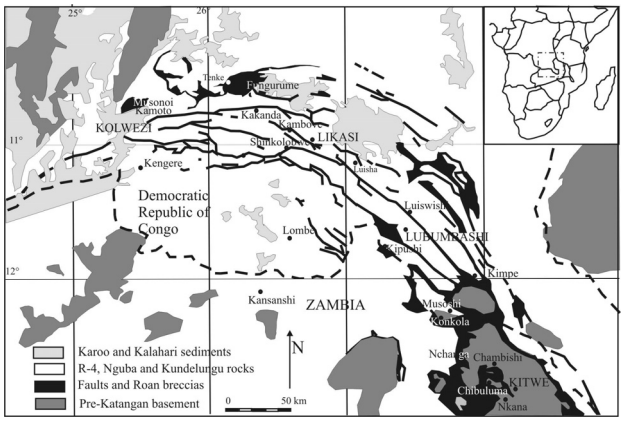


Figure 1. Location of mineral occurrences in the Copperbelt (modified after François, 1973)

The Katangan basin closed during the Lufilian orogeny, leading to the development of predominantly north-verging folds, thrusts and nappes (François 1973). Syn- to post-tectonic intrusives and rhyolites in central Zambia were dated by Hanson *et al.* (1993). Synorogenic granites yielded U/Pb zircon ages of 566 ± 5

Ma and 559 ± 18 Ma and a synorogenic rhyolite an age of 551 ± 18 Ma. The age of the post-orogenic rhyolite is 538 ± 1.5 Ma. Metamorphism associated with the Lufilian orogeny varied from amphibolite facies in Zambia to sub-greenschist grade in the northern part of the Lufilian arc in the Democratic Republic of Congo. SHRIMP U-Pb data of metamorphic monazite from the Chambishi basin provide ages of 592 ± 22 Ma, 531 ± 12 Ma and 512 ± 17 Ma, which correspond respectively to the ages of eclogite facies metamorphism, high-pressure talc-kyanite whiteschist metamorphism, and of a regional metamorphic and mineralization pulse (Rainaud *et al*. 2005). This study discusses the relationship between Copperbelt ore deposits and geodynamics, based on the literature and new observations.

## 2 RELATIVE AND ABSOLUTE TIMING OF ORE DEPOSITS

A detailed petrographic analysis has been carried out on the Cu-Co ore deposit of Musonoi and Kamoto (Fig. 1) in the Lufilian fold-and-thrust-belt (Dewaele *et al.* 2006b). The authors concluded that mineralization began early during diagenesis of the Lower Roan rocks with the precipitation of framboidal pyrite. Pyrite precipitation largely coincided with a first phase of dolomitisation. Dolomites formed as a primary precipitate in a sabkha environment and due to reflux of evaporated seawater (Bartholomé *et al*. 1973). This dolomite partly created a porous network that was subsequently occluded by the precipitation of quartz, carrolite, chalcopyrite, bornite, digenite and chalcocite. The ore minerals also occur disseminated in the host-rock, with chalcopyrite, and probably other ore sulphides replacing earlier formed pyrite. Large carrolite crystals deform the host-rock layering on a microscale and are much larger than the dispersed pyrite crystals observed. This suggests that carrolite precipitated in a non-consolidated host-rock. Anhydrite nodules are pseudomorphosed to dolomite, which itself was subsequently replaced by quartz and sulphides. Microthermometry of primary fluid inclusions in authigenic quartz associated with the first main ore stage indicates relatively high fluid temperatures (average homogenisation temperature of 160°C) and thus a deep origin of the metal-bearing fluid. Mineralization continued during burial as reflected in later generations of coarse-grained dolomite and sulphide minerals in veins and their surrounding host-rock. Replacement of anhydrite nodules and layers by dolomite, and the associated precipitation of sulphides and quartz have also been observed in the Zambian Copperbelt (*e.g*. Sweeney & Binda 1989). A diagenetic origin of the Konkola deposit is suggested by Re-Os dating of chalcopyrite in the deposit hangingwall at 816 ± 62 Ma (in Selley *et al*. 2005). This age predates the transition of the Roan to the Nguba at ~750 Ma, however, the error in the determination does not exclude a late Roan to early Nguba age.

In addition to the diagenetic mineralization, structural and petrographical studies show that several metal-rich deposits formed during and after the Lufilian orogeny. These deposits include Kipushi and Dikulushi in the Katangan Copperbelt (de Magnée & François 1988; Dewaele *et al*. 2006a) and Kansanshi and Nchanga in the Zambian Copperbelt (Torrealday *et al*. 2000, McGowan *et al.* 2003). A multistage system of diagenetic and orogenic mineralization is possibly present at Nkana-Mindola, where stratiform sulphides could have formed before folding, but where the major part of the ore deposit formed during folding and hydrofracturing post-dating the folding. Both at Chambishi and Nkana, thick mineralized quartz veins filled by quartz and coarse-grained sulphides occur along reverse faults (*e.g*. Annels 1989). A detailed study carried out by Greyling *et al*. (2005) indicates that the fluid inclusions from a lateral secretion quartz vein immediately post-dating stratiform copper mineralization have a diagenetic origin. A five point Re-Os isochron of sulphides from the Nkana, Chibuluma and Nchanga ore deposits yields an age of 583 ± 24 Ma (Barra *et al.* 2004). This age overlaps with the oldest biotite (~586 Ma) and monazite (~592 Ma) ages (Rainaud *et al*. 2005) and with synorogenic magmatic rocks (~560 Ma). However, also a younger Re-Os molybdenite age of 525.7 ± 3.4 Ma has been reported from Nkana (Barra *et al*. 2004).

Late hydrothermal alteration and veining at the Musoshi stratiform copper deposit in the Democratic Republic of Congo has been dated by U-Pb rutile and uraninite ages (Richards *et al.* 1988). Six rutile samples gave a U-Pb concordia upper intercept of 514 ± 2 Ma, which was confirmed by nine analyses of five uraninite vein samples that showed an age of 514 ± 3 Ma. This hydrothermal activity is interpreted to be related to the compressional deformation

and metamorphism associated with the Lufilian orogeny. The Kansanshi copper deposit in northern Zambia, containing high-angle, sheeted quartz-carbonate-sulphide veins with envelopes of disseminated sulphides, also has been dated. Re-Os dating of a molybdenite-monazite vein set indicates an age of 502.4 ± 1.2 Ma, 10 million years younger than the dominant chalcopyrite veins (512.4 ± 1.2 Ma; Torrealday *et al.* 2000). A major mineralization event occurred during and after peak metamorphism and mineralising fluids responsible for the formation of many of these deposits may have been metamorphic in origin.

## 3 RELATION BETWEEN GEODYNAMICS AND ORE DEPOSIT FORMATION

Sulphides occur disseminated in the host-rock, as replacement of dolomite pseudomorphs after anhydrite or as a first cement in pores in the dolomite host-rock (*e.g.* Kamoto-Principal, Musonoi and Luiswishi in the DRC; Dewaele *et al.* 2006; El Desouky *et al.* 2007) Depending on the ore district, they formed during early or late diagenesis. Ore deposition in the Zambian Copperbelt and possibly in Katanga was controlled by extensional faults cross-cutting the basement and Lower Roan (Annels 1989; Selley *et al.* 2005). These faults were mainly active during the early Roan, before deposition of the rocks host to ore (Selley *et al*. 2005). Recent modelling of fluid flow in extensional settings indicates that exhalative and near-surface ores are likely to form when extension ceases and the thermal structure becomes the driver for fluid flow (Oliver *et al*. 2006). Active extension or extensional reactivation of basin-bounding faults is generally destructive with respect to fluid upflow and generation of near-surface deposits.

An important period of magmatic activity, characterised by the formation of volcanic and pyroclastic rocks, occurred during early Mwashya time. Large lithologic and thickness variations suggest that differential subsidence took place during this period (François 1973). Therefore, it is plausible that this period with an increased geothermal gradient may have caused mineralization or remobilisation of earlier formed mineralization (Selley *et al*. 2005).

Petrographic and structural evidence and radiometric dating indicate that an important stage of ore deposition took place during metamorphism and tectonic activity between 580 and 510 Ma (Selley *et al* 2005). Metamorphic fluids were expelled within a compressional regime and mineral precipitation occurred along cleavage planes, in the hinges of anticlines, the core of synclines and in fractures cutting the folds. Finally, recent studies in the foreland also indicate that mineralization continued after the Lufilian orogeny (Dewaele *et al.* 2006a).

## REFERENCES


Annels A.E. (1989) Ore genesis in the Zambian Copperbelt, with particular reference to the northern sector of the Chambishi Basin. In: Boyle RW, Brown AC, Jefferson CW, Jowett EC, Kirkham RV (eds) Sediment-hosted stratiform copper deposits. *Geological Association of Canada Special Paper* 36, pp 427-452.

Barra F, Broughton D, Ruiz J, Hitzman M (2004) Multistage mineralization in the zambian Copperbelt based on Re-Os isotope constraints. T*he Geological Society of America, 2004 Denver Annual Meeting.* Abstracts with program vol 36 (5).

Bartholomé P, Evrard P, Katekesha F, Lopez-Ruiz J., Ngongo M. (1973) Diagenetic ore-forming processes at Kamoto, Katanga, Republic of the Congo. In: Amstutz GC, Bernard AJ (eds) *Ores in sediments*. Springer, Berlin, pp 21-41.

Cailteux JLH, Kampunzu AB, Lerouge C, Kaputo AK, Milesi JP (2005) Genesis of sediment-hosted stratiform copper-cobalt deposits, central African Copperbelt. *Journal of African Earth Sciences* 42: 134-158.

de Magnée I, François A (1988) The origin of the Kipushi (Cu, Zn, Pb) deposit in direct relation with a Proterozoic salt diaper. Copperbelt of Central Africa, Shaba, Republic of Zaïre. In: Friedrich GH, Herzig PM (eds) *Base Metal Sulfide Deposits.* Springer, Berlin, pp 74-93.

Dewaele S, Muchez Ph, Heijlen W, Boutwood A, Lemmon T, Tyler R (2006a). Reconstruction of the hydrothermal history of the Cu-Ag vein-type mineralization at Dikulushi, Kundelungu foreland, Katanga, D.R.Congo. *Journal of Geochemical Exploration* 89: 376-379.

Dewaele S, Muchez Ph, Vets J, Fernandez-Alonzo M, Tack L (2006b) Multiphase origin of the Cu-Co ore deposits in the western part of the Lufilian fold-and-thrust belt, Katanga (Democratic Republic of Congo). *Journal of African Earth Sciences* 46 : 455-469.

El Desouky H, Haest M, Muchez Ph, Dewaele S, Cailteux J, Heijlen W (2007) Fluid evolution in the Katanga Copperbelt, DRC. *This volume*.

François A (1973) L'extrémité occidentale de l'arc cuprifère Shabien. Etude géologique. *Mémoire du Département Géologique Gécamines, Likasi (République du Zaïre),* pp 1-65.

Greyling LN, Robb LJ, Master S, Boiron MC, Yao Y (2005) The nature of early basinal fluids in the Zambian Copperbelt: A case study from the

Chambishi deposit. *Journal of African Earth Sciences* 42: 159-172.

Hanson RE, Wardlaw MS, Wilson TJ, Mwale G (1993) U-Pb zircon ages from the Hook granite massif and Mwembeshi dislocation: Constraints in Pan-African deformation, plutonism, and transcurrent shearing in central Zambia. *Precambrian Research* 63: 189-209.

Kampunzu AB, Cailteux J (1999) Tectonic evolution of the Lufilian Arc during Neoproterozoic Pan African orogenesis. *Gondwana Research* 2, 401-421.

Kampunzu AB, Tembo F, Matheis G, Kapenda D, Huntsman-Mapila P (2000) Geochemistry and tectonic setting of mafic igneous units in the Neoproterozoic Katangan basin, central Africa: implications for Rodinia break up. *Gondwana Research* 3, 125-153.

Kampunzu AB, Tembo F, Matheis G, Kapenda D, Huntsman-Mapila P (2000) Geochemistry and tectonic setting of mafic igneous units in the Neoproterozoic Katangan basin, central Africa: implications for Rodinia break up. *Gondwana Research* 3: 125-153.

Key RM, Liyungu AK, Njamu, FM, Somwe V, Banda J, Mosley PN, Armstrong R.A. (2001) The western arm of the Lufilian Arc in NW Zambia and its potential for copper Mineralization. *Journal of African Earth Sciences* 33: 503-528.

McGowan RR, Roberts S, Foster RP, Boyce AJ, Coller D (2003) Origin of the copper-cobalt deposits of the Zambian Copperbelt: an epigenetic view from Nchanga. *Geology* 31: 494-500.

Oliver NHS, McLellan JG, Hobbs BE, Cleverley JS, Ord A, Feltrin L (2006) Numerical models of extensional deformation, heat transfer, and fluid flow across basement-cover interfaces during basin-related mineralization. *Economic Geology* 101: 1-31.

Porada H, Berhorst V (2000) Towards a new understanding of the Neoproterozoic-Early Palaeozoic Lufilian and northern Zambezi Belts in Zambia and the Democratic Republic of Congo. *Journal of African Earth Sciences* 30: 727-771.

Rainaud C, Master S, Armstrong RA, Phillips D, Robb LJ (2005) Monazite dating and $^{40}Ar$-$^{39}Ar$ thermochronology of metamorphic events in the Central African Copperbelt during the Pan-African Lufilian Orogeny. *Journal of African Earth Sciences* 42: 183-199.

Richards JP, Krogh TE, Spooner ETC (1988) Fluid inclusion characteristics and U-Pb rutile age of late hydrothermal alteration and veining at the Musoshi stratiform copper deposit, Central African Copper Belt, Zaire. *Economic Geology* 83: 118-139.

Selley D, Broughton D, Scott R, Hitzman M, Bull S, Large R, McGoldrick P, Croaker M, Pollington N, Barra F (2005) A new look at the geology of the Zambian Copperbelt. *Economic Geology 100th Anniversary Volume*, pp 965-1000.

Sweeney MA, Binda PL (1989) The role of diagenesis in the formation of the Konkola Cu-Co orebody of the Zambian Copperbelt. In: Boyle RW, Brown AC, Jefferson CW, Jowett EC, Kirkham RV (eds) Sediment-hosted stratiform copper deposits. *Geological Association of Canada Special Paper* 36, pp 499-518.

Torrealday HI, Hitzman MW, Stein HJ, Markley RJ, Armstrong R, Broughton D (2000) Re-Os and U-Pb dating of the vein-hosted mineralization at the Kansanshi copper deposit, Northern Zambia. *Economic Geology* 95: 1165-1170.

# Fluid evolution in the Katanga Copperbelt, DRC

H. El Desouky, M. Haest & Ph. Muchez
*Geodynamics & Geofluids Research Group, K.U.Leuven, Celestijnenlaan 200E, B-3001 Leuven, Belgium*

S. Dewaele
*Department of Geology and Mineralogy, Royal Museum for Central Africa, Leuvensesteenweg 13, B-3080 Tervuren, Belgium*

J. Cailteux
*Department of Research and Development, Groupe G. Forrest International, Lubumbashi, Congo*

W. Heijlen
*School of Earth and Environment, University of Leeds, Woodhouse Lane, Leeds, LS2 9JT, UK*

ABSTRACT: Three main mineralization phases in the Lufilian EFTB and two phases in the Lufilian foreland can be recognized. The first phase in the EFTB is mainly stratiform, has a diagenetic origin and is caused by a hydrothermal fluid with a minimum temperature of 105˚C and salinity between 8 and 18 wt% NaCl eq. The second is a late diagenetic to syn-orogenic phase overprinting the earlier one and caused by a fluid with a minimum temperature of 320˚C and salinity between 38 and 47 wt% NaCl eq. The final phase in the EFTB is late to post-orogenic and represented by vein-type polysulphide ore deposits (e.g. Kipushi). Although the early sulphide stages of this third phase are formed from a fluid with similar temperature and salinity to the syn-orogenic fluid, the youngest stages were formed from fluids with lower temperature and salinity. In the Lufilian foreland, the first mineralization phase is caused by a diagenetic to syn-orogenic fluid with a temperature of 80 to 170˚C and a salinity of 18 to 24 wt% $CaCl_2$ eq. The second phase is related to a fluid with a varying temperature (45 to 180˚C) and salinity (1.9 to 13 wt% NaCl eq.).

KEYWORDS: Copperbelt, fluid inclusion microthermometry, Lufilian orogen, stratiform ore deposits, vein-type deposits

## 1 INTRODUCTION

The Central African Copperbelt in Zambia and the Democratic Republic Congo (DRC) forms one of the largest metallogenic districts of the world. The Congolese part of the Copperbelt in Katanga represents the main part of the External Fold-and-Thrust Belt (EFTB) portion of the arcuate-shaped NW-SE elongated and NE directed Lufilian arc. To the NE of the Lufilian arc, a triangular-shaped area is located (the Lufilian foreland).

The EFTB is characterised by the presence of stratiform Cu-Co mineralization concentrated in two main ore bodies (upper and lower), hosted in the lower part of the late Proterozoic Mines Subgroup (Cailteux *et al.* 2005). Later vein-type mineralizations are commonly associated with the stratiform mineralization or form their own deposits (*e.g.* Kipushi). The foreland is characterised by stratiform and vein-type Cu-Ag mineralization (*e.g*. Dikulushi).

The aim of this research is to study the evolution of the temperature and chemistry of the mineralizing fluids in the Congolese Copperbelt and Lufilian foreland. The study focuses on four deposits in the Copperbelt (Luiswishi, Kamoto, Musonoi and Kipushi) and two areas in the foreland (Lufukwe and Dikulushi).

## 2 GEOLOGIC SETTING

The Katanga Supergroup, which hosts Cu-Co mineralization in the Lufilian arc and Cu-Ag mineralization in the foreland, is ~5 to 10 km thick and is commonly sub-divided into three Groups (Roan, Nguba and Kundelungu), based on the regional occurrence of two diamictites (Cailteux *et al*. 2005). The Roan Group is mainly composed of dolomites and dolomitic siltstones, while the Nguba and Kundelungu Groups are composed of clastic sedimentary rocks with few carbonate units. The Katanga Supergroup was deformed during the Lufilian orogeny (Cailteux *et al*. 2005).

The Luiswishi deposit is located ~26km NW of Lubumbashi, while Kamoto and Musonoi belong to the Kolwezi area ~200km NW of

Lubumbashi. In the two areas, the Cu-Co ores are hosted in the Mines Subgroup of the Roan Group. The Kipushi Cu-Zn deposit is located ~20km west of the city of Lubumbashi, only few hundred meters away from the border with Zambia. The Cu-Zn mineralization is mainly occurred in carbonates from the Lower Nguba (Likasi Subgroup).

The Lufukwe anticline is located in the Lufilian foreland, ~200km NE of Lubumbashi. The anticline hosts stratiform Cu-Ag mineralization concentrated in the lower 10 to 15m of the Monwezi sandstone (Nguba Group). Dikulushi is a Cu–Ag vein-type deposit, situated ~80km N of Lufukwe and ~300km NE of Lubumbashi. Mineralization is hosted in sediments of the Kalule Subgroup of the Kundelungu Group.

## 3 PETROGRAPHY AND FLUID INCLUSION MICROTHERMOMETRY

### 3.1 *External Fold-and-Thrust Belt (EFTB)*

At Luiswishi, Kamoto and Musonoi the Cu-Co mineralization formed after early diagenetic pyrite and widespread dolomitization of the host rock. The ore minerals are dominantly carrolite, bornite, digenite and chalcocite at Kamoto and Musonoi, and dominantly chalcopyrite and carrolite at Luiswishi. The ore minerals are always associated with a quartz phase.

Two Cu-Co mineralization types were recognised at Luiswishi, Kamoto and Musonoi. The first is stratiform and represented by disseminated sulphides that are mainly concentrated in mm to cm thick lenticular bands and in nodules with dolomite and authigenic quartz pseudomorphs after anhydrite and gypsum. This stratiform mineralization is mainly hosted in the lower and upper ore bodies (Cailteux *et al.* 2005). In the second Cu-Co mineralization type, the ore minerals are concentrated in mm to cm thick straight to irregular veins that crosscut the bedding and also occur associated with cement in a tectonic breccia that was likely formed during the Lufilian orogeny. The veins and the breccia cement are composed of dolomite and quartz. This type of mineralization is not restricted to the sediments of the upper and lower ore bodies.

In the stratiform mineralization, two types of lenticular bands and nodules can be distinguished. In type one (I), dolomite precipitated first and was replaced by microflamboyant (Milliken 1979) authigenic quartz and sulphides. All crystals are anhedral, fine- to medium-grained. In type two of stratiform lenticular bands and nodules (II), the authigenic quartz and sulphides precipitated before dolomite and the crystals are coarse-grained, free-growing euhedral to subhedral. The first type of lenticular bands and nodules is most common at Kamoto and Musonoi and fairly represented at Luiswishi. The second type of bands and nodules and the second type of Cu-Co mineralization (veins and breccias) are common at Luiswishi, but less common at Kamoto and Musonoi.

A microthermometric study has been carried out on authigenic quartz associated with Cu-Co mineralization in type I lenticular bands and nodules at Kamoto and Musonoi. Small (≤5 μm) primary two phase (L+V) aqueous fluid inclusions are present in the quartz and show a first melting temperature (Tfm) around –20°C, indicative for an $H_2O$-NaCl system. The final ice melting temperature ($Tm_{ice}$) ranges between –11.8 and -8.4°C (n =7) for Kamoto and between -14.8 and -5.4°C (n =9) for Musonoi. These values correspond to a salinity of 12.2 to 15.2 and 8.4 to 18.4wt% NaCl eq. respectively. The homogenization temperature (Th) varies between 127 to 192°C (n =11) at Kamoto and 105 to 188°C (n =6) at Musonoi.

At Luiswishi, microthermometric analyses were performed on authigenic quartz in mm- and cm-sized nodules of type II and in quartz associated with the second Cu-Co mineralization type (veins and breccia). Primary fluid inclusions (up to 15μm) in these quartz phases are three phase (L+V+S) aqueous inclusions. The solid phase is mostly halite with few large inclusions that enclose small prismatic and rounded highly birefringent crystals in addition to halite. The homogenization (Th) and halite dissolution ($Ts_h$) temperatures for inclusions from the type II nodules are between 324 and 419°C (n =42) and between 305 and 396°C (n =93) oC respectively. Similar Th (341 to 439 °C; n =45) and $Ts_h$ (311 to 391°C; n =78) values are obtained for the inclusions in the veins. The inclusions in the quartz cementing the breccia show Th values between 359 and 427 °C (n =37) and $Ts_h$ values between 328 and 373 °C (n =69). In an $H_2O$-NaCl system, these $Ts_h$ values correspond to a salinity of 38.6 to 47 wt% NaCl eq. in the nodules, of 39 to 46.5 wt% NaCl eq. in the veins and of 40.4 to 44.6 wt% NaCl eq. in the breccia.

The Kipushi Cu-Zn deposit formed along a

late to post-tectonic fault zone. It occurs as vein-type mineralization along the fault zone and as associated stratiform lodes at lithological contacts. Dolomite and quartz associated with the main stage of sulphide mineralization at Kipushi contain primary assemblages of multi-phase fluid inclusions having L+V+H and trapped, rounded solid inclusions. Microthermometric study of these inclusions is hampered by the fact that most decripitate before Th or even Tsh. Therefore, minimum Th of such assemblages (for inclusions that homogenised before decrepitation) are between 229 and 324°C (n =18), with Tsh between 149 and 360°C (n =35), *i.e.* salinities between 29.6 and 43.3 wt% NaCl eq. Late sphalerite, which formed as the youngest ore mineral, has L+V primary inclusions with Th between 80 and 167°C (n = 19). In these inclusions hydrohalite was always the latest phase to melt during cryometric runs, at metastable temperatures >0.1°C. This indicates salinities > 23.2 wt% NaCl eq.

### 3.2 *Lufilian foreland*

At the Lufukwe anticline the stratiform Cu-Ag mineralization is interpreted to be of post-orogenic origin (El Desouky *et al.* 2006). The Monwezi sandstone (host rock) underwent strong compaction and cementation by authigenic quartz, followed by intense feldspar dissolution, which resulted in a well-developed secondary porosity (El Desouky *et al.* 2006). Copper sulphide minerals are concentrated in the dissolution cavities and partially replace the detrital grains. The ore minerals are hypogene chalcopyrite, bornite and chalcocite and supergene digenite, covellite and little native copper.

Microthermometric analyses were carried out on primary aqueous fluid inclusions in pre-mineralization authigenic quartz and in secondary trails crosscutting both detrital and authigenic quartz. The trails are preferentially developed near to and radiating from ore minerals, hence they likely developed from micro-crack healing during mineralization. The primary fluid inclusions in the authigenic quartz are two phase (L+V) aqueous inclusions with Th between 80 and 130°C (n =14) and Tfm values below -40°C (likely $H_2O$-NaCl-$CaCl_2$ composition). $Tm_{ice}$ values are between -16.4 and -24.8°C (n =10), corresponding to a salinity between 18.8 and 23.4 wt.% $CaCl_2$ eq. In contrast, the two phase (L+V) aqueous fluid inclusions in secondary trails have a Tfm around -20°C and $Tm_{ice}$ between -1.1 and -4.9°C (n =38), which corresponds to salinity between 1.9 and 7.7 wt.% NaCl eq. The Th is between 120 and 180°C (n=74). The secondary inclusions are characterised by increasing Th with increasing salinity. This trend indicates the mixing of a higher salinity mineralizing fluid with a colder low salinity fluid.

The Dikulushi ore deposit consists of two vein-type mineralization phases: (1) a polysulphide assemblage (Zn-Pb-Fe-Cu-As) and (2) a Cu-Ag assemblage. The polysulphide phase is interpreted to have formed during the Lufilian orogeny, while the vein Cu-Ag phase is thought to have a post-orogenic origin (Haest *et al.* 2007). Sphalerite and coarse-grained dolomite, associated with the syn-orogenic polysulphide assemblage, contain primary two-phase (L+V) aqueous fluid inclusions. The Tfm values of these inclusions are below -40°C (likely $H_2O$-NaCl-$CaCl_2$ composition). The $Tm_{ice}$ ranges between -26.1 and -18.4°C (n =26), corresponding to a salinity between 20.2 and 24 wt% $CaCl_2$ eq. The Th is varying between 135 and 172°C (n =33).

Quartz, calcite and barite have been investigated from post-orogenic Cu-Ag mineralization. Two-phase (L+V) aqueous primary fluid inclusions show Tfm values around -25°C, indicative for another monovalent cation in addition to NaCl ($H_2O$-NaCl-X composition). The $Tm_{ice}$ varies between -9.1 and -3.9°C (n =57), indicative for a salinity between 6.3 and 13.0 wt% NaCl eq. The Th values are between 46 and 82°C (n =35).

## 4 DISCUSSION AND CONCLUSION

The results of the fluid inclusion microthermometry are summarized in Table 1. The data presented indicate the presence of three main mineralization phases in the Lufilian EFTB and two mineralization phases in the Lufilian foreland. The first phase in the EFTB resulted in the first stratiform Cu-Co mineralization type (type I lenticular bands and nodules). This phase formed due to the migration of a fluid with a temperature above 105°C and a salinity between 8.4 and 18.4 wt% NaCl eq. The presence of early pervasive dolomite before the Cu-Co sulphides is interpreted as an indication for an early to intermediate diagenetic origin of this first main stratiform mineralization phase.

The similarity in Th and salinity of the fluid inclusions associated with the Cu-Co minerali-

zation in type II nodules, veins and breccia indicates that they formed from a similar mineralising fluid with a minimum temperature of 320 $^{o}$C and salinity between 38 and 47 wt% NaCl eq. This fluid caused the second Cu-Co mineralization phase in the EFTB, which is represented by the second stratiform mineralization type (type II lenticular bands and nodules) and the second type of Cu-Co mineralization (veins and breccia). This later mineralizing period has probably a late diagenetic (*e.g*. pseudomorphs of type II nodules) to syn-orogenic (tectonic breccia) origin. The very high temperature of this fluid points to a deep basinal origin, likely migrating upwards from the basement, or to a hydrothermal fluid heated by pre- or syn-orogenic magmatic activity. It is possible that this fluid introduced metals and/or remobilised the disseminated mineralization of the earlier phase and re-precipitated them in economic ore deposits (*e.g.* Luiswishi). Although the ores of the first main mineralization phase are generally limited to the lower and upper ore bodies, the ores of the second phase occur both within and outside of the ore bodies. When the two phases occur together, the second phase severely overprints the earlier one (*e.g*. Luiswishi). The major vein-type Cu-Zn deposit of Kipushi has fluid inclusion characteristics (Th and salinity) similar to the syn-orogenic fluids, although later mineralization phases from this deposit tend to show a decrease in salinity and temperature. However, new Rb-Sr and Re-Os dating studies on main stage sulphides gave concordant ages of ~450Ma (Schneider *et al*. 2007), which is well after the main phase of Lufilian deformation and metamorphism.

Table 1. Summary of fluid inclusion results:

| | | Locality | Salinity | Th (°C) |
|---|---|---|---|---|
| Post-orog | Arc | Kipushi (late stage) | > 23.2 [(a)] | 80 - 167 |
| | | Kipushi (early stage) | 29.6 - 43.3 [(a)] | 229 - 324 |
| | For. | Dikulushi (Cu-Ag) | 6.3 - 13.0 [(a)] | 46 - 82 |
| | | Lufukwe (stratiform Cu-Ag) | 1.9 - 7.7 [(a)] | 120 - 180 |
| Syn-orog | Arc | Luiswishi (breccia) | 40.4 - 44.6 [(a)] | 359 - 427 |
| | | Luiswishi (veins) | 39.0 - 46.5 [(a)] | 341 - 439 |
| | | Luiswishi (nodules II) | 38.6 - 47.0 [(a)] | 324 - 419 |
| | For. | Dikulushi (polysulphide) | 20.2 - 24.0 [(b)] | 135 - 172 |
| | | Lufukwe (pre-mineralization) | 18.8 - 23.4 [(b)] | 80 - 130 |
| Pre-orog | Arc | Kamoto (nodules I) | 12.2 - 15.2 [(a)] | 127 - 192 |
| | | Musonoi (nodules I) | 8.4 - 18.4 [(a)] | 105 - 188 |

(a) wt% NaCl eq. (b) wt% $CaCl_2$ eq. orog = orogenic, Arc = EFTB

The first mineralization phase in the Lufilian foreland is characterised by a saline (18.8 to 24 wt% $CaCl_2$ eq. hydrothermal fluid with a temperature of 80 to 130$^{o}$C. Although the fluid was present during burial (*e.g*. Lufukwe) it seems only to have caused mineralization during the Lufilian orogeny (*e.g*. the polysulphide phase at Dikulushi). The second phase in the Lufilian foreland is represented by post-orogenic stratiform and vein-type Cu-Ag mineralization, which are related to a mineralizing fluid with a varying temperature (46 to 180$^{o}$C) and salinity (1.9 to 13 wt.% NaCl eq.).

## ACKNOWLEDGEMENTS

The research of H. El Desouky and M. Haest was financed by the Katholieke Universiteit Leuven, Belgium. H. Nijs carefully prepared the thin, polished and doubly polished sections. Anvil Mining Congo and the Forrest Group Company are thanked for their support, access to ore deposits and availability of the samples.

## REFERENCES

Cailteux JLH, Kampunzu AB, Lerouge C, Kaputo AK, Milesi JP (2005) Genesis of sediment-hosted stratiform copper–cobalt deposits, central African Copperbelt. J*ournal of African Earth Sciences* 42: 134-158.

El Desouky H, Muchez Ph, Dewaele S, Boutwood A, Tyler R (2006) Late diagenetic to post-orogenic origin of the stratiform Cu mineralization at Lufukwe, Lufilian foreland, Democratic Republic Congo. *Poster and abstract on DVD-ROM, SEG* 2006 Conference Proceedings, 14-16 May 2006, Colorado, USA.

Haest M, El Desouky H, Muchez Ph and Dewaele S (2007) Contributions from structural analysis and remote sensing to the timing of mineralization in the Lufilian belt and its foreland. *This volume*.

Milliken K (1979) The silicified evaporite syndrome-two aspects of silicification history of former evaporite nodules from southern Kentucky and northern Tennessee. *Journal of Sedimentary Petrology* 49: 245-256.

Schneider J, Melcher F, Brauns M (2007) Concordant ages for the carbonate-hosted Kipushi base metal deposit from direct Rb-Sr and Re-Os dating of sulphides. *This volume.*

# Contributions from structural analysis and remote sensing to the timing of mineralization in the Lufilian arc and its foreland.

M. Haest, H. El Desouky & Ph. Muchez
*Geodynamics & Geofluids Research Group, K.U. Leuven, Celestijnenlaan 200E, bus: 2408, B-3001 Heverlee, Belgium*

S. Dewaele
*Department of Geology and Mineralogy, Royal Museum for Central Africa, Leuvensesteenweg13, B-3080 Tervuren, Belgium*

ABSTRACT: The Lufilian arc and its foreland host numerous stratiform and vein-type Cu mineralizations that formed during different stages. The main phase of the stratiform Cu-Co mineralization formed during diagenesis prior to the Lufilian orogeny. The Lufilian orogeny was characterised by folding and thrusting that extended north into the foreland. The folds were crosscut by faults at an angle to the fold axis. These oblique faults were preferential sites for vein-type polysulfide mineralization in the Lufilian arc and its foreland. NE-oriented faults developed subsequently and these were favourable fluid conduits for remobilisation and enrichment of the former mineralization.

KEYWORDS: Copperbelt, structural analysis, remote sensing, geodynamics

## 1 INTRODUCTION

The Lufilian arc in D.R.Congo and Zambia forms one of the largest Cu provinces known on earth. It includes stratiform Cu-Co (e.g. Kamoto and Musonoi) and high-grade Cu-Pb-Zn-Fe-Ag vein-type deposits (e.g. Kipushi, Lombe and Kengere). The Lufilian foreland, north of the Lufilian arc, is characterised by minor stratiform Cu-Ag mineralization (*e.g.*. Lufukwe) and some high-grade vein-type Cu-Ag deposits (*e.g.* Dikulushi) (fig. 1).

The aim of the current study is to reconstruct a sequence of formation for the different types of mineralization in the Lufilian fold-and-thrust belt and its foreland. This sequence is based on the structural setting of some selected mineralization, which is obtained from remote sensing analysis at Dikulushi and Lufukwe, from detailed structural analysis on the field at Dikulushi, and from the available literature.

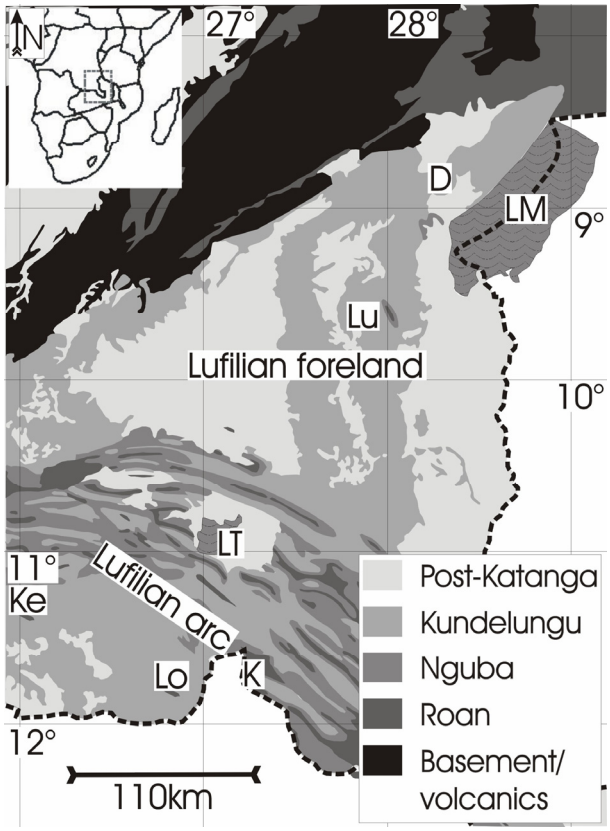


Fig. 1. Geological map of the southern part of Katanga (Ke: Kengere; Lo: Lombe; K: Kipushi; Lu: Lufukwe; D: Dikulushi; LT: Lake Tschangalele; LM: Lake Mweru) (Modified after Lepersonne, 1974).

## 2 GEOLOGIC SETTING

The Lufilian arc and its foreland are composed of sediments belonging to the Katanga Supergroup. The Katanga Supergroup is a ~7km thick sequence that is subdivided in three

groups, based on the regional occurrence of two diamictites.

Sedimentation of the Roan Group started after intrusion and erosion of the Nchanga granite (877±11 Ma) (Armstrong *et al*. 2005). The Roan Group consists of dolomites and dolomitic siltstones, with carbonaceous shales and fine pyroclastic layers in the upper part. The Nguba, with the "Grand Conglomérat" at its base, was deposited on top of the Roan after ~750 Ma. The Nguba and the overlying Kundelungu Groups are separated from each other by the "Petit Conglomérat", which was deposited around ~620 Ma. Both groups contain dominantly siliciclastic rocks, with few carbonate layers, above the two diamictites. The top of the Kundelungu consists of coarse-grained sandstones (~Plateaux Subgroup) that were deposited after 573±5 Ma.

The Lufilian orogeny was characterised by a northeast-oriented transport direction, with folding and thrusting in the Lufilian arc and its foreland (Trefois & Fernandez 2000). At the end of the Lufilian orogeny the folds were crosscut by faults at an angle to the axial surfaces (François 1974).

## 3 MINERAL DEPOSITS

### 3.1 *Lufilian foreland*

#### 3.1.1 Stratiform mineralization

Stratiform Cu-Ag mineralization at Lufukwe is contained in the Monwezi sandstone of the Nguba Group. This sandstone underwent first a

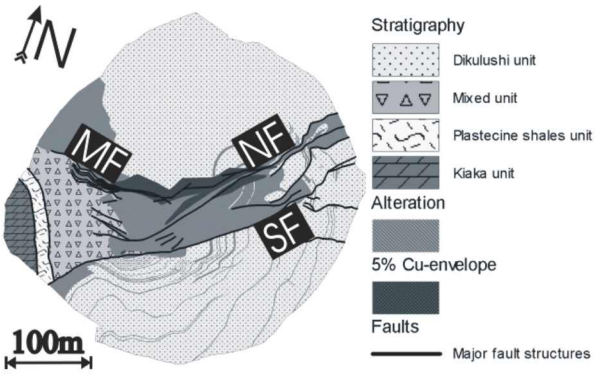


Fig. 2. Geological map of the Dikulushi quarry, with the 5% Cu-envelope, based on borehole data and the alteration (MF: Main fault corridor; NF: Northern fault; SF: Southern fault).

phase of compaction and silica cementation, followed by feldspar dissolution that created a secondary porosity. In this secondary porosity developed the mineralization. Satellite image interpretation shows that the NW-oriented Lufukwe anticline is crosscut by WNW-oriented strike-slip faults that displace the layers from the Katanga Supergroup, except those of the Plateaux subgroup. Only strike-slip faults, with an overall NE- to ENE-orientation crosscut the Plateaux subgroup. The highest grade bore hole intersections are close to NE- to ENE-oriented faults, which suggests an association of the mineralization with these strike-slip faults.

#### 3.1.2 Vein-type mineralization

The Dikulushi Cu-Ag deposit is situated at the north-eastern end of the Dikulushi anticline. Four lithologically distinct units are observed in the quarry (Dikulushi unit, Mixed unit, Plastecine shales Unit, and Kiaka Unit, fig. 2), which belong to the Kundelungu Group. The bedding in the Dikulushi unit has a mean orientation of ~098/48. It becomes irregular, in a strongly faulted zone around the mineralization (fig. 2).

Three separate groups of layer discordant faults are observed. The first group of sub vertical NNW-oriented faults are covered with slickenlines pointing to a dip-slip movement. The second group of steeply south-dipping (~70°) EW-oriented faults build up the Main fault corridor (MF in fig. 2) and part of these faults underwent a reverse oblique-slip movement. The third group of discordant faults are steeply south-dipping (~70°) NE-oriented faults. These faults form a NE-oriented fault corridor that is bordered to the north by the Northern fault (NF in fig. 2) and to the south by the Southern fault (SF in fig. 2). The Southern fault underwent an important phase of dextral strike-slip movement.

The Dikulushi ore body is positioned in the zone between the Main fault corridor (MF) and the Northern fault (NF). It has an ENE-orientation and dips 70° to the southeast. It remains open to a depth of 400m and originated from two distinct mineralization phases. The first polysulphide Cu-Fe-Pb-Zn-As mineralization phase precipitated in a complex set of EW- and NE-oriented faults and is dominantly observed in the western part of the quarry. At depth this mineralization extends further to the east. The polysulphide mineralization contains quartz with an undulose extinction, saddle dolomite, and calcite with bent twins as gangue minerals. The second phase of mineralization is dominantly located near the surface, a1ong NE-

oriented faults in the east of the quarry that cut through the set of EW- and NE-oriented faults and contain an orthorhombic chalcocite, with a high Ag-content. At depth, this orthorhombic chalcocite surrounds remnant blebs of bornite. Calcite without bent twins, quartz, and barite are associated with the orthorhombic chalcocite.

### 3.2 *Lufilian fold- and thrust-belt*

#### 3.2.1 Stratiform mineralization

The stratiform Cu-Co mineralization at Kamoto and Musonoï mainly occurs in two separate levels in the Mines Subgroup of the Roan Group. The main phase of the stratiform mineralization is interpreted to have formed during diagenesis, before the Lufilian orogeny (Bartholomé *et al*. 1972, Dewaele *et al.* 2006).

#### 3.2.2 Vein-type mineralization

The Zn-Cu-Pb-Ag mineralization at Kipushi is located near the western end of the Kipushi anticline. This mineralization is associated with the steeply west-dipping (~70°) NNE-oriented Kipushi fault that cuts across the WNW-ESE trend of the anticline. The hanging wall west of the fault consists of shales and sandstones, which belong to the Kundelungu Group. The footwall consists of the dolomitised Kakontwe limestone and the "Série Récurrente", belonging to the Nguba Group. The Kipushi ore body is located along the Kipushi fault for a length of 200 to 500m and extends to a depth below 1800m (De Magnée & François 1988).

The ore body developed during different mineralization stages which broadly change from early Zn-dominated to later Cu-dominated. The Cu-bearing mineralization remobilised certain parts of the Zn-bearing mineralization and formed during two separate phases. A Co-rich chalcopyrite with molybdenite precipitated first and a Ag-rich bornite precipitated later. At the surface malachite and chalcocite with a high Ag content are present. At depth bornite and chalcopyrite dominate (Intiomale & Oosterbosch 1974).

The Pb-Zn mineralization at Kengere and the Pb-Zn-Cu-Ag mineralization at Lombe are situated along NS- and NNE-oriented faults respectively. Both faults crosscut folds, with an axial breccia (Unrug 1988).

## 4 MINERALIZATION IN THE LUFILIAN ARC AND ITS FORELAND

The main phase of Cu-Co mineralization in the stratiform deposits of Kamoto and Musonoi developed during diagenesis (Bartholomé *et al.* 1972. The Cu-Co mineralization has, however, been overprint by later phases (Bartholomé *et al.* 1972, Dewaele *et al.* 2006).

The Lufilian orogeny began after deposition of the major part of the Kundelungu sediments and led to folding and thrusting in the Lufilian arc. It also resulted in the formation of anticline structures in the Lufilian foreland, which are interpreted as the surface expressions of detachments at depth (Trefois & Fernandez 2000). Injection of the Plastecine shales at the contact between the Kiaka and the Dikulushi units brecciated and folded the overlying units. This injection lies subparallel to the axial surface of the Dikulushi anticline. As such, the injection of the Plastecine shales could be derived from an underlying detachement that formed the Dikulushi anticline. Similar detachments developed in the Lufilian belt. Dechow & Jensen (1965) proposed that the southern limb of the Kipushi anticline was thrust on the northern limb, based on the observed axial breccia. The vein-type deposits of Lombe and Kengere are also associated with axial breccias that could be the surface expressions of such detachment faults. The folds were crosscut by faults at an angle to their axial surfaces at the end of the Lufilian orogeny (François 1974) or possibly postdating the Lufilian orogeny. The mineralizations of Kipushi, Lombe and Kengere in the Lufilian belt and of Dikulushi in the Lufilian foreland are all positioned along such crosscutting faults.

The orthorhombic, Ag-rich chalcocite of the second mineralization phase at Dikulushi occurs associated with NE-oriented faults. The polysulphides of the first mineralization phase probably became remobilised and enriched during the second phase. The remobilisation and enrichment are indicated by the remnant bornite blebs surrounded by chalcocite at depth and the high Ag-content of the orthorhombic chalcocite respectively. The stratiform mineralization at the Lufukwe anticline is associated with subparallel NE- to ENE-oriented faults. This mineralization also contains Ag, in addition to Cu. Thus, the structural setting and the mineralogy of the mineralization at the Lufukwe anticline and the second mineralization at Dikulushi are

similar. The upper parts of the mineralization at Kipushi also are reported to be rich in Ag (Intiomale & Oosterbosch, 1974).

## 5 CONCLUSIONS

Stratiform Cu-Co mineralization in the Lufilian belt mainly occurs in two distinct levels in the Mines Subgroup. The main phase of the Cu-Co mineralization formed during diagenesis before the Lufilian orogeny.

The Lufilian orogeny developed folds and thrusts that were afterwards crosscut by faults at an angle to the axial surfaces. Along these faults developed polymetallic (Zn-Cu-Pb) vein-type mineralization (Kipushi – Lombe – Kengere) in the Lufilian arc.

Another possibly related (?) phase of dominantly Cu-Zn-Pb mineralization at Dikulushi in the Lufilian foreland is similarly associated with NE- and EW-oriented faults that crosscut a fold at an angle to its axial surface.

Subsequent remobilisation produced a Cu-Ag rich mineralization along NE-oriented faults at Dikulushi and in the Lufukwe anticline in the foreland and at Kipushi in the Lufilian arc.

## ACKNOWLEDGEMENTS

Prof. Dr. Ali Aït Kaci, Mr. Roger Tyler, Mr. Nick Franey, Mrs. Amanda Boutwood and Mr. Terry Lemmon of Anvil Mining are thanked for their geologic expertise and the logistic support during the different field surveys to Dikulushi.

## REFERENCES

Armstrong RA, Master S, Robb LJ (2005) Geochronology of the Nchanga Granite, and constraints on the maximum age of the Katanga Supergroup, Zambian Copperbelt. *Journal of African Earth Sciences* 42: 32-40.

Bartholomé P, Evrard P, Katekesha F, Lopez-Ruiz J and Ngongo M (1972) Diagenetic ore-forming processes at Kamoto, Katanga, Republic of the Congo. In: *Amstutz GC and Bernard AJ (eds), Ores in Sediments*: Berlin, Springer-Verlag, p. 21-41.

De Magnée I, François A (1988) The origin of Kipushi (Cu, Zn, Pb) deposit in direct relation with a Proterozoic salt diapir. Copper belt of Central Africa, Shaba, Republic of Zaïre. In: Friedrich GH, Herzig PM (eds), *Base metal sulfide deposits. Springer-Verlag,* Berlin, pp 74-93.

Dechow E, Jensen ML (1965) Sulfur isotopes of some Central African sulfide deposits. *Economic Geology* 60: 894-941.

Dewaele S, Muchez P, Vets J, Fernandez-Alonzo M, Tack L (2006) Multiphase origin of the Cu-Co ore deposits in the western part of the Lufilian fold-and-thrust belt, Katanga (Democratic Republic of Congo). *Journal of African Earth Sciences* 46: 455-469.

François A (1974) Stratigraphie, tectonique et minéralisations dans l'arc cuprifère du Shaba (République du Zaïre). In : Bartholomé P (ed) Gisements Stratiformes et Provinces Cuprifères. Liège, *La Société Géologique de Belgique*, pp 79-101.

Intiomale MM, Oosterbosch R (1974) Géologie et Géochimie du gisement de Kipushi, Zaïre. In : Bartholomé P (ed), Gisements Stratiformes et Provinces Cuprifères. *La Société Géologique de Belgique,* Liège, pp 123-164.

Lepersonne J (1974) Carte Géologique du Zaïre au 1:2.000.000 et notice explicative. In : Rapport annuels, 1975. Tervuren, *Royal museum for Central Africa.*

Trefois P, Fernandez M (2000) Updating the geological map of Katanga (D.R. of Congo) with space imagery combined to archive data compilations. *Fourteenth International Conference on Applied Geologic Remote Sensing: Las Vegas, Nevada*, Veridian ERIM International.

Unrug R (1988) Mineralization Controls and Source of Metals in the Lufilian Fold Belt, Shaba (Zaïre), Zambia, and Angola. *Economic Geology* 83: 1247-1258.

# A Re-Os study of noble metal-rich black shales from the Polish Kupferschiefer

J. Pašava & A. Vymazalová
*Czech Geological Survey, Klárov 131/3, 118 21 Praha 1, Czech Republic*

J. Mao
*Institute of Mineral Resources, Chinese Academy of Geological Sciences, Beijing 100037, China*

A. Du, W. Qu
*Institute of Rock and Mineral Analyses, Chinese Academy of Geological Sciences, Beijing 100037, China*

W. Korzekwa
*KGHM Cuprum Ltd. Pl. Jana Pawla II 1, 50-136 Wroclaw, Poland*

ABSTRACT: Six samples of Permian noble metal-rich black shales from the Polkowice mine were analyzed for Re-Os isotopes, noble metals, and selected major and trace elements. Negative correlations between common Re and Os and common Os and $C_{org.}$ indicate that noble metal-rich black shales have not remained in a closed system, especially with respect to Os. The $^{187}Os/^{188}Os$ vs $^{187}Re/^{188}Os$ plot defines an errorchron with an age of 279 ± 14 Ma (MSWD = 8). The initial $^{187}Os/^{188}Os$ ratio of 1.17 ± 0.28 (if not altered) is within the variation range of present-day seawater, and excludes any significant contribution from mantle or meteoritic PGE sources.

KEYWORDS: black shales, Kupferschiefer, Poland, Re-Os isotopes, platinum-group elements

## 1 INTRODUCTION

The $^{187}Re$- $^{187}Os$ isotope system has been successfully applied to generate whole rock isochrons in organic carbon-rich sediments analogously to Rb-Sr or Sm-Nd (Ravizza & Turekian 1989 and others). Provided that there is no appreciable detrital Re and Os and subsequent hydrothermal redistribution, euxinic sediments preserve the $^{187}Os/^{188}Os$ isotopic ratio of the seawater composition. The initial Os isotope ratio of such systems is a powerful tool in elucidating the source of PGE. However, the behaviour of the Re-Os isotope system in organic carbon-rich sediments during many fundamental post-depositional geological processes such as low-grade metamorphism and/or hydrothermal alteration is poorly understood (Creaser 2003).

In this paper we present new Re-Os isotopic data from black shales from the Polkowice mining area (Fig. 1) that were enriched by noble metals during post-depositional processes and discuss them in the light of previous geochronological studies, behaviour of Re and Os during noble metal enrichment, and possible sources of platinum group elements (PGE).

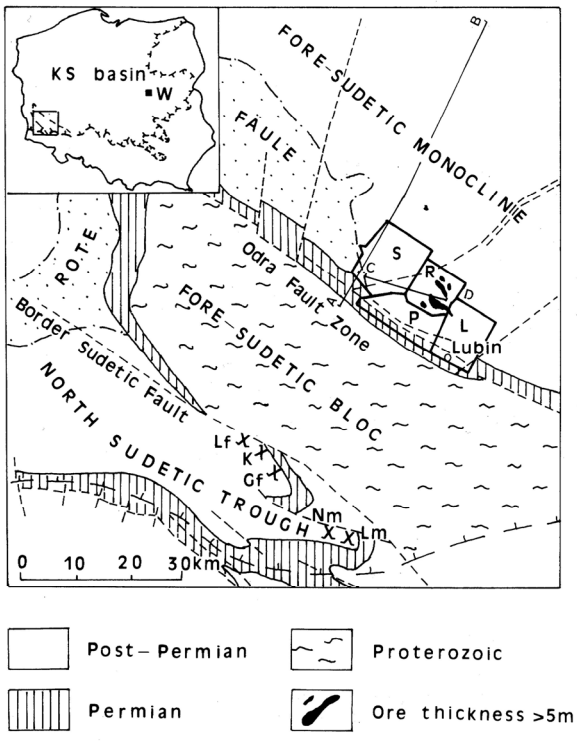


Figure 1. Location and geological setting of the Lubin – Sieroszowice district (*after* Wodzicki & Piestrzynski 1994). S – Sieroszovice, R – Rudna, P – Polkowice, L – Lubin, K – Konrad, Lf – Lubichowa field, Gf – Grodzic field, Lm – Lena mine, Nm – Nowy Kosciol mine, W – Warsaw.

## 2 GENERAL GEOLOGY

The geology of the pre-Permian basement of the Polish Zechstein basin consists of three provinces: (1) the Precambrian East European platform, (2) the epi-Caledonian platform, and (3) the epi-Variscan platform (Oszczepalski & Rydzewski 1987). The Sudetes and the Sudetic foreland were folded during the Variscan orogeny, with peak metamorphism during the late Carboniferous (*c*. 325 Ma). At the end of the Variscan orogeny, the intracontinental basins (*e.g*., Polish basin) were filled with Early Permian pyroclastics, lava flows, and clastic sediments (red beds of the Rotliegendes). In the Polish Zechstein basin, fluviatile or eolian sediments, forming the Weissliegendes strata, were deposited during late Rotliegendes-early Zechstein time. At the end of Rotliegendes time, Poland was eroded to a peneplain; only the Mazury elevation, the Sudetes and the fore-Sudetic block, the Wolsztyn highlands, and the Pomeranian elevation were topographic highs and supplied clastics to fill the depressions. The uppermost Weissliegendes sandstone was reworked and redeposited by the invading Zechstein sea, and those reworked sediments represent the first influence of the Zechstein transgression following a long period of arid to semiarid conditions. The Kupferschiefer, a bituminous calcareous or dolomitic shale, overlies these clastic rocks.

### 2.1 *Noble metal-rich mineralization*

Noble metal-rich mineralization occurs as a separate horizon 0.5 to 1.5m below the copper horizon and is often related to Rote Fäule facies (see summary in Kucha 2003). Widespread replacement of earlier Cu-Fe sulphides by haematite coeval with the emplacement of noble metals was documented by Kucha (2003). Along with different mineral replacements, Cu, Ag, Pt, Pd, U and REE are remobilized and such a behavior results in much lower contents of mobile metals on the oxidized side of the redox interface versus the reduced side (Kucha 2003, Bechtel *et al*. 2001). This produced a relatively thin reduced zone adjacent the redox interface with U and high contents of noble metals, and a much thicker and laterally extensive oxidized zone free of U, with low Pt and Pd but still high values of Ag-free gold (Kucha 2003).

Kucha & Pawlikowski (1986) interpreted the younger timing and stratigraphically lower position of noble metal mineralization with respect to the Kupferschiefer horizon as due to the influx of geopressured brines during salt doming. This occurred during the Triassic, Lower Jurassic and Lower Cretaceous and these authors concluded that noble-metal mineralization is about 60-50 Ma younger than the main Cu mineralizing event (about 240-230 Ma as indicated by remnant haematite magnetization – Jowett 1986).

## 3 SAMPLES AND ANALYTICAL METHODS

Six samples of noble metal-rich calcareous black shale (each 5-7cm thick and 0.5kg in weight) represent a typical 0.35m thick section of noble metal-rich black shale that is sharply separated from footwall red sandstone and hangingwall dolomite. These fresh-looking samples were taken in the Polkowice West mining area (Area P-2, Section G-33, Heading G-40E/cross heading 10, depth 830 m) and represent to a different degree calcareous black shales. Based on a sum of PGE we distinguish low PGE ($\sum$PGE < 0.5 ppm – samples 1, 2 and 6) and high PGE (($\sum$PGE > 0.5 ppm - samples 3, 4 and 5) samples (Table 1).

Table 1. Re and PGE abundances (in ppb), Re and Os isotope ratios, and model ages for noble metal-rich black shales from Polish Kupferschiefer (Polkowice mine).

| Sample | 1 | 2 | 3 | 4 | 5 | 6 |
|---|---|---|---|---|---|---|
| common Re* | 421.8 | 558.3 | 212.1 | 255 | 287.5 | 403.1 |
| common Os* | 1.1228 | 1.4848 | 2.0722 | 1.5903 | 1.4841 | 0.8812 |
| Ir | 0.269 | 0.383 | 0.592 | 0.748 | 0.494 | 0.109 |
| Ru | 3.174 | 3.774 | 3.007 | 3.317 | 2.323 | 3.555 |
| Rh | 0.307 | 0.291 | 0.57 | 0.436 | 0.192 | 0.171 |
| Pt | 181.5 | 229.7 | 793.3 | 637.4 | 433.7 | 102 |
| Pd | 34.14 | 40.55 | 266.24 | 129.84 | 74.82 | 17.64 |
| $\sum$PGE | 220 | 276 | 1066 | 773 | 513 | 124 |
| $^{187}Os/^{188}Os$ | 9.427 | 10.068 | 3.428 | 4.819 | 5.344 | 11.412 |
| $^{187}Re/^{188}Os$ | 1797 | 1798 | 489 | 767 | 926 | 2187 |
| Model Age (Ma) | 276.21 | 297.28 | 280.01 | 287.27 | 271.76 | 281.21 |

The Re-Os isotope analyses were done in the Re-Os laboratory of the National Research Center of Geoanalysis, Chinese Academy of Geological Sciences (Beijing). $CrO_3$–$H_2SO_4$ were used for sample dissolution and ICPMS (TJA X-series) for Os and Re isotope determination. Detailed description of the methodology is given in Du *et al.* (2004) and Mao *et al.* (2002).

The analytical reliability was tested by re-

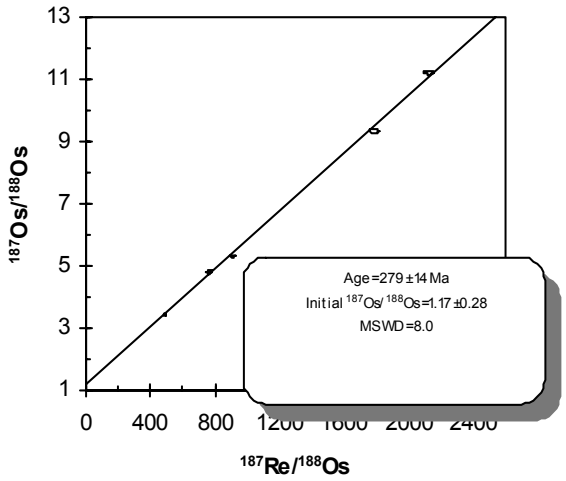


Figure 2. Re/Os vs. Os/Os plot for Polish noble metal-rich black shales (sample no. 2 with highest initial $^{187}Os/^{188}Os$ ratio was not included in age calculations).

peated analyses of the Certified Reference Materials GBW04435 (HLP) (Du *et. al* 2004).

Analytical uncertainty includes 1), the calculated standard deviation of all available data, and 2), an estimate of the factors affecting the accuracy of Re-Os dating. The Isoplot package of Ludwig (1999) was used to calculate isochrons and the Re-Os age. The results are shown in Table 1.

## 4 DISCUSSION

Significant discrepancies still exist in the literature regarding the timing of Kupferschiefer sedimentation (Menning 1995). The potash salts of the Zechstein 1 and 2 have a recalculated K/Ar age of 258 ± 19 Ma (Menning 1995), Bechtel *et al*. (1999) suggested an age around 250 Ma for Cu-mineralized Kupferschiefer in Poland while Jowett (1986) argued for 240-230 Ma based on remnant haematite magnetization. Pätzold *et al.* (2002) suggested a Re/Os age 204.3 ± 0.5 Ma for Kupferschiefer mineralization in the Mansfeld district while Brauns *et al.* (2003) reported a Re/Os age of 257.3 ± 1.6 Ma for Cu-mineralized Kupferschiefer black shale from Sangerhausen (Germany). Large ranges in age estimates of 249 to 267 Ma for base metal low- or non-mineralized samples were reported by Bechtel *et al*. (1999) based on K/Ar dating of different size fractions of illite. These authors also reported a wide range of K/Ar ages of illite (from 227 to 281 Ma) from noble metal-rich black shales in the Polish Zechstein basin, and explained their results in terms of mixing of diagenetic and detrital illites, the latter derived from the Variscan Mountains and Caledonian to Precambrian uplands. Our best fit derived from Re-Os data gives the age of 279 ± 14 Ma (Fig 2), which is somewhat comparable with illite ages in noble metal rich shales and about 20 Ma older than the expected age of the Kupferschiefer sedimentation. Our age is also significantly older than that suggested for noble metal mineralization by Kucha (2003), and 50-60 Ma younger than major Cu mineralization (240-230 Ma) as indicated by remnant haematite magnetization, (Jowett 1986).

Noble metal-rich mineralization in black shale resulted from the infiltration of chloride- and noble metal bearing oxidizing solution (Jowett 1986, Bechtel *et al*. 2001). Post-depositional redistribution of common Re and Os is clearly documented by variance in lowest common Re (212-287 ppb) and highest Os (1.48-2.07 ppb) values in high PGE samples (LUP-3-3, 3-4 and 3-5, Table 1), by significant positive correlations between common Os and most PGEs, and by a negative relationship between $C_{org.}$ and Os and common Re and Os in high PGE samples. Substantial loss of radiogenic Os during weathering of black shales was documented by Peucker-Ehrenbrink & Hannigan (2000). Rhenium is significantly mobile and soluble in hydrothermal fluids and Os can be transported in hydrothermal fluids (Hattori 2002). She also noted that low-temperature fluids likely contain radiogenic $^{187}Os$ which is not accompanied by non-radiogenic Os isotopes, because fluids and water may more readily leach radiogenic Os in Re minerals.

Our data document that $^{187}Os$ decreases with increasing PGE values (Table 1), suggesting loss of $^{187}Os$ (and also $C_{org.}$, Re and other metals – Bechtel *et al.* 2001) corresponds with input of REE and other elements into noble metal-rich black shale through oxidizing mineralized solutions. This redistribution of metals naturally resulted in the significant shift of $^{187}Os/^{188}Os$ and $^{187}Re/^{188}Os$ values in our samples (Table 1). If correct, the initial $^{187}Os/^{188}Os$ ratio of 1.17 ± 0.28 for noble metal-rich black shales from Polkowice is inconsistent with a mantle or meteoritic source component, and in contrast suggests a continental source. Our low PGE samples are characterized by Pt/Os (116-160), Pt/Ir (600-936), Pd/Os (20-30), and Pd/Ir (106-162) while high PGE samples show higher values of Pt/Os (292-400), Pt/Ir (852 to 1342), Pd/Os (50-129), and Pd/Ir (151-450). All these values are higher than typical upper con-

tinental crust (Peucker-Ehrenbrink & Jahn 2001) and global MORB (Crocket 2002), and reflect most likely post-depositional redistribution of metals.

## 5 CONCLUSION

Noble metal-rich black shales from the Polkowice mining district resulted from post-depositional enrichment that led to the redistribution of various elements. As a result, low- and high-PGE mineralized black shales display significant differences in abundances of Re, PGE and other elements and also Re-Os isotopic composition. High PGE samples are characterized by much lower Re but higher Os values (with lower $^{187}Os$) than those of low PGE samples. We suggest that the less radiogenic character of high-PGE samples most likely resulted from the interaction of black shales with basinal brines that leached Re and $^{187}Os$.

The initial $^{187}Os/^{188}Os$ value of 1.17 ± 0.28 and trace element (*e.g*. Pt/Os) ratios for our samples are inconsistent with a mantle or meteoritic PGE source, and indicate an origin of Os from continental crust.

## ACKNOWLEDGEMENTS

This work was financially supported by the European Commission in the frame of Bioshale European project (6th Framework program - NMP2-CT-2004-505710). The MS benefited from comments by B. Lehmann and D. Broughton.

## REFERENCES

Du A, Wu S, Sun D, Wang S, Qu W, Markey R, Stein H, Morgan J, Malinovskiy D (2004) Preparation and Certification of Re-Os Dating Reference Materials: Molybdenite HLP and JDC *Geostandard and Geoanalytical Research* 28 (1): 41-52

Bechtel A, Elliott WC, Wampler JM, Oszczepalski S (1999) Clay mineralogy, crystallinity and K-Ar ages of illites within the Polish Zechstein basin: Implications for the age of Kupferschiefer mineralization. *Econ Geol* 94: 261-272

Bechtel A, Ghazi AM, Elliott WC, Oszczepalski S (2001) The occurrences of the rare earth elements and PGEs in relation to base metal zoning in the vicinity of Rote Faule in the Kupferschiefer of Poland. *Appl Geoch* 16(3): 375-386

Brauns CM, Pätzold T, Haack U (2003) A Re-Os study bearing on the age of the Kupferschiefer mineralization at Sangerhausen. *Abstracts, XVth International Congress of Carboniferous and Permian Stratigraphy, Utrecht,* p. 66.

Creaser RA (2003) A review of the Re-Os isotope system with application to organic-rich sedimentary rocks. In Lentz DR (ed) Geochemistry of sediments and sedimentary rocks: evolutionary considerations to mineral deposit-forming environments. *GAC, Geotext* 4, pp 79-83

Crocket JH (2002) Platinum-group element geochemistry of mafic and ultramafic Rocks. In: Cabri LJ (ed) The Geology, Geochemistry, Mineralogy and Mineral Beneficiation of Platinum-Group Elements, *CIM Special Vol*. 54, 177-210

Hattori KH (2002) A review of Re-Os isotope geochemistry of PGM and platinum mineralization. In: Cabri LJ (ed) *The Geology, Geochemistry, Mineralogy and Mineral Beneficiation of Platinum-Group Elements, CIM Special Vol.* 54, 251-271.

Jowett EC (1986) Genesis of Kupferschiefer Cu-Ag deposits by convective flow of Rotliegende brines during Triassic rifting. *Econ Geol* 81: 1823-1837.

Kucha H (2003) Geology, mineralogy and geochemistry of the Kupferschiefer, Poland. In Kelly JG, Andrew CJ, Ashton JH, Boland MB, Earls G, Fusciardi L, Stanley G (eds) *Europe`s major base metal deposits*. IAEG, Dublin, pp 215-235.

Kucha H, Pawlikowski M (1986) Two-brine model of genesis of strata bound Zechstein deposits - Kupferschiefer type) Poland. *Min Dep* 21: 70-80.

Ludwig K (1999) Isoplot/Ex, version 2.0: a geochronogical toolkit for Microsoft Excel. *Geochronology Center.*

Mao J, Lehmann B, Du A, Zhang G, Ma D, Wand Y, Zeng M, Kerrich R (2002) Re-Os dating of polymetallic Ni-Mo-PGE-Au mineralization in Lower Cambrian Black Shales and its geologic significance. *Econ Geol* 47: 151-1061.

Menning M (1995) A numerical time scale for thr Permian and Triassic periods: an integrated time analysis. In Scholle PA, Peryt TM, Ulmer-Scholle DS (eds) T*he Permian and Northern Pangea,* Springer, Heidelberg. pp77-97.

Oszczepalski S, Rydzewski A (1987) Palaeogeography and sedimentary model of the Kupferschiefer in Poland. Lect Not Earth Sci 10: 189-205.

Pätzold T, Brauns CM, Haack U (2002) A Re-Os study bearing on the age of Kupferschiefer mineralization at Mansfeld (Germany). Abstract Symposium "*Highly siderophile elements in terrestrial and meteoritic samples: implications for planetary differentiation and igenous processes*", Nancy, August 26-28, 2002.

Peucker-Ehrenbrink B, Jahn B (2001) Rhenium-osmium isotope systematics and platinum element concentrations: Loess and the upper continental crust. *Geochemistry Geophysics Geosystems* 2: 1525-2027.

Peucker-Ehrenbrink B, Hannigan RE (2000) Effects of black shale weathering on the mobility of rhenium and PGE. *Geology* 28: 475-478.

Ravizza G, Turekian KK (1989) Application of the $^{187}Re$- $^{187}Os$ system to black shale geochronometry. *Geochim Cosmochim Acta* 53: 3257-3262.

Wodzicki A, Piestrzynski A (1994) An ore genetic model for the Lubin – Sieroszowice mining district, Poland. *Min Dep* 29: 30-43

# Geochemical characteristics of organic matter and its relation to ore mineralization in Kupferschiefer, Lubin-Sieroszowice deposit, SW Poland

D. Więcław, J. Pieczonka, M.J. Kotarba & A. Piestrzyński
*Faculty of Geology, Geophysics and Environmental Protection, AGH-University of Science and Technology, Kraków, Poland*

ABSTRACT: In the Lubin-Sieroszowice polymetallic deposit, organic matter (OM) plays an important role in the major stage of precipitation of both copper minerals and precious metals. Two different genetic types of OM have been recognized and investigated. The first, sapropelic type of OM is more important and is related to the sedimentary stage of the Kupferschiefer strata. The reduced zone of the ore deposit is characterized by elevated amounts of this type of OM (up to 14.2 wt. %) and base metals like Cu, Ni, Co, V, Fe, Pb, Zn and Ag (*e.g*. Cu content up to 16.7 wt. %). In the oxidized zone (Rote Fäule), OM was almost completely destroyed during the secondary oxidation stage (SOS) that is also responsible for the reduction and deposition of precious metals (Au, Pt and Pd). The second type of OM is connected with U-rich thucholite, and is related to an active redox barrier locally developed by the SOS solution. This barrier existed below the lower border of the copper sulphide deposit. Thucholite precipitated from the reduced side of the barrier.

KEYWORDS: Kupferschiefer, organic matter, oxidation, copper mineralization, thucholite

## 1 INTRODUCTION

The upper Permian Kupferschiefer of the Polish Zechstein Basin contains the world-class Lubin-Sieroszowice copper deposit, and is rich in organic matter. The deposit is classified as stratabound, and red-bed associated. Geochemical characteristics of organic matter present in Kupferschiefer shales were described previously, in particular for zones where Cu, Ag, Pb, Zn, noble metals and other elements are concentrated (*e.g*. Sawłowicz *et al.* 2000, Bechtel *et al*. 2001, Kotarba *et al.* 2006). Geology, mineralogy and genesis of this deposit are also well described (e.g. Wodzicki & Piestrzyński 1994).

The geochemical characteristics of organic matter (OM) versus zones of secondary oxidization and the influence of these on precipitation of base and as well precious metals ores are discussed in this paper. For the purpose of this study, we sampled 34 clayey or dolomitic shales in the Kupferschiefer strata. The samples were collected from mines (Fig. 1): Lubin (L, 7 samples), Rudna (R, 9 samples), Sieroszowice (S, 6 samples) and Polkowice (P, 12 samples). In this paper the identification of reduced, transition and oxidizing zones in the deposit was developed for the first time based on organic matter characteristics. 15 samples were collected from the reduction zone, 14 samples from the transition zone and 5 – from the oxidized zone (Polkowice mine). Thirteen thucholite grains were investigated.

## 2 GEOLOGICAL SETTING

The Polish Zechstein Basin is a part of the Southern Permian Basin (Fig. 1) in Europe. The Kupferschiefer strata were deposited in anoxic or suboxic shallow shelf conditions. Sulphide copper mineralization transgresses sedimentary strata, as it occurs in Permian Weissliegendes sandstone that overlies Rotliegendes old red type sandstone, Kupferschiefer organic shale and Werra dolomite, both of Zechstein age. Major ore minerals are chalcocite, digenite, covellite, bornite, chalcopyrite, tennantite, galena, pyrite and native silver (Piestrzyński 1996). In the last decade, a zone of precious metals has been discovered below the copper ores. This horizon hosts a new type of Au, Pt and Pd mineralization, classified as a red-bed related precious metal deposit (Piestrzyński *et al.* 2002).

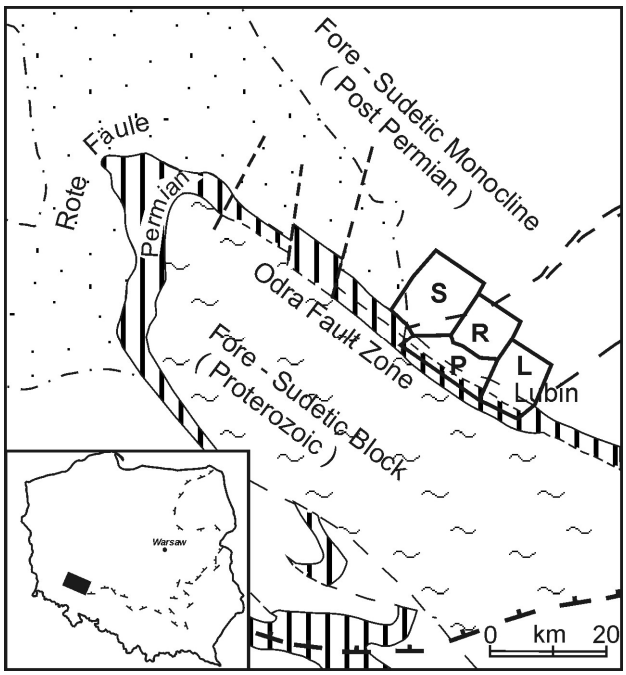


Figure 1. Sketch geological map of the Lubin mining district After Wodzicki And Piestrzyński (1994) and location of mines: S - Sieroszowice, R - Rudna, P - Polkowice, L - Lubin.

## 3 METHODS

Pyrolysis assay was done with a Delsi Model II Rock-Eval® instrument equipped with an organic carbon module. Bitumens were extracted with dichloromethane:methanol mixture (93:7 v/v) and then separated into saturated hydrocarbons, aromatic hydrocarbons, resins, and asphaltenes. Stable carbon isotope analyses were performed by on-line system on a Finnigan Delta Plus mass spectrometer. Analytical results are presented in the standard δ-notation relative to PDB. The analysis of metals was made by ICP-MS method on samples treated with $HClO_4$-$HNO_3$-HCl-HF at 200°C in microwave oven with a Perkin Elmer SCIEX ELAN 6000 spectrometer at ACTLABS Laboratories Ltd., Canada. Chemical composition of thucholite was measured with ARL SEMQ microprobe at 20 kV, 120 μA beam current using following standards and spectral lines: S Kα and Fe Kα ($FeS_2$), Cu Kα (100%), U Mα (100%), Th Mα (100%), Ca Kα ($CaCO_3$), Pd Lα (100%), Au Lα (100%), Pt Mα (100%), Pb Mα (PbS), Si Kα ($SiO_2$), Al Kα (feldspar).

## 4 RESULTS AND DISCUSSION

The sedimentary-hosted organic matter occurs in all zones (reduced, transition and oxidized) in changeable amounts. The reduced zone preserves the original characteristics of OM from sedimentation. It is rich in organic carbon (TOC content ranges from 9.0 to 14.2 wt. %, average 11.5 wt. %) and characterized by high HI/OI ratios (Fig. 2). Data from Rock-Eval pyrolysis (Fig. 3) and stable carbon isotope analyses (Fig. 4) show the presence of sapropelic Type-II kerogen at a maturity level corresponding to the initial stage of low-temperature thermogenic processes. In this reduced zone, elevated amounts of metals, including Cu, Ag, Pb, Zn, Ni, Co, V and Fe were observed. Cu dominates with abundances ranging from 1.7 to 16.7 wt. % (average 7.6 wt. %) (Fig. 5A).

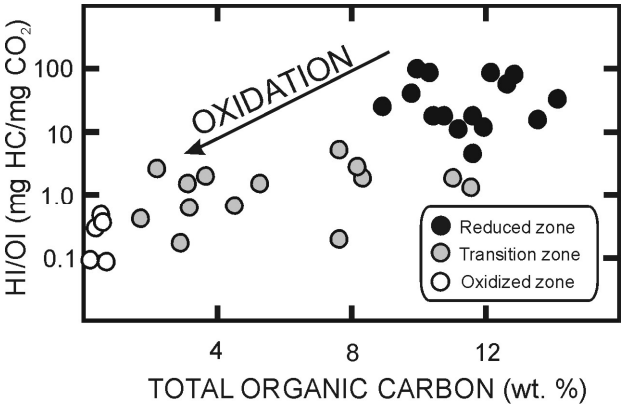


Figure 2. HI/OI ratio vs. total organic carbon.

Galena and sphalerite accompany copper sulphides, sometimes in significant amounts (Fig. 5B). Only traces of precious metals were found in this zone (Fig. 5C).

Organic matter in the transition zone has characteristics intermediate between the reduced and oxidized zones. TOC ranges from 1.7 to 11.6 wt. % (average 5.8 wt. %). With decreasing TOC, the HI/OI ratio decreases (Fig. 2) and maturity increases (Fig. 3), a result of partial oxidation of OM hot brines during the secondary oxidation stage (SOS). The influence of these oxidation processes on stable carbon isotope compositions in extractable hydrocarbons is insignificant (Fig. 4).

The transition zone is especially important for copper mining, because here, similar to the reduced zone, elevated amounts of Cu can be encountered (Fig. 5A); however, the concentration of unwanted Zn and Pb does not exceed 0.1 wt. % (Fig. 5B). Au, Pt and Pd occur in variable amounts (Fig. 5C).

The OM in the oxidized zone *(i.e.* the haematitic Rote Fäule, Fig. 1) is almost compl-

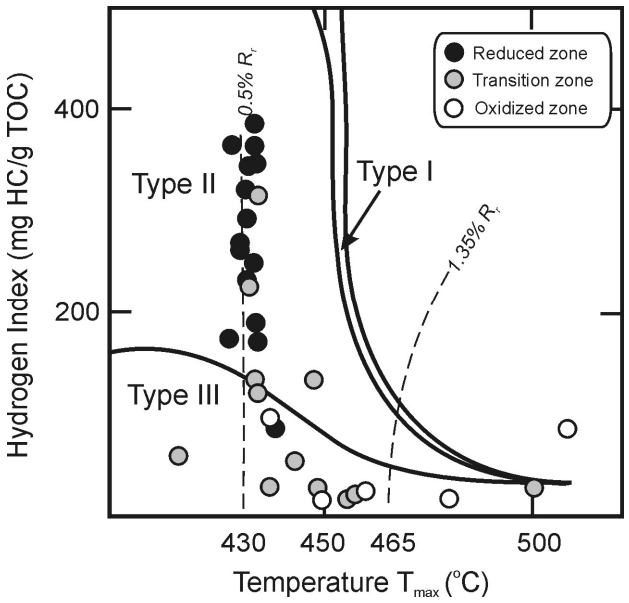


Figure 3. Rock-Eval hydrogen index vs. $T_{max}$ temperature for recognition of genetic type and maturity of organic matter of Kupferschiefer. Genetic curves for kerogen from Espitalié *et al.* (1985).

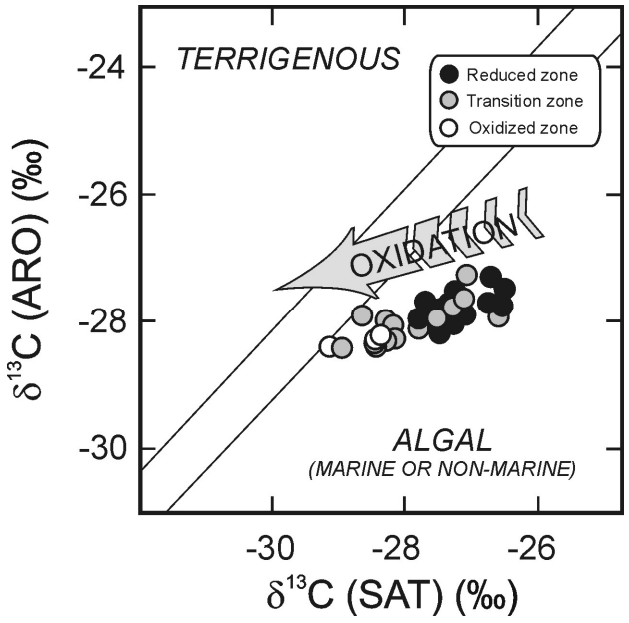


Figure 4. Stable carbon isotope composition of aromatic hydrocarbons vs. saturated hydrocarbons. Genetic fields after Sofer (1984).

etely destroyed (TOC content varies from 0.04 to 0.97 wt. %, average 0.40 wt. %), corresponding with a decrease in the HI/OI ratio (Fig. 2), an increase in maturity (Fig. 3), and an increase in the light isotope $^{12}$C content of extractable hydrocarbons (Fig. 4). In the oxidized zone, base metals occur only in trace amounts (Fig. 5 A & B), whereas gold abundances are commonly greater than 1 ppm (Fig. 5C). Organic matter is responsible for the reduction and deposition of precious metals (Au, Pt and Pd) (Piestrzyński *et al.* 2002).

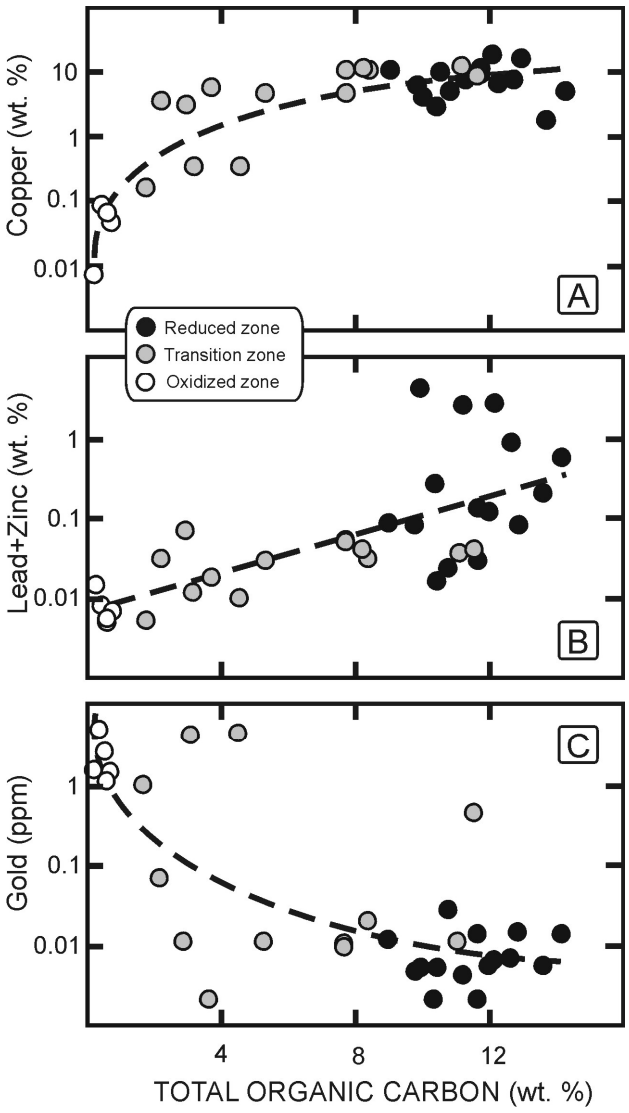


Figure 5. Correlation of (A) copper, (B) lead + zinc and (C) gold concentration with TOC content in Kupferschiefer.

A second type of organic matter is connected with U-rich thucholite, consisting of mixed uraninite, hydrocarbons, and sulphides. It occurs at the redox boundary in the lowermost part of the copper deposit. Thucholite is a hydrothermal origin (Piestrzyński 1989), contains a complicated structure of organic compounds and characterise very different chemical composition: Al – up to 0.21 wt. %, Si – up to 0.51 wt. %, S – up to 3.81 wt. %, Ca – 0.46-1.77 wt. %, Fe – 0.05-3.89 wt. %, Cu – 0.07-3.15 wt. % and U – 0.18-65.35 wt. % (Piestrzyński 1989). No Pt, Pd or Au were detected (Pieczonka *et al.* 2006).

## 5 CONCLUSIONS

Organic matter in the Kupferschiefer played an important role in the genesis of the Lubin-

Sieroszowice ore deposit. It occurs in two different genetic types. The first, more important, sedimentary-hosted sapropelic organic matter participates as reducing agent in precipitation of base metal ores in the reduced zone as well as in precipitation of precious metals in the oxidized zone. The second type of organic matter is connected with U-rich thucholite, related to an active redox barrier locally existing below the lower contact of the copper sulphide deposit.

## ACKNOWLEDGEMENTS

Financial support of this work was provided through the Polish Ministry of Science and Higher Education (Grant No. 6 T12 2003 C/06148), KGHM PM S.A. and AGH-University of Science and Technology (Grant No. 11.11.140.300). Review comments and suggestions by D. Broughton were very helpful.

## REFERENCES

Bechtel A, Gratzer R, Püttmann W, Oszczepalski S (2001) Variable alternation of organic matter in relation to metal zoning at the Rote Fäule front (Lubin-Sieroszowice mining district, SW Poland). *Org Geochem* 32: 377-395.

Espitalie J, Deroo G, Marquis F (1985) La pyrolyse Rock-Eval et ses applications. *Revue IFP* 40-41: 563–579, 755–784.

Kotarba MJ, Peryt TM, Kosakowski P, Więcław D (2006) Organic geochemistry, depositional history and hydrocarbon generation modelling of the Upper Permian Kupferschiefer and Zechstein Limestone strata in south-west Poland. *Marine Petrol Geo*l 23: 371-386.

Pieczonka J, Więcław D, Kotarba MJ, Piestrzyński A (2006) Forms of organic matter and mineralization in Kupferschiefer, Lubin-Sieroszowice deposit, SW Poland. In: *Understanding the genesis of ore deposits to meet the demands of the 21st century, 12th Quadrennial IAGOD Symposium, Moskow, PDF* 284.

Piestrzyński A (1996) Ore Minerals. In: Piestrzyński A, Jasiński AW, Kotlarski J, Maślanka W, Siewierski S, Speczik S, Śmieszek Z (eds) Mongrafia KGHM Polska Miedź S.A. CBPM „*Cuprum*", Wrocław, pp 200-237 (in Polish).

Piestrzyński A (1989) Uranium and thorium in copper ore deposits on the Fore-Sudetic Monocline (SW Poland). *Mineral Polon* 20: 41-57.

Piestrzyński A, Pieczonka J, Głuszek A (2002) Redbed-type gold mineralisation, Kupferschiefer, southwest Poland. *Mineralium Deposita* 37: 512-528.

Sawłowicz Z, Gize AP, Rospondek M (2000) Organic matter from Zechstein copper deposits (Kupferschiefer) in Poland. In: Glickson M, Mastalerz M (eds.) *Organic matter and mineralization: thermal alteration, hydrocarbon generation and role in metallogenesis.* Kluwer Academic Publ. Dordrecht, pp 220-242.

Sofer Z (1984) Stable carbon isotope compositions of crude oils: applicaton to source depositional environments and petroleum alteration. *AAPG Bull* 68: 31-49.

Wodzicki A, Piestrzyński A (1994) An ore genetic model for the Lubin-Siroszowice mining district, Poland. *Mineralium Deposita* 29: 30-43.

# The significance of footwall and hanging wall ore in the German Kupferschiefer of Richelsdorf and Spremberg / Weisswasser

S. Walther & G. Borg
*Petrology and Economic Geology Research Group, Institute for Geosciences, Martin-Luther-University Halle-Wittenberg, Germany*

J. Kopp
*Federal Geological Survey of Brandenburg, Germany*

ABSTRACT: The sediment-hosted copper mineralization in the basal Zechstein sequence (Kupferschiefer *sensu lato*) is locally discordant to bedding and stratigraphy. Investigations of the footwall and hanging wall of the Kupferschiefer *sensu stricto*, the Weissliegend sediments and the Zechstein Limestone respectively, were carried out to characterize the coarse-clastic-hosted and carbonate-hosted "Kupferschiefer mineralization" in Germany. Replacement of the carbonate matrix of the Weissliegend sandstone and locally of individual lithic clasts, as well as sulphide veinlets within the Zechstein Limestone document the epigenetic, ore-forming stage of the German Kupferschiefer.

KEYWORDS: Kupferschiefer, sediment-hosted copper deposits, sand ore, epigenetic, replacement

## 1 INTRODUCTION

The origin of the sediment-hosted copper mineralization within the basal units of the Zechstein (Upper Permian) in Germany has been discussed controversially for a long time. The main subject of interest has been focused on the 40 to 90cm thick stratum of the Kupferschiefer, which is commonly a $C_{org.}$-rich black mudstone to marl at the base of the Zechstein.

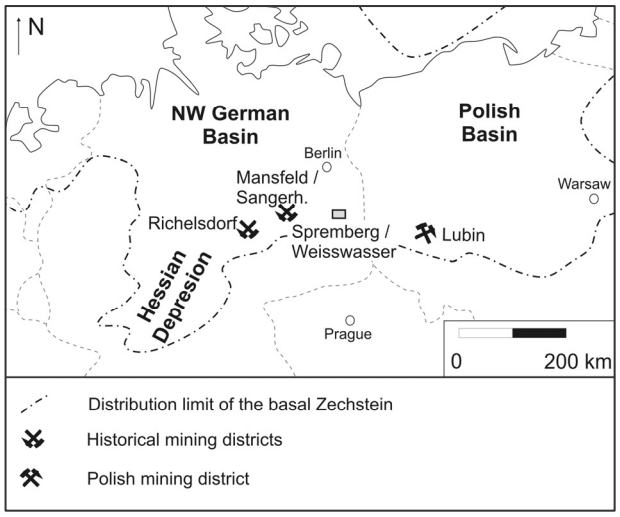


Figure 1. Distribution of the Zechstein (after Kiernowski *et al*. 1995 & Vaughn *et al.* 1989)

Recently, more attention has been paid to the mineralization occurring in the underlying "Weissliegend" and "Grauliegend" sandstones and conglomerates and in the overlying Zechstein Limestone (*e.g*. Kopp *et al*. 2006). Even though Schmidt & Friedrich (1988), Schmidt *et al*. (1986) and Borg (1991) describe the occurrence of ore minerals within the Weissliegend sandstone, mineralogical and genetic description of these ore types are scarce to absent.

The Kupferschiefer extends from Poland through the Spremberg/ Weisswasser area and Mansfeld/Sangerhausen into the Hessian Depression (Fig. 1).

## 2 CHARACTERISATION OF FOOTWALL AND HANGING WALL ORE

### 2.1 *Footwall Sediments*

The footwall sediments of the Kupferschiefer comprise greyish to white sandstones and conglomerates known as Weissliegendes or Grauliegendes. In the area of Spremberg/ Weisswasser, the footwall units consist of siltstone, sandstone and conglomerate, commonly with a carbonate cement. Within these sedimentary units, bornite, chalcocite and chalcopyrite have replaced the carbonate cement and filling the interstitial spaces between clasts (Fig. 2).

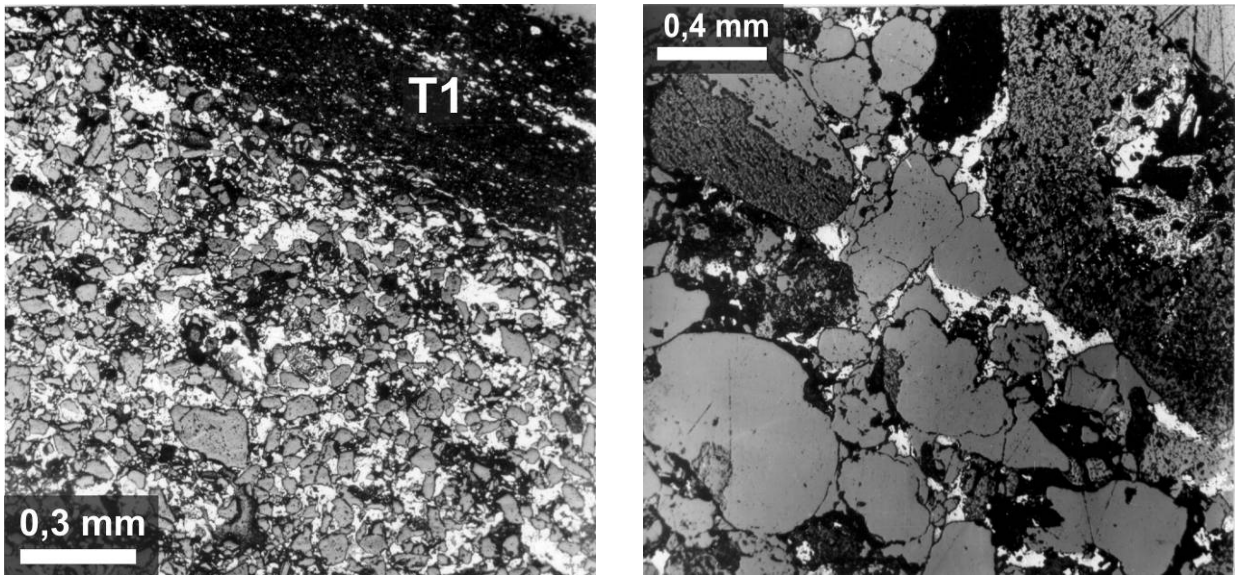


Figure 2. Photomicrographs of polished sections with bornite and chalcopyrite (white) replacing the carbonate matrix of the footwall sandstone. The black shale of the Kupferschiefer is visible in the upper right of the left picture (T1). (drill core samples Cu Sp 82/60 and Cu Sp N5/71).

In the Richelsdorf area, the footwall units comprise mainly conglomerate and conglomeratic sandstone, partially interbedded with finer-grained sandstone. Copper ore minerals such as chalcopyrite and chalcocite occur within these rocks. Chalcopyrite and chalcocite locally replace even clasts within the conglomerate (Fig. 3). The footwall mineralization typically shows a systematic metal zonation (Fig. 4).

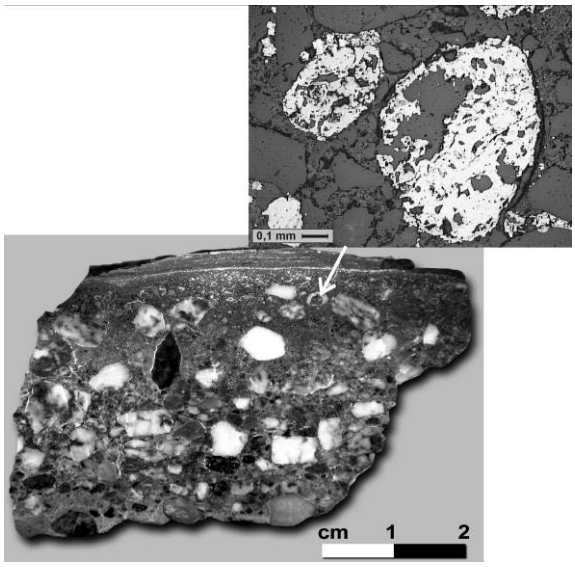


Figure 3. Hand specimen of Weissliegend conglomerate overlain by Kupferschiefer (main picture) with chalcopyrite and chalcocite partly replacing lithic clasts, shown in photomicrograph of a polished section (insert picture); Richelsdorf district.

*2.2 Hanging wall sediments*

The hanging wall sediments (Zechstein Limestone) in both investigated areas comprise mainly calcareous and dolomitic mudstones and marls. These rocks are typically associated with compact micritic carbonates. Ore minerals appear within small veinlets, which "truncate" the host rock along zones of weakness (Fig. 5).

Bornite and subordinately chalcopyrite and covellite are the main copper ore minerals in the Zechstein Limestone in the Spremberg/Weisswasser area. In the Richelsdorf area, in contrast, mineralisation of the examined hanging wall sediments consists predominantly of disseminated galena and sphalerite, reflecting the typical ore mineral zonation pattern of the Kupferschiefer.

## 3 COMPARISON WITH POLISH KUPFERSCHIEFER

Oszczepalski (1999) described the mineralization in the sedimentary units at and below the base of the Zechstein strata of the Polish Kupferschiefer (Lubin district, Fore Sudetic Monocline). Here, the mineralization occurs within the Weissliegend (locally up to 11m below the Kupferschiefer), the Kupferschiefer *sensu stricto* and the Zechstein Limestone, thus crosscutting the stratigraphy (Wodzicki & Piestrzynski 1994). Within the Weissliegend sediments, sulphides fill pore spaces, replace the carbonate cement and "corrode" detritic

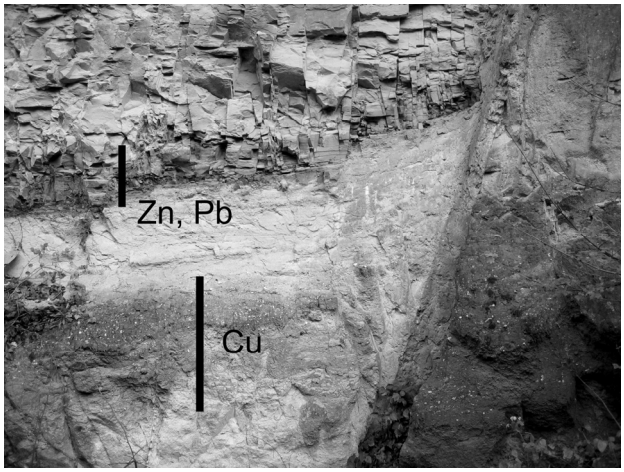


Figure 4. Footwall Cu mineralization in Weissliegend conglomerate approx. 1m below a Zn-Pb zone in the Kupferschiefer. The zonation suggests an ascending migration of ore fluids, not supergene remobilisation. Quarry at Münden, Richelsdorf area.

clasts (Oszczpalski 1999). The mineral zonation, as observed in the Polish Kupferschiefer (Jowett *et al*. 1987, Piestrzynski 1997, and Oszczepalski 1999) has also been recognized in the German Kupferschiefer (*e.g.* Rentzsch 1974, Borg 1991 and Kopp *et al*. 2006).

## 4 DISCUSSION

Over the past decades, many controversial models have been discussed for the origin of the Kupferschiefer mineralization. Syngenetic to very early diagenetic models have been particularly proposed for the German Kupferschiefer (Wedepohl 1965, Rentzsch 1991), whereas for the Polish Kupferschiefer an epigenetic, late diagenetic model has been convincingly established (*e.g*. Jowett *et al*. 1987, Oszczepalski 1999, Wodzicki & Piestrzynski 1994). A multi-stage origin of the copper ores is discussed for both the Polish and German Kupferschiefer by several authors (Borg 1991, Piestrzynski 1997, Schmidt & Friedrich 1988, Blundell *et al.* 2003, Rentzsch & Friedrich 2003, Hitzman *et al*. 2005).

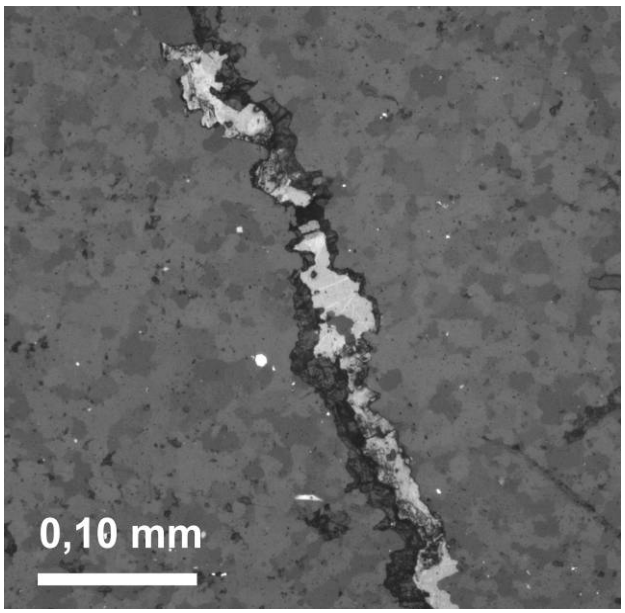


Figure 5. Bornite veinlet within Zechstein carbonate (polished section, drill core Cu Sp 75/60)

Although footwall ore, locally termed "sand ore" had been mined and documented, these ores had attracted little academic interest in the German Kupferschiefer districts. The epigenetic replacement structures, found within the Weissliegend sediments in the Richelsdorf and Spremberg/Weisswasser districts illustrate a mineralization event, long after diagenesis and thus clearly argue against a synsedimentary origin of the mineralization. A multi-stage late-diagenetic to epigenetic ore forming process seems to be likely although a synsedimentary non-economic deposition of some of the ore minerals should not be excluded.

Multiple sources for the metals, contained within the Kupferschiefer ores, have been identified and these include bi-modal volcanics of the Lower Permian (Borg 1991) and clastic basin fill and Variscan basement rocks (Rentzsch & Friedrich 2003).

## 5 CONCLUSIONS

The footwall of the Kupferschiefer in the investigated areas consists mainly of conglomerate and sandstone. Mineralization occurs as replacement of carbonate cement and locally of lithic clasts.

The hanging wall units comprise marly mud- and siltstone, interbedded with micritic thick-bedded carbonate units.

Ore textures in the Weissliegend Sandstone and the Zechstein Limestone show evidence of an epigenetic origin of these ores. The metallogenetic similarities between the Kupferschiefer in Poland and Germany are striking and common ore forming processes can be assumed.

## ACKNOWLEDGEMENTS

We thank the Federal Geological Surveys of Hessen, Brandenburg and Sachsen for access to drill core and archives. Anglo American Corpo-

ration is acknowledged for logistical support of the project.

## REFERENCES

Blundell DJ, Karnkowski PH, Alderton DHM., Oszczepalski S, Kucha H (2003). Copper mineralization of the Polish Kupferschiefer; a proposed basement fault-fracture system of fluid flow. *Econ. Geol*. 98/7: 1487-1495.

Borg G (1991). The significance of Rotliegend volcanics for the metal provinces of the Kupferschiefer Basin. *Zentralblatt für Geologie und Paläontologie*, Teil I, 4: 929-943.

Hitzman M, Kirkham R, Broughton D, Thorson J, Selley D (2005). The sediment hosted stratiform copper ore system. *Soc. Econ. Geol.* 100th Anniversary Volume: 609-642.

Jowett EC, Rydzewski A, Jowett RJ (1987). The Kupferschiefer Cu-Ag ore deposits in Poland: a reappraisal of the evidence of their origin and presentation of a new genetic model. *Can. J. Earth Sci*. 24/10, 2016-2037.

Kiersnowski H, Paul J, Peryt TM, Smith DB (1995). Facies, Palaeogeography, and sedimentary history of the Southern Permian Basin in Europe. In: Scholle PA, Peryt TM, Ulmer-Scholle DS (eds.). The Permian of Northern Pangea – Part 2: Sedimentary Basins and Economic Resources, Springer, Berlin: 119-136.

Kopp J, Simon A, Göthel M (2006). Die Kupferlagerstätte Spremberg-Graustein in Südbrandenburg. Brandenburg. *Geowiss. Beitr.* 13 (2006) 1/2: 117-132.

Oszczepalski S (1999). Origin of the Kupferschiefer polymetallic mineralization in Poland. *Mineralium Deposita* 34/5-6: 599-613.

Piestrzynski A (1997). Genetic model of the Kupferschiefer type deposits. In: Abstracts, 18th IAS regional European meeting of Sedimentology; *Gaea Heidelbergensis* 3: 272-273.

Rentzsch J (1974). The Kupferschiefer in comparison with the deposits of the Zambian Copperbelt. In: Bartholome P (ed). Gisements stratiformes et provinces cupriferes. *Societe Geologique de Belgique*, Liege: 395-418.

Rentzsch J. (1991). Die Rote-Fäule-Fazies als wichtigster erzkontrollierender Faktor der Vererzung des Typs Kupferschiefer. Zbl. *Geol. Paläont.;* Teil I / 4: 945-956.

Rentzsch J, Friedrich G (2003). Zur Herkunft der Metalle der Kupferschiefervererzung in Deutschland – Metallbilanz im Präzechstein und in der Erzführenden Zone an der Zechsteinbasis. Hall. Jb. *Geowiss*. B 25: 1-20.

Schmidt FP, Friedrich G (1988). Geologic setting and genesis of Kupferschiefer mineralization in West Germany. Spec. publ. *Soc. Geol. Appl. Mineral Deposits* 5: 25-59.

Schmidt FP, Schumacher C, Spieth V, Friedrich G (1986). Results of recent exploration for copper-silver deposits in the Kupferschiefer of West Germany. Spec. publ. *Soc. Geol. Appl. Mineral Deposits 4*: 572-582.

Vaughan DJ, Sweeney MA, Friedrich G, Diedel R, Haranczyk C (1989). The Kupferschiefer: An overview with an appraisal of the different types of mineralization. *Econ. Geol.* 84/5: 1003-1027.

Wedepohl KH (1965). Untersuchungen an Proben von Kupferschiefer aus Nordwestdeutschland und Diskussion seiner Bildungsbedingungen. *Freiberger Forschungshefte* C193: 107-121.

Wodzicki A, Piestrzynski A. (1994). An ore genetic model for the Lubin-Sieroszowice mining district, Poland. *Mineralium Deposita* 29/1: 30-43.

# Ore mineral zoning and enrichment due to oxidation in the Lubin-Sieroszowice deposit (Fore Sudetic Monocline, Poland)

A. Emetz
*Institute of Geochemistry, Mineralogy and Ore Formation of M.P. Semenenko, National Academy of Sciences of Ukraine*

W. Puettmann
*Johann Wolfgang Goethe-University, Institute of Atmospheric and Environmental Sciences, Department of Environmental Analytical Chemistry, Frankfurt am Main, Germany*

P. Lenik
*University on Science and Technology, Cracow, Poland*

ABSTRACT: The paper presents results of ore mineral mapping of the Lubin-Sieroszowice stratiform copper deposit (Poland), and documents lateral zoning in the ore mineral distribution in the ore sandstones. Mineralization formed in front of a mobile oxidation zone due to redeposition of ore metals (predominantly Cu and Ag) by oxidized fluids with enrichment of the ore body and mineral replacement in the sequence: covellite → digenite → chalcocite → bornite → chalcopyrite.

KEYWORDS: Kupferschiefer shale, Cu ores, stratabound, sulphide mineral zoning, ore enrichment

## 1 INTRODUCTION

The Lubin-Sieroszowice Cu-Ag deposit in Poland is a giant strata-bound Cu-Ag deposit hosted within the Kupferschiefer black shale and adjacent dolomites and sandstones..The deposit has been the subject of intensive scientific study since its discovery in 1957, including investigations into ore mineral zoning. Earlier works (*e.g.* Konstantynowicz 1972) demonstrated a lateral, northwest to southeast mineral zoning of chalcocite-bornite-chalcopyrite. The distribution of the economic metals (*i.e*. Pb, Zn and Cu) has been mapped in detail both for the deposit and for the whole Fore Sudetic territory (Jowett *et al* 1987b; Oszczepalski *et al,* 1999, 2002). Other workers emphasized the presence of vertical zoning (Jowett *et al* 1987b), or multiple, overlapping mineral zones without clear regularities (Wodzicki & Piestrzynski 1994). The presented research deals with major ore mineral distribution developed in front of the Rote Fäule haematitic-goethitic zone, which is considered the influx zone for oxidized ore-forming fluids introduced from red-bed strata below the ore units (Oszczepalski *et al* 1999).

## 2 TECHNIQUES

More than 1000 polished sections were studied by optical microscopy. The samples include 33 vertical profiles across the stratabound orebody taken in the underground mines. In the profiles, the samples were selected every 20 to 40cm, a sufficient distance to document the variations in the ore mineral composition. Mineralogical zones were delineated according to the dominant ore minerals. In constructing ore mineral distribution maps, borders between lateral zones were drawn in compliance with the dominant ore mineral in the vertical profile across the Weissliegend sandstone, independent of ore composition in the overlying shale and limestone.

## 3 GEOLOGY AND ORE BODY POSITION

The geological setting, position of the ore zone and description of the ore bearing beds in the deposit have been given previously (Konstantynowicz *et al* 1972; Jowett *et al* 1987b; Kwolek 2000, *et al*). Briefly, the deposit is located in the Fore-Sudetic Monocline, bordered to the southwest by the Middle Odra fault zone on the Fore Sudetic block, consisting of Precambrian and early Palaeozoic metamorphic rocks. The strata-bound ore body, 4 m in average thickness, is located in the basal beds of the Zechstein (late Permian) carbonate-evaporite strata, covering the Rotliegend (early Permian) cross-bedded terrestrial units. The ores occur in (from bottom to top) the Weissliegend sand-

stone, Basal limestone, Kupferschiefer black shale, and Werra limestone. The Permian beds of the Fore Sudetic Monocline dip slightly eastward (2-6$^{o}$) and are stepwise faulted by 50 to 100m faults, striking W – E, and by numerous low-amplitude faults, which developed subparallel to the Middle Odra faults.

The Werra limestone is covered by the Lower Anhydrite series of the lowermost of four (Z1, Z2, Z3, Z4) Zechstein carbonate-evaporite cycles. Triassic, Jurassic and Cretaceous beds successively overlie the column eastward.

On the west side of the deposit, the ore body is destroyed due to the development of an oxidation zone consistent with the overall reddening (so-called Rote Fäule facies) of the ore-bearing sequence. The facies is well recognized due to development of secondary haematite and goethite, which pseudomorphed sulphides (Oszczepalski 1994). In concordance with the configuration of the Rote Fäule, the ore body changes its vertical position laterally across the deposit (Fig. 1). In the western part of the deposit, the ores occur only in the Werra limestone over the reddened barren Kupferschiefer shale or the Rote Fäule facies developed in the lowermost part of the Werra limestone. Eastward, the ores progressively descend into the Kupferschiefer shale and the Weissliegend grey sandstone. Farther southeast the ore body gradually pinches out.

## 4 ORE ZONING

In the ore body, pyrite, sphalerite, galena, chalcocite, digenite, covellite, bornite and chalcopyrite are the most common sulphides, whereas marcasite, tennantite, djurleite and native silver form rich mineralization locally. Sulphides mostly occur as disseminations, nests, and veinlets. In dense shale and calcareous beds, a vertical ore mineral zoning is recognised in many places and was described by Wodzinski & Piestrzynski 1994. In non-fractured (veined) places, mineral zones are successively distributed in sequence from top to bottom: pyrite-sphalerite-galena-chalcocite-bornite (± chalcopyrite) from the earliest to latest sulphides. Chalcopyrite occurs in different amounts as an associated mineral with a later origin. The zones are laterally persistent and traceable in many places. Borders between the sulphide zones are represented by transitional or mixed mineralization, and relics of the minerals of the upper zones are documented in the lower levels. In the shale these transitional zones often do not exceed several cm in thickness. Replacement textures are common and include incrustations of foraminifera shells and buried algal forms, pseudomorphs and overgrowths of Cu, Pb and Zn sulphides after framboidal pyrite, and later sulphides after earlier sulphides.

The vertical sulphide zoning reflects reaction of the ascending fluids with the carbonate-rich environment. Syn-ore dolomitization with partial dissolution of calcite in limestone and shale indicates that the ore-forming solutions were relatively acidic. The minerals of the lower zones are everywhere observed in the upper levels because of the occurrence of numerous fractures in the brittle rocks and due to variation of the limestone permeability throughout the deposit. In such fractures, clear regularity in mineral composition is often absent, but the zoning can be inferred from adjacent disseminated mineralization. Generally, in such zones the mineral-forming sequence and replacements are similar to that noted above (from earlier to later): pyrite-sphalerite-galena-chalcocite-bornite-chalcopyrite-tennantite. A significant part of the mineralization containing arsenides clearly relates to the formation of Co-Ni-Ba (with As) and Cu-As-Ag Rücken-type veins (Schmidt & Friedrich 1985).

On the reduced side of the Rote Fäule facies, mostly in the Kupferschiefer shale, electrum occurs in association with digenite (Oszczepalski *et al,* 2002). To the east and south where ore occurs in the Weissliegend sandstone (Fig. 1), the ore body increases in thickness but farther southeast the mineralization passes into sub-economic Cu-Pb-Zn ores, predominantly represented by bornite, with galena and sphalerite in the black shale.

Vertical zoning is also observed in profiles across the Weissliegend sandstone, and can be correlated laterally. However, in many profiles in the western part of the deposit the ore mineral distribution in the Kupferschiefer and Werra limestone does not correspond with sulphide mineralogy in the Weissliegend sandstone. This difference reflects different mineral-forming conditions affected by the contrast of the rock permeability and lithology, and different timing of ore mineralization. Consequently, ore mineral zoning in the Weissliegend sandstone trends approximately N-S, subparallel to the strike of the Rote Fäule boundary, and forms the sequence (proximal/ youngest to distal/oldest) covellite - digenite - chalcocite -

bornite, with chalcopyrite locally dominant in the Lubin mine (Fig. 1). Relics of earlier Cu, Pb and Zn sulphides and tennantite, although uncommon, occur within the various mineral zones.

Anhydrite-gypsum cement in sandstone and nests in carbonaceous rocks (Konstantynowicz 1972) are common in covellite, digenite and chalcocite zones. The cement often contains syngenetic sulphides.

Cu sulphides form micro-aggregates and nests in sandstones. In the shale, they occur as thin blebs, pseudomorphs after framboidal pyrite, foraminifera and algae. Morphologically, the majority of digenite and covellite blebs do not differ from chalcocite blebs which they completely replaced.

The eastern part of the chalcocite zone in sandstone and often in adjacent rocks is characterized by partial chalcocite replacement by djurelite, annilite, and other relatively Cu-depleted sulphides. Their presence is interpreted as evidence for Cu leaching from chalcocite by acidic solutions originating from the Rote Fäule. Chalcocite contains fine inclusions of domeykite, possibly formed during dissolution of arsenides with partial redistribution of As in the ores. Over some eastern parts of the chalcocite zone, the organic shale contains native copper, which may reflect the introduction of Cu-oversaturated fluids into highly reduced black shale.

The most intense bornite mineralization in sandstone occurs close to the chalcocite zone, and can be subdivided into bornite rich and bornite-poor sub-zones. The bornite rich subzone is easily recognized in the profiles and directly confines the chalcocite zone from east and below. It contains the areas where bornite does not contain chalcopyrite emulsion, which is common in the bornite-poor subzone. Overgrowths of later bornite on chalcopyrite and earlier bornite containing chalcopyrite emulsion are observed in this sub-zone. Consequently, the bornite rich sub-zone corresponds to the peripheral area of Cu enrichment relative to the Rote Fäule front. Galena and sphalerite occur irregularly in sandstone in the bornite-poor subzone, and are probably related to the most distal enrichment of the ore body.

Native silver and stromeyerite are concentrated mainly as thin blebs which replace chalcocite, digenite and bornite within the black shale, predominantly in the chalcocite and rich bornite zones. The later position of native silver in relation to Cu sulphides and tennantite and its zonal distribution and abundance with respect the lateral sulphide zoning suggests that Ag was precipitated during the same processes that led to Cu enrichment.

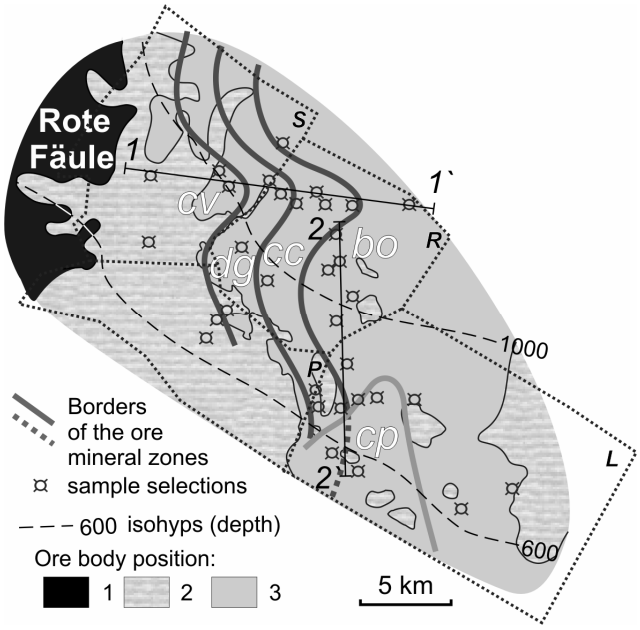


Figure 1. Lateral ore zoning in the Weissliegend sandstone (zones: cv – covellite, dg – digenite, cc – chalcocite, bo – bornite, cp – chalcopyrite) and position (1 – oxidized (destroyed); 2 – without ores in sandstone; 3 – including ores in sandstone) of the Lubin-Sieroszowice deposit.

## 5 CONCLUSIONS

Major enrichment of the Lubin-Sieroszowice deposit occurred due to oxidation in front of the developing Rote Fäule goethite-haematite front. Lateral covellite-digenite-chalcocite-bornite ore mineral zoning developed via formation of successive replacement of pre-existing and more distal sulphide ores as the front migrated eastwards. Vertical zoning partially developed in the Weissliegend sandstone suggests that zoning was controlled by a sub-horizontal boundary such as a stratified fluid column (*i.e.* groundwater table). $\delta^{34}S$ and $\delta^{18}O$(SMOW) of anhydrite and gypsum in the ore body range from -31.7 to 16.3‰ and from 0.1 to 11 ‰, respectively (Michalik 2001). These data suggest conversion of sulphur from $^{32}S$-rich sulphides to sulphates by waters containing isotopically light oxygen. Consequently, the lateral ore zoning is interpreted as originating from descending oxygenated meteoric waters, although other sources of these oxidizing fluids can not be excluded. The ore-forming environment in the permeable sandstone was therefore chiefly controlled by redox-potential and metal concentra-

tions slowly changing laterally. In the overlying dense organic and calcareous beds the redox-potential was controlled by the contrasting rock permeability, but supersaturation in metals occurred because of vertically dependent neutralization reactions. Consequently, the zoning developed due to mobilization, transport and redeposition of metals by oxidizing fluids, and defines an eastward-moving fluid flow regime oblique to that of the NW trending Odra fault zone. The age of this oxidation process has been estimated by palaeomagnetic dating at 250-220 Ma (Jowett *et al*., 1987a).

ACKNOWLEDGEMENTS

We thank D. Broughton for his suggested edits to this manuscript, which improved its scientific quality. Also, the authors thank Prof. Adam Piestrzynski for his generous donation of ore samples and equipment for mineralogical research. INTAS 04-83-3551 YS Fellowship grant supported the first author research work.

REFERENCES

Jowett EC, Pearce GW, Rydzewsky A (1987a): Mid-Triassic paleomagnetic age of the Kupferschiefer mineralization in Poland based on a revised apparent polar wander path of Europe and Russia. *J. Geoph. Res*. 92: 581-598.

Jowett CE, Rydzewski A, Jowett RJ (1987b): The Kupferschiefer Cu-Ag ore deposits in Poland: a reappraisal of the evidence of their origin and presentation of a new genetic model. *Can. J. Earth Sci.* 24: 2016-2037.

Konstantynowicz E (1972): Genesis of Permian Cu deposits in Poland. *Sovetskaya Geologiya* 8: 101-117.

Kwolek K (2000): Age of the tectonic movements in the dislocation element Poznan-Kalish, Fore Sudetic Monocline. *Przeglad Geologiczny* 48: 804-814.

Michalik M (2001) Diagenesis of the Weissliegend sandstones in the South-Western margin of the Polish Rotliegend basin. *Prace Mineralogichne* 91: pp. 172.

Oszczepalski S (1994): Oxidative alteration of the Kupferschiefer in Poland: oxide-sulphide parageneses and implications for ore-forming models. *Geological Quarterly* 38: 651-672.

Oszczepalski S (1999): Origin of the Kupferschiefer polymetallic mineralization in Poland. *Mineral. Deposita* 34: 599-613.

Oszczepalski S, Nowak GJ, Bechtel A, Zak K (2002): Evidence of oxidation of the Kupferschiefer in the Lubin-Sieroszowice deposit, Poland: implications for Cu-Ag and Au-Pt-Pd mineralization. *Geological Quarterly* 46: 1-23.

Schmidt F-P, Friedrich G (1985): Geological setting and genesis of Kupferschiefer mineralization in West Germany. In: Friedrich F H, Herzig P M (eds): *Base metal sulphide deposits in sedimentary and volcanic environments,* Springer-Verlag: 25-59.

Wodzicki A, Piestrzynski A (1994): An ore genetic model for the Lubin-Sieroszowice mining district, Poland. *Mineral. Deposita* 29: 30-43.

# Kupferschiefer – A hunt for new reserves

S. Speczik, S. Oszczepalski, M. Karwasiecka & G.J. Nowak
*Polish Geological Institute, Rakowiecka 4, 00-975 Warsaw, Poland*

ABSTRACT: Previous results suggested that the present day geothermal field of the Kupferschiefer horizon corresponds strictly with the ore series depth in a fashion steadily consistent with the strata inclination of the Fore-Sudetic Monocline. Recent studies on organic matter as well as on the geothermal field in SW Poland revealed that areas with overlapping high grade Cu-Ag mineralization and low temperature anomalies within the present day geothermal field can be delineated. Therefore, we believe that some deeper mineral resources may become ore reserves accessible in future.

KEYWORDS: Kupferschiefer, exploration, palaeogethermal field, subsurface temperatures

## 1 INTRODUCTION

During nearly 40-years of copper mining, the immense reserves of the Lubin-Sieroszowice area have been gradually diminished. Therefore, a need exists to re-evaluate adjacent reserve and prospective areas that were encountered in SW Poland. The investigations should be based not only on base metal distribution pattern but also on recent results of organic matter alteration trends. Recent results show a clear trend displaying an increase of organic matter thermal maturity from low grade Cu-Pb-Zn mineralization towards high grade Cu-Ag and Au-Pt-Pd mineralization and Rote Fäule units, which might be used as a new practical exploration guide (Speczik *et al.* 1997, 2003).

New technologies allow the mining industry to operate at greater depths. Depths below 1200 m are the main technological barrier for copper production, due to relatively high geothermal gradient within the deposits area. Also, nearly all known reserve and prospective areas are located deeper than recently operated.

Until now, it was generally assumed that temperatures of the Zechstein footwall gradually increase with depth, following the inclination of strata. However, recent findings have shown that this tendency is not uniform over the area studied, and places with temperatures lower than expected may locally exist.

The above considerations suggest that future re-evaluations of reserve and prospective areas should take into consideration three major factors: (1) economically accepted grade of mineralization; (2) maximum values of organic matter thermal maturity (that coincide with the richest Cu-Ag and Rote Fäule-related Au-Pt-Pd mineralization); and (3) the lowest values of present day subsurface temperatures at the depth of the Kupferschiefer.

## 2 ZONING PATTERN

Metal zonation is the most characteristic feature of the Kupferschiefer ore system (Fig. 1). Centers of this system are occupied by Rote Fäule alteration, which are successively surrounded by Cu-, Pb-, Zn- and pyrite-bearing zones (Oszczepalski, Rydzewski 1997). The largest Rote Fäule area, rimmed with the Lubin-Sieroszowice, Konrad-Wartowice and Lena Cu-Ag deposits, encompasses the western part of the area studied. Numerous oxidized fields are also known to occur in the central and eastern parts of the area studied. A few prospective areas appear adjacent to recognised Rote Fäule alteration. In areas with the highest

copper concentrations, chalcocite and bornite predominate over the other sulphides, whereas in areas distant from the Rote Fäule, chalcopyrite, galena and sphalerite successively prevail.

Au, PGE, Co, Bi, Se, Re and REE show a clear tendency towards higher concentrations closer to the Rote Fäule. The variability in V, Hg, and U contents is similar. An increase in CaO/MgO, $K_2O/Na_2O$ and V/Cr ratios in the same direction is also observed. Element zoning pattern is consistent with the interaction of the oxidising fluid passage from underlying Rotliegend aquifer and argues for efficient metal redistribution during formation and expansion of the Rote Fäule. Most of the base metals (Cu, Ag, Pb, Zn, Co, Mo, Ta and As) were removed from the altered lithologies, whereas Au, Pt, Pd, Se, Re, REE (partly V, U and Hg) concentrated within the oxidized rocks (*e.g.* Speczik *et al.* 1997; Bechtel *et al.* 2001; Kucha & Przybyłowicz 1999; Oszczepalski *et al.* 2002).

## 3 ORGANIC MATTER DISTRIBUTION

The organic matter content significantly decreases towards the Rote Fäule areas. Oxidized shales contain 0.07-3.33 % $C_{org}$ (0.55 % on average), Cu-bearing shales - 0.19-14.70 % (5.13 %), whereas Pb-Zn and pyritiferous shales contain 1.57-16.09 % (6.34 % $C_{org}$). Rock-Eval pyrolysis reveals that hydrogen index (HI) values, in contrast to oxygen index (OI) and $T_{max}$ (the temperature of maximum hydrocarbon generation) variations, clearly parallel this trend, averaging between 96 in oxidized shales, through 208 in Cu shales up to 293 within Pb-Zn-bearing shales shales. OI averages in the range from 165 within oxidized shales to 21 within the Pb-Zn shales, and $T_{max}$ varies from 450°C in the oxidized rocks, through 442°C in Cu shales to 438°C in Pb-Zn shales.

Consistent with the trend in $C_{org}$ content, amounts of bitumen, hydrocarbon, n-alkane, isoprenoid, porphyrin and resin also decrease towards the Rote Fäule, whereas concentrations of aromatic hydrocarbons, PAH, PAHS, phenantrenes and asphaltenes show the opposite trend. Stable isotope records display a clear tendency of $^{13}C$-enrichment in the oxidized kerogen, accompanied by a depletion of $^{13}C$ and $^{18}O$ in the carbonates.

Petrologic studies indicate that the most labile components (alginite, bituminite, sapropelic mass, gelinite) are present almost exclusively in the black shales, whereas the stable and secondary components (recycled vitrinite, vitrinite-like maceral, bituminous-mineral matrix, solid bitumen) predominate in the oxidized rocks (Nowak *et al.* 2001; Oszczepalski *et al.* 2002; Speczik *et al*. 2003).

Vitrinite reflectivity ($R_o$) contours typically correspond with base metal zoning (Fig. 1). The highest $R_o$ values (0.7-1.4 %) are observed in the Rote Fäule areas, fall to 0.6-1.3 % within the Cu zone, and finally to 0.5-0.9 % within the Pb- Zn- and pyrite zones. In contrast to the deeply buried Kupferschiefer (NE part of the area studied), $R_o$ values seem not to be depth-related around the Fore-Sudetic Block. Furthermore, the $R_o$ contours are markedly undulating in a fashion consistent with the extents of the Rote Fäule and metal zones, implying that the altering, ore-bearing solutions caused laterally extensive hematitic alteration, maturity variations, and localisation of orebodies. Elevated $R_o$ values are postulated to be caused by post-depositional thermal and chemical changes in indigenous vitrinite composition caused by post-sedimentary oxidation.

The change in vitrinite reflectance is about 100 % when compared with values in barren black shales. As a result, the organic matter in the reduced shales corresponds to liptinitic-type II kerogen, whereas organics in the oxidized shales were transformed due to oxidation into degraded aromatic-rich type III kerogen.

Maximum palaeotemperatures estimated from $R_o$ measurements significantly decline from 95-135°C in the oxidized shales, through 60-126°C in Cu-bearing rocks, decreasing to 65-100°C in Pb-Zn-bearing shales. These data suggest a maximum palaeotemperature that reached a highest value of around 135°C in the Rote Fäule alteration, indicating feeder areas, consistent with the previous results. Based on a normal heat flow, the maximum burial temperature of the mineralized horizon in Lubin area, was in the range 60-80°C that indicate the highest temperatures occurred as the effect of ascendant fluids. A high local heat flow during the late Permian-to-early Jurassic provided a heat source that influenced the temperature of the brine and enhanced fluid motion (Blundell *et al.* 2003).

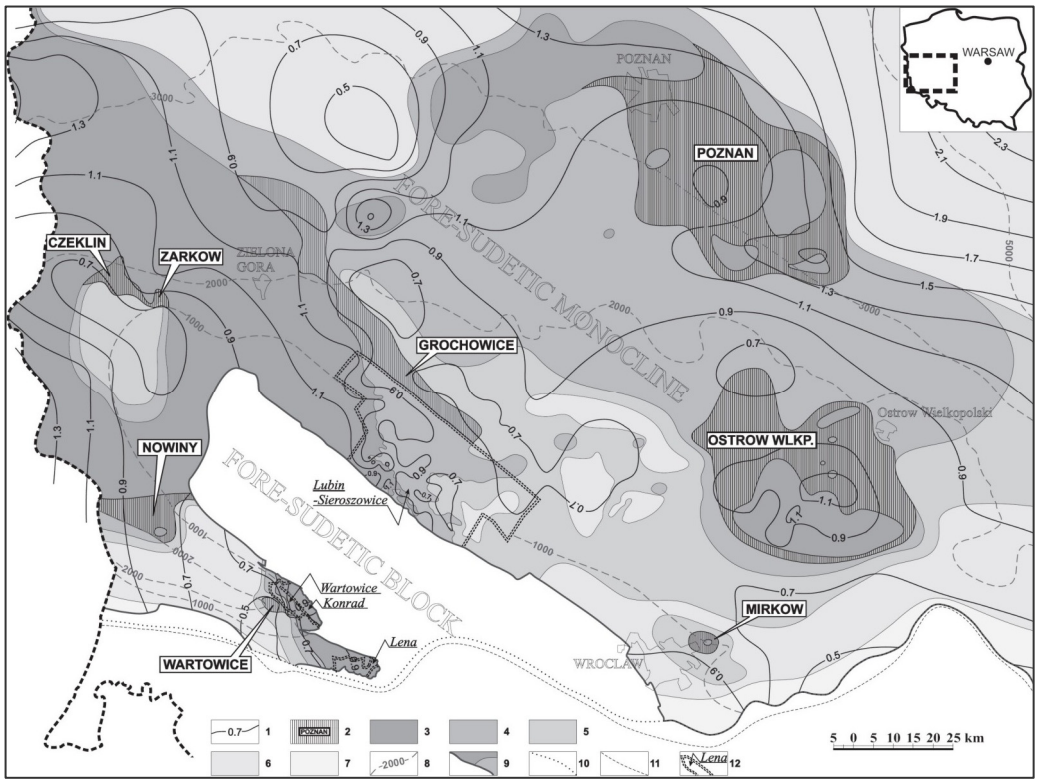


Figure 1. Kupferschiefer deposits, prospective areas, metal zoning and variation of vitrinite reflectance in SW Poland. 1 – Vitrinite reflectivity (in % $R_o$); 2 – Prospective areas; 3 – Rote Fäule zone; 4 – Cu zone; 5 – Pb zone; 6 – Zn zone; 7 – Pyrite zone; 8 – Depth of the Kupferschiefer (in m); 9 – Present Zechstein; 10 – Original Zechstein; 12 – Cu-Ag deposits.

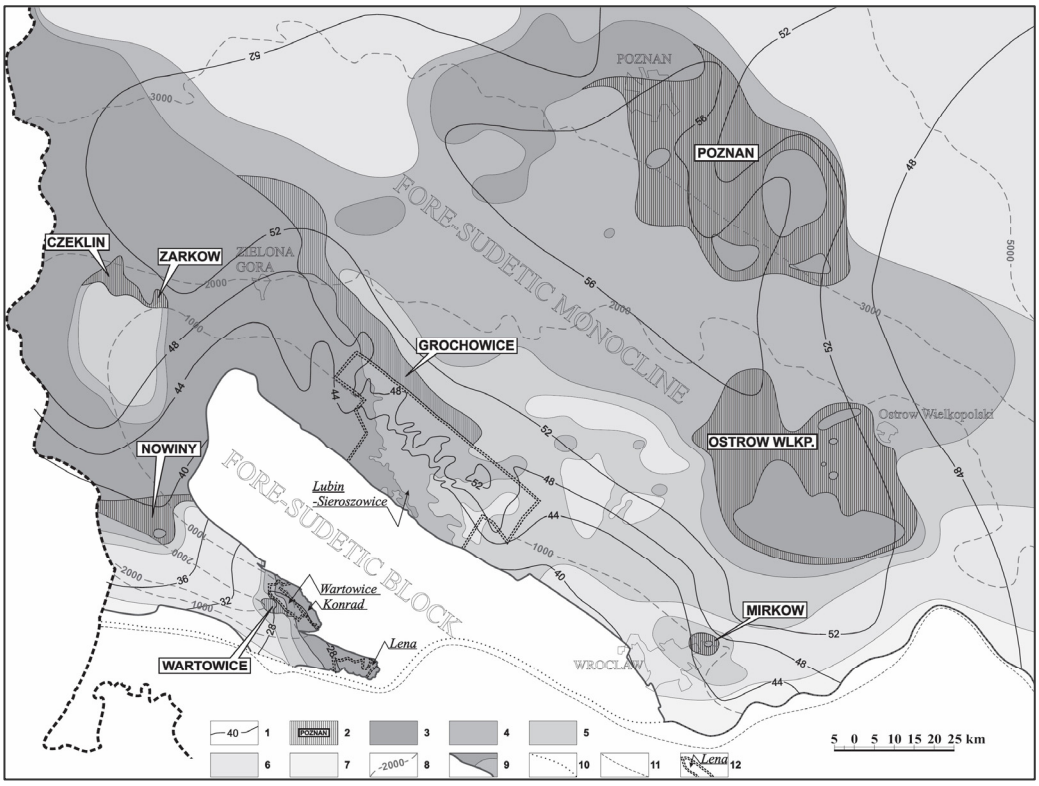


Figure 2. Present day temperatures at the depth of 1250m. 1 – Isotherms (in $^{o}$C); for other explanations see Figure 1.

## 4 PRESENT DAY GEOTHERMAL FIELD

To hold the scale of production on an economically acceptable level, KGHM Polish Copper SA will have to either import concentrates or move operations below 1200m. The temperature at depths between 1250 and 2000m that host copper resources will be the major technological and economical barrier. The temperature contour maps at 1250m (Fig. 2), 1500, 1750 and 2000m (not shown) have been constructed based on well temperature logs and new thermal conductivity measurements. The isotherms on these maps allow us to discern many places with anomalously lower than expected geothermal field values, suggesting low present day heat flows. They include areas situated N of Lubin–Sieroszowice deposit, W of the Fore-Sudetic Block and a vast region in the vicinity of Ostrów Wielkopolski. Those areas are characterized by relatively low values of present day temperatures at the ore unit that do not exceed 60$^{o}$C at 1500m level.

## 5 CONCLUSIONS

All of the Rote Fäule/ore centres located around the Fore-Sudetic Block are characterized by vitrinite reflectance maxima (predominantly >0.9 % $R_o$) and maximum palaeotemperatures exceeding 90$^{o}$C. This implies the highest maturity of the organic matter in areas of intense hematitization and the richest Au-Pt-Pd mineralization. A slightly lower degree of alteration is typical for Cu-Ag ores, while Pb-Zn zones reveal very low or lack of oxidation. Such a pattern suggests that the Rote Fäule/ore centres acted as conduits for hydrothermal mineralizing solutions. The zonation of organics, vitrinite reflectance and polymetallic mineralization in relation to the oxidized rocks may be genetically linked to intensity of ascendant circulation and interaction of hydrothermal ore fluids with reduced sediments. Thermal maturity variations indicate that mineralizing processes increased $R_o$ values of indigenous vitrinite. As a result, the redox interface forms the most important exploration guide for both Cu-Ag ores and Rote Fäule-related Au-Pt-Pd mineralization.

Our preliminary results show that the present day geothermal field is not uniform in SW Poland and that there is no strict correlation between subsurface temperatures and the depth of ore reserves, due to variations in recent heat flows. Local areas with geothermal anomalies encourage searching for technologies and new mining techniques that will allow extraction of ores from deeper than current operational levels.

## ACKNOWLEDGEMENTS

Partial support was provided by KGHM Polish Copper SA.

## REFERENCES

Bechtel A, Gratzer R, Püttmann W, Oszczepalski S (2001) Variable alteration of organic matter in relation to metal zoning at the Rote Fäule front (Lubin-Sieroszowice mining district, SW Poland). *Organic Geochemistry* 32: 377-395.

Blundell DJ, Karnkowski P, Alderton DHM, Oszczepalski S, Kucha H (2003) Copper mineralization of the Polish Kupferschiefer: A proposed basement fault-fracture system of fluid flow. *Economic Geology* 98: 1487-1495.

Kucha H, Przybyłowicz W (1999) Noble metals in organic matter and clay-organic matrices, Kupferschiefer, Poland. *Economic Geology* 94: 1137-1162.

Nowak GJ, Speczik S, Oszczepalski S (2001) Petrographic composition of organic matter in the Kupferschiefer horizon of Poland. *Mineral Deposits*, Balkema, Rotterdam: 67-70.

Oszczepalski S, Nowak GJ, Bechtel A, Zák K (2002) Evidence of oxidation of the Kupferschiefer in the Lubin-Sieroszowice deposit, Poland: Implications for Cu-Ag and Au-Pt-Pd mineralization. *Geological Quarterly* 46: 1-23.

Oszczepalski S, Rydzewski A (1997) Metallogenic Atlas of the Zechstein Copper-bearing Series in Poland. *Polish Geological Institute.* Warsaw.

Speczik S, Oszczepalski S, Nowak GJ, Grotek I, Niczyporuk K (2003) Organic matter alteration trends in the Polish Kupferschiefer: Ore genetic implications. *Mineral Exploration and Sustainable Development,* Millpress, Rotterdam: 853-856.

Speczik S, Rydzewski A, Oszczepalski S, Piestrzyński A (1997) Exploration for Cu-Ag and Au-Pt-Pd Kupferschiefer-type deposits in SW Poland. *Mineral Deposits,* Balkema, Rotterdam: 119-122.

# Comparison between stratabound Copper-Silver mineralization of Mitu Formation, Peru, and Polish Kupferschiefer Deposit

J. Pieczonka & A. Piestrzyński,
*AGH-University of Science and Technology, av. Mickiewicza 30, 30-059 Krakow, Poland,*
P. Lutyński
*Amera Resources Corporation AMS - TSX-V,Vancouver, B.C., V6C 3N6, Canada,*

ABSTRACT: Permian stratabound sulphide and oxidized copper-silver mineralization has been recently discovered within the Mitu Formation in central Peru. Sulphide mineralization is represented by association of chalcocite, covellite bornite and minor native silver overprinted by an oxide assemblage composed of malachite, azurite and brochantite. Mineralization is hosted in volcaniclastics (greenschist metamorphic facies), sandstone, and shale. Copper and silver mineralization is commonly associated with the presence of organic matter and is similar to the Polish, Permian age, world class, stratabound Lubin – Sieroszowice copper-silver deposit.

KEYWORDS: economic stratabound copper mineralization, new discovery, Mitu Formation, Peru

## 1 INTRODUCTION

The Mitu Formation is a part of a relatively well-recognized Permian sequence in Peru consisting mainly of clastic and volcanoclastic rock units. This paper discusses some geological and metalliferous similarities and differences between the Mitu Formation and the Polish Kupferschiefer. Samples for this study were collected from two mineral exploration properties, Cocha and Mitu, located in the Junin district in central Peru, at an elevation between approximately 4000 and 4600m. Three lithologically different rock types collected from the Mitu Formation have been studied: sandstone (Fig. 1, *e.g.* sample no 426202 and 246200), shale (sample 426201) and volcaniclastic, commonly metamorphosed to greenschist facies. The stratigraphy of the Cocha property is represented by metamorphic basement rocks overlain with unconformity by volcaniclastics, locally metamorphosed into a green schist or zeolite facies, and consequently overlain by sandstone and limestone. At the Mitu property the stratigraphy consists of metamorphic basement overlain by sandstones with intercalations of shale and limestones.

## 2 MITU FORMATION

The Permian age Mitu Formation represents a suite of andesite and rhyolite flows intercalated with volcanogenic agglomerate and tuff (Norman *et al*. 1953) and subsequently overlain by fine-grained sandstone and arkose with several intercalations of mudstone (Kobe 1990). The Mitu Formation forms a NNW-SSE belt parallel to the main geological structure of Peru and varies in thickness from the south to the north, reaching in some places up to 4000m.

The Mitu Formation is discordantly underlain by Copacabana Formation (Permian + Pennsylvanian) and overlin by the Pucara Formation (Lower Mesozoic). In many sections the Mitu Formation forms tectonic contacts with other strata (Piestrzyński *et al.* 2006). Mitu sandstone represents well sorted, generally fine grained clastic sediment composed of plagioclase, quartz, sericite, carbonate, organic matter, micro-clasts of volcanogenic rocks (dacite, andesite), siliciclastic material, minor zircon, clinozoisite, apatite, microcline, muscovite, and probably zeolites. This unit probably represents wackes and arkoses mixed with flow fragments or tuffite – lahar type of clastic material. Shale compositions are very similar to the sandstone, only finer grained. Volcaniclastics are represented by fine ash tuff, lapilli tuff and tuff agglomerates, and possibly also lahars that in the mineralized zones are commonly metamorphosed to greenschist facies. Microscopic studies reveal silicification (Fig. 4), albitization,

younger sulphidization, and oxidation (Piestrzyński *et al.* 2006).

Geochemical surface rock sampling reveals the presence of up to 9.3% copper and 1000 g/t silver in sandstones. The same rock analysis assayed up to 0.01 ppm Au, 0.25 g/t Pd, 0.005 g/t Pt, 0.05 g/t Re, 0.78 g/t Se and up 752 g/t As (Piestrzyński *et al.* 2006). The 2006 drilling performed in the discovery outcrop area of the Cocha property intersected over 30m assaying 2.67% Cu and 24.1 g/t Ag (*Amera Resources Corporation* 2006).

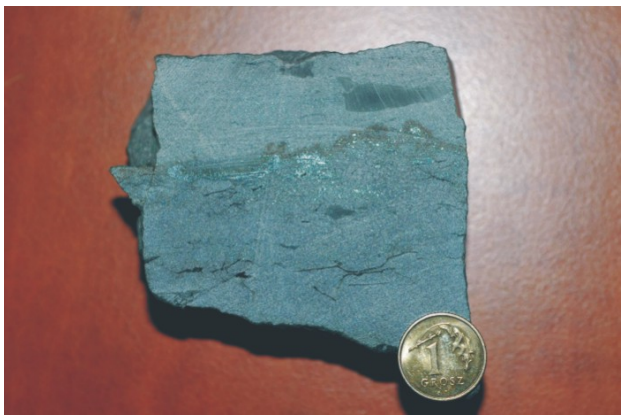

Fig. 1 Chalcocite rich sandstones from the Mitu Formation, black is organic matter, Peru, sample 425201

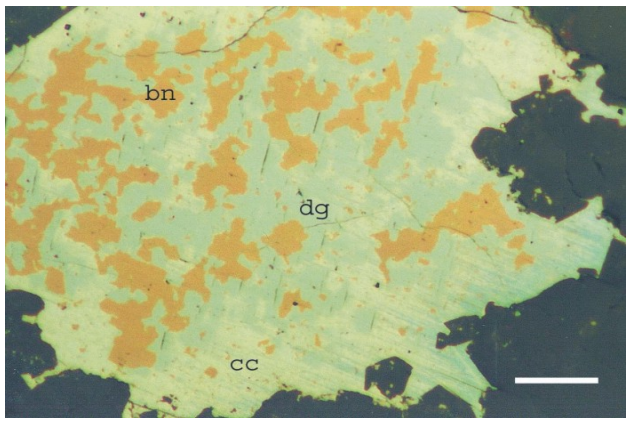


Fig. 2 Intergrowth of bornite (bn) digenite (dg) and chalcocite (cc), reflected light, scale bar 50 μm, sample 425201.

Table 1. SEM-EDS composition of chalcocites and bornites.

| sample | Cu *Kα* | Fe *Kα* | S *Kα* | Ag *Lα* | Hg *Mα* |
|---|---|---|---|---|---|
| 342/4 | 78.55 | 0.23 | 21.22 | 0 | n.a. |
| 342/3 | 78.50 | 0.72 | 20.55 | 0.24 | n.a. |
| 342/3 | 62.88 | 10.65 | 26.32 | 0.15 | n.a |
| 342/1 | 62.86 | 10.75 | 26.39 | 0 | n.a. |
| 341c/5 | 60.83 | 10.42 | 26.28 | 0.38 | 2.09 |
| 341c/4 | 61.01 | 10.13 | 25.65 | 1.17 | 2.04 |

n.a.- not analysed

Sulphidization probably developed in one stage and is characterized by chalcocite, bornite, digenite, covellite, and minor chalcopyrite. The petrogenetic position of native silver is not clear, as. Silver has been found only in small fissures in the host rocks. Chalcocite is a major copper sulphide. It forms nest and micro-vein structures, usually less than 100 μm in size, filling almost all free spaces in sandstone as well as cracks and nests in organic matter (coal). The largest sulphide nest observed, in the richest copper section, is less then 2 mm in diameter. Chalcocite also forms intergrowths with bornite, covellite and digenite (Fig. 2) and is commonly replaced by covellite. In some samples sphalerite, galena and native silver also have been detected.

All investigated samples collected on the surface are partly oxidized. Oxidation is developed along fissures and micro-cracks and is represented by iron hydroxides, malachite, brochantite, and probably atacamite. One hand-size sample from the Mitu Formation represents mica-plagioclase schist with minor quartz, chlorite, haematite, and carbonates. This rock contains also macro-clasts of volcanogenic rocks.

The EDS compositions of chalcocites show its stoichiometric composition with minor amounts of silver (Tab. 1). Chemical composition of some bornite grains is variable; some grains contain elevated amounts of silver and mercury (Tab. 2), and in reflected light, these grains show bi-reflectance and are anisotropic. According to Kanzawa *et al.* (1978) such optical properties are characteristic of low-bornite with pseudotetragonal symmetry.

Analyzed bornites represent the low temperature variety occurring in temperature below 170°C (Kanzawa *et al.* 1978). The chemical composition of native silver is shown in Table 2. Analyzed silver grains are characterized by a very low admixture of other metals like Au, Fe, Hg and Cu (Tab. 2). The structural position of silver and its chemical composition suggest a younger stage of deposition. The source of silver could be primary bornite and or other Cu-

sulphides containing low silver admixtures (compare Tab. 1).

## 3 ORGANIC MATTER

The investigated samples are rich in organic matter (Fig. 3 & 4). In some samples, fragments of organic matter are visible macroscopically. Two different types of organic matter from the Mitu Formation were investigated. The first type, more common, is para-anthracite high (C) (according to international classification ECE/ENERGY/50), that is characterized with a random reflectivity ranging from R° = 2.16% up to R° = 2.53%, and an average of R° = 2.34% (all measurements were made on metavitrinite). This difference is confirmed by bireflectance of metavitrinite observed under a microscope. The second type of organic matter is dispersed in sandstone (Fig. 4). Results of 150 single measurements of the random reflectivity showed a wide distribution of this parameter ranging between 1.2 and 2.8% (Piestrzyński *et al*. 2006).

Table 2. SEM-EDS composition of native silver.

| sample | Cu *Kα* | Fe *Kα* | Au *Mα* | Ag *Lα* | Hg *Mα* |
|---|---|---|---|---|---|
| 341c/3 | 0.65 | 0.19 | 0.16 | 98.30 | 0.71 |
| 341c/2 | 0.59 | 0.23 | 0.07 | 98.25 | 0.87 |
| 341c/1 | 0.85 | 0.32 | 0 | 98.24 | 0.59 |

Table 3. Rock Eval data samples from the Mitu Formation in wt%, $T_{max}$ in °C.

| Sample | TOC | $T_{max}$ | $S_1$ | $S_2$ | $S_3$ | PI | HI | OI |
|---|---|---|---|---|---|---|---|---|
| 246200 | 0.06 | 518 | 0.08 | 0.12 | 1.94 | 0.40 | 200 | 3233 |
| 425201 | 0.71 | | 0.16 | 0.05 | 1.15 | 0.76 | 7 | 162 |
| 425202 | 0.17 | 453 | 0.26 | 0.21 | 0.67 | 0.55 | 124 | 394 |
| 425203 | 0.16 | | 0.13 | 0.08 | 1.92 | 0.62 | 50 | 1200 |

S1- hydrocarbons content (mg HC/g of rock), S2- residual HC potential, S3-content of $CO_2$ (mg$CO_2$/g of rock), TOC- total organic carbon content, PI- production index, HI- hydrogen index, OI- oxygen index

This differentiation allows the identification of several macerals each having different average random reflectivity. Based on this, the following macerals have been recognized: metaalginite – R° = 1.33%, metafunginite and metasecretynite - R° = 1.69%, metainertinite - R°=2.05% and metavitrinite - R° = 2.52%. Examination of the organic matter suggests high non-homogenity of organic matter and a contact type of thermal flux (around 210°C) in the

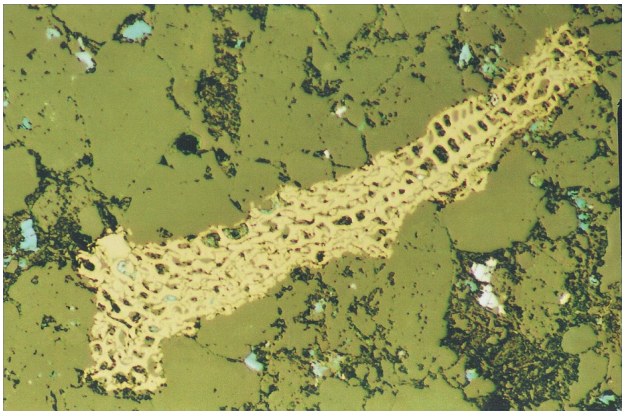

Fig. 3 Cataclastic type of para-anthracite, reflected light, scale bar 50 μm, sample 42521.

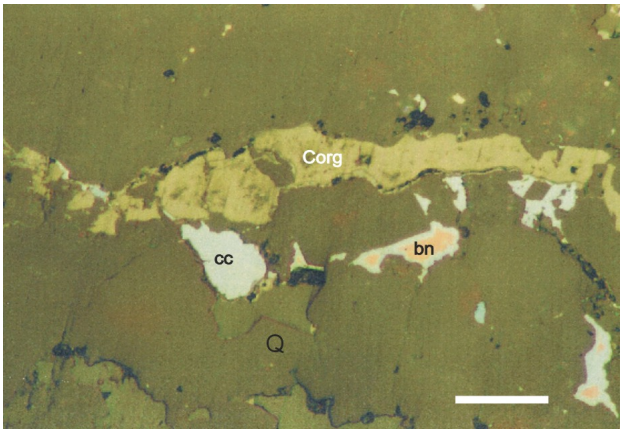


Fig. 4 Vein type of organic matter (Corg), chalcocite (cc), bornite (bn). Reflected light, scale bar 50 μm, sample 42521

local environment (Piestrzyński *et al.* 2006). In the Polish Kupferschiefer two genetic types of organic matter have been identified: sapropelitic liptinite with minor vitrinite and inertinite (Nowak *et al.* 2001), and thucholite. Sapropelitic organic matter is characterized by reflectivities ranging between 0.72-1.13%. It corresponds to a low degree of maturation and temperatures below 130°C (Nowak *et al.* 2001). Thucholite represents a metaliferous type of kerogen, and deposition of this material is related to the secondary, hydrothermal stage of oxidation that took place in the Polish Kupferschiefer (Piestrzyński *et al.* 2002).

## 4 DISCUSSION AND CONCLUSIONS

Investigated samples from the Mitu Formation show a similar style of copper sulphide mineralization and the same hydrothermal genesis as for the Polish Kupferschiefer. However, the temperature responsible for metamorphic changes in the Mitu Formation was higher:

a maximum temperature of 210°C was calculated from the reflectivity of vitrinite-type organic matter (Piestrzyński *et al.* 2006). This temperature should be related to sulphidization, however presence of low-temperature bornite suggests that deposition of sulphide was shifted in time in relative to the maturation of organic matter. In the Polish Kupferschiefer copper deposit, the presence of low chalcocite suggests a temperature below 103°C for the mineralized fluids – the last stage of a hydrothermal activity. A similar temperature is suggested by the temperature of maturation of sapropelitic organic matter (Nowak *et al*. 2001). Sulphides from the Mitu Formation were deposited at a higher temperature, probably related to the zeolite facies, but not higher than the upper limit for low bornite. High HI and OI indexes of organic matter (Tab. 3) show, that organic matter could have stimulated deposition of copper sulphides. Bulk chemical analyses of the Mitu and the Kupferschiefer type of deposits showed several similarities and small number of differences (Piestrzyński *et al.* 2006). Green schist – zeolite facies; however, according to different reflectivity of organic matter, contact metamorphic alterations are more probable. The temperature of the discoloration in both cases is the same. In polished sections from the Kupferschiefer deposit, red internal reflections have been found as a remnant of the red-bed environment (Wodzicki & Piestrzyński 1994, Piestrzyński *et al.* 2002). Bleaching effect was developed simultaneously with a development of anoxic environment that took place during the reduction of metals from the oxidized fluids. Also, hydrothermal models of ore mineralization as a post-depositional effect are postulated for both units (Piestrzyński *et al*. 2006). The oxidation effect observed in all samples is younger and represents a supergene mineralization; however sulphide grains from the Mitu Formation do not show typical structures developed during oxidation. It can also be concluded that oxide association from the Mitu Formation is a result of a different stage of the development of the deposit. Host rocks of the Mitu Formation, in comparison to the Polish redbed-related copper deposit, are characterized by an intensive alteration that took place at higher temperature.

The Mitu Formation appears to be a good exploration target for the stratabound copper deposits in Peru; however, a detail regional geological study is needed.

ACKNOWLEDGEMENT:

Authors express sincere thanks to Prof. M. Wagner from the AGH-University of Sciences and Technology for his help in investigation of organic matter. The two first authors are also sincere to Amera Resources Corporation AMS - TSX-V, Vancouver for its financial support in Peru. Grant AGH 11.11.140.300.

## REFERENCES

Amera Resources Corporation (2006) Amera Intersects 30.23 Metres of 2.67% Copper and 24.1 g/t Silver on 100% Owned Cocha project. In: *http://www.ameraresources.com/s/NewsReleases.asp?ReportID=154314*.

Kanzawa Y, Koto K, Morimoto N (1978) Stability and crystal structure of the intermediate form. *Canadian Mineralogists* 16: 397-404.

Kobe HW (1990) Stratabound Cu-(Ag) deposits in the Permian Mitu Red-bed Formations, Central Peru. In: *Stratabound Ore Deposits in the Andes (L. Fonbote et al. eds.)*, Springer-Verlag Berlin Heidelberg: 123-127.

Norman D, Newell ND, Chronic J, Roberts T (1953) Formations and Geologic history. Memoir Â·36, *Geological Society of America.* pp111.

Nowak GJ, Speczik S, Oszczepalski S (2001) Petrographic composition of organic matter in the Kupferschiefer. InMineral Deposits at the beginning of the 21st centuary, A. Piestrzyński et al. Eds, *Proceeding of the joint biennial SGA-SEG Meeting /Kraków, Poland/*: 67-70.

Piestrzyński A, Pieczonka J, Głuszek A (2002) Redbed-type gold mineralisation, Kupferschiefer, southwest Poland. *Mineralium Deposita* 37: 512-528.

Piestrzyński A, Pieczonka J, Dunin-Borkowski S, Lutyński P, Wagner M, Durand A, (2006) Mitu-Kupferschiefer formations: similarities and differences, Peru-Poland. *Sociedad Geologica del Peru, Publication Especial* no 7: 772-775.

Wodzicki A, Piestrzyński A (1994) An ore genetic model for the Lubin-Sieroszowice mining district, Poland. *Mineral. Deposita* 29: 30-43.

# Aynak: A world-class sediment-hosted copper deposit, Afghanistan

A.J. Benham & J.S. Coats
*British Geological Survey, Keyworth, Nottingham, NG12 5GG, UK*

Peter Kovac
*Geological Institute Slovak Academy of Science, Bratislava, Slovakia*

ABSTRACT: The Aynak copper deposit, 30 km south of Kabul in Afghanistan, was discovered by Soviet geologists in the 1970s. Extensive exploration from 1974-89 included drilling, trenching and adits. This delineated several large ore bodies and smaller lenses with a total "drill-indicated resource" of 240 Mt at 2.3% Cu (ESCAP, 1995). Mineralization consists of disseminated bornite and chalcopyrite in a stratabound cyclic sequence of metamorphosed sediments of late Precambrian age. A model proposes copper was leached from underlying volcanic rocks by circulating brines and then moved up faults to deposit copper sulphides within the overlying sediments.

KEYWORDS: Sediment-hosted copper deposit, Afghanistan

## 1 INTRODUCTION

The largest and best-known copper deposit in Afghanistan is the world-class Aynak sediment-hosted stratiform copper (SHSC) deposit, approximately 30km south of Kabul (Figure 1). Aynak occurs within the Kabul Block, a north-north-east-trending lenticular shaped block, approximately 200km long and 5km wide. This block, which also contains several other copper deposits including Darband and Jawkhar, is one of a series of microplates that broke off from Gondwana around 250 Ma and accreted onto the margins of Laurasia.

## 2 PREVIOUS EXPLORATION

Soviet and Afghan geologists undertook extensive exploration in the Aynak area during two phases, from 1974 to 1976 and again from 1978 to 1989. This work included several hundred boreholes, seventy trenches and nine exploratory adits as well as ground-based geophysical surveying and mapping. During this work, the Soviets identified four principal and 28 smaller lens-like mineralized zones at Central Aynak, and 20 zones in Western Aynak. The major mineralized zones at Central Aynakwere traced for 1850m along strike and 1200m down dip with a maximum thickness of 210m. At the Western Prospect, mineralization was traced for 2230m along strike, 1640m down dip with a maximum thickness of 214m. A Soviet "drill-indicated resource" of 240 Mt at 2.3% Cu was calculated for both deposits, assuming a cut-off grade of 0.4% Cu (ESCAP, 1995).

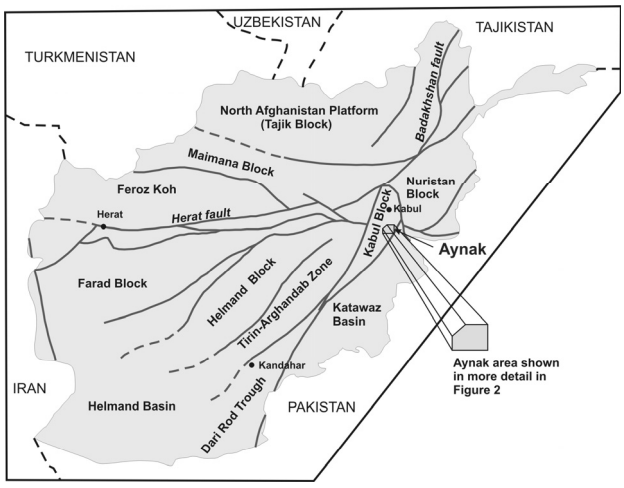


Figure 1. Structural map of Afghanistan and location of the Aynak copper deposit. Aynak area shown in more detail in Figure 2.

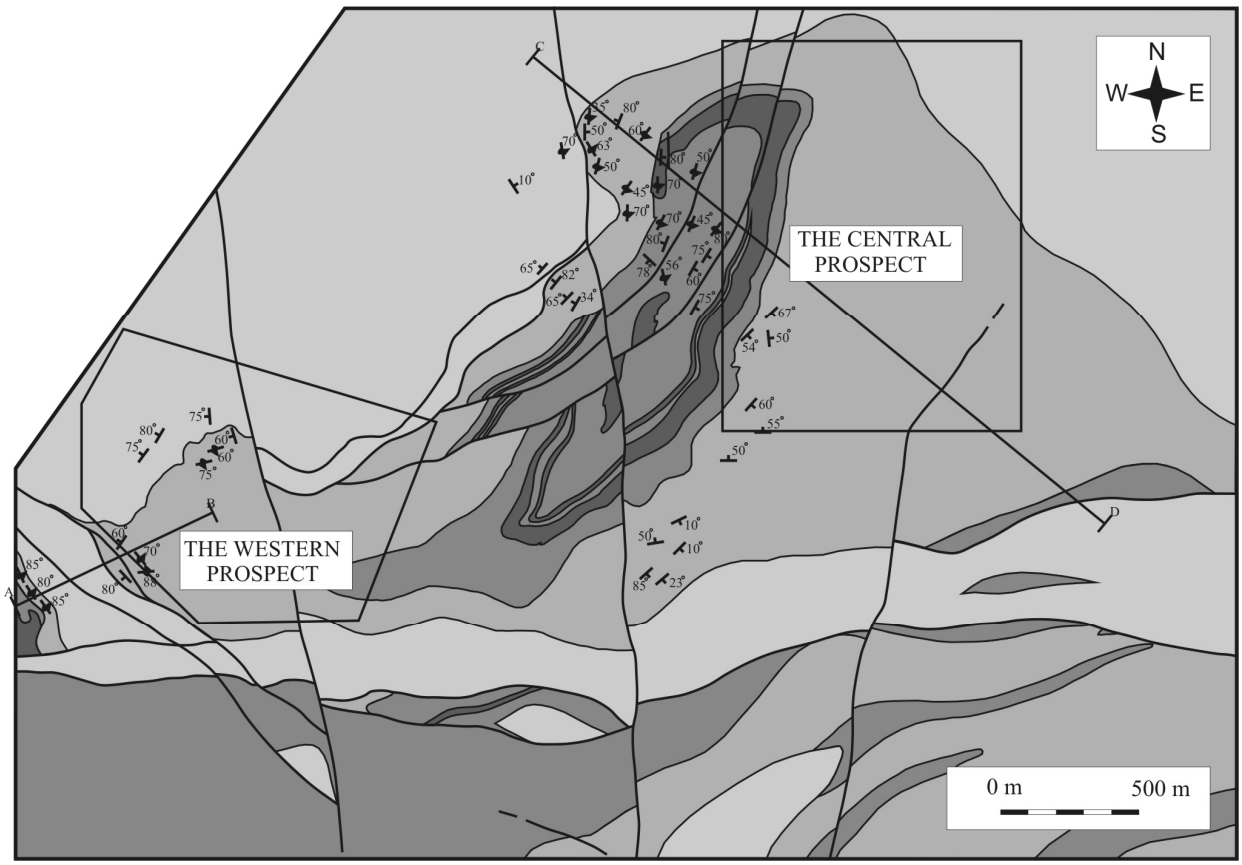


Figure 2: Simplified geological map of the Aynak Area

## 3 STRUCTURE

The structure at Aynak is dominated by the Aynak anticline. The anticline is asymmetrical and approximately 4 km in length and up to 2.5 km wide. The south-eastern limb dips gently to the south-east but the north-western limb is steeply dipping and in places overturned, with dips of 45-70$^{o}$ to the south-east. The periclinal closure of the anticline at its western end is asymmetrical. Here, the southern limb is overturned and the axial plane is inclined towards the north-north-east. Several sets of later faults cut across the folds. As a result of folding, Aynak is divided into two prospects. The Central Aynak prospect is located on the shallow-dipping eastern limb of the anticline and the Western Aynak prospect occurs in the area of the periclinal closure at the western end of the structure (Figures 2 and 3)

## 4 MINERALIZATION

The mineralization at Aynak is stratabound and consists of disseminated bornite and chalcopyrite hosted within a cyclic succession of metamorphosed dolomites, marls, siltstones and carbonaceous pelites of the Loy Khwar Formation. Primary mineral zonation is apparent with the central part of the deposit containing mainly bornite, grading out to chalcopyrite, then pyrite and pyrrhotite. Cobalt concentrations, although very low, increase towards the periphery of the deposit. The host sediments were deposited in Vendian-Cambrian times in a shallow sea on the northern margin of Gondwana.

## 5 METALLOGENIC MODEL

Detailed studies into the genesis of the deposit have yet to be carried out. However, due to the style, size and grade of the deposit at Aynak, it may be analogous to the deposits of the Zambian Copperbelt. A metallogenic model is proposed in which the copper is leached from underlying volcanic rocks by circulating evaporitic brines and seawater. The heated brines are channelled up marginal faults into the overlying sediments where they reacted with reduced interstitial fluids and hydrocarbons, depositing copper sulphides in the dolomite host rock (Figure 4).

ACKNOWLEDGEMENTS

This paper is published with the permission of the Director of the British Geological Survey (NERC). The authors would like to thank Tim Colman who helped in the preparation of this paper and provided useful comments and feedback.

REFERENCE

ESCAP, 1995. Atlas of Mineral Resources of the ESCAP Region: *Geology and mineral resources of Afghanistan,* Vol. 11. 1995 United Nations 85pp.

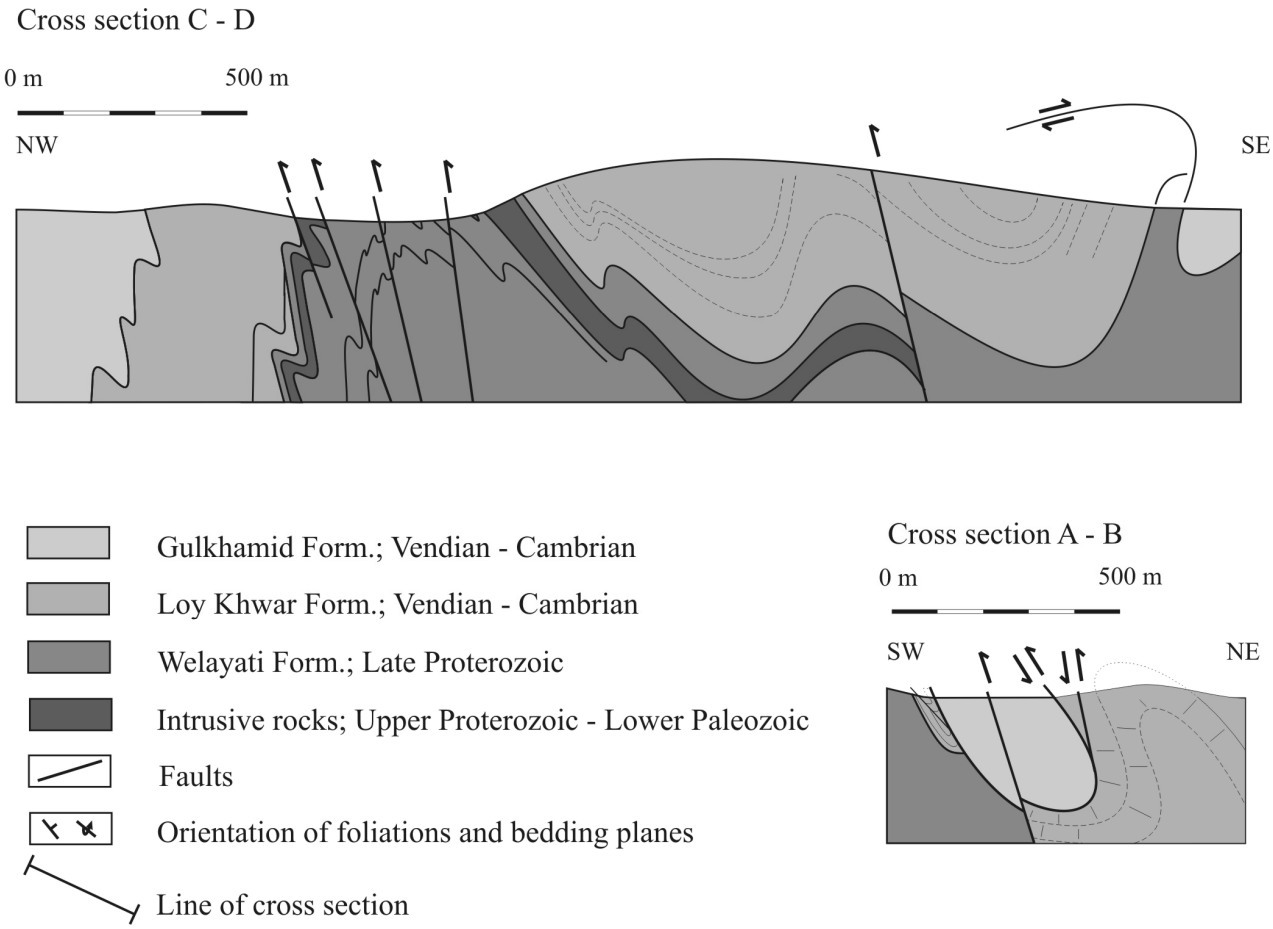


Figure 3. Simplified cross sections through the Aynak area.

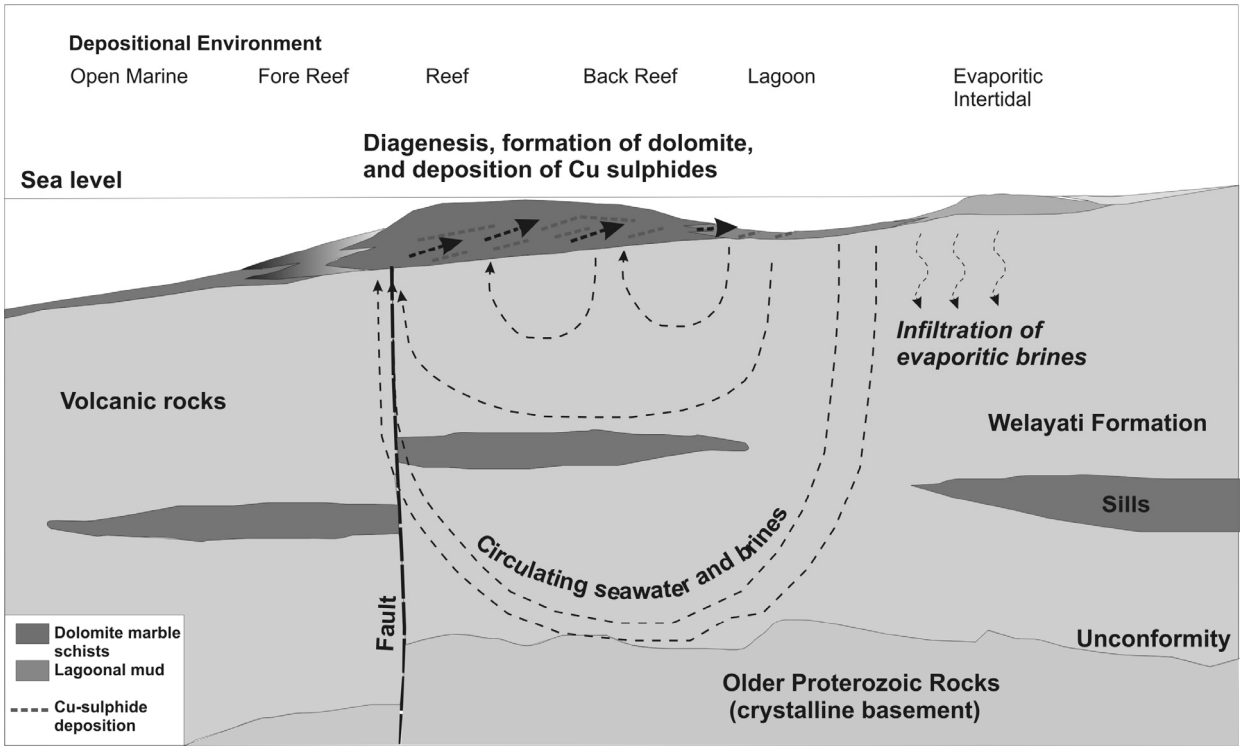


Figure 4. Proposed metallogenic model for the formation of copper mineralization at Aynak.

# Exploration potential for sediment-hosted copper deposits in the Adelaide Fold Belt, South Australia

G.R. Baglin
*International Base Metals Limited, Sydney, NSW, Australia*

M.E. I'Ons
*Photogeological Consultant, Tenterfield, NSW, Australia*

R.V. Kirkham
*Private Consultant, Delta, British Columbia, Canada*

K.J. Maiden, C.L. Seabrook
*Copper Range Limited, Adelaide, SA, Australia*

J.P. Thorson
*Private Consultant, Parker, Colorado, USA*

A.H. van Herk
*International Base Metals Limited, Sydney, NSW, Australia*

ABSTRACT: The Proterozoic Adelaide Fold Belt (AFB) of South Australia displays many similarities with geological environments that are known to host large stratiform sediment-hosted copper deposits. The general characteristics of geology and basin development in the AFB have produced all the features necessary for the generation of these deposits. Little exploration for copper has been undertaken in the region since the 1980s and whilst previous explorers have investigated some areas, many targets remain insufficiently tested due to poor understanding of the style of deposit. Copper Range Limited ("Copper Range") and it's consulting geologists have developed a new approach to understanding the distribution of copper in the AFB. The company's recent field investigations in the region have resulted in the generation of new exploration models based on up-to-date research of sediment-hosted copper deposits. Initial exploration has confirmed the potential of this target style.

KEYWORDS: Copper, Adelaide Fold Belt, Flinders Ranges, sediment-hosted, exploration

## 1 INTRODUCTION

The AFB contains in excess of 800 known occurrences of copper mineralization. The majority of these are historic workings and were mined during the 19th century and generally consist of small pits and shafts. Two significant deposits at Burra and Kapunda (Fig. 1) were mined more extensively, producing approximately 180,000 and 14,500 tonnes of copper metal respectively. However, sustained exploration for copper in the region has not been undertaken since the 1970s-1980s when companies such as Utah Development Co. focused on known occurrences and specific stratigraphic situations. These exploration programs were based on a syngenetic or early diagentic model and exploration never pursued the potential of the epigenetic replacement-type model that is generally accepted today. Consequently, the general sentiment seems to consider the AFB to have been fully explored and not generally acknowledged to have the potential for further significant economic discoveries (*e.g.* Bull 2003).

In contrast, Copper Range geologists believe that previous exploration was unsuccessful because it was based on erroneous concepts, that the region has been under-explored and that excellent potential remains for discovery of stratabound copper deposits of substantial size.

## 2 REGIONAL GEOLOGY

The thick sedimentary sequence within the AFB was deposited during broad subsidence and the development of successive rift valleys. The largely clastic sedimentary rocks in the fold belt comprise the Warrina and Heysen

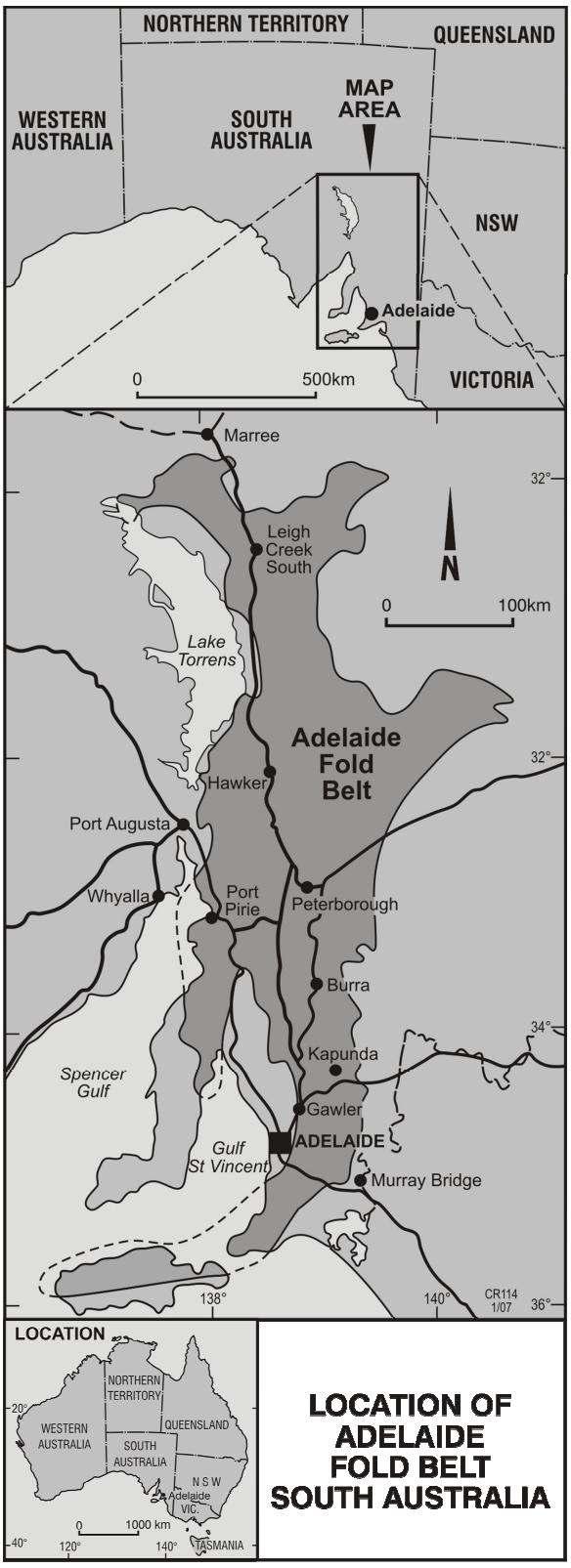


Figure 1. Location of the Adelaide Fold Belt, South Australia

Supergroups that regionally host the copper mineralization. Lowermost in the succession, the Callana Group sediments accompany rift-related basic volcanics (basalts) on which thick sequences ofmixed evaporitic clastics and carbonates accumulated. These rocks are overlain by the Burra Group sandstones, dolomites and limestones that were deposited in transgressive-regressive cycles with some fluvial input. The base of the overlying Umberatana Group is marked by a glacial conglomerate (Sturtian) and comprises thick basinal clastic sequences of shale, siltstone and sandstone with minor carbonate. A second glaciation (Marinoan) was followed by a marine transgression during which sediments of the Wilpena Group were deposited. Deposition ceased with the onset of the Delamerian Orogeny marked by granite intrusions in the south at about 500 million years and subsequent folding and thrusting. Two separate tectonic events are recognized in the Flinders Ranges, with early east-west compression producing linear north-south trending folds and a north-south compression producing strong east-west folds accompanied by low-grade metamorphism.

## 3 EXPLORATION POTENTIAL

Sediment-hosted copper deposits such as the Polish Kupferschiefer, the Zambian Copperbelt and the Paradox Basin, Utah comprise pene-concordant zones of copper sulphides within siliciclastic or dolomitic sedimentary rocks (Hitzman *et al.* 2005). An epigenetic model for these deposits is now generally accepted, in which copper is precipitated from circulating brines within the sedimentary sequence (*e.g.* Kirkham 1989). Several geological features of sedimentary basins are therefore essential to the generation of such deposits. These include:

1. A thick sedimentary sequence deposited in a rift-basin setting;
2. Metal-rich source rocks, such as volcanics or redbeds, from which copper can be leached;
3. The presence of evaporite units within the sedimentary sequence to generate basin-wide circulation of saline fluids; and
4. Organic or sulphide-rich sequences capable of serving as an *in-situ* reductant for the precipitation of copper from low temperature brines.

All of these features are present within the AFB.

Other additional features may also be favorable for the genesis of sediment-hosted copper deposits. These may be the direct result of the four features outlined above, or may be related

to subsequent events in basin development. In either case, these conditions are considered encouraging for exploration success and are well developed within the AFB.

5. Widespread alteration of the sediments indicating the production and extensive circulation of aqueous fluids;
6. Numerous stratiform copper occurrences, particularly at stratigraphic levels where a reducing unit occurs; and
7. Post-mineralization events that may have resulted in upgrading a deposit, such as remobilization by later tectonic events or supergene enrichment.

A significant hindrance to exploration in the AFB is the extensive weathering that has occurred over much of the Australian continent. Long periods of sub-aerial erosion and deep supergene oxidation have effectively masked the original nature of lithologies making it difficult to establish, for example, their primary oxidizing or reducing potential. These complications may have contributed to the AFB being ineffectively explored during the 1970s-1980s and more recently overlooked as a significant province for sediment-hosted copper deposits.

## 4 CURRENT EXPLORATION TARGETS

Since the inception of Copper Range in mid-2005, the company has established an extensive tenement position within the AFB, focused around the historic mining centers of Burra and Kapunda, and clusters of old workings near Hawker in the Flinders Ranges (Fig. 1). Several targets are described here in order to demonstrate similarities with other sediment-hosted copper provinces and highlight the existing potential of the region. Exploration is ongoing in all areas.

Hawker Project Area: The Company's review of data from previous exploration and interpretation of satellite imagery has led to the identification of a number of target areas, including:

- Bedded copper which is evident in outcrop or in small-scale mine workings, but has not been subjected to more recent exploration;
- Zones of alteration which, in at least one case, appear to contain hematite after chalcocite;
- Copper (and zinc and cobalt) geochemical anomalies;
- Areas where significant structures intersect favorable lithologies.

During September 2006, a reconnaissance drilling program at the Birthday prospect identified stratiform zones of copper-bearing lithologies that are similar to those found in many other sediment-hosted copper occurrences globally. The prospect area also displays significant diapirism, which has been interpreted to have resulted from salt deformation in evaporite-bearing strata (Rowan & Vendeville *in press*).

At Wyacca, old workings display copper oxides and minor chalcopyrite replacing calcareous beds at the base of the Tapley Hill Formation (Preiss 1999). They occur along projected strike of quartz-veined fault zones that cross-cut and offset an underlying quartzite unit that contains small amounts of fine-grained disseminated chalcopyrite. These features suggest that copper-bearing fluids may have collected and focused at the top of the quartzite and leaked up fault-related fracture systems, providing cross-stratal fluid flow that is critical in many other systems (Hitzman *et al*. 2005).

Kapunda Project Area: High grade quartz lodes containing malachite and chalcocite were the principal ore zones mined from the Kapunda Mine subsequent to its discovery in 1842. The host rocks are highly weathered and leached carbonaceous siltstones and shales, which also contain malachite, probably after chalcocite, in the supergene zone along fractures and as disseminations in siltstone and shale. Drilling by Utah Development (Lambert *et al.* 1980) documented stratiform zones of disseminated chalcopyrite in a local Mine Series dolosiltstone lithology discovered below the weathered zone. Mineral and vein textures from that core indicate very early, pre-deformation deposition of copper. Fluid inclusions and isotope studies indicate that copper, carried by a mildly oxidizing highly saline aqueous fluid, replaced initial biogenic iron sulphide. The features are comparable with copper mineralization within the carbonaceous shales and siltstones of the Nonesuch Formation at White Pine, USA, and the Kupferschiefer shale. Considerable exploration potential exists in the vicinity of the Kapunda Mine for fine-grained sediment-hosted copper in deeper, un-weathered porous and permeable horizons that acted as receptive hosts to metal-bearing fluids flowing along cross-cutting structures.

## 5 CONCLUSIONS

The AFB of South Australia displays all the general characteristics of geology and basin development considered necessary for the generation and emplacement of stratiform sediment-hosted copper deposits: A rift-basin geological history with a thick sedimentary sequence; breccia diapirs derived from evaporites probably containing considerable salt; metal-bearing source rocks from which copper could have been leached; and reductant-bearing strata capable of precipitating copper from low temperature brines.

Known mineralization displays a range of characteristics similar to other sediment-hosted copper deposits globally. Initial exploration by Copper Range has validated this exploration model and has targeted several areas that show both short and long term potential to develop into drillable prospects. However, exploration programs face significant challenges posed by deep weathering and confusing stratigraphy.

## ACKNOWLEDGEMENTS

The authors thank the generous financial and academic support of Copper Range Limited.

## REFERENCES

Bull S (2003) Comparison of Cu mineralised basins: the Zambian Copperbelt, the Polish Kupferschiefer, the Adelaide Fold Belt and the Yeneena Basin. *ARC/AMIRA* P544 Final Report October 2003.

Hitzman M, Broughton D, Kirkham R, Thorson J and Selley D (2005) The sediment-hosted stratiform copper ore system. In: Hedenquist JW, Thompson JFH, Goldfarb RJ, Richards JP (eds) *Economic Geology 100th Anniversary Volume*, pp 609-642.

Kirkham RV (1989) Distribution, settings, and genesis of sediment-hosted stratiform copper deposits. In: Boyle RW, Brown AC, Jefferson CW, Jowett EC and Kirkham RV (eds), *Sediment-hosted stratiform copper deposits. Geol Assoc Canada, Special Paper* 36, pp 3-38.

Lambert IB, Donnelly TH and Rowlands NJ (1980) Genesis of Upper Proterozoic stratabound copper mineralization, Kapunda, South Australia. *Mineralium Deposita,* 15, pp 1-18.

Preiss WV (1999) Parachilna, South Australia. 1:250 000 Geological series sheet SH54-13, with explanatory notes. *Geol Surv South Australia*, 52 pp

Rowan MG and Vendeville BC (*in press*) Foldbelts with early salt withdrawal and diapirism, physical model and examples from the northern Gulf of Mexico and the Flinders Ranges, Australia. *Marine and Petroleum Geology,* August 2007.

# Bitumen linked to stratabound Cu deposits in northern Chile: Source of the fluids which transported organic matter

A. Rieger
*Department of Earth and Environmental Sciences, University of Munich, Luisenstrasse 37, 80333 Munich, Germany*

ABSTRACT: The association of bitumen and stratabound copper sulphide hosted in Lower Cretaceous lava flows is found in a north-south belt 10km east of Copiapó, in northern Chile. The bitumen-bearing lavas are intercalated with limestones of the Pabellón Formation (upper Barremian to early upper Aptian). Four calcite generations have been recognized and related to two main hydrothermal events. The first calcite generation (calcite I) crystallized together with unaltered bitumen. Analyses of stable isotopes on calcite I were performed to characterize the fluid source, with which the organic matter migrated into the volcanic rock. Isotope ratios in calcite I range between +13.50 and +19.33‰ $\delta^{18}O_{V\text{-}SMOW}$, and between -4.50 and -20.07‰ $\delta^{13}C_{V\text{-}PDB}$. The calculated $\delta^{18}O$- and $\delta^{13}C$-values of the fluid in equilibrium with calcite I at 95 to 150°C suggest a meteoric or modified meteoric origin for the fluid.

KEYWORDS: meteoric fluids, stable isotope

## 1 INTRODUCTION

Stratabound copper sulphide deposits hosted in a ~70m thick basaltic andesite lava occur about 10km southeast of Copiapó, Chile (Fig. 1).

Nine small mines, currently not operating, with an average tonnage of 100,000 Cu-tonnes, mined mainly copper sulphides with ore grades between 1.95% and 5.1% Cu (Cisternas & Frutos 1996; Cisternas & Hermosilla 2006). Bitumen plays a decisive role in the genesis of these Cu-deposits (*e.g.* Rieger *et al. in review*). A similar relationship between bitumen and Cu-mineralization has been reported in the largest Chilean stratabound deposit El Soldado, located 1,000 southwards of the studied area (Wilson & Zentilli 1999).

The objective of the present study is to determine the source of the fluid that transported the organic matter into the basaltic andesite. Samples of calcite intergrown with bitumen were selected from the mines San Pedro, San Vicente, Manto Gloria and Manto Delicias (Fig.1).

## 2 GEOLOGICAL SETTING

During the late Jurassic to early Cretaceous, an arc-backarc system developed in northern Chile (26 to 29°S). Volcanic and volcaniclastic arc deposits (Bandurrias Group; Marschik & Fontboté 2001) interfingered with shallow marine carbonate sediments (Chañarcillo Group; Segerstrom 1960) deposited to the east.

Early Cretaceous plutons of the Coastal Batholith of northern Chile represent the root zone of the volcanic arc (*e.g.* Marschik & Fontboté 2001; Marschik & Söllner 2006). The Chañarcillo Group is subdivided from bottom to top into the Abundancia, the Nantoco, the Totoralillo and the Pabellón Formations. The upper Barremian to early upper Aptian Pabellón Formation contains the basaltic andesite which hosts the bitumen-bearing Cu-deposits. The marine back arc sequence is unconformably overlain by late Cretaceous continental sediments and volcaniclastic deposits (Cerrillos Formation; Aguirre 1985)

.

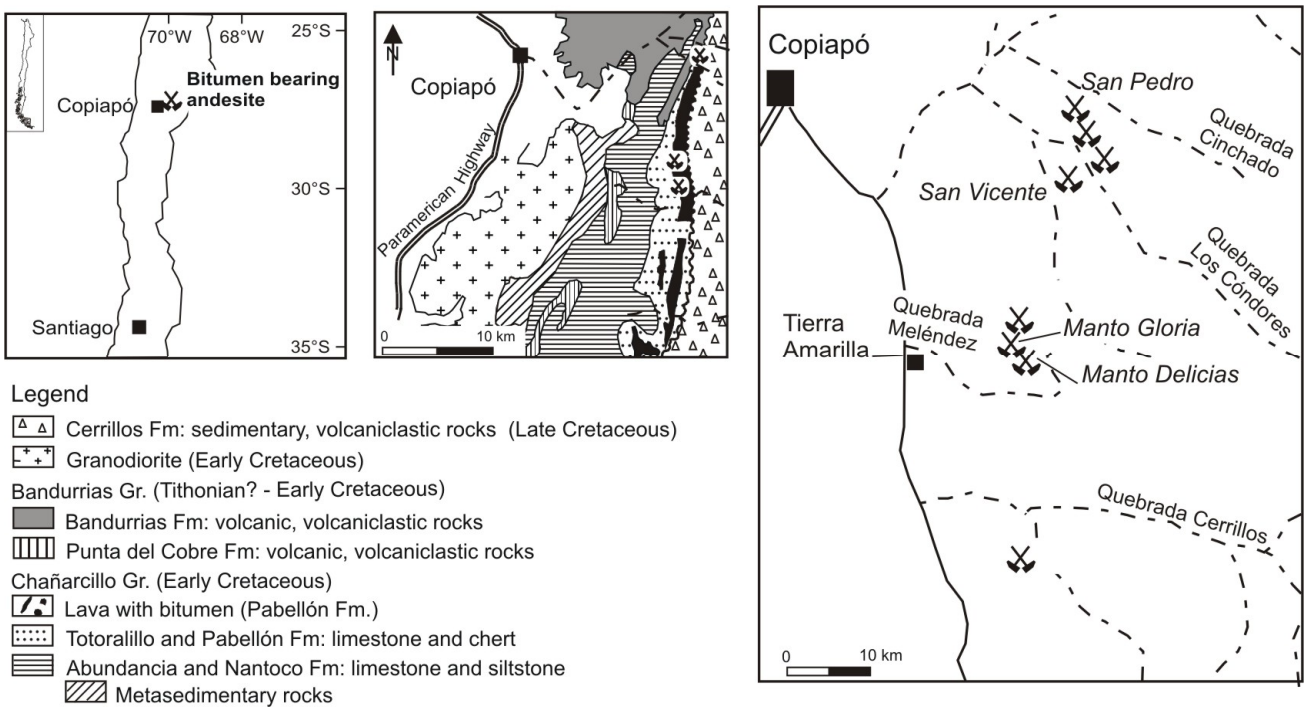


Fig. 1: Schematic geological map of Cretaceous units near Copiapó (modified after Segerstrom, 1968). The study area is situated in the Atacama region, about 10 km E of Copiapó between 27°15'-27°29'S and 70°12'-70°17'W.

## 3 BITUMEN MIGRATION AND ORE FORMATION

The bitumen-bearing stratabound Cu-deposits formed from two main hydrothermal events: an early Fe-rich hydrothermal event and a Cu-rich hydrothermal event (*e.g.* Cisternas & Hermosilla 2006).

The early Fe-rich hydrothermal can be divided into a migration-and-trapping sub-event, and a Fe-sulphide sub-event. The migration-and-trapping sub-event started with the release of organic matter from the source rock. Biomarker analyses of bitumen suggest oil expulsion at temperatures between 64 and 87°C (Rieger *et al. in review*). These temperatures might have been the initial temperature conditions of the migration of the organic matter-bearing fluid. This fluid migrated into the basaltic andesite of the Pabellón Formation, where the organic matter was trapped in primary and secondary porosity of the lavas.

This sub-event ended with solidification of the organic matter and crystallization of the first generation of calcite (calcite I). Calcite I contains bitumen inclusions and aqueous fluid inclusions. Homogenization temperatures of oil inclusions vary from 115 to 140°C (Cisternas *et al.* 1999b). Cisternas & Hermosilla (2006) reported homogenization temperatures between 115 and 307°C in aqueous fluid inclusions in calcite I of the early Fe-rich hydrothermal event.

Biomarker content in the bitumen suggests a maximal temperature of 150°C for the migration-and-trapping sub-event (Rieger *et al. in review*).

In the Fe-sulphide sub-event, the precipitation of pyrite, marcasite, hydrothermal chlorite, and the partial alteration of bitumen took place (Cisternas & Hermosilla 2006). Studies of bitumen reflectivity suggest temperatures around 134°C for the Fe-sulphide crystallization (Cisternas & Hermosilla 2006). Based on a single $\delta^{34}S$ analysis ($\delta^{34}S=0.6‰_{CDT}$) on pyrite cogenetic with bitumen, Cisternas and Hermo-silla (2006) suggested a magmatic source for the sulphur.

During the Cu-rich hydrothermal event, Cu was introduced into the system, leading to formation of chalcopyrite, bornite, tetrahedrite, chalcocite, digenite and covellite. During this hydrothermal event, another three generations of calcite formed (calcites II, III, and IV), and thermo-chemical alteration of the bitumen into pyrobitumen took place (Cisternas & Hermosilla 2006). Trapping of fluid inclusions in calcites II, III, and IV occurred between 116 to 400°C. The fluids have salinities from 3.5 to 25.3 wt% $NaCl_{eq}$ (Cisternas & Hermosilla

2006). Calculated oxygen and carbon isotopes of the hydrothermal fluid in equilibrium with calcites III and IV suggests a meteoric origin of the hydrothermal fluids (Cisternas & Hermosilla 2006).

## 4 RESULTS

Homogenization temperatures were measured in aqueous fluid inclusions in calcite I intergrown with fresh bitumen or in calcite I with coexisting aqueous and bitumen inclusions. Aqueous fluid inclusions have homogenization temperatures from 95 to 150°C, and salinities between 17 and 24 wt% $NaCl_{eq}$ (n=60). The fluids contain $NaCl \pm MgCl_2 \pm CaCl_2$ in solution.

Stable isotope compositions of calcite ($\delta^{18}O$ and $\delta^{13}C$) were measured at the Laboratory of Isotope Hydrology, University of Arizona, Tucson, USA, to characterize the source of the fluid entrapped in the basaltic andesite together with the organic matter. Repeated internal standardizations yielded a degree of accuracy of 0.1‰ for $\delta^{18}O$ and 0.06‰ for $\delta^{13}C$. The stable isotopic composition of oxygen and carbon is presented using the delta notation normalized to $\delta^{18}O_{V\text{-}SMOW}$ and $\delta^{13}C_{V\text{-}PDB}$.

The $\delta^{18}O$-values of calcite I, spatially associated with bitumen, are between +13.50 and +19.33‰ (Table 1). $\delta^{13}C$ of the studied calcite shows values of -4.47 to -20.04‰.

Table 1. Composition of oxygen ($\delta^{18}O_{V\text{-}SMOW}$) and carbon ($\delta^{13}C_{V\text{-}PDB}$) stable isotope of calcite and calculated composition balanced with fluids. For oxygen 1000lnα is 17.62 at 95°C and 12.64 at 150°C. For carbon 1000lnα is 4.36 at 95°C and 1.5 at 150°C.

| Sample | Corrected $\delta^{18}O_{V\text{-}SMOW}$ [‰] | $\delta^{18}O_{fluid}$ at 95°C [‰] | $\delta^{18}O_{fluid}$ at 150°C [‰] | Corrected $\delta^{13}C_{V\text{-}PDB}$ [‰] | $\delta^{13}C_{fluid}$ at 95°C [‰] | $\delta^{13}C_{fluid}$ at 150°C [‰] |
|---|---|---|---|---|---|---|
| San Pedro | +19.33 | +1.71 | +6.69 | -20.04 | -24.40 | -21.54 |
| San Pedro | +17.33 | -0.29 | +4.69 | -13.49 | -17.85 | -14.99 |
| San Pedro | +17.16 | -0.46 | +4.52 | -13.00 | -17.36 | -14.50 |
| San Vicente | +18.19 | +0.57 | +5.55 | -9.19 | -13.55 | -10.69 |
| San Vicente | +17.73 | +0.11 | +5.09 | -8.81 | -13.17 | -10.31 |
| Manto Gloria | +14.20 | -3.42 | +1.56 | -4.47 | -8.83 | -5.97 |
| Manto Delicias | +13.50 | -4.12 | +0.86 | -8.62 | -12.98 | -10.12 |

## 5 DISCUSSION

The trapping temperatures of bitumen inclusions and aqueous fluid inclusions in calcite I suggest that the migration-and-trapping subevent occurred within a temperature range of 95 to 150°C. This is in agreement with the biomarker content, which could only be preserved at temperatures below 150°C (Rieger *et al. in review*).

The calculated $\delta^{18}O_{fluid}$ and $\delta^{13}C_{fluid}$ values of a fluid in equilibrium with calcite I, based on the homogenization temperatures reported here, are between -4.12 and +6.69‰, and -24.40 and -5.97‰, respectively. The isotopic composition of the fluid $\delta^{18}O_{fluid}$ and $\delta^{13}C_{fluid}$ was calculated using the fractionation factors of Friedman & O'Neil (1977) and of Ohmoto & Rye (1979). This fluid isotope signature is suggestive of a fluid of meteoric or modified meteoric origin ($\delta^{18}O_{V\text{-}SMOW}$ values of sediments range between +10 and +44‰; Hoefs 1997). In contrast, the fluid isotope signature of the El Soldado deposit has been considered as compatible with a metamorphic, rather than a magmatic origin (Wilson *et al.* 2003).

Homogenization temperatures in calcite I over 150° reported by Cisternas & Hermosilla (2006) are consistent with the formation temperature of the subsequent Fe-sulphide subevent. These authors suggested that a fluid of magmatic source contributed sulphur to the solution ($\delta^{34}S$=0.6‰$_{CDT}$, n=1 on pyrite).

Without excluding a magmatic sulphur source, sulphur could have been acquired during the migration of the fluid through evaporites such as are in the Nantoco Formation. A similar process is proposed to explain the moderate salinity of the fluid. Sulphur could in part also derive from organic activity in the source rock. Sulphur could be transported in form of complex aromatic compounds in the bitumen-bearing fluid.

The lower $\delta^{13}C_{fluid}$ values could reflect the isotopic interaction of fluid and oil/bitumen during migration coincident with the early hydrothermal event. Carbonate with this signature also could originate via mixing of inor-

ganic carbon and carbon from oxidation of organic matter.

## 6 CONCLUSIONS

The results obtained in this research point to a migration of organic matter at temperatures of 64 to 150°C, in moderately saline fluids of meteoric or modified meteoric origin. The fluid salinity could have resulted from interaction with evaporites such those of the Nantoco Formation. More studies are necessary to determine the sulphur source.

## ACKNOWLEDGEMENTS

Financial support by the Deutsche Akademische Austauschdienst (DAAD) and Fondecyt grants 1010825 is gratefully acknowledged. I want to express my gratitude to Dr. Mark Barton and Dr. David Dettman of the University of Arizona, Tucson, for the access to stable isotope facilities.

## REFERENCES

Aguirre L (1985) The southern Andes. In: Nairn AEM, Stehli FG, Uyeda S (eds) the Pacific Ocean. The ocean basins and margins 7A: 265-376.

Cisternas ME, Frutos J (1996) Importancia metalogenética del volcanismo extensional del Cretácico Inferior en la región de Copiapó, Chile. *Congreso brasileiro de geología* 7: 303-306.

Cisternas ME, Haggan T, Parnell J (1999) Andesite-hosted copper sulphide-bitumen mineralization in back arc Andean basin, north central Chile In: Stanley CJ et al. (eds) Mineral deposits, processes to processing, *Balkema*; Rotterdam 1: 223-226.

Cisternas ME, Hermosilla J (2006) The role of bitumen in strata-bound copper deposit formation in the Copiapó area, northern Chile. *Miner. Dep*. 41: 339-355.

Friedman I, O'Neil JR (1977) Compilation of stable isotope fractionation factors of geochemical interest. In: Fleischer M (ed) Data of geochemistry. *U.S. Geological Survey*, Professional Paper 440-KK, pp12.

Hoefs J (1997) Stable isotopes geochemistry. *Springer* Berlin Heidelberg, 201p.

Marschik R, Fontboté L (2001) The Punta del Cobre Formation, punta del cobre-candelaria area, northern Chile. *J. S. Am. E. Sci*. 14: 401-433.

Marschik R, Fontignie D, Chiaradia M, Voldet P. (2003) Geochemical and Nd-Sr-Pb-O isotope characteristics of granitoids of the Early Cretaceous Copiapó plutonic complex (27°30'S), Chile. *J. S. Am. E. Sci*. 16: 381-398.

Marschik R, Söllner F (2006) Early Cretaceous zircon U-Pb isotope ages for the Copiapó plutonic complex and implications for the IOCG mineralization at Candelaria, Atacama Region, Chile. *Miner. Dep*. 41: 785-801.

Ohmoto H, Rye RO (1979) Isotope of sulphur and carbon. In Barnes HL (ed) Geochemistry of hydrothermal deposits. New York, *Wiley Interscience*: 509-567.

Rieger A, Schwark L, Cisternas, ME, Miller H, (in review) Genesis and evolution of bitumen hosted in Lower Cretaceous lavas and its implications for strata-bound copper deposits, North Chile. *Econ. Geol.*

Segerstrom K (1960) Cuadrángulo Quebrada Paipote, provincia de Atacama. Instituto de investigaciones geológicas, Santiago, carta geológica de Chile no. 2, 35 p.

Segerstrom K (1968) Geología de las hojas copiapó y ojos del salado, provincia de Atacama, IIG: Santiago, 58 p.

Wilson N, Zentilli M (1999) The role of orga-nic matter in the genesis of the El Soldado volcanic-hosted manto type Cu Deposit, Chile. *Econ. Geol.* 94:1115-1136.

Wilson N, Zentilli M, Spiro, B (2003) A sulphur, carbon, oxygen, and strontium isotope study of the volcanic-hosted El Soldado manto type copper deposit, Chile: The essential role of bacteria and petroleum. *Econ. Geol.* 98: 163-174.

# Sediment-hosted cupriferous mineralization in the Quebec Appalachians, Canada: the Transfiguration deposit

A.R. Cabral
*Department of Geology: Exploration Geology, Rhodes University, Grahamstown, South Africa*

G. Beaudoin
*Département de géologie et de génie géologique, Université Laval, Québec, QC, G1K 7P4, Canada*

ABSTRACT: Transfiguration is a red bed-type cupriferous deposit in the Quebec Appalachians, Canada. Mineralization occurs as sulphide disseminations and veinlets within a greyish sandstone unit of the Lower Silurian Robitaille Formation. Overlying red beds are barren. The deposit can be explained by a diagenetic fluid-mixing model, in which: (i) the greyish sandstone unit is the result of ponding of reduced groundwater (recorded as a calcrete horizon) over a Taconian unconformity; (ii) early pyrite, commonly plumbiferous, formed by bacterial sulphate reduction (BSR); (iii) BSR pyrite and mobile hydrocarbon served as reducing agents for metal deposition as Cu, Pb and Zn sulphides; (iv) underlying pre-Taconian rocks leaked hydrocarbon-bearing fluid into the Robitaille Formation; (v) fluid leakage from the pre-Taconian basement (reducing fluid) and superjacent red-bed unit (oxidising fluid) probably took place during the Salinic disturbance.

KEYWORDS: red bed-Cu deposit, Transfiguration, Quebec Appalachians

## 1 INTRODUCTION

About 1/4 of the world's Cu production comes from sediment-hosted stratiform deposits (*e.g*. Hitzman *et al*. 2005). Several occurrences of sediment-hosted Cu are known in the Gaspé Peninsula, Quebec Appalachians, but they are poorly recorded. We succinctly present data on one of those deposits, known as Transfiguration.

## 2 GEOLOGICAL SETTING

Transfiguration is a Cu–Pb–Zn–Ag deposit hosted by Lower Silurian continental red beds of the Robitaille Formation, Chaleurs Group (Fig. 1). The red beds rest on deformed pre-Taconian rocks of the Humber Zone, above a Taconian unconformity (*e.g.* Malo 2004).

The Robitaille Formation is a terrestrial succession deposited on subaerial lava flows and volcaniclastic gravels of the Pointe-aux-Trembles Formation, which are underlain by deep-water turbidite to shallow-water sediments of the Cabano Group. Platformal limestones of the Sayabec Formation overlie the Robitaille Formation. The late Llandoverian to late Wenlockian Sayabec platform is transgressed by late Wenlockian deep-water, fine-grained siliciclastic sediments (Saint-Léon Formation and equivalents). This transgression is affected by synsedimentary faults related to the late Silurian–early Devonian Salinic disturbance (*e.g*. Bourque *et al*. 2001).

## 3 DEPOSIT GEOLOGY

Outcrops are scarce at Transfiguration and its geology has been disclosed by exploration trenches and drill cores. The deposit stratigraphy comprises, from bottom to top: (a) sheared slate (Cambro-Ordovician basement, *i.e.* pre-Taconian rocks); (b) calcrete nodules in greenish sandstone; (c) polymictic conglomerate; (d) greyish sandstone; and (e) reddish sandstone.

The sandstones consist of quartz arenite, sub litharenite and quartzwacke, made up of fine-grained, moderately to poorly sorted detrital grains. Strata are gently folded and continuous. The stratigraphic continuity is disrupted by a NNW-striking transcurrent fault in the central area of the deposit.

Pyrite interstitial to detrital grains, in amounts varying from trace to a few modal per cent, is disseminated in greyish and greenish sandstones.

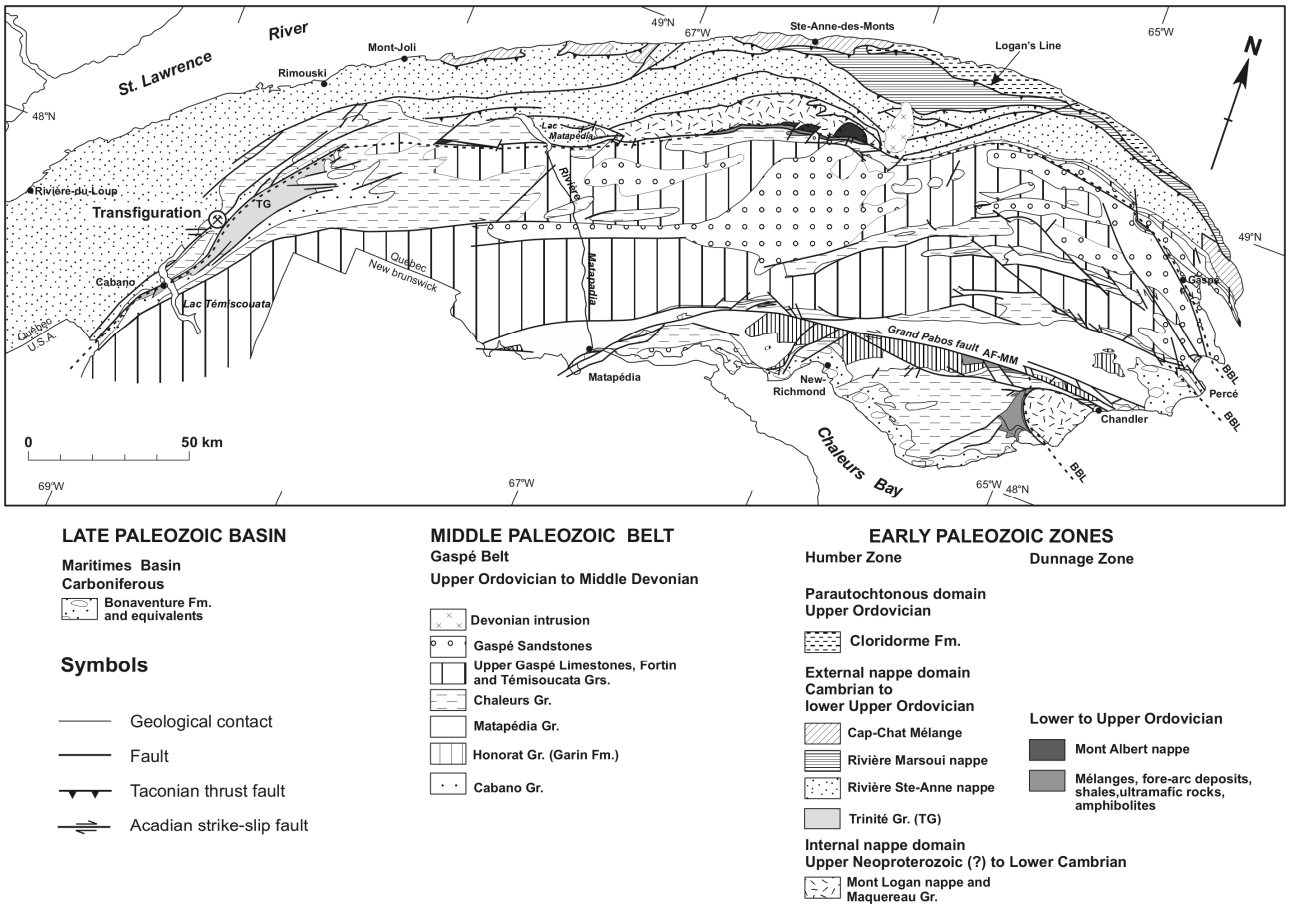


Figure 1. Major stratigraphic units (Malo 2004) and location of study area, Transfiguration.

Calcrete nodules form a stratigraphic marker. Individual nodules vary in width from a few mm up to 5cm. They are composed of micritic and sparry calcite, being characterised by microstructures such as calcite-filled cracks (crystallaria), floating grains and circumgranular cracks. These microstructures are typical of alpha-type calcrete (Wright 1990).

## 4 MINERALIZATION

Mineralization occurs as sulphide disseminations and minor veinlets within the greyish sandstone and conglomerate between the Taconian unconformity and the superjacent red-sandstone unit. Fault-related barite veins with sphalerite dissemination in the adjacent sandstone are locally observed at the contact between the calcrete horizon and the pre-Taconian rocks. Some intervals are enriched in Pb and Zn (*e.g.*, 3.4m @ 0.25% Cu, 3.0% Pb, 2.0% Zn, 18.2 g/t Ag, A. Hupé, *unpublished data,* 2001).

Pyrite and, subordinately, marcasite are the earliest sulphides. Chalcopyrite replaces pyrite. This early pyrite is commonly plumbiferous, with Pb-rich core and Pb-poor margin. The Pb content in pyrite is as high as 2.2 wt% and co-varies with Fe. Galena, which post-dates pyrite, is also found as inclusions in authigenic albite. Chalcopyrite veinlets, <2 mm in width, have euhedral albite with tiny, <5 μm long, hydrocarbon-bearing fluid inclusions.

Silver seems to be in solid solution in Cu sulphides. The major argentiferous phase is idaite, with values to 11 wt% Ag. Pyrite and marcasite may contain a few hundred ppm Ag.

Some remarkable microstructures present in mineralized intervals are displacive calcite growth, feldspar destruction and quartz dissolution by dolomite associated with chalcopyrite precipitation, with or without albite.

### 4.1 *Bulk-rock chemistry*

Assay values reach 2.4% Cu and 3.6% Pb in selected samples. Copper is correlated with $Fe^{3+}/Fe^{2+}$ (r=0.84, Fig. 2). Maximum contents of Ag and Re are 226 ppm and 501 ppb, respectively. About 1% Zn, 55 ppm Cd and 16% Ba are associated with fault-related vein at the con-

tact between pre-Taconian rocks and the overlying calcrete horizon.

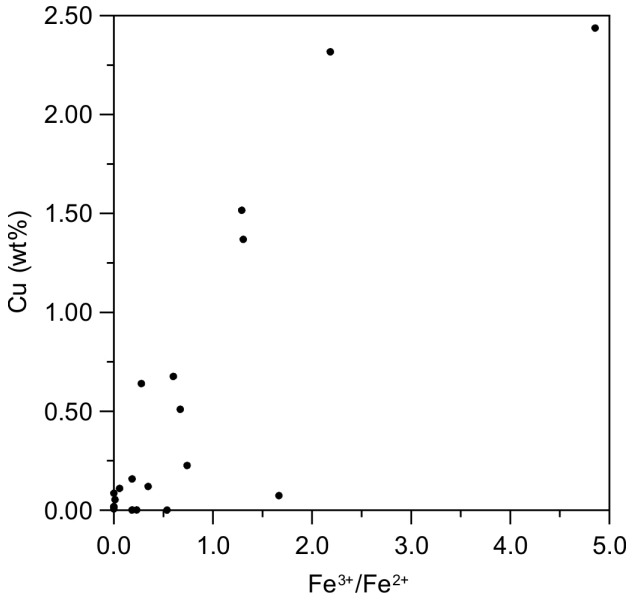


Figure 2. Cu vs. $Fe^{3+}/Fe^{2+}$ plot of bulk-rock chemical analyses.

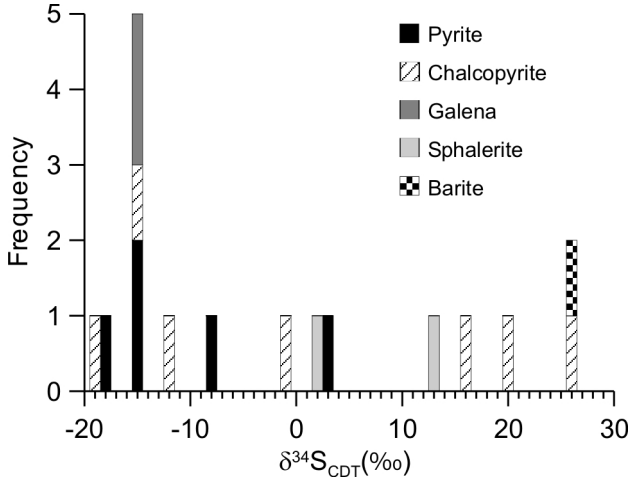


Figure 3. Histogram of $\delta^{34}S$ values of sulphides and barite.

## 4.2 *Stable isotopes*

Sulphide, sulphate and carbonate concentrates were analysed for stable isotope ratios at G.G. Hatch Isotope Laboratories, University of Ottawa. Sulphide $\delta^{34}S$ shows values ranging from -19 to 25‰, with a mode at -15‰ (Fig. 3). The highest sulphide $\delta^{34}S$ value (25.1‰) is close to that of vein barite (26.2‰). Chalcopyrite coexisting with albite that hosts hydrocarbon-bearing fluid inclusions has low $\delta^{34}S$ ratios (-15.2 and -1.2‰).

Disseminated and vein carbonates, as well as calcrete, have $\delta^{13}C$ and $\delta^{18}O$ ratios varying from -7.5 to -1.1‰ (VPDB), and from 14.7 to 21.3‰ (VSMOW), respectively.

# 5 DISCUSSION AND CONCLUSION

The nodular calcrete horizon is interpreted to represent palaeogroundwater seepage and ponding over the Taconian unconformity. Because continental red beds are not originally deposited as red sediments (Brown 2005; and references therein), the calcrete horizon and greyish arenaceous rocks were never reddened. Consequently, the difference in colour between the upper and lower sandstone units can be understood as two hydrologic systems, above and below the water-table: the upper, reddening sediments and the lower, reducing groundwater ponding over the Taconian unconformity (Fig. 4a).

In Llandoverian times (Fig. 4a), the drainage was probably conditioned by the Cambro-Ordovician organic carbon-rich basement, upon which reduced groundwater ponded to form nodular calcretes. The light carbon isotope composition of calcrete calcite is consistent with degradation of organic matter.

Mineralized intervals occur within the greyish sandstone unit and have no obvious connection with redox boundaries. The negative sulphide $\delta^{34}S$ values can be attributed to bacterial reduction of pore-water sulphate (*e.g.* Machel *et al.* 1995). Interestingly, the existence of plumbiferous pyrite is in accordance with Pb removal by sulphate-reducing bacteria (*e.g.* Massadeh *et al*. 2005).

Mineralized intervals also occur at the basal contact with pre-Taconian rocks where crosscut by faults. The highest sulphide $\delta^{34}S$ value (25.1‰) is close to that of vein barite (26.2‰), suggesting thermochemical reduction of Silurian sea-water sulphate (*e.g.* Machel *et al*. 1995). It appears that cupriferous fluids were canalised by faults into the subjacent greyish unit where it percolated laterally (*cf*. Lisbon Valley Cu deposit, Hitzman *et al*. 2005).

In Ludlovian times (Fig. 4b), synsedimentary faulting related to the Salinic disturbance triggered pulses of hydrocarbon-bearing fluids from pre-Taconian rocks into lowermost Silurian rocks (*e.g.* Lavoie & Morin 2004). It is suggested that pseudomorphic replacement of early pyrite by chalcopyrite and sulphide precipitation took place in response to the interac-

tion between red bed-derived cupriferous fluid and hydrocarbon-bearing basinal brine from pre-Taconian rocks. Mixing between the two fluids induced redox reactions, which are probably expressed by the positive correlation between Cu and $Fe^{3+}/Fe^{2+}$ ratios (Fig. 2).

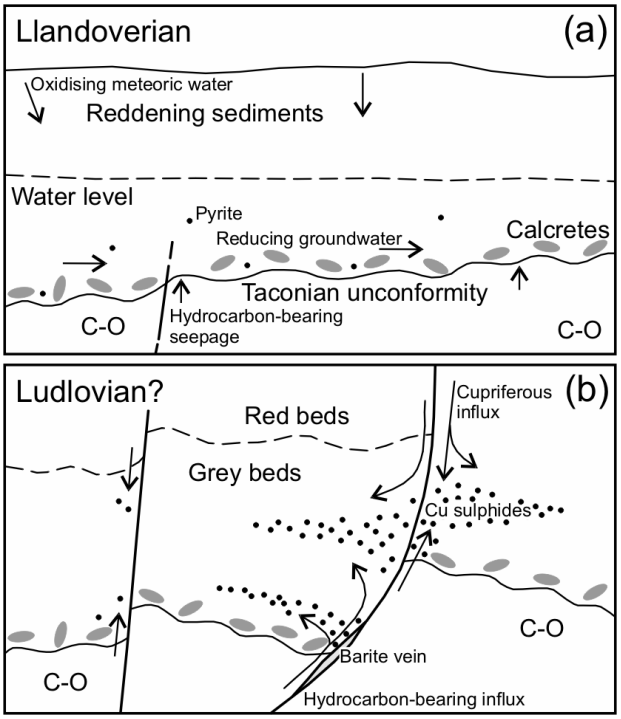


Figure 4. Diagenetic fluid-mixing model for Transfiguration. Arrows indicate fluid migration paths. (a) Ponding of reduced groundwater on the Cambro-Ordovician basement (C-O); calcrete development and formation of BSR pyrite below the water level. (b) Faulting related to Salinic tectonics triggered leakage of hydrocarbon-bearing fluid from the basement, concomitant with cupriferous fluid influx from the overlying red beds. Sulphides were deposited by reaction with early BSR pyrite and by interaction between ascending and descending fluids.

## ACKNOWLEDGEMENTS

The results reported here come from a research project financed by Diversification de l'Exploration Minérale au Québec (Divex). Ressources Appalaches, particularly Alain Hupé, provided access to drill cores and internal reports.

## REFERENCES

Bourque PA, Malo M, Kirkwood D (2001) Stratigraphy, tectono-sedimentary evolution and paleogeography of the post-Taconian–pre-Carboniferous Gaspé Belt: an overview. *B Can Petrol Geol* 49: 186-201.

Brown AC (2005) Refinements for footwall red-bed diagenesis in the sediment-hosted stratiform copper deposits model. *Econ Geol* 100: 765-771.

Hitzman M, Kirkham RV, Broughton D, Thorson J, Selley D (2005) The sediment-hosted stratiform copper ore system. In: Hedenquist JW, Thompson JFH, Goldfarb RJ, Richards JP (eds.) *Economic Geology 100th anniversary volume. Society of Economic Geologists,* pp 609-642.

Lavoie D, Morin C (2004) Hydrothermal dolomitization in the Lower Silurian Sayabec Formation in northern Gaspé–Matapédia (Québec): constraint on timing of porosity and regional significance for hydrocarbon reservoirs. *B Can Petrol Geol* 52: 256-269.

Machel HG, Krouse HR, Sassen R (1995) Products and distinguishing criteria of bacterial and thermochemical sulfate reduction. *Appl Geochem* 10: 373-389.

Malo M (2004) Paleogeography of the Matapédia basin in the Gaspé Appalachians: initiation of the Gaspé Belt successor basin. *Can J Earth Sci* 41: 553-570.

Massadeh AM, Al-Momani FA, Haddad HI (2005) Removal of lead and cadmium by halophilic bacteria isolated from the Dead Sea shore, Jordan. *Biol Trace Elem Res* 108: 259-270.

Wright VP (1990) A micromorphological classification of fossil and recent calcic and petrocalcic microstructures. In: Douglas LA (ed.) *Soil micromorphology: a basic and applied science*. (Developments in Soil Science 19) Elsevier, Amsterdam, pp 401-407.

# Periodicity of copper accumulation in the Earth's sedimentary record

I.F. Gablina & Yu.M. Malinovsky
*Geological Institute RAS, Moscow, Russia*

ABSTRACT: Specific features of distribution of cupriferous sandstones and shales in the Earth's sedimentary record are considered from early Proterozoic to Tertiary time. Genetic links of cupriferous sandstones and shales with arid red-bed molassoid formations are described, and causes of decreasing Cu accumulation from the Proterozoic to the Cenozoic are analyzed. Periodicity of the development of ore-generating red-bed formations is discussed. It is shown that periods of maximum Cu accumulation in the Earth's history coincided with maximum development of red-bed formations on the Panotia and Pangea supercontinents; the time of their appearance corresponds to the Wilson cycle (400-450 Ma).

KEYWORDS: Genesis, red-bed copper deposits, periodicity.

## 1 DISTRIBUTION OF CUPRIFEROUS SANDSTONES AND SHALES

Exogenic copper deposits (cupriferous sandstones and shales) are known to occur in sedimentary rocks from the early Proterozoic to Tertiary age inclusive. Their share makes up 32.6% of the world copper reserves (Pervago 1975). The major part of reserves is found in large and gigantic deposits, the copper reserves in which amount to 10 million tonnes or more. Judging by the maximum copper concentration, three main stages may be identified in the Earth's history: late Precambrian, late Palaeozoic, and Mesozoic--Cenozoic. In accumulated copper quantities, each subsequent stage is much inferior to the preceding stage: 21% in Precambrian formations, about 10% in Palaeozoic, and 1.6% in Mesozoic-Cenozoic (Yanshin 1972).

Maximum copper concentration is associated with late Proterozoic deposits (late Riphean--Vendian). Deposits of that age are known virtually in all continents, among them the African Copperbelt, White Pine in USA, deposits in Afghanistan (Ainak), India, and China.

A second peak of copper accumulation, less productive than the preceding one, is recorded in the Carboniferous-Permian. Deposits of this age contain Dzhezkazghan deposits in Kazakhstan ($C_{2-3}$), Lubin-Sieroszowice in Poland, Mansfeld in Germany ($P_2$), and others.

Mesozoic-Cenozoic sequences incorporate the following deposits: Koroko in Bolivia (Paleogene--Neogene), Boleo in Mexico (Neogene), relatively small deposits and occurrences in Jurassic, Cretaceous, and Palaeogene red-bed formations in China (Narkelyun *et al*., 1983), Lower Cretaceous Cu-bearing deposits of the Tadjik Depression and Neogene deposits of the Fergana Valley (Naukat).

## 2 FORMATION OF CUPRIFEROUS SANDSTONES AND SHALES

The main feature of localization and structure of cupriferous sandstones and shales, common for gigantic and small ore occurrences, is their connection with molassoid red-bed formations and localization of mineralization in gray-coloured organically-rich pyrite-bearing deposits, which replace red-coloured formations in vertical or lateral direction.

Spatial connection of cupriferous sandstones and shales with red-bed formation is determined by specific aspects of copper geochemical behavior in the exogenic environment. As

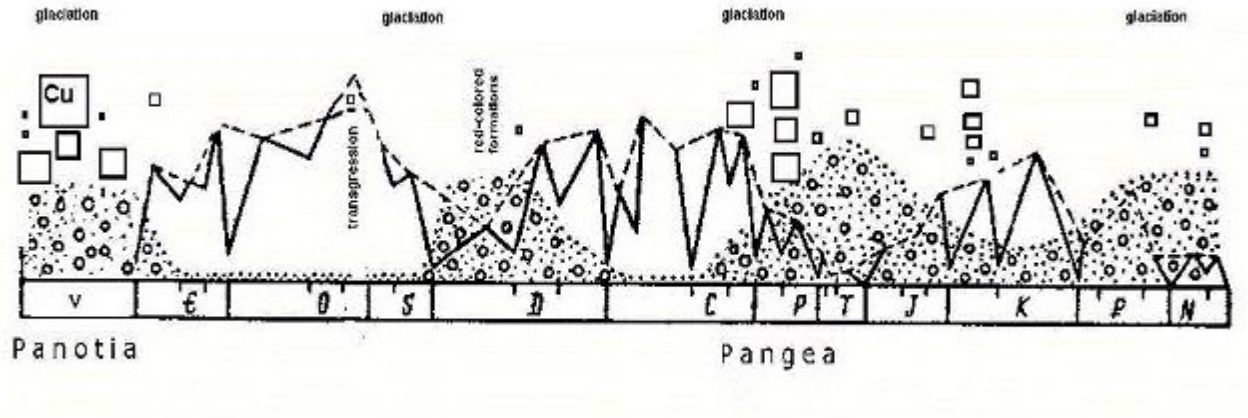


Fig.1 Copper deposits in sandstones and shales against a background of large-scale global changes. Red-bed formations are shown by specks (after Anatol'eva A.I., 1978), deposits – by squares. The size of the square approximately corresponds to copper reserved in a deposit.

reported by Perel'man (1959, 1968), Rose (1976), and Lur'e (1988), arid red-bed formations serve as a source and transport medium for copper. Stratal waters of these formations are characterized by a slightly oxidizing medium, in which copper ($Cu^{+}$) is mobile, mostly in the form of chloride complexes. The red colour of the rocks originates and is preserved by an oxidizing environment during sedimentation and subsequent lithogenesis. Since the Proterozoic, arid red-bed formations occur nearly in all periods, with greatest abundance in the Late Proterozoic, Devonian, Permian, Triassic, Palaeogene, and Neogene (Fig. 1).

However, the conditions of formation of Phanerozoic and Precambrian red-bed deposits were different. Precambrian red-beds are associated with the proliferation of photosynthetic cyanobacteria (Cloud 1978; Melezhik 1987). By the beginning of the Proterozoic, the oxygen content in the atmosphere was similar to the present content due to the activity of organisms (Krylov 1983). Red-beds formed in the oxidizing medium do not contain reducing agents. On the contrary, analogous Phanerozoic red-beds associated with the appearance of higher plants on the continent are geochemically more complicated. In many cases, they contain relics of organic remains, indicating that the oxidizing process was incomplete. On that basis, Lur'e (1988) identified two principally different types of red-beds: ore-generating and non-ore-generating. In ore-generating formations, copper ($Cu^{+}$) was mobile (Eh of 0 ±0.2V). In non-ore-generating formations, copper was immobile, either at a higher Eh ($Cu^{2+}$ stability field) or lower Eh (stability field of sulphide copper). Examples of the latter include the Devonian redbeds of the northwestern Russian Platform, Permian, and Triassic of the middle Pechora, Neogene of the Kara-Kum, and others (Borisenko 1980). Thus changes of the conditions of copper accumulation in the Earth's history are associated with the evolution of living matter.

The genetic model that best explains regularities of localization of cupriferous sandstones and shales, implies that copper and other metals are removed from red-bed formations by underground waters and concentrated on hydrogen sulfide geochemical barriers in the sulphide form. The formation of cupriferous sandstones and shales occurs in geochemical barriers of two types: syngenetic and epigenetic.

Syngenetic barriers are known in shallow-sea, lagoon, boggy, river bed, and deltaic facies settings. The first two facies types developed throughout the history of formation of cupriferous sandstones and shales. They also are the most laterally continuous. The majority of Precambrian and late Palaeozoic deposits occur in shallow-sea beds (*e.g.* most African Copperbelt deposits, White Pine, occurrences in the Siberian platform, Mansfield, Lubin-Sieroszowice, cupriferous sandstones of the Kazanian stage in West Fore-Urals). The maximum copper accumulations in Precambrian sedimentary strata correspond in age to the period of growth and rapid spreading of stromatolite-formers on the Earth (blue-green algae) in the Middle Riphean. Their activity generated organic-enriched deposits, widespread on vast former water areas. Two other syngenetic barrier facies types (boggy and river-bed) appeared only in the Devonian, concurrently with the development of

vegetation. These facies types significantly increased in abundance during and after the Permian. They mainly host average to small-sized deposits.

Epigenetic biogeochemical barriers develop during catagenesis, when reducing agents (oil waters, bitumen, oil, gas) penetrate reservoir rocks in red-bed formations. As a rule, these are clastic and coarse-clastic facies (deltaic, alluvial, prolluvial, alluvial fans, *etc.*) that show signs of local catagenetic alterations: clarification, pyritization, calcitization, and in some cases, bituminization (Gablina 1983, 1986). During Earth history, epigenetic barriers are associated with two indispensable conditions: availability of organic matter and proximity of carbonaceous formations with red-coloured molassoid beds. The Dzheskazghan ($C_{2-3}$) and Graviika in the Igarka area of Siberia (late Proterozoic) are examples of deposits connected with epigenetic barriers.

Minor ore occurrences and average-sized deposits may be associated with different types of barriers. However, development of giant deposits needs large sedimentary-rock basins with red-coloured coarse-clastic rocks; vast areas of geochemical barriers or thick oil-gas source strata, conjugated with red-beds; and long-term sulphide forming processes (Gablina 1997).

## 3 GLOBAL PERIODICITY OF COPPER ACCUMULATION

The periodicity of accumulation of cupriferous sandstones and shales can be considered with respect to global biological and environmental changes. This approach clearly links unique and large deposits with the Panotia and Pangea supercontinents (Fig. 1). The Panotia supercontinent provided conditions for the formation of large deposits of the late Proterozoic, and possibly Udokan. Large deposits of the late Paleozoic occur within Pangea.

Taking into consideration the genetic model for cupriferous sandstones and shales, the link with supercontinents is quite natural. Large deposits require thick layers of red-bed ore-generating deposits and carbonaceous geochemical barriers. The latter are made up of carbonaceous phases of biosphere rhythms, which always appear against the background of ocean level rise. Red-bed formations are generated at the final calcium phase of biosphere rhythms, which follows directly after the carbonaceous (Malinovsky 2006). Formation of thick red-beds is associated with climatic aspects of a supercontinent, including the formation of gigantic ice covers and the near-absence of the humid tropical belt. In lower and middle latitudes of supercontinents, the climate was continental and arid (Zharkov 2004). Many red-beds accumulated when world ocean levels were low and during initial extension of the continental crust. However, the long lasting glaciation in the Middle Ordovician--Silurian, which was not accompanied by low ocean levels and extensive continental glaciation, did not stimulate development of large copper deposits. Thus, broad continental glaciation corresponds with a greater abundance of large copper deposits. This also applies to Phanerozoic ore-bearing and oil-gas deposits (Malinovsky 1982).

Minima of cupriferous sandstone and shale deposits occur in the Early Ordovician, Early Carboniferous, and Late Cretaceous, a periodicity of about 180 Ma., equivalent to the Bertran cycle. These periods are characterized by maximum world ocean levels and maximum extent of humid tropical zones at the very beginning of glacial eras. Deposit maxima are concurrent with the Wilson cycle for the formation of supercontinents (400-450 Ma.).

## 4 CONCLUSIONS

The conditions for the formation of cupriferous sandstones and shales evolved parallel to the appearance of primary arid red-bed formations, which are ore-generating for copper. Changes of the conditions of copper accumulation in the Earth's history are associated with the evolution of living matter on the planet. The maximum copper concentration in the Riphean—Vendian coincide with the period of flourishing blue--green algae and the formation of large areal reducing barriers. The appearance of on-land vegetation in the Phanerozoic increased the number of deposit facies types, through the formation of small local geochemical barriers, resulting in small ore occurrences. Maxima of cupriferous sandstones and shales coincided with maximum development of red-bed formations on the Panotia and Pangea supercontinents, with a periodicity equivalent to the Wilson cycle (400-450 Ma).

## ACKNOWLEDGEMENTS

The authors acknowledge the support of the Russian Foundation for Basic Research (project

no. 05-05-64952), and Division of Earth Sciences-2. The authors thank S.Aivasova for translation, and D. Broughton for valuable comment.

## REFERENCES

Anatol'eva AI (1978) Main boundaries of the evolution of red-bed formations. *Nauka, Novosibirsk*, 192 p.

Borisenko EN (1980) Geochemistry of gley catagenesis in rocks of the red-bed formations. *Nauka, Moscow*, 164 p.

Cloud P (1978) Paleoecological significance of the banded iron-formation. *Econ. Geol.* vol. 68. pp 1135-1143.

Gablina IF (1983) Cupriferous accumulation condition in red continental formations. *Nauka, Moscow*, 111 p.

Gablina IF (1986) Genetic types of copper mineralization in the Igarka area, West of the Siberian platform. In: Friedrich G.H. et al. (eds) *Geology and metallogeny of copper deposits.* Springer-Verlag Berlin Heidelberg, pp 524-539.

Gablina IF (1997) Formation condition of large cupriferrous sandstone and shale deposits. *Geology of ore deposits,* vol. 39 pp 4: 320-333

Krylov LN (1983) Organic world of the Precambrian and its influence on sedimentation processes. In: *Biochemical aspects in the formation of sedimentary rocks and ores: Abstracts of papers,* p 23.

Lur'e AM (1988) Genesis of the cupriferous sandstones and shales. *Nauka, Moscow*, 182 p.

Malinovsky YuM (1982.) Synphse stratigraphy of the Phanerozoic. *Nedra, Moscow,* 176 p.

Malinovsky YuM (2006) Self-regulation of the biosphere and great glaciations. *Science in Russia* pp 4: 35-40.

Meleszik VA (1987) Early Precambrian red-bed formations – the result of biochemical activity of organisms. In: Materials of the 3rd All-Union symposium on paleontology of the Precambrian and Early Cambrian. A*bstracts of Papers. Petrozavodsk,* pp 66-67.

Narkelyun LF, Salikhov VS, Trubachev AI et al. (1983) Cupriferous sandstones and shales of the world. *Nedra, Moscow,* 414 p.

Perel'man AI (1959) Some questions about geochemical evolution in sedimentary deposits of cupriferous sandstone. *Transactions of IGEM, Issue 28.AS SSSR, Moscow,* pp 5-21.

Perel'man AI (1968) Geochemistry of epigenetic processes. *Nedra, Moscow,* 331 p.

Pervago VA (1975) Formation and geologo-economic assessment of industrial types of the base metals deposits. *Nedra, Moscow*, 272 p.

Rose AW (1976) The effect of cupriferous chloride complexes in the origin of red-bed copper and related deposits. *Econ. Geol.*, vol. 71, pp 1036-1048.

Yanshin AL (1972 ) Principles of identifying geological formations. In: Anatol'eva A.I. Pre-Mesozoic red-bed formations. *Nauka, Novosibirsk*, pp 5—12.

Zharkov MA (2004.) Paleogeographic reconstructions and sedimentation settings in the Permian and Early Triassic.. In: Semichatov M.A., Chumakov N.M. (eds) Climate in epochs of large biosphere reconstructions. N*auka, Moscow,* pp 158-180.

# A common basin-scale, gravity-driven, evolved-meteoric water model for the White Pine sulphide-facies copper mineralization and Keweenaw native copper lodes, northern Michigan

Alex C. Brown
*Dept. of Civil, Geological and Mining Eng., École Polytechnique de Montréal*
*P.O. Box 6079, Sta. Centre-Ville, Montréal, Québec, Canada*

ABSTRACT: Oxygen-rich, gravity-driven meteoric water descending into the Copper Harbor Conglomerates of the Lake Superior rift district are proposed to have become saline by the assimilation of evaporites and then to have reddened and leached copper from this aquifer under moderately oxidizing conditions to form the early diagenetic White Pine sulphide-facies mineralization in the basal units of the overlying reduced pyritic Nonesuch Formation. Some 20-35 Ma later, this circulation and leaching system may have extended into deep-basin basalts and interbedded sandstone-conglomerates and have carried hot cupriferous brines into up-dip aquifers of the Portage Lake Volcanics where native copper could deposit under cooler, oxygen-depleted, sulphide-free conditions. These concepts suggest that one basin-scale meteoric-water system could account for both types of economic copper in the Keweenaw district of northern Michigan.

KEYWORDS: Copper mineralization, sulphide-facies, native copper lodes, meteoric water, aquifers, metamorphogenic water, salinity, gravity-driven model, White Pine, Keweenaw, northern Michigan

## 1 INTRODUCTION

The Keweenaw district of northern Michigan is the site of two distinct deposit types: a) disseminated sediment-hosted stratiform copper (SSC) mineralization in basal carbonaceous sulphide-rich beds of the Nonesuch Formation in the White Pine district, and b) about 100km to the northwest, native copper lode (NCL) mineralization in porous amygdaloidal and flow-top breccias of basaltic flows and interbedded conglomerates of the Portage Lake Volcanics (PLV) on the Keweenaw Peninsula proper.

Sulphide-facies copper emplacement at the White Pine SSC deposit is generally interpreted to have taken place during early diagenesis of the 1080 Ma-old (Ohr 1993) Nonesuch "black shales", by the introduction of copper from a vast reservoir of cupriferous chloride brines residing in the footwall Copper Harbor Conglomerate redbeds (White 1960; Brown & Trammell 1965; White & Wright 1966; Brown 1971). In contrast, NCL mineralization has been attributed to the leaching of copper from basalts by metamorphogenic fluids generated during compaction and metamorphism of deeply buried basalts along the synclinal axis of the Midcontinent Rift (Butler & Burbank 1928; Stoiber & Davidson 1959; Weege *et al*. 1972; Jolly 1974; Livnat *et al.* 1983). The two deposit types are separated stratigraphically by 100's to 1000's of metres of Copper Harbor redbeds, as well as the Porcupine Volcanic dome in the White Pine area. In this communication, the two distinctive types and timings of copper mineralization are linked in a common long-term basin-scale circulation of gravity-driven evolved-meteoric water.

## 2 A REVISED ORIGIN FOR SSC-TYPE MINERALIZATION AT WHITE PINE

The genesis of the White Pine SSC deposit is dependent on the circulation of a low-temperature cupriferous brine in the footwall aquifer. The brine is presumed to have formed by the leaching of evaporites or the assimilation of downward draining evaporitic fluids in

a hot, arid, intracontinental rift setting. The copper is presumed to have been leached under oxidizing conditions from common labile mineral constituents of the footwall redbeds (Zielinski *et al.* 1983; Walker 1989).

Of the possible causes of brine circulation (*e.g.*, gravity-driven meteoric recharge, sediment compaction, anomalous heat flow), meteoric recharge from highlands adjacent to the rift basin is particularly attractive (Brown 2005, 2006; Fig. 1). In this conceptual model, descending meteoric water becomes saline by the assimilation of evaporitic salt and evolves

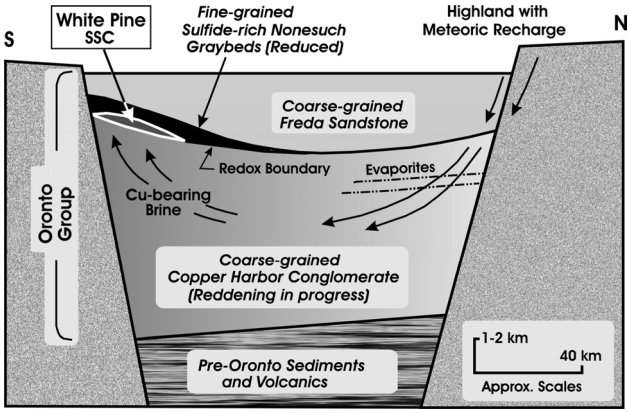


Figure 1. Basin-scale genetic model for the White Pine sediment-hosted stratiform copper deposit (modified after Brown 2005). See text for explanation.

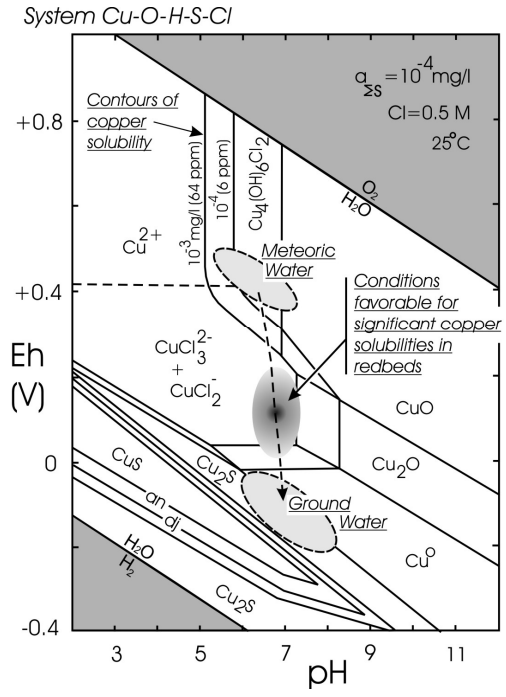


Figure 2: Eh-pH stability diagrams for the system Cu-O-H-S-Cl (after Brown 2005). See text for explanation.

slowly from the oxygen-rich, slightly acid Eh-pH conditions (Garrels 1960) of surface waters equilibrated with the atmosphere (upper ellipse of Fig. 2), to the oxygen-depleted conditions of deep groundwaters (lower ellipse of Fig. 2) which have lost oxygen during the diagenetic reddening of initially non-red coarse-grained rift sediments (Zielinski *et al.* 1983; Walker 1989; Brown 2006) and which approach near-neutral pHs by equilibration with silicates and/or carbonates.

In contrast to our long-held dictum that the simple presence of a hematitic pigment in redbeds assures that conditions would be suitably oxidizing for copper solubility (and transport) in a chloride brine, the optimum conditions for copper solubility (middle ellipse of Fig. 2) fall within a rather restricted area (Eh ≈ 0.1 ± 0.1 v, pH ≈ 7; Rose 1976, 1989; Brown 2003, 2005) along the path of meteoric water evolving to deep groundwater. Because that path results from aquifer reddening, the timing of copper leaching and subsequent emplacement in the basal Nonesuch greybeds at White Pine can be related directly to the diagenetic reddening of immature Copper Harbor Conglomerate sediments, a process considered in turn to extend over several millions of years of early diagenetic time (Walker 1989).

## 3 PRIOR EXPLANATIONS FOR NCLs ON THE KEWEENAW PENINSULA

Extensive descriptions of "regional hydrothermal metamorphism" in amygdaloidal basalts on the Keweenaw Peninsula led Stoiber & Davidson (1959) to propose a metamorphogenic origin for associated native copper lodes (NCLs). White (1968), Jolly (1974) and Livnat *et al.* (1983) gave more precise quantitative analyses for this ore-forming system. Briefly stated, hot metamorphogenic fluids leached important trace amounts of copper from basalts in the neighborhood of the rift axis, and these cupriferous fluids then rose along PLV aquifers (amygdaloidal and brecciated flow tops and interbedded sandstone-conglomerate units) and deposited native copper in up-dip sulphide-free portions of those aquifers under the cooler, hydrated levels of pumpellyite metamorphism (Fig. 3).

Unfortunately, in this model, the origin of the high salinity of the metamorphogenic brine is not explained; the 3 molar salinity suggested in Jolly (1974) is unlikely to have resulted dur-

ing metamorphic dewatering of basalts, given that metamorphic waters generally do not have salinities above 1 molar even under mesothermal conditions (Robert & Kelly 1987). High salinities may have resulted from metamorphism of sediments associated with shallow marine environments (Yardley & Graham 2002). The metamorphogenic model also lacks an explanation for the rise of its dense brine from deep sites along the rift axis.

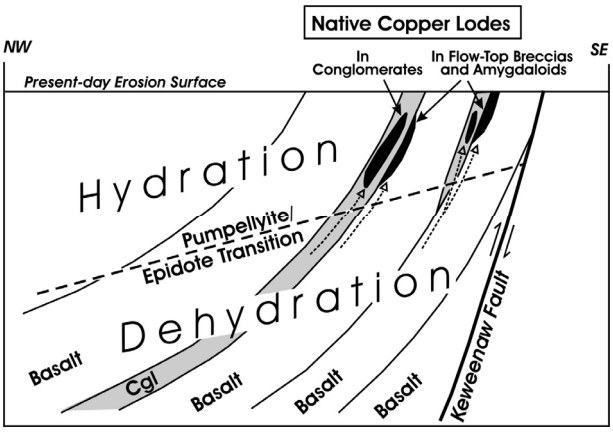


Figure 3: Setting and genesis of native copper lodes in basalts and conglomeratic sediments of the Portage Lake Volcanics (modified after Brown 2006). See text for explanation.

## 4 GENESIS OF NATIVE COPPER LODES VIA A METEORIC BRINE

The evolved meteoric brine which formed the White Pine SSC may be appropriately extended to explain the origin of native copper lodes on the Keweenaw Peninsula (Brown 2006). The salinity of the brine would again be derived from the leaching of subsurface evaporites or the mixing with downward draining brines from surface evaporite pans. The basin-scale circulation of the brine would be assured by highland recharge (Fig. 4). From the reconstructed development and evolution of the Midcontinent Rift System in the Lake Superior region, this recharge may have been associated with tilting of the host Portage Lake Volcanics toward the axis of the rift during Grenvillian compression which took place at ~1060 to 1045 Ma (Bornhorst *et al.* 1988; Cannon *et al*. 1993), 20 to 35 Ma after the circulation of the SSC-forming brine.

The descending, oxygen-rich, meteoric brine would have lost oxygen by progressive reddening of deep basin aquifers, including the amygdaloidal and brecciated flow tops of basalts and interbedded sandstones and conglomerate of the PLV. As the brine lost oxygen, it would have evolved first toward conditions suitable for the leaching and transport of copper, and eventually to the highly reduced conditions typical of groundwater. Significantly, under the sulphur-free conditions which prevailed during NCL deposition, these final highly reduced conditions coincide with the stability field of metallic copper, and thus the evolved cupriferous brine would have precipitated native copper in the PLV (Brown 2006). Furthermore, iron oxides become soluble under these reduced conditions, and thus the influx of a highly reduced, native copper-depositing solution should have been accompanied by the leaching of the earlier formed haematitic pigment. This effect is seen in the

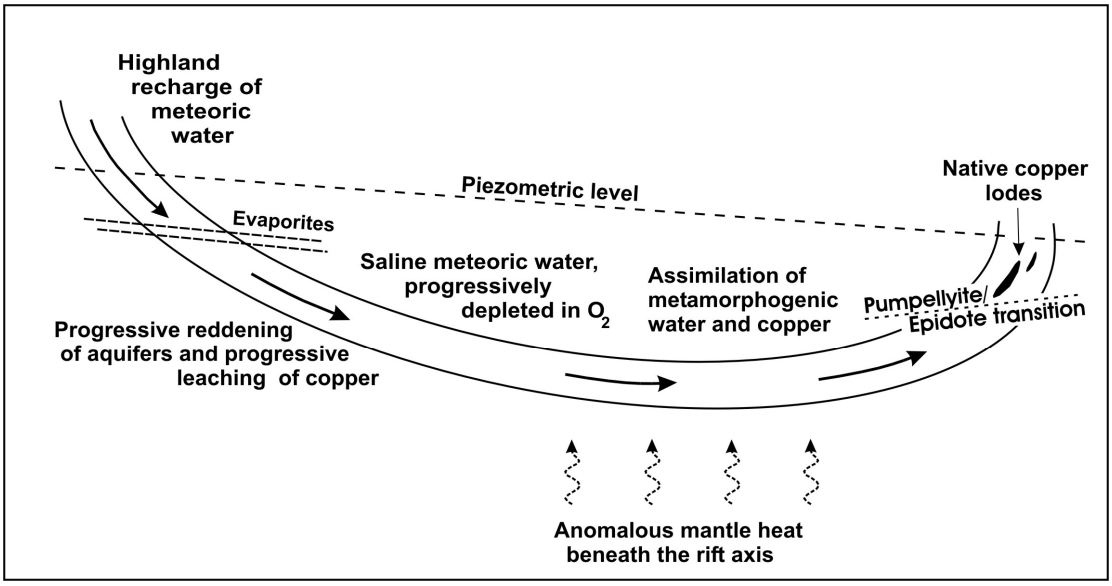


Figure 4: The origin of native copper lodes from meteoric (and metamorphic) brines flowing within the Keweenaw rift basin (after Brown 2006). See text for explanation.

Keweenawan native copper lodes as hydrothermally bleached host rock where native copper has been deposited (Butler & Burbank 1929; Weege *et al*. 1972; Brown 2006).

## 5 CONCLUDING COMMENTS

The linkage of both SSC and NCL mineralizations to a single gravity driven meteoric flow model which is in turn tied to the diagenetic reddening of aquifers and the leaching of copper from those aquifers provides a succinct global model for the principal copper deposit types of the Keweenaw district.

The White Pine deposit also encompasses a late, structurally controlled native copper mineralization (representing ~13% of the total mine production) which may been contemporaneous with the emplacement of Keweenawan native copper mineralization (Mauk 1993).

## ACKNOWLEDGEMENTS

This work has been sponsored by an individual grant from the Natural Sciences and Engineering Research Council of Canada.

## REFERENCES

Bornhorst TJ, Paces JB, Grant NK, (1988) Age of native copper mineralization, Keweenawan Peninsula, Michigan. *Econ. Geol*. 83: 619-625.

Brown AC (1971) Zoning in the White Pine copper deposit, Ontonogan, County, Michigan. *Economic Geology* 66: 543-573.

Brown AC (2003) Redbeds: source of metals for sediment-hosted stratiform copper, sandstone copper, sandstone lead, and sandstone uranium-vanadium deposits, *in* Lentz, D.R., ed., Geochemistry of Sediments and Sedimentary Rocks: Evolutionary Considerations to Mineral Deposit-Forming Environments: *Geological Association of Canada*, Geotext 4: 121-133.

Brown AC (2005) Refinements for footwall redbed diagenesis in the sediment-hosted stratiform copper deposits model. *Econ Geol* 100: 765-771.

Brown AC (2006) Genesis of native copper lodes in the Keweenaw district, northern Michigan: a hybrid evolved meteoric and metamorphogenic model. *Economic Geology* 101 (in print).

Brown AC, Trammel JW (1966) Zoning of the White Pine copper deposit, Ontonagon Co., Michigan. *Economic Geology* 61: 1308 (abstr.)

Butler B.S.,Burbank W.S. (1929) The copper deposits of Michigan. U.S. Geological Survey, Professional Paper 144, 238 p.

Cannon WF, Peterman ZE, Sims PK, (1993) Crustal-scale thrusting and origin of the Montreal River monocline – a 35 kilometer-thick cross section of the Mid-continent rift in northern Michigan and Wisconsin: *Tectonics* 12: 728-744.

Garrels RM (1960) Mineral Equilibria. Harper and Brothers, New York, 254 p.

Jolly WT (1974) Behavior of Cu, Zn and Ni during prehnite-pumpellyite rank metamorphism of the Keweenawan basalts, northern Michigan. *Economic Geology* 69: 1118-1125.

Livnat A, Kelly WC, Essene EJ, Rye RO (1983) P-T-X conditions of sub-greenschist burial metamorphism and copper mineralization, Keweenaw Peninsula, northern Michigan (abs.): *Geological Society of America* Abstracts 15: 629.

Mauk JL (1993) Geological and geochemical investigations of the White Pine sediment-hosted stratiform copper deposit, Ontonagon County, Michigan: *Unpublished PhD thesis,* University of Michigan, Ann Arbor, 194 p.

Ohr M (1993) U-Pb, Rb-Sr, and Sm-Nd dating of diagenesis and mineralization in the Late Proterozoic Nonesuch Formation, northern Michigan: *Unpublished PhD dissertation*, Univ. of Michigan, Ann Arbor, p. 97-142.

Robert F, Kelly WC (1987) Ore-forming fluids in Archean gold-bearing quartz veins at the Sigma mine, Abitibi greenstone belt, Quebec, Canada. *Economic Geology* 82: 1464-1482.

Rose AW (1976) The effect of cuprous chloride complexes in the origin of red-bed copper and related deposits: *Economic Geology* 71: 1036-1048.

Rose AW (1989) Mobility of copper and other heavy metals in sedimentary environments, *in* Boyle RW, Brown AC, Jefferson CW, Jowett EC, Kirkham RV, eds, Sediment-Hosted Stratiform Copper Deposits. *Geol. Assoc. Canada,* Spec. Paper 36, p. 97-110.

Stoiber RE, Davidson ES (1959) Amygdule mineral zoning in the Portage Lake Lava Series, Michigan copper district; Part I, Part II. *Economic Geol.* 54: 1250-1460, 1444-1460.

Walker TR (1989) Application of diagenetic alterations in redbeds to the origin of copper in stratiform copper deposits, *in* Boyle et al, eds, Sediment-Hosted Stratiform Copper Deposits. *Geological Association of Canada,* Special Paper 36, p. 85-96.

Weege RJ, Pollock JP, the Calumet Division Geol. Staff (1972) The geology of two new mines in the native copper district of Michigan. *Economic Geology* 67: 622-633.

White WS (1960) The White Pine copper deposit (discussion). *Economic. Geology*. 55: 402-410.

White WS (1968) The native-copper deposits of northern Michigan, *in* Ridge JD, ed, Ore Deposits of the United States, 1933-1967 (Graton-Sales Volume): *Amer. Inst. of Mining, Metal. and Pet. Eng.*, p. 303-326.

White WS, Wright JC (1966) Sulphide-mineral zoning in the basal Nonesuch Shale, northern Michigan. *Economic Geology* 61: 1171-1190.

Yardley WD, Graham JT (2002) The origins of salinity in metamorphic fluids. *Geofluids* 2: 249-256.

Zielinski A, Bloch S, Walker TR (1983) The mobility and distribution of heavy metals during the formation of first cycle red beds: *Economic Geology* 78: 1574-1589

# Organic and mineral characteristics of Kupferschiefer ore from Lubin mine (Poland): implications for bioleaching of the ore.

J. Gouin, T. Augé, L. Bailly & P. D'Hugues
*BRGM, BP 6009, 45060 Orléans cedex 2, France.*

J.R. Disnar & D. Keravis
*ISTO, UMR 6113, CNRS-University of Orleans, BP 6759, 45067 Orleans cedex 2, France.*

ABSTRACT: The ore mineral and organic matter content of the Lubin black shale (LBS) are compared with copper concentrate (LC) obtained by flotation. Study of a mineralized profile shows a good correlation between the S, TOC and Cu, Co and Ag content, suggesting syngenetic bacterial sulfate reduction (BSR) accumulation. The presence of disseminated and fracture filling rather than framboidal Cu-minerals, suggests formation via diagenetic processes. Compared to the black shale, the LC shows a lower HI and a higher OI, and a much more diverse ore mineral content. The black shale ore is composed of 15 vol. % sulphide, this proportion reaches 27 % in the LC whereas the TOC is similar in the LC and LBS. The ore mineral diversity in the LC is due to the contribution of mineralized sandstone and dolomite adjacent the black shale ore.

KEYWORDS: mineralization, organic matter, black shale deposit, copper concentrate

## 1 INTRODUCTION AND GEOLOGICAL SETTING

The Lubin mine belongs to the Kupferschiefer organic and copper-rich black shale deposit, which covers about 54.5% of Poland (Piestrzyński & Sawlowicz 1999). This deposit is located in southwestern part of Poland (Fig. 1). It is the largest copper deposit in Europe and one the largest in the world as regard to the copper reserves.

In the framework of the European BioShale project (*http://bioshale.brgm.fr*), aiming at evaluating biotechnology for beneficiation of black shale ore, we had the opportunity to study the Lubin black shale and various samples in order to characterize the product before and after the bioleaching treatment.

The Lubin ore deposit is of the stratabound polymetallic type, with a size of about 550km². The Kupferschiefer mineralization occurs between the uppermost Lower Permian Rotliegendes terrestrial redbeds and the Upper Permian Zechstein marine sequence (Oszczepalski 1999), in the southwestern part of Poland, within the North Sudetic basin and the Foresudetic Monocline. These polymetallic ore-bearing sediments are developed in two distinct facies, a reduced one which consists of an organic-rich black shale containing base metal sulphides and an oxidized one (Rote Fäule) which consists of red-coloured organic-deficient shale containing most of the precious metals (Oszczepalski 1999; Piestrzyński *et al*. 2002).

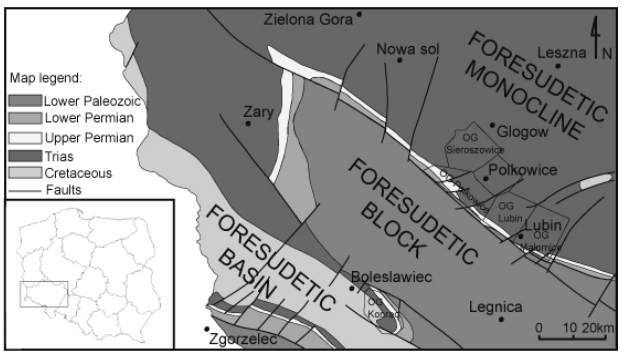


Figure 1. Geological map of Southwestern Poland, location of the Lubin deposit.

Results are presented for a 110cm thick profile through the reduced zone in the Lubin mine (LUP2-1 lowermost sample: boundary dolomite, LUP2-2 to 9: black shales, LUP2-10 to 12 uppermost sample: dolomites), analyzed to study sulphide distribution and relationships between metal enrichments and organic matter.

An "average black shale sample" (LBS) and the Lubin copper concentrate (LC) were also analyzed to compare the black shale ore and the industrial metal-enriched material for copper recovery. The Lubin copper concentrate (LC) is the final industrial product of the Lubin mine, obtained by flotation processes of a composite run of mine constituted by the three main formations of the Kupferschiefer: dolomite, black shale and sandstone.

## 2 MINERALIZATION

The most mineralized part of the orebody is the Kupferschiefer laminated black shale, with an average copper content of 7.1% (Piestrzyński & Sawlowicz 1999) on an average thickness of about 80cm. It shows a high organic content (TOC of 7-8% in average), clay minerals (illite), calcite/dolomite, detrital quartz and feldspars, and base metal sulphides. The organic matter is mainly represented by amorphous material of bituminite type, with vitrinite in various proportion and inertinite particles (Koch 1996). The main ore minerals are chalcocite, digenite, covellite, bornite, chalcopyrite, pyrite, tennantite, galena, sphalerite and silver minerals (Piestrzyński *et al*. 2002).

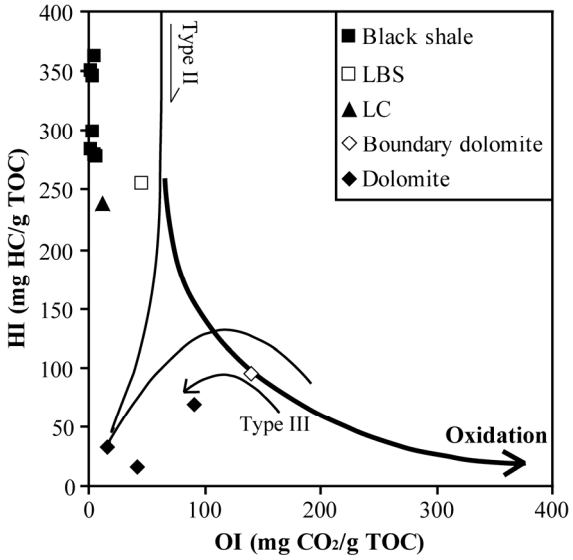


Figure 2. Hydrogen Index vs. Oxygen Index for recognition of genetic type of organic matter. Genetic paths after Espitalie *et al.* (1985).

## 3 METHODS

Rock-Eval Pyrolysis assay performed with a "Turbo" model RE6 pyrolyzer. Sulphide minerals were analyzed using a Camebax SX50 electron probe microanalyzer (EPMA) in routine conditions. For LBS and LC samples, sulphides minerals were concentrated by bromoform densimetric separation. The heavy fraction was compacted with a hydraulic press to obtain a disk which was then polished and analyzed by counting point technique with EPMA with a step of 200µm in same conditions as described above in order to accurately determine the proportion of each mineral.

Chemical analysis of the bulk samples was carried out by atomic absorption spectrophotometry and induced coupled plasma spectrophotometry. Loss of ignition was measured by heating the samples at 1000°C for 1h.

## 4 LUBIN PROFILE

### 4.1 *Organic matter characterization*

Two different types of organic matter (OM) can be distinguished in the profile of the reduced zone between black shale and dolomite samples. The black shale horizon is rich in OM, the TOC ranges from 5.27% to 13.7% (Fig. 2). This OM is typically of marine origin (type II kerogen) with high values of hydrogen index (HI up to 361 mg HC/g TOC) and low values of oxygen index (OI below 10 mg $CO_2$/g TOC) (Fig. 2). To the contrary, in all dolomite samples, the OM seems to be of terrigenous origin (type III kerogen). The TOC and HI are much lower (up to 1.11% and 93 mg HC/g TOC) and OI much higher (above 10 mg $CO_2$/g TOC). This is probably due to the low TOC contents with an artificial contamination of OI by carbonate material (Katz 1983).

### 4.2 *Metal distribution*

The boundary dolomite (LUP2-1) and the upper dolomite (LUP2-10 to 12) are poor in organic matter, and show very low metal contents: less than 1 wt.% Cu, less than 2 wt.% S, and less than 100-200 ppm As, Co, Ni, Ag. Organic-rich black shales (LUP2-2 to 9) exhibit, to the contrary higher contents of S (up to 7.5 wt.%), Cu (up to 14.4 wt.%) and hundreds of ppm As, Co, Ni, Ag.

The highest TOC, and metal content is observed in sample 2, except for S, and, there is a global tendency of decrease in metal contents toward the top of the profile (Fig. 3). Some enrichments in As, Co, Ni are observed in the middle of the profile corresponding to a higher content in cobaltite-gersdorffite group minerals.

The top of the profile is marked by an enrichment in S, Cu, Ag.

The metal patterns are globally in agreement with the S and TOC content, indicating that these metals were accumulated by bacterial sulphate-reduction during shale ore formation (Sun & Püttmann 1997). This process would however result in the formation of framboidal texture for the Cu-minerals as described by Sawlowicz (1990). With the exception of framboidal pyrite occurrences in black shale (mostly in algal filaments), the mineralization occurs as fine-grained disseminations and as fracture fillings indicating a base metal enrichment of diagenetic origin (Sun & Püttmann 1997).

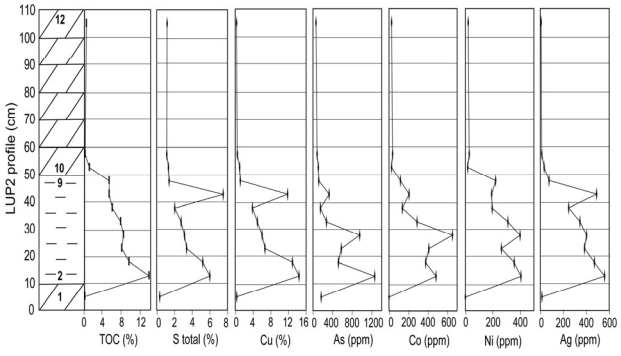


Figure 3. TOC and major elements distribution in LUP2.

## 5 COMPARISON OF LBS VS. LC

### 5.1 *Geochemistry*

LBS has a TOC value of 6.89%, lower than the mean value for the black shale ore of the profile (TOC = 7.98%), whereas TOC for LC is in the range with 7.63%. The OM, which composes LBS and LC is of marine origin as supported by the HI (254 and 237 mg HC/g TOC respectively) and OI (47 and mg $CO_2$/g TOC) (Fig. 2). Compared to the black shale of the profile, the two samples (LBS and LC) exhibit lower HI and higher OI (Fig. 2). LBS sample was probably collected in a more oxidized zone. Table 1 shows that the Lubin black shale has a similar composition to the average black shale of the profile. Compared to black shale ore, LC is enriched in total S and base metals, and depleted in V. The highest metal content in LC, (As - Pb - Zn being more than 10-times higher in the concentrate than in black shale ore), point to a probable input of metals from sandstones and/or dolomites, and the V depletion seems to be due to an effect of dilution (by the contribution of dolomite and sandstone in the concentrate) or a stronger affinity with gangue minerals.

Table 1. Geochemical data of average LUP2 black shales, LBS and LC.

| | Avg. LUP2-BS | LBS | LC |
|---|---|---|---|
| TOC (%) | 7.98 | 6.89 | 7.63 |
| $S_{tot.}$ (%) | 3.9 | 2.56 | 12.5 |
| Ag (ppm) | 372.3 | 340 | 910 |
| As (ppm) | 522.6 | 206 | 4930 |
| Co (ppm) | 334.5 | 234 | 1384 |
| Cu (%) | 7.73 | 8.6 | 17.1 |
| Ni (ppm) | 292.6 | 304 | 534 |
| Pb (ppm) | 121.1 | 112 | 4.74 % |
| V (ppm) | 1084.3 | 1530 | 854 |
| Zn (ppm) | 117.6 | 10 | 8330 |

### 5.2 *Sulphide quantification*

As mentioned previously, LC is enriched in metal compared to black shale ore. This is confirmed by the fraction of heavy minerals (mainly sulphides) extracted from each sample. LBS is composed of 15% of sulphides and 85% of gangue minerals (OM, quartz, clay minerals, carbonates), whereas LC contains 27% of sulphides and 73% of gangue minerals.

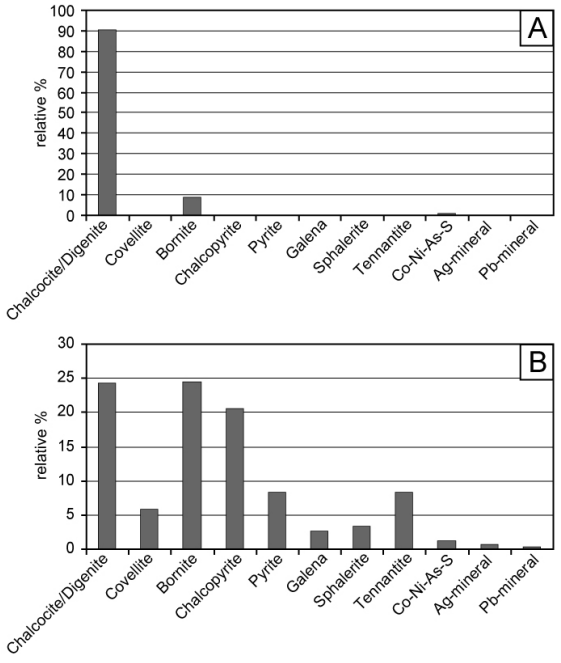


Figure 4. Relative proportion of each mineral phase in the heavy fraction in A) LBS and B) LC.

The differences observed in the chemical composition are reflected by the mineral composition. The sulphide fraction of LBS is

mainly composed of 3 main minerals (Fig. 4): chalcocite/digenite (>90%) - the distinction between the two was not possible with the technique used - and bornite (9%), with traces of Co-Ni-sulpharsenides (0.6%).

On the contrary, the sulphide fraction of LC is composed of about 11 minerals (Fig. 4). The four most abundant minerals are chalcocite/digenite (24.4%), bornite (24.5%) and chalcopyrite (20.6%), representing roughly 70% of the sulphide fraction. Three other minerals representing more than 20% of the sulphide fraction are pyrite (8.3%), tennantite (8.3%), covellite (5.8%). Less common minerals include galena (2.7%), sphalerite (3.3%), Co-Ni-sulpharsenides (1.2%). Rare Ag- and Pb-bearing minerals represent less than 1% of the sulphide fraction, and are poorly characterized.

The LBS is composed of 85% gangue minerals, 13.6% chalcocite/digenite, 1.4% bornite and 0.1% Co-Ni-sulpharsenide. The LC is more complex. It contains 73% gangue minerals, 6.6% chalcocite/digenite and bornite, 5.6% chalcopyrite, 2.2% pyrite and tennantite, 1.6% covellite, and less than 1% of other minor minerals (Table 2).

Table 2. Mineral composition and relative proportions in LBS and LC.

| | LBS | LC |
|---|---|---|
| Chalcocite/Digenite (%) | 13.6 | 6.6 |
| Covellite (%) | | 1.6 |
| Bornite (%) | 1.4 | 6.6 |
| Chalcopyrite (%) | | 5.6 |
| Pyrite (%) | | 2.2 |
| Galena (%) | | 0.7 |
| Sphalerite (%) | | 0.9 |
| Tennantite (%) | | 2.2 |
| Co-Ni-sulpharsenide (%) | 0.1 | 0.3 |
| Ag-mineral (%) | | 0.2 |
| Pb-mineral (%) | | 0.1 |
| Gangue (%) | 85 | 73 |

## 6 CONCLUSIONS

The black shale from the reduced zone of Lubin mine is rich in OM (marine origin) and base metals. The element enrichment (Cu, S, Co, Ni, Ag, V) is correlated with the presence of OM. Some metals such as Pb, Zn, As are however preferentially concentrated in sandstone and/or dolomite.

The black shales and Cu–concentrate from Lubin have similar organic material, but are different with regard to their metal contents and mineralization.

Some Cu-bearing sulphides, such as chalcopyrite, are known to degrade poorly during industrial bioleaching processes. It is thus important to quantify the sulphide, content and composition, in the black shale ore and Cu-concentrate to evaluate bioleaching efficiency for metal recovery.

## ACKNOWLEDGEMENTS

This work was financially supported by the European Commission in the frame of Bioshale European project (6th Framework program - NMP2-CT-2004-505710), in collaboration with CUPRUM (Poland).

## REFERENCES

Espitalie J., Deroo G. Marquis F. (1985) La pyrolyse Rock-Eval et ses applications. *Revue IFP* 41: 755-784.

Katz B.J. (1983) Limitations of « Rock-Eval » pyrolysis for typing organic matter. *Organic Geochemistry* 4: 195-199.

Koch J. (1996) Organic petrographic investigations of the Kupferschiefer in northern Germany. *Int. J. of Coal Geol*. 33: 301-3116.

Oszczepalski S. (1999) Origin of the Kupferschiefer polymetallic mineralization in Poland. *Mineralium Deposita* 34: 599-613.

Piestrzynski A. and Sawlowicz A. (1999) Exploration for Au and PGE in the Polish Zechstein copper deposits (Kupferschiefer) : *J. of Geochem. Expl.* 66: 17-25.

Piestrzynski A., Pieczonka J. and Gluszek A. (2002) Redbed-type gold mineralization, Kupferschiefer, south-west Poland : *Mineralium Deposita* 37: 512-528.

Sawlowicz Z. (1990) Primary copper sulphides from Kupferschiefer, Poland : *Mineralium Deposita* 25: 262-271.

Sun Y. and Püttmann W. (1997) Metal accumulation during and after deposition of the Kupferschiefer from the Sangerhausen Basin, Germany : *Applied Geochem.* 12: 577-592.

# Lead isotope and trace element patterns of German and Polish Kupferschiefer – a provenance study of bronze artifacts

M. Frotzscher & G. Borg
*Petrology & Economic GeologyResearch Group, Institute for Geological Sciences, Martin-Luther-University Halle, Germany*

E. Pernicka, B. Höppner & J. Lutz
*Curt-Engelhorn-Center for Archeometry, Reiss-Engelhorn-Museums, Mannheim, Germany*

ABSTRACT: The outstanding importance of the Early Bronze Age "Skydisk of Nebra" gave reason to investigate Central European copper occurrences in order to find out which occurrence might have been the source for its copper. Lead isotope ratios (by MC-ICP-MS) and trace element contents (Ag, As, Sb, Co, Ni, Bi, by energy-dispersive XRF) of German and Polish Kupferschiefer are presented and compared with data from the "Skydisk" and other artifacts found at Nebra. Trace element ratios and lead isotope data show clear differences between Kupferschiefer ore and Nebra artifacts. As a consequence, the investigated Kupferschiefer occurrences can be excluded as a copper source for the Nebra finds.

KEYWORDS: lead isotope, trace element, Kupferschiefer, "Skydisk of Nebra"

## 1 INTRODUCTION

The "Skydisk of Nebra", found in 1999 at Mittelberg near Wangen (Saxony-Anhalt, East Germany), is the earliest astronomical illustration in Europe and thus one of the most important Bronze Age finds. It had been buried at Mittelberg in the Early Bronze Age (1600 BC) as part of a hoard together with two swords, two hatchets, and other bronze artifacts. At present, a DFG-financed multidisciplinary research group investigates a number of archeological, archeometallurgical, archeoastronomical, and geological questions connected with the "Skydisk of Nebra" and the associated artifacts.

One of the projects has the aim to find out which Mid European copper occurrence could have provided the copper for the "Skydisk" and the other finds from Nebra. The study is focussed on occurrences, which crop out at surface and thus could have been easily exploited by Early Bronze Age miners. To characterize the different copper occurrences, lead isotopes and a number of trace elements (Ag, Co, Ni, As, Sb, Bi), which are not lost during smelting are used. Lead isotope compositions were measured by multicollector ICP-MS (Axiom, data corrected for Tl and Hg, 3 runs per sample). Trace elements together with the copper content are measured by energy-dispersive XRF (powder disks, detection limit for above mentioned trace elements about 10-50 ppm).

Amongst the investigated copper occurrences there are the Kupferschiefer-outcrops at the southern rim of the Harz Mountains and Kyffhäuser, in the vicinity of Dobis and Könnern (Saxony-Anhalt, East Germany), and in the North Sudetic Syncline in Southwest Poland. The data of several Kupferschiefer samples from these localities is compared with trace element and lead isotope data of the "Skydisk" and the other Nebra finds (data taken from an unpublished Diploma thesis by Daniela Nickel at University Freiberg). The Kupferschiefer south of the Harz Mountains was seen as a possible copper source, due to its proximity to Nebra. Besides our own analyses, lead isotope data of the Kupferschiefer from the literature is compared with the Nebra finds.

## 2 SAMPLES

Field samples have been taken from five localities in Saxony-Anhalt and Lower Saxony (Fig. 1). From an outcrop at Dobis come two samples of mineralized Weißliegend Conglomerate and two samples of Kupferschiefer. At Könnern, four Kupferschiefer samples from dumps have been taken. Five Kupferschiefer samples and one sample of "Sand Ore" are

from underground at the "Röhrigschacht" in Wettelrode (near Sangerhausen at the southern rim of the Harz Mountains) and two Kupferschiefer samples are from an outcrop nearby. Three samples (two of mineralized Weißliegend Conglomerate and one of Kupferschiefer) come from a dump near Rottleberode further west. From Bad Lauterberg (Lower Saxony), the westernmost of the sample points, there are two Kupferschiefer samples from the entrance of a small gallery, immediately at the former outcrop of the Kupferschiefer.

Two samples have been obtained from the Mineralogical Collection of University in Freiberg (Germany). These are a sample of mineralized Weißliegend Conglomerate from Rottleben at the southern rim of the Kyffhäuser (Fig. 1) and one sample of copper marl from Leszcyna in the North Sudetic Syncline.

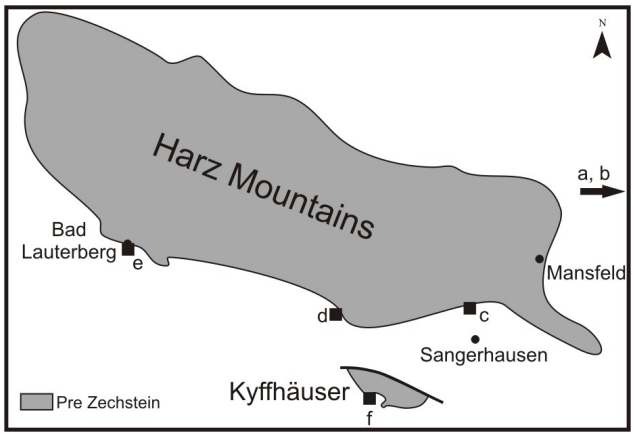


Figure 1. Sketch map of the Harz region (a and b point to Dobis and Könnern, c = Wettelrode, d = Rottleberode, e = Bad Lauterberg, f = Rottleben south of Kyffhäuser).

## 3 RESULTS AND DISCUSSION

Most of the 23 samples listed above have been measured for both trace elements and lead isotopes. The two samples from Kyffhäuser and from the North Sudetic Syncline have not yet been analyzed for lead isotopes.

### 3.1 *Trace elemental characterization*

Trace elements Ag, Co, Ni, As, Sb and Bi are typically used for determining the provenance of bronze artifacts because these elements pass from ore into crude copper during smelting (Pernicka 1987). However, bronze artifacts, consisting of 90% to 97% copper and up to 10% tin cannot be directly compared with copper ores. For this reason the metal ratios Ag/Cu, As/Cu, Sb/Cu, Co/Cu, Ni/Cu and Bi/Cu are used.

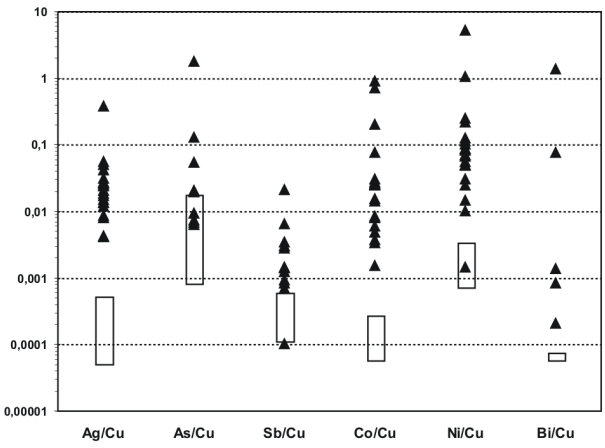


Figure 2. Comparison of element ratios between samples (black triangles) and artifacts (indicated by open rectangles).

Figure 2 shows these trace elements to copper ratios for all samples (black triangles). There is a relatively large variation between different localities and also between samples from the same locality. This gives an insight into the strong lateral and vertical variability in the chemical composition of the Kupferschiefer. For comparison with the Nebra finds, the variation within the group of artifacts (including the "Skydisk") is indicated by rectangles of different spread. It can be seen that there is almost no overlap. The As/Cu ratios of some samples fall into the variation of the artifacts but in most cases the Kupferschiefer tends to have higher relative trace element contents, especially for Ag and Co. It is important to note that a number of values are omitted in the diagram because the trace element contents are below detection limit and thus are difficult to display on a logarithmic scale. This includes for the artifacts (total number is 30) 8 values for Co, 11 values for Ag, 9 values for Sb, and all except one value for Bi (resulting in a small rectangle for the Bi/Cu values of the artifacts). For the Kupferschiefer samples (total number is 23) 13 values for As, 11 values for Sb, and 18 values for Bi are affected. So especially for Bi, there are values both from samples and artifacts below detection limit. But nevertheless, the trace element pattern of the Kupferschiefer is clearly different from the Nebra finds.

### 3.2 *Lead isotopical characterization*

Smelting of copper ores does not cause an isotope fractionation of lead (Pernicka 1987). As a consequence, the isotope ratios $^{206}Pb/^{204}Pb$, $^{207}Pb/^{204}Pb$, and $^{208}Pb/^{204}Pb$ can be used to characterize bronze artifacts. Lead iso-

tope ratios of 21 Kupferschiefer samples (and samples from mineralized Weißliegend Conglomerate) have been analyzed. The results are displayed in the following diagrams. Figs 3 and 4 compare lead isotope ratios of samples from the different localities to those of the "Skydisk" and the other Nebra finds. Similar to the XRF data, the lead isotope ratios show a clear difference between Kupferschiefer ores and the Nebra artifacts. However, the samples seem to form two clusters, one including the samples from Dobis, Könnern and Wettelrode, the other including samples from Rottleberode and Bad Lauterberg.

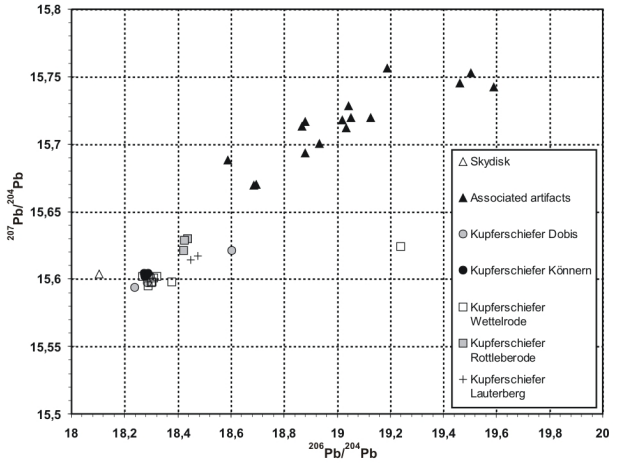


Figure 3. $^{207}Pb/^{204}Pb$ vs. $^{206}Pb/^{204}Pb$ diagram comparing Kupferschiefer samples from different localities with the "Skydisk of Nebra" and its associated artifacts.

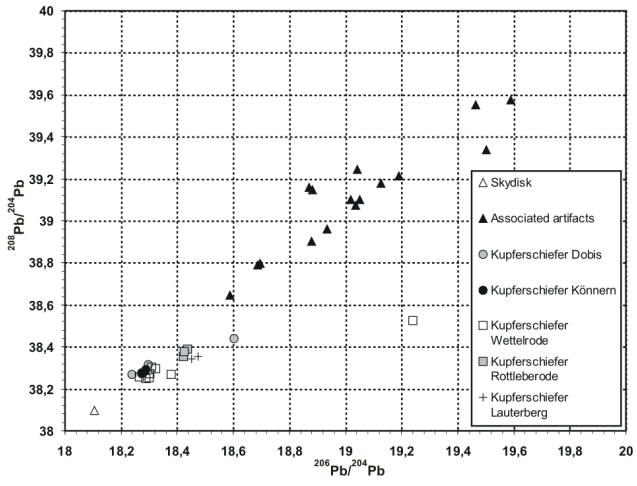


Figure 4. $^{208}Pb/^{204}Pb$ vs. $^{206}Pb/^{204}Pb$ diagram comparing Kupferschiefer samples from different localities with the "Skydisk of Nebra" and its associated artifacts.

One sample of Weißliegend Conglomerate from Dobis and the sample of "Sand Ore" from Wettelrode are characterized by higher $^{206}Pb/^{204}Pb$ contents (Fig. 3 and 4).

In the following two diagrams (Fig. 5 and 6) lead isotope data from literature is additionally shown. This includes data from the Kupferschiefer at Mansfeld (Niederschlag *et al*. 2003; Wedepohl *et al.* 1978), Eisleben (Wedepohl *et al*. 1978), Sangerhausen (Hammer *et al*. 1987; Wedepohl *et al.* 1978), Bad Lauterberg (Leveque & Haack 1993), from "Richelsdorfer Gebirge", "Weserbergland" and Lubin (Wedepohl *et al.* 1978), and also from the Zechstein at Kyffhäuser (Leveque & Haack 1993).

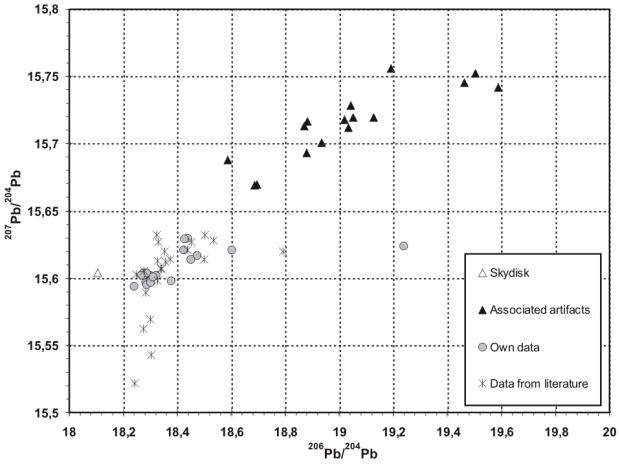


Figure 5. $^{207}Pb/^{204}Pb$ vs. $^{206}Pb/^{204}Pb$ diagram of artifacts, Kupferschiefer samples and Kupferschiefer data from literature.

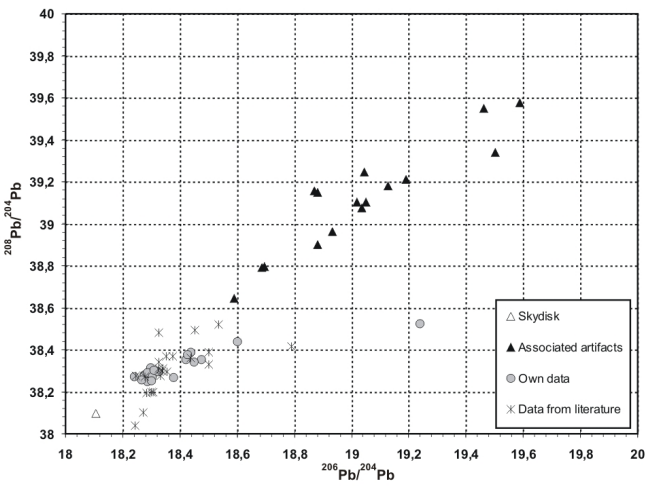


Figure 6. $^{208}Pb/^{204}Pb$ vs. $^{206}Pb/^{204}Pb$ diagram of artifacts, Kupferschiefer samples and Kupferschiefer data from literature.

Most of this literature data (with Lubin tending to higher $^{206}Pb/^{204}Pb$ contents) plots in the same range as our measured Kupferschiefer

samples. The signature of the published data is also different from that of the Nebra finds.

## 4 CONCLUSIONS

Trace element data as well as lead isotope data of the Kupferschiefer at the southern rim of the Harz Mountains and near Dobis and Könnern (Saxony-Anhalt, East Germany) is clearly different from data of the "Skydisk of Nebra" and its associated artifacts. As a consequence, these occurrences can be excluded as a copper source for the Nebra finds. XRF data of the Kupferschiefer at the southern rim of Kyffhäuser and in the North Sudetic Syncline (Southwest Poland) suggests that these localities can also be excluded, but this has still to be confirmed by lead isotope measurements. Lead isotope data from literature also shows no correlation with the "Skydisk" and the other artifacts from Nebra.

The present data is available for provenance studies of other artifacts and thus offers an excellent opportunity for future metallurgical comparisons.

## ACKNOWLEDGEMENTS

This study would not have been possible without the support of the Deutsche Forschungsgemeinschaft (DFG-FOR550). We also thank Volkmar Kästner and Udo Theuring from the Mining Museum "Röhrigschacht Wettelrode" for their guidance and admittance of sampling in Wettelrode, Karin Rank from the Mineralogical Collection of the University Freiberg for the samples from collection material and Wilfried Ließmann for his guidance in Bad Lauterberg.

## REFERENCES

Hammer J, Hengst M, Pilot J, Rösler HJ (1987) Pb-Isotopenverhältnisse des Kupferschiefers der Sangerhäuser Mulde – Neue Untersuchungsergebnisse. *Chemie der Erde* 46: 193-211.

Leveque J, Haack U (1993) Pb Isotopes of Hydrothermal Ores in the Harz. *Monograph series on mineral deposits* 30: 197-210.

Niederschlag E, Pernicka E, Seifert T, Bartelheim M (2003) The determination of lead isotope ratios by multiple collector ICP-MS: A case study of Early Bronze Age artefacts and their possible relation with ore deposits of the Erzgebirge. *Archaeometry* 45, 1: 61-100.

Pernicka E (1987) Erzlagerstätten in der Ägäis und ihre Ausbeutung im Altertum: Geochemische Untersuchungen zur Herkunftsbestimmung archäologischer Metallobjekte. *Jahrbuch des Römisch-Germanischen Zentralmuseums Mainz* 34, 2: 607-714.

Wedepohl KH, Delevaux, MH, Doe BR (1978) The potential source of lead in the Permian Kupferschiefer Bed of Europe and some selected Paleozoic mineral deposits in the Federal Republic of Germany. *Contributions to Mineralogy and Petrology* 65, 3: 273-281.

# CARBONATE-HOSTED ZN-PB DEPOSITS

EDITED BY:

PATRICK REDMOND

JAMIE WILKINSON

# The composition of Irish-type Zn-Pb ore fluids

J.J. Wilkinson & S.J. Collins
*Department of Earth Science and Engineering, Imperial College London, South Kensington Campus, Exhibition Road, London, SW7 2AZ*

T. Jeffries
*Department of Mineralogy, The Natural History Museum, Cromwell Road, London, SW7 5BD*

ABSTRACT: Laser ablation ICP-MS analyses of fluid inclusions from the Irish orefield provide compositional information on sediment-hosted ore fluids. Results from sphalerite and quartz samples within deposits indicate Zn and Pb contents of several hundred ppm and Ba contents of several thousand ppm. This contrasts with samples distal to deposits which are typically an order of magnitude lower. Both spatial and temporal heterogeneities exist in fluid chemistry indicating a complex evolution. Deposit formation may be linked to the influx of anomalously metal-rich batches of fluid.

KEYWORDS: fluid inclusions, laser ablation, ICP-MS, zinc, lead, orefluid, Ireland

## 1 INTRODUCTION

The composition of ore forming fluids is in general quite poorly known, yet is critical for a quantitative understanding of ore genesis. Models for metal sources, fluid flow and depositional mechanisms are all dependent on knowledge of the metal content of the fluids involved, in addition to intensive variables such as temperature, pressure, pH and redox state. Recent developments in laser ablation inductively-coupled plasma mass spectrometry (LA-ICP-MS) have enabled the determination of trace metal concentrations in fluid inclusions, providing new insights into processes of metal transport and deposition in ore systems (*e.g.* Landtwing *et al*., 2005).

Clastic sediment-hosted stratiform (Sedex) ore deposits are major repositories of Zn, Pb and Ba but the nature of the ore fluids, even in terms of their basic thermal and salinity properties, are arguably the most poorly known of any hydrothermal ore type. The Irish Carboniferous carbonate-hosted Zn-Pb deposits can be considered to be a carbonate-hosted end-member of the sedimentary-exhalative (Sedex) deposit class. A Sedex-type genetic model is widely, if not universally, accepted for these deposits (*e.g.* Wilkinson *et al*., 2005).

One of the great advantages of studying the Irish orefield is that it has not been subjected to significant tectonic or metamorphic overprinting as is the case for other Sedex deposits such as the Proterozoic examples of the McArthur basin in Australia, or other Phanerozoic examples such as Sullivan or Red Dog. This means that hydrothermal minerals which may have trapped primary ore fluids in the form of fluid inclusions are well-preserved and amenable for analysis.

Here we present data on the trace element chemistry of ore fluids from the Irish orefield obtained by LA-ICP-MS analysis of single fluid inclusions. Arguably, this is the first time that detailed data on sediment-hosted ore fluids have been obtained. The results provide new insights into metal sources and metal fractionation during extraction, transport and deposition, and the probable importance of ore fluid heterogeneity in large hydrothermal provinces.

## 2 FLUID INCLUSION DATA IN IRELAND

Fluid inclusion data have been acquired in a number of studies of the Irish Zn-Pb deposits, including Samson and Russell (1987), Banks & Russell (1992) and Everett *et al.* (1999a). Substantial data were collected by PhD students working at Imperial College: Sally Eyre, Kate Everett and Michael Lee. Here, we only present data from these studies and additional unpublished results obtained by our group. Basic homogenization temperature and salinity data mostly from primary or pseudosecondary fluid

inclusions hosted by quartz, dolomite, calcite and sphalerite are shown in Figure 1, and are subdivided according to sample type. The results show the very wide spread in salinity characteristic of fluids mobilized in the Irish hydrothermal system, with homogenization temperatures (approximately equivalent to trapping temperatures) of 44-276°C (excluding two outliers). Data from the ore deposits, regional carbonate-hosted hydrothermal veins and breccias and Lower Palaeozoic basement-hosted veins largely overlap, with the exception of some lower salinity (<8wt% NaCl equiv.) inclusions, hosted by the Type 1 veins of Everett *et al.* (1999a), that predate mineralized veins. Apart from the very low homogenization temperatures derived from the Harberton Bridge and Kinnitty prospects, the only notable

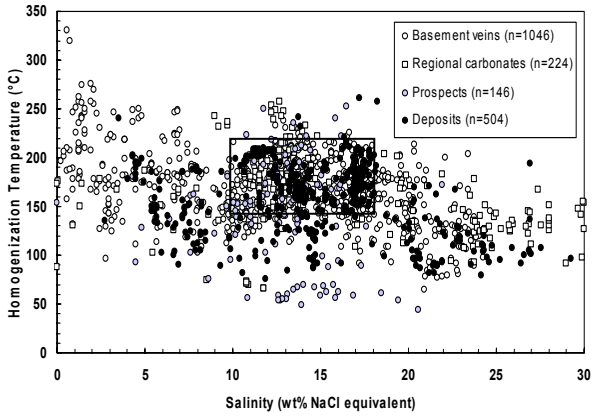


Figure 1. Summary of microthermometric data for fluid inclusions from the Irish orefield (sources listed in text). The concentration of data in the range 10-18wt% NaCl equiv. and 140-220°C (boxed) represents the "principal orefluid" as defined by Everett *et al.* (1999a, b). Ore deposit data outside this range (at both higher and lower salinity) are mostly from Navan.

difference between prospects and deposits is the general lack of fluids in excess of 17.5wt% NaCl equivalent in the former.

## 3 METHODS

### 3.1 *Sampling*

Samples for fluid inclusion analysis by LA-ICP-MS were selected from previous collections (Table 1). Priority was given to samples that were well-constrained by previous analyses, particularly those that contained well-developed fluid inclusions with prior microthermometric data. Some of the samples had also been previously analysed by bulk extraction methods for fluid chemistry (Everett *et al.*, 1999a,b; Wilkinson *et al.*, 2005).

Table 1. List of samples analysed by LA-ICP-MS

| Locality | Region | Type | Sample No. | Mineral |
|---|---|---|---|---|
| Ballycar | SW Midlands | L. Palaeozoic | BAL 5 | Quartz |
| Birdhill | SW Midlands | L. Palaeozoic | BIR 7 | Quartz |
| Fantane Quarry | SW Midlands | L. Palaeozoic | KEL 7 | Quartz |
| | | | KEL 9 | Quartz |
| | | | KEL 9B | Quartz |
| | | | KEL 16 | Quartz |
| Latteragh Quarry | SW Midlands | L. Palaeozoic | BOR 2B | Quartz |
| | | | LGH 2 | Quartz |
| Dunleer | NE Midlands | L. Palaeozoic | DUN 2 | Quartz |
| Navan | N Midlands | L. Palaeozoic | N840 – 2 | Dolomite |
| Keel | N Midlands | Prospect | KEEL | Quartz |
| Silvermines | SW Midlands | Deposit | Upper G | Sphalerite |
| | | | 75-85-104/71' | Sphalerite |

### 3.2 *LA-ICP-MS analysis*

After petrographic characterization and microthermometry, single fluid inclusions were analysed by LA-ICP-MS. Analyses were carried out at the Natural History Museum, London, using a New Wave UP213AI, 213 nm aperture laser ablation system linked to a Thermo Element PlasmaQuad 3 ICP-MS, according to procedures summarised by Stoffell *et al.*

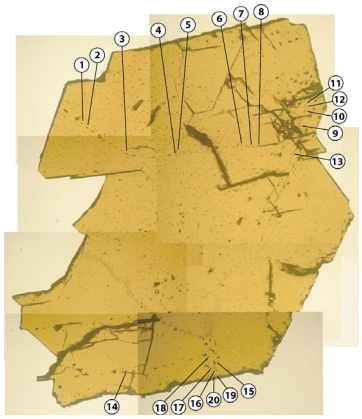


Figure 2. Sphalerite sample "Upper G" from Silvermines showing locations of fluid inclusions analysed (see Table 2 for results). Inclusions #1-8 are located on a primary growth zone; #9-12 are pseudosecondary that terminate at the growth zone; #13 and #15-20 are secondary inclusions; #14 is unclassified.

(2004). External calibration was carried by ablating multielement solutions held within pure quartz glass capillaries; chloride estimated from

freezing point depression measurements was used as the internal standard.

In addition to analysis of fluid inclusions in quartz, preliminary data were also acquired from inclusions hosted by sphalerite (Fig. 2) in order to assess possible compositional differences between fluids precipitating gangue minerals and those precipitating sulphides. Due to a contribution from the host for some elements (*e.g.* Mn, Pb; see Fig. 3) a background correction for these was applied. To our knowledge, this is the first ever report of fluid composition data from single fluid inclusions in sphalerite.

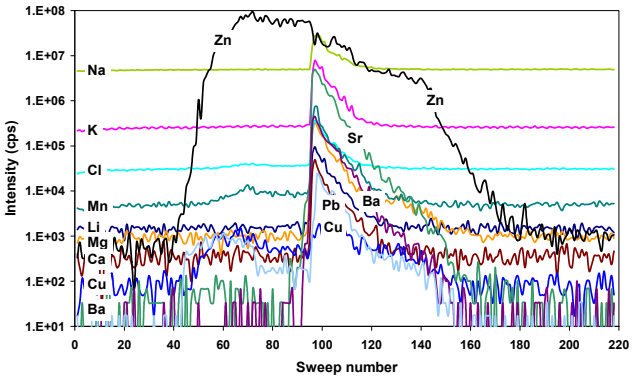


Figure 3. Time resolved spectrum showing ablation of fluid inclusion in sphalerite. The Zn signal rises when the laser is turned on indicating ablation of the host. The fluid signal when the inclusion is breached is clearly seen. Some elements (*e.g.* Mn, Pb, Cu) are present in the host at low concentration.

## 4 RESULTS

### 4.1 *Sphalerite from Silvermines*

Two samples of sphalerite from Silvermines were analysed. Full results from one of these (sample "Upper G") are listed in Table 2. The earliest inclusions (9-12) display elevated concentrations of Li, Mg, Ca, Mn, Sr and Ba relative to later inclusions. Pb concentrations for all inclusions range from 5-190 ppm; the early inclusions show higher Pb contents than those in the secondary trails.

### 4.2 *Regional comparison of metal contents*

Preliminary fluid compositional data have been obtained from seven other localities in the Irish Midlands (Table 1). These samples fall into two groups: Northern Midlands deposits (Keel and Navan), and Lower Palaeozoic-hosted footwall veins, distal to the Silvermines deposit.

Inclusions from both Northern Midlands samples display low Pb and high Zn concentrations, and at Keel also high Ba (Table 3). In the Southwest Midlands, Lower Palaeozoic-hosted veins contain fluid inclusions with low metal concentrations, confirming previously bulk inclusion analyses (Wilkinson *et al.,* 2005). These data contrast with the very high Pb and Ba concentrations determined in the sphalerite-hosted inclusions from Silvermines (unfortunately Zn cannot be determined in these inclusions).

Table 2. Fluid inclusion compositions (ppm) from sphalerite sample "Upper G" from Silvermines.

| Inc | Type | Li | Mg | Cl | K | Ca | Mn | Sr | Ba | Pb |
|---|---|---|---|---|---|---|---|---|---|---|
| 1 | P | 222 | 309 | 75498 | 1125 | 11691 | 955 | 177 | 647 | 108 |
| 2 | P | 376 | 500 | 74814 | nd | 19603 | 555 | 368 | 1339 | 31 |
| 3 | P | 583 | 612 | 73435 | 6587 | 17242 | 589 | 356 | 1984 | 41 |
| 4 | P | 174 | 169 | 74814 | 1519 | nd | nd | 147 | 700 | 177 |
| 5 | P | 348 | 238 | 75498 | 1795 | nd | nd | 186 | 524 | nd |
| 6 | P | 401 | 442 | 75498 | 5129 | 13891 | 1091 | 301 | 1645 | 31 |
| 7 | P | 361 | 341 | 75498 | 2668 | nd | 912 | 246 | 1591 | 133 |
| 8 | P | 290 | 391 | 75498 | 1412 | nd | 942 | 288 | 1215 | 190 |
| 9 | PS | 663 | 1114 | 103487 | 3648 | 43102 | 1119 | 6252* | 51194* | nd |
| 10 | PS | 1151 | 1688 | 102944 | 8709 | 67921 | 1371 | 6065* | 31404* | 100 |
| 11 | PS | 938 | 1251 | 103487 | 1845 | 46559 | 1487 | 856 | 8053 | 145 |
| 12 | PS | 611 | 492 | 103216 | 941 | 117024 | 1676 | 4348 | 6355 | 121 |
| 13 | S | 610 | 676 | 104564 | 1613 | 39281 | 599 | 2219 | nd | 41 |
| 14 | P? | 313 | 455 | 87852 | 2399 | nd | nd | 380 | 1072 | 134 |
| 15 | S | 962 | 1148 | 76179 | 6190 | 31549 | 552 | 997 | 2646 | 6 |
| 16 | S | 349 | 391 | 76179 | 1832 | 23883 | 254 | 484 | 1200 | 5 |
| 17 | S | 423 | 701 | 76179 | 2420 | 19356 | 608 | 654 | 971 | nd |
| 18 | S | 410 | 726 | 76179 | 2538 | nd | 631 | 430 | 1941 | nd |
| 19 | S | 653 | 728 | 76179 | 2115 | 27661 | 728 | 605 | 2400 | 9 |
| 20 | S | nd | nd | nd | nd | nd | nd | nd | nd | nd |

P = primary; PS = pseudosecondary; S = secondary; nd = not determined. *Anomalous values, possibly due to synchronous ablation of trapped barite with fluid inclusions.

| Location | Zn | Ba | Pb |
|---|---|---|---|
| Navan | 379 | n.d. | 6 |
| Keel | 841 | 1038 | 31 |
| Southwest Midlands L. Palaeozoic-hosted | 52 | 328 | 42 |
| Silvermines | nd | 4312 | 232 |

Table 3. Mean composition of "principal orefluids" (ppm)

## 5 DISCUSSION

The significant temporal and spatial heterogeneities in fluid inclusion chemistry are striking. Despite the fact that most of the inclusions analysed in this study would fall in the "princi-

pal orefluid" field in terms of microthermometric properties (Fig. 1) they show marked differences in total metal content and metal ratios. This indicates extreme chemical variability exists on the large scale in the ore system. Nonetheless, this result is perhaps not surprising given the similar variability that can be found in modern geothermal systems such as Yellowstone (McCleskey *et al.*, 2004).

Perhaps an important, although very preliminary, finding is that fluids appear to be significantly more Zn-rich at Navan and Keel than those from Silvermines, which have elevated Pb values (although Zn concentrations are presently unknown). This might imply a different lithological source for metals in the Northern Midlands, perhaps even Precambrian basement as suggested by recent Nd isotope data (Walshaw *et al.,* 2006). It is also noteworthy that extremely high average Ba concentrations are observed at Silvermines and Keel (2054 and 1038 ppm respectively), both proximal to the only two significant barite accumulations in the orefield, Ballynoe and Garrycam.

The enrichment in metals observed in deposit samples compared with those from vein systems distal to deposits is also of note. This suggests either that parts of the hydrothermal system involved fluids that were barren or that these represent the depleted "exhaust" of the ore system. The coincidence of elevated metals and ore deposits seems to be intuitive, and yet such a relationship has rarely been documented. The existence of true "orefluids" containing anomalously high metal concentrations would simplify existing models for ore formation that either require excessively long time-scales or unusually high fluid fluxes.

## 6 CONCLUSIONS

LA-ICP-MS analyses of individual fluid inclusions show that significant spatial and temporal heterogeneity exists in the Irish orefield. High metal concentrations are observed in primary inclusions associated with orebodies. Secondary inclusions and samples distal from mineralization contain lower metal concentrations, suggesting that ore formation involves fluid batches anomalously enriched in metals.

## ACKNOWLEDGEMENTS

We thank the many colleagues and friends who have collaborated with us, and the operators and staff at Navan, Lisheen and Galmoy for generous access and assistance. CSA, Glencar, Noranda, Minco, BHP and Rio Tinto provided field support and access to drillcore. Significant contributions were made to this work by the late Dave Johnston and Kate Everett.

## REFERENCES

Banks DA, Russell MJ (1992) Fluid mixing during ore deposition at the Tynagh base-metal deposit, Ireland. *Eur Jour Mineral* 4: 921–931.

Everett CE, Wilkinson JJ, Rye DM (1999a) Fracture-controlled fluid flow in the Lower Palaeozoic basement rocks of Ireland: Implications for the genesis of Irish-type Zn-Pb deposits, *in* McCaffrey KJW, Lonergan L, Wilkinson JJ, eds, Fractures, Fluid Flow and Mineralization: *Geol Soc London Spec Pub* 155: 247–276.

Everett CE, Wilkinson JJ, Boyce AJ, Ellam RM, Fallick AE, Gleeson SA (1999b) The genesis of Irish-type Zn-Pb deposits: Characterisation and origin of the principal ore fluid, *in* Stanley CJ et al., eds, *Mineral Deposits: Processes to Processing, Proc SGA and IAGOD,* London: Balkema, vol. 2, 845–848.

Landtwing MR, Pettke T, Halter WE, Heinrich CA, Redmond PB, Einaudi MT, Kunze K (2005) Copper deposition during quartz dissolution by cooling magmatic–hydrothermal fluids: the Bingham porphyry. *Earth Planet Sci Lett* 235: 229–243.

McCleskey RB, Ball JW, Nordstrom DK, Holloway JM, Taylor HE (2004) Water-chemistry data for selected hot springs, geysers and streams in Yellowstone National Park, Wyoming, 2001-2002. *USGS Open File Report* 2004-1316.

Samson IM, Russell MJ (1987) Genesis of the Silvermines zinc-lead-barite deposit, Ireland: Fluid inclusion and stable isotope evidence. *Econ Geol* 82: 371–394.

Stoffell B, Wilkinson JJ, Jeffries TE (2004) Metal transport and deposition in hydrothermal veins revealed by 213nm UV laser ablation microanalysis of single fluid inclusions. *Amer Jour Sci* 304: 533–557.

Wilkinson JJ, Everett CE, Boyce AJ, Gleeson SA, Rye DM (2005) Intracratonic crustal seawater circulation and the genesis of sub-seafloor Zn-Pb mineralization in the Irish orefield. *Geology* 33: 805–808.

Walshaw RD, Menuge JF, Tyrell S (2006) Metal sources of the Navan carbonate-hosted base metal deposit, Ireland: Nd and Sr isotope evidence for deep hydrothermal convection. *Miner Deposita* 41: 803–819.

# Fluid inclusion and stable isotope characteristics of carbonate replacement Pb-Zn-Ag deposits in the Lavrion district, Greece

T.A. Bonsall & P.G. Spry
*Department of Geological & Atmospheric Sciences, Iowa State University, Ames, Iowa 50011, U.S.A.*

P. Voudouris
*Department of Mineralogy & Petrology, University of Athens, 15784 Athens, Greece*

K. St. Seymour & S. Tombros
*Department of Geology, University of Patras, 26500 Rion, Greece*

V. Melfos
*Department of Mineralogy, Petrology & Economic Geology, Aristotle University of Thessalonika, Greece*

ABSTRACT: Carbonate replacement Pb-Zn-Ag deposits (CRDs) in the Lavrion district are spatially related to an Upper Miocene granodiorite intrusion and various sills and dikes of intermediate to acid composition. The mineralogy of CRDs includes base-metal sulphides as well as sulphosalts containing Ag, Bi, Sn, Sb, As, and Pb, particularly at Plaka and Kamariza. Fluid inclusion studies suggest the CRDs were deposited from moderate-temperature (132$^{o}$-365$^{o}$C), $CO_2$-poor, and low- to moderately-saline (1 to 20 wt% NaCl equivalent) fluids. Sulphur isotope compositions of sulphides and sulphates suggest a magmatic contribution to the ore fluids and a marine seawater origin for barite. Carbon and oxygen isotope compositions of calcite intergrown with sulphides reflect variable exchange of the ore-bearing fluid with the upper and lower marble host and with proximity to the Plaka granodiorite. The CRDs resemble carbonate-hosted sulphide deposits in Mexico, central Colorado, and northern Greece.

KEYWORDS: Lavrion, fluid inclusions, stables isotopes, carbonate replacement Pb-Zn-Ag ores

## 1 INTRODUCTION

The famous Lavrion silver district, Greece, was actively mined for over 3000 years and produced ~ 25 million oz of Ag before it closed in the early part of the 1970s. Although there are >50 base metal occurrences in the district, much of the mining centered around Plaka and Kamariza. The district consists of four different mineralization types: intrusion-hosted, carbonate replacement, vein, and skarn, with all four types occurring at Plaka (Fig. 1). Of these ore types, the most important economically is the carbonate replacement Pb-Zn-Ag type, which is found at locations such as Kamariza, Esperanza, Sounio, Villia, Avlaki, and Megala Pefka (Fig. 1). Skarn- and vein-types (*e.g.*, Vein 80) are spatially related to intrusion-hosted mineralization in and adjacent to the Plaka granodiorite (Fig. 1). Prior to the discovery of the intrusion-related mineralization at Plaka, Kalogeropoulos & Mitropoulos (1983) proposed, on the basis of fluid inclusion data, that the carbonate replacement deposits (CRDs) in the Lavrion district were Mississippi Valley-type (MVT) deposits. The aim of this study is to determine the origin of the CRDs and their genetic relationship, if any, with the granodiorite intrusion near Plaka and other minor porphyritic dikes and sills (intermediate to acid composition) that are exposed at the surface or occur in underground locations throughout the district.

## 2 REGIONAL GEOLOGY

The Lavrion district is part of the Cycladic-Pelagonian base and precious metal belt that trends northwest from Milos Island, Greece, to Bulgaria. In the Lavrion area, a Mesozoic metamorphic autochthonous sequence, which consists of an upper and lower marble and intercalated schist (Kessariani schist), was overthrust by an Upper Cretaceous allochthonous phyllitic nappe. The formation of the Plaka granodiorite (7-10 Ma; Altherr *et al.* 1992) is synchronous with extensional detachment faulting.

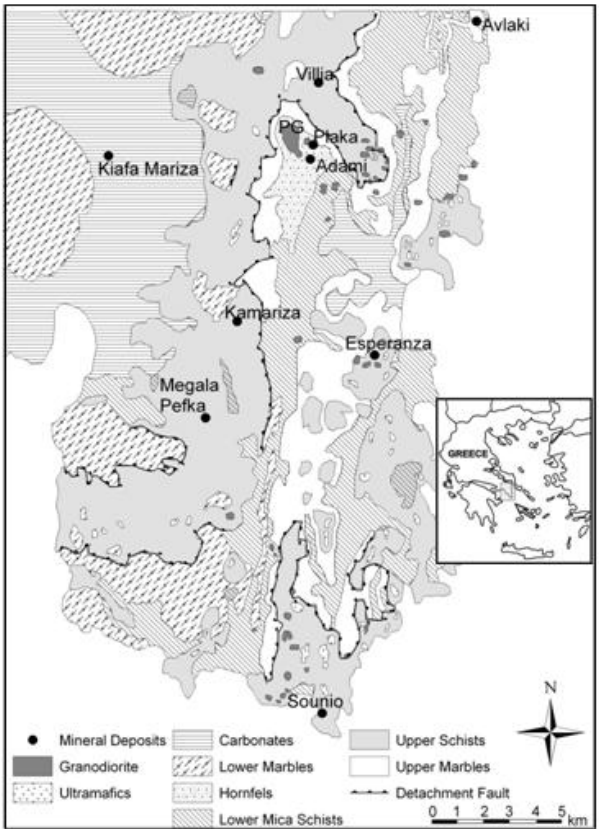


Figure 1. Geological map of the Lavrion district. PG = Plaka granodiorite.

.

## 3 MINERALOGY

Although famous for containing more than 400 secondary minerals, the primary ores in the Lavrion district are also complex, with >60 sulphides and sulphosalts (containing Ag, Bi, Sn, Sb, As, and Pb). Pyrite, molybdenite, chalcopyrite, pyrrhotite and scheelite occur in intrusion-hosted mineralization whereas magnetite, pyrrhotite, scheelite, sphalerite, chalcopyrite, galena, bismuthinite, and native bismuth are present in skarn-type mineralization. Carbonate replacement ores are hosted in marble at contacts with the Kessariani schist and with granodiorite dikes and sills. Replacement orebodies (up to 10s of meters in length) are generally conformable to bedding but locally crosscut bedding.

For ores in the Kamariza area, Voudouris and Economou-Eliopoulos (2003) showed that pyrite and arsenopyrite formed first, followed by sphalerite, galena, Bi-Cu-Pb-Sb-Ag-sulphosalts, enargite, petrukite, chalcopyrite and native gold. Away from Plaka and Kamariza, primary sulphide mineralization is dominated by sphalerite, galena, pyrite, marcasite, chalcopyrite, pyrrhotite and arsenopyrite with considerably fewer sulphosalts. Calcite, quartz, and fluorite are intergrown with sulphides and may occur at various stages in the paragenetic sequence. Primary barite and secondary gypsum are less common gangue minerals. In places, particularly along the western margin of the district, sulphides are essentially absent and barite is the dominant sulphur-bearing mineral.

## 4 FLUID INCLUSION STUDY

Approximately 230 microthermometric measurements of primary and secondary fluid inclusions were made. Preliminary measurements of primary aqueous liquid-vapour inclusions and aqueous liquid-vapour inclusions with variable liquid to vapour ratios and up to three daughter crystals in quartz from quartz-molybdenite veins at the Plaka granodiorite show homogenization temperatures ($T_h$) of 268 to >460°C, and salinities that range from 10.4 to 42.8 wt.% NaCl equivalent (Fig. 2). The spatial relationship among vapour-rich, vapor-poor, low salinity and high salinity fluid inclusions suggest that the precipitation of molybdenite was associated with phase separation.

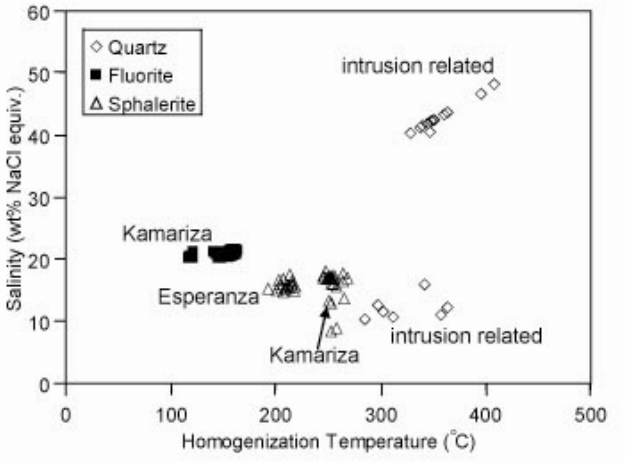


Figure 2. Salinity-homogenization temperature plot for fluid inclusions in ore and gangue minerals from the Lavrion district.

Primary two phase liquid-vapour inclusions with liquid:vapour ratios of ~4:1 were measured in sphalerite and fluorite from the Kamariza area (Jean Baptiste, Ilarion, and Serprieri deposits). These show $T_h$ values of 233 to 265°C and salinities of 7.2 to 18.0 wt% NaCl equivalent. Similar inclusions from the

Esperanza deposit exhibit $T_h$ values of 183 to 221°C and salinities of 14.8 to 17.6 wt% NaCl equivalent (Fig. 2). Fluid inclusions from both locations show low eutectic temperatures of ~ -42.0 to -32.0°C suggesting the presence of $Ca^{2+}$, in addition to $Na^{+}$ and $K^{+}$, in the hydrothermal solutions. The data obtained here overlap those obtained by Knoll (1988; 250 to 365°C and 1 to 15 wt% NaCl equivalent) and Kalogeropoulos & Mitropoulos (1983; 132 to 208°C and 16 to 20 wt% NaCl equivalent) from fluid inclusions in fluorite from the Plaka and Kamariza areas.

## 5 STABLE ISOTOPE STUDY

Sulphur, carbon and oxygen isotope data were obtained from different minerals collected from Kamariza, Adami (Vein 80), Sounio, Esperanza, Avlaki and Villia. Sulphur isotope compositions of both sulphides (galena, sphalerite, and pyrite; n = 54) and sulphates (barite and gypsum; n = 8) were measured. Carbon and oxygen isotope compositions of calcite samples (n = 61) from the lower and upper marbles and intergrown with sulphides in CRDs were acquired. The sulphur isotope data are reported as per mil variations relative to Cañyon Diablo Troilite (CDT) whereas those for carbon and oxygen isotope data are reported relative to VPDB and VSMOW, respectively.

Calcite samples yielded $\delta^{13}C$ and $\delta^{18}O$ values of -9.4 to 5.2‰ and 2.5 to 30.0‰ respectively (Fig. 3), and reflect variable exchange of ore fluids with the upper and lower marble host rocks, over a range of temperature, and with the Plaka granodiorite. Carbon and oxygen isotope compositions of most carbonates in sulphides are isotopically lightest with increasing proximity to the Plaka granodiorite (Fig. 3). For example, those from the Villia deposit, which is closest to the Plaka granodiorite, exhibit values of $\delta^{13}C$ = -5.4 to -1.8‰ and $\delta^{18}O$ = 2.7 to 7.7 ‰, respectively. They are isotopically distinguished from carbonate that formed after sulphide deposition, which is characterized by $\delta^{13}C$ and $\delta^{18}O$ values of -9.4 to -7.3‰ and 20.6 to 24.9‰, respectively

Sulphur isotope compositions of sulphides from Vein 80 (Adami mine) ranged from -3.2 to 2.0‰ (n = 7) and are isotopically heavier than sulphides in CRDs in the Kamariza area (-5.0 to -0.8‰; n = 25) (Fig. 4). Sulphides from all other CRDs show positive values of 2.1 to 9.4‰ (n = 22), with the isotopically heaviest

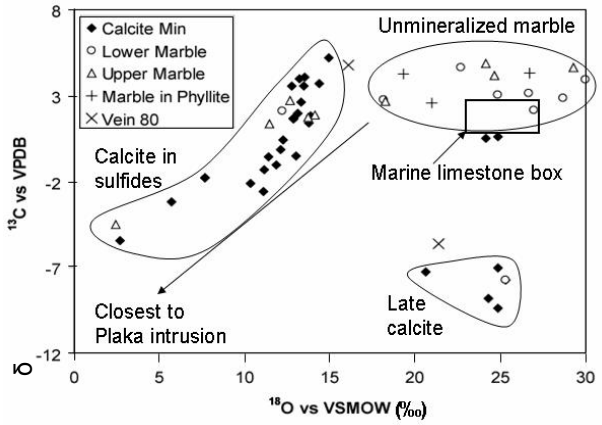


Figure 3. Plot of C and O isotope compositions of calcite from the Upper and Lower Marbles and intergrown with CRD sulphides.

sulphide being sphalerite from the northernmost deposit (Avlaki). The only other negative value of $\delta^{34}S$ (-2.2‰) was obtained from galena from the Megala Pefka deposit. Sulphur isotope compositions of barite from CRDs range from 17.2 to 23.7‰ whereas those for two samples of secondary gypsum yielded $\delta^{34}S$ values of -0.9 and -0.8‰. Although the mean of sulphide $\delta^{34}S$ values center around zero per mil, consistent with a magmatic sulphur contribution, sulphur isotope values of barite are consistent with its derivation from late Miocene seawater whereas those for gypsum suggest that they formed by oxidation of primary sulphides.

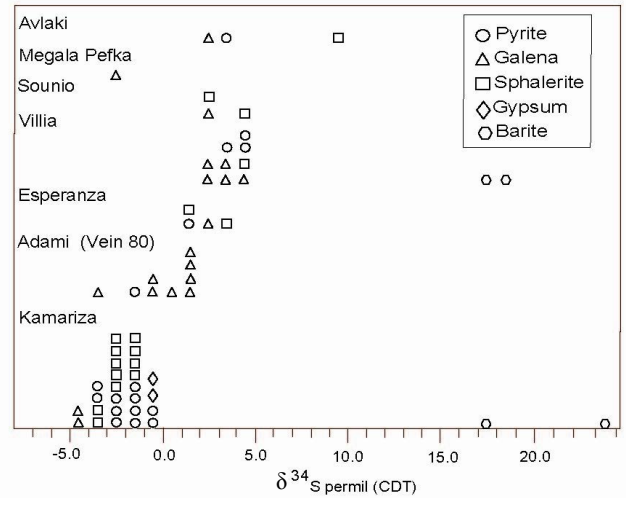


Figure 4. Sulphur isotope compositions of sulphides and sulphates from the Lavrion district.

## 6 CONCLUSIONS

Carbonate replacement deposits formed as part of a complex ore system in the Lavrion district that mimic those associated with manto-

style CRDs in Mexico, northern Greece and central Colorado. Carbonate replacement deposits in the Lavrion district show a complex mineralogy (including the presence of a wide variety of sulphosalts), a spatial relationship with igneous intrusions/apophyses, fluid inclusions in sphalerite and fluorite with moderately high $T_h$ values, and a likely involvement of magmatic fluids and components (S, Ag, Bi, Cu, Pb, Sb). These characteristics are distinct from MVT deposits. Magmatic contributions (fluids and ore components) are likely highest for CRD mineralization in the Plaka and Kamariza areas and diminish on the margins of the Lavrion district.

ACKNOWLEDGEMENTS

Special thanks go to Ch. Solomos and A. Tsolakos for their assistance with underground sampling in the Lavrion area. This contribution was improved by the editorial comments of Jamie Wilkinson. His efforts were greatly appreciated.

REFERENCES

Altherr R, Kreuzer H, Wendt I, Lenz H, Wagner G, Keller J, Harre W, Hondorf A (1982) A late Oligocene/Early Miocene high temperature belt in the Attic-Cycladic crystalline complex (SE Pelagonian, Greece). *Geol. Jahrbuch,* 23: 97-164.

Kalogeropoulos S, Mitropoulos P (1983) Fluid inclusion characteristics of fluorite from Laurium (Greece). *Ann. Geol. Pays. Hellen*., 31: 130-135.

Knoll O (1988) Ore mineralogy and fluid inclusion studies on Pb-Zn-ores from Lavrion, Greece. *Unpubl. MSc Thesis, University of Hamburg*, 72 p.

Voudouris P, Economou-Eliopoulos M (2003) Mineralogy and chemistry of Cu-rich ores from the Kamariza carbonate-hosted deposit (Lavrion), Greece. In: Eliopoulos DG et al. (eds) *Mineral exploration and sustainable development,* Millpress, Rotterdam, pp 1039-1042.

Voudouris P (2005) Gold and silver mineralogy of the Lavrion deposit, Attika, Greece. In: Mao J et al. (eds) *Mineral deposit research: Meeting the global challenge.* Springer, Berlin, pp 1089-1092.

# The Origin of Sulphur in MVT Deposits

G.M. Anderson
*Department of Geology, University of Toronto, Toronto M5S 3B1, Canada*

J. Thom
*Department of Earth and Ocean Sciences, University of British Columbia, Vancouver V6T 1Z4, Canada*

ABSTRACT: Data on first order rate constants for the thermochemical sulphate reduction (TSR) reaction cover a range of $10^0$ to $10^{-4}$ $y^{-1}$ at 150°C. The rate equation has not been definitely established, but using a reasonable guess and rate constants within this range, two types of models are used to calculate the amounts of ZnS precipitated and the amounts of carbonate dissolved and precipitated as a function of time. Both the Constant Stirring Tank Reactor (CSTR) and the reactive transport model of sulphide precipitation by TSR show that rates in the upper part of the experimental range are fast enough to form small to medium sized ore deposits in geologically reasonable times, and, being very slow, this has implications for what the ores should look like. There are however reasons to doubt that the experimental data are really applicable to natural situations.

KEYWORDS: MVT kinetics TSR CSTR reactive transport

## 1 INTRODUCTION

Any genetic hypothesis for MVT (Mississippi Valley-Type) deposits must account for the source of both the metals and the sulphur in the ore minerals.

For the sulphur, one possibility is sulphate reduction, presumably without the aid of bacteria because of the high temperatures involved. Thermochemical sulphate reduction (TSR) reaction has been studied experimentally by a number of authors, and is known to be an extremely slow process. In most hypotheses, $H_2S$ produced by TSR is trapped and later intersected by a metal-bearing solution. This is one variant of the "mixing hypothesis" (Beales & Jackson, 1966). Another variant of this idea would be derivation of the sulphur *during* mineralization, rather than before.

This possibility has been widely dismissed because it is assumed that TSR is too slow to provide sufficient sulphide during the mineralizing event. It is the purpose of the work reported here to summarize the available data on the rate of TSR and to examine more closely the idea that sulphide might be supplied during ore deposition.

## 2 THERMOCHEMICAL SULPHATE REDUCTION

Sulphate reduction in the absence of bacteria (TSR) has been carried out experimentally at temperatures as low as 175°C (Orr, 1982; Goldhaber & Orr, 1995), but most experiments have been at 250°C or higher because reaction rates are slow. We performed experiments similar to those of Orr (1982), and obtained similar results. Data have been interpreted by all authors as showing that TSR is a first order reaction, and these data are shown in the form of an Arrhenius plot in Figure 1 (references in Goldhaber & Orr, 1995).

The rate constants in $y^{-1}$ units at a typical MVT temperature of 150°C range from about log $k$ = 0 to log $k$ = -4 (estimated from Figure 1). This wide range is probably due to the various reductants, pH, and other experimental conditions used. These rate constants are for a rate equation which has not been investigated to any great extent, but because (1) it appears to be first order; (2) the rate increases with the activities of both $H^+$ and $H_2S$ which are on opposite sides of the reaction and so their effects may therefore cancel; and (3) the reductant activity in most experiments was constant and so would not affect the rate, the rate equation may

be as simple as

$$\text{rate} = k \times [SO_4]^n \qquad (1)$$

where $[SO_4]$ is the sulphate concentration, $k$ is the rate constant, and $n = 1$. In any case this is the equation used in the model calculations described below. We have used two types of models to evaluate the quantity of ZnS deposited as a function of time and TSR rate constant.

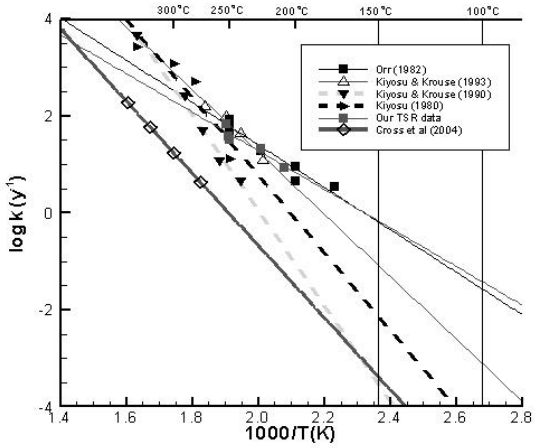


Figure 1 Arrhenius plot of most available rate constant data (in $y^{-1}$ units) for TSR. Results from this study are labeled "Our TSR data".

## 2.1 *The CSTR Model*

We first consider the flow of Zn and sulphate in and out of a box, representing a vein system at 150°C, as shown in Figure 2. The accumulation of ZnS in the vein is equal to the difference between the amount of Zn entering and leaving the vein. In the vein, methane reduces sulphate to $H_2S$ at a rate given by equation (1), precipitating ZnS. Assuming that the ore is not zinc-limited, *i.e.*, that all $H_2S$ generated precipitates ZnS, the amount of ZnS precipitated equals the amount of $H_2S$ generated and the amount of sulphate reduced. Therefore the difference between Zn(*in*) and Zn(*out*) of the box is the same as the sulphate(*in*) and sulphate(*out*) of the box. One could also assume that the $H_2S$ is generated not in the vein but elsewhere, and enters the vein during the fluid flow. This raises additional problems, but however and wherever the $H_2S$ is generated, we assume it appears in the vein at our calculated rates.

The equations governing this situation are those for the "Constant Stirring Tank Reactor" or CSTR model, discussed in many Chemical Engineering texts, for example Schmidt (2005, Chapter 3). Mass balance considerations for a first order reaction lead to the equation

$$SO_4(in) - SO_4(out) = SO_4(in) - \frac{SO_4(in)}{1 - t \times k}$$

where $(SO_4)$ is the sulphate concentration in molality, $t$ is the residence time in years, and $k$ is the rate constant in $y^{-1}$ units. The residence time is the time an element of solution spends in the box, and is defined as $V/r$, where $V$ is the volume of fluid in the box in $m^3$, and $r$ is the volumetric flow rate in $m^3/y$. The volume of fluid in the box is the total volume times the porosity (assumed to be 0.2), and the volumetric flow rate is defined as $F \cdot A$ where $F$ is the specific discharge or Darcy flow rate $m^3/(m^2y)$) and $A$ is the inlet area ($m^2$), or the area over which the solution flows into the box.

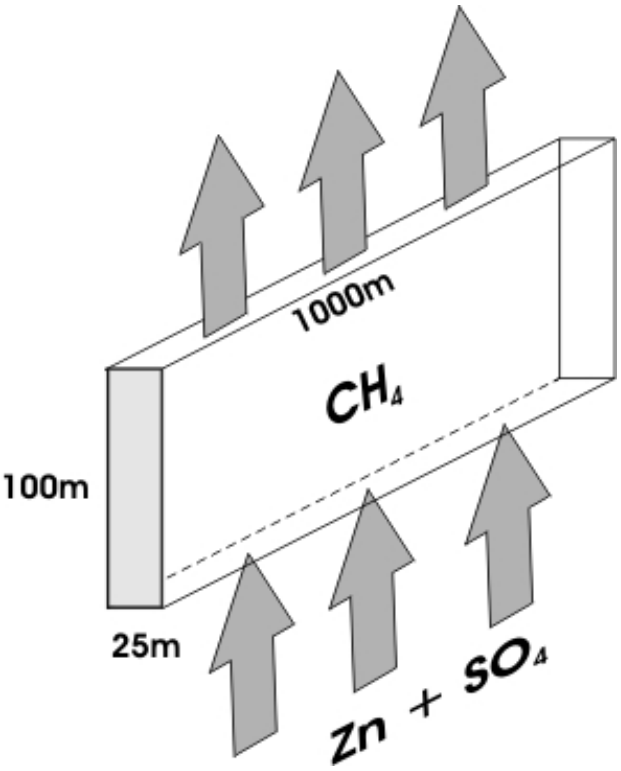


Figure 2 The flow model. The inlet fluid has a composition of 3m NaCl, 0.01m Zn, and 0.025m $SO_4^{2-}$. The shaded cross-section of the box (vein) is the 2D section shown in Figure 4.

This results in the moles of sulphate reduced, hence the moles of ZnS precipitated, per kg of solution per year. Multiplying by the number of kg of fluid per year and the number of years, and converting moles of Zn to kg, gives the mass of Zn precipitated in a given

number of years. The results of these calculations for log $k$ = -1 are shown in Figure 3. Clearly these conditions will easily produce an ore deposit in geologically reasonable times. With a log $k$ of -4, all three curves are well below the dotted reference line, and intermediate $k$ values obviously produce intermediate values.

## 2.2 *Reactive Transport Model*

Another way to evaluate this is with a reactive transport model, such as used by Corbella et al. (2004). This type of model uses a number of cells in 1, 2 or 3 dimensions, into which fluids can be introduced and in which reactions with other phases can take place. Corbella *et al*. used a 2D section approximately the same size as the cross-section of the box (vein) in Figure

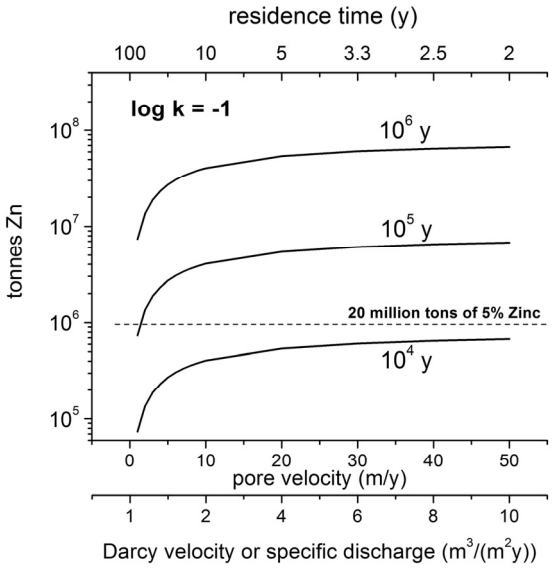


Figure 3 Tonnes of Zn precipitated as a function of time and fluid flow at a rate constant of $10^{-1}y^{-1}$. The position of an ore deposit of 20 million tonnes of 5% Zn is shown as a reference.

2 (they used 26.5m by 110m), having a lower relatively impermeable unit, an upper permeable limestone unit, and a fault admitting a brine along the right side. They showed that mixing of the brine with a less concentrated pore fluid in the limestone results in carbonate dissolution independent of any sulphide precipitation, as has been documented in other contexts. If the brine carries zinc and the pore fluids contain $H_2S$, sulphide precipitation results not only in additional carbonate dissolution but carbonate precipitation as well, because the dissolved calcium diffuses outward to other parts of the vein where it precipitates because the pore fluid is already saturated with carbonate.

We used the same section, but changed the brine composition to that used in the CSTR model to compare results. Figure 4 shows some of these results. Only the left half of a symmetrical situation is shown, *i.e*, one should imagine a mirror image on the right side of each section. The ZnS precipitated and calcite dissolved are tightly constrained at the point where the fault intersects the permeable carbonate. Calcite is precipitated farther from the fault. The distribution of precipitated carbonate depends greatly on the assumed flux of carbonate pore fluid towards the fault, the brine flux, and the rate of sulphate reduction. The amount of ZnS precipitated is very close to that given by the CSTR model for the same conditions, but the reactive transport model, having a ½ meter fault width and thus a 500 $m^2$ fluid inlet area for a 1 km vein length gives up to 50 time less ZnS than the CSTR model results shown in Figure 2. Nevertheless, the conclusion that some experimental TSR rates are fast enough to produce ore still holds.

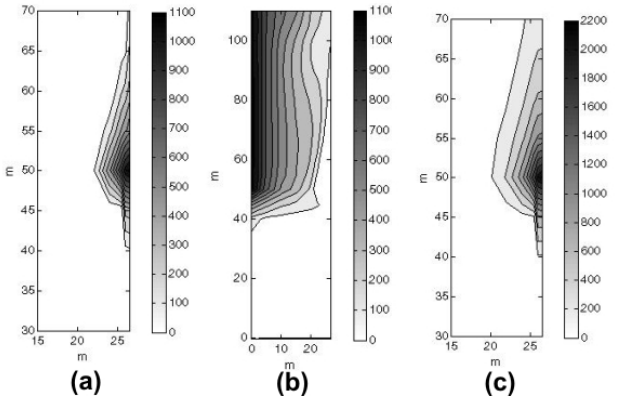


Figure 4 A 2D section of limestone. The lower half is impermeable, the upper half is permeable. A fault ½ m wide admitting a brine runs along the right side. The brine carries the same Zn and sulphate as in the CSTR model, and $H_2S$ is produced by TSR in the carbonate unit using log $k$ = -1. (a) moles calcite dissolved per $m^3$ (b) moles calcite precipitated per $m^3$ (c) moles ZnS precipitated per $m^3$. Note that (a) and (c) show only part of the section.

It is interesting to note the difference between these conclusions and those of Anderson & Garven (1987) with respect to sulphide precipitation and carbonate dissolution / precipitation. They used a titration model (a zero-dimension model having no spatial coordinates) and concluded that sulphide precipitation results in carbonate dissolution, and that carbon-

ate cannot precipitate if sulphide is precipitating. The 2D model used here and by Corbella *et al*. (2004) on the other hand shows that carbonate dissolution and precipitation can happen simultaneously, just in different parts of the vein.

## 3 CAVEATS

Obviously, the parameters used such as the dimensions, the fluid compositions and the flow rates are fairly arbitrary, and might be changed within certain limits. Many of these changes would not change the main conclusions. For example, if the vein length is 100m rather than 1000m, the amount of ore is reduced by 1/10, but Figure 3 shows that the conclusion that rate constants in the upper part of the possible range are still fast enough to produce ore during deposition.

However, it is by no means clear that experimental results for TSR are directly applicable to natural situations. The reductant in nature appears to be hydrocarbons such as methane and related alkanes (*e.g*., Worden and Smalley, 1996), but no experimental work has used these reductants, which may well be less reactive than the reductants which have been used, such as toluene and acetic acid. And as mentioned, no concerted attempt at determining the rate law has been made. The one we use here (equation 1) may be inadequate.

## 4 CONCLUSIONS

Using a possible rate law and reasonable values of other flow parameters, we have shown that contrary to common belief, TSR is fast enough to form ore deposits during ore deposition, using values in the upper part of the measured range of rate constants. However despite the fact that TSR is invoked in a great many studies of MVT deposits, our knowledge of what exactly this reaction is and at what rate it proceeds under various geological conditions is extremely weak.

Obviously a deposit or parts of a deposit in which the ore was produced by TSR would have formed much more slowly than one formed by traditional fluid mixing models and the sphalerite crystals might be centimeter-sized rather than colloform. However we know next to nothing about the factors controlling ZnS crystal growth, and how long it takes to grow a crystal of a given size. Having such knowledge would help greatly in interpreting the origins of MVT deposits.

## ACKNOWLEDGEMENTS

We thank Terry Seward for supporting the early stages of this work at ETH in Zürich, Carlos Ayora for helpful comments, and David Parkhurst for help with using the USGS 3D reactive transport program PHAST.

## REFERENCES

Anderson GM, Garven G (1987) Sulphate-sulphide-carbonate associations in Mississippi Valley-type lead-zinc deposits. *Econ. Geol.* 82: 482-488

Beales FW, Jackson SA (1966) Precipitation of lead-zinc ores in carbonate reservoirs as illustrated by Pine Point ore field, Canada. *Inst. Mining and Metallurgy Transactions*, sec. B: B8278-8285

Corbella M, Ayora C, Cardellach E (2004) Hydrothermal mixing, carbonate dissolution and sulphide precipitation in Mississippi Valley-type deposits. *Min. Deposita* 39: pp 344-357

Goldhaber MB, Orr WL (1995) Kinetic controls on the thermochemical sulphate reduction as a source of sedimentary $H_2S$. In: Vairavamurthy MA, Schoonen MAA (eds) Geochemical Transformations of Sedimentary Sulphur; ACS Symposium Series 612; *Amer. Chem*. Soc.: Washington, DC, pp 412–425

Orr WL (1982) *Abstracts with Program; 95th GSA Meeting, New Orleans* 14: p 580

Schmidt LD (2005) *The Engineering of Chemical Reactions*, 2nd ed. Oxford University Press, New York, 618 pp

Worden RH, Smalley PC (1996) $H_2S$-producing reactions in deep carbonate gas reservoirs: Khuff formation, Abu Dhabi. *Chem. Geol*. 133: 157-171

# Formation of Irish-type base metal deposits by multiple deep hydrothermal convection cells: Evidence from a regional fluid inclusion and Sr-Nd isotope study

J.F. Menuge & J.S. Daly
*School of Geological Sciences, University College Dublin, Belfield, Dublin 4, Ireland.*

R.D. Walshaw
*Leeds Electron Microscopy and Spectroscopy Centre (LEMAS), University of Leeds, Woodhouse Lane, Leeds, LS2 9JT, UK.*

ABSTRACT: Controversy regarding the age and genesis of Irish–type deposits centres around two competing genetic models: an upper crustal convection cell model associated with Lower Carboniferous extension; and a regional topographic fluid flow model driven by an Hercynian compressional tectonic regime. Elucidation of ore-fluid geochemistry and crustal pathways is integral to testing these models. Data are presented for a regional scale, integrated fluid inclusion and Sr-Nd isotope study of six Irish-type deposits and a single sub-Carboniferous-hosted basement mineral vein, covering an area in excess of 24,000 km$^2$. The data confirm the presence of previously documented hydrothermal fluid types in deposits and basement-hosted carbonate veins across the study area. These fluids are proposed to have formed via mixing of bittern waters with less saline fluids. Sr and Nd isotopic characterisation of these hydrothermal fluids indicates that a major component of the dissolved metal load has not just been acquired from sub-Carboniferous Lower Palaeozoic basement, but from crustal material with a $T_{DM}$ age of ~2 Ga. Ore forming fluids must therefore have accessed greater crustal depths than previously thought. The data provide no support for significant involvement of the Old Red Sandstone or for genetic models involving regional lateral fluid flow; rather, they are consistent with genetic models involving deep crustal convection.

KEYWORDS: Irish, base metal deposits, fluid inclusions, Sr isotopes, Nd isotopes, convection

## 1 INTRODUCTION

Healthy controversy regarding the age and genesis of Irish–type deposits (Hitzman 1995) centres around two competing genetic models: an upper crustal convection cell model associated with Lower Carboniferous extension (Russell 1978); and a regional topographic fluid flow model driven by an Hercynian compressional tectonic regime (Hitzman 1995). Crucial considerations in testing the two models are accurate geochemical characterisation of the hydrothermal fluids involved and elucidation of their crustal flow pathways. Previous petrographic, isotopic (C, O, S) and fluid inclusion studies of individual ore deposits invoke the involvement of two and occasionally three distinct fluids in ore formation at several sites (Samson & Russell 1987; Banks & Russell 1992; Eyre 1998; Everett *et al*. 1999b; Gleeson *et al*. 1999; Banks *et al*. 2002; Wilkinson *et al*. 2005). Although advancing the understanding of these deposits on a local scale, a paucity of

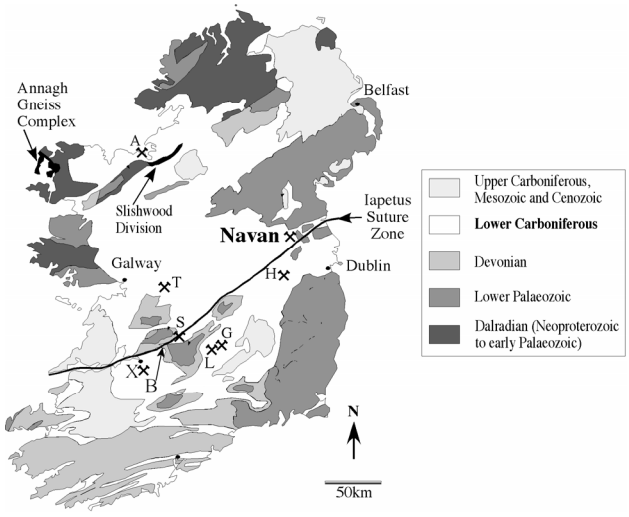


Figure 1. Geological Map of Ireland with study localities shown. A – Abbeytown, B – Birdhill (basement-hosted vein), G – Galmoy, H – Harberton Bridge, L – Lisheen, S – Silvermines, T – Tynagh, X – Irish-type deposit in Co. Limerick, exact locality confidential.

directly comparable data between studies (Everett *et al.* 1999a, b; Johnson *et al.* 2000; Wilkinson *et al.* 2005) inhibits coherent understanding of the orefield and genetic processes on a regional scale.

Here, we present data from a regional scale, integrated crush-leach fluid inclusion, Rb-Sr and Sm-Nd isotopic study of gangue mineralization from six Irish-type deposits and one Silurian basement hosted carbonate vein (Fig. 1).

## 2 FLUID INCLUSION DATA

### 2.1 *Microthermometry*

Microthermometric data (Fig. 2) augment and significantly extend the established array of temperature and salinity data. The same two principal fluid types as reported by previous workers (see section 1) are identified across the study area with extensive evidence in several deposits of mixing between these two fluid end-members. The presence of an additional, third fluid type, also previously reported (Banks & Russell 1992; Everett *et al.* 1999b) is observed in two localities. These three discrete hydrothermal fluids are: (1) a moderate salinity, moderate $T_h$ fluid (~10-15 wt% NaCl equiv., $T_h$~100 to 200°C); (2) a hypersaline brine (19.6 -24.8 wt% NaCl equiv., $T_h$~50-150°C); and (3) a very dilute fluid (0.5-3.4 wt% NaCl equiv., $T_h$~120-190°C).

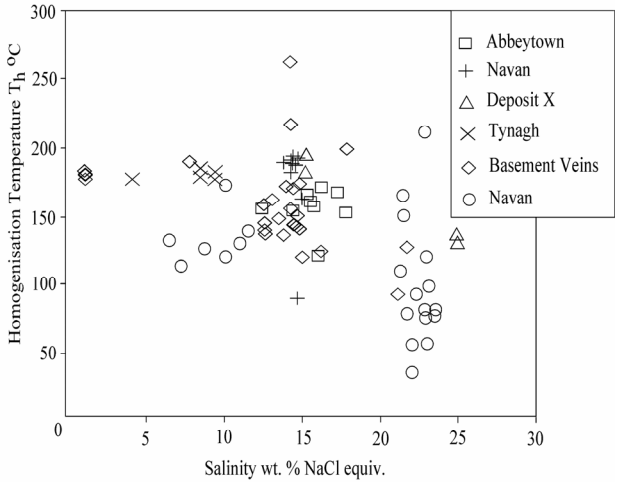


Figure 2. Th vs salinity plot of new microthermometric data from six localities.

### 2.2 *Crush-Leach Geochemistry*

Modelling of crush-leach geochemical data using the LogCl/LogBr (Bohlke & Irwin 1992) (Fig. 3) and Na deficit - Ca excess (Davisson & Criss 1996) (Fig. 4) methods indicates that all hydrothermal fluids are seawater derivatives. These are considered to be mixtures between bittern fluids and less concentrated basinal fluids, although the additional involvement of a component of halite dissolution cannot be ruled out.

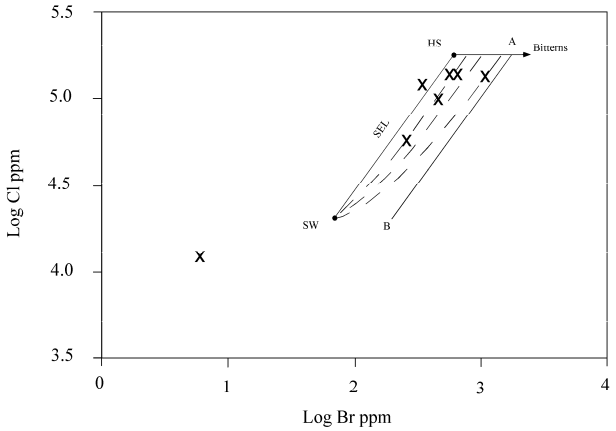


Figure 3. Log Cl vs log Br plot for four Irish base metal deposits. Also plotted are the seawater evaporation line (SEL) and four dilution trends. SW - seawater, HS - halite saturation. Line A-B represents dilution of a bittern fluid of arbitrary composition with meteoric water. Dashed lines represent bitterns diluted with seawater.

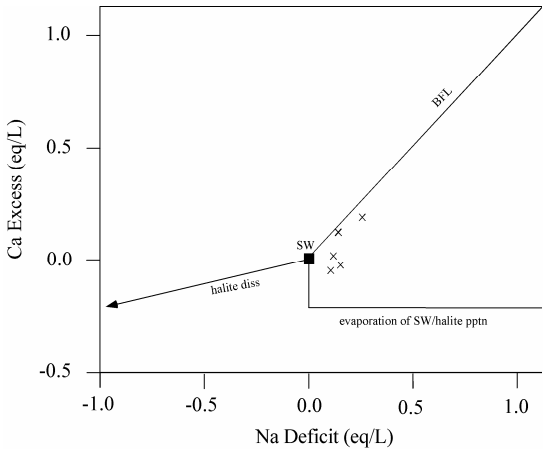


Figure 4. Na deficit - Ca excess plot showing crush-leach data. SW – seawater, BFL – basinal fluid line.

## 3 RB AND SR ISOTOPES

Rb-Sr and Sm-Nd isotope data from calcite, dolomite, barite and fluorite spanning the parageneses of these deposits define a range in $^{87}Sr/^{86}Sr_{350Ma}$ of 0.7083 to 0.7135 and in $\varepsilon_{Nd350Ma}$ of -7.3 to -16.5. In each individual deposit at least a component if not the majority of the gangue-hosted Sr and Nd is too radiogenic,

or unradiogenic, respectively, to have been derived solely from Carboniferous carbonate host-rocks or seawater and requires an input from sub-Carboniferous basement lithologies. The gangue mineral Sr and Nd isotopic compositions are therefore interpreted in terms of binary mixing between two principal isotopic end-members (although the potential for additional components exists). The first of these is proposed to be a sub-Carboniferous basement-derived component while the second is in isotopic equilibrium with Lower Carboniferous carbonate host-rocks. Identical isotope systematics have also been documented at the Navan deposit (Walshaw *et al.* 2006).

The derivation of metals from sub-Carboniferous basement in Ireland is not a new idea (O'Keeffe 1986; LeHuray *et al*. 1987) but these studies invoked the Lower Palaeozoic succession as the principal source. Our finding, that a component of the Nd within these deposits is sufficiently unradiogenic to require a crustal source reservoir with a $T_{DM}$ age of ~2 Ga, is inconsistent with this interpretation. North of the Iapetus Suture Zone (ISZ), the only viable source candidates are the Proterozoic Annagh Gneiss Complex and the Dalradian Supergroup (Walshaw *et al*. 2006). South of the ISZ a suitable pre-Monian candidate has yet to be identified. The Nd isotope evidence therefore provides evidence that hydrothermal fluids accessed greater crustal depths than previously suggested.

No regional trends are discernible in the Sr and Nd isotope data (Table 1). However, similarities in the isotopic characteristics of each of these deposits suggest a common origin, including localities like Abbeytown and Harberton Bridge – previously regarded as anomalous – and one which involves deep crustal circulation of hydrothermal fluids. In accord with Everett *et al*. (2003), no support is found for large scale metal sourcing from, or fluid flow through, the Old Red Sandstone (Hitzman 1995).

## 4 CONCLUSIONS

Sr and Nd isotope analyses of gangue mineralization from six Irish-type deposits show that these minerals contain a component which can only have been derived from sub-Carboniferous basement lithologies. In certain cases this Sr and Nd is too radiogenic or unradiogenic, respectively, to be sourced from Lower Palaeozoic lithologies and requires input from a crustal reservoir with a $T_{DM}$ age of ca 2 Ga. North of the ISZ, this reservoir might be provided by the Proterozoic Annagh Gneiss complex or the Dalradian Supergroup, while to the south of the ISZ it is proposed that the pre-Monian basement contains as yet unidentified material with $T_{DM}$ greater than 2 Ga. Hydrothermal fluids are therefore inferred to have accessed deeper crustal levels than previously evidenced, consistent with the activity of crustal convection cells as described by Russell (1978). The data provide no support for significant involvement of the Devonian Old Red Sandstone.

Fluid inclusion data confirm the presence of previously documented ore fluids. Modeling of crush leach geochemical data indicates all these fluids to be seawater derivatives with the principal genetic process being dilution of bitterns by other less saline fluids. A component of halite dissolution remains possible.

Together, fluid inclusion and Sr and Nd isotopic data show regional similarities across the entire study area, suggesting a common origin for the deposits. This origin is proposed to involve deep crustal convection of hydrothermal fluids and thus lends support to the genetic model of Russell (1978).

## ACKNOWLEDGEMENTS

This research was funded by Forbairt under basic research grant SC/93/004. We thank staff, past and present at Tara Mines, Lisheen, and Galmoy for providing access to mine workings and drill core samples and for helpful discussions. Aaron Johnson and Kevin Shelton at University of Missouri, Columbia, are thanked for assistance with crush-leach analyses.

## REFERENCES

Banks DA, Russell MJ (1992) Fluid mixing during ore deposition at the Tynagh base metal deposit, Ireland. *European J. Mineral* 4: 921-931

Banks DA, Boyce AJ, Samson IM (2002) Constraints on the Origins of Fluids Forming Irish Zn-Pb-Ba Deposits: Evidence from the Composition of Fluid Inclusions. *Econ Geol* 97: 471-480

Bohlke JK, Irwin, JJ (1992) Laser microprobe analysis of Cl, Br, I and K in fluid inclusions: implications for sources of salinity in some ancient hydrothermal fluids. *Geochim Cosmochim Acta* 56: 203-225

Davisson ML, Criss RE (1996) Na-Ca-Cl relations in basinal fluids. *Geochim Cosmochim Acta* 60: 2743-2752

Everett CE, Rye DM, Wilkinson JJ, Boyce AJ, Ellam RM, Fallick A, Gleeson SA (1999a) The genesis of Irish-type Zn-Pb deposits: Characterisation and origin of the principal ore fluid. In: Stanley CJ et al. (eds) *Mineral Deposits: Processes to Processing*. Balkema, Rotterdam, pp 845-848

Everett CE, Wilkinson JJ, Rye DM (1999b) Fracture controlled fluid flow in the Lower Palaeozoic basement rocks of Ireland: Implications for the genesis of Irish-type Zn-Pb deposits. In: McCaffrey KJW, Lonergan L, Wilkinson JJ (eds) *Fractures, fluid flow and mineralization.* Geological Society, London, Special Publication 155, pp 247-276

Everett CE, Rye DM, Ellam RM (2003) Source or Sink? An Assessment of the Role of the Old Red Sandstone in the Genesis of the Irish Zn-Pb Deposits. *Econ Geol* 98: 31–50

Eyre SL (1998) Geochemistry of dolomitization and Zn-Pb mineralization in the Rathdowney Trend, Ireland. *Unpublished Ph.D. thesis, University of London*, 414 pp

Gleeson SA, Banks DA, Everett CE, Wilkinson JJ, Samson IM, Boyce AJ (1999) Origin of mineralising fluids in Irish-type deposits: Constraints from halogens. In: Stanley CJ et al. (eds) *Mineral Deposits: Processes to Processing*. Balkema, Rotterdam, pp 857-860

Hitzman MW (1995) Geological setting of the Irish Zn-Pb-(Ba-Ag) orefield. In: Anderson K, Ashton J, Earls G, Hitzman M, Tear S (eds), Irish Carbonate-Hosted Pb-Zn Deposits. *Society of Economic Geologists, Guidebook Series*, Vol 21, pp 3-23

Johnson AW, Shelton KL, Gregg JM, Somerville ID, Wright WR (2000) Fluid inclusion evidence for the presence of multiple fluids in the Zn-Pb hosting Carboniferous carbonate rocks in the Irish Midlands: Initial findings. In: Hagni D (ed.) *Studies on ore deposits, mineral economics and applied mineralogy: with emphasis on Mississippi Valley-Type base metal and carbonatite-related fluorspar deposits.* University of Missouri – Rolla Press, Rolla, USA, pp 18-30

LeHuray AP, Caulfield JBD, Rye D, Dixon PR (1987) Basement controls on sediment-hosted Pb-Zn deposits: a lead isotope study of Carboniferous mineralization in Central Ireland. *Econ Geol* 82: 1695-1709

O'Keeffe WG (1986) Age and postulated source rocks for mineralization in central Ireland, as indicated by lead isotopes. In: Andrew CJ, Crowe RWA, Finlay S, Pennell WM, Pyne JF (eds) *Geology and genesis of mineral deposits in Ireland.* Irish Association for Economic Geology, Dublin, pp 617-624

Russell MJ (1978) Downward-excavating hydrothermal cells and Irish-type ore deposits: importance of an underlying thick Caledonian prism. *Trans Instit Mining Metall* 87: B168-171

Samson IM, Russell, MJ (1987) Genesis of the Silvermines zinc-lead-barite deposit, Ireland: Fluid inclusion and stable isotope evidence. *Econ Geol* 82: 371-394

Walshaw RD, Menuge JF, Tyrrell S (2006) Metal sources of the Navan carbonate-hosted base metal deposit, Ireland: Nd and Sr isotope evidence for deep hydrothermal convection. *Miner Deposita* 41: 803-819

Wilkinson JJ, Everett CE, Boyce AJ, Gleeson SA, Rye DM (2005) Intracratonic crustal seawater circulation and the genesis of subseafloor zinc-lead mineralization in the Irish orefield. *Geology* 33: 805-808

# Updates on the Geology and Metallogenesis of the Lisheen Zn-Pb Deposit in Ireland

J.F. Güven, M.J. Passmore & D.M.W. Harney
*The Lisheen Mine, Moyne, Thurles, Co. Tipperary, Ireland*

ABSTRACT: The Lisheen carbonate-hosted zinc and lead deposit in Ireland consists of largely flat-lying massive sulphide orebodies hosted within Lower Carboniferous carbonates. Mineralization is polyphase, showing evidence of varying fluids and fluid pathways, and appears to be strongly influenced by extensional fault structures that formed at a detachment horizon at or near the base of the Waulsortion limestone, possibly following the extensional event. Further episodes post-mineralization have significantly complicated the orebody geometry, which represents challenges to mining methods, ground conditions and dilution at Lisheen.

KEYWORDS: Lisheen, zinc, lead, geology, metallogenesis

## 1 INTRODUCTION

The Lisheen carbonate-hosted Zn-Pb deposit is located in County Tipperary in central Ireland. It contains 17.9 million tonnes of massive sulphides averaging 15.8% Zn and 2.6% Pb. The deposit is largely flat lying at a depth of 130-200m from surface. It exhibits a high level of variability in grade, geometry and geotechnical character due to complex geological controls that governed its genesis.

The Lisheen mine is owned and operated by Anglo American plc and employs about 350 permanent staff. It is an underground, trackless operation, accessed via a decline. Production started in September 1999 and, at an annual production rate of 1.6 million tonnes of ore, is scheduled to continue until early 2014. Three separate mining methods are employed: Room and Pillar, Drift and Fill and Long Hole Stoping. Selection of the mining method is mainly determined by ore thickness but other factors including grade continuity, geological complexity and economic value are also considered. The majority of development is planned in ore.

## 2 GEOLOGICAL SETTING

The Lisheen deposit is hosted by Lower Carboniferous (Courceyan) carbonates. Boreholes show that these form a thin-skinned package overlying a structurally complex, Lower Palaeozoic basement, which, as indicated by aeromagnetic data, exhibits a strong NE-SW trending Caledonian grain. The regional Carboniferous geology mirrors this grain, as do deposit and prospect occurrences. This trend of structurally controlled deposits, which also includes the Galmoy orebodies some 10km to the northeast, is referred to as the Rathdowney Trend (Hitzman *et al*. 1992).

The Lisheen deposit is largely hosted by hydrothermal breccias (Black Matrix Breccia; Hitzman *et al.* 1992, Hitzman *et al*. 2002, Wilkinson *et al*. 2005). These are developed at or proximal to the base of a 200m thick, massive biomicrite unit, the Waulsortian Limestone Formation, which in the mine area is extensively dolomitised. This unit lies conformably above a package of medium to thick-bedded, laterally persistent, argillaceous bioclastic limestones (ABL) that form the lithological footwall to the mineralization. The contact between these units is transitional over 5-10m and lithologies often exhibit some degree of lateral lithological and thickness variability. Some 90 m below the top of the ABL is a 70m thick Oolitic Member, which contains economic sulphides where normal faulting has juxtaposed it with Waulsortian hosted mineralization.

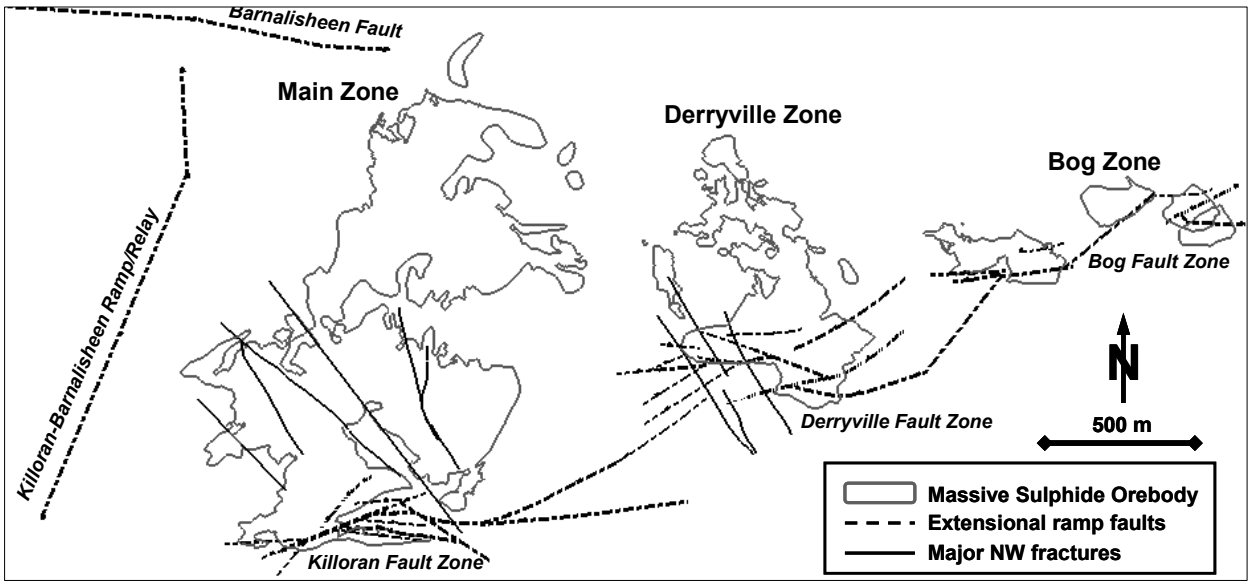


Figure 1: Structural map of Lisheen, showing the orebodies and the larger extensional ore-controlling faults. Numerous smaller ore-controlling faults extend into the hanging walls of these structures.

## 3 STRUCTURAL SETTING

The Lisheen deposit comprises three main orebodies, i.e. Main Zone, Derryville Zone and the three Bog Zone pods, as well as a number of smaller satellite bodies (Fusciardi *et al.* 2003). These orebodies are sited in the hanging walls of extensional faults with displacements of the order of 200m referred to as the Killoran, Derryville and Bog faults, respectively. They form a series of left-stepping, northerly dipping, en echelon structures (Fig. 1) that exhibit a classic ramp-relay geometry. These faults are considered to be the primary control on the location of the orebodies. The ore is thickest in their immediate hanging walls and mineralization is largely absent in the ramp-relay zones. The detailed geometry of the deposit, however, is controlled by much smaller displacement, low-angle listric faults and slides with short strike length. These faults appear to be confined to the Waulsortian – ABL contact zone and are thought to collectively relay displacement northwards, to a parallel en echelon system some 2km to the north (Barnalisheen Fault). Locally, they form a complex system of relaying listric faults and show a close spatial relationship with hydrothermal breccia development.

## 4 ALTERATION AND MINERALIZATION

Breccia development and mineralization are largely thought to have post-dated faulting. Feeder fluids from Lower Palaeozoic basement rocks are believed to have accessed the host breccias through the larger displacement faults and moved northwards utilising the smaller structures developed at the Waulsortian – ABL contact. In gross terms, the scale of the structure determines the degree of breccia development, the availability of the mineralising fluid and consequently the grade and distribution of mineralization. Transitional facies at the base of the Waulsortian Limestone Formation also appear to have influenced the geometry and intensity of breccia development. In many areas, different fluid pathways were formed in this lithologically variable unit, resulting in the development of two or more breccia-hosted ore horizons.

The classic Black Matrix Breccia (BMB) has previously been described in detail by Redmond (1995), Hitzman *et al.* (2002) and Wilkinson *et al.* (2005). It consists of pale angular to irregular dolomitic clasts in a dark, microcrystalline dolomite matrix. It exhibits both matrix and clast support. However, volumetrically the majority of BMB consists of a variably altered precursor dolostone containing extremely amorphous remnant clast structures. It is clear from selected exposures that the BMB developed by a combination of progressive hydrothermal alteration and collapse. Laminated hydrothermal dolomite containing ‘drop stones’ is recorded within the breccias.

## 5 MINERALOGY

Mineralogically, the orebodies comprise numerous massive sulphide lenses typically composed of pyrite and sphalerite with lesser amounts of galena. Nickel is present locally, mainly as niccolite, in strong association with 'feeder faults' (Fusciardi *et al*. 2003) where it can be present in percentage grades. Significant tennantite bodies with crosscutting chalcopyrite veins are also present in Main Zone adjacent to the Killoran Fault.

The mineral textures and quantities vary considerably with some lenses being completely pyritic and others being almost devoid of iron. Stacked lenses of varying compositions are also seen and often these are separated by very thin and impersistent shaley seams. Grades always vary more greatly in the vertical sense than they do laterally and often there is a 'pyrite cap' developed at the top of economic sulphide lenses. The lenses typically exhibit sharp upper contacts with the host lithology and a more diffuse lower contact. Late sulphide veins often crosscut sulphide lenses.

Much of the textural variability can be explained by the progressive replacement of BMB by a mineralization front to form massive sulphide as is seen in many exposures, which supports earlier presumptions by Hitzman *et al.* (2002) and Wilkinson *et al.* (2005). Other textures such as finely banded sulphides prevalent in the transitional facies may betray strong lithological control. Colloform sphalerite and botryoidal pyrite imply local open space filling.

## 6 METAL DISTRIBUTION

On a larger scale, significant zinc-rich and iron-rich domains can be identified. These zones appear to exhibit different trends that can be broadly matched to mapped structural trends. Although little work has been done to date, many of the large and small-scale spatial relationships mentioned above suggest a complex interaction between fluid evolution and structural evolution. Pyrite bodies seem to be strongly associated with the large ENE trending extensional faults, whereas zinc and lead trends are principally controlled by the network of smaller structures and associated breccias at the Waulsortian – ABL contact.

The notion of syn-extensional mineralization as a mechanism to explain some of the large- and small-scale metal distribution is tempting. However, the Oolite-hosted mineralization, which is present only in the footwall of all the large extensional structures in juxtaposition with BMB-hosted hanging wall ores, seems to suggest that most if not all of the displacement, had occurred prior to the onset of mineralization.

The Oolite ore exhibits repeated and variable mineralization phases including Fe, Fe+Zn+Pb, Zn+Pb, Ni and Cu, in fact, most of the phases present in the BMB-hosted ore. These are punctuated by successive brecciation events. Most of the sulphides are fragmental. Large host-rock blocks are supported with the fragmental sulphide in an exotic argillaceous matrix. These textures may indicate synchronous mineralization and faulting. Alternatively, the features could be explained by massive dissolution due to the passage of hydrothermal fluids resulting in the collapse and brecciation of host rock, mineralization and in some cases lithified restite laminates. Elevated nickel and copper grades within the oolite ore suggests that it was proximal to the main feeder system in each of the Lisheen ore zones.

## 7 POST-ORE EVENTS

Two post-mineralization structural episodes have significantly complicated the local orebody geometry. A compressional event, most probably related to the Variscan orogeny at the end of the Carboniferous, has inverted, to some degree, many of the pre-existing normal structures. Folds are commonly developed, centred on or sub-parallel to the smaller extensional faults. The complex geometry of these folds is probably governed by the contrasting ductility of the host lithologies and the original normal fault geometry. Larger compressional features are present where there has been buttressing against the footwall of early extensional structures. Here, thrusting has severely impacted orebody geometry and in Bog Zone East has duplicated the ore horizon. Underground mapping indicates that compressional features generally post-date the mineralization. However, locally stratabound, pale, low-iron zinc mineralization is commonly developed within ABL-cored folds. It is not yet established, whether this mineralization represents a remobilisation into bedding flexures opened during compression or is associated with the extensional faults on which the folds may have developed.

A second structural episode produced sub-

vertical, NW dextral wrench faults with widespread associated NNW accommodation faults. Folding is developed locally adjacent to some of the larger structures. Most of these structures have minimal displacements and short strike length, although some can be mapped across the mine. They are typically filled with a white or pink coarse dolomite or a calcite gangue and rarely with insignificant small sphalerite and galena crystals. These structures locally dislocate the orebody and are clearly post-ore. They are extensively karstified and severely impact geotechnical conditions.

## 8 CONCLUSIONS

The petrology of the Lisheen orebodies indicates a complex relationship between structural history, lithology, and mineralising fluids. Mineralogy, metal distribution and alteration seen across the mine suggest the orebody is polyphase with evidence of varying fluid chemistry and fluid pathways. The exact timing of mineralization is still unclear, but appears to be strongly influenced by extensional fault structures that have formed at a detachment horizon at or near the base of the Waulsortion limestone. These listric faults may have developed syn-mineralization although the presence of Oolite-hosted economic sulphides in juxtaposition with Waulsortion hosted ore suggests mineralization could be post extensional faulting.

The structural history of the Lisheen deposit significantly affects ore extraction, in particular selection of the appropriate mining method, ground conditions and dilution. Hence, good structural understanding and continuous geological modelling, facilitated by regular underground mapping and diamond drilling, are of vital importance to the mining operation.

## ACKNOWLEDGEMENTS

The authors would like to thank Anglo American and The Lisheen Mine for permission to publish this paper. Special thanks go to Leo Fusciardi, John Elmes and Jamie Wilkinson for constructive comments on the manuscript.

## REFERENCES

Fusciardi LP, Güven JF, Stewart DRA, Carboni V, Walsh JJ (2003) The geology and genesis of the Lisheen Zn-Pb deposit, Co. Tipperary, Ireland. In: Kelly JG, Andrew CJ, Ashton JH, Boland MB, Earls G, Fusciardi LP, Stanley C (eds) *Europe's Major Base Metal Deposits.* Irish Association for Economic Geology, Dublin: 455-482.

Hitzman MW, O'Connor P, Shearley E, Schaffalitzky C, Beaty DW, Allan JR, Thompson T (1992) Discovery and geology of the Lisheen Zn-Pb-Ag prospect, Rathdowney Trend, Ireland. In: Bowden AA, Earls G, O'Connor PG, Pyne JF (eds) *The Irish Minerals Industry 1980-1990.* Irish Association for Economic Geology, Dublin: 227-246.

Hitzman MW, Redmond PB, Beaty DW (2002) The Carbonate-hosted Lisheen Zn-Pb-Ag deposit, County Tipperary, Ireland. *Economic Geology* 97: 1627-1655.

Redmond P (1995) Structural controls on mineralization and dolomitisation of the Lisheen Zn-Pb-Ag deposit, Co. Tipperary, Ireland. *Extended Abstract, International Field Conference on Carbonate Hosted Lead-Zinc Deposits, St. Louis, Missouri*: 251-253.

Wilkinson JJ, Eyre SL, Boyce AJ (2005) Ore-forming processes in Irish-type carbonate-hosted Zn-Pb deposits: Evidence from mineralogy, chemistry, and isotopic composition of sulfides at the Lisheen Mine. *Economic Geology* 100: 63-86.

# Age and origin of the Earth's oldest carbonate-hosted Pb-Zn-(F) deposits

J. Gutzmer, C.R. McClung & N.J. Beukes
*PPM Group, Department of Geology, University of Johannesburg, P.O. Box 524, Auckland Park 2006, South Africa*

D. Banks
*School of Earth Sciences, University of Leeds, Woodhouse Lane, Leeds LS2 9JT, UK*

H. Zwingmann
*John de Laeter Centre of Mass Spectrometry, CSIRO Petroleum Resources and School of Applied Geology, Curtin University, GPO Box U1987 WA, Australia*

M.O. Schaefer
*Anglo American Ltd., Exploration Division, 45 Main Street, Marshalltown, Johannesburg 2000, South Africa*

ABSTRACT: Pb-Zn deposits hosted by dissolution collapse breccias in dolostones of the Neoarchaean Transvaal Supergroup in Griqualand West, South Africa are regarded as the Earth's oldest examples of MVT deposits. This association is based on numerous lines of geological, mineralogical-textural and geochemical similarities. K-Ar ages of 2.038±0.040 Ga and 2.059±0.041 Ga for hydrothermal illite intergrown with ore-forming sphalerite has provided the first accurate age constraints for these deposits. These ages are within error of the intrusive age of the Bushveld Complex as well as the age of stratabound fluorite deposits in the dolostones of the Transvaal Supergroup in the Transvaal region. Based on these results, a metallogenetic model is proposed that identifies the intrusion of the Bushveld Complex as the driving mechanism for long-lived hydrothermal systems active on a subcontinental scale. These systems gave rise to fluorite deposits in dolostones proximal to the intrusion, where fluids had a distinct magmatic contribution. Fluorite-poor Pb-Zn deposits, in contrast, formed in the distal tectonic foreland of the Bushveld intrusion, reflecting the migration of pre-existing aqueous fluids and brines along suitable basement aquifers.

KEYWORDS: MVT, Transvaal Supergroup, Palaeoproterozoic, K-Ar geochronology

## 1 INTRODUCTION

Neoarchaean (2.52-2.65 Ga) stromatolitic dolostones of the Transvaal Supergroup of South Africa are host to Pb-Zn-(F) deposits that have long been described as the oldest known examples of Mississippi Valley-type (MVT) deposits, *i.e.* epigenetic carbonate (dolostone)-hosted Pb-Zn deposits that are not associated with igneous activity (Leach *et al*. 2005). A Palaeoproterozoic mineralization age (1.9 to >2.35 Ga) has been proposed for these Pb-Zn-(F) deposits, based on geological field relationships (Martini *et al*. 1995) and Rb-Sr geochronological evidence (Duane *et al.* 2004). These very broad age constraints identify the deposits unequivocally as the oldest known MVT-type Zn-Pb-(F) deposits, but they are insufficient to link their origin to specific tectonic or palaeoenvironmental events.

## 2 GEOLOGICAL SETTING

Carbonate-hosted Pb-Zn-(F) deposits occur in the Campbellrand/Malmani Subgroup of the Transvaal Supergroup. Important examples occur in three districts (Fig. 1), each centering around one prominent deposit, namely the Pering (Gutzmer 2006; Huizenga *et al*. 2006), and Bushy Park deposits (Schaefer 2002) in the Griqualand West region, and the Witkop deposit in the Zeerust area of the Transvaal region (Poetter 2001).

The Witkop deposit is located within the contact metamorphic aureole of the Bushveld Igneous Complex (Fig. 1). Mineralization is dominated by stratabound fluorite that replaces diagenetic dolomite cements in stromatolitic dolostones of the uppermost stratigraphic unit of the Malmani Subgroup. Occurrences of breccia-hosted fluorite with significant base-metal

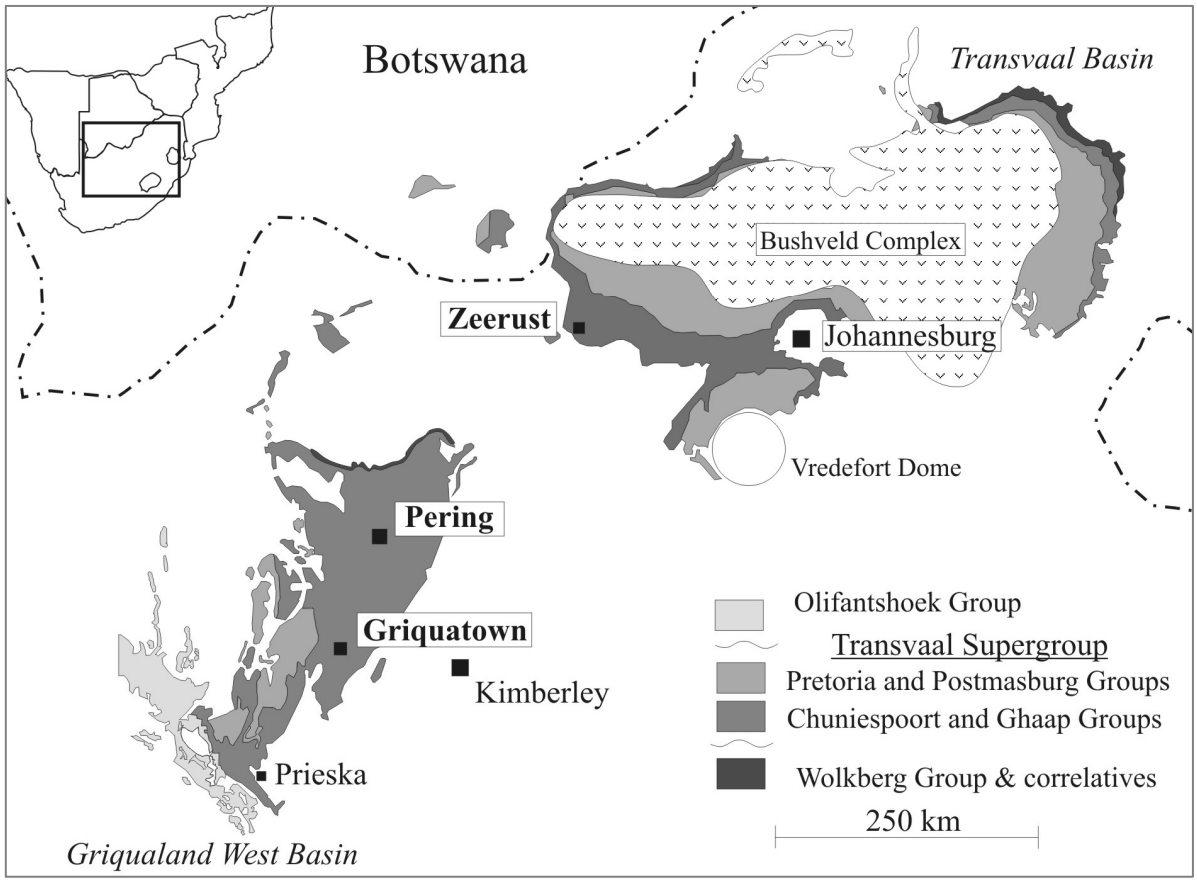


Figure 1. Occurrence of important Pb-Zn-F deposits in the Neoarchean dolostones of the Chuniespoort and Ghaap Groups of the Transvaal Supergroup.

sulphide mineralization are of minor importance. Fluorite is associated with minor sphalerite, galena, pyrite, pyrrhotite, sparry calcite, dolomite, quartz and bitumen.

The Pering and Bushy Park deposits are hosted by the 2.4 km thick platform dolostones of the Campbellrand Subgroup in Griqualand West (Fig. 1). The dolostones are virtually unmetamorphosed, and have experienced only minor regional folding and normal faulting. Mineralization at Bushy Park is confined to a ring-shaped, subvertical breccia body, whereas the Pering deposit is best described as a series of interconnected pipe-shaped breccia bodies, surrounded by minor stratabound mineralization. Both deposits are Zn-dominated, of medium size and low average grade (<20Mt, ≤ 6wt% Zn+Pb).

Base-metal mineralization at the Pering deposit can be subdivided into a quantitatively predominant early stage that is collomorphous or fine-granular and replacive, followed by a later stage of coarse-grained open-space infill (Gutzmer 2006). At Bushy Park, mineralization occurs exclusively as coarse-grained open-space infill. The mineralogy of both deposits is simple, with sphalerite and galena the only important sulphide minerals, accompanied by minor pyrite and chalcopyrite. Sparry dolomite, calcite and quartz are the most common gangue minerals. Pyrobitumen is a widespread, but quantitatively very minor, component in both deposits. Fluorite is absent (Bushy Park) or present in trace amounts only (Pering). Notable is the presence of fine-grained illite and chlorite at Bushy Park, and of phlogopite at Pering as part of the main stage sulphide mineralization (Fig. 2). Aggregates of fine-grained illite from Bushy Park were selected for K-Ar dating.

## 3 FLUID INCLUSIONS AND CHEMISTRY

Studies of primary and pseudo-secondary fluid inclusions in sphalerite, quartz and hydrothermal carbonate reveal the presence of three different fluid end members: a high-salinity aqueous fluid ($CaCl_2$-NaCl brine, >20wt% NaCl equiv.), a low-salinity (<5wt% NaCl equiv.) fluid of inferred meteoric origin, and a carbonic ($CH_4$-$CO_2$-$HS^-$) fluid. Pressure-corrected mineralization temperature ranges are 121-239°C for Bushy Park and 157-210°C for

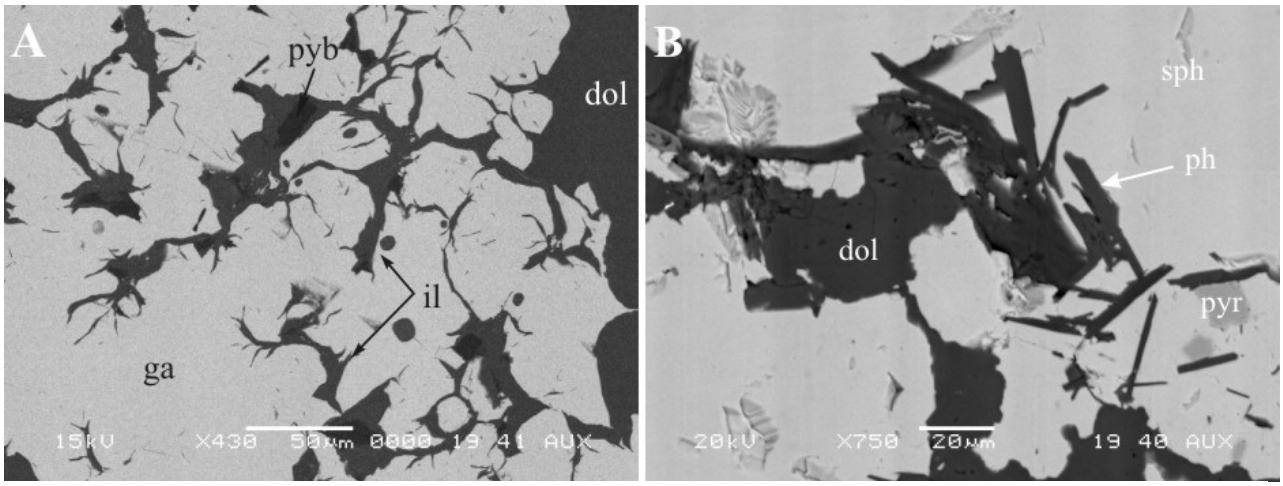


Figure 2. Backscattered electron photomicrographs illustrating the cogenetic occurrence with base metal sulphides of illite at Bushy Park (A) and phlogopite at Pering (B). Abbreviations: ga - galena, il – illite, pyb - pyrobitumen, ph – phlogopite, sph – sphalerite.

Pering. Liquid-vapour homogenization temperatures uncorrected for pressure are in the range 98-180°C for the Zeerust area, with some inclusions containing halite and calcite daughter crystals homogenizing above 250°C (Poetter 2001; Kesler *et al.* 2006).

Crush-leach analysis of fluid inclusions dominated by a single fluid type, were carried out on quartz, calcite, dolomite and sphalerite. Na/Br *vs* Cl/Br molar ratios from Pering (240-360 *vs* 240-440) and Bushy Park (80-280 *vs* 200-360) are lower than modern sea-water and plot on or close to the evaporation trend of modern seawater. Their restricted range of ratios are indicative of a single fluid source and contrast with inclusions from Zeerust (80-600 *vs* 200-800) that have a significantly larger range of values and are indicative of more than one fluid. LA-ICP-MS analysis of single inclusions (analyzed at Leeds using the protocols in Allan *et al.* 2005) shows they are dominated by Na and Ca, with lesser amounts of K and Mg. Pb, Zn and Cu concentrations are *c.* 400, 2000 and 200 ppm for the Pering and Bushy Park deposits. The Zeerust deposit has lower concentrations of Pb and Zn (*c.* 200 and 600 ppm respectively) but significantly higher Cu (*c.* 2500 ppm). These are significantly higher than present day oilfield brine values (Carpenter *et al.* 1974).

## 4 GEOCHRONOLOGY

Millimeter-sized monomineralic illite aggregates from Bushy were hand-picked and yielded K-Ar ages of 2.038±0.040 Ga and 2.059±0.041 Ga. These ages are within error of a Sm-Nd isochron age for fluorite from the Zeerust District (2.06 Ga; Kesler *et al.* 2003), and also similar to radiometric age constraints for the Pering deposit (Duane *et al.* 2004).

Another three illite aggregates, with significant intergrowth of quartz and calcite, yielded younger ages (1.568±0.031 Ga, 1.843±0.037 Ga and 1.728±0.035 Ga). Since the latter samples contained impurities, the older ages are considered more reliable. These K-Ar ages supersede the age of 2.145±0.007 Ga of Schaefer (2002), determined by Ar-Ar step heating on similar illite aggregates. The difference between K-Ar and Ar-Ar ages is attributed to Ar recoil loss commonly observed for microcrystalline illite (Dong *et al.* 1995)

## 5 DISCUSSION AND CONCLUSIONS

Textural, mineralogical and geochemical attributes of the Pering and Bushy Park deposits are very similar to those recorded for Phanerozoic MVT deposits. Owing to their fluorite-dominant nature and the presence of unusually saline fluids, the Witkop deposits of the Zeerust area are markedly different and a genetic link to the intrusion of the Bushveld Complex appears likely. We propose to extend this igneous association to the deposits in Griqualand West. This link is based on (a) a mineralization age that is within error of the intrusive age of the Bushveld Complex (2.06 Ga); and (b) the absence of an alternative tectonic-hydrothermal event of suitable age and magnitude. The Kheis Orogeny, a regional tectonic event that has often been associated with the origin of the carbonate-hosted Pb-Zn deposits in Griqualand

West (Duane *et al.* 2004), has recently been assigned an age of 1.0-1.3 Ga (Van Niekerk 2006) and can thus be excluded as a driving mechanism for fluid flow. The Vredefort meteorite impact event, with an age of 2.023 Ga (Kamo *et al*. 1996), has a similar age, but may have been too short-lived to account for the sustained mobilization of sedimentary brines required for the formation of MVT deposits.

The proposed metallogenetic model places the Pering and Bushy Park deposits into the distal tectonic foreland of the Bushveld intrusion. The intrusion of this *ca*. 7 km thick laccolith thickened the crust of the Kaapvaal Craton and generated a substantial thermal and topographic anomaly. This would have resulted in long-lived hydrothermal systems on the subcontinental scale, driving aqueous fluids away from the Bushveld instrusion. The fluids may have had a magmatic contribution (Zeerust), but in the distal foreland they were more likely represented by pre-existing aqueous fluids and brines that mobilized and transported metals along suitable basement aquifers. Once these metal-bearing brines came into contact with the dolostones of the overlying Transvaal Supergroup, they interacted with resident fluid reservoirs of meteoric and carbonic origin. Carbonic fluids acted both as reductants and as a source of reduced sulphur, thus resulting in metal deposition and the formation of igneous-induced carbonate-hosted Pb-Zn-(F) deposits carrying all the hallmarks of MVT deposits.

## REFERENCES


Allan MM, Yardley BWD, Forbes LJ, Shmulovich KI, Banks DA**,** Shepherd TJ (2005) Validation of LA-ICP-MS fluid inclusions analysis with synthetic fluid inclusions. *Am Mineral*, 90: 1767-1775.

Carpenter AB, Trout ML, Pickett EE (1974) Preliminary report on the origin and chemical evolution of lead-and zinc-rich oilfield brines in central Mississippi. *Economic Geology,* 69: 1191-1206.

Dong H, Hall CM, Peacor DR, Halliday AN (1995) Mechanism of argon retention in clays revealed by laser $^{40}Ar$–$^{39}Ar$ dating. *Science*, 267: 355-359.

Duane MJ, Kruger FJ, Turner AM, Whitelaw HT, Coetzee H, Verhagen B (2004) The timing and isotopic character of regional hydrothermal alteration and epigenetic mineralization in the western sector of the Kaapvaal Craton (South Africa). *Journal of African Earth Sciences,* 38: 461-476.

Gutzmer J (2006) The Paleoproterozoic carbonate-hosted Pering Pb-Zn deposit, South Africa: I. Styles of brecciation and mineralization. *Mineralium Deposita*, 40; 664-685.

Huizenga J-M, Gutzmer J, Banks D, Greyling L (2006) The Paleoproterozoic carbonate-hosted Pb-Zn deposit, South Africa. II: fluid inclusion, fluid chemistry and stable isotope constraints. *Mineralium Deposita*, 40: 686-706.

Kamo SL, Reimold WU, Krogh TE, Colliston WP (1996) A 2023 Ma age for the Vredefort impact event and observations from shocked metamorphosed zircons in pseudootachylite breccias and granophyre. *Earth and Planetary Science Letters,* 144: 369-388.

Kesler SE, Reich M, Jean M (2006) Geochemistry of fluid inclusion brines from Earth's oldest Mississippi Valley-type deposits, Transvaal Supergroup, South Africa. *Chemical Geology,* doi: 10.1016/j.chemgeo.2006.11.001.

Leach DL, Sangster, DF, Kelley KD, Large RR, Garven G, Allen CR, Gutzmer J, Walters S (2005) Sediment-hosted lead-zinc deposits: A global perspective. *Society of Economic Geologists, 100th Anniversary Volume:* 561-607.

Poetter PA (2001) Origin and exploration potential of sedimentary-hosted MVT F-Zn-Pb deposits in the Neoarchean platform dolostones of the Transvaal Supergroup, Northwest Province, South Africa. *Unpubl. MSc thesis, WWU Muenster,* pp. 193.

Martini JEJ, Eriksson PG, Snyman CP (1995) The Early Proterozoic Mississippi Valley-type Pb-Zn-F deposits of the Campbellrand and Malmani Subgroups, South Africa. *Mineralium Deposita,* 30: 135-145.

Schaefer MO (2002) Origin and Exploration potential of MVT Pb-Zn deposits in Griqualand West, Northern Cape Province, South Africa: *Unpubl. PhD thesis, Rand Afrikaans University,* pp. 367.

Van Niekerk HS (2006) The origin of the Kheis Terrane and its relationship with the Archean Kaapvaal Craton and the Grenvillian Namaqua Province in Southern Africa. *Unpubl. PhD thesis, University of Johannesburg,* pp. 402.

# A scale integrated structural analysis of the Mount Isa Zn-Pb-Ag deposit and its implications for genesis and exploration

Toby P. Davis
*School of Earth Sciences James Cook University, Townsville, Queensland 4811, Australia*

ABSTRACT: The structural geology of the Mount Isa Zn-Pb-Ag deposit, which is part of one of the largest base metal accumulations on Earth, has been examined at a range of scales to better understand its genesis, which has been enigmatic to date. The key to determining the genesis of this deposit is in establishing the proportionality of features over a range of scales. At the deposit scale there is widespread close correlation between the metal distribution and folding. Structurally controlled sulphide deposition, as defined by micro-scale sulphide-structural overprinting relationships, is ubiquitous and the distribution of all sulphide textural styles follows $F_4$ trends. These features are inconsistent with established pre-deformation mineralization models, including one that incorporate remobilization, and require re-evaluation of the genetic and, consequently, exploration models for this style of mineralization so that future exploration can proceed on a sound footing
.

KEYWORDS: Mount Isa, sediment hosted Zn-Pb-Ag, copper, remobilisation, syn-tectonic mineralization.

## 1 INTRODUCTION

The Mount Isa Zn-Pb-Cu-Ag deposit is one of the largest and most enigmatic base metal accumulations on Earth. This study is a scale integrated analysis of the structural geology of the Mount Isa Zn-Pb-Ag orebody ranging from the mine scale metal distribution to micro structures of the complete range of sulphide textures present in the deposit. The aim is to determine the role of regional deformation in the formation of these ores and the implications this has for choosing appropriate exploration strategies. A comparison with the nearby copper orebodies is included because the base metal and copper deposits are potentially related. Prior to mining the entire base metal deposit contained in excess of 405 million tonnes of ore including 150 Mt at 7 % Zn, 6% Pb and 150 g/t Ag and 255 Mt at 3.3 % Cu (Forrestal 1990, McGoldrick and Large 1998, Waring et al. 1998) in spatially separate copper and Zn-Pb-Ag orebodies.

The Mount Isa base metal deposit is located on the western margin of the Leichhardt River Fault Trough in the Western Fold Belt of the Mount Isa Inlier, north-western Queensland, Australia (Fig. 1). It lies east of, and adjacent to the Mount Isa and Paroo faults and is traversed by folds that formed during the Isan Orogeny (1610-1500 Ma). The orebody is hosted by the Urquhart Shale, a dolomitic sedimentary sequence in the Upper Mount Isa Group.

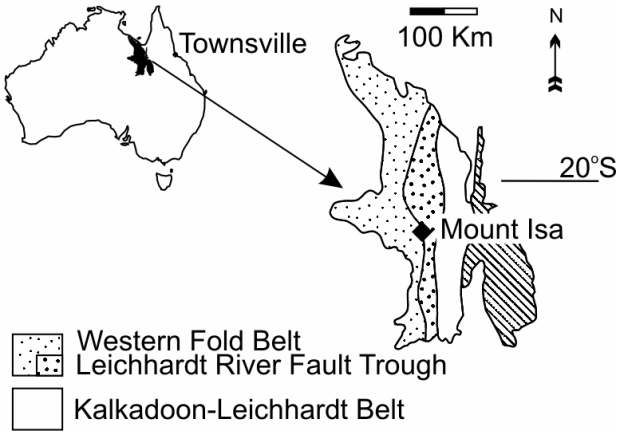


Figure 1: The Mount Isa Inlier and its main tectonic units

The Zn-Pb-Ag orebody contains a series of conformable lenses that consist of centimetre scale bedding parallel sulphide bands and breccias and belongs to the stratiform sediment hosted Zn-Pb-Ag class of deposits (Fig. 2). Other deposits in this class include Red Dog

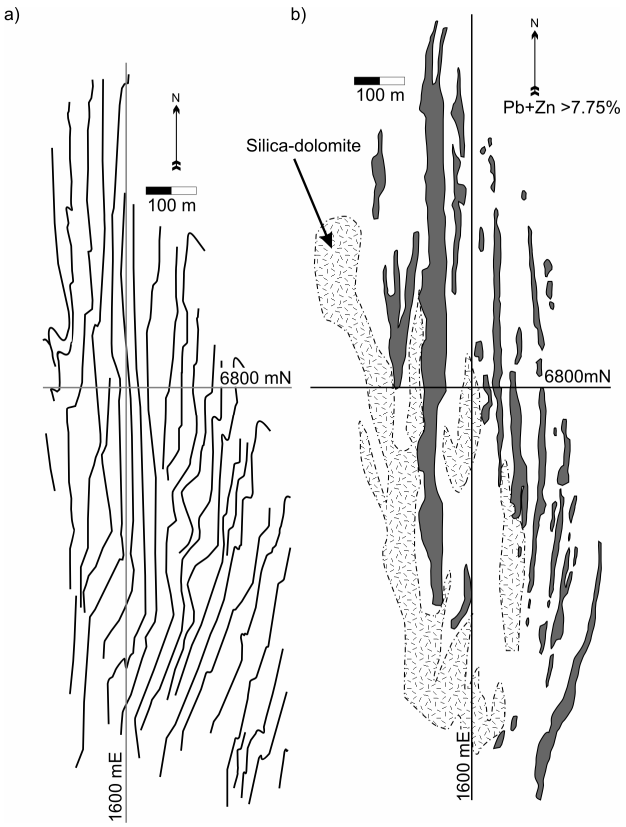


Figure 2: a) Bedding plan in the Lead Mine at Level 9 (3080 mRL). NNW-SSE-striking fold zones are defined by bedding orientations that deviate from the dominant N-S to NNE-SSW-striking fabric. b) Level 12 (2910 mRL) plan of Pb+Zn > 7.75 % and silica-dolomite alteration in the Mount Isa Lead mine.

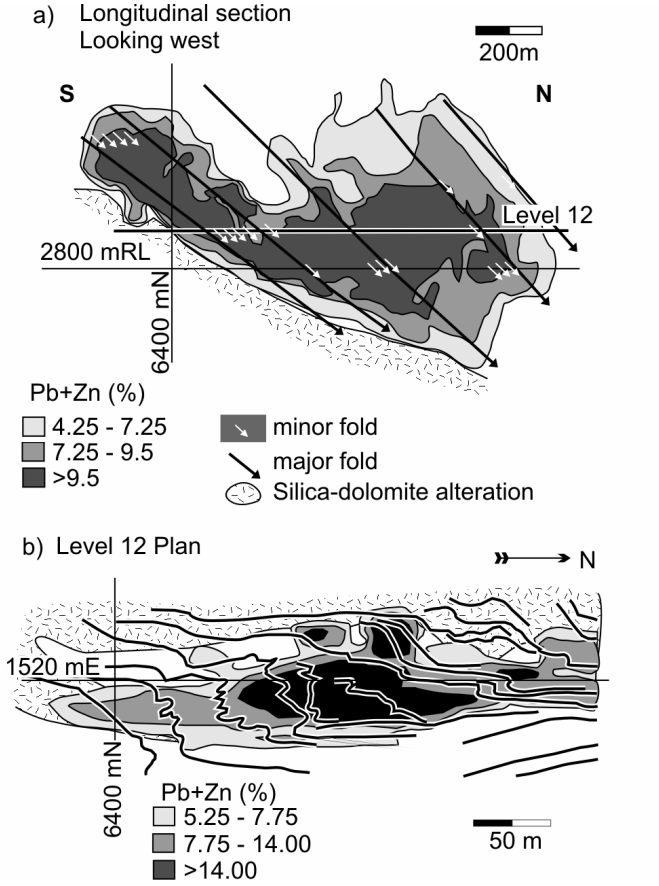


Figure 3: Relationship between the metal distribution and tectonic structures in the Zn-Pb-Ag deposit. a) Longitudinal section looking west orebody C. b) Plan through level 12, demonstrating the metal distribution is centred on disharmonic folds.

(Alaska), Sullivan (Canada), HYC (Northern Territory), Century (Queensland), and George Fisher-Hilton (Queensland). In contrast to the Zn-Pb-Ag orebody, the copper orebodies at Mount Isa are discordant at the mine scale and consist of cross-cutting breccias.

## 2 PREVIOUS WORKERS

The genesis of the Mount Isa base metal deposit is controversial because of apparently conflicting features between and within the copper and Zn-Pb-Ag orebodies. Early workers (Blanchard & Hall 1937) considered the deposits to be epigenetic but model was superseded by pre-deformation mineralization models, including exhalative and diagenetic depositional styles, to explain the conformable nature of sulphide bands within the Zn-Pb-Ag ores (Murray 1961; Neudert 1986; McGoldrick & Large 1998;). In these models, various discordant ore textures documented by the earliest workers were attributed to remobilisation (McDonald 1970). Evidence of syntectonic sulphide deposition presented by Perkins (1997) has largely been dismissed as an effect of remobilisation because of the ambiguity of these features. However, remobilisation has never been documented at Mount Isa.

## 3 STRUCTURAL GEOLOGY

The mine-scale fabric is dominated by NNE-SSW-striking bedding in the south that progressively rotates to N-S in the north of the mine (Fig. 2). This fabric is traversed by numerous NNW-SSE-striking, asymmetric and ENE-verging folds that formed in $D_4$. The Zn-Pb-Ag orebody contains ten sheet-like Zn-Pb-Ag ore lenes located around the northern margin of the discordant quartz-dolomite bodies, locally referred to as silica-dolomite, which host the breccia-hosted copper ores. The ore lenses are up to 1.2 km long and plunge in the range of 23-60° towards 323-348°, which is parallel to the plunge of $F_4$ fold hinges. Longitudinal sections show the ore lenses contain NNW-plunging high grade shoots that are parallel to their mar-

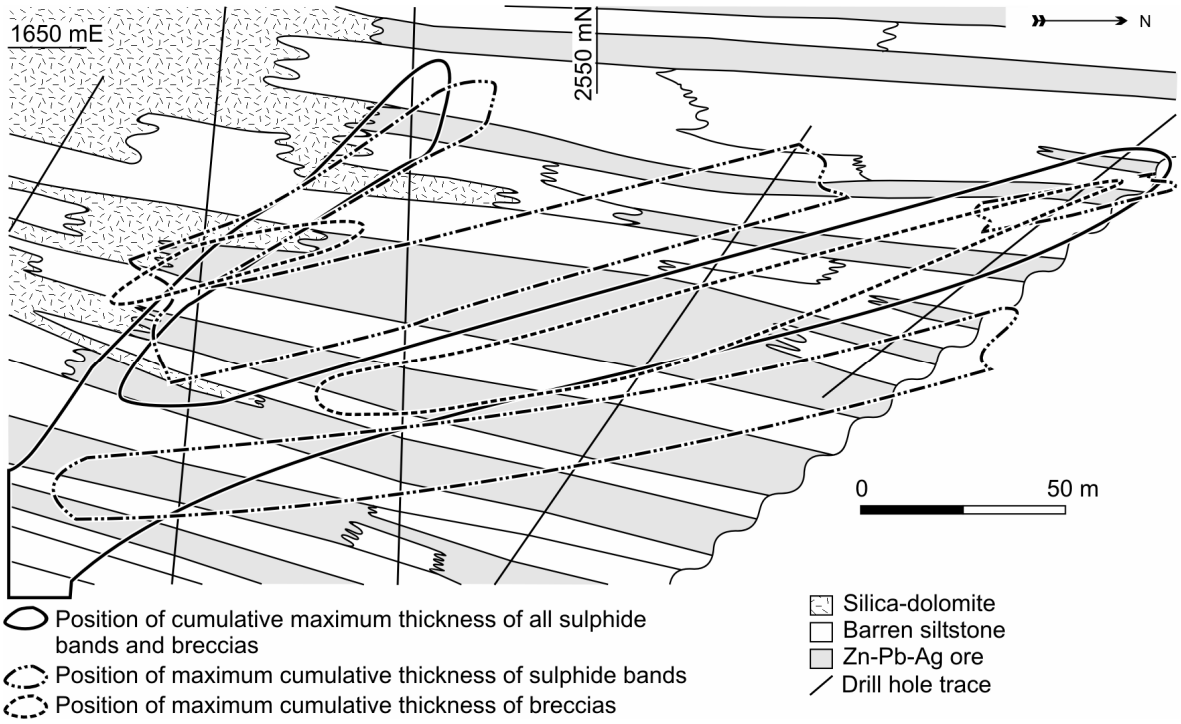


Figure 4: Plan showing cumulative thickness contours of sulphide textural groupings. Note that the NNW-SSE orientation of the contours is the same as the orientation of the hinges of $F_4$ folds. The combined thickness of all bands and breccias has a NNW-SSE-striking peak plus a NW-SE striking one north of the silica-dolomite alteration front. Sulphide bands (microcrystalline and fine grained styles excluding microbreccias) display two NNW-SSE-striking peaks that straddle the combined styles peak. Breccias have a NNW-SSE-striking cumulative thickness peak coincidental with the combined styled peak and a peak area north of the silica-dolomite alteration front.

gins and are centred on NNW-plunging disharmonic folds. Similarly orientated folds are located along the margins of the ore lenses but these folds are continuous across them (Fig. 3).

Metal zonation patterns throughout the Zn-Pb-Ag orebody show Pb:Zn contours are parallel to F4 fold hinges and silica dolomite fronts. The remarkably continuous nature of the lead distribution and the simple and parallel shapes of the Pb:Zn contours indicate deposit is undeformed and there has not been any differential remobilisation of sulphide minerals.

## 4 TEXTURAL ANALYSIS

The Mount Isa Zn-Pb-Ag orebody consists of conformable sulphide bands and breccias whose enveloping surfaces are parallel to layering at hand specimen and exposure scales. The range of textural variation in the bands and breccias and their distribution has been determined by systematically logging drill core throughout the orebody. Sulphide bands were classified by the dominant sulphide mineral and its grain size into the following categories; microcrystalline pyrite bands, microcrystalline sphalerite bands, fine grained sphalerite bands and microbreccias, galena bands, and nodular layers. All bands contain the same paragenetic sequence; Fe-dol, cte-qz, py, sp, gn, cp with sulphides overprinting tectonic structures. Microcrystalline pyrite is the earliest sulphide phase in the sequence and overprints several generations of crenulation cleavages.

Breccias are classified according to the pattern of brecciation into foliation fill, fold clast and rounded clast breccias. These contain the same paragenetic sequence as the banded ore styles described above, which clearly overprints tectonic structures including foliations and folds.

The deposit is zoned with respect to the ore textures described above (Fig. 4). It contains a core of breccias surrounded by sulphide band textural styles. All ore textural styles have NNW-SSE-trending distribution, which is the same orientation as fold-hosted mine-scale high-grade shoots.

## 5 DISCUSSION

The Zn-Pb-Ag orebodies at Mount Isa formed in the fourth regional deformation without remobilisation from a pre-existing accumu-

lation in the vicinity. The structural controls on mineralization are demonstrated by the ubiquitous relationship between the metal distribution and folding at mine scale, sulphide-foliation overprinting relationships in all ore textural styles at micro scales and the distribution of ore textural styles through the deposit.

Synchronous copper and Zn-Pb-Ag mineralization is indicated by the similarity of ore-structural relationships at a range of scales. Their spatial separation is the result of processes a change in the size of ore mineral host structures between the orebodies which impacted on the chemistry of the mineralising system by difference in the fluid-rock ratio between the two orebodies.

Bedding-parallel sulphide textures in the Zn-Pb-Ag orebody are not diagnostic of pre-deformation mineralization as previous proposed and such features can form by structural processes as is the proposed at Mount Isa. The bedding parallel nature of sulphide accumulations reflects the strong influence of rock type on strain partitioning which controlled the localisation of fluid flow. These rock type-based competency domains occur at a range of scales from individual beds to formation scale. At Mount Isa, shale and shale dominated packages experienced higher progressive strains which resulted in these units being mineralized.

The scale integrated nature of this study and the widespread spatial distribution of the data mean that the features presented here are representative of the deposit. In the past, features demonstrating tectonically controlled sulphide deposition have had a questionable representivity, which has meant they were able to be dismissed as being the products of remobilisation without actual evidence of this process being presented. Remobilisation processes can be confidently discounted as having a significant influence of the formation of the Mount Isa Cu-Zn-Pb-Ag deposit.

## REFERENCES


Blanchard R and Hall G (1937) Mount Isa ore deposition *Econ Geol* 32: 1042-1057

Davis TP (2004) Mine-scale structural controls on the Mount Isa Zn-Pb-Ag and Cu orebodies. *Econ Geol* 99: 543-559

Forrestal PJ (1990) Mount Isa and Hilton Silver-Lead-Zinc Deposits. In: Hughes FE (ed) Geology of the Mineral Deposits of Australia and Papua New Guinea: *Australasian Institute of Mining and Metallurgy, Melbourne*, 927-934

McDonald J A (1970) Some effects of deformation on sulfide-rich layers in lead-zinc orebodies, Mount Isa, Queensland. *Econ Geol* 65: 273-358

McGoldrick P J, and Large R R (1998) Proterozoic stratiform sediment-hosted Zn-Pb-Ag deposits: *AGSO J Geol and Geophys* 17: 189-196

Murray W J (1961) Notes on Mount Isa geology: *Proc AusIMM* 197: 105-136

Neudert M (1986) A depositional Model for the Upper Mount Isa Group and implication for ore formation: *Unpubl PhD. Thesis, Australian National University, Canberra,* 324 p

Perkins W G (1997) Mount Isa lead-zinc orebodies: replacement lodes in a zoned syndeformational copper-lead-zinc system?: *Ore Geol Rev* 12: 61-110

Waring C L, Heinrich C A, and Wall V J (1998) Proterozoic metamorphic copper deposits: *AGSO J Aust Geol Geophys* 17: 239-24

# Recent Research on Black Shale Hosted Base-Metal Deposits of the Mount Isa Region, Northern Australia

Andy Wilde
*pmd*CRC, School of Geosciences, Monash University, Clayton, Victoria, Australia*
*Now at Gold Fields, Minns Office Park, Oxford, UK*

Stafford McKnight
*School of Science & Engineering, University of Ballarat, Victoria, Australia*

ABSTRACT: Recent research as part of the co-operative research Centre in Predictive Mineral Discovery has addressed a number of issues pertaining to the giant base-metal deposits of the Mount Isa Region of northern Australia. This paper focuses on the Mount Isa copper deposits and the Century Zinc deposit, currently the world's second largest zinc mine. New insights into ore genesis and spatial distribution of alteration will contribute towards more cost-effective exploration.

KEYWORDS: Mount Isa, Century, ore genesis, alteration

## 1 INTRODUCTION

The Mount Isa region of northern Australia is host to several giant base-metal deposits hosted in weakly metamorphosed Proterozoic black shale, notably at Mount Isa, McArthur River and Century. In this paper we present a new genetic model for copper mineralization at Mount Isa and discuss bulk chemical and mineralogical (transmission electron microscopy, X-ray diffraction, and short wave infra-red) data for the Century deposit.

## 2 CHEMICAL PROCESSES IN THE MOUNT ISA CU-CO DEPOSITS

It has been previously proposed that the extraordinary spatial coincidence of giant copper and lead-zinc deposits at Mount Isa is due to the emplacement of copper into host-rocks (Urquhart Shale) made chemically favorable by enrichment in dolomite and/or pyrite, and mechanically favourable by the presence of layers of ductile lead and zinc sulphide ore. Several recent studies, however, suggest that copper and much, if not all, of the lead-zinc ore are contemporaneous. Reaction path modelling suggests that the presence of dolomite is not a prerequisite for economic copper grades (Wilde *et al.* 2005, *in press*). Furthermore, the pyrite-rich rocks are no more effective at precipitating copper than pyrite-absent rocks, consistent with several lines of evidence demonstrating that pyrite was not consumed during ore formation.

High grade (>2.5%) copper was preferentially emplaced into brecciated and silicified rocks whereas dolomite-rich rocks typically contain much lower copper grades. Early quartz is often euhedral and contains numerous growth zones defined by disordered carbon and fluid inclusions containing $CH_4$. Late dolomite (dolomite II) often infills vuggy porosity defined by this euhedral quartz. Chalcopyrite, however, postdates both phases and there is textural evidence of both dolomite and quartz dissolution during chalcopyrite formation.

The fluid that produced the early quartz was significantly more reduced and less saline than the oxidized brine believed to have introduced copper and to have formed a newly-discovered anhydrite body at the northern end of the mine. The paucity of quartz in the anhydrite body reflects heating, consistent with derivation from an oxidized bittern brine introduced from above as proposed in several previous studies (*e.g.* Matthai *et al.* 2004).

Reduction of this oxidized brine by the carbonaceous and silicified Urquhart Shale appears to be the most likely depositional process. Many other rock types in the region therefore have the capacity to reduce oxidized ore-forming brines, thus ore can be anticipated in these other units, provided that sufficient porosity and permeability existed.

## 3 ABSOLUTE AGE OF THE MOUNT ISA CU-CO DEPOSITS

Although most authors agree that copper was emplaced after the peak of metamorphism at Mount Isa, there are few data with which to constrain the absolute age of ore deposition. Re-Os isotopic analyses of whole rocks and sulphide separates define an imprecise Re-Os isochron age of 1370 ± 80 Ma and initial $^{187}Os/^{188}Os$ ratio of 0.20 ± 0.25 (MSWD = 49; Gregory et al. 2005). The new data suggest that copper ore formation was much younger than the 1523 to 1505 Ma range inferred using $^{40}Ar/^{39}Ar$ dating of biotite presumed but not proven to be of hydrothermal origin (Perkins *et al.* 1999). Previously published Rb-Sr analyses of hydrothermally-altered tuff samples from the orebodies (Farquharson & Richards 1975) define a recalculated isochron age of 1323 ± 12 Ma. The initial $^{87}Sr/^{86}Sr$ of 0.7418 ± 0.0061 is very radiogenic and is consistent with a hydrothermal resetting event at this time.

## 4 CENTURY ZN DEPOSIT – A ROLE FOR HYDROCARBON LIQUID?

Ore textures from the giant zinc and lead deposits at Century and McArthur River are ultrafine grained with grain dimensions commonly less than one micron. Such grains are below the resolution of light microscopy and also pose problems for scanning electron microscope and electron microprobe analysis. Monte-Carlo modelling for samples of this type and composition and standard instrument conditions shows that the resolution is greater than one micron for back-scattered electron imaging and X-ray analysis (McKnight & Wilde 2004). This poor resolution limit is due to the large electron beam interaction volume and is responsible for early reports describing sphalerite from Century as "porous" and "non-porous" (Broadbent *et al.* 1998) and for the failure to image finely dispersed bitumen with which much of the zinc sulphide is intimately intergrown. Several orders of magnitude improvement in resolution (~1nm) is achieved by high voltage (300kV) transmission electron microscopy (TEM) of thin foils produced from polished sections by argon ion milling followed by a finishing chemical thinning treatment. So called "porous" sphalerite is seen to be composed of myriads of sphalerite tetrahedral crystallites and other forms, ranging down to 100nm in size "floating" in bitumen of intermediate maturation. "Non-porous" sphalerite displays a distinctive cryptocrystalline texture comprising grains up to several microns possibly formed by solid state processes. Negative crystals, daughter crystals, and lattice defects as small as 5nm are readily imaged.

TEM observations of Century ore suggest that significant zinc mineralization was the product of the migration of hydrocarbon-rich fluids prior to or during peak maturation. Comparison of the textures shown by the two sphalerite types suggests they are related and it is proposed that the distinctive texture displayed by "non-porous" sphalerite has been derived by Ostwald ripening of a "porous" type precursor.

## 5 HYDROTHERMAL ALTERATION AROUND THE CENTURY ZN DEPOSIT

The Century ore zone is depleted in $SiO_2$, $K_2O$, MgO and CaO relative to all comparable rocks of the host McNamara Group, while $Fe_{tot}$ and MnO are greatly enriched. Zn shows a good inverse correlation with $SiO_2$, with rocks containing 20% Zn invariably containing less than 45% $SiO_2$. K depletion is probably due to K-feldspar dissolution, since this is more abundant in unmineralized rocks.

Fe enrichment at Century is due to the presence of pyrite in shale layers or ferroan carbonate in siltstones (siderite, sideroplesite or pistomesite). Carbonate minerals in rocks distal to the deposit tend to contain higher proportions of dolomite, accounting for higher bulk MgO and CaO. The presence of ferroan carbonate does not, however, define a halo around Century; indeed, siderite and Fe-Mg carbonates are abundant in oolitic ironstone of the overlying South Nicholson Group.

Short-wave infra-red spectra were obtained from the surface and from drillholes both in the open pit and beyond. The "MicaXT" parameter is a measure of the smectite component in white mica, relative to the muscovite component. MicaXT is often a good guide to the presence of hydrothermal alteration systems, for example in mesothermal gold systems of the Yilgarn and Carlin-type gold systems. At Century, mineralised rocks are clearly differentiated by a MicaXT parameter >2.0, with virtually no overlap with other sample groups.

Over 200 conventional X-ray diffraction determinations were made on samples from the

surface and from drillholes. These define a distinct halo around Century based on illite crystallinity. Comparison with the results after glycolation suggest that the halo is due to relatively low levels of interlayered smectite relative to the unaltered rocks, and hence that the deposit is associated with a palaeo-thermal anomaly. The clay-mineral halo also corresponds to variations in Pb isotopic characteristics of small lead-zinc occurrences in the district and, together with bulk chemistry, provides a powerful means of locating undiscovered deposits.

ACKNOWLEDGEMENTS

We acknowledge the discussion and input of many colleagues in the *pmd**CRC that helped in the development of ideas in this work. In particular, we thank Peter Jones and Klaus Gessner.

REFERENCES

Broadbent GC, Myers RE, Wright JV (1998) Geology and origin of shale-hosted Zn-Pb-Ag mineralization at the Century deposit, northwest Queensland, Australia. *Economic Geology,* 93: 1264-1294.

Farquharson RB, Richards JR (1975) Isotopic remobilization in the Mount Isa tuff beds. *Chemical Geology,* 16: 73-88.

Gregory MJ, Wilde AR, Schaefer BF, Keays RR (2005) Potassic alteration and veining and the age of copper emplacement at Mount Isa, Australia: in Mao J. and Bierlein F. (eds), Mineral Deposit Research: Meeting the Global Challenge: *Proc. 8th Biennial SGA Meeting Beijing China,* Springer: 755-758.

McKnight S, Wilde A (2005) Application of High Voltage Transmission Electron Microscopy to Ultra-Fine Grained Ores: The Century Deposit, Queensland: In Hancock, H. and others (eds), *Structure, Tectonics and Ore Mineralisation Processes: EGRU Contribution* #64, p. 84.

Matthäi SK, Heinrich CA, Driesner T (2004) Is the Mount Isa copper deposit the product of forced brine convection in the footwall of a major reverse fault? *Geology,* 32: 357-360.

Perkins C, Heinrich CA, Wyborn LAI (1999) $^{40}Ar/^{39}Ar$ geochronology of copper mineralization and regional alteration, Mount Isa, Australia: *Economic Geology*, 94: 23-36.

Wilde AR, Gregory MJ, Duncan RJ, Gessner K, Kuhn M, Jones P (2005) A geochemical process model for the Mt Isa Cu-Co-Ag deposits: in Mao J. and Bierlein F. (eds), *Mineral Deposit Research: Meeting the Global Challenge: Proc. 8th Biennial SGA Meeting Beijing China,* Springer: 199–203.

Wilde AR, Jones PA, Gessner K, Aillères L, Gregory MJ, Duncan RJ (2007) A geochemical process model for the Mt Isa copper orebodies: *Economic Geology*, 101: *in press.*

# Reactive flow models for shale-hosted ore mineralization, Anarraaq Zn-Pb-Ag deposit, Red Dog district, Alaska

C. Schardt & G. Garven
*Department of Earth and Planetary Sciences, The Johns Hopkins University, MD, USA*

K.D. Kelley & D.L. Leach
*U.S. Geological Survey, Denver, CO, USA*

ABSTRACT: The Red Dog district in northern Alaska is host to the high-grade, carbonate/shale-hosted Zn+Pb Anarraaq deposit. Using geological observations and fluid inclusion data, numerical heat and fluid flow simulations and coupled reactive flow simulations were conducted to gain more insight into the possible controls of ore body formation. Results suggest that the ore body and associated base metal zonation formed by the mixing of oxidized, saline, metal-bearing hydrothermal fluids (< 200°C) with reducing, $HS^-$ rich porewaters. Forward modeling results also predict the distribution of pyrite and quartz in agreement with field observations and suggest a reaction front moving from the initial mixing interface into the host rocks. Heuristic mass balance calculations suggest that metal accumulations comparable to those found in the ore district may develop in less than 1 million years.

KEYWORDS: reactive fluid flow, base-metals, zinc, lead, Red Dog

## 1 INTRODUCTION

The Red Dog district in the Brooks Range of northern Alaska hosts several high-grade Zn+Pb+Ba deposits, such as the Anarraaq deposit, with an estimated 223 Mt of ore averaging about 14% Zn and 4% Pb (Leach *et al.* 2005). The hydrogeology of these deposits is poorly understood as the ore bodies are presently situated in a highly deformed series of structural allochthons, thrusted during the Mesozoic to Tertiary Brookian Orogeny. The aim of this study is to determine the most likely chemical and physical conditions leading to the formation of the Anarraaq deposit and why this district contains such an unusual accumulation of base metals.

## 2 GEOLOGY AND MODEL SETUP

The deposit is hosted by radiolarian shale, mudstone, and carbonates, and is covered by at least 65m of barite. The mineralogy of the sulphide zone is dominated by sphalerite, galena, and iron sulphides with some carbonate. Three types of mineralization are distinguished: a low grade zone (< 8% Zn + massive pyrite + marcasite), banded sulphides (~ 14% Zn + laminated sphalerite + galena + iron sulphides), and a massive zone (~ 20% zinc, Kelley et al. 2004). Fluid inclusion and isotope studies suggest that hydrothermal fluids (T< 200°C, salinity > seawater) used the Endicott sandstone or fractured basement as fluid flow pathways to migrate into the shales and mixed there with reduced, HS-rich pore fluids to precipitate the base metals of the Red Dog deposits (Leach *et al*. 2004).

Based on these and other geological data a 600 x 330m model cross-section has been con-

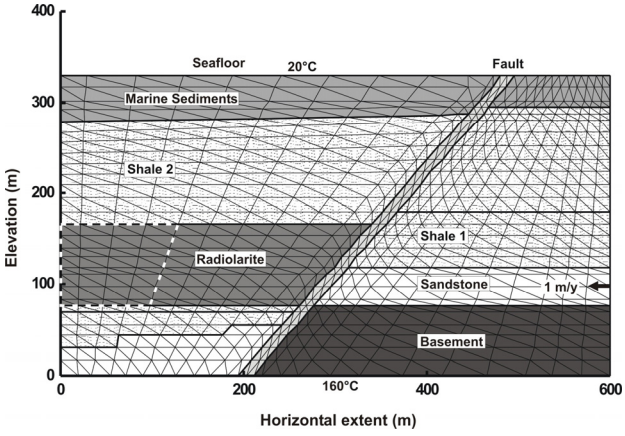


Figure 1. Numerical mesh and hydrostratigraphy of the model domain

structed for the Anarraaq deposit that includes most of the rock units described and a 40m-wide fault zone (Fig. 1). Initial and boundary conditions assume a temperature gradient (20°C-160°C) from top to bottom and a fluid injection rate from the right side of 1 m/yr. Side and lower boundaries are impermeable to heat and fluid exchange and initial fluid velocities are zero. All model units are assigned physical rock properties (permeability, porosity, thermal conductivity) and chemistry based on whole rock analysis. The injected fluid has been defined as an oxidizing ($SO_4^{2-} > HS^-$), saline (3 *m* NaCl), metal-bearing (3 ppm Pb, 30 ppm Zn) fluid that migrates through the Endicott sandstone, mixes with the pore fluids in the calcite-rich radiolarite, and precipitates base metals.

## 3 RESULTS

To investigate the validity of the proposed mixing scenario, three $HS^-$ source models were tested to simulate the formation of the base metal sulphides. The temperature and fluid flow field under constant conditions show almost linear isotherms and fluids migrating through the sandstone unit into the radiolarite unit, where mixing occurs (Figure 2). Fluids eventually migrate upwards and discharge through the fault.

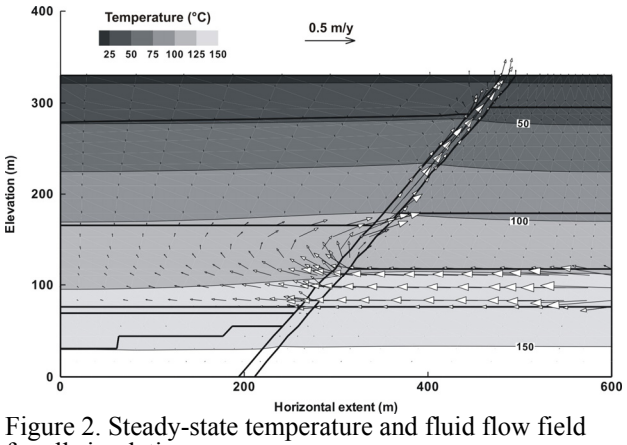

Figure 2. Steady-state temperature and fluid flow field for all simulations.

### 3.1 *Constant source*

The constant $HS^-$ source model defines the entire radiolarite unit as a constant source of $HS^-$ (100 μmol/L). Results show that significant base metal precipitation occurs at the radiolarite-fault interface, where the injected fluid mixes with the pore fluids. Because the entire radiolarite possesses a constant chemistry, no fluid migration into the radiolarite is observed. Maximum metal concentrations reach 125 and 9 mMol/L bulk porous medium (b.p.m.) ZnS and PbS respectively after 10,000 years.

### 3.2 *Half source*

In the half source model only a portion of the radiolarite unit is defined as a constant $HS^-$ source (stippled region in Figure 1); all other conditions are the same. In this scenario, mixing occurs within the radiolarite and base metal precipitation occurs within the right half of the radiolarite unit as a reaction front moving from the fault towards the edge of the $HS^-$ source, where the highest base metal concentrations are predicted. ZnS and PbS precipitated initially are dissolved and reprecipitated for the most part near the $HS^-$ source interface, because of local undersaturation. The overall concentrations of ZnS and PbS precipitated are significantly lower than in the constant source model (4.1 and 0.26 mMol/L b.p.m. respectively) with PbS showing a more widespread distribution than ZnS.

### 3.3 *Flush source*

This model assumes an initial $HS^-$ concentration in the radiolarite unit at the start, which is then replaced by the injected fluids. In this scenario, $HS^-$ drops to the same level as in the injected fluid in less than 1,000 years and fluids migrate and mix throughout the entire radiolarite unit. Reaction fronts for both ZnS and PbS are observed moving at different speeds through the radiolarite with concentrations < 0.1 mMol/L b.p.m. After 10,000 years most of the ZnS has been removed from the radiolarite unit, whereas PbS is still abundant (Fig. 3). Results show a mineralogical zoning of pyrite > sphalerite > galena progressing from the right to the left of the radiolarite.

Although none of these models by themselves predict sufficient amounts of accumulated base metal or the distribution and zonation patterns observed in the Anarraaq ore body, they may be able to explain the general features of the mineralization.

## 4 DISCUSSION

### 4.1 *Replacement of calcite by sulphides*

Textural evidence and chemical data suggest that sulphide mineralization at Anarraaq formed by the replacement of carbonate-rich sediments rather than by exhalative processes (Kelley *et*

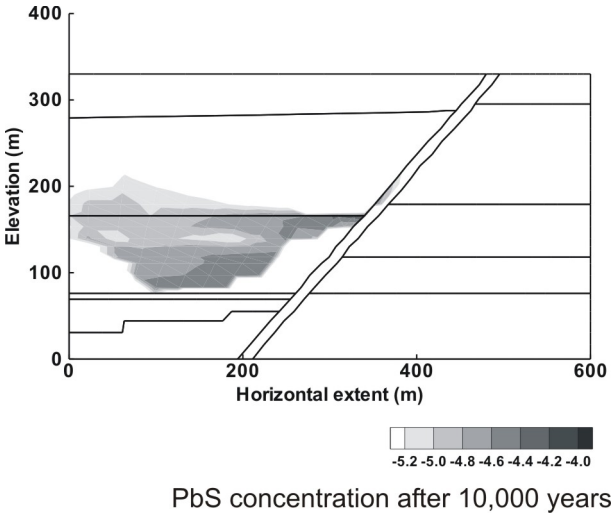


Figure 3. Galena distribution for the Flush source model (mol/L b.p.m.)

*al.* 2004). It is therefore of interest to explore whether the models can predict the concurrent dissolution of calcite and precipitation of sphalerite and galena to account for the formation and size of the Anarraaq ore body. Using discrete points in the numerical mesh, calculated porosity values show a significant decrease (~ 9%) for the constant model after about 4,000 years, which is due to the continuous accumulation of significant amounts of ZnS and PbS. $CaCO_3$ records continuous dissolution while $SiO_2$ exhibits precipitation once albite begins to dissolve after about 16,000 years.

Results from the half source model show similar steady dissolution and precipitation patterns except that the amounts of base metals are significantly smaller and consequently porosity changes are insignificant (< 0.1%). In addition, K-feldspar is predicted to dissolve at the expense of albite.

Due to the widespread dissolution and reprecipitation of ZnS and PbS in the flush model, predicted porosity changes are even smaller. Quartz shows early and steady precipitation, and muscovite is predicted to precipitate instead of albite. Overall, the predicted porosity changes are determined by both dissolution (calcite, K-feldspar) and precipitation (albite, quartz) and are judged sufficient to accommodate the replacement of calcite by sulphides under certain conditions (Constant source).

### 4.2 *Zonation in the Anarraaq ore body*

Results from each source model may provide insights into the formation of individual ore zones in the Anarraaq ore body.

The massive sulphide zone at Anarraaq has the highest ZnS content and is best represented by the constant source model. This implies that a constant or long-lasting $HS^-$ source is needed to ensure the accumulation of significant amounts of base-metal sulphides. This could have been achieved by either continuous bacterial sulfate reduction within, or thermochemical sulphate reduction of, the organic-rich shale that hosts the mineralization.

Findings from the half source model are broadly consistent with the banded sulphide zone. This zone contains lower Zn and Pb grades and up to 50 % quartz in individual layers of sphalerite. These features can be explained by the location of the $HS^-$ source away from the inflow zone, enabling fluids to mix and replace the $HS^-$-rich fluids in the non-source portion of the model.

The low-grade iron sulphide zone at Anarraaq is characterized by minor amounts of base metal sulphides and is made up mostly of massive pyrite and marcasite. The flush model best fits the nature and distribution of sulphides in this zone. Although the iron content of the injected fluids has been kept low ($6.1 \times 10^{-6}$ mol/L), pyrite precipitates early and migrates quickly to the left of the model section (~ 1,000 years). In addition, the model also predicts minor amounts of PbS and ZnS and the precipitation of quartz. The predicted movement of a base metal precipitation front through the radiolarite because of dissolution and precipitation could be the cause of the observed widespread but very low-grade distribution of base-metal sulphides.

It is interesting to note that modeling results predict a different timing of the migration and accumulation of pyrite, sphalerite, and galena towards the left of the model. Most of the pyrite is predicted to precipitate in the low-grade iron sulphide zone in less than 3,000 years, whereas galena and sphalerite reach their highest concentrations much later.

### 4.3 *Formation time of the ore deposit*

The computed total weight percent of accumulated ZnS and PbS for each model as a function of time is applied to ore grades of the entire ore body volume (750m x 90m x 350m; Figure 4). Although the half source and flush models were only run for 10,000 years, at their predicted base metal accumulation rates it will clearly take much longer to form the deposit compared to the constant source model results. These scenarios are therefore judged less likely

to have been the dominant conditions in the hydrothermal system.

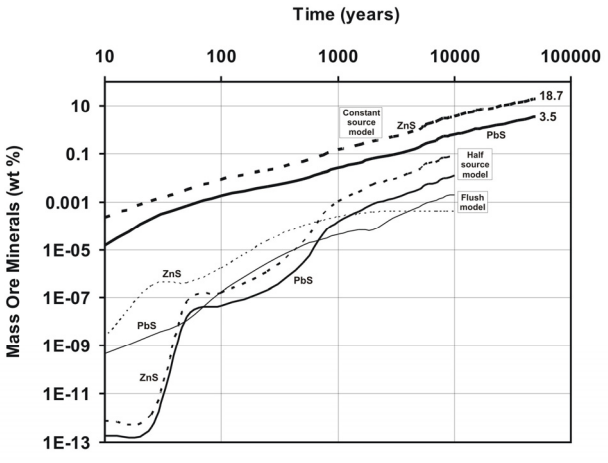


Figure 4. Predicted ore mass accumulation as a function of simulation time and source model.

The constant source model on the other hand predicts that ZnS + PbS concentrations similar to those of the Anarraaq deposit (18% and 5% respectively) will be reached after about 50,000 years. If reasonable deposition efficiency is assumed (20%), the formation time for the Anarraaq ore deposit is about 250,000 years.

Overall, the ore zonation may have evolved by mixing of the initial fluid with an $HS^-$-rich pore fluid source, precipitating most of the base metals and dissolving large amounts of calcite. Migrating further, the fluid precipitated much less ZnS and PbS and increasing amounts of quartz. The spent fluid, reacting with lower concentrations of $HS^-$, precipitated more quartz, and most of the pyrite due to dissolution and reprecipitation processes.

## 5 CONCLUSIONS

Reactive-coupled flow simulations have been used to simulate the formation of the Anarraaq Zn-Pb ore deposits based on field observations, fluid inclusion data, and isotope studies. Results suggest that a long-lasting $HS^-$ source is required to enable the formation of ore grades comparable to those observed in the field in a reasonable time frame, i.e. less than one million years. The formation of the ore deposit by the mixing of relatively oxidized, metal-bearing (33 ppm Zn+Pb), saline fluids with reduced pore fluids in the host rocks under these conditions is therefore considered a likely scenario.

## ACKNOWLEDGEMENTS

This project was supported by the Mineral Resources Program of the USGS. We thank Julie Dumoulin and Chris Potter at the USGS and Teck Comico geologists for providing geological and geochemical information that in part formed the foundation for the modeling.

## REFERENCES

Kelley KD, Dumoulin JA, Jennings S (2004) The Anarraaq Zn-Pb-Ag and Barite Deposit, Northern Alaska: Evidence for Replacement of Carbonate by Barite and Sulphides: *Economic Geology* 99: 1577-1591.

Leach DL, Marsh E, Empso P, Rombach CS, Kelley KD, Anthony M (2004) Nature of Hydrothermal Fluids at the Shale-Hosted Red Dog Zn-Pb-Ag Deposits, Brooks Range, Alaska: *Economic Geology* 99: 1449-1480.

Leach DL, Sangster DF, Kelley KD, Large RR, Garven G, Allen CR, Gutzmer J, Walters S (2005) Sediment-Hosted Lead-Zinc Deposits: A Global Perspective: *Economic Geology 100th Anniversary Volume,* 561-608.

# A regional S and Pb isotope study of carbonate hosted Zn-Pb mineralization, Mackenzie Mountains, NWT, Canada.

Sarah A. Gleeson,
*Department of Earth & Atmospheric Science, University of Alberta, Edmonton AB T6G2E3, Canada*

R.J. Sharp
*Transpolar consultants, 60 Hawkmount Hts, NW, Calgary, AB T3G 3S5, Canada.*

K. Dewing
*Geological Survey of Canada, 3303-33 Street NW, Calgary, AB, T2L2A7, Canada*

D. Krstic,
*Department of Earth & Atmospheric Science, University of Alberta, Edmonton AB T6G2E3, Canada*

E.L. Turner
*Department of Earth Sciences, Laurentian University, Sudbury ON, P3E 2C6, Canada*

L. Ootes
*Northwest Territories Geoscience Office, Box, 1500, 4601b-52nd Ave, Yellowknife, NT X1A 1W1 Canada*

ABSTRACT: The carbonate strata of the Mackenzie Mountains of Northwestern Canada are host to a large number of mineralized base-metal occurrences, including the Neoproterozoic-hosted Gayna River deposit. Here, we present S and Pb isotopic data on sulphides and sulphates from Gayna River and 7 other smaller showings hosted by Lower Cambrian and Silurian-Ordovican units. The S isotope data suggest that the source of S in all the deposits is variable and may be derived locally. The Pb isotope data have consistent values for most of the showings suggesting a single Pb source for the mineralization. These data allow a model of a regional hydrothermal fluid flow event(s) in the Mackenzie Mountains in the Devonian-Carboniferous that deposited base metals in units of varying ages.

KEYWORDS: Base metals, carbonate-hosted, Mackenzie Mountains, Sulphur isotopes

## INTRODUCTION

The Mackenzie Mountains are located in northwestern Canada and run along the border of the Northwest and Yukon territories. They were thrust into their present day exposures during the Late-Cretaceous to Tertiary Laramide Orogeny. Broadly, five stratigraphic packages can be identified within the orogenic belt; the Mesoproterozoic Mackenzie Mountain Supergroup, the Neoproterozoic Windermere Supergroup, the latest Proterozoic-Cambrian succession, the Upper Cambrian-Silurian units and finally, the Devonian succession. These form a carbonate platform in the eastern Mackenzie Mountains. Deep-water equivalents to west of the Mackenzie platform are preserved in the Selwyn basin, which hosts a series of shale-hosted deposits such as Faro and Howard's Pass.

Carbonate-hosted mineralization is widespread throughout the Mackenzie platform. Over 100 base-metal mineralized showings have been identified in units ranging from Neoproterozoic to Devonian in age. However, the possibility of a genetic relationship between the showings has not been previously addressed. In this paper, we present the results of a preliminary sulphur and lead isotope study on the Neoproterozoic-hosted Gayna River deposit, the largest mineralized occurrence in the Mackenzie Mountains, and 7 other smaller showings, hosted in Lower Cambrian and Silurian-Ordovician sediments to test the possibility of a regional base metal mineralizing event.

## 2 MINERALIZATION

The largest mineralized occurrence is found at Gayna River where the mineralization is hosted by Neoproterozoic carbonates (Figure 1). The Gayna River deposit is made up of over 100 mineralized showings on the property. The main phase of mineralization is dominated

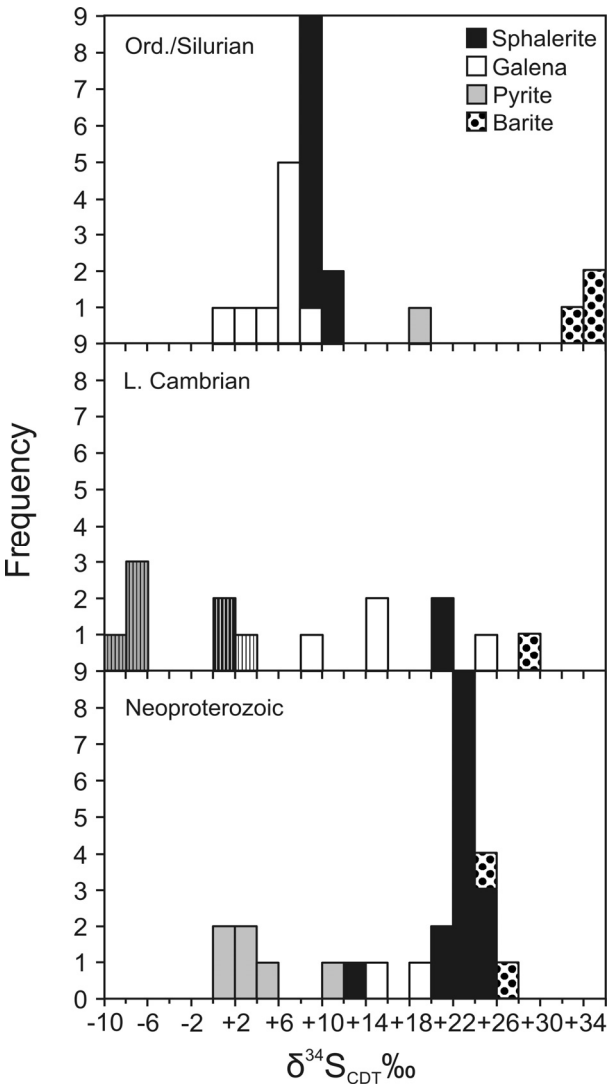


Figure 1 Sulphur isotope data from Neoproterozoic, Lower Cambrian and Silurian-Ordivcian hosted Zn-Pb occurrences in the Mackenzie mountains. Data from the Lower Cambrian hosted Tic showing is highlighted by **a** vertical stripe

by multi-coloured sphalerite and galena, occurring as cements in carbonate breccias and/or as fracture or vug fills. The sulphides are commonly associated with coarse white and saddle dolomite, although barite, quartz and pyrobitumen are also present; the latter two occur late in the paragenesis.

The other showings discussed here are hosted by Lower Cambrian Sekwi Formation (Majesty, AB, Tic and Ice) and Ordovician-Silurian strata (Bear and Keg), but have many features in common. The mineralization at these sites is dominated by sphalerite and galena, although tetrahedrite is also found in many locations. Keg and Tic are the only showings that contain significant pyrite mineralization. The gangue minerals found in all these showings are dominated by dolomite, calcite and quartz. Barite also occurs at the AB and Bear showings.

All the mineralized occurrences are structurally controlled at the outcrop scale. Preliminary fluid inclusion work suggests that all the mineralization formed at temperatures between 165-210°(modal Th is approx. 180°C) from fluids that varied in salinity from 10-30 wt% NaCl equiv. (Carriere & Sangster, 1999; Gleeson, 2006) including the mineralization at Gayna River.

## 3 METHODS

Sulphur isotopic analyses of sulphides and sulphates were carried out at the University of Calgary using the techniques described by Robinson & Kukusabe, (1975). Precision on the analyses is 0.3‰. The Pb isotope compositions of galena were determined by the method detailed in Clark & Thorpe (1990). The analytical uncertainties, as calculated on the basis of repeated measurements of standards are not greater than 0.044, 0.072 and 0.088% for the ratios $^{206}Pb/^{204}Pb$, $^{207}Pb/^{204}Pb$ and $^{208}Pb/^{204}Pb$, respectively, at the 2σ uncertainty level.

## 4 RESULTS

### 4.1 *Sulphur isotopes*

The bulk of the sulphur isotope data from the Neoproterozoic hosted mineralization come from Gayna River. Pyrite occurs early in the paragenesis and has $\delta^{34}S$ values that range from +0.7 to +11.3‰. Galena and sphalerite have values that that vary from 14.4 to 25.7‰ and the barite at Gayna River has values of 23.6 and 26.5‰ (Table 1, Figure 1). One analysis from sphalerite at the Tet showing yielded a value of 13.6‰. The data from the Lower Cambrian deposits are variable. In particular, sulphides from the Tic deposit have the lightest isotopic compositions measured in the study; these range from -8.3 to 1.9‰. In contrast, values from sphalerite and galena at the AB showing range from 14.0 to 21.2‰. The single barite analysis from AB yielded a $\delta^{34}S$ value of 29.2‰. Sphalerite samples from the Majesty and Ice showings have $\delta^{34}S$ values of 12.3 and 24.3‰ respectively (Table 1). At the Bear deposit, hosted by Ordovician-Silurian strata, the sulphur isotopic values of the galena and sphalerite range from +3.1 to 10.4 and 11.1 to

| Location | Host-rock age | Mineral | $\delta^{34}S$ (‰) |
|---|---|---|---|
| Gayna River | Neoproterozoic | Pyrite | 0.7 to11.3 |
| | | Galena | 14.4, 18.3 |
| | | Sphalerite | 18.2 to 25.7 |
| | | Barite | 23.6, 26.5 |
| Tet | Neoproterozoic | Sphalerite | 13.6 |
| Majesty | L. Cambrian | Sphalerite | 12.3 |
| AB | L. Cambrian | Galena | 14.0, 15.9 |
| | | Sphalerite | 20.3, 21.1 |
| | | Barite | 29.2 |
| Tic | L. Cambrian | Pyrite | -6.6 to -8.3 |
| | | Galena | 3.6, 8.3 |
| | | Sphalerite | 1.7, 1.9 |
| Ice | L. Cambrian | Sphalerite | 24.3 |
| Bear | Ord./Silurian | Galena | 3.1 to 10.4 |
| | | Sphalerite | 11.1 to 12.1 |
| | | Barite | 32.2 to 35.7 |
| Keg | Ord./Silurian | Pyrite | 20.4 |
| | | Galena | 9.6 |

Table 1. A summary of the results of the sulphur isotope study. The data are displayed as a range where the number of samples analysed is greater than 2.

12.1‰ respectively (Table 1; Figure 1). The barite sampled here has the highest $\delta^{34}S$ values. observed in the study and range from 32.2 to 35.7‰. Pyrite from the Keg showing has a high $\delta^{34}S$ value of +20.4‰ and the sole datum from galena has a value of +9.6‰

### *4.2 Pb isotopes*

The Pb isotope data from the Lower Cambrian and Ordovician–Silurian showings have relatively consistent values of $^{206}Pb$-$^{204}Pb$, $^{207}Pb$-$^{204}Pb$ and $^{208}Pb$-$^{204}Pb$ that range between 18.699 and 18.769, 15.671 to 15.711 and 38.331 to 38.940 respectively (Table 2). There is more variation in the Neoproterozoic hosted deposits. Although most of the Pb-Pb data for the Gayna River deposits also falls within this range, there are 3 galenas samples from the deposit that have lower $^{206}Pb$-$^{204}Pb$, $^{207}Pb$-$^{204}Pb$ and $^{208}Pb$-$^{204}Pb$ ratios. The single galena sample from the Majesty showing has similar $^{207}Pb$-$^{204}Pb$ and $^{208}Pb$-$^{206}$ Pb ratios to the other mineralized occurrences but has a higher $^{206}Pb$-$^{204}Pb$ ratio.

## 5 DISCUSSION

The sulphur isotopic composition of the barite at Gayna River is consistent with values measured on marine evaporite minerals of Ordovician to Late Devonian in age, although a pre-Varanger source of sulphur cannot be ruled out. The pyrite at Gayna River occurs early in the paragenesis and may represent early remobilization of diagenetic pyrite from the host-rocks. The isotopic composition of the sphalerite and galena is consistent with derivation from seawater sulphate and coeval galena and sphalerite from a single sample appear to be isotopic equilibrium at temperature of 180°C.

Table 2. A summary of the Pb isotope results from the study

| Location | $^{206}Pb/^{204}Pb$ | $^{207}Pb/^{204}Pb$ | $^{208}Pb/^{204}Pb$ |
|---|---|---|---|
| Gayna River | 18.433-18.851 | 15.621-15.686 | 38.035-38.570 |
| Majesty | 19.218 | 15.713 | 38.800 |
| AB | 18.720, 18.722 | 15.681, 15.702 | 38.859, 38.940 |
| Tic | 18.762-18.769 | 15.689-15.704 | 38.711-38.764 |
| Ice | 18.711 | 15.711 | 38.331 |
| Bear | 18.699-18.709 | 15.680-15.682 | 38.625-38.652 |
| Keg | 18.718 | 15.671 | 38.634 |

The available data from the Lower Cambrian hosted showings are sparse. A single barite $\delta^{34}S$ value is higher than those seen at Gayna and has a Lower Palaeozoic seawater sulphate source. Of the Lower Cambrian hosted mineralization, the Tic showing has a distinctive sulphur isotopic signature. Here, the low values may suggest a bacteriogenic source for the sulphides, whether this could be from remobilization of earlier diagenetic pyrite or through the introduction of $H_2S$ in a second, cooler fluid is unknown.

The strongly positive values for $\delta^{34}S$ from the barite at the Bear showing suggest that the sulphur was likely derived from either Cambrian or Devonian evaporites. Open system thermochemical reduction of this sulphate at temperatures of around 180°C cannot produce the relatively low values of $\delta^{34}S$ of the sulphides recorded here, and may suggest that there is another source of sulphur at Bear.

On the whole, with the exception of a small number of samples found in Gayna River and the galena from the Majesty showing, the Pb isotopic composition of the galenas show little variation and there is no significant difference in the values as a function of the age of the

host-rocks to the mineralization. This suggests that much of the Pb in the mineralizing system may have come from a single, homogenous source. These data plot on modeled growth curves for shale-hosted deposits in the Yukon in the Devonian-Carboniferous (Godwin & Sinclair 1982). These Pb isotopic data also have values that are comparable to the "least radiogenic Pb in Cordilleran carbonate hosted deposits of Nelson *et al*. (2002), which are also ascribed to a late Devonian timing for mineralization. This suggests that the mineralization may represent a hydrothermal fluid flow event(s) in the Mackenzie Mountains in the Devonian-Carboniferous that deposited base metals in units of varying ages.

The small number of galena samples with lower $^{206}Pb$-$^{204}Pb$ values from Gayna River may have a different lead source, the values are comparable with Godwin & Sinclair's (2002) data for Cambrian hosted deposits suggesting that Pb in the Gayna River system may be derived from a mixture of sources.

In summary, our data supports the hypothesis of a Devonian-Carboniferous fluid flow event, which carried an isotopically relatively homogenous Pb along active fault zones to the sites of mineralization. Precipitation occurred where this fluid interacted with a source of reduced sulphur, this source is different at different showings and may suggest that availability of sulphur is the major control on deposit size in the Mackenzie Mountains.

## ACKNOWLEDGEMENTS

The authors thank Eagle Plains Resources for financial and logistical assistance in the field and for payment for analyses.

## REFERENCES

Carriere JJ, Sangster D (1999) A multi-disciplinary study of carbonate hosted zinc-lead mineralization in the Mackenzie Platform, Yukon and Northwest Territories, Canada. *Geological Survey of Canada, Open file report* 3700.

Clark T, Thorpe RI, (1990). Model lead ages from the Labrador Trough and their stratigraphic implications. In: Lewry J.F., Stauffer M.R. (Eds.), The Early Proterozoic Trans-Hudson Orogen of North America: *Geological Association of Canada, Sp. Paper* 37: 413–431.

Gleeson SA (2006) A microthermometric study of fluid inclusions in sulphides and carbonates from Gayna River and the Bear base metal prospects, Mackenzie Mountains, NWT. *Northwest Territories Geoscience Office Open Report 2006-005*. 1-10.

Godwin CI, Sinclair AJ (1982) Average lead isotope growth-curves for shale-hosted zinc-lead deposits, Canadian Cordillera. *Economic Geology* 77 (3): 675-690.

Nelson J, Paradis S, Christensen J, Gabites J (2002) Canadian Coredilleran Mississuppi Valley-type deposits: A case for Devonian Mississippian back-arc hydrothermal origin. *Economic Geology*, 97 (5) 1013-1036.

Robinson BW, Kusakabe M (1975) Quantitative preparation of sulfur dioxide for $^{34}S/^{32}S$ analyses, from sulphides by combustion with cuprous oxide. *Analytical Chemistry* 47:1179–1181

# Carbonate-hosted Zn-Pb deposits in southern British Columbia, Canada - Potential for Irish-type deposits

S. Paradis
*Geological Survey of Canada, Sidney, British Columbia, Canada*

ABSTRACT: Carbonate-hosted Pb-Zn deposits of the Kootenay Arc are hosted by deformed Lower Cambrian shallow water platformal carbonates of the Badshot Formation or its equivalent the Reeves member of the Laib Formation. The deposits range in size from 6 to 10 Mt and contain 3-4% Zn, 1-2% Pb, 0.4% Cd and traces of Ag. They are essentially stratabound and stratiform lenticular concentrations of sulphides (sphalerite, galena, pyrite, occasional pyrrhotite and rare arsenopyrite) in isoclinally folded dolomitized or silicified carbonates. The origin of these deposits is enigmatic. Some of them are analogous in their geological setting and features to the Irish-type carbonate-hosted Zn-Pb deposits.

KEYWORDS: Irish-type deposits, carbonate-hosted, Zn-Pb, Kootenay Arc, Canada

## 1 INTRODUCTION

Carbonate-hosted Zn-Pb deposits of the Kootenay Arc in British Columbia, Canada (Figure 1) are commonly referred to as "Kootenay Arc-type deposits" (Höy, 1982; Nelson, 1991). They are hosted in miogeoclinal carbonates of the Lower Cambrian Badshot Formation and Reeves member of the Laid Formation.

Several deposits are past-producers (*e.g.* Reeves MacDonald, Jersey, HB, and Bluebell) and others have been intensively explored (*e.g.* Duncan and Wigwam). The largest deposits range in size from 6 to 10 million tonnes and contained 3-4% Zn, 1-2% Pb, 0.4% Cd and traces Ag (Höy 1982; Höy & Brown 2000). None of these deposits are presently in production.

The origin of these deposits is enigmatic because of the intense deformation that has modified most of their original features. However, several of the less deformed deposits share a number of syngenetic-diagenetic characteristics with Irish-type carbonate-hosted Zn-Pb deposits.

## 2 REGIONAL GEOLOGIC SETTING

The Kootenay Arc in the southeastern Canadian Cordillera refers to an arcuate geomorphic feature defined by a curving belt of complexly deformed rocks extending at least 400km long from near Revelstoke in the northern part of the Arc to the southwest across the Canadian-U.S.A boundary (Fyles 1964). The Arc lies between the Purcell Anticlinorium in the Purcell Mountains on the east, and the Monashee metamorphic Complex on the west (Figure 1). It consists of a thick succession of thrust imbricated Proterozoic to early Mesozoic miogeoclinal to basinal strata of sedimentary and volcanic protoliths (Brown *et al.* 1981).

Three phases of folding are recognized within the Kootenay Arc. Large amplitude (10 km-scale) west-verging recumbent folds were deformed by two phases of upright, tight to isoclinal folds, under conditions of lower greenschist to amphibolite facies metamorphism (Fyles 1964; Warren & Price 1993). This polyphase deformation has produced a pervasive transposition of bedding that locally obscures the stratigraphic relationships (Colpron & Price 1995). Colpron & Price (1995) have outlined a regionally consistent stratigraphic succession along the Kootenay Arc that is summarized below.

The lower part of the stratigraphic section along the Kootenay Arc is composed of Eocambrian siliciclastic rocks and carbonates of

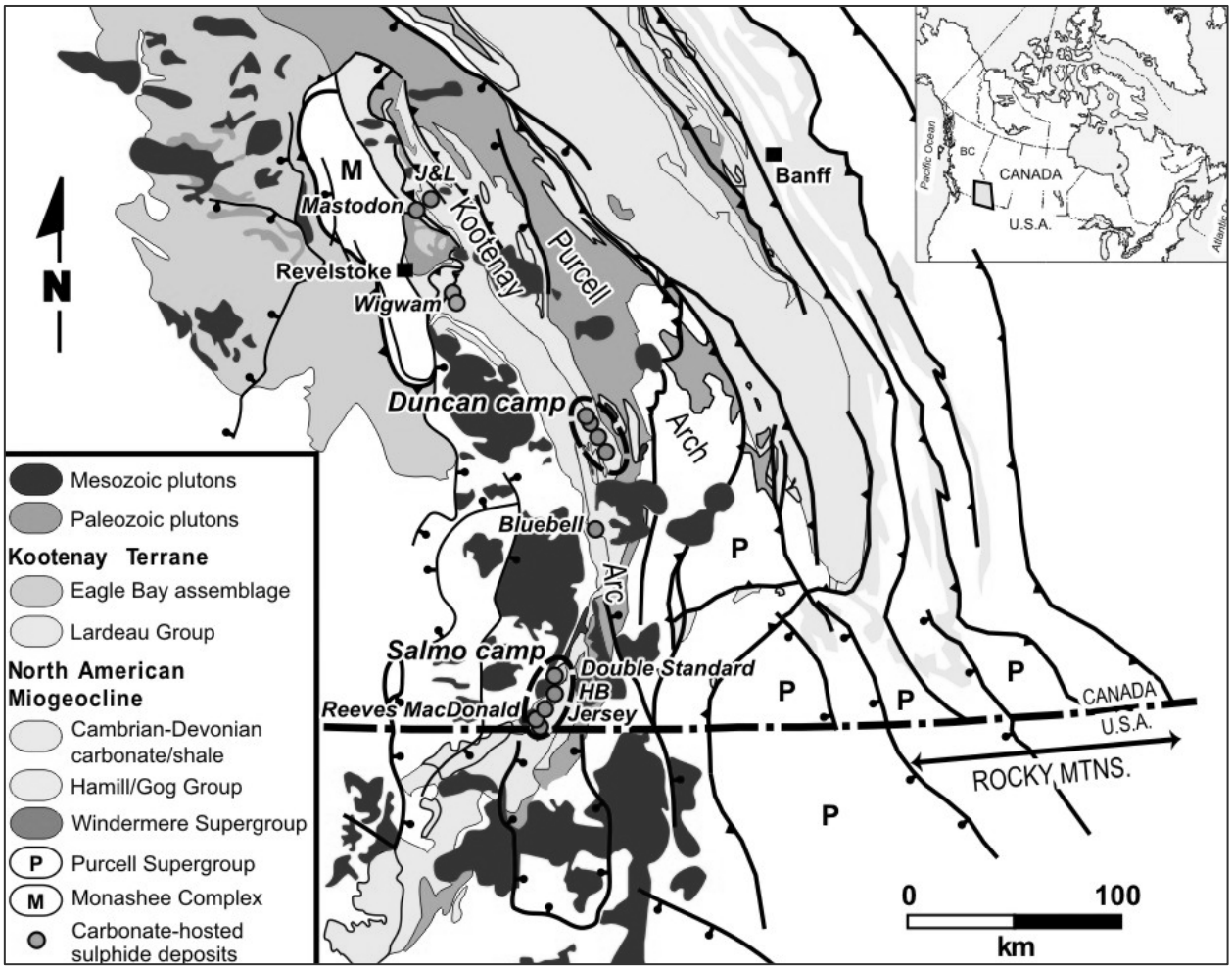


Figure 1. Simplified geologic map of southeastern British Columbia showing the location of the carbonate-hosted Zn-Pb deposits.

the Hamill Group and Mohican Formation. These rocks are overlain by the Lower Cambrian Archaeocyathid-bearing carbonates of the Badshot Formation and its equivalent, the Reeves member of the Laib Formation (Fyles & Eastwood 1962; Fyles 1964; Read & Wheeler 1976).

The Badshot Formation is characterized by cliff-forming, white to medium grey, commonly laminated marble or dolomitic marble. Locally, grey calcareous schist is interlayered with the carbonates. The Badshot and the Reeves carbonates host the Zn-Pb sulphide deposits. They are overlain with apparent conformity by the lower Palaeozoic siliciclastic, basinal shales and mafic volcanic rocks of the Lardeau Group (Colpron & Price 1995).

## 3 SULPHIDE DEPOSITS

The carbonate-hosted Zn-Pb deposits are distributed along the whole length of the Kootenay Arc, with two main districts, the Salmo and Duncan camps. The Bluebell deposit, described as a fracture-controlled replacement deposit (Ransom 1977; Höy 1980, 1982), is located between the Salmo and Duncan camps and smaller deposits are distributed in the northern part of the Kootenay Arc (Figure 1).

Dolomitized, brecciated, and silicified carbonates host all the Zn-Pb deposits. The dolomite is medium to dark grey, fine-grained, poorly banded and texturally different from the barren, generally well-banded limestone. It forms an envelope that completely or partially surrounds the sulphide mineralization.

The deposits are stratiform and stratabound. They consist of disseminated to massive sulphide aggregates forming lenses, irregular and well layered bands and laminae in dolomite or silicified carbonates. They are irregular in outline with the sulphide laminae following bedding of the host carbonates. The sulphide lami-

nae and the host carbonates are deformed into mesoscopic folds that mimic the large-scale (regional) structures. The deposits are commonly elongated parallel to the regional structural grain.

The main sulphides are sphalerite, galena and pyrite. Pyrrhotite and traces of arsenopyrite are observed in some deposits. The dominant gangue minerals are dolomite, calcite, quartz, and rarely barite. Sulphide mineralization appears to have formed primarily by replacement of the host carbonates, with minor open space filling of breccia zones, fractures and vugs. Common sulphide textures are fine- to medium-grained disseminations, banded encrustations, crystalline galena and sphalerite, and colloform sphalerite.

A brief description of the Salmo and Duncan camps is given below. It is based on recent field investigations by the author and descriptions of Fyles and Hewlett (1959), Fyles (1964, 1970), Höy (1982), and Legun (2000).

### 3.1 *Salmo camp*

The Salmo camp is also known as the Mine Belt (Fyles & Hewlett, 1959). The principal deposits are Reeves MacDonald, Jersey and HB mines. Production from these deposits is listed in Table 1. They are hosted in fine-grained, poorly banded dolomite of the Reeves member, which is texturally different from the barren, generally well-banded limestone of the Reeves member. The mineralized dolomite is dark-grey, poorly banded and mottled with black flecks, wisps and bands outlined by concentration of carbon. This textured dolomite generally hosts the sulphide deposits, whereas the more massive dolomite is only sparsely mineralized (Fyles 1970).

The deposits lie within secondary isoclinal folds along the limbs of anticlinal structures. They are stratiform, tabular and lenticular disseminations of pyrite, sphalerite, and galena in dolomitized zones. Brecciated zones are common within the more massive sulphide mineralization. They consist of limestone and dolomite fragments cemented by sulphides (Fyles & Hewlett 1959; Legun 2000).

The deposits, their enveloping dolomite and the limestone host rock are folded. It is apparent that the dolomitization was controlled by the Reeves syncline and that sulphide mineralization followed the same structure as the dolomite (Höy & Brown, 2000). The upper portion of several deposits is deeply oxidized and consists of extensive zinc-enriched iron oxide gossans, which overlie the sulphide deposits.

Table 1. Production and reserve of the main carbonate-hosted Zn-Pb deposits of the Kootenay Arc.

| Deposit | Production (Reserves) |
|---|---|
| Reeves MacDonald | 5.85 Mt at 1% Pb, 3.42% Zn, 3.4 g/t Ag |
| Jersey | 8.4 Mt at 1.95% Pb, 3.83% Zn |
| HB | 6.7 Mt at 0.77% Pb, 4.1% Zn, 4.8 g/t Ag |
| Duncan | (9 Mt at 2.7% Pb, 2.9% Zn) |
| Bluebell | 4.82 Mt at 5.2% Pb, 6.3% Zn, 45 g/t Ag |
| Wigwam | (632,814 t at 2.14% Pb, 3.54% Zn) |

### 3.2 *Duncan camp*

Several complexly deformed and faulted sulphide bodies occur in a thick section of dolomite or silicified carbonates of the Badshot Formation within the Duncan camp. Höy (1982) interpreted the Badshot carbonates in this area as an "extensively brecciated and locally dolomitized, bank margin facies developed on a shoal complex". The dolomite is either massive or it displays the same textures as dolomitic envelopes enclosing the sulphide deposits in the Salmo camp.

Some 20 mineralized zones occur on the hinge of a phase 2 fold, which is on the east limb of the phase 1 Duncan anticline (Höy 1982). None of the deposits have been mined; however, one of the mineralized zones has reserves of 9 Mt grading 2.7% Pb and 2.9% Zn (Muraro, 1962).

Mineralization consists mainly of fine-grained pyrite and subordinate sphalerite, galena, and pyrrhotite concentrated in layers in the dolomitized and silicified carbonates. The sulphide bodies are vertical lenses and sheets of sulphides with gradational but in general well-defined margins. The attitude of the sulphide bodies is essentially parallel to that of the enclosing formations, *i.e.*, the largest dimension is parallel to the strike and the intermediate dimension is parallel to the dip (Fyles 1964).

## 4 ORIGIN OF THE KOOTENAY DEPOSITS AND POTENTIAL FOR IRISH-TYPE DEPOSITS

The origin of the deposits is enigmatic. Fyles & Hewlett (1959) interpret these deposits as replacement zones controlled by phase 2 folds and locally by faults and breccia zones associated with them. Sangster (1970) and Addie (1970) believe these deposits are syngenetic, formed by sulphides accumulation in small basins within a deep-water carbonate platform. Muraro (1962) suggests that these deposits formed by pre-metamorphic, pre-tectonic hydrothermal replacement of the host rock controlled by stratigraphy. Höy (1982) suggests largely a syngenetic-diagenetic origin, with sulphide accumulating simultaneously with shallow-water carbonates, and local accumulation of sulphides in cavities or breccia zones of the lithified Reeves or Badshot carbonates.

All of the authors agree that the genesis of these deposits is difficult to ascertain because of the intense deformation that has modified most of the original features. Our preliminary investigation of the Salmo and Duncan deposits suggests that these deposits share many geological characteristics with the Irish-type carbonate-hosted massive sulphide deposits of Ireland. Some of these characteristics are: 1) stratabound nature, *i.e.*, sulphides are hosted in dolomitized or silicified carbonates; 2) simple mineralogy, *i.e*., sphalerite, galena, and iron oxides; 3) occurrence along or immediately adjacent to faults that may have formed conduits for upward-migrating hydrothermal fluids; 4) banded and layered appearance of the sulphides; and 5) the presence of complex textures ranging from replacement of host carbonates by sulphides to some open-space fillings.

## ACKNOWLEDGEMENTS

This project is being carried out under the umbrella of the Cordilleran Targeted Geoscience Initiative-3 (TGI-3) of the Geological Survey of Canada.

## REFERENCES

Addie GG (1970) The Reeves MacDonald Mine, Nelway, British Columbia. In: Pb-Zn Deposits in the Kootenay Arc, N.E. Washington and adjacent British Columbia. *Dept Nat Res, State of Washington, Bull* 61 pp 79-88

Brown, RL, Fyles JT, Glover JK, Höy T, Okulitch AV, Petro VA, Read PB (1981) Southern Cordillera Cross-section – Cranbrook to Kamloops. *Geol Ass Can, Field Guides to Geology and Mineral Deposits*, pp 335-371

Colpron M, Price RA (1995) Tectonic significance of the Kootenay terrane, southeastern Canadian Cordillera: An alternative model. *Geology* 23: 25-28

Fyles JT (1964) Geology of the Duncan Lake area, British Columbia. BC Min Energy, *Mines and Pet Res Bull* 49, 87 p

Fyles JT (1970) Geological Setting of Pb-Zn Deposits in the Kootenay Lake and Salmo Areas of B.C. In: Pb-Zn Deposits in the Kootenay Arc, N.E. Washington. *Dept of Nat Res, State of Washington Bull* 61, pp 41-53

Fyles JT, Hewlett CG (1959) Stratigraphy and structure of the Salmo lead-zinc area. *BC Dept of Mines Bull* 41, 162 p

Fyles JT, Eastwood GPE (1962) Geology of the Ferguson area, Lardeau district, British Columbia. *BC Dept of Mines Bull* 45, 162 p

Höy T (1980) Geology of the Riondel area, central Kootenay Arc, southeastern British Columbia. *BC Min Energy, Mines and Pet Res Bull* 73, 89 p

Höy T (1982) Stratigraphic and Structural Setting of Stratabound Lead-Zinc Deposits in Southeastern British Columbia. *Can Inst Mining Metall Bull* 75: 114-134

Höy T, Brown D (2000) Introduction to regional stratigraphy and tectonics; Bluebell and Reeves MacDonald. In: Höy T, Brown D, Lydon J (eds) Sullival and other Zn-Pb deposits, southeastern BC. *GeoCanada 2000, Field Trip Guidebook* 17, pp 19-37

Legun A (2000) Geology and regional setting of major mineral deposits in the Kootenay district. In: Legun A, *et al* (eds) Geology and regional setting of major mineral deposits in southern BC. Geol Surv *Can Open File 2167, 8th IAGOD symposium*, pp 5-27

Muraro TW (1962) Stratigraphy, structure and mineralization at the Duncan Mine, Lardeau district, British Columbia. *MSc thesis, Queen's University, Canada*

Nelson JL (1991) Carbonate-hosted Lead-Zinc Deposits of British Columbia. In: McMillan WJ, Höy T, MacIntyre DG, Nelson JL, Nixon GT, Hammack JL, Panteleyev A, Ray GE, Webster ICL (eds) Ore Deposits, Tectonics and Metallogeny in the Canadian Cordillera. *BC Ministry of Energy, Mines and Petroleum Resources, Paper* 1991-4, pp 71-88

Ransom (1977) An outline of the geology of the Bluebell Mine, Riondel, BC. In: Höy T (ed) Lead-zinc deposits of southeastern BC, *Geol Ass Can Fieldtrip Guidebook* 1, pp 44-51

Read PB, Wheeler JO (1976) Geology of Lardeau W/2 (82K w/2). *Geol Surv Can Open File Map* 432,

Sangster DF (1970) Metallogenesis for some Canadian Lead-zinc Deposits in Carbonate Rocks. *Geol Ass Can Proceedings* 22, pp 27-36

Warren MJ, Price RA (1993) Tectonic significance of stratigraphic and structural contrasts between the Purcell anticlinorium and the Kootenay Arc, east of Duncan Lake (82K). In: Geological Fieldwork 1992, *BC Ministry of Energy, Mines and Petroleum Resources Paper* 1993-1, pp 9-1

# The peridiapiric-type Pb-Zn deposit at Fedj el Adoum, Tunisia: geology, petrography, and stable isotopes

Salah Bouhlel
*Department of Gelology, Faculté des Sciences de Tunis*
*El Manar University, 2092, Tunis, Tunisia*

Craig A. Johnson & David L. Leach
*U.S. Geological Survey, Box 25046, Denver CO 80225, USA*

ABSTRACT: The Fedj el Adoum peridiapiric-type (PDT) Pb-Zn deposit is hosted by dolostone and clay breccias of the Transition Zone Formation (TZF), which is underlain by diapiric evaporites of Triassic age and overlain by marly limestones of Cretaceous (Albian) age. The TZF was deposited in Early Albian time on the crest and flanks of the salt diapir as a result of halite and anhydrite dissolution. The ore deposit (1.5 Mt of 17% Zn+Pb) was formed in two main stages, possibly by two different fluids. The first stage was Zn>Pb and had $\delta^{34}S$-$H_2S$ of 18±6‰ (VCDT), whereas the second stage was Pb>Zn and had $\delta^{34}S$-$H_2S$ of -3±8‰. The $H_2S$ in the first stage was produced by thermochemical sulphate reduction, whereas the $H_2S$ in the second stage was produced dominantly by bacterial sulphate reduction. The second stage was also characterized by the presence of methane, the oxidation of which produced calcite with $\delta^{13}C$ values as low as -48 ‰ (VPDB).

KEYWORDS: Salt diapirs, Pb-Zn, carbon isotopes, sulphur isotopes, calcite, methane

## 1 INTRODUCTION

Numerous peridiapiric-type (PDT) Pb-Zn deposits occur in the Diapir Belt of Northern Tunisia (Fig.1). The ore-bearing formation is a brecciated dolostone that is referred to as the Transition Zone Formation (TZF). The deposits are similar to Mississippi Valley-type deposits in many respects (Rouvier *et al.*, 1985; Bouhlel, 2005 and references therein). Fedj el Adoum, the type-example of this deposit type in Tunisia, is located on the northeast side of the Jaouada salt diapir, and contains ~1.5 Mt of ore grading 17% Zn+Pb. This paper describes the host rock and ore petrology, presents new carbon and sulphur isotope data, and discusses the origin of the TZF, sources of ore sulphur, and the sulphate reduction pathways that allowed the ores to form.

## 2 GEOLOGIC SETTING

Fedj el Adoum is located in a NE-SW-trending rift system, the el Kef Rift, that started forming in Late Jurassic time and reached its maximum activity in the Cretaceous (Aptian to Cenomanian). From the early Cretaceous, the el Kef Rift was subdivided by SW-NE faults into several en echelon half grabens that deepened to the NW (Chaari *et al.*, 2004). Salt diapirism occurred during late-Aptian and continued during the Upper Cretaceous through to recent times. During lower-Albian the Triassic salts intruded the overlying rocks mostly along SW-NE faults to form SW-NE-elongated diapirs (Bouhlel, 1993).

By Middle Albian time, approximately 50 of these diapirs had been emplaced beneath, or had pierced, the basin floor. The TZF formed at this time as a result of water-rock interactions and salt dissolution.

The Pb-Zn occurrences are located where NW-SE trending faults intersect the SE margins of the diapirs, and also at their axial ends. The distribution is thought to reflect flow of the hydrothermal fluids along the preexisting faults.

Upper Albian time was characterized by transgression and rapid sedimentation. Sediment thicknesses decreased from south to north within individual half grabens (from 6 to 2km in the Fedj el Adoum half graben) as a consequence of continued extension and salt halokinetics. In the Middle Miocene, the area ex-

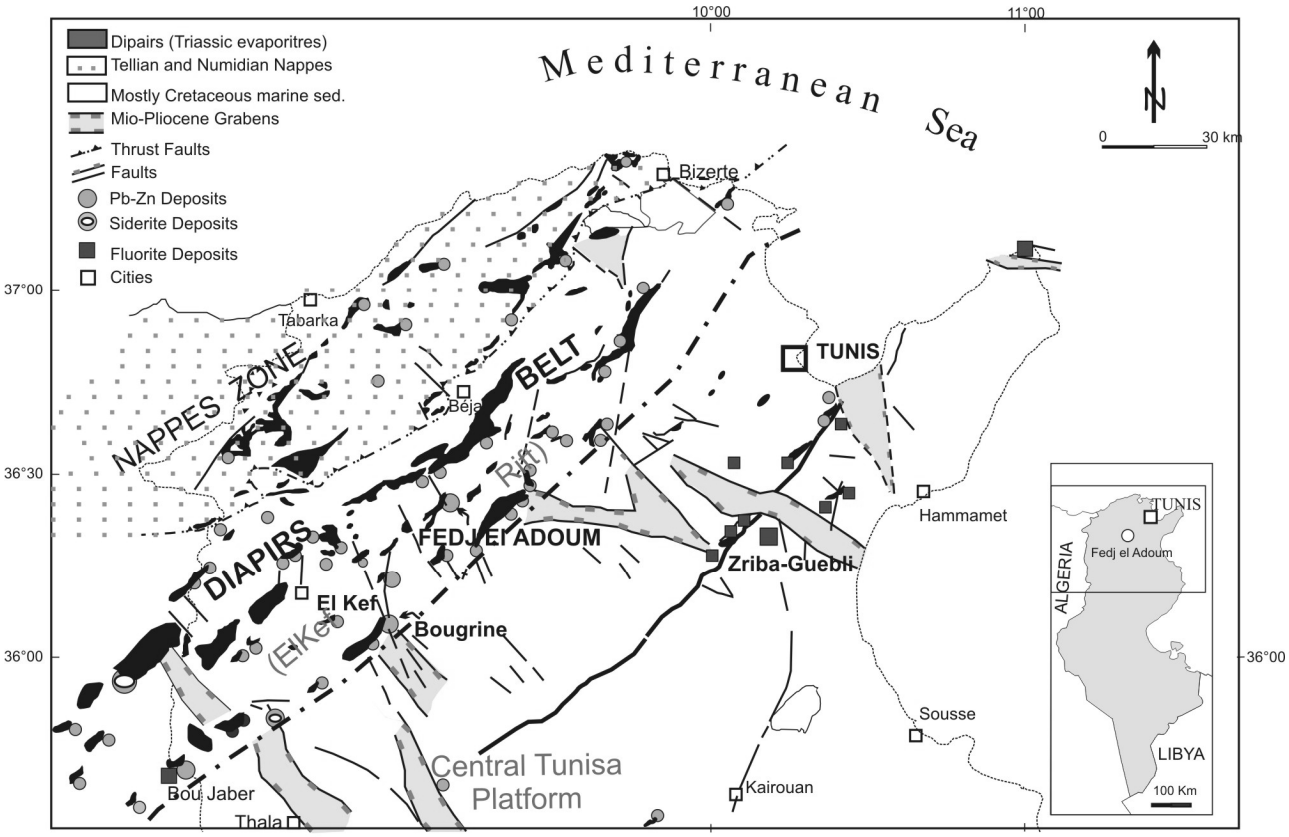


Figure 1. Map of lead-zinc-, siderite-, fluorite- deposits, exposed Triassic diapirs, structural and paleo-geographic zones of northern Tunisia

perienced compression related to the Alpine orogeny. NW-to-SE thrusting occurred in Late Miocene time. By the Pliocene, the area had emerged, and was subjected to intensive subaerial erosion.

## 3 DESCRIPTION OF TZF AND MINERALIZATION

On a regional scale, the TZF has the appearance of an intraformational breccia, 30 to 70m in thickness, that is situated between underlying Triassic gypsum (after anhydrite) and overlying Upper Albian marly limestones. It hosts most of the Pb-Zn deposits in the area.

At Fedj el Adoum, the TZF consists of several breccia-types, but is dominated by dissolution breccias and crackle-to-mosaic breccias. Slump and collapse features are common. The clasts, which are Triassic in age, include grey dolostone, light-grey de-dolomitized dolostone, green to black compacted clays, and bipyramidal quartz. The dolostone clasts are either dolomicrite or dolosparite. Dolomicrite is frequently laminated, like the dolomicrite that is found as interbeds within the underlying Triassic evaporites. Dolosparite is composed of dolomite crystal aggregates (90% of the rock) in a matrix of black shale, iron sulphide crystals, and organic matter.

The upper part of the unit, which lies against the Albian limestone, is a 0-20m thick horizon of compacted, dolostone-rich breccia with green shale matrix. The lower part, which is in contact with Triassic evaporite, consists of a 1-2m thick shaly horizon with interbedded 2-10 cm thick lenticular dolostone layers.

The variety of breccias within the TZF are related to halite and anhydrite (or gypsum) dissolution, and subsequent collapse of the overlaying soft units as the salt diapir approached or pierced the sea floor, and to subsequent tectonics at the diapir margins.

The TZF hosts at least four types of mineralization: Zn-rich ore, zebra calcite, Pb-rich ore, and native sulphur. They have the following characteristics:

*1. Zn-rich ore*:

Zn>>Pb, stratabound, lens-shaped orebodies, conformable to the banding in the TZF. This mineralization type accounts for 80% of the resource at Fedj el Adoum. Highest grades occur at the lower part of the TZF. Mineralization oc-

curs as replacements of dolostone or as open space fillings. Alternating dark- and white-yellow bands, 1 to 5cm in thickness, are common. The dark bands consist of Triassic dolostone fragments, and the cream-colored bands are colloform, very fine, microcrystalline sphalerite. The youngest colloform bands may be incrusted with honey-to-yellow, minute sphalerite crystals cemented by small amounts of white sparry calcite. The Zn-rich ore is relatively poor in calcite.

*2. Zebra calcite*:

Irregular patches of disseminated, massive, or zebra calcite, occurring as mm- to m-thick open space fillings. Zebra calcite consists of mm- to cm-scale alternations of dark calcite and white calcite. The dark calcite is equigranular pseudospar with crystal sizes ranging from 0.5 to 1 mm. Crystals are generally polyhedral, rhombohedral, or lenticular. The white calcite may be massive or scalenohedral in form growing toward open cavities. Individual crystals can reach 20 cm in length.

*3. Pb-rich ore:*

Pb>>Zn, veins, stockwork, or massive mineralization. This mineralization type accounts for 20% of the Fedj el Adoum resource. This ore cross-cuts all layering in the TZF including Zn-rich ore. Highest grades occur in a dolostone-rich subzone in the upper TZF against the hanging wall limestones. Galena is coarse-grained and massive. Sphalerite postdated galena, is microcrystalline, and forms mm-scale textures. Post-sulphide sparry calcite filled residual porosity.

*4. Native sulphur:*

Late, minor occurrences as open space fillings, locally forming zebra textures in which sulphur is intergrown with calcite or aragonite. Sulphur-rich occurrences are most common in the lower part of the TZF against the anhydrite/gypsum footwall.

## 4 CARBON AND SULPHUR ISOTOPES

We determined the carbon isotope composition of the Triassic dolostone (n=5) and several generations of ore calcite. The dolostone has $\delta^{13}C$ (VPDB) values of about 1‰, within the range of Triassic marine carbonates in the region (0±5‰). Calcite that precipitated with sphalerite in banded Zn-rich ore gave a $\delta^{13}C$ value of 1‰. The $\delta^{13}C$ values of cacite that predated the Pb-rich ore were -20±4‰. Calcite that post-dates the Pb-rich ore calcite had $\delta^{13}C$ values of -9 to 3‰. Calcite from the native sulphur stage had $\delta^{13}C$ values of about -30‰, and aragonite from the banded native sulphur ores ranged from -43 to - 48‰.

These data suggest that the Zn-rich ore formed in the presence of normal marine bicarbonate, whereas the later ore stages involved carbonate from oxidation of organic compounds. Ore formation culminated in the oxidation of hydrocarbons or methane.

Sulphur isotope compositions were determined on sphalerite (n=17), galena (n=15), and anhydrite/gypsum (n=8). The sulphide $\delta^{34}S$ values fall into two distinct groupings. Banded Zn-rich ores contain heavy sulphur (18±6‰), and vein and stockwork Pb-rich ores contain lighter sulphur (-3±8‰). The highest $\delta^{34}S$ values exceed the 15-18‰ range that characterizes the Triassic anhydrite. This may implicate a source of isotopically heavy $H_2S$, possibly sour gas transported from depth. The isotopically heaviest sulphides correspond with the highest Zn+Pb grades. The lighter sulphur in the vein and stockwork Pb-rich ore may reflect isotopically light $H_2S$ produced locally through bacterial sulphate reduction. This would be consistent with the production of methanogenic calcite ($\delta^{13}C$ as low as 48‰) at the site of ore deposition.

## 5 SYNTHESIS AND CONCLUSIONS

The Fedj el Adoum deposit formed by the following sequence of events:

1. In the Lower Albian, Triassic salt intruded its cover sediments along SW-NE faults. Near to or on the sea floor, halite was dissolved leading to the formation of the TZF on the crest and flanks of the diapir.
2. Hydrologic conditions changed, and a deep-sourced Zn>>Pb fluid and deep sourced $H_2S$ entered the TZF leading to the formation of Zn-rich banded ore.
3. Following deposition of the Zn-rich ore, hydrological conditions changed again and methane entered the TZF. Anhydrite was dissolved by shallowly-circulating meteoric water. Sulphate was reduced to $H_2S$ through bacterial sulphate reduction, using methane or hydrocarbons as the reductant and producing low $\delta^{13}C$ calcite.

4. Metal ratios in the hydrothermal fluids changed to Pb>>Zn, and biogenic sulphate reduction continued.

5. Methane-bearing fluids continued to enter the TZF and bacterial sulphate reduction became more important. The absence of metals and more oxygenated conditions led to the oxidation of hydrogen sulphide to form native sulphur.

6. Subaerial exposure of the diapir crest led to dissolution of halite by meteoric water and conversion of anhydrite to gypsum.

We conclude that, in the salt diapir environment, structural analysis, petrography, and isotopic analysis of carbon and sulphur can provide useful tools for Zn-Pb exploration.

ACKNOWLEDGEMENTS:

Support of this study by Fulbright Scholar Grant (2003/2004) to S. Bouhlel is gratefully acknowledged. We wish to think Pr. H. Belayouni (University of Tunis) for long time discussion on the Tunisian PDT Pb-Zn deposits.

REFERENCES

Bouhlel, S. 1993 Gîtologie, minéralogie et essai de modélisation des minéralisations de Pb-Zn-Sr-Ba-F-(S°) associées aux carbonates jurassiques et crétacés et aux diapirs triasiques (Tunisie septentrional) : *Unpubl. thesis, Doctorat D'Etat, Univ. de Tunis II,* pp293.

Bouhlel S. 2005 Carbonate-hosted Mississippi Valley-type Pb-Zn deposit in Tunisia (eastern Atlasic foreland belt). In *Mineral Deposit research : Meeting the global challenge. SGA* 3: 19-22

Chaari G., Belayouni H. and Soussi M. 2004 The Geodynamic and petroleum system of Jebel Gorra area, Dome Zone: New play concept for Northern Tunisia (Abstract). *The 9th Tunisian Petroleum Exploration and Production Conference. Tunis:* 16-17.

Rouvier, H., Perthuisot, V. and Mansouri, A., 1985, Pb-Zn deposits and salt-bearing diapirs in Southern Europe and North Africa: *Econ. Geol.,* 80: 666-687.

# Classification of low-temperature carbonate-hosted (MVT) Zn-Pb deposits

E. Schroll
*University of Vienna, Vienna, Austria*

ABSTRACT: Low-temperature hydrothermal sedimentary Zn-Pb deposits are divided into SEDEX type (hosted in siliclastic rocks) and MVT type deposits (hosted in carbonate rocks) without transitions between these two types. However, carbonate-hosted Zn-Pb deposits that form in the surface and near-surface do exist. Evidence for biogenic sulphate reduction at the place of ore formation supports a near-surface origin for some deposits. A new classification of carbonate-hosted MVT deposits is proposed in this paper, with respect to biogenic sulphate reduction and to special genetic groups of Zn-Pb mineralization.

KEYWORDS: lead, zinc, isotope geochemistry, Irish type, Alpine type, SEDEX

## 1 INTRODUCTION

In the past, a terminology of low-temperature Zn-Pb deposits was developed on the basis of regional knowledge of Zn-Pb deposits. In Northern America, in the Upper Mississippi Valley Zn-Pb province the term Mississippi Valley type (MVT) was introduced (Brown 1967). The Appalachian type (Hoagland 1976) was later included into this MVT type. In Europe, two types were distinguished: the Bleiberg-type (Maucher & Schneider, 1967), better known as Alpine type (APT; Maynard 1983), and the Irish type (IRT; Hitzman & Beaty, 1987; Wilkinson, 2003). This discussion about classification and terminology has contined since the Behre-Symposium 1967. However, recently the MVT classification became popular for describing *all* low-temperature Zn-Pb-deposits (Leach & Sangster, 2003; Leach *et al.*, 2005). However, the authors of a major review paper on sedimentary Zn-Pb-deposits (Leach *et al.* 2005) are aware of the difficulties of this classification. It is also important that geomicrobiology (Southam & Saunders, 2005) be integrated into any new classification.

## 2 DEFINITION

### 2.1 *Sedex*

The SEDEX (sedimenary exhalative) type is defined as tabular Zn-Pb-Ag deposits that contain laminated stratiform mineralization, hosted by shale, carbonate or organic-rich rocks. Igneous rocks are absent or volumetrically minor, and the deposits are formed in intra- and or epicratonic settings or at passive continental margins (Leach *et al* 2005). The physical and chemical properties of siliclastic rock series favour ore deposition on the sea floor and quartz is the common gangue mineral.

Generally, biogenic processes are thought to have a minor influence on ore precipitation in SEDEX environments except for distal mineralization. However, the term “exhalative” should be reserved to clearly volcanic processes. Therefore, substitution of “exhalative” by “extrusive” would be preferable.

Moreover, the use of SMS or SHMS (sedimentary massive ore or sedimentary-hosted massive) would be advantageous instead of the term SEDEX.

### 2.2 *MVT*

According to Leach *et al.* (2005), MVT deposits are characterized by the following: an epigenetic origin, lacking association with igneous rocks, mainly carbonate wall rocks, a simple mineral association (sphalerite, galena, iron sulphides, dolomite, calcite, minor barite

and rarely fluorite), occurrence on platform carbonate sequences at flanks of basins or foreland thrust belts, commonly strata-bound, locally stratiform, large ore districts, saline brines as ore fluids, temperatures of ore precipitation 75 to 200°C, tectonic control by faults and fractures, dissolution collapse breccias, lithological unconformities, coarserly crystalline to fine-grained sulphides, massive to disseminated, replacement and lesser space filling, dolomitization, and host rock dissolution and brecciation.

It would appear that Brown's (1970) historical conclusion that no single classification scheme can provide rigorous classification criteria is renewed by this definition.

## 3 DISCUSSION

The above-mentioned classification is exclusively descriptive and mainly focussed on the classic MVT deposits in the Ozark Province. The existence of deposits with extrusive character (SEDEX) is neglected. Although the physical and chemical properties of carbonate rock series diminish the chance that Zn-Pb deposits form on the sea floor this process cannot be doubted. Geochronological age dating is still problematic and has not proven very useful in the study of these deposits and the interpretation of age data is often hampered by post-mineralization (*e.g.* diagenetic) processes.

The discrimination of surface or near-surface deposition needs to be based on geological, mineralogical and textural evidence. Near-surface mineralization can be partly extrusive (*e.g.* Bleiberg, Schroll *et al.* 2006). Mineralizating systems may be long lasting. Near-surface mineralization is to be expected in miogeosynclines or in carbonate platforms.

The large number of "MVT-deposits" demands definition of subtypes. Each carbonate hosted province, *e.g.* classical MVTs in the Ozark Province, IRT or APT, is genetically inhomogeneous. Differences have been described among ore deposits in the MVT-Ozark Province (Leach 1994). The uneconomic Kildare Group is exceptional in the Irish Midlands (Hitzman & Beaty 1996). The Zn-Pb deposits in the Alpine Triassic show regional groupings and diversities, but economic deposits exhibit geochemical and isotopic similarities (Schroll 2005). However, detailed investigations based on geochemical and isotopic data, in addition to geological and mineralogical descriptions have shown the existence of more or less affiliated deposits within each group of carbonate-hosted Zn-Pb deposits. In other words a common denominator can be found for each group of deposits.

The trace elements contents and associations in the ores are not only of economic importance but are controlled by thje temperature of leaching and diversity of fluid-rock interactions. For example; the element association Ge, Cu, Ga, Ag, and Cd is typical for the MVT-Ozark Province, but not for all deposits that were classified as MVT by Leach *et al.* (2005). For instance, the above mentioned element association is found only in the Gorno district in the Alpine Triassic and all other ore deposits in this region are characterised by As, Ge and Tl (Schroll 2005).

The MVT definition of Leach *et al*. (2005) also emphasizes rare occurrences of fluorite in these deposits. However, in the Alpine Triassic deposits fluorite contents are highly variable; from geochemical background to ore grade values. The latter are characterised by fine-grained primary fluorite and concordant deposit geometries (Hein & Schneider 1985).

Lead isotopes are important indicators of the origin of lead and other metals, and they can also help to constrain palaeohydrogeological systems (Heijlen & Muchez, 2003). The sulphur isotope distribution should be another essential parameter for the classification of subtypes. Biogenic processes are also a characteristic feature of some subtypes formed in the low-temperature range. Micro-organisms are restricted to the surface and near-surface environment with biogenic processes being limited by the oil window and the coalification of organic matter. Hydrogen sulphide from sour gas also shows biogenic and non-biogenic characteristics (Machel *et al* 1995). The detection of remnants from sulphate reducing bacteria, fossil bacteria and micro-mineralization confirms that hydrogen sulphide was produced in place (Kucha *et al.* 2001, 2005; Schroll & Rantitsch 2005). Bacterial activity and open or closed system behaviour of sulphate reduction may also exist in surface-near cavity systems (*e.g.* in the Upper Silesian-Cracow province).

Brown (1967) observed that fluid inclusions in diagenetically re-crystallized mineral phases

are rare. In contrast, plentiful fluid inclusions are found in typical MVT deposits.

Table 1: Proposal for the classification of low-temperature Pb-Zn deposits (mostly below 250°C) hosted by carbonate rocks

| | |
|---|---|
| 1. | Epigenetic origin |
| 1.1 | Pre-burial settings in biogenic environment above oil window, in miogeosynclinal or platform setting |
| 1.1.1 | External ore sediments ± near-surface deposition (Alpine type (APT), Irish type (IRT), Appalachian type) |
| 1.1.2 | Pre-burial setting, strongly influenced by diagenesis ± metamorphism (Alpine Province) |
| 1.1.3 | Distinctly post-sedimentary (Upper-Silesian-Crakow type) |
| 1.2 | Burial settings in non-biogenic environment below oil window, mainly in platform setting |
| 1.2.1 | Subterraneous deposition of Pb-Zn, includin sandstone (Mississippi Valley type) |
| 1.2.2 | Subterraneous deposition of polymetallic ores containing germanium minerals (Kipushi type) |
| 2. | Syngenetic origin |
| | Uneconomic extensive ores in undisturbed carbonate rock series |
| 3 | Special affiliations |
| 3.1 | Affiliated with salt diapirism (to 1.1 and 1.2) |
| 3.2 | Affiliated with siliceous crust, hosted by palaeo-karstic unconformities characterized by carbonate and siliclastics rocks ( SC-type, to 1.2) |

Special subtypes of the MVT family are the polymetallic Kipushi-(or Tsumeb)-type (Höll et al. 2006), the diapire type (Kyle and Saunders 1996), the Siliceous-Crust (SC)-type (Brigo *et al.* 2001), and last but not least the uneconomic type of extensive ores in undisturbed carbonate rock series (Laznicka 1985). The Kipushi type is characterized by germanium thiosulphates, the diapire type by the immediate connection with halite-bearing evaporites, specific hydrogeological conditions and thermal history and the formation of a "siliceous crust- type" by anomalous silification caused by mobilization of silica from clastic sediments. The "extensive ore type" includes lateral secretion origin on various scale.

## 3 CONCLUSION

These comments are intended aimed at finding common denominators in the complex system of carbonate-hosted Zn-Pb deposits. A comprehensive classification should be based on descriptive facts and data and avoid geographic terminology. Based on the above discussion, a proposal is made to classify low-temperature carbonate-hosted Zn-Pb deposits in Table 1.

## ACKNOWLEDGEMENTS

I am grateful to H. Kucha for discussion and his input in various ÖAW projects. The Austrian Academy of Sciences (ÖAW) supported these projects through grants of the Kommission für Grundlagen der Mineralrohstoffforschung. J.G. Raith is thanked for improving the English.

## REFERENCES

Brigo L, Gamana G, Rhodigera F., Potenza, R. (2001): Carbonate-hosted siliceous.crust type mineralisation of Carnic Alps (Italy, Austria). *Ore Geology Reviews,* 12: 199-214.

Brown JS (1970): Mississippi Valley type lead-zinc ores. A review and sequel to the "Behre Symposium". *Mineralium Deposita*, 5:103-119.

Heijlen W, Muchez Ph (2003) Paleohydrological and geodynamic framework of carbonate-hosted Zn-Pb mineralization in Europe and North America: Insights from fluid composition and Pb isotope systematics. In: Eliopoulis D et al. (eds): *Mineral Exploration and Sustainable Development.* Vol. 2, pp 681-684, Millpress, Rotterdam.

Hein UF, Schneider H-J (1985): Fluorine anomalies accompanying the Alpine Pb-Zn deposits compared to the geochemistry of their fluorites. In: Schneider H-J (ed): Mineral deposits of the Alps and the Alpine epoch in Europe. *Proceedings IV. ISMIDA 1981, SGA Spec. Publ. 3,* 198-212, Springer, Berlin-Heidelberg.

Heyl AV (1967: Some aspects of genesis of stratiforme lead-zinc-baryte-fluorite deposits in the United States. In: Brown, JS (ed): Genesis of stratiform lead-zinc-barite-fluorite deposits in carbonate rocks (the so-called Mississippi Valley type deposits), *Econ. Geol. Monogr.* 3, 20-32, Econ. Geol. Publ., Lancaster.

Hitzman MW, Beaty DW (1996): The Irish Zn-Pb- (Ba) orefield. In: Sangster DF (ed): Carbonate-hosted lead-zinc deposits *Soc. Econ. Geol. Special Paper* 4, 112-143, Soc. Econ . Geologists, Littleton, 1997.

Hoaghland AD (1976): Appalachian zinc-lead deposits. In: Wolf KH (ed):*Handbook of stratabound and stratiform ore deposits II. Regional studies and specific deposits,* vol. 6, Elsevier, Amsterdam, pp 497-534.

Höll R, Kling M, Schroll E (2006): Metallogenesis of germanium – a review. *Ore Geology Reviews* www.elsevier,com/locate/oregeorev), 36 pp.

Kucha H, Schroll E, Stumpfl EF (2001): Direct evidence for bacterial sulphur reduction in Bleiberg-type

deposits. In: Piestrzysjki A. et al. (eds): *Mineral Deposits at the Beginning of the 21th Century,* 149–152, Swetz & Zeitlinger Publ., Lisse 2001.

Kucha H, Schroll E, Stumpfl EF (2005): Fossil sulphate-reducing bacteria in the Bleiberg lead-zinc deposit, Austria. *Mineralium Deposita,* 40: 123–126.

Laznicka P (1985): *Empirical metallogeny. Vol. 1 Part A*, Elsevier, Amsterdam, 1002 pp.

Leach, DL (1994): Genesis of the Ozark Mississippi Valley type Metallogenetic Province, Missouri, Arkansas, Oklahoma, USA. In: Fontboté L, Boni M (eds). *Sediment hosted Zn-Pb ores,* pp. 104-138, Springer, Berlin-Heidelberg- New York.

Leach DL, Bechstädt Th, Boni M, Zeeh S (2003): Triassic-hosted MVT Zn-Pb ores of Poland, Slovakia and Italy. In: Kelly JG et al. (eds.):*Europe´s major base metal de-posits,* 169-213, Irish Assoc. Econ. Geol., Dublin.

Leach DL, Sangster F, Kelley KD, Large RR, Garven G, Allen CR (2005): Sediment-hosted lead-zinc deposits. *One Hundredth Anniversary Volume,* 561-608, Soc. Econ. Geologists, Littleton.

Machel HG (2001): Bacterial and thermochemical sulfate reduction in diagenetic settings *Sedimentary Geology*, 140: 143-175.

Maucher A, Schneider H-J (1967): The Alpine lead-zinc ores. In: Brown JS (ed): Genesis of stratiform lead-zinc-barite-fluorite deposits in carbonate rocks (the so-called Mississippi Valley type deposits), *Econ. Geol. Monogr.* 3, 71-89, Econ. Geol. Publ., Lancaster.

Maynard, J. B. (1983): *Geochemistry of sedimentary ore deposits.* Springer, New York-Heidelberg-Berlin, 305 pp.

Schroll, E., Rantitsch, G. (2005): Sulfur isotope patterns in the Bleiberg deposit (Eastern Alps) and their implications for genetically affiliated deposits. *Mineralogy and Petrology* 148: 1-18.

Schroll E (2005): Alpine type Pb-Zn-deposits (APT) hosted by Triassic carbonate rocks. In: Mao I and Bierlein FP (eds): *Mineral Deposits Research: Meeting the Global Challenge,* Vol 1, 175–178, Springer, Berlin- Heidelberg- New York.

Schroll E, Köppel V, Cerny I (2006): Isotopic and chemical data from the Pb-Zn deposit Bleiberg (Austria) – constraints on the age of mineralization. *Mineralogy and Petrology,* 86: 129-156.

Southam G, Saunders A (2005): The microbiology of ore deposits. *Economic Geology*, 100: 1067-2084.

Wilkinson JJ (2003): On diagenesis, dolomitisation and mineralization in the Irish Zn-Pb orefield. *Mineralium Deposita,* 38: 968-983.

# Characterisation of colloform layering in primary sulphides using electron backscatter diffraction and S isotope studies

C.D. Barrie, A.P. Boyle & D.J. Prior
*Department of Earth and Ocean Sciences, University of Liverpool, Liverpool, L69 3GP, UK*

A.J. Boyce
*S.U.E.R.C., Scottish Enterprise Technology Park, Rankine Avenue, East Kilbride, Glasgow, G75 OQF, UK*

J.J. Wilkinson
*Department of Earth Science and Engineering, Imperial College, London, SW7 2AZ, UK*

ABSTRACT: Colloform textures are abundant in nature, particularly in ore deposits. How do colloforms develop through time, and what are the environmental controls and possible mechanisms of formation? Our studies of electron backscatter diffraction (EBSD) combined with sulphur isotope analyses address these questions. A sample of colloform sphalerite from the Galmoy deposit in Ireland, which shows dramatic positive and negative variation in sulphur isotopes across the layers, also reveals that the crystallographic preferred orientation (CPO) of individual layers varies. Initial results suggest that where layers have a positive $\delta^{34}S$ signature they develop either a <100> or <110> CPO whereas layers with a negative $\delta^{34}S$ will develop a <111> CPO. This suggests that environmental factors may play an important role in controlling preferred crystal growth development of sulphide minerals within colloform layers.

KEYWORDS: electron backscatter diffraction, colloform, Galmoy, crystallographic preferred orientation, S-Isotopes

## 1 INTRODUCTION

Pyrite often forms primary depositional structures involving the aggregation of microcrystals. Ohfuji *et al*. (2005) documented evidence for some pyrite framboids achieving their raspberry-shape forms by self-organisation of the microcrystals. Wilkin *et al,* (1996) suggested variations in microcrystal size distribution relative to the host framboid diameter reflected differences in redox conditions, leading to wide use of pyrite framboids as palaeoenvironmental indicators. Freitag *et al.* (2004) found evidence for crystallographic organisation within layers of a pyrite colloform involving <100> and <110> preferred orientation pyrite textures associated with microcrystal size variations, raising the possibility that there may be a relationship between crystallographic self-organisation and environmental factors such as redox state. Unlike framboids, colloforms have not been used as palaeoenvironmental indicators, but they are potentially much more interesting because they have the potential to preserve a sequence of conditions in their layers rather than the single snapshot given by a framboid.

To test the potential of these structures we have systematically collected petrographic, crystallographic, chemical and *in situ* laser S isotope data. Here, we present the results of the first such study using a sample from the Galmoy ore-body in Ireland. The sample is dominated by a large sphalerite colloform with local grains of galena and pyrite (Figure 1).

## 2 METHODS

*In situ* laser S isotope analyses were carried out using standard techniques on a polished block (Wagner *et al*, 2002; Figure 1). For electron backscatter diffraction (EBSD) analysis, the sample was SYTON$^{TM}$ -polished on a polyurethane lap for 1 hour, to remove any surface damage caused by the mechanical polishing, and then given a thin carbon coat to minimize charging effects and maximize the crystallographic signal.

All crystallographic orientation data were collected by EBSD at Liverpool University us-

ing a CamScan X500 crystal probe SEM with a thermionic field emission gun. (Ohfuji *et al*, 2005). EBSD data was collected on rectilinear grids with a typical spacing of 2-5μm to produce crystallographic orientation maps. Post processing allows of EBSD allows calculation of grain sizes, shapes and shape orientations as well as CPO's. All of the CPO data were plotted on pole figures as 1 point per individual grain in order to remove the biased effects which large grains with many data points would have upon the data set.

## 3 RESULTS

### 3.1 *S-Isotope and Fe-Zn analysis*

S-isotope analysis along two transects (ST1 and ST2 in Figure 1) of the sphalerite colloform demonstrates consistent within-layer $\delta^{34}S$ signatures (Figure 2), which vary from a positive $\delta^{34}S$ at the basal layer (first formed part), through a highly negative $\delta^{34}S$ zone related to the very pale layer (figure 1) to another positive $\delta^{34}S$ zone and then entering another negative $\delta^{34}S$ at the top layer (youngest). The Fe:Zn concentration shows no associated variation; there is negligible or no Fe present within the majority of sphalerite layers. The exception is the topmost negative $\delta^{34}S$ zone 4 (Figure 2) where Fe content increases to a maximum of 7.5%.

### 3.2 *Crystallographic and textural analysis*

Ten layers have been investigated in detail for textural and crystallographic variations. Sphalerite microcrystals in the colloform are subhedral and range in size from 14 to 85μm. They tend to be elongate oriented normal to colloform layering with average shape ratios of about 2:1. Each layer is characterized by a particular grain size (Figure 2) between fine grained (<20μm) through relatively coarse grained (>40μm) to coarse (~85μm). Boundaries between individual sphalerite layers (Figure 2B, C, and D) are sharp and often marked by a grain size change. Grain size is relatively coarse in zone 1, the base of zone 3, and the layer in zone 4 (Figure 2).

Sphalerite crystallographic orientation also varies along the transect with four different types of CPO developed: <100>, <111>, <110> or no preferred directions (see pole figures in Figure 3i, ii, iii for examples). These CPO textures are defined by development of a common crystallographic axis (arrows in Figure 3) with the other axes being distributed in girdles around the common one. For example, in Figure 3i there is a common <111> axis at the top of each pole figure about which all of the other <111> axes and the <100> and <110> axes appear rotated to form girdles. This is referred to as a <111> CPO. Similar CPO relationships occur for <100> and <110> axes in other layers, though <100> tends to be weaker developed (Figure 3ii) than the other two and is detected principally by the lack of a CPO in either <111> or <110>. The clearest CPO is that developed in the <110> direction (Figure 3iii) in a fine grained sphalerite layer (<20μm). Figure 2 summarises the distribution of CPOs with each set of layered zones, as well as grain size and $\delta^{34}S$.

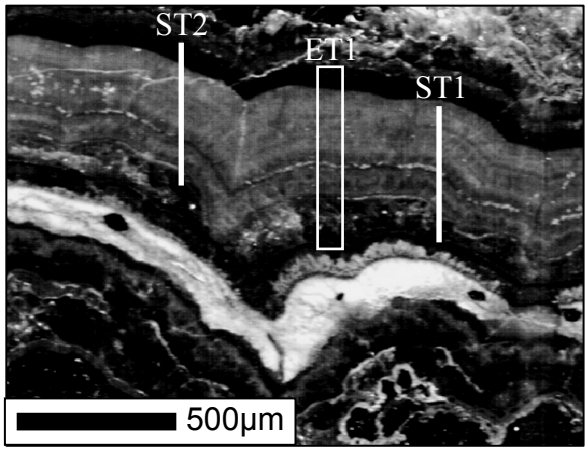


Figure 1: Incident light Image of the Galmoy sample. ST1 and ST2 represent S-isotope analysis transects and ET1 the EBSD analysis transect

## 4 DISCUSSION

The results demonstrate that each layer is characterized by a particular grain size, crystallographic orientation and $\delta^{34}S$ signature (Figure 2). Previous work on the Irish ore deposits (Wilkinson *et al*, 2005) has suggested that there is a dual source for the sulphur forming the ore deposits. Where the $\delta^{34}S$ is lower than -3 this is suggested to have resulted from a bacteriogenic source of the sulphur whereas a $\delta^{34}S$ more positive than this suggests a hydrothermal source for the sulphur. Our S isotope results (Figure 2) show significant variation from a highly negative to positive $\delta^{34}S$. They indicate that colloform zone 2 formed using bacteriogenic sulphide, layers in zone 3 with hydrothermal sulphide and zone 4 a return to bacteriogenic processes. These broad shifts also correlate with sphalerite CPO: negative $\delta^{34}S$ signature is

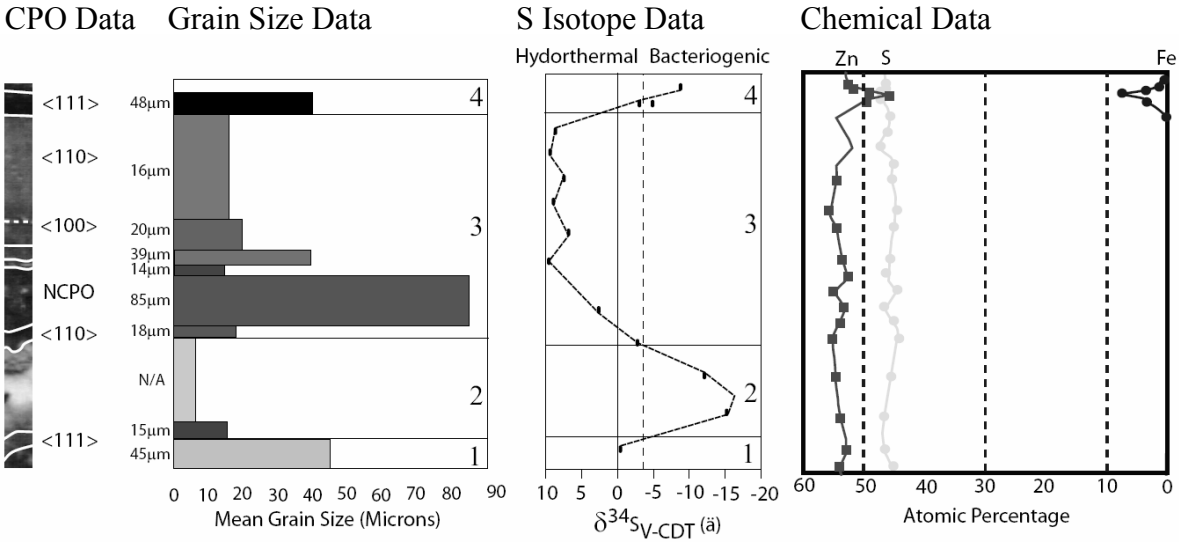


Figure 2: Summary of CPO, grain size, S-isotope and chemical data gathered across all of the layers analysed in the Galmoy sample. Data is split up into 4 zones corresponding to positive and negative S isotope signatures, NCPO represents a random orientation of grains.

associated with the <111> CPO, whereas positive $\delta^{34}S$ signature is associated with either <100> or <110> CPO. However, some layers do not show a preferred orientation (NCPO in Figure 2) and so other factors must play a role in CPO development. Similarly, there is no obvious relationship between grain size and either CPO or $\delta^{34}S$, although our results indicate zone 2 hosts the lightest $\delta^{34}S$ and the smallest crystals (also the most porous texture). Apart from zone 4, there is no significant variation in Fe:Zn ratio. The correlation of <111> CPOs with negative $\delta^{34}S$ suggest there is some positive relationship involving sulphur sources, perhaps echoing Chekroun *et al* (2004) who documented changing carbonate crystal morphology associated with bacteria.

The most likely situation, from current results, suggests that the sulphur source may be a significant control on the preferred orientation which develops, but that there have to be some other factors. The independence of the grain size changes suggest factors such as crystal morphology and growth rate as well as supply rate of sulphur and zinc may play an important role, and perhaps also affect CPO development.

## 5 CONCLUSIONS

The colloform sphalerite sample analysed records a series of events in terms of changing $\delta^{34}S$, grain size and crystallographic orientation. $\delta^{34}S$ data suggest a relatively simple history involving switches between a hydrothermal and a bacteriogenic sulphur source. There appears to be a correlation between some aspects of the crystallographic orientation of layers with this switching of sulphur sources. However, grain size variations do not exhibit similar correlation suggesting the history was more complex than the $\delta^{34}S$ data alone suggest. It has been suggested that gold distribution within pyrite grains is related to development of particular crystal orientations (Chouinard *et al*, 2005), thus analysis of layered colloforms and determination of the crystal preferred orientations developed may also provide a useful tool in understanding gold and other trace element distribution within ore bodies. This work continues.

## ACKNOWLEDGEMENTS

This work forms part of the Ph.D. project of C.D.B., which is funded by the University of Liverpool. Isotope analysis was carried out at the Scottish Universities Environmental Research Centre (S.U.E.R.C.) and is funded by Natural Environment Research Council facilities grant IP/907/0506.

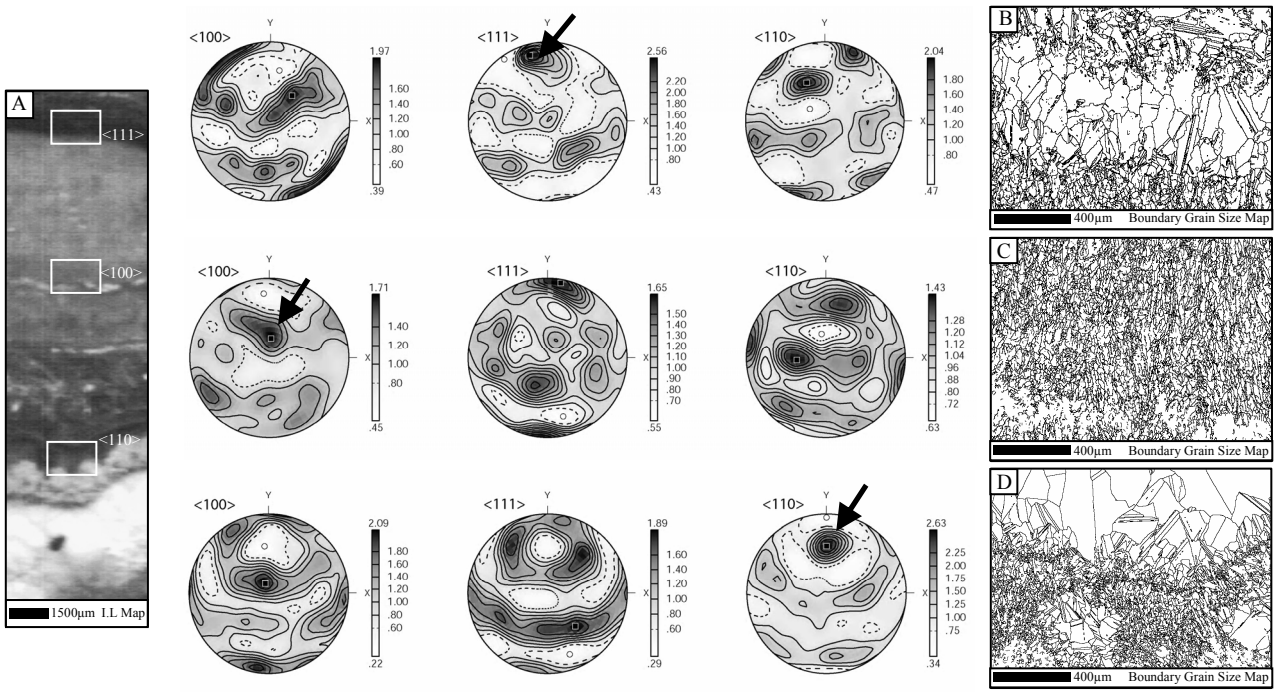


Figure 3: Summary of Crystallographic analysis. A. Incident light Image of area mapped with EBSD, boxes highlight layers which pole figures are shown for; i: <110> CPO, ii: <100> CPO and iii: <111> CPO. Arrows highlight crystal growth axis. B,C and D.: Boundary maps highlighting grain size changes between layers

## REFERENCES


Chekroun, K.B., Rodriguez-Navarro, C., Gonzalez-Munoz, M.T., Arias, J.M., Cultrone, G. and Rodriguez-Gallego, M., 2004, Precipitation and growth morphology of calcium carbonate induced by myxococcus xanthus: implications for recognition of bacterial carbonates, *Journal of Sedimentary Research* 74, 868-876

Chouinard, A., Paquette, J. and Williams-Jones, A., 2005, Crystallographic controls on trace element incorporation in auriferous pyrite from the pascua epithermal high-sulfidation deposit, Chile-Argentina: *The Canadian Mineralogist* 43, 951-963

Freitag, K., Boyle, A.P., Nelson, E., Hitzman, M., Churchill, J and Lopez-Pedrosa, M., 2004, The use of electron backscatter diffraction and orientation contrast imaging as tools for sulphide textural studies: example from the greens creek deposit (Alaska). *Mineralium Deposita* 39, 103-113

Ohfuji, H., Boyle, A.P., Prior, D.J., Rickard, D., 2005, Structure of framboidal pyrite: An electron backscatter diffraction study. American Mineralogist 90, 1693-1704

Wagner, T., Boyce, A.J. and Fallick, A.E., 2002, Laser combustion analysis of $\delta^{34}S$ of sulfosalt minerals: determination of the fractionation systematics and some crystal-chemical considerations. *Geochimica Cosmochimica Acta* 66, 2855-2863

Wilkin, R.T., Barnes, H.L and Brantley, S.L., 1996, The size distribution of framboidal pyrite in modern sediments: An indicator of redox conditions. *Geochimica et Cosmochimica Acta* 60, 3897-3912

Wilkinson, JJ, Eyre, SL, Boyce, AJ, 2005, Ore-forming processes in Irish-type carbonate-hosted Zn-Pb deposits: Evidence from mineralogy, chemistry, and isotopic composition of sulfides at the Lisheen mine, *Econ Geol.* 100, 63 – 86

# DATING MINERAL DEPOSITS

EDITED BY:

DAVE SYMONS

PATRICK WILLIAMS

# Concordant ages for the carbonate-hosted Kipushi base metal deposit from direct Rb-Sr and Re-Os dating of sulphides

Jens Schneider
*Ore Fluids Research Group, K.U. Leuven, Belgium*

Frank Melcher
*Federal Institute for Geosciences and Natural Resources (BGR), Hannover, Germany*

Michael Brauns
*Institut für Geowissenschaften und Lithosphärenforschung, JLU Giessen, Germany*

ABSTRACT: Concordant ages of 451 Ma for the carbonate-hosted Kipushi base metal (+ Ge, Ag) deposit in the Neoproterozoic Lufilian Arc, DRC (Africa), obtained from direct Rb-Sr and Re-Os dating of epigenetic Zn-Cu-Ge sulphides, are reported. The homogeneous Pb isotopic composition of these sulphides indicates that both Cu-Ge- and Zn-rich orebodies of the Kipushi deposit formed from the same mineralizing fluid system. The 451 Ma age gives evidence that the ore-forming solutions did not evolve from metamorphogenic fluids mobilised syntectonically during the Pan-African-Lufilian orogeny but rather generated in a postorogenic, extensional setting prevailing in the late Ordovician. The concordant Re-Os and Rb-Sr ages obtained in this study provide independent proof of the significance of direct Rb-Sr dating of sphalerite which has been repeatedly questioned.

KEYWORDS: Kipushi base metal deposit, geochronology, Rb-Sr, Re-Os, Copperbelt

## 1 INTRODUCTION

Precise constraints on the timing of mineralization are of fundamental importance in understanding the genesis of hydrothermal base metal deposits. Among the few available isotope geochronological methods applicable to sulphide deposits, Rb-Sr dating of sphalerite and Re-Os dating of Cu-Fe sulphides have attained increasing attractivity as these techniques allow for direct dating of ore-forming constituents. However, it has been repeatedly suspected that detrital silicate inclusions control the Rb-Sr system of sphalerite, thereby casting doubt on the reliability and significance of the method (*e.g.* Bradley *et al.* 2004).

Here we present a comparative geochronological study on the giant carbonate-hosted Kipushi base metal deposit, Democratic Republic of Congo (DRC), Africa, that involves direct Re-Os and Rb-Sr dating of sulphides from epigenetic, Cu-Ge- and Zn-dominated orebodies. Applying two different isotopic dating methods to sulphide ore minerals from the same deposit will provide internal, independent control on the ages so obtained. This is supported by complementary Pb isotope analyses of the dated sulphides that will help to assess their paragenetic relationship.

## 2 GEOLOGY

The world-class Kipushi base-metal deposit is located in the southeast DRC within the northern extension of the Central African (Zambian) Copperbelt. Kipushi is the largest among a number of Zn-Cu-Pb deposits situated in the Copperbelt, original ore reserves are estimated to have been 70 Mt @ 8.8% Zn, 4.8% Cu, 0.5% Pb, 160 g/t Ag (Höll *et al.*, 2007), with sphalerite, bornite and galena being the principle ore minerals. Abundant germanium sulphides such as reniérite make the Kipushi deposit one of the largest known Ge anomalies in the world, production between 1925 and 1986 amounted to *ca.* 120 t Ge. The geology and ore mineralization of the Kipushi deposit has been described in detail by De Vos *et al.* (1974), Intiomale & Oosterbosch (1974) and De Magneé & Francois (1988). The host rocks

belong to the Katangan system, a Neoproterozoic, > 9 km thick marine succession in the foreland of the Pan-African Lufilian Arc (Fig. 1) which has been subdivided into the Roan and Kundelungu Supergroups. The Kipushi deposit is situated in the upper Katangan Kundelungu Supergroup (760-500 Ma) that consists of alternating carbonate rocks, shales, sandstones, and diamictites. The orebodies at Kipushi occur within the Kipushi anticline along the Kipushi fault zone at the contact between Kundelungu sediments with a breccia body that occupies the core of the Kipushi anticline and contains megaclasts and fragments derived from Roan/Kundelungu units. Economic Zn-Cu-Pb sulphide mineralization is epigenetic and forms (i) discordant bodies (Cu+Zn *ca*. 20%) filling cavities and voids in the breccia body and adjacent Kundelungu dolomites along the Kipushi fault, and (ii) Zn-rich (*ca.* 40%), "pipe-like" structures in massive, upper Kundelungu carbonate rocks. Broadly stratiform horizons of Cu-poor (*ca*. 2%) ores are confined to both sides of the boundary between upper and lower Kundelungu strata (De Magneé & Francois 1988).

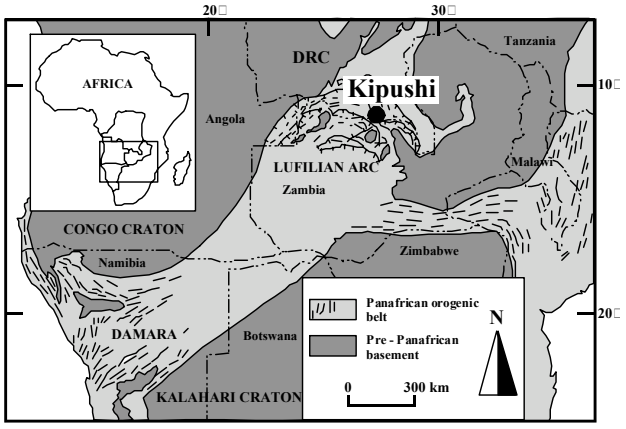


Figure 1. Map of southern central Africa showing major geotectonic units and location of the Kipushi deposit (modified after Kamona *et al*. 1996).

Various contrasting models have been suggested for the genesis of the Kipushi deposit. Using structural criteria, Kampunzu *et al.* (1998) favoured a synorogenic ore emplacement during deformation in the Lufilian Arc (*ca.* 560-550 Ma) from tectonic brines and interpreted ore Pb isotope data from the literature to reflect binary mixing of distinct crustal Pb components. Conversely, de Magneé & Francois (1988) suggested a postorogenic formation of the deposit based on galena Pb-Pb model ages of *ca*. 425 Ma and by reference to U-Pb ages in the range of 525-500 Ma obtained for epigenetic uraninite from Copperbelt mineralization. Walraven & Chabu (1994) and Kamona *et al.* (1999) refined these estimates and interpreted galena Pb-Pb model ages of *ca*. 455 Ma to reflect the age of mineralization at Kipushi, in agreement with U-Pb zircon ages of 458-427 Ma for syenites located farther south. From galena Pb isotope data, Kamona *et al*. (1999) suspected a significant mantle component in the Kipushi ore lead.

## 3 SAMPLING AND METHODS

Two cores from drillholes 1270 and 787 (stored at BGR Hannover, Germany) that intersect economic-grade, Zn- and Cu-Ge-rich portions of the Kipushi deposit, respectively, were sampled at different depths for this study. All samples were crushed, sieved (grain size interval 400-250 μm), and precleaned in deionized water. For Rb-Sr isotopic analysis, four sphalerite separates and one bornite sample were produced by handpicking of material extracted from core 1270, whereas the Re-Os work was performed on two reniérite and two bornite separates handpicked from samples of drillcore 787. Sulphide sample residues from crush-leach experiments were analysed for Rb-Sr in this study, details on sample preparation are given in Schneider et al. (this volume). Pb was extracted from these samples subsequently to Rb-Sr chemical separation using 1 ml HCl 6 N.

The procedures for Re-Os isotopic analysis are fully described in Brauns (2001) and Woodhead & Brauns (2004) and involved Carius tube digestion of reniérite and bornite separates spiked with a mixed $^{185}Re$-$^{190}Os$ tracer using inverse aqua regia. Osmium as the $OsO_4$ species was then directly distilled from the Carius tubes, condensed on *ca.* 2 μl of chilled sulfuric acid and finally collected in 0.5 ml of 7 N HBr. Rhenium was recovered from the remaining solutions with 0.5 N - 4 N $HNO_3$ on anion exchange columns. Osmium was further purified using microdistillation techniques. Lead was separated from aliquots of the sample solutions used for Re chemistry.

All isotopic measurements were performed on FINNIGAN MAT 261/262 mass spectrometers. Sr, Rb, Pb and Re were measured in static multicollection mode on Faraday detectors us-

ing P-TIMS and N-TIMS methods, respectively, whereas Os isotope ratios were determined by N-TIMS using an ion-counting system. Details on mass spectrometry techniques and error propagation procedures are given in Schneider *et al.* (2003) and Woodhead & Brauns (2004). Total procedural blanks amounted to 10-50 pg Sr, 5 pg Rb, 0.1 pg Os, and 5 pg Re. All data were blank-corrected. Pb isotope ratios were corrected for instrumental mass fractionation using a mean discrimination factor of 0.085 ± 0.006 (2σ) %/[amu]. Isochron regressions were calculated after Ludwig (2003) using the ISOPLOT/Ex version 3.00 program and errors on the ages are quoted at the 2σ level.

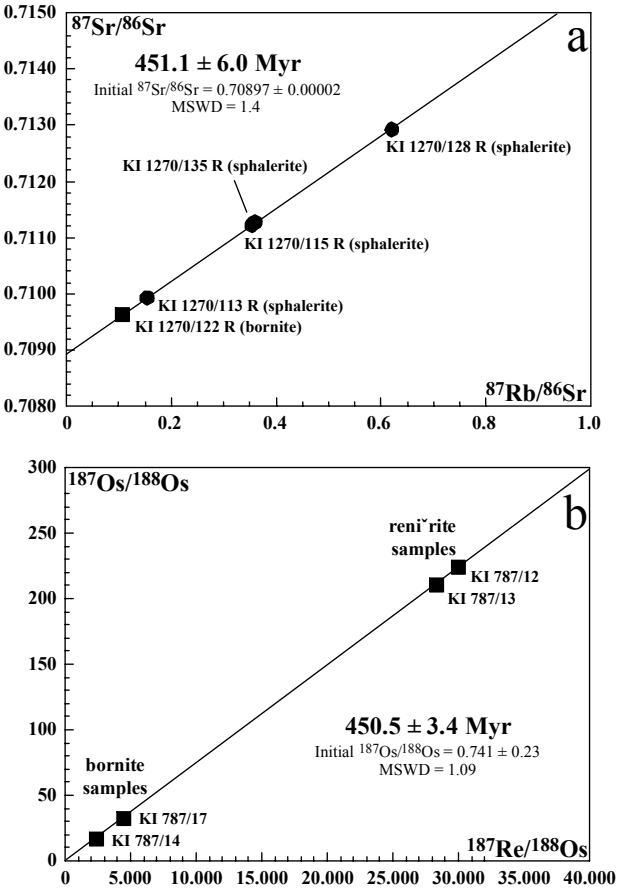


Figure 2. (a) Rb-Sr isochron diagram for crushed sphalerite and bornite residues, (b) Re-Os isochron diagram for bornite and reniérite samples.

## 4 RESULTS AND DISCUSSION

The crushed sulphide residues from drillcore 1270 area have variable $^{87}Rb/^{86}Sr$ ratios between 0.10 and 0.62 and $^{87}Sr/^{86}Sr$ ratios ranging from 0.7099 to 0.7129. The elemental concentrations are 1.9-22.4 ppb Rb and 8.8-275.5 ppb Sr, respectively. Bornite and reniérite samples from drillcore 787 have Re = 17.6-49.4 ppb and Os = 87-256 ppt, resulting in high $^{187}Re/^{188}Os$ ratios between 2,255 and 29,820 and highly radiogenic $^{187}Os/^{188}Os$ ratios ranging from 32.8 to 224. Both data sets yield well-defined Rb-Sr and Re-Os isochron regressions (MSWD = 1.4 and 1.09) giving concordant ages of 451.1 ± 6 and 450.5 ± 3.4 Ma, respectively, within errors (Fig. 2). No linear data arrangement is observed in the $^{87}Sr/^{86}Sr$ vs. 1/Sr space (not shown), indicating that the line in Fig. 2a is not a pseudo-isochron produced by binary mixing of distinct Sr components. Bornite has the lowest Rb-Sr isotope ratios of the sample set. The same applies to the Re-Os isotope systematics, where reniérite samples show much higher $^{187}Re/^{188}Os$ and radiogenic $^{187}Os/^{188}Os$ ratios (Fig. 2b). Fig. 3 shows a comparative Pb-Pb diagram for all analysed sulphide samples and literature data for Kipushi galena (Walraven & Chabu 1994, Kamona *et al.* 1999).

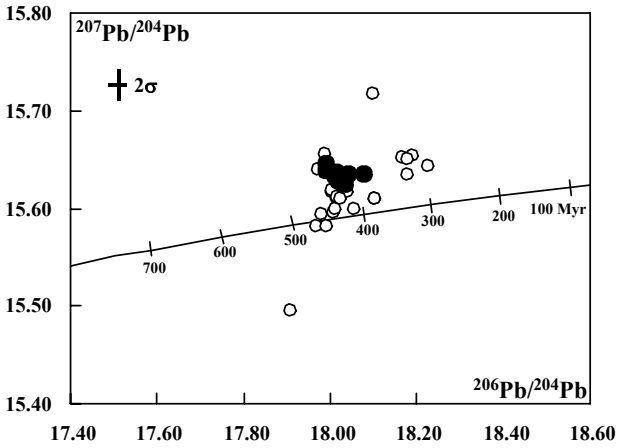


Figure 3. Pb-Pb diagram showing all sulphides analysed for Rb-Sr and Re-Os in this study (filled circles) and literature data for Kipushi sulphides (see text for references). Growth curve shown represents average crustal lead evolution after Stacey & Kramers (1975)

The sulphide samples depicted in Fig 2. display remarkably uniform Pb isotope signatures, indicating that the Cu-Ge- and Zn-dominated portions of the Kipushi deposit are paragenetic and have formed contemporaneously from the same fluid system. Their lead is of crustal origin and shows no indication of a mantle component. Considering the slightly enhanced $^{207}Pb/^{204}Pb$ ratios, the Pb partly evolved in ancient cratonic reservoirs. The Pb isotope population of our sample largely corresponds to the mean of the depicted literature data. We therefore suspect that the linear trends observed in

these data reflect instrumental mass fractionation rather than mixing of distinct Pb components.

## 5 CONCLUSIONS

Economic-grade sulphides from the Kipushi Zn-Cu-Pb (+Ge) deposit have been dated directly by two independent isotopic methods for the first time, yielding a concordant age of 451 Ma. This age is in agreement with previously published galena Pb-Pb model ages but much more precise and based on the analysis of complete parent/daughter isotope systems. Our study demonstrates that both Zn- and Cu-Ge-dominated orebodies at Kipushi formed during late Ordovician extension, clearly refuting models of mineralization by tectonic brines during the Pan-African-Lufilian orogeny. Moreover, the concordant Re-Os and Rb-Sr ages obtained in this study provide independent proof of the accuracy and significance of direct Rb-Sr dating of sphalerite.

## ACKNOWLEDGEMENTS

This study was supported by BGR Hannover, Germany, through Hochschulvergabeprojekt Nr. 80, SP "Metalle kurzer Reichweite".

## REFERENCES

Bradley DC, Leach DL, Symons D, Emsbo P, Premo W, Breit G, Sangster DF (2004) Reply to discussion on „Tectonic controls of Mississippi Valley-type lead-zinc mineralization in orogenic forelands“ by S.E. Kesler, J.T. Christensen, R.D. Hagni, W. Heijlen, J.R. Kyle, K.C. Misra, P. Muchez and R, van der Voo, *Mineralium Deposita*. 39: pp 515-519

Brauns CM (2001) A rapid, low-blank technique for the extraction of osmium from geological samples. *Chem Geol* 176: pp 379-384

De Magneé I, Francois A (1988) The origin of the Kipushi (Cu, Zn, Pb) deposit in direct relation with a Proterozoic salt diapir. Copperbelt of Central Africa, Shaba, Republic of Zaire. In: Friedrich GH, Herzig PM (eds) *Base metal sulphide deposits in sedimentary and volcanic environments.* Springer-Verlag, Berlin Heidelberg New York, pp 74-93

De Vos W, Viaene W, Moreau J, Wautier J (1974) Minéralogie du gisement de Kipushi Shaba, Zaire. In: Bartholomé P (ed) Gisements stratiformes et provinces cupriféres. *Centen Soc Géol Belg,* Liège, pp 165-183

Höll, R, Kling M, Schroll E (2007) Metallogenesis of germanium - a review. *Ore Geol Rev*: in press

Intiomale M, Oosterbosch R (1974) Géologie et Géochemie du gisement de Kipushi Zaire. In: Bartholomé P (ed) Gisements stratiformes et provinces cupriféres. *Centen Soc Géol Belg, Liège*, pp 123-164

Kamona AF, Leveque J, Friedrich G, Haack U (1999) Lead isotopes of the carbonate-hosted Kabwe, Tsumeb, and Kipushi Pb-Zn-Cu sulphide deposits in relation to Pan-African orogenesis in the Damaran-Lufilian Fold Belt of Central Africa. *Mineral Deposita* 34: pp 273-283

Kampunzu AB, Wendorff M, Kruger FJ, Intiomale MM (1998) Pb isotopic ages of sediment-hosted Pb-Zn mineralisation mineralization in the Neoproterozoic Copperbelt of Zambia and Democratic Republic of Congo (ex-Zaire): re-evaluation and implications. *Chron Rech Min* 530: pp 55- 61

Ludwig KR 2003, Isoplot/Ex version 3.00. A geochronological toolkit for Microsoft Excel.: *Berkeley Geochron Center Spec Pub* 4: pp 1-43

Schneider J, Haack U, Stedingk K (2003) Rb-Sr dating of epithermal vein mineralization stages in the eastern Harz Mts. (Germany) by paleo-mixing lines. *Geochim Cosmochim Acta* 67: pp 1803-1819

Stacey JS, Kramers JD (1975) Approximation of terrestrial lead isotope evolution by a two-stage model. *Earth Planet Sci Lett* 26: pp 207-221

Walraven F, Chabu M (1994) Pb-isotopic constraints on base metal mineralization at Kipushi (Southeastern Zaire). *J Afr Earth Sci* 18: pp 73-82

Woodhead J, Brauns M (2004) Current limitations to the understanding of Re–Os behaviour in subduction systems, with an example from New Britain. *Earth Planet Sci Lett* 221: pp 309-323

# Timing of gold mineralization at Kalgoorlie, Western Australia

Noreen M. Vielreicher, David I. Groves & Neal J. McNaughton
*Centre forExploration Targeting, The University of Western Australia, 35 Stirling Highway, Western Australia, 6009*

Lawrence W. Snee
*USGS, Denver, Colorado 80225, USA*

ABSTRACT: New geochronological data from hydrothermal phosphate minerals indicate that the majority of gold mineralization at Kalgoorlie, including Fimiston-, Oroya- and some Charlotte-style lodes, are broadly the same age at 2.65-2.63 Ga. This giant ore system formed after *c*. 2.69 Ga basic magmatism, intrusion of the Golden Mile Dolerite sill at *c.* 2680-2675Ma, as well as deposition of volcanosedimentary Black Flag Beds and coeval felsic porphyry dyke intrusion at *c*. 2.67 Ga. Mineralization overlapped but outlasted hornblende-phyric and lamprophye dyke intrusion and peak regional metamorphism at *c*. 2.65-2.64 Ga. It was broadly coeval with both ductile and brittle deformation, which were probably related to a prolonged regional deformation event that was accompanied by dynamic mineral growth. Subsequent localised brittle faulting was accompanied by hydrothermal activity that led to some late Charlotte-style gold mineralization after 2.62 Ga.

KEYWORDS: SHRIMP geochronology, orogenic gold, Golden Mile, Kalgoorlie

## 1 INTRODUCTION

The Kalgoorlie operations comprise the Fimiston (or Super) Pit and Mt Charlotte underground mine at Kalgoorlie-Boulder, ~600km east of Perth, in the Yilgarn craton, Western Australia. The giant ore system includes >2,000 lodes in an area of >5km strike-length, 2km width and >1km depth, known as the Golden Mile. More than 50Moz gold has been mined since discovery in 1893. About 9.788Moz gold remained as proven and probable reserves (as of 31 December, 2005; *www.infomine.com/minesite/minesite.asp?site =Kalgoorlie, 2006*).

Despite over a century of mining and much research, there is still debate on the significance and timing of events that led to the formation of the ore system. The timing of events is reviewed here in light of new geochronological data, which includes U-Pb and Ar dates for zircon, mica, monazite and xenotime from dyke, ultramafic and ore samples.

## 2 STRATIGRAPHY

The Kalgoorlie Terrane consists of two mafic-ultramafic volcanic sequences overlain by mafic to felsic volcanic and volcaniclastic rocks. Both sequences are intruded by felsic to ultramafic sills, dykes and stocks. In the Golden Mile, the lowermost exposed unit is the Hannans Lake Serpentinite, which is *c.* 2.7 Ga based on ages of zircon from interbedded sedimentary units (Krapez *et al.* 2000). This is overlain by the Devon Consols and Paringa Basalts, which are separated from the underlying serpentinite by the Kapai Slate, which contains 2692±4 Ma zircons (Claoue-Long *et al.* 1988). Zircons from the Paringa Basalt are dated at 2690±5 Ma (www rses.anu.edu.au/oregen /Admin/CHStratigraphy.html).

A >1km sequence of volcanosedimentary Black and White Flag Beds with >2.8 Ga to *c.* 2655 Ma zircons overly the basalts. (Krapez *et al.* 2000). The sequence is intruded by differentiated dolerite sills. The tholeiitic Golden Mile Dolerite, main host to gold at the Golden Mile, contains *c.* 2675 Ma zircons (Claoue-Long *et al*. 1988; Woods 1997; Heath 2003). However, the main magmatic Zr phase in the Dolerite is baddeleyite rimmed by zircon, suggesting that zircon is post-magmatic. Hence, the dolerite must be older than *c.* 2675 Ma. The sill also cuts basal units of the Black Flag Beds (dated at *c.* 2687±8 Ma south of Kalgoorlie), but is unconformably overlain by younger (*c*. 2667Ma)

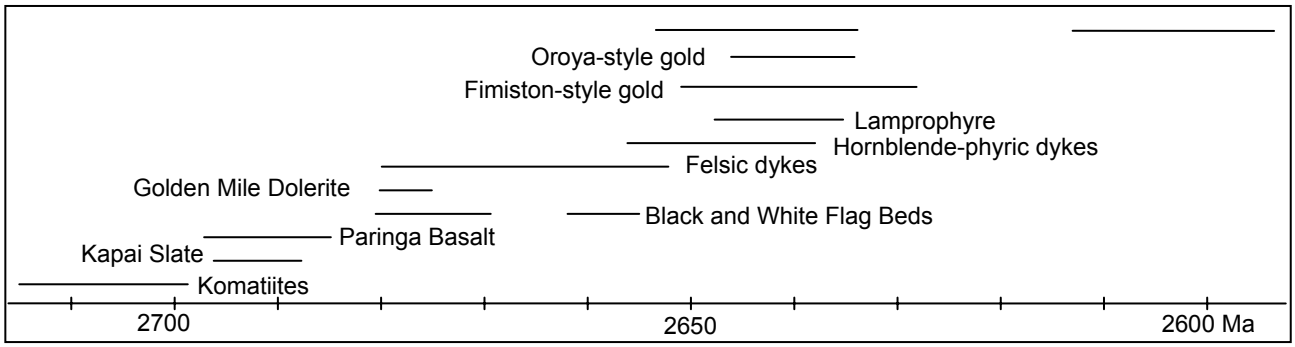


Figure 1 Timing of main rock units and events at Kalgoorlie. See text for discussion and references.

units of the Black Flag Beds (Krapez *et al*. in press). Hence, the sill must have intruded between 2.68 and 2.675 Ga.

Several calc-alkaline porphyritic and lamprophyre dykes intrude the sequence (*e.g*. Mueller *et al.* 1988; Woods 1997). The older feldspar-quartz phyric dykes intruded before gold mineralization. Hornblende-phyric dykes and associated lamprophyres both host and cross-cut gold lodes (Fimiston- and Oroya-style; see below), and as such, are probably coeval with gold mineralization. Several zircon dates (Kent & McDougall 1995; Woods 1997; Yeats *et al*. 1999; Gauthier *et al.* 2004) have been interpreted to record dyke intrusion between 2.68 Ga and 2.66 Ga. However, zircon morphology combined with geochronological data indicates a complex growth history. New data suggest that the feldspar dykes intruded at, or after, *c.* 2675-2670 Ma, coeval with hydrothermal zircon growth in the Golden Mile Dolerite and felsic volcanism in the Black Flag Beds, whereas the hornblende-phyric and lamprophyre dykes intruded at *c.* 2.65-2.64 Ga. New $^{40}Ar/^{39}Ar$ ages for metamorphic fuchsite in Hannans Lake Serpentinite and new metamorphic/ hydrothermal zircon ages from the feldspar dykes overlap the period of intrusion of the later dykes.

## 3 DEFORMATION

The deformation history at Kalgoorlie is hotly discussed (*e.g.* Mueller *et al.* 1988; Swager 1989; Clout *et al.* 1990; Ridley & Mengler 2000; Bateman *et al*. 2001; Weinberg *et al*. 2005; and references therein). All workers recognise early thrusting and folding, followed by sinistral and dextral shearing and late faulting.

There are up to four fabrics documented. Despite several interpretations of the significance and timing of these fabrics and specific deformation events, it is generally agreed that the main, penetrative foliation ($S_n$) formed at the same time as, or after, peak metamorphism, but before pervasive carbonate alteration. The $S_{n+1 \text{ and } +2}$ foliations and shear/fracture cleavage ($S_{n+3}$) are coeval with, or postdate, carbonate-pyrite alteration and K-Na metasomatism. The $S_{n+1 \text{ to } 3}$ foliations are defined by white mica of a similar composition indicating similar P-t conditions of formation and a broad synchroneity in the fabric formation despite local mutual cross-cutting relationships. Therefore, deformation was prolonged and accompanied by continuous dynamic mineral growth.

No direct absolute ages are available for deformation. However, the relationship of some dykes and other intrusive units with specifc structures provide some, albeit less reliable, indirect age constraints. The feldspar dykes are generally deformed by $S_{n+1 \text{ to } +3}$ foliations, whereas the hornblende and lamprophyre dykes are variably deformed by these foliations and locally cross-cut temporally associated structures (*e.g*. Mueller *et al.* 1988; Gauthier *et al*. 2004; McNaughton *et al.* 2005). Hence, the $S_{n+1}$ to $S_{n+3}$ foliations are indirectly constrained to be broadly coeval with intrusion of the *c.* 2.65-2.64 Ga hornblende-phyric and lamprophyre dykes.

## 4 MINERALIZATION

The Golden Mile deposit comprises Fimiston-, Oroya- and Charlotte-style ore lodes that are hosted within a complex array of ductile to brittle shear zones and quartz veins that are hosted mainly by the Golden Mile Dolerite, and to a lesser extent, by the Paringa Basalt and Black Flag shales. The Mt Charlotte deposit comprises lodes hosted primarily in the Golden Mile Dolerite, adjacent to, and in the footwall of, steeply N-striking faults. Charlotte-style lodes have also been mined from the Golden Mile deposit (*e.g*. Golden Pike lodes).

Due to the different styles, and local cross-cutting relationships, Fimiston-style lodes are structurally older Oroya-style lodes, with Charlotte-style gold-bearing brittle vein arrays and breccias having formed last. All ore styles are associated with a similar sericite-carbonate-pyrite assemblage, although roscoellite and telluride minerals are most common in high-grade Fimiston-style (Green Leader) and Oroya-style lodes.

## 5 TIMING OF GOLD MINERALIZATION

Fimiston-style gold lodes are variably described as forming after, or broadly synchronous with, intrusion of *c*. 2.65–2.64Ga calc-alkaline hornblende dykes. Similarly, Oroya-style gold mineralization (petrogenetically similar to Fimiston-style) is constrained in time by 2642±5Ma monazite and zircon in a syn-mineralization lamprophyre dyke (McNaughton *et al*. 2005). New data on ore-related *c.* 2.65-2.63 Ga monazite in a Fimiston-style lode, supports the formation of Oroya-style mineralization at broadly the same time as Fimiston-style lodes.

Charlotte-style lodes are hosted in structurally younger brittle vein arrays and breccias. Interestingly, new data from ore-related xenotime in different Charlotte-style lodes do not record a similar age. Instead, xenotime from Mt Charlotte is *c.* 2.65-2.63 Ga, whereas that from Golden Pike is younger than *c.* 2.62 Ga. Hence, at least some Charlotte-style mineralization at Mt Charlotte temporally overlaps Fimiston- and Oroya-style gold mineralization. The xenotime data indicate that, despite the similar structural setting, style and associated alteration, the Charlotte-style gold lodes did not form at the same time across the district.

Importantly, the Golden Pike xenotime is from a weakly mineralised pyrite-carbonate-sericite altered sample. Hence, the weak alteration may not be related to one of the main gold styles but rather a late hydrothermal event. 2.60-2.59 Ga and Palaeoproterozoic events are recorded in zircons in dykes, and monazite in the lodes, and may be related to late brittle cross-faulting and local hydrothermal activity.

Argon isotopic data from mineralized samples from the Golden Mile and Mt Charlotte record at least two events at 2.63 Ga and 2.60 Ga (Kent & McDougall., 1995; Phillips & Miller, 2006; this study). The data are interpreted to record the waning stages of the main gold mineralization event, and the later localised Charlotte-style mineralization that accompanied brittle cross-faulting (*cf.* Witt *et al*. 1996).

## 6 CONCLUSIONS AND IMPLICATIONS

In light of the new geochronological data, it is evident that the main Golden Mile gold mineralization, including Fimiston- Oroya- and Charlotte-style lodes, formed at *c.* 2.65 and 2.63 Ga. Gold mineralization was broadly coeval with regional ductile-brittle deformation and occurred after peak regional metamorphism and synchronous intrusion of calc-alkaline hornblende-phyric and lamprophyric dykes (Figure 1). Later gold mineralization occurred locally in brittle faults and vein arrays after *c*. 2.62 Ga.

Based on the absolute and relative timing within the regional geological framework, the current geometry of the deposit has probably not changed significantly since the time of the main gold mineralization event.

## ACKNOWLEDGEMENTS

The authors thank AMIRA and the sponsors of AMIRA P680, as well as acknowledge the support of an ARC SPIRT grant.

## REFERENCES

Bateman RJ, Hagemann SG, McCuaig TC, Swager CE (2001) Protracted gold mineralization throughout Archean orogenesis in the Kalgoorlie camp, Yilgarn craton, Western Australia: structural, mineralogical and geochemical evolution. *West Aust Geol Surv, Rec* 2001/17:63-98.

Claoue-Long JC, Compston W, Cowden A (1988) The age of the Kambalda greenstones resolved by ion-microprobe: implications for Archaean dating methods. *Earth Planet Sci Lett* 89: 239-259.

Clout JMF, Cleghorn JH, Eaton PC (1990) Geology of the Kalgoorlie gold field. In: FE Hughes (Ed) *Geology of the Mineral Deposits of Australia and Papua New Guinea. Australas Inst Min Metall Monogr* 14: 411-431.

Gauthier L, Hagemann S, Robert F, Pickens G (2004) New constraints on the architecture and timing of the giant Golden Mile gold deposit, Kalgoorlie, Western Australia. In: J. Muhling et al. (eds) *SEG 2004 – Predictive Mineral Discovery Under Cover, Extended Abstracts. UWA Publication* 33: 353-356.

Heath CJ (2003) Fluid flow at the giant Golden Mile deposit, Kalgoorlie, Western Australia. *PhD Thesis (unpublished), ANU,* 173p.

Kent AJR, McDougall I (1995) $^{40}$Ar-$^{39}$Ar and U-Pb age

constraints of the timing of gold mineralization in the Kalgoorlie Gold Fields, Western Australia. *Econ Geol* 90: 845-859.

Krapez B, Brown SJ, Hand J, Barley ME, Cas RA (2000) Age constraints on recycled crustal and supracrustal sources of Archaean metasedimentary sequences, Eastern Goldfields Province, Western Australia; evidence from SHRIMP zircon dating. *Tectonophysics* 322: 89–133.

Krapez B, Hand J (in press) Late Archaean deep-marine volcaniclastic sedimentation in an arc-related basin: the Kalgoorlie Sequence of the Eastern Goldfields Superterrane, Yilgarn Craton, Western Australia. *Prec Res*

McNaughton NJ, Mueller AG, Groves DI (2005) The age of the giant Golden Mile deposit, Kalgoorlie, Western Australia: ion-microprobe zircon and monazite U-Pb geochronology of a syn-mineralization lamprophyre dike. *Econ Geol* 100:1427-1440.

Mueller AG, Harris LB, Lungan A (1988) Structural controls of greenstone-hosted gold mineralization by transcurrent shearing: A new interpretation of the Kalgoorlie Mining District, Western Australia. *Ore Geol Rev* 3: 359-387.

Phillips D, Miller JM (2006) $^{40}$Ar-$^{39}$Ar dating of mica-bearing pyrite from thermally overprinted Archean gold deposits. *Geology* 34(5): 397 - 400.

Ridley JR, Mengler F (2000) Lithological and structural controls on the form and setting of vein stockwork ore bodies at the Mt Charlotte gold deposit, Kalgoorlie. *Econ Geol* 95: 85-98.

Swager CP (1989) Structure of Kalgoorlie greenstones – regional deformation history and implications for the structural setting of the Golden Mile gold deposits. *Geol Surv West Aust Rep* 25: 59-84.

Weinberg RF, vanderBorg P, Bateman RJ, Groves DI (2005) Kinematic history of the Boulder-Lefroy Shear Zone system and controls on associated gold mineralization, Yilgarn Craton, Western Australia. *Econ Geol* 100:1407-1426.

Witt WK, Swager CP, Nelson DR (1996) $^{40}$Ar-$^{39}$Ar and U-Pb age constraints on the timing of gold mineralization in the Kalgoorlie Gold Fields, Western Australia – a discussion. *Econ Geol* 91: 1354-1371.

Woods BK (1997) Petrogenesis and geochronology of felsic dikes in the Kalgoorlie terrane, Kalgoorlie, Western Australia. *BSc (Honours) Thesis (unpublished), CUT,* 108p.

Yeats CJ, McNaughton NJ, Ruettger D, Bateman RJ, Groves DI, Harris JL, Kohler E (1999) Evidence for diachronous Archean lode gold mineralization in the Yilgarn Craton, Western Australia: a SHRIMP U-Pb study of intrusive rocks. *Econ Geol* 94: 1259-1276.

# SIMS U-Pb geochronology of hydrothermal ore formation

Neal J. McNaughton, Birger Rasmussen & Ian R. Fletcher
*Centre for Exploration Targeting, School of Earth and Geographical Sciences, The University of Western Australia, Crawley WA 6009, Australia*

ABSTRACT: Reliable U-Pb isotope dating of hydrothermal ore deposits and events in their host terrains are being advanced by new developments and analytical techniques. Precambrian deposits and terrains, in particular, are best dated using U-Pb methods applied to U-bearing minerals which form during ore formation and other geological events. The REE-phosphates monazite and xenotime, appear common, although minor, in most hydrothermal systems, and are more isotopically robust than all(?) other datable minerals. However, due to the typically small grain size of these minerals, advanced SIMS-based (secondary ion mass spectrometry) geochronology, coupled with a detailed understanding of the petrography of the samples within a paragenetic framework of ore deposition, has emerged as the best and most flexible approach to reliable geochronology of hydrothermal ore deposits. Herein we outline the status of SIMS-based geochronology and petrology of ore deposits and environs, and highlight some recent examples for gold, iron and uranium deposits and their host terrains.

KEYWORDS: SIMS, U-Pb geochronology, monazite, xenotime, lode-gold, iron ores, uranium

## 1 INTRODUCTION

SIMS (secondary ion mass spectrometry) U-Pb dating methods have been developed to routinely date a wide range of U-bearing minerals: *e.g*. zircon, baddleyite, titanite, perovskite, rutile, monazite, xenotime. These minerals form by igneous, diagenetic, metamorphic, alteration and/or hydrothermal processes and can potentially be used for geochronology of these events. Importantly, hydrothermal monazite and xenotime have been found to be common constituents in ore assemblages in some deposit types, and have an exceptionally wide range of formation environments. One limitation, however, is that these minerals typically form as small grains and are often not large enough to be spatially resolved by in-situ SIMS analysis. The current practical lower size limitation for SIMS is ~10 microns, although successful dating of very U-rich minerals with a 3 micron analysis area has been achieved (Stern *et al*. 2005). Importantly, analytical precision is inversely related to the size of the analytical area, such that 10-12 microns is probably the minimum practical diameter for the SIMS analysis area for most routine applications.

SIMS U-Pb geochronology in the 10-12 micron range requires both (i) that datable minerals grow to this size during a single event, and (ii) that careful petrography can relate the mineral growth to the event. Petrographic interpretations at this scale largely rely on textural relationships as imaged by a scanning electron microscope, and on relating these textures to ore paragenesis at the deposit and regional scale. In most cases, identifying datable minerals and determining their paragenesis is achievable, but time-consuming.

Below we highlight examples where coupled SIMS-petrographic studies have made significant advances in dating a range of hydrothermal ore deposits and, within the chronological framework of the host terrain, impacted on deposit models and exploration strategies.

## 2 CHRONOLOGICAL FRAMEWORK OF THE HOST TERRAIN

In order to understand the formation of ores it is just as important to reliably know the chronology of their geological context as it is to

know the age of mineralization. In many cases, the chronological context is best established by:

i) chronostratigraphy, through analyses of volcanic and authigenic minerals; augmented by detrital minerals;
ii) intrusive ages for both felsic and mafic bodies, and their contact aureoles;
iii) the timing of metamorphism, deformation and fluid flow.

Precambrian volcanic units often host datable magmatic minerals, such as zircon, which may form either during emplacement or be included as contaminating xenocrysts/xenoliths. Textural discrimination of xenocrysts, coupled with age data, are usually sufficient to resolve the age of volcanism, establishing this method as the most applied dating technique in Precambrian terrains. Authigenic xenotime may also form in siliciclastic sediments during earliest diagenesis, and its age is used as a proxy for sedimentation, particularly in sandstones where the larger pore spaces allow larger grains of xenotime to grow (McNaughton *et al.* 1999, Kositcin *et al*. 2003, Rasmussen et al. 2004, Vallini *et al.* 2005).

Geochronology of igneous intrusions potentially provides minimum ages for terrain formation, and dates magmatic events in the terrain history. However, despite the propensity for zircon populations in felsic dykes to be dominated by xenocrysts (*e.g*. Baggott *et al*. 2005), and mafic rocks to be generally devoid of datable minerals, the contact metamorphic effect of the intrusions, particularly the higher temperature mafic ones, are datable via contact metamorphic monazite and xenotime (*e.g*. Rasmussen & Fletcher, 2002; Rasmussen *et al*. 2006).

Similarly, monazite and xenotime form in response to a range of regional metamorphic conditions, and may be petrographically related to both metamorphic and deformational events allowing age constraints to be placed on those events (*e.g.* Rasmussen *et al.* 2001, Dawson *et al.* 2003). Further, since both monazite and xenotime readily form at low temperatures, they may form prior to metamorphism in response to externally initiated fluid-flow events (*e.g*. Vallini *et al.* 2005, Rasmussen *et al*. 2005).

The nature of these pre-metamorphic events is somewhat cryptic, and for the most part can only be seen in age data, where it is preserved due to the resistance of the phosphates to isotopic disruption by later events.

## 3 DIRECT DATING OF HYDROTHERMAL ORE DEPOSITION

### 3.1 *Lode-gold deposits*

Many previous studies of Archaean and Palaeoproterozoic lode-gold deposits have identified monazite and xenotime which are related to their ore paragenesis and provided a means to date the mineralization event (*e.g*. Brown *et al.* 2002, Pigois *et al*. 2003, Vielreicher *et al*. 2003, *this volume*, Salier *et al.* 2004, 2005).

A recent example is the Tom's Gully gold deposit, in the Pine Creek Orogen of northern Australia (Rasmussen *et al*. 2006). Previous interpretations of this deposit envisaged mineralisation to be driven by either the intrusion of Mt Bundey Granite, part of the ~1.83 Ga Cullen Batholith (Stuart-Smith *et al*. 1993), or a regional orogenic event about 100 Ma later (Sener *et al.* 2005). SHRIMP analyses of zircons separated from the Mt Bundey Granite and in situ SHRIMP analysis of monazite from the associated Mount Goyder Syenite confirm an intrusive age of ~1825 Ma. In situ analyses of monazite and xenotime from metasediments in the contact aureole, which hosts the Au deposit, give an equivalent age. However, monazite intimately associated with Au in the mineralized quartz reef is dated at 1780+/-10 Ma, requiring ore formation to be distinct from both granite intrusion and the proposed regional ~1.73 Ga orogenic event.

### 3.2 *Iron ores*

In the Pilbara Craton, authigenic monazite and xenotime in metasedimentary rocks record a complex pattern of hydrothermal alteration, probably associated with two cryptic thermotectonic events (Rasmussen *et al.* 2005). The first, at 2.43–2.40 Ga is seen only in the west of the craton whereas the other records a metamorphic front that progressed northeast across >100,000 $km^2$ of the craton between 2215 Ma and 2145 Ma. Both monazite and xenotime are intergrown with iron-ore minerals at Tom Price and their age spectra (B. Rasmussen, *unpubl. data*) indicate multiple additional mineralization and/or remobilization events.

### 3.2 *Unconformity related U-mineralization*

In the Tanami Region of northwestern Australia, a highly uraniferous authigenetic xenotime cement in conglomerates gives a mimimum age of 1632+/-3 Ma for the Birrindudu Group (Vallini *et al.* 2007), which is similar to

the age of unconformity-related uranium deposits in the nearby Pine Creek Orogen. Similarities between the geological setting and apparent formation processes suggest that the age may be a valid proxy age for more deeply buried uranium mineralization, or the precursor to, or source for, later unconformity-associated ore deposition. The relationship between anomalously U-rich xenotime cements and U-ores in unconformity-related sandstones/conglomerates has not been fully explored or understood.

## 4 SUMMARY

Monazite and xenotime are minerals which form during a large number of geological processes and over a wide temperature range, in particular during the deposition of many types of hydrothermal ores. They are ideal for in situ U-Pb geochronology by SIMS, particularly in Precambrian terrains, and will provide the backbone of ore deposit geochronology in the future.

## ACKNOWLEDGEMENTS

This contribution summarizes many previous studies into the applications of SIMS geochronology to ore deposit research: all colleagues are thanked. Support from ARC, UWA and the WA SHRIMP consortium is acknowledged.

## REFERENCES

Baggott MS, Vielreicher NM, Groves DI, McNaughton NJ, Gebre-Mariam M (2005) Zircons, dikes and gold mineralization at Jundee-Nimary: post ca 2.66 Ga Archean lode gold in The Yandal Belt, Western Australia. Economic *Geology* 100: 1389-1405.

Brown SM, Fletcher IR, Stein HJ, Snee LW, Groves DI (2002) Geochronological constraints on pre-, syn- and postmineralization events at the world-class Cleo deposit, Eastern Goldfields Province, Western Australia. *Econ. Geol.* 97: 541–559.

Dawson GC, Fletcher IR, Krapez B, McNaughton NJ, Rasmussen B (2003) 1.2 Ga thermal metamorphism in the Albany-Fraser Orogen of Western Australia: consequence of collision or regional heating by dyke swarms? *J. Geol. Soc., London* 160: 29-37.

Kositcin N, McNaughton NJ, Griffin BJ, Fletcher IR, Groves DI, Rasmussen B (2003) Textural and geochemical discrimination between xenotime of different origin in the Archaean Witwatersrand Basin, South Africa. *Geochim et Cosmochim Acta.* 67: 709-731.

McNaughton NJ, Rasmussen B, Fletcher IR (1999) SHRIMP U-Pb dating of diagenetic xenotime in siliclastic sedimentary rocks. *Science* 285: 78-80.

Pigois J-P, Groves DI Fletcher IR, McNaughton NJ, Snee LW (2003). Age constraints on Tarkwaian palaeoplacer and lode-gold formation in the Tarkwa-Damang district, SW Ghana. *Mineralium Deposita* 38: 695-714.

Rasmussen B, Fletcher IR (2002) Indirect dating of mafic intrusions by SHRIMP U–Pb analysis of monazite in contact metamorphosed shale: an example from the Capricorn Orogen, Western Australia. *Earth Planetary Sci. Lett.* 197: 287–299.

Rasmussen B, Fletcher IR, Bengtson S, McNaughton NJ (2004) SHRIMP U-Pb dating of diagenetic xenotime in the Stirling Range Formation, Western Australia: 1.8 billion year minimum age for the Stirling biota. *Precamb. Res.* 133: 329-337.

Rasmussen B, Fletcher IR, McNaughton NJ (2001) Dating low-grade metamorphism by SHRIMP U-Pb analysis of monazite in shales. *Geology* 29: 963-966.

Rasmussen B, Fletcher IR, Sheppard S (2005) Isotopic dating of the migration of a low-grade metamorphic front during orogenesis. *Geology* 33: 773-776.

Rasmussen B, Sheppard S, Fletcher IR (2006) Testing ore deposit models using in situ U-Pb geochronology of hydrothermal monazite: Paleoproterozoic gold mineralization in northern Australia. *Geology* 34: 77-80.

Salier BP, Groves DI, McNaughton NJ, Fletcher IR (2004) The world-class Wallaby gold deposit, Laverton, Western Australia: an orogenic-style overprint on a magmatic-hydrothermal magnetite-calcite alteration pipe? *Mineralium Deposita* 39: 473-494.

Salier BP, Groves DI, McNaughton NJ, Fletcher IR (2005) Geochronological and stable isotope evidence for widespread orogenic gold mineralization from a deep-seated fluid source at ca 2.65 Ga in the Laverton Gold Province, Western Australia. *Economic Geology* 100: 1363-1388.

Sener AK, Young C, Groves DI, Krapež, B, Fletcher IR (2005) Major orogenic gold episode associated with Cordilleran-style tectonics related to the assembly of Paleoproterozoic Australia? *Geology* 33: 225-228.

Stern RA, Fletcher IR, Rasmussen B, McNaughton NJ, Griffin BJ (2005) Ion-microprobe (NanoSIMS 50) Pb-isotope geochronology at <5 micron scale. *International Journal of Mass Spectrometry* 244: 125-134.

Stuart-Smith PG, Needham RS, Page RW, Wyborn LAI (1993) Geology and mineral deposits of the Cullen Mineral Field, Northern Territory. *Australian Geological Survey Organisation Bulletin* 229: 145p.

Vallini DA, Groves DI, McNaughton NJ, Fletcher IR (2007) Uraniferous diagenetic xenotime in northern Australia and its relationship to unconformity-associated uranium mineralisation. *Mineralium Deposita* 42: 51-64.

Vallini DA, Rasmussen B, Krapez B, Fletcher IR, McNaughton NJ (2005) Microtextures, geochemistry and geochronology of authigenic xenotime:

constraining the cementation history of a Palaeoproterozoic metasedimentary sequence. *Sedimentology* 52: 1-22.

Vielreicher NM, Groves DI, Fletcher IR, McNaughton NJ, Rasmussen B (2003) Hydrothermal monazite and xenotime geochronology: a new direction for precise dating of orogenic gold mineralization. *SEG Newsletter* 53: 1 and 10-16.

# Isochrons or antichrons? The behaviour of Pb and U in complex ore deposits.

K.A. Bassano & J. Hergt
*pmd*CRC, School of Earth Sciences, The University of Melbourne, Parkville. Australia.*

R. Maas & J. Woodhead
*The University of Melbourne, Parkville. Australia.*

ABSTRACT: The Pb-Pb step-leaching technique has been applied to magnetite and chalcopyrite from Australian iron-oxide Cu-Au ore deposits at Copper Blow (Curnamona Province) and Ernest Henry (Mount Isa Inlier) in an attempt to assess the reliability of the approach in constraining their ages of mineralisation. The majority of the resulting Pb-Pb step-leaching data arrays are highly scattered and produce age estimates with significant uncertainties. The lack of agreement between the data obtained from this study and the generally 'accepted' ages for mineral deposition at these deposits is best explained by open-system behaviour in the Pb/U isotope system. In this study, the combination of U/Pb geochronology with trace element ICPMS, SEM and LA-ICPMS analysis provides evidence for this open-system behaviour. These techniques reveal the presence of U-rich inclusions at a range of scales.

KEYWORDS: Pb-Pb step-leaching, U, ore minerals, direct dating.

## 1 INTRODUCTION

Complex ore deposits are generally open-systems that have potentially experienced many generations of alteration by hydrothermal fluids. As a result, isotopic systems can be reset, either partially or completely, resulting in highly variable isotopic ratios within the same deposit.

This study aimed to constrain the ages of chalcopyrite and magnetite from well-studied complex ore deposits utilising Pb-Pb step-leaching (PbSL). This is a digestion technique based on sequential acid treatment of a mineral resulting in the selective recovery of radiogenic and common Pb components from the crystal lattice, making single-phase Pb-Pb dating possible. Developed originally by R. Frei (*e.g.* Frei & Pettke 1996; Frei *et al*. 1997) and colleagues at Bern, the technique has had mixed success. Initial studies produced reliable age estimates for silicates and mixed sulphides, however there is some conflict surrounding the validity of PbSL isochrons, with some authors claiming that isochrons might be the product of initial Pb heterogeneity and/or Pb mixing due to post crystallisation U or Pb introduction. To determine whether the isochrons obtained from PbSL in the current study are the result of U/Pb open-system behaviour we utilised U/Pb, SEM, LA-ICPMS and trace element analysis.

## 2 RESULTS

In this study PbSL was applied to chalcopyrite and magnetite from Copper Blow (Broken Hill) and Ernest Henry (Mt Isa Inlier). Studies of chalcopyrite from Copper Blow (a small ironstone-hosted high grade Cu-rich deposit located close to the Broken Hill main lode; Williams & Skirrow 2000) yielded promising results. Lead isotope ratios obtained, particularly in the second leach step, indicate the presence of radiogenic Pb with $^{206}Pb/^{204}Pb$ ratios ranging up to ~57. Results for magnetite from the same deposit display greater spread in the $^{206}Pb/^{204}Pb$ (~23 to 183). The PbSL age estimates obtained from these minerals are the same (magnetite: 1011±52 Ma; MSWD=250; chalcopyrite: 1053±310 Ma; MSWD=213), to within error, although the uncertainties are large. These results are ~550 Ma younger than the 'inferred' age of ~1630-1600Ma for the Copper Blow ore body (Burton 1994). Unlike the $^{206}Pb/^{204}Pb$ and $^{207}Pb/^{204}Pb$ ratios of these samples, $^{208}Pb/^{204}Pb$ displays very little

variation, retaining values that are only slightly higher than Broken Hill common Pb (~37 to 38). This indicates that the hydrothermal fluid from which these phases grew carried U but not Th.

Studies at Ernest Henry (iron-oxide Cu-Au deposit, eastern Mt Isa Block; Mark *et al.* 2000) indicate the presence of highly radiogenic Pb in both chalcopyrite and magnetite. Chalcopyrite shows a large spread in $^{206}Pb/^{204}Pb$ (~18 to 257). Data arrays produce a very well constrained 'isochron' and generate an age estimate of 1591±46Ma (MSWD=3486). Magnetite shows an even greater range (~214 to 965) but the resulting age (1044±450) has a large error caused by considerable scatter in the data. Analyses of both of these minerals did not produce age estimates within error of the 'accepted' age for ore deposition at Ernest Henry (~1529Ma; Mark *et al.* 2006). Further analyses of these samples with modified leaching protocols produced consistently scattered data sets.

In summary, the PbSL ages obtained in this work display large uncertainties and are consistently young compared to expected/known mineral formation ages. One exception is the Ernest Henry chalcopyrite, which yielded a PbSL age older than the known formation age.

## 3 EVALUATION OF ISOCHRONS

To understand the 'age estimates' obtained using PbSL, U/Pb geochronology was carried out on splits of the same samples. Data for chalcopyrite and magnetite from Copper Blow are all discordant indicating loss of Pb or addition of U. Age estimates obtained are inconsistent between samples and within aliquots of the same sample indicating small-scale heterogeneity presumably caused by open-system Pb and/or U isotopic behaviour. Magnetite data from Ernest Henry are variably discordant between samples and within different aliquots of the same sample and indicate either a gain in U or loss of Pb. Ernest Henry chalcopyrite aliquots show the greatest data scatter. All samples are discordant, indicating that the mineral has gained Pb or lost U.

Trace element ICPMS provided evidence for links between U and radiogenic Pb with non-lattice-bound chemical components indicating that these elements might be hosted within impurities. Although no specific minerals can be confidently identified, uraninite, carbonates, phosphates and possibly sulfates appear to be likely candidates.

Scanning Electron Microscopy (SEM) was employed to determine whether small-scale U-rich inclusions could explain the sample heterogeneity. Investigation of Ernest Henry magnetite exposed microscopic U-rich inclusions in some grains, which may be the reason for the large quantity of radiogenic Pb in this magnetite (Fig. 1). The heterogeneous distribution of these inclusions, and the timing of their introduction, might explain the scatter in the Pb isotope data and the young apparent age of the 1044±450 Ma "isochron". SEM imaging of Ernest Henry chalcopyrite and the Copper Blow samples did not reveal any U-rich inclusions.

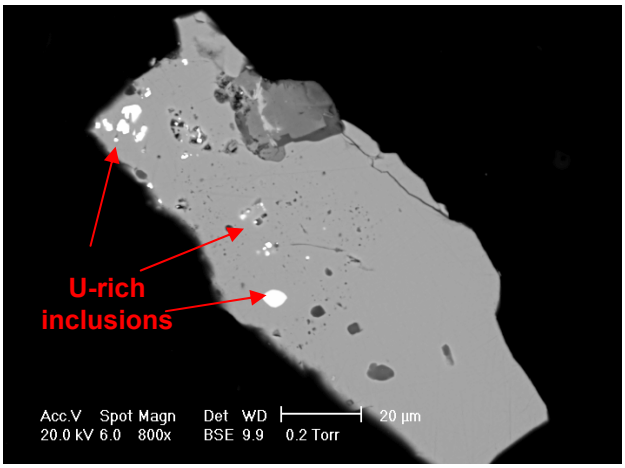


Figure 1: SEM image of Ernest Henry magnetite with U-rich inclusions.

Contrary to SEM, *in situ* laser ablation Pb isotope depth profiling analysis of magnetite from Copper Blow revealed significant $^{206}Pb$-rich spikes against a low $^{206}Pb/^{204}Pb$ background, suggesting the presence of very small U "hotspots" or thin U-rich zones (Fig. 2). *In situ* Pb isotope analysis of Copper Blow chalcopyrite did not show $^{206}Pb$-rich spikes but revealed Pb isotope variations on a grain scale. Similar analysis of Ernest Henry chalcopyrite revealed a generally well-constrained Pb-isotope array although some scatter in the data outside analytical uncertainties is evident suggesting open-system behaviour has occurred.

## 4 CONCLUSIONS

Ore deposits are complex and have

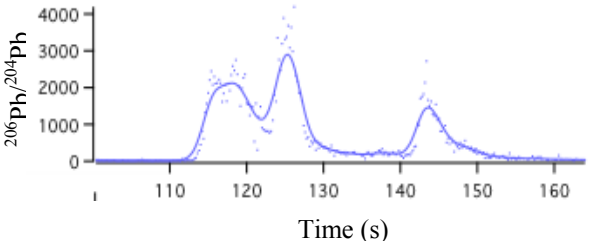


Figure 2: Time-resolved $^{206}Pb/^{204}Pb$ trace for linear scan across surface of Copper Blow magnetite.

potentially experienced many alteration and remobilisation events at different times. This kind of open-system behaviour will inevitably lead to geochemical heterogeneity even within a single phase and, as demonstrated here, may occur at the grain or sub-grain scale. In this study a number of techniques were applied to Pb-Pb step-leached samples to examine the nature and scale of this heterogeneity. U/Pb geochronology, ICPMS trace element analysis, SEM and LA-ICPMS all indicate that the samples have experience open-system U/Pb behaviour. This open system behaviour is reflected in PbSL isochrons that are highly scattered and produce age estimates that do not agree with the accepted ages of ore deposition in these examples. It is important to note that, despite the relatively well-constrained PbSL 'isochron' for chalcopyrite from Ernest Henry, some heterogeneity in Pb isotope compositions occurs on the sub-grain scale and the PbSL 'isochron' yields an age estimate at odds with the currently accepted value. We suggest that even in cases where the PbSL approach appears to produce an isochron, further detailed analysis similar to that conducted in our study is required to determine the veracity of the age estimate. That is, caution should be exercised when distinguishing 'isochrons' from 'antichrons' in complex ore systems.

## ACKNOWLEDGMENTS

The authors would like to thank the many members of the *pmd**CRC who have provided us with the well-constrained materials required for this study. We also wish to thank the AusIMM Education Endowment Fund for funding to present this work.

## REFERENCES

Burton GR (1994) Metallogenic studies of the Broken Hill and Euriowie Blocks, New South Wales. 3. Mineral deposits of the southeastern Broken Hill Block. *Geological Survey of New South Wales, Bulletin* 32(3), 100p

Frei R, and Pettke T (1996) Mono-sample Pb-Pb dating of pyrrhotite and tourmaline; Proterozoic vs. Archean intracratonic gold mineralization in Zimbabwe. *Geology* 24: 823-826.

Frei R, Villa IM, Nagler ThF, Kramers JD, Przybylowicz WJ, Prozesky VM, Hofmann BA, Kamber BS (1997) Single mineral dating by the Pb-Pb step leaching method: Assessing the mechanisms. *Geochimica et Cosmochimica Acta* 61: 393-414.

Mark G Oliver HS Williams PJ Valenta RK Crookes RA (2000) The Evolution of the Ernest Henry Fe-oxide Hydrothermal System; in *Hydrothermal Iron Oxide Copper-Gold and Related Deposits: A Global Perspective, Volume 1,* Ed TM Porter, 123-136, PGC Publishing: Adelaide.

Mark G, Stein H, Salt C (2004) Re-Os isotopic evidence for two periods of sulfide mineralisation in the vicinity of Ernest Henry Cu-Au deposit, northwest Queensland, Australia. 17th Australian Geological Convention Abstracts, *Geological Society of Australia, Melbourne,* 96.

Mark G, Oliver NHS, Williams PJ (2006) Mineralogical and chemical evolution of the Ernest Henry Fe oxide-Cu-Au ore system, Cloncurry district, northwest Queensland, Australia. *Mineralium Deposita* 40: 769-801.

Williams PJ and Skirrow RG (2000) Overview of iron oxide-copper-gold deposits in the Curnamona Province and Cloncurry district (Eastern Mount Isa Block), Australia in *Hydrothermal Iron Oxide Copper-gold and Related Deposits: A Global Perspective, Volume 1,* Ed TM Porter, 102-122, PGC Publishing:Adelaide.

# Application of the geomagnetic polarity sequence to dating mineral deposits

H. Ueno
*Department of Environmental Security Systems, Chiba Institute of Science*

ABSTRACT: The geomagnetic polarity sequence from rocks and ores is used for the determination of mineralization ages. The mineralization age of the Hishikari gold deposits is restricted within the Jaramillo normal chron from 1.07 to 0.99 Ma. The Kasuga gold deposits were mainly formed in C2Ar reversed chron. The polarity sequence of the Chichibu pyrometasomatic deposits and accumulated radiometric ages reveal that the mineralization events occurred in the C3r reversed chron and hydrothermal alteration continued until following C3n.4n normal chron. It is noteworthy that the mineralization age can be restricted within a short time period by this method.

KEYWORDS: reversed polarity, normal polarity, haematite, hydrothermal alteration, mineralization

## 1. INTRODUCTION

A radiometric age determination from minerals concerned with mineralization gives directly the mineralization age. Usually the procedure of age determination includes uncertainty. If different means are employed, we may get more exact ages. The palaeomagnetic method is treated here as one of the means.

There are two palaeomagnetic approaches. One is the age determination using the secular variation of the geomagnetic field as illustrated by Symons *et al*. (2000). It is effective for Pre-Cambrian time. Another technique use both the age and its interval of the polarity change of the geomagnetic field. In this paper the latter is performed by comparing to the geomagnetic polarity time scale. The geomagnetic polarity time scale after the Jurassic has been constructed (Gradstein, 2004) and the scale since 10 Ma has been very accurately revised (Cande & Kent, 1995).

The basic technique is to correlate a polarity magnetization of rocks or ores with the established geomagnetic polarity time scale. Radiometric ages and other geological information are indispensable to this procedure.

## 2. PRINCIPLE AND METHOD

The direction of the geomagnetic field changes with historic time. The change constitutes geomagnetic secular variations. It contributed to prove the continental drift theory. On the other hand, the geomagnetic field repeatedly changes its polarity over a short time. The present configuration of the geomagnetic field is referred to as normal polarity, and the opposite configuration is defined as reversed polarity. The established record of the geomagnetic field polarity is called the geomagnetic polarity time scale.

Around ore deposits, there may be igneous rock bodies including the host rock. They have a thermal remanent magnetization which is acquired during cooling from above the Curie temperature of the rock forming Fe-Ti oxide minerals. An ore containing ferromagnetic minerals acquires a chemical remanent magnetization. During hydrothermal alteration processes involving crystallization or recrystallization of ferromagnetic minerals, a chemical remanent magnetization may also be acquired (Ueno, 1982; Ueno *et al.*, 2003).

Remanent magnetizations were measured by a Schonstedt SSM-2A spinner magnetometer. In order to clean out the secondary magnetization and to reveal the original remanent magnetization, alternating field and/or thermal demagnetization were carried out for each specimen.

The polarity obtained from laboratory test-

ing is correlated with the geomagnetic polarity time scale (Ueno, 1975; Takeda *et al*., 2001). Some possible cases of correlation are listed below with convenient names such as R1, N1, R2, N2, RN, NR, RNR and NRN. R1 (or N1) is an event having reversed (normal) polarity magnetization and geochronogical information that falls in one chron of reversed (normal) polarity. R2 (or N2) are two or more events that are correlated with one reversed (normal) polarity chron. RN and NR are events that occur in two polarity chrons. RN includes the change from reversed to normal. Changing from normal to reversed is NR. RNR denotes changing from reversed through normal to reversed chrons and NRN includes normal-reversed-normal chrons.

## 3 PRACTICAL APPLICATION

### *3-1 Hishikari gold deposits [Example of N1]*

The Hishikari gold mine (32°04'N:130°42'E) has been operated since 1985. The annual gold production is 7.5 tonnes. The ore deposits consist of high grade gold silver bearing quartz-

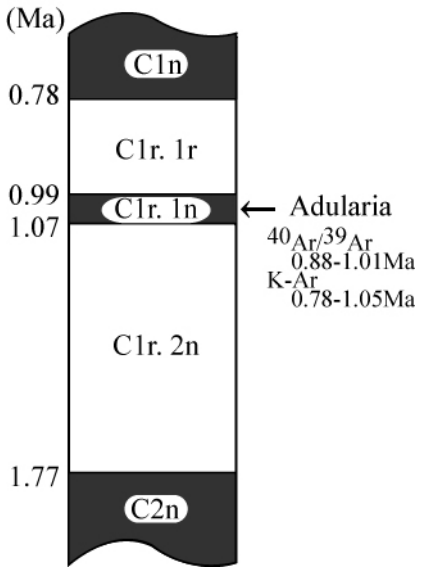


Figure 1. Correlation of the Hishikari gold deposits, southern Kyushu, Japan.

adularia veins, and are classified into low-sulphidation type. The largest of the three ore deposits, Honko is discussed here. Many absolute radiometric ages of adularia from ore veins have been reported. K-Ar ages are 0.78 to 1.05 Ma [n=13] (*Metal Mining Agency Japan and Sumitomo Metal Mining Co. Ltd. 1987*). Most $^{40}Ar/^{39}Ar$ ages range from 0.88 to 1.01 Ma [n=14] (Sanematsu *et al*., 2005).

The haematite bearing ores have normal polarity magnetization. It is clear that the normal polarity of the ores is correlated with the Jaramillo normal chron, C1r.1n [1.07-0.99 Ma], because the normal chron, C1n [0.78-0.00] is too young and the Olduvai normal chron, C2n [1.95-1.77] is too old.

Thus, the mineralization of the Honko deposit of the Hishikari gold mine is constrained within the period of 1.07 to 0.99 Ma. The remanent magnetizations of volcanic rocks in the Hishikari mining district and genetic consideration based on them will appear as another paper.

### *3.2 Kasuga gold deposits [Example of RN]*

The gold deposits (31°16'N:130°16'E) are composed of strongly silicified bodies including haematite as a magnetic carrier. The argillic zone forms an envelope around silicified bodies. It seems that the argillic zone was formed prior to silicification by mono-ascending hydrothermal fluid (Tokunaga, 1954). This concentric zoning is defined as Stage I. Stage II is characterized by formation of the breccia zone and precipitation of quartz and haematite.

The magnetization of the argillic zone is a stable reversed polarity with weak to medium magnetic intensity. The K-Ar sericite age of from the zone is 4.2±0.2 Ma. This reversed polarity seems to be correlated to C2Ar chron. The weakly silicified zone, which is slightly later than the argillic zone, has a stable reversed polarity magnetization with medium intensity. The strongly silicified zone also has a stable reversed polarity with medium to strong intensity. These reversed polarity magnetizations are also correlated to the C2Ar chron. Ore samples from Stage II show the well grouped normal polarity magnetization. The timing of Stage II falls in the C2An.3n chron following C2Ar chron, because no big gap may exist between Stage I and Stage II. The mineralization of the Kasuga gold deposits lies over the 3.58 Ma boundary between C2Ar and C2An.3n chrons. It is possible to determine the exact age using the RN relation as shown by this example.

### *3.3 Chichibu pyrometasomatic deposits [Example of NRN]*

The palaeomagnetic approach to examine the timing of formation of the Chichibu py-

rometasomatic deposits (36°01'N:138°49'E) has been reported (Ueno & Tonouchi, 1987). Here, the application as NRN is reconsidered using new radiometric ages.

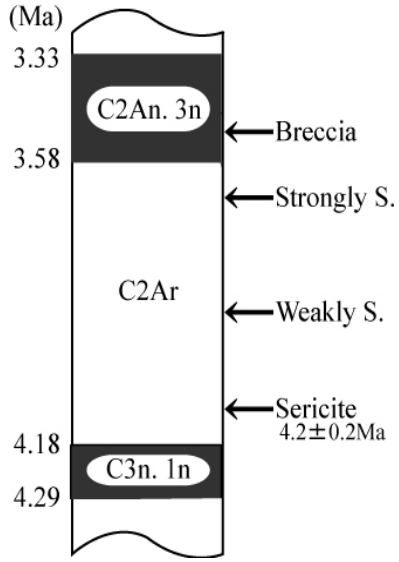


Figure 2. Correlation of the Kasuga gold deposits, southern Kyushu, Japan.

*Zones: Argillic(sericite), Weakly silicified, Strongly silicified, and Breccia.*

The quartz diorite A body intruded in the southeast portion of the mining area during a normal polarity chron (here called Jn normal chron for convenience) of the late Miocene and acquired a normal polarity magnetization. After the change of the polarity from Jn normal to reversed (called Kr), the quartz diorite C body intrudes and acquires a reversed polarity magnetization. In the same reversed polarity chron, skarnization, mineralization and weak hydrothermal alteration occur, and ores containing haematite or pyrrhotite and weakly altered quartz diorite acquired reversed polarity chemical remanent magnetizations. After the change of the polarity from Kr reversed one to normal one (called Ln), extremely altered quartz diorite from later strong hydrothermal alteration acquired a normal polarity magnetization. Events of the Chichibu pyrometasomatic deposits contain three chrons of Jn normal, Kr reversed and Ln normal.

Ueno & Tonouchi (1987) did not dare to correlate these chrons with the geomagnetic polarity time scale because of too few radiometric ages and their uncertainty. The correlation is tried now using published radiometric ages including new data. In this step available radiometric ages are abundant (Metal Mining Agency of Japan, 1975; Ueno *et al*, 1978; Ueno & Shibata, 1986; Ueno & Tonouchi, 1987;

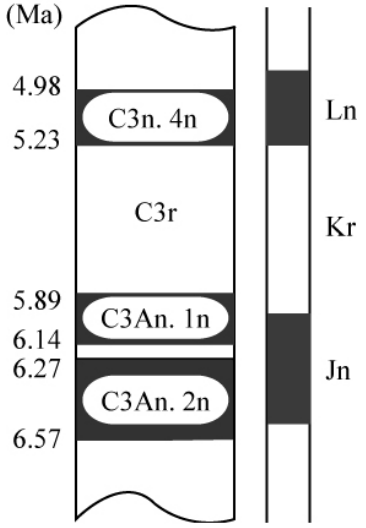


Figure 3. Correlation of the Chichibu pyrometasomatic deposits, central Japan.

*Details in the text.*

Saito *et al*., 1996). The quartz diorite A body: K-Ar Biotite age 6.44 Ma (n=6), K-Ar Hornblende age 6.81 Ma (n=4). The quartz diorite C body: K-Ar Biotite age 6.1 Ma (n=3), FT age < 8.1 Ma. Now it is possible to correlate Jn-Kr-Ln with C3An.1n (or C3An.2n)-C3r-C3n.4n. Thus, the mineralization age of the Chichibu pyrometasomatic deposits is restricted to the C3r chron between 5.89 and 5.23 Ma.

## 4 CONCLUSION

The geomagnetic polarity sequence has been correlated with the geomagnetic polarity time scale (Cande & Kent, 1995). The results for the Hishikari gold deposits indicates that the normal polarity magnetization falls in the Jaramillo normal polarity chron of 1.07 to 0.99 Ma. The main mineralization age of the Kasuga gold deposits is restricted within C2Ar reversed chron of 4.18 to 3.58 Ma, and the breccia zone is formed in following C2An.3n normal chron. The Chichibu pyrometasomatic deposits were examined using magnetizations of plutonic rocks, haematite and pyrrhotite ores, and hydrothermally altered rocks. Published radiometric

ages, including new data, show that the mineralization age of the Chichibu pyrometasomatic deposits was within the C3r reversed chron between 5.89 and 5.23 Ma.

## ACKNOWLEDGEMENTS

Experimental measurements were mainly performed at Tohoku University and Kagashima University. The author wishes to thank the collaborators at the time.

## REFERENCES

Cande SC, Kent DV (1995) Revised calibration of the geomagnetic polarity time scale for the late Cretaceous and Cenozoic. *Jour. Geophys*. Res. 100: 6093-6095.

Gradstein F, Ogg J, Smith A (2004) *A Geologic Time Scale*. Cambridge: Cambridge Univ. Press pp 589.

Metal Mining Agency of Japan (1975) Report on the regional geological survey, Chichibu district. *Ministry International Trade and Industry, Tokyo* (in Japanese).

Metal Mining Agency of Japan, Sumitomo Metal Mining Co., Ltd. (1987) Discovery and development of Hishikari mine. *Mining Geol.* 37: 227-235 (in Japanese).

Saito K, Takahashi M, Onozuka N (1996) A K-Ar investigation of the Chichibu quartz diorite and some discussions on its cooling history. *Jour. Geomag. Geoelect.* 48:1103-1109.

Samematsu K, Duncan R, Imai A, Watanabe K (2005) Geochronological constraints using $^{40}Ar/^{39}Ar$ dating on the mineralization of the Hishikari epithermal gold deposits, Japan. *Resource Geol.* 55: 249-266.

Symons DTA, Symons TB, Sanguster DF (2000) Paleomagnetism of the Society Cliffs dolomite and the age of the Nanisivik zinc deposits, Baffin Island, Canada. *Minerallium Deposita* 35: 672-682.

Takeda T, Shimada N, Ueno H (2001) Paleomagnetic constraints on the Nansatsu-type gold deposits in southern Kyushu, Japan. *Resource Geol*. 51: 239-248.

Tokunaga M (1954) Geology and ore deposits of the Kasuga and Akeshi mine in the Makurazaki district, Kagoshima Prefecture. *Mining Geol.* 4: 205-212. ( in Japanese)

Ueno H (1975) Paleomagnetism and origin of the Sennin haematite deposits in northeastern Japan. *Econ. Geol.* 70: 547-553.

Ueno H (1982) Hydrothermal alteration and magnetic polarity of the Torigoe dacite lava around the Kosaka Kuroko deposits in the Hokuroku district, Japan. *Sci. Rept. Tohoku Univ. ser* 3, 13: 1-12.

Ueno H, Kitazono S, Takeda T (2003) Opaque mineralogy in the alteration zones of ore deposits. In: Eliopoulos et al. (eds) *Mineral Exploration and Sustainable Development.* Millpress, Rotterdam 1035-1038.

Ueno H, Shibata K (1986) Isotope ages of quartz diorite bodies around the Chichibu pyrometasomatic deposits. Jour. Japanese Assoc. Mineral. Petrol. *Economic Geol.* 81: 77-82.

Ueno H, Tonouchi S, Shibata K (1978) Paleomagnetical evidence for the genesis of the Chichibu pyrometasomatic deposits, Japan. *Abstract of IAGOD Fifth Symposium held at Snowbird, USA* p194.

# Evidence for a Hercynian age for Cobalt-Arsenide-(Gold) Mineralization, Bou Azzer, Anti-Atlas, Morocco from new U-Pb, Sm-Nd and Re-Os age determinations

Thomas Oberthür, Frank Melcher & Friedhelm Henjes-Kunst
*Bundesanstalt für Geowissenschaften und Rohstoffe, Stilleweg 2, D-30655 Hannover, Germany*

Holly Stein, Aaron Zimmerman
*AIRIE Program, Department of Geosciences, Colorado State University, Fort Collins, CO 80523-1482 USA and Geological Survey of Norway, Leiv Eirikssons vei 39, 7491 Trondheim, Norway*

Axel Gerdes
*Institute of Geosciences, Petrology & Geochemistry, Senckenberganlage 28, D-60054 Frankfurt, Germany*

Mustapha El Ghorfi
*REMINEX Exploration, Route de Casablanca, Lot. Elhamra Nr. 235 - Marrakech - 40 000, Morocco*

ABSTRACT: The age of Co-As-(Au) mineralization in the Bou Azzer inlier was determined using different isotopic systems on mineralization-related ore and gangue minerals. Coexisting brannerite (U-Pb) and carbonates (Sm-Nd) yield consistent ages of 302 ± 9 Ma and 308 ± 31 Ma, respectively. These dates are regarded as the best estimate for the age of the Co-As mineralization. Re-Os data for drilled ore separates containing micron-scale molybdenite yield inconsistent, older ages (350-400 Ma). These are attributed to complex and disturbed Re-Os systematics, possibly involving excess radiogenic Os derived from an older source. The new age data suggest that Co-As mineralization at Bou Azzer was formed during and towards the end of the Hercynian Orogeny.

KEYWORDS: Dating, U-Pb, Re-Os, Sm-Nd, Co-As-(Au) ores, Bou Azzer, Anti-Atlas, Morocco

## 1 INTRODUCTION

The dating of mineralization is problematic as ores of base and noble metals are commonly barren of minerals that offer chances for direct age determinations.

The Anti-Atlas of Morocco hosts a large number of ore deposits (Au, Ag, Cu, Co). However, the age(s) of the mineralization within the context of crustal development is still controversial and mineralization ages between 685 Ma and 215 Ma have been proposed by various authors. At Bou Azzer, we had the opportunity to date the mineralization using several less conventional methods applied to different mineralization-related minerals (brannerite, molybdenite and carbonates). This paper reports new age data with the aim of constraining the timing of Co-As-(Au) mineralization at Bou Azzer within the larger context of crustal evolution of the Anti-Atlas.

## 2 GEOLOGY AND MINERALIZATION

The Bou Azzer-El Graara inlier (Fig. 1) of the Anti-Atlas represents a window into the Proterozoic basement surrounded by a discordantly overlying infra-Cambrian to Palaeozoic cover sequence. The inlier is a segment of a Pan-African (685-580 Ma) orogenic belt, located along the main Anti-Atlas thrust, an E-W trending fault zone which constitutes the northern boundary of the West African Craton (*ca*. 2.0 Ga; Leblanc 1981).

The Co-As-(Au) ores are hosted in variably steep shear zones, which occur mainly on or close to the contact of serpentinites and diorites. Mineralization has been traced locally for ~1km within structures that can be followed up to 5km. Payable ore zones are usually between 0.2 and 2m wide. The pristine ores are mainly Co-Ni-Fe arsenides and sulpharsenides. Currently, about 150,000 t of ore with grades of ~1% Co, 1% Ni and 3-4 g/t Au is mined annually at a number of mines.

## 3 ORE PETROLOGY

Samples of primary ores were collected in the underground workings of the Bou Azzer Co-As district. Major ore minerals are skutterudite [$CoAs_3$], safflorite [$CoAs_2$], niccolite [NiAs], rammelsbergite [$NiAs_2$], löllingite [$FeAs_2$], various sulpharsenides (cobaltite, gersdorffite,

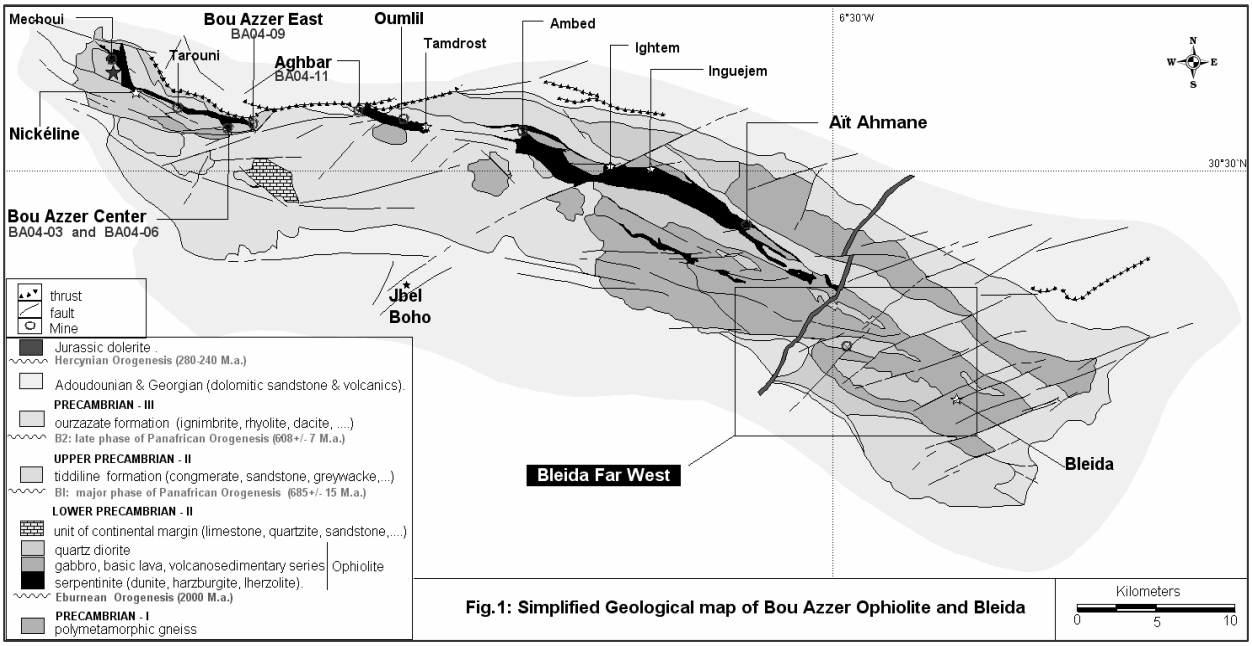


Figure. 1: Location of mines in the Bou Azzer inlier (after Leblanc 1981).

arsenopyrite) and subordinate base metal sulfides. Of particular interest are the ubiquitous, granular and webby-looking mats of micron-scale anhedral molybdenite [$MoS_2$] and up to 200 µm sub-idiomorphic grains of brannerite [$UTi_2O_6$] in the ores. Both minerals often occur together either in quartz-carbonate (mainly calcite) gangue (Fig. 2), or in the outer zones of skutterudite, suggesting a temporal relation to the main Co-As mineralization.

## 4 METHODS

### 4.1 *U-Pb (brannerite)*

Brannerite grains were measured *in situ* in polished sections by LA-ICPMS at the University of Frankfurt, using a Thermo-Finnigan Element II sector field ICP-MS coupled to a New Wave UP213 ultraviolet laser system. Spot size varied from 4 to 12 µm. Raw data were corrected for background signal, common Pb, laser induced elemental fractionation, instrumental mass discrimination, and time-dependant elemental fractionation. Analytical reproducibility (Manangotry monazite reference standard) for $^{206}Pb/^{238}U$ and $^{207}Pb/^{206}Pb$ was usually better than 0.7%.

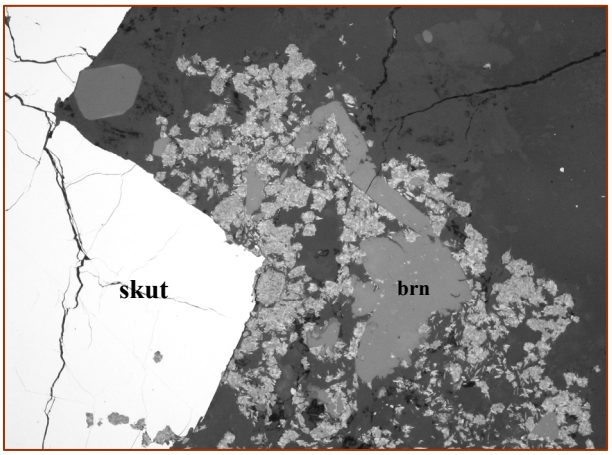


Figure. 2: Ore from Bou Azzer. Skutterudite (skut), molybdenite (mo), brannerite (brn) and carbonate (carb). Reflected light, in air, width = 375 µm.

### 4.2 *Re-Os (ore mixtures with molybdenite)*

Molybdenite was not visible to the eye for routine extraction of a pure or silica-diluted separate. Instead, in a non-conventional hit-or-miss fashion, a powder was obtained from ore-rich samples in the hope that molybdenite would be present in the mixture, common Os would be minimal, and thus direct dating of the mixture using the model age approach would be possible (Stein *et al.* 2001). Re and Os concentrations were determined at AIRIE, Colorado State University (CSU). A Carius-tube digestion using $HNO_3$-HCl equilibrated with a mixed-double Os spike was used. Os is recovered by distillation into HBr and purified by micro-distillation. Re is recovered by anion exchange. Isotopic compositions were determined by NTIMS on NBS 12-inch radius, 90° sector mass spectrometer at AIRIE-CSU.

### 4.3 *Sm-Nd (carbonate)*

For Sm-Nd dating, clean carbonate fractions were obtained by hand picking from coarsely crushed ores. Powdered carbonate samples of

optically homogenous carbonate were dissolved in hot dilute acetic acid. Sm-Nd element fractions were purified by conventional cation exchange chromatography in a first step and using columns with HDEHP-coated Teflon powder in a second step. Sm and Nd were measured on a ThermoFinnigan Triton multicollector mass spectrometer in static mode using a double Re filament assembly. Procedural blanks are negligible at <0.1% of the relevant sample concentration.

## 5 RESULTS

### 5.1 *U-Pb dating of brannerite*

The results of the U-Pb LA-ICPMS analyses of brannerite are shown in Fig. 3.

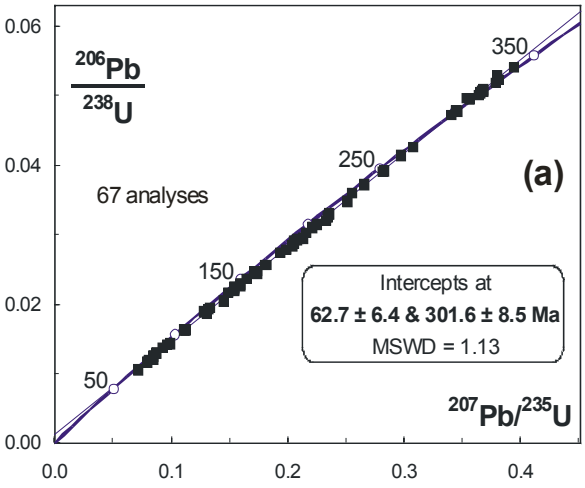


Figure. 3: U-Pb data for brannerite (errors not shown).

The upper intercept is interpreted as a mineralization age of 301.6 ± 8.5 Ma. The lower intercept at 62.7 ± 6.4 Ma may point to a later remobilisation event.

### 5.2 *Re-Os analyses of ore mixtures*

| AIRIE Run # | Re (ppm) | $^{187}$Os (ppb) | Os$_{common}$ (ppb) | Age (Ma) |
|---|---|---|---|---|
| MDID-542 (BA0406) | 0.1553 (1) | 0.571 (1) | 0.010 (19) | 350.4 ± 1.3 |
| MDID-543 (BA0411) | 10.84 (5) | 45.6 (1) | 7.38 (19) | 400.2 ± 2.5 |
| MDID-560 (BA0406b) | 0.345 (1) | 1.346 (8) | 0.004 (13) | 371.0 ± 2.7 |

Table 1: Re-Os analyses of ore mixtures.

A total of six Re-Os analyses were acquired from "blind" drilling of ore material from two deposits (Bou Azzer and Aghbar). Three of these results had ppb level common Os that exceeded measured radiogenic Os by up to 30 times. These samples are unsuitable for the molybdenite model age approach and are not co-linear in isochron space. The other three samples with subordinate common Os have Re concentrations suggesting the presence of molybdenite in the analyzed mixture (Table 1). The ages obtained, however, are not in agreement, spanning 350-400 Ma. This is highly unusual for molybdenite when separates can be drilled from visible crystalline samples. Thus, we conclude that the Re-Os systematics in the analyzed mixture reflect a complex pre-Hercynian history. One possible explanation is the incorporation of excess radiogenic Os in the ores, derived from older rocks (and sulphides) during serpentinization.

### 5.3 *Sm-Nd dating of carbonate*

Among the investigated nine carbonates, five samples from the eastern part of the ore district (Buismas, Oumlil, Ait Ahmane – filled ellipses) are roughly co-linear (MSWD of 2.1) on a Sm-Nd isochron diagram (Fig. 4) corresponding to an age of 308 ± 31 (2σ) Ma. An initial Nd isotope ratio corresponding to $\varepsilon_{Nd}$ +1 suggests a component of Nd from a primitive source. Another subset of three samples (Bou Azzer filon 7) yields a similar isochron age, but projecting to a lower, more crustal-like initial $\varepsilon_{Nd}$ of -5 (dashed line in Fig. 4). Outlying point Ba 04-09 is from Bou Azzer East.

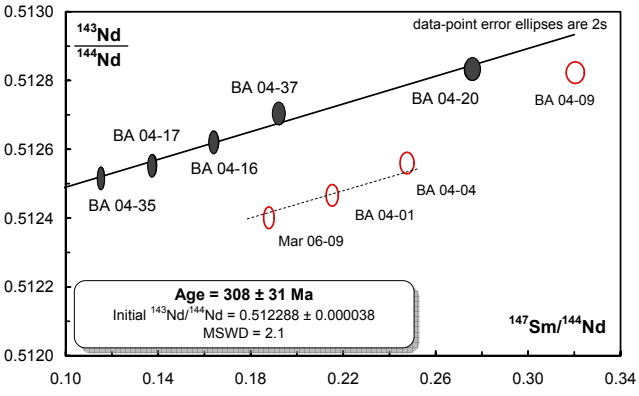


Figure. 4: Sm-Nd isochron plot for carbonates.

## 6 DISCUSSION

The complex crustal evolution of the Anti-Atlas is disputed (*e.g.* Cheilletz *et al.* 2002, Gasquet *et al.* 2005), as is the timing of various types of mineralization. Previous work on Anti-

Atlas ore deposits reveals a variety of possible mineralization ages. For example, the silver ores of the famous Imiter deposit were emplaced at 550 Ma (Cheilletz *et al.* 2002, Levresse *et al.* 2004), whereas the gold mineralization of the Iourirne Mine is dated at 300 Ma (Gasquet *et al*. 2005).

Regarding the Co-As ores of Bou Azzer, Leblanc (1981) proposes a late Pan-African, post-B1 (~685 Ma) age. Levresse (2001) gives a maximum mineralization age of 533 ± 2 Ma (age of the Aghbar trachyte which is cut by the mineralization). Ledent (1960) arrived at an age of 240 ± 10 Ma (Pb-Pb) for syn-mineralization brannerite (which we re-interpreted using the $^{207}Pb/^{206}Pb$ ratio to *ca.* 325 Ma), whereas En-Naciri et al. (1997) report a SIMS U-Pb age of *ca.* 550 Ma for brannerite. Levresse (2001) obtained an age of 215 ± 8 Ma (i.e. end of the Triassic) using $^{40}Ar/^{39}Ar$ dating of adularia from filon 7, Bou Azzer Mine.

Different isotope systems used in the present work point to formation of coexistent brannerite and carbonates at 302 ± 8 (2σ) Ma (weighted average of two isochron ages). The consistent dates are regarded as the best estimate of the age of Co-As mineralization in the Bou Azzer inlier. Re-Os dating of ore mixtures containing poorly crystalline micro-scale molybdenite yield inconsistent older ages (350-400 Ma), possibly reflecting excess radiogenic Os derived from recrystallization and metamorphism of older material.

U-Pb and Sm-Nd age data suggest that Co-As mineralization in the Bou Azzer inlier is Hercynian (Variscan) age. Notably, Gasquet *et al.* (2005) also describe hydrothermal activity in the Anti-Atlas at ~330-300 Ma. The Co-As mineralization likely formed at <300°C by percolating basinal brines (En Naciri *et al*. 1997) during and towards the end of the Hercynian Orogeny.

## ACKNOWLEDGEMENTS

Thanks to the Geology Department at the Bou Azzer Mine, especially Mr. Mhaili and Mr. Mustapha Souhassou. Reminex Exploration provided logistical support for field work. Thanks also to Siegrid Gerlach, Kirsten Fromme and Peter Macaj for assistance with Sm-Nd analysis. M. ElG acknowledges support from the SEG Foundation.

## REFERENCES

Cheilletz A, Levresse G, Gasquet D, Azizi Samir MR, Zyadi R, Archibald DA (2002) The Imiter epithermal deposit (Morocco): new petrographic, microtectonic and geochronological data. Importance of the Precambrian-Cambrian transition for major precious metal deposits in the Anti-Atlas. *Mineral Deposita* 37: 772-782.

En-Naciri A, Barbanson L, Touray JC (1997) Brine inclusions from the Co-As(Au) Bou Azzer district, Anti-Atlas, Morocco. *Econ Geol* 92: 360-367.

Gasquet D, Levresse G, Cheilletz A, Azizi-Samir MR, Mouttaqi A (2005) Contribution to a geodynamic reconstruction of the Anti-Atlas (Morocco) during Pan-African times, with emphasis on inversion tectonics and metallogenic activity at the Precambrian-Cambrian transition. *Precamb Res* 140: 157-182.

Leblanc M (1981) Ophiolites précambiennes et gîtes arséniés de Cobalt (Bou Azzer - Maroc). *Notes et mémoires du service géologique du Maroc* N°280, 306 pp.

Ledent D (1960) Age absolu d'une brannérite de Bou-Azzer (Sud-Marocain). *Académie des Sciences Belgique, Brussels:* 1309-1311.

Levresse G (2001) Contribution à l'établissement d'un modèle génétique des gisements d'Imiter (Ag-Hg), Bou Madine (Pb-Zn-Cu-Ag-Au) et Bou Azzer (Co-Ni-As-Ag-Au) dans l'Anti-Atlas marocain. *PhD thesis (unpubl), CRPG-CNRS Nancy*, 191 pp.

Levresse G, Cheilletz A, Gasquet D, Reisberg L, Deloule E, Marty B, Kyser K (2004) Osmium, sulphur, and helium isotopic results from the giant Neoproterozoic epithermal Imiter silver deposit, Morocco: evidence for a mantle source. *Chem Geol* 207: 59-79.

Stein HJ, Markey RJ, Morgan JW, Hannah JL, Scherstén A (2001) The remarkable Re-Os chronometer in molybdenite: how and why it works. *Terra Nova* 13: 479-486.

# Re-Os ages for molybdenites from the Variscan Strzegom-Sobótka granite massif (SW Poland)

S.Z. Mikulski,
*Department of Economic Geology, Polish Geological Institute, 4 Rakowiecka St., 00-975 Warsaw, Poland*

H.J. Stein[1,2] & A. Zimmerman[1]
[1] *AIRIE Program, Department of Geosciences, Colorado State University, Fort Collins, CO 80523-1482 USA*
[2] *Norges Geologiske Undersøkelse, Leiv Eirikssons vei 39, 7491 Trondheim, Norway*

ABSTRACT: New Re-Os isotopic analyses of molybdenite from the western and central parts of the Strzegom-Sobótka granite massif yield ages from 298 ± 1 to 296 ± 2 and 257 ± 1 Ma, respectively. These new data, together with our previous ages for the more westerly Paszowice quarry (309 ± 1 to 304 ± 1 Ma) suggest a magmatic-related mineralization history spanning at least 50 Ma. (Upper Carboniferous to Upper Permian). Furthermore, there appears to be a systematic decrease in ages from west to east across the Strzegom-Sobótka granite massif.

KEYWORDS: molybdenite, Re-Os, Strzegom-Sobótka granites, Fore-Sudetic block, SW Poland, Bohemian Massif

## 1 INTRODUCTION

In the late Variscan Strzegom-Sobótka granitoids massif (SSM), numerous occurrences of molybdenite mineralization have been documented, primarily in quarry exposures (Pendias & Walenczak 1956; Salacinski 1978; Chilinska & Lindner 1978; Kanasiewicz & Mikulski 1982). Re-Os ages for molybdenite from the Strzegom-Sobótka granite were acquired from the westernmost part of the massif from samples taken at the Paszowice quarry (Mikulski & Stein 2005). Those molybdenites yield Re-Os ages from 309 ± 1 to 304 ± 1 Ma. They are characterized by markedly low Re concentrations (<1 ppm), interpreted as possibly related to metamorphic processes and the development of shear zones in an uplifted orogen. Low Re molybdenite, derived from metamorphic processes, has been attributed to exhumation of orogens (Bingen & Stein 2003; Stein 2006).

Here we present new Re-Os data for molybdenite collected from the western and central parts of Strzegom-Sobótka granite massif (Fig. 1) and compare these with existing age data.

## 2 THE STRZEGOM-SOBÓTKA GRANITOID MASSIF

The Strzegom-Sobótka massif is situated in the central part of the Fore-Sudetic block, which resides in the northeastern part of the Bohemian Massif, Saxothuringian Zone of the European Variscan belt. Palaeozoic crystalline rocks exposed in the Western Sudetes continue under Cenozoic cover across the Sudetic Marginal Fault into the Fore-Sudetic block and reach the Odra Fault Zone, which defines the northeastern boundary of the massif (Fig. 1).

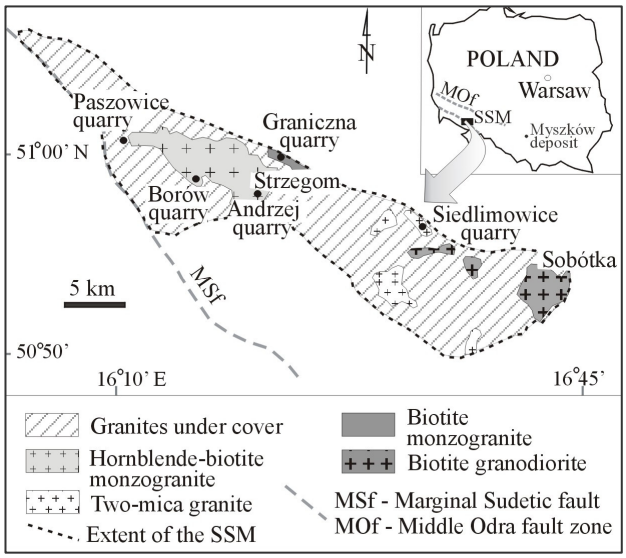


Figure 1. Simplified geologic sketch map of the Strzegom-Sobótka granite massif after Kural & Morawski (1968) with quarries where molybdenite samples were collected for Re-Os studies

Metamorphosed crystalline rocks of the Fore-Sudetic block were subject to post-orogenic magmatic-volcanic processes during the Carboniferous and early Permian. Although the SSM is poorly exposed, four main petrologic varieties are recognized (Majerowicz 1972; Maciejewski & Morawski 1975; Puziewicz 1985; 1990): *(1,2)* hornblende-biotite monzogranite and biotite monzogranite (west SSM), *(3)* two-mica monzogranite (central SSM), and *(4)* biotite granodiorite (east SSM).

Only the two-mica granite is peraluminous; other types are metaluminous (Puziewicz 1990). Two main stages of granite intrusions were defined on the basis of Rb-Sr dating. The first stage of two-mica intrusions (324 ± 7 Ma) was followed by a second stage with biotite granodiorite and monzogranites dated at *ca*. 280 Ma (Pin *et al.* 1989; Oberc-Dziedzic *et al*. 1996; Kennan *et al.* 1999). Recent investigations yield ages of 309.1 ± 0.8 Ma and 306.4 ± 0.8 Ma for two-mica granite (ID-TIMS monazite and xenotime, respectively; Turniak & Bröcker 2002), 308.4 ± 1.7 Ma for biotite granodiorite (Pb-evaporation zircon; Turniak *et al.* 2005), and a range of Pb/Pb ages from 299 ± 8 (Paszowice) to 307.2 ± 4.4 Ma (Graniczna) for hornblende-biotite and biotite monzogranites (zircon; Turniak *et al.* 2005). According to Turniak *et al*. (2006) K-Ar cooling ages for hornblende-biotite from biotite monzogranites range from 291.0 ± 4.4 to 305.2 ± 4.9 Ma.

## 3 SAMPLE DESCRIPTION

Five molybdenite samples for Re-Os dating were collected within the Strzegom-Sobótka massif from the following quarries (Fig. 1):

- Borów (2), MDID-684 and MDID-666
- Andrzej (1), MDID-667
- Graniczna (1), MDID-698
- Siedlimowice (1), MDID-699, MDID-759

Molybdenite from *Borów quarry* consists of fine-grained flakes that form irregularly distributed aggregates up to 10 mm in diameter. Samples with up to 1.32% Mo have been reported from this quarry (Pendias & Walenczak 1956). Molybdenite occurs as intergrowths with plagioclase, biotite, hornblende and K-feldspar. Biotite is commonly chloritized, K-feldspar is sericitized and plagioclases are albitized. In the vicinity of molybdenite, the quartz content of the monzogranite decreases notably. Native bismuth and rarely chalcopyrite are found in paragenetic association with molybdenite. Ilmenite and rutile form elongate micrograins, usually in biotite.

Molybdenite from the abandoned *Andrzej quarry* occurs in gray quartz veins up to 3cm thick. They generally strike NW-SE and dip steeply to the NE. These veins cut pegmatitic rocks with characteristic micrographic intergrowths of quartz and K-feldspar. Molybdenite blades are curved and form separate aggregates up to 30mm in diameter. Fine-grained euhedral pyrite and rarely single anhedral grains of chalcopyrite may occur with the molybdenite.

Molybdenite from *Graniczna quarry* occurs as disseminated aggregates up to 20mm in diameter within biotite monzogranite. Rosette aggregates 5-10mm in diameter are common. Larger molybdenite crystals are curved and intergrown with K-feldspar or/and plagioclase. Native bismuth may occur between parallel flakes of molybdenite or along K-feldspar cleavage. Native bismuth may be replaced by bismuthinite. Rare chalcopyrite and pyrite may be associated with molybdenite and ilmenite and rutile with biotite. At the Graniczna quarry, Mo mineralization occurs within scattered molybdenite-rich pockets up to a few cubic meters. Chemical analyses of Mo-bearing samples reveal up to 1.2 % Mo (unpublished data). Within these pockets the granite is strongly sericitized, chloritized and albitized.

Molybdenite from *Siedlimowice quarry* occurs in quartz-sericite rock that interfingers with two-mica peraluminous granite. The molybdenite sample from Siedlimowice is the easternmost Mo-mineralization known in the SSM. Molybdenite occurs as thin (<2mm) wafers (up to 25mm in diameter) on fractured surfaces and within cataclastic rocks. Molybdenite is commonly associated with native bismuth showing replacement by bismuthinite. Ilmenite is also present, and pyrite is rare.

## 4 METHODS AND RESULTS

Re-Os dating of molybdenite is described in Stein *et al*. (2001). We present six Re-Os analyses for five molybdenite samples using procedures outlined in Markey *et al.* (2003). Analyzed molybdenite samples were between 44 and 195 mg at near 100% purity. Separates were acquired from targeted drilling of specific molybdenite occurrences. Molybdenite was

added to inverse *aqua regia* and a mixed Re-double Os spike ($^{185}$Re, $^{188}$Os-$^{190}$Os). The mixture was sealed in a Carius tube and digested overnight. Instead of a distillation procedure to isolate Os, chloroform solvent extraction was used. Re was isolated using standard anion chromatography. Re and Os aliquots were measured on both a single Faraday cup/SEM NBS NTIMS unit and a multiple Faraday cups/single SEM NTIMS unit with consistent ages. The molybdenites have Re concentrations ranging from 6 to 58 ppm. Re-Os ages are 299 to 294 Ma, with one molybdenite analyzed twice (two mineral separates) at 257 ± 1 Ma.

Table 1. Re-Os data for molybdenite from the Strzegom-Sobótka granite massif

| AIRIE Run # and Quarry | | Re, ppm | $^{187}$Os, ppb | Age, Ma |
|---|---|---|---|---|
| MDID-684 | B | 11.033 (9) | 34.48 (5) | 298 ± 1 |
| MDID-666 | B | 12.34 (1) | 38.5 (2) | 297 ± 2 |
| MDID-667 | A | 6.97 (1) | 21.62 (9) | 296 ± 2 |
| MDID-698 | G | 57.59 (8) | 179.62 (8) | 297 ± 1 |
| MDID-699 | S | 10.173 (8) | 27.39 (1) | 257 ± 1 |
| MDID-759* | S | 5.975 (7) | 16.13 (7) | 257 ± 1 |

Footnotes to Table 1:

(1) Assumed initial $^{187}$Os/$^{188}$Os for age calculation = 0.2 ± 0.1

(2) Absolute uncertainties at 2σ for last digit indicated

(3) Decay constant used for $^{187}$Re is 1.666 x $10^{-11}$yr$^{-1}$ (Smoliar *et al*. 1996) and age calculated using $^{187}$Os = $^{187}$Re ($e^{\lambda t}$ – 1)

(4) Ages corrected for Re blank = 4.88 ± 0.06 pg, total Os = 0.69 ± 0.01 pg, $^{187}$Os/$^{188}$Os = 0.37 ± 0.01 for MDID-666 and MDID-667

(5) For others, blanks are Re = 0.72 ± 0.01 pg, total Os = 0.730 ± 0.002 pg, $^{187}$Os/$^{188}$Os = 0.257 ± 0.001

(6) 2σ ages include all analytical and $^{187}$Re decay constant error

(7) B = Borów, A = Andrzej, G = Graniczna, S = Siedlimowice

(8) MDID-759* represents a second analysis using a ***new*** mineral separate thereby unequivocally affirming age accuracy

## 5 DISCUSSION

Re-Os dating of four molybdenite samples from three quarries in the western part of the Strzegom-Sobótka granitoid massif yields ages from 298 ± 1 to 296 ± 2 Ma. Both rosette and quartz vein occurrences of molybdenite yield ages within a narrow range. Re contents in Strzegom-Sobótka molybdenite samples are moderately low (6-58 ppm; this study), and those from the Paszowice quarry are notably low (<1 ppm Re; Mikulski & Stein 2005). Stein (2006) shows that low Re molybdenite can be precipitated during high-T metamorphism associated with dehydration melting in exhuming terranes. In a recent Re-Os study of molybdenites with similar Re concentrations from the Myszków Mo-W deposit (Fig. 1), a metamorphic-metasomatic derivation with rapid exhumation was proposed (Stein *et al*. 2005). We suggest a post-magmatic origin for Strzegom-Sobótka molybdenites associated with fluids exsolved during slow cooling of monzogranites. Molybdenite from the Siedlimowice quarry indicates a distinctly younger Re-Os age (257 ± 1 Ma). At Siedlimowice, molybdenite occurs in cataclastic rocks within two-mica granites in a down-thrown block of the SSM. This younger age dates cataclasis in this part of the Strzegom-Sobótka massif as late Permian.

Comparison of these results with Re-Os ages for molybdenite from the Paszowice quarry (309-304 Ma; Mikulski & Stein 2005) indicates that molybdenite crystallization is younger from west to east in the SSM, correlating with the present level of erosion, with deeper levels outcropping in the west.

## ACKNOWLEDGEMENTS

Special thanks to Dr. T. Woroncowa-Marcinowska from the PGI Geological Museum for the molybdenite sample from the Graniczna quarry. Analytical work was supported by the National Committee Scientific Research, Grant 4 T12B 029 30 and by the U.S. National Science Foundation.

## REFERENCES

Bingen B, Stein H (2003) Molybdenite Re-Os dating of biotite dehydration melting in the Rogaland high-temperature granulites, S Norway. *Earth and Planetary Science Letters* 208: 181-195.

Chilinska H, Lindner M (1978) Prospects of ore occurence in the Strzegom-Sobótka granite massif. *Biuletyn Instytutu Geologicznego* 308: 9-24.

Kanasiewicz J, Mikulski SZ (1989) On the occurrence possibility of the molybdenum deposit of the Cu-Mo formation on the Strzegom granites massif. *Przeglad Geologiczny* 37: 129-133.

Kennan PS, Dziedzic H, Lorenc MW Mierzejewski MP (1999) A review of Rb-Sr isotope patterns in the Carboniferous granitoids of the Sudetes in Poland. *Geologia Sudetica* 32: 49-53.

Kural S, Morawski T (1968) Strzegom-Sobótka granitic massif. *Biuletyn Instytutu Geologicznego* 227: 33-85.

Maciejewski S, Morawski T (1975) Petrographic diversity of granites of the Strzegom massif. *Kwartalnik Geologiczny* 19: 47-65.

Majerowicz A (1972) The Strzegom-Sobótka granite massif. *Geologia Sudetica* 6: 7-96.

Markey R, Hannah JL, Morgan JW, Stein HJ (2003) A double spike for osmium analysis of highly radiogenic samples. *Chemical Geology* 200: 395-406.

Mikulski SZ, Stein HJ (2005) The Re-Os age for molybdenite from the Variscan Strzegom-Sobótka massif (SW Poland). In: Mao J, Bierlein FP (eds). *Mineral Deposit Research: Meeting the Global Challenge*. Springer: 789-792.

Oberc-Dziedzic T, Zelazniewicz A, Cwojdzinski S (1999) Granitoids of the Odra Fault Zone: late- to post-orogenic Variscan intrusions, SW Poland. *Geologia Sudetica* 32: 55-71.

Pendias H, Walenczak Z (1956) Signs of mineralization in the northwestern part of Strzegom Massif, Lower Silesia. *Biuletyn Instytutu Geologicznego* 227: 209-228.

Pin C, Puziewicz J, Duthou JL (1989) Ages and origins of a composite granitic massif in the Variscan belt: a Rb-Sr study of the Strzegom-Sobótka Massif. *Neues Jahrbuch Mineralogische Abhandlungen* 160: 71-82.

Puziewicz J (1985) Origin of chemical, structural and textural variations in aplites from Strzegom granite (Poland). *Neues Jahrbuch Mineralogische Abhandlungen* 153: 19-31.

Puziewicz J (1990) Strzegom-Sobótka granitic massif (SW Poland). Summary of recent studies. *Archiwum Mineralogiczne* 45: 135-154.

Salacinski R (1978) Ore mineralization and its origin in the granitoids of the Strzegom massif. *Biuletyn Instytutu Geologicznego* 308: 41-90.

Smoliar MI, Walker RJ, Morgan JW (1996) Re-Os ages of group II1, IIIA, IVA and IVB iron meteorites. Science 271: 117-133.

Stein HJ (2006) Low-rhenium molybdenite by metamorphism in northern Sweden: recognition, genesis, and global implications. *Lithos* 87: 300-327.

Stein HJ, Markey RJ, Morgan JW, Hannah JL, Scherstén A (2001) The remarkable Re-Os chronometer in molybdenite: how and why it works. *Terra Nova* 13: 479-486.

Stein HJ, Markowiak M, Mikulski SZ (2005) Metamorphic to magmatic transition captured at the Myszków Mo-W deposit, southern Poland. In: Mao J, Bierlein FP (eds). *Mineral Deposit Research: Meeting the Global Challenge*. Springer: 833-836.

Turniak K, Bröcker M (2002) Age of the two-mica granite from the Strzegom Massif: new data from U/Pb monazite and xenotime study. *Mineralogical Society of Poland Special Papers* 20: 211-213.

Turniak K, Tichomirowa M, Bombach K (2005) Zircon Pb-evaporation ages of granitoids from the Strzegom-Sobótka massif (SW Poland). *Mineralogical Society of Poland - Special Papers* 25: 241-245.

Turniak K, Hałas S, Wojtowicz A (2006) New K-Ar cooling ages of granitoids from Strzegom-Sobótka massif, SW Poland. *Proceedings – IX Ogólnolnopolska Sesja Naukowa Datowanie Mineralów i Skal, Gdansk* 23-24.10. 2006: 63-65.

# The Rigròs F-(Ba) vein system (Catalan Coastal Ranges, NE Spain): fluid geochemistry and timing of ore deposition

À. Piqué & À. Canals
*Dept. de Cristal·lografia, Mineralogia i Dipòsits Minerals, Universitat de Barcelona, Spain*

F. Grandia
*Enviros Spain, S.L., Valldoreix, Spain*

J. M. Fuenlabrada
*C.A.I. de Geocronología, Universidad Complutense de Madrid, Spain*

D. A. Banks
*School of Earth and Environment, University of Leeds, UK*

ABSTRACT: The Rigròs F-(Ba) vein system is hosted by a late Hercynian granodiorite in the Catalan Coastal Ranges. At least two warm (~110ºC) fluids were involved in the main fluorite precipitation stage, one of them had a salinity ~22 wt % NaCl eq, while the other was less saline (~16 wt % NaCl eq). Both fluids are polysaline (Na-Ca-K-Mg-Cl) and show geochemical features of evolved basinal brines after interaction with Triassic evaporites and late Hercynian granitic rocks. Sm-Nd dating of fluorite yields an age of 137 ± 25 Ma, which coincides with the late Jurassic – early Cretaceous rifting episode in the East Iberian basins.

KEYWORDS: Fluorite, hydrothermal fluids, Sm-Nd dating, early Cretaceous, rifting

## 1 INTRODUCTION

F-Ba base-metal low temperature hydrothermal systems are widespread throughout the Palaeozoic basement of Europe and N Africa. The Catalan Coastal Ranges (CCR; NE Spain) host many veins of this type, with the Rigròs system as an outstanding example. This system is located in the Montseny-Guilleries Massif (45 km to the NE of Barcelona) and consists of fluorite-rich and metal-poor veins. The fluorite stock of the massif has been estimated in 3.5 to 4 Mt @ 40-50% $CaF_2$ (Font 1983).

In this work, new geochemical data (microthermometry, *crush-leach* and LA-ICP-MS of fluid inclusions, together with Sr isotopes of fluorite) are presented in order to better understand the physico-chemical processes that led to vein formation. Additionally, these data are complemented with an age determination of vein fluorite that has allowed relating the hydrothermal event to the major tectonic events that affected the CCR.

## 2 THE RIGRÒS MINERALIZATION

The Rigròs vein system is hosted in a late Hercynian granodiorite-monzogranite of calcalkaline affinity. The host rocks close to the vein are affected by propylitic and sericitic alteration.

The main deposit consists of a near-vertical, N50-90º trending vein that measures 0.5-3.5m thick, 700m long and 250m of known vertical extension. It is asymmetric with banded structures and, to a lesser extent, brecciated. Smaller veins, up to 0.5m thick, are also present around the main one.

The vein mineralogy is made up of fluorite, quartz and minor amounts of barite, calcite, galena, sphalerite, chalcopyrite and pyrite. Barite occurs mainly in the central and upper levels, while quartz predominates in the lower levels and at the walls of the vein system (Font 1983). The paragenetic sequence, deduced from transmitted, reflected and cathodoluminescence microscopy of thin sections, is illustrated in Fig. 1. It is interesting to note that fluorite II replaces fluorite I and that they were only distinguished by cathodoluminescence.

## 3 FLUID GEOCHEMISTRY

The geochemistry of ore fluids was characterized from microthermometry, *crush-leach* and LA-ICP-MS analyses of fluid inclusions in fluorite, from Sr isotopes and REE in fluorite and from Sr and S isotopes in barite.

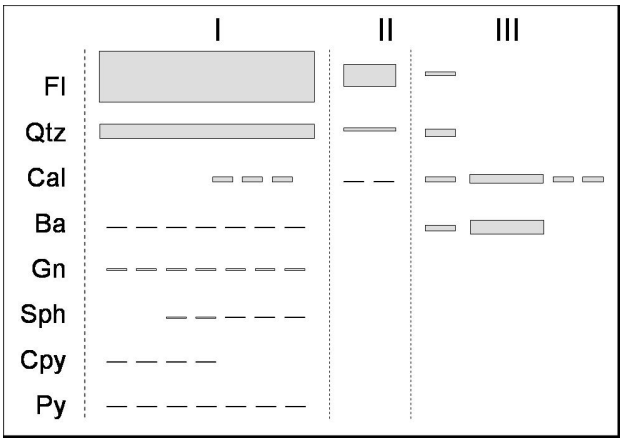


Figure 1. Paragenetic sequence of the minerals precipitated during the hydrothermal events recorded in the Rigròs vein system.

Two populations of fluid inclusions (FI) were determined in fluorite I: A-type FI, found in the main and smaller veins, have $T_{mi}$ up to -22ºC (n=173), with a peak at -19ºC; and B-type FI, only found in the main vein, define a clear peak of $T_{mi}$ around -13ºC (n=85). In both populations most $T_h$ are between 80 and 140ºC (n=145), with a sharp peak at 110ºC. In fluorite II from the main and smaller veins, FI have $T_h$ between 75 and 140ºC (n=149), with a mode at 93ºC, and $T_{mi}$ between -20 and 0ºC (n=224), with a peak at -13ºC. All measured fluid inclusions have eutectic temperatures between -65 and -55ºC.

Relative concentrations of Cl, Br, Na, K and Li in fluid inclusions were obtained from *crush-leach* analysis of 11 samples of fluorite. Cl/Br molar ratios are between 299 and 969 and Na/Br between 114 and 431, with the highest values in fluorite with A-type FI (Fig. 2). Na/K and Na/Li molar ratios in this fluorite (9 to 21 and 73 to 166, respectively) are lower than in fluorite with B-type FI (22 to 43 and 190 to 246, respectively).

Individual fluid inclusion analysis (n=263) was carried out on 7 samples of fluorite I by LA-ICP-MS. The elements analyzed were Mg, K, Mn, Fe, Zn, Ag, Ba and Pb, and Na was the internal standard. The results allow a distinction to be made between A-type and B-type fluids, the former being more enriched in K than Mg and the opposite the latter (Fig. 3). In all samples, the molar abundance of analyzed metals is Fe > Mn ~ Zn > Pb > Ag.

Absolute element concentrations were obtained following the procedures of Allan *et al.* (2005). The Ca/Na ratios, needed for this calculation, were approximated by charge balance of *crush-leach* data. The ranges of mean concentrations in A-type and B-type FI from fluorite I (all in ppm) are Na = 23500 to 37800; Ca = 28700 to 36700; K = 1500 to 5500; Mg = 900 to 2300; Fe = 90 to 1100; Ba = 60 to 460; Mn = 40 to 100; Zn = 40 to 190; Pb = 35 to 190; and Ag = 10 to 15.

$^{87}Sr/^{86}Sr$ ratios of fluorites (n=7) are between 0.7123 and 0.7126. These values are within the range of previously reported data for barites from the same deposit ($^{87}Sr/^{86}Sr$ = 0.7122 to 0.7126; Canals & Cardellach 1993). The $\delta^{34}S$ of these barites are between +17.4‰ and +18.5‰ (Canals & Cardellach, 1993).

Chondrite normalized REE patterns of fluorites are bell shaped (Canals 1989) and, with respect to a granodiorite from the CCR (Enrique 1990), they are enriched in MREE. Most samples of fluorite have small negative Eu and Ce anomalies.

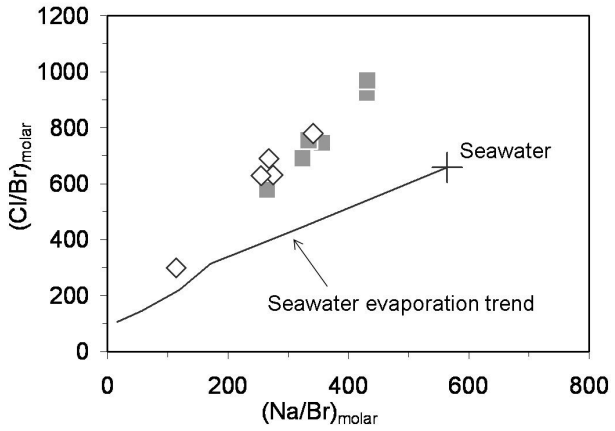


Figure 2. Cl/Br versus Na/Br molar ratios of leachates from fluorites with A-type (■) and B-type FI (◇).

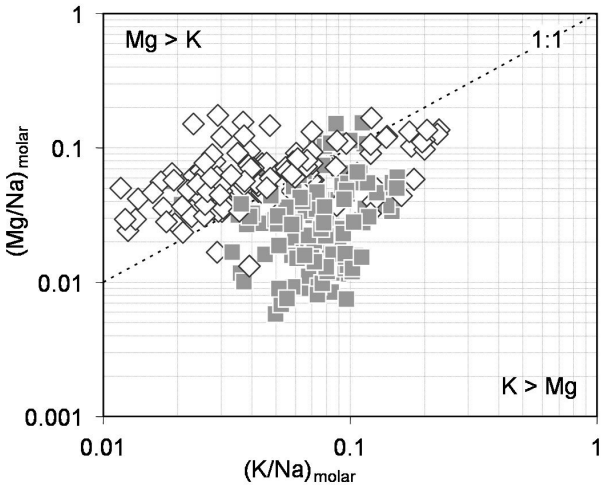


Figure 3. Mg/Na versus K/Na molar ratios of A-type (■) and B-type FI (◇) in fluorite I.

## 4 Sm-Nd DATING

Sm-Nd isotope analyses were carried out on 11 fluorite samples from Rigròs. Sm and Nd concentrations range from 3.04 to 6.89 ppm and from 6.87 to 14.66 ppm, respectively. The $^{147}Sm/^{144}Nd$ ratio varies from 0.1717 to 0.3537.

The fluorites define a Sm-Nd isochron, yielding an age of 137 ± 25 Ma (MSWD = 0.40) and an initial $^{143}Nd/^{144}Nd$ ratio of 0.512078 ± 0.000046 (Fig. 4). The mean age value corresponds to the Valanginian (early Cretaceous) and, if the error bar is considered, the age is between the Callovian (Middle Jurassic) and Aptian (early Cretaceous).

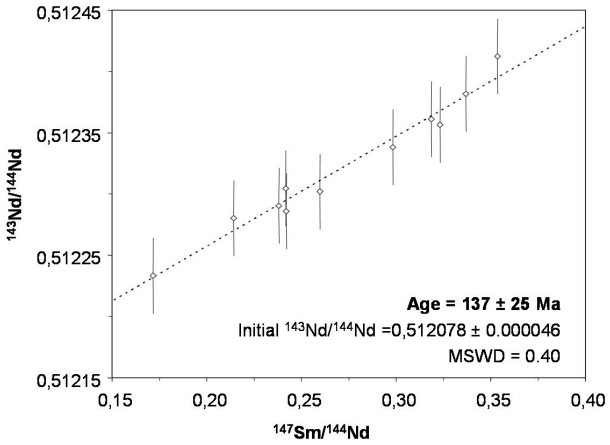


Figure 4. Sm-Nd isochron of fluorite samples from the Rigròs vein system. Error bars are 2σ.

## 5 DISCUSSION AND CONCLUSIONS

At the time of ore formation (Callovian to Aptian) sedimentary rocks were deposited at Rigròs in a shallow marine environment, as revealed by the extensive development of carbonate platforms. These rocks overlie alluvial, shallow marine and evaporitic sequences deposited during the Triassic.

The presence of evaporite horizons is relevant in terms of brine formation and metal transport, as brine infiltration from the Triassic down to the crystalline basement is a plausible process to explain the origin of the ore-forming fluids at Rigròs. *Crush-leach* data support the interaction of fluids with evaporites. The relatively wide ranges of the Cl/Br ratios in the fluid inclusions can be explained by mixing between a seawater-derived fluid, with some degree of evaporation, and a fluid resulting from halite dissolution, or simply by a seawater-derived brine that subsequently leached evaporites. A contribution of halogens from the crystalline basement by water-rock interaction is likely to be insignificant and would be masked in any case by the high salinity of the sedimentary brines.

In a Cl/Br vs Na/Br graph (Fig. 2), the Rigròs fluids plot to the left of the seawater evaporation trend, implying a loss of Na. This loss was compensated by an increase of Ca, K and Li in A-type fluids and by an increase of Ca and Li in B-type fluids. Therefore, A-type fluids seem to have undergone a higher degree of interaction with rocks.

The concentrations of ore metals in the Rigròs fluids are of the same order of magnitude as those reported for modern sedimentary formation brines (*see e.g.* Yardley (2005) for references), which are furthermore considered the current equivalents to brines in Mississippi Valley-type deposits.

Sulphur isotope values of barites are within the range of Triassic to early Jurassic evaporite values from NE Spain (+10‰ to +19‰; Utrilla *et al.* 1992), supporting an origin of sulfate from leaching of these evaporites.

$^{87}Sr/^{86}Sr$ ratios of fluorites and barites are higher than those of Mesozoic seawater (Burke et al. 1982) and of the initial ratio of late Hercynian granitoids from the CCR (0.71026; Del Moro & Enrique 1996). This $^{87}Sr$-enrichment is believed to be caused by water-granite interaction during the early Cretaceous, without excluding a significant contribution of Sr from seawater.

The REE patterns of the Rigròs fluorites may reflect leaching of the granite because they are very similar to those found in granite-aquifer waters and from granite leaching experiments (Möller *et al*. 1997).

The age of the Rigròs vein system coincides with the late Jurassic – early Cretaceous (end of Oxfordian – Middle Albian) rifting episode that occurred in the East Iberian basins (Salas *et al.* 2001), related to the opening of the Central Atlantic.

The proposed model for the genesis of the Rigròs vein involves the circulation of hydrothermal fluids through fracture systems affecting the Mesozoic cover and the crystalline basement. Fluid migration and mineral precipitation was related to a rifting episode that occurred during the middle Mesozoic (late Jurassic – early Cretaceous). Hydrothermal fluids were evolved polysaline brines (Na-Ca-Cl) generated in a evaporitic environment. Some

geochemical features of these fluids were subsequently acquired during interaction with basement rocks. Finally, although the mixing of fluids has been proposed as a mechanism of ore precipitation for similar veins in Western and Central Europe, any evidence for this process found at Rigròs can be interpreted instead as the result of an evolution through time of the hydrothermal system.

## ACKNOWLEDGEMENTS

This study was financed through a CICyT project (BTE2003-01346) and the stay of À.P. at the University of Leeds to perform the LA-ICP-MS and *crush-leach* analyses was funded by the FPU program, both from the Spanish Ministry of Education and Science.

## REFERENCES

Allan MM, Yardley BWD, Forbes LJ, Shmulovich KI, Banks DA, Shepherd TJ (2005) Validation of LA-ICP-MS fluid inclusion analysis with synthetic fluid inclusions. *Am Miner* 90: 1767-1775 DOI 10.2138/am.2005.1822

Burke WH, Denison RE, Hetherington EA, Koepnick RB, Nelson HF, Otto JB (1982) Variation of seawater $^{87}Sr/^{86}Sr$ throughout Phanerozoic time. Geology 10: 516-519

Canals À (1989) Fisico-química de los fluidos del filón Rigròs (Girona): datos de inclusiones fluidas y tierras raras. *Bol Soc Esp Mineral* 12: 283-293

Canals À, Cardellach E (1993) Strontium and sulphur isotope geochemistry of low-temperature barite-fluorite veins of the Catalonian Coastal Ranges (NE Spain): a fluid mixing model and age constraints. *Chem Geol* 104: 269-280 DOI 10.1016/0009-2541(93)90156-D

Del Moro A, Enrique P (1996) Edad Rb-Sr mediante isocrona de minerales de las tonalitas biotítico-hornbléndicas del Macizo del Montnegre (Cordilleras Costeras Catalanas). *Geogaceta* 20, 2: 491-494

Enrique P (1990) The Hercynian intrusive rocks of the Catalonian Coastal Ranges (NE Spain). *Acta Geol Hisp* 25, 1-2: 39-64

Font X (1983) Estudio de las mineralizaciones del Montseny-Guilleries (Barcelona y Girona) y su aplicación en la prospección geoquímica de redes de drenaje. *Unpublished PhD thesis, Universitat de Barcelona*, 317 pp

Möller P, Stober I, Dulski P (1997) Seltenerdelement-, yttrium-gehalte und bleiisotope in thermal- und mineralwässern des Schwarzwaldes. *Grundwasser* 3: 118-132 DOI 10.1007/s767-1997-8533-0

Salas R, Guimerà J, Mas R, Martín-Closas C, Meléndez A, Alonso A (2001) Evolution of the Mesozoic Central Iberian rift system and its Cainozoic inversion (Iberian Chain). In: Ziegler et al. (eds) Peri-Tethys Memoir 6: Peri-Tethyan rift/wrench basins and passive margins. *Mém Mus Nat Hist Natur* 186: 145-185

Utrilla R, Pierre C, Ortí F, Pueyo JJ (1992) Oxygen and sulphur isotope compositions as indicators of the origin of Mesozoic and Cenozoic evaporites from Spain. *Chem Geol* 102: 229-244 DOI 10.1016/0009-2541(92)90158-2

Yardley BWD (2005) Metal concentrations in crustal fluids and their relationship to ore formation. *Econ Geol* 100: 613-632 DOI 10.2113/100.4.613

# Dating of orogenic gold in the Svecofennian domain of southern Finland

K. Saalmann, P. Peltonen & I. Mänttäri
*Geological Survey of Finland, P.O. Box 96, FI-02151 Espoo, Finland*

U. Kuronen
*Polar Mining Oy, P.O. Box 15, FI-83501 Outokumpu, Finland*

ABSTRACT: Most gold occurrences in Finland can be classified as orogenic gold. The absolute age of mineralization is not well constrained yet and neither is it well known whether the Svecofennian orogeny comprises several episodes of mineralization of various age. The study areas are located in the Häme belt and Pirkanmaa belt that belong to two different arc terranes. Structural studies of both areas suggest that they can be classified as orogenic gold occurrences. A multi-mineral approach of applying various isotope systems on different samples and minerals is used i.e. U/Pb of zircon, monazite and titanite as well as $^{40}Ar/^{39}Ar$ analyses of biotite and hornblende from auriferous quartz veins. Samples comprise host rocks, spatially associated pre- and post-mineralization veins and dykes, and hydrothermal and/or metamorphic minerals formed in the wall rock alteration zones.

KEYWORDS: orogenic gold, Svecofennian orogeny, U/Pb dating, $^{40}Ar/^{39}Ar$ dating

## 1 INTRODUCTION

Many gold occurrences in Finland can be classified as orogenic gold linked to shear zones and thus to specific deformation episodes in the tectonic evolution of the Fennoscandian Shield.

Although the relative age of many prospects to the main deformation episodes is often known, the true age of mineralization is not well constrained. Hence, determination of the age of these shear zones is critical for understanding the formation, origin and location of regional mineralization episodes as well as their genetic relationships. Mineralization in most orogenic gold occurrences in the Palaeoproterozoic Svecofennian domain in southern Finland took place between 1.84–1.79 Ga; however, few ages are based on direct dating of mineralization but rather attempt to bracket the timing of mineralization indirectly (Eilu *et al*. 2003). Therefore, the possibility of the existence of mineralization episodes of various age cannot be excluded.

Despite the fact that individual gold deposits have different origins and structural settings, no systematic study exists on whether or not structurally controlled gold deposits in southern Finland are linked to the same tectonic regime and event. Although the tectonic evolution is well established, including a large number of age data, in particular in the Uusimaa belt, the age of gold mineralization in both the Southern Svecofennian Arc Complex (SSAC) and the Central Svecofennian Arc Complex (CSAC) has not been intensely studied yet. The determination of whether or not the majority of these deposits formed nearly synchronously during a widespread shearing event or if gold mineralization was diachronous and took place at different times in different terranes has important consequences for constraining genetic models and for finding new targets.

Host rocks, spatially associated pre- and post-mineralization veins and dykes, and wall rock alteration minerals can be used to bracket the age of mineralization. Hydrothermal phosphate minerals, like monazite, are common in ore-mineral assemblages in orogenic deposits and occur either in ore-bearing veins or in altered wall rocks. As a consequence, we use a multi-mineral approach by applying various isotope systems on different samples and minerals.

## 2 GEOLOGIC SETTING

The two study areas are located in the Häme belt and Vammala Migmatite Zone, Pirkanmaa belt (Fig. 1), and they belong to two different

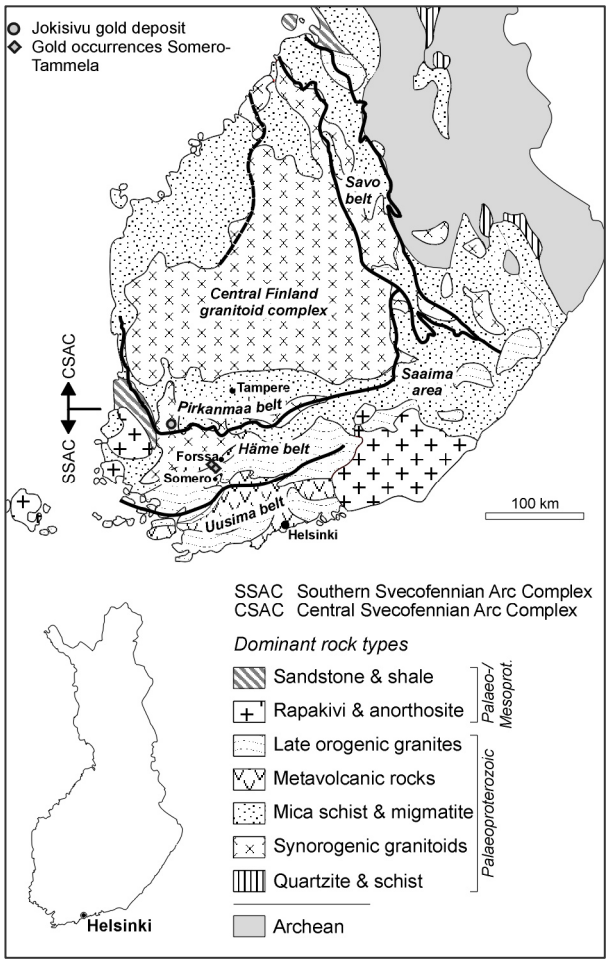


Fig. 1: Simplified geological map of southern Finland. The study areas are located in the Häme belt between Forssa and Somero and in the Jokisivu deposit farther NW.

arc terranes the SSAC and CSAC, respectively.

The critical Somero-Tammela gold zone in the northern Häme belt comprises calc-alkaline amphibolite facies metavolcanic and metasedimentary rocks of the Forssa Group, which is part of a continental volcanic arc complex. The gold occurrences are hosted by quartz veins and shear zones that truncate a sequence of felsic to mafic metavolcanic rocks. The structural geology implies that the mineralization is closely related to quartz veins and WSW-ENE to SW-NE trending shear zones and faults formed during dextral transpression (D3). Elevated gold concentrations, spatially associated with shear zones and faults, can be observed typically in brittle reactivated shear zones. Quartz veins are accompanied in many places by sulphidization of the wall rock. Biotite occurs at the margins of some quartz veins and, together with sulphide minerals, in shear zones adjacent to quartz veins. The biotite flakes as well as the sulphide minerals are enriched in layers and are aligned in the shear zone foliation, illustrating the close relationship of shearing and mineralization.

The Somero-Tammela gold zone provides typical examples of mesothermal orogenic gold (*sensu* Groves *et al*. 1998) formed during the later retrograde stages of orogenic evolution that give rise to formation of auriferous quartz veins and deformation at the brittle-ductile boundary (Saalmann, this volume). Transpressional deformation in southern Finland is related to the so-called "post-collisional stage" (Ehlers et al. 1993) at 1.84–1.81 Ga after collision of the SSAC with the CSAC in the north (Fig. 1). However, the age of mineralization in this area has not been determined yet.

The Jokisivu gold deposit is located farther north in the Pirkanmaa belt, which formed as part of the CSAC. The deposit is under feasibility study and test mining by Polar Mining Oy/Dragon Mining NL. The deposit comprises two ore zones, and the current in situ resource estimate is 1.5 Mt of gold at the average grade of 6.8 g/t Au (Haga 2005, FINGOLD database, GTK).

The deposit is hosted by metamorphosed quartz-diorite/gabbro. It is interpreted to form a subvolcanic or shallow intrusion sub-parallel to the compositional layering of the wall rocks (mica gneiss) either before deformation or after the initial deformation of the wall rocks. The overall structure, alteration types and mineralogy, as well as mineralization stages, are well known (*e.g*. Luukkonen *et al.* 1992, Luukkonen 1994). The absolute age of gold deposition, however, is not established. Gold occurs in SE-NW to ESE-WNW striking sheared quartz veins and surrounding mineralized alteration zones with a width of a couple of metres to few decimetres, and the whole occurrence consists of a series of stacked vein systems. The shear zone, quartz veins and dominant foliation in the mica gneisses were affected by regional scale folding around SW-NE to SSW-NNE striking and 40-60° NE-plunging axes. In contrast to the metasedimentary rocks, the quartz diorite was not affected by intense migmatization accompanying folding. However, folds are exposed in the Jokisivu deposit as the northwestern part of the ore zone bends to the S and SE, suggesting that it is also affected by the regional-scale folding. Thus the mafic rocks deformed in a less ductile way than the surrounding metasedimentary rocks but have been boudinaged and disrupted. Nevertheless these structural relationships suggest that mineralization occurred

close to (possibly shortly after) the regional metamorphic peak conditions. A number of barren pegmatite dykes intrude along-strike of the deposit following the general strike of the ore zone. Thick and very coarse-grained dykes, which can be followed tens of metres along strike, cut the ore zone and run sub-parallel to the quartz veins and the alteration zone. The dyke thickness ranges from a couple of cm to several dm. The foliation in the wall rocks does not deflect around the coarse and thick dykes, suggesting an emplacement after foliation development. Since the dykes also cut quartz veins locally, they post-date vein intrusion. They are also affected by the regional scale folding and, therefore, might have intruded during folding, possibly in the later stages.

## 3 ISOTOPIC DATING IN PROGRESS

A series of samples of pre-, syn- and late- to post-mineralization rocks have been taken to gain absolute ages of mineralization events and gold deposition by using a variety of techniques.

### *3.1 Somero-Tammela gold zone*

The maximum age of gold deposition in the area is provided by the crystallization age (U/Pb zircon) of a fine-grained felsic volcanic rock, which is part of the host rocks. A $^{40}Ar/^{39}Ar$ cooling age of biotite from unsheared granodiorite as well as an unsheared felsic tuff, both from host rocks unaffected by mineralization, can be compared with $^{40}Ar/^{39}Ar$ cooling ages of mineralization related hydrothermal biotite.

Direct dating of the mineralization was attempted by $^{40}Ar/^{39}Ar$ cooling ages of hydrothermal biotite and amphibole and, if available, U/Pb data for hydrothermal zircon or monazite. Samples for zircon and monazite dating have been taken from altered wall rocks of auriferous quartz-tourmaline veins and from a sheared and altered intermediate metavolcanic rock that is truncated by numerous narrow quartz veins. This rock gives high gold contents. Biotite formed in quartz veins as well as biotite and hornblende in alteration zones around quartz veins containing sulphide minerals were sampled for $^{40}Ar/^{39}Ar$ analysis. Their ages are expected to be close to the age of mineralization.

A quartz feldspar dyke cuts the dominant foliation of the country rocks and has the same strike as auriferous quartz veins, suggesting a contemporaneous intrusion. Moreover, the wall rocks show the same mineralization as many quartz veins. Thus the age of this dyke is proposed to be close to the age of quartz vein formation and of gold deposition In addition, biotite has been separated from in the mineralized wall rock of this dyke for $^{40}Ar/^{39}Ar$ analysis.

### *3.2 Jokisivu (Vammela migmatite zone, Pirkanmaa belt)*

With ages of the host rocks (quartz diorite) and of unmineralized pegmatite dykes that postdate the auriferous quartz veins, the age of gold deposition can be bracketed. For this purpose unaltered samples of the quartz diorite from outside the ore zone have been taken for U/Pb zircon analysis to provide the maximum age of mineralization. The barren pegmatite that partly follows the ore zone but postdates the mineralization gives the minimum age of gold deposition in the sheared quartz veins.

Samples of intensely altered quartz diorite from the ore zone surrounding the quartz veins have been taken in order to further bracket the age for gold mineralization by dating metamorphic and/or mineralization-related hydrothermal minerals (titanite, zircon).

## ACKNOWLEDGEMENTS

This is a contribution to the project "Geological and metallogenic bedrock modelling", Geological Survey of Finland. The authors would like to thank Polar Mining Oy/Dragon Mining NL for the permission to study the Jokisivu gold deposit.

## REFERENCES

Dragon Mining NL (2005) Press release, 24 February 2005. available from Internet pages: http://www.dragon-ming.com.au/pages/ASX/2005/24feb2005_vammala_production_centre.htm

Ehlers, C., Lindroos, A., Selonen, O. (1993) The late Svecofennian granite–migmatite zone of southern Finland — a belt of transpressive deformation and granite emplacement. *Precambr. Res*. 64: 295–309.

Eilu, P., Sorjonen-Ward, P., Nurmi, P. & Niiranen, T. (2003) A review of gold mineralization styles in Finland. *Economic Geology* 98: 1329-1354.

FINGOLD public database, Geological Survey of Finland (GTK). ed. by P. Eilu.; Internet-link: http://en.gtk.fi/ExplorationFinland/Commodities/Gold/gtk_gold_map.html

Groves, D.I., Goldfarb, R.J., Gebre-Mariam, M., Hagemann, S.G. & Robert, F. (1998) Orogenic gold deposits: A proposed classification in the context of their crustal distribution and relationship to other gold deposit types. *Ore Geology Reviews* 13: 7-27.

Luukkonen, A., Grönholm, P. & Hannila, T. (1992) Eräiden Etelä-Suomen kulta- ja sen seuralaismetalliesiintymien geologiset pääpiirteet. Summary: Main geological features of certain gold and tungsten-tin-gold prospects in southern Finland.- *Geol. Surv. Finland, Report of Investigation* 113: 1-9.

Luukkonen, A. (1994) Main geochemical features, metallogeny and hydrothermal alteration phenomena of certain gold and gold-tin-tungsten prospects in southern Finland. *Geol. Surv. Finland, Bulletin* 377: 1-153.

Saalmann, K.: Orogenic gold in southwestern Finland. *This volume*.

# Age of the Silvermines Irish-type Zn-Pb deposit from direct Rb-Sr dating of sphalerite

Jens Schneider
*Ore Fluids Research Group, K.U. Leuven, Belgium*

Albrecht von Quadt
*Swiss Federal Institute of Technology, Institute of Isotope Geochemistry and Mineral Resources, Zurich, Switzerland*

Jamie J. Wilkinson
*Imperial College, Department of Earth Science and Engineering, London, United Kingdom*

Adrian J. Boyce
*Scottish Universities Environmental Research Centre, East Kilbride, United Kingdom*

ABSTRACT: A well-defined Rb-Sr isochron age of 360 ± 5 Ma is presented for sphalerite from the carbonate-hosted, stratabound Silvermines Irish-type (IRT) Zn-Pb deposit in the Irish Midlands, constraining the age of mineralization to early Tournaisian (Courceyan). The age is in agreement with an early, syndiagenetic-exhalative origin for the Silvermines system and is inconsistent with models of gravity-driven flow of mineralizing fluids in the Irish orefield and entirely epigenetic (burial diagenetic) interpretations of the ores. The initial $^{87}Sr/^{86}Sr$ ratio of the isochron identifies Lower Carboniferous seawater as an important contributor to the ore-forming fluids.

KEYWORDS: Irish-type Zn-Pb deposits, Silvermines, geochronology, Rb-Sr, sphalerite

## 1 INTRODUCTION

Irish-type (IRT) zinc-lead (± barite) deposits hosted by Lower Carboniferous limestones of the Irish Midlands form a class of stratabound base metal mineralization that are distinct in many features from other carbonate-hosted Zn-Pb deposits (*e.g*. Hitzman & Beaty 1996; Wilkinson 2003). Among the most striking differences is the presence of both epigenetic-replacive mineralization styles and stratiform orebodies displaying textures suggestive of a syndiagenetic-exhalative origin (Banks 1985; Boyce *et al*. 1983a, 2003).

Due to the complex nature of IRT deposits and despite numerous studies, their genesis is still a matter of controversy. An entirely epigenetic, post-lithification formation of IRT ores has been proposed (Hitzman & Beaty 1996; Peace & Wallace 2000; Reed & Wallace 2004). Hitzman & Beaty (1996) explained the origin of IRT deposits by gravity-driven fluid flow due to uplift of the Hercynian orogen during the Visean, invoking the upper Devonian Old Red Sandstone as the principal fluid aquifer and source of base-metals.

Alternative models favour an earlier onset of ore deposition during Tournaisian crustal extension that allowed deep penetration of seawater-derived fluids into, and extraction of metals from the Lower Palaeozoic basement. This is believed to have resulted in both exhalative seafloor ore deposition and syndiagenetic, sub-seafloor mineralization of the Lower Carboniferous host limestones (*e.g.* Russell 1986; Boyce *et al*. 2003; Wilkinson 2003, Wilkinson *et al.* 2005). Hydrothermal activity is thought to have continued until at least the Arundian stage of the Visean (*e.g*. Anderson *et al.* 1998: Wilkinson 2003; Wilkinson *et al*. 2003).

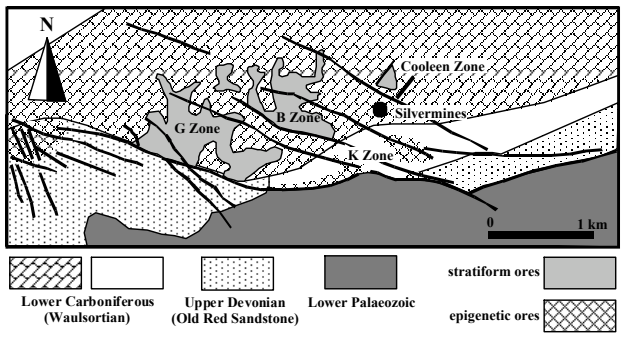


Figure 1. Simplified geological map of the Silvermines area showing the main structural elements and mineralization types (modified after Lee & Wilkinson 2002).

Critical uncertainties in these models arise largely from a poor knowledge of the absolute age of mineralization. Previous attempts to constrain the timing of IRT deposits, mostly

based on geological criteria, have yielded ambiguous results. Here we present an isotopic age for the Silvermines IRT deposit, Co. Tipperary, obtained from direct Rb-Sr dating of ore-stage sphalerite.

## 2 GEOLOGY AND AGE CONSTRAINTS

The Silvermines deposit and associated mineralization (Fig. 1) has been extensively decribed by Boyce *et al*. 1983a; Taylor (1984), Andrew (1986), Mullane and Kinnaird (1998), Everett *et al.* (1999), and Lee & Wilkinson (2002). Four types of mineralization are known in the Silvermines area (Fig. 1): (i) stratiform massive sulphide and barite bodies in Lower Carboniferous carbonate units (Ballynoe open pit, B, Upper G, and Cooleen Zones); (ii) epigenetic-replacive sulphides (Lower G and K Zones); (iii) base-metal and barite veins in altered portions of the Old Red Sandstone; and (iv) sulphide-quartz-carbonate veins in the Lower Palaeozoic basement which have been implicated as feeder conduits (Everett *et al*. 1999).

The mineralized Lower Carboniferous sequence consists of interbedded dolomitised, muddy, and partly brecciated carbonate rocks of Courceyan age (Fig. 2), with the Waulsortian Limestone being the principal host rock. The structural pattern of the area is characterised by a system of interrelated WNW-NW-trending synsedimentary faults (Fig. 1) that exerted a major control on the development of sedimentation and mineralization (Boyce *et al*. 1983b; Andrew 1986).

## 3 SAMPLING AND METHODS

Five sphalerite samples from the Silvermines G and Cooleen Zones (SILV 10, CLN 1-4; Fig. 1) were extracted from selected hand specimens and drillcore. One additional sphalerite sample (LGH 3) was taken from a quartz-carbonate vein exposed in the Lower Palaeozoic basement at Latteragh, 12km east of Silvermines.

All samples were crushed and sieved and for each analysis between 50 and 100 mg of sphalerite were carefully handpicked from 400-250 µm grain size fractions. To remove possible carbonate contaminants, the sphalerite separates were repeatedly leached in 1 N HCl and washed with deionised water prior to analysis. The dry samples were then weighed and crushed in 400 µl of deionised water using a clean boron-carbide mortar and pestle (*e.g.* Christensen *et al*. 1995) in order to remove possible multistage inclusion fluids that may disturb the Rb-Sr system of the host sphalerite. The fluid inclusion leachates were separated by centrifuging and collected for separate Rb-Sr analysis. The crushed sphalerite residues were then leached again for 10 min using 1 N HCl and repeatedly washed with deionised water and centrifuged. To eliminate concentration errors due to material loss, the residues were dried on a hot plate, cooled and carefully weighed into new Teflon vials and allowed to decompose in 2 ml of 6 N HCl on a hot plate. Vial tops were lifted repeatedly to release $H_2S$. Complete dissolution of all samples was achieved within one week.

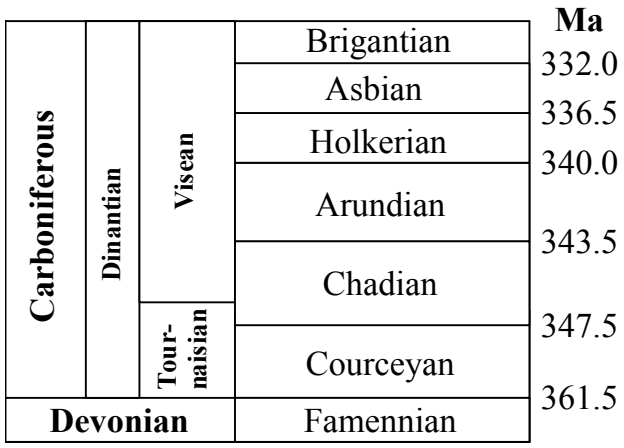


Figure 2. Lower Carboniferous timescale showing main stages, substages and absolute ages according to the recently updated global time scale (Menning *et al.* 2006).

All sample solutions were totally spiked using a mixed $^{87}Rb$-$^{84}Sr$ tracer. Rubidium and strontium were separated with 3 N $HNO_3$ using EICHROM Sr resin on 50 µl Teflon columns. The first 600 µl of $HNO_3$ wash were collected for Rb and further purified using standard ion-exchange procedures. Sr was stripped from the 50 µl columns with 1 ml of deionised water.

Rb and Sr isotopic measurements were performed on a six collector FINNIGAN MAT 262 mass spectrometer running in static multi-collection mode. Total procedural blanks amounted to 40 pg Sr and 2-5 pg Rb. All data were blank-corrected. Rb-Sr isochron regressions were calculated after Ludwig (2003) using the ISOPLOT/Ex version 3.00 program and errors on the ages are quoted at the 2σ level.

## 4 RESULTS AND DISCUSSION

The crushed sphalerite residues from the Silvermines area have $^{87}Rb/^{86}Sr$ ratios between 0.008 and 0.744 and $^{87}Sr/^{86}Sr$ ratios ranging from 0.70796 to 0.71174. Fig. 3 shows a $^{87}Sr/^{86}Sr$ vs. $^{87}Rb/^{86}Sr$ correlation diagram for the samples. The five Silvermines sphalerites define a statistically well-supported five-point isochron, with a slope yielding an age of 359.9±1.7 Ma (MSWD = 1.6, initial $^{87}Sr/^{86}Sr$ = 0.70793 ± 1). On a $^{87}Sr/^{86}Sr$ vs. 1/Sr plot (not shown) there is no discernible linear data arrangement, indicating that the line in Fig. 3 is not a pseudo-isochron produced by binary mixing of distinct Sr components. The four samples from the Cooleen Zone display the highest isotope ratios whereas sample SILV 10 from the G Zone plots close to the initial $^{87}Sr/^{86}Sr$ ratio. Isochron regression including the sample of vein sphalerite LGH 3 is still statistically acceptable (MSWD 2.2) and yields 360 ± 5.2 Ma with an initial $^{87}Sr/^{86}Sr$ ratio of 0.70794 ± 3, indistinguishable from the five-point regression within errors. This implies that the sulphide-bearing veins in the Lower Palaeozoic do represent conduits for mineralizing fluids as previously inferred from fluid inclusion and isotopic evidence (Everett *et al*. 1999; Wilkinson *et al*. 2005). The initial $^{87}Sr/^{86}Sr$ ratio of 0.7079 is very close to values observed for stratiform barite from the Ballynoe pit and within the range expected for Carboniferous seawater (Wilkinson *et al*. 2005). This indicates a significant seawater component in the mineralizing fluids as suggested by fluid inclusion halogen data (Banks *et al.* 2002; Wilkinson *et al*. 2005). The age indicates that the use of pressure solution features and textural relationships for constraining the timing of mineralization in sediment-hosted deposits may be unreliable, especially where extensive recrystallisation has occurred.

## 5 CONCLUSIONS

The 360 Ma date provides the first reliable absolute age of the IRT deposits, constraining mineralization in the Silvermines area to the early to middle Courceyan (Fig. 2). This is consistent with an early syndiagenetic-exhalative, near-seafloor formation of ores at Silvermines as previously inferred (Lee & Wilkinson 2002; Boyce *et al*. 2003). Our age clearly disproves models of entirely epigenetic, post-lithification ore-forming processes in the Irish Midlands (Peace & Wallace 2000; Reed & Wallace 2004) and implies gravity-driven fluid flow is unlikely to be the principal driving force for IRT mineralization (Hitzman & Beaty 1996). However, we do not exclude a diachronous evolution of mineralization across the Irish orefield, including the development of epigenetic ores even in some parts of the Silvermines deposit. More detailed direct Rb-Sr geochronology of sphalerite will reveal whether the timing of different textural stages of IRT mineralization can be resolved.

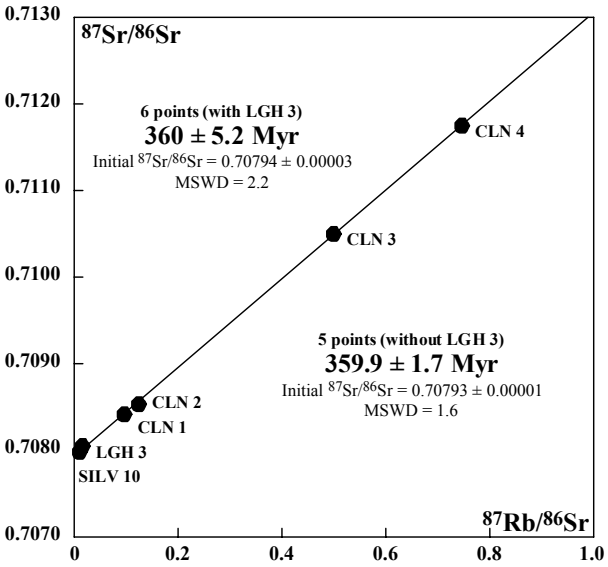


Figure 3. Rb-Sr isochron diagram for crushed sphalerite residues showing ages calculated only for Silvermines samples (n = 5) and including the vein sphalerite (LGH 3) from Latteragh (n = 6).

## ACKNOWLEDGEMENTS

We would like to thank Mike Lee for providing samples, many helpful discussions, and support in the field. Kellys of Fantane Concrete Ltd. are thanked for providing access to their quarries. The invaluable help of Manfred Menning (GFZ Potsdam, Germany) is greatly acknowledged.

## REFERENCES

Anderson IK, Ashton JH, Boyce AJ, Fallick AE, Russell MJ (1998) Ore depositional processes in the Navan Zn+Pb deposit, Ireland. *Econ Geol* 93: 535-563

Andrew CJ (1986) The tectono-stratigraphic controls to mineralization in the Silvermines area, County Tipperary, Ireland. In: Andrew CJ, Crowe, RWA, Finlay S, Pennell WM, Pyne J (eds) *Geology and genesis of mineral deposits in Ireland:* Dublin, Irish Association for Economic Geology: 377-417

Banks DA (1985) A fossil hydrothermal worm assemblage from the Tynagh lead-zinc deposit in Ireland. *Nature* 313: 128-131

Boyce AJ, Coleman ML, Russell MJ (1983a) Formation of fossil hydrothermal chimneys and mounds from Silvermines, Ireland. *Nature* 306: 545-550

Boyce AJ, Anderton R. and Russell MJ (1983b) Rapid subsidence and early Carboniferous mineralization in Ireland. *Trans Inst Min Metall* 92: B55-66

Boyce AJ, Little CTS, Russell MJ (2003) A new fossil vent biota in the Ballynoe barite deposit, Silvermines, Ireland: Evidence for intracratonic seafloor hydrothermal activity about 352 Ma. *Econ Geol* 98: 649-656

Everett CE, Wilkinson JJ, Rye DM (1999) Fracture-controlled fluid flow in the Lower Palaeozoic basement rocks of Ireland: Implications for the genesis of Irish-type Zn-Pb deposits. In: McCaffrey KJW, Lonergan L, Wilkinson JJ (eds) Fractures, fluid flow, and mineralization. *Geol Soc London Spec Pub* 155: 247–276

Hitzman MW, Beaty DW (1996) The Irish Zn-Pb-(Ba) orefield. In: Sangster DF (ed) Carbonate-hosted lead-zinc deposits. *SEG Spec Pub* 4: 112-143

Lee MJ, Wilkinson JJ (2002) Cementation, hydrothermal alteration, and Zn-Pb mineralization of carbonate breccias in the Irish Midlands: Textural evidence from the Cooleen zone, near Silvermines, County Tipperary: *Econ Geol* 79: 653-662

Ludwig KR 2003, Isoplot/Ex version 3.00. A geochronological toolkit for Microsoft Excel.: *Berkeley Geochron Center Spec Pub* 4: 1-43

Menning M, et al. (2006) Global time scale and regional stratigraphic reference scales of Central and West Europe, East Europe, Tethys, South China, and North America as used in the Devonian-Carboniferous-Permian Correlation Chart 2003 (DCP 2003). *Palaeogeogr, Palaeoclimat, Palaeoecol* 240: 318-372

Mullane MM, Kinnaird JA (1998) Synsedim-entary mineralization at the Ballynoe barite deposit, near Silvermines, Co. Tipperary, Ireland. *Trans Inst Mining Metall* 107: B48-61

Peace WM, Wallace MW (2000) Timing of mineralization at the Navan Zn-Pb deposit: A post-Arundian age for Irish mineralization. *Geology* 28: 711-714

Reed CP, Wallace, MW (2004) Zn-Pb mineralization in the Silvermines district, Ireland: a product of burial diagenesis. *Mineral Deposita* 39: 87-102

Russell MJ (1986) Extension and convection: a genetic model for the Irish Carboniferous base metal and barite deposits. In: Andrew CJ, Crowe, RWA, Finlay S, Pennell WM, Pyne J (eds) *Geology and genesis of mineral deposits in Ireland*: Dublin, Irish Association for Economic Geology: 545-554

Taylor S (1984) Structural and paleotopo-graphical controls of lead-zinc mineralization in the Silvermines ore bodies, Republic of Ireland. *Econ Geol* 79: 529-548

Wilkinson JJ (2003) On diagenesis, dolomitisation and mineralization in the Irish Zn-Pb orefield. *Mineral Deposita* 38: 968-983

Wilkinson JJ, Boyce AJ, Everett CE, Lee MJ (2003) Timing and depth of mineralization in the Irish Zn-Pb orefield. In: Kelly JG, Andrew CJ, Ashton JH, Boland MB, Earls G, Fusciardi L, Stanley G (eds) *Europe's Major Base Metal Deposits*. Dublin, Irish Association for Economic Geology: 483-497

Wilkinson JJ, Everett CE, Boyce AJ, Gleeson, SA, Rye DM (2005) Intracratonic crustal seawater circulation and the genesis of sub-seafloor zinc-lead mineralization in the Irish orefield. *Geology* 33: 85-88

# Palaeomagnetic age of the Magcobar Ba deposit, Silvermines, Ireland

D.T.A. Symons, S.J. Pannalal & K. Kawasaki,
*Dept. of Earth and Environmental Sciences, University of Windsor, Windsor, ON, Canada*

D.F. Sangster,
*Consultant, North Gower, ON, Canada*

G.A. Stanley,
*Geological Survey of Ireland, Dublin, Ireland*

ABSTRACT: Palaeomagnetic analysis has been done on 183 specimens from 16 sites in barite and Lower Carboniferous Waulsortian (352±3 Ma) pyritic and carbonate hostrocks of the Magcobar pit in the Silvermines Zn-Pb-Ba district of the Irish Midlands. Alternating field and thermal step demagnetization and saturation isothermal remanence analyses show that the characteristic remanent magnetization (ChRM) is carried by single domain magnetite with minor haematite. Breccia and fold tests show that the ChRM is post-brecciation and post-folding. The paleopole for the ChRM is located at 43.0°S, 19.9°W (dp = 1.2°, dm = 2.4°), giving an age of 269±4 Ma on the apparent polar wander path. Thus the Magcobar barite deposit, and likely the Silvermines Zn-Pb deposits also, was formed epigenetically at 269±4 Ma.

KEYWORDS: barite, Magcobar, Silvermines, Irish Midlands, ore genesis, palaeomagnetism

## 1 INTRODUCTION

Lower Carboniferous carbonate rocks of the Irish Midlands are host to numerous Pb-Zn-Ag-Ba deposits (Fig. 1). One of these, Magcobar (~5.5x$10^6$ tonnes of 84% barite), is the up-dip extension of the now inaccessible Silvermines deposit which produced ~17.7x$10^6$ tonnes of Pb-Zn-Ag ore (Andrew 1986).

Palaeomagnetic methods have been used elsewhere to provide direct ages for similar Zn-Pb-Ba mineralization (Leach *et al*. 2001; Symons *et al*. 2002) and here we use palaeomagnetism to date the Magcobar barite.

## 2 GEOLOGY

All Magcobar's barite and most of the Silvermines' base metal sulphides were hosted in the basal portion of the 100-200m thick Tournasian (Courceyan) (352±3 Ma, Gradstein *et al.* 2004) Waulsortian Limestone. It was deposited as mudmounds at depths of <200m and contains slumps, fractures and breccias indicative of synsedimentary growth faults (Andrew 1986, 1995). Subsequent regional replacive dolomitization is attributed to burial and alteration by formational waters expelled from the Munster Basin. Hydrothermal dolostone breccia bodies follow feeder faults, cut the replacive dolomite, and extend up into 344±2 Ma Chadian strata where they surround the Ba and Pb-Zn zones. These zones abut, and extend ~400m from, major faults that presumably

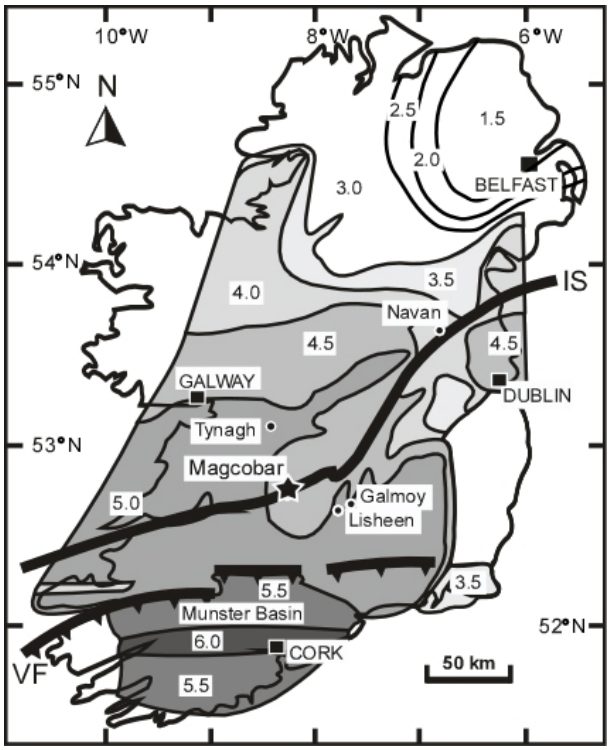


Figure 1. Location of Magcobar in Ireland with the colour alteration index (CAI) isopleths for conodonts in Carboniferous rocks (Jones, 1992), the Iapetus suture (IS) and the Variscan Front (VF).

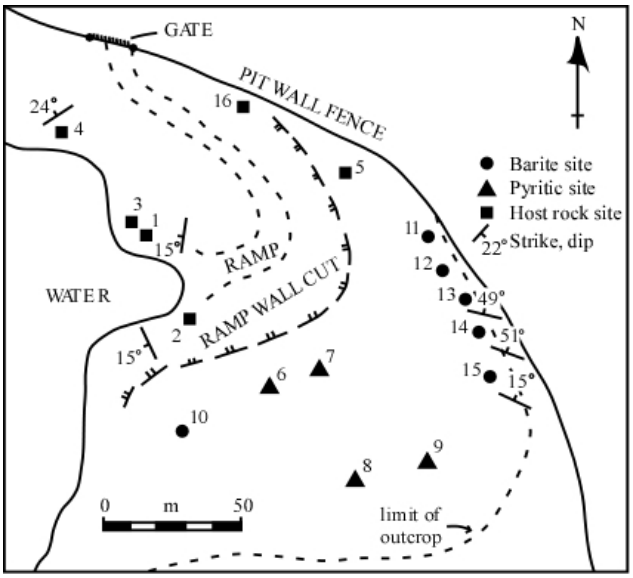


Figure 2. NE corner of the Magcobar pit (52°47.48'N, 8°15.27'W) with sampling sites.

acted as hydrothermal fluid conduits. Paragenetically, barite has been interpreted to predate most sphalerite and galena (Hitzman & Beaty 1996) or mostly postdate them (Reed & Wallace 2004). Also, magnetite, haematite and pyrrhotite have been reported in the paragenetic sequence of the ore mineralization (Hitzman & Beaty 1996; Rhoden 1960).

## 3 EXPERIMENTAL METHODS

Palaeomagnetic methods, instrumentation and references follow those given in Symons *et al*. (2002). Oriented specimens (183) were collected from ore-grade barite (6 sites), massive and disseminated pyritic and dolomitic rocks (4 sites) and hanging-wall carbonates (6 sites) in the Magcobar pit (Fig. 2) where the strata are folded into a NNW-plunging anticline. The

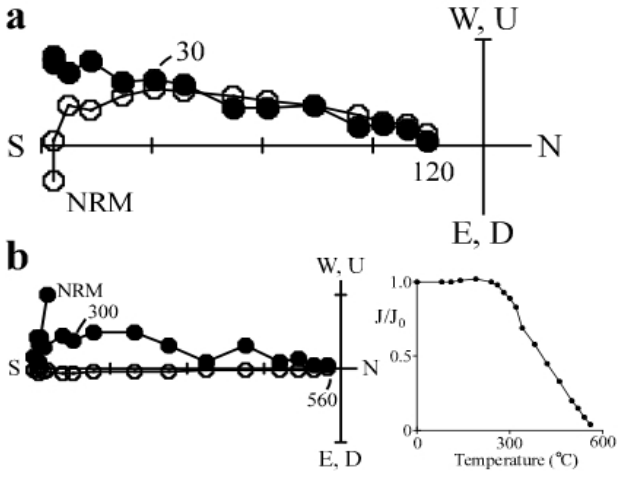


Figure 3. Vector component plots for barite ore specimens (a) 110801 on AF and (b) 150601 on Th step demagnetization.

specimens' natural remanent magnetizations (NRMs) had median NRM intensities of: barite ore, ~$5.9 \times 10^{-3}$ A/m; pyritic rocks, ~$8.7 \times 10^{-5}$ A/m; and, host carbonates, ~$1.1 \times 10^{-7}$ A/m.

One specimen per site was alternating field (AF) demagnetized in 14 steps to 120 mT and showed the removal of a modern viscous remanent magnetization (VRM) by ~20 mT, and then isolation of a stable shallowly-upward SSW characteristic remanent magnetization (ChRM) (Fig. 3a). A second specimen per site was thermally (Th) demagnetized in 22 steps to 670°C and showed removal of the VRM by ~260°C and then isolation of the ChRM component up to 460 to 560°C, showing that the ChRM is carried mostly by magnetite (Fig. 3b). The remaining specimens were AF demagnetized in 13 steps to 130 mT. Ten representative specimens were pulse magnetized in 16 steps to 900 mT and then AF demagnetized in 9 steps to 130 mT to obtain saturation isothermal remanent magnetization acquisition and decay curves that show the ChRM is carried by single-domain magnetite with minor haematite.

Specimen ChRM directions were well defined, incorporating ~8.8 step directions with a

Table 1 Characteristic remanence directions of sites

| Site | Lith. | Bedding | | Spec. | | Demag. | | ChRM | | | |
|---|---|---|---|---|---|---|---|---|---|---|---|
| | | Str.° | Dip° | n | n' | ds | mad° | D° | I° | $\alpha_{95}$° | k |
| 1 | Da | 199 | 15 | 7 | 7 | 6.9 | 6 | 187 | -20 | 7 | 87 |
| 2 | Da | 154 | 15 | 9 | 9 | 6.6 | 6 | 188 | -14 | 7 | 52 |
| 3 | Da | 199 | 15 | 9 | 9 | 7.8 | 6 | 186 | -16 | 3 | 272 |
| 4 | Db | 237 | 24 | 12 | 11 | 7.1 | 5 | 185 | -8 | 5 | 91 |
| 5 | Db | | | 14 | 14 | 7.2 | 4 | 189 | -9 | 5 | 77 |
| 6 | Pm | | | 11 | 11 | 4.6 | 7 | 184 | -8 | 3 | 186 |
| 7 | Pd | | | 8 | 6 | 3.7 | 7 | 184 | -11 | 11 | 38 |
| 8 | Pd | | | 11 | 6 | 6.7 | 6 | 183 | -16 | 4 | 231 |
| 9 | Pd | | | 9 | 3 | 7.7 | 4 | 195 | -8 | 25 | 26 |
| 10 | Bmr | | | 14 | 13 | 8.8 | 5 | 192 | -12 | 3 | 212 |
| 11 | Baw | | | 12 | 10 | 8.0 | 4 | 194 | -11 | 3 | 256 |
| 12 | Bmr | | | 10 | 10 | 9.0 | 4 | 186 | -18 | 4 | 134 |
| 13 | Bmg | 282 | 49 | 13 | 10 | 9.0 | 4 | 190 | -11 | 4 | 193 |
| 14 | Bmg | 300 | 51 | 14 | 14 | 9.2 | 4 | 192 | -9 | 3 | 142 |
| 15 | Bmg | 295 | 15 | 14 | 6 | 9.0 | 5 | 193 | -14 | 6 | 136 |
| 16 | Dc | | | 16 | 16 | 7.3 | 5 | 190 | -15 | 5 | 56 |

*Notes: Lithology (Lith.): barite (B), dolomite (D), pyretic rock (P), argillaceous (a), brecciated (b), clasts (c), disseminated (d), gray (g), massive (m), red (r), white (w), Attitude is right hand convection. Specimens (Spec.) collected (n) and used in average (n'). Demagnetization (Demag.) gives average number of steps per specimen (ds) and the mean angular deviation (mad*). Characteristic remanent magnetization (ChRM) by declination (D*), inclination (I*), radius of 95% confidence ($a_{95}$*) and precision parameter (k).*

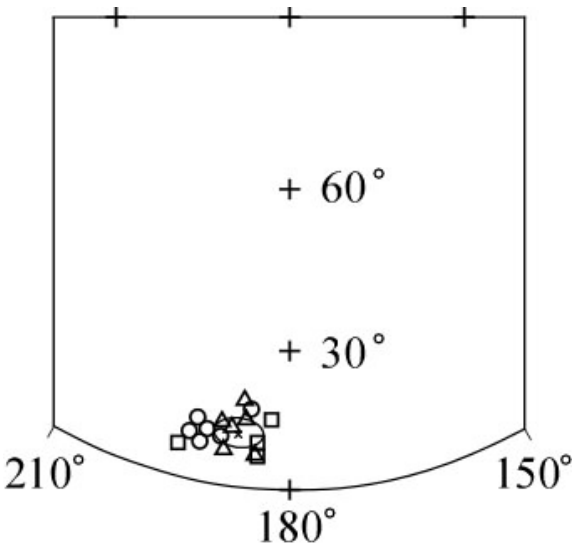


Figure 4. Site mean remanence directions on upper hemisphere of an equal-area stereonet: hostrocks ○, pyritic rocks □, and barite △ with the mean (x) and cone of 95% confidence for all 16 sites.

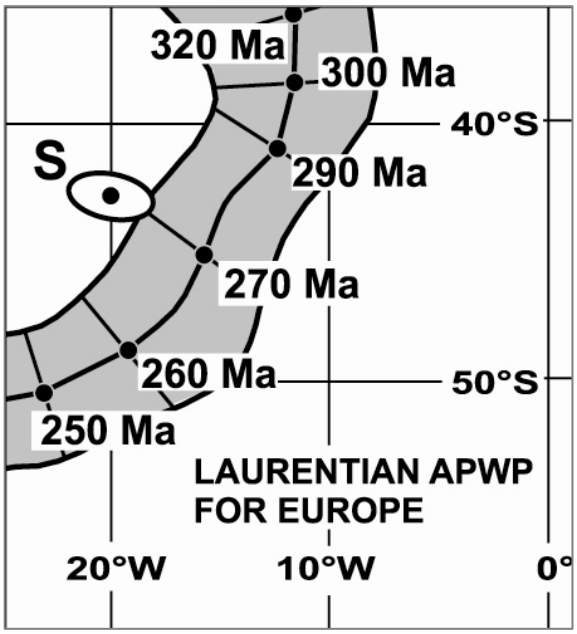


Figure 5. European apparent polar wander path (Torsvik *et al*. 1996) with the Magcobar paleopole.

mean angular deviation of only 5.1° on average. The specimen directions were averaged to get the site directions (Table 1). Four hostrock sites (1-4) and three barite ore sites (13-15) with bedding attitudes were used for a palaeomagnetic fold test. Unfolding the tilts causes the precision parameter (k) for the 7 directions to decrease from 281 to 10, showing with >>99% confidence that the ChRM is postfolding. Ten sedimentary breccia clasts from site 16 have significantly clustered ChRM vectors with a cone of 95% confidence ($\alpha_{95}$) of 7.0° and k = 48.0, showing with >>99% confidence that the clasts were magnetized after brecciation. When the site mean ChRM directions are grouped by lithology, the barite ore, pyritic rocks and host carbonate populations are statistically indistinguishable at 95% confidence (Table 2), and so they may be combined to give a ChRM direction at D = 188.5°, I = -12.5° (N = 16, $\alpha_{95}$ = 2.4°, k = 235) [declination, inclination, (number of sites, radius of 95% confidence, precision parameter)] (Fig. 4). This post-folding ChRM direction gives a palaeopole at 43.0°S, 19.9°W (semi-axes of 95% confidence, dp = 1.2° & dm = 2.4°) that falls on the robust apparent polar wander path (APWP) for Laurentia in European co-ordinates (Torsvik *et al.* 1996) at 269±4 Ma (2σ) (Fig. 5).

## 4 DISCUSSION

The early Permian 269±4 Ma age for the Magcobar Ba ore indicates that it, and likely the Silvermines Zn-Pb ores also, are epigenetic. This conclusion is supported by the post-brecciation and post-folding results found for the palaeomagnetic breccia and fold tests, respectively. Although intense to the south, deformation in the Carboniferous strata north of the Variscan Front in Ireland (Fig.1) is relatively mild, resulting in gentle open folds from N-S compression with ENE-WSW dextral shear except next to faults (Graham 2001). This Variscan deformation is observed in ~305 Ma strata in Ireland. Thus the fold test shows that the barite ore postdates the Carboniferous sedimentation in the Irish Midlands.

In general, carbonate alteration indices (CAI; Fig. 1), fluid inclusions, and isotope values show that the Carboniferous host rocks at Magcobar and early non-sulphide minerals in the paragenetic sequence have been exposed to temperatures of ~220-300°C, sphalerite and ga-

Table 2: Unit Mean ChRM directions.

| Unit | Sites | N | ChRM | | | |
|---|---|---|---|---|---|---|
| | | | D° | I° | $\alpha_{95}$° | k |
| Carbonate rocks | 1 - 5, 16 | 6 | 187.3 | -13.5 | 4.0 | 288 |
| Pyritic rocks | 6 - 9 | 4 | 186.5 | -10.6 | 7.6 | 146 |
| Barite ore | 10 - 15 | 6 | 191.0 | -12.7 | 3.5 | 361 |
| All host rocks | 1 - 9, 16 | 10 | 187.0 | -12.3 | 3.3 | 219 |
| All sites | 1 - 16 | 16 | 188.5 | -12.5 | 2.5 | 295 |

*Notes: Abbreviations as in Table 1 except (N) is the number of site mean ChRM directions averaged.*

lena to ~100-200°C, and barite to 80±10°C (Jones, 1992; Hitzman & Beaty 1996), indicating that the barite is coeval with, or postdates, cooling from the regional Variscan thermal event.

The 269±4 Ma palaeomagnetic age agrees with the 271±24 Ma lead isotope model age for Magcobar/Silvermines (Boast *et al.* 1981) but is much more precise. Slightly older K-Ar ages of 295-320 Ma on clay minerals from Magcobar (Halliday & Mitchell 1983) have been attributed to argon leakage during tectonism (Andrew 1995).

## 5 CONCLUSION

The Magcobar barite, and most likely the Silvermines sulphide ores, was deposited at 269±4 Ma and is therefore epigenetic. This agrees with, and provides an age for, the epigenetic evidence cited by Reed & Wallace (2004) for Silvermines but runs counter to synsedimentary genetic models for "Irish-type" ore deposits (*eg*. Lee and Wilkinson, 2002).

## ACKNOWLEDGEMENTS

The authors thank A.Chertov for technical help and the Natural Sciences and Engineering Council of Canada for funding this research.

## REFERENCES

Andrew CJ (1986) The tectono-stratigraphic controls to mineralization in the Silvermines area, County Tipperary, Ireland. In: Andrew CJ, et al., (ed) *Geology and genesis of mineral deposits in Ireland.* Irish Assoc Econ Geol: 377-417.

Andrew CJ (1995) The Silvermines District, Co. Tipperary, Ireland; Irish Carbonate-hosted Zn-Pb deposits; *Soc Econ Geol Guidebook Series* Vol 21: 247-258.

Boast AM, et al. (1981) Lead isotope variation in the Tynagh, Silvermines and Navan base-metal deposits, Ireland. *Trans Inst Min Metal, Sect B,* 90: 115-119.

Gradstein FM, Ogg JG, Smith GA, and 37 others (2004) *A geological time scale 2004*. Cambridge University Press: p 500.

Graham JR (2001) Variscan structures. In Holland, CH, (ed) *The Geology of Ireland,* Dunedin Academic Press, Edinburgh: 314-329.

Halliday AN, Mitchell J G (1983) K-Ar ages of clay concentrates from Irish orebodies and their bearing on the timing of mineralisation. *R Soc Edinb. Earth Sci.* 74: 1-14.

Hitzman MW, Beaty DW (1996) The Irish Zn-Pb-(Ba) orefield. In: Sangster DF (ed) Carbonate-hosted lead-zinc deposits. *Soc Econ Geol Sp. Pub.* No.4: 112-143.

Jones GL (1992) Irish Carboniferous conodonts record maturation levels and the influence of tectonism, igneous activity and mineralization. *Terra Nova* 4: 238-244.

Larter RCL, Boyce AJ, Russell MJ (1981) Hydrothermal pyrite chimneys from the Ballynoe baryte deposit, Silvermines, County Tipperary, Ireland. *Miner Deposita* 16: 309-318.

Leach DL, Bradley D, Lewchuk MT, Symons DTA, de Marsily G, Brannon J (2001) Mississippi Valley-type lead-zinc deposits through geological time: Implications from recent age dating research. *Miner Deposita* 36: 711-740.

Lee MJ, Wilkinson JJ (2002) Cementation, hydrothermal alteration, and Zn-Pb mineralization of carbonate breccias in the Irish Midlands; textural evidence from the Cooleen Zone, near Silvermines, County Tipperary. *Econ Geol* 97: 653-662.

Reed CP, Wallace MW (2004) Zn-Pb mineralisation in the Silvermines district, Ireland: a product of burial diagenesis. *Miner Deposita* 39: 87-102.

Rhoden NH (1960) Mineralogy of the Silvermines district, Co. Tipperary, Eire. *Mineral Mag* 32: 128-139.

Symons DTA, Smethurst MT, Ashton JH (2002) Paleomagnetism of the Navan Zn-Pb deposit, Ireland. *Econ Geol* 97: 997-1012.

Torsvik TH, Smethurst MA, Meert JG, Van der Voo R, McKerrow WS, Brasier MD, Sturt BA, Walderhaug HJ (1996) Continental break-up and collision in the Neoproterozoic and Palaeozoic - A tale of Baltica and Laurentia. *Earth Sci Rev* 40: 229-258.

# New data on mineralogy, zoning, age and mineralization conditions of cobalt deposits in the Altai-Sayan orogenic area

I.G. Tretjakova, A.S. Borisenko, V.I. Lebedev & E.A. Naumov
*Institute of Geology and Mineralogy, Siberian Branch of Russian Academy of Sciences, Novosibirsk, Russia*

ABSTRACT: Hydrothermal cobalt deposits are widespread in the Altai-Sayan orogenic area (ASOA). Three main types of hydrothermal cobalt ores (Co-As, Ni-Co-As(±Bi, Ag), and Cu-Co) occur in this region. The Co-As deposits formed at 300-350°C, Ni-Co-As deposits at 200-180°C, and Cu-Co deposits at 70-230°C. Most of the cobalt deposits are characterized by high concentrations of high salinity fluid inclusions (up to 30-35 wt. % NaCl equivalent). Commonly the hydrothermal cobalt mineralization zoned: arsenic → sulphosalts→ Pb-Zn (Co-bearing) → barite and they display. Atomic absorption spectroscopy of cobalt ores from the ASOA revealed high concentrations of Au, Ag, and PGE. Three main epochs of mineralization were respectively: Late-Mesozoic ($J_3$-$K_1$) (Rb-Sr dating), early-Mesozoic ($P_2$-$T_1$) (Ar-Ar dating) and Middle-Palaeozoic (D-$C_1$) (U-Pb and Ar-Ar methods).

KEYWORDS: cobalt deposits, metal zoning, age, dating, Altai-Sayan Orogen

## 1 TYPES OF COBALT DEPOSITS OF ALTAI-SAYAN REGION

Hydrothermal and hydrothermal-metasomatic cobalt deposits are widespread in the Altai-Sayan orogenic area (ASOA). Three main types of the hydrothermal cobalt ores (Co-As, Ni-Co-As(±Bi, Ag) and Cu-Co) occur in this region.

Typical examples of *Co-As deposits* in ASOA are Vladimirovskoe (NE Altai), Karakul, Karaoug (SE Altai), earlier cobalt skarn mineralization in Hovoo-Aksy deposit (Tuva). They occur as ore zones with sulfide-arsenide mineralization, containing cobaltite, glaucodot, safflorite, danaite, and skutterudite within the hosted by exoscarn and hornfels contact areas of the granitoid intrusions.

*Ni-Co-As (±Bi, Ag)* deposits are widespread in the Altai-Sayan region. They are as at in Tuva (Hovoo-Aksy, Askhatin-Gol, Khuren-Taiga, Kyzyl-Ouk), Altai, Hakasia and NW Mongolia. Ores of these deposits consist of arsenic minerals (niccolite, cobaltite, rammelsbergite, skutterudite, fahlore with subordinate loellingite, safflorite, Ag and Sb sulphosalts).

*Cu-Co* deposits revealed occur in the Tuva (Uzun-Oi, Mogenburen, Kaat-Taiga), Khakasia (Kharadgul, Butrakhta), NW Mongolia, SE Altai and others regions of the ASOA. These mostly occur peripherally to the Ni-Co-As and Co-As deposits. They are characterized by Cu-sulphosalts and sulphides, such as pyrite, chalcopyrite, galena, and sphalerite. Ni and Co minerals occur as sulphides, sulphoarsenides and arsenides.

## 2 FLUID INCLUSION STUDY

A fluid inclusion study constrained some physical and chemical conditions of the cobalt mineralization. Arsenical ores formed at quite low-temperatures (up to 200-180°C) in the Ni-Co-As deposits. Co-As ores formed at higher temperature (up to 300-350°C). Vein and disseminated ores formed at similar conditions. High homogenization temperatures (up to 350°C) are common in quartz-sulphide-sulphoarsenide veins of the Karakul deposit (SE Altai) and skarn-hosted cobalt mineralization in skarn at the Hovoo-Aksy deposit. Most Cu-Co deposits formed at low-temperatures (up to 70-230°C). Most cobalt deposits in Altai-Sayan region are characterized by high salinity

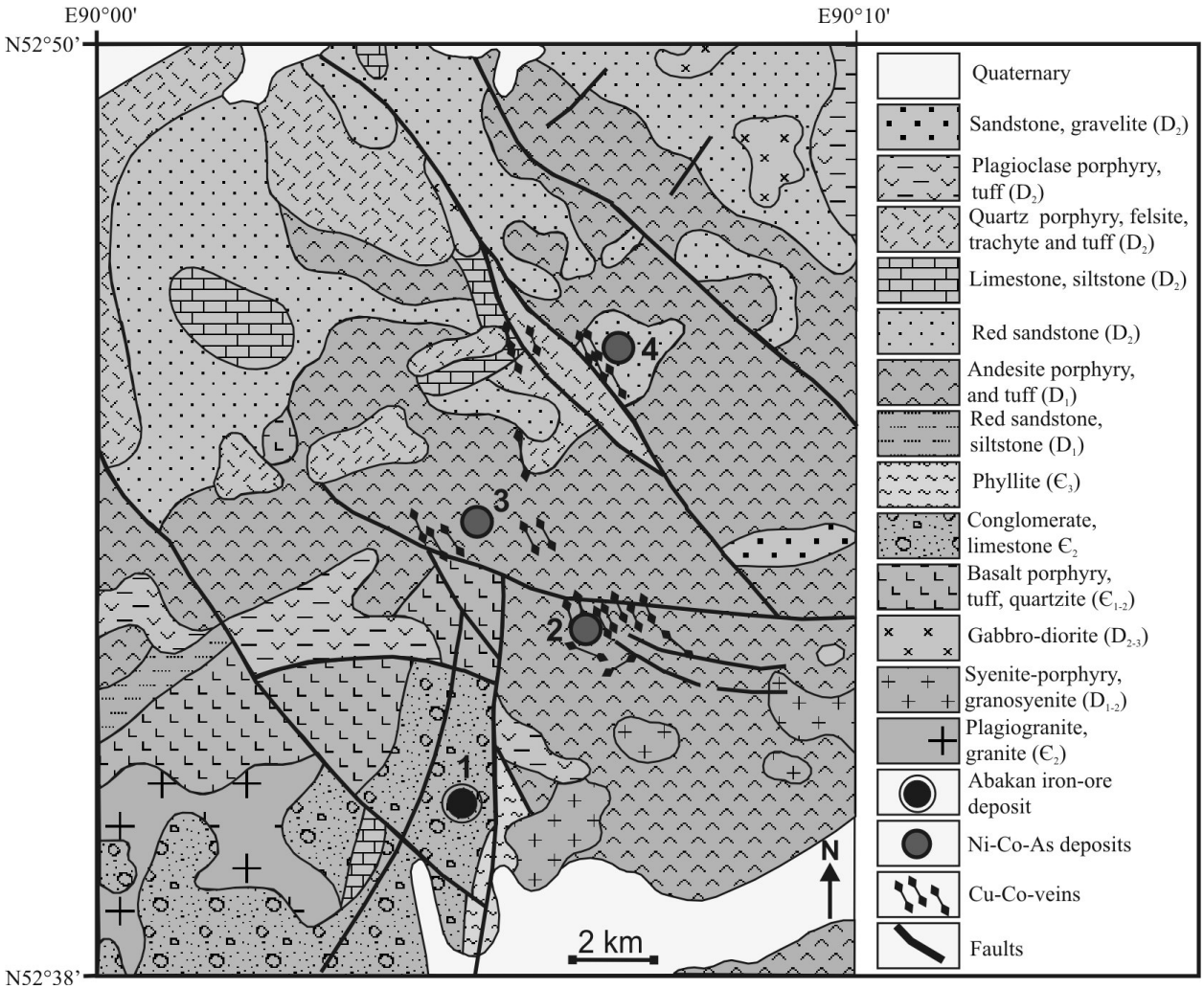


Figure.1 Geological scheme of Abakan deposit.
1 – Abakan iron-ore deposit, 2 – Kharadgul-1 deposit, 3 – Kharadgul-2 deposit, 4 – Butrakhta deposit

fluid inclusions (up to 30-35 wt.% NaCl equivalent).

## 3 METAL AND MINERAL ZONING

The hydrothermal cobalt districts are characterized by occurrences of different types of cobalt ores (viz. Co-As, Ni-Co-As, Cu-Co etc.). As a rule, occurrences are zoned, commonly in the sequence: arsenic → sulphosalts→ Pb-Zn (Co-bearing) → barite. Geochemical and temperature features allow the zoned cobalt deposits to be subdivided into two types, namely:

1. High temperature cobalt mineralization (Co-As → Cu-Co-As → Pb-Zn (Co-bearing) → Ba)
2. Low-temperature nickel-cobalt mineralization (Ni-Co-As → Cu-Co-As → Cu, Pb, Zn, Ba (Co-bearing) → Ba).

For example, the main type of hydrothermal cobalt mineralization at Abakan is Ni-Co-As mineralization, but Cu-Co–sulphosalt veins are widespread around the periphery (Fig. 1).

## 4 AU, AG, AND PGE IN COBALT DEPOSITS

The hydrothermal cobalt deposits revealed ores have high concentrations of Au, Ag, and PGE (Kharadgul - Au up to 1.2 ppm, Ag up to 486 ppm; Vladimirovskoe - Pt up to 0.12 ppm, Pd up to 1.08 ppm.). Table 1 shows that high concentrations of PGE are typical in high-temperature Co-As deposits, that are usually related to basic intrusions, whereas high contents of Au and Ag occur in low-temperature Ni-Co-As ores, related to granites.

## 5. AGE OF COBALT DEPOSITS OF THE ASOA

Dating of cobalt deposits (Vladimirovskoe, Askhatin-Gol, Abakan ore cluster) was carried out on sericite from ore quartz-sericite-

| Deposit | Type of mineralization | Location | Au (ppm) | Ag (ppm) | Pt (ppm) | Pd (ppm) |
|---|---|---|---|---|---|---|
| Karakul | Co-As | Altai | 0.03-3.2 | 5.0-26 | up to 0.15 | up to 0.11 |
| Vladimirovskoe | Co-As | Altai | 0.043-0.54 | 4.3-160 | up to 0.12 | up to 1.08 |
| Abakanskoe | Co-As | Khakassia | up to 0.2 | up to 3.1 | 0.01 | up to 0.02 |
| Mogenburen | Cu-Co-As | Tuva | up to 0.0058 | up to 140 | - | - |
| Mergen-bulak | Cu-Co-As | Mongolia | up to 0.024 | 12-1200 | - | - |
| Sergievskoe | Cu-Co-As | Mongolia | up to 0.46 | up to 34 | - | - |
| Kharadgul | Cu-Co-As | Khakassia | 0.45-1.2 | 84-493 | 0.01 | up to 0.016 |
| Hovoo-Aksy | Ni-Co-As | Tuva | up to 1 | up to 290 | - | - |
| Askhatin-Gol | Ni-Co-As | Tuva | up to 1 | 70-1700 | - | - |
| Akol | Ni-Co-As | Tuva | 0.015 | up to n*1000 | - | - |
| Sagsai | Hg(Co-bearing) | Mongolia | up to 4.5 | up to 140 | - | - |

Table 1. Concentrations Au, Ag, PGE in cobalt deposits of Altai-Sayan Orogenic Area.

carbonate veins (Ar-Ar-method). $^{40}Ar/^{39}Ar$ isotope analysis of minerals was carried out on a Noble gas 5400 mass spectrometer. Mineral fractions no less than 0.15 mm in size were wrapped in Al foil and, after pre-pumping, were sealed in quartz vials and irradiated in the cadmium-plated channel of the water-cooled and water-moderated research reactor at Tomsk Polytechnical University. K/Ar standard biotite MCA-11 calibrated with LP-6 biotite and MMhb-1 hornblende was included between every two samples for neutron gradient monitoring. The neutron gradient did not exceed 0.5% on sample size. $^{40}Ar/^{39}Ar$ stepwise heating experiments were accomplished in a quartz reactor heated by an external furnace. A blank of $^{40}Ar$ exposed to 1200 °C for 40 min did not exceed $n\times10^{-9}$ STI. Released gases were purified by exposure to a Ti getter and two SAES getters.

Three main epochs of cobalt mineralization were respectively late-Mesozoic ($J_3$-$K_1$), early-Mesozoic ($P_2$-$T_1$) and Middle-Palaeozoic (D-$C_1$).

*The late-Mesozoic ($J_3$-$K_1$)* mineralization age boundaries determined based from geologic data. Cobalt and associated polymetallic (Cu, Pb, Zn) and barite mineralization are superimposed on the Jurassic ($J_{1-2}$) conglomerates of Karginsk graben (SW Tuva, NW Mongolia). To the East of this region Co-mineralization is associated with Ulatai-Choz alkalic intrusions, that have been dated at 118-120 Ma (Rb-Sr dating, Nikiforov *et al.*, 2006).

*Early-Mesozoic ($P_2$-$T_1$)* Ni-Co-As deposits occur in the Yustyd ore cluster (SE Altai) and Cu-Co-sulphosalt deposits and South-Chua ridge formed. This mineralization overprinted Paleozoic rocks, but the orebodies are intruded by 246-240 Ma lamprophyre dikes (Ar-Ar dating, Vrublevskii *et. al.*, 2004). Moreover, results from the Yustyd ore cluster (Askhatin-Gol deposit) revealed superimposition of Ag-Sb mineralization (238 Ma. Ar-Ar dating) on Ni-Co-As.

*Middle-Palaeozoic (D-$C_1$)* hydrothermal events formed early skarn assemblages of Hovoo-Aksy Co-As deposit (Tuva), Vladimirovskoe (NE Altai) Co-As deposit, Karakul (SE Altai) Cu-Co-As deposits and probably cobalt mineralization of the Abakan ore cluster (Khakassia). The age of granites of Yustyd ore cluster (355.7±8.6 Ma) was determined by U-Pb-method (zircon). The age of Sn-W(Ni), Cu-Co-W and Co-As mineralization related to these granites is 352±6 Ma (Ar-Ar-method).

## ACKNOWLEDGEMENTS

The work was supported by RFBR (grant 07-05-00803, 07-05-00988, 06-05-64789) and grant of the Ministry for Russian Science and Education DSP.2.1.1.702

## REFERENCES

Nikiforov A.V., Bolonin A.V., Pokrovskiy B.G., Sugorakova A.M., Chugaev A.V., Likhin D.A. Geochemistry of isotopes (O, C, S, Sr) and Rb-Sr dating of the Central Tuva carbonatites // "*Geology of ore deposits*" – 2006. – Vol. 48. - №5. – P. 296-320.

Vrublevskii V.V.; Gertner I.F.; Polyakov G.V.; Izokh A.E.; Krupchatnikov V.I.; Travin A.V.; Voitenko N.N. Ar-Ar isotopic age of lamproite dikes of the Chua complex, Gornyi Altai // "*DOKL EARTH SCI*". - 2004. - Vol. 399A. - Iss. 9. - P. 1252-1255.

.

# Geochronology of gold deposits associated with Variscan granitoids in central west Iberia

F.J. López-Moro, M.C. Moro & S.M. Timón
*Geology Department, Salamanca University, Spain*

J.S. Cózar
*CIEMAT, Avd. Complutense, 22, 28004, Madrid, Spain*

ABSTRACT: Uraninites from unaltered Variscan granites and metasomatized granites from central west of Iberia have been analyzed for chronological purposes (chemical age method). A common hydrothermal history was revealed despite the large distances between the districts studied, different metasomatic processes and the different ages of emplacement of granites. Uraninite ages and textural relationships were established during three hydrothermal events: the first (around 277 Ma) involved strong alkali metasomatism, the second (around 250 Ma) was related to silica and sulphide deposition, and finally, the main gold stage, which is of uncertain age.

KEYWORDS: uraninite, chemical ages, hydrothermal event, gold deposit

## 1 INTRODUCTION

Uraninite can be used for dating purposes due to its high contents in Pb and U, which are easily measured by electron microprobe. However, it is a scarce mineral and its chemistry is easily reset with pH and oxidation variations, giving rise to U or Pb losses or gains. It is consequently an inappropriate phase for dating the emplacement age of an altered plutonic rock. Nevertheless, these characteristics can be advantageous for dating different superimposed hydrothermal stages.

Uraninites from different metasomatized and unaltered hosted rocks have been analyzed to date the post-Variscan hydrothermal history of the western part of the Iberian massif, which contains As and Au deposits in the Pino district and W, As and Au deposits in El Cabaco and Los Santos districts (Fig. 1).

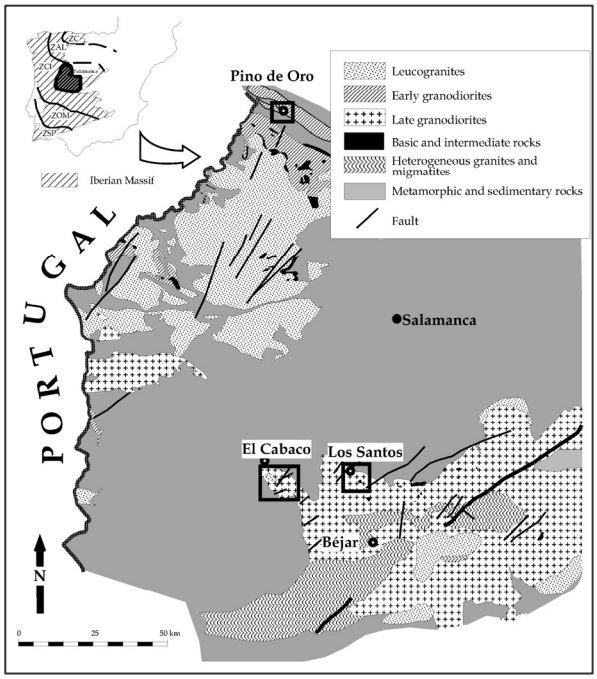


Fig. 1. Geological sketch with the location of studied ore districts

## 2 SAMPLES

### 2.1 *Uraninites from the Pino district.*

Uraninites studied from the Pino district occur enclosed in plagioclase, K feldspar and quartz of a peraluminous two-mica granite affected by ductile shearing, as well as in alkali-enriched brecciated granites (episyenites). In this case, albite is the main host of uraninite.

Two textural-uraninite generations can be distinguished in episyenites: i) one early, fine-grained and enclosed in albite, and a later, coarser-grained type, associated with sulphides. Gold is syn- to post- brittle shearing and post-dates sulphide deposition.

2.1 *Uraninites from the El Cabaco district*

Uraninites occur in the most differentiated facies of the batholith, that is, a fine-grained muscovite- and cordierite-bearing biotite granite. The uraninite is hosted by plagioclase and K-feldspar in fresh and weakly altered granites and by plagioclase, white mica or quartz in strongly altered granites. As in the Pino district, uraninite is scarce in unaltered granite but quite abundant in some metasomatized granite facies, suggesting it is hydrothermal. In most cases, veins show clear evidence of a complex geological history, involving successive openings and sealing with several related alteration processes. Thus, veins hosted by granitoids frequently show abundant muscovite making up a selvage-style greisen, which is commonly enveloped by a K-feldspar-enriched reddish rim, which, could represent a previous alkali alteration similar to episyenitization in the Pino district.

2.1 *Uraninites from the Los Santos district*

In the Los Santos skarn zone, uraninite occurs in similar granites to those in the El Cabaco district, and, more extensively in Ca-metasomatic rocks that formed by interaction between Variscan granites and Lower Cambrian limestones. Two major groups of metasomatic rocks can be distinguished, namely prograde and retrograde skarn. Uraninite is hosted by calcic plagioclase in prograde endoskarn, in association with epidote, scheelite and sulphides in retrograde endoskarn, and included in allanite in prograde-hedenbergite exoskarn.

## 3 METHODOLOGY

Uraninite detection was initially carried out using a Geiger counter on hand specimens. Secondly, the method of Basham & Easterbrook (1977) was applied to samples where traces of α particles were previously detected. Finally, the presence of uraninite was confirmed by optic and scanning electron microscopy.

All uraninites considered were analyzed by a scanning electronic microscope with an X Link eXL X-ray analytical system. The arithmetical average of measured deviations was of 1 % for U and 0.31 % for Pb. According to the methodology of Kempe (2003) samples showing a strong negative correlation trend defined by data points fitting on a single correlation line were used for dating (Fig. 2).

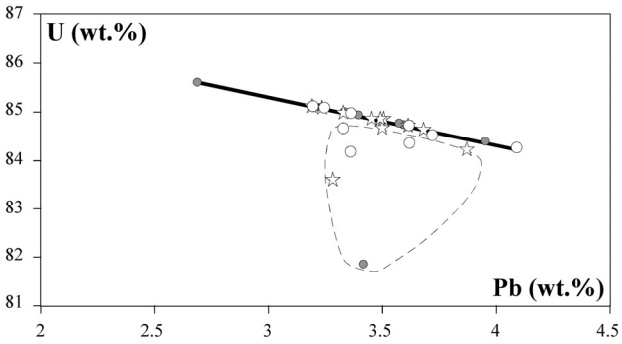


Fig.2. U-Pb diagram showing strongly correlated analyses (bold-straight line) and poorly correlated ones (fine-dash line). Stars: samples from the Pino district; white circles: samples from the El Cabaco district; grey small circles: samples from the Los Santos district.

Finally, the on-line application of Brugger (2003) was performed for dating.

## 4 RESULTS AND DISCUSSION

4.1 *The Pino district*

The ages obtained range from 287 to 247 ± ~20 Ma (Fig. 3), most of them between 273 and 247 Ma. It is worth emphasizing the lack of ages corresponding to granite cooling (324 ± 12 Ma from K-Ar in biotites, Toros 1981) as well as ductile shearing (around 306 ± 9 Ma, U-Pb in monazite, Valle-Aguado *et al*. 2005). Our preferred explanation for the lack of primary granite ages is that magmatic uraninites were reset during subsolidus events. The presence of quite similar ages in deformed granites and in some episyenites could support this possibility. Likewise, episyenitization has been dated in the Spanish Central System in 277 ± 6 Ma (Caballero *et al.*, 1996), that is, a similar age to some of the episyenite uraninites in the Pino district.

Another key point is, even allowing for error, the lack of overlap between the oldest ages and the youngest in episyenites. This confirms the presence of two different uraninite types: i) an older type associated with episyenitization and ii) a second type, associated with sulphides and with ages around 245 Ma. The youngest uraninite ages in the Pino district probably reflect a young extensional event, as inferred from mantle magmatism in the area (245 ± 19 Ma, K-Ar whole-rock age, Toros 1981). This age is very similar to the episyenitization process dated by K-Ar in the Guarda batholith in Portugal (Bobos *et al*., 2005), but in the current case this process appears to be older (Fig. 3).

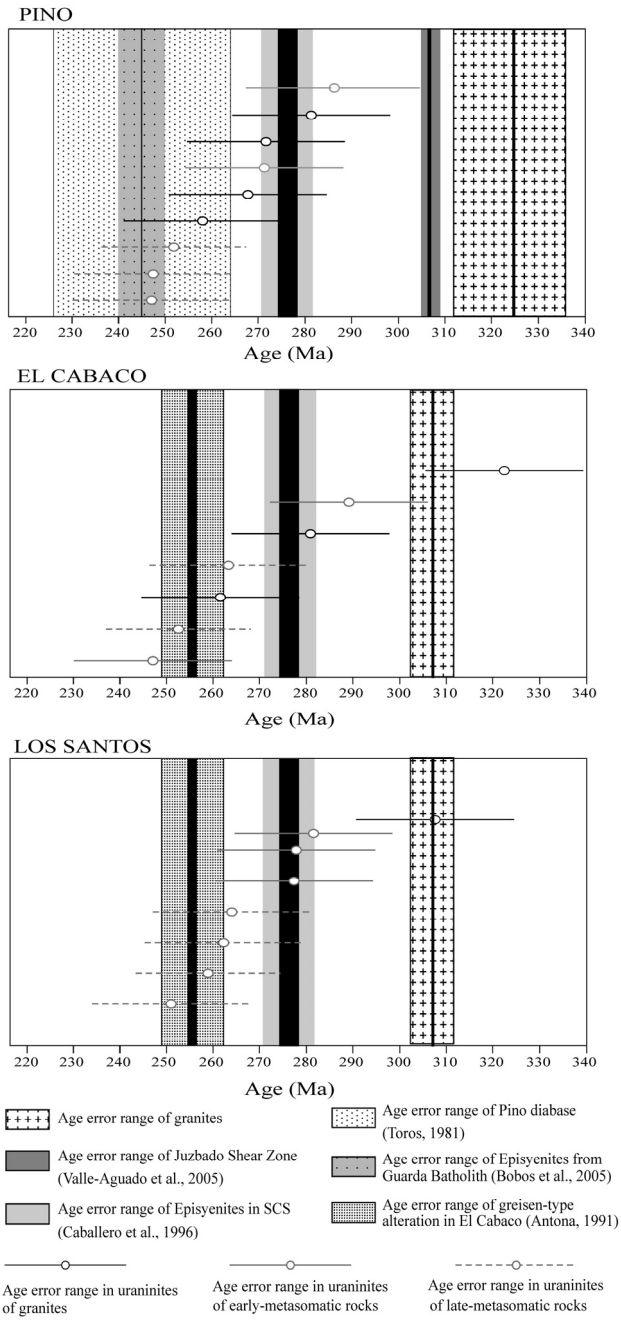


Fig. 3. Comparative graph showing the chemical ages obtained in the three studied districts. Different hydrothermal and geological events are included for comparative proposes. The black ribbon represents the obtained ages for the corresponding hydrothermal/geological event.

Finally, taking into account textural data, the main episode of gold mineralization occurred after 245 Ma.

### 4.2 *The El Cabaco and the Los Santos districts*

Both districts are grouped here since they are located in the same geological setting (Fig. 1). Three sets of ages have been obtained:

i) The oldest ages (307-319 ± 20 Ma) could correspond to granite emplacement, in accordance with U-Pb ages in zircons (~306 Ma, Zeck *et al.*, 2004) (Fig. 3).

ii) The youngest ages (247-265 ± 20 Ma) occur in uraninites located in the greenish muscovite-enriched selvage of sulphide-bearing quartz veins of El Cabaco, and in the retrograded skarn of Los Santos. These ages are similar to those of muscovites of the greenish muscovite-enriched selvage obtained in the El Cabaco district (255-256 ± 5 Ma, K-Ar method, Antona, 1991). From a textural point of view, gold is later than As-Fe sulphides, as in the Pino district (*i.e.* deposited after 255 Ma).

iii) Intermediate values (277-287 ± 20 Ma). In the Los Santos district these ages were obtained from uraninites in prograde skarn. Such ages are uncommon in the El Cabaco district and they have been found in the reddish metasomatized zone or in "unaltered" granite (reset uraninites?). Therefore, intermediate ages relate to two different kinds of alterations in the El Cabaco and the Los Santos districts, but also to the episyenitization process in the Pino district.

## 5 CONCLUSIONS

In the studied gold districts, a common hydrothermal history can be emphasized, despite the large distances between some of them, differences in the alteration processes and the different ages of emplacement of granites. This rules out a close relationship between granites and the subsequent hydrothermal history. In the cases studied, at least three hydrothermal events can be inferred: an early process about 277 Ma involving strong alkali metasomatism, a second event (around 250 Ma) associated with sulphide and in some cases wolframite/scheelite deposition, and finally the deposition of gold of uncertain age, but after 250 Ma.

## ACKNOWLEDGEMENTS

This work was supported by the Comunidad de Castilla y León (Research Project Ref. SA015A06). The authors are in debt to Regional Government of Castilla y León for the facilities to study drill holes from the Pino and El Cabaco areas.

## REFERENCES


Antona F (1991) Fluidos mineralizadores en los yacimientos de oro de Saucelle y El Cabaco (Salamanca) *PhD Thesis Univ Salamanca*.

Basham IR, Easterbrook GD (1977) Alpha-particle autoradiography of geological specimens by use of cellulose nitrate detectors. *Trans. Inst. Min. Metall,* B86: 95-98.

Bobos I, Jaques L, Noronha F, Clauer N, Liewig N (2005). Geochemistry, geothermometry, and K-Ar dating of episyenitic rocks associated with the Guarda uraniferous granites, Portugal. *8th SGA Meeting*, 3-1, 225-228.

Brugger J (2003) http://geolog008.geology.adelaide.edu.au/UraniniteDating/UraniniteDating.html

Caballero JM, González-Casado JM, Casquet C, Galindo C, Tornos F (1996). Episienitas de la Sierra de Guadarrama: un proceso hidrotermal regional de edad Pérmico Inferior ligado al inicio de la extensión alpina. *Cuad. Geol. Iberica* 20: 183-201.

Kempe U (2003). Precise electron microprobe age determination in altered uraninite; consequences on the intrusion age and the metallogenic significance of the Kirchberg Granite (Erzgebirge, Germany). *Contrib Mineral Petrol* 145: 107-118.

Toros M (1981) Les granitoïdes et les gîtes d'étain associés dans leur contexte lithostraigraphique et métamorphique à l'ouest de Zamora (Massif Hespérique, Espagne). *PhD Thesis Univ Lausanne*.

Valle-Aguado B, Azevedo MR, Schaltegger U, Martínez Catalán JR, Nolan J (2005) U-Pb zircon and monazite geochronology of Variscan magmatism related to syn-convergence extensión in Central Northern Portugal. *Lithos* 82: 169-184.

Zeck HP, Wingate MTD, Pooley GD, Ugidos JM (2004) A sequence of Pan-African and Hercynian events recorded in zircons from an orthogneiss from the Hercynian Belt of Western Central Iberia-an ion microprobe U-Pb study. *J Petrol* 45: 1613-1629.

# New Geochronological Constraints on the Einasleigh Cu Deposit, Georgetown Inlier, Queensland, Australia

P.M. Evins, T. Baker, K.L. Blake, B. Giles, & P.J. Williams
*EGRU, James Cook University, Townsville, Australia*

T. Lees & P.W. Gregory
*Copper Strike Ltd., Melbourne, Australia*

N. J. Pearson
*GEMOC, Macquarie University, Sydney, Australia*

D. Selby
*Department of Earth Sciences, Durham University, Durham, UK*

ABSTRACT: Proterozoic terranes in Australia contain several world class copper, lead and zinc deposits, however, in the Georgetown inlier there has been only limited base metal production. Recent exploration at the historic Einasleigh copper deposit has identified significant high grade copper (0.9 Mt at 3.3 % Cu). New U-Pb zircon and EMPA monazite age data from host rocks to the deposit support regional work that has identified a protracted, multiphase metamorphic history from *ca.* 1650 to 1500 Ma. A Re-Os age of molybdenite in the ore and monazite in related alteration suggests the ore in its current structural setting formed at *ca*. 1400 Ma. This does not coincide with a widely recognised Proterozoic metallogenic event but does coincide with Re-Os age data from the Mount Isa copper-lead-zinc system.

KEYWORDS: Proterozoic, Georgetown inlier, copper deposit, geochronology

## 1 INTRODUCTION

Proterozoic rocks in Australia that formed between 1.8 and 1.5 billion years ago contain some of the largest concentrations of copper, lead and zinc in the world. These include the world class mineral deposits of the Mount Isa and Broken Hill regions (Fig. 1). The Georgetown inlier of north Queensland also contains rocks of the same age as Mount Isa and Broken Hill, but has until recently been considered a poor cousin to those metal-rich terranes. New exploration has identified several copper prospects in the vicinity of the historic Einasleigh copper mine, which produced a reported 130,000 tonnes containing 6% Cu, 0.5 g/t Au, 30 g/t Ag and 1.2 % Zn. The exploration has added a further 940,000 tonnes at 3.3 % copper, 0.18 g/t gold and 15 g/t silver to this resource.

The research reported here focuses on new geological and geochronological data from recent drilling and mapping in the vicinity of the Einasleigh mine. Several geochronological techniques have been applied including U-Pb zircon and Re-Os molybdenite chronometers supported by extensive electron microprobe analysis (EMPA) of monazite and uraninite. The data highlight a complex, multi-staged history for the deposit and its host rocks and suggests the ore in its current structural setting may have formed at *ca*. 1400 Ma.

## 2 REGIONAL GEOLOGY

The Early to Middle Proterozoic Georgetown inlier comprises highly deformed and metamorphosed sedimentary and igneous rocks (Fig. 2). The oldest rocks in the region, the Etheridge Group, formed at around 1700 Ma (Black *et al*., 2005; Bodger & Hansen, 2004) and experienced lower greenschist to granulite facies metamorphism, the latter particularly evident in the Einasleigh Metamorphics that host the Einasleigh copper deposit. Overlying the Etheridge Group are the Langlovale and Croyden Volcanic Groups that were deposited at around 1550 Ma. Also at around 1550 Ma, extensive S-type granitic magmatism intruded the Georgetown inlier (*e.g*., Forsayth Granite). Most studies in the region infer a similar age (~1550 Ma) for high temperature, low pressure peak metamorphism based on the zircon ages obtained from S-type granitoids (Black & Withnall, 1993) and metamorphic rims on zir-

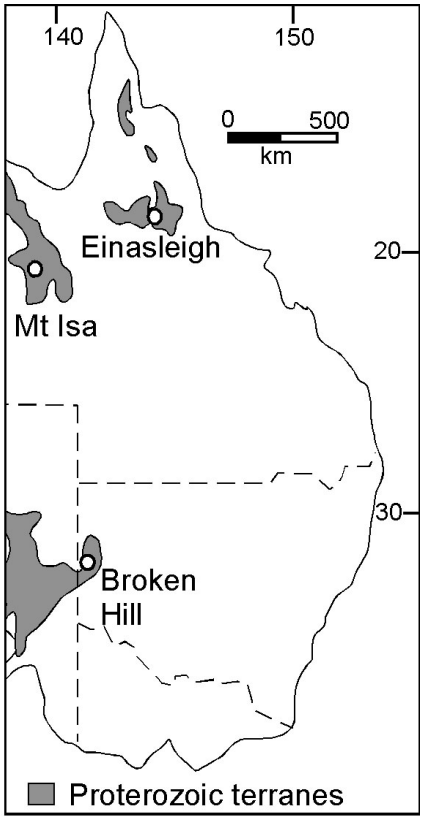


Figure 1. Map of eastern Australia showing selected Proterozoic terranes and location of Einasleigh copper deposit.

con from mafic rocks (Black *et al*., 1998).

Bodger & Hansen (2004) and Cihan *et al.* (2006) have identified a more complex regional metamorphic history with the latter recognising two stages of prolonged medium pressure-temperature metamorphism from *ca.* 1655 to 1625 and 1625 to 1586 Ma based on EMPA dating of monazite. Cihan *et al*. (2006) also identified metamorphic monazite that grew during the regional S-type granite intrusion that had ages of *ca*. 1542 Ma and suggests this period possibly extended for another 30–50 Ma based on the monazite ages obtained from the younger foliations.

## 3 DEPOSIT GEOLOGY

The Einasleigh copper deposit is located near the junction of the Copperfield and Einasleigh rivers (Fig. 2). Exposed Einasleigh Metamorphics consist of migmatized biotite gneiss, amphibolite and calc-silicate layers. The gneissic foliation (composite $S_1$ and $S_2$; Hills, 2003) has a dominant NNE-SSW strike and subvertical dip. Locally granite pegmatites occur oriented parallel to, and crosscutting, the foliation.

The immediate host rocks to the main deposit located south of the Breccia Fault are dominantly biotite quartzofeldspathic gneiss that is silicified at the margins of the ore. The ore consists of massive zones of pyrrhotite-chalcopyrite with lesser pyrite, molybdenite and sphalerite. Alteration assemblages within the ore include early skarn (pyroxene-garnet-magnetite±barite±apatite), which is overprinted by biotite-hornblende-epidote-pyrrhotite-chalcopyrite±molybdenite±sphalerite. Three main styles of ore occur including (1) skarn (garnet-magnetite-pyroxene-sulphide-barite) with disseminated chalcopyrite (typically <1% Cu to <3% Cu), (2) structurally-controlled chalcopyrite-pyrite-pyrrhotite, often replacing biotite-matrix breccia at its margins and/or in structural positions such as contacts with amphibolite or pegmatite, and (3) massive chalcopyrite-pyrrhotite-pyrite, forming high grade ore (>3% Cu), typically with relict fragments of altered host rock.

Gregory *et al.* (2005) suggest that the ore sits on the steep eastern limb of a possible local $F_3$ fold and, although it clearly crosscuts the gneissic fabric, the ore appears to anastomose parallel to the foliation and plunges moderately to the south (Fig. 2). Definitive structural evidence for the fold was not found in oriented drill core and in detail much of the ore appears to be controlled by the marginal breccia to the-massive sulphide. Later stage veins postdate the ore and contain pyrite-iron rich chlorite-calcite-siderite±sphalerite±arsenopyrite±tellurides.

## 4 GEOCHRONOLOGY

### 4.1 *U-Pb Zircon*

U-Pb dating of zircons hosted in small scale felsic intrusions was carried out at Macquarie University using LA-ICPMS techniques (Jackson *et al.*, 2004). Sample E9 is from a pegmatite that was emplaced parallel to the main gneissic foliation. U-Pb dating of zircons in this sample provides a crystallization age of 1560 ± 5 Ma, consistent with the peak of regional metamorphism.

A later pegmatite generation, sample E8, cuts the earlier pegmatite and gneissic foliation and has an age of 1544 ± 14 Ma. Sample E1 represented a microgranite dyke that cuts garnet-pyroxene skarn. Zircon rims gave a crystallization age of 1564 ± 15 Ma whereas inherited zircon cores have an age of 1690 ± 15 Ma. One zircon recorded an age of *ca*. 2400 Ma and another *ca*. 1440 Ma. We interpret the age data

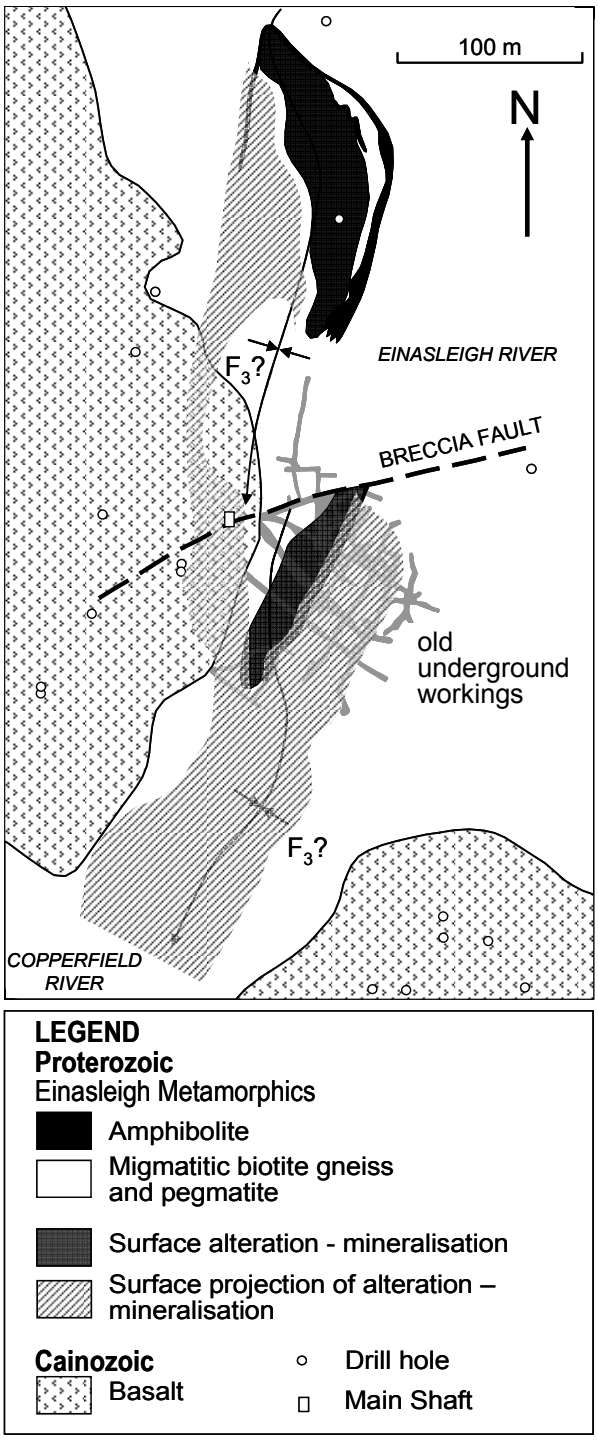


Figure 2. Map of Einasleigh copper deposit (adapted from Gregory *et al.*, 2005)

and field relationships as indicating that at least some of the skarn assemblages in the region formed before 1564 ± 15 Ma (pre- to syn-peak metamorphism).

### 4.2 *Re-Os Molybdenite*

Molybdenite from the main chalcopyrite-pyrrhotite ore was selected for Re-Os dating at Durham University and gave an age of 1394 ± 10Ma. The molybdenite is locally visible in hand specimen (up to 0.5cm) and in thin section where finer grains are intergrown with chalcopyrite-pyrrhotite.

### 4.3 *EMPA Monazite and Uraninite*

EMPA analysis of monazite and uraninite (Fig. 3) were carried out as a complimentary study due to its cost effectiveness and excellent in situ spatial resolution. Monazite was identified in different textural locations including least altered host rocks and alteration associated with mineralization. Outside of alteration and ore zones, monazite grains primarily record metamorphic growth ages predominantly at *ca.* 1590 Ma but spanning an age range from 1540 to 1682 Ma. The latter may be due to detrital monazite whereas the former likely records the last major metamorphic events in the region (Hills, 2003; Cihan *et al.* 2006).

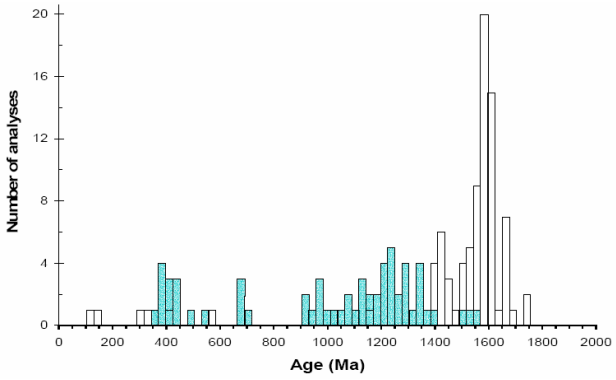


Figure 3. Histogram of all EMPA monazite (white) and uraninite (grey) age data

Three samples yield monazite ages at *ca.* 1400 to 1430 Ma and are related to alteration and brecciation associated with mineralization. Late veins with no mineralization contain rare monazite grains that record ages between 100 and 600 Ma that may be related in part to younger intrusive events in the region.

Uraninite is a common accessory phase in the ore samples at Einasleigh. Uraninite ages are consistently younger than monazite ages and reflect Pb-loss in uraninite (*cf.* Evins *et al.* 2005).

## 5 DISCUSSION AND CONCLUSIONS

The new U-Pb zircon and EMPA monazite age data from the Einasleigh copper deposit host rocks and felsic intrusion presented in this paper supports regional studies in the George-

town inlier that recognise a protracted, multi-phase metamorphic history from *ca*. 1650 to 1500 Ma (Cihan *et al*., 2006). This is consistent with the prolonged period of orogenesis identified in the Mount Isa inlier, suggesting the events may be correlated. However, the *ca.* 1400 Ma event recorded for the age of molybdenite in the ore and monazite in related alteration at Einasleigh has not been widely identified as a significant age for metallogenesis in Australian Proterozoic terranes. Nonetheless, Gregory *et al.* (2004) carried out preliminary Re-Os isotopic analysis from the Mount Isa copper and lead-zinc orebodies and generated a Re-Os isochron age of 1370 ± 80 Ma. In contrast an $^{40}Ar/^{39}Ar$ geochronological study by Perkins et al. (1999) indicated that biotite associated with the main copper ore formed at *ca*. 1523 to 1505. However, they also carried out dating of sericite and hornblende from fault zones in the mine and in Mount Isa fault zone that record Ar-Ar ages between 1440 and 1325 Ma. This may suggest that there was a significant fluid flow and/or uplift event occurring both in the Georgetown and Mount Isa inliers at around 1400 Ma that affected copper ore.

## ACKNOWLEDGEMENTS

This research was funded through a James Cook University collaborative research grant supported by Copper Strike Ltd. We thank Copper Strike for their permission to publish the paper. This study used instrumentation at Macquarie University funded by ARC LIEF and DEST Systemic Infrastructure Grants, Macquarie University and Industry.

## REFERENCES

Black LP, Withnall IW (1993) The ages of Proterozoic granites in the Georgetown Inlier of northeastern Australia, and their relevance to the dating of tectonothermal events. Australian Geological Survey Organisation, *Journal of Geology and Geophysics*, 14/4: 331–341.

Black LP, Gregory P, Withnall IW, Bain JCH (1998) U-Pb zircon age for the Etheridge Group, Georgetown region, N Queensland: implications for the relationship with the Broken Hill and Mt Isa sequences. *Australian J. of Earth Sciences,* 45: 925–935.

Black LP, Withnall IW, Gregory P, Oversby BS, Bain JHC (2005) U-Pb zircon ages from leucogneiss in the Etheridge Group and their significance for the early history of the Georgetown region, north Queensland. Australian *Journal of Earth Sciences*, 52: 385-402.

Bodger SD, Hansen D (2004) Metamorphic evolution of the Georgetown Inlier, northeast Queensland, Australia; evidence for an accreted Paleoproterozoic terrane? *Journal of Metamorphic Geology*, 22: 511-527.

Cihan M, Evins P, Blake K, Lisowiec N (2006) Absolute time constraints on deformation and accompanying metamorphism from in-situ electron microprobe dating of monazite in the Robertson River Metamorphics, NE Australia. *Precambrian Research,* 145: 1-23.

Evins LZ, Jensen KA, Ewing RC (2005) Uraninite recyrstallization and Pb loss in the Oklo and Bangombe natural fission reactors, Gabon. *Geoch. et Cosmo. Acta,* 69: 1589-1606.

Gregory MJ, Wilde AR, Keays RR, Schaefer BF (2004). Preliminary Re-Os dating of the Mount Isa copper ores, NW Queenland. In Barnicoat, A.C., and Korsch, R.J., editors, Predictive Mineral Discovery Cooperative Research Centre – *Extended Abstracts from the June 2005 Conference. Geoscience Australia, Record* 2004/9: 79-80.

Gregory P, Hills QG, Mackee GL, Mclean N (2005) Possible structural controls on the newly discovered extensions to the Einasleigh copper-gold-silver-(molybdenum-zinc) mineralization, Einasleigh, North Queenland. *STOMP Abstract Volume, EGRU Contribution* 64: 57.

Hills Q (2003) The deformational and metamorphic history of the Georgetown Inlier, North Queensland: implications for the 1.7 to 1.5 Ga tectonic evolution of northeastern Proterozoic Australia, *PhD thesis, Monash University, Australia,* pp212.

Jackson SE, Pearson NJ, Belousova E, Griffin WL (2004) The application of laser ablation-inductively coupled plasma-mass spectrometry (LA-ICP-MS) to in situ U-Pb geochronology. *Chemical Geology*, 211: 47-69.

Perkins C, Heinrich CA, Wyborn LAI (1999) $^{40}Ar/^{39}Ar$ geochronology of copper mineralization and regional alteration, Mount Isa, Australia. *Economic Geology*, 94: 23-36.

# FELSIC INTRUSION-RELATED MINERAL DEPOSITS

EDITED BY:

DAVID COOKE

BERND LEHMANN

LAURIE MEINERT

# Basins, breccias and basement – diverse settings for porphyry deposits

David R. Cooke, Anthony C. Harris & David P. Braxton
*CODES, the ARC Centre of Excellence in Ore Deposits, University of Tasmania, Hobart, Tasmania, 7001, Australia*

Kirstie A. Simpson
*Geological Survey of Canada, Natural Resources Canada, Vancouver, British Columbia, Canada*

ABSTRACT: Porphyry Cu-Au and Cu-Mo deposits commonly form in volcano-sedimentary basinal settings. These basins can be inverted by compressional tectonism prior to the onset of mineralisation. Porphyry systems can also form in volcanic conduits – large-scale matrix-rich breccia pipes that may have been the subsurface pipe facies of maar-diatreme volcanoes, and in blind breccia pipes. Crystalline basement rocks and zoned plutonic complexes also host porphyry systems. Varied host rocks and surficial landforms will affect the nature of fluid flow and the morphology of hydrothermal alteration zones in the shallow crust, implying that greater diversity is required in our models of porphyry ore systems for research and mineral exploration.

KEYWORDS: porphyry, copper, gold, volcanic, sedimentary, basin, basement, breccia

## 1 INTRODUCTION

Porphyry Cu-Au and Cu-Mo deposits are generally emplaced at depths of 1-3 km below the Earth's surface (*e.g.*, Cooke *et al.* 2004). Their environments of formation are diverse. Sillitoe (1973) provided important insights into how porphyry systems operate at different levels in the crust, emphasizing high-level and deeper-lever geological features. The landforms that occur above porphyry deposits are typically eroded, and it can be difficult to determine their exact nature in ancient systems. This is why subsequent papers by Sillitoe (*e.g.*, Sillitoe & Thompson 2006) do not show volcanic landforms above porphyry deposits. Despite this, a common misconception remains that porphyry ore formation occurs beneath stratovolcanoes. It is in fact difficult to provide examples where a genetic link between a stratovolcano and a porphyry ore deposit can be demonstrated convincingly. This paper reviews the diversity of environments that some porphyry Cu-Au and Cu-Mo deposits are known to have formed in, and discusses the implications for mineral exploration, fluid flow modeling and ore genesis.

## 2 PORPHYRY DEPOSITS HOSTED IN VOLCANO-SEDIMENTARY BASINS

### 2.1 *Bajo de la Alumbrera*

In the 1970s studies of the Farallón Negro Volcanic Complex (Argentina), host to the Bajo de la Alumbrera porphyry Cu-Au deposit, led to the genetic model for formation of porphyry ore deposits located in the core of, or beneath the flank of, a large polygenetic stratovolcano. Workers previously interpreted the volcano-sedimentary succession to preserve a large (15 to 20km diameter) stratovolcanic complex (Llambías 1972; Sillitoe 1973; Sasso, 1997; Sasso & Clark 1998; Proffett 2003; Halter *et al.* 2004). In contrast, recent studies of the facies architecture of the volcanic complex have found that thick, sheet-like coarse-grained volcano-sedimentary deposits, not lavas, dominate the Farallón Negro Volcanics (Harris *et al.* 2006). Specifically, constructional facies (*i.e.*, lavas) make up less than 30% of the stratigraphy. Furthermore, where lavas are present, they do not form thick stacked sequences representative of a proximal stratocone sequence. Instead, the host rocks to Bajo de la Alumbrera are dominated by locally-derived volcanogenic sedimentary material (with some extra-basinal sources; *i.e.*, crystalline basement) that were deposited within a low relief, multiple-vent-bearing volcano-sedimentary basin (Harris *et al.* 2006).

At Bajo de la Alumbrera, minor felsic eruptions produced nested lava domes, lava flows and associated pyroclastic deposits that were

coeval with the earliest phases of porphyry intrusion (*ca* ~8.0 to 7.8 Ma; Harris et *al.* 2004, 2006). It is not known whether later, strongly mineralized porphyry intrusive phases (*ca* 7 Ma; Harris *et al*. 2004) were emplaced coeval with volcanism, due to the current level of erosion within the district.

Geologic features which show that the Farallón Negro volcanics did not form in a steep-sided polygenetic stratovolcano setting include 1) the dominance of extensive coarse-grained sedimentary basin-fill deposits; 2) volumetrically minor coherent units (*e.g.*, lavas), 3) the presence of peperites on the lower contacts of individual lava units, and 4) lacustrine deposits occurring in areas previously thought to be proximal to the summit region of the stratovolcano. The recognition of peperites (Fig. 1) at most stratigraphic levels is particularly significant. While these features are described in submarine, lacustrine, and subaerial environments, peperites are not found in abundance in high-standing subaerial stratovolcanoes, and if present, would require special circumstances to permit magma interaction with unconsolidated and generally wet sediment within the volcanic edifice (Harris *et al*. 2006).

### 2.2 *Northparkes*

The late Ordovician to early Silurian North-Parkes porphyry Cu-Au deposits (NSW, Australia) are hosted within clastic and coherent facies of the Goonumbla and Wombin Volcanics (Lickfold *et al.* 2003, 2007). The Goonumbla Volcanics contain abundant coarse grained subaqueous mass flow deposits, and coherent units within this sequence locally have peperitic margins, indicating emplacement within wet, unconsolidated sediments (Kolkert 1998; Simpson *et al*. 2005). Based on facies characteristics, the most likely environment of deposition for the volcano-sedimentary sequence is a submarine basinal environment.

Cu-Au mineralization at Northparkes is spatially and genetically associated with quartz monzonite porphyry complexes that have intruded the host volcano-sedimentary sequence. The mineralized intrusive complexes have pipe-like geometries (Fig. 2). The quartz monzonite porphyries were emplaced into the host volcano-sedimentary sequences after deformation, because the subaqueous mass flow deposits of the Goonumbla Volcanics have dips of 30-40, whereas the mineralized intrusive complexes have sub-vertical orientations (Fig. 2).

The Northparkes Cu-Au deposits most likely formed in an inverted, originally submarine, volcano-sedimentary basin. Intrusion occurred synchronous with, or soon after deformation, based on the fact that age determinations (Lickfold *et al*. 2003, 2007) cannot separate the timing of emplacement for the mineralized intrusions and the youngest volcano-sedimentary unit (Wombin Volcanics). As for Bajo de la Alumbrera, models of formation involving a stratovolcano are not consistent with the facies characteristics of the host succession. A similar geological environment is likely for the nearby Cadia porphyry Cu-Au deposits (*e.g*., Wilson *et al.* 2003).

## 3 PORPHYRY DEPOSITS HOSTED IN BRECCIA PIPES

Some porphyry deposits have formed in large-scale, polymictic, matrix-rich breccia pipes. These pipes may have been subsurface facies to maar-diatreme volcanoes. Examples of porphyry deposits that may be hosted in breccia-filled volcanic conduits include the Grasberg (PNG; MacDonald & Arnold, 1994) and Boyongan (Philippines; Braxton 2007) porphyry copper-gold deposits. In both cases, mineralizing intrusions were emplaced into pre-existing, large-scale, discordant, matrix-rich breccia bodies. The breccia at Grasberg has a broadly inverted cone-shaped geometry, consistent with a breccia pipe that has breached the surface (*e.g.,* McCallum 1985).

The Boyongan example is of particular interest, because this breccia-hosted porphyry system underlies a recent stratovolcano complex (Braxton, 2007). The Maniayo Andesite has a 2km diameter eruptive crater, a resurgent dome, and a series of andesitic lavas that are intercalated with fine-grained lacustrine sediments. The volcanic edifice and fluvio-lacustrine material have buried the Boyongan porphyry deposit, and are totally unrelated to mineralization. Maniayo volcanism began occurred almost two million years after hypogene mineralization ceased. Volcanism also post-dated the development of significant supergene oxidation at Boyongan. Application of a stratovolcano model to Boyongan would be totally inappropriate, based on detailed analysis of the host succession and unconformity relationships.

For some porphyry deposits, mineralization occurred entirely in breccia pipes (e.g., Mt. Polley, British Columbia), but it is not clear

Figure 1: Biotite-phyric dacite breccia comprising fluidal igneous lobes and smaller ragged clasts supported in a volcaniclastic sedimentary breccia. The igneous-sedimentary contact is seen across the top of the image. The peperitic contact implies that the sedimentary material was unconsolidated and probably wet at the time of emplacement. Bajo de la Alumbrera, Argentina.

whether these breccia pipes vented, due to the current level of erosion and lack of surficially-derived material in the pipes. If these breccias did not vent, then they would have no surficial expression, possibly apart from hydrothermal alteration features.

## 4 PORPHYRY DEPOSITS HOSTED IN PLUTONIC COMPLEXES

There are some porphyry systems hosted within large, zoned plutonic complexes (McMillan & Panteleyev 1988). Probably the best-known examples are the Highland Valley porphyry Cu-Mo deposits, which occur within a large, zoned plutonic complex in southern British Columbia, Canada. Other examples include the Cu-Mo-Au prospects in the Yeoval Monzodiorite, NSW, Australia. In both cases, mineralization occurred entirely by plutonic rocks, which vary from equigranular to porphyritic facies. The mineralized intrusions are the most fractionated phases of zoned, large-scale plutonic complexes, and occur near the centre of zoned plutons.

## 5 PORPHYRY DEPOSITS HOSTED IN UPLIFTED BASEMENT COMPLEXES

The giant Eocene-Oligocene porphyry Cu-Mo deposits of northern Chile crop out within the Domeyko Cordillera. The Domeyko fault system has been important in localizing porphyry intrusions and mineralization throughout the Cordillera. Although the Domeyko Fault currently has a major component of strike-slip movement, it began life as a series of basin-bounding normal faults for the Jurassic back-arc sedimentary units exposed to the west of the cordillera (Gow & Walshe 2005). This basin-bounding normal fault was inverted during compressive tectonism during the Eocene. Consequently, all along the Cordillera, porphyry intrusive complexes have been emplaced along into uplifted Palaeozoic basement blocks (*e.g.*, Collahuasi, Masterman *et al.*, 2005) and/or inverted Jurassic – Cretaceous sedimentary basins. Evidence for volcanism coeval with porphyry mineralization is extremely limited throughout the Cordillera. Instead, there is strong evidence for rapid uplift and exhumation synchronous with mineralization in this fold belt setting (*e.g.*, Masterman *et al*. 2005), suggesting that the near-surface landforms would have comprised tectonically uplifted mountain ranges, rather than volcanic landforms.

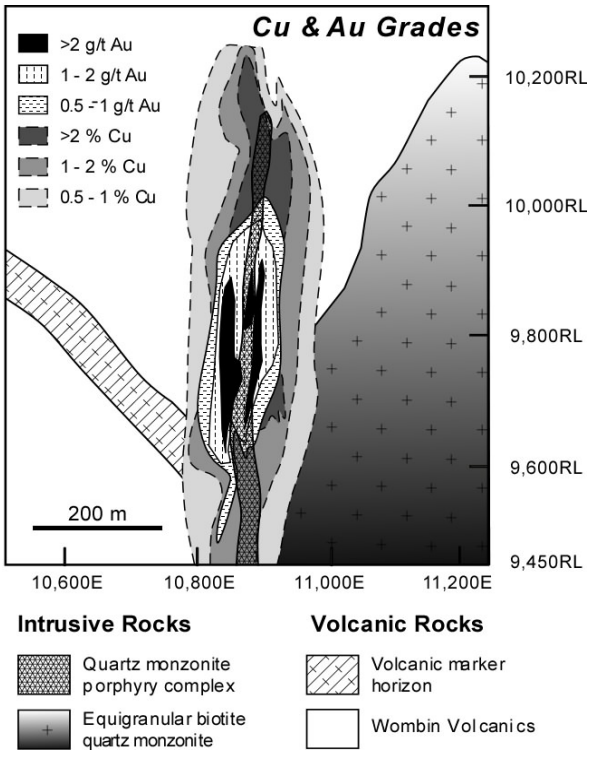


Figure 2: Simplified geology of the E26 porphyry Cu-Au deposit, Northparkes, Australia, showing the steep dip of the host volcano-sedimentary sequence (Goonumbla Volcanics) and the near-vertical mineralizing intrusive complex. Diagram modified after Cooke *et al.* (2007)

## 6 CONCLUSIONS

Stratovolcanic settings are an uncommon environment for porphyry ore formation. Based on our observations, volcano-sedimentary ba-

sins appear to be a more common geological setting for porphyry systems than previously recognised. Given the complex array of environments in which porphyry deposits can form, there is a need for more diverse exploration models. These models will need to account for geologically-controlled variations in near-surface hydrothermal features that could be used to vector downwards towards porphyry ore zones. Hydrological models of fluid flow in porphyry systems will also need to account for this diversity of geological environments. The near-surface facies architecture profoundly affects the nature of hydrothermal fluid flow and subsequent alteration and mineralization in the upper parts of porphyry systems.

## ACKNOWLEDGEMENTS

We thank our past and current research colleagues and students who have contributed significantly to our understanding of the diverse geological environments of porphyry mineralization. In particular we thank Paddy Waters and AngloAmerican Ltd. for providing permission to discuss the Boyongan case study. CODES is the Australian Research Council's Centre For Excellence in Ore Deposits.

## REFERENCES

Braxton, D.P., 2007, Boyongan & Bayugo porphyry Cu-Au deposits, NE Mindanao, Philippines: geology, geochemistry, and tectonic evolution: *Unpublished PhD thesis, University of Tasmania*, 277 p.

Cooke D.R., Wilson A.J., and Davies A.G.S. 2004. Characteristics and genesis of porphyry copper-gold deposits, in Cooke, D.R., Deyell, C., and Pongratz, J., *24 Carat Gold Workshop: CODES spec. publ. No 5*, University of Tasmania, 17-34.

Cooke, D.R., Wilson, A.J., House, M.J., Wolfe, R.C., Walshe, J.L., Lickfold, V., and Crawford, A.J., 2007. Shoshonitic magmatism and the formation of the Northparkes porphyry Cu-Au deposits, NSW, Australia. *Australian Journal of Earth Sciences,* 54, 307-325.

Gow, P.A., and Walshe, J.L., 2005. The Role of Pre-existing Geological Architecture in the Formation of Giant Porphyry-Related Cu +/- Au Deposits: *Economic Geology*, 100, 819-833.

Halter, W.E., *et al*, 2004, From andesitic volcanism to the formation of a porphyry Cu-Au mineralizing magma chamber: the Farallón Negro Volcanic Complex, northwestern Argentina: *Journal of Volcanology and Geothermal Research,* v. 136, p. 1-30.

Harris, A.C., Allen, C.M., Bryan, S.E., Campbell, I.H., Holcombe, R.J., and Palin, M.J., 2004, Measuring the longevity of regional volcanism hosting the Bajo de la Alumbrera Cu-Au deposit: Implications for the genesis of porphyry ore deposits: *Mineralium Deposita*, v. 39, p. 46-67.

Harris, A.C., Bryan S.E., Holcombe, R.J., 2006, Volcanic setting of the Bajo de la Alumbrera porphyry Cu-Au deposit, Farallon Negro Volcanics, Northwest Argentina. *Economic Geology* 101, pp 71-94

Kolkert, R. 1998. Carbonate-base metal veins peripheral to the Goonumbla Cu-Au deposits - vectors to mineralized centers? *BSc (Hons) thesis, University of Tasmania, Hobart* (unpublished).

Lickfold V., Cooke D.R., Smith S.G. & Ullrich, T.D. 2003. Endeavour Cu-Au porphyry deposits, Northparkes, N.S.W.: Intrusive history and fluid evolution. *Economic Geology* 98, 1607-1636

Lickfold V., Cooke D.R., Crawford A. J. & Fanning, C.M. 2007. Shoshonitic magmatism and the formation of the Northparkes porphyry Cu-Au deposits, NSW, Australia. *Australian Journal of Earth Sciences,* 54, 279-306.

Llambías, E.J., 1972, Estructura del grupo volcanico Farallón Negro, Catamarca, Argentina: *Revista de la Asociation Geologica Argentina,* 27: 161-169.

MacDonald, G.D., and Arnold, L.C., 1994, Geological and geochemical zoning of the Grasberg Igneous Complex, Irian Jaya, Indonesia: *Journal of Geochemical Exploration*, v. 50, p. 143–178.

Masterman, G.J., Cooke, D.R., Berry, R.F., Walshe, J.L., Lee, A.W. and Clark A.H., 2005. Fluid Chemistry, Structural Setting, and Emplacement History of the Rosario Cu-Mo Porphyry and Cu-Ag-Au Epithermal Veins, Collahuasi District, Northern Chile: *Economic Geology*, 100, 835-862.

McCallum, M.E., 1985 Experimental Evidence for Fluidization Processes in Breccia Pipe Formation: *Economic Geology*, 80, 1523-1543.

McMillan, W.J., and Panteleyev, A., 1988. Porphyry copper deposits. in Roberts, R.G., and Sheahan, P.A., Ore Deposit Models. *Geoscience Canada, Reprint Series* 3, p. 45-58.

Proffett, J.M., 2003, Geology of the Bajo de la Alumbrera porphyry Cu-Au deposit, Argentina: *Economic Geology*, v. 98, p. 1535-1574.

Sasso, A.M., 1997, Geological evolution and metallogenetic relationships of the Farallón Negro volcanic complex, NW Argentina: *Unpublished Ph.D. Thesis, Queens University,* 842 p.

Sasso, A.M., and Clark, A.H., 1998, The Farallón Negro group, northwest Argentina: magmatic, hydrothermal and tectonic evolution and implications for Cu-Au metallogeny in the Andean back-arc: *Society of Economic Geologists Newsletter*, v. 34, p. 1, 8-18.

Simpson C.J., Cas R.A.F. & Arundell M. C. 2005. Volcanic evolution of a long-lived Ordovician island-arc province in the Parkes region of the Lachlan Fold Belt, southeastern Australia. *Australian Journal of Earth Sciences* 52, 863-886.

Wilson AJ, Cooke DR, Harper BL (2003) The Ridgeway gold-copper deposit: a high-grade alkalic porphyry deposit in the Lachlan Fold Belt, NSW, Australia. *Economic Geology* 98 pp 1637-1656.

Sillitoe, R.H., 1973. The tops and bottoms of porphyry copper deposits. *Economic Geology,* 68, 799-815.

Sillitoe, R.H., and Thompson, J.F.H., 2006. Changes in Mineral Exploration Practice: Consequences for Discovery. *Society of Economic Geologists Special Publication 12*: *Wealth Creation in the Minerals Industry*: Integrating Science, Business and Education.

# Possible adakitic porphyries and their tectonomagmatic and metallogenic implications: Evidence from the northern Loei Fold Belt, Thailand and Laos

T. Kamvong, Khin Zaw & S. Meffre
*CODES ARC Centre of Excellence in Ore Deposits, University of Tasmania, Tasmania, Australia*

ABSTRACT: The northern Loei Fold Belt (LFB) is an important ore province of mainland Southeast Asia. Most of the economic ore deposits of LFB are porphyry, skarn Cu-Au, and epithermal Au-Ag deposits associated with Permian-Triassic continental arc magmatism. Here we present evidence of the possible existence of adakitic porphyries in the northern LFB which are mainly associated with porphyry-related skarn Cu-Au deposits. Purely based on geochemical characteristics, almost all porphyritic intrusions within the study area display features of adakitic affinity. Due to the close relationships of these possible adakitic porphyries and Cu-Au mineralization in the area, we propose that this adakitic magma is important in controlling economic mineralization in the northern LFB. Further Sr-Nd-Pb isotopic studies are in progress in order to define the adakitic signatures of the rock suites which are associated with Cu-Au mineralization.

KEYWORDS: Loei Foldbelt, Southeast Asia, adakitic porphyries, slab melting

## 1 LOEI FOLD BELT OF MAINLAND SOUTHEAST ASIA

The Loei Fold Belt (LFB) is a major Cu-Au metallogenic and magmatic belt in mainland Southeast Asia (Fig. 1). The LFB extends across western Cambodia and Ko Chang Island, up through central Thailand and into the northwestern Laos. It is considered to form by eastward subduction of the Palaeo-Tethys oceanic crust beneath the Indochina terrane during the Indosinian Orogeny. The LFB consists of continental margin volcano-plutonic suites which are closely associated with Cu-Au mineralization. To date, LFB hosts several economic Cu-Au deposits, such as Chatree (LS epithermal Au-Ag), Puthep 1 (porphyry-related skarn Cu), Phu Thap Fah (Au skarn) and Phu Kham (porphyry-related skarn Cu-Au). Although it contains many economic ore deposits, its tectonomagmatic evolution is poorly understood.

The aim of this paper is to present new data on the geochemistry of the northern LFB porphyritic intrusions that mostly display a geochemical affinity with adakite. We also discuss the significance of adakitic signatures of the rocks in relation to tectonomagmatism and metallogeny at the northern LFB.

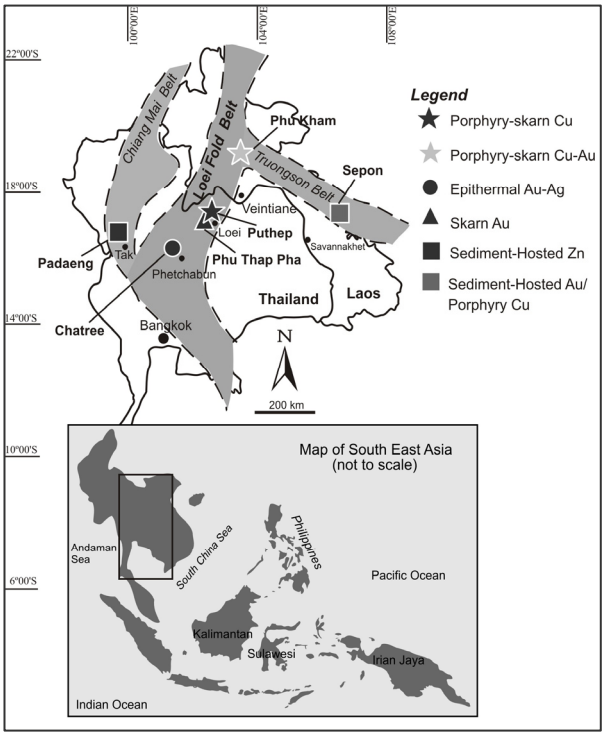


Figure 1. Location map of the LFB.

Table 1 Main geochemical features of typical adakites compared to results from the Phu Kham and PUT 1 intrusive suites in the northern Loei Fold Belt.

| Characteristics | Adakites* | Phu Kham | Puthep 1 |
|---|---|---|---|
| high $SiO_2$ (wt%) | ≥56 | 58.2–69.9 | 61.9–65.7 |
| high $Al_2O_3$ (wt%) | ≥15 | 15.0–19.0 | 16.1–17.4 |
| low MgO (wt%) | <3 | 0.9–3.8 | 1.8–3.1 |
| high Sr (ppm) | >300 | 133–377 | 586–917 |
| low Y (ppm) | <15 | 9.1–21.0 | 10.1–15.9 |
| low Yb (ppm) | <1.9 | 0.8–2.2 | 0.9–1.6 |
| high Sr/Y | >20 | 7.5–33.6 | 43.4–65.0 |
| high La/Yb | >20 | 11.0–37.8 | 8.9–18.5 |
| Eu anomaly | positive and/or absent | usually absent | absent |
| HFSE (ppm) | depletion | depletion | depletion |

* From Defant & Drummond (1990), Martin (1999), Castillo (2006)

## 2 BACKOUND: ADAKITE

Adakite is a petrogenetic term, which was originally identified at Adak Island in the Aleutian arc to describe the tectonic setting (*i.e.* slab-melts), and was introduced by Defant & Drummond (1990). After the published work of Kay (1978), Defant & Drummond (1990) proposed that adakites are magmatic arc rocks with a special and unusual tectonomagmatic evolution. Adakite is characterised by high $SiO_2$, $Al_2O_3$ and Sr contents, high Sr/Y and La/Yb ratios, but depleted in MgO, Y, Yb, and HREE contents (Defant & Drummond 1990; Table 1). In terms of their genesis, adakite is derived from direct partial melting of a young (≤25 Ma) and hot subducted oceanic slab (Defant & Drummond 1990). However, recent workers have proposed alternative models of adakitic generation. These are: (1) partial melting of thickened lower crust; (2) AFC processes from parental basaltic melts; (3) partial melting of delaminated mafic lower crust; and (4) partial melting of a stalled slab in the mantle. Therefore, it clearly appears that adakites are not always produced by melting of a subducted oceanic slab, and investigators should interpret with caution when the term adakite is used for genetic interpretation.

Recently, Castillo (2006) suggested that adakites can form in late Palaeozoic to Cenozoic arc settings where unusual tectonic conditions can lower the solidus of older slabs. In addition to their petrogenesis, adakites have a close spatial and temporal relationship with Cu-Au mineralization worldwide, especially in the Pacific Rim. This finding suggested that there may be a genetic link between adakites and Cu-Au mineralization (Mungall 2002; Wang *et al*. 2006).

## 3 RESULTS FROM THE NORTHERN LOEI FOLD BELT PORPHYRIES

In this study, 30 intrusive rocks (diorite porphyry, monzodiorite porphyry), which are closely related in space and time with porphyry-related skarn Cu-Au, from the PUT 1 (northeastern Thailand) and Phu Kham (northern Laos) deposits in the northern LFB have been analysed for major and trace elements using XRF and ICP-MS techniques at University of Tasmania. Most of the analysed rocks show compositions that approach fresh intrusive rocks, and these results (Table 1) are used in the following discussions.

Porphyritic intrusions from the northern LFB have relatively high contents of $SiO_2$ (58.2–69.9 wt%; mean = 63.7), $Al_2O_3$ (15.0–19.0 wt%; mean = 16.6) and Sr (133–917 ppm; mean = 486.5) but relatively low contents of MgO (0.9–3.8 wt%; mean = 2.4), Y (9.1–21.0 ppm; mean = 12.6) and Yb (0.8–2.2 ppm; mean = 1.2). The rocks also show LILE- enrichment but strongly depleted in HFSE. Chondrite-normalized REE patterns show that all samples of the northern LFB porphyritic are strongly fractionated, with LREE enrichment and HREE depletion ($(La/Yb)_N$ = 5.6–25.2). Moreover, REE patterns display a weak concavity in the MREE and are almost absent in the Eu anoma-

lies (Eu/Eu* ~ 1).

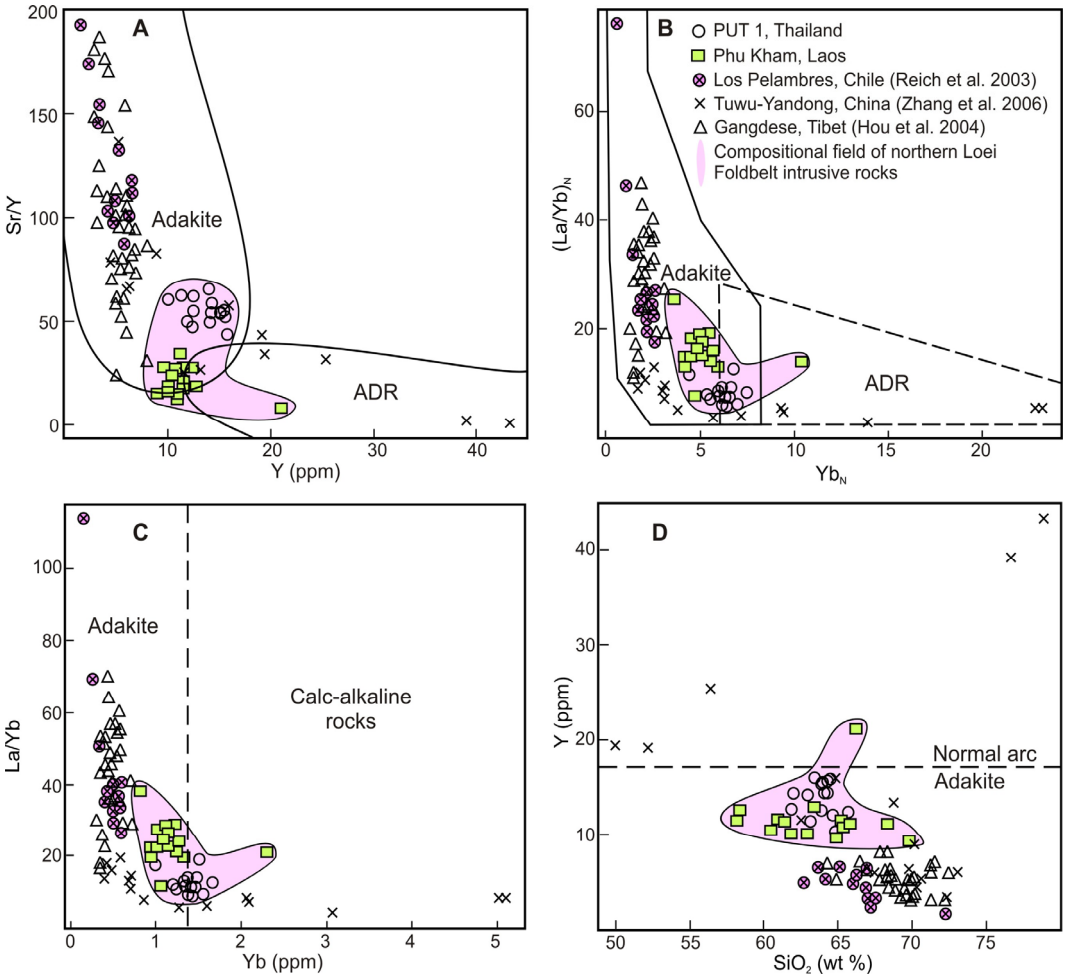


Figure 2. Adakitic discrimination diagrams for the northern LFB rocks. A: Sr/Y vs. Y diagram (Defant and Drummond 1990). B: $(La/Yb)_N$ vs. $(Yb)_N$ diagram (Martin 1999). C: La/Yb vs. Yb diagram (Samaniego *et al.* 2002). D. Y vs. $SiO_2$ diagram (Defant & Drummond 1993). ADR (arc andesite, dacite, rhyolite) fields are defined by Defant & Drummond (1990) and Martin (1999)

.

## 4 TECTONOMAGMATIC IMPLICATIONS

Based on the adakitic criteria defined by Defant & Drummond (1990; 1993), Martin (1999) and Samaniego *et al.* (2002), almost all porphyritic intrusive rocks within the study area display a geochemical affinity with adakite (Fig. 2). Commonly absent Eu anomalies and strong HREE depletions suggests that adakitic signatures in the study area require a plagioclase-free residuum to plagioclase fractionation and amphibole- and garnet-bearing residuum in the source of adakitic magmas, respectively. Besides, the rocks also show relatively low Nb/Ta and high Zr/Sm ratios, suggesting melting in the garnet amphibolite stability field (Foley *et al*. 2002).

These geochemical characteristics imply that adakitic signatures in the study area were most likely derived by partial melting of a subducted oceanic slab and suggest a basaltic source transformed to garnet amphibolite sources (Defant & Drummond 1993). However, based on the fact that several petrogenetic models of adakite generation have been proposed, Further Sr-Nd-Pb isotopic studies are in progress to understand how the adakitic signatures of the studied rocks developed in the northern LFB.

## 5 METALLOGENIC IMPLICATIONS

Because adakite or adakitic rocks are formed in magmatic arcs, they have been recognised associated with many Cu-Au deposits, particularly in the Pacific Rim (*e.g*. Oyarzún *et al*. 2001). Thus, adakitic magma seems to show a genetic link with Cu-Au mineralization (Oyarzún *et al*. 2001; Mungall 2002; Wang *et al*. 2006).

At Phu Kham and PUT 1, the porphyritic rocks with adakitic characteristics display a close spatial and temporal relationship with the economic Cu-Au mineralization. A large amount of magnetite, haematite and titanite has been observed in the rocks together with gold and sulphides. This evidence infers that the porphyries were formed under high $fO_2$ conditions, indicating a favorable setting to generate Cu-Au mineralization (Mungall 2002; Wang *et al*. 2006).

Overall, due to the close relationships of adakitic signatures of the studied rocks and Cu-Au mineralization in the area, we propose that the adakitic magmatism is important in controlling economic mineralization at the Phu Kham and PUT 1 deposit in the northern LFB.

## ACKNOWLEDGEMENTS

The study is conducted as a part of the first author's PhD research supported by the ARC Linkage grant from the Australian Research Council to Khin Zaw. This research is also funded through Hugh E. McKinstry and Newmont Mining Corporation Grants from the Society of Economic Geologists to Kamvong. We also acknowledge Pan Australian Resources Ltd for support and permission to publish.

## REFERENCES

Castillo PR (2006) An overview of adakite petrogenesis. *Chinese Science Bulletin* 51: 258-268.

Defant MJ, Drummond MS (1990) Derivation of some modern arc magmas by melting of young subducted lithosphere. *Nature* 347: 662-665.

Defant MJ, Drummond MS (1993) Mount St. Helens: potential example of the partial melting of the subducted lithosphere in a volcanic arc. *Geology* 21: 547-550.

Foley S, Tiepolo M, Vannucci R (2002) Growth of early continental crust controlled by melting of amphibolite in subduction zones. *Nature* 417: 837-840.

Hou ZQ, Gao YF, Qu XM, Rui ZY, Mo XX (2004) Origin of adakitic intrusives generated during mid-Miocene east-west extension in southern Tibet. *Earth and Planetary Science Letters* 220: 139-155.

Kay RW (1978) Aleutian magnesian andesites; melts from subducted Pacific Ocean crust. *Journal of Volcanology and Geothermal Research* 4: 117-132.

Martin H (1999) Adakitic magmas: modern analogues of Archaean granitoids. *Lithos* 46: 411-429.

Mungall JE (2002) Roasting the mantle; slab melting and the genesis of major Au and Au-rich Cu deposits. *Geology* 30: 915-918.

Oyarzun R, Marquez A, Lillo J, Lopez I, Rivera S (2001) Giant versus small porphyry copper deposits of Cenozoic age in northern Chile; adakitic versus normal calc-alkaline magmatism. *Mineralium Deposita* 36: 794-798.

Reich M, Parada MA, Palacios C, Dietrich A, Schultz F, B L (2003) Adakite-like signature of Late Miocene intrusions at the Los Pelambres giant porphyry copper deposit in the Andes of central Chile: metallogenic implications. *Mineralium deposita* 38: 876–885

Samaniego P, Martin H, Robin C, Monzier M (2002) Transition from calc-alkalic to adakitic magmatism at Cayambe Volcano, Ecuador; insights into slab melts and mantle wedge interactions. *Geology* 30: 967-970.

Wang Q, Xu J, Jian P, Bao Z, Zhao Z, Li C, Xiong X, Ma J (2006) Petrogenesis of adakitic porphyries in an extensional tectonic setting, Dexing, south China; implications for the genesis of porphyry copper mineralization. *Journal of Petrology* 47: 119-144.

Zhang L, Xiao W, Qin K, Zhang Q (2006) The adakite connection of the Tuwu-Yandong copper porphyry belt, eastern Tianshan, NW China; trace element and Sr-Nd-Pb isotope geochemistry. *Mineralium Deposita* 41: 188-200.

# Alkalic epithermal or porphyry? Hydrothermal alteration and vein paragenesis at the E41 gold deposit Cowal district, New South Wales, Australia

Wojciech Zukowski, David R. Cooke & Cari L. Deyell
*ARC Centre of Excellence in Ore Deposits, University of Tasmania, Private Bag 79, Hobart, 7001, Tas, Australia*

Paul McInnes
*Barrick Australia Limited, Cowal Gold Mine, New South Wales, Australia*

ABSTRACT: Epithermal and porphyry styles of mineralization and alteration occur within the Endeavour 41 (E41) gold prospect of the Ordovician Cowal district, New South Wales, Australia. The deposit is located in an Ordovician subaqueous volcano-sedimentary succession that has been intruded by multiple sills and dykes. Gold is associated with quartz-pyrite and quartz-sphalerite-carbonate veins. Alteration facies include potassic, calcic-potassic, phyllic and propylitic mineral assemblages. The nature and distribution of these assemblages has been controlled by rock types, structure and geometry of the mineralised zones. The paragenetic sequence is complex, with certain minerals (*e.g*. epidote, pyrite, sericite, quartz and carbonate) forming at several stages in the deposit evolution. Early hydrothermal alteration produced actinolite-magnetite-albite-chlorite and garnet-epidote-carbonate assemblages. Syn-mineralization alteration facies are characterised by K-feldspar, sericite (muscovite/illite), chlorite, epidote and arsenopyrite, whereas late alteration comprises epidote-carbonate-prehnite. The hydrothermal system evolved from early high-temperature actinolite-magnetite-albite-chlorite and garnet alteration and vein facies, characteristic of an alkalic porphyry environment, to assemblages more typical of an epithermal style gold deposit (*e.g*. quartz, carbonate, chalcedony, adularia, gold, sphalerite, galena and illite). The paragenetic history of the E41 gold prospect appears to record the transition from deep to shallow-level magmatic-hydrothermal activity, and implies un-roofing of the system synchronous with mineralization.

KEYWORDS: alkalic, epithermal, porphyry, alteration, vein paragenesis

## 1 INTRODUCTION

Endeavour 41 (E41) is one of three economically significant gold deposits that occur in the Cowal district, part of the Junee-Narromine belt of the Ordovician Macquarie Arc, NSW, Australia (Fig. 1). E41 has features characteristic of both epithermal and porphyry environments. Some of the alteration facies are similar to those occurring in alkalic porphyry systems, and imply that the district is similar to the major alkalic porphyry Cu-Au deposits in the Macquarie Arc: Cadia (Wilson, 2003) and Northparkes (Lickfold, 2003). This paper documents the complex vein paragenesis and alteration facies of E41 in relation to the local intrusive history.

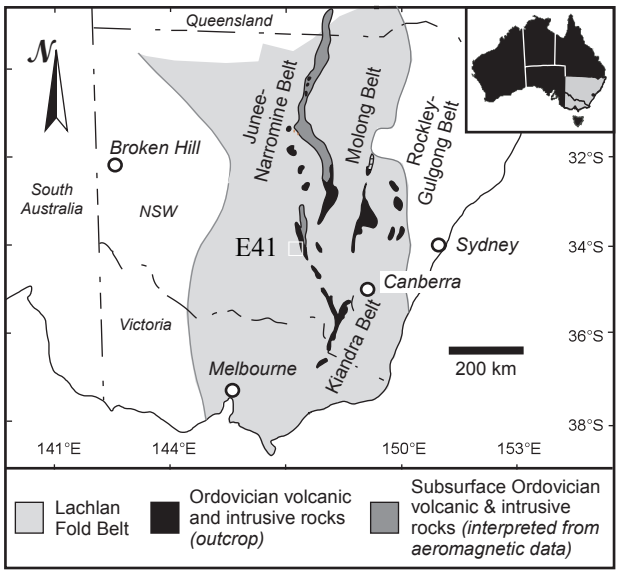


Figure 1. The Ordovician Macquarie Arc, NSW

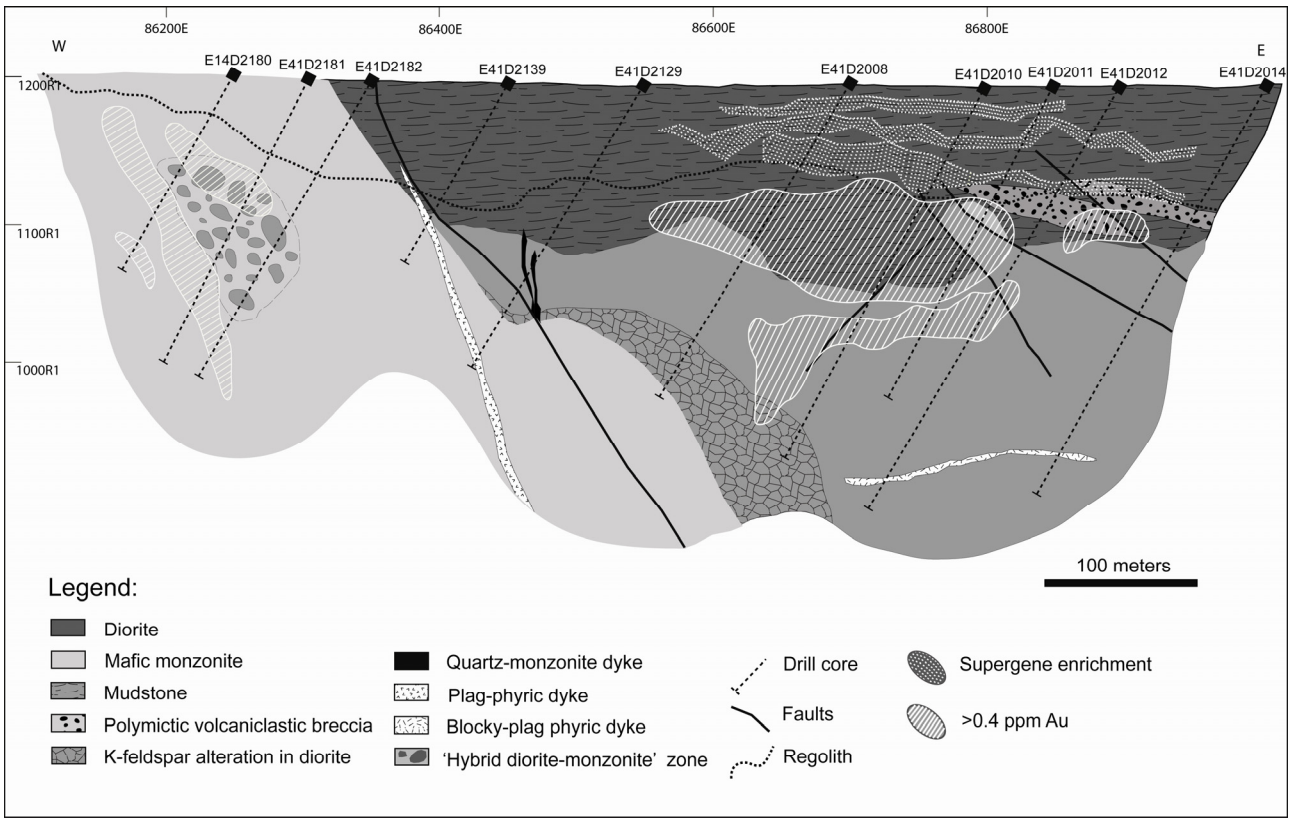


Figure 2. Interpreted geology of long section 34900N (E-W) through the E41 gold deposit. Mineralized zones in the eastern part of the deposit are located at the contact between the diorite sill and volcaniclastic beds. An elongated zone of mineralization characterizes the 'west pod' of the deposit, which is hosted in mafic monzonite. A 'patchy' texture in the west pod is interpreted to be a direct consequence of potassic metasomatism induced by intrusion of mafic monzonite into diorite, and is associated with domains of hybrid diorite-monzonite rock.

## 2 GEOLOGICAL SETTING

The Lake Cowal Volcanic Complex, a middle Ordovician volcanic arc succession, is part of the Junee-Narromine belt of NSW's Macquarie Arc (Fig. 1). Two zones of hypogene gold mineralization have been discovered at E41 (west and east pods), which are hosted by volcaniclastic and coherent igneous facies (Fig. 2). The volcaniclastic facies include: (1) mudstone; (2) sandstone; and (3) polymictic volcaniclastic breccia/sandstone. The volcaniclastic packages have been intruded by sills and numerous dykes. The earliest and volumetrically most significant coherent unit is a heterogeneous diorite complex – the Muddy Lake Diorite, which is spatially associated with mineralization in east pod (Fig. 2). West pod mineralization is hosted in equigranular, medium grained mafic monzonite (Fig. 2), and is spatially associated with a hybrid diorite-monzonite zone (Fig. 2). Other pre-mineralization intrusions include several dyke facies which have been truncated by mineralised veins and overprinted by alteration facies intimately associated with gold mineralization (Table 1). The exact timing of pyroxene-phyric mafic dykes and quartz monzonite dykes remains enigmatic although absence of well-mineralized veins within those dykes and intensive K-feldspar-haematite alteration associated with mineralization suggest a pre- to syn-mineralization timing. Post-mineralization dykes include hornblende-quartz phyric, vesicular, plagioclase-phyric and hornblende-phyric dyke facies. These dykes are characterised by a lack of the alteration assemblages that are intimately associated with mineralization.

## 3 HYDROTHERMAL ALTERATION

The E41 hydrothermal system evolved from early high temperature mineral assemblages to low temperature alteration facies. Early hydrothermal alteration of the diorite produced an actinolite-magnetite-albite-chlorite assemblage. Actinolite, magnetite and chlorite have pseudomorphed former mafic minerals. The altered diorite contains abundant secondary K-feldspar as halos around mineralized veins and as char-

acteristic ‘patchy’ domains. The ‘patchy’ texture is only observed in the diorite near the mafic monzonite contact (Fig. 2).

Multiple generations of epidote, pyrite, quartz, sericite and carbonate alteration characterise E41. Sericite alteration facies are particularly complicated. Green ‚waxy’ sericite (muscovite ± illite) occurs as halos around mineralized veins. There are also domains of pervasive illite alteration. Sericite has also selectively replaced plagioclase phenocrysts within the mafic monzonite. Late stage alteration minerals include ankerite, carbonates, epidote, chalcedony and prehnite.

| Vein stage | Description |
|---|---|
| Stage 0 | Actinolite-magnetite-chlorite replace former clinopyroxene/and amphibols |
| Stage 1 | Irregular epidote veins, veinlets and/or patches locally with pyrite and carbonate |
| Stage 2 | Parallel sided/or irregular and wispy magnetite-albite-pyrite-quartz-chalcopyrite veins with weak albite halos |
| Stage 3A | Parallel sided quartz-pyrite, occasionally with carbonate. Associated with K-feldspar, K-feldspar-epidote, chlorite or sericite halos |
| Stage 3B | Parallel sided quartz-pyrite-K-feldspar veins, locally K-feldspar halos |
| Stage 4 | CBMS; sphalerite, galena, arsenopyrite, chalcopyrite, pyrite, quartz, carbonate. Associated with sericite and/or sericite/arsenopyrite pyrite halos. Irregular, parallel sided, multi stage opening veins, occasionally brecciated |
| Stage 5 | Irregular, wispy veinlets and clots of epidote and carbonate or epidote-carbonate-prehnite. Locally pyrite associated with those veins |
| Stage 6 | Wispy/irregular carbonate-hematite veins and veinlets |
| Stage 7 | Irregular gypsum veins |
| Stage 8 | Irregular ankerite veinlets, often late infills in 3A, 3B and 4 stage |

Table 1. Characteristic features of veins at E41

## 4 VEIN PARAGENESIS

The E41 paragenetic sequence has been determined from systematic core logging on two perpendicular cross sections (N- and E-trending). The complex vein paragenesis has been grouped into nine stages (Table 1). Additional pre-mineralization features of uncertain timing include garnet-epidote-carbonate veins which occur in the volcaniclastic units.

Gold mineralization at E41 is typically associated with quartz – pyrite ± carbonate veins, and also carbonate - base-metal sulphide veins (CBMS), comprising pyrite, sphalerite, galena, carbonate, arsenopyrite and quartz. The well-mineralized veins have typically been re-opened. Many quartz – pyrite ± adularia ± carbonate veins have been reactivated and infilled with CBMS stage mineral assemblages. These veins typically have the highest gold grades. Some multi-stage veins consist of two or three stages - typically stages 3A, 3B and 4 – that are in some cases brecciated and/or are associated with larger faults.

## 5 DISCUSSION

The complex paragenetic sequence at E41 demonstrates that the hydrothermal system evolved from early high temperature porphyry-like conditions (actinolite-magnetite-albite-chlorite and garnet alteration and vein facies) to conditions more typical of an epithermal setting (lower temperature quartz, carbonate, chalcedony, adularia, gold, sphalerite, galena and illite-bearing veins and alteration assemblages).

The early vein and alteration assemblages at E41 may have an alkalic porphyry affinity. For example; quartz – magnetite – chalcopyrite - actinolite veins characterise the core of the Ridgeway porphyry Cu-Au deposit in the Cadia district of NSW, and were genetically associated with an early monzonite intrusion (Wilson *et al.*, 2003). Actinolite also defines the highest temperature subzone of propylitic alteration halos adjacent to the mineralized potassic centres of several porphyry copper deposits and geothermal fields (*e.g.*, Tintic, Norman *at al*. 1991; Batu Hijau, Garwin, 2002; Palinipinon, Rae *et al.*, 2004). The presence of these mineral associations characterise an environment proximal to a magmatic centre.

## ACKNOWLEDGEMENTS

Thanks to Stuart Matthews, Paul McInnes and all staff at the Cowal gold mine. Thanks also to Amber Henry, Kirstie Simpson and other sponsors and team members of the alkalic project.

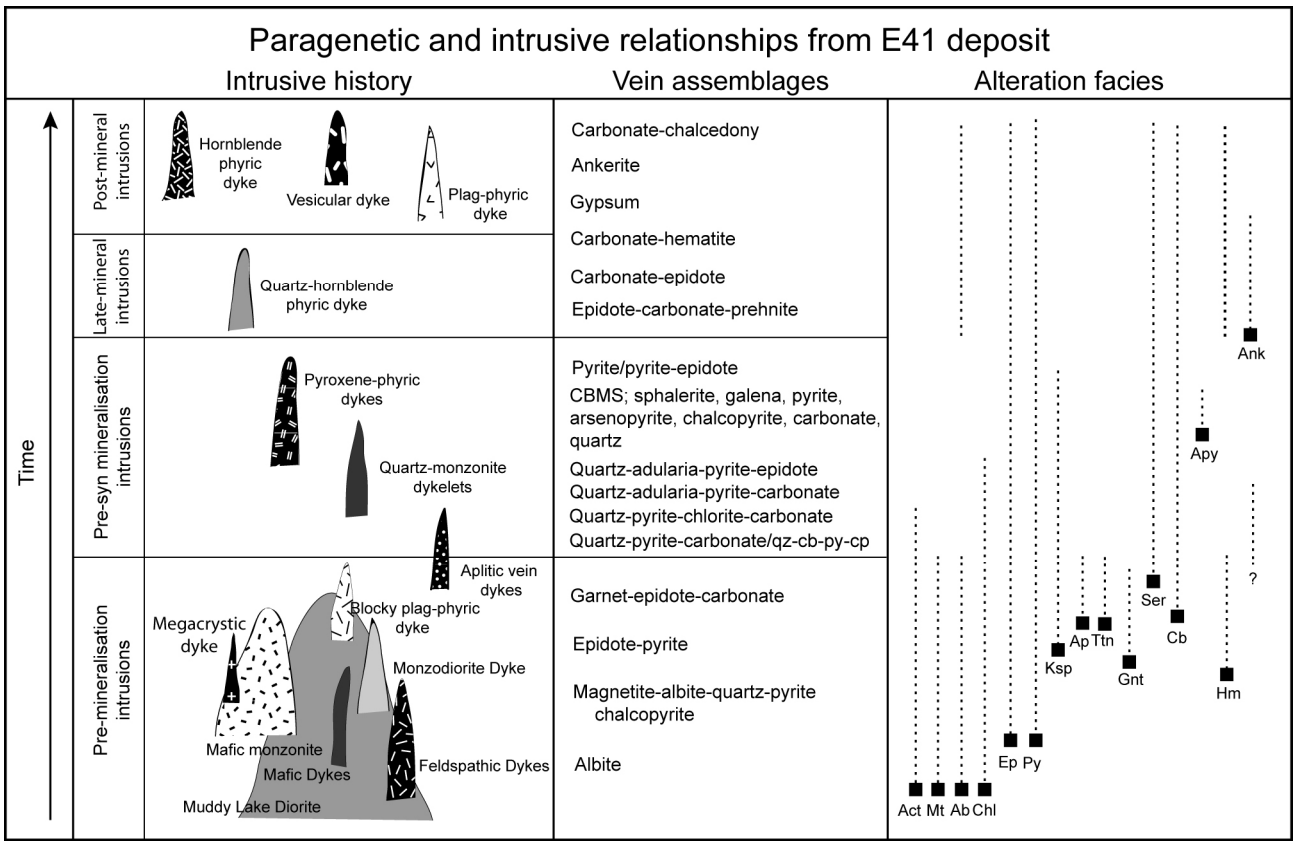


Figure 3. Alteration facies, vein assemblages and the intrusive history of E41. Note the presence of high temperature minerals early, and lower-temperature mineral assemblages during mineralization and post mineralization events.

## REFERENCES


Garwin S., 2002, The geological setting of intrusion-related hydrothermal systems near the Batu Hijau porphyry copper-gold deposit, Sumbawa, Indonesia: *Society of Economic Geologists, Special Publication* No. 9, p. 333–366.

Lickfold V., Cooke D.R., Smith S. G., and Ullrich T.D., 2003, Endeavour Cu-Au Porphyry Deposits, Northparkes, NSW, Intrusive History and Fluid Evolution: *Economic Geology,* v. 98, p.1607-1636

Norman D.K., Parry, W.T., and Bowman, J.R., 1991, Petrology and geochemistry of propylitic alteration at Southwest Tintic, Utah: *Economic Geology,* v. 86, p. 13-28.

Rae A.J., Cooke, D.R., Phillips, D., Yeats, C., Ryan, C. and Hermoso, D., 2003, Spatial and temporal relationships between hydrothermal alteration assemblages at the Palinpinon geothermal field, Philippines: implications for porphyry and epithermal ore deposits: *Society of Economic Geologists Special Publication* No 10, p. 223-246.

Wilson A.J., 2003, The geology, genesis and exploration context of the Cadia gold-copper porphyry deposit, NSW, Australia. *Unpublished Ph.D. thesis, University of Tasmania.*

Wilson A.J., Cooke D.R. & Harper B.L., 2003, The Ridgeway gold-copper deposit: a high-grade alkalic porphyry deposit in the Lachlan Fold Belt, NSW, Australia, *Economic Geology*, v.98, p. 1637-1666

# Cooling, fractionation and mixing of magmas in the super-giant Oyu Tolgoi Cu-Au porphyries; SHRIMP-RG trace element geochemistry of zircons

Alan J. Wainwright & Richard M. Tosdal
*Mineral Deposit Research Unit, Department of Earth and Ocean Sciences, The University of British Columbia, Canada*

Joseph L. Wooden & Frank K. Mazdab
*U.S.G.S.-Stanford Ion Probe Laboratory, Stanford, CA*

ABSTRACT: Trace element geochemistry of zircons from five late Devonian intrusions associated with the Oyu Tolgoi Igneous Complex (OTIC) has been measured by SHRIMP-RG. Th/U and Yb/Gd ratios in addition to Hf and Y concentrations indicate the presence of mutiple magmatic groups and that discrete melts influenced the same pluton. The TiO2-in-zircon thermometer estimates that temperatures for the spot analyses range from 699°C to 863°C and zircons typically exhibit a transition from high-T cores with low Hf toward low-T rims with high Hf. The zircon chemistry suggests that OTIC intrusions are derived from a multi-component, fractionating, cooling magmatic system.

KEYWORDS: zircon, porphyry, trace element, copper, Mongolia

## 1 INTRODUCTION

The super-giant Oyu Tolgoi porphyry copper-gold deposits, located in the South Gobi region (Mongolia), are associated with Late Devonian medium- to high-K calc-alkaline intrusive phases that define the Oyu Tolgoi Igneous Complex (OTIC). The deposits are aligned in a 6.5 kilometer-long, north-northeast-trending corridor and are divided into five zones: South Oyu, Southwest Oyu, Central Oyu and the Hugo Dummett deposits (North and South). District measured and indicated resources include 1.15 Gt grading 1.27% copper and 0.48 g/t gold at a 0.60% copper equivalent cut-off grade. There is an additional inferred resource of 1.44 Gt grading 1.11% copper and 0.28 g/t gold at a 0.60% copper equivalent cut-off grade (*Ivanhoe Mines press release*, 2006).

Specific geochemical characteristics and magma chamber events appear to be associated with the genesis of porphyry copper deposits (PCD). For example, there is a link between elevated oxidation state of arc magmas and the formation of porphyry Cu-Au deposits (*e.g.* Candela, 1992). Furthermore, the injection of sulfur-undersaturated mafic magma into an intermediate porphyry root system has been proposed as a means of forming PCDs (*e.g.* Hattori & Keith, 2001).

Zircon is a robust mineral chronometer and preserves additional information that is otherwise lost due to pervasive alteration of PCD-related intrusions. We have used SHRIMP-RG trace element geochemistry of zircons to investigate the evolution of the OTIC and possible linkages to the development of super-giant copper-gold deposits in the district.

## 2 GEOLOGIC SETTING

The Oyu Tolgoi district is located within a sequence of Paleozoic rocks in the Gurvansayhan island arc terrane. The Cu-Au deposits are hosted in an inlier of Devonian volcanic and volcaniclastic rocks and late Devonian intrusions that are surrounded by disconformably-overlying Carboniferous volcanic and sedimentary rocks (Wainwright *et al*., 2005) (Fig. 1). Geochemistry of the late Devonian intrusions suggests that OTIC rocks have at least 2 petrogenetic lineages and that magma recharge events may have occurred (Wainwright, *unpublished data*).

## 3 RESULTS

We have generated SHRIMP-RG data from five samples and each of the main porphyry deposits are represented (Table 1). All of the samples are equigranular to porphyritic quartz monzodiorites that range in age from ~374 Ma

to ~362 Ma (Wainwright, *unpublished data*). A review of the applied techniques is given in Mazdab and Wooden (2006). We analyzed a variety of different growth zones that include oscillatory-zoned core-to-rim pairs, sector-zoned areas and discordant cores. Furthermore,

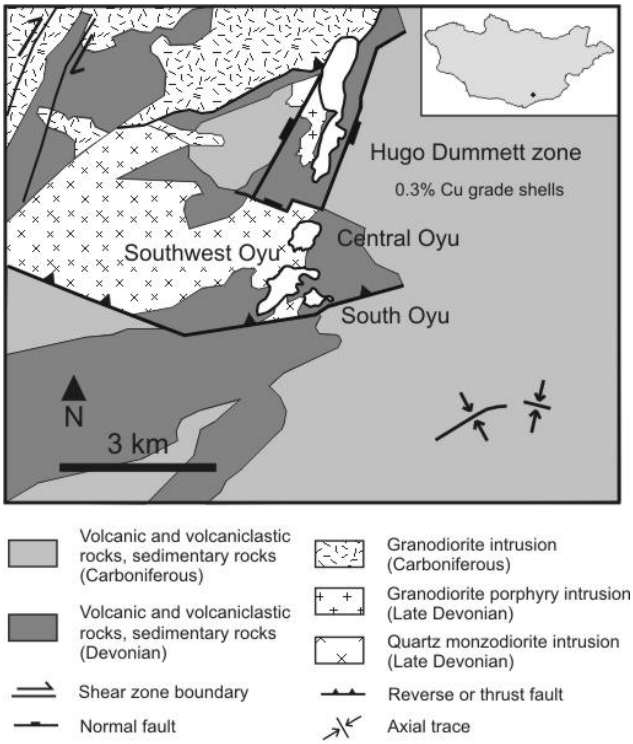


Figure 1. Simplified geologic map of the Oyu Tolgoi porphyry Cu-Au district.

on some of the larger grains, we performed core-to-rim traverses with three or more analytical spots.

The Y versus Yb/Gd plot (Fig. 2a) separates the data into three groups:

1. High Y, low Yb/Gd with zircon spots from all samples except AJW-03-178.
2. Moderate Y, moderate Yb/Gd with analytical spots from all rocks.
3. Low Y and high Yb/Gd dominated by zircon spots from sample AJW-03-178 with some analyses from AJW-03-182.

On the Th/U vs. Yb/Gd plot (Fig. 2b); most data points define an array that increases in Th/U with decreasing Yb/Gd. Some spot analyses from AJW-03-178, AJW-03-182 and AJW-04-385 are distinct from the rest of the spot analyses (high Yb/Gd).

The TiO2-in-zircon thermometer (Watson and Harrison, 2005) suggests that temperatures in the OTIC zircons range from 699°C to 863°C (using a TiO2 ≈ 0.7; Claiborne *et al.*, 2006).

| Sample | Location | U-Pb Age |
|---|---|---|
| AJW-03-181 | Central Oyu | ~370 Ma |
| AJW-04-385 | 100m west of Central Oyu | ~362 Ma |
| AJW-03-178 | Southwest Oyu | ~370 Ma |
| AJW-03-182 | South Oyu | ~374 Ma |
| AJW-04-356 | Hugo Dummett zone | ~370 Ma |

Table 1. Sample locations.

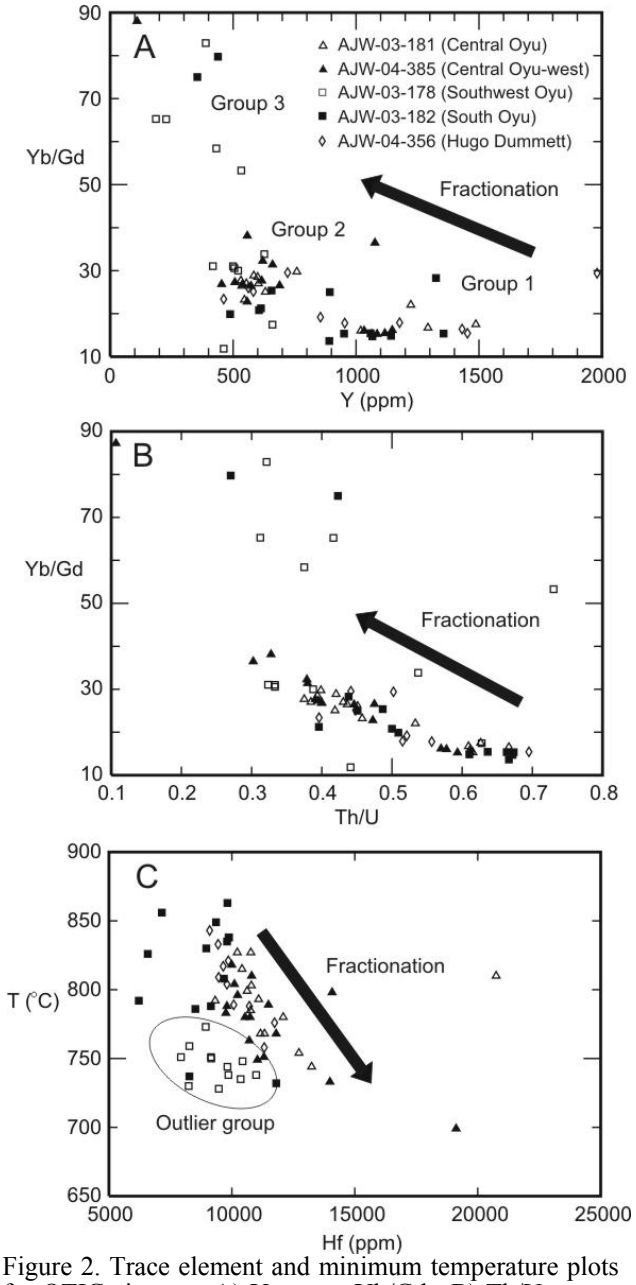


Figure 2. Trace element and minimum temperature plots for OTIC zircons. A) Y versus Yb/Gd. B) Th/U versus Yb/Gd. C) Hf versus minimum temperature.

Zirconium has a much higher zircon/melt partition coefficient compared to Hf and as mag-

mas undergo cooling and fractional crystallization, Hf will increase in the melt relative to Zr (Wooden *et al*., 2006). The Hf versus T plot (Fig. 2c) suggests that there is a correlation between increasing Hf and decreasing T. The zircon spots from sample AJW-03-178 (Southwest Oyu) do not fit this trend as they have both low minimum T as well as low Hf.

Cores tend to be high-T and low Hf compared to their corresponding rim analyses (Fig. 3). However, there are some exceptions where low-T, high Hf cores are surrounded by high-T, low Hf growth zones as well as grain traverses where T and Hf behave discordantly.

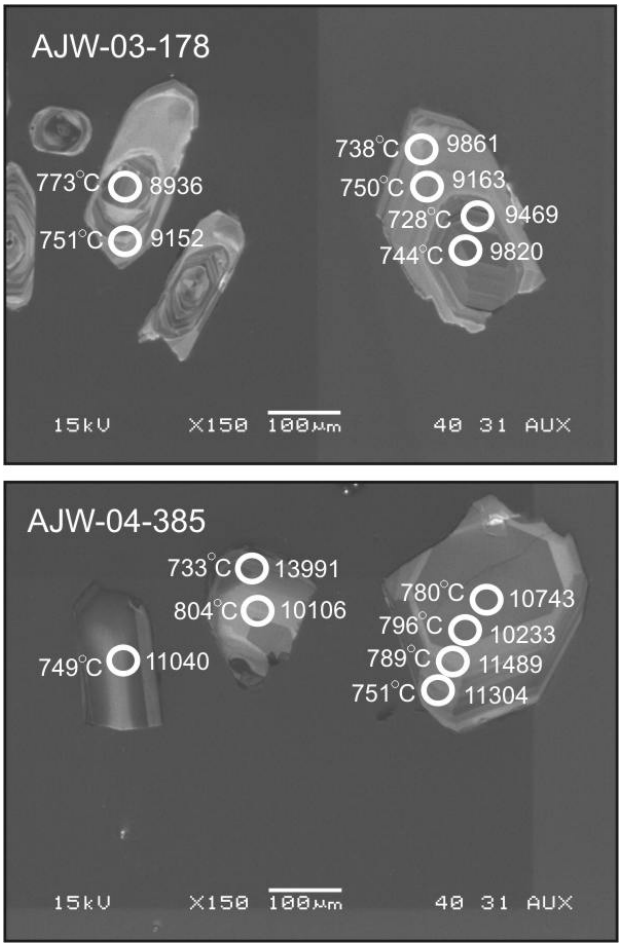


Figure 3. Cathode-luminescence images of zircons (Samples AJW-03-178 and AJW-04-385) with minimum temperatures (left) and hafnium concentration in ppm (right).

## 4 DISCUSSION

Data from three samples (AJW-03-181, AJW-04-385 and AJW-04-356) lie on similar fractionation trends (Fig.2) suggesting that they may be derived from the same parent magma. Conversely, zircons from AJW-03-178 (Southwest Oyu) and some zircons from AJW-03-182 (South Oyu) yield different trace element data suggesting that the grains were derived from a fundamentally unique source or that the melts were mixed with material that did not influence the other group. These are the southernmost samples, so there appears to be a geographic correlation with the zircon chemistry as well. Data from sample AJW-03-182 may be transitional between that of AJW-03-178 and the other set which suggests the possibility that mixing occurred between two end-members.

The presence of zircons with different Yb/Gd ratios and Y concentrations that were derived from a single rock sample provides evidence for source heterogeneity, mixing of material from multiple sources or mixing of discrete melts that experienced distinctive fractionation histories. Furthermore, core-to-rim pairs suggest that early, high-T, unfractionated melt environments evolved toward low-T, fractionated environments.

Ongoing research will address linkages between OTIC zircon geochemistry and U-Pb age, wholerock geochemistry as well as metal tenor of the porphyries.

## 5 CONCLUSIONS

Zircon geochemistry suggests that the OTIC intrusions are derived from a multi-component, fractionating, cooling magmatic system.

## ACKNOWLEDGEMENTS

Thanks to Ivanhoe Mines and SEG.

## REFERENCES

Candela, P.A. 1992. Controls on ore metal ratios in granite-related ore systems; an experimental and computational approach. *Special Paper – Geological Society of America* Vol. 272: 317-326.

Claiborne, L.L., Miller, C.F., Walker, B.A., Wooden, J.L., Mazdab, F.K. & Bea, F. 2006. Tracking magmatic processes through Zr/Hf ratios in rocks and Hf and Ti zoning in zircons: An example from the Spirit Mountain batholith, Nevada. *Mineralogical Magazine* Vol. 70 (No. 5): 517–543.

Hattori, K.H. & Keith, J.D. 2001. Contribution of mafic melt to porphyry copper mineralization: evidence from Mount Pinatubo, Philippines, and Bingham Canyon, Utah, USA. *Mineralium Deposita* Vol. 36: 799-806.

Mazdab, F.K. & Wooden, J.L. 2006. Trace element analysis in zircon by ion microprobe (SHRIMP-RG): technique and applications. *Geochimica et*

*Cosmochimica Acta Supplement*, Vol. 70 (No. 18): 405.

Wainwright, A.J., Tosdal, R.M., Forster, C., Kavalieris I., Crane D. & Kirwin D. 2005. Stratigraphic and U-Pb constraints on the Oyu Tolgoi porphyry Cu-Au deposits, Mongolia. *Geological Society of Nevada Conference, 15–18th May, 2005, Reno, Nevada*. Poster.

Watson E.B. & Harrison T.M. 2005. Zircon thermometer reveals minimum melting conditions on earliest Earth. *Science* Vol. 308: 841-844.

Wooden J.L., Mazdab F.K., Barth A.P., Miller C.F. & Lowery L.E. 2006. Temperature (Ti) and compositional characteristics of zircon: Early observations using High Mass Resolution on the USGS Stanford SHRIMP-RG. *Geochimica et Cosmochimica Acta Supplement* Vol. 70 (No. 18): 707.

# Fluid saturation in the Habo South porphyry Cu-Au (Mo) system, Southern China: application of petrology to mineral exploration

Anthony C. Harris, Noel C. White & David R. Cooke
*ARC Centre of Excellence in Ore Deposits, University of Tasmania, Hobart, Tasmania, 7001, Australia*

Charlotte Allen & Ian H. Campbell
*Research School of Earth Sciences, Australian National University, Canberra, 2006, Australia*

ABSTRACT: The Habo South porphyry Cu-Au-(Mo) deposit, China, occurs in a series of granitic intrusions that have been overprinted by extensive K-feldspar-biotite alteration. Veins of quartz, quartz-magnetite, quartz-biotite, and sulphides occur widely. Several igneous phases have been affected by the mineralization, and host rock textures indicate that all phases were saturated with volatiles. A formation age of 36-34 Ma has been obtained by ELA-ICPMS on zircons from the deposit. This suggests a trend to younger ages of porphyries along the Red River Fault Zone. Average $Ce^{4+}/Ce^{3+}$ ratios of 240 (with some to >1000) imply highly oxidized and evolved magmas, consistent with intrusions related to porphyry systems elsewhere along the Red River Fault Zone.

KEYWORDS: porphyry, copper, magmatic-hydrothermal, zircon, Red River Fault Zone, Habo South, China

## 1 INTRODUCTION

The geological setting in which porphyry ore deposits reside influences the composition of the associated magma, the character of the resultant hydrothermal alteration and their metal endowment (Sillitoe 1997). Porphyry Cu-Mo and Cu-Au-(Mo) systems in Tibet and Yunnan are localized along a crustal scale deformation zone in a convergent intracontinental setting. Such environments are not typical of classical porphyry Cu deposits (*see* Cooke *et al.* 2005).

The salient geological features of a new porphyry deposit discovered in Yunnan Province, southern China, are documented here. We have combined basic petrographic observations with advanced microanalysis to highlight the prospectivity of the Habo system. Just as soil and rockchip geochemistry are part of everyday exploration activities, heavy mineral trace element chemistry (from drainage samples) may be useful in the prioritization of porphyry prospects.

Rather than discriminating regions of metal anomalism, zircon microanalysis (including the determination of $Ce^{4+}/Ce^{3+}$ ratios) may assist explorers in identifying productive intrusive suites (*e.g.*, Liang *et al*. 2006).

## 2 GEOLOGIC SETTING

The Habo South porphyry Cu-Au-(Mo) deposit (White *et al*., this volume) is hosted by a large (up to 10 km across) granitoid body that intruded late Palaeozoic metasedimentary rocks. The Tertiary granitoids were emplaced in a crustal scale deformation zone, referred to as the Red River-Ailao Shan Fault Zone, which extends over 1000km between eastern Tibet and the Tonkin Gulf in Vietnam, crossing Yunnan Province (Fig. 1A). The Red River Fault Zone represents the northwest-striking boundary between the Indochina and South China terranes. Suturing of these terranes occurred after the late Triassic and as a result of the Indo-Asian collision (Leloup *et al.*, 1995).

## 3 DEPOSIT GEOLOGY

At Habo, the bulk of the Cu-Fe- and Fe-sulphides occur in pervasive and fracture-controlled potassic (quartz ± magnetite-biotite-K-feldspar) alteration assemblages that have overprinted several porphyritic granitic intrusions. These intrusions form large (km-scale) stocks, cut by narrow (10s of meters wide) dykes (Fig. 1B). Individual porphyritic dykes

are up to several hundred metres long. Typically, medium to coarse-grained (up to 20mm) K-feldspar, quartz and plagioclase phenocrysts characterize the rocks, with lesser amounts of biotite and hornblende. Pyroxene is rare. Different porphyry phases are subdivided on the type, size and abundance of phenocrysts. For example, some porphyritic granite (and syenogranite) phases contain large pink K-feldspar and distinct quartz eyes, or they may be mafic mineral-bearing. Other intrusions include unmineralised (but weakly biotite-K-feldspar altered) lamprophyre dykes.

### 3.1 *Intrusion geology*

Biotite-quartz and K-feldspar alteration assemblages obscure the primary igneous textures and mineralogy of most granitic phases. Quartz (± biotite) veins are best developed where they have overprinted quartz-eye K-feldspar-phyric porphyries (up to 20-30 volume percent crystals). Our study has subdivided three quartz-eye K-feldspar-phyric phases, including one that is pyroxene-bearing. In this latter variety, secondary biotite and K-feldspar alteration assemblage are poorly developed.

In most porphyries, K-feldspar (typically 1-3 mm; <40 %) occurs as twinned euhedral phenocrysts. Coarse-grained (up to 12mm) 'megacrysts' of K-feldspar (rarely perthitic) are abundant; these crystals poikilitically enclose plagioclase, quartz, K-feldspar and biotite crystals. Quartz eyes (1-4 mm) are common and are either round or irregularly shaped (embayed). Phenocrysts of plagioclase (<5 mm; <25%) are found as subhedral and euhedral twinned clusters. Isolated euhedral oscillatory-zoned plagioclase (<5%) also occurs. Biotite phenocrysts (1-3mm; <3%) form euhedral laths. Hornblende is rare, or, more commonly, absent. Where seen, pyroxene occurs as isolated euhedral crystals. Accessory minerals include apatite, zircon and magnetite. The groundmass is cryptocrystalline to very fine-grained (<0.2mm), and comprises quartz and feldspar.

The wallrocks to the Habo intrusions consist of equigranular granite, with medium-grained (2-5mm, up to 10mm) K-feldspar and quartz with lesser plagioclase. Biotite and amphibole comprise less than 2 % of the leucogranite. K-feldspar crystals have poikilitically enclosed euhedral and zoned plagioclase. Resorption textures are evident in amphibole and plagioclase. The groundmass comprises fine-grained (<1 mm) intergrowths of anhedral quartz, K-feldspar and biotite. Xenoliths of metamorphic rocks are found throughout.

A variety of subtle primary igneous textures occur in the quartz-eye K-feldspar-phyric porphyries and the granite wallrock. Interconnected miarolitic cavities and miarolitic pods are associated with pegmatites and aplites. Miarolitic pods occur as small (<4mm) sugary elliptical aggregates of anhedral quartz crystals (making them distinctly different from homogenous quartz phenocrysts). Although they typically occur randomly distributed throughout the groundmass, the miarolitic pods also occur locally in linear quartz and biotite zones (up to 15mm long). Coarse-grained (cm-scale crystals) pegmatite veins cut both the porphyries and the granite host.

### 3.2 *Hydrothermal alteration*

The zone of intense hydrothermal alteration (and associated veins) at Habo is at least 750m across. Most disseminated sulphide mineralization occurs in the potassic (quartz, biotite and lesser K-feldspar) alteration zone. Biotite and K-feldspar occur as irregular fracture-controlled or pervasive alteration assemblages. Some of the earliest quartz veins are texturally similar to those described as A veins (Lowell & Guilbert, 1970). Typically, these veins are diffuse and consist of saccharoidal quartz. More classical quartz (± biotite) stockworks overprint these transitional veins and appear related to pervasive biotite alteration assemblages. Phyllic (quartz - muscovite ± pyrite) assemblages have overprinted parts of the potassic alteration assemblages and formed late in the deposit's development. Rare selective propylitic (chlorite-illite-epidote-calcite) alteration also occurs.

## 4 ZIRCON MICROANALYSIS

We have undertaken a reconnaissance microanalytical survey of zircons from the Habo district. Heavy mineral separates from a single drainage sample panned from a small stream draining the Habo South deposit (including multiphase altered porphyries) were analyzed following a procedure described in Harris *et al.* (2004a). U–Th–Pb isotopic and trace element compositions of zircons were analyzed at the Australian National University, Canberra, using Excimer laser ablation inductively coupled plasma mass spectrometry (ELA-ICPMS). Acquired data included the determination of $Ce^{4+}/Ce^{3+}$ ratios, which has been shown to be

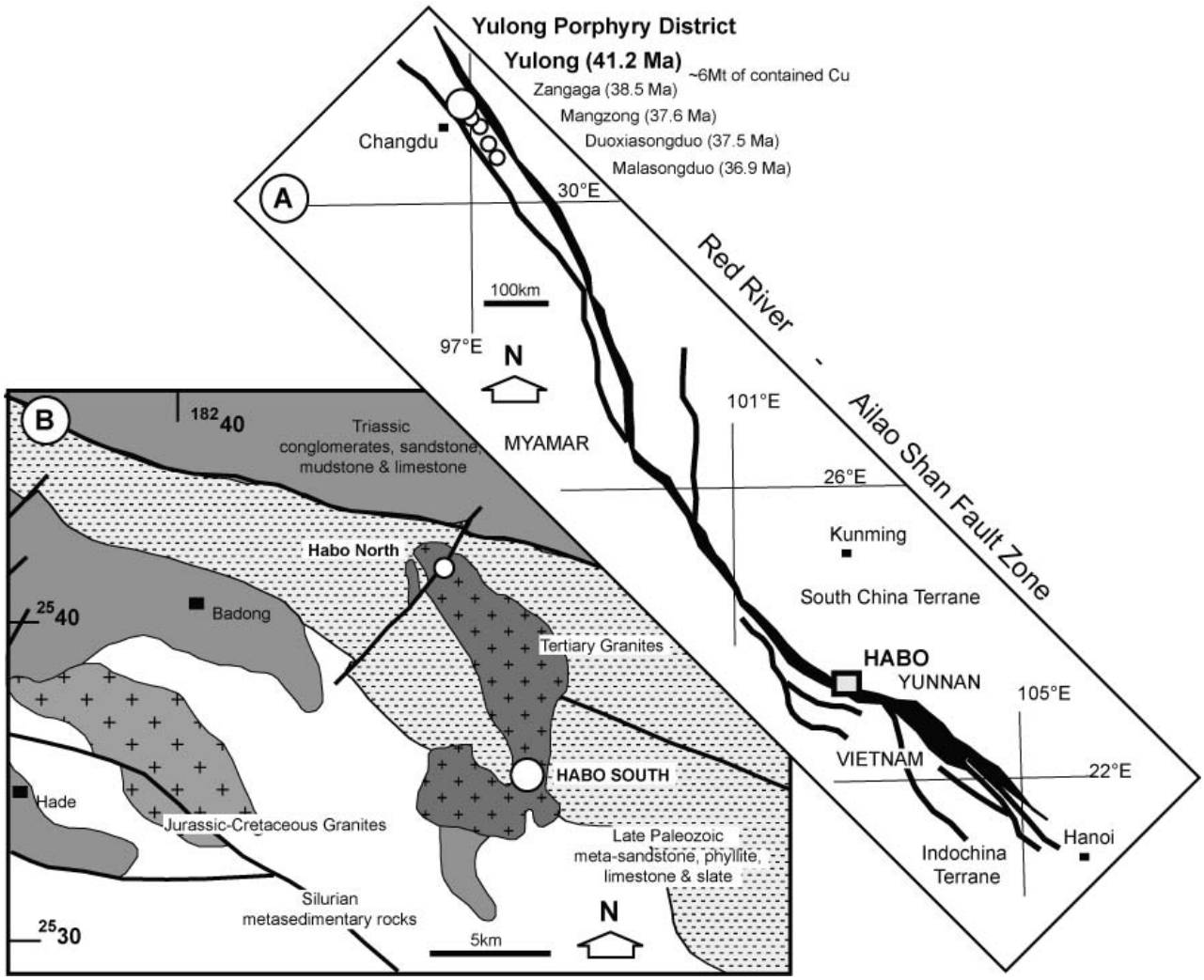


Figure 1.A. Schematic overview of the Red River-Ailao Shan Fault Zone (modified after Wang *et al*. 2000 and Liang *et al.* 2006). The Habo porphyry-related alteration centre lies several hundred kilometers to the southeast of the Yulong Tertiary porphyry ore deposit. B. Habo district geology; Tertiary granites have intruded the Red River Fault Zone.

important in the discrimination of productive and non-productive porphyries in other parts of the Red River Fault Zone (*e.g*., Liang *et al.* 2006).

The zircons form two morphologic populations: the first population consists of clear prismatic euhedral crystals up to 200 μm long; the second, less abundant population consists of clear stubby euhedral crystals that exhibit some resorption. The majority of these zircons yield ages between 36.7 and 34.2 Ma (with a mean of 35.3 Ma for 21 concordant analyses out of 28 zircons). A high MSWD implies that multiple zircon populations exist in this age range. A single zircon yielded a slightly older age of 42.8 Ma. This reconnaissance study also encountered an old (Grenville-age) crystalline basement zircon dated at 1.0 Ga.

Zircons with ages between 36.7 and 34.2 Ma have an average $Ce^{4+}/Ce^{3+}$ ratios of 240 (see Ballard *et al.* 2002). These values are comparable to those reported elsewhere (Liang *et al*. 2006), especially for those determined for economic porphyry ore deposits (*e.g.* Yulong). Some zircons have unusually high $Ce^{4+}/Ce^{3+}$ ratios (in excess of 1000); these same zircons have high concentrations of $HfO_2$ (>1.3 wt.%) and U (>1300ppm) and low P (<130 ppm) values and Th/U ratios (<0.45) compared to other analyzed zircons. When combined with calculated crystallization temperatures (based on the concentration of Ti in zircon; $a_{Ti} = 1$; Watson & Harrison 2005), it appears that these anomalous zircons are from lower temperature (~650°C) more fractionated and oxidized magmas. This result is consistent with the abundance of magnetite throughout the deposit. Other zircons with lower $Ce^{4+}/Ce^{3+}$ ratios have calculated crystallization temperatures of 660-770°C.

## 5 DISCUSSION AND CONCLUSION

Typically, porphyry Cu-Au-(Mo) deposits occur in subduction-related, continental-arc and island-arc settings (*e.g.* Cooke *et al.* 2005) and are less commonly reported in continental collision orogenic belts (*e.g*. Hou *et al.* 2003; Liang *et al*. 2006). Such environments, while known for granite-related Mo, W and Sn deposits, are not widely considered prospective for porphyry Cu deposits. Tertiary porphyry ore systems in Tibet and Yunnan (along the Red River Fault Zone) are exceptions, having formed in intracontinental convergent environments related to the Indo-Asian collision (Liang *et al*. 2006). Known resources can be as much as several million tons of contained metal (*e.g.*, the Yulong porphyry Cu-Mo deposit; Hou *et al*. 2003).

At Habo, a new porphyry-style Cu-Au-(Mo) system is still being explored (White et al., this volume). While the full extent of the system is still not known, exploration pits, trenches and adits are helping to define an alteration centre at least 2 $km^2$ in extent. Here sulphide-bearing hydrothermal alteration assemblages are developed in and around multiphase granitic and syenogranitic intrusions. U-Pb zircon geochronology shows that these intrusions cluster at 36–34 Ma. These ages match Rb-Sr model ages for the Habo intrusive complex (*i.e*. 37.3 Ma; Yunnan Geology, 2000, unpublished). Older U-Pb ages (41–37 Ma) have been determined for porphyry ore systems in eastern Tibet (Liang *et al*. 2006). Zhang & Schärer (1999, and references there in) determined slightly younger U-Pb crystallization ages for syntectonic leucogranitic veins in the Red River Fault Zone in Yunnan (33–22 Ma). Our results suggest that porphyry-related mineralization centres may young south-east along the Red River belt (over 600km), thus extending the findings of Liang *et al*. (2006). Microtextural evidence shows that fluid saturation was attained in most magma batches emplaced into the South Habo deposit. This is implicit in the abundance of 'slushy' textures, including interconnected miarolitic cavities and miarolitic pods (*see* Harris *et al.* 2004b). While these textures imply the presence of a considerable volume of magmatic volatiles, they do not imply metal fertility at economic levels. At Habo this is yet to be determined. Despite this, microanalytical work on zircons confirms that these wet and potentially ore-forming silicic magmas were oxidized (yielding extreme $Ce^{4+}/Ce^{3+}$ ratios; see Ballard *et al*. 2002) and more evolved (based on trace element compositions) compared to other apparently barren intrusions along the Indo-Asian collision zone.

## REFERENCES


Ballard JR, Palin JM, Campbell IH, (2002) Relative oxidation states of magmas inferred from Ce(IV)/Ce(III) in zircon: application to porphyry copper deposits of northern Chile: *Contribution to Mineralogy and Petrology* 144 pp 347-364

Cooke DR, Hollings P, Walshe JL, (2000) Giant porphyry deposits: characteristics, distribution and tectonic controls: *Economic Geology* 100 pp 802-818

Harris AC, Allen CA, Bryan SE, Campbell IH, Holcombe RJ, Palin MJ (2004a) Measuring the longevity of regional volcanism hosting the Bajo de la Alumbrera Cu-Au de-posit: Implications for the genesis of porphyry ore deposits: *Mineralium Deposita* 39 pp 46-67

Harris AC, Kamenetsky VS, White NC, Steele DA (2004b) Volatile phase separation in silicic magmas at Bajo de la Alumbrera porphyry Cu-Au deposit, NW Argentina: *Resource Geology* 54 pp 341-356

Hou ZQ, Ma HW, Zaw K, Zhang YQ, Wang MJ, Wang Z, Pan GT, Tang RL (2003) The Himalayan Yulong porphyry copper belt: product of large-scale strike–slip faulting in eastern Tibet. *Economic Geology* 98:125–145

Leloup PH, Lacassin R, Tapponnier P, Schärer U, Dalai Z, Xiaohan L, Liangshang Z, Shaocheng J, Trinh PT (1995) The Ailao Shan-Red River shear zone (Yunnan, China), Tertiary transform boundary of Indochina: *Tectonophysics* 251 pp 3-84

Liang H, Campbell IH, Allen C, Sun W, Liu C, Yu H, Xie Y, Zhang Y (2006) Zircon Ce4+/Ce3+ ratios and ages for Yulong ore-bearing porphyries in eastern Tibet: *Mineralium Deposita* 41 pp 152-159

Lowell JD, Guilbert JM (1970) Lateral and vertical alteration-mineralization zoning in porphyry ore deposits: *Economic Geology* 65 pp 373-408

Sillitoe RH (1997) Characteristics and controls of the largest porphyry copper-gold and epithermal gold deposits in the circum-Pacific region: *Australian Journal of Earth Sciences* 44: 373-388

Wang P, Lo C, Chung S, Lee T, Lan C, Thang T (2000) Onset timing of left-lateral movement along the Ailao Shan-Red River Shear Zone: $^{40}Ar/^{39}Ar$ dating constraint from the Nam Dinh Area, NE Vietnam: *Journal of Asian Earth Sciences* 18 281-292

Watson EB Harrison TM (2005) Zircon thermometer reveals minimum melting conditions on earliest Earth: *Science* 308 pp 841-844

White NC, Yang K Li W (this volume) Discovery of the Habo Porphyry Cu-Au-(Mo) System in Southern China: Its lessons for Exploration Everywhere. In: *Proceedings of the 9th Biennial SGA Meeting*

Zhang LS, Schärer U (1999) Age and origin of magmatism along the Cenozoic Red River shear belt, China: *Contributions to Mineralogy and Petrology* 134 pp 67-85

# Fe-rich magmatic volatiles in the Ridgeway Au-Cu porphyries: evidence from magnetite-quartz comb-layered textures

Anthony C. Harris, Ana Liza G. Cuison, Zhaoshan Chang, David R. Cooke & Natalee Bonnici
*ARC Centre of Excellence in Ore Deposits, University of Tasmania, Hobart, Tasmania, 7001, Australia*

Kevin Faure
*National Isotope Centre, GNS Science, Lower Hutt, New Zealand*

Cameron Cross
*Cadia Valley Operations, Newcrest Mining Limited, Orange, 2800, Australia*

ABSTRACT: Magnetite (± quartz) comb-layered textures occur in intrusions intimately associated with ore-bearing hydrothermal alteration assemblages at the Ridgeway alkalic porphyry Au-Cu deposit. These magnetite-rich textures imply that extremely Fe-rich magmatic volatiles accumulated within these silicic intrusions. Our micro-textural and micro-analytical study suggests that these Fe-rich magmatic volatiles transported and deposited ore-forming metals (including Cu, Zn, Mo, Pb, and Au). The occurrence of thickly stacked magnetite-quartz comb-layered textures implies that large volumes of these volatiles streamed through the Ridgeway intrusions. Their recognition highlights the specialized nature of the magma suite associated with the formation of an extremely high-grade Au porphyry deposit.

KEYWORDS: comb-layered textures, magnetite, porphyry, gold, alkalic, magmatic-hydrothermal

## 1 INTRODUCTION

Porphyry Cu-Au deposits owe their origins to fluids sourced via magma degassing and volatile exsolution from crystallisation of magmas intruded into the upper parts of the Earth's crust. Geochemical studies of districts hosting porphyry ore deposits reveal that repeated influx of hydrous magmas combined with continued open-system fractional crystallisation results in the episodic exsolution of magmatic volatiles. Physical models constraining this volatile exsolution are supported by textural features, including comb-layered textures (Carten *et al*. 1988; Kirkham & Sinclair 1988; Lowenstern & Sinclair, 1996). Such textures are typically quartz-rich (*e.g*., Wilson *et al.* 2003). We present new petrographic observations of magnetite-rich comb-layered textures found in the Ridgeway alkalic porphyry Au-Cu deposit, central New South Wales (Australia). Such features imply that exsolved fluids spanning the magmatic-hydrothermal transition can be unusually Fe rich.

## 2 DEPOSIT GEOLOGY

Ridgeway is a high-grade, Au-rich alkalic-type porphyry ore deposit (77 Mt averaging 1.87 g/t Au and 0.63 % Cu) hosted by late Ordovician volcano-sedimentary rocks of the Forest Reefs Volcanics. Wilson *et al*. (2003) have described the deposit geology and paragenesis of Ridgeway in detail. Metal-rich veins (comprising quartz-bornite-chalcopyrite-magnetite-calcite) are centered on narrow (<50 m) multiphase pipe-like alkaline monzonite and monzodiorite intrusions. Typically, medium to coarse-grained (up to 20mm) plagioclase phenocrysts characterize the rocks, with lesser amounts of orthoclase and clinopyroxene, minor hornblende, biotite and magnetite. The groundmass is quartzo-feldspathic (± magnetite), with orthoclase being the dominant feldspar. Accessory minerals include apatite, zircon and titanite. Different porphyry phases have been subdivided on the basis of crosscutting intrusion, vein, and alteration relationships (Wilson *et al*. 2003). Other criteria used, included the presence or absence of quartz vein xenoliths and characteristic vein stages.

At Ridgeway, hydrothermal alteration is broadly zoned from an inner calc-potassic (actinolite-biotite-orthoclase) and potassic (orthoclase-biotite-quartz) core, outwards through propylitic (chlorite-haematite-magnetite-epidote-albite-pyrite ± calcite) and sodic (albite-pyrite) assemblages. Sulphide minerals are

similarly zoned from a bornite > chalcopyrite (plus gold) core, outwards and upwards through a chalcopyrite-rich to an outer pyrite-rich domain. Chalcopyrite ± pyrite zones also occur in the deepest parts of the system, and are spatially related to the monzonites.

Fluid inclusion studies show that high temperature (up to 500°C) and saline (over 30 wt.% NaCl equivalent) fluids caused the bulk of the alteration (Wilson *et al*. 2003). An extreme pressure of entrapment is implicit in the non-boiling salt-rich inclusions that homogenize by halite-dissolution. Wilson *et al*. (2003) concluded that the fluids were directly sourced from volatile exsolution from a silicic melt crystallizing under relatively high pressure conditions.

## 3 COMB-LAYERED TEXTURE

Quartz comb-layered textures and related features such as vein-dykes, have been reported at Ridgeway (Wilson, 2002; Lickfold *et al*. 2003; Wilson *et al.* 2003; Wilson *et al*. 2004). These textures occur in most of the monzonites, and are best preserved in the late-stage least-altered phases. Comb-quartz layers are planar or crenulate and range from 1 to 300mm thick. Apical terminations of the quartz crystals are typically oriented perpendicular to the intrusion contact. Crystal morphology is consistent with low-temperature α-quartz. This quartz is intergrown with magnetite, chalcopyrite and lesser pyrite. Aphanitic to porphyritic igneous rock separates the coarse-grained prismatic quartz layers.

We have recently discovered that magnetite (± quartz) comb-layered textures also occur in the Ridgeway monzonites. These textures define alternating bands of magnetite (± quartz) and igneous material. The magnetite forms asymmetric crenulate bands; distinctly apical terminated crystals oppose an irregular base (Fig. 1A and B). Like other comb-quartz layered textures (reported elsewhere), the occurrence of prismatic α-quartz with magnetite, implies crystal-growth at temperatures below 600°C (at 100 MPa).

The inter-layer igneous material comprises aplite and coarser-grained porphyry. The aplite is characterized by myrmekitic intergrowths of K- and Na-feldspar plus quartz that occur as overgrowths to the coarse prismatic magnetite and quartz. Macroscopically, these granophyric bands are narrow, less than a few millimeters across. Such intergrowths are common in high level silicic intrusions, implying that the bulk composition was close to the minimum melting conditions in the orthoclase-albite-quartz-$H_2O$ system.

The quartz- and magnetite-rich comb-layered textures occur as flat-lying zones that extend laterally for 30m within in the apical regions of the porphyries (Lickfold *et al*. 2003; Wilson *et al.* 2003). They also occur as pipe-like features with a vertical extent of approximately 150m. Single comb-layered textured zones are up to 3m thick. The thickness of single bands, combined with the high aspect ratio of crystals (2-3 to 1), implies magmatic volatiles accumulated within the monzonites during their emplacement.

Chalcopyrite and pyrite occur with the magnetite comb-layered textures, either as coarse-grained (up to 3cm) zoned euhedral crystals or as disseminations throughout the aplitic groundmass. Cu-Fe sulphides occur with Ag-rich tellurides in quartz-chlorite-apatite ± rutile veinlets (micron-scale) cutting these textures.

### 3.1 *Isotope geochemistry*

We have analysed oxygen isotopic compositions of co-existing magnetite and quartz to constrain the temperature of formation of magnetite-rich comb-layered textures, because there are no workable fluid inclusions. Using $CO_2$ laser/$BrF_5$ extraction, we measured the $\delta^{18}O$ values of coexisting magnetite-quartz for two contrasting examples of comb-layered textures; *i.e.*, one more magnetite-rich than the other. The magnetite-rich example returned quartz-magnetite $\delta^{18}O$ values of 10.4 and 3.3 per mil, respectively. Similar values were determined for the more quartz-rich comb-layered texture (10.8 and 3.0 ‰, respectively). Using these quartz-magnetite $\delta^{18}O$ pairs and the fractionation factor of Zheng (1999), the calculated equilibration temperatures suggested that the magnetite-rich comb-layered textures were slightly hotter (600°C) compared to quartz-rich comb-layered texture (560°C).

### 3.2 *Microanalysis*

Scanning electron microscopic imaging of magnetite comb-layered textures have revealed internal complexities in otherwise homogenous magnetite. The leading edge of the apical termination of the magnetite crystals consists of a narrow (0.2 mm) zone of finer-grained magnetite that is brecciated with a jig-saw fit texture

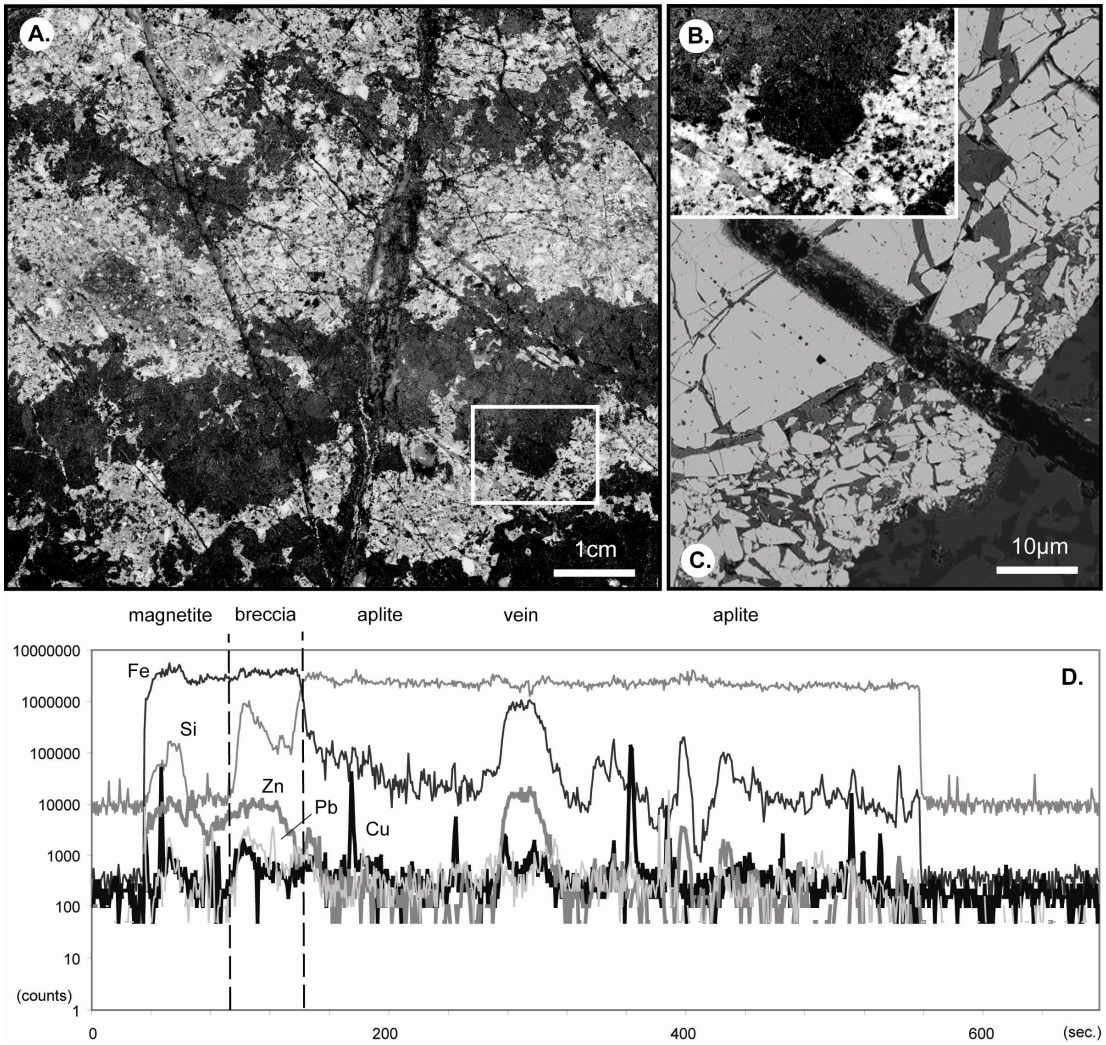


Figure 1 Magnetite comb-layered textures. A. Crenulate bands of comb-layered magnetite. B. Asymmetric character of euhedral magnetite crystals. C. SEM image of magnetite comb-layered texture showing brecciated magnetite. D. LA-ICP-MS line scan across magnetite-aplite texture showing subtle variations of Cu, Pb and Zn in the brecciated magnetite zone and throughout the aplite.

(Fig. 1C). Igneous material (comprising myrmekitic feldspar-quartz intergrowths) forms the breccia cement. Chalcopyrite and pyrite are also common as breccia infill. These breccia zones are absent from along the margins of quartz-rich band in comb-layered textures.

Laser-ablation ICP-MS line scans show that anomalous counts in trace elements, including those important to ore-formation, along the leading edge of the magnetite (*e.g.*, Cu, Zn, Mo, Pb, Sn, W ± Au and Ag). It appears that these elements are enriched in the brecciated margins to the magnetite bands and in the myrmekitic zones immediately adjacent to the prismatic magnetite and quartz in the comb-layered textures (Fig. 1D). Microscopic imaging has found euhedral chalcopyrite along aplitic band adjacent to these textures.

## 4 DISCUSSION AND CONCLUSIONS

Degassing and volatile exsolution from a crystallizing magma system supplies the fluid and metal needed for the formation of porphyry ore deposits. The abundance of miarolitic cavities and comb-layered textures indicate that fluid saturation was attained in most magma batches that once intruded Ridgeway. Comb-layered textures crystallize from pockets of volatiles that exsolve and accumulated inside the convecting and crystallizing magma batches (*e.g.*, Lowenstern & Sinclair 1996). Other studies show that these textures record the episodic accumulation and release of magmatic volatiles from a magma (Harris *et al*. 2005). Formation of quartz-rich comb-layered textures requires that the volatile phase is silica-rich and quartz-saturated (Carten *et al*. 1988). By contrast, the

bands of asymmetric magnetite (± prismatic quartz) crystals found in comb-layered textures at Ridgeway, implies that unusually Fe-rich volatiles are also exsolved directly from a silicic magma.

At Ridgeway, it appears that perhaps hotter conditions (up to 50°C) of formation existed for magnetite-rich compared to quartz comb-layered textures (calculated from limited $\delta^{18}O$ values). The presence of α-quartz implies that crystal-growth in the fluid pockets occurred close to 600°C at depths between 2 and 4km. Increasing fluid pressures caused fracturing of the carapace and crystal growth ceased. Rapid under-cooling and devolatilisation of the adjacent magma then occurred, causing aplite deposition.

There is microscopic textural evidence for catastrophic release of volatiles from the Fe-rich fluid pockets in the Ridgeway monzonites. Graphic overgrowths of the prismatic magnetite and quartz crystals imply pressure quenching associated with fluid expulsion. The explosive release of these fluids caused *in situ* brittle fragmentation of the magnetite rims, but not the more ductile quartz crystals. Melt that infiltrated the breccia crystallized rapidly, forming granophyric textures. Metals (including Cu, Zn, Mo, Pb, and Au) were deposited outboard of the aplite during decompression and/or adiabatic cooling of the magmatic volatile phase. Metal deposition occurred at near-magmatic temperatures (over 550°C). Residual fluid phases cause subsequent low-temperature hydrothermal alteration.

## ACKNOWLEDGEMENTS

This work has been made possible through the financial and logistical support of Newcrest Mining Limited and CODES. In particular we thank John Holliday, Geoffrey Smart, Geoffrey Merrel, Dean Collett, Colin McMillian and Ross Large. Newcrest is thanked for providing permission to publish these research results. CODES is the Australian Research Council's Centre For Excellence in Ore Deposits.

## REFERENCES

Carten RB, Ceraghty EP Walker BM (1988) Cyclic development of ignoues features and their relationship to high-temperature hydrothermal features in the Henderson porphyry molybdenum dpoeist, Colorado. *Economic Geology* 83, pp. 266-296

Harris AC, Kamenetsky VS, White NC, Steele DA (2004) Volatile phase separation in silicic magmas at Bajo de la Alumbrera porphyry Cu-Au deposit, NW Argentina. *Resource Geology* 54 pp 341-356

Harris AC, Cooke DR, White NC, Dunlap WJ, Allen CM, Campbell I, Reiners PW (2005) Timing of volatile and magma ascent in the formation of the Bajo de la Alumbrera porphyry Cu-Au deposit. In: *Proceedings of the 8th Biennial SGA Meeting.* Springer Heidelberg New York, pp 393-396

Holliday JR, Wilson AJ, Blevin PL, Tedder IJ, Dunham PD, Pfitzner M (2002) Porphyry gold-copper mineralisation in the Cadia district, eastern Lachlan Fold Belt, New South Wales, and its relationship to shoshonitic magmatism. *Mineralium Deposita* 37, pp 100-116.

Kirkham RV, Sinclair WD (1988) Comb quartz layers in felsic intrusions and their relationship to porphyry deposits. In: Taylor RP, Strong DF (eds) Recent advances in the geology of granite-related mineral deposits. *Canadian Institute of Mining and Metallurgy Special Volume* 39, pp 50-71

Lickfold V, Wilson AJ, Harris AC, Cooke DR (2003) The alkalic Au-Cu porphyry deposits of NSW, Australia: Evidence for coexisting melt and hydrothermal fluids in comb quartz layers. In: *Proceedings of the 7th Biennial SGA Meeting*. Millpress Rotterdam, pp 315-318

Lowenstern JB, Sinclair WD (1996) Exsolved magmatic fluid and its role in the formation of comb-layered quartz at the Cretaceous Logtung W-Mo deposit, Yukon Territory, Canada: *Transactions of the Royal Society of Edinburgh: Earth Sciences*, 87 pp 291-303

Zheng YF (1999) On calculations of oxygen isotope fractionation in minerals: *Episodes,* 22 pp 99-106

Wilson AJ (2003) The geology, genesis and exploration context of the Cadia gold-copper porphyry deposits, New South Wales, Australia. *Ph.D. thesis, University of Tasmania, Hobart*, p 335

Wilson AJ, Cooke DR, Harper BL (2003) The Ridgeway gold-copper deposit: a high-grade alkalic porphyry deposit in the Lachlan Fold Belt, NSW, Australia. *Economic Geology* 98 pp 1637-1656

Wilson AJ, Cooke DR, Richards T (2004) Veins, pegmatites and breccias: examples from the alkalic Cadia Quarry Au–Cu porphyry deposit, NSW, Australia. In: *CODES special publication* no. 5. University of Tasmania, Hobart, pp 45-56

Shannon JR, Walker BM, Carten RB, Geraghty EP (1982) Unidirectional solidification textures and their significance in determining relative ages of intrusion at the Henderson mine, Colorado. *Geology* 10 pp 293-297

# A regional comparison of gold-bearing hydrothermal breccia pipes, north Queensland, Australia

J.L.Graham, T. Baker & T.G. Blenkinsop
*EGRU, School of Earth and Environmental Sciences, James Cook University, Townsville, Qld 4811, Australia*

ABSTRACT: Carboniferous to Permian aged intrusion-related gold systems have historically produced about 7.5Moz within the Kennedy Igneous Province in north Queensland. Gold deposits that are associated with breccia pipes include Kidston, Mt Leyshon, Mt Wright and Empire Stockworks. The formation of these deposits involved emplacement of porphyritic intrusions which caused structurally controlled brecciation, ponding of mineralized fluids beneath earlier granites, and a transition to sheeted vein and dyke emplacement under the influence of regional strain. The orientation of extensional sheeted veins, dykes and the reactivation of NE and NW orientated structures during breccia pipe emplacement and gold mineralization infers the prevailing compression or transpression direction was N-S to NW-SE.

KEYWORDS: Intrusion-related gold, Kennedy Igneous Province, hydrothermal breccia pipes

## 1 INTRODUCTION

Major Carboniferous to Permian age gold deposits in north Queensland, Australia, are associated with hydrothermal breccia pipes (Beams, 1998). The gold deposits share characteristics with intrusion-related gold (IRGS) class of deposit because (1) they display a strong gold-bismuth trace-element correlation; (2) they have a temporal and spatial relationship with weakly to moderately oxidized, rhyolitic to andesitic intrusions of the Kennedy Igneous Province (KIP); (3) occur in fractionated magmatic belts associated with ± Mo, W, and Sn (*cf*. Thompson *et al*., 1999), and (4) they are located inboard of the subduction trench and related to back-arc extension and strike-slip movement in a continental setting (Vos *et al*., 2006).

This paper summarizes previous studies of gold-bearing breccias at Kidston (3.5Moz), Mt Leyshon (3Moz) and Mt Wright (1Moz) and presents new data collected from Empire stockworks (0.2Moz). The aim of this study is to highlight the similarities between these deposits, which strengthens their magmatic association and allows connections to be made between ore genesis and regional tectonics. Exploration criteria for this important class of deposits are highlighted by the comparison.

## 2 GOLD BRECCIA SYSTEMS OF NORTH QUEENSLAND

### 2.1 *Kidston*

The Kidston breccia pipe formed at ~332 Ma (Perkins & Kennedy, 1998). The pipe is located at the intersection of NW and N-NE faults, and at the NW-SE striking, steeply dipping contact between the Devonian-Silurian aged Oak River Granodiorite and the mid-Proterozoic Eiansleigh Metamorphics (Figure 2A, Baker & Andrew, 1991). It lies above a gravity low between the Newcastle Range Volcanics and the Lochaber ring complex to the south inferring the presence of a source intrusion at depth (Baker & Andrew, 1991). The breccia pipe is thought to have been emplaced at about 3.5km (Baker & Andrew, 1991). Brecciation was related to the release of volatiles from a fractionating magma and synchronous emplacement of dacite to rhyolite intrusions and post-ore andesite dykes (Baker & Andrew, 1991).

Rowe (1997) suggested breccia development, internal dyking and sheeted vein formation occurred during NW-SE regional compression in conjunction with vertical extensional emplacement of flat veins in the basal units of the pipe, resulting from collapse of the magmatic-hydrothermal system.

Early, deep, pre-breccia Mo mineralization occurs in uneconomic stockworks identified in breccia clasts which is post dated by breccia gold mineralization located in cavity fill with sulphide-carbonate alteration and late stage quartz veins. The quartz veins post date the rhyolite dykes and are sub-parallel to the pipe walls (Mustard, 1986). The trace element geochemistry of the ore comprises variably zoned Ag-As-Sb-Cu-Pb-Zn-Bi (Davis, 1998).

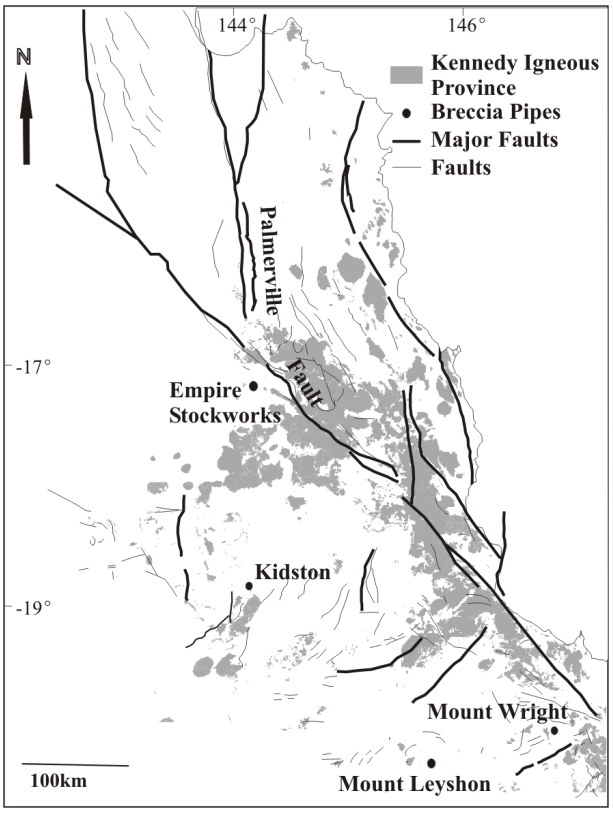


Figure 1: Map of the Kennedy Igneous Province and location of four breccia pipe hosted gold deposits. NE- and NW-trending structures were important for intrusion and breccia pipe emplacement (after Bain & Draper, 1997).

## 2.2 *Mount Leyshon*

The main breccia pipe at Mount Leyshon is located at the intersection of the NE-trending Mount Leyshon-Tuckers corridor, NW-trending lineaments, and at the contact between the Mid-Ordovician Fenian Granite and the Cambrian Puddler Creek Formation (Figure 2B Wormald *et al*, 1993). The main breccia pipe has been re-brecciated by the mineralized Mount Leyshon breccia, which formed ~ 292 – 281 Ma (Allan, 2006 *and references therein*). Breccia emplacement is interpreted to have been controlled by N-S regional compression which resulted in strike slip movement on NW and NE orientated structures (Allan, 2006).

The Mt Leyshon breccia is a clast supported, angular to sub-angular polymict breccia with clasts of the previous breccias and rhyolite intrusions. It was emplaced at depths between 1.5 and 3.4km (Allan, 2006). An intrusive sequence from early rhyolite to dacite to syn-gold andesitic tuffisite dykes suggests reverse fractionation. Early Mo mineralization pre-dates gold and forms on the margins of the quartz porphyry (Allan, 2006). Gold mineralization is associated with quartz-K-feldspar-carbonate-sulphide cavities and with breccia cement (Allan, 2006) rather than in sheeted veins. Gold has a strong correlation with Bi and is characterized by Zn-Cu-Pb-Mo-Bi-Au-Ag±Sb-As-Te signature (Allan, 2006).

## 2.3 *Mount Wright*

The Mt Wright breccia pipe formed at 303.9 ± 3.8 Ma (U-Pb zircon age on syn-ore rhyolite; Furniss, 1998) and intruded the contact between the Ordovician Millaroo Granite and Glenell Granodiorite (Davies, 1998). The complex is hosted in a NW-trending structural corridor (Furniss, 1998 and references therein). The pipe is about 80m by 200m wide and at least ~1.1km deep (Figure 2C). A strong structural control is inferred from the dominant NE-trending dykes close to Mt Wright and the NW-trending bounding faults to the breccia complex (Furniss, 1998). The breccia pipe was emplaced at depths of <2 km based on breccia textures (Furniss, 1998).

Breccia textures range from matrix supported milled clasts with abundant rock flour and lithic fragments to clast supported breccias with angular fragments, less fine-grained matrix and some open space (Furniss, 1998). Quartz-feldspar porphyritic rhyolite dykes and breccias contain clasts of earlier rhyolite and granite and at least three phases of flow banded rhyolite intrusions are recognized (Furniss, 1998). No magmatic-hydrothermal transition textures were observed in the rhyolite dykes.

Cross cutting mineralized veins are located at depth in the clast dominated rhyolite breccias. Mineralization occurs in sericite-altered feldspar phenocrysts, breccia matrix and open space voids. The ore-bearing alteration comprises sericite, quartz, siderite and muscovite (Furniss, 1998). Distal alteration includes chlorite, epidote, sericite and quartz. Feldspar has been sericitised, chloritised or replaced by sulphide and carbonate (Furniss, 1998). The trace

element assemblage includes Au-Ag-As-Bi-Cu-Zn (Harvey, 1998).

### 2.4 *Empire Stockworks*

Empire Stockworks is a series of parallel N-trending sheeted gold veins hosted on the eastern contact of the Empire Breccia Pipe (EBP; 500m diameter, Figure 2D). The Pinnacles Breccia Pipe is a younger pipe to the east which contains sub-economic mineralization. Regionally small breccia pipes or fault controlled elongate bodies are located within NW- and NE-trending structures.

The gold mineralization is hosted in a rhyolite porphyry dyke (likely to be *ca* 320-310 Ma; *cf*. Perkins & Kennedy, 1998)**.** The EBP is hosted in the Silurian Nundah Granodiorite near the moderately SE- dipping, NE-striking contact with the Dargalong Metamorphics. The EBP contains polymictic clasts of local host rock assemblages which are sub-angular and spherical to tabular in shape. Intrusion of dacite, rhyodacite and rhyolite stocks are common in the pipe. Late rhyolite intrusive dykes pre-date the mineralization and andesite dykes post date all phases at Empire Stockworks.

Low grade (<1 g/t Au), sheeted veins with gold mineralization are rarely located in the breccia pipe and cavity or replacement style mineralization is absent. Higher grade (~2 – 3 g/t Au), gold mineralization is associated with steeply dipping sheeted veins that are N-trending.

Late fine comb textured veins and the presence of porphyritic intrusives infer a shallow emplacement level for the mineralization. These veins comprise equigranular, quartz-albite with median sutures comprising carbonate – arsenopyrite – chalcopyrite -pyrite and minor bornite. Alteration associated with gold mineralization comprises sericite-albite-carbonate vein selvedges and pervasive replacement of feldspar in the Nundah Granodiorite. Early Cu-As-Pb-Zn phases are associated with the EBP and late sheeted vein mineralization at Empire Stockworks contains Au-Ag-Bi-Cu-Mo-Sb-W.

Very little trace-element data is available in the resource region and consequently zonation has not been identified. Shallow or distal comb textured stibnite veins and base metal occurrences are common in the region.

## 3 KEY CONTROLS ON BRECCIA FORMATION

The major KIP intrusions and related regional dyke swarms have a dominant NW-trend that appear in part to exploit structures like the Palmerville Fault (Figure 1). In addition NE-trending belts of KIP intrusions can be recognized at the regional to local scale. The major breccia bodies occur at the intersection of NW- and NE-trending structures, particularly in the older crustal elements to the west of the Palmerville fault (Figure 1). The major breccia pipes appear to form at the contacts of Ordovician to Silurian aged granites and metamorphic rocks that may have acted as a competency contrast. Furthermore, the older intrusions may also have operated as a cap to the breccia pipes, concentrating and pooling ore-bearing fluids and prevented venting and loss of metals and volatiles.

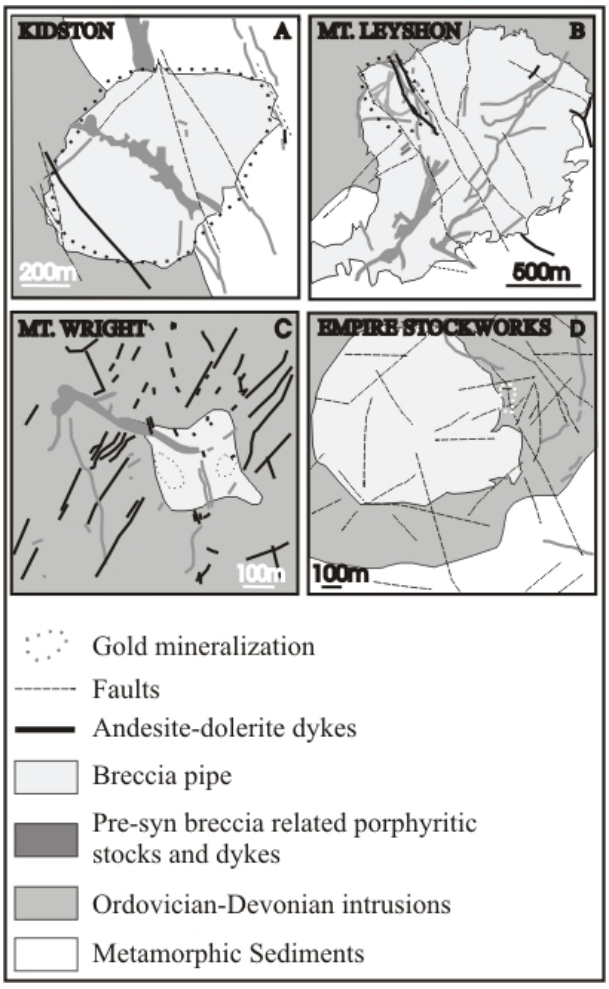


Figure 2: Common features of the hydrothermal breccia pipes A) Kidston B) Mount Leyshon, C) Mount Wright D) Empire Stockworks (after Rowe, 1997, Wormald *et al*., 1993 and Furniss, 1998).

These deposits have a strong gold-bismuth trace-element correlation, and temporal and spatial relationships with weak to moderately oxidized, rhyolite to andesite dykes. A genetic link between magmatism and mineralized fluids is evident from the presence of hydrothermal-magmatic transitional features such as brain rock textures in dykes and stocks, quartz-carbonate cavities in the breccia intimately associated with intrusion of dykes and the intrusion of the breccia pipe by flow banded felsites at the pipe rim.

The similarity in orientation of extensional sheeted veins, dykes and reactivation of the NE- and NW- orientated structures at the local to regional scale infers that the regional stress regime controls the breccia pipe emplacement, the late emplacement of dykes, and the mineralized sheeted veins. The prevailing stress regime is interpreted to be N-S to NW-SE directed compression or transpression.

## ACKNOWLEDGEMENT

This research and review of deposits was conducted as a part of a PhD project supported by an Australia Research Council Linkage Project partnered by TeckCominco Pty Ltd. Field support from local companies including Chillagoe Gold, Kagara Zinc is appreciated as is the time given by John Nethery, Alan Graham and John Skinner.

## REFERENCES

Allan, M.M., 2006. Hydrothermal processes in the Mt Leyshon intrusive complex, Australia: Microanalytical insights. *Unpublished PhD thesis, University of Leeds*, pp. 321.

Baker, E. M. and Andrew, A. S., 1991, *Geological, Fluid Inclusion, and stable isotope studies of the Gold-Bearing Breccia Pipe at Kidston, Queensland, Australia*, pp.810-830.

Bain, J.H.C., Draper, J.J. (eds), 1997, North Queensland Geology, *AGSO Bulletin* 24), pp.225-325.

Beams, S.W. (ed), 1998, *Contributions of the Economic Geology Research Unit* 52, pp.1-32.

Davis, G., 1998, The Geology and Geochemistry of Three North Queensland Breccia Prospects, *Unpublished Msc Thesis, James Cook University,* pp.41.

Furniss, R., 1998, Paragenesis and Petrology of the Mount Wright Intrusive Complex, Mineralization and associated alteration, *Unpublished Msc, James Cook University*, pp.176.

Harvey, K.J., 1998, Mount Wright gold deposit, In: Berkman, D.A. and MacKenzie, D.H. (eds), *Geology of Australian and Papua New Guinean Mineral Deposits,* The Australasian Institute of Mining and Metallurgy, pp. 675-678.

Mustard, H., 1986, Geology and Genesis of the Kidston Gold Deposit, Australia, In: *Proceedings of Gold '86 Symposium*, Toronto, pp. 405-415.

Perkins C. and Kennedy, A.K., 1998, Permo-Carboniferous gold epoch of northeast Queensland, *Australian Journal of Earth Sciences*, 45, 185-200.

Rowe, E.G., 1997, The structural controls and mineralogical zoning of the sheeted vein envelope within the Kidston breccia pipe, North Qld, *Unpublished Msc Thesis, James Cook University,* pp. 193.

Thompson, J.F.H, Sillitoe, R.H., Baker, T., Lang, J.R., Mortensen, J.K., 1999, Intrusion-related gold deposits associated with tungsten-tin provinces, *Min. Dep.*, 34, p323-334.

Vos, I.M.A., Bierlein, F.., Phillips, D., 2006, The Palaeozoic tectono-metallogenic evolution of the northern Tasman Fold Belt system, Australia: Interplay of subduction rollback and accretion, *Ore Geology Reviews, in press,* www.elsevier.com/locate/oregeorev.

Wormald, P.J., Orr, T.O.H. amd Hodkinson, I.P., 1993, The Mount Leyshon Gold Mine (NE Queensland), an intrusive breccia and igneous complex, Geological Society of Australia *Field Excursion Guidebook, Charters Towers,* pp. 223-231

# Infill paragenesis and hydrothermal alteration in the Northeast Zone of the Mt. Polley magmatic-hydrothermal breccia complex, British Columbia, Canada

Heidi E. Pass[1], David R. Cooke[1], Claire Chamberlain[2], Kirstie Simpson[3], Chris Rees[4], Lee Ferreira[4], Patrick McAndless[4] & Steve Roberston[4]

[1]*ARC Centre of Excellence in Ore Deposits, University of Tasmania, Private Bag 79, Hobart, 7001, Tas, Australia*

[2]*Mineral Deposit Research Unit, The University of British Columbia, Vancouver, BC, Canada*

[3]*Geological Survey of Canada, Vancouver, BC, Canada*

[4]*Imperial Metals Corporation, Vancouver, BC, Canada*

ABSTRACT: The late Triassic Mt. Polley breccia complex in British Columbia, Canada, contains four Cu-Au orebodies and several exploration targets associated with silica-undersaturated alkalic monzonite porphyries. Core logging of the Northeast ore zone (NEZ) has defined four mineralization and alteration events relative to breccia-formation: pre-, main-, late- and post-mineralization stages. Main stage alteration and mineralization assemblages are zoned laterally and vertically through the breccia body. Spatially restricted bornite-rich, pyrite-deficient cores are associated with high-grade ore (>1% Cu), and occur within broader chalcopyrite-rich zones. Alteration assemblages include potassic, calc-potassic, propylitic and sodic.

KEYWORDS: alkalic, hydrothermal breccia, porphyry, Mt. Polley, Canada, copper-gold

## 1 INTRODUCTION

Alkalic Cu-Au porphyry deposits (Lang *et al*., 1995) are of increasing economic significance (Cooke *et al*., in press; Deyell & Tosdal, 2005; Wilson *et al*., in press) however, the quality of individual deposit descriptions available for alkalic systems varies greatly and little effort has been made towards developing a coherent model. Alkalic porphyry deposits share some features with the well studied calc-alkalic style of deposits however, other aspects of their geology set them apart. In order to advance the understanding of alkalic system characteristics and integrate the information into a holistic model for alkalic porphyry deposits a collaborative research project between the University of Tasmania (CODES) in Australia, University of British Columbia (MDRU) in Canada and the Geological Survey of Canada, investigating shallow- and deep-level alkalic mineral deposits has been initiated.

The work presented herein is part of PhD research being conducted at the Mt. Polley alkalic porphyry Cu-Au system in British Columbia, Canada. This study aims to establish the paragenesis of hydrothermal breccia infill/veining and alteration of Mt. Polley through a combination of core logging, fieldwork and geochemical laboratory work. Results will contribute to the understanding of sources and composition of mineralizing fluids, principal ore forming processes, understanding genetic links between alkalic porphyry and epithermal environments and also to assist in vectoring towards ore within and around such systems.


Figure 1. Location of Mt. Polley Cu-Au porphyry deposit (★) in British Columbia, Canada

## 2 LOCATION

The Mt. Polley Cu-Au mine is located 650km northeast of Vancouver, British Columbia, Canada in the Quesnel terrane (Figure 1), one of two accreted island arc terranes in the province that host mineralized alkalic associated deposits of late Triassic age (Logan & Mihalynuk, 2005).

## 3 DEPOSIT GEOLOGY

The Mt. Polley mine consists of four Cu-Au porphyry deposits and several exploration targets. Proven and probable reserves are 59.9 Mt @ 0.36% Cu, 0.27 g/t Au (0.52 Moz Au), measured and indicated resources are 73.6 Mt @ 0.36% Cu, 0.30 g/t Au (0.71 Moz Au) and inferred resources are 22.3 Mt @ 0.30% Cu, 0.30 g/t Au (0.22 Moz Au) *(Imperial Metals Corporation, 2007)*.

Mineralization is associated with a monzonitic intrusive complex and occurs as several deposits localized within high-grade magmatic-hydrothermal breccia complexes. This project focuses on the Northeast Zone (NEZ; Figure 2), which is currently being mined.

Ore-related mineralization and alteration was spatially and temporally related to breccia formation, with Cu-sulphides principally occurring as breccia cement. Equigranular to porphyritic (augite ± hornblende ± plagioclase ± K-feldspar) monzonitic host rocks are the dominant clast-type within the breccia. The mineralized breccia has been intruded by monzonitic and more mafic dykes.

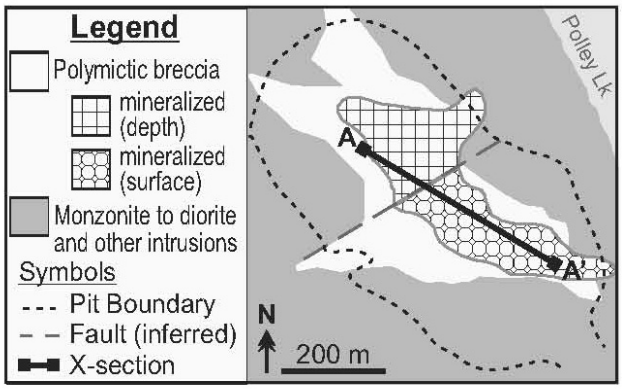


Figure 2. NEZ ore deposit trace, pit outline and location of long section (A-A') in Figure 4. Abbreviations: Lk - Lake.

## 4 PARAGENESIS

Four mineralization and alteration events have been recognized in the NEZ. Their timing is described here relative to the main-stage breccia-forming event: pre-, main-, late- and post-mineralization stages (Figure 3). Evidence of early hydrothermal activity is preserved as altered and veined clasts within the breccia.

Main-stage breccia formation is associated with cementation and alteration of clasts. Late-stage mineralization and alteration is evidenced by Cu-sulphide bearing veins and associated al-

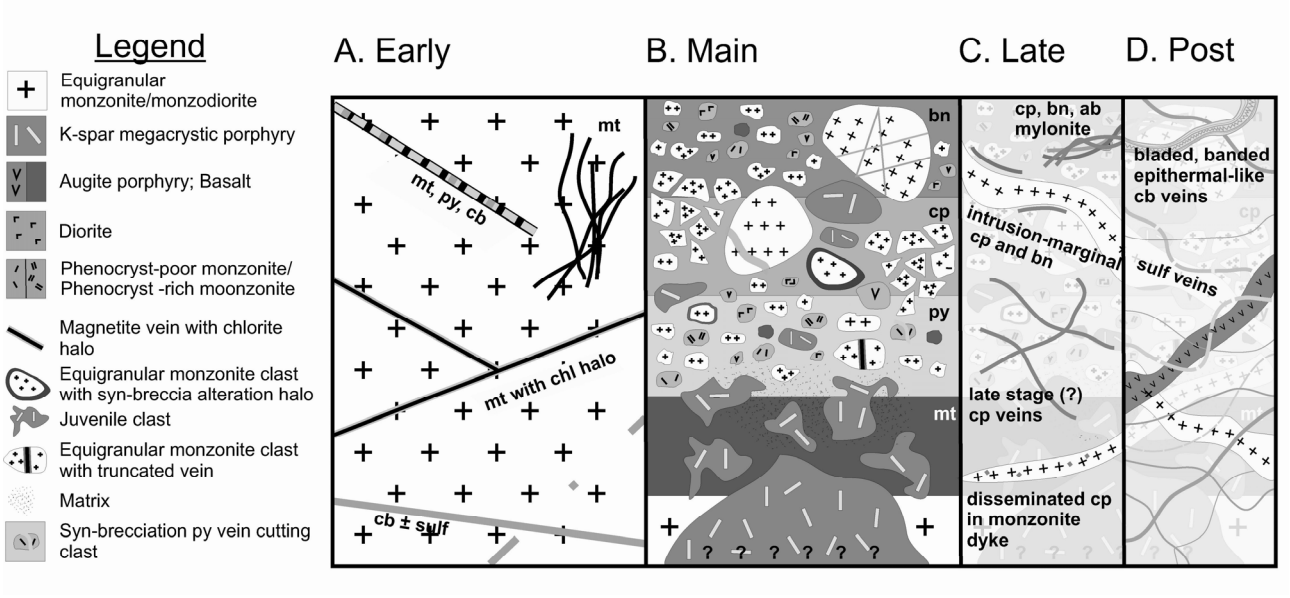


Figure 3. Paragenesis of the NEZ: A. Early: hydrothermal veining/fracturing in monzonite/diorite host rock. B. Main: brecciation event initiated by megacrystic K-feldspar-phyric intrusion as indicated by juvenile clasts; production of clasts and space; infill and cementation; lithification. C. Late: Cu-sulphide mineralization cross-cutting breccia; chalcopyrite ± albite veins. D. Post: dykes, faulting, sulfate and carbonate veining. Abbreviations: ab – albite; bn – bornite; cb – carbonate; cp – chalcopyrite; chl - chlorite; mt - magnetite; py – pyrite; sulf – sulphate.

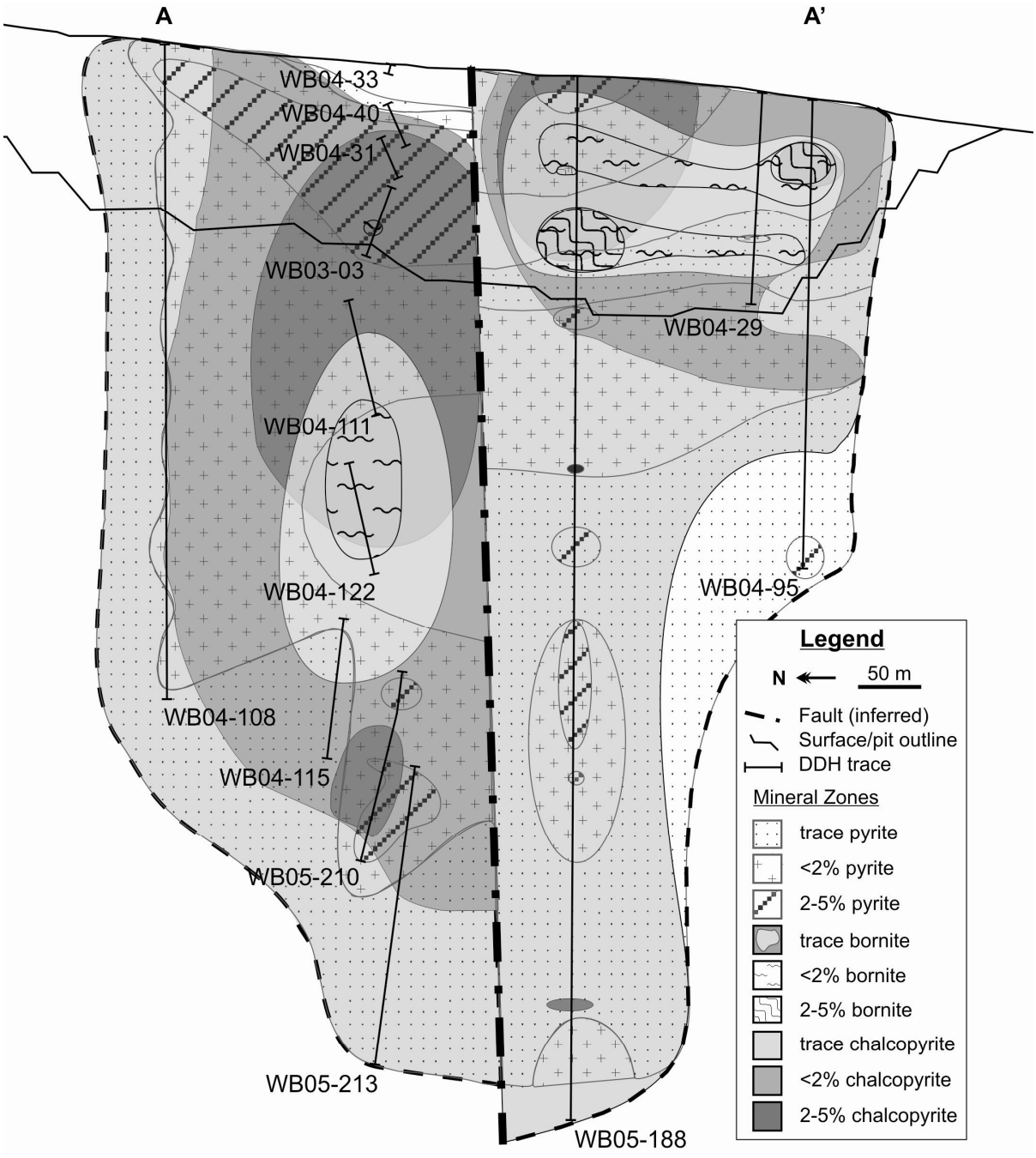


Figure 4. Long section (A-A') showing sulphide mineral zonation based on field observations

teration selvages that have cut the breccia and post-breccia monzonitic intrusions. Post-mineralization carbonate and sulphate veins and intrusions have cut all previous hydrothermal features and lack Cu-sulphides.

## 5 ALTERATION AND MINERAL ZONATION

Main stage alteration and mineralization assemblages are zoned laterally and vertically through the breccia body. Based on detailed logging of a long-section through the NEZ (Figures 2 and 4), chalcopyrite is ubiquitous throughout the section, occurring in high concentrations locally towards the center.

Within these chalcopyrite-rich zones, spatially restricted bornite-rich, pyrite-deficient cores are associated with high-grade ore (>1% Cu). In contrast, the outer margins of the chal-

copyrite zone are associated with pyrite and low grades (Figure 4). Gold is not visible in hand specimen but correlates well with Cu assay data.

Initial observations indicate that a garnet-bearing calc-potassic alteration assemblage occurs predominantly to the north, near the present-day surface. Potassic and propylitic alteration appear to overlap with each other and occur throughout the long section. Sodic alteration appears erratically at several locations. These patterns suggest that syn-mineralization alteration zones have been disrupted by altered post-breccia intrusive units and faults.

## 6 FUTURE WORK

Questions specific to Mt Polley that will guide laboratory work during this on-going PhD study include:

1. Was the bulk of the ore at Mt. Polley introduced during the main stage brecciation event, or did other paragenetic stages contribute significant volumes of Cu and Au?
2. What constraints on fluid compositions and fluid evolution can be determined from the observed infill and alteration mineralogy?
3. What are the isotopic characteristics of the ore and gangue minerals and what are their implications for ore genesis and exploration?

## ACKNOWLEDGEMENTS

Many thanks for the support and guidance from the people at Mt. Polley Mine and Imperial Metals: Linda Bingham, Michelle Brereton, Brenda Emerson, Lee Ferreira, Natasha Gainer, Patrick McAndless, Chris Rees, Steve Roberston and Gary Roste.

This work forms part of a larger MDRU-CODES research project investigating shallow- and deep-level alkalic mineral deposits, in collaboration with the GSC. Funding and field support is provided by Amarc Resources Ltd., AngloGold-Ashanti, Barrick Gold Corp., Imperial Metals Corp., Lysander Minerals Corp., Newcrest Mining Ltd., Newmont Mining Corp., Novagold Resources Inc., Teck Cominco Ltd., NSERC-CRD and Geoscience BC.

## REFERENCES

Cooke, D. R., Wilson, A. J., House, M. J., Wolfe, R. C., Walshe, J. L., Lickfold, V., and Crawford, A. J., in press, Alkalic porphyry Au-CU and associated mineral deposits of the Ordovician to Early Silurian Macquarie Arc, NSW: Australian Journal of Earth Science.

Deyell, C. L., and Tosdal, R. M., 2005, Alkalic Cu-Au Deposits of British Columbia: Sulphur Isotope Zonation as a Guide to Mineral Exploration, Geological Fieldwork 2004: Victoria, BC, British Columbia Geological Survey Branch, p. 191-208.

Imperial Metals Corporation, 2007, "Imperial Reports 2006 Production and Updated Mount Polley Reserve" (Fri. March 2, 2007 News Release), viewed March 29, 2007 http://www.imperialmetals.com/s/News-2007.asp?ReportID=175026&_Type=&_Title=Imperial-Reports-2006-Production-and-Updated-Mount-Polley-Reserve.

Lang, J. R., Stanely, C. R., Thompson, J. F. H., and Dunne, K. P. E., 1995, Na-K-Ca magmatic hydrothermal alteration in alkalic porphyry Cu-Au deposits, British Columbia, Mineralogical Association of Canada, Short course 23, p. 339-336.

Logan, J. M., and Mihalynuk, M. G., 2005, Regional Geology and Setting of the Cariboo, Bell, Springer and Northeast Porphyry Cu-Au Zones at Mount Polley, South-Central British Columbia, Geological Fieldwork 2004, Paper 2005-1: Victoria, BC, p. 249-270.

Wilson, A. J., Cooke, D. R., Harper, B. J., and Deyell, C. L., in press, Sulfur isotopic zonation in the Cadia district, southeastern Australia: exploration significance and implications for the genesis of alkalic porphyry gold-copper deposits: Mineralium Deposita.

# Trace element remobilization at the Ok Tedi porphyry Cu-Au deposit, Papua New Guinea.

Michiel van Dongen
*Pmd*CRC, School of Geosciences, Monash University, Clayton, 3800 VIC, Australia*

Andrew G. Tomkins
*School of Geosciences, Monash University, Clayton, 3800 VIC, Australia*

Roberto F. Weinberg
*School of Geosciences, Monash University, Clayton, 3800 VIC, Australia*

ABSTRACT: The Ok Tedi Complex hosts a world-class porphyry copper-gold deposit. Samples from the Ok Tedi Complex and the neighbouring Mount Ian Complex were analyzed for major and trace elements using XRF and HR-ICP-MS, and the isotopic composition of S in sulphides was analyzed by Elemental Analyzer. Major element geochemistry indicates that both complexes are alkaline and contain rocks ranging in composition from picrobasalts to trachytes. Trace element signatures suggest both complexes have a common parental magma. REE values are significantly lower for felsic, mineralized rocks than for both unmineralized equivalents and more mafic rocks in general. This suggests that original magmatic signatures have been lost due to intense alteration, which is complicating the unraveling of the magmatic history. Destruction of monazite, xenotime and possibly apatite were the main cause of REE modification of the mineralized rocks at Ok Tedi.

KEYWORDS: Ok Tedi, porphyry copper, magmatic evolution, REE, sulphur

## 1 INTRODUCTION

This study investigates the geochemistry of the Ok Tedi Complex and its relationship with the neighbouring Mount Ian Complex. The Ok Tedi Cu-Au deposit of Western Papua New Guinea was discovered in 1968 and mined since the early eighties. Its resources are 854 Mt at 0.64 wt% Cu and 0.78 g/t Au, and production was 2.86 Mt Cu and 706 t Au until 2003. This study provides a detailed geological and geochemical framework for understanding the magmatic genesis of the rocks that are parental to these deposits. This is important because it is unclear to what extent common magmatic processes such as magma mixing occur during the genesis of porphyry copper deposits (Sillitoe, 1997).

## 2 GEOLOGY

The deposits are situated in the Mio-Pliocene fold-and-thrust belt of Western Papua New Guinea. The deposits consist of chalcopyrite, chalcocite and minor bornite, deposited in quartz veins and stockworks in a central part of a porphyrytic monzonite intrusion. This intrusion itself is part of the larger Ok Tedi Complex, which consists mainly of equigranular monzodiorite. In addition, Au and Cu are found in massive magnetite and sulphide skarns in the adjacent country rock. The area consists of shallowly dipping continental margin marine sediments of Cretaceous to Middle Miocene age overlying stable Palaeozoic metamorphic and granite rocks of the West Papuan platform (Bamford, 1972; Fig. 1).

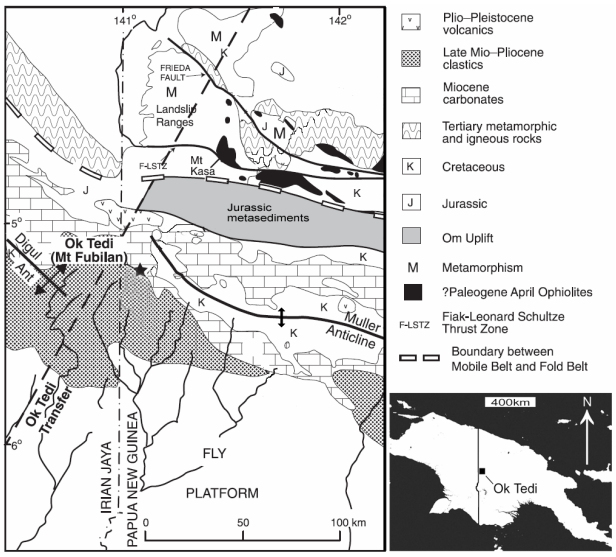


Figure 1. Regional geology and location of the Ok Tedi deposit. Modified from Hill *et al.* (2003).

The sedimentary package comprises Cretaceous marine mudstone and glauconitic sandstone of the Ieru Formation, late Oligocene-early Miocene Darai Limestone and Middle Miocene calcareous mudstone, siltstone and limestone of the Pnyang Formation. Minor tuffaceous sandstone was deposited as part of the Pnyang Formation during the Middle Miocene. Subsequent detrital volcaniclastic sediments, derived from a rapidly eroding stratovolcano during the late Miocene to Pliocene, form the Birim formation. The final sedimentary phase was the clastic and volcaniclastic alluvial flood plain deposits of the Anwin Formation (Rush & Seegers, 1990).

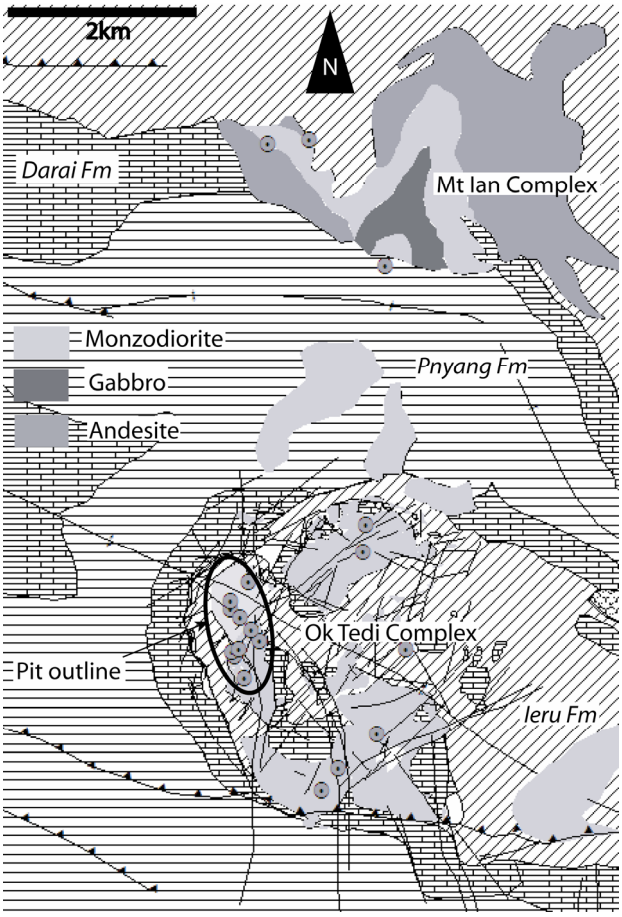


Figure 2. Geology of the Ok Tedi Complex and the Mount Ian Complex.

The Ok Tedi Intrusive Complex (OTC) is Middle Miocene to Pleistocene in age (Page & McDougall, 1972). Two units of this calc-alkaline complex are present at Mt Fubilan (corresponding to the pit outline on Fig. 2). The main stock is the Fubilan monzonite porphyry (FMP), which hosts the Cu-Au vein stockworks. This porphyry intruded sediments and parts of the 2.6 Ma Sydney monzodiorite stock. Skarns are associated with both intrusions. The FMP is about 850m in diameter, but tapers downward. It has been extensively altered by a hydrothermal event dated by K-Ar in biotite at 1.2-1.1 Ma (Page & McDougall, 1972).

The hydrothermal activity has produced K-feldspar and biotite alteration spatially associated with the main Cu-bearing stockwork veins, within a larger alteration zone characterized by chlorite, pyrite and magnetite. The latter extends over large parts of the OTC, though in varying intensity. Calc-silicate alteration is spatially associated with massive magnetite and sulphide skarns. A leached oxide cap was present (Rush & Seegers, 1990) but has been mined out.

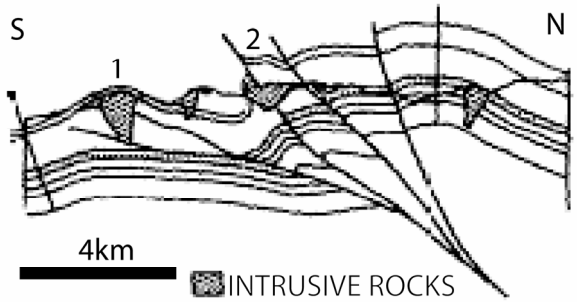


Figure 3. Cross-section modified from Mason *et al.* (1997) showing similarities in structural setting between Ok Tedi Complex (1) and Mount Ian Complex (2).

The Mount Ian Complex (MIC) intruded Darai limestone north of the OTC and consists of a core of Pliocene gabbro, diorite, monzonite and surrounding "intrusive andesite porphyry". K-Ar dating of MIC gabbro resulted in an age of 2.0-1.7 Ma, whereas one "andesite" sample had an age of 12.9 Ma (Page, 1975). Some parts are altered and contain secondary biotite and pyrite (Arnold *et al*, 1979). Despite its petrological similarities to the OTC, the MIC is not Cu-Au mineralized.

A strong structural control is noted by field evidence from pre-, syn- and post-emplacement slip along fault- and thrust planes and mineralized skarn formation on some of these planes in the OTC.

A comparison of the structural setting between the OTC and MIC (Fig. 3) suggests that their setting is equally favorable for mineralization. Some other explanation is thus required for the lack of mineralization in the MIC.

## 3 METHODS

Field study consisted of pit wall analysis, core logging and sampling. Samples were analyzed by XRF at CSIRO Land and Water, Adelaide, for whole rock major and trace element geochemistry. Selected samples were dissolved by High Pressure Dissolution with HF. Rare Earth and other trace elements were determined following Elburg *et al*. (2002) using HR-ICP-MS at the School of Geosciences, Monash University. Sulphides of selected samples were separated using tetra-bromide liquid (specific gravity 2.96) and washed with ethanol. After drying, they were combusted with $VO_5$. The S isotopic composition of the gas was determined using an Elemental Analyzer.

## 4 RESULTS

Rock samples have been classified using the IUGS TAS classification (Fig. 4), although this is a scheme for volcanic rocks. All samples are from medium-to-coarse grained plutonic rocks. The OTC is an alkaline intrusive complex and predominantly has a chemical composition of trachyandesites to trachytes. Deep-seated alkaline gabbroic dikes and enclaves of basaltic to basaltic trachyandesitic composition are also present. The MIC is less alkaline and less evolved than the OTC. Its intrusive rocks have picrobasaltic, trachybasaltic, trachyandesitic and trachydacitic compositions.

Trends in major oxides with increasing silica show decreasing MgO, CaO, $TiO_2$ and $P_2O_5$ and increasing alkali oxides. XRF trace element trends with increasing silica show increasing Rb, Ba and Zr, decreasing Y and Ce, increasing then decreasing Sr and variable S, Th, Cu and Zn.

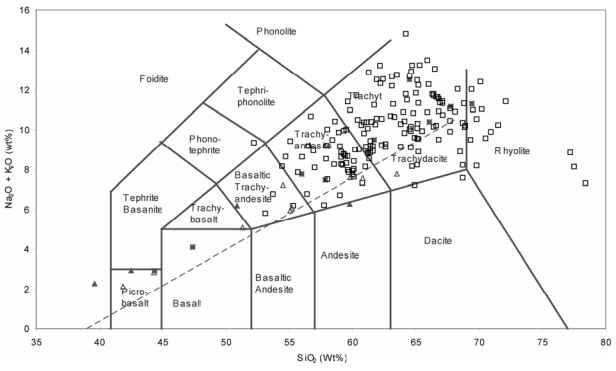


Figure 4. TAS plot showing OTC (filled black squares) and MIC (filled black triangles) rocks and their IUGS classification. Open symbols represent data from Doucette (2000).

Samples are enriched in REE relative to C1 chondrites (Fig. 5), with LREE enrichment, typical of arc andesites. Although MIC samples and the OTC picrobasaltic gabbro have similar signatures, most OTC rocks (near Mt Fubilan) are depleted relative to MIC samples and OTC picrobasaltic gabbro. Most OTC rocks have significant positive Eu anomalies, whereas MIC rocks and the OTC picrobasaltic gabbro have small negative Eu anomalies.

Sulphur isotopic compositions of sulphide separates are between –0.8 and 5.1 (Fig. 6).

## 5 DISCUSSION

### *5.1 Whole rock geochemistry*

The alkaline character of the rocks in the MIC and OTC (Fig. 4) is characteristic of many major circum-Pacific gold-copper occurrences (Sillitoe, 1997). Incompatible element ratios of Zr/Y and Nb/Y of mafic OTC and MIC are similar, suggesting a common source. The REE values of OTC monzonites and monzodiorites are substantially lower than the other samples. This suggests remobilization by fluids, *i.e*. the effects of hydrothermal alteration (Poitrasson *et al,* 1995). This decrease in REE can at least in part be ascribed to the disappearance of monazite and xenotime, causing a significant decrease in P, Y and La. Using field relationships and published data, relative ages were assigned to the samples. This produces complex chemical patterns over time that need further examination and interpretation in order to interpret the magmatic evolution of the rock suite correctly.

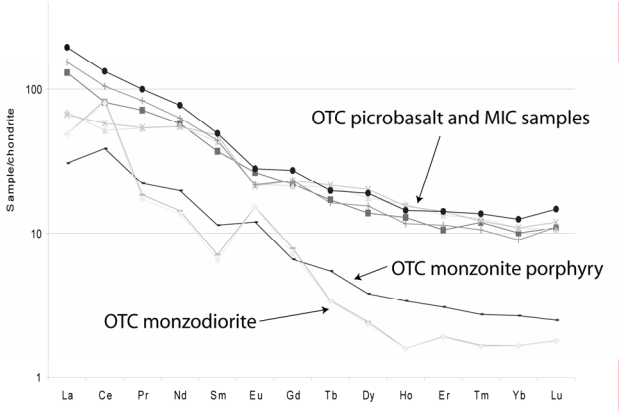


Figure 5. Chondrite (C1) normalized spidergram of REE from the OTC and MIC. Normalizing values are from (Sun & McDonough, 1989).

## 5.2 *Sulphur isotope geochemistry*

The range of sulphur isotopic values (Fig. 6) is similar to those of typical sulphides from porphyry copper deposits, although slightly higher. Since sulphide from the mantle has a $\delta^{34}S$ of approximately zero, a large part of the sulphur is interpreted to have an orthomagmatic source. The slight shift towards positive values may reflect mixing with crustally sourced sulphur, *e.g.* from surrounding sediments.

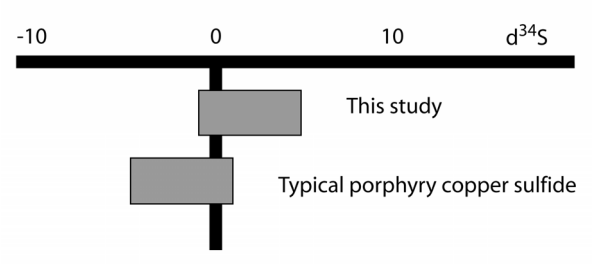


Figure 6. Sulphur isotopic composition of sulphide separates relative to Canon Diablo Troilite. Typical sulphide sulphur isotopic values are from Rollinson (1993)

## 5.3 *Implications for porphyry copper genesis*

The sulphur isotope results suggest a largely magmatic source for the sulphur. This could imply that a large part of the sulphur in this system is provided by mafic magma replenishment, which is consistent with the conclusions of Hattori & Keith (2001). In our attempt to substantiate this possibility by means of comparison of REE patterns, we found that REE mobility through destruction of accessory phases strongly disrupts the original signature. Caution should be taken when interpreting geochemical signatures of ore deposits associated with intense alteration.

## ACKNOWLEDGEMENTS

Ok Tedi Mining Limited is thanked for site access and logistical support. The Australasian Institute of Mining and Metallurgy is acknowledged for the Bicentennial Gold'88 Award towards travel financing. The Predictive Mineral Discovery Co-operative Research Centre is acknowledged for financial support.

## REFERENCES

Arnold, G.O., Griffin, T.J. & Hodge, C.C. 1979. Geology of the Ok Tedi and Southern Atbalmin 1:100000 Sheet. *Geological Survey of Papua New Guinea Report 79/3*: 41-56.

Bamford, R.W. 1972. The Mount Fubilan (Ok Tedi) porphyry copper deposit, Territory of Papua and New Guinea. *Economic Geology* Vol. 67: 1019-1033.

Doucette, J.D. 2000. *A petrochemical study of the Mount Fubilan Intrusion and associated ore bodies, Papua New Guinea.* Unpublished PhD thesis: 373p.

Elburg, M.A., van Bergen, M., Hoogewerff, J., Foden, J., Vroon, P., Zulkarnain, I. & Nasution, A. 2002. Geochemical trends across an arc-continent collision zone: magma sources and slab-wedge transfer processes below the Pantar Strait volcanoes, Indonesia. *Geochimica et Cosmochimica Acta* Vol. 66: 2771-2789.

Hattori, K. & Keith, J.D. 2001. Contribution of mafic melt to porphyry copper mineralization: evidence from Mount Pinatubo, Philippines, and Bingham Canyon, Utah, USA. *Mineralium Deposita* Vol. 36: 799-806.

Hill, K.C., Kendrick, R.D. & Crowhurst, P.V. 2002. Copper-gold mineralisation in New Guinea; tectonics, lineaments, thermochronology and structure. *Australian Journal of Earth Sciences* Vol. 49: 737-752.

Mason, R.A. 1997. Structure of the Alice Anticline, Papua New Guinea: serial balanced cross-sections and their restoration. *Journal of Structural Geology* Vol. 19: 719-734.

Page, R.W. & McDougall, I. 1972. Ages of mineralization of gold and porphyry copper deposits in the New Guinea Highlands. *Economic Geology* Vol. 67: 1034-1048.

Page, R.W. 1975. Geochronology of late Tertiary and Quaternary mineralized intrusive porphyries in the Star Mountains of Papua New Guinea and Irian Jaya. *Ecnomic Geology 70* Vol. 70: 928-936.

Poitrasson, F., Pin, C. & Duthou, J.L. 1995. Hydrothermal remobilization of rare earth elements and its effects on Nd isotopes in rhyolites and granite. *Earth and Planetary Science Letters* Vol. 130: 1-11.

Rollinson, H. 1993. *Using geochemical data: Evaluation, presentation, interpretation.* Harlow, Essex, England: Longman Scientific & Technical.

Rush, P.M. & Seegers, H.J. 1990. Ok Tedi copper-gold deposits. *AusIMM Monograph Series 14, Geology of the mineral deposits of Australia and Papua New Guinea* Vol. 2: 1747-1754.

Sillitoe, R.H. 1997. Characteristics and controls of the largest porphyry copper-gold and epithermal gold deposits in the circum-Pacific region. *Australian Journal of Earth Sciences* Vol. 44: 373-388

Sun, S.S. & McDonough, W.F. 1989. Chemical and isotopic systematics of oceanic basalts; implications for mantle composition and processes. *Magmatism in the ocean basins:* 313-345. London: Geological Society of London.

# Spatial distribution of geochemical indicators in the Jalama Batholith, Spain, as vectors for Sn-W mineralization

Concepción Fernández-Leyva
*Geological Survey of Spain*

Juan Locutura
*Geological Survey of Spain*

Casilda Ruiz
*The Madrid School of Mines, Polytechnical University of Madrid (UPM) Spain*

ABSTRACT: The granite batholith of Jálama (Central Iberian Zone) is one of numerous granites with associated Sn and W mineralization in the Hesperian Massif. Three types of granites have been distinguished: inhomogeneous granitoides, porphyritic granites and leucogranites. Ratios of Rb/Sr, $P_2O_5$*100/Th, $Na_2O/(Na_2O+K_2O+CaO)$ and fluorine abundance are used as indicators of mineralization potential. Contour maps show the spatial distribution of these indicators and their relation to the mapped granite facies, the mineralization potential, and distribution of Sn and/or W mineralization. These distribution patterns suggest that leucogranites and the subfacies at the margin of the porphyritic granites have the best mineral potential in the Jálama batholith.

KEYWORDS: granites, tin-tungsten, Central-Iberian Zone, Jálama batholith, Spain

## 1. GEOLOGICAL SETTING AND GEOCHEMISTRY OF THE JÁLAMA BATHOLITH

The granite batholith of Jálama is one of numerous granites associated with Sn and W mineralization in the Iberian Hercynian Basement. It forms an enclave in the southern part of the Central Iberian Zone (CIZ) of the Hesperian Massif, and is emplaced in the Late Precambrian Greywacke-Schist Complex.

Three major granite units have been established by field mapping, petrographic study and geochemical caracterisation: inhomogeneous granitoids (IG), porphyry granites (PG) and leucogranites (Lc) (Fig. 1). The inhomogeneous granitoids and the porphyry granites correspond to granite/monzogranites, while the leucogranites are alkali feldspar granites, according to the classification of La Roche (1992). The inhomogeneous granitoids are two-mica granites. The porphyritic granites, of variable porphyritic character, have more muscovite and less biotite than the inhomogeneous granitoids.

The leucogranites have a medium to fine grain size, with a high content of muscovite.

The granites of the Jálama batholith correspond to peraluminous and subalkaline rocks, with elevated contents of P and F. Major

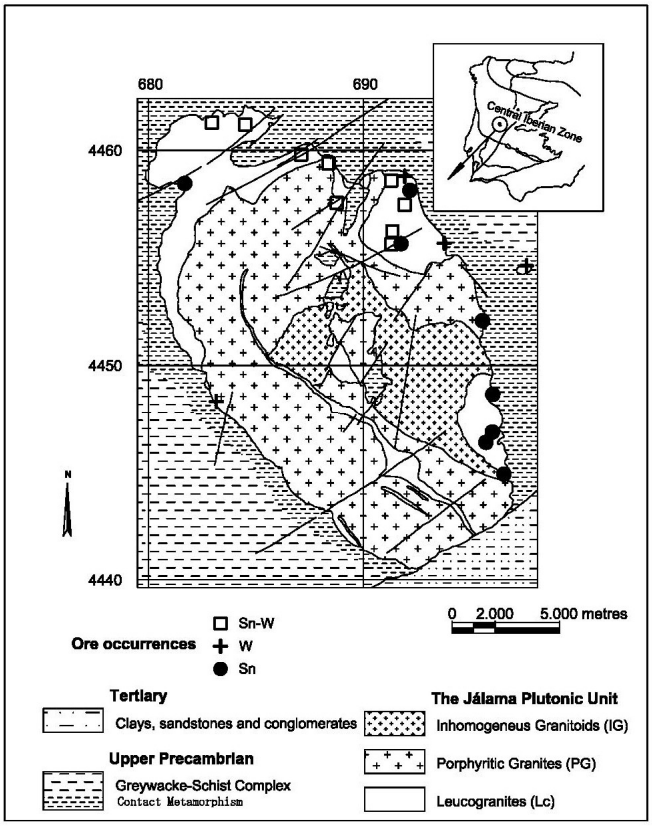


Figure 1. Schematic geological map

and trace elements show regular variation trends from inhomogeneous granitoids to leucogranites. The three granitic units show subparallel REE patterns. There is a decrease in total REE and an increase in the negative Eu anomaly from the inhomogeneous granitoids to leucogranites. All granites exhibit a high K/Na ratio, high normative corundum, A/CNK> 1.1, $(Sr^{87}/Sr^{86})_0 > 0.707$ and values of Th+U < 50 ppm which are characteristics of S-type granites (White & Chappell, 1988; Scheepers, 2000).

Whole-rock Rb-Sr isochrons mainly indicate an early intrusion of the inhomogeneous granitoids (319±10 Ma), followed by porphyritic granites (279±9 Ma) (Ruiz *et al*., 2007). The initial $^{87}Sr/^{86}Sr$ ratios (IG: 0.711±0.001; PG: 0.719±0.001) suggest that the granites resulted from partial melting of pre-existing crustal material.

## 2 MINERALIZATION POTENTIAL OF GRANITIC UNITS OF THE JALAMA BATHOLITH

In the Jalama batholith the Sn and/or W mineralizations are basically present in the form of cassiterite and/or wolframite in intragranitic quartz veins, some of which gave rise to mining operations of some importance in the last century. Such mineralizations are associated with the leucogranites and the subfacies at the margin of the porphyritic granites. The internal porphyritic granites and the inhomogeneous granitoids do not show mineralization.

The average Sn content and the variations of trace elements such as Sr, Ba, Rb, Th and P have been applied as geochemical criteria to determine the mineralization potential in the granitic units of the Jálama batholith (Ruiz *et al.*, 2007). Low values for the ratios Ba/Rb, K/Rb and Sr/Rb and high values for the ratio $P_2O_5$*100/Th correspond to fertile granites, such as the leucogranites and the subfacies at the margin of the porphyritic granites.

On the other hand, the porphyritic granites and the inhomogeneous granitoides do not have these features.

## 3 SPATIAL DISTRIBUTION OF GEOCHEMICAL INDICATORS IN THE JÁLAMA BATHOLITH

Once the magmatic variation trends and mineralization potential indicators of the Jálama batholith facies were established, the spatial distribution of these indicators and their relation with granite facies and distribution of Sn and/or W mineralizations was studied.

We have elaborated contour maps of the geochemical indicators. These maps are made on the basis of different variable grids obtained through the Inverse Weighted Distance (IWD) method, with a search radius of 5000m.

The ratios Rb/Sr, $P_2O_5$*100/Th, $Na_2O/(Na_2O+K_2O+CaO)$ and fluorine abundance have been selected as indicators of mineralization potential.

Contour maps of Rb/Sr and $P_2O_5$*100/Th indicators (Figures 2 and 3) show distribution patterns that are related to the facies of leucogranites and the subfacies at the margin of the porphyritic granites, pointing to the mineral potential of these facies. According to Scheepers (2000), mineralized S-type granites are enriched in P/Th. Both contour maps, and particularly the Rb/Sr map, are coherent with the corresponding distribution of mineral occurrencesof the Jálama batholith (Ruiz *et al.*, 2007).

The $Na_2O/(Na_2O+K_2O+CaO)$ index (Figure 4), shows distribution patterns very similar to those considered before. Once again, the leucogranites and the subfacies at the margin of the porphyritic granites are discriminated because of their high values. This indicator could also quantify processes of tardimagmatic albitization, related to these facies, a fact that was not considered so far.

Finally, the spatial distribution of fluorine has been considered as it is a very important element in granitic magmatic differentiation. F contents are generally high compared to barren granites (Olade, 1980).

The distribution of F (Figure 5) is consistent with the distribution of leucogranites in the northeastern border and the centre of the batholith, that have W-Sn mineralization.

## 4. CONCLUSIONS

Ratios of Rb/Sr, $P_2O_5$*100/Th, $Na_2O/(Na_2O+K_2O+CaO)$ and fluorine abundance have been selected as indicators of mineralization potential in the Jálama batholith. The spatial distribution of these indicators shows a close relation with mapped rock facies and distribution of Sn and/or W occurrences,

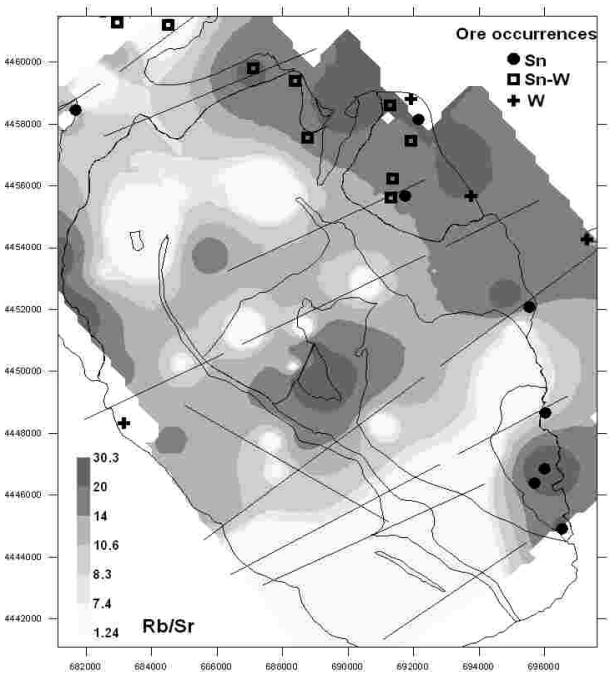


Figure 2. Contour map of Rb/Sr

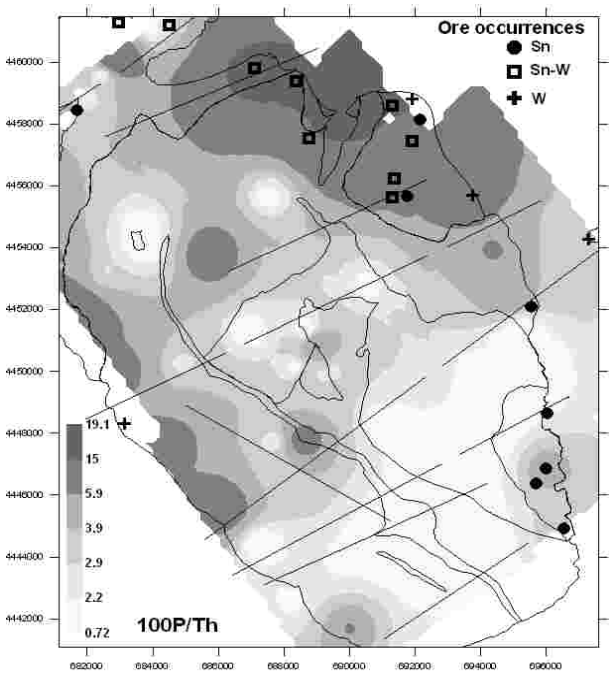


Figure 3. Contour map of $100P_2O_5/Th$

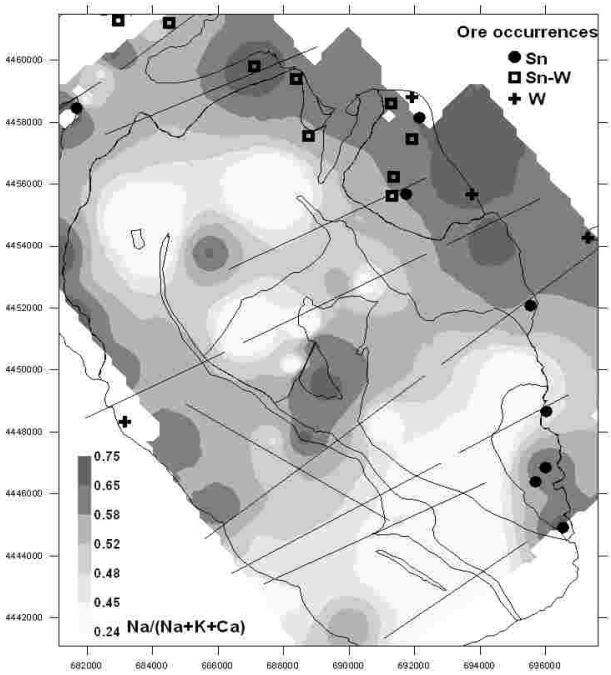


Figure 4. Contour map of Na/(Na+K+Ca)

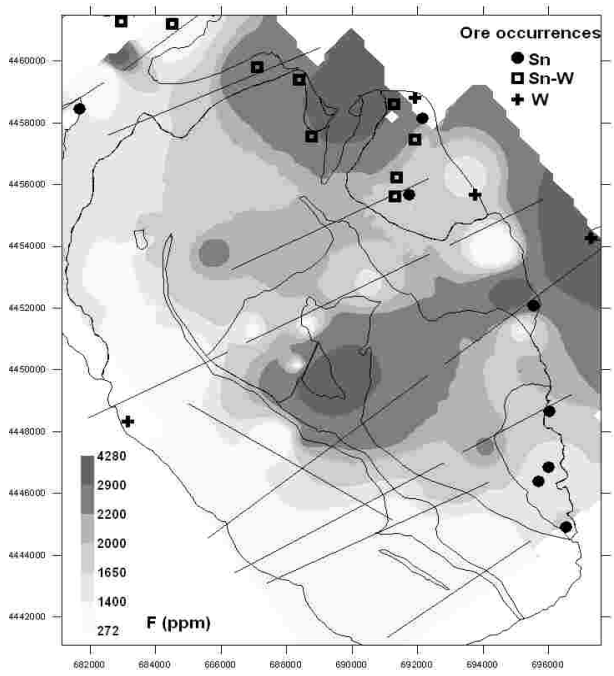


Figure 5. Contour map of F content

Contour maps of Rb/Sr and $P_2O_5$*100/Th indicators show distribution patterns that are in line with the mineralization potential of leucogranites and the subfacies at the margin of the porphyritic granites. High ratios characterize areas with the presence of Sn-W mineralization.

The $Na_2O/(Na_2O+K_2O+CaO)$ index shows distribution patterns that are very similar to Rb/Sr and $P_2O_5$*100/Th. This indicator could also quantify processes of tardimagmatic albitization.

The spatial distribution of fluorine is consistent with the occurrence of leucogranites in the northeastern border and the centre of the batholith, where mineralizations of W-Sn are concentrated.

ACKNOWLEDGEMENTS

Financial support for this work was provided by the Geological Survey of Spain (IGME).

REFERENCES

La Roche H (1992) Un homologue cationique du triangle Q-A-P (quartz-feldspath alcalin-plagioclase), figure majeure de la pétrologie des roches plutoniques. *C.R. Acad. Sci. Paris* 315: 1687-1693.

Olade M A (1980) Geochemical characteristics of tin bearing and tin-barren granites. Nothern Nigeria. *Economic Geology* 75, 71-82.

Ruiz C (2007) Geochemistry, geochronology and mineralization potential of the granites in the Central Iberian Zone: The Jálama batholith. *Chemie der Erde* (2007) DOI 10.1016 /j.chemer.2006.11.001.

Scheepers R (2000) Granites of the Saldania mobile belt, South Africa: radioelements and P as discriminators applied to metallogeny. *J.Geochem. Explor.* 68: 69-86.

White AJR, Chappell BW (1988) Some supracrustal (S-type) granites of the Lachlan Fold Belt. *Trans. Roy. Soc. Edinburgh 79*: 169-181.

# Geochemistry and geothermometry of altered rocks associated with the Gerês granite, northern Portugal

L. Jaques, F. Noronha & I. Bobos
*GIMEF – Centro de Geologia, Faculdade de Ciências, Rua do Campo Alegre, 4069-007 Porto, Portugal*

ABSTRACT: Hydrothermal alteration has caused albitization and quartz dissolution within the Gerês granite, Portugal. Altered domains within the granite are characterized by a core zone of albitization, and a peripheral zone that contains epidote + vermicular chlorite + calcite + hematite. Homogenization temperatures from authigenic quartz range from 171 to 279ºC, with a mode around 220ºC. The altered rocks from Gerês have very low U and W contents, and W - Mo mineralization in the area is inferred to pre-date albitization and epidote alteration.

KEYWORDS: albite, epidote, geochemistry, fluid inclusions, Gerês, Portugal.

## 1 INTRODUCTION

The late Hercynian granites of Central and Western Europe in the Variscan belt are associated with W, Mo and minor Sn mineralization. Alkaline hydrothermal fluids are known to have flowed along fracture systems within the granitoids, causing dissolution of primary quartz and deposition of secondary albite. These altered rocks, locally described as "episyenites", are common throughout the European Hercynian belt in the French Massif Central (Leroy 1971, Cuney 1978, Cathelineau 1986), the Bohemian Massif (Hecht *et al*. 1999) and the Iberian Massif (Caballero *et al*. 1996, Recio *et al.* 1997). The Gerês region was prospected by JEN during the 1960s for uranium mineralization, based on the occurrences of albitized, quartz-deficient altered granitoids. The altered rocks have been described by Ávila-Martins & Saavedra (1976) and Cheilletz & Giuliani (1982).

This paper documents the geochemistry of hydrothermal alteration in the Gerês granite, in order to determine the nature of the hydrothermal fluids and to evaluate possible relationships with tungsten mineralization.

## 2 GEOLOGY

The Hercynian orogenic belt contains metamorphosed sedimentary rocks and granitoids

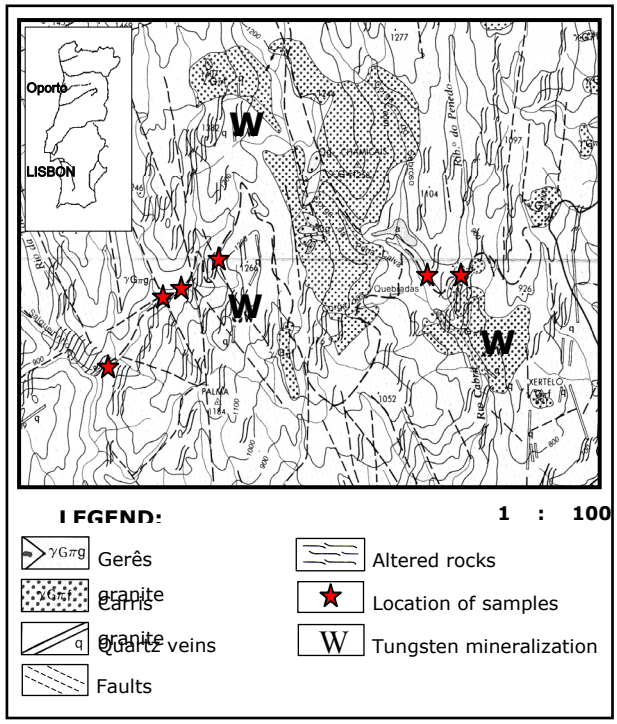


Figure 1. Geological map of the Gerês region (after Noronha & Ribeiro 1983).

that formed during the collision of two major continents in the late Palaeozoic (Matte 1991). In the Iberian Massif, the late orogenic (post-tectonic) granitic massif of Gerês (age: ~ 300 Ma) is located at the northern border between Portugal and Spain (Fig. 1). The granite is related to W-Mo mineralization.

The discordant massif includes four major granitic units, which have intruded synorogenic granitoids and metasedimentary rocks of Silurian age (Noronha & Ribeiro 1983, Mendes & Dias 1996). The Gerês granite has a coarse to medium grained porphyritic texture. The contact between the altered rocks and the granitic protolith has a net texture, controlled by N- and ENE-trending faults. The altered rocks occur as elongated pipes that are several tens of metres in diameter.

## 3 MATERIALS AND METHODS

In order to characterize the effects of alteration at Gerês, we have completed petrographical and geochemical analyses. Electron microprobe analyses (EMPA) were conducted using a Cameca Camebax electron microprobe. Major, trace and rare earth element compositions of whole-rock samples were determined by inductive-coupled plasma mass spectrometry (ICP-MS). Chondrite-normalization was carried out according to Taylor & McLennan (1985). Estimating the gains or losses of elements during mass transfer was determined by Gresens method (Grant, 1986). Microthermometry analyses were performed using Chaixmeca and Linkam TH600 heating-freezing stages. The volatile species and the solid inclusions analyses were carried out with a LABRAM micro-Raman spectrometer.

## 4 RESULTS

### 4.1 *Post-Magmatic Alteration Stages*

The Gerês granite mainly consists of quartz, feldspars and biotite. Mineralogical and petrographical studies have identified two distinct alteration products of $Na^+$ and $Ca^{2+}$-metasomatism: albitization and epidotization.

Albitized rocks are characterized by a "chessboard" texture of albite in thin section. Alteration of magmatic biotite to chlorite, and sericitization of feldspars are also characteristic. Primary K-feldspar has been reddened due to hematite dusting, giving the K-feldspar a cloudy appearance in thin section. Cavities that were produced by dissolution of primary quartz have been subsequently filled with albite, microcline and haematite.

The outer margins of the altered domains are characterized by epidote + vermicular chlorite + calcite + haematite. Small aggregates of adularia and hydrothermal quartz have been identified in the epidotized granites.

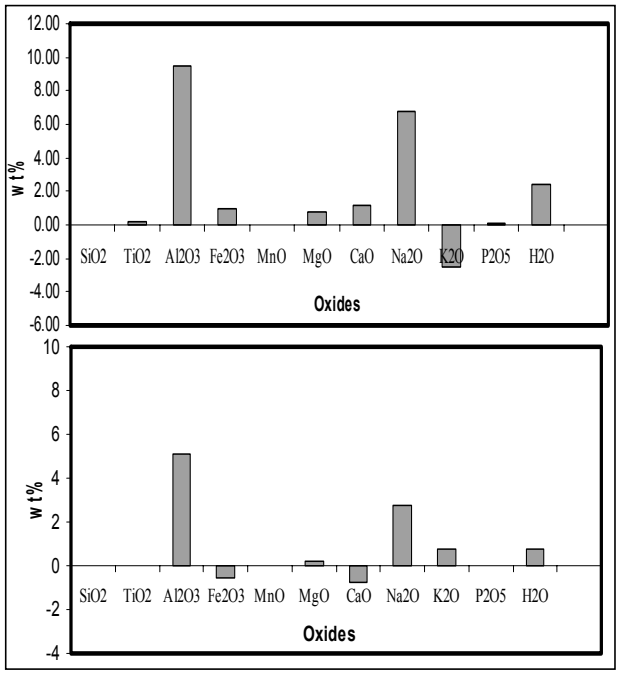


Figure 2. Gains and losses of major elements caused by alteration of the Gerês granite

### 4.2 *Geochemistry*

The altered rocks at Gerês have average uranium concentration of 15 ppm, whereas W averages 2.7 ppm. Although we have not detected any significant mineralization in our altered samples, our geochemical data provides evidence for mobilization of some major and trace elements during hydrothermal alteration at Gerês (Figs. 2, 3 and 4).

Although there is textural evidence for dissolution of primary quartz at Gerês, no net loss or gain of silica occurred during hydrothermal alteration (Fig. 2). Bulk geochemical results show a decrease in $K_2O$, associated with en-

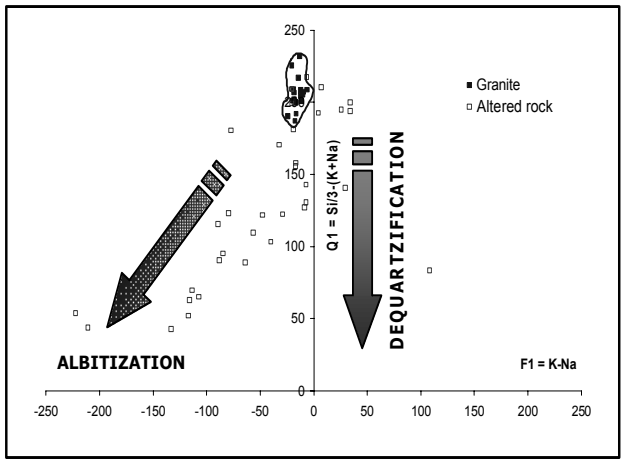


Figure 3. Main alteration trends in the Q1-F1 diagram: 1) albitization and 2) quartz dissolution.

richment of $Na_2O$ and $Al_2O_3$, which is directly related to albitization. Increased CaO is associated with epidote and calcite alteration.

The $Q_1$–$F_1$ diagram (Fig. 3) shows the main geochemical trends related to: 1) albitization and 2) quartz dissolution. The effects of albitization are also evident on Figure 4. $Na_2O$ enrichment in the altered Gerês granite was accompanied by depletion of $K_2O$ (Fig. 4).

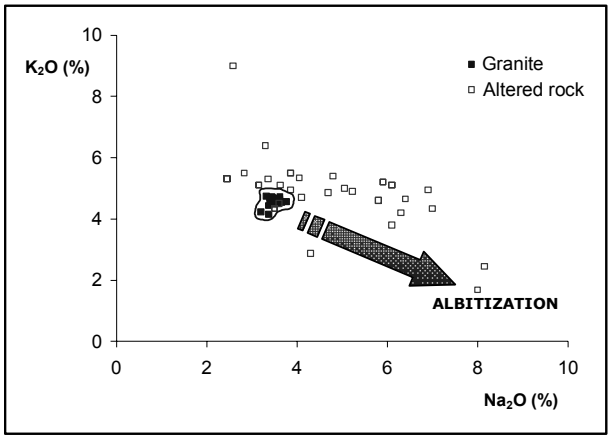


Figure 4. $Na_2O$-$K_2O$ plot showing the albitization trend for the Gerês granite.

Chondrite normalized REE patterns (Fig. 5) show relative depletion of HREE and some enrichment in LREE in the altered rocks, which is similar to results obtained by Hecht *et al.* (1999). Crystallization of late-stage apatite in cavities may explain this relationship. However, there is no evidence for alteration of primary REE-bearing accessory minerals (*i.e.*, zircon, allanite or monazite).

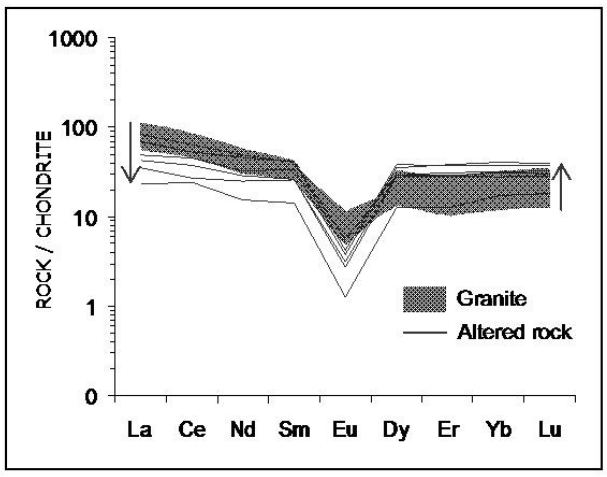


Figure 5. Chondrite-normalized REEs patterns of altered rocks compared with the compositional range of the granitic rocks.

### 4.3 *Fluid Inclusions*

Microthermometric analyses were performed on primary and pseudosecondary fluid inclusions (FIs) in authigenic quartz crystals that had crystallized in open spaces near the centre of the albitized zones. The FIs are two-phase, containing liquid and gas, and are aqueous fluids ($H_2O$–NaCl system). No volatile species were detected in the FIs by micro-Raman analyses. The FIs all homogenized to the liquid phase, with homogenization temperature from 171 to 279ºC, and a mode around 220ºC.

## 5 DISCUSSION

Brittle deformation in the Gerês granite provided flow paths for hydrothermal fluids that caused albitization and epidotization. Textural and mineralogical features provide evidence for the leaching of primary magmatic quartz, and albitization of feldspars. Secondary vugs have been infilled by authigenic quartz, sericite, adularia, epidote, vermicular chlorite, calcite and hematite. Quartz dissolution and albitization are inferred to have been contemporaneous on textural grounds. $Na_2O$ contents increased during albitization, whereas $SiO_2$ remained constant.

Cathelineau (1986) estimated temperatures of hydrothermal alteration from 400 to 250 ºC for the types of alteration observed at Gerês. Our fluid inclusion data are mostly lower than this range, but are uncorrected for pressure. The presence of epidote at Gerês is consistent with Cathelineau's temperature estimate. The altered Gerês granite contains very low U and W contents, and appears to have been unrelated to W-Mo mineralization that occurs elsewhere in the district.

## ACKNOWLEDGEMENTS

We are indebted to David Cooke for his helpful review comments. The investigation was made possible through the POCTI Project (0039/2003), developed at the "Centro de Geologia da Universidade do Porto". L. Jaques thanks the Portuguese Foundation of Sciences for the financial support (SFRH/BD/4646/2001).

## REFERENCES

Ávila-Martins J, Saavedra J (1976) The study of the episyenitization process of the Serra de Gerês granite (North of Portugal). Memórias e Notícias,

*Publicações do Museu e Laboratório Geológico e Mineralógico da Universidade de Coimbra* pp 82: 79-93

Caballero JM, González-Casado JM, Casquet C, Galindo C, Tornos F (1996) Episyenitic rocks from Sierra de Guadarrama: a regional hydrothermal process of the Lower Permian related to the Alpine orogeny. *Cuadernos de Geologia Ibérica* pp 20: 183-201

Cathelineau M (1986) The Hydrothermal Alkali Metasomatism Effects on Granitic Rocks: Quartz Dissolution and Related Subsolidus Changes. *Journal of Petrology* pp 27: 945-965

Cheilletz A, Giuliani G (1982) The role of deformation and the geneses of the feldspathic episyenitic rocks from Lovios – Gerês Mountains (Galice) and Zaer (Central of Morocco). *Mineralium Deposita* pp 17: 387-400

Cuney M (1978) Geologic Environment, Mineralogy, and Fluid Inclusions of the Bois Noirs-Limouzat Uranium Vein, Forez, France. *Economic Geology* pp 73: 1567-1610

Dias G, Leterrier J, Mendes A, Simões PP, Bertrand JM (1998) U-Pb zircon and monazite geochronology of post-collisional Hercynian granitoids from the Central Iberian Zone (Northern Portugal). *Lithos* pp 45: 349-369

Giuliani G, Cheilletz A (1983) Structural petrology and metallogeny: examples of feldspathic episyenitic rocks and intragranite mineralisations. *C. R. Acad. Sci. Paris - Série II* pp 296: 845-848

Grant JA (1986) The Isocon Diagram - A Simple Solution to Gresen's Equation for Metasomatic Alteration. *Economic Geology,* pp 81: 1976-1982

Hecht L, Thuro K, Plinninger R, Cuney M. (1999) Mineralogical and geochemical characteristics of hydrothermal alteration and episyenitization in the Königshain granites, northern Bohemian Massif, Germany. *Journal of Earth Sciences* 88: 236-252

Leroy J (1971) No mineralized episyentic rocks in the two mica granite from the Saint-Sylvestre (Limousin-France). Equilibrium between minerals and solutions. *Unpublished Thesis, Univ. Nancy* I, pp 87

Matte P (1991) Accretionary history and crustal evolution of the Variscan belt in Western Europe. *Tectonophysics* pp 196: 309-337

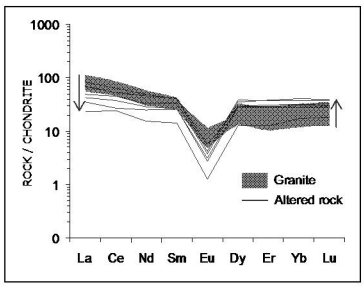

# Magnetite-apatite deposits of the Bafq district, Central Iran: monazite geochronology and ore formation

Farhad M. Torab[1,2] & Bernd Lehmann[2]
*1-Department of Mining Engineering, Yazd University, Yazd, Iran*
*2-Institute of Mineralogy and Mineral Resources, Technical University of Clausthal, 38678 Clausthal-Zellerfeld, Germany.*

ABSTRACT: The Bafq mining district is in the early Cambrian Kashmar-Kerman volcano-plutonic arc in Central Iran and hosts important Kiruna-type magnetite-apatite deposits. Apatite has partially undergone hydrothermal overprint which involves leaching of sodium, chlorine, and rare-earth elements (REE). The REE are then remobilized into monazite (and minor allanite, parisite and xenotime) which nucleates as inclusions within apatite or as individual crystals outside of apatite. The monazite has generally very low $ThO_2$ content (<1 wt%), but there are some high-Th cores which allow chemical Th-U-total Pb dating by electron microprobe. These cores yield an isochron age of 515 ±21 Ma (initial PbO intercept = 68 ppm), or 529 ±21 (forced initial PbO = 0), which is contemporaneous with the formation of the volcano-plutonic host rocks of the magnetite-apatite mineralization, and coincides with sedimentation of late Proterozoic to Cambrian evaporitic rocks in Central Iran. Monazite age and mineralogical and geochemical data suggest that the magnetite-apatite deposits are likely related to large-scale brine circulation induced by Cambrian felsic magmatism.

KEYWORDS: Magnetite, apatite, monazite geochronology, IOCG deposits, Bafq district, Iran

## 1 INTRODUCTION

The Bafq metal province in Central Iran hosts important Kiruna-type magnetite-apatite ore deposits. There are 34 aeromagnetic anomalies identified so far, and individual deposits range up to several hundred million tonnes of iron ore with variable amounts of apatite and locally high REE content. Among these deposits, Choghart, Chador-Malu, Se-Chahun and Esfordi are currently mined (Torab & Lehmann, 2006) (Fig. 1).

We report on the relationship of apatite and monazite, constrain the age of the mineralization on the basis of monazite geochronology, and propose a tentative genetic model for the ore deposits.

## 2 GEOLOGICAL SETTING

Central Iran is an assemblage of several Precambrian fragments of Gondwanaland. The major tectono-metamorphic terranes are the Lut, Tabas, and Yazd Blocks. Their boundaries are defined by large regional-scale faults (Fig. 1). The Tabas and Yazd Blocks are separated by a more than 1000km-long, and up to 80km-wide, arcuate and structurally complex belt composed of variably deformed supracrustal rocks, i.e. the Kashmar-Kerman Tectonic Zone which represents an early Cambrian active continental margin environment (Ramezani & Tucker, 2003). This magmatic arc hosts the Bafq metal province, located between Bafq and Saghand (Fig. 1).

The basement of the Bafq district consists of Precambrian high- to low-grade metamorphic rocks (Haghipour, 1977), and is unconformably overlain by an early Cambrian volcano-sedimentary sequence of dolomite and volcanic rocks (Esfordi Formation). The volcanic rocks range mainly from rhyolite to rhyodacite, and are high-K calc-alkaline in composition. Their U-Pb zircon ages are in between 529 to 554 Ma (Ramezani & Tucker, 2003). The metamorphic and volcano-sedimentary sequences are intruded by Cambrian plutonic rocks which vary in composition from granite to granodiorite and gabbro-diorite with calc-alkaline signature. These plutonic rocks have been dated in the Saghand area from 525±7 Ma to 533±1 Ma (U-Pb on zircon; Ramezani &

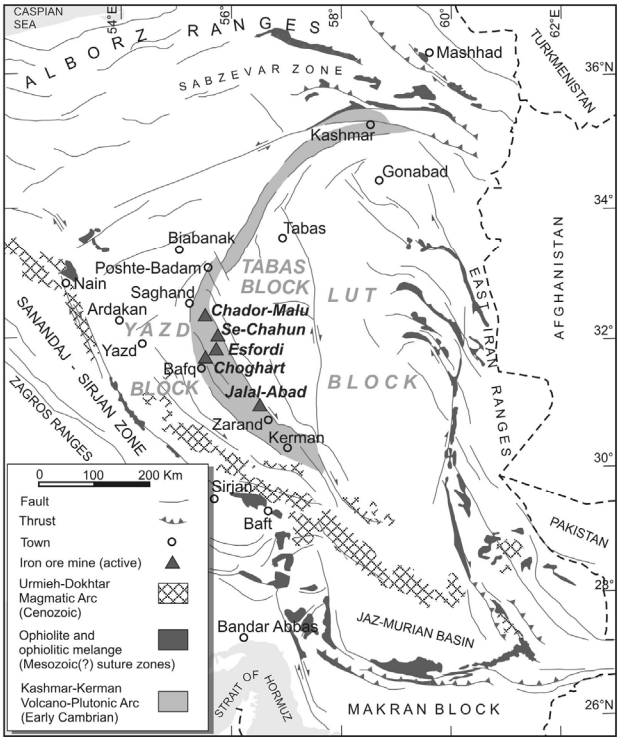


Figure 1. Structural map of Central Iran (modified from Ramezani & Tucker, 2003) and location of major magnetite-apatite deposits in the Bafq mining district

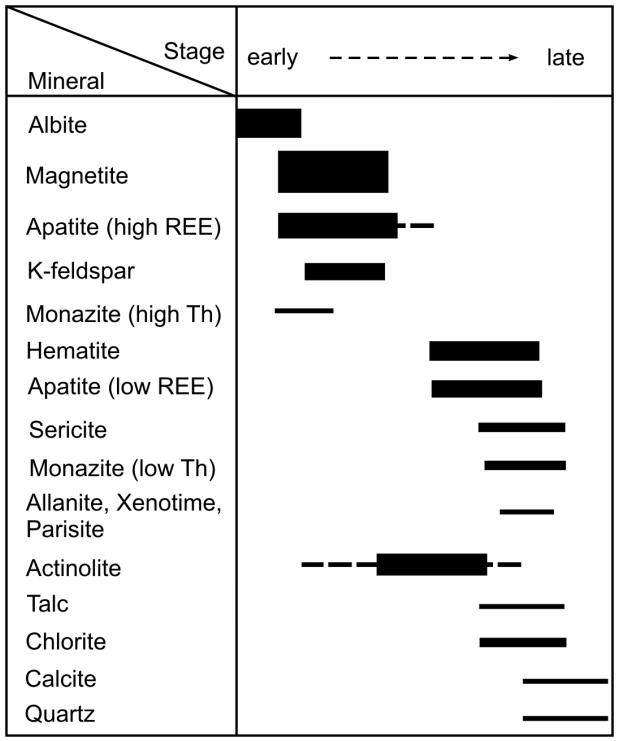


Figure 2. Paragenesis of ore minerals and associated alteration assemblage.

Tucker, 2003). The magnetite-apatite ore systems are mainly replacive in the volcano-sedimentary Esfordi Formation and display a characteristic alteration zoning (Torab & Lehmann, 2006). Their geological framework is similar to the Chilean iron ore belt in the Andean Coastal Cordillera, which, however, formed in the Cretaceous.

## 3 MINERALOGY

The magnetite-apatite deposits show a spectrum of mineralization styles such as massive orebodies, metasomatic replacements, veins and stockworks. Fig. 2 summarizes the paragenetic sequence of ore minerals and alteration assemblages. Although the main iron mineral is magnetite, all gradations towards hematite (martitization) can be recognized. Some primary haematite is found in drill core.

Apatite, the second most abundant mineral after magnetite, is characterized by fluorapatite with small amounts of hydroxyl, but no chlorine or carbonate. Fine- and coarse-grained apatite occurs in varying proportions with magnetite, ranging from sporadic grains to relatively pure apatite veins.

Other hydrothermal minerals are actinolite, quartz, calcite, albite, K-feldspar, sericite, chlorite, talc, sphene, and epidote. Monazite, and relatively rare parisite, allanite and xenotime, occur particularly in those deposits with high apatite content.

## 4 APATITE-MONAZITE RELATIONSHIP

Under high-contrast BSE imaging, some apatite crystals show a heterogeneous pattern with two different domains: dark and bright phases (Fig. 3A). The difference between both phases is mainly due to different concentration of REE and some trace elements, such as Si, Na, Cl, and F (Fig. 4).

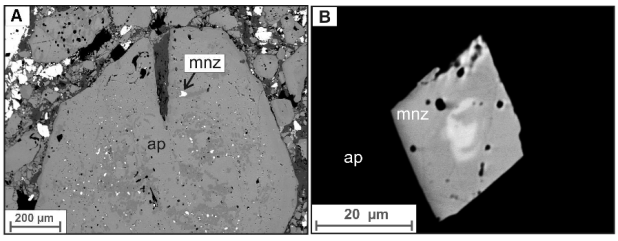


Figure 3. BSE images: A- Euhedral crystal of apatite (ap) with numerous small monazite (mnz) inclusions in the dark apatite phase. B- Euhedral monazite (mnz) crystal overgrown on a high-Th monazite core.

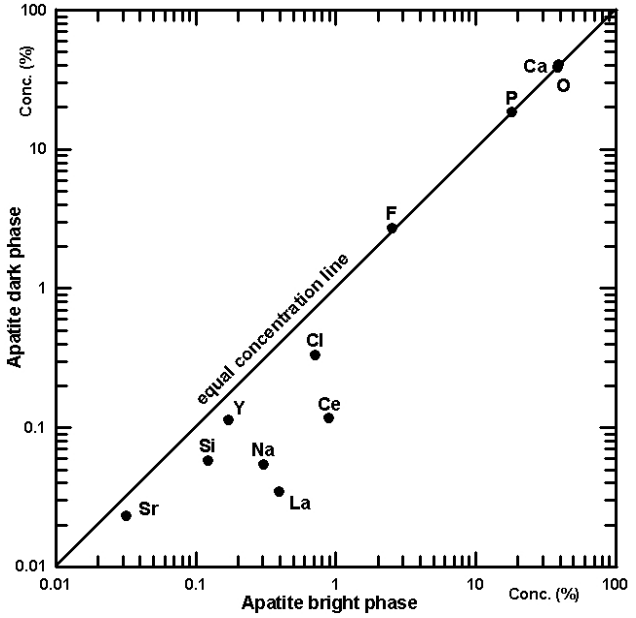


Figure 4. Comparison between element concentration in bright and dark BSE domains of apatite crystals.

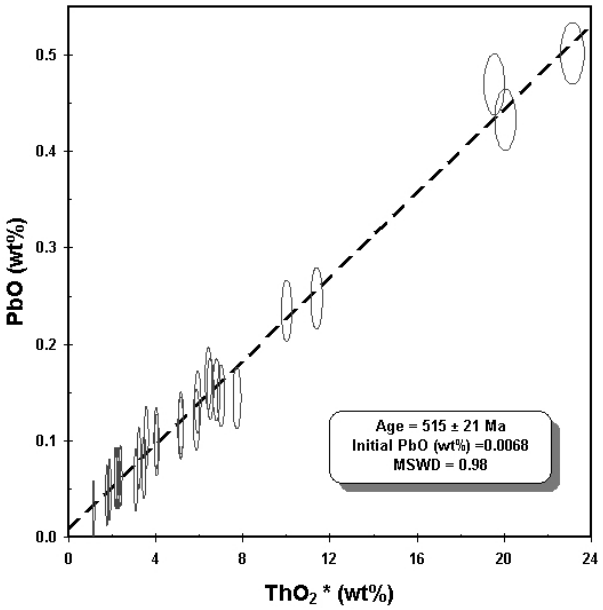


Figure 5. Plot of PbO vs. $ThO_2$* for 27 analytical points of high-Th monazite cores. $ThO_2$* is the measured $ThO_2$ content plus $ThO_2$-equivalent $UO_2$.

The dark (REE-poor) domains host abundant monazite inclusions suggesting a process of REE redistribution with depletion in the host apatite and concomitant nucleation of monazite crystals. The same overprint process also leads to nucleation of other rare REE minerals, such as allanite, xenotime and parisite, and crystallization of major alteration components such as actinolite, talc, and chlorite along the apatite grain boundaries.

Monazite also occurs as relatively large (up to 200 μm), isolated grains along apatite grain boundaries, intergrown with magnetite and silicate minerals. Most of these monazite crystals are homogeneous and do not show significant zoning.

Some samples from the Choghart deposit have individual (usually euhedral) monazite crystals with an irregularly shaped core of relatively high Th content (Fig. 3B). We believe that this core is a high temperature microcrystal of monazite which has been affected by epitactic hydrothermal overgrowth.

## 5 MONAZITE GEOCHRONOLOGY

We used the chemical Th-U-total Pb dating method by electron microprobe analysis. Most monazite is below the analytical detection limit of Th, U and Pb. However, relatively rare high-Th core zones from the Choghart deposit (see *e.g.* Fig. 3B) were found suitable for electron microprobe analysis. The age of each analytical point was calculated according to the iteration method of Suzuki & Adachi (1991). The calculated data (PbO versus $ThO_2$*) define an isochron with a reliable age of 515 ± 21 Ma, and an initial PbO of 0.0068 wt%.

On the assumption that monazite has no initial lead (Parrish, 1990), the isochron can be forced to pass through the origin. Then the slope of the line slightly increases and the age becomes 529 ± 21 Ma. Therefore, according to these two different ways of estimation, the age of the high-Th monazite is estimated in between 515± 21 and 529± 21 Ma.

## 6 METALLOGENIC OUTLOOK

The magnetite-apatite deposits of the Bafq metal district are in an early Cambrian volcano-plutonic arc. The geotectonic situation places the ore deposits in a geological framework similar to the Cretaceous Chilean iron belt in the Coastal Cordillera of the South American Andes.

Our calculated monazite age (515± 21 to 529± 21 Ma) of the ore overlaps with the Cambrian age of the volcano-plutonic host rock sequence (U-Pb, 525± 7 to 533± 1 Ma, Ramezani & Tucker, 2003).

Extensive circulation of sodium-rich saline fluids is reflected in widespread sodic alteration (albitization). This alteration is earlier than the magnetite-apatite mineralization and occurs at deeper levels. Potassic alteration occurs in up-

flow zones. In this situation, due to cooling and reaction with dolomitic country rocks, magnetite and apatite precipitate. This process is succeeded by actinolitization (especially in dolomitic host rocks), and lower temperature hydrolytic and sericitic alteration in volcanic rocks. Low-Th hydrothermal monazite forms at this stage due to apatite metasomatism.

Both late Proterozoic and Cambrian evaporites are widespread in Central Iran (Zharkov, 1984; Banerjee & Mazumdar, 1999). The shallow felsic magmatism of the Cambrian volcano-plutonic arc is likely to have set up convection systems with large-scale metal leaching by highly saline waters as described by Barton & Johnson (1996). These systems formed ore deposits of the iron-phosphorus end-member of the IOCG family.

This study suggests a new exploration potential for the more than 1000km-long Kashmar-Kerman Tectonic Zone in Central Iran which may host other iron oxide-apatite deposits. Our bulk-rock chemical data from the magnetite-apatite systems display very low abundances of uranium, copper and gold. However, given suitable depositional conditions (*e.g.* sulphide traps), other members of the IOCG deposit spectrum may be present.

## ACKNOWLEDGEMENTS

The authors would like to thank the managers of the Choghart, Esfordi and Chador-Malu mines for access to the deposits, sampling and support during field work.

Special thanks are also due to Klaus Herrmann for his kind assistance with electron microprobe analysis, Ulf Hemmerling for help with sample preparation, and Fred Türck for computer support.

## REFERENCES

Banerjee DM, Mazumdar A (1999) On the Late Neoproterozoic-Early Cambrian transition events in parts of east Gondwanaland. *Gondwana Research* 2: 199-211.

Barton MD, Johnson DA (1996) Evaporitic-source model for igneous-related Fe oxide-(REE-Cu-Au-U) mineralization. *Geology* 24: 259-262.

Haghipour A (1977) Geological map of the Biabanak-Bafq area (scale 1:500,000). *Geological Survey of Iran.*

Parrish RR (1990) U-Pb dating of monazite and its application to geological problems. *Canadian Journal of Earth Sciences* 27: 1431-1450.

Ramezani J, Tucker RD (2003) The Saghand region, Central Iran: U-Pb geochronology, petrogenesis and implications for Gondwana tectonics. *American Journal of Science* 303: 622-665.

Suzuki K, Adachi M (1991) Precambrian provenance and Silurian metamorphism of the Tsubonosawa paragneiss in the South Kitakami terrane, Northeast Japan, revealed by the chemical Th-U-total Pb isochron ages of monazite, zircon and xenotime. *Geochemical Journal* 25: 357-376.

Torab FM, Lehmann B (2006) Iron oxide-apatite deposits of the Bafq district, Central Iran: an overview from geology to mining. *World of Mining - Surface and Underground* 58: 355-362.

Zharkov MA (1984) *Paleozoic salt bearing formations of the world*. Berlin: Springer-Verlag. pp 427.

# Fluorine concentration in fluids related to the Los Santos scheelite skarn deposit (NW Spain)

S.M. Timón & M.C. Moro
*Dpio. Geología, Cristalografía y Mineralogía. Facultad de Ciencias, Universidad de Salamanca, Spain*

ABSTRACT: Fluorine-bearing minerals such as chondrodite, norbergite, clintonite, chlorite and F-rich mica in the Los Santos dolomite marbles indicate that F metasomatism has accompanied the contact metamorphism. The low HF concentration of $10^{-2.46}$ to $10^{-3.03}$ mol/dm$^3$ estimated using experimentally calibrated phlogopite and biotite fluorimeters, is similar to that calculated in other marbles and skarns related to magmatic or hydrothermal fluids equilibrated with a granite rock.

KEYWORDS: fluorine, skarn deposits, tungsten, Los Santos, Spain

## 1 INTRODUCTION

Fluorine contents of phlogopite, pargasite, chlorite and humite-group minerals present in dolomite marbles, as well as fluorine in biotite in siliceous hornfelses, and the occurrence of fluorapatite and fluorite, suggest that F has played an important role during the Los Santos skarn formation. Fluorine is a common constituent in mineralized skarn systems, especially if the skarn is related to leucogranites and pegmatites. The concentration of HF in fluids broadly correlates with the composition of granitoids, skarn type, and physico-chemical conditions. The study of this halogen element is important because it affects the structure of granitic melts and minerals like mica, and can play an important role in mobilization of ore elements, such as U, W, Mo, Be, Sn, REE that may form soluble fluoride complexes in hydrothermal fluids (Zhu & Sverjensky, 1991).

The aim of this paper is to show the distribution of fluorine between coexisting phases in the Los Santos dolomite marbles, to determine the HF concentration in the hydrothermal fluid and to compare it with that of other marbles and mineralized skarns. Finally, we shall discuss the origin of fluorine.

## 2 GEOLOGIC SETTING

The Ávila Batholith is the most extensive continuous outcrop of granitoids in the Iberian Variscan Belt. The study zone is located in the northwestern part of this igneous complex, where granodiorites and monzogranites outcrop. In the Los Santos area, they are crosscut by fine-grained granites, tourmaline-bearing aplites and pegmatites. The emplacement of granitoid bodies, during the late- to post- main Variscan tectonic events, caused contact metamorphism of late Vendian-early Cambrian metasedimentary rock accompanied by intense metasomatism and development of the Los Santos tungsten skarn. This W-bearing calcic mesozonal reduced skarn is one of the more significant scheelite mineralization of the Iberian Peninsula, the total tonnage is about 2.5 Mt at 0.58%$WO_3$ (Crespo *et al*. 2000).

Contact metamorphism accompanied by metasomatism generated the following mineral assemblages: cordierite, K-feldspar, andalusite ± sillimanite in the metapelitic rocks; diopside, forsterite, phlogopite ± clintonite ± pargasite and humites (norbergite and chondrodite) and spinel-bearing assemblages in the dolomite marbles; and diopside, grossular, vesuvianite ± wollastonite in the calcic marbles. Mineral assemblages of marbles and hornfelses indicate pressure conditions ranging from 2.0 to 2.5 kb, and maximum temperatures between 630 and 640ºC. $^{13}C$ and $^{18}O$ depletions in calcic marbles are consistent with hydrothermal fluid-rock interaction during metamorphism. Microthermometric analyses of fluid inclusions from vesuvianite indicate that the fluid is water

dominant with minor contents of $CO_2$ (± $CH_4$ ± $N_2$) (Timón *et al*. in press). This previous metasomatic column is superimposed by an important hedenbergite skarn that, according to Einaudi *et al*. (1981), can be classified as a calcic reduced tungsten skarn.

## 3 PARTITIONING OF FLUORINE BETWEEN COEXISTING PHASES

Humite group minerals can appear in metamorphosed impure carbonate rocks during low-pressure contact metamorphism and metasomatism, involving the introduction of fluorine and reaction with pre-existing silicates (Piazolo & Markl, 1999). Other authors point out that humites can also form in regionally metamorphosed zones not spatially related to an igneous body, by isochemical reactions involving (OH-F) silicates, such as calcic amphibole, chlorite, phlogopite, and $H_2O$-$CO_2$-rich fluids (Moore & Kerrick, 1976). The study of humites from Los Santos shows evidence that supports the first hypothesis but not the second. Rice (1980a,b) argues that the prograde sequence clinohumite → chondrodite→ norbergite is inconsistent with the isochemical model. He suggests that the formation of norbergite results from metasomatic introduction of fluorine into the system after the formation of clinohumite and/or chondrodite. Norbergite formation requires high fluorine content and if a high ratio of F/(F+OH) is already present in the protolith, norbergite will form first (Rice, 1980b). The order of preference of F relative to OH is:

norbergite $X_F = 0.45$ > chondrodite $X_F = 0.41$ > phlogopite $X_F = 0.08$ > clintonite $X_F = 0.05$ > pargasite $X_F = 0.045$ > chlorite $X_F = 0.0108$

This sequence of partitioning of F during prograde metamorphism is in accordance with that described by Rice (1980a), *i.e*. clinohumite > phlogopite > tremolite > chlorite.

## 4 ESTIMATION OF HF CONCENTRATION IN THE FLUID

The fluorine concentration in the hydrothermal fluid has been estimated using the experimentally calibrated mineral fluorimeters by Aksyuk & Zhukovskaya (1994) and Aksyuk (2000) at high temperature and pressure.

### 4.1 *Phlogopite fluorimeter*

Aksyuk & Zhukovskaya (1994) give the following equation to estimate the HF concentration in a fluid equilibrated with F-phlogopite at a temperature interval of 500 to 700ºC and 1 to 4 kbar pressure:

$$\log M_{HF}\,(T, P) = X_{Mg}\,[\log (X_F/(1\text{-}X_F)) - 1722/T - 0.2112] + \log a_{H2O}$$

where $M_{HF}(T, P)$ is concentration of HF in the fluid in mol/dm$^3$ at absolute temperature (K) and pressure of interest; $X_{Mg}$ is the mole fraction of Mg in the octahedral sites and $X_F$ is the mole fraction of F in the hydroxyl sites of phlogopite; $a_{H2O}$ is the activity of water in fluid expressed as $\gamma_{H2O}X_{H2O}$, where $X_{H2O}$ is mole fraction and $\gamma$ is an activity coefficient of water at T-P of fluid. Transition from $M_{HF}$ (mol/dm$^3$) units to $m_{HF}$ (mol/kg of $H_2O$) can be obtained dividing $M_{HF}$ by the density of water at T-P of interest.

This fluorimeter has been used for the chemical data of the phlogopite in dolomite marbles. Phlogopite has $X_{Mg}$ ranging from 0.86 to 0.93, and $X_F$ = 0.05-0.19. The calculations have been made at 640ºC, estimated maximum temperature for the contact metamorphism in the study zone, and using $a_{H2O} = 1$. The analyses of fluid inclusions indicate the fluid is water dominant, therefore an ideal HF-$H_2O$ solution can be assumed in which other components ($CO_2$, $CH_4$, $N_2$) have a negligible effect on F distribution between fluid and phlogopite (Aksyuk & Zhukovskaya, 1994). Bearing in mind all these considerations, the values obtained from log $M_{HF}$ range from -2.73 to -3.03.

The HF concentration in fluid associated with the Los Santos marbles is similar to the HF concentration estimated for phlogopite formation in marbles of different localities: for example, phlogopites with $X_F = 0.2$ and $X_{Mg} = 0.975$ were described in magnesian skarns of the magmatic stage in the Spanish Central System, where the conditions were estimated as 660ºC and 2-3 kbar (Casquet & Tornos, 1984). Assuming $a_{H2O} = 1$, the phlogopite fluorimeter gives log $M_{HF} = -2.59$. In fluids associated with marbles of the Adirondack Mountains (USA), at 650ºC and 6 kbar, phlogopite gives $X_F = 0.57$, $X_{Mg} = 0.97$, and $a_{H2O} = 0.07$, and log $M_{HF}$ is -3.05 (Aksyuk & Zhukovskaya, 1994).

### 4.2 *Biotite fluorimeter*

Aksyuk (2000) gave the equation of the biotite fluorimeter as follows:

$$\log M_{HF}\,(bt) = \log (X_F/(1\text{-}X_F)) - 1722/T - 1.107\,X_{Mg} + 0.216\,(Al\text{-}2) + 0.8958 + \log a_{H2O}$$

This equation takes into account the composition of biotite solid solution and fluid: $X_F$ = F/4; $X_{Mg}$ = Mg/$S_{oct}$; F, Mg and Al are numbers of the chemical formula of biotite calculated for 22 oxygen atoms; $S_{oct}$ is the sum of cations in octahedral sites in the formula of biotite; and $a_{H2O}$ is the activity of water in the fluid under the given P-T conditions.

In siliceous hornfelses of Los Santos, $X_F$ of biotite varies from 0.02 to 0.06, $X_{Mg}$ from 0.36 to 0.37, and the Al content is ~ 2.6. The biotite fluorimeter gives a log $M_{HF}$ ranging from -2.46 to -2.96.

## 5 DISCUSSION

The geological, chemical, isotopic and fluid inclusion study of the Los Santos W skarn deposit suggest that deep fluids of likely magmatic/metamorphic origin were dominant at least during the formation of the early skarn (Timón, *unpublished data*). These fluids and metals probably derive from the adjacent granitoids, from the host metasediments and a deep but unexposed leucogranite. Tornos *et al.*, (2001) proposed that this highly evolved granite probably is equivalent to those granites hosting the widespread W-Sn veins in the Iberian Variscan Belt.

The estimate of the HF concentration related to different granites, pegmatites, marbles and skarn deposits, shows that there are two trends of fluorine behaviour in the magmatic fluid: (1) a high F- trend, typical of rare metal leucogranite, Li-F granite and pegmatite, and related W, Be, U, Th, REE, Ta, Nb, Li and Sn skarn deposits; the HF concentration in the fluids associated with these rocks is $10^{-1.5}$ to $10^{-1}$ mol/dm$^3$ and remains constant, although formation temperatures vary from 900 to 500ºC; (2) a low F-trend, characteristic of barren diorite, tonalite, granodiorite, and granite plutons and porphyry Cu and Mo deposits, as well as F-poor phlogopite, scheelite, and other base metal skarn deposits. The HF concentration in the fluids related to these rocks decreases with the formation temperature. At low temperature, the HF concentration is lower than in the high F-trend, e.g., at 500ºC, it ranges from $10^{-3}$ to $10^{-2.6}$ mol/dm$^3$.

The diagram $M_{HF}$-T (Fig. 1) shows the zones defined by the two trends of fluorine evolution described previously, the HF concentration in samples from marbles and skarn formation, taken from Aksyuk (2000), and the values of log $M_{HF}$ calculated from the micas of the Los Santos marbles.

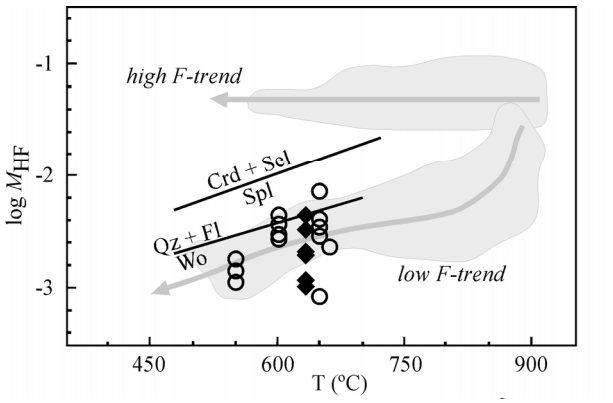


Figure 1. The HF concentration (M. mol/dm3) in fluids related to the high F and low F granitoid trends, marbles and skarn formations (open circles) (Data were taken from Aksyuk, 2000). Black rhombus correspond to the HF values estimated using the phlogoptite and biotite fluorimeters in the Los Santos marbles.

As can be observed, log $M_{HF}$ ~ -2.7 mol/dm$^3$ in the fluid related to the Los Santos skarn formation plots into the low F-trend. This fact reveals an apparent contradiction: supposing that the fluid derived from the unexposed leucogranite plays a decisive role in the formation of the Los Santos skarn, it could be expected that the HF concentration belongs to the high F-trend.

The comparative study realized by Aksyuk (2000) about the behaviour of fluorine in skarn-granitoid fluid systems from different localities shows that the HF concentration in most skarn fluids is relatively low (at 500ºC, log $M_{HF}$ ~ -2.8), although the formation temperatures of associated granitoids were different and although the fluid may be originally derived from granitoids of either the high or low F trends. The calculated skarn fluid values lie close to and below those of the low F trend of granitoid systems. The explanation should be sought in the skarn assemblages themselves which represent a mineral buffer for the ore-forming fluid (Aksyuk, 2000). For example, the coincidence of the plot of the calculated skarn fluid values and the location of the Qz-Wo-Fl-$H_2O$-HF equilibria, shows that the activity ratios of Ca, Si, and F species in the fluid were probably close to those of the skarn equilibria (Fig. 1). In the Los Santos exoskarn it is common to find fluorite (± calcite). Therefore, the activity of Ca and solubility of fluorite in the fluid could have been a buffer in the same way as to the previous assemblage. Decreasing temperature and/or the HF concentration in the fluid during exoskarn

formation may cause a breakdown of fluoride complexes, resulting in the deposition of ore components.

ACKNOWLEDGEMENTS

This work was supported by the Comunidad Autónoma de Castilla y León (Research Project Ref. SA015A06)

REFERENCES

Aksyuk AM & Zhukovskaya TN (1994) Experimental calibration of phlogopite fluorimeter at 500-700 ºC and 1-4 kbar, and estimated HF concentrations of fluids associated with marble: Some examples. *Geochim Cosmochim Acta* 58: 4305-4314.

Aksyuk AM (2000) Estimation of fluorine concentrations in fluids of mineralized skarn systems. *Econ Geol* 95: 1339-1347.

Crespo JL, Rodríguez P, Moro MC, Cabrera R, Conde C, Fernández A, Rodríguez I (2000) El yacimiento de scheelita de Los Santos (Salamanca). *Geotemas* 1-4: 25-28.

Casquet C, Tornos F (1984) El skarn de W-Sn del Carro del Diablo (Sistema Central Español). *Bol Geol Min* CXVI: 58-79.

Einaudi MT, Meinert, LD, Newberry RJ (1981) Skarn deposits. In: Skinner B (ed) *Econ Geol, 75th Anniv Vol,* 317-391.

Moore JN, Kerrick DM (1976) Equilibria in siliceous dolomite of the Alta aureole, Utah. *Am J Sci* 276: 502-524.

Piazolo S, Markl G (1999) Humite- and scapolite-bearing assemblages in marbles and calc-silicates of Droning Maud Land, East Antarctica: new data for Gondwana reconstructions. *J Metamorph Geol* 17: 91-107.

Rice JM (1980a) Phase equilibria involving humite minerals in impure dolomitic limestones, Part I. Calculated stability of clinohumite. *Contrib Mineral Petr* 71: 219-235.

Rice JM (1980b) Phase equilibria involving humite minerals in impure dolomitic limestones. Part II. Calculated stability of chondrodite and norbergite. *Contrib Mineral Petr* 75: 205-223.

Timón SM, Moro MC, Cembranos ML, Fernández A, Crespo JL (in press) Contact metamorphism in the Los Santos W skarn (NW Spain). *Mineral Petro*l DOI 10.1007/s00710-006-0166-0.

Tornos F, Galindo C, Spiro BF (2001) Isotope geochemistry of Los Santos (Spanish Central System) calcic scheelite skarn: constraints on the source of the fluids and tungsten. In: Piestrzynsky et al., (eds) *Mineral Deposits at the Beginning of the 21st Century*. Swets & Zeitlinger Publishers Lisse, 921-924.

Zhu C, Sverjensky DA (1991) Partitioning of F, Cl and OH between minerals and hydrothermal fluids. *Geochim Cosmochim Acta* 55: 1837-1858.

# Preliminary results of geochemical and ore-microscopic studies of Mo-Cu mineralization from the Bedkowska Valley near Kraków (Poland)

S.Z. Mikulski[1], M. Markowiak[2] & S. Oszczepalski[1]
[1]*Polish Geological Institute, 4 Rakowiecka St., 00-975 Warsaw, Poland*
[2]*Polish Geological Institute, 1 Królowej Jadwigi St., 41-200 Sosnowiec, Poland*

ABSTRACT: Mo-Cu mineralization occurs in steeply dipping quartz veins which cut an almost 1 km thick sequence of Ediacarian clastic metasedimentary rocks and Variscan porphyritic dykes. High-temperature molybdenite is associated with chalcopyrite and pyrite, and overprinted by base metal sulphides with carbonates. The quartz-sulphide mineralization is associated with only narrow metasomatic alteration haloes within the nearest surroundings of veins. Geochemical investigations revealed no statistically significant correlation between Mo, Cu and W. Our observations suggest an origin of the main stage of molybdenite (-chalcopyrite-pyrite) in quartz veins from post-magmatic-contact metamorphic hydrothermal processes during rapid late Variscan uplift.

KEYWORDS: molybdenite, Mo, Cu mineralization, geochemistry, Bedkowska Valley, Poland

## 1 INTRODUCTION

The regional NW-trending Hamburg-Kraków tectonic zones in south-central Poland hosts a late Carboniferous volcano-plutonic belt. This zone between Lubliniec-Kraków separates two geotectonic blocks: the Upper Silesian Block and the Malopolska Block (Bula 2000; Bula *et al.* 2002).

Drilling in the years 1985-1993 revealed several areas with intensive Mo-Cu sulphide mineralization with scheelite, and the Myszków Mo-W-Cu deposit was discovered.. Several stages of molybdenite mineralization in quartz veins and stockworks were described as closely spatially associated with granodiorite intrusions (Slósarz 1985; Piekarski 1995) and classified as of calc-alkaline porphyry type formed at about 300 Ma (Podemski *et al.* 2001).

Recent Re-Os studies of molybdenite from Myszków detected moderate-low concentration of Re what argues against a subduction-related porphyry origin and may indicate crustal melting (Stein *et al.*, 2005). We present preliminary results of geochemical and ore-microscopic studies of drillcore from the borehole WB-102A, located in the Bedkowska Valley about 60 km SE from the Myszków deposit (Fig. 1).

## 2 GEOLOGICAL SETTING

The Bedkowska Valley is located *ca.* 15 km NW from Kraków on the Malopolska Block between Beblo, Jerzmanowice and Bedkowice. Ten boreholes were drilled along a line of SW-NE direction perpendicular to the trend of the regional shear zone.


Fig. 1. Location of the WB-102A borehole with schematic extent of granodiorite intrusions between Myszków and Kraków

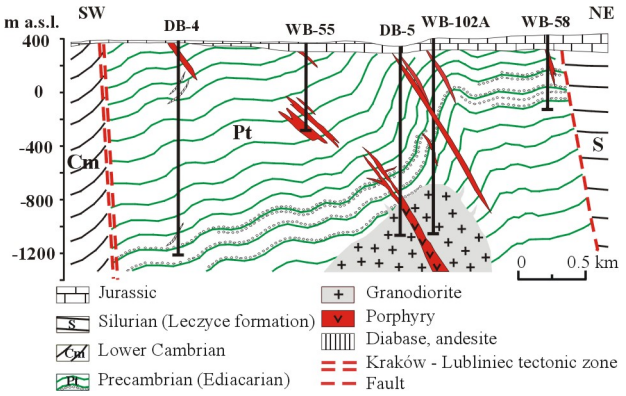


Fig. 2. Geological cross-section through the Bedkowska Valley modified from Piekarski & Markowiak 1988 unpublished

The Bedkowska Valley is intimately associated with the Lubliniec-Kraków tectonic zone to the west, and with another tectonic fault to the east, which separates (under Mesozoic cover) Ediacarian from Silurian clastic rocks of the Lapczyce formation (Fig. 2).

Three major rock units can be distinguished in the Bedkowska Valley:

- Cenozoic cover of Quaternary sands and loams up to a several meter thick;
- Mesozoic calcareous sedimentary rocks of Middle and Upper Jurassic age with intercalation of Lower Jurassic clastic sediments of up to a few dozens of meter in thickness;
- Ediacarian clastic sedimentary rocks.

The latter rock complex is represented by primarily clayey to muddy to sandy metasediments with minor metaconglomerates that were regionally metamorphosed under greenschist facies condition (Bula 2000). The metaconglomerate contains fragments of poorly rounded rocks from 0.5 to 5 cm in size, representing various rock types (sedimentary, magmatic and metamorphic) and fragments of quartz veins as well. Ediacarian clastic rocks occur at shallow levels, from 13 to 100m below surface. They are strongly folded and penetrated by a late Carboniferous narrow granodiorite intrusion and numerous subvolcanic dykes of dacite and rhyolite porphyries and veins of diabase, andesite, and quartz. Granodioritic-dacitic intrusive rocks were encountered at a depth of ca. 1.1 km only in two boreholes (WB-102A and DB-5). The medium-grained granodiorites are peraluminous, with initial $^{87}Sr/^{86}Sr$ ratios from 0.705-0.706 and belong to the calc-alkaline series. Geochemical characteristics indicate that these granites were derived from inhomogeneous crustal sources. The metasedimentary rocks were subject of variable contact metasomatic alteration within a zone up to 1.5km away from the intrusion margin (Markowiak & Habryn, 2003, unpubl.) under conditions corresponding to the orthoclase-cordierite facies of thermal metamorphism (Koszowska & Wolska, 2000).

## 3 PRELIMINARY RESULTS OF ORE MICROSCOPY

Ore mineralization in the borehole WB-102A is represented mainly by pyrite, chalcopyrite and molybdenite. Less frequent are marcasite, galena, sphalerite, arsenopyrite and scheelite. These ore minerals are of epigenetic type and occur in veins (2-30mm thick) and impregnations. Veins dip almost vertical or steeply (55-85°). The veins are commonly scattered throughout the whole sequence of folded Ediacarian metasedimentary rocks, as well as within porphyry dykes, andesite veins and granodiorite. Sulphides occur also in narrow streaks, veinlets and as impregnation. It is possible to observe several quartz veinlet generations with sulphides, which intersect cores at different horizons. The most common paragenetic mineral associations are:

- Quartz-feldspar-molybdenite;
- Quartz-chlorite-molybdenite-pyrite-chalcopyrite;
- Quartz-scheelite;
- Carbonate- quartz-base metal sulphides;
- Marcasite-chlorite.

Molybdenite occurs in form of irregular aggregates in association with pyrite or chalcopyrite. Aggregates are embedded in white-milky mosaic quartz (Fig. 3). Molybdenite may also occur as veinlets infilling fractures and very fine euhedral crystals (0.1-0.2 mm in diameter) on fractured surfaces. The association of molybdenite with minute wolframite inclusions and fine euhedral cassiterite crystals were rarely observed. Less frequently molybdenite occurs at a depth below 1.1 km where quartz veinlets cut granodiorite. Instead, more abundant scheelite appears there. Chalcopyrite and molybdenite mineralization is widespread and commonly associated with sericitization, silicification, chloritization and pyritization. Additionally, molybdenite is often accompanied by pink K-feldspar. Hydrothermal alteration is found almost exclusively within the nearest surroundings of the quartz-molybdenite veinlets into metasedimentary rocks and porphyry dykes as well. Biotitization was noticed in deeper parts of the drillhole near granodiorite intrus-

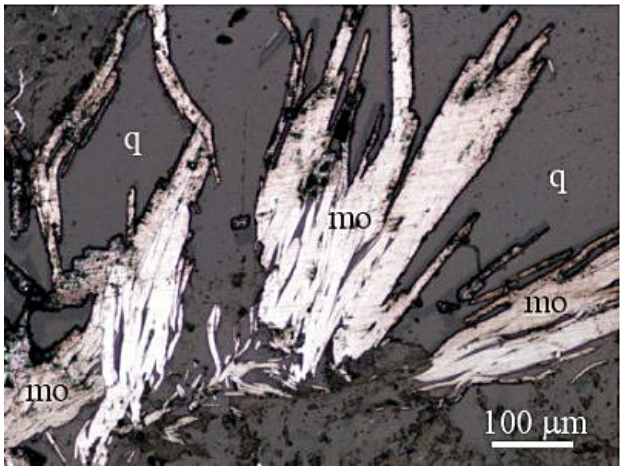


Fig. 3. Molybdenite flakes form irregular aggregates in quartz vein cutting shale. Borehole WB-102A, depth 920m. Symbol explanation: mo – molybdenite; mg – magnetite; q – quartz

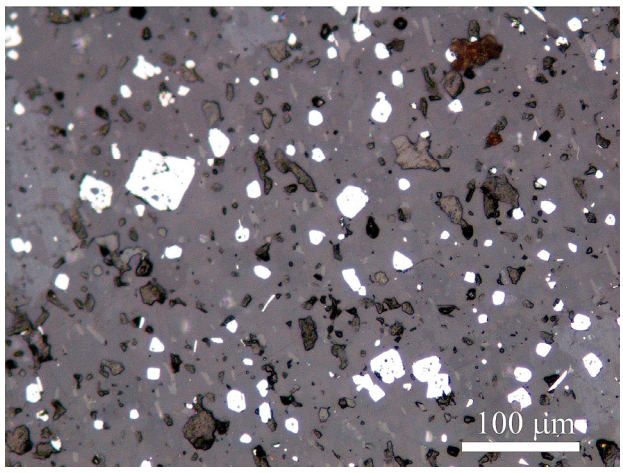


Fig. 4. Abundant disseminated euhedral fine-grained magnetite (white) in black shale. Borehole WB-102A, depth 922m

ions. In some horizons of black shales appears dense finely dispersed magnetite mineralization, less frequently pyrrhotite and chalcopyrite microlites. Euhedral magnetite grains up to 10-50 µm in diameter are equally distributed in dark shale (Fig. 4). Disseminated magnetite in black shale is considered as of metamorphic origin, and is intersected by quartz-pyrite and quartz-molybdenite veins and chalcopyrite-pyrite-pyrrhotite streaks. Carbonate (ankerite, calcite) and base metal sulphides are subordinate and cemented brecciated rocks. They also overprint older fractured quartz-molybdenite-Cu-sulphide veins. Chalcopyrite, pyrite and traces of sphalerite, and galena and Cu-Pb-Bi-S sulphosalts occur in quartz-ankerite veinlets.

The Cu-Mo quartz-vein mineralization in the Bedkowska Valley was considered by Haranczyk (1978; 1985) as of porphyry-style origin. However, its is also possible to interpret this mineralization as result of hydrothermal remobilization during complex post-magmatic and contact metamorphic processes during uplift of the Variscan orogen.

## 4 GEOCHEMICAL INVESTIGATION OF THE ORE MINERALIZATION

The vertical distribution of metals is shown in Figure 4. Typically, granodiorite rocks are not enriched in metallic elements when compared to granite averages. Most metal enrichment has been observed only in the upper part of the section studied which is represented by the metasedimentary sequence, highly fractured and veined with quartz and carbonates. Cu and Mo mean values are higher in the metasedimentary rock unit in comparison to average shale. Copper values are highest in the metasedimentary rocks and porphyry dikes, reaching up to 0.35 % Cu. Elevated Cu contents have been also revealed in an andesite layer (0.34 % Cu at the depth of 402.5 m) and locally in conglomerates (up to 918 ppm).

Copper content averages 630 ppm in conglomerates, 274 ppm in other metasedimentary rocks and 260 ppm in porphyries, contrasting with granodiorite that contains barely 15 ppm Cu on average. Locally, quartz veinlets contain as much as *ca*. 540 ppm Cu. Molybdenum contents up to 1477 ppm Mo at the topmost part of the section studied, where it is mostly concentrated in quartz veinlets that cut the metasedimentary sequence, gradually decrease with depth, reaching ≤13 ppm in granodiorite. Mo also is enriched in a few samples of metasedimentary rocks, ranging up to 634 ppm. In contrast to copper and molybdenum, W, Pb and Zn concentrations are low. The source of Cu, Mo and other metals could also be Ediacarian clastic rocks as earlier postulated by Piekarski (1982) and Stein *et al*. (2005).

W reaches as high as 236 ppm in granodiorite, but Pb and Zn contents are highest in mudstones (436 and 765 ppm, respectively). Other metals are erratic in occurrence.

The ratio of base metal (Cu + Pb + Zn) contents to W + Mo contents indicates that the distribution of these metals is not vertically zoned relative to the granodiorite intrusion, however, this ratio seems to show a tendency to an increase in andesites and porphyries.

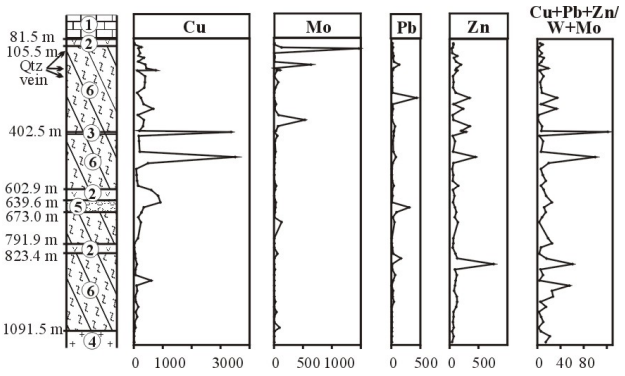


Fig. 4. Variation of Cu, Mo, Pb and Zn contents (in ppm) in the WB-102A section. 1 – Limestone; 2 – Dacite porphyry; 3 – Andesite; 4 – Granodiorite 5 – Metaconglomerate; 6 – Ediacarian metasedimentary rock complex (mudstone, claystone and sandstone); Qtz –quartz

Metasedimentary rocks show strong positive correlation between Pb and Zn, whereas W, Cu and Co correlate in porphyries.

In granodiorite, W shows a positive correlation with Bi, and Cu with Pb. There is no statistically significant correlation between W and Mo, Cu and Mo, nor Cu and W.

## 5 CONCLUSIONS

The preliminary data on ore mineralization in clastic Ediacarian metamorphic rocks cut by Upper Carboniferous granodiorite and rhyolite porphyry dykes from the borehole WB-102A in the Bedkowska Valley indicate:

1) Epigenetic and multiple character of hydrothermal sulphide mineralization. Molybdenite-chalcopyrite-pyrite mineralization in quartz veins dominates, overprinted by less frequent base metal sulphides and carbonate;
2) Metasomatic alteration (sericitization, feldspathization, silicification, chloritization and carbonatization) occurs mostly in the nearest surroundings of quartz-sulphide veins;
3) Geochemical investigation does not indicate any correlation between Mo and Cu and any spatial zonation of ore distribution to granodiorite intrusion. Molybdenite is generally associated with quartz-feldspar veins scattered in detritic rocks. Scheelite occurs only in quartz veinlets and patches within granodiorite.

## ACKNOWLEDGEMENTS

The analytical work was supported by the PGI project 6.57.0001.00.0. and NFOSiGW project 2.58.0000.00.0.

## REFERENCES

Bula Z (ed.), Habryn R, Kurek S, Krieger R, Markowiak M, Wozniak P (2002) The Geological Atlas of the Palaeozoic (without Permian) rocks contact between the Upper Silesian and Malopolska Blocks. PGI Warszawa.

Bula Z (2000) The Lower Palaeozoic of the Upper Silesia and West Malopolska. Prace *Panst. Inst. Geol.* v. 171:5-71.

Haranczyk C (1978) Mineralizacja polimetaliczna w utworach paleozoicznych Wsch. obrzeżenia *GZW. Prace IG* 83: 171-182.

Haranczyk C (1985) Paragenezy mineralne w złozach krakowidów i ich pokrywy. *Roczn. Pol. Tow. Geol.* v. 53: 91-126.

Koszowska E, Wolska A (2000) Mineralogical and geochemical study of thermally altered country rocks of granodiorite intrusion in the Bedkowska Valley near Cracow (S Poland). *Ann. Soc. Geol. Poloniae.* v. 70 (4): 261-281.

Piekarski K (1982) Molybdenum schists in the vicinities of Myszków (Eng. Sum.) *Przegl. Geol.* v. 7: 335-340.

Piekarski K (1995) Geologic setting and ore mineralization characteristics of the Myszków area (Poland). *Geol. Quart.* v. 39(1): 31-42.

Podemski M (ed.), (2001) Palaeozoic porphyry molybdenum-tungsten deposit in the Myszków area, Southern Poland. *Polish Geological Institute Special Papers* 6: 1-87.

Slósarz J (1985) Stages and zonality of ore mineralization in Palaeozoic rocks of the environs of Myszków. *Ann. Soc. Geol. Pol.* 53:267-288.

Stein HJ, Markowiak M, Mikulski SZ (2005) Metamorphic to magmatic transition captured at the Myszków Mo-W deposit, southern Poland. *In*: *Mineral Deposit Research: Meeting the Global Challenge* (*eds*. Jingwen Mao, Frank P. Bierlein): 833-836. Springer.

# Microanalysis of ore forming fluids at El Teniente, Chile

V. H. Vry & J. J. Wilkinson
*Department of Earth Science and Engineering, Imperial College London, South Kensington Campus, Exhibition Road, London, SW7 2AZ*

T. Jeffries
*Department of Mineralogy, The Natural History Museum, Cromwell Road, London, SW7 5BD*

J. Seguel
*Superintendencia Geología, El Teniente, CODELCO-CHILE, Millán 1040, Rancagua, Chile.*

D. Cooke
*Centre for Excellence in Ore Deposits, University of Tasmania, Private Bag 79, Hobart, Tasmania 7001, Australia*

ABSTRACT: El Teniente is the world's largest copper deposit yet despite its significance and well constrained geology, relatively little is known about ore-forming processes. In particular, few data exist on the nature and chemistry of the hydrothermal ore forming fluids involved. This study utilises laser ablation inductively coupled plasma mass spectrometry (LA-ICP-MS) to yield compositional information on the fluid inclusions trapped during mineralization.

KEYWORDS: LA-ICP-MS, El Teniente, Porphyry Copper, ore formation

## 1 INTRODUCTION

El Teniente is located on the western margin of the Andean Cordillera, in the central Chilean porphyry belt, along with several other late Miocene-Pliocene copper deposits *e.g.* Los Pelambres and Rio Blanco-Los Bronces (Figure 1). El Teniente hosts over 12 billion tonnes of copper ore with grades averaging >0.67% (Cannell *et al.*, 2005) making it the world's largest copper deposit in terms of contained metal (Cooke *et al.,* 2005). The deposit is also rich in molybdenum, with average Mo grades of 0.019% (Skewes *et al.*, 2002). However, despite its significance in terms of size and copper production, and quite well-constrained geology, relatively little has been published on ore forming processes.

Fluid inclusion microanalysis is important in the study of ore deposits since it represents the only direct means of determining the composition of ancient ore forming solutions. Such studies can therefore make a significant contribution to the understanding of how, why and potentially where hydrothermal ore deposits form. This project aims to constrain the composition of hydrothermal fluids involved in mineralization at El Teniente using LA-ICP-MS microanalysis of single fluid inclusions. The main objectives are to: (1) identify metal concentration changes between successive fluid


Figure 1. Map of Chile showing locations of major porphyry deposits. El Teniente is situated in the central Chilean porphyry belt, south of Santiago.

generations to determine if there are specific, copper-rich stages and if the metal budget of these fluids is anomalous in relation to other porphyry systems; and (2) determine copper sulphide depositional mechanisms. Here, we present a summary of the geology of the deposit and present a framework of hydrothermal precipitation and alteration that will form the basis of our detailed fluid evolution study.

## 2 SUMMARY OF GEOLOGY

Over 80% of the mineralization at El Teniente is hosted in an andesitic sill and stock complex which forms part of the mid-late Miocene Farellones Formation (Figure 2). This was later intruded by a series of felsic intrusives (the Teniente Plutonic Complex), the oldest of which is the Sewell Tonalite, followed by the younger Teniente Dacite porphyry (Figure 3). It has been suggested that the Teniente Dacite porphyry is responsible for the mineralization at El Teniente, making this a typical porphyry copper deposit (Howell & Molloy, 1960; Camus, 1975; Cannell *et al*., 2005). Others have argued that copper mineralization was emplaced by several hydrothermal brecciation events and classify El Teniente as a breccia hosted deposit in line with several other Chilean breccia hosted deposits, *e.g.* Los Pelambres and Rio Blanco-Los Bronces (Skewes *et al.* 2002). The central feature of the deposit is a late to post-mineralization, 1200m wide (at surface) breccia pipe (Cannell *et al.*, 2005), the Braden Formation, consisting of two breccia facies: a mineralized outer tourmaline breccia and an inner barren breccia (Figure 3). The youngest rocks in the vicinity of the deposit are late, post-mineralization felsic intrusives; dacite and latite porphyries; and lamprophyre dikes (Figure 3). The most important hypogene minerals at El Teniente are chalcopyrite, pyrite, bornite and molybdenite (Camus, 1975), with supergene processes producing abundant chalcocite plus minor covellite.

## 3 ALTERATION

Alteration stages at El Teniente were first described by Camus (1975) who designated three alteration types: potassic, quartz-sericite and propylitic. The presence of potassic alteration was defined by the occurrence of secondary biotite and K-feldspar ± anhydrite, quartz, sericite, carbonate, chlorite, rutile and apatite. This alteration affects all rocks within the El Teniente area, excluding the Braden Formation and the post mineralization lamprophyre dikes, and it is most significant in the mine andesites. Quartz-sericite alteration comprises quartz, sericite, pyrite ± minor tourmaline, anhydrite, calcite and chlorite. This alteration is best developed in the quartz diorites (Sewell Tonalite) and to a lesser degree in the mine andesites.

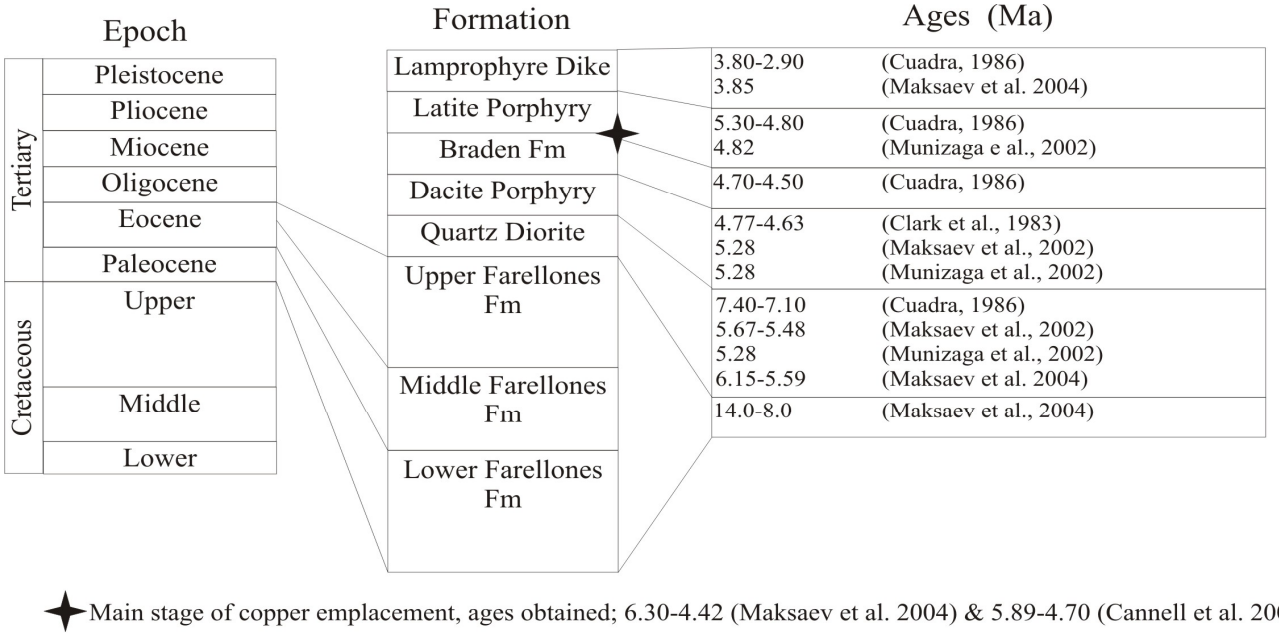


Figure 2. Stratigraphic column showing the main formations at El Teniente and published ages from U-Pb, $^{40}Ar/^{39}Ar$, Re-Os, and Fission track dating (from Clark *et al.*, 1983; Cuadra, 1986; Maksaev *et al.*, 2002; Munizaga *et al.*, 2002; Maksaev *et al.,* 2004).

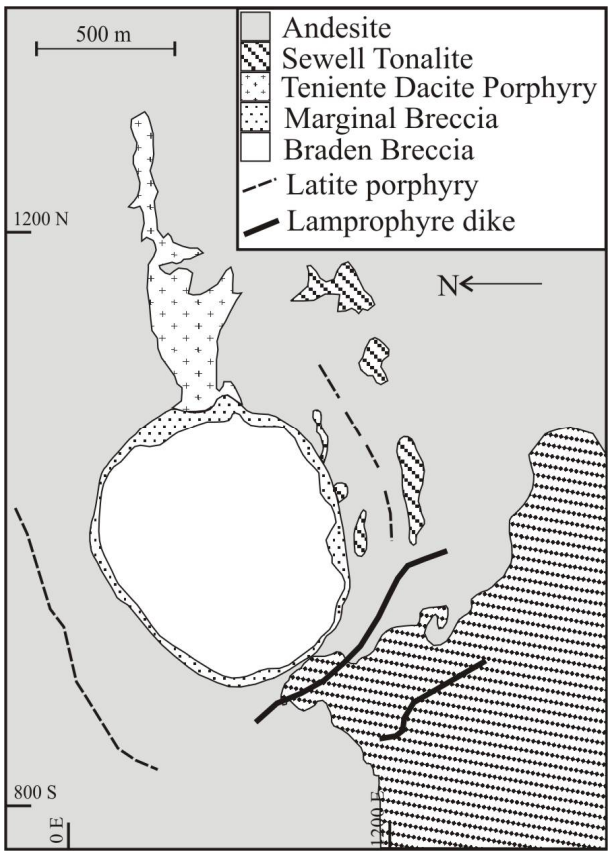


Figure 3: Simplified geological map of El Teniente level 5 (2,284 m above sea level).

Propylitic alteration forms a halo surrounding all other types of alteration and consists of chlorite, epidote, calcite, magnetite, pyrite ± sericite, quartz and anhydrite.

Skewes *et al.* (2002) defined four alteration stages: late magmatic, principal hydrothermal, late hydrothermal and *posthuma* stages. They suggested that the most pervasive and earliest (late magmatic) alteration was widespread secondary biotite, which occurred simultaneously with the formation of biotite breccias. This alteration corresponds to the potassic alteration of Camus (1975) and, based on its distribution, has been linked to the intrusion of the Sewell Tonalite and the Teniente dacite porphyry (Skewes *et al.*, 2002). The principal hydrothermal alteration can be correlated with the quartz-sericite alteration of (Camus, 1975) and is most intense in the upper levels of the deposit, at the edges of the Sewell Tonalite and surrounding the Teniente Dacite Porphyry. The intensity of this alteration decreases with depth (Skewes *et al.*, 2002). Late hydrothermal alteration is spatially related to the formation of the Braden Breccia and Latite ring dikes, and corresponds to the development of tourmaline in the deposit (Skewes *et al*., 2002). Its intensity decreases with depth. Posthuma alteration represents the last stage of hypogene alteration, and is limited to the central rock-flour Braden Breccia (Skewes *et al.*, 2002).

This alteration history was recently revised into four alternative alteration stages: pre-mineralization, late magmatic, principal hydrothermal and late hydrothermal (Cannell *et al*., 2005). This classification is similar to that documented by Skewes *et al.* (2002), the main difference being the addition of a pre-mineralization stage and the combination of the late hydrothermal and Posthuma stages. Cannell *et al.* (2005) also documented ten vein stages associated with the four alteration stages.

## 4 METHODS

### 4.1 *Samples*

Preliminary analyses are being carried out on a suite of vein samples from the pre-mineralization, late magmatic and principal hydrothermal stages (Cannell *et al*., 2005).

### 4.2 *SEM-Cathodoluminescence imaging*

In addition to conventional petrography, samples are being examined using an SEM-mounted cathodoluminescence detector which enables resolution of multiple stages of quartz precipitation and recrystallization. This approach allows identification of fluid inclusions related to specific paragenetic stages, enabling a fluid chronology to be defined (*e.g.* Landtwing *et al*., 2005).

### 4.3 *Laser Ablation ICP-MS*

Analyses are being carried out at the Joint Analytical Facility at the Natural History Museum, London, using a New Wave UP213AI, 213 nm aperture laser ablation system (Jeffries *et al.* 1998) linked to a Thermo Element PlasmaQuad 3 ICP-MS, according to procedures summarised by Stoffell *et al*. (2004). Operating conditions (laser parameters and inclusion ablation protocol, mass spectrometer dwell-times and sweep-time) will be optimised for the determination of Cu, Mo, Zn, Pb and Au using synthetic fluid inclusions.

## 5 SUMMARY

New data on the chemistry of ore fluids from the supergiant El Teniente system should enable key questions regarding the origin of the deposit to be addressed. In particular, we

should be able to determine if there was an anomalous ore fluid metal budget, whether depositional mechanisms were unusually efficient, or whether there were just multiple Cu-bearing fluid events. The link between evolving ore fluid chemistry and the chemistry of rock alteration have never been investigated in detail in porphyry systems, and the El Teniente deposit, hosted largely by mafic rocks of more distinctive chemistry, will provide an opportunity to try and understand this interrelationship.

## ACKNOWLEDGEMENTS

We thank Clara Buckroyd and Barry Stoffell for helpful discussions and Codelco El Teniente for approving access to the deposit.

## REFERENCES

Camus, F. (1975) Geology of the El Teniente Orebody with Emphasis on Wall-Rock Alteration. Economic Geology, 70(8), 1341-1372.

Cannell, J., Cooke, D. R., Walshe, J. L., and Stein, H., (2005) Geology, Mineralization, Alteration, and Structural Evolution of the El Teniente Porphyry Cu-Mo Deposit: *Economic Geology*, v. 100.

Clark, A. H., Farrar, E., Camus, F., and Quirt, G. S., (1983) K-Ar Age Data for the El Teniente Porphyry Copper Deposit, Central Chile. *Economic Geology*, 78, 1003-1006.

Cooke, D. R., Hollings, O., and Walshe, J. L., (2005) Giant Porphyry Deposits: Characteristics, Distribution, and Tectonic Controls. *Economic Geology,* 100 (5), 801-818.

Cuadra, P., (1986) Geochronologia K-Ar Del Yacimiento El Teniente Y Areas Adyacentes. *Rivista Geológica de Chile,* 27, 3-26.

Howell, F. H. and Molloy, J. S. (1960) Geology of the Braden Orebody, Chile, South America. *Economic Geology,* 55 (5), 863-905.

Jeffries, T., Jackson, S. E., and Longerich, H. P., (1998) Application of a frequency quintupled Nd:YAG source (λ=213 nm) for laser ablation inductively coupled plasma mass spectrometric analysis of minerals, 13, 935-940.

Landtwing, M., Pettke, T., Halter, W. E., Heinrich, C.A., Redmond, P. B., Einaudi, M. T., AND Kunze, K., (2005) Copper Deposition During Quartz Dissolution by Cooling Magmatic-Hydrothermal Fluids: The Bingham Porphyry. *Earth and Planetary Science Letters,* 235, 229-243.

Maksaev, V., Munizaga, F., McWilliams, M. O., Fanning, M., Mathur, R., Ruiz, J., and Thiele, K., (2002) El Teniente porphyry copper deposit in the Chilean Andes; new geochronological timeframe and duration of hydrothermal activity. Abstracts with Programs- *Geological Society of America*, 34 (6), 336.

Maksaev, V., Munizaga, F., McWilliams, M. O., Fanning, M., Mathur, R., Ruiz, J., and Zentilli, M., (2004) New Chronology for El Teniente, Chilean Andes, from U-Pb, $^{40}Ar/^{39}Ar$, Re-Os, and fission track dating: Implication for the Evolution of a Supergiant Porphyry Cu-Mo Deposit. *Special Publication of the Society of Economic Geologists*, 11, 15-54.

Munizaga, F., Maksaev, V., Mathur, R., Ruiz, J., McWilliams, M. O., and Thiele, K., (2002) Understanding molybdenite Re-Os ages from the El Teniente porphyry copper deposit, Chile. Abstracts with Programs- *Geological Society of America*, 34 (6), 336-337.

Skewes, A. M., Arevalo, A., Floody, R., Zuniga, P. H., and Stern, C., (2002) The Giant El Teniente Breccia Deposit: Hypogene Copper Distribution and Emplacement: *Special Publication of the Society of Economic Geologists.*

Stoffell, B., Wilkinson, J. J., and Jeffries, T. E., (2004) Metal transport and deposition in hydrothermal veins revealed by 213nm UV laser ablation microanalysis of single fluid inclusions. *American Journal of Science*, vol. 304, pp. 533-557.

# Mafic enclaves associated with felsic intrusions of the Zhireken porphyry Mo-Cu deposit (Russia)

Anita N. Berzina
*Institute of Geology and Mineralogy, Novosibirsk, Russia*

Victor O. Gimon
*Institute of Geology and Mineralogy, Novosibirsk, Russia*

Adel P. Berzina
*Institute of Geology and Mineralogy, Novosibirsk, Russia*

Alexander F. Korobeinikov
*Tomsk Polytechnic University, Tomsk, Russia*

ABSTRACT: The mafic microgranular enclaves (MME) associated with Upper Jurassic felsic porphyry ore-bearing rocks from the Zhireken porphyry Mo-Cu deposit (Eastern Transbaikalia, Russia) are intermediate in composition (54% $SiO_2$) and often contain the same minerals as the host granite porphyries, however their chemical compositions are different. Accessory magnetite in MME has higher $Cr_2O_3$ and Cu contents and apatite has higher Cl and S compared to the host porphyries. Mafic enclaves show relatively high Pt and Re content. Mafic melt may have made substantial contributions for the overall budget of sulphur and ore metals in evolving felsic magma and hydrothermal fluid of the Zhireken deposit.

KEYWORDS: mafic enclaves, porphyry Cu-Mo deposits, Zhireken

## 1 INTRODUCTION

Large-scale porphyry Cu-Mo deposits contain great quantities of sulfur as sulphide minerals. Typically, felsic magmas have a low solubility for sulphur and are incapable to supply significant amounts of sulphur required to form porphyry Cu-Mo deposits. In recent years, there have been some papers discussing injection of mafic magma into a compositionally evolved chamber as a potential sulfur and metal source for porphyry-related mineralization (Keith *et al*. 1998; Hattori & Keith 2001; Maughan *et al.* 2002, and others). In this respect, the ore-bearing complex of porphyry Mo-Cu Zhireken deposit (Eastern Transbaikalia, Russia) showing evidence of magma mixing is of certain interest.

## 2 GEOLOGICAL SETTING

The Zhireken porphyry Mo-Cu deposit (Fig. 1) is situated in the northern part of the Mongol-Okhotsk fold belt within the Bushulei Pluton. The deposit was discovered in 1945, explored in 1958-1966 and is mined now as an open pit. The Bushulei pluton is composed

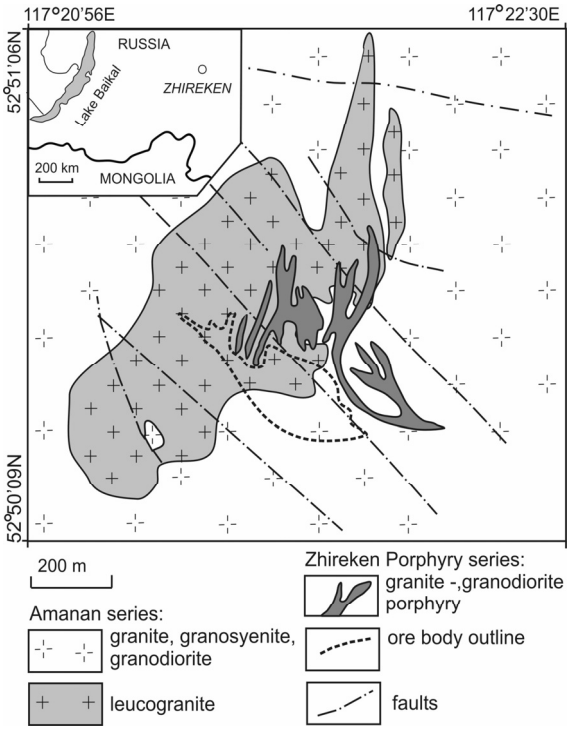


Figure 1. Geological map of the Zhireken deposit.

mainly of collision-related calk-alkaline granites and leucogranites with minor granodiorites and granosyenites (Amanan Series) of normal to elevated alkalinity. The age of Amanan se-

ries of rocks is 188 to 168 Ma (Ponomarchuk *et al*. 2004). The ore-bearing porphyries (Zhireken Porphyry Series) occur as stocks and dikes in surrounding Amanan biotite granites and leucogranites and are represented predominantly by granite and granodiorite porphyry. Small dikes of quartz diorite porphyries and kersantites are of minor importance and occur before and after the emplacement of granite porphyry stockwork (0.12 km$^2$). $^{40}Ar/^{39}Ar$ ages of porphyries are 160 to 158 Ma (Ponomarchuk *et al.* 2004). Re-Os dates for molybdenite conducted by AIRIE at Colorado State University yield an age of 162-163 Ma (Berzina *et al*. 2003). The deposit has contained metal reserves of 100 Kt Mo and 100 Kt Cu with average grade of 0.1 % Mo and 0.1 % Cu. Molybdenite is a dominant commercial mineral; chalcopyrite, chalcosine and fahlores are secondary. The average Cu/Mo ratio in ores is 1-2. The granite porphyries show Sr isotopic value indicating mantle-crust interaction - $(^{87}Sr/^{86}Sr)_0$=0.70642 (Sotnikov *et al.* 2000).

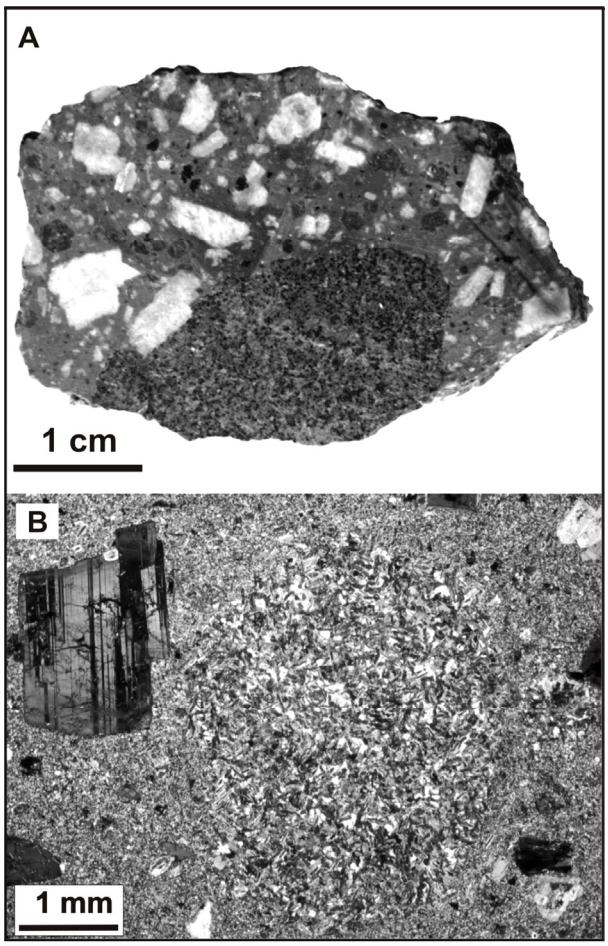


Figure 2. Photographs of MME from the Zhireken deposit. (A) Typical view of MME with oval shape. (B) Photomicrograph of MME lodged in granite porphyry.

## 3 HOST ROCKS AND MAFIC MICROGRANULAR ENCLAVES

### 3.1 *Field occurrence and petrography of MME*

The coexistence of felsic and mafic magmas at the Zhireken deposit is confirmed by the occurrence of small rounded and oval enclaves of dark-colored rocks in ore-related granite porphyries. Mafic microgranular enclaves (MME) up to 5-10 cm in diameter occur in the groundmass of the porphyries (Fig. 2a). The smallest are 5 mm across (Fig. 2b). They are fine grained, exhibiting a general hypidiomorphic granular texture. MME are darker than host granite porphyry, with which they show sharp contacts. Biotite, K-feldspar and quartz fill interspaces between lath-shaped crystals of plagioclase. Biotite is the sole ferromagnesian phase with a composition typically similar to that of the host granite porphyry. The plagioclase in mafic enclaves is enriched in anorthite component as compared to the groundmass and phenocrysts of the porphyries. Major element geochemistry indicates that MME are metaluminous (A/CNK=0.92), while host porphyry rocks are peraluminous (A/CNK=1.07).

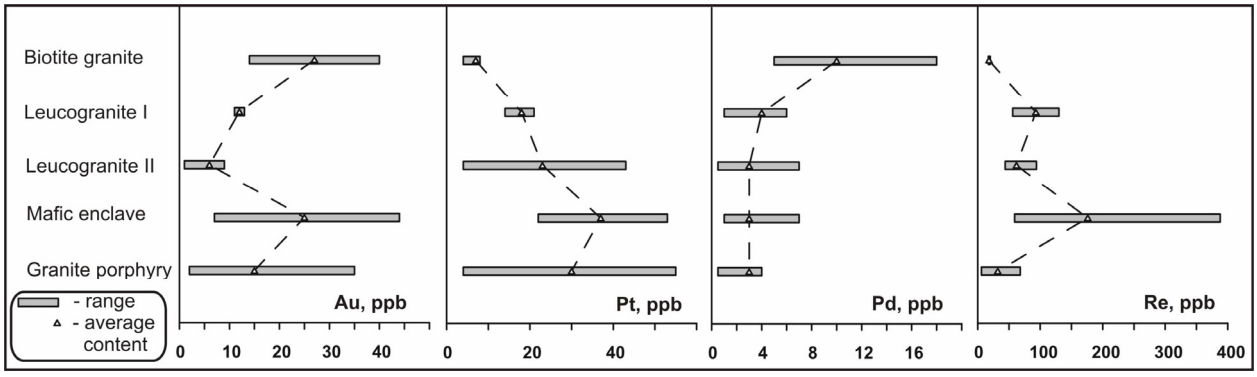


Figure 3. Au, Pt, Pd and Re abundances in mafic microgranular enclaves and felsic rocks from the Zhireken deposit.

Phenocrysts in granite porphyries make up 40-50% of rock volume and are represented mainly by K-feldspar, plagioclase (albite-oligoclase) and quartz with minor biotite. The fine-grained (0.01-0.05 mm) groundmass of the porphyry is composed from the same minerals. The accessory minerals are magnetite, apatite and celestine. MME and kersantite dikes have shoshonitic affinity unlike host granite porphyries that are located in the high-K calc-alkaline field (Peccerillo & Taylor, 1976).

The presence of quartz and K-feldspar phenocrysts (often with reaction rims) in diorite porphyrite and kersantite dikes also indicate the mixing of felsic and basic magmas during the formation of the Zhireken ore-bearing porphyry complex. The quartz grains (up to 2-3 mm) are usually rounded and corroded, and, in some cases, are granulated into aggregates. The quartz in MME contains crystallized melt inclusions similar in composition and texture to the granite porphyry groundmass. K-feldspar is present as large (up to 1 x 1.5cm) resorbed segregations with thin plagioclase rims. Granite porphyries often include partially resorbed plagioclase crystals of reticulate structure with more calcic rims. According to experimental data (Tsuchiyama 1985) such a structure occurs during partial dissolution of sodic plagioclase in mafic melt.

### 3.2 *Geochemistry of the MME*

Chemical composition of apatite and magnetite was determined with electron microprobe ($Cr_2O_3$, Cl, S) and LA-ICP-MS (Cu, Mo, Co, Ni) at the Institute of Geology and Mineralogy (Novosibirsk, Russia). Au, Pt, Pd and Re were analysed by inversion voltammetry in Tomsk Polytechnic University (Russia).

The mafic microgranular enclaves are chemically distinct from the host granite porphyries and are somewhat similar to that of the late kersantite dikes (Table 1). The $SiO_2$ contents of the enclaves is 54.6 wt.%, which is lower than the $SiO_2$ content of the host granite porphyry (70.6 wt.%).

Accessory magnetite in mafic enclaves (Table 2) shows high $Cr_2O_3$ (up to 3.2 %); it also contains Cu (1500 ppm), Mo (1-2 ppm) and Co, Ni (both, 30-50 ppm). The concentrations of Mo are higher (3-10 ppm) in the accessory magnetite of granite porphyries while $Cr_2O_3$ (0.27-0.40%) and Cu (up to 100 ppm) are notably lower than those in mafic enclaves. The concentrations of Cl are higher in apatite from mafic enclaves (up to 0.4-0.5 %) and lower in that from the porphyries (0.1%). Elevated contents of Pd and Pt in molybdenites and in flotation molybdenum concentrate from the Zhireken deposit (684 and 299 ppb, respectively; Sotnikov *et al.* 2001) as well as high temperatures of formation of porphyry rocks (1020-910°C, melt inclusions; 850-790°C, biotite geothermometer; Sotnikov *et. al.* 1985) indirectly suggest a contribution from primitive mafic melt derived from the mantle. MME show the-highest average Pt (37 ppb) and Re (176 ppb) contents among the rocks of Zhireken deposit

Table 1. Major element analyses (wt%) of the igneous rocks, Zhireken deposit

| Sample | GP | MME | Ks |
|---|---|---|---|
| $SiO_2$ | 70.60 | 54.62 | 59.00 |
| $TiO_2$ | 0.25 | 0.96 | 0.86 |
| $Al_2O_3$ | 13.40 | 13.80 | 14.60 |
| $Fe_2O_3$ | 1.01 | 3.84 | 2.61 |
| FeO | 3.23 | 3.63 | 4.67 |
| MnO | 0.03 | 0.08 | 0.06 |
| MgO | 0.57 | 5.66 | 4.91 |
| CaO | 1.20 | 2.94 | 3.02 |
| $Na_2O$ | 3.33 | 3.50 | 4.33 |
| $K_2O$ | 4.50 | 3.48 | 3.67 |
| $P_2O_5$ | 0.05 | 0.28 | 0.22 |
| SrO | n.a. | 2.80 | n.a. |
| $SO_3$ | n.d. | 2.20 | 0.30 |
| LOI | 0.99 | 1.76 | 1.60 |
| Total | 99.16 | 100.45 | 100.07 |

*n.a.* – not analyzed; *n.d.* – not detected; *LOI* – loss of ignition; *GP* – granite porphyry; *MME* – mafic microgranular enclave, *Ks* – kersantite

Table 2. Chemical composition of magnetite and apatite from MME and host granite porphyries

| Element | GP | MME |
|---|---|---|
| | *magnetite* | |
| $Cr_2O_3$, % | 0.27-0.40 | 3.20 |
| Cu, ppm | 100 | 1500 |
| Mo, ppm | 3-10 | 1-2 |
| Co, ppm | n.a. | 30-50 |
| Ni, ppm | n.a. | 30-50 |
| | *apatite* | |
| Cl, % | 0.1 | 0.4-0.5 |
| S, ppm | 600-1000 | 5700-7200 |

Table 3. Au, Pt, Pd and Re content in MME and felsic rocks from the Zhireken deposit

| Element | Gr | LcI | LcII | MME | GP |
|---|---|---|---|---|---|
| Au, ppb | 27 | 12 | 6 | 25 | 15 |
| Pt, ppb | 12 | 18 | 23 | 37 | 30 |
| Pd, ppb | 10 | 4 | 3 | 3 | 3 |
| Re, ppb | 18 | 93 | 62 | 176 | 32 |

*Gr* – biotite granite, Amanan Series, *LcI, LcII* - leucogranite I phase and II phase, Amanan Series; *MME* – mafic enclave, *GP* – granite porphyry

(Table 3, Fig. 3). The Au content in MME on average is comparable to that from the earliest phases of Amanan Series (biotite granites), while late phases of Amanan Series (leucogranites I and II), and granite porphyries, hosting MME show lower Au content. Pd concentrations in whole-rock samples are relatively low with equal average contents in MME and granite porphyries.

Unusually high chromium, up to 190 ppm, in granite porphyries, containing MME further suggests input from mafic melt. Apatite from mafic microgranular enclaves contains 5700-7200 ppm of sulphur that corresponds to 630-800 ppm of sulphur in related melt, assuming the distribution coefficient of Baker & Rutherford (1996). Concentration of sulphur in apatite from granite porphyries varies from 600 to 1000 ppm which is consistent with 65-110 ppm of sulphur in the melt. $\delta^{34}S$ values for sulphide minerals (pyrite, molybdenite and chalcopyrite) vary from -0.6 to 4.1‰ (Sotnikov *et al.* 2004), which corresponds to the magmatic sulfur source at Zhireken. The mafic magma was also saturated with copper, as evidenced by high copper content (1500 ppm) in magnetite from mafic inclusions.

## 4 CONCLUSIONS

Studies of the Zhireken deposit show that mafic melt may have made substantial contributions for the overall budget of sulphur and ore metals in evolving felsic magma and hydrothermal fluid. We suggest that injection of mafic component into already existing subvolcanic felsic magma chambers is one of the main factors controlling productive Cu-Mo systems.

## ACKNOWLEDGEMENTS

This work was supported by Russian Foundation for Basic Research (grants 06-05-64254, 07-05-00664) and NSH-4933.2006.5. We thank L. Meinert for detailed review and language improvement.

## REFERENCES

Baker L.L., Rutherford M.J. (1996). Crystallization of anhydrite-bearing magmas. *Trans. R. Soc. Edinb. Earth Sci.* 87, pp. 243-250.

Berzina A.N., Stein H.J., Zimmerman A., Sotnikov V.I. (2003). Re-Os ages for molybdenite from porphyry and greisen Mo-W deposits of southern Siberia (Russia) preserve metallogenic record. In: D. Eliopoulos et al. (Eds), Mineral Exploration and Sustainable Development. *Proc. of the 7th SGA Meeting, Athens, Greece.* Millpress, Rotterdam. 1, pp. 231-234.

Hattori K.H., Keith J.D. (2001). Contribution of mafic melt to porphyry copper mineralization: evidence from Mount Pinatubo, Philippines, and Bingham Canyon, Utah, USA. *Miner. Deposita.* 36, pp. 799-806. DOI: 10.1007/s001260100209.

Keith J.D., Christiansen E.N., Maughan D.T., Waite K.A. (1998). The role of mafic alkaline magmas in felsic porphyry Cu and Mo systems. Geol. Assoc. Can. Short Course Note, *Geological Association of Canada*, St. John's, Newfoundland, pp. 211-243.

Maughan D.T., Keith J.D., Cristiansen E.H., Pilsipher T., Hattory K., Evans N.J. (2002). Contribution from mafic alkaline magmas to the Bingham porphyry Cu-Au-Mo deposit, Utah, USA. *Miner. Deposita*,. 37, pp. 14-37. DOI: 10.1007/s00126-001-0228-5.

Peccerillo. A., Taylor S.R. (1976). Geochemistry of Eocene calk-alkaline volcanic rocks from the Kastamonu area, northern Turkey. *Contr. Mineral. Petrol.* 58, pp. 63-81. DOI:10.1007/BF00384745

Ponomarchuk V.A., Sotnikov V.I., Berzina A.N. (2004). Isotopic and geochronological heterogeneity of granite porphyry from the Zhireken porphyry Cu–Mo deposit (Eastern Transbaikalia). *Geochemistry International*. 42 (6), pp.587-590.

Sotnikov V.I., Poliveev A.G., Berzina A.N. (1985). Physicochemical formational characteristics of ore-bearing granitic rocks, the Zhireken Cu-Mo deposit. *Doklady Academii Nauk SSSR* 283, pp. 1463-1465. (in Russian).

Sotnikov V.I., Ponomarchuk V.A., Berzina A.N., Berzina A.P., Kiseleva V.Yu., Morozova I.P. (2000). Evolution of $^{87}Sr/^{86}Sr$ in igneous rocks of porphyry copper-molybdenum ore clusters (based on studies of accessory apatite). *Russian Geology and Geophysics.* 41 (8), pp. 1078-1088.

Sotnikov V.I., Berzina A.N., Economou-Eliopoulos M., Eliopoulos D.G. (2001). Palladium, platinum and gold distribution in porphyry Cu±Mo deposits of Russia and Mongolia. *Ore Geol. Rev*. 18, pp. 95-111. DOI:10.1016/S0169-1368(01)00018-X.

Sotnikov V.I., Ponomarchuk V.A., Pertseva A.P., Berzina A.P., Berzina A.N., Gimon. V.O. (2004). Geochemistry of sulphur isotopes in Cu-Mo porphyry systems within Siberia and Mongolia. *Russian Geology and Geophysics*, 45 (8), pp. 913-923.

Tsuchiyama A. (1985). Dissolution kinetics of plagioclase in the melt of the system diopside-albite-anorthite, and origin of dusty plagioclase in andesites. *Contr. Mineral. Petrol.* 69 (1), pp.1-16. DOI:10.1007/BF01177585.

# Rhenium concentrations in the host rocks and ores at the Aksug and Sora porphyry Cu-Mo deposits (Russia)

Anita N. Berzina
*Institute of Geology and Mineralogy, Novosibirsk, Russia*

Alexander F. Korobeinikov
*Tomsk Polytechnic University, Tomsk, Russia*

ABSTRACT: Whole-rock analyses of 48 rock samples, ranging from gabbro to granite, combined with mineral separate analyses of molybdenite, chalcopyrite and magnetite and sulphide flotation concentrates, have been used to constrain the distribution of Re at the Sora porphyry Mo-Cu and Aksug Cu-Mo deposits (Siberia, Russia). Re contents in rocks have been significantly modified by hydrothermal processes. Higher Re concentrations are associated with phyllic alteration. The deposits studied show comparable Re contents in syn-mineral porphyries, while Re concentration in molybdenite differs greatly, most likely due to changes in physical and chemical conditions (pH, $fO_2$, salinity).

KEYWORDS: rhenium, porphyry Cu-Mo deposits, Sora, Aksug

## 1 INTRODUCTION

The Re contents of molybdenites from porphyry Cu-Mo deposits vary widely, from ppm to percentages (Giles & Shilling 1972, Todorov & Staikov 1985, *etc*.). Very little is known, however, about the actual abundances of Re in whole-rock samples from porphyry Cu-Mo deposits. To investigate the possible causes of variations in Re abundances, a suite of intrusive rocks ranging from gabbro to granites, from two Russian porphyry Cu-Mo deposits have been analyzed for their whole-rock Re contents. Re abundances in mineral separates and sulphide flotation concentrates have also been analyzed.

## 2 GEOLOGICAL SETTING

Southern Siberia is part of the Central Asian mobile belt. The region contains a number of porphyry Cu-Mo deposits. The Aksug pluton and associated Early Devonian porphyry Cu-Mo ores are located in the Tuvinian terrane. This terrane comprises an island-arc complex, including early Cambrian basalts, andesites and rhyolites, which were intruded by Middle Cambrian collisional-related gabbros, diorites and tonalites (Berzina *et al.* 1994). The Aksug pluton is composed mainly of sodic, calc-alkaline quartz diorites and tonalites, with subordinate diorites and gabbro. The syn-mineral porphyry series consists of quartz diorite-, tonalite- and granodiorite porphyries. Major stockwork Cu-Mo mineralization is confined to the porphyry stock, which has been cut by post-mineralization plagiogranites and aplite dikes and minor intrusions. The average Cu/Mo ratio in Aksug ores is high (40-70). Phyllic (quartz-sericite) and propylitic alteration assemblages are predominant at the deposit, whereas early potassic (K-feldspar-biotite) alteration is subordinate. The deposit is dominated by a mantle source component with $(^{87}Sr/^{86}Sr)_0$ varying from 0.70454 to 0.70496 (Sotnikov *et al*. 2000).

The early Devonian Sora Mo-Cu porphyry deposit is located in the Kuznetsk Alatau terrane, an island-arc complex of Vendian-early Cambrian age, consisting of trachyrhyolite and trachyandesite subvolcanic rocks and high-K calc-alkaline monzonites, diorites and gabbros (Berzina *et al*. 1994). The Cambro-Ordovician Uibat pluton consists of monzodiorites, granosyenites and leucogranites, and is inferred to have been emplaced in a collisional setting. Pre-mineral dikes include microdiorites, diorite porphyries, spessartites and syenite porphyries. Cu-Mo mineralization produced veins, disseminations and hydrothermal breccia ores, and

was related to intrusion of the granite porphyry stock. The stock has undergone potassic alteration, locally strong albitization, and minor subsequent phyllic (quartz-sericite) alteration. Numerous post-mineral Devonian dikes define the final stage of magmatic activity at Sora. The range of Cu/Mo ratios in the Sora ores is 2-4. All magmatic rocks of the Sora deposit are characterized by a dominant mantle source component, with $(^{87}Sr/^{86}Sr)_0$ in accessory apatites varying from 0.70407 to 0.70494 (Sotnikov *et al*. 2000).

## 3 ANALYTICAL METHODS

Re contents in whole-rock samples, chalcopyrite separates and copper flotation concentrates have been measured using inversion voltammetry based on impregnated carbon electrode (Goltz 2004) at the Geological Analytic Centre "Zoloto-Platina" (Tomsk Polytechnic University, Russia). 5-10 g of powdered whole-rock sample and 200-300 mg of sulphide concentrate was used for each run (detection limit for Re was 1 ppb). Re concentrations in magnetite were determined by LA-ISP-MS at the Institute of Geology and Mineralogy (Novosibirsk, Russia) with a detection limit of 1 ppb. Cu and Mo contents were determined by the AAS method at the Institute of Geology & Mineralogy (Novosibirsk, Russia) with a detection limit of 1.5 ppm.

## 4 WHOLE-ROCK Re ABUNDANCE

The samples analyzed include rocks from plutons, hosting porphyry stocks and dikes, pre, syn- and post-mineral porphyry rocks and altered rocks. The measured concentrations of Re are summarized in Table 1.

Re abundances in whole-rock samples from Aksug and Sora are relatively high, mostly above the average crustal abundance estimate of 0.188 ppb (Rudnik & Gao 2003) or 2 ppb (Sun *et al.*, 2003). Re concentrations for the Aksug samples range from 9 to 89 ppb, with an average content of 35 ppb. The Re contents of the Sora rocks overlaps the Aksug rock field, but with a larger range, varying from 1 to 89 ppb. The average Re concentration of the Sora whole-rock samples is a little lower (29 ppb).

Most of the samples selected for this study do not contain visible sulphides, and so the impact of mineralization on the whole-rock Re contents should be minimal. Mo contents in the samples varied from below detection limit (1.5 ppm) for both deposits to 100 ppm at Aksug, and to 1.2 % at Sora. Cu contents ranged from 109 ppm to 0.9 % at Aksug, and from 6.5 ppm to 0.2 % for the Sora samples. There is no correlation of Re with Cu. The correlation between Re and Mo content is difficult to estimate as the molybdenum content in the majority of samples is below detection limits.

Table 1. Rhenium content in whole-rock samples.

| Rock type | Re, ppb | |
|---|---|---|
| | range | average |
| AKSUG DEPOSIT | | |
| Aksug pluton (outside the ore zone) | 38-62 | 50 (2)* |
| Aksug pluton (within the ore zone) | 21-89 | 46 (4) |
| Syn-mineral porphyries | 22-32 | 25 (4) |
| Post-mineral plagiogranite | | 49 (1) |
| Potassic alteration | 9-19 | 14 (2) |
| Phyllic alteration | 10-49 | 29 (4) |
| SORA DEPOSIT | | |
| Uibat pluton (outside the ore zone) | 2-46 | 14 (7) |
| Uibat pluton (within the ore zone) | 37-55 | 44 (3) |
| Pre-mineral porphyry | 40-66 | 57 (4) |
| Syn-mineral stocks and dikes | 20-52 | 31 (4) |
| Post-mineral dikes | 21-89 | 51 (4) |
| Phyllic alteration | | 49 (1) |
| Albitic alteration | 1-19 | 10 (2) |

* - in brackets - number of samples analyzed

Re abundance in rocks from the Aksug deposit (Table 1) show that the average contents of Re in rocks of the Aksug pluton (gabbro, quartz diorite, tonalite) are similar to the late-mineral plagiogranites (48-49 ppb Re) that have undergone minor mineralization and metasomatic alteration. The average Re concentration in the Aksug syn-mineral porphyries (tonalite-, granodiorite porphyry) is lower (25 ppb). Samples from zones of intense alteration show wide Re dispersion (9-49 ppb). Rhenium concentrations in rocks with superimposed potassic alteration are typically lower than abundances from quartz-sericite altered rocks, varying from 9 to 19, and from 10 to 49 ppb, respectively (Table 1, Fig. 2). There is no clear correlation between Re and $SiO_2$ content in the Aksug samples, but it is evident that evolved phases typically show higher Re contents, particularly in the rocks from the Aksug pluton.

Rhenium abundances in rocks from the Sora

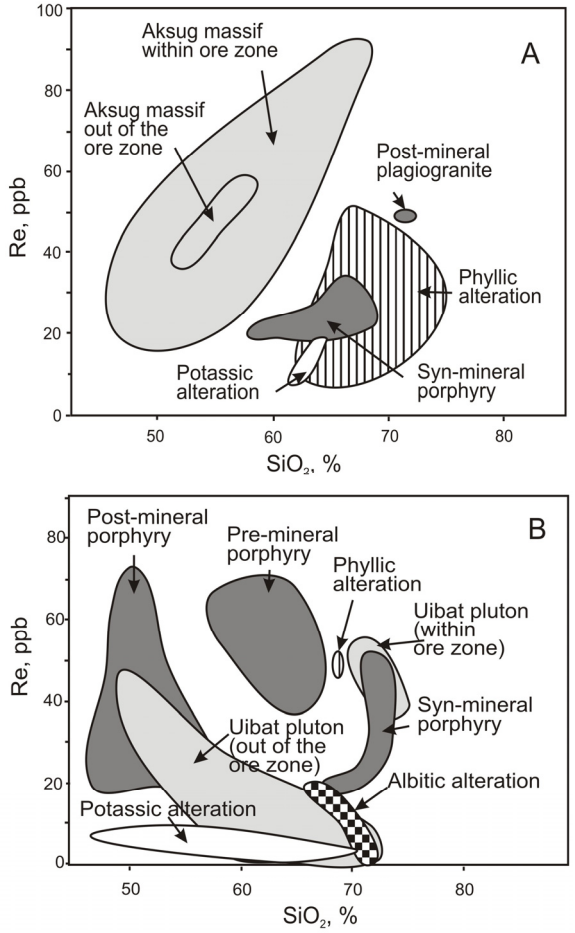


Figure 2. Re vs. $SiO_2$ content in whole-rock samples from the Aksug (A) and Sora (B) deposits.

deposit (Table 1) are somewhat different to those from Aksug. Rhenium contents in unaltered rocks from the Uibat pluton (gabbro, quartz monzonite, granosyenite, leucogranite) are on average lower than those in the altered and unaltered pre-, syn- and post-mineral porphyries. Rhenium concentrations in samples from the Uibat pluton, collected from outside the ore zone, where porphyry stocks and dikes don't occur are typically lower than abundances in the same rocks located adjacent to the porphyry stocks, with average contents of 14 and 44 ppb, respectively. Rhenium concentration in the mineralized porphyries range from 20 to 89 ppb. Rhenium abundances in the pre-mineral (quartz monzonite-, syenite-, granodiorite porphyry) and post-mineral dikes (trachyte and diabase porphyry) are typically higher than that in syn-mineral granite porphyries, with average contents of 57, 51 and 31 ppb, respectively. As at Aksug, the low Re abundances for Sora samples (2-9 ppb) are associated with rocks that have undergone intense potassic alteration. Relatively low Re contents (1-19 ppb) are also associated with rocks that have undergone intense albitic alteration. Rhenium concentration in the one sericite-altered sample analyzed is significantly higher (49 ppb).

Evolved rocks of the Uibat pluton (granosyenite, leucogranite) have lower Re concentrations (2-9 ppb) than the gabbro and diorites. Where the leucogranites occur within the ore zone, they have markedly higher Re abundances (37-55 ppb). There is no obvious correlation between $SiO_2$ and Re content in the Sora porphyry series intrusions.

## 5 RHENIUM IN MINERAL SEPARATES AND FLOTATION CONCENTRATES

The Re contents of magnetite from the Aksug gabbro (Aksug pluton) varies from below detection limit (1 ppb) to 6 ppb. No Re was detected in magnetite from Aksug porphyry rocks. Chalcopyrite separates from Sora contain Re from 101 to 1600 ppb. The lower Re contents are typical of chalcopyrites from K-feldspar altered rocks. The highest values (1600 ppb) were obtained from chalcopyrite in the hydrothermal breccias. The Re content in copper flotation concentrate from Sora is 563 ppb Re (Cu ~ 14%). Aksug concentrates have comparable values of 131-321 ppb Re (Cu ~ 10 %) and 930-1120 ppb Re (Cu ~ 20%). Rhenium contents in molybdenites from Aksug and Sora were reported by Berzina *et al.* (2005). Molybdenite is the main rhenium-hosting mineral. Its separates show a large enrichment of Re relative to whole-rock samples and other ore minerals, averaging 460 and 14 ppm for the Aksug and Sora deposits, respectively.

## 6 DISCUSSION

Some unmineralized samples, notably from zones of intense potassic and albitic alteration at both deposits have low Re abundances, while porphyries from zones of phyllic alteration have higher Re contents comparable to the weakly altered porphyries. Lower Re concentrations were previously detected in molybdenites from K-feldspar altered rocks at Sora (Berzina *et al*., 2005). These data support the possibility that Re contents in rocks have been significantly modified by hydrothermal processes. Recent experimental studies (Xiong & Wood 2002) showed that Re solubility depends strongly on pH and chloride concentration, increasing greatly with increasing chloride concentration and decreasing with increasing pH at

400-500°C in equilibrium with the K-feldspar-muscovite-quartz pH buffer. Such conditions are directly relevant to porphyry Cu-Mo deposits. Thus, low-pH fluids, associated with phyllic alteration, were probably capable of dissolving and transporting more Re than the higher-pH fluids associated with potassic alteration.

Average Re abundances in porphyry rocks related to ore formation are higher for the Sora samples than those from Aksug. At the same time, molybdenite samples from Aksug have significantly higher Re contents than Sora molybdenites. Evidently, Re content in molybdenites from these two deposits does not correlate positively with Re in the porphyritic intrusions. Differences in Re concentrations for the Aksug and Sora molybdenites were most likely determined by physical and chemical fluid conditions (pH, $fO_2$, salinity). Aksug formed under relatively oxidizied conditions with elevated chlorine activity in the fluid compared to Sora (Berzina *et al*., 2005). Such conditions were favorable for accumulating higher Re contents in Aksug molybdenites. The relatively high solubility of Re in high-temperature, chloride-rich fluids (Xiong & Wood 2002) could be responsible for the extraction of Re from rocks, thereby modifying the original content, which then could be redeposited with sulphides.

Perhaps such processes took place at Aksug, which resulted in lowered Re abundances in syn-mineral porphyries and elevated Re concentrations in molybdenites compared to Sora.

## 7 CONCLUSIONS

Rhenium abundances in whole-rock samples of the Aksug and Sora deposits vary widely and were significantly modified by hydrothermal processes. Higher Re contents are associated with phyllic alteration at both deposits. Re contents of molybdenites from Aksug and Sora do not correlate with Re in the whole-rock samples. Higher Re contents in molybdenites from Aksug may be due to more highly oxidized, saline mineralizing fluids than at Sora, which proved more favorable for Re transportation.

## ACKNOWLEDGEMENTS

This work was supported by RFBR grant (06-05-64254) and NSH-4933.2006.5. We thank D. Cooke for his detailed review.

## REFERENCES

Berzina A.N, Sotnikov V.I, Economou-Eliopoulos M., Eliopoulos D.G. (2005) Distribution of rhenium in molybdenite from porphyry Cu-Mo and Mo-Cu deposits of Russia (Siberia) and Mongolia. *Ore Geol. Rev.* 26 (1-2), pp. 91-113. DOI 10.1016/j.oregeorev.2004.12.002

Berzina A.P., Sotnikov V.I., Berzina A.N. and Gimon V.O. (1994) Features of magmatism in Cu-Mo deposits in various geodynamic settings. *Russian Geology and Geophysics*. 35(7-8), pp. 204-217.

Giles D.L., Shilling J.H. (1972) Variation in rhenium content of molybdenite. *International Geological Congress, 24th Session,* Section 10, Montreal, pp. 145-152.

Goltz L.G. (2004). Determination of Re and Re associated with Mo using inversion voltammetry. In V.V. Malakhov (Ed): Analytics of Siberia and Far East. *Proc. of the VII All-Russian scientific conference.* Novosibirsk, v. 2, p.94. (In Russian).

Rudnik R.L., Gao S. (2003) Composition of the continental crust. In: R.L. Rudnick (Ed), *Treatise on Geochemistry*. V. 3. The Crust. Elsevier-Pergamon, Amsterdam. pp.1-64. DOI 10.1016/B0-08-043751-6/2F03016-4.

Sotnikov V.I., Ponomarchuk V.A., Berzina A.N., Berzina A.P., Kiseleva V.Yu., Morozova I.P. (2000) Evolution of $^{87}Sr/^{86}Sr$ in igneous rocks of porphyry Cu-Mo ore clusters (based on studies of accessory apatite). *Russian Geology and Geophysics*. 41(8), pp. 1078-1088.

Sun W., Bennet V.C., Eggins S.M., Kamenetsky V.S., Arculus R.J. (2003) Enhanced mantle-to-crust rhenium transfer in undergassed arc magmas. *Nature.* 422, pp. 294-297. DOI 10.1038/nature01482.

Todorov T., Staikov, M. (1985) Rhenium content in molybdenite from ore mineralizations in Bulgaria. *Geologica Balcanica*, 15 (6), pp. 45-58.

Xiong Y., Wood S. (2002) Experimental determination of the hydrothermal solubility of $ReS_2$ and the Re-$ReO_2$ buffer assemblage and transport of rhenium under supercritical conditions. *Geochem. Trans.* 3, pp. 1-10. DOI 10.1186/1467-4866-3-1.

# INTEGRATED EXPLORATION & NEW DISCOVERIES

EDITED BY:

COLIN ANDREW

JULIAN MISIERWICZ

# The West Musgraves, Western Australia: a potential world-class Ni – Cu – PGE sulphide and iron oxide Cu – Au province?

D.I. Groves[1,2], I. Groves[1], S. Gardoll[1], W. Maier[2] & F.P. Bierlein[2]
1 *Redstone Resources, Suite 3, 110 – 116 East Parade, East Perth WA 6004, Australia*
2 *Centre for Exploration Targeting, University of Western Australia, 35 Stirling Highway, Crawley WA 6009, Australia*

ABSTRACT: The West Musgraves lies near the triple-point junction of the West Australian, North Australian and South Australian cratons. Largely Mesoproterozoic amphibolite-granulite facies gneisses are intruded by large layered mafic intrusions of the *ca.* 1080 Ma Giles Complex. These are intruded by smaller, sulphide-bearing mafic bodies and A-type granites, which appear restricted to a NE- to ENE-trending structural corridor. Despite limited past access for exploration companies, there are large nickel laterite deposits at Wingellina, and significant Ni-Cu-PGE sulphide deposits at Nebo-Babel. Recent exploration has defined several Cu, Ni and PGE anomalies in soil and surface gossans on the flow-through margin of a concentrically zoned intrusion. High-resolution aeromagnetic surveys also highlight magnetic 'bullseyes' that resemble anomalies above the Olympic Dam and Prominent Hill IOCG deposits, further adding to the potential metallogenic significance of the province.

KEYWORDS: Musgrave Block, Giles Complex, nickel-copper-PGE sulphides, IOCG

## 1 INTRODUCTION

The West Musgraves represent one of the last frontiers for first-pass mineral exploration in Australia. Situated in a remote part of west-central Australia, access to land by mining and exploration companies was difficult in the past because of access restrictions imposed by traditional owners. Recently, such access has proved possible through structured arrangements with regional land councils. The Wingellina lateritic Ni deposit (227 Mt at 1.0% Ni and 0.07% Co) had been known since 1955, but little exploration had been carried out elsewhere in the Musgraves until Western Mining Corporation discovered the Babel and Nebo Ni-Cu-PGE sulphide deposits (2.4 Mt Ni+Cu, 2.57 Moz PGE) in 2000. This represented the most significant Ni-sulphide discovery globally in the past decade. Since then, Redstone Resources has acquired approximately 7000 km² of ground in the West Musgraves and, in 2006, started regional exploration. This paper presents some of the data collected in this period that further enhance the potential for the West Musgraves to become a significant metallogenic province.

## 2 TECTONIC SETTING AND REGIONAL GEOLOGY

The Musgrave Block occupies a unique tectonic niche in the Precambrian Shield of Australia, with the West Musgraves lying near the triple-point junction of the West Australia, North Australia and South Australia cratons at the western extremity of that Block (Fig. 1). Although the oldest rocks dated are Mesoproterozoic (< 1650 Ma; Scrimgeour *et al*. 1999), there is likely to be at least some Archaean or Palaeoproterozoic lithosphere beneath the West Musgraves because of the multiply-reworked nature of the margins of the cratons and the presence of thick layered mafic intrusions in the Musgrave Block. Its tectonic setting is similar to that of several giant Ni-Cu-PGE sulphide ore bodies globally (*e.g.* Sudbury, Jinchuan, Noril'sk) and similar to that of Precambrian iron oxide Cu-Au (IOGC) deposits (Groves & Bierlein 2007).

The Musgrave Block is an east-west trending orogenic belt comprising a variety of high-grade *ca.* 1600 - 1300 Ma basement lithologies of sulphur-poor amphibolite- to granulite-facies felsic gneisses of mixed intrusive, volcanic and

sedimentary protoliths (Glikson *et al.* 1995). These are intruded by the Giles Complex, mafic dykes, and granitoids associated with the waning stages of the Musgrave Orogeny at *ca.* 1200 - 1120 Ma, which also produced the high-grade metamorphism (Scrimgeour *et al*. 1999).

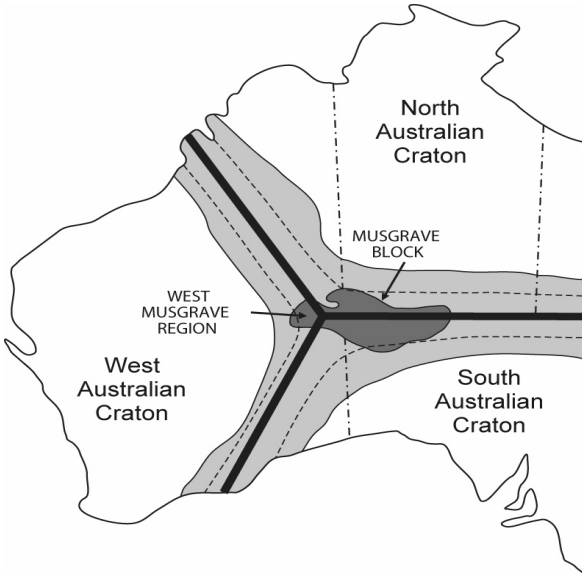


Figure 1. Schematic diagram showing the tectonic setting of the Musgrave Block and West Musgraves at the triple-point junction of the West Australian, North Australian and South Australian cratons.

The *ca.* 1080 Ma Giles Complex consists of partly deformed and recrystallised, layered mafic-ultramafic intrusions, mafic and felsic dykes, and coeval bimodal mafic and felsic volcanic rocks (Glikson *et al*. 1995), which are part of the Warakurra Large Igneous Province of central Australia. The Complex, similar in extent to the Bushveld Complex of South Africa, is interpreted to have been emplaced at 33 to 16km, with the shallower intrusions in the West Musgraves ranging from olivine gabbronorites to gabbronorites, leuco-gabbronorites and troctolites.

Morphologically, the intrusions range from large layered bodies through more circular to irregular or tube-like bodies, as at the Nebo-Babel Ni-Cu-PGE sulphide deposit (Seat *et al*. in press; Fig. 2). The mafic lavas and dykes in the region are largely S-undersaturated, whereas, based on available geochemistry (*e.g.* Cu/Zr ratios) and reconnaissance petrology, the Giles intrusions are variably S-saturated. Sulphur saturation appears to be the result of differentiation, with sulphides commonly associated with mafic units that are enriched in Zr, Fe and P (*e.g.* Seat *et al.* 2007), suggesting extreme fractionation. At present, the distribution of S-undersaturated and S-saturated units is unclear, but it appears that in the large layered sills S saturation is only reached during late crystallisation, whereas many of the smaller mafic intrusions were S-saturated on intrusion. The S does not appear to have been derived from the local S-poor country rocks.

## 3 STRUCTURAL CORRIDOR CONCEPT AND METALLOGENIC POTENTIAL

Prior to recent exploration in the West Musgraves, geological maps (Glikson *et al.* 1995) lacked lithological and structural continuity, with isolated outcropping areas (20-30%) depicted in areas of more continuous cover. Low-level, close-spaced aeromagnetic surveys have enabled a more coherent understanding of the solid geology of the region (Fig. 2). It now appears that most of the exposed, relatively well-described portions of the Giles Complex represent the layered sheets or sills of mafic-ultramafic rocks, whereas the smaller, more circular to irregular mafic intrusions are largely confined to a NE- to ENE-trending structural corridor (Fig. 2) largely covered by thin regolith.

This distinction has important economic implications. In the large layered sills, S saturation may only be achieved during the late stages of differentiation, notably in V-rich magnetite layers. This could result in Ni-Cu-PGE concentrations, but most likely in thin layers such as those mined in the 'reefs' of the Bushveld Complex (Cawthorn *et al.* 2005), but uneconomic elsewhere. In contrast, the smaller intrusions may be derived from differentiated S-saturated magma (*e.g.* Nebo-Babel; Seat *et al.* 2007), providing opportunity for trapping of Ni-Cu-PGE sulphides during dynamic emplacement in these geometrically complex intrusions (*c.f.* Jinchuan, Voisey's Bay) and/or along magma flow-through zones such as in the Platreef of the Bushveld Complex (Cawthorn *et al.* 2005).

The structural corridor also appears to be the locus for emplacement of circular A-type granite bodies. Their A-type affinity, associated high Fe, F, U, and REE, and potential occurrence adjacent to a lithospheric boundary (c.f. Groves and Bierlein 2007) all point to IOCG potential in the region. The structural corridor

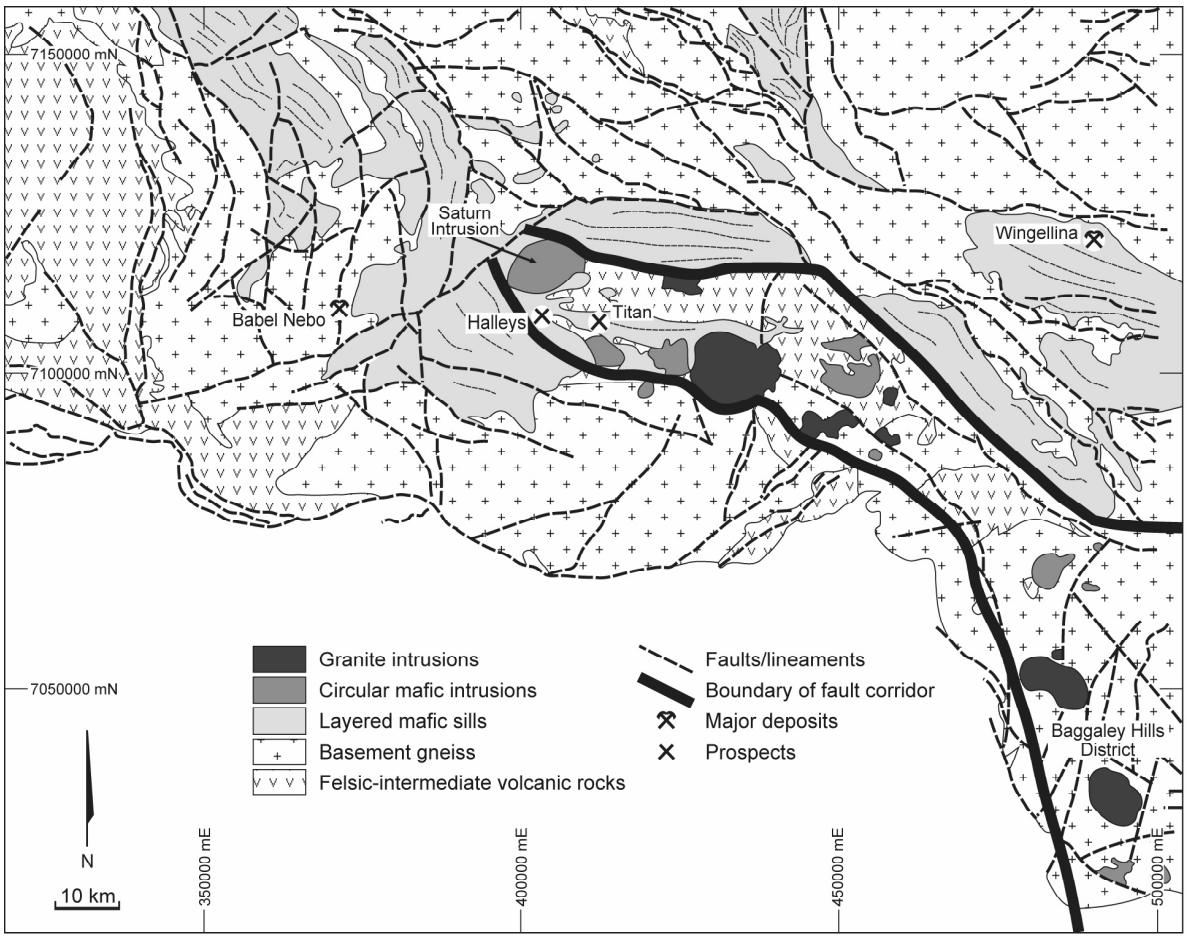


Figure 2. Geological map of the West Musgraves, as interpreted from surface outcrop and aeromagnetic data. Map emphasizes the NE- to ENE-trending structural corridor which encloses numerous subcircular to irregular mafic and granitic intrusions. The major Ni deposits are show, as are the new Ni-Cu-PGE prospects.

resembles that controlling the world-class Carajas IOCG province of Brazil (Groves & Bierlein 2007), and it broadly coincides with an interpreted lineament on which the giant Olympic Dam IOCG deposit also lies to the southeast (O'Driscoll 1990).

Much of the West Musgraves is essentially virgin ground in terms of modern exploration. Importantly, most of the exposed bedrock is of the less-prospective rock units. By contrast, the units with the greatest metallogenic potential, although under cover, are generally overlain by only thin regolith which largely retains the *in situ* geochemical signature of the underlying units. The Nebo-Babel deposit, for example, was initially located below a soil lag geochemical anomaly with peak values of 950 ppm Cu, 748 ppm Ni and 12 ppb PGE, broadly coincident with gravity, magnetic and EM anomalies (see summary in Seat *et al.* 2007).

It is evident from the Nebo-Babel discovery that the smaller, more complex and differentiated (high Zr, P, Fe) mafic intrusions are one important target. Another target type is represented by magma flow-through zones on the discordant margins of the bodies such as the concentrically-zoned Saturn Intrusion within the structural corridor (Fig. 2). Geometrical irregularities along such zones may concentrate Ni-Cu-PGE sulphides due to magma dynamics.

Initial regional soil-geochemical exploration along the discordant south western margin of the Saturn Intrusion highlights its dynamic importance, with discontinuous Ni, Cu and PGE anomalies along its length. At Halleys (Fig. 2), such exploration has defined a 1.5km-long zone of anomalous Cu-Ni-PGE soil geochemistry with peak values of 1915 ppm Cu, 940 ppm Ni and 72 ppb Pt+Pd, approximately 2x, 1.25x and 6x the peak values for Cu, Ni and Pt+Pd respectively in soils above Nebo-Babel. Limonitic gossan at Halleys contains up to 9000 ppm Cu, 5200 ppm Ni, 500 ppm Co and 250 ppb Pt+Pd, with analyses of the entire PGE suite confirming its derivation from magmatic sulphides (Fig. 3), as does a coincident down-dip

EM anomaly. Further to the east at Titan (Fig. 2), there are also significant Cu-PGE soil anomalies at a potentially higher crustal level of the flow-through contact. Although exploration is in its infancy, these results, together with the prior discovery of Nebo-Babel, highlight the Ni-Cu-PGE potential of the West Musgraves in at least two magmatic scenarios.

The region considered most prospective for IOCG deposits is the Baggeley Hills district (Fig. 2). A high-definition aeromagnetic survey has defined several magnetic 'bullseyes', similar to those over IOCG deposits (*e.g.* Olympic Dam and Prominent Hill, South Australia; Carajas district, Brazil), associated with magnetic felsic intrusions interpreted to be A-type granites. No geochemical surveys have been carried out to date over these geophysical targets.

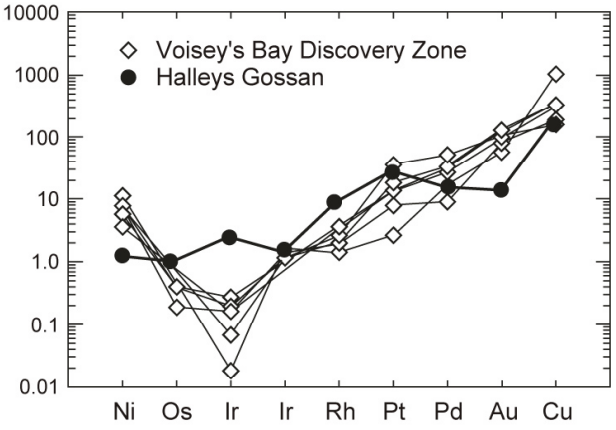


Figure 3. Chondrite-normalised Ni, PGE, Au and Cu spidergram showing geochemical data for the Halleys gossan compared to those from the Voisey Bay Discovery Zone.

## 4 CONCLUSIONS

The West Musgraves in the Musgrave Block represents one of the last exploration frontiers in Australia, being remote, having restricted access for more than 30 years, and being largely covered by thin regolith that provides a barrier to traditional prospecting. Initial exploration, over only a fraction of its surface area, has already resulted in the largest Ni-Cu-PGE sulphide discovery of the last decade and the definition of several other promising Ni-Cu-PGE targets within a newly-defined structural corridor. The province also shows potential for IOCG deposits based on its tectonic setting, contained A-type granites, known F, U and REE anomalism, and presence of aeromagnetic 'bullseyes' adjacent to interpreted oxidised A–type granite intrusions. The West Musgraves thus has the potential to become a new world-class Ni-Cu-PGE and IOCG province.

## ACKNOWLEDGEMENTS

We are grateful to Redstone Resources staff, particularly Anthony and Rodney Ailakis for their role in ground acquisition and vision for the West Musgraves. Staff of the Geological Survey of Western Australia are thanked for informal but informative discussions and for field support for Wolfgang Maier.

## REFERENCES

Cawthorn RG, Barnes SJ, Ballhaus C, Malitch KN (2005) Platinum group element, chromium and vanadium deposits in mafic and ultramafic rocks. *Economic Geology 100th Anniversary Volume:* 215-250

Glikson AY, Ballhaus CJ, Clarke GL, Sheraton JW, Stewart AJ, Sun S-S (1995) Geological framework and crustal evolution of the Giles Complex, western Musgrave Block, Western Australia. Australian Geological Survey Organisation *Journal of Geology and Geophysics* 16: pp 41-68

Groves DI, Bierlein FP (2007) Geodynamic settings of mineral deposit systems. *Journal of the Geological Society London* 164: pp 19-30

O'Driscoll EST (1990) Lineament tectonics of Australian ore deposits. In: Hughes FE (ed) Geology of the Mineral Deposits of Australia and Papua New Guinea, *The Australian Institute of Mining and Metallurgy,* pp 33-41

Scrimgeour IR, Close DF, Edgoose CJE (1999) Petermann Ranges SG – 52-7 1:250,000 *Geological Map Series Explanatory Notes 52-7: Northern Territory Geological Survey*

Seat Z, Beresford SW, Grguric BA, Waugh RS, Hronsky JMA, Gee MAM, Groves DI, Mathison CI (2007) Architecture and emplacement of the world-class Nebo-Babel gabbronorite-hosted magmatic Ni-Cu- PGE system, West Musgraves, Western Australia. *Mineralium Deposita* (in press)

# An integrated approach to exploration and exploitation of Ni-Cu (PGE) deposits in dynamic magmatic systems

Christoph Gauert
*Centre for Sustainable Usage of Earth Resources, Dept. of Geology, University of the Free State, P.O. Box 339, Bloemfontein 9300, R.S.A.*

ABSTRACT: The exploration and exploitation history of the Uitkomst Complex Ni-Cu-(PGE) deposit in the Mpumalanga Province in South Africa is used to illustrate the ore-forming potential of dynamic magmatic systems. A within-plate tectonic setting along a crustal lineament, a possible Bushveld Complex connection through a subvolcanic feeder sill, and sulphur-bearing country rocks of the lower Transvaal Sequence created promising geochemical and geophysical footprints for a fertile magmatic system. S isotope ratios of sulphide minerals and incompatible trace element ratios of chilled marginal rocks exhibit evidence for crustal contamination. Pathfinder minerals such as zinc-enriched spinels and Ni-depleted olivine assist in regional exploration. Integration of remote sensing, aeromagnetic and geo-electric data, regional stream sediment as well as lithogeochemical and metamorphic data in a geographical information system appears to be the successful route in reconnaissance exploration – both Brown- and Greenfield - to generate targets in a similar environment. Ranking of targets through mineral project evaluation and innovative processing techniques such as Activox® make low-grade and high tonnage deposits viable operations under current metal prices.

KEYWORDS: Exploration, Ni-Cu-(PGE) deposits, dynamic magmatic systems, geochemical and geophysical footprints, pathfinder minerals, integrated G.I.S, innovative evaluation and processing

## 1 INTRODUCTION

Metal deposits cropping out at surface have already been found in most countries through their prospecting history. The deposits now being searched for are largely concealed by weathered and sealed outcrops, they are covered by soils, drift, or some other cover and it requires sophisticated methods to find them. Large economic deposits (>50Mt) at high grade underlying an surface area of 2 $km^2$ up to 1000m of depth are minute and thus are not easy to target. Mineral economics requires from such exploration campaigns that favourable ore should be high to medium grade Ni-Cu(-PGE) mineralization hosted by (ultra-) mafic igneous rocks in subvolcanic feeder sill positions.

Market mechanisms determine commodity prices in such fashion, that even under current favourable circumstances, the optimum target should have a size of more than 100 Mt of ore at a grade of at least 0.5 % equivalent of Ni + Cu + PGEs. Economically viable deposits should have a low waste to ore ratio, and are possibly situated not far from existing mines and infrastructure.

## 2 CHOICE OF EXPLORATION AREA

Factors governing the choice of exploration areas are (i) principal plate tectonic regimes of formation of this type of deposit, (ii) geological and metallogenic models and (iii) the deposits' worldwide distribution. The principal exploration strategy is to initially use remote sensing techniques such as satellite images and hyperspectral scans and the evaluation of past exploration literature. Reconnaissance techniques comprise airborne (electro-) magnetics, and stream sediment or overburden sampling procedures depending on the climate of the area. Analytical techniques are then applied to meaningful geochemical data which can be used for trace element modelling. Prospecting includes field recognition of mineralized chilled margins of intrusions, abnormal rocks such as gossans,

alteration halos and contact-metamorphic features, coupled with an understanding of the mineralogy of economic deposits. Findings compiled in a G.I.S. system will allow target generation. The feasibility study of a prospect focuses on drilling techniques, three-dimensional statistics and visualisation of assay results.

This case study considers the Uitkomst Complex, hosting the Nkomati Ni-Mine and subsequent exploration projects for this deposit type in the Mpumalanga Province of South Africa. The sulphide-bearing lower Transvaal Supergroup sediments are ideal country rocks for mineralised mafic to ultramafic intrusions. The shape, geochemical trends, and the ore body's shallow dip add to the characteristics of a subvolcanic feeder sill (conduit), replenishing a higher volcanic reservoir. Satellite complexes to the Bushveld Complex appear to be controlled by major crustal lineaments. The sulphide solubility of the melt decreases during progressive crystallization (Naldrett & Von Gruenewaldt, 1989), and assimilation of sulphur-rich country rock leads to appearance of an immiscible sulphide melt. At Uitkomst, considerably higher magma volumes than indicated by the cross section cause a dynamic magma system and Ni, Cu and PGE are scavenged due to high partition coefficients into sulphides of these metals. Additionally to Ni and Cu, genetic models of both chromite and PGE mineralization in layered mafic intrusions also have to be adapted to this case.

## 3 SUBVOLCANIC, COUNTRY ROCK AND ORE FOOTPRINTS

'Footprints' of magmatic Ni-Cu (PGE) systems (Lesher *et al*., 2004) applicable to such exploration are tectonic and magmatic settings (within plate volcanism along crustal lineaments), and volcanic and subvolcanic 'footprints'. The ore localization is facilitated by sulphur-bearing country rocks, geo-electric, also downhole anomalies, and geochemical 'footprints' such as Ni, Cr, Co and Zn stream sediment anomalies. The worldwide distribution of Ni-Cu-PGE deposits can be classified into 'petro-tectonic setting' (Naldrett, 1999), grade-tonnage diagrams, tectonic settings and parental magmas. Only a few magmatic Ni-Cu-(PGE) deposits form in isolation from each other. Cratons often contain multiple mineralized provinces, belts, and assemblages/terranes. There exists a scale-dependant relation of deposits to magmatic eruptions with distinctive footprint (small), same broad magmatic event (intermediate) or common magmatic processes (large). Economic deposits are almost exclusively associated with dynamic (replenished) magmatic systems (Lesher, 2004), and so is Uitkomst. As a mineralized sub-volcanic sill complex it is 0.8 to 1.6km wide and about 12km long.

Magma-country rock interaction depends on setting, mode of emplacement, nature of country rock, and degree of metamorphism and deformation. The amount of contamination and/or chalcophile element depletion depends on the stratigraphic architecture of the system and the fluid (thermo-) dynamics of the magma/lava (Lesher, 2004). The physical, chemical and thermal characteristics and the sulphur and metal content of the contaminant, the high initial sulphur saturation state of magma, the assimilation: crystallization ratio, the amount of lava replenishment and the effective magma : sulphide ratio of the system decide about the 'ore-fertility' of the system.

Promising litho-types in mapping are troctolites and wehrlites. The amount of nickeliferous pyrrhotite, and the liberation size required for beneficiation of net-textured ore determine its quality. $\Delta^{34}S$ isotope ratios of ore sulphides strongly deviating from zero reflect contamination by host-rock sulphur. Mapping of brecciated intrusive contacts with hornfels-calc-silicate contact aureoles in pelitic country rocks is a powerful tool in Ni-Cu-PGE exploration when targeting differentiated mafic to ultramafic igneous rocks. Pathfinder minerals such as zinc-enriched spinels and Ni-depleted olivine have proven to assist in regional exploration for Uitkomst-style deposits.

## 4 GEOCHEMICAL FOOTPRINTS

Lithogeochemical footprints of fertile igneous rocks on various Ni-Cu prospect use V/Cr and Ti/Zr ratios as fractionation indicators and to determine derivation from an initial magma source. Incompatible trace element patterns of prospective intrusive rocks were normalized to Bushveld Complex initial magma (B1) and compare similarly to known mineralized rocks (Gauert, 2001). Cu/Pd and Cu/Pt ratios well below mantle values can be used to assess potential for platinum reefs (Maier *et al.*, 1998). Fractionation models using Y, Zr, Cr and Ni

(De Waal *et al.*, 2001) facilitate in establishing whether open or closed system conditions prevail in intrusions, such as the conduit situation for the Uitkomst Complex. Meaningful discrimination of litho-geochemical grab samples of gabbroic rocks from igneous provinces such as the eastern Kapvaal Craton could be achieved effectively by multivariate statistics such as canonical variance analysis based on factors calculated from logarithms of: $Al_2O_3$, $FeO_{tot}$, CaO, MgO, $Na_2O$, $K_2O$, Rb, Sr, Nb, Y, Mg#, and Cr/Ni, Ti/Y, and Cr/Zr ratios.

## 5 FEASIBILITY STAGE

At the feasibility stage results of systematic and infill drilling allows subsequent application of 3D-statistics to perform reserve calculations. Detailed studies of the mineralogy of economic deposits determine metallurgical and processing techniques by mineral interlocking and liberation size. The occurrence of deleterious substances can cause problems. Mineral project evaluation and selection criteria - depending on development of cash flow in constant money, sensitivity analysis, and a 'hurdle rate' - may result in a ranking of mineralizations. The life of the small Nkomati Mine until 2007 is in the process to be drastically extended by introducing the innovative Activox® hydrometallurgical process (Lion Ore Australia, 2004). It results in low capital cost compared to smelting, is an environmentally friendly process, and it enables the treatment of a range of concentrates including high impurities and low grades without $SO_2$ emissions and at high base metal recoveries.

## 6 CONCLUSIONS

The booming of non-OECD (Organization for Economic Co-operation and Development) economies causing a mineral/metal crisis positively affects mineral exploration industry through high commodity prices. A short static lifetime of many metals and fossil fuel is a further incentive for mineral exploration. The optimum target is a high quality product with ≥ 100 Mt at high grade near the surface. The choice of exploration area is governed by the cost of infrastructure, transport, environmental considerations, taxation and political factors. There are favourable plate tectonic regimes of deposit formation, metallogenetic, empirical & grade-tonnage models. Lithogeochemical ratios, contact metamorphic effects and mineral chemistry of indicator minerals have high application value as vectors to ore in both 'Brown' and 'Greenfield' exploration. Stream sediment anomalies with log-normal distributions offer excellent tools to narrow down targets, and so does soil sampling with help of auguring at smaller scale. Lithogeochemical relational databases using multivariate statistics and norm calculations help to identify fertile intrusions. Open file reports, metallogenetic maps, geochemical and geophysical, remote sensing, and detailed mapping (Joubert *et al.*, 2006) will generate targets for integrated G.I.S.-based exploration projects. The outlook on exploration and exploitation of Ni-Cu(PGE)-bearing systems is: The demand exists and successful mining is a challenge.

## ACKNOWLEDGEMENTS

Thanks to the Dept. of Geology, Univ. of the Free State for useful scientific discussion and to African Rainbow Minerals Ltd., and to Nkomati Mine Management for logistic help.

## REFERENCES

De Waal, S.A., Maier, W., Armstrong, R., Gauert C.D.K. 2001. Chemical constraints on the differentiation and emplacement of the Uitkomst Complex, Mpumalanga Province, S. Africa, *Canadian Mineralogist*, v.39, p.557-571.

Gauert, C. 2001. The importance of a magmatic conduit mechanism for the formation of the sulphide and oxide mineralization in the Uitkomst Complex, South Africa, *J. of Afr. Earth Sc.,* v. 32/2, p.149-161.

Joubert, L.P., Gauert, C.D., Davidson, M. and Van Lente, B. 2006. The role of post-intrusive, deformational processes in ore reserve consideration at Nkomati Nickel Mine, Mpumalanga Province, South Africa. *Abstract volume of Colloquium of African Geology* 21, Associacao Geologica Mineira de Mocambique, Maputo, p.288-291.

Lesher, C.M. 2004. Footprints of magmatic Ni-Cu(PGE) systems SEG 2004 Perth, Western Australia, Session: Cutting-Edge Developments in Economic Geology. Conference abstract volume, 117-120.

Maier, W.D., Barnes, S.-J. & De Waal, S.A. 1998. Exploration for magmatic Ni-Cu-PGE sulphide deposits: a review of recent advances in the use of chemical tools, and their application to some South African ores. *S.A. Journal of Geology*, V.101, 237-253.

Naldrett, A.J. and von Gruenewaldt, G. 1989. Association of platinum-group elements with chromitite in layered intrusions and ophiolite complexes. *Economic Geology,* 84,180-7.

Naldrett A.J. 1999. World class Ni-Cu-PGE deposits: key factors in their genesis, Miner. Dep., 34, 227-240.

| Setting criteria after Lesher (2004) | Applicable to Uitkomst Complex type Ni-Cu-(PGE) deposits in Mpumalanga and Limpopo Provinces, RSA |
|---|---|
| **Tectonic setting** | |
| intracontinental rift | NW-SE Uitkomst Lineament of the Bushveld Complex |
| rifted continental margin | n/a |
| rifted arc, convergent margin | n/a |
| **Magma type** | |
| Al (un-)depleted komatiite | n/a |
| komatiitic basalt | n/a |
| continental flood & tholeiitic basalts | mixture of B1 & fractionated B2-Bushveld-type magma |
| quartz diorite | Uitkomst initial magma more evolved than a normal basalt |
| **Volcanic/subvolcanic settings** | |
| subvolcanic feeder sill | Shallowly dipping magma conduit |
| feeder / exit dyke | n/a |
| volcanic vent, lava channel | n/a |
| melt sheet | n/a |
| **Influence on country rocks** | |
| sulphide veins injected into footwall rocks | locally at Uitkomst, high Cu and Pd contents |
| contact metamorphism | extensive at Uitkomst (20 to 300m) |
| brecciation of country rocks | extensive shearing at the base of the Complex |
| **Form, distrib., timing of sulphide segregation** | |
| stratiform to stratabound, at or near the base of host unit | massive sulphide lenses at base and channel-like disseminated mineralization internal to host unit, early magmatic segregation |
| Veins in country rocks assoc. with above | magmatic-hydrothermal |
| Semi-massive within shears and fault zones | tectonically mobilised |
| **Geochemical footprints** | |
| fractionation indicators | Mg#, V/Cr ratios, Ti/Zr for magma lineage, Y and Cr modeling. |
| stream sediment geochemistry | High Ni, Cr, Co, Cu, Zn and Pb |
| pathfinder minerals | RIM: chrome-spinel chemistry, Ni-depleted olivine |
| **Geophysical footprints** | |
| geo-electrical response (electr. conductivities) | strong geoelectric response near disseminated to massive sulphide ore |
| magnetic response | difficult to follow under country rock cover |

# Burkina Faso, an emerging mineral producer in West Africa

A. Nare
*Wentworth Resources Pty. Ltd, Ouagadougou, Burkina Faso*

ABSTRACT: Despite its vast mineral potential, mining only accounts for a small amount of Burkina Faso's GDP. The main mineral commodity produced is gold, all of which is extracted by small-scale gold miners. However, the mining industry is expected to take an increasingly important place in the country's economy with several gold mines currently being developed and mineral exploration steadily intensifying.

KEYWORDS: Burkina Faso, Palaeoproterozoic, mineral, potential, gold, base-metals, mining.

## 1 GEOGRAPHICAL AND GEOLOGICAL SETTING OF BURKINA FASO

Burkina Faso is a landlocked nation in West Africa. It covers an area of approximately 274,000km² with a resident population estimated at some 14 million. Burkina Faso is one of the poorest countries in the world, with more than 80% of the population relying on subsistence agriculture, and with only a small fraction directly involved in industry and services.

Figure 1. Geological map of Burkina Faso with major gold deposits.

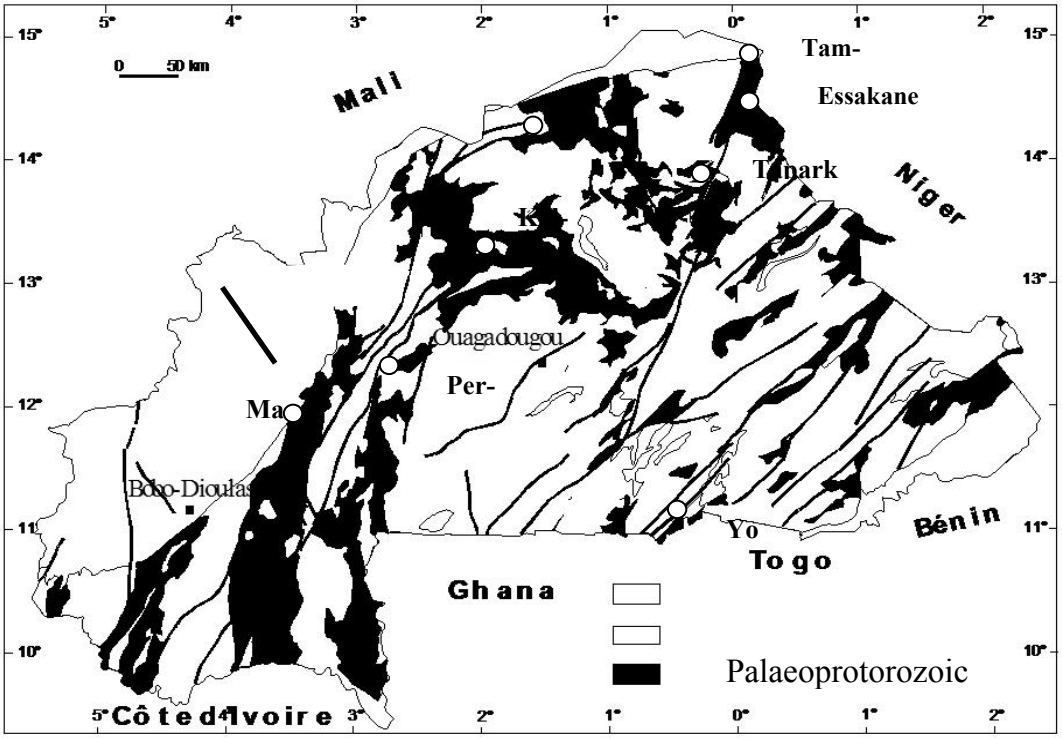

| Deposits | Metal | Companies | Reserves & Resources |
|---|---|---|---|
| TAPARKO/BOUROUM | Au | HRG (SOMITA) | 7.98Mt @ 2.87g/t |
| | | | 0.80Mt @ 4.15g/t |
| YOUGA | Au | BMC (ETRUSCAN) | 6.60Mt @ 2.70g/t |
| KALSAKA | Au | CLUFF MINING (KALSAKA MINING SA) | 13.7Mt @ 1.40g/t |
| MANA | Au | SEMAFO | 13.0Mt @ 2.24g/t |
| ESSAKANE | Au | GOLDFIELDS / OREZONE | 40.5Mt @ 2.0g/t |
| INATA | Au | GOLDBELT | 29.5Mt @ 2.0g/t |
| GUIRO | Au | STREMCO SA | 0.35Mt @ 10.2g/t |
| SEGUENEGA | Au | OREZONE | 9.33Mt @ 2.80g/t |
| BONDIGUI | Au | OREZONE | 6.22Mt @ 2.88g/t |

Table 1. Gold potential in Burkina Faso

The geology of Burkina Faso is dominated by Palaeoproterozoic rocks, which underlie most of the country. Younger rocks crop out only in the far west and southeast of the country, respectively as part of the Taoudenni and Volta sedimentary basins. The majority of the Palaeoproterozoic terrane consists of granitoïds, with subordinate migmatitic gneisses, cut by a large number of, predominantly, northeast to north-northeast trending greenstone belts hosting the volcano-sedimentary rock sequences of the Birimian Supergroup.

These greenstone belts host the majority of the country's mineral occurrences, notably gold, zinc, manganese, copper, nickel and antimony. Neoproterozoic phosphate rocks occur in the southeast of the country close to the borders with Benin and Niger, while small bauxite occurrences and marble deposits are found in the westernmost Neoproterozoic and Palaeozoic sedimentary cover.

## 2 THE MINERAL POTENTIAL OF BURKINA FASO AND ITS IMPORTANCE IN THE LOCAL ECONOMY

### 2.1 *Mineral Potential*

During the geological evolution of the Palaeoproterozoic basement, the emplacement of the primary ore deposits took place at various stages, notably :

During the sedimentary and magmatic events of the Birimian (2240-2170Ma):

- deposition of polymetallic volcanic-hosted massive sulphides (VHMS) (*eg.* Perkoa: 6.3Mt @ 14.5% Zn) and manganese-bearing volcano-sedimentary (exhalative?) deposits (*eg* : Tambao: 19Mt @ 55% Mn and Kiere : 0.6Mt @ 54%Mn);
- emplacement of porphyry-type copper-gold mineralization in the Gaoua district genetically related to diorite-quartz diorite porphyry complexes.

During the "Late-Eburnean" tectonic events (2100Ma), mainly comprising gold mineralization associated with cross-cutting regional and local faulting.

### 2.2 *Mining Development*

Despite the vast mineral potential of the country, mining only accounts for a small amount of Burkina Faso's GDP. The only metal commodity produced is gold, all of which is extracted by small-scale gold miners. This is however likely to change rapidly.

There are currently two gold and one zinc mines under construction, respectively at Taparko-Bouroum (High River Gold Mines Ltd. ) and at Youga (Etruscan Resources Inc.) for gold, and at Perkoa for zinc (AIM Resources plc). Four (gold) projects have completed a feasibility study and/or have applied for mining permits, namely the Kalsaka (Cluff Gold plc, exploitation permit already granted), Inata (Goldbelt Resources Inc.), Mano River Resources plc (Semafo Inc.) and Guiro-Diouga

(Stremco S.A.) gold projects. Three projects are in an advanced (say resource definition) stage, namely Essakane (Goldfields and Orezone Resources), Séguénéga and Bondigui (both Orezone Resources).

In addition intensive exploration is being carried out over several other exploration permits. In June 2006 some 230 exploration permits had been granted in Burkina Faso and there are over 25 foreign companies actively exploring in the country.

ACKNOWLEDGEMENTS

Special thanks go to Guy Franceschi, for his constructive review and comments, and to Goldcrest Resources Ltd, who supported the preparation of this paper.

REFERENCES

Carte Géologique et Minière au 1/1000000 du Burkina Faso_2003_CASTAING C et Al.

Mining Journal_Special Publication_ Burkina Faso

Paléoprotérozoïque_Birimien du Burkina Faso_Prof.Martin LOMPO

# Targeting Gold Deposits along a Regional Shear Zone: A Case Study from the Archaean Golden Pride Deposit in Tanzania

I.M.A. Vos & M.H.D. Christie
*Resolute Mining Ltd, Perth, Australia*

S.H. Halley
*Mineral Mapping Pty Ltd, Perth, Australia*

ABSTRACT: Exploring for gold deposits along regional shear zones can be challenging because of the presence of cover. A case study from the Archaean Golden Pride deposit in Tanzania demonstrates how the utilization of PIMA results combined with multi-element geochemistry can aid in locating the position of regional shear zones and the generation of targets along such shear zones.

KEYWORDS: gold, exploration, alteration, geochemistry, PIMA.

## 1 INTRODUCTION

The Golden Pride gold deposit (Total Resource: ~3 Moz Au) is situated in the central part of the E-W striking Nzega Greenstone Belt in the Archaean Lake Victoria Goldfields of Tanzania.

The Golden Pride Au deposit is hosted in the immediate hanging-wall of the regional, ~150km long, steeply south-dipping Bulangamirwa Shear Zone within intensely deformed and altered meta-sedimentary rocks of the Nyanzian System (Borg, 1990).

The occurrence of this well-sized orebody along a regional-scale shear may infer the presence of additional Au occurrences under cover along the strike of the structure. However, identification of the Bulangamirwa Shear Zone in the field is hampered by the presence of surficial cover sediments. Also, the shear zone unfortunately can not be effectively delineated in geophysical (*e.g.* airborne magnetics) imaging.

As a result of the above, alternative methods were required to; 1) effectively delineate the position of the shear zone, and 2) generate 'vectors to ore' to define targets along the strike of the shear zone. To achieve these aims, a study on the alteration and geochemical signature of the Golden Pride deposit was carried out utilizing PIMA (Portable Infrared Mineral Analyser) and litho-geochemistry. The results of this study could then be applied to regional exploration.

## 2 METHODS

To define the alteration signature of the Golden Pride Au deposit, a total of ~15,000 samples from drilling were measured with PIMA (see Thompson *et al*., 1999 for a discussion on its application to exploration). In addition, a total of 152 samples from drill holes along two selected sections through the ore deposit were analysed using a full ICP-OES/MS multi-element (ME) suite. On the basis of the results of these studies, an air core (AC) program was designed along the strike of the Bulangamirwa Shear Zone on 1km-spaced fences centered on the interpreted position of the shear zone and collar locations approx. 80m apart. Each hole was drilled to blade refusal and an end-of-hole (EOH) sample of fresh rock was obtained. PIMA and ME analyses were carried out on the obtained samples, which were then interrogated in light of the results from fingerprinting the Golden Pride Au deposit.

## 3 FINGERPRINTING THE GOLDEN PRIDE AU DEPOSIT

PIMA analysis results from the Golden Pride Au deposit indicate:

1) Short wavelength micas are spatially associated with the Bulangamirwa Shear Zone;
2) High mica abundance can be used the map the presence of felsic porphyry units;
3) There is no visible zonation in chlorite chemistry within the rocks associated

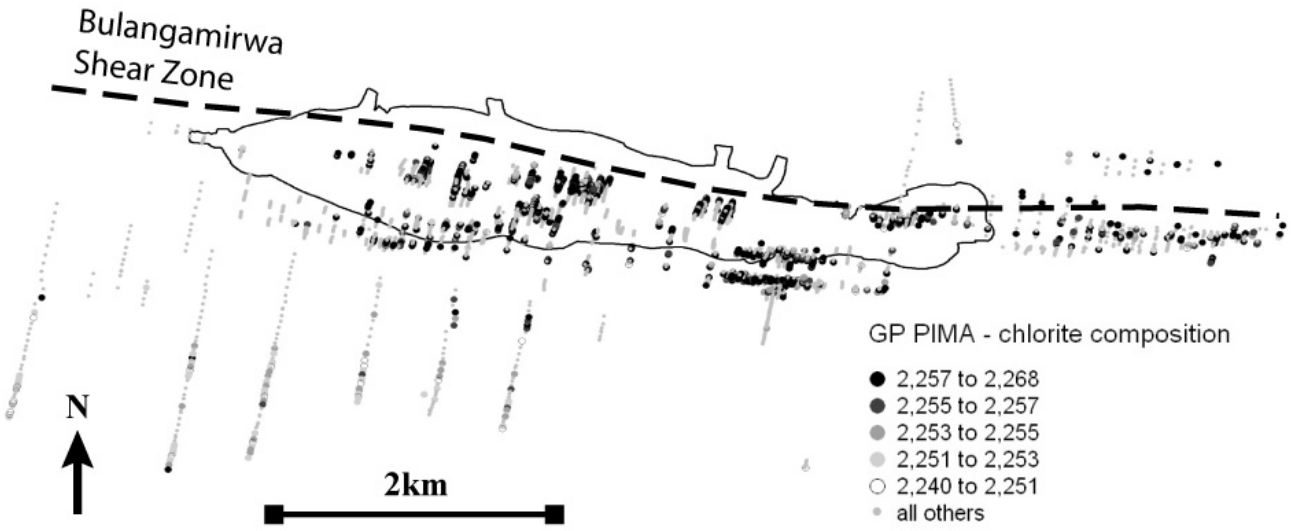


Figure 1. Alteration signature of the Golden Pride Au deposit (approx. outline of pit in black) showing contrast in chlorite composition associated with gold mineralization. Proximal to mineralization Fe-rich chlorite dominates while distal to mineralization Mg-rich chlorite dominates.

with the Golden Pride Au deposit; and,

4) Biotite and chlorite alteration minerals in the samples are iron-rich. More distal to the deposit, however, the composition of chlorite minerals is more Mg-rich (Fig. 1).

The ME results of rocks sampled as part of this study indicate that a strong relationship exists between a number of pathfinder elements (As, Li, Sb, W) and Au mineralization at the

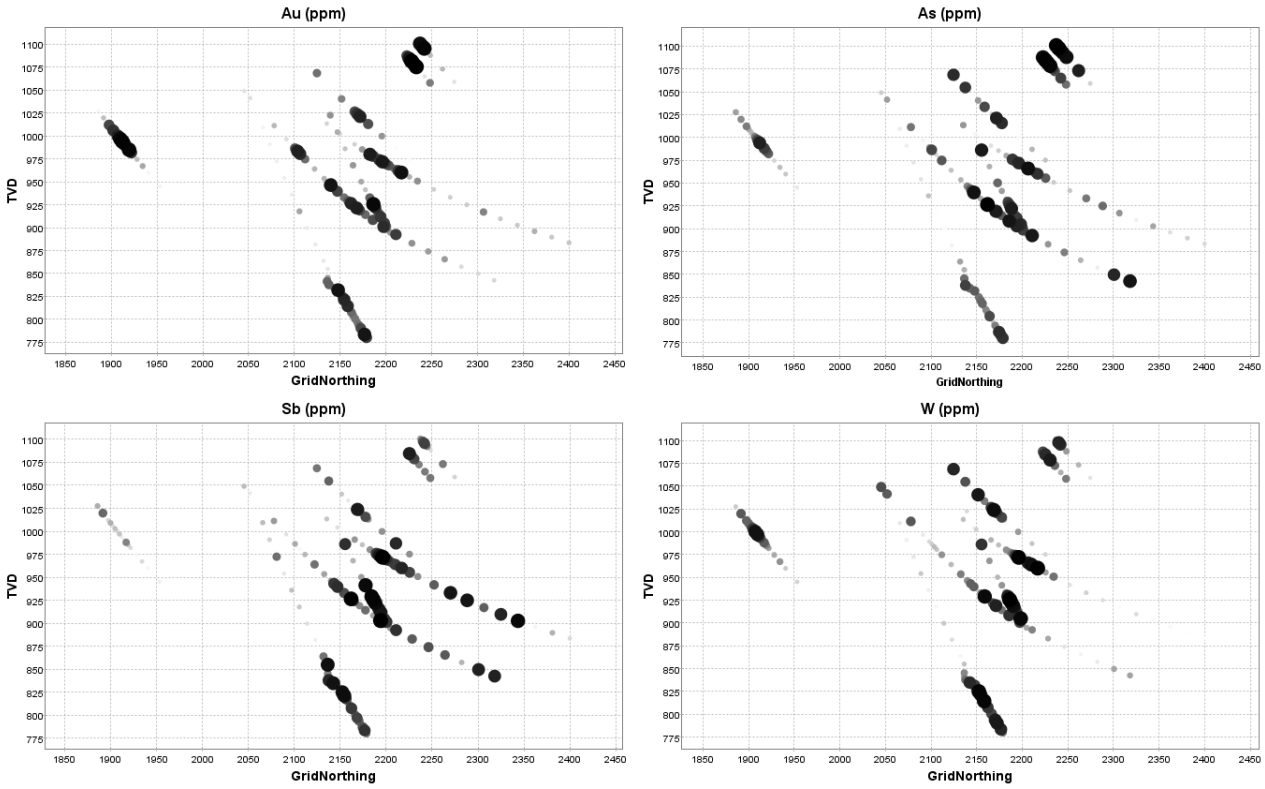


Figure 2. Pathfinder element signatures associated with Au mineralization in the Golden Pride deposit. Note that Sb has a wide dispersion around the ore zone, while W is only well defined within the ore zone. Values range from light grey (low) to black (high) and represent relative abundances (*i.e*. values are not normalized against average crustal abundances).

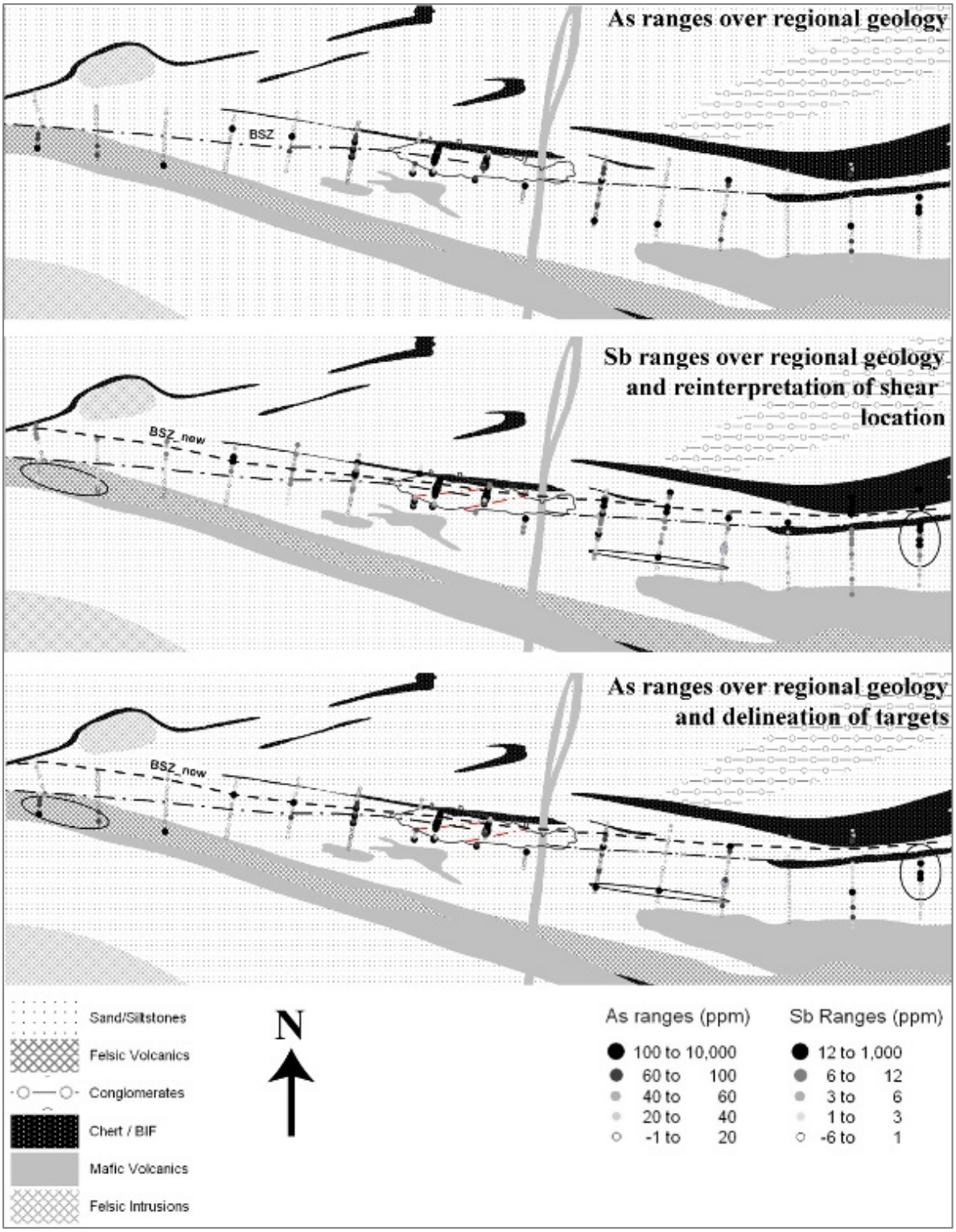


Figure 3. Location of AC holes across the Bulangamirwa Shear Zone with projected As ranges (top). A combination of As and Sb ranges resulted in the re-interpretation of the location of the shear zone (middle) and where pathfinder elements are anomalously high, potential drill targets can be generated (bottom).

Golden Pride deposit (Fig 2.).

In particular, Sb and Li haloes were found to exceed over 500m width, as a result of which the current study did not get out of the hydrothermal system. Tungsten was identified as a proximal indicator mineral, producing restricted haloes around gold mineralization.

The signature of short wavelength micas, Fe-rich chlorites of the Golden Pride deposit and its close association with As and Sb can be interpreted to reflect an acid-reduced hydrothermal environment, where gold has a rela-

tively low solubility as a bi-sulphide complex.

## 4 REGIONAL TARGETING

Based on results from PIMA analysis at the Golden Pride Au deposit, it was inferred that the Bulangamirwa Shear Zone could be identified along strike as a zone of short wavelength mica and long wavelength chlorite. Unfortunately, it was found that the majority of EOH samples collected from the AC drilling program did not penetrate to fresh rocks and therefore the results of this study were only partially beneficial.

On the basis that As and Sb generally have anomalous values in the vicinity of regional shear zones (as is generally accepted for the Yilgarn craton in Australia), As and Sb results from ME analysis of EOH samples from AC drilling were used to determine their proximity to the Bulangamirwa Shear Zone (Fig. 3: top and centre). These results allowed a refined interpretation of the position of this shear zone along the portion of the Nzega Greenstone Belt covered by the AC program.

In addition to this, potential areas of gold mineralization could be defined from anomalous values of Li and W in close proximity to the Bulangamirwa Shear Zone (represented by high values of Sb and As) and a number of targets could be generated that can be drilled in follow-up programs (Fig. 3: bottom).

## CONCLUSIONS

PIMA and ME analysis has successfully enabled the identification of the characteristics of the Golden Pride Au deposit. The recognition of this footprint aided in delineation of the location of a regional shear zone and potential targets along that shear zone. The successful application of this technique around the Golden Pride Au deposit and along the Bulangamirwa Shear Zone demonstrates its strength and applicability in exploration for gold deposits in Tanzania and Archaean greenstone belts elsewhere, in particular where gold deposits may be present under cover.

## ACKNOWLEDGEMENTS

Resolute Mining Ltd. is gratefully acknowledged for allowing presentation of project results.

## REFERENCES

Borg G (1990) A preliminary report on the geology of the Siga Hills, NW - Tanzania. Part I: Regional geology, geophysics, geochemistry and distribution of gold within the project area. (With contributions by D. Eberle). - Tanzanian-German Technical Cooperation, BGR internal report, Archive No. 108564. pp77

.

# Spatial data mining techniques as mineral exploration tools: Examples from gold exploration in the northern Fennoscandian Shield, Finland

V.M. Nykänen & V.J. Ojala
*Geological Survey of Finland, Bedrock and Mineral Resources, Rovaniemi, Finland*

ABSTRACT: Geoscientific information systems (GIS) can be used to quantitatively analyse and integrate spatially referenced information from geological, geophysical and geochemical surveys for decision-making processes in mineral exploration. Excellent coverage of well documented, precise and good quality data enables testing of variable exploration models in an efficient and cost-effective way with high-tech computer aided GIS tools. These data and techniques have been applied to mineral exploration in the Northern Fennoscandian Field, Finland, to provide mineral potential or prospectivity assesments for gold. The techniques have been used to test for orogenic gold deposits and for IOCG deposits.

KEYWORDS: spatial data mining, neural networks, weights-of-evidence, logistic regression, fuzzy logic, mineral exploration, gold, orogenic gold, IOCG, Fennoscandian Shield

## 1 INTRODUCTION

Digital geoscientific data from the Geological Survey of Finland (GTK) are being used as spatial evidence in exploration targeting, *i.e*. ranking areas based on their exploration importance. Spatial data mining or spatial analysis techniques including neural networking, weights-of-evidence, logistic regression and fuzzy logic, have been used as tools in GTK's mineral exploration and geological mapping. Gold exploration has been the main test bench for these techniques due to the excellent data coverage within prospective volcanic belts and especially due to the increased activity in gold exploration in Finland during recent years. We describe some successful case histories where spatial modelling methods have been used to assist Au-potential mapping. The projects have shown that by using these modelling techniques exploration targets can be generated by quantitatively analyzing extensive amounts of data from various sources, and by ranking targets based on their exploration potential.

## 2 STUDY AREA

The study area is located in the Northern Fennoscandian Shield (Figure 1), which is the north-westernmost part of the East European Craton. The Archaean bedrock in the Fennoscandian Shield is divided into three adjacent cratonic nuclei known as Norrbotten, Karelia and Kola These nuclei, which may have originated separately, were fragmented between 2.51 and 2.4 Ga, and finally amalgamated by *ca*. 1.9 Ga (Lahtinen *et al.*, 2005). Between 1.9 and 1.8 Ga, a number of juvenile volcanic arcs and microcontinents were accreted to the Archaean craton, mostly along the south-western margin of the Archaean craton. This process of cratonisation resulted in the formation of the present-day Fennoscandian Shield by 1.77 Ga (Lahtinen *et al.*, 2005).

## 3 SPATIAL DATA MINING

'Data mining' is defined as the automated processes of discovering patterns or unexpected correlations among different datasets. Spatial data mining applies these techniques to spatially referenced data (Miller & Han, 2001). The spatial modelling techniques included in ArcSDM software (Sawatzky *et al.*, 2004) belong to the predictive modelling group of spatial data mining. These techniques have been

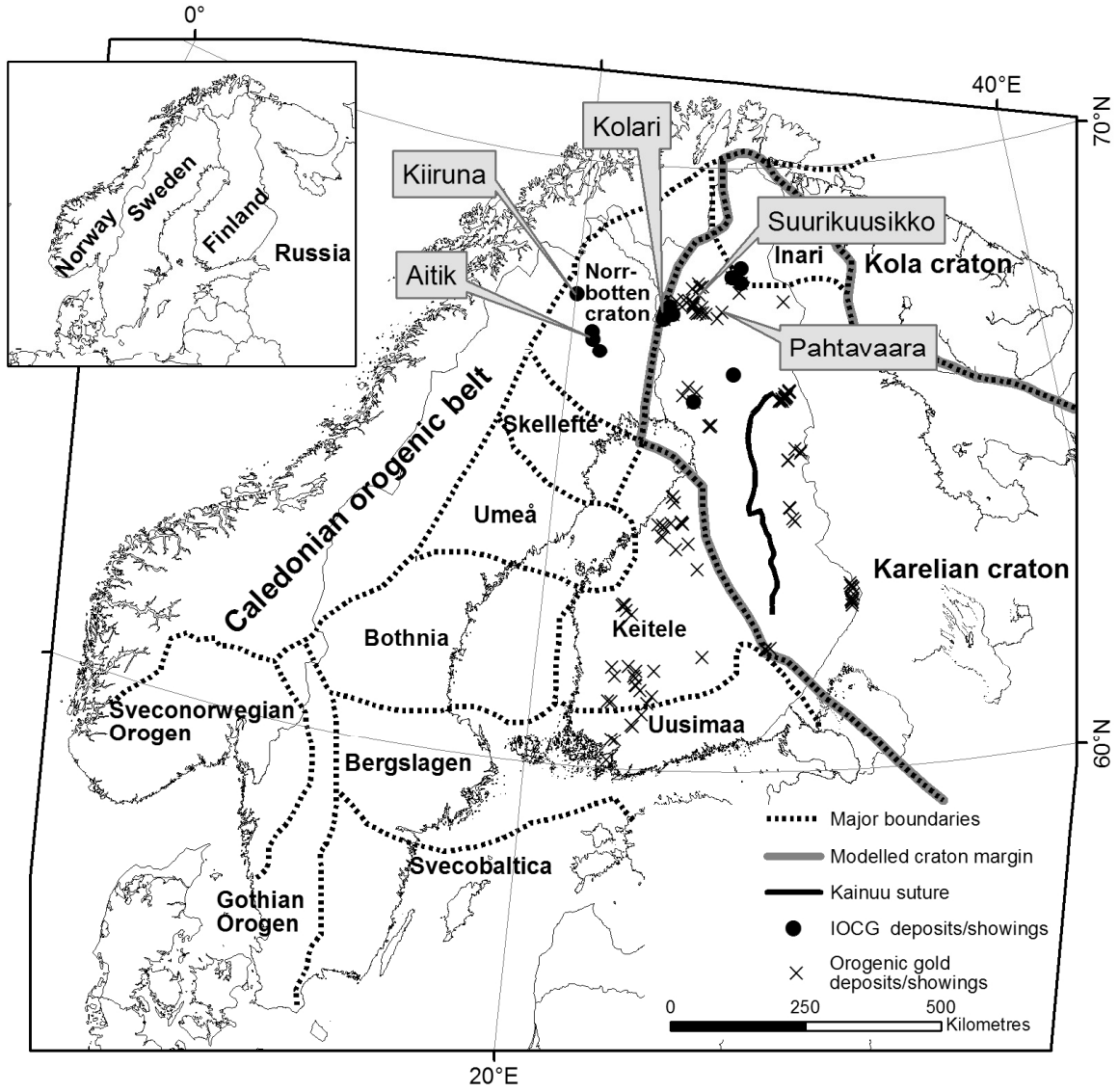


Figure 1. Location of the study area. Boundaries of the major geologic units from Lahtinen *et al.* (2005).

applied also to mineral exploration. In this paper we use neural networking, weights-of-evidence, logistic regression and fuzzy logic for mineral exploration by integrating geological, geophysical and geochemical data sets in various ways.

Bonham-Carter (1994) divides the spatial modelling techniques into two main classes based on their approach: in the data driven (or empirical) spatial modelling approach the known mineral occurrences are used as 'training sites', whereas in the knowledge-driven (or conceptual) approach the decisions to rank the importance of each input data set is defined by expert opinions. Alternatively, or in addition, the known mineral occurrences or deposits can be used to validate the modelling results. Both approaches have been used in the modelling presented in this paper. The two deposit types modelled are briefly described and referenced below.

## 4 GOLD DEPOSITS

### 4.1 *Orogenic gold*

Based Weihed *et al.*'s 2005 conclusions, all orogenic gold deposits in the Fennoscandian Shield have similar features to orogenic gold deposits worldwide (Groves *et al.*, 1998); *i.e.* they are structurally controlled, being located in second- to lower-order shear or fault zones within local compressional to transpressional structures at the time of mineralization. The FinGOLD database (Eilu, 1999) includes more than thirty drilled gold occurrences with at least

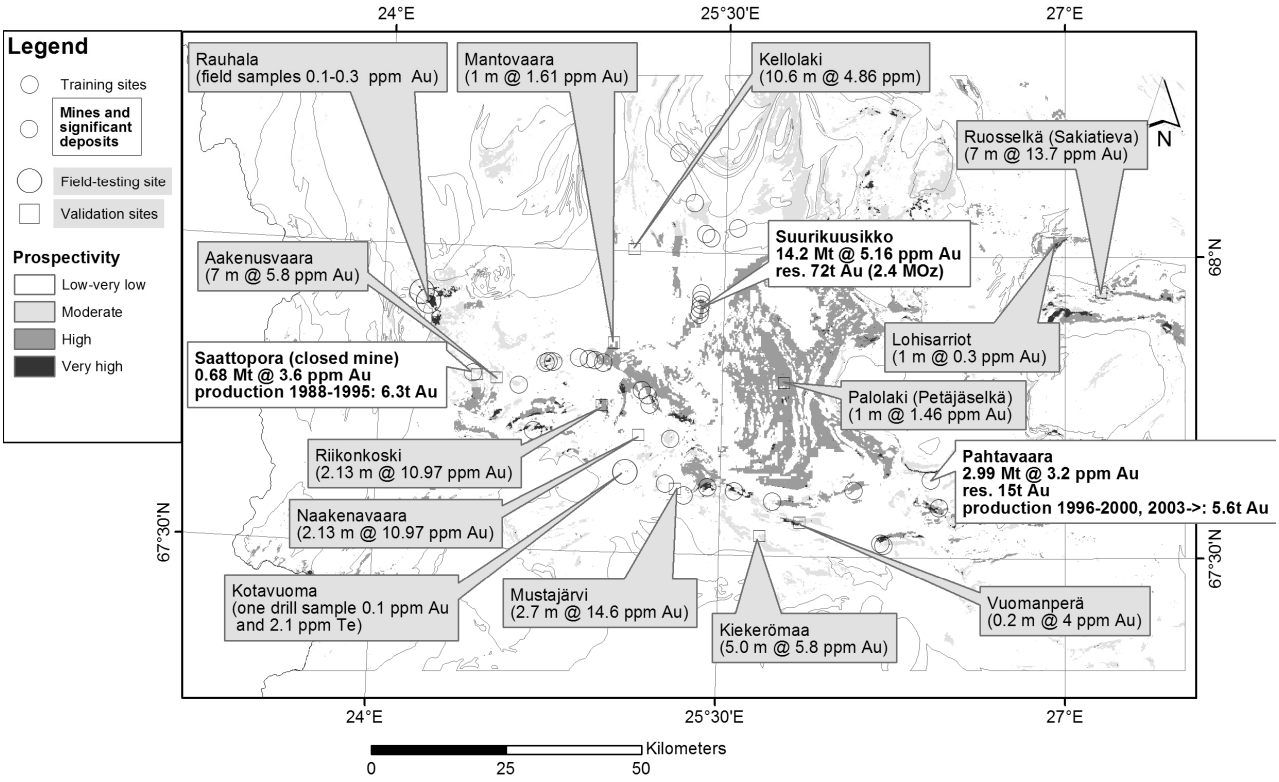


Figure 2. Prospectivity map for orogenic gold within the Central Lapland Greenstone Belt. Modified from Nykänen *et al.* (*in press* a). The labeled gold deposits and occurrences (grey labels) were used as validation sites. The white labels represent active and closed gold mines.

1m of 1 ppm Au within the Central Lapland Greenstone Belt (CLGB) area (Figure 1 and 2).

The data used for the modelling of orogenic gold deposits (after Charoy *et al.*, 2001) presented in this paper include airborne geophysics (magnetic and electro-magnetic), gravity, regional till geochemistry and several derivatives of a 1:200 000 scale bedrock geology map. The modelling techniques implemented include neural networking, weights-of-evidence, logistic regression and fuzzy logic (Nykänen *et al*., *in press* a).

### 4.2 *Deposits with IOCG affinities*

The northern region of the Fennoscandian Shield is recognised as an economically important metallogenic province dominated by numerous small Fe-oxide and Au-Cu deposits, some with IOCG affinities (Weihed *et al.,* 2005). These deposits mainly occur within or close to (<100 km) the margin of the Archaean craton (Figure 1), above Archaean continental crust and subcontinental lithospheric mantle, and are hosted by juvenile Palaeoproterozoic volcano-sedimentary sequences formed during rifting of the Archaean craton (Weihed *et al.*, 2005).

The data used in the modelling of IOCG deposits include airborne geophysics, gravity, mineral indications data base, regional till geochemistry and derivatives of a 1:1M scale bedrock geology map. The technique used for this modelling was fuzzy logic (Nykänen *et al.*, in press b).

## 5 RESULTS

The results of the orogenic gold modeling define less than 5% of the area of the Central Lapland Greenstone belt as highly prospective for gold exploration. The models successfully predict the known gold occurrences which were used as validation sites. The modelling results are currently being field tested by the GTK. Based on these studies there are approximately six that are undergoing further exploration.

The conceptual IOCG model delineates areas favourable for deposits with IOCG affinities. The known IOCG deposits in Finland are located within these areas highlighted by the

models. Some of these areas are under active exploration by mining companies.

The first spatial modelling results for orogenic gold within the Central Lapland greenstone belt are being published by Nykänen & Salmirinne (*in press*) and the model has been enhanced by Nykänen *et al*. (i*n press* b). New data from ongoing exploration campaigns is used to refine the moels. The recent developments and the new implementations of neural networks and some new data sets are presented in the current paper.

## REFERENCES


Bonham-Carter GF (1994) Geographic Information Systems for Geoscientists – Modelling with GIS. *Computer Methods in the Geosciences* 13. Pergamon Press, New York.

Eilu P (1999) FINGOLD – a public database on gold deposits in Finland. *Geological Survey of Finland,* Report of Investigation 146.

Groves DI, Goldfarb RJ, Gebre-Mariam M, Hagemann SG, Robert F & Arne DC (1998) Orogenic gold deposits; a proposed classification in the context of their crustal distribution and relationship to other gold deposit types; Mesothermal gold mineralization in space and time. *Ore Geology Reviews* 13, 7-27.

Lahtinen R, Korja A, Nironen M (2005) Palaeoproterozoic tectonic evolution. In: Lehtinen M, Nurmi PA, Rämö OT (eds.) *Precambrian Geology of Finland – Key to the Evolution of the Fennoscandian Shield.* Elsevier Science, B.V., Amsterdam, pp. 481-532.

Miller HJ, Han J (2001). Geographic Data Mining and Knowledge Discovery: an overview. In: Miller HJ, Han J (eds.) *Geographic Data Mining and Knowledge Discovery*. Taylor & Francis, pp. 3-32.

Nykänen VM, Groves DI, Ojala VJ, Gardoll S, (in press a) Combined conceptual/empirical prospectivity mapping for orogenic gold in the Northern Fennoscandian Shield, Finland. *Australian Journal of Earth Sciences,* Thematic Issue on Conceptual Targeting.

Nykänen VM, Groves DI, Ojala VJ, Eilu P., Gardoll S, (in press b) Reconnaissance-scale conceptual fuzzy-logic prospectivity modelling for iron-oxide-copper-gold deposits in the Northern Fennoscandian Shield, Finland. A*ustralian Journal of Earth Sciences,* Thematic Issue on Conceptual Targeting.

Nykänen VM, Salmirinne H, (in press), Prospectivity analysis of gold using regional geophysical and geochemical data from the Central Lapland Greenstone Belt, Finland In: Nurmi P, Ojala VJ (eds.) Gold in the Central Lapland Greenstone Belt. *Geological Survey of Finland, Special Paper*.

Sawatzky DL, Raines GL, Bonham-Carter GF, Looney CG (2004) ARCSDM3.1: ArcMAP extension for spatial data modelling using weights of evidence, logistic regression, fuzzy logic and neural network analysis. After Charoy *et al*. (2001)http://www.ige.unicamp.br/sdm/ArcSDM31/. (Accessed 26th January, 2007).

Weihed P, Arndt N, Billström K, Duchesne EJ-C, Eilu P, Martinsson O, Papunen H, Lahtinen, R (2005) Precambrian geodynamics and ore formation: The Fennoscandian Shield. *Ore Geology Reviews* 27, 273-322.

# Application of Palaeo-Stress Modelling for Orogenic Gold Exploration in the Central Lapland Greenstone Belt

V. J. Ojala & V. Nykänen
*Geological Survey of Finland, Rovaniemi, Finland*

ABSTRACT: Palaeo-stress modelling applies geomechanical modelling codes to define dilatant (low stress) sites in a rock mass. UDEC code was applied to determine the palaeo-stress pattern caused by the fault network geometry and rheology within the Central Lapland Greenstone Belt at 1:250 000 scale to target orogenic gold mineralization. The spatial correlation of the modelling result to the known gold occurrences was quantified using logistic regression methods in ArcGIS. The minimum principal stress distributions of the models, which simulate E-W compression, have the highest positive weight, contrast and confidence. The maximum spatial association pattern in the best model cover 1.3% of the study area and include 11% of the known gold occurrences.

KEYWORDS: Central Lapland greenstone belt, gold, stress modelling, UDEC

## 1 INTRODUCTION

Palaeo-stress modelling as a targeting tool for structurally controlled mineralization is based on rock mechanics principles and geomechanical modelling for identifying areas that experienced minimum stress and maximum dilation during deformation (Holyland & Ojala 1997). It is assumed that the mapped rock geometries are represent the plan view through the crust that existed at the time of mineralization. This is the case for the orogenic gold deposits, which are typically structurally late (Groves *et al.* 2000).

The Palaeoproterozoic Central Lapland greenstone belt (CLGB) is reminiscent of the late Archaean greenstone terrains of the Superior and Yilgarn cratons in terms of scale, lithological diversity, structural architecture, alteration history, and metamorphic grade. Research and exploration during past two decades has shown that the belt is prospective for structurally controlled orogenic gold and it has the potential to become a significant gold producer. Discoveries include the Suurikuusikko gold mine with the current published resource estimate standing currently at about 2.4Moz Au (14.2Mt @ 5.16 g/t). Available indirect ages suggest that the gold mineralization occurred 1.85-1.79Ga, most likely about 1.80Ga. Palaeo-stress modelling of CLGB was to model the area at 1:250,000 scale to select targets for orogenic gold exploration. The structural interpretations of the stress field orientation during the mineralization vary and four different far field stress orientations were modelled. To quantify the spatial correlations of results to the known orogenic gold occurrences and the effectiveness of the results for targeting orogenic gold mineralization, the logistic regression model in the Arc-GIS software was used. In addition, GIS modelling was to estimate which far field orientation was the most likely operational during the gold mineralization.

## 2 MODELLING APPROACH

This study utilised the distinct element method (UDEC program, Itasca Consulting Group, Starfield & Cundall 1988), which is a recognized discontinuum modelling approach for simulating the behaviour of jointed rock masses. In the distinct element method, a rock mass is represented as an assembly of discrete blocks. Faults and contacts are viewed as interfaces between distinct bodies. The contact forces and displacements between the stressed assemblies of blocks are found through a series of calculations which trace the movements of the blocks. Movements result from the propaga-

tion of disturbances, which were caused by applied loads, through the block system. In UDEC models, the fault geometry is predetermined and development of new structures cannot be modelled. A failure of a pre-existing weakness, or intact rock, can be initiated by an increase of differential stress, by an increase in the pore fluid pressure, or by combination of both. In most cases, stress changes lead to decrease of mean stress or, more commonly, decrease of minimum stress (σ3), which was used in this study to indicate the areas of dilation, fluid flow and potential gold mineralization.

### 2.1 *Geometry and geomechanical model*

Typically, the geological map interpretation is the largest source of uncertainty for the deformation simulation used for structural targeting. The other severe limiting assumption of two-dimensional stress modelling is that the plane of a map does not accurately reflect the stress pattern in an area with complex three-dimensional geometry. In many terrains, like CLGB, this may not be a critical restriction, since the vast majority of the observed structures are upright and the majority of gold deposits are hosted in steep structures, although significant exceptions do occur.

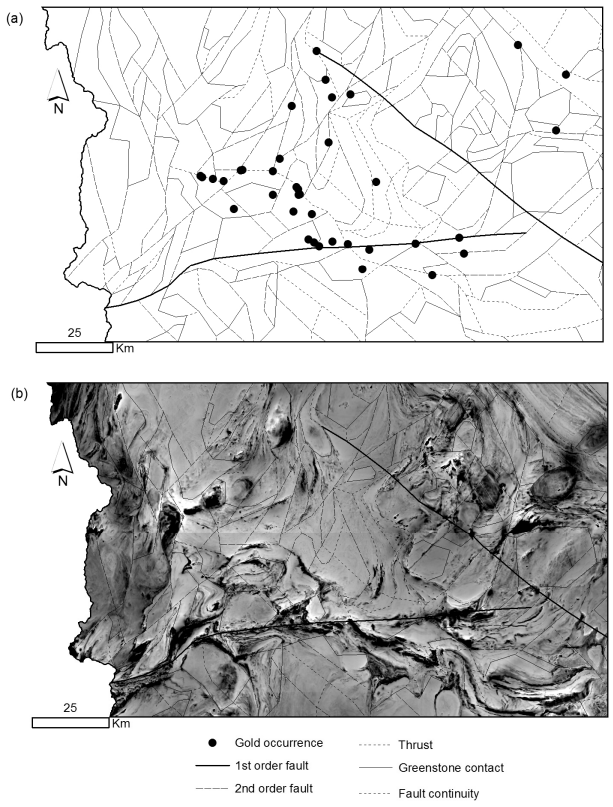


Figure 1. a) A digitized geomechanical interpretation of the discontinuities in the Central Lapland greenstone belt. The geology is simplified to facilitate modelling. The known gold occurrences are shown for reference. b) An aeromagnetic map of the model area overlain with the modeled discontinuity network

Geomechanical interpretation (Fig. 1) was done at 1:250 000 scale. Fault and rock geometries were interpreted and simplified from 1:100 000 and 1:200 000 scale geological (*eg.* Lehtonen *et al.* 1998) and geophysical (processed low altitude aeromagnetic and EM) maps. Discontinuities were divided to faults and contacts. Faults were further divided into first and second order faults, and thrusts using their length, continuity and timing as the main division, and rock contacts to greenstone and granitoid contacts with increasing shear stiffness. Dominating rock type between the discontinuities was used to define material properties for the rock blocks. Since the model is two dimensional, all faults and contacts are treated as vertical.

### 2.2 *Far-field stress orientations*

Determination of palaeo stress directions is closely related to the understanding the geological history of the area, quality of geological maps and reconstruction of the geometry during the mineralization. In many cases, this is not difficult as in linear greenstone belts and fold belts main principal stress direction and tectonic transport is typically perpendicular to the general structural grain. Furthermore, geomechanical modelling is not very sensitive for small differences in stress directions. In addition, several stress directions can be simulated and the result combined. Several tectonic transport directions and block rotations during the late structural evolution (D3 and later) in the CLGB can be interpreted. Consequently, it was decided to model all four main compression directions (N-S-, E-W, NE-SW, NW-SE).

### 2.3 *Material properties*

The selection of material properties of rocks is a difficult element in the generation of the palaeo stress model because of high uncertainty in the property database. It should be considered when performing an analysis, that the problem involves a data-limited system and the field data will never be known completely. However, as with the geometry, with the appropriate selection of properties important insight to the physical problem can still be achieved. Furthermore, the relative scale of the rock properties is reasonably well known. The rock properties for the simulations were estimated from the published data (Clark 1966) to approximate rock properties at the estimated

temperature-pressure conditions (70 - 100 MPa, 300±50°C) during mineralization. Although the real rock properties are not very well known for the pressure-temperature conditions during mineralization, it is likely that the relative scale of rock properties was similar to that indicated by geomechanical tests. Rocks were modelled as Mohr-Coulomb material and the modelling considers only elastic and elasto-plastic stresses and strains, and, therefore, deformation dilatency due to viscous strains is not considered.

## 3 MODELLING RESULTS

The solid geology model was digitized and the parameter values described above were given to the rock blocks, faults, and lithological contacts. The far field stresses were then applied to the model boundaries and the computation of the resulting deformation begun in UDEC. After sufficient cycles of calculations were completed, the model reached steady state, and the resulting stress pattern was calculated. The results were exported from UDEC into the ArcGIS and the minimum principal stress (σ3) values were converted into ArcGIS grids. The spatial resolution of the grid is about two kilometres at 1:250 000 scale. As the discontinuities cause the stress variations in UDEC models, most of the σ3 anomalies are along the faults and are related to fault bends and intersections. Many of the known gold occurrences are near or within anomalous stress zones but visually it is difficult to quantify the spatial correlation between σ3 and gold occurrences.

To quantity the spatial association between the modelled σ3 distribution and the orogenic gold occurrences within the CLGB the mean values and the standard cumulative descending weights were calculated following the weights-of-evidence methodology (Raines & Bonham-Carter 2006). The modelled σ3 values were reclassified into 12-13 classes using standard deviation method of GIS software. This classification method shows how much a feature's attribute value varies from the mean. The GIS software calculates the mean values and the standard deviations from the mean and the class breaks are then created using these values. A pair of weights was calculated for each map class of the input σ3 values. A positive weight (W+) was calculated for presence of each class at the training site, and a negative weight (W-) for absence of that class. The weights are a function of the number of the training sites within a map class and the area of the corresponding map class. The magnitude of the weights depends on this measured spatial association between the map class and the training sites. A weight of zero indicates no spatial association between the training sites and a particular map class. The layers were reclassified into binary patterns by using the maximum contrast value, which is the arithmetic difference between the weights in the cumulative weights

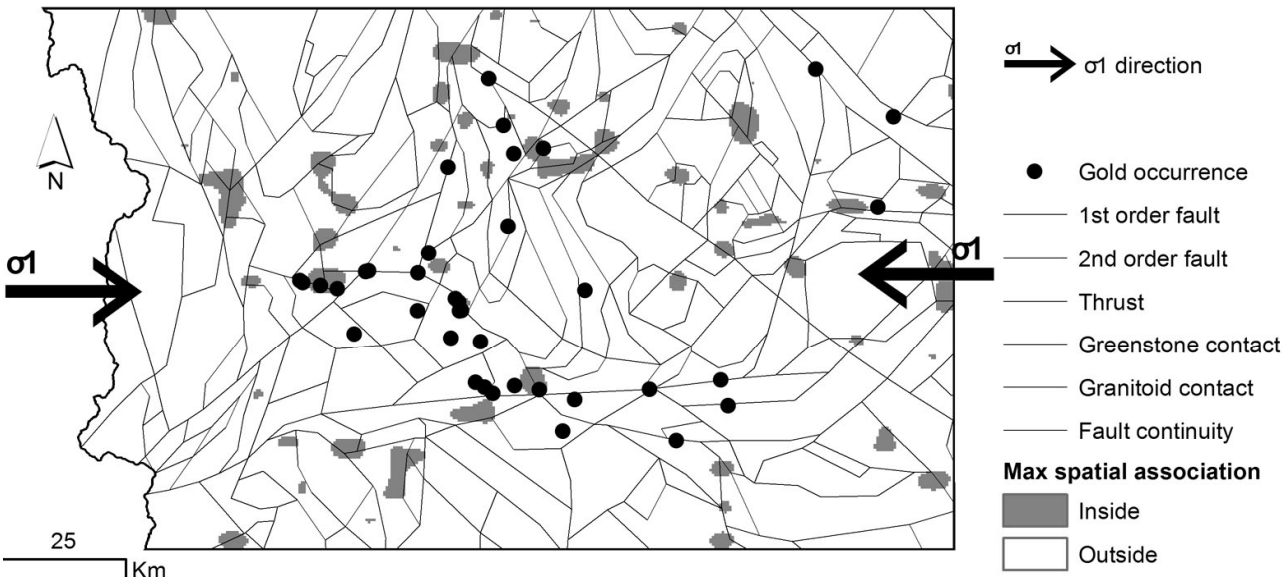


Figure 2. E–W compression simulation of CLGB, maximum spatial association binary pattern between modelled σ3 and gold occurrences.

calculation. The σ3 values in the stress models with the compression in E-W and NE-SW direction have stronger spatial association with gold occurrences than those simulating N-S or NW-SE shortening. The area of maximum spatial association pattern for the best E-W is only 1.3% of the total study area, and the pattern includes four (11%) of the 37 known gold occurrences.

The models were ranked based on the maximum contrast value, which quantifies the spatial association between the gold occurrences and the map classes. The confidence of the weights calculation was estimated by calculating the studentised contrast (Contrast/Standard deviation of the contrast), which is the measure of the certainty that the contrast is not zero (Bonham-Carter 1994). Confidence values above 1.96, which is about a 97.5% confidence level, were considered acceptable (Raines 1999). All E-W and NE-SW models are above these levels, and only one N-S model and none of the NW-SE stress models bypass this rule. This indicates that the correlations of the E-W and NE-SW models with the known gold occurrences are more reliable than the correlations of the NW-SE and N-S models with the gold occurrences. Consequently, E-W and NE-SW models could be considered as the best predictors for the structurally controlled orogenic gold mineralization in CLGB.

## 4 CONCLUSIONS

Palaeo stress modelling of CLGB suggests that:

a) the modelled geometry has a control on the distribution of the orogenic gold mineralization,
b) the modelled geometry is reasonably accurate,
c) modelling scale is reasonably representative,
d) fault and material properties are representative,
e) modelled geology has not significantly changed since mineralization,
f) stress field during the mineralization was probably E-W or NE-SW as suggested by previous studies,
g) modelled stress anomalies are viable exploration targets

## REFERENCES


Bonham-Carter, G.F. 1994. Geographic Information Systems for Geoscientists – Modelling with GIS. *Computer Methods in the Geosciences* 13. Pergamon Press, New York, 398 p.

Clark, S. P. (1966) Handbook of Physical Constants. Memoir 97, *The Geological Society of America Incorporated*, New York, 600 p.

Groves, D.I., Goldfarb, R.J., Knox-Robinson, C.M., Ojala, V.J. Gardoll, S. Yun, G. & Holyland, P.W. 2000. Late-kinematic timing of orogenic gold deposits and significance for computer-based exploration techniques with emphasis on the Yilgarn Block, Western Australia. *Ore Geology Reviews.* 17: 1-38.

Holyland, P. W. & Ojala, V. J. 1997. Computer-aided structural targeting in mineral exploration : two- and three-dimensional stress mapping. *Australian Journal of Earth Sciences* 44:421-432.

Lehtonen, M., Airo, M.-L., Eilu, P., Hanski, E., Kortelainen, V., Lanne, E., Manninen, T., Rastas, P., Räsänen, J. & Virransalo, P. 1998. Kittilän vihreäkivialueen geologia : Lapin vulkaniittiprojektin raportti. Summary: The stratigraphy, petrology and geochemistry of the Kittilä greenstone area, northern Finland : a report of the Lapland Volcanite Project. *Geologian tutkimuskeskus*. Tutkimusraportti 140. 144 p.

Raines G.L. 1999. Evaluation of weights of evidence to predict epithermal-gold deposits in the Great Basin of the Western United States. *Natural Resources Research* 8: 257-276.

Raines G.L. & Bonham-Carter G.F. 2006. Exploratory spatial modelling: demonstration for Carlin-type deposits, central Nevada, USA, using Arc-SDM. In: Harris J.R. (Ed.) GIS for the Earth Sciences. *Geological Association of Canada. Special Publication* 44: 23-52.

Starfield, A. M. & Cundall, P. A. (1988) Towards a methodology for rock mechanics modelling. *International Journal of Rock Mechanics and Mining Sciences and Geomechanics,* Abstracts 25: 99-106.

# Discovery of the Habo Porphyry Cu-Au-(Mo) System in Southern China: Its lessons for Exploration Everywhere

Noel C. White[1,2,3], Kaihui Yang[1] & Wenchang Li[2,4]

*1. Asia Now Resources Corporation, Toronto, Canada; 2. China University of Geosciences, Beijing, China; 3. CODES, University of Tasmania, Hobart, Australai; 4. Yunnan Geological Survey, Kunming, China.*

ABSTRACT: A new major porphyry Cu-Au-(Mo) system has been discovered at Habo, SE Yunnan Province, China, and is still being evaluated. The deposit occurs in an area with a long history of exploration and remained undiscovered despite being covered by several surveys, and in spite of its occurrence in an area a high relief. Poor outcrop due to soils and leaf litter from dense vegetation kept it hidden until it was detected by systematic exploration aimed at porphyry targets. The history of its exploration and discovery provide lessons for explorers in China and elsewhere.

KEYWORDS: porphyry copper, mineral exploration, Red River fault zone

## 1 INTRODUCTION

A major new porphyry Cu-Au-(Mo) system has been discovered at Habo in southern China in a well-populated area with easy access. Despite occurring in steep terrain, the Habo South porphyry system outcrops poorly, and is obscured only by thin soil cover and leaf litter. Exploration is still at an early stage but it is clear that a major mineralized system is present, and its economic potential will take considerable time to assess fully. The full extent of the system is still not known, but it covers an area of at least 2km$^2$, possibly much more, based on exploration pits, trenches and adits, and the extent of geochemical anomalies. It is likely that Habo South is only one of several centres of mineralization in the Habo district.

While so far this discovery can only be called a technical success, technical success is the first essential step towards economic success. Irrespective of whether it is ultimately proved to host an economic resource, the discovery of the Habo South porphyry system provides several important lessons for exploration geologists and managers, and highlights several crucial requirements for exploration success.

## 2 GEOLOGY OF THE HABO REGION

The Habo project is in Yunnan Province of southern China, approximately 350km by road from the provincial capital, Kunming. The Habo South porphyry mineralized system occurs at latitude E102°35', longitude N22°53', about 25 kilometers from the border with Vietnam.

The Habo intrusive complex that hosts the porphyry Cu-Au-(Mo) system occurs in the Red River Fault Zone, a major crustal suture that extends from Tibet along the centre of Yunnan Province and crosses into Vietnam. The Red River suture closed in the late Triassic (Yang, 1998), and closure was followed by large scale (>300km) left lateral movement in the Tertiary as a result of the Indo-Asia collision (Leloup *et al*., 1995). The latter event is indicated by the Tertiary high-grade metamorphic belt and a number of felsic intrusions dated to range from 42 to 4Ma (Yunnan Geology, *unpublished*), along with the large strike-slip shear zones of the Red River suture (Scharer *et al*, 1994).

Habo occurs where the major N-S Yanshanian (Jurassic-Cretaceous) arc, characterised in this region by tin granites, is cut by the Red River suture. The Habo intrusive complex with a Rb-Sr model age of 37.3Ma (Yunnan Geology, 2000, unpublished; *cf.* Harris et al., this volume) intrudes late Palaeozoic sedimentary rocks, dominantly fine-grained siliciclastic rocks with minor limestone. These rocks are strongly folded with low metamorphic grade.

Mesozoic granitoids and Tertiary lamprophyres also intrude the host sequence. Proterozoic high-grade metamorphic rocks outcrop further north in the district, and xenoliths occur in intrusions.

The geological setting for the Habo porphyry deposit is not a conventional setting that would be regarded as prospective for porphyry deposits. It is related to a major crustal shear zone with large strike-slip movements related to continental collision, where magmatism has continued long after terrain docking. Numerous porphyry Cu-(Au-Mo) deposits have been found in this setting, mainly in far NW Yunnan and Tibet. The most important deposits found to date are Yulong and Pulang (Hou *et al*, 2003) in addition a number of porphyry Cu-Au prospects along the Red River belt. Chinese geologists have long recognized that the prospective porphyry belt extends SE along the Red River suture and exploration has been conducted along this belt for many years.

## 3 HISTORY OF EXPLORATION

The early exploration history of the area is summarized in Table 1. The regional stream geochemical survey carried out in 1969-71 detected anomalous Cu, Au and Mo in and around the Habo intrusive complex. Soil sampling at 1:50,000 scale was carried out on parts of the complex, confirming large anomalous areas at Habo North and Habo South. Yunnan Geology and Mineral Resources Company (YGMR) applied for title over the whole area, and licenses were granted in April 2000. In the following year soil geochemical sampling was carried out at 1:25,000 scale. In 2002 a trench was dug in the anomalous area at Habo South, but only minor secondary copper was found in pervasively altered rocks lacking apparent veining. Moreover, the pervasive alteration was not recognized, and the minor copper mineralization was interpreted as structure-related veins.

In 2002, Kaihui Yang investigated possible projects to bring into a new company to be listed on the Toronto Stock Exchange (since listed as Asia Now Resources Corporation). He learned of the Habo project and commenced discussion for a possible joint venture between Asia Now and YGMR on the property; The JV agreement was signed in January 2004, and the exploration licenses were transferred to the JV company in April 2005.

Table 1: History of Exploration at Habo

| Year | Work |
|---|---|
| 1969-1971 | Geological mapping, stream geochemistry and heavy mineral surveys at 1: 200,000 scale by Geological Survey Team under Yunnan Bureau of Geology and Mineral Resources (Yunnan Geology), published as Yuanyang Map Sheet F-48-13 by Geological Publishing House, 1975. |
| 1983-1986 | 1:50,000 scale soil geochemical survey conducted by Geophysical Prospecting Team under Yunnan Geology. |
| 1983-1989 | Yunnan Geological Survey Team under Yunnan Geology conducted a regional stream sediment survey, and a series of geochemical maps (15 elements) was printed on Oct. 1, 1989. |
| 1997-1998 | Yunnan No.4 Geological Team under Yunnan Geology examined the soil anomalies and found a number of veins with gold and base metal mineralization. |
| 1998-1999 | Yunnan No.1 Geological Team under Yunnan Geology conducted a regional geological survey program at a scale of 1:50,000 (unpublished). |
| 1999-2000 | Yunnan Geology applied for exploration licenses January 1, 1999; exploration license granted 27 April, 2000. Yunnan No. 1 Geological Team explored gold veins in the Habo region. |
| 2000-2001 | 1:25,000 scale soil geochemical survey conducted by No. 807 Geological Team under Yunnan Geology |
| 2002-2003 | Asia Now Resources Corp. and Yunnan Geology discuss JV (agreement signed January 2004) |
| 2005 | Exploration licenses transferred to JV company 27 April, 2005 |

On 8 January 2004, Kaihui Yang, Noel White and Yunsheng Zhang visited Habo South and examined the trench dug by YGMR personnel. Adjacent to the trench we found porphyry float with strong quartz-magnetite veining, however it occurred uphill from the trench, suggesting the source was in a very restricted area at or near the top of the ridge. The next day we examined the Habo North anomaly. Following this visit, it was decided to focus work on the Habo North anomaly because of the coincidence of Cu, Au and Mo in soils, and because the size and shape of the anomaly was suggestive of a porphyry target. Over the following year, soil sampling, pitting and trenching at Habo North failed to find anything of significance, and there was a view that the project was not living up to our hopes. The Habo

North anomaly remains unexplained and requires further work.

Following a review of the results of work on Habo North, attention was refocused on Habo South, and a program of mapping, ground magnetic lines, soil sampling, pitting, and trenching commenced in mid 2005. Early trench mapping and sampling produced encouraging results, however the full appreciation that a discovery had been made dates from a field visit on 27 August 2005. The party consisted of Kaihui Yang, Noel White and Yunsheng Zhang. In the previous week there had been heavy rain in the area, and a few days before our visit a large tree on the upper slopes had fallen and slid down the hillside, cleaning off soil and exposing bedrock for about 300m. The succeeding rain washed the surface clean in time for our visit. With superb continuous exposure it was clear that a large porphyry system was present, as the exposed rock showed intense potassic alteration and high density of quartz-magnetite-sulphide (now limonite) stockwork.

Although the cleaned surface made the discovery obvious, it was already apparent in the trenching and sampling that had been done, yielding wide zones with elevated Cu, Au and Mo geochemistry in altered and veined rocks. Fortuitously, the trench dug in 2002 was located in a relatively vein-free part of the system; it was surrounded by intensely altered and veined porphyry. At that stage the system could be inferred to extend 800m N-S and 600m E-W, with no boundaries apparent. Early follow-up work aimed to determine the extent of the system by additional trenching and pitting. That work continues, and only one possible boundary has been located. We now believe the system is at least 2 km N-S and 1.2 km E-W, still with no clear margins.

In 2006 onset of the rainy season restricted the work that could be safely done in the area. Man-portable drill rigs could not be safely carried into the area during this period, so exploration continued with excavation of a series of short adits driven to sample fresh bedrock and to allow comparison with surface results. A total of 8 adits have been excavated so far, revealing the high intensity of sulphide veins that occurs even in the absence of quartz veins. With the end of the rainy season drilling has now commenced.

The Habo South system forms a ridge 600m high. The prominent parts are dominantly underlain by potassic alteration, with variable density of sulphide, quartz, and quartz-magnetite veinlets. Very steep slopes appear to correspond to zones of phyllic alteration. Several lithologies occur, with the most extensive a medium-grained porphyritic granite, and a subordinate similar phase distinguished by having large rounded quartz eyes. A minor phase that intrudes the granite consists of coarse pink K-feldspar (similar to that in the granite) in a fine-grained groundmass. Rock analyses by Yunnan Geology (2000, unpublished) indicate high alkali contents in the altered granites (Table 2). These three phases are all mineralized; some younger unmineralized lamprophyre dykes also occur. Harris *et al*. (this volume) describe the petrology of the host rocks at Habo South.

Table 2: Rock Analyses from Habo

| | Sample 1 | Sample 2 | Sample 3 | Sample 4 |
|---|---|---|---|---|
| $SiO_2$ | 58.46 | 68.27 | 64.96 | 58.06 |
| $TiO_2$ | 0.77 | 0.29 | 0.54 | 0.72 |
| $Al_2O_3$ | 13.23 | 15.22 | 14.58 | 12.20 |
| $Fe_2O_3$ | 2.15 | 1.68 | 2.47 | 1.94 |
| FeO | 3.25 | 1.27 | 1.67 | 3.92 |
| MnO | 0.10 | 0.03 | 0.05 | 0.09 |
| MgO | 5.44 | 1.23 | 2.23 | 6.78 |
| CaO | 5.26 | 1.10 | 2.43 | 5.62 |
| $Na_2O$ | 3.30 | 3.50 | 4.51 | 2.31 |
| $K_2O$ | 6.18 | 5.80 | 5.66 | 6.20 |
| $P_2O_5$ | 0.49 | 0.14 | 0.28 | 0.46 |
| LOI | 0.43 | 1.18 | 0.38 | 0.66 |
| Total | 99.06 | 100.2 | 99.36 | 99.06 |

Sample 1: Med-coarse grained granite (Sanduobang)
Sample 2: Quartz porphyritic granite (Habo Nanshan)
Sample 3: Quartz-porphyritic granite (Ashu)
Sample 4: Fine-grained granite (Ashu Pingshan)

Note that the samples in Table 2 were named syenite or quartz syenite and the potassic alteration was not recognized. Based on our observations, the so-called syenite is granite with pervasive potassic alteration including hydrothermal K-feldspar and biotite.

## 4 SIGNIFICANCE OF THE DISCOVERY

It is beyond doubt that a large porphyry Cu-Au-(Mo) system exists at Habo, but its economic significance remains unknown. However, discovery of major porphyry systems is an

essential precursor to discovery of major porphyry ore deposits. Thus, even without economic evaluation, this discovery is very significant:

- It occurs in a geological belt that does not fit the widely-held perceptions of belts favorable for porphyry deposits; it is a post-collisional porphyry system, not a conventional arc system.
- The region has high relief, on average reasonable outcrop, and variable population density; despite being thoroughly walked over, a major mineralized system remained unrecognized.
- Despite the high relief of the area, the mineralized system outcrops poorly, being covered by thin soil and leaf litter in a generally densely vegetated part of the region.
- This system occurs in a moderately populated part of China, and has had a long history of geological investigations, yet still the system remained undiscovered; most of China has had less work, and much of it has scarcely been explored: the potential for major discoveries in other parts of China is immense!

## 5 LESSONS FOR EXPLORATION

There are several important lessons for exploration, not only in China.

- Good geology deserves good exploration, without the constraint of excessive commitment to conventional models; this deposit belongs to a new class of post-collisional porphyry deposits that do not closely fit conventional models for where to look for porphyry deposits.
- Once a target has been selected and a project area defined, it is important to complete work on the whole project area to a logical decision stage: early work on what was judged to be the best anomaly in the area was not encouraging; if we had stopped then, Habo South would not have been found.
- It is essential that exploration is managed by people with good familiarity with the targets sought; in porphyry systems potassic alteration can be mistaken for fresh rock (here K-feldspar-altered granite was mapped as syenite and quartz syenite), thin quartz±magnetite veins are not seen as significant, sulphide stockworks may not be recognized in weathered rock, and wide zones with 0.2-0.4 g/t Au may be regarded as unimportant (these actually happened!).
- Visitors to Habo South now would conclude that it was *impossible* to miss that the area hosts a porphyry system; however, at the time of our first visit, there was very little to see and what little there was had been missed through geological mapping and several stages of geochemical sampling (both stream and soil); 10cm of rotted leaves is a very effective cover!

## ACKNOWLEDGEMENTS

Important contributions to the work that led to the discovery of the Habo porphyry system were made by Yunsheng Zhang, Mark Zhu and Weiguang Yang.

## REFERENCES

Hou ZQ, Ma HW, Zaw K, Zhang YQ, Wang MJ, Wang Z, Pan GT, Tang RL (2003) The Himalayan Yulong porphyry copper belt: product of large-scale strike-slip faulting in Eastern Tibet. *Economic Geology* 98, pp. 125-145.

Leloup PH, Lacassin R, Tapponnier P, Scharer U, Zhong D, Liu X, Zhang L, Ji S, Trinh PT (1995) The Ailao Shan-Red River shear zone (Yunnan, China), Tertiary transform boundary of Indochina. *Tectonophysics* 251, pp. 3-84.

Scharer U, Zhang LS, Tapponnier P (1994) Duration of strike-slip movements in large shear zones: The Red River belt, China: *Earth and Planetary Science Letters* 126, pp. 329-397.

Yang K (1998) A plate reconstruction of the eastern Tethyan orogen in southwestern China. In: Flower M (ed), Mantle Dynamics and Plate Interaction in East Asia, *Geodynamics* 27, pp. 269-287: American Geophysical Union.

# Building the Resource Base for a New Copper Operation - the Lady Annie project, Northwest Queensland

K.J. Maiden
*CopperCo Limited, Sydney, Australia*

S. Pooley
*CopperCo Limited, Perth, Austral*

ABSTRACT: CopperCo Limited was formed in 2004 as a new company focussed on copper in Northwest Queensland. The company's focus has been on the development of an SX- EW copper operation based on oxide copper resources in the Lady Annie - Mount Kelly area. Since its formation, the company has discovered three new deposits, has outlined resources in excess of 22 million tonnes at 0.9% Cu and has completed a feasibility study for a 19,000 tonne per annum copper operation. CopperCo expects to be producing cathode copper in July 2007.

KEYWORDS: Lady Annie, Mount Kelly, oxide copper, Mount Isa Block

## 1. INTRODUCTION

The Mount Isa Block, in Northwest Queensland, is Australia's premier base metal province. Based on its world-class deposits, the region boasts a strong mining industry and well-developed infrastructure.

Geologically, the Mount Isa Block is divided into the Eastern and Western Successions. The Eastern Succession contains important iron oxide-copper-gold (IOCG) deposits (including Ernest Henry, Osborne and Selwyn) and Broken Hill-type silver-lead-zinc deposits (notably Cannington). The Western Succession contains stratiform silver-lead-zinc deposits (Mount Isa, George Fisher, Century) and sediment-hosted copper deposits (notably the giant Mount Isa deposit) (Fig, 1). (Qld DME, 2000)

This paper outlines the approach taken to build the resource base for a new copper operation in the Western Succession.

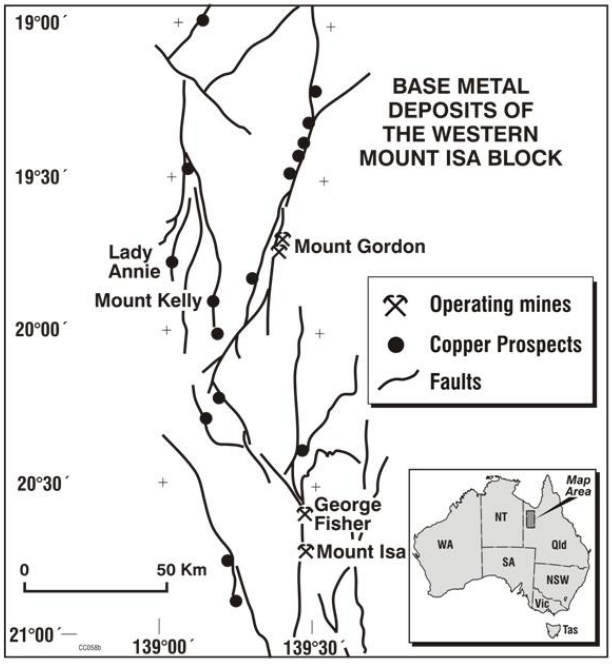


Fig 1: Structural setting of base metal deposits in the Western Mount Isa Block

## 2. GEOLOGICAL SETTING

The Proterozoic evolution of the Mount Isa Block involved several cycles of rifting, with associated igneous activity, and basin subsidence. From around 1590 Ma, the sequence was subjected to compressive deformation and metamorphism in the Isan Orogeny (Qld DME, 2000).

Copper deposits in the Western Succession are related to faults, which were active late in the Isan Orogeny. The deposits are associated with intense brecciation and alteration of the host rocks. The style of mineralization varies from veins and stockworks to breccia fillings, disseminations and massive replacements.

The Lady Annie project area lies ~ 100km north of Mount Isa. The sequence is dominated by siltstones and dolomitic siltstones, folded around north-trending axes and cut by an extensive fault array.

Copper was discovered at Lady Annie in 1919 and high grade oxide copper ore was mined on a small scale between 1937 and 1963. At Mount Kelly, 20km southeast of Lady Annie, small scale mining dates from the 1950s.

At Lady Annie, a zone of high grade chalcocite mineralization lies below the oxide copper zone on the western side. At Mount Kelly, drill holes have intersected zones of chalcopyrite at depth. Much of the previous exploration in the area has been directed towards sulphide copper targets.

## 3. CREATING A VIABLE PROJECT

*Focus on oxide copper targets:* Prolonged rock weathering during the Tertiary resulted in development of a regionally-developed lateritic weathering surface, underlain by a deep weathering profile, to depths of 60m or more. Where this deep weathering has affected primary copper mineralization, oxide copper concentrations have resulted.

The oxide copper mineralization is mainly malachite with subordinate tenorite, cuprite, azurite and chrysocolla, in zones up to 40m thick. Critically for mineral processing, most of the carbonate from the host rocks has been leached out of the oxidised material, leaving a soft host rock consisting largely of kaolinite, quartz and iron oxides.

For a small company, seeking early cash flow, an exploration focus on oxide copper targets provides a number of advantages:

- Shallow targets can be cheaply explored and rapidly assessed, leading to early resource definition;
- Rapid development of shallow deposits provides early cash flow;
- Cathode copper can be produced at competitive costs.

At Lady Annie, drilling during 2002 defined a resource 8.9 million tonnes (Mt) at a grade of 1.17% Cu. At Mount Kelly, drilling during 2003 intersected up to 40m of oxide copper at the Mount Clarke prospect.

*Plan for a central processing plant:* Economies of scale suggest that a viable project should have a minimum 15,000 tonnes per annum (tpa) solvent extraction – electrowinning (SX-EW) copper plant. For a 10-year operation, the minimum resource requirement is

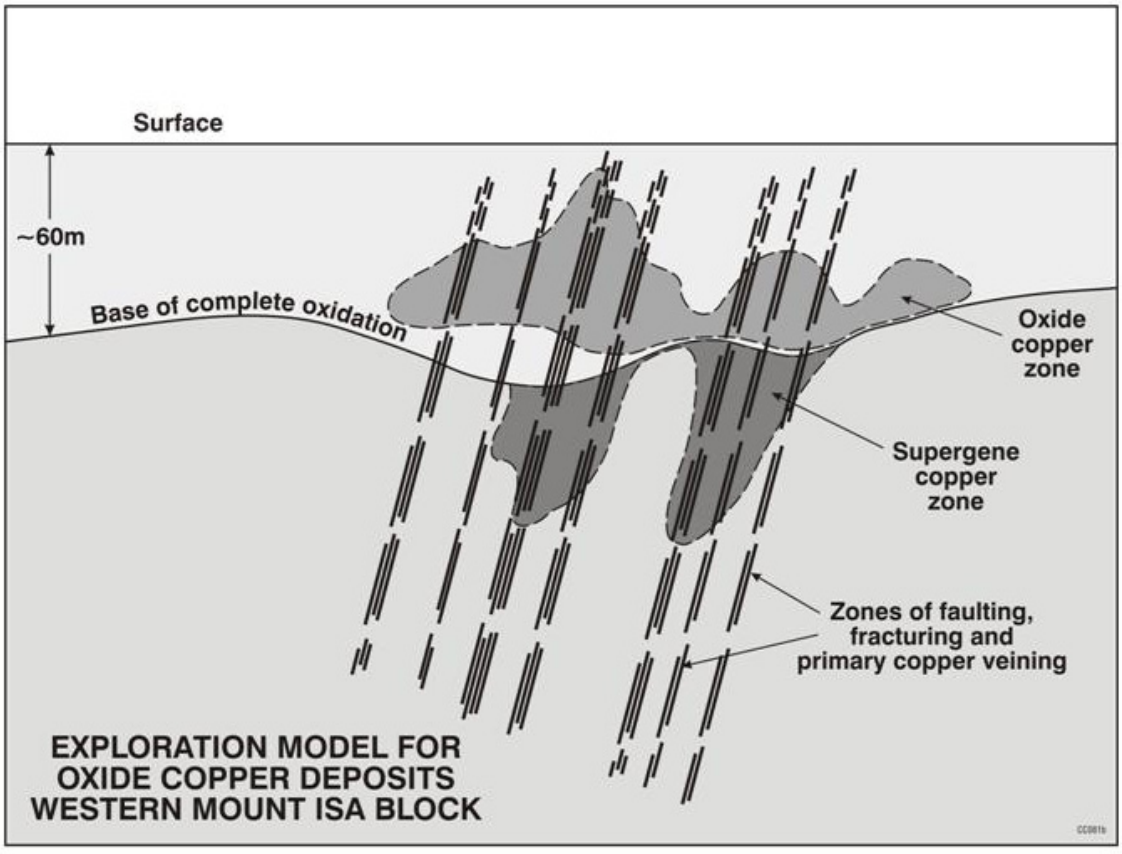


Figure 2. Exploration model for oxide copper deposits

150,000 tonnes of contained copper, *i.e.* 15 Mt at a grade of ~ 1% Cu.

By late 2003, the area had a known resource at Lady Annie, an emerging resource at Mount Kelly, and other under-explored prospects, all accessible via the one road. A central processing plant could access feed from multiple deposits, but the deposits and prospects were held by competing companies.

*Consolidation of assets:* Following a lengthy period of negotiation, a critical piece of financial engineering resulted in the creation of a new company, CopperCo Limited. In 2004, the company listed on the Australian Stock Exchange (ASX), raised significant capital and merged the assets of four companies, acquiring:

- The Lady Annie oxide copper resource;
- The Mount Kelly oxide copper resource;
- 2,500 $km^2$ of prospective tenements.

Critically, the CopperCo management team has expertise in evaluation, development and management of copper SX-EW operations and a track record of producing shareholder value. The new company has the goal of becoming a substantial Australian-based copper producer.

## 4. EXPLORATION AND EVALUATION

*Exploration programme:* Drilling commenced at both Lady Annie and Mount Kelly in November 2004. In the following 14 months, CopperCo completed 40,000m of reverse circulation and diamond drilling. This included infill and extension drilling on the known deposits as well as testing of additional targets.

*Copper deposits:* The deposits occur as subhorizontal oxide copper concentrations, up to 40m thick, covered by up to 60m of overburden. The deposits all lie in complex structural zones of fault splays and intersections, reflecting the primary structural controls on the precursor sulphide copper concentrations.

In detail, the distribution of oxide copper is partly controlled by primary features, occurring as vein and breccia fillings, especially within and adjacent to faults. In addition, there has been significant redistribution of copper within the weathered rock, where it occurs as fracture fillings in brittle rock types (especially quartzitic rocks) and in zones of secondary permeability where primary carbonate has been leached out of dolomitic siltstone.

*Resource definition:* At Lady Annie, drilling has confirmed an oxide copper resource of 11.3 Mt at 1.0% Cu. Other targets close to the known deposit remain to be tested. In the Mount Kelly project area, drilling showed a significant resource at the Mount Clarke prospect and identified additional oxide copper deposits - Flying Horse, Mount Kelly Workings and Swagman.

The combined Lady Annie – Mount Kelly resource now stands at 22.2 Mt at 0.9% Cu. Additional transition and sulphide copper resources are not included in this figure.

*Feasibility study:* A review of the metallurgical testwork and other aspects of the feasibility study is beyond the scope of this paper.

In summary, CopperCo has completed a bankable feasibility study (including mine planning, metallurgical work, environmental, geotechnical and hydrological studies), acquired the necessary permits (Mining Lease applications, environmental management plan, access agreements, Native Title agreements) and raised funding for project development and ongoing exploration.

The company is now nearing completion of construction of mines, processing facilities and related infrastructure. Open-cut mining of the orebodies will use conventional load and haul methods. The leach pads and SX-EW processing plant are to be located near Mount Kelly, with truck haulage from Lady Annie. The company is targeting initial copper production of 19,000 tpa and expects to be producing cathode copper (*i.e*. copper metal) by July 2007.

Financial analysis indicates a robust project, with cash costs of less than US$0.70/lb. The projected mine life is eight years. Exploration of the project area is continuing, both in close proximity to the known resources and regionally, where there are numerous targets to be tested. It is expected that further discoveries from ongoing exploration will extend the project life.

## 5. CONCLUSION

Success in creating a viable project has come from:

- A focus on oxide copper resources, with their potential to produce copper at competitive costs and early cash flow
- Expertise in design and management of copper SX-EW projects

- Planning for a central processing plant, drawing feed from multiple sources
- Investors prepared to back the project
- An intensive evaluation program, including 40,000m of drilling and comprehensive metallurgical testwork
- Tight control on all aspects of the feasibility study.

ACKNOWLEDGEMENTS

The authors acknowledge the support of CopperCo Limited in preparing this paper.

REFERENCES

Qld Dept Mines & Energy, Taylor Wall & Associates, SRK Consulting Pty Ltd and ESRI Australia, 2000. *Northwest Queensland Mineral Province Report, Queensland Dept Mines and Energy*.

# Mineral chemistry of iron oxides: application to mineral exploration

Georges Beaudoin, Céline Dupuis
*Université Laval, Québec, (QC) Canada G1K 7P4*

Patrice Gosselin
*Geological Survey of Canada, 490 de la Couronne, Québec (QC) Canada G1K 9A9*

Michel Jébrak
*Université du Québec à Montréal, Montréal (QC) Canada H3C 3P8*

ABSTRACT: The mineral chemistry of iron oxides (magnetite and haematite) display a range of composition that can be related to the mineral deposit type from which it formed. An efficient and optimized electron microprobe analytical method allows routine analysis of iron oxides. Discriminant diagrams such as the Ti/V *vs* Ti or the (Ni+Ca)/(Cr+Mn) vs Ti/V are efficient to distinguish iron oxides formed in IOCG deposits from those formed in Kiruna, porphyry Cu-Au, and Fe-Ti deposits.

KEYWORDS: iron oxide, mineral chemistry, electron microprobe, mineral deposit

## 1 INTRODUCTION

Iron oxides (haematite and magnetite) are common minerals found in magmatic and metamorphic rocks and can be accessory to major minerals in a range of mineral deposit types. Spinel is used as a petrogenetic mineral because its chemical composition is controlled by that of the environment in which it formed (Barnes & Roeder 2001). Zincian spinel gahnite in metamorphosed VMS deposits also displays a chemistry largely controlled by the chemistry of the metamorphic hostrocks (Heiman *et al.* 2005). The range in chemical composition of the various deposit type environments likely controls the chemical composition of iron oxides in mineral deposits, such that this compositional variety can be used to fingerprint mineral deposit types.

Magnetite is a member of the spinel group minerals. Spinel group minerals display a wide range of chemical compositions owing to several solid-solution substitutions of divalent and trivalent cations (Deer *et al*. 1997). In the "magnetite series", *magnetite* ($Fe^{2+}Fe_2^{3+}O_4$) forms a complete solid solution with *magnesioferrite* ($Mg\ Fe_2^{3+}O_4$), and partial solid solutions with *franklinite* ($ZnFe_2^{3+}O_4$), *jacobsite* ($MnFe_2^{3+}O_4$) and *trevorite* ($Ni\ Fe_2^{3+}O_4$). Solid solutions also exist with the "chromite series" where the trivalent cation is $Cr^{3+}$ in *chromite* ($FeCr_2O_4$) and *magnesiochromite* ($MgCr_2O_4$). Finally, the "spinel series" are characterized by $Al^{3+}$ as the trivalent cation of the four (4) end-members: *spinel* ($MgAl_2O_4$), *hercynite* ($Fe^{2+}Al_2O_4$), *gahnite* ($ZnAl_2O_4$) and *galaxite* ($MnAl_2O_4$). *Haematite* ($Fe_2O_3$) forms a complete solid solution with *ilmenite* ($FeTiO_3$) at high temperature (950 ºC). *Haematite* also forms limited solid solution with *magnetite* ($Fe_3O_4$), *corundum* ($Al_2O_3$), and *bixbyite* ($(Mn, Fe)_2O_3$) (Deer *et al*. 1997).

## 2 SAMPLES AND ANALYTICAL METHOD

Representative samples (61) of 9 deposit types were investigated: iron-oxide copper-gold (IOCG), Kiruna, banded iron formation (BIF), Cu-Au porphyries, volcanogenic massive sulphides (VMS), iron skarns, Ni-Cu massive sulphides, Fe-Ti, and Cr. Polished thin sections were analyzed using U. Laval CAMECA SX-100 5-WDS electron microprobe under a beam of 15 kV at 100 nA, using a range of natural and synthetic standards. After counting over the peak for 20 to 30 s, background is measured on both sides for 10 s. These settings yield minimum detection limits (mdl) as low as 20 ppm for elements such as K, Ca, Al, Si, Ti and Mg, 50 ppm for Mn, Cr and V, 200 ppm for Cu and Ni and 400 ppm for Zn. The optimized analytical routine allows analysis of one spot in ~20 min.

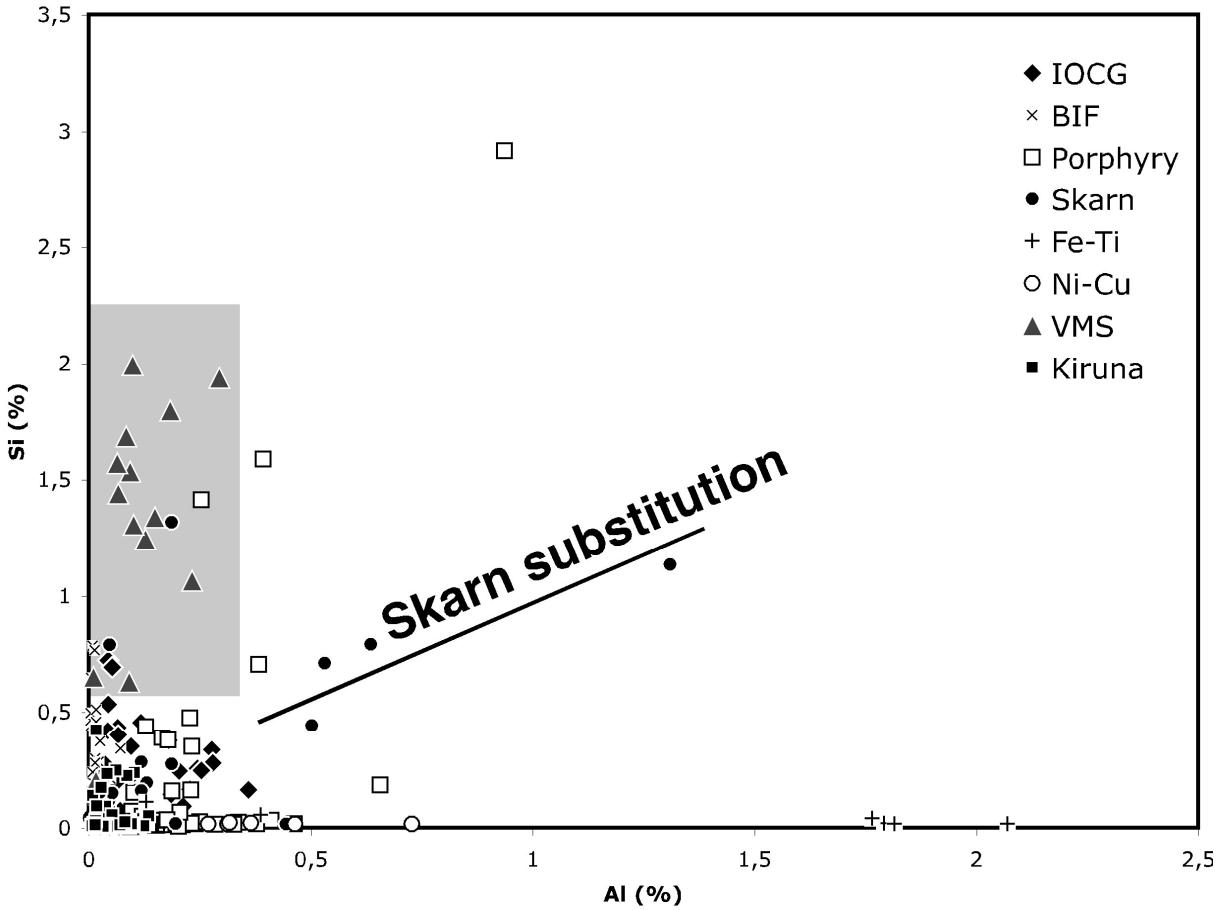

Figure 1. Si vs Al in wt. % for iron oxides from a range of deposit types.

## 3 CHEMICAL COMPOSITION OF IRON OXIDES

Although we initially measured the chemical composition for 28 elements, we find that only 12 elements have average grade (x) either commonly above minimum detection limit (mdl), with x/mdl > 1.2, and sufficient concentration variability with a relative standard deviation (s) where s/x > 0.15 to allow for use as a discriminant element. The average composition of magnetite and/or haematite from several deposit types outlines elements that are characteristically enriched or depleted. BIF are characterized by high Mn whereas VMS are rich in Si and have low Mg. Magnetite from an ophiolitic chromitite is characterized by low Al and high Cr. Iron skarns are characterized by high Ca, whereas highest Ti are measured in magnetite from Fe-Ti deposits. Although a low-Ti magnetite is considered characteristic of IOCG deposits, our data indicates that this is a feature shared also by BIF, VMS and skarns which have lower Ti content than IOCG. The abundance of V is higher in Kiruna and porphyry deposits than in IOCG deposit, a feature that is discussed in more detail below.

## 4 DISCRIMINANT DIAGRAMS

Over the last 30 years petrogenetic discriminant diagrams have evolved from a few to a wide range of grids that are used either for all rock types or have specific application to a rock type or process. We take the same approach here; that is to identify elements, element ratios or element combinations that empirically plot one or several deposit types in distinct fields.

A first approach is to use binary diagrams. An example is the Si-Al diagram (Fig. 1) which shows that iron oxides in VMS deposits are characterized by high Si (> 0.5 wt. % Si) but are poor in Al. Fe-Ti deposit iron oxides are characterized by trace Si but are aluminous with Al greater than 1.5 wt. % (Fig. 1). An interesting feature is the Si-Al covariation for Fe-skarn deposits, suggesting a substitution between Si and Al for analyses with Al greater than 0.5 % in Fe-skarns (Fig. 1).

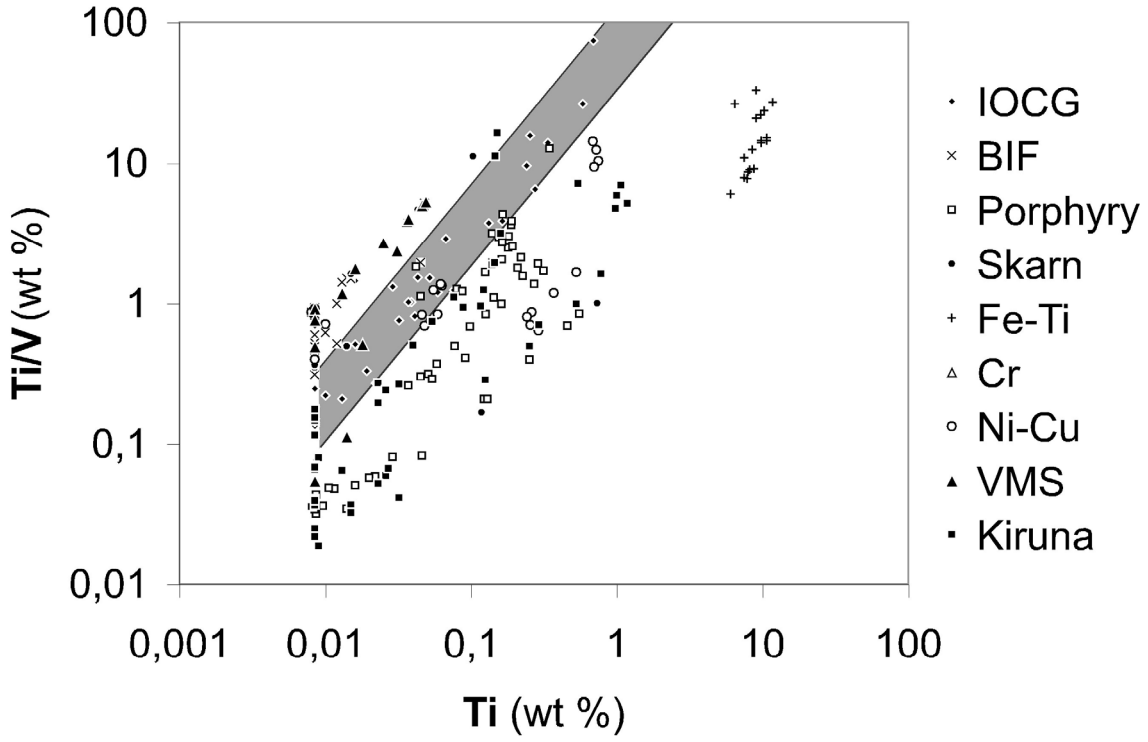


Figure 2. Ti/V vs Ti diagram for individual analyses of magnetite and haematite. The gray field outlines the composition of samples from IOCG deposits. This diagram shows that 90 % of porphyry, 100 % of Kiruna and 86% of Ni-Cu deposit analyses plot below the IOCG field. For Ti/V above the IOCG field, the diagram discriminates 95 % of VMS, 100 % of skarn and 98 % of BIF deposit analyses.

The Ti vs Ti/V is a useful diagram to distinguish individual analyses of magnetite or haematite from IOCG versus other deposit-types (Fig. 2). In the Ti/V vs Ti diagram, IOCG deposits form a narrow log-linear array. This IOCG array defines a field that allow distinction of IOCG from porphyry-Cu-Au, Ni-Cu, and Kiruna Fe-P deposits, all three characterized by lower Ti/V. This distinction is particularly useful because Kiruna deposits are commonly considered to be a variant of IOCG deposits (Williams *et al*. 2005). Fe-Skarn, VMS and BIF deposits plot above the IOCG array (Fig. 2). Finally Fe-Ti titanomagnetites plot at Ti > 6 wt%.

The (Ni+Ca)/(Cr+Mn) vs Ti/V is useful to discriminate IOCG from porphyry Cu-Au and Kiruna deposits (Fig. 3). Whereas the Ti/V vs Ti plot does not distinguish between Kiruna and porphyry Cu-Au deposits (Fig. 2), the (Ni+Ca)/(Cr+Mn) ratio of Kiruna deposits is systematically higher than that of iron oxides from porphyry Cu-Au deposits (Fig. 3). Thus combination of the Ti/V vs Ti and (Ni+Ca)/(Cr+Mn) vs Ti/V diagrams is efficient to distinguish between three deposit types that may share several features in the field. BIF and Fe-Ti deposits also have distinct composition in this diagram, but skarn, Ni-Cu and VMS deposit do not show a systematic composition. We also show the composition of some IOCG-like deposits that plot outside the IOCG field (Fig. 3) either in the fields of Kiruna deposits (San Fernando) or porphyry deposits (Armagosa and Murdie Island). Samples from the Fort Constatine Fe deposit (Cloncurry, Australia) plot near the boundary between porphyry and Kiruna deposit-types (Fig. 3).

## 5 CONCLUSION

These preliminary results demonstrate the potential of using iron oxides chemical composition to fingerprint mineral deposit types. As for petrogenetic diagrams, it is likely that a collection of discriminant diagrams will have to be devised to allow distinction of a wide range of mineral deposit types based on analysis of iron oxides. The electron microprobe is a widely available instrument that allows fast, efficient

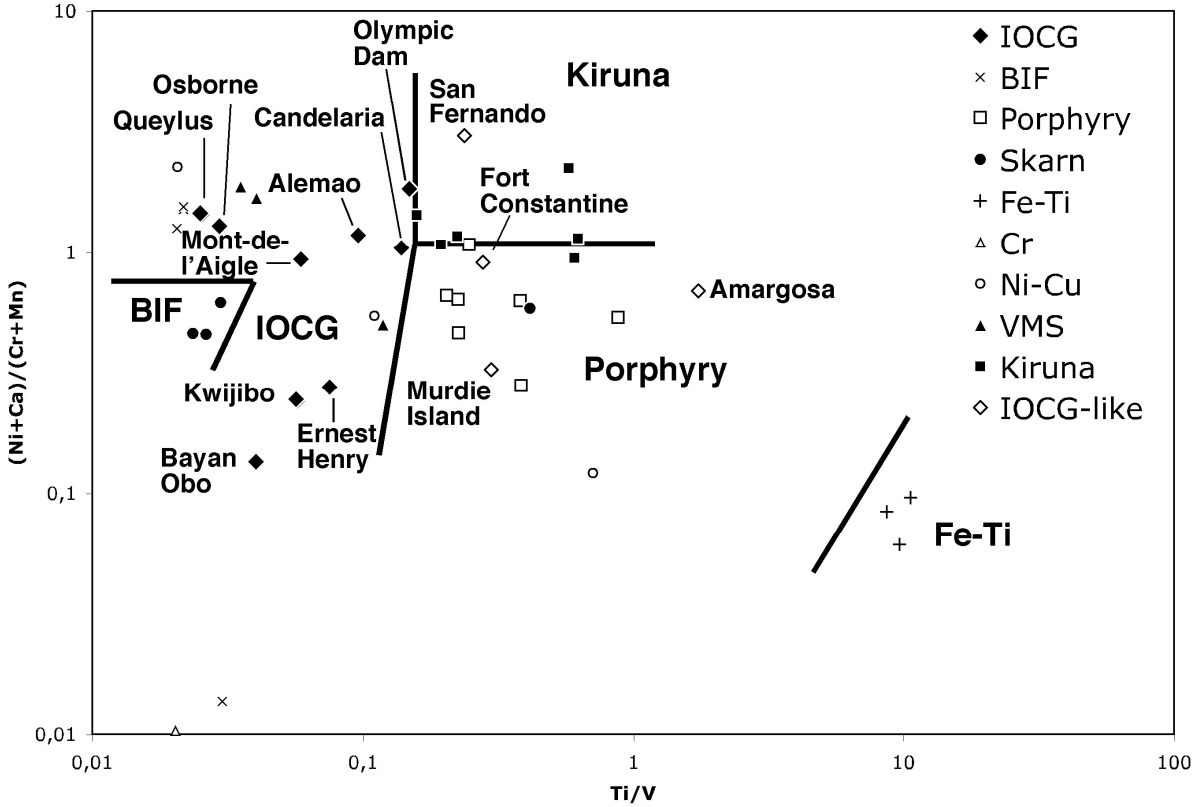


Figure 3. (Ni+Ca)/(Cr+Mn) vs Ti/V in wt. % for average composition per deposit. Compositional fields for Fe-Ti, BIF, Porphyry, Kiruna and IOCG deposit types.

and low cost analysis of iron oxides for application to mineral exploration.

## ACKNOWLEDGEMENTS

This work is funded by the DIVEX network of Valorisation Recherche Québec. We thank Marc Constantin, Mark Cruise, Renan Furic, Michel Gauthier, Alain Hupé, Doug Kirwin, Jochen Kolb, Peter Lightfoot, Larry Meinert and Ricardo Presnell for donating samples.

## REFERENCES

Barnes SJ, Roeder PL (2001) The range of spinel compositions in terrestrial mafic and ultramafic rocks. *J. Petrology* 42: 2279-2302.

Deer WA, Howie RA, and Zussman J (1997) Rock-forming minerals, Vol. 5B: Non-silicates: sulphates, carbonates, phosphates, halides, *Geological Society, London.*

Heimann, A., Spry, P. G., and Teale, G. S., 2005, Zincian spinel associated with metamorphosed Proterozoic base-metal sulfide occurrences, colorado: a re-evaluation of gahnite composition as a guide in exploration: *Canadian Mineralogist*, v. 43, p. 601-622.

Hitzman M.W., Oreskes N. O., Einaudi M.T. (1992) Geological characteristics and tectonic setting of Proterozoic iron oxide (Cu-U-Au-REE) deposits. *Precambrian Research* 58: 241-287.

Williams PJ, Barton MD, Johnson DA, Fontboté L, de Haller A, Mark G, Oliver NHS, Marschik R (2005) Iron oxide copper-gold deposits: Geology, space-time distribution, and possible modes of origin. *Economic Geology 100th Anniversary Volume:* 371-405.

# Arsenic concentrations in groundwater as a potential exploration tool for gold in the Pirkanmaa region, Finland

T. Ruskeeniemi, N. Kärkkäinen, B. Backman, M. Talikka & S. Vuori
*Geological Survey of Finland, Espoo, Finland*

K. Loukola-Ruskeeniemi & A. Parviainen
*Helsinki University of Technology, Espoo, Finland*

ABSTRACT: An environmental study has produced information applicable to gold exploration in the Pirkanmaa region, Finland. The correlation between the distribution of gold occurrences and elevated arsenic concentrations in drilled wells suggest that it is worth considering the use of hydrogeochemical data as one of the regional screening tools when ore potential targets are defined. The benefits of this "non-destructive" approach are underlined when dealing with sensitive, populated or conserved areas. In addition, the collected information of natural background values in groundwater will be useful if the prospect is further developed.

KEYWORDS: arsenic, groundwater, gold deposit, exploration tool, environmental study, Finland

## 1 INTRODUCTION

The history of arsenic research in Pirkanmaa is a good example of the common interests, which seemingly contradicting activities may have. In this case, environmental research benefits from exploration activities, and vice versa. The Pirkanmaa region (14,700 km$^2$ with 450,000 inhabitants) in southern Finland was the target of gold exploration already in the 1980´s. During the exploration phase, high arsenic concentrations were observed in bedrock in the gold potential areas.

Thus, after 1992 when arsenic analyses for groundwater became routine, the regional hydrogeochemical mapping was focused in southern Finland. In some cases elevated arsenic concentrations were found also in drilled bedrock wells close to gold findings. Likewise, anomalous arsenic concentrations were reported in the glacial till deposits (Koljonen *et al*. 1992). Meantime, the gold exploration activities increased and more chemical analytical data were obtained from bedrock and soils.

One of the Finland's largest cities, Tampere, the capital of the Pirkanmaa region, is located within the arsenic anomaly. Due to the urgent need and the extensive background information, the Pirkanmaa region was appraised as a suitable test area for developing risk assessment and risk management procedures for arsenic. In 2004, the EU Life Environment program granted funding for a three-year project "Risk assessment and Risk Management procedure for Arsenic in the Tampere region" or 'RAMAS' (www.gtk.fi/projects/ramas).

## 2 GEOLOGY AND METALLOGENY OF THE STUDY AREA

The crystalline bedrock in Finland is part of the Precambrian Fennoscandian craton and consists mainly of Late Archean (3.8–2.5 Ga) and Palaeoproterozoic (2.5–1.6 Ga) rocks that are exposed at the current erosion level. The two major collisions of tectonic plates that lead to the formation of the Finnish bedrock occurred at 2.8–2.7 Ga and 1.9–1.8 Ga ago. The bedrock has been a subject to erosion ever since.

The Pirkanmaa area is located in the middle of the Paleoproterozoic Svecofennian domain, which formed 1920-1870 Ma ago as a result of several orogenic and extensional events (Lahtinen *et al*. 2005). The bedrock of the domain is predominantly composed of metasedimentary rocks, metavolcanic rocks of island-arc type and granitoids, which cut the former rock types (Kähkönen 1989, Nironen 1997, Kilpeläinen 1998). The supracrustal rocks were subjected to deformation and metamorphosis after their formation.

The Pirkanmaa region can be divided in three geologically distinct units based on the dominant rock types encountered in the area. The main geological subdivisions in the study area are: the Central Finland Granitoid Complex (CFGC) in the north, the Tampere Belt (TB) in the centre, and the Pirkanmaa Belt (PB) in the south. The CFGC mainly consists of tonalites, granites and granodiorites with minor proportions of supracrustal rocks and mafic plutonic rocks. The TB is predominantly composed of turbiditic metasedimentary rocks and felsic-intermediate arc-type metavolcanic rocks and plutonic intrusions that cut the supracrustal sequence (Ojakangas 1986, Kähkönen 1989, Kähkönen & Leveinen 1994). In the PB area, mafic and ultramafic plutons and granitoids cut the migmatitic metasedimentary rocks, sporadically containing graphite-bearing gneiss interlayers.

The volcanic-sedimentary belt (TB & PB) is enriched in gold, arsenic, silver, cobalt, copper, lithium, molybdenum, phosphorus, antimony, uranium, and zinc (Koljonen *et al*. 1992). Pirkanmaa has a long mining history including the Ylöjärvi Cu-W-As, Kylmäkoski Ni-Cu, Vammala Ni-Cu, Haveri Au-Cu and Orivesi Au mines. Arsenic is one of the enriched elements in most of the mined deposits. The occurrence of arsenic is, however, unpredictable. Generally, arsenic concentrations are insignificant in mafic and ultramafic Ni-Cu ores, as in the Vammala mine (Eilu & Lahtinen 2004), but the Kylmäkoski Ni-Cu ore is atypical in this respect. Some parts of the Kylmäkoski ore contain more than 1000 mg/kg of arsenic. The arsenic may have assimilated from the surrounding sedimentary rocks when the intrusion forced its way through. However, in the two gold ores Haveri and Orivesi, the arsenic levels are variable, but generally well below 100 mg/kg. The Ylöjärvi Cu-W-As mine is the only mine in Finland that produced arsenic concentrate. Currently, there are no mines in the study area, but active exploration is carried out by several companies and by the Geological Survey of Finland (GTK).

Within the last 2.4 Ma, numerous glacial and interglacial periods have occurred and thick continental ice sheets have repeatedly covered northern Europe. During the glacial maximum of the Weichselian glaciation, some 18 000 years ago, the ice cover extended to central Europe. The majority of the overburden observed today in Finland was deposited about 10 000 years ago, during and after the last glaciation. The average thickness of the overburden that comprises till, sand, gravel, silt, and clay deposits is 3–4 m. Arsenic and some of the heavy metals are variably enriched in the till and some other soil types (*e.g*. Backman *et al* 2006).

## 3 GOLD EXPLORATION

Gold exploration in the Pirkanmaa area has been active during the past twenty years (http://en.gtk.fi/ExplorationFinland/Commodities/Gold.html).

Previously, the Pirkanmaa Belt was not regarded of interest for gold exploration, because the bedrock mainly consists of migmatitic graywackes, potassium granites, pegmatites and small mafic-ultramafic intrusions. However, when the nation-wide geochemical survey on till (one sample/16 $km^2$) revealed a 60km long and 20km wide NW-SE-oriented arsenic anomaly with some randomly distributed gold (Koljonen *et al*.1992), the exploration became strongly motivated. As a consequence, GTK's exploration at Pirkanmaa Belt started in 1986. The task is not easy since the arsenic anomaly is controlled neither by lithological units nor major fault zones. Targets from the Pirkkala municipality, 20km SW from the City of Tampere, were chosen for more detailed geochemical surveys. Distinct gold anomalies were encountered, with gold concentrations reaching up to 883 ppb Au (and 13500 ppb As) in the fine fraction of till (Rosenberg 1997). There were also gold-rich erratic boulders and mineralized outcrops in this area. Glacial transportation distance of till material is short, only about 200m. Drilling of the gold anomalies resulted in the discovery of several minor gold occurrences with the highest assays of 1-2 ppm Au.

Later, boulders and outcrops with visible gold and higher gold assays (up to > 500 ppm Au) were found in many places south from the original anomaly. Further exploration including geochemical and geophysical surveys, heavy mineral studies and tentative diamond core drilling, resulted to the detection of several gold occurrences in shear zones and quartz vein systems from various localities containing up to 15.7 ppm Au per one meter of drill core (Kärkkäinen *et al.* 2003, Rosenberg 1997).

Gold occurs in native form, as grains between silicates and as inclusions in major sulphide minerals, arsenopyrite or pyrrhotite.

Visible gold is common, and the amount of sulphides varies being sometimes minor.

The style of gold mineralization varies in the Pirkkala area. In some places the mineralization is closely associated with a small quartz dioritic intrusion and is hosted by quartz-vein bearing shear zones within this rock type. The second type is composed of narrow (1 – 10m), gently dipping shear zones in graywackes and the third type is characterised by quartz veins or network cutting competent metagraywackes surrounded by mica schist or gneisses. There are still unexplored geochemical Au anomalies in this region. Recent regional exploration includes heavy mineral studies and geochemical till sampling close to the bedrock surface and, as a new application, review of arsenic anomalies in groundwater.

## 4 ARSENIC IN GROUNDWATER

Shallow groundwater and surface waters have generally very low arsenic concentrations even in anomalous surroundings (Backman *et al.* 2006). This is due to the geochemical properties of arsenic and it's tendency for retention to soil particles and iron or manganese oxyhydroxides in oxidized conditions. In contrast, arsenic in bedrock is readily transferred to deep groundwater via water-rock interaction.

The close association of arsenic in drilled wells and the arsenic source in bedrock is striking. Practically all elevated arsenic concentrations are from wells located in the Tampere and Pirkanmaa Belts, where gold (and arsenic) potential rock types dominate. The low arsenic levels in the Granitoid Complex rocks in the northern part of the Pirkanmaa region are reflected in low concentrations in the well waters. Arsenic concentrations exceeding the health limit value (10µg/L) by ten- or hundred-folds are rather common in drilled bedrock wells in the southern part of the study area (Backman *et al*. 2006). The concentration range is from negligible to more than 2000 µg/L, which is large enough to be effective in discriminating anomalies from the background levels.

## 5 ARSENIC IN GROUNDWATER AS AN INDICATOR OF GOLD ANOMALIES

The solubility of gold in natural waters is extremely low meaning that the analyses are susceptible for analytical errors and contamination during sampling. The significantly higher dissolution rate of arsenic-bearing phases and it's well-known coupling with gold in ore-forming processes makes arsenic an applicable pathfinder element also in hydrogeochemical studies. In the Finnish metamorphosed rocks the major load of arsenic is incorporated in arsenopyrite. Arsenic seems to transfer relatively easily to soluble form in the long-term, low-temperature water-rock interaction processes. Arsenic also tends to remain in the soluble form since the reducing conditions prevailing deeper in the bedrock do not favor sorption processes, which would scavenge arsenic from the water.

Due to the strong geologic control it is relatively easy to define the areas where the probability to come up against an arsenic-rich well is high. However, the arsenic anomalies are very difficult to predict in detail. Nearby wells may have very different arsenic levels and most of the wells in the risk area are healthy, *i.e*. they contain arsenic less than 10µg/L (Backman *et al.* 2006). The explanation for this is probably found from the nature of the "aquifers" in crystalline bedrock. All the rock types encountered in the area are metamorphozed, crystalline hard rocks. The low porosity of these rocks allows storage and conductive flow of groundwater only along a discrete fracture network. The fractures or fracture zones may cross from one rock mass to another, but hydrogeological and hydrogeochemical compartmentalization is also common. Further, arsenic and gold are not always accompanying each other as the Kylmäkoski Ni-Cu mine (atypical positive anomaly) and Orivesi Au mine (weak anomaly) demonstrate.

However, the very obvious correlation between interesting gold occurrences and arsenic in wells observed in Pirkanmaa suggests that it is worth considering the use of hydrogeochemical data as one of the regional screening tools when ore potential targets are defined. In Pirkanmaa such screening carried out in cooperation with the exploration department of the Geological Survey of Finland and the RAMAS project has already drawn attention to certain areas, which have not been targets for exploration activities before. Time will show to which direction these prospects will develop.

Similar relationship between gold and arsenic in natural spring water has been reported earlier from Kittilä, northern Finland (Loukola-Ruskeeniemi *et al.* 1999).

Water sampling from drilled wells provides a "non-destructive" method to survey sensitive,

populated or conserved areas where conventional exploration is difficult. Compared to lithogeochemical or till geochemical sampling the benefit in water sampling is that water is already homogenized and it reflects the chemistry of a large rock mass. Besides, now that the sustainable use of ores and the environmental aspects are highlighted everywhere, it is beneficial to collect baseline information from the exploration area in case it is needed in future licensing applications. Even if the exploration does not advance to positive result, the collected data may be used for other purposes as in this case, for environmental risk assessment in the Pirkanmaa area.

## REFERENCES


Backman B, Luoma S, Ruskeeniemi T, Karttunen V, Talikka M, Kaija J (2006) Natural Occurrence of Arsenic in the Pirkanmaa region in Finland. Espoo: *Geological Survey of Finland.* pp82.

Eilu P, Lahtinen R (2004) Arseeni kallioperässä ja malmiutuneissa vyöhykkeissä (Anomalous arsenic in bedrock and ores in Finland). In: Loukola-Ruskeeniemi K, Lahermo P (eds.). *Arsenic in Finland: Distribution, environmental impacts and risks; in Finnish with English synopsis and abstracts. Espoo: Geological Survey of Finland:* 29-44.

Kilpeläinen T (1998) Evolution and 3D modelling of structural and metamorphic patterns of the Palaeoproterozoic crust in the Tampere-Vammala area, southern Finland. Espoo: *Geological Survey of Finland. Bulletin* 397. pp124.

Koljonen T, Gustavsson N, Noras P, Tanskanen H (1992) The Geochemical Atlas of Finland, Part 2–Till. Espoo: *Geological Survey of Finland*. pp218.

Kähkönen Y (1989) Geochemistry and petrology of the metavolcanic rocks of the early Proterozoic Tampere Schist Belt, southern Finland. Espoo: *Geological Survey of Finland. Bulletin* 345. pp104.

Kähkönen Y, Leveinen J (1994) Geochemistry of metasedimentary rocks of the Paleoproterozoic Tampere Schist Belt, southern Finland. In: Nironen, M. and Kähkönen, Y. (eds.) Geochemistry of Proterozoic supracrustal rocks in Finland. Espoo: *Geological Survey of Finland. Special paper* 19: 117-136.

Kärkkäinen N, Lehto T, Tiainen M, Jokinen T, Nironen M, Peltonen P, Valli T (2003) Ni and Au exploration within the South and Western Finland Arc Complexes in 1998-2002. Phase I – Final Report. *Geological Survey of Finland, Report* M 19/21, 12/2003/1/10 (in Finnish).

Lahtinen R, Korja A, Nironen M (2005) Paleoproterozoic tectonic evolution of the Fennoscandian Shield–a plate tectonic model. *In*: Lehtinen, M., Nurmi, P. & Rämö, O. T. (eds.) *Precambrian Geology of Finland – Key to the Evolution of the Fennoscandia Shield.* Amsterdam: Elsevier Science B.V: 483-504.

Loukola-Ruskeeniemi K, Tanskanen H, Lahermo P (1999) Anomalously high arsenic concentrations in spring waters in Kittilä, Finnish Lapland. In: Autio S (ed.) Geological Survey of Finland, Current Research 1997-1998. Espoo: *Geological Survey of Finland. Special Paper* 27: 97-102.

Nironen M (1997) The Svecofennian orogen: a tectonic model. *Precambrian Research* 86: 21-44.

Ojakangas RW (1986) An Early Proterozoic metagraywacke-slate turbidite sequence: the Tampere schist belt, southwestern Finland. *Bulletin of Geological Society of Finland* 58: 241-261.

Rosenberg P (1997) Research report on the ore exploration carried out in the claims Luitamo I-II (nro 5059/1-2) and Tikkarinvuori I (nro 5299/1), Pirkkala in 1992-1995. *Geological Survey of Finland,* Report M06/2123/-97/1/10 (in Finnish).

# The use of geochemistry exploration to identify lithium bearing pegmatite-aplite veins in Northern Portugal

A.M.C. Lima, R.C. Vieira, T. Martins, F. Noronha & F. Da Silva
*GIMEF – Centro de Geologia da Universidade do Porto, R. Campo Alegre, 687, 4169-007 Porto, Portugal*

ABSTRACT: The Barroso-Alvao region (BA) and Almendra-Barca d'Alva region (AB) have high mineral resources potential for LCT (Li, Cs, Ta) pegmatites. Both pegmatite fields are located in the NW part of the Iberian Pegmatitic Belt. Pegmatite veins are hosted in low- to medium-grade metamorphic rocks and are surrounded by highly evolved synorogenic two-mica granitoids. The lithium mineralization occurs within pegmatite-aplite veins mainly in the form of lepidolite, spodumene, petalite and accessory montebrasite-amblygonite, cookeite and eucryptite. Based on successful geochemical exploration results obtained in the BA region, similar methodologies are now being applied to the AB region with successful identification of lepidolite, petalite and spodumene bearing pegmatite-aplite veins.

KEYWORDS: Lithium minerals, stream sediment, geochemical exploration, pegmatites

## 1 INTRODUCTION

The Barroso-Alvao (BA) and Almendra-Barca d'Alva (AB) regions have high potential for mineral resources, especially LCT (Li, Cs, Ta) pegmatites. The lithium mineralization in these veins occurs mainly as lepidolite, spodumene, petalite and accessory montebrasite-amblygonite, cookeite and eucryptite.

During the 1980s, the Portuguese Geologic Survey (presently INETI) undertook extensive stream sediment exploration campaigns for metals in the AB region. Similar campaigns were undertaken in the BA region during the 1990s. The results led to the identification of anomalous lithium zones (background of 99 ppm) within drainage catchments. These anomalous zones were integrated with geological mapping and were followed up by geological exploration at 1/10,000 scale.

Several pegmatite veins were identified by the detailed exploration.

## 2 GEOLOGICAL SETTING

The BA pegmatite field is located in the NW part of the Iberian Peninsula. Aplite-pegmatite veins from this region are hosted metasedimentary rocks that have undergone medium-grade metamorphism. These lithologies are of Ordovician to Silurian age and belong to the Galiza-Trás-os-Montes geotectonic zone (Ribeiro *et al.*1979). Different types of Hercynian granite bodies surround this pegmatite field, including highly evolved syntectonic two-mica granitoids (Cabeceiras de Basto Massif and Serra do Barroso Massif) and biotitic post-tectonic granites (Vila Pouca de Aguiar Massif).

Aplite-pegmatite veins from the Almendra-Barca d'Alva (AB) region are hosted by low- to medium-grade metasedimentary rocks occurring within the "Complexo Xisto-Grauváquico". They are of pre-Ordovician age and belong to the Centro-Ibérica geotectonic zone (Ribeiro *et al.*1979).

The Meda-Penedono-Lumbrales Massif, a syntectonic two mica granite body, is located within the vicinity of this pegmatite field..

The pegmatite veins are defined on the basis of the lithium mineral they host:

(i) Aplitic veins commonly converted to kaolinite. In those cases, petalite is difficult to identify. These veins contain low-grade (<3 kg/t) cassiterite (I) mineralization and were intensively exploited during the last century.

(ii) Aplite-pegmatite veins mineralized with spodumene.

(iii) Aplite-pegmatite veins mineralized with

petalite.

(iv) Aplite-pegmatite veins mineralized with lepidolite and cassiterite (II).

All of these Li-rich granitic pegmatites are of the LCT-type (*i.e.*, Li–Cs–Ta) family (Černý 1982, 1991a). Silicates (spodumene, petalite, lepidolite and, less commonly, eucryptite), phosphates (mainly of the amblygonite–montebrasite and lithiophylite–triphylite series) and clay mineral cookeite are the main Li carriers.

Using the system of Charoy *et al.* (2001), spodumene and petalite bearing dykes are not evenly distributed. Local swarms of several dykes of various size can be traced continuously for a few hundred meters (up to 1 km) along strike, and up to 100 meters in outcrop width. Their average thickness is variable, ranging from less than a few meters up to ten meters. All pegmatite dykes display irregular patterns in outcrop: some are flat-lying; others have gently or steeply dipping attitudes along strike. The largest usually pinch and swell in accordance with the ductility of their host rocks.

As a consequence of weathering, the internal structure of the pegmatites is not easy to establish at outcrop scale. All of them are texturally composite with aplitic and largely granular pegmatitic components. Both textures are intermixed together in variable proportions and spatial relations appear to be contemporaneous.

Overall, the pegmatites seem to be texturally unzoned. Aplitic zones are texturally uniform, with only a few tapered K-feldspar phenocrysts present. An aborted comb-layered fabric involving elongate crystals of alkali feldspars may be sporadically encountered. Contacts between pegmatite bodies and enclosing schists are sharp. The host micaceous schists at the footwall are commonly very disturbed, and are often strongly folded and silicified.

## 3 STREAM SEDIMENT GEOCHEMISTRY

Stream sediment geochemistry has been used over the past fifty years with remarkable success in identifying areas of high mineral potential (Fletcher 1997).

In 1979/80 the Portuguese Geological Survey (SFM) carried out a stream sediment sampling campaign in the AB region. In total, 631 samples were collected over an area covering 210 square kilometers (Viallefond 1981). On the basis of a pilot study, the less-than 80 mesh fraction sample was analysed by optical spectroscopy by the BRGM-France for 10 major elements and 25 trace elements. The elements considered in this study were Li, B, Sn, W, Nb and Be (Viegas *et al.* 1985).

In 1993/94 the Portuguese Geological Survey (IGM) completed a stream sediment sampling campaign in the BA region. In total, 665 samples were collected over an area covering 227 square kilometers. Following a pilot study, the less-than 80 mesh fraction was analysed for Li (by Atomic Absortion), Ta and Nb (by X-ray Florescence), Sn and W (by Colorimeter) (Pires 1995).

## 4 DISCUSSION

From the work of Pires (1995), a number of Li anomalies in the BA region without known spodumene or lepidolite mineralization were identified. The anomalous geochemistry was incorporated with an updated pegmatite geological map. Geological exploration at 1/10,000 scale was carried out to investigate the lithium anomalies. Following this work (Lima *et al.* 2003; Noronha & Lima 2005) the source of the anomalies were determined to be petalite mineralization.

On the basis of these results, it was decided to investigate the old stream sediment data from the AB region.

The background threshold was determined to be at the 50 percentile. Values above the 75 percentile are regarded as highly anomalous responses. Figure 1 and figure 2 show the location of the stream sediment geochemical data with data above the 75 percentile (135 ppm in BA region and 96 ppm in AB region). They also illustrate their spatial relationship with the Li-bearing pegmatites that have been identified so far.

## 5 CONCLUSIONS

This simple methodology, which combines stream sediment geochemistry with geological mapping, has led to the discovery of petalite-bearing pegmatite veins and has consequently augmented the Li resources in the BA area.

Based on the successful results obtained in the BA region, the same methodology is being applied to the AB area and is leading to the successful identification of new lepidolite, petalite and spodumene bearing pegmatite-aplite veins.

## ACKNOWLEDGEMENTS

We would like to thank to INETI (Dr. Luis Martins) for all the geochemical data. Tania Martins and Romeu Vieira have both a PhD grant from Portuguese Science and Technology Foundation (FCT). The present article is integrated in the Centro de Geologia da Universidade do Porto activities, with financial support from POCI 2010.

## REFERENCES

Černý P (1991) Rare-element granitic pegmatites, Part I. Anatomy and internal evolution of pegmatite deposits. *Geoscience Canada,* 18/2, pp 49-67

Charoy B, Noronha F, Lima AMC (2001) Spodumene-Petalite-Eucryptite: mutual relationships and alteration style in pegmatite-aplite dykes from Northern Portugal. *Canadian Mineralogist*, 39, pp 729-746

Fletcher WK (1997) *Proceedings of Exploration 97: Fourth Decennial International Conference on Mineral Exploration*, edited by A.G. Gubins, pp 249-260

Lima AMC, Vieira R, Martins T, Noronha F (2003) - Aplicação de Geoquímica de Sedimentos de Linhas de Água na Prospecção de Filões Aplitopegmatíticos Litiníferos no Campo Aplitopegmatítico do Barroso-Alvão (Norte de Portugal), I*V Congresso Ibérico de Geoquímica. Universidade de Coimbra,* pp 458-460

Noronha F, Lima AMC (2005) Li stream sediment geochemistry at Barroso pegmatite field (Portugal) 15th Annual V M Goldschmidt Conference, *GEOCHIMICA ET COSMOCHIMICA ACTA* 69 (10): A883-A883, Suppl. S MAY 2005

Pires M (1995) Prospecção Geológica e Geoquímica. Relatório interno da Prospecção de Jazidas Litiníferas e de Metais Associados entre as Serras de Barroso e Alvão – Ribeira de Pena. *IGM, Lisboa*, 1995, 46 pp

Ribeiro A, Antunes MT, Portugal Ferreira M, Rocha RB, Soares AF, Zbyszewski G, Moitinho de Almeida F, Carvalho D, Monteiro JH (1979) Introduction à la géologie générale du Portugal. *Serv. Geol. Portugal*

Viallefond L (1981) Prospection Geochimique Portugal: resultats analytiques et interpretation de l'echantillonnage realise par le SFM sur la Feuille 15A – Region de Almendra. Note GMX nº 732. *BRGM, Orleans,* 6p

Viegas L, Lima LP, Soares J, Fonseca EC (1985) Aplicação da análise estatística multivariada ao estudo de amostras de sedimentos na região de Escalhão- Barca D'Alva (NE de Portugal) *Boletim da Sociedade Geológica de Portugal*. Vol. XXIV, pp 161-169

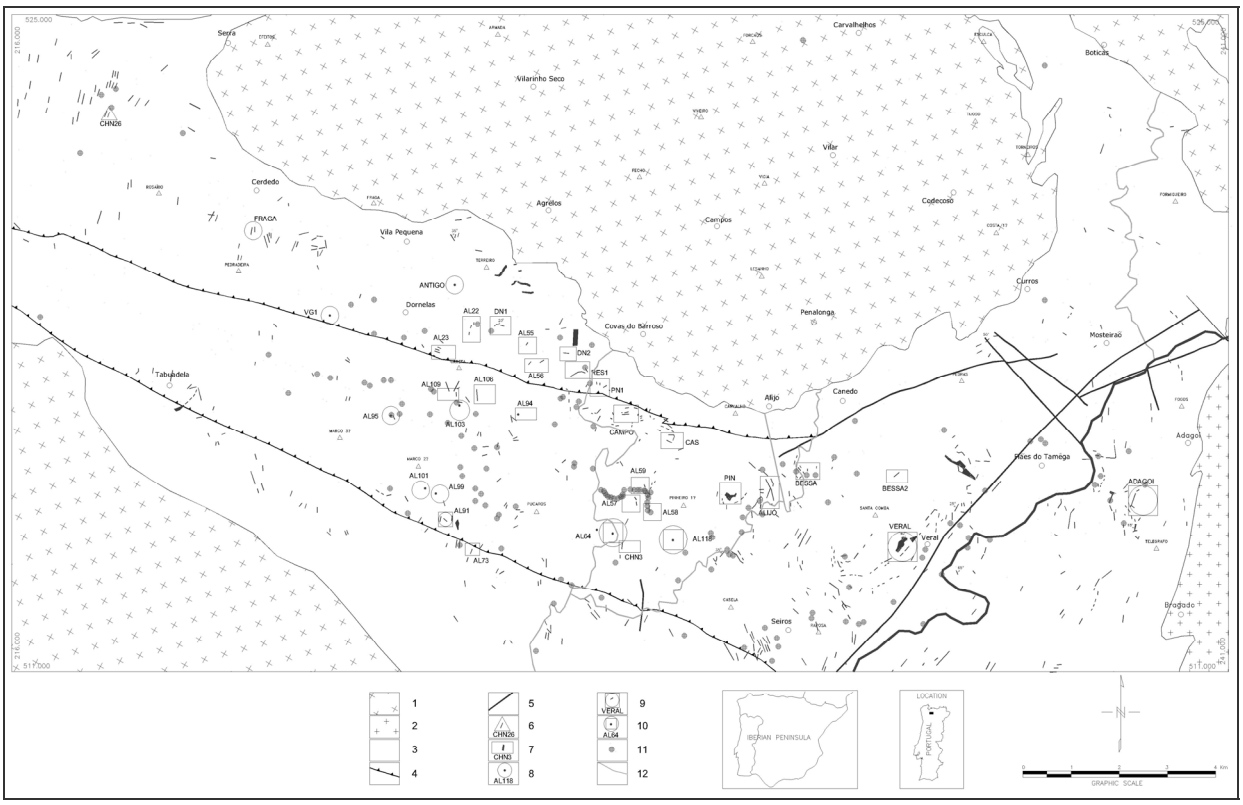


Fig. 1 – Simplified map of geology from BA region. 1 – Synorogenic granites (biotitic and two-micas); 2 – Post-tectonic biotitic granite; 3 – Metasediments; 4 – Thrust; 5 – Fault; 6 – Vein with lepidolite; 7 - Vein with spodumene; 8 - Vein with petalite; 9 - Vein with dominant spodumene and accessorial petalite; 10 - Vein with dominant petalite and accessorial spodumene; 11 – stream sediment sample with more than 135 ppm of Li; 12 – Important river.

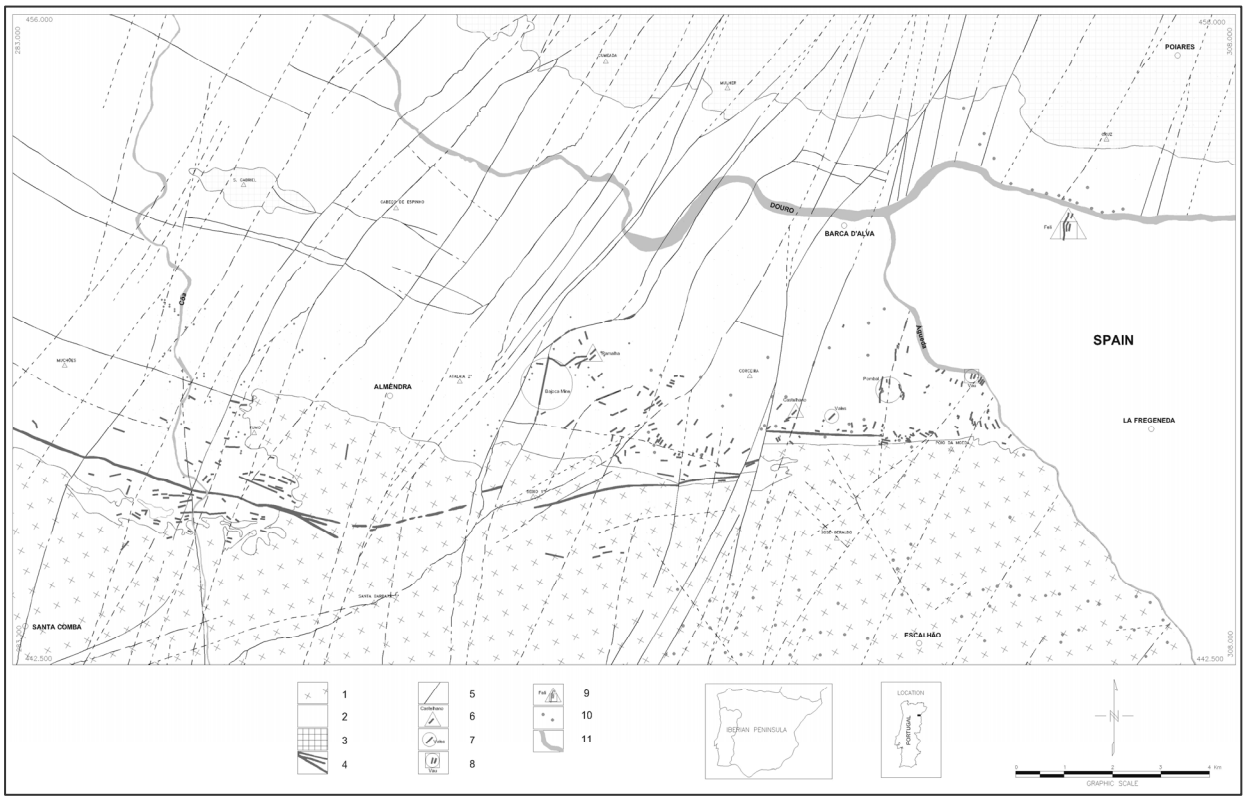


Fig. 2 – Simplified map of geology from AB region . 1 – Synorogenic granites (two-micas); 2 CXG; 3 – Quartzites; 5 – Fault; 6 – Vein with lepidolite; 7 - Vein with petalite; 8 - Vein with dominant spodumene and accessorial petalite; 9 - Vein with dominant lepidolite and accessorial spodumene; 10 – stream sediment sample with more than 96 ppm of Li; 11 – Important river.

# Gold Mineralization Types in the Borborema Province, NE Brazil: Geological Controls and Exploration Models

S.G. Hagemann
*Centre for Exploration Targeting, School of Earth and Geographical Sciences, M006, The University of Western Australia, 35 Stirling Highway CRAWLEY Western Australia 6009, Australia*

K. Petersen jr
*Ore Targeting Worldwide, Belo Horizonte, Minas Gerais, Brazil*

R. Smakman, V.E. do Carmo
*Crusader do Brasil, Campinas Grande, Paraiba, Brazil*

ABSTRACT: The Borborema Province in NE Brazil contains multiple different gold mineralization types including orogenic-hypozonal shear zone, mesozonal reef-type, mesozonal granitoid-hosted, -thin skinned thrusting related gold, and reduced gold-skarn. The two different gold deposit types and various styles of orogenic gold mineralization are hosted in supracrustal and granitoid host rocks, metamorphosed to greenschist-amphibolite grade, and structurally controlled. Exploration models, taking into account models for the different gold mineralization types and styles, tries to predict the location of mid-size (>100, 000 oz) gold deposits.

KEYWORDS: gold, mineralization styles, Borborema, gold exploration model

## 1 INTRODUCTION

Gold mineralization in the Borborema Province has been the target for garimpeiros the past 70 years with extensive small-scale exploration exploitation (~20 t Au) from a variety of gold mineralization styles. In the mid-1970's more systematic gold exploration by mining companies resulted in the development of small deposits (<10 t Au) such as the Sao Francisco mine (State of Rio Grande do Norte), and Cachoeiras de Minas and Itajubatiba mines (both located in the State of Paraiba). In 2006, Crusader do Brasil Mineração Ltda. acquired significant land-holdings in the Transversal domain of the Borborema Province (Fig.1) with the goal to target a variety of structurally controlled gold mineralization types and styles.

This contribution provides a geological framework of the Transversal domain, descriptions of the gold mineralization styles and exploration models that take into account the complex geological setting.

## 2 REGIONAL GEOLOGY

The Borborema Province consists of microplates of Archaean to Neo-Proterozoic granitic, gneissic and migmatitic terranes, that are surrounded by Proterozoic fold belts. The dominant Neoproterozoic mountain building event produced a complex structural pattern consisting of the E-W trending, about 500 km long Patos and Pernambuco crustal-scale lineament systems (Fig. 1).These multiply reactivated fault zones are linked by anastomosing networks of NE- and E-trending, about 70 km long, secondary subsidiary strike-slip shear zones (Vauchez *et al.* 1995). Syn-tectonic, en cornue shape granitic stocks were emplaced preferentially within, or at the margins of, the secondary shear zones where they intersect lithological boundaries. (Weinberg *et al.* 2004). The metamorphic grade of the metasedimentary, metavolcanic, and metagranitic gneisses appears to be controlled by the proximity to first-order fault zones (Neves *et al*. 2000); with medium- to high-grade metamorphism (amphibolite to lower granulite facies) close to the Patos fault zone and low- to medium-grade metamorphism (greenschist to lower amphibolite facies) near the Jurú-Belém fault zone (Fig. 1).

## 3 GOLD MINERALIZATION TYPES AND STYLES

Gold mineralization in the Borborema Province is hosted either in Proterozoic fold belts

(mainly of Brasiliano age) in supracrustal or granitic rocks or in Archaean basement in high-grade metamorphic metasedimentary, metavolcanic, and metagranitic rocks (Table 1). Based on desktop analyses, reconnaissance mapping including the analyses of geological characteristics of gold deposits, garimpos and mineralized rocks, and conceptual modeling the following types of gold mineralization are interpreted: (1) Orogenic gold: (a) hypozonal shear zone, (b) mesozonal reef-type, (c) mesozonal granitoid-hosted, and (d) mesozonal thin-skinned thrust related. (2) Skarn gold (reduced)

### 3.1 *Orogenic-hypozonal shear zone gold*

Hypozonal shear zone style gold mineralization is best characterized by the Boqueirão dos Cochos (BC) garimpos (Fig. 1). The host rocks are mainly schists with intercalated gneiss (after tonalites) and amphibolite lenses. Locally the gneisses contain migmatites. Several bodies of augen-orthogneisses include granodiorites and monzogranites. The metamorphic grade is estimated to be amphibolite to lower granulite facies. The BC garimpos are located in, and controlled by, a lower-order ductile shear zone that is interpreted to be part of the second-order Boqueirão dos Cochos shear zone, which connects towards the north with the first-order transcrustal Patos fault zone. The main Damião garimpo is located in strongly foliated quartz-feldspar-biotite gneiss and displays up to 20cm wide quartz veins, in places with a pegmatitic texture that strikes about E-W and dips 50$^{o}$ to the south. The quartz vein has an approximate extension of 50m. Hydrothermal alteration minerals that semi-concentrically envelop the quartz vein include biotite, quartz, plagioclase, and garnet. Native gold occurs in recrystallised quartz within the vein and in the wallrock. A pegmatite dyke strikes parallel to the vein and is composed mainly of quartz and feldspar.

### 3.2 *Orogenic-mesozonal reef-type gold*

Orogenic-mesozonal gold mineralization is the most common type of gold mineralization in the Borborema Province and is expressed by two gold mines, the São Francisco and Cachoeiras de Minas mines that were both active during the 1970 to 1980. Both are small deposits (production and reserves < 10 tonnes Au produced) with grades of 2.3 and 3.7 g/t Au, respectively (Couthinho 1994). Gold mineralization is characterized by ductile-brittle shear zone systems that display a consistently dextral configuration from regional- to camp- to ore body-scale. The ore bodies are mostly defined by the central shear veins (S-structures) and locally characterized by up to 2.5 m wide, massive quartz veins. Locally they display distinct crack-seal textures. Hydrothermal alteration surrounding the central shear veins is defined by carbonate, sericite, magnetite, tourmaline, pyrite, galena, and gold.

### 3.3 *Orogenic-mesozonal granitoid-hosted gold*

This style of gold mineralization is characterised by only a restricted number of gold garimpos (Couthinho 1994). Gold mineralization is controlled by ductile-(brittle) shear zones. Gold is located in quartz +/- tourmaline shear veins which are surrounded by thin (<1 m) potassic alteration zones (Couthinho 1994).

### 3.4 *Mesozonal thin-skinned thrust-related*

This newly discovered mineralization style is located near the town of Ibiara (Fig. 1). The host rocks are: a) quartz±garnet phyllite, and (b) biotite-muscovite-quartz phyllite with fine granulations. In interpreted mineralized areas, the predominant lithology is a green-grey sericite (muscovite)-chlorite-quartz phyllite. The main foliation that controls the orientation of hydrothermal veins trends NE and EW and dips 20$^{o}$ to 50$^{o}$ SE and S, respectively. Foliation parallel veins are dominant with locally sigmoidal shape and small voids. They are locally surrounded by strongly foliated feldspar alteration zones which, in many localities, are partly or completely kaolinized. Pyrite and locally gold is observed in the veins, as well as in the altered wallrocks. The widths of the alteration halos are variable (mm to cm), locally alteration haloes lack distinct quartz veins. On a regional scale gold mineralization is interpreted to be associated with thin-skinned thrust zones, expressed by mylonites, intensely foliated host rocks and quartz veins that occur within the phyllite units.

### 3.5 *Reduced gold-skarn*

The Itajubatiba gold mine (now abandoned) is located about 60km west of the town of Patos and located in metamorphosed marble, tonalite, syenogranite, pegmatite, and amphibolite of probable Neoproterozoic age (Neto 1995). According to Neto (1995) and Neto *et al.* (1999), the hydrothermal alteration consists of pyroxene-plagioclase-amphibole and amphibole-quartz and quartz veins in the endoskarns (located in the marble) and pyroxene-plagioclase-

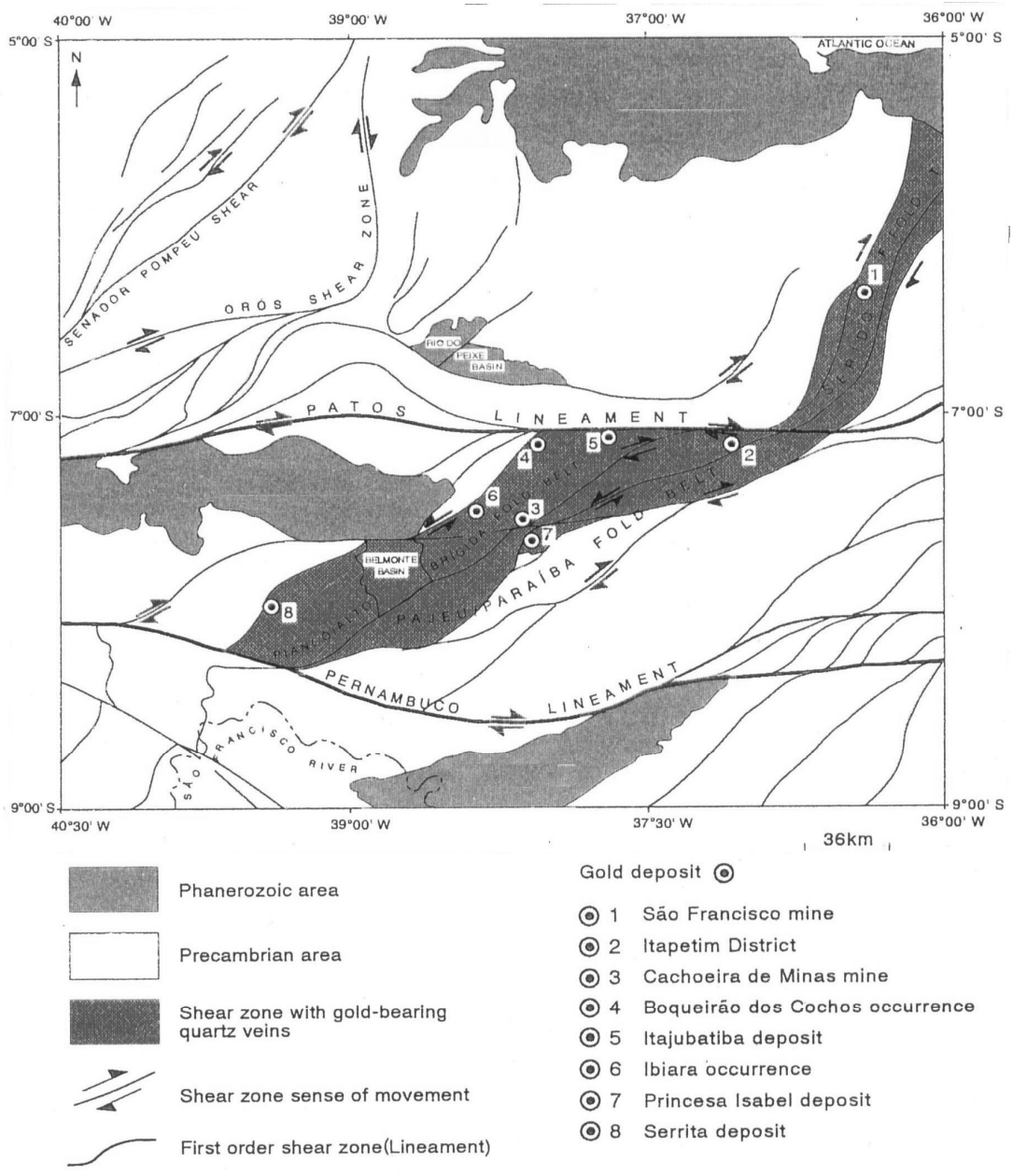


Figure 1 – Detail of the Borborema Province and main gold deposits (after Coutinho, 1994

garnet-amphibole-titanite-apatite in the exoskarn (located in the tonalite and syenogranite). Ore minerals in the early stage consist of magnetite and in the late stage of pyrrhotite, pyrite, chalcopyrite, arsenopyrite, and gold. Temperatures of prograde and retrograde alteration are constrained between 500° and 800°C and 400° to 500°C, respectively. Tungsten concentrations of <20 ppm, molybdenum of about 104 ppm, W/Mo ratio of >5 and Au content of an average of 0.5 to 2.0, locally up to 6.3 ppm are reported by Neto *et al*. (1999).

## 4 EXPLORATION MODEL

The exploration model developed for the orogenic gold types is based on the observation that gold mineralization is epigenetic, structurally controlled with ductile-brittle shear zones that host quartz reefs and contains semi-concentric hydrothermal alteration zones that consists of medium- and high-temperature hydrothermal alteration minerals. The gold-skarn type mineralization is also structurally controlled, hosted in meta-limestone, meta-amphibolite and granitoids and contains characteristic high-temperature alteration minerals. The following exploration strategy is employed:

(1) Detailed structural and alteration mapping to identify the primary structural brittle-ductile shear zone geometry, including the

movement sense, dip of the shear zone plane, plunge of lineations and fold axes that may exert a geometric control of ore bodies. Hydrothermal alteration mineral identification and mapping to characterize the width and length of the hydrothermal footprint, thus constrain the extent of the initial drilling program.

(2) ASTER interpretation and selected soil sampling to identify regional hydrothermal alteration zones and (concealed) mineralized areas, respectively. Pathfinder elements such as Cu, Pb, W, and Bi are used to further identify vectors towards gold mineralization.

(3) Airborne- and ground-based magnetic surveys to identify structural elements of the shear zone that are not exposed, *e.g*., the tension direction in the brittle Riedel model.

(4) GIS is employed for all data-sets and throughout all phases of exploration in order to: (a) highlight anomalies in individual data-sets, and (b) identify through overlay of the different anomalies, targets that may be tested via RAB or RC drilling.

(5) Using all datasets a structural, alteration, and mineralization model is developed that allows the prediction of targets that are subsequently tested by RC and Diamond drilling.

## 5 CONCLUSIONS

The Borborema Province contains several gold mineralization types including orogenic gold and gold-skarn that are structurally controlled and epigenetic in nature. Orogenic gold type mineralization displays a significant variation with mesozonal reef, granite-hosted, and thin-skinned thrust-related styles, and hypozonal shear zone style. The structural model of a brittle-ductile to ductile shear zone geometry for the gold mineralization types can be conceptually applied at the regional- (100 km), deposit-, and ore shoot-scale.

## ACKNOWLEDGEMENTS

Geologists at Crusader do Brasil Mineração Ltda. are thanked for their support.

## REFERENCES

Coutinho MG (1994) The geology of shear-zone hosted gold deposits in northeast Brazil. *PhD thesis, Royal Holloway and Bedford New College, University of London*, pp 359

Neto SJA (1995) Geologic studies at the Itajubatiba gold mineralization (PB): tectono-metamorphic evolution, metasomatism and fluid characterization (in Portuguese). *MSc Dissertation, São Paulo State University (UNESP), Brazil,* pp 188

Neto SJA, Sonnet P, Legrand JM, Melo jun G (1999) Bonfim and Itajubatiba gold deposits, NE Brazil: C and O isotope evidence for skarn origin. In: Stanley CJ (ed) *Mineral deposits: processes to processing*. Balkema, p 1439-1442

Neves BB, Santos EJ, van Schmus WR (2000) Tectonic history of the Borborema Province, Northeastern Brazil. In: *Tectonic evolution of South America,* p 151-182

Vauchez A, Neves S, Caby R, Corsini M, Egydio-Silva M, Arthaud M, Amaro V (1995) The Borborema shear zone system, northeast Brazil. *Journal of South American Earth Sciences* 8:247-266

Weinberg RF, Sial AN, Mariano G (2004) Close spatial relationship between plutons and shear zones. *Geology* 32: 377-380

# RESOURCE ESTIMATION - CLASSIFICATION SYSTEMS

EDITED BY:

JOHN CLIFFORD

GORDON RIDDLER

# The importance of correct sampling and assaying practices in resource evaluation: case studies from selected gold projects

S.C. Dominy
*Snowden Mining Industry Consultants Ltd, Weybridge, England and University of Ballarat, Victoria, Australia*

ABSTRACT: Poorly designed sampling and assaying protocols can result in high resource risk by artificially increasing grade variability (*i.e.* the nugget effect). Sample collection, preparation and assay protocols that suit the orebody, together with QA/QC systems, will reduce these errors. All current reporting codes (*e.g.* JORC, PERC, etc) require the Competent Person (CP) to consider the quality and implication of sampling and assaying programmes. Where these are deemed to be deficient, the CP must act accordingly, and consider this uncertainty in his/her resource classification. High sampling errors beget higher resource uncertainty; despite this fact, sampling is often deemed a second class citizen and does not receive the attention it deserves.

KEYWORDS: gold sampling; sampling errors; economic impact; resource uncertainty

## 1 INTRODUCTION

Sampling is a critical component in all stages of a mining project, from exploration to exploitation. It includes the sampling of material in-situ and broken rock. In all cases, the aim is to gain a representative sample to accurately describe the material in question. Field sample collection is followed by sample reduction in both mass and fragment size to provide an assay charge. This process is challenging in the gold environment, and particularly when coarse gold is present (Gy 1982; Dominy *et al*. 2000; Dominy & Petersen 2005).

## 2 SAMPLING ERRORS

### 2.1 *Introduction*

Five principal sampling errors are recognized (Gy 1982): Fundamental Sampling Error; Grouping and Segregation Error; Materialization Error; Preparation Error and Analytical Error.

### 2.2 *Fundamental Sampling Error (FSE)*

The FSE is the smallest residual error that can be achieved even after 'homogenization' of a sample lot. Effectively it can never be removed. When FSE is not optimized for each sampling and sub-sampling stage, it often becomes a major component of the sampling nugget variance. Experience shows that nugget effect is often artificially high because sample protocols are not optimized (Dominy 2004).

The FSE can be recognized as a type of loss function during sampling. Put simply, the higher the FSE, the greater uncertainty due to misclassification of ore and waste, and hence the greater the potential for financial loss.

### 2.3 *Grouping and Segregation Error (GSE)*

The GSE is an error related to the grouping of the fragments by increments in the lot to be sampled. Once a sample is broken, there will then be segregation of particles. This could be fines within a coarse stockpile, or coarse gold grains within an assay pulp. The GSE can be reduced by taking smaller sample increments, and by attempting to homogenize samples. The latter is extremely difficult, if not impossible for gold deposits.

### 2.4 *Materialization Error (ME)*

The ME comprises the Delimitation (DE) and Extraction (EE) Errors, which are introduced during sample selection/collection. DE refers to the need for proper delimitation of a sample; for example, an even channel sample or the full width of a moving belt. EE is related to the need for all particles within the delimited zone to be removed. For example, collection of

a sample from a core with good recovery (*e.g.* 90% or more: Annels & Dominy 2003).

The ME's are directly related to the actions of the sampler and/or sampling equipment, and can be controlled by good sampling practice and properly designed and maintained equipment.

### 2.5 *Preparation Error (PE)*

The PE refers to issues during sample preparation such as contamination, dust losses, unintentional human error, and sabotage. Clean and efficient laboratories can minimize such errors, as well as a strong emphasis on QA/QC.

### 2.6 *Analytical Error (AE)*

The AE reflects errors during the analysis process, such as calibration errors, machine drift and human error. Good procedures and well trained staff usually minimize AE.

## 3 CASE STUDIES

### 3.1 *Introduction*

A series of cases studies follow that document some of the sampling issues that can be found in the gold industry. Each case study is reported anonymously, and in the context of the sampling errors. The issues presented should not be considered to be exhaustive.

### 3.2 *Case Study 1: Core Quality Issues*

A shear-zone style deposit located in the FSU was characterized by high-grade gold-quartz-sulphide veins up to 0.3m in width. The global deposit grade was reported as 5.7 g/t Au. There was little coarse gold present, though the deposit was nuggety due to the pod-like nature of the sulphide mineralization within the veins. The resource had been diamond drilled on a relatively fine grid and had limited underground development in it. The original Russian estimate contained C1, C2 and 'P' resources (Russian Reporting Code). A more recent estimate defined Measured, Indicated and Inferred Mineral Resources (JORC).

During an audit, it was found that there was poor documentation with regard to QA/QC and that the (total) core recovery was generally between 44% and 71% with a mean of 61%. The present owner had drilled a number of confirmatory diamond holes, whose recovery was still poor between 65% and 83%.

The low recoveries indicated that there was a large amount of core (sample) loss, and that the actual sample collection process was prone to a high EE. Checks made on limited remaining core showed that loss was related to the sheared and altered nature of much of the mineralization. The remaining half core was highly fragmented and friable, testifying to the difficulty in cutting the original sample.

This was clearly of concern to the group undertaking the audit and as a result, the Measured blocks were reallocated to the Indicated and Inferred categories, and the Indicated Resources to the Inferred category.

As a result of the resource downgrade, the company concerned was unable to raise the finance required for project development. They had to find additional funds for diamond drilling to confirm their expectations of the deposit. The impact on the project was related to loss of confidence and delaying the development

### 3.3 *Case Study 2: Compositing Problems*

A 1m to 4m wide structurally complex gold vein in North America was evaluated using diamond drilling. All drill cores were logged and 1m lengths submitted for fire assay.

A subsequent resource estimate yielded a diluted global resource of 5 g/t Au. This figure was disappointing to the operator, who was expecting a figure closer to 10-15 g/t Au to support a medium-sized underground operation. The project was put on hold.

A later independent review found, that in the drive to collect 1m core samples, any core on the footwall of the vein that was less than 0.5m was sampled, bagged, and subsequently discarded and not sent for assay. Geological studies reveled that the footwall of the structure contained a discrete high-grade vein bearing visible-gold. This entire mineralization had been virtually excluded from the estimate with a loss of approximately 55% of the gold inventory. The project staff had apparently been told by a consultant, that 1m supports were critical - they had taken this quite literally. The remaining footwall mineralized core was collected and assayed by screen fire assay and the resource re-estimated. The new diluted global grade was 12.8 g/t Au, much closer to expectation.

This example shows the clear need for proper training of staff and for good communication between all parties. A plan was required to ensure that all sample composites were close to, but not exactly 1 m. Though this perceived need was rather dependent upon the choice of estimation method (*i.e.* 2D vs. 3D). The issue

of compositing is often ignored during sampling programme design.

### 3.4 *Case Study 3: What Coarse Gold?*

An Australian greenstone-hosted narrow vein deposit was found to have a coarse gold problem. The vein had a mean width of 2.2m, with a global resource grade of about 10 g/t Au.

Checks of diamond core and RC field and laboratory duplicates indicated a very high variability. The issue had been ignored as there was apparently no indication of visible gold within drill core.

An initial review of metallurgical data indicated that a gravity recoverable gold yield of 55% was achievable. A number of samples were taken from high-grade core intersections (>30 g/t Au), sectioned, and inspected under a transmitted light microscope. This revealed the presence of gold particles up to 1,000 μm in size, with most in the 7μm to 300μm range.

A series of fifty quarter-core samples were taken for 1 kg screen fire assay (75μm screen) and it was found that between 15% and 65% of the gold in the samples reported to the screen (mean 30%). A comparison was made between the new screen fire assay grades and the original 30 g fire assays, and it was found that the new screen fire assays overstated the original fire assays by up to 35%.

A number of key drill holes were re-logged, and it was found that visible gold was common.

In this case, despite the QA/QC duplicate data indicating a problem, the issue was ignored. The sampling protocol used was inappropriate in a coarse gold environment, and in fact led to an overall underestimation of gold grade. The pulps were prone to a high GSE. The timely identification of visible gold in core should have been achieved and acted upon.

### 3.5 *Case Study 4: Gold Segregation in Pulps*

An underground vein operation in North America was known to contain coarse gold particles up to 1,200μm in size. The vein had an average width of 2.5m and a historical production grade of 26 g/t Au. From drill core or underground chip samples a 1 kg sample was pulverized and a 30 g sub-sample taken for fire assay.

The mine had been operating for a number of years, and no sampling or laboratory QA/QC systems existed. With new owners, new systems were introduced to the pre-existing laboratory. It was shown that the pulp duplicates had a poor precision; where 90% of the data was ±70% (using Half Absolute Relative Difference) or worse.

A number of exhaustive tests were undertaken on 1 kg pulp lots, where the pile was mixed, flattened and 40 consecutive 50 g subsamples taken for fire assay. The variability was very high, and in one instance the range between the minimum and maximum values was almost 500 g/t Au.

These findings confirmed that the pulps were exceptionally heterogeneous due to the poor comminution of gold particles during pulverization. In addition, the level of GSE within the pulps was excessive. This problem was exacerbated by the two laboratory technicians who each treated the pulp sub-sampling in a different way. One homogenized the pulp by 'matting', and then simply scooped off 30 g from the top of the pile, thereby missing gold that had segregated to the bottom of the pile. The other placed the pulp on the mat, gave a shake, flattened the pile and cut a series of sample lines through the pile with a greater chance of picking up segregated gold at the pile base.

In short, one technician was understating and the other overstating the gold grade. The recent mine records were revisited and it was found that during a prolonged leave of absence by the 'overstating' technician, a number of stopes had been abandoned due to unexpected low grades. These blocks were re-sampled and assayed using a new protocol, and found to be in ore grade. They were subsequently mined out and recovered nearly 20,000 ozs Au.

A screen fire assay protocol was introduced. The key learning here is that coarse gold needs to be treated differently, pulps cannot be homogenized, GSE can be problematic, and that proper protocols and procedures must be set up. This is a clear example of the potential for misclassification and financial loss.

### 3.6 *Case Study 5: Grab Sampling*

Dump sampling was used as tool to define ore and waste in a shear-zone hosted underground gold operation in Australia. The operation consistently had reconciliation problems, with a general undercall with respect to the resource grade of between 20% and 30%.

Each stock pile represented about 500 t of stoped rock. Twenty 3 kg samples were taken from around the edge of the stockpile, at a

fragment size of generally no greater than 12 cm. Each sample was sent to the laboratory for a 500 g LeachWELL bottle-roll.

An exhaustive test taking two hundred 3kg grab samples was undertaken to check grade variability. Out of two hundred samples, the lowest grade combination of twenty samples was 0.2 g/t Au, and the highest grade combination 38.9 g/t Au.

Given two hundred grab samples in the test study, there are a number of permutations possible if exhaustive 20-set sample batches are drawn. A test run was undertaken where one thousand random sets of twenty samples were taken. In this case, the lowest and highest grade lots were 0.4 g/t Au and 49.6 g/t Au. Some 60% of the grades were below cut-off, implying a 60% chance of the stockpile being misclassified as waste based on grab samples.

Additional studies also indicated that the ore contained quantities of coarse gold. The existing laboratory protocol also had a high potential for GSE in the pulps.

This study showed that the use of grab samples to assess grade is highly problematic. The majority of stockpiles were set to the mill as ore, though this did not reflect the reality of negative reconciliation with respect to grade.

The sensitivity study did not reveal that each grab sample or group of twenty grab samples did not represent the actual stockpile. Grab sampling is prone to chronic FSE, GSE, DE and EE. Gy calculations indicated that a 25 t sample was required – clearly impractical. More time should have been spent on geology, resource drilling and resource modeling.

## 4 DISCUSSION & CONCLUSION

Incorrect sampling generates losses that do not always appear obvious. As professionals we are often preoccupied with the effects and not the aetiology of problems.

In the case studies presented, issues relating to the following have been discussed:

- use of grab samples resulting in misclassification (FSE, GSE, EE & DE);
- poor core quality leading to poor sample quality and higher resource risk (EE & FSE);
- bad laboratory practice leading to misclassification (GSE, EE & DE);
- non-recognition of the presence of coarse gold and higher resource uncertainty (FSE & GSE); and
- use of inappropriate assay methods (AE).

Throughout a sampling and assaying programme, QA/QC protocols should be a primary feature. Protocols must be set up to cover field collection, laboratory preparation and analysis which are based on the actual nature of the ore and not so-called 'industry standard practice'.

Within the gold mining industry there are still many issues not recognized or not addressed, which lead to uninformed decisions during resource estimation and classification.

## REFERENCES


Annels AE, Dominy SC (2005) Core recovery and quality: important factors in mineral resource estimation. *Trans Inst Min Metall* 112: B305-B312.

Dominy SC, Johansen GF, Annels AE, Cuffley, BW (2000) General considerations of sampling and assaying in a coarse gold environment. *Trans Inst Min Metall* 109: B145-B167.

Dominy SC (2004) Fundamental sampling error and its relationship to the nugget effect in gold deposits. In: *Proceedings of the Mining and Resource Geology Symposium 2004*. EGRU Contribution No 62, 30-45 (James Cook University, Townsville)

Dominy SC, Petersen JS (2005) Sampling coarse gold-bearing mineralisation - developing effective protocols and a case study from Southern Greenland. In: *Proceedings of the Second World Conference on Sampling and Blending 2005*. Australasian Institute of Mining & Metallurgy: Melbourne, 151-165.

Gy PM (1982) *Sampling of Particulate Materials - Theory and Practice*. Elsevier, Amsterdam. pp431.

# Resource Estimation of Witwatersrand Rock Dumps

M.W. Grodner
*TWP Consulting(PTY), LTD, Johannesburg, South Africa*

ABSTRACT: The early mining of the Witwatersrand gold fields in South Africa was focused on very high grade ore. Much of this ore was accessed via on-reef drives. This material was dumped as development waste, along with ore from slightly lower grade areas and true waste material on rock dumps. Many of these historical "waste" rock dumps thus contain significant amounts of gold. This paper demonstrates that even though it is likely that a given dump will contain gold, it is not possible to calculate an accurate resource estimate, even with extensive sampling. Issues with regards these estimates and the potential risks and rewards are scrutinized. These risk evaluations are not only important for the owner, but also for potential buyers and investors. It is emphasised that in areas where accurate mining and dumping records exist, the ability to determine a resource estimate is more likely.

KEYWORDS: Witwatersrand gold, rock dumps, resource estimation

## 1 INTRODUCTION

Material mined during different economic circumstances may be stockpiled or dumped as waste rather than being processed for the minerals present there-in. At a later stage it may become viable to process this. To determine the profitability, the quantity and the quality of material in the dump must be determined. This includes tonnage, particle size & type distribution, mineralisation style and grade characteristics. This information could be used to determine the value of the material on a dump.

Of recent, accurate records of strategic stockpiles and rock dump material that has been mined but not processed has been collected. However, the older dumps such as the ones examined in this paper, have little or no historical information. This is investigated, using an example of rock dumps of the old Witwatersrand gold mines.

In this example, an evaluation of the dump cannot occur by using mining and dumping records to develop a grade distribution model of the dump. Issues with regards the estimates of the historical rock dumps and conclusions are scrutinized. From this the potential of exploiting these dumps is defined. These risk evaluations are not only important for the owner, but also for potential buyers and investors.

## 2 BACKGROUND

Mining has occurred in the Witwatersrand goldfields for over 120 years (Pretorius, 1986). Much of the earlier mining was from surface outcrops or with shallow vertical shafts. From these points, irregular and scattered on-reef drives following the strike of the reef and narrower stopes were developed. These not only generated significant amounts of gold, but also dumped a large amount of "waste" material on surface. This material was often created during the development of on-reef declines and strike drives and hence also contains reef. The dumps also contain material from slightly lower grade areas, which was not considered worthwhile processing. There is thus a large amount of gold in the old dumps which could be economically exploitable. Before an accurate estimate of the value of this can be made, the

quality and quantity of auriferous material must be determined. This process and results based on a case study are presented below. In this study the validity of a gold "resource" was investigated for potential investors.

## 3 ESTIMATION OF VOLUMES AND TONNAGES

The owners calculated dump volumes from detailed surveying. A conversion factor of a bulk density of 1.65 was been used to determine the tonnage from this volume, which has been shown to be a suitable estimate for Witwatersrand rock dumps. A significant uncertainty is the topography of the surface underneath the dump. To accurately determine the tonnage, the dump floor topography must be known. The total quoted dump tonnage was 8.66 million tonnes, where-as a total tonnage of 7.46 million tonnes was calculated from the available data. The calculated tonnages included additional tonnes as a result of extraction of 2 m of the soil beneath the dump - there is a potential that gold has percolated down through the dump into the soil. Even if these additional tons are included, it was found that there was still a shortfall of 1 million tonnes. In addition some 5.48 million tonnes were listed by the owner for other dumps, but this data could not be verified.

## 4 ESTIMATION OF ROCK TYPE DISTRIBUTION

The main source of material on the dumps is from on-reef declines and strike drives with a shale footwall and quartzite hangingwall. The reef is only about 10 to 20 cm thick and the on-reef development required a wider (180 cm) height, hence mining of especially the footwall was necessary.

If one considers the mining height, then conservatively 80 to 90% of the dump should consist of the quartzite and shale. Off-reef mining can reduce the amount of ore to less than 10%. On the dumps the light grey quartzite and the carbonaceous shale are common. Conversely it is very difficult to find pieces of reef despite its easily recognisable rust-colour due to the oxidation of the pyrite. The relative abundances of the different rock types are different at different sites and size fractions. The owners undertook an extensive exercise in an attempt to alleviate the problems of size distribution and the grades of the different fragment sizes. Large bulk-samples were taken to determine the composition of the fragment size distribution. The contribution of each rock type to each of these size fragments was measured.

But these samples only represent a portion of a single time-slice of the dump, both in terms of mining and historical dumping. As there is no geological or historical model of the dump there is no justifiable confidence in the representativeness of the samples in terms of fragment size distribution and the percentage of different rock size per fragment size.

## 5 ESTIMATION OF GOLD GRADE

Development occurs in both high and low grade areas, with the stopes being selectively mined. The historically quoted shaft head-grades are thus likely to be a lot higher than those that would have been dumped. This precludes the use of historical information. The problems associated with fragment size and rock type distributions are also applicable to the grade estimation.

## 6 SAMPLING ISSUES

The uncertainties, listed above need to be quantified. The heterogeneity of rock (shale, quartzite or reef) in each sample is defined as:

$$C_l = N_f \sum \frac{(a_i - a_L)^2}{a_L^2} * \frac{M_i}{M_L^2}$$

$C_l$ = heterogeneity
$N_f$ = no. rock fragments
$a_i$ = weight of rock$_{(i)}$in sample
$a_L$ = weight of rock$_{(i)}$ in dump
$M_i$ = weight of ave. rock $_{(i)}$ in sample
$M_L$ = weight of ave. rock $_{(i)}$ in dump

The rock types that contributed to the dumps during mining, the distribution of the various rock underground and the different dumping of material in space and time are unknown. Hence heterogeneity cannot be determined. Rock-types have different strengths and will thus break into different size fractions, resulting in an uncertainty of the fragment size distribution of the rock. The different size fragments would be segregated through the different dumps at different rates.

These factors are necessary to define the different portions of the dump. For each unique portion of the dump, with respect to the mineralization, the fundamental sampling error (S) is a product of the fragment shape, fragment size, the mineralogical factor, the liberation factor and the size of the coarse fragments. The relationship is:

$$S_{FE}^2 = \sum_1^n IH_L$$

$IH_L$ (taking into account $C_l$) is the heterogeneity uncertainty in the representativeness of the sample and is dependant on fragment shape error (f), fragment size errors (g), liberation factor (l) and size of the coarse fragments. The only factor that can be defined is the fragment shape error ($f_{quartz}$ = 0.47). There are differences in the fragment sizes (g) on the different dumps. The fragment size distribution measured during site visits is only applicable to that unique portion of that specific dump. Even this data shows that the fragment size distribution is non-linear.

Liberation factor (l) is one of the most complex issues, being dependant on rock type contribution and distribution, rock fragment size distribution (with associated amount of oxidation), the original distribution of the grade in the orebody, the redistribution of the rock within the dump through dumping in different places at different times and finally the differential movement of fines, which are described as being gold-rich through different parts of the dump. The only way to solve such a complex, multi-parametric problem is to reduce the uncertainties of the various constituents by defining their characteristics through sampling. Unfortunately, as shown above the sampling of dumps are very difficult and the uncertainties are high. As such, the characteristics of the material that is present when the estimation exercise is undertaken are poorly defined. The potential problems can be broken into:

1) Fundamental error (S);
2) Nugget effect errors;
3) Grouping & segregation errors;
4) Delimitation error;
5) Analytical error and
6) Extraction error.

The aspects of the fundamental error are described in detail above. Points 2 and 3 are also partially covered by the discussion, but still remain an issue. A mineralogical and liberation factor for gold in the Witwatersrand can be determined as it occurs as native Au. Problems exist with the estimation of the shape, size and volume of each fragment. The nugget effect occurs both on a large scale (reef versus waste rock) and a small scale (mineralised versus un-mineralised portion of reef). A similar type of problem exists with the segregation error, as during different parts of the dump's existence, various rock-types would have been grouped together contributing to the delimitation errors. Over- or under-representation of the portions of the dump (for example grade variation between fines and large fragments) will produce sample errors. As the impact of the various errors is cumulative, the result will be an un-representative sample. Therefore, the statistical characteristics of the dumps cannot be determined. The only reasonable measurement of gold grade is to examine it after it has been processed. Not only is this reactive in terms of dump mining and processing, but possible sampling and errors also exist at this stage.

A mineral resource may be defined as the results which would have a reasonable and realistic prospect for eventual economic extraction (SAMREC, 2006). It has been claimed that the dumps may present such a "resource". An inferred mineral resource is that part of the resource for which the tonnage, grade and mineral content can be estimated to a low level of confidence. This confidence is derived from geological evidence or sampling (SAMREC, 2006). In the present situation, no geological modeling is possible. As shown above, the sampling of these dumps cannot be assumed to indicate any grade-continuity. The dump material may not be reported as resources, let alone a reserve.

## 7 CONCLUSIONS

If no record of the dump "growth" is available, it has been implied that statistical evaluation will be able to determine the worth of a dump. In the case presented, the owners have suggested that over 10 tonnes of gold could be recovered from the dumps. To confirm this, the sampling and measurement methods used to determine the volume, the rock-type, fragment size distribution and the gold content of were examined. The validity of the sampling methods to determine these

aspects is shown to be in-adequate. No reasonable estimate based on sampling can be made of the "resource". Any sample only defines a small unique part of such a dump and is dependant on factors from original variability of the rock, the uncertainty of dumping in space and time to fragment size distribution. As such no representative sample can be taken. The heterogeneity of the potential gold grades in each rock type in each sample increases the variance of the fundamental sample error to levels beyond which the sample can be considered representative.

Sampling cannot define the grades and distribution of such historical dumps. This makes the level of risk un-definable.

This is in contrast to rock dumps and stockpiles (strategic dumps of material to ensure that processing remains within specified parameters) that have the records of the grade, location and volume of the material in the dump. When this occurs, it is possible to build up a model of the ore distribution, much like a geological model. The statistical characteristics of the original material can be combined to determine the characteristics of such a dump. This information can be then used to account for this material in the NPV of the mine.

## ACKNOWLEDGEMENTS

TWP Consulting is thanked for permission to present this work. Basic information is derived from the study of an anonymous rock dump owner. Much of the sampling theory was presented by F. Pitard at a course at the University of the Witwatersrand.

## REFERENCES

Pretorius, DA (1986) The goldfields of the Witwatersrand Basin. *In Mineral Deposits of Southern Africa,* 489-493.

SAMREC (2006) *South African Code for the reporting of exploration results, mineral resources and mineral reserves.* Prepared under the joint auspices of the SAIMM and the GSSA.

# Quality and grade parameters in aggregate resource and reserve definition

C.A. Jeffrey
*Department of Geology, University of Leicester, LE1 7RH*

ABSTRACT: Unlike metal deposits the concept of grade and quality are not well defined for construction materials sources despite these representing over half of all the mineral products worked and sold worldwide. Evaluation of deposits for construction material production requires an assessment of the deposits ability to supply a range of products defined mainly by their mechanical properties and particle size distributions. A number of grade parameters are suggested that allow quantification of sand and gravel quality based on their ability to meet individual product specifications. Combined with hypothetical yield calculations for target products these provide a description of deposit quality analogous to terms used elsewhere in the mining industry. Hard rock aggregates can be described in grade terms using the most important mechanical property for a given application and the proportion of the rock mass capable of being processed into that product. Introduction of the international reporting code and review of the guidance on aggregate reserve definitions present an opportunity to develop these ideas.

KEYWORDS: Reserve definition, aggregates, quality, grade, Reporting Code

## 1 INTRODUCTION

Aggregates deposits, encompassing both crushed rock and sand & gravel account for around 50% of the mineral matter extracted worldwide. This ranges from local and artisanal scale to international companies. In the UK, Europe, USA and parts of S. America the trend is towards internationalization and consolidation of production into fewer larger companies. In the UK four out of five of the largest companies are know headquartered outside of the UK.

The companies are multinational, integrated and also involve other activities including cement manufacture, metalliferous and industrial mineral mining. The companies shares are traded on a number of different stock exchanges and attract a wide range of international and institutional investors. It is therefore interesting to note that within the current reporting codes for aggregates there is little or no definition of what constitutes good or high quality aggregate reserves, and there is no real attempt at a definition of what might be the 'grade' of an aggregate deposit (Institution of Materials, Minerals & Mining Working Group 2001). These concepts are widely understood in metalliferous and industrial minerals operations but investors currently have few ways to compare the quality of the aggregate resource / reserve base in different companies. It is also a potential legal issue in that many local authorities in the UK have cited assumption against mineral working in certain areas unless they are 'high quality' deposits. There is however no objective measure or definition of this and opinion is the best that can be offered.

The introduction of international reporting codes and potential revision of the current wording on aggregate reserve definition provides an opportunity to consider whether additional guidance or further underpinning information may be applied to this issue. There are clear parallels and differences between the practice in the metal mining and other mineral sectors which can be examined. A number of crucial differences however exist between aggregates and many other minerals particularly the very local nature of the market into which most are sold, the pre-existing particle size distributions in sand and gravels that largely con-

trol their potential to economically make a specific graded product and the low unit value of the products.

## 2 GRADE AND QUALITY CONCEPTS

Estimating the quantity of reserves for aggregate deposits is generally achieved within acceptable limits using standard methods of drilling & trenching and incorporating the results in computerised volumetric calculations (Wardrop 1999). The assessment of quality or grade is however less easily described.

Quality in crushed rock deposits is usually demonstrated by mechanical and associated test results and how these meet industry or customer specifications. This is not the same as saleability which also reflects local competition and market demand. 'Grade' in other mining sectors usually indicates the proportion of economically interesting components in the in-situ material but may also be expressed in a qualified form to account for mining and processing recovery. For crushed rock aggregates most of the rock mass can generally be rendered saleable and the grade should really reflect the minor proportion that is largely unsaleable as fines, combined with an indication of product split. The gradings of the crushed materials can be adjusted by the processing to address different markets within the constraints of its physical property suitability.

This approach is particularly important where low and high value products are co-produced. The grade will be important in high value products such as high PSV gritstones used for road surfacing where the proportion of such material recovered from the deposit frequently only represents 30-50% of the deposits. The remainder is either waste or low grade fill products.

Grade and quality in the context of naturally particulate materials such as sand & gravels is significantly more complex. Here again the description as high quality materials reflect their physical performance in a range of product specific tests but grade is more hard to define. Grade could be the recoverable component i.e. the sand & gravel fractions excluding the fine silt and clay that would be discarded during washing or oversize that is not to be crushed and re-incorporated. A good deposit would therefore be 'clean' but must also be capable of supplying material that meets relevant specification requirements (Smith & Collis 1993). In this context the best materials are those that with typical processing can produce as close a match as possible to that required by a particular specification or market requirement.

Assuming that a sand contains at least some proportion on all of the sieves used in grading analysis it could theoretically be processed to any grading, the only difference being the amount of the deposit consumed to make a tonne of product. The yield figure for a given product and the closeness of the processed grading to an ideal in-specification grading are therefore the main contenders for a grade measurement. Gravels are generally screened to single size products so their grade is basically the same as the overall gravel component.

## 3 GRADE PARAMETERS FOR SANDS

A series of parameters have been developed that assess the 'closeness of fit' of the processed sand grading to the centerline of a specification envelope. These are a development of the regional scale assessment method described by Laxton (1992). These reflect the sum of the positive or negative difference in abundance on each sieve between the sample and the ideal specification centre line or a particular customers specification. The value is termed the 'Centre line Proximity Factor'. Since the positive and negative divergencies can cancel out, a sand grading that significantly crosses the centre line can return a low value implying a close match the value is also calculated as an absolute value. The center line is used as the target as this represents the grading where the maximum variation can occur due to deposit variability or processing problems without the sand falling out of specification. Other target lines reflecting material performance or contract conditions can also be used. Other factors have also been developed for quality mapping and contouring around the deposit but these are not values to be used in a reserve context.

A spreadsheet based approach (CACTUS) has also been developed to assess the 'theoretical yield' of a grading in making a particular target specification. This assumes that if the sand were split into individual sizes and then recombined to the new target grading one of the size fractions would eventually become exhausted. The proportion of the material used before this point reflects the yield of the product. This is of course not how most sands are processed. The sands are processed to give

multiple gradings with individual sizes fractions shared amongst the two (or more products). Such an approach is difficult to model and presents no opportunity for independent scrutiny of the results. The approach suggested is repeatable by external practitioners, does reflect the ease of making the primary product, and is capable of giving yields for a range of different target products. This is vital as local markets may only accept certain gradings for which the yield from the deposit is low. This deposit is clearly of 'lower grade' than one which can supply this grading with ease. A fine grained sand deposit might for example be expected to be simultaneously a low grade concreting sand source but a high grade asphalt sand.

It is therefore proposed that to define the grade of a sand and gravel site the theoretical yield and closeness of fit to a specification centerline or other appropriate target grading be cited.

## 4 CONCLUSIONS

The concept of 'grade' for aggregates is complex and inextricably linked to saleability in a local market. The intrinsic quality parameters of the deposit and a 'grade', may however be described by the use of hypothetical yield calculations, 'closeness of fit' factors to individual specifications and mechanical or other appropriate test results. These clearly are not perfect methods but are a first attempt at establishing some guidance that could inform the process of quoting aggregate reserve quality under reporting codes or in legal settings.

## ACKNOWLEDGEMENTS

I would like to thank Gordon Riddler for his interest and encouragement in this area over many years, Eddie Bailey for his keen industrial perspective and the MIRO MIST scheme for funding that allowed the initial consideration of these ideas.

## REFERENCES

European Committee for Standardisation (2002) Aggregates for bituminous mixtures and surface treatments, BS EN 13043

Institution of Materials, Minerals & Mining (I.M.M.M) Working Group 2001. *Code for reporting of Mineral Exploration results, Mineral Resources and Mineral Reserves (The Reporting Code).*

Laxton J.L., 1992. A particle-size classification of sand and gravel deposits as a basis for end use assessment. *Engineering Geology*, 32, pp 29-37

Smith M.R. and Collis L. (Eds) 1993. Aggregates: Sand, gravel and crushed rock aggregates for construction purposes – *Geol. Soc. Eng. Geol. Spec. Publ.* 9, 2nd Ed. Geological Society, London. 339pp

Wardrop D. R. 1999. A study on the accuracy of sand and gravel reserve estimates. *Quarterly Journal of Engineering Geology,* 32, 81-86.

# The Study of Mineral Deposit Anatomy, an Essential Foundation for Deposit Evaluation and Exploration

W. A. Sheppard
*LiaMin Consulting, Dublin Ireland*

ABSTRACT: Based on empirical geological studies, Mineral Deposit Anatomy ('MDA') incorporates i) Preliminary Assessment, ii) Data Collection, iii) Analysis and Modelling and iv) Template Development. Case studies presented show that MDA can be applied to deposits of a wide range of styles within diverse geological environments. Such studies can impact substantially on i) exploration modelling and targeting, ii) priorities for evaluation drilling, iii) the degree of confidence in Resource modelling, iv) metallurgical data interpretation and v) mine planning.

KEYWORDS: Geology, Mineral Deposits, Base Metals, Gold

## 1 INTRODUCTION

Mineral Deposit Anatomy ('MDA') is the structured study of the nature and interrelationship of the diverse component parts of a mineral deposit. MDA aims to establish an objective framework for the integration of mineral deposit data to ensure optimum evaluation and exploration. This paper presents three differing case histories that illustrate the value of MDA in deposit exploration and evaluation.

## 2 STUDY STRATEGY

### 2.1 *Preliminary assessment*

The critical first phase of any MDA project is to i) review the state of current knowledge, iii) assess the range of data available and iii) undertake a reconnaissance review of the host rocks and mineralization. An open mind is essential at this stage. It is important to become aware of any shortcoming in the available database and of any important aspects of the deposit geology that may have been overlooked.

### 2.2 *Data Collection*

Even where previous data collection has been thorough, considerable independent data collection is necessary to i) become familiar with the deposit geology, ii) gain a clear understanding of previous nomenclature and procedures and iii) check the consistency of previous data collection. Mindful of the likely need for data integration into a number of software systems and the probable use of the data by numerous geoprofessionals, templates for drill core and outcrop data collection need to be i) within a readily available software package, ii) quantitative to semi-quantitative and iii) largely numerical in nature. During this stage in the MDA process, lithological coding tends to evolve as the full range of lithological variation becomes apparent.

### 2.3 *MDA Analysis and Modelling*

Cross-section, long-section and plan presentation and interpretation are initially undertaken prior to development of 3-D models. The fundamental aims of MDA Analysis are to establish i) the controls of deposit location, ii) the deposit geometry, iii) the component parts of the deposit and their spatial relationship and iv) geological factors that will influence exploration, evaluation and mine planning. Features likely to emerge from analysis include i) host rock correlation and structural non-sequences, ii) mineral and geochemical vectors and iii) classification of the types of mineralization that make up the deposit.

### 2.4 *Project Template Preparation*

Once the MDA model is established, ongoing data collection needs can be assessed and the logging and mapping templates refined. In

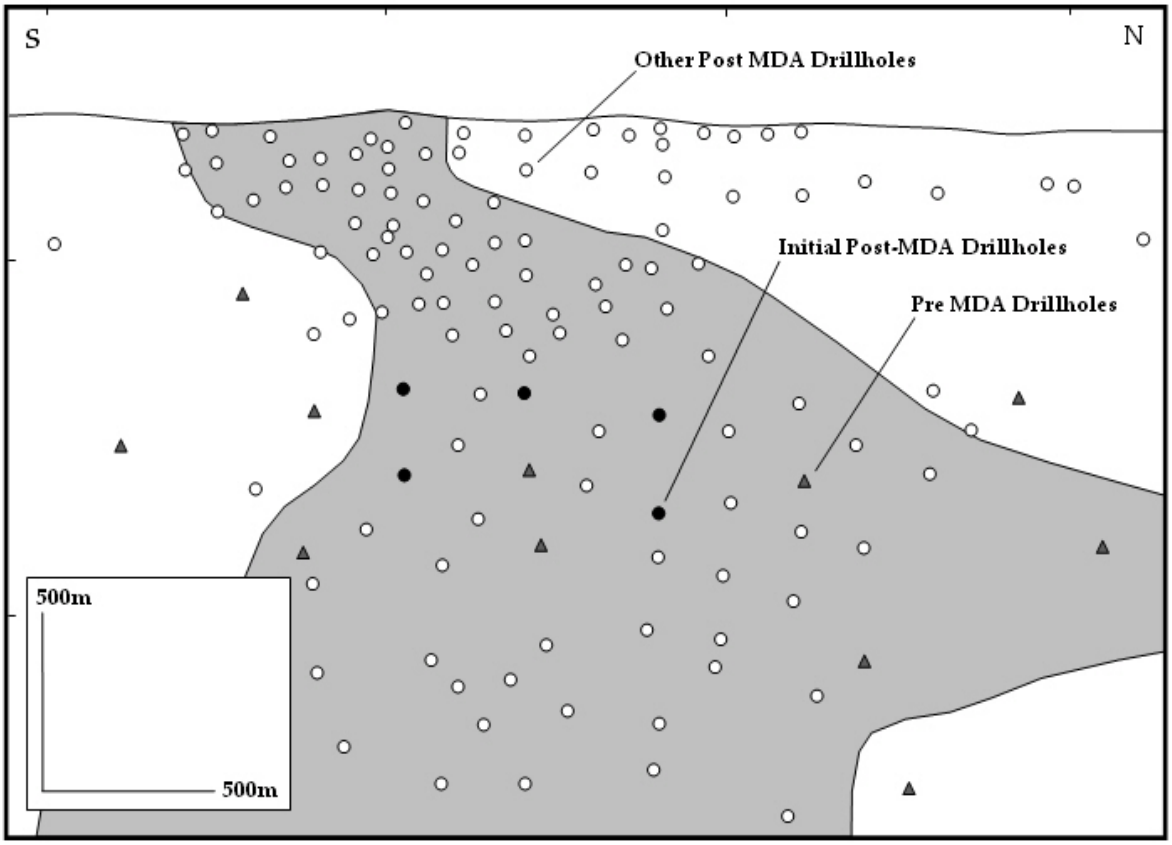


Fig.1 Long-Section of the Dugald River deposit showing the defined Resource area in grey

a major drill programme, it is vital that ongoing production logging is focused on essential data collection to ensure an appropriate balance between data collection and interpretation.

## 3 CASE HISTORIES

### 3.1 *Dugald River*

The Dugald River Zn-Pb deposit is located 90km northeast of Mount Isa in Western Queensland, Australia (Fig.1). Prior to MDA study, the deposit was described as a stratabound zinc-lead sulphide accumulation in graphitic black shale (Connor, *et al* 1990). Evaluation had included a 54 diamond drillhole programme that defined a low grade Resource of 60Mt at 10% Zn, 1% Pb and 30g/t Ag (Connor, *et al* 1982).

Preliminary assessment highlighted structural complexity within the deposit area and a wide range of sulphide textures within the deposit. During data collection particular attention was given to the definition and logging of these sulphide textures. Mapping revealed discontinuous folds of variable plunge, a vertical stretching direction and locally a cross-cutting relationship between the mineralized body and the host rocks. Long-section presentation and interpretation proved particularly informative during MDA analysis (Fig.1).

Much of the deposit consisted of planar to irregularly banded sphalerite-pyrite mineralization within shale, but it became clear that it was within sulphide breccias in the southern part of the deposit that the true potential of the Dugald River deposit lay. Given the presence of vertical stretching, a programme of down-dip drill testing was justified. Early results from follow up drilling were very positive. Drilling ultimately defined 38Mt at 13% Zn, 2.1% Pb and 42g/t Ag (Newbery *et. al.*, 1993), a very significant increase in grade.

### 3.2 *Lomero-Poyatos*

The Lomero-Poyatos polymetallic deposit (Fig.2) is an auriferous Volcanic Hosted Massive Sulphide ('VHMS') deposit located close to the northern boundary of the Iberian Pyrite Belt in the Andalucia Province in southwest Spain (Tornos, 2006). The deposit includes both massive and semi-massive sulphide mineralization. Much shearing is apparent in open-pit outcrop and in drill core. MDA study of the deposit was undertaken to develop a tec-

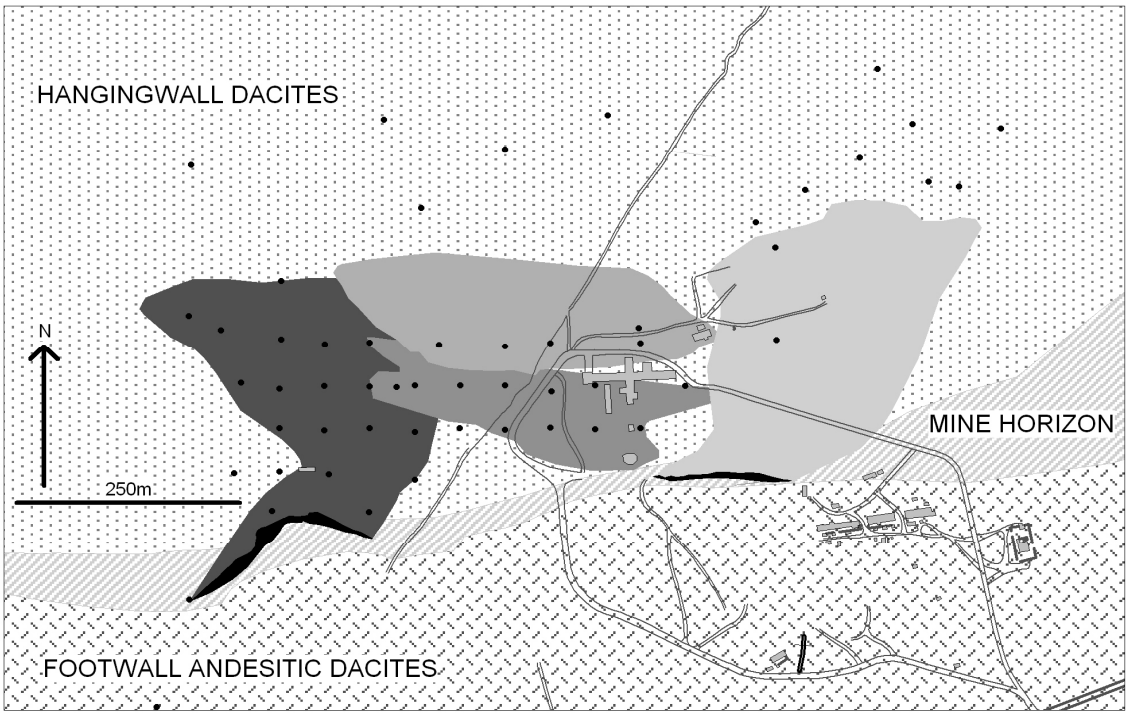


Fig.2 Plan of the Lomero-Poyatos area showing the en echelon massive sulphide bodies in shades of grey

tonostratigraphic framework for the deposit and clarify the deposit's geometry.

Data collection included 1:5,000 scale mapping, the relogging of nine available drillholes, the reinterpretation of geological plans of the old mine workings and ground magnetic surveying. Drill core logging used a 45 data-column template. Particular attention was given to volcanic textures with fragment and matrix characteristics logged independently.

MDA analysis established that the deposit consisted of four en echelon massive sulphide bodies underlain, and locally overlain, by semi-massive sulphide (Fig.2). The improved geometric understanding greatly increased the confidence with which the Resource was modelled.

Locally, conformable hangingwall and footwall contacts were observed between all lithological units. The sequence was largely right-way-up and lacked major repetitions. Two points of significance were noted. First, the immediate hangingwall sequence consisted of magnetitic mass flow deposits with auriferous clasts of massive sulphide. Second, the three hangingwall dacitic units progressively cut out eastwards. The middle dacite unit displayed a lateral and up-sequence transition from massive volcanic through hyaloclastic breccias to epiclastic units related to a domal volcanic centre. MDA study enhanced the prospectivity of Fixed Loop EM anomalies down dip of the deposit.

Ground magnetic data facilitated the correlation of the stratigraphic sequence away from the deposit. A clear association between volcanic centres and massive sulphide deposits was established. Syn-volcanic faulting was interpreted to control massive sulphide deposit and volcanic centre location.

### 3.3 *Passendro*

AXMIN Inc is currently evaluating a series of structurally controlled gold deposits at Passendro within the Bambari Greenstone Belt in the Central African Republic (Fig.3). At the time of commencement of MDA, more than eight prospect areas had been outlined within an area of about 10km$^2$.

An extended period of preliminary assessment incorporated i) the creation of a geological map of the study area, ii) the definition of a controlling duplex structure and iii) the establishment of a stratigraphic sequence consisting of a single basic to acid metavolcanic sequence overlain by Banded Iron Formation (BIF) units. The need for tighter geological control on Resource modelling was recognized.

Data collection focused on the Katsia and Main Zone prospects. Over 5,000m of drill core were logged using a 48 column logging

template designed for the project. Aspect ratio data from stretched porphyroblasts and fragments was routinely collected.

MDA analysis was based on the compilation of geological cross sections on a spacing of 40m to 80m. The four styles of mineralization defined were i) gold associated with ductile and brittle-ductile shear zones, ii) gold within BIF units or associated with BIF contacts, iii) tourmaline-quartz vein related gold and iv) gold within disseminated tourmaline-bearing schists.

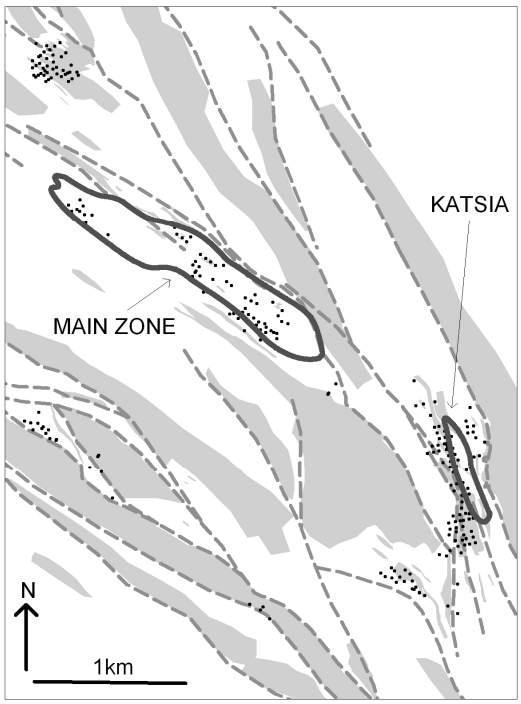


Fig.3 Plan of the Passendro area showing areas of BIF in grey and the Katsia and Main Zone mineralized envelopes in dark grey.

The established host rock sequence was defined in both prospect areas. Clearer ore zone definition within both prospects resulted from MDA studies enabling the recognition of areas with high potential for Resource addition. In particular the subdivision of the extensively mineralized Main Zone facilitated focused vector analysis by long-section for each defined mineralized zone. At Katsia, previous ore-zone correlations were revised. The possible metallurgical and mining characteristics of each mineralization type were highlighted. Independent study of each from a metallurgical and mining stand point was urged.

At the conclusion of the study, i) a reference set of some 30 boxes of core was compiled, ii) logging routines were revised to afford greater time for interpretation, iii) lithological coding was altered to better reflect the stratigraphic sequence identified and iv) coding for each type of mineralization was adopted.

## 4 CONCLUSIONS

MDA analysis and modelling is a structured strategy for geological assessment of mineral deposits incorporating i) Preliminary Assessment, ii) Data Collection, iii) Analysis and Modelling and iv) Template Development. As shown here, it can be applied to deposits of a wide range of styles throughout diverse geological environments. The outcome of such studies can impact substantially on i) exploration modelling and targeting, ii) priorities for evaluation drilling, iii) the degree of confidence in Resource modelling, iv) metallurgical data interpretation and v) mine planning.

## ACKNOWLEDGEMENTS

Zinifex Limited, AXMIN Inc and Cambridge Mineral Resources plc are thanked for permission to present this paper. Structural geological input by D. Coller is acknowledged.

## REFERENCES

Connor AG, Johnson IR and Muir MD 1990 Dugald River zinc-lead deposit *in* Geology of the Mineral Deposits of Australia and Papua New Guinea (Ed. FE Hughes), 949 - 953. *The Australian Institute of Mining and Metallurgy*: *Melbourne.*

Newbery SP, Carswell JT, Allnutt SL and Mutton AJ 1993. The Dugald River zinc-lead-silver deposit: an example of a tectonised Proterozoic stratabound sulphide deposit *in World Zinc The Australian Institute of Mining and Metallurgy: Melbourne.*

Tornos F 2006. Environment of formation and styles of volcanogenic massive sulphides: The Iberian Pyrite Belt. *Ore Geology Reviews* 28, 259-307.

# Multifractal Analysis of Production Data

A. Ford & T.G. Blenkinsop
*School of Earth and Environmental Sciences, James Cook University, Townsville Qld 4811, Australia*

ABSTRACT: Mineral deposits form by transport of elements/minerals from a relatively large mass, low concentration source to high grades focused in a small mass of crust. The de Wijs model is a simple mathematical description of this process. The modified version of this model proposed by Turcotte predicts that concentration process will generate a multifractal distribution of elements/minerals. Several studies have shown that this description is valid by analyzing the distribution of grades from geochemical exploration surveys, which sample a wide range of crustal mineral/element concentrations. We demonstrate that the model can also be applied to analyze the distribution of gold from production data. Databases from gold deposits hosted in veins from the Eastern goldfields of the Yilgarn craton and the Victorian goldfields, both in Australia, and the Zimbabwe craton in southern Africa, are either multifractal or depart from mulitfractality in a way that can be predicted by sampling the only highest grade proportion of a multifractal dataset. The gold deposit databases can be regarded as a high-grade sub-sample of the complete multifractal.

KEYWORDS: de Wijs model, multifractals, production data

## 1 INTRODUCTION

The most general process in the formation of mineral deposits is the transport and concentration of elements/minerals from a source region, where they will typically have a background concentration, to a depositional site where they form a mineral deposit in a much smaller volume of crust at a much higher concentration than the source. For example, Phillips *et al.* (1987) estimate that the Golden Mile, Kalgoorlie gold deposits of the Eastern Goldfields, Australia, formed by concentration of gold into 3 $km^3$ from a source of 320 $km^3$. This process can be described by the de Wijs model (de Wijs 1951; de Wijs 1953), in which a mass of crust is divided into two and an element or mineral is concentrated into one half of the crustal mass by an enrichment factor Phi, leaving a depleted mass of crust with an enrichment factor 2 - Phi. Repetition of this process leads to an exponential relationship between grade and tonnage; Turcotte (1986) argued that grade-tonnage relationships are actually power law (fractal) and demonstrated that a slight modification of the de Wijs model, in which the depleted fraction of the crust is left unaffected by subsequent steps, leads to a power law grade-tonnage relationship. Fractals have also been used to describe the spatial distribution of mineral deposits (*eg*. Blenkinsop & Sanderson 1999; Carlson 1991).

While these fractal studies are important, fractal analysis is typically restricted to two variables at most, such as the x and y coordinates of a deposit location, or grade and tonnage. Multifractal analysis can overcome this limitation by including the distribution of grades at deposit locations to provide a much more complete description of mineral distributions. Moreover, multifractal distributions of elements/minerals are predicted from the modified de Wijs model (Agterberg 2001; Xie & Bao 2004). Several studies have used geochemical exploration survey data to demonstrate that a variety of metals do indeed have a multifractal distribution (Agterberg *et al.* 1996; Cheng 1999; Cheng *et al.* 1994; Xu & Cheng 2001).

This study aims to determine whether gold distribution can be described as a multifractal using production data from three study areas,

and to compare these data with the predictions of the modified de Wijs model. Such a multifractal description would have considerable importance in understanding the genesis of gold deposits.

## 2 DATA, MULTIFRACTAL ANALYSIS, AND MODEL

Due to the availability of large amounts of high quality data, study areas in the Eastern Goldfields of the Yilgarn craton and the Victorian goldfields, both in Australia, and Zimbabwe craton in southern Africa were selected for analysis of recorded gold production (ore tonnage and grade) data (Bartholomew 1990; Western Australia Department of Industry and Resources 2005; Victoria Department of Primary Industries 2006). Each database was filtered to include only vein-hosted gold deposits in order to focus on a single population. These deposits are the predominant deposit type in each study area.

The method of moments technique was used to determine whether the datasets could be described by a continuous multifractal model (Evertsz & Mandelbrot 1992). A grid of equal sized boxes with side length $E$ was placed over the study area with the number of boxes ($N(E)$) noted. If a box contained a single data point, the value (grade) of that data point was applied to the whole box, and if a box contained more than one data point, the values of each point in the box were averaged and the average value was assigned to the box. A partition function $\chi_q(E)$ was then calculated for a range of $q$ values, the mass exponent function $\tau(q)$ was then estimated and the function $\alpha$ evaluated in order to determine the multifractal spectrum $f(\alpha)$. Techniques for evaluating these parameters are detailed in several studies (*e.g.* Agterberg *et al*. 1996; Evertsz & Mandelbrot 1992).

Using the methodology outlined by Xie and Bao (2004), a 128x128 grid was generated after seven iterations of the de Wijs model with an enrichment factor of 0.2. Partition functions $\chi_q(E)$ were generated for a range of $q$ using the method of moments technique. In order to simulate the effect of having only the highest population, approximately 90% of the data with the lowest concentration values was removed from the 128x128 grid and the partition functions were recalculated.

## 3 RESULTS

Multifractal analysis of grade data from each of the three study areas indicates that data from the Eastern Goldfields and the Zimbabwe craton could be described by a multifractal model. The non-linearity of the partition function graph seen in Fig. 1 as required by the theory outlined by Evertsz & Mandelbrot (1992) precluded the Victorian data from being described as multifractal.

Figure 2a shows the partition functions for the output of the model. They are clearly mulitfractal, as predicted.

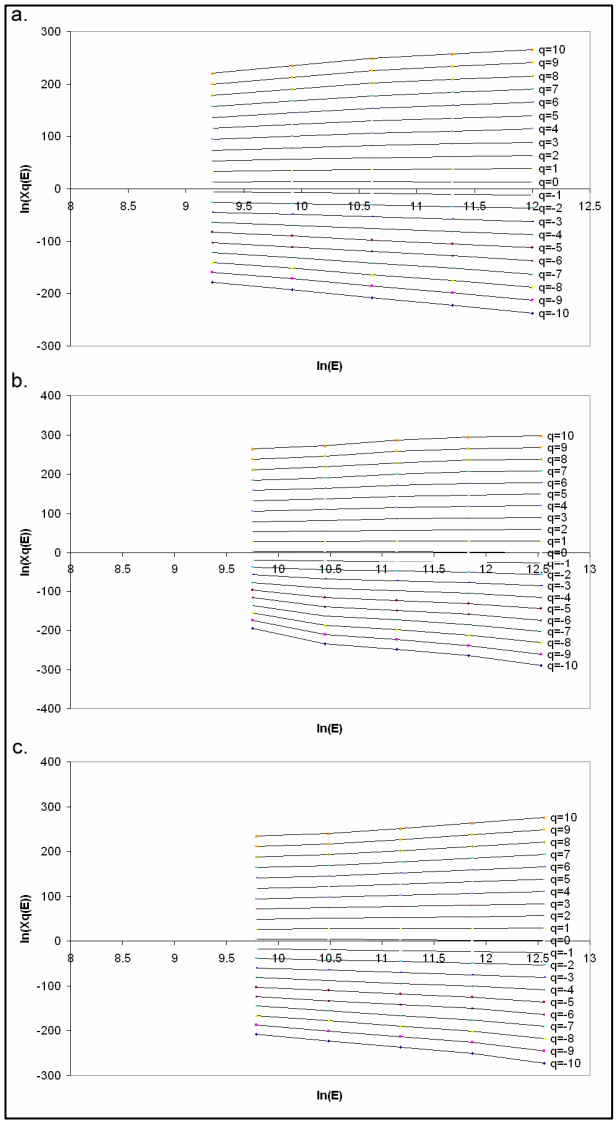


Figure 1: Relationship between natural log of partition function $\chi_q(E)$ and natural log of box size $E$ for (a) grade in Eastern Goldfields, (b) grade in Victorian goldfields, (c) grade in Zimbabwe craton.

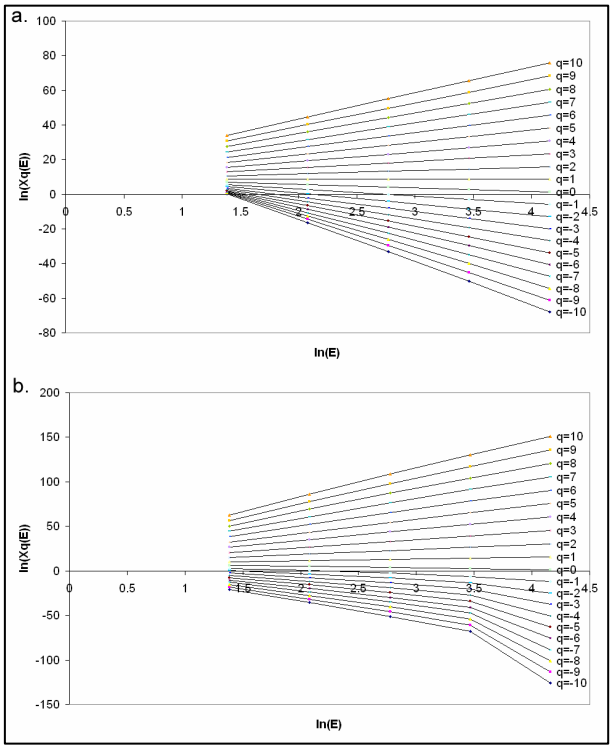


Figure 2: Relationship between natural log of partition function $\chi_q(E)$ and natural log of box size $E$ for (a) 128x128 cell de Wijs model, (b) de Wijs model with the lowest 90% of concentration values removed.

## 4 DISCUSSION & CONCLUSIONS

The production data for Figure 1a and 1c is multifractal – as predicted by the de Wijs model. However the data for Figure 1b may not be multifractal because it is only the high grade part of the distribution. To test this, we selected just the high-grade parts of the de Wijs model output. These were not multifractal in the same way as the Victorian grade data (Fig. 2b). The effect on the graphs of the partition function from the modified de Wijs model is similar to the effect seen on the graphs shown in Figure 1.

Though the results of previous studies would indicate that production data in terms of ore grade are multifractal, in practice production data is only available from the highest grade end of the spectrum. Previous studies have shown that element concentration data is multifractal, It is suggested that the differing conclusions reached for case in Figure 1b are due to the difference in data collection techniques, as geochemical datasets tend to contain a full spectrum of data as opposed to production data which is collected from mineral deposits that are at the upper grade end of the spectrum.

The results of the case study suggest that production data has the potential to be described by multifractals. Using a modified de Wijs model it is shown that incompleteness of production datasets can affect the linearity of the partition function graphs, thus multifractals can not describe some of the data. The more complete the data set, the more likely it is that a multifractal description can be applied.

The link between the data and the modified de Wijs model opens up the possibility to deduce the enrichment factors for the different data sets. This could have important implications for the genesis of the gold deposits.

## ACKNOWLEDGEMENTS

This work is published with the permission of the Chief Executive Officer, predictive mineral discovery Cooperative Research Centre (pmd*CRC). This study is part of the PhD research of AF at James Cook University which is supported by a pmd*CRC scholarship.

## REFERENCES

Agterberg FP (2001) Multifractal simulation of geochemical map patterns In: Merriam DF, Davis JC (eds) *Geologic modeling and simulation: Computer Applications in the Earth Sciences.* Plenum Press, New York, pp 31-39.

Agterberg FP, Cheng Q, Wright DF (1996) Fractal Modelling of Mineral Deposits In: Elbrond J, Tang X (eds) *Proceedings of the International Symposium on the Application of Computers and Operations Research in the Minerals Industries.* Montreal, pp 43-53.

Bartholomew DS (1990) *Gold Deposits in Zimbabwe.* Geological Survey of Zimbabwe.

Blenkinsop TG, Sanderson DJ (1999) Are gold deposits in the crust fractals? A study of gold mines in the Zimbabwean craton In: McCaffrey KJW, Lonergan L, Wilkinson JJ (eds) *Fractures, Fluid Flow and Mineralization*. Geological Society, London, pp 141-151.

Carlson CA (1991) Spatial distribution of ore deposits. *Geology* 19: 111-114.

Cheng Q (1999) Spatial and scaling modelling for geochemical anomoly separation. *Journal of Geochemical Exploration* 65: 175-194.

Cheng Q, Agterberg FP, Ballantyne SB (1994) The separation of geochemical anomalies from background by fractal methods. *Journal of Geochemical Exploration* 51: 109-130.

de Wijs HJ (1951) Statistics of ore distribution: (1) Frequency distribution of assay values. *Journal of the Royal Netherlands Geological and Mining Society* 13: 365-375.

de Wijs HJ (1953) Statistics of ore distribution: (2) Theory of binomial distribution applied to sampling and engineering problems. *Journal of the Royal Netherlands Geological and Mining Society* 15: 12-24.

Evertsz CJG, Mandelbrot BB (1992) Multifractal Measures (Appendix B) In: Peitgen H-O, Jürgens H, Saupe D (eds) *Chaos and Fractals: New Frontiers of Science.* Springer-Verlag, New York, pp 921-953.

Phillips GN, Groves DI, Brown IJ (1987) Source requirements for the Golden Mile, Kalgoorlie: significance to the metamorphic replacement model for Archean gold deposits. *Canadian Journal of Earth Sciences* 24: 1643-1651.

Victoria Department of Primary Industries (2006) *Mines and Mineral Occurrences Database* Victoria Department of Primary Industries.

Western Australia Department of Industry and Resources (2005) *Mines and Mineral Deposits of Western Australia* Department of Industry and Resources.

Xie S, Bao Z (2004) Fractal and Multifractal Properties of Geochemical Fields. *Mathematical Geology* 36: 847-864.

Xu Y, Cheng Q (2001) A fractal filtering technique for processing regional geochemical maps for mineral exploration. *Geochemistry: Exploration, Environment, Analysis* 1: 147-156.

# 3D implicit geological modeling by Marching cube algorithm and its application in study on Anqing copper-iron deposit, China

L.M. Liu, A.L. Cai, H.Y. Yang, C.L. Wang, Z.M. Shu & Y.L. Zhao
*Computational Geoscience Research Centre, School of Geoscience and Environmental Engineering, Central South University, Changsha, China*

ABSTRACT: This paper presents the researches of how to model 3 dimensional shape in geo-fields through three-dimensional interpolation and isosurface constructing from limited and scatted exploration data. The Kriging algorithm is used as the 3 dimensional interpolation method to convert the insufficient and irregularly-scattered data set into sufficient grid data set. The isosurfaces are extracted from the grid data set by using of Marching cube algorithm and rendered by using of the OpenGL. Through programming for the computation by VC++.net, and integration and test of the programs, a practicable 3D geological modeling software, 3DIMS (3 dimension isosurface modeling soft) is developed. The 3DIMS is applied in the Anqing copper-iron deposit to demonstrate ore grade 3D distribution. The modeling results in the Anqing deposits show visually that high grade of Cu must be in the high grade iron zones, and high grade of Cu and S are spatially related to F1 fault, suggesting that deposition of chalcopyrite might be related to magnetite, and F1 might be conduit for Cu-bearing fluids. The 3DIMS can be extended to model all kinds of 3D data in geofield.

KEYWORDS: 3D model, isosurface, interpolation, Marching cube, Anqing copper-iron deposit

## 1 INTRODUCTION

The 3D geological modeling, as an important tool for mineral exploration and research, can be performance by two ways, explicit and implicit. The explicit modeling is to construct surfaces of a solid through manual manipulation and digitization. The implicit modeling is to extract surface of a solid from a volume function of the solid. These surfaces are implied to exist in a continuous volume function, therefore are referred to as "implicit surfaces". Since geological data is inherently volumetric, the implicit representation of surfaces is an ideal one (Cowan *et al*. 2003). The core of implicit modeling is the algorithms of interpolation, necessary for constructing the volume function, and of isosurface extraction, necessary for producing 3D shape. In this paper, the Kriging and the Marching cube are used as algorithms respectively of interpolation and isosurface-extraction, and the VC++.net and OpenGL are used to develop a 3D geological modeling system. This modeling system is used to study the 3D zoning of Fe and Cu contents in ore bodies in the Anqing deposit, south China.

## 2 THEORY AND METHOD FOR 3D MODELING

### 2.1 *Kriging and Marching cube algorithums*

Kriging is a geostatistical interpolation algorithum that considers both the distance and the degree of variation between known data points when estimating values in unknown areas (Matheron 1963). Estimating value $Z_v^*$ of any estimating point's true value is a linear combination a set of value of surrounding points, writing as

$$Z_v^* = \sum_{i=1}^{n} \lambda_i Z(x_i) \qquad (1)$$

where $Z(x_i)$ is value of point $x_i$ and $\lambda_i$ is its weight. The $\lambda_i$ can be valued through analyzing variogram and solving the semivariogram equation.

The Marching Cubes algorithm was designed by William E. Lorensen and Harvey E.

Cline to extract surface information from a 3D field of values (Lorensen & Cline 1987). The basic principle behind the algorithm is to subdivide space into a series of small cubes. The algorithm then instructs us to 'march' through each of the cubes testing the corner points and replacing the cube with an appropriate set of polygons. The sum total of all polygons generated will be a surface that approximates the one the data set describes. The first step for realizing isosurface construction is to classify eight vertexes of every cube according to whether vertex is inside or outside the isosurface. The second step is to determine the isosurface jointing mode according the vertex status. After triangle isosurface jointing mode being determined inside the cube, intersection X of isosurface with cube's edge can be obtained by using linear interpolation:

$$X = i + [F_t - F(i,j,k)]/[F(i+1,j,k) - F(i,j,k)] \quad (2)$$

where $F_t$ is threshold value and $F(i,j,k)$ is value of vertex ($i,j,k$). Because the gradient is perpendicular to the isosurface, so the gradient at the iso-value point, P, can be treated as its normal vector at the point P in the whole data field. Because the data field is three-dimension orthogonal, the gradient at vertex in every cube can be calculated by using of central difference, the linear interpolation is then used to calculated the gradient at point P as following,

$$g_x = \frac{F(x_0 + a, y_0, z_0) - F(x_0 - a, y_0, z_0)}{2a} \quad (3)$$

$$g_y = \frac{F(x_0, y_0 + b, z_0) - F(x_0, y_0 - b, z_0)}{2b} \quad (4)$$

$$g_z = \frac{F(x_0, y_0, z_0 + c) - F(x_0, y_0, z_0 - c)}{2c} \quad (5)$$

where the *a, b* and *c* indicate the edge length of the cube, and $g_x$ $g_y$ and $g_z$ indicate gradient at the vertex ($x_0$, $y_0$, $z_0$).

## 2.2 *Isosurface Rendering by OpenGL and programming by VC++.net*

The isosurface created by Marching cube algorithm is a series of jointing triangle faces which need to render through considering illumination, material and elimination of the hidden faces that exist in the real world. The OpenGL, open graphics library, as a robust three-dimension graphics and model library offers many general functions to process illumination, material and elimination of the hidden faces through convenient programming interface (Mason *et al.* 2005).

The VC++.net is used to program for computation of interpolation, isosurface extraction and isosurface rendering. By integration and test, a 3D modeling system, 3DIMS (3 dimensional isosurface modeling software), with graphics user interface (GUI) is developed and can conveniently be used to auto-create 3D model from 3D data.

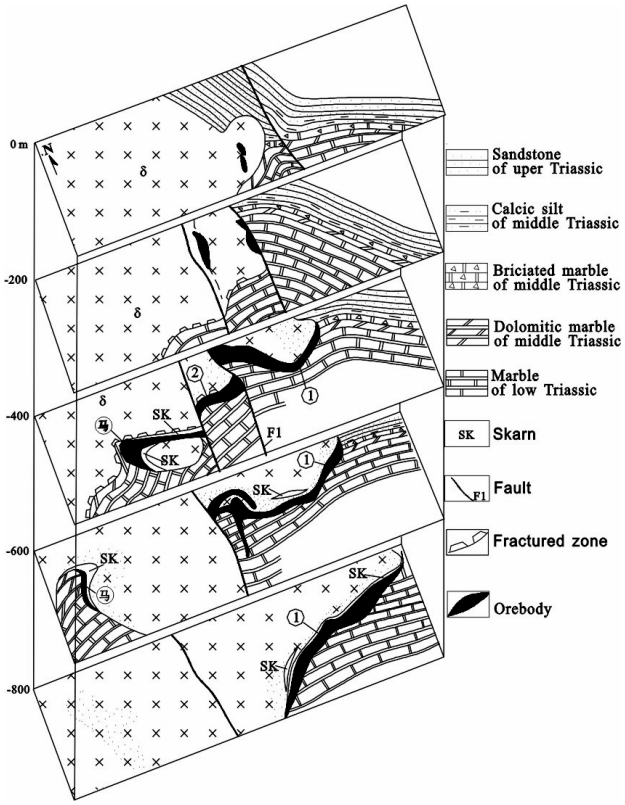


Figure1. Geological map of different level of Anqing deposit

# 3 APPLICATION IN STUDY ON ANQING DEPOSIT

## 3.1 *Features of the Anqing deposit*

The Anqing deposit, located in middle part of the lower Yangtze River metallogenic belt (Pan & Dong 1999), south China, is a is a typical Fe-Cu skarn, with measured reserves of 520 kt copper and 21.8 Mt iron. The orebodies, including iron orebodies with more than 35% Fe content and less than 0.3% Cu, copper orebodies with more than 0.3% Cu but less than 35% Fe, and iron-copper orebodies with more than 0.3% Cu and more than 35% Fe, are located

along the contact zone of Yushan diorite intrusive (of 147.24Ma Rb-Sr age) with sedimentary carbonate of middle Triassic (Fig.1). The average grade of 1.164% Cu and 47.65% Fe demonstrates its economic and scientific importance. Ores in the Anqing deposit are mainly copper-bearing magnetite, secondly copper-bearing skarns and copper-bearing diorite. Both Cu and Fe are profitable elements in this deposit. The spatial distribution pattern of Cu and Fe is important for study and development of the deposit.

### 3.2 *3D grade isosurface modeling in Anqing deposit and its implication*

The contents of Cu, Fe and S in 24476 samples from 1371 drills in the Anqing mine are used to model 3D grade isosurface. After the data are inputed as Access database, the 3D isosurface of Cu Fe and S at any threshold can be auto-created by using of the our 3DIMS, which give a 3D visualization of ore grade distribution. Figures 2, 3 and 3, respectively of Cu isosurface at 1.5%, Fe isosurface at 35% and S isosurface at 1.5%, present 3D models of high grade ore distribution.

Theoretically, the space inclosed by the isosurface of 35% Fe grade should be iron and copper-iron orebodies determined by cut grade of 35% Fe. But comparing with the hand-drawn sections, difference in detail is also obvious, the inclosed isosurfaces being thicker in thickness direction and more stretch in dip and strike direction than the real orebodies, which means the modeling orebodies become plumper than the real orebodies. These differences are mainly resulted from two aspect reasons, effects of fault and strata to anisotropy being not considered in the Kriging interpolation, and the isosurface jointing adjacent points being always auto-produced as most round face which is distinct from the real border of orebody

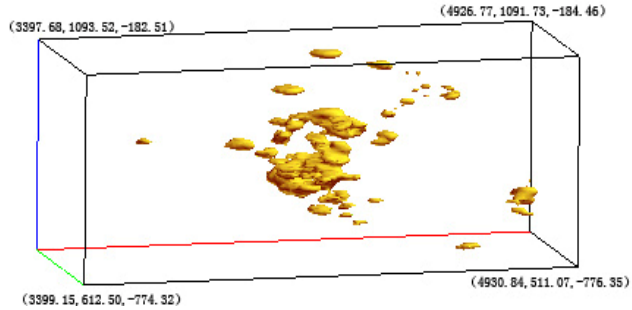


Figure 2. Isosurface of 1.5% Cu grade

Compared Fig. 2 with Fig.3, it is demonstrated that high grade copper ores must be distributed in the high grade iron orebodies. It suggests that the deposition of main copper-bearing mineral, chalcopyrite, should be related with magnetite.

Compared Fig. 2, 3 and 4 with 1, it is obvious that the high grade of Cu and S ores are spatially with the fault F1, but high grade Fe is not spatially related with fault F, suggesting that the F1 should play an important role in copper mineralization, maybe acting as conduit for copper-bearing fluid. The copper and iron in the orebodies might be differently sourced.

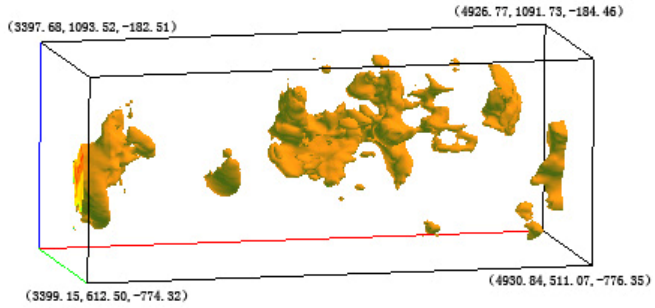


Figure 2. Isosurface of 35% Fe grade

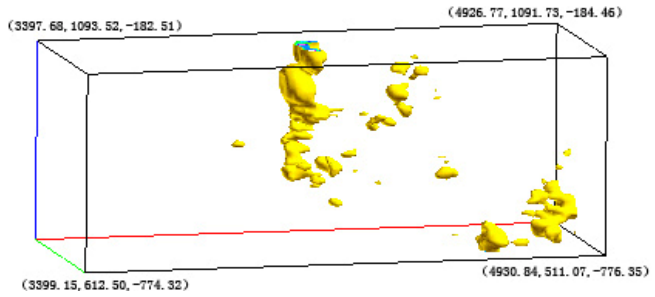


Figure 4. Isosurface of 5% S grade

## 4 CONCLUSION

By using of VC++.net to program computation of 3D interpolation by the Kriging algorithm, isosurface extraction by Marching cube algorithm and isosurface rendering by OpenGL, a practicable 3D isosurface modeling software, 3DIMS, has been developed. The 3DIMS is applied in the Anqing copper-iron deposit to model 3D orebodies and ore grade distribution. The isosurfaces of Cu, Fe, S and other contents at any threshold can be easily auto-created from irregularly scattering drill data. The 3D modeling results in the Anqing deposits demonstrate

visually that high grade of Cu must be in the high grade iron deposit, and high grade of Cu and S are spatially related to F1 fault, suggesting that deposition of chalcopyrite might be related to magnetite, and F1 might be conduit for Cu-bearing fluids. The 3DIMS can be extended to model all kinds of 3D data in geofield.

ACKNOWLEDGEMENTS

The Anqing Copper Mine, Tongdu Copper Limited Co. is acknowledged for the financial data support.

REFERENCES

Cowan EJ, Beatson RK, Ross HJ, McLennan T (2003) J. Practical Implicit Geological Modeling. In: Dominy S (ed), *5th International Mining Geology Conference.* The Australasian Institute of Mining And Metallurgy, 2003/8: 89-99

Matheron G (1963) Principles of geostatistics. *Economic Geology* 58:pp1246-1266

Lorensen WE, Cline HE (1987) Marching Cube:A High Resolution 3D Surface construction Algorithm. *Computer Graphics* 21: pp163-169

Mason W, Neider J, Davis T, Shreiner D (2005) *OpenGL Programming Guide: The Official Guide to Learning* OpenGL 4th Edition. Moston: Addison-Wesley Professional, PP784

Pan Y, Dong P (1999) The lower Changjiang (Yangtze / Yangtze River) metallogenic belt, easter central China: intrusion- and wall rock-hosted Cu-Fe-Au,Mo,Zn,Pb,Ag deposits. *Ore Geol Rev.* 15: pp177-242

# International Mineral Resource and Ore Reserve Reporting

Paul Gribble
*Principal Adviser, Geology, Rio Tinto Operational and Technical Excellence*

Niall Weatherstone
*Chief Adviser Study Reviews, Rio Tinto Operational and Technical Excellence*

ABSTRACT: This paper looks briefly at the historical development of global resource and reserve reporting and then seeks to describe recent, current and future changes and developments. An overview of recent techniques and tools for classification and risk analysis is given.

KEYWORDS: Resource & Reserve Classification, CRIRSCO

One of the first attempts at formal resource and reserve classification, and one of the forerunners of the JORC Code, was the USBM Circular 831, US Geological Survey bulletin 1450A produced in 1976. This set out the dual viewpoint of classification of geological, physical and chemical attributes of a deposit, paired with the profitability of extracting and marketing the contained mineral(s) at costs and the economic situation at a given time. At the same time, definitions were given to a wide range of terms, together with guidelines for classification. The various categories were illustrated graphically, giving an overall picture and concepts that we would be familiar with today.

In response to the Bre-X saga and the advent of Sarbanes Oxley, the development of national reporting codes has accelerated in recent years. This has been accompanied by concerted moves to reconcile and converge international reporting in mining and other extractive industries.

Using the JORC code as a model, national codes or guidelines have recently been produced in USA (SME Guidelines), Canada (NI 43-101), Peru (Lima SX Code), Chile (IIMCh Code), South Africa (SAMREC) and the UK/Ireland/Western Europe (Reporting Code, 2001). These national codes have been brought together under the auspices of the Committee for Mineral Reserves International Reporting Standards (CRIRSCO). Formed in 1994 with the support of the Council of Mining and Metallurgical Institutes (CMMI), CRIRSCO is the committee representing the national reporting organisations (NROs) of most of the countries listed above. Their combined efforts have resulted in the reporting standards in most 'western' countries using almost identical resource and reserve definitions with a high degree of compatibility. CRIRSCO aims to provide a unified approach to reporting for the mining industry, aiding the understanding of investors and regulators, thereby promoting confidence in reporting. CRIRSCO has recently produced an International Template that reflects the best of each of the CRIRSCO type national codes and guidelines as they are updated; it is hoped that the template will be a vehicle for countries to develop compatible resource and reporting codes. CRIRSCO has recently become a part of the CMMI.

The significant exception in compatibility in reporting is the USA Securities and Exchange Commission (SEC), which adheres to its own standard (Industry Guide 7) that is only partly compatible with the CRIRSCO type codes. A comparison of Industry Guide 7 with Circular 831 well illustrates how far the SEC has moved away from a comprehensive reporting system that had at least some of its origins in the USA, to one that is so relatively poorly defined. The USA is represented on CRIRSCO and it is hoped that in time the continued submissions to the SEC by the mining industry will bear fruit.

The development of CRIRSCO type codes continues. The UK, Ireland and Western European reporting code is being updated with

the formation of the Pan European Reserves Reporting Committee (PERC) that supersedes the original Working Group on Reserves and Resources of the IoM3. An updated reporting code will be produced later this year. PERC is the European equivalent of the Australasian JORC in Australasia, SAMREC in South Africa, and similar reserves standards bodies in the USA, Canada, and Chile, and with them is a constituent member of CRIRSCO. PERC serves as the NRO for UK and Europe providing a forum representing a broad spectrum of national interests concerning public reporting. In common with its international counterparts PERC recognises the need for the accredited competent person, the coordination and application of reporting standards at national and international level, and for a single point of contact on these issues.

This year has also seen the release of the updated SAMREC code from the SAIMM. The definitions in this edition of the SAMREC Code are either identical to, or not materially different from the international definitions given in the CRIRSCO template.

The emergence of Russia and China as hosts to a wealth of mineral resources has resulted in their interest in attracting 'western' finance to assist in their development. Investors, encouraged by the simplicity and transparency of CRIRSCO type codes, are looking for 'translation' of the categorisation and status of these deposits into the terms in common usage in the 'CRIRSCO community'. Russia has its own prescriptive reporting code developed in the Soviet era. A committee set up by PERC, representing CRIRSCO, and Russian experts is currently working on interpretation of the Russian code to be able to compare it with CRIRSCO standards. In the same way, a committee set up by JORC is working with China in development of their reporting code. This is in earlier stages of development.

In the background is the United Nations Economic Commission for Europe (UN ECE) that has been developing its Framework Classification (UNFC) since 1992. This aims at a global reporting system for hydrocarbon and solid mineral extraction, catering for both governmental and industry requirements. Whilst few mining companies report their reserves and resources using the UNFC, the system is being examined or has been accepted at least in principle by some governments, including India, China and Russia. At present the categories and definitions for resources and reserves are not aligned with the CRIRSCO template.

Since 2004, discussions between CRIRSCO and the Society of Petroleum Engineers (SPE) have found common ground during joint discussions with the International Accounting Standards Board (IASB).

The IASB is investigating the development of a new Accounting Standard for the Extractive Industries as a part of its International Financial Reporting Standards (IFRS). In this standard, the major assets of an exploration or mining company, its mineral resources and reserves might be valued using fair value methods and carried on, for example balance sheets. Such a move is obviously highly relevant to the companies concerned and engagement of CRIRSCO and the SPE with the IASB is considered essential. Discussions have centred on demonstrating the similarities and significant differences between the hydrocarbon and mineral reporting systems. This project, carried out on behalf of the mining industry, is one of CRIRSCO's most important responsibilities. CRIRSCO's initial involvement was to provide the IASB Board and its research team with information on reporting standards used by the mineral industry worldwide and, more specifically, on definitions for mineral resources and reserves.

Following these discussions with the IASB it became apparent that such organisations view the resources and reserves of solid minerals and hydrocarbons as essentially the same, and therefore definitions should be identical. Following a request from the IASB discussions took place between the SPE and CRIRSCO with regard to possible convergence of definitions. Whilst the two industries share a similar basis, significant differences also exist

Where to for the future?

The prospects for a compatible Russian code are promising; it is hoped that China moves in the same direction. Current trends suggest that the reporting of all mineralised material might become a feature of the CRIRSCO type codes, catering for the needs of all sectors.

CRIRSCO compatible codes encourage resource and reserve practitioners to discuss confidence in their estimates. Techniques for assessing confidence in resource and reserve estimation continue to advance. These include confidence interval work and it's implications

for long term mine planning, and the optimisation of drill spacing.

Recent developments in confidence interval estimation enable the rapid creation of models of the reliability of estimates. This provides a range of 'upside' and 'downside' potential to the estimate and adds another tool to the classification process for both resources and reserves. By the same token, the technique enables a risk assessment, both positive and negative, of the uncertainty associated with the estimate and thus the classification; a valuable addition to the strategy for further exploration or development of the mineralization.

Confidence intervals in themselves are not new; the ideas were developed a few years ago, but have recently been integrated into specialist software. The technique is based on a modified version of simple Kriging, and takes into account the sample distribution as well as sample distance. Previous work has been completed using conditional simulation that can produce similar results. This, however, is very time consuming requiring at least 100 simulations that, even with modern powerful computers, might take days to calculate. The new method allows for direct calculation Essentially, the process converts sample values to Gaussian values, and allows for change of support. A Gaussian variogram is calculated and Gaussian block values and Kriging variance are calculated that are then back transformed to raw values. Confidence intervals reflect the inability to exactly define an unknown value, estimating the probability that a value estimated into a block lies within a certain grade range, thus indicating the potential reliability of an estimate. Bivariate techniques are currently in development. The resulting distribution can be used as an indicator of resource classification.

Uncertainty in a project can be assessed by sensitivity analysis of a series of assumptions and estimates in a model. This can be a business, mining or geological model. Traditionally, such analyses have considered variation of single factors such as the product price or the extraction and process costs. Uncertainty within the resource is rarely considered as it has always been more difficult to model.

The implications of confidence interval work in mine planning can be demonstrated by pit optimisation of successive models of varying uncertainty in the estimate. Essentially, the method used is to import the confidence levels for each block into Whittle and represent them as elements. A spread of optimal pits and potential pit values is obtained and an overview of the financial robustness of a project obtained. By this method risk is integrated into open pit design and long term planning. Estimates of risk for the project can be made together with predictions of uncertainty in, for example, the input grade to the mill during mine life.

Recent work has been completed to optimise drill spacing. Essentially the technique simulates a model of values from limited drill hole data, from which a variety of planned drill hole grids are used to re-estimate values and the results compared with the simulation. As would be expected, closer spaced grids improve confidence in the estimate, but this technique quantifies the likely transfer of material between categories using percentage differences. Thus the cost versus benefit of drilling one grid against another can be evaluated, in terms of category upgrade and thus in value to the project. Clearly this technique can also be used as an indicator of resource classification.

## ACKNOWLEDGEMENTS

This paper is based partly on CRIRSCO and PERC documents prepared by, or in conjunction with, other members of the committees. The authors gratefully acknowledge their assistance. The authors' ability to contribute to CRIRSCO activities is only possible through the generous support of their employer, Rio Tinto plc and their support is also gratefully acknowledged.

The assistance of John Forkes, Faye Jones and Georg Gestrich, without which description of new techniques would not have been possible.

## REFERENCES

Forkes, J. (2002): An alternative approach for generating confidence intervals for block grade estimates, Rio Tinto Technical Services, unpublished.

Gestrich, G, (2006), Incorporating resource risk into pit optimisation studies, TU Berlin MSc thesis, unpublished.

Jones, F, (2007), personal communication.

Stephenson, P R and Weatherstone, N, (2006), Developments in International Mineral Resource and Reserve Reporting, International Mine Management Conference, Melbourne.

# Conceptual Modeling for Reasonable Exploration & Exploitation of Solid Mineral Resources in China

Li Li, Pei Rongfu, Wang Yonglei & Wang Haoling
*Institute of Mineral Resources, CAGS, Beijing 100037, China*

ABSTRACT: The concept of 'double control' and reasonable area in mineral exploration and exploitation modeling is presented. 'Double control' includes two controlling factors, namely the degree of geological study and the economic feasibility. Geological research combined with economic analyses is crucial to the evaluation of mineral resources. The application of this model is tested in mineral exploration and exploitation.

KEYWORDS: mineral exploration and exploitation; mining industry; model of double control and reasonable area

## 1 INTRODUCTION

Efficient exploration and exploitation of mineral resources plays an important role in sustainable development of the mining industry. With the objective of improving living standards world-wide, demand for solid mineral resources probably will continue to increase for the foreseeable future. Many of the large-super large, high grade, close to surface and close to market mineral deposits have been depleted or are currently in production. More and larger deposits have to be discovered to meet increased demand for mineral commodities.

Over the past several years, the demand of base-metals increased significantly in China (Li Li *et al*., 2006). The output also increased (Figure 1). According to data, there is an emergent need for iron ore and aluminum in China. Mining plays a backbone role in China's national economy. At present, the mining sector is providing 93% of energy, 80% of raw materials for industry and 70% of means of production for agriculture (Shao, 2005). The sustainable development of the mining industry is an increasingly important problem facing the sector. Our ability to meet the continuing and growing demand for minerals is greatly affected by concerns about reasonable exploration and exploitation of mineral resources. The purpose of this paper is to present a conceptual model about reasonable exploration and exploitation of solid mineral resources.

## 2 EXPLORATION MODELS

The simplified model (Figure 2) (Pei *et al.*, 1994; Pei *et al*., 1998; Pei & Xiong, 1999) is divided into a series of stages. Efficient exploration and exploitation of mineral resources is highly dependent on the quality control exercised at each stage of the process. At each step in the resource modeling process it is necessary to define the specific objectives, the meth-

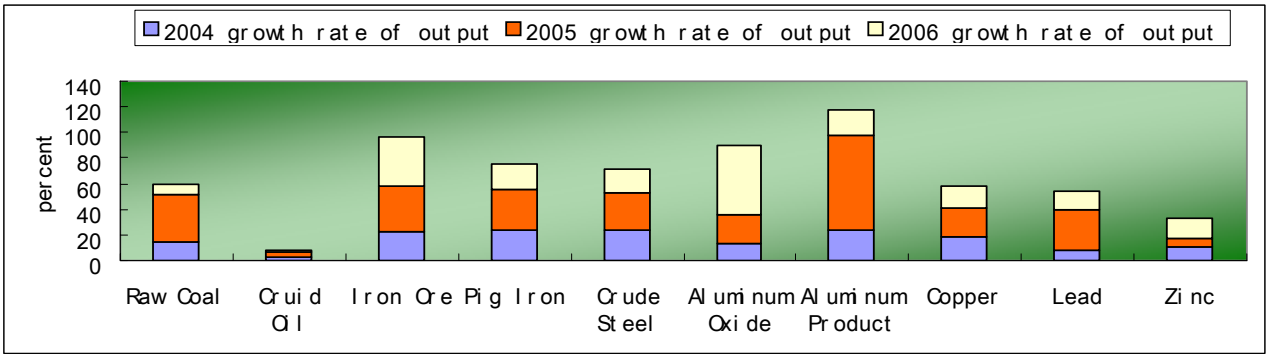


Figure 1 Chinese mineral resources growth rate of output

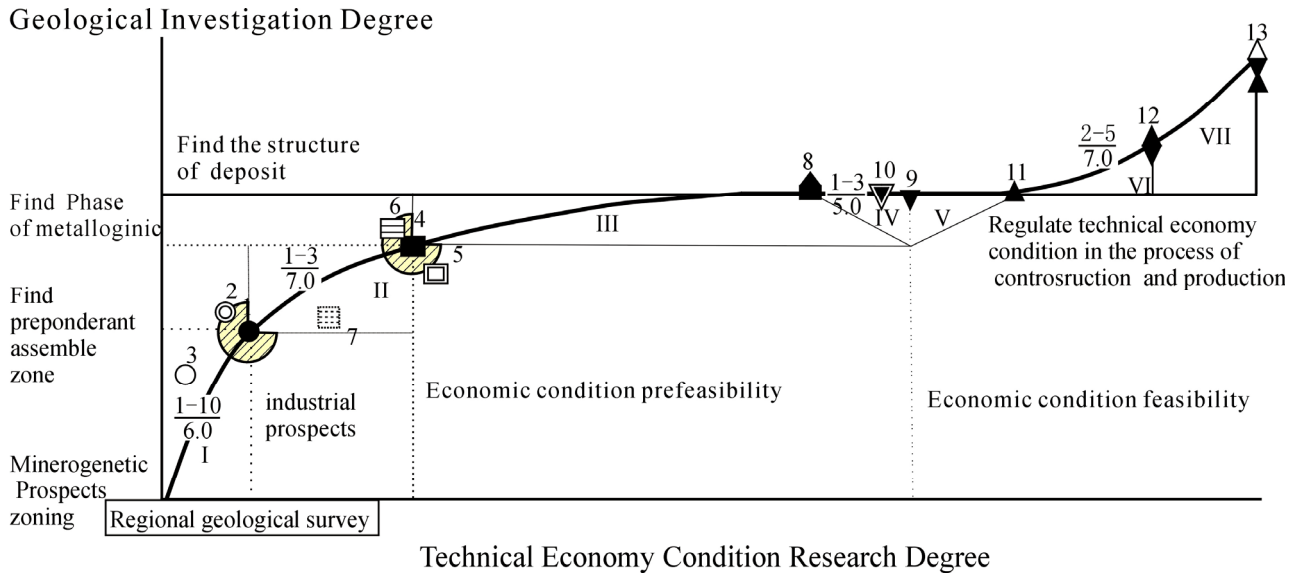


Figure 2 A model about reasonable exploration & exploitation of mineral resource

I..Geologic reconnaissance. II. Mineral reconnaissance in detail. III. Mineral exploration. IV. .Feasibility study in detailed for mine construction. V..Mine construction. VI. Complementary mineral exploration based on mine construction needed. VII. Deposit research in detailed during the production stage.
1.approved detailed investigation deposit. 2.uncertain industrial prospects deposit ; 3.without geological and industrial prospect deposit ; 4.approved mineral exploration deposit ; 5.metallogenic in complex condition and exploitation in feasible technical economy condition deposit. 6.find metallographic phase and future exploitation in feasible technical economy condition deposit. 7.metallogenic in complex condition and exploitation in infeasible technical economy condition deposit. 8.approved mine construction design deposit. 9..mine construction on schedule ; 10.measure up feasible technical economy condition deposit ( future mine construction. 11.investor commence capital construction of a mine. 12.accomplished capital construction mine. 13. put into production and sustainable broaden perspective mine. 1-3/5.0 working period month or year/Investments percent

odology proposed to achieve those objectives and to establish a set of validation tools to assess the outcome. Resource estimation is a complex process involving different specialists with relevant experience using a multidisciplinary approach (Zhao, 2000). We propose that the double control theory, which comprises geological and economic factors, is an effective management tool. Geological quality is a function of deposit grade, deposit size, and "other" geological factors. Mineral deposits of the same deposit type have similar geological quality attributes. Economic quality is measured relative to a benchmark. As geologists we must understand the economic impact of our plays and prospects. Geological analyses and economic analyses are crucial to the evaluation of resource.

The resource classifications are directly related to the appraisal stages of the project. For an inferred resource, geological and grade continuity are assumed, but not established. At the inferred category, scoping-stage evaluations can be carried out to determine if further exploration or technical investigations are warranted. At the indicated category, geological and grade continuity have been reasonably established, but short-range grade variability is not well known. The information is sufficient to carry out pre-feasibility stage assessments and assess the economic viability of the deposit. At the measured category, the geological continuity of the deposit and the local grade continuity including short-range variability have been established with a high degree of confidence.

As geoscientists, we recognize the importance of the economic assessment. We may vary drastically in our methodologies and in agreeing on which economic indicators to rely upon.

According to actual condition, we choose a kind of indicator to evaluate mine value. When the amount of geological work is comparatively small, we use mine potential value (Vq), Formula of mine potential value Vq=Q' (reserves)×P(price). Wit h increased geological data, we apply mine abstraction value (Vt), Vt=Q'(reserves)×ε(total recovery)×P. With a high degree of geological data, we use mine gross profit (S), formula:

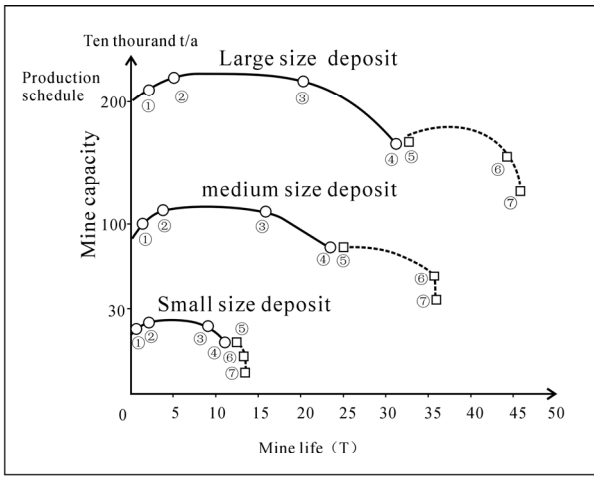


Figure 3 The process of reasonable exploitation of mineral resources

$$S=\frac{Q\times\varepsilon 1}{1-\rho}\left[\bar{\alpha}\times(1-\rho)\times\varepsilon''\times P-C\right]$$

Q'—reserves, $\bar{\alpha}$ —average grade, ρ—mining dilution ratio, ε1—mining recovery rate, ε''—ore processing recovery rate, C—ore cost per tonne, P—price per tonne.

## 3 EXPLOITATION MODELLING

Models of the process of reasonable exploitation of mineral resources are illustrated in Figure 3. We divide exploitation process into seven stages. These comprise trial-production stage, development stage, production steady stage, production decline stage, supplementary exploration stage, closure of mine stage, and reclamation stage.

Trial-produce stage pre-production stage. Development stage: Basic construction is completed, preproduction reaches definite scale. Usually this stage of large size deposit begins when it achieves 30 percent of design capacity end to 100 percent, this needs about 5 years. The stage of medium size deposit begins when it reaches 50 percent of design capacity end to 100 percent. The stage of a small size deposit begins when it reaches 100 percent of the mine design capacity. Medium size mine and small size mines need about 2-3 years to reach this point. Production steady stage: reached mine design capacity, output of mine remains steady. Economic benefit of the stage is best of all. Production decline stage: Reserves depletion. Condition of exploitation runs down and production cost increases. Output of mine decreases year by year. Supplementary exploration stage: increased demonstrated reserves and output. Closure of mine stage: The process of closure. Reclamation stage: compared to the US, Germany, Canada, Brazil and Spain, where the rate of land reclamation is between 50% and 70%, the average rate of land reclamation in China is merely around 12% .

## 4 DISCUSSION

In order to test the model, a total of 52 iron deposits, both economic and uneconomic, were studied (Table 1). According to data of 52 iron mines, we contrast mine design capacity with actual mine capacity and design Figure 4 graphically illustrates the distribution of the deposits included in the study. The abscissa represents mine life, and the ordinate represents mine capacity. Curve ‘A’ shows large size deposits, Curve ‘B’ shows medium size deposits, Curve ‘C’ shows small size deposits. A total of 52 iron deposits, including 19 large size deposits and 26 medium size deposits and 7 small size deposits, are considered in the analysis. Determination of whether a known deposit was reasonable was based on having reported capacity and mine life and mine operating cost.

Through contrasting mine design data with actual data we get the result of exploration with the result of exploitation and reflect it graphically. On the graph a “blue” point represents a good-quality deposit, while a “red” point falls short of that quality. Based on the above analysis, we get 24 good quality deposits (including 8 large size, 14 medium size, and 2 small size), we will input the geological factors and economic factors into assessment software as study sample then we input factors about the rest of the deposits into assessment software to obtain results.

Table1 Data of 52 iron mines

| MINE | Design mine capacity (10000T/Y) | Actual mine capacity (10000T/Y) | Design Mine life (YEAR) | Design mine life (YEAR) |
|---|---|---|---|---|
| A1 | 300 | 300 | 40 | 46 |
| A2 | 110 | 100 | 16 | 71 |
| A3 | 600 | 500 | 5 | 52 |
| A4 | 220 | 150 | 25 | 65 |
| A5 | 250 | 250 | 21 | 55 |
| A6 | 600 | 470 | 33 | 66 |
| A7 | 50 | 45 | 15.24 | 36.44 |
| A8 | 700 | 251 | 40 | 56 |
| A9 | 100 | 111.69 | 32 | 43 |
| A10 | 500 | 150 | 27 | 37 |
| A11 | 400 | 27.3 | 50 | 51 |
| A12 | 700 | 700 | 25 | 25 |
| A13 | 590 | 269.5 | 26 | 26 |
| A14 | 400 | 150 | 48 | 48 |
| A15 | 1350 | 907.35 | 60 | 60 |

| | | | | |
|---|---|---|---|---|
| A16 | 460 | 460 | 58 | 56 |
| A17 | 1800 | 1058 | 25 | 17.4 |
| A18 | 300 | 550 | 53 | 39.5 |
| A19 | 500 | 408 | 87 | 69 |
| B1 | 70 | 70 | 7 | 53 |
| B2 | 80 | 26.75 | 22 | 58.91 |
| B3 | 50 | 50 | 27 | 63 |
| B4 | 50 | 38 | 16 | 36.2 |
| B5 | 72 | 87 | 21 | 34 |
| B6 | 40 | 35 | 40 | 50 |
| B7 | 50 | 38 | 26 | 35.6 |
| B8 | 230 | 120 | 27 | 36 |
| B9 | 28 | 60 | 23 | 30.5 |
| B10 | 50 | 41 | 25 | 32 |
| B11 | 50 | 56 | 48 | 54 |
| B12 | 40 | 33.89 | 17 | 22 |
| B13 | 100 | 96.3 | 20 | 23 |
| B14 | 65 | 44 | 18 | 21 |
| B15 | 70 | 96 | 20 | 21 |
| B16 | 110 | 110 | 10 | 10 |
| B17 | 73.8 | 82 | 35 | 35 |
| B18 | 140 | 84.7 | 44 | 44 |
| B19 | 30 | 55 | 18 | 17.2 |
| B20 | 60 | 74.48 | 29 | 26.46 |
| B21 | 70 | 75.75 | 24 | 21 |
| B22 | 30 | 100 | 28 | 23 |
| B23 | 50 | 70 | 23.17 | 18 |
| B24 | 50 | 55 | 28 | 21 |
| B25 | 90 | 10 | 25 | 17 |
| B26 | 40 | 53 | 62 | 50.73 |
| C1 | 5 | 5 | 16 | 53 |
| C2 | 100 | 45 | 20 | 33 |
| C3 | 30 | 20 | 30 | 30 |
| C4 | 30 | 20 | 13 | 13 |
| C5 | 10 | 4.5 | 20 | 20 |
| C6 | 20 | 20 | 20 | 20 |
| C7 | 20 | 50 | 20 | 15 |

## 5 SUMMARY

Mineral deposits are the products of various geological processes. The most common measure of geological quality is recoverable ore reserve tonnage and grade. Mineral deposits of the same deposit type have similar geological quality attributes. The key geological quality features of deposit types have been considered. Economic quality is a relative benchmark. The benchmark relevant to the present study is exploration success measured by the net present value. The higher the Net Present Value the better the quality of the deposit. Geological condition is complex in China (Pei *et al.*, 2001), there are so many type of iron deposit. Part of those deposits cannot be exploited, due to their processing and metallurgy characteristics, exploitation technology and disadvantage traffic condition and climate condition ore carry cost too high or climate is too bad. In the above discussion, we obtain a curve about reasonable exploration & exploitation, our study is still going on. We need to research more commodities and more deposits. We will test this model further and revise it.

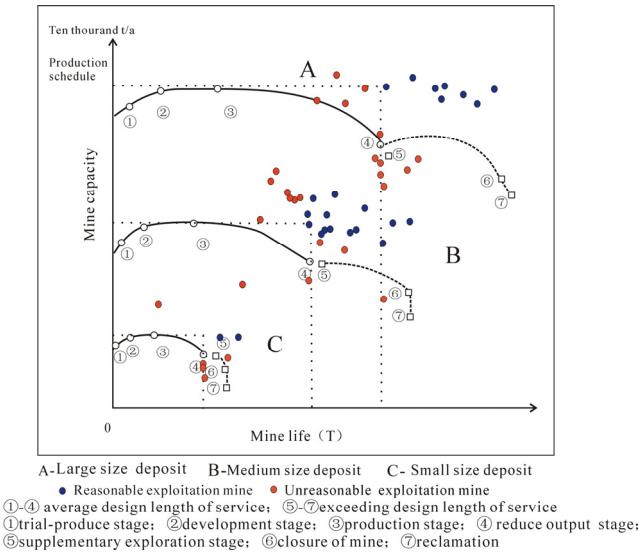


Figure 4 Instances of exploitation of iron mine

## ACKNOWLEDGEMENT

The study is supported by China prospect for mine about replacement resources exploration of crisis mines Project (2005110413). I would like to thank Prof. Pei for supporting my application to the Ph.D. program and his valuable guidance in setting up the technical, financial framework which has kept me on track.

## REFERENCES

Li Li, Zhang Changqing, Wang Yonglei. 2006. Sustainable Development of Mineral Resources, China. In: *The Symposium of National Deposits Conference*. Beijing: Geology Publishing, 846-849.

Zhao Pengda. 2000. Theories and methods of mineral exploration. Wuhan: Press of China *Univ. of Geosc*., 5-7, 24-25.

Pei Rongfu, Wu Liangshi, Xiong Qunxiao et al. 1994. Guidance of derivative deposits and tracing of metallogenetic path for prospecting concealed giant ore deposits. *Mineral Deposits,* 13:380-382.

Pei R F, et al. 1998. Metallogenic preferentiality and exceptional metallotect convergence of giant ore deposits in China. *Geol. Pub. House*, 262-284.

Pei R F and Xiong Q Y. 1999b. Hierarchy systematic metallogeny of a metallogenetic province and assessment of mineral exploration. In: Chen Y C, ed. Modern theories and methods on exploration and assessment of mineral resources. Beijing: *Seismological Press*. 134~142.

Pei R F. 2001. Geological assessment of mineral resources potential for hard_identified concealed large and rich ore deposits. *Beijing: Geol. Pub. House*, 72-75.

Meldrum A.H 2001. Mining in the 21st century: Making the grade and the survival of the fittest , Proceedings of the Joint Sixth SGA-SEG, Swets & Zeitlinger *Publishers Lisse, ISBN90,* 3-6

# Mineral Resource classification of the Sishen South Iron Ore deposits, South Africa

V. Lickfold, P. J. Mienie & L. Jacobs
*Kumba Iron Ore (Pty) Ltd*

ABSTRACT A confidence matrix was developed in order to determine the overall reliability of each deposit at Sishen South, Northern Cape, South Africa, based on both the quality and quantity of data used in the estimation process (geoscientific confidence) as well as the in-depth deposit-specific geological knowledge and an assessment of the risk associated with each deposit (risk rating). The resultant reliability index (related to the mineral resource classification category) is then a combination of the two components and essentially represents the geologists' overall understanding of the geological and grade continuity of that particular orebody; continuity here being the most important criteria for confidence in terms of the SAMREC classification of Mineral Resources. Geoscientific confidences of 77% and 34% have been determined for Leeuwfontein and Kapstevel, two of the Sishen South deposit. Risk ratings for the two deposits were determined as 15%. The Mineral Resource classification is then calculated by subtracting the risk rating from the geosceintific confidences to give a reliability, which corresponds to specific SAMREC Mineral Resource categories; Leeuwfontein is classified as an Indicated Resource whereas Kapstevel is classified as an Inferred Resource.

KEYWORDS: Geoscientific confidence, risk rating, resource classification

## 1. INTRODUCTION

Extensive iron- and manganese-bearing lithologies are exposed in a narrow north/south belt, between Sishen and Postmasburg in the Northern Cape Province of South Africa. Numerous shallow manganese and iron ore deposits were initially mined here from early 1900's until the 1930's. The landscape is dotted with abandoned workings along two sub-parallel ridges, which stretch from Beeshoek in the south to Sishen in the north. Other major iron ore occurrences in the region include the Sishen South deposits immediately south of the Beeshoek Mine.

Today this 'belt' provides the bulk of South Africa's iron ore needs and enables the country to be a major role player in the domestic and iron ore export market.

Current Mineral Resource and Ore Reserve estimates for the Sishen South deposits, which are the subject of a Feasibility Study for a 9 million tonne (Mt) per annum open pit operation, are shown in Table 1.

Table 1 The 2006 Mineral Resource and Ore Reserve estimates of the Sishen South iron ore deposits (Kumba Iron Ore Annual Report, 2006)

| Resource category | Tonnes (Mt) | Grade (%Fe) | Reserve category | Tonnes (Mt) | Grade (%Fe) |
|---|---|---|---|---|---|
| Measured | 156 | 65.4 | Proved | 134 | 65.4 |
| Indicated | 150 | 64.8 | Probable | 31 | 64.2 |
| Inferred | 67 | 62.9 | | | |
| **TOTAL** | **373** | **64.7** | **TOTAL** | **166** | **65.2** |

## 2. GEOLOGICAL SETTING

Iron ore at Sishen South is preserved in chemical and clastic sediments of the Proterozoic Transvaal Supergroup. These sediments define the western margin of the Kaapvaal Craton in the Northern Cape Province of South Africa.

The Transvaal Supergroup rocks overly a basement of Archaean granite gneisses and greenstones and/or lavas of the Ventersdorp Supergroup. In the Sishen – Postmasburg region, the oldest rocks of the Transvaal Supergroup form a carbonate platform sequence

known as the Campbell Rand Subgroup. The upper part of the Transvaal Supergroup comprises a banded iron formation unit, the Asbestos Hills Subgroup, which has been conformably deposited on the carbonates. The upper portion of the banded iron formation (Kuruman Formation, ) has, in places, been enriched to ore grade (*i.e.* Fe > 55%). The ores found within this formation comprise the bulk of the higher-grade iron ores in the region.

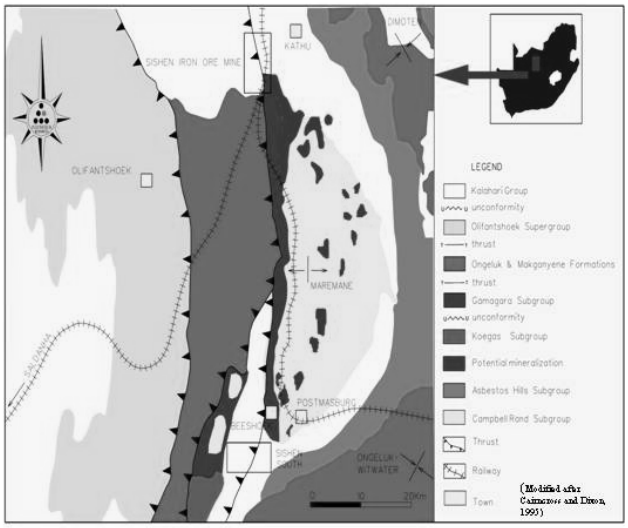


Figure 2 Location of the Sishen South iron ore deposits, Northern Cape Province, South Africa

A thick sequence of younger clastic sediments of the Gamagara Subgroup unconformably overlies the banded iron formations (). Some of the conglomerates comprise almost entirely hematite and are of lower-grade ore quality.

The stratigraphy has been deformed by thrusting from the west, which produced a series of open, north/south plunging, anticlines, synclines and grabens. Karstification of the dolomitic units took place prior to and after deposition of the iron formations. This process led to the development of several deep sinkholes (*e.g.* Leeuwfontein), which further complicate the structure of the Sishen South deposits.

Multiple episodes of supergene-enrichment and/or structurally-associated Fe-rich fluid movement through the banded iron formations are thought to have resulted in the development ore-grade Fe concentrations within the Kuruman and Gamagara Formation sediments comprising the Sishen South deposits.

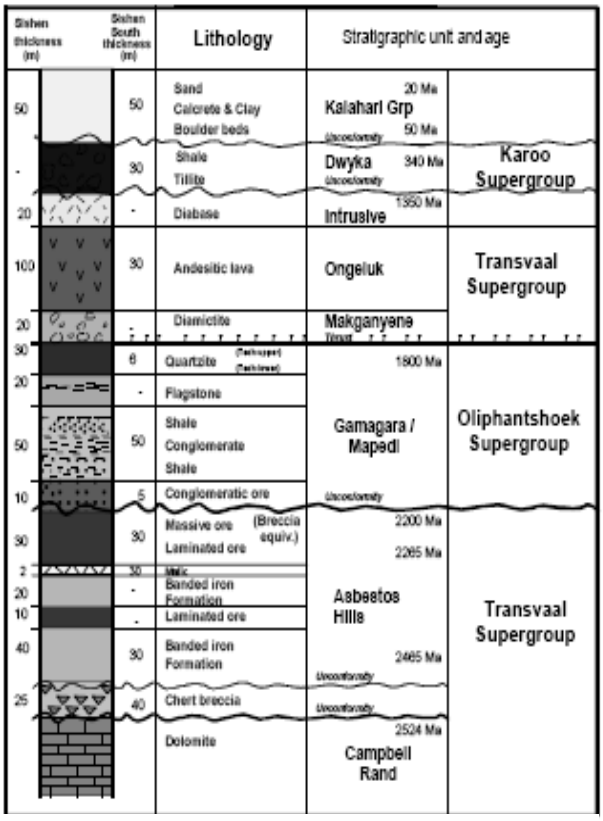


Figure 1 Stratigraphic columns of the rocks in the vicinity of the Sishen South iron ore deposits (after Cairncross & Dixon, 1995)

## 3. MINERAL RESOURCE ESTIMATION

### *3.1 Process overview*

Mineral resource estimation at Sishen South is largely based on drilling results. All exploration drilling data is stored in a relational database so that de-surveyed sample points can be used for estimation purposes.

The database is regularly validated and records kept of any errors that were highlighted and subsequently corrected. A final check of all data to be used for geological model building and subsequent block modelling is conducted when all exploration data has been captured immediately prior to the modelling.

Data is extracted from the database and imported into a sectional interpretation database from which geological cross-sections can be extracted and interpretation captured. Plots showing borehole and geological intersections are produced so that interpretation can be done and crosschecked in both directions with previous and following sections before being finally captured. Interpretations on the 50m-based sections are first made perpendicular to strike (east/west) and then confirmed parallel to strike

(north/south). Before these sections are transferred to the block-modelling step in the process, a final validation of geological solids produced, data and interpretation is conducted.

### *3.2 Geological data*

Based on the solids created during the geological interpretation and modelling stages, one-metre composite samples are prepared per rock type per deposit. The data are studied geostatistically and variography parameters determined for use in the block model.

The block model is set up with blocks roughly estimating the smallest mining unit, which in the case for Sishen South is 20m x 20m x 10m. Material type is assigned to each block according to the solids modelled in the geological interpretation (based on the centroid rock type) and blocks are defined as 'ore' or 'waste'. Grades are interpolated into the ore blocks using ordinary kriging and tonnages are estimated using the Fe grade and a well-established Fe%-density algorithm.

### *3.3 Mineral Resource classification*

#### 3.3.1 Drilling grid

Exploration at Sishen South was planned to increase the confidence of all the deposits to Indicated, based on the classification as described in the SAMREC Code (2000).

Until recently, geoscientific confidence at Sishen South was almost entirely based on the borehole spacing, which was designed according to the initial understanding of the geological and grade continuity of the orebodies. Based on this initial understanding, parts of orebodies covered by a borehole gird of ~200m were classified as Inferred, those of ~100m as Indicated and <100m as Measured. The geologist could downgrade part of a deposit in areas with greater than anticipated geological complexity or uncertainty.

Despite the drilling grid criteria forming the basis of the resource confidence categories at Sishen South, it is essence a clinical process that leaves little or no discretion to the geologist in terms of applying his/her knowledge of the local geology. It was therefore decided to incorporate the local knowledge of the different orebodies into the resource classification process by adding a confidence matrix.

#### *3.3.2 Confidence matrix*

A confidence matrix was developed in order to determine the overall reliability of each Sishen South deposit based on both data used in the estimation process as well as the in-depth deposit-specific geological knowledge. Although a subjective component, the matrix also incorporates a risk component, which allows a much greater interpretation of 'geoscientific confidence' than purely the drilling grid.

The 'geoscientific confidence' table appraises the *amount and quality* of the data available for the estimation process. Geological (mapping, borehole logging, co-ordinates, etc.); drilling (material recovery, potential contamination) and quality assurance – quality control (assay, geology and co-ordinate) and geostatistical data as well as validation and estimation process steps are evaluated (

Figure 3). Note that the low confidence here can be used to drive exploration in a specific direction so that status can be improved with new information.

| | | Leeuwfontein | | Kapstevel | |
|---|---|---|---|---|---|
| | weight | rating | score | rating | score |
| Geology | 25 | 2 | 5 | 6 | 15 |
| Drilling | 25 | 2 | 5 | 8 | 20 |
| Geophysics | 5 | 2 | 1 | 2 | 1 |
| Geotechnics | 10 | 2 | 2 | 8 | 8 |
| Groundwater | 5 | 2 | 1 | 8 | 4 |
| Sable database | 10 | 2 | 2 | 6 | 6 |
| Sectional data (GEMCOM) | 5 | 2 | 1 | 8 | 4 |
| Geostatistics | 5 | 8 | 4 | 8 | 4 |
| 3D resource modelling | 10 | 2 | 2 | 4 | 4 |
| | 100 | | 23 | | 66 |
| | | % confidence | 77 | % confidence | 34 |

| Confidence rating | |
|---|---|
| Perfect | 0 |
| Substantial | 2 |
| Sufficient | 4 |
| Some | 6 |
| Limited | 8 |
| None | 10 |

**Score**

Calculated by multiplying the weight by the rating and dividing it by 10, the rating to be applied if there was no information (and thus no confidence)

Figure 3 An example of a geoscientific confidence table

It can be seen from

Figure 3 that the weighting applied to geological information is higher than that for groundwater. Also, that for drilling information, there is more information for Leeufontein than there is for Kapstevel. The components adding to the overall 'confidence' number are rated so that the smaller the number (*e.g.* 5 *vs* 15 for Leeuwfontein *vs* Kapstevel for geology), the higher the confidence. The % confidence is calculated by subtracting the total score from 100, resulting in a 77% information confidence for Leeuwonftein and a 34% confidence for Kapstevel.

Figure **2** The risk table comprises a *risk assessment* for each orebody. It makes provision for deleterious elements, clay occurrence, stripping ratio, host rock, dewatering requirements, structural complexity, drilling method (different methods have different reliabilities in terms of

material representativity) and bulk density (Figure 4). It is clear from Figure 4 that despite the particular risks associated with each deposit specifically, the overall risk rating is the same (15%) for both Leeuwfontein and Kapstevel.

These are the risk areas critical for the Sishen South deposits and are thought to have a place in the 'geoscientific' confidence of the Mineral Resources that are classified. Each risk is weighted according to how significant it is to each deposit.

By combining the assessment of the amount and quality of the data available with the assessment of the local geological conditions, the confidence index is compared with the clinical drilling classification and the resource reliability downgraded accordingly, should the geoscientific confidence index not meet the specifications of the original drilling grid and estimated continuity for Inferred, Indicated and Measured Mineral Resources (Figure 6).

| Criteria | Rating | Criteria | Rating |
|---|---|---|---|
| **1 Stripping Ratio** | | **6 Structural complexity** | |
| <1 | 0 | Structurally not complex | 1 |
| 1 - 2 | 1 | Structurally complex | 2 |
| > 2 | 2 | Structurally very complex | 3 |
| **2 Groundwater** | | **7 QA/QC** | |
| low risk | 1 | low risk | 1 |
| Medium risk | 2 | Medium risk | 2 |
| High risk | 3 | High risk | 3 |
| **3 Host rock** | | **8 Drilling method** | |
| low risk | 0 | low risk | 1 |
| Medium risk | 1 | Medium risk | 2 |
| High risk | 2 | High risk | 3 |
| **4 Deliterious elements** | | **9 Bulk density** | |
| Lower than product quality std | 0 | low risk | 1 |
| Meets product quality std | 1 | Medium risk | 2 |
| Higher than product quality std | 2 | High risk | 3 |
| **5 Clay** | | | |
| No known clay occurences | 1 | | |
| Occur in insignificant amounts | 2 | | |
| Occur in significant amounts | 3 | | |

| Risk Rating | |
|---|---|
| 0 - 5 | 2% |
| 6 - 8 | 5% |
| 9 - 10 | 10% |
| 11 - 12 | 15% |
| >12 | 20% |

**Kapstevel**

| Risk | Rating | Comments |
|---|---|---|
| 1 Stripping Ratio | 2 | orebody occur at depth > 70m |
| 2 Groundwater | 3 | A substantial amount of groundwatering |
| 3 Host rock | 1 | Very limited info available |
| 4 Deliterious elements | 0 | Very low P, K and $SiO_2$ values |
| 5 Clay | 1 | Insignificant amounts of clay |
| 6 Structural complexity | 1 | No major problems with structural interpretations |
| 7 QA/QC | 1 | Refinement of system in progress |
| 8 Drilling method | 1 | Diamond drilling only |
| 9 Bulk density | 1 | Bulk density study completed |
| | 11 | |

**Leeuwfontein**

| Risk | Rating | Comments |
|---|---|---|
| 1 Stripping Ratio | 2 | Average depth of resource > 70m |
| 2 Groundwater | 1 | substantial dewatering info available |
| 3 Host rock | 1 | subvertical dips with gabbro in contact with iron ore |
| 4 Deliterious elements | 1 | Acceptable P, K and $SiO_2$ values |
| 5 Clay | 1 | Insignificant amounts of clay |
| 6 Structural complexity | 1 | No major problems with structural interpretations |
| 7 QA/QC | 1 | Refinement of system in progress |
| 8 Drilling method | 2 | Diamond drilling with limited percussion |
| 9 Bulk density | 1 | Bulk density study completed |
| | 11 | |

Figure 4 An example of an orebody risk assessment

The resultant confidence index (related to the mineral resource classification category) is then a combination of the two tables and essentially represents the geologists' understanding of the geological and grade continuity of that particular orebody; continuity here being the most important criteria for confidence in terms of the SAMREC classification of Mineral Resources. Overall classification is then calculated by subtracting the risk rating (15% in both cases) from the geoscientific confidences (77% and 34% respectively for Leeuwfontein and Kapstevel) and plotting these in the respective SAMREC categories (Figure 6).

| DRILL SPACING | CATEGORY | RELIABILITY |
|---|---|---|
| 200m x 200m | Inferred | 30% - 50% |
| 100m x 100m | Indicated | 50% - 70% |
| <100m | Measured | >70% |

Figure 5 Mineral Resource categories in terms of % reliability

It is thus clear from Figure 6 that Leeuwfontein can be classified as an Indicated Mineral Resource whereas Kapstevel can only be classified as an Inferred Mineral Resource when the geoscientific confidence is combined with the risk rating to establish an overall reliability for each deposit.

| Property | Geoscientific Confidence % | Risk Rating % | Reliability % | SAMREC Classification |
|---|---|---|---|---|
| Leeuwfontein | 77 | 15 | 62 | Indicated |
| Kapstevel | 34 | 15 | 19 | Inferred |

Figure 6 Overall classification based on the confidence matrix and drilling grid approach

### *3.3.3 Conclusion*

Mineral Resource classification at Sishen South has moved from the original drilling grid basis to include consideration of the amount and quality of the geoscientific data used for estimation purposes. It also comprises an assessment of the risk, or incorporation of the local, in-depth knowledge of the local geology, so that the overall reliability for each deposit is incorporated into the Mineral Resource classification.

## REFERENCES


Cairncross, B. and Dixon, R (1995). *In* Minerals of South Africa, Singapore 1995, 60p

*Kumba Iron Ore Annual Report* 2006 (see web for details).

SAMREC Code. *The South African mineral resource committee (SAMREC) under the auspices of the South African Institute of Mining and Metallurgy* (2000).

# Inferred Resource Estimation in the Navan Orebody

John H. Ashton
*Chief Mine and Exploration Geologist, Boliden Tara Mines Limited, Navan, Co Meath, Ireland.*

ABSTRACT: Resource estimation methodology used for the Navan carbonate-hosted Zn-Pb orebody is outlined. Over the last ten years, annual resource updates have allowed assessments of the accuracy of Inferred Resource estimates (based on widely spaced surface drilling), by comparison with Indicated Resources calculated from closely spaced underground drilling. This information is used to discuss the usage and applicability of JORC resource classification in an underground carbonate-hosted Zn/Pb mining operation.

KEYWORDS: Zn, Pb, inferred, indicated, resources, JORC, reconciliation.

## 1 INTRODUCTION

Boliden Tara Mines Limited currently mines 2.6Mtpy from Europe's largest Zn-Pb orebody at Navan, Co. Meath using underground open stoping techniques. The orebody is a Zn-Pb carbonate-hosted, faulted, stratabound base metal deposit that exhibits complex development of both sulphide textures and ore boundaries. Experience based on over 30 years of mining has led to an estimation system that uses stratigraphic slicing to estimate resources and is designed to model the stratabound, irregular nature of the ore.

Resource evaluation is largely based on diamond drilling information (Fig. 1). Initial, widely spaced (>80m spacing) surface drill holes are used to estimate Inferred Resources. Indicated Resources are estimated following the development of hanging-wall drifts and underground diamond drilling designed to give a hole spacing of the order of 20-25m.

Up to end 2006, some 65.5Mt grading 8.4% Zn, 2.0% Pb of ore had been mined and JORC classified Mineral Resources and Ore Reserves are tabulated in Table 1. The high tonnage of Inferred Resources contains material that will be mined over mine life but, under the JORC Code, is excluded from Ore Reserves. A mine life schedule is updated annually that comprises the Ore Reserves plus a conservatively scheduled and diluted portion of the Inferred Resources. An essential facet of this process is an understanding of the confidence levels and accuracy of the Inferred Resource estimates.

A relatively new section of the orebody developed to the southwest of the main orebody and extending to locally 1000m deep, is known

| **JORC Mineral Resources** (undiluted) | | | | **JORC Ore Reserves** (diluted, recoverable, scheduled) | | | |
|---|---|---|---|---|---|---|---|
| | **Mt** | **Zn %** | **Pb %** | | **Mt** | **Zn %** | **Pb %** |
| **Measured** | 0.7 | 5.0 | 3.0 | **Proven** | 3.9 | 9.3 | 2.0 |
| **Indicated** | 7.2 | 6.0 | 2.4 | **Probable** | 12.8 | 8.1 | 1.8 |
| ***Measured + Indicated*** | ***7.9*** | ***5.9*** | ***2.5*** | ***Total Ore Reserves*** | ***16.7*** | ***8.4*** | ***1.8*** |
| **Inferred** | 9.2 | 8.0 | 1.8 | The Ore Reserves are additional to the Mineral Resources | | | |
| ***Total Mineral Resources*** | ***17.1*** | ***7.0*** | ***2.1*** | | | | |

Table 1. JORC Classified Mineral Resources and Ore Reserves at Navan as of 31/12/2006.

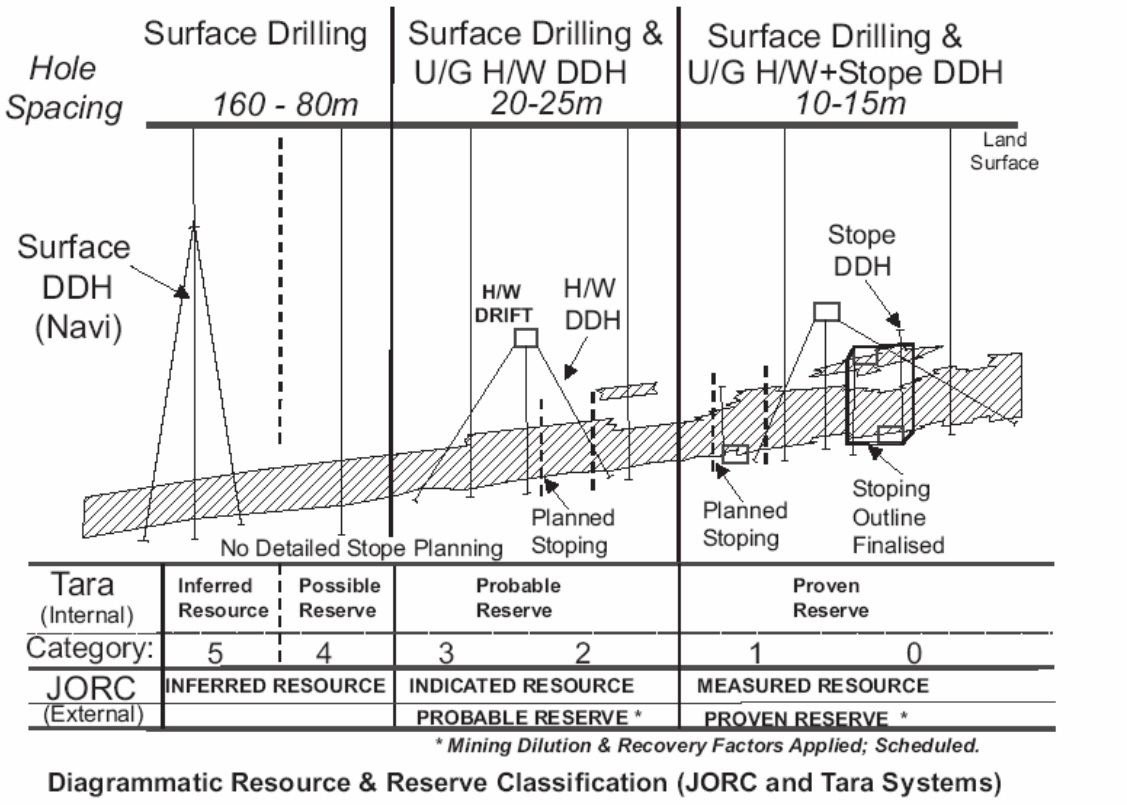


Figure 1. Schematic section showing resource and reserve classification schemes (in-house and JORC) used at Navan in comparison to diamond drilling density. The category number is an internal classification system designed to give detailed information in relation to confidence level of a resource.

as the South-West Extension (SWEX). This area comprises several stratabound ore lenses that have been upgraded from Inferred to Indicated Resources via annual campaigns of underground diamond drilling as mining has progressed southwestwards and down-dip, progressively delineating new mining blocks.

Regular assessment of trends in tonnage and grade losses/gains between Inferred and Indicated Resources in these mining blocks has been extremely useful in assessing the accuracy of Inferred Resource estimation and allows critical evaluation of JORC resource definitions.

## 2 GEOLOGICAL SETTING

The Navan orebody comprises a complex series of locally superimposed tabular, locally stratiform, but dominantly stratabound lenses of sphalerite, galena, pyrite and barite hosted by Courceyan-Chadian Carboniferous limestones (Ashton *et al.* 2003). The lenses are extremely complex on a local basis and display a range of textural styles ranging from disseminated and laminated to chaotic re-brecciated sulphides and vein/stockwork style mineralization (Anderson *et al.*, 1998). The lenses typically occur in calcareous horizons that are locally capped by impervious siltstones and dolomites with additional subtle controls resulting from the detailed petrography of the host limestones (Anderson *et al.* 1998, Ashton *et al.* 2003).

Distinctive sandstone, shale and silt horizons occur within the host rocks and define a series of marker horizons that are used for structural interpretation and as basis for assay compositing. In general the lenses dip to the southwest in conformity with the host stratigraphy at angles of around 15-20$^{o}$. The orebody is cut by several major northeast trending faults and a host of smaller structures.

## 3 RESOURCE ESTIMATION

Early resource estimation methods used at Navan comprised a system of manual selection of ore-grade intervals in drill holes and application of a type of inverse-distance weighting to arrive at block tonnages and grades. As the mine developed down-dip and production experience was gained it became obvious that this methodology tended to overestimate the tonnage and grade in areas where the mineralization was erratic in terms of thickness and grade.

Detailed reconciliation studies were per-

formed in the early 80's between various estimation techniques, applied at differing levels of drill-hole density. These confirmed that manual-selection of mineralized intersections for input to block interpolation methods was inadequate to deal with the highly irregular nature of parts of the orebody.

As a result of these findings and also for speed of calculation, a stratigraphic slicing system was introduced for the bulk of resource estimation at Navan. The system was designed in-house, with specialized geostatistical assistance from Mr A.G.Royle at Leeds University and after initial implementation on IBM and later VAX minicomputers is currently operational on a PC network.

Briefly the stratigraphic slicing system involves:

a) Reorganization of drill hole assays to form slice composite values. Particular slices in a hole are then stratigraphically equivalent to similar numbered slices in other holes.

b) Definition of the block size and shape required (40x40m square blocks for Inferred, maximum of 20x20m for Indicated).

c) Calculation of tonnages and grades for each slice in each block required (kriging or inverse distance interpolation). This is preceded by 2D search of slice composite data in each slice.

d) Selection of slice tonnages and grades for inclusion into resources based on cutoff criteria.

This system has worked well since its introduction in the early 1980s and manual controls on both slice composite location and selection of slices to form a resource are considered to be important elements in its operation (see also Ashton & Harte 1989, Annels 1991).

## 4 RECONCILIATION STUDIES

Rapid underground development of the SWEX section of the orebodies has taken place since 1995. Hanging-wall drifts mined above the ore lenses have been used for closely spaced diamond drilling to upgrade Inferred to Indicated Resources. Typically, diamond drilling spacing for Inferred Resources varies from 80x80m to 160x80m while underground drill spacing is of the order 20x20m.

Comparison between Inferred and Indicated Resources for identical areas in annual drilling campaigns gives an indication of the accuracy of Inferred Resource estimation. The following are the major conclusions:

a). Globally, Indicated Resources are higher in tonnage and grade than the Inferred Resources. This gives confidence in the accuracy of the method and also for preparation of long-term mining plans.

b) On a local mining block level (block tonnages ranging between ~0.2 and 1Mt), large changes in tonnages and grades are evident. These clearly show that widely spaced drilling does not give a good local estimate of tonnages and grades. Similar conclusions are evident from geological interpretation of the underground drilling that shows that in some places the surface drilling missed significant areas of high-grade ore whilst in others, surface drill ore intersections were not confirmed by underground drilling.

These results, while encouraging for long-term tonnage and grade forecasting purposes are not so useful for short to medium-term scheduling and underline the need for closely spaced diamond drilling well in advance of mining block development.

## 5 JORC CLASSIFICATION COMMENTS

The JORC classification system is a widely used and internationally recognized scheme for Mineral Resource and Ore Reserve classification. The scheme does not allow inclusion of Inferred Resources into Ore Reserves and thus creates difficulties for working mines in creating 'life of mine' schedules that are an essential part of any mining business plan.

The type of reconciliation study outlined above for the Navan orebody is if great use in incorporating Inferred Resources into long-term schedules because it creates a degree of confidence in the global accuracy of such figures. Additionally, the knowledge of the variability of Inferred Resources estimated for local mining blocks assists in confirmation that the correct confidence level classification of these resources is indeed Inferred, rather than Indicated.

## 6 CONCLUSIONS

Reconciliation studies between resources estimated for identical areas but based on differing drill hole densities is a powerful method of assessing the accuracy of the estimation methods employed.

These investigations also give valuable information for resource classification purposes

and in helping the geologist select the correct confidence level for JORC classification. Furthermore this type of information helps the mine planner to arrive at realistic long-term mining schedules and points to the requirements and timing of access development and infill drilling delineation activities.

ACKNOWLEDGEMENTS

Boliden Tara Mines Limited is thanked for permission to present this contribution. Mine Geology Department staff are thanked for their input to development of the resource estimation methods and reconciliation studies.

REFERENCES

Anderson, I.K., Ashton, J.H., Boyce, A.J., Fallick, A.E. and Russell, M.J. (1998) Ore Depositional processes in the Navan Zn-Pb deposit, Ireland. *Econ. Geol.*, 93, 535-563.

Annels, A.E. (1991) Mineral Deposit Evaluation a Practical Approach. *Chapman & Hall,* 436p. (Navan Case History).

Ashton, J.H., Holdstock, M.P., Geraghty, J.F.,O'Keeffe, W.G., Martinez, N., Peace, W. and Philcox, M.E. (2003) The Navan Orebody - discovery and geology of the South West Extension. In: *Europe's Major Base Metal Deposits,* Irish Association for Economic Geology, 405-436.

Ashton, J.H. and Harte, G. (1989) Technical computerisation at Tara Mines Ltd., Navan, Ireland. *Trans. Instn. Min. Metall. (Sect A: Appl. Min. industry),* 98, A85-97.

# Lisheen Mine: Lessons Learnt from the Development of the Mineral Resource and Ore Reserve Model from Discovery to Maturity

Leonardo P. Fusciardi [1], Dirk Harney [2], John F. Güven [2]

*[1] Anglo Base Metals, 1st Floor, 45 Main Street, Johannesburg 2001, South Africa*
*[2] The Lisheen Mine, Killoran, Moyne, Thurles, Co. Tipperary, Ireland*

ABSTRACT: The Lisheen orebody was discovered in April 1990. Over time information levels increased; starting with original step-out drilling, infill drilling to support a Feasibility Study, definition drilling to support operational planning and underground mapping and grade control to support day-to-day mining operations. Reconciliation at each step in the chain of information has enabled a series of learning experiences relevant to the Lisheen orebody and other orebodies where selective tabular mining is carried out. The lessons learnt focus on: managing unanticipated change in the mineral resource estimate; acquiring sufficient data to accurately forecast reserve modifying factors; correctly classifying mineral resources and ore reserves and communicating small scale changes in the geological model. They also point to the need for effective tactics during mine start-ups to manage the differences which inevitably arise between any estimate of mineral resources and ore reserves and the reality encountered during actual mining.

KEYWORDS: Lisheen, Resource Estimating, Classification, Mining Reserve, Dilution

## 1 INTRODUCTION

The Lisheen Mine is located 10km northeast of the town of Thurles, County Tipperary, Ireland (). The mine was discovered in 1990 by Chevron Mineral Corporation of Ireland and Ivernia West plc. In 1990, Anglo purchased Chevron's 50% interest, and in 2003, Anglo purchased the remaining interest from Ivernia West to take over 100% ownership of the property. Production commenced in September 1999 and the current mining reserve contains some 11.7Mt of ore grading at 12.45% zinc equivalent. Nominal production rates are 1.6Mtpa of ore and this is processed into approximately 345,000t of zinc and lead concentrates each year.

The orebody comprises discrete lenses of massive zinc and lead sulphide situated at depths ranging between 165m and 205m below surface (Figure **2**). The broad geometry favours the use of a combination of Room and Pillar, Drift and Fill and Long Hole mining methods. A trackless mechanised fleet is employed underground and broken ore is trucked to a central crusher and conveyed to surface via an access decline. A paste backfill plant facilitates secondary and tertiary mining. Zinc and lead concentrates are trucked to customised port facilities at the Port of Cork for shipping to

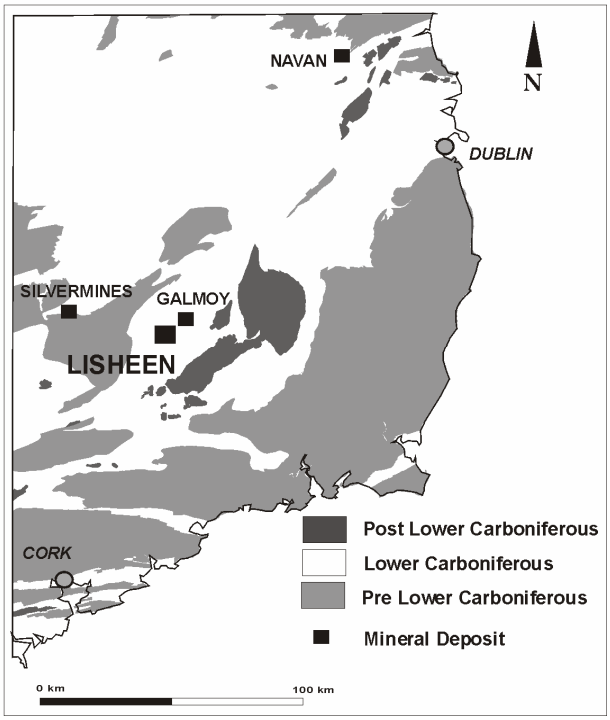


Figure 1: Location and Regional Geology

smelters in Europe and North America. Tailings are stored in a 78-hectare Tailings Management Facility.

## 2 PHASE 1: DISCOVERY

The orebody was discovered by Ivernia West plc on April 10th 1990 as part of a Joint Venture with Chevron Mining Corporation of Ireland. The outer limits of the orebody were largely defined between 1990 and 1993 by diamond drilling from surface and extensive campaigns of ground electromagnetic surveys. Minorco Ireland Ltd purchased Chevrons portion in 1993.

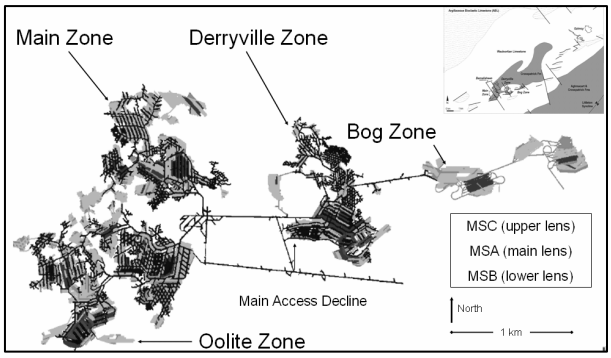


Figure 2 Lisheen mining layout

## 3 PHASE 2: FEASIBILITY TO CONSTRUCTION

Minorco carried out two infill drilling campaigns and published two resource estimates; one in 1995 for the project Feasibility Study, and another in 1999 to improve confidence in the areas scheduled for early mining. The estimation methodology was predominantly 2-dimensional. Drill intersects were composited on the basis of a minimum mining height of 3.0m with an additional 0.6m allowed for dilution. Two composites were generated if there was more than 5m separation between mineralized intercepts in a single drill hole. Composites greater than 4.5% zinc equivalent (Zn+Pbx0.5) defined the orebody and were included for resource estimating purposes. Vertical thickness and grade accumulations were kriged within the geological limits and this formed the basis for the pre-mining resource at Lisheen. Given that dilution had already been incorporated, the conversion to a mining reserve was based on using mostly room and pillar mining with an 85% extraction ratio.

Final permitting was granted in late 1997 and construction of the underground mine and surface facilities commenced shortly thereafter. Underground mine development was hampered by unanticipated water inrushes on the main decline however, despite this, production commenced on schedule in late 1999.

## 4 PHASE 3: START-UP OF OPERATIONS

The areas selected for initial mining were thick, high grade and geotechnically sound areas of east Main Zone and west Derryville Zone. The first exposures of the orebody led to several significant changes to the geological modelling and resource reserve estimating process. The key changes are as follows:

1. During mining, the orebody was seen to comprise of continuous massive sulphide lenses containing the majority of the metal, enveloped in a patchy (but often high grade) zone of disseminated mineralization. The 2D compositing approach had mixed these two different ore-types (as well as diluting waste) together leading to mis-interpretation of the geology and variograms with very high nugget effects.
2. Highly variable orebody elevations were predicted in the Feasibility, however, their impact during start-up when limited headings were available was greater than anticipated.
3. The “pinch and swell” nature of the orebody margins was in contradiction to that modelled using the 2D method of estimating where vertical thicknesses were kriged from the nearest hole to the ore boundary.

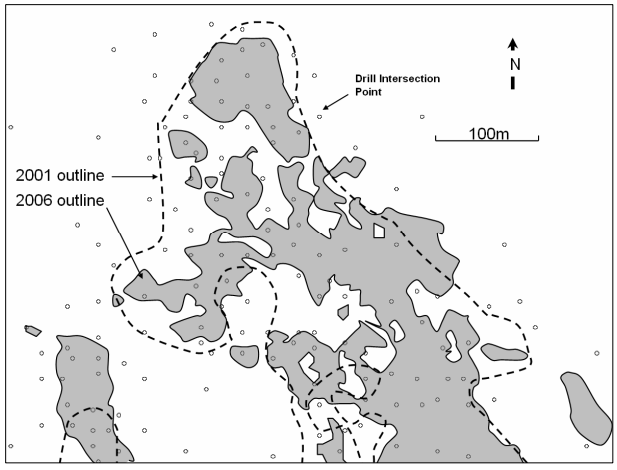


Figure 3 Plan of Derryville North demonstrating the presence of waste embayments and ore enclosures (solid shade) not picked up in the orebody defined by the original wide spaced drilling grid (dashed line)

4. Numerous small enclosures of waste were encountered between the pre-Feasibility drilling grid (Figure **3**). These regularly led to ore ton-

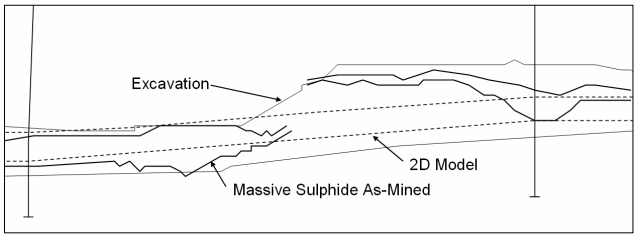


Figure 4 Section comparing 2D model with actual massive sulphide horizon. Illustrates that correlating economic composites was not geologically valid

nage losses. Following two years mining experience a discount factor for further unanticipated waste enclosures was added into all areas of Inferred resources remaining at Lisheen. This discount was finally removed in 2005 when the infill drilling of the orebody had been largely completed.

5. Despite identifying the differences between massive and disseminated ores, a mismatch between that defined as massive sulphide (criteria: >30% total Zn+Pb+Fe sulphides) using borehole assays, and that visually identified as massive sulphide by grade control technicians mapping underground exposures led to a 10% drop in volume in the geological wireframe in areas which used mapping information in the model. Following a detailed assessment, the criteria for defining massive sulphide was changed to >40% sulphide.

6. The 2D compositing methodology led to incorrect correlation between different lenses and portions of lenses. Headings designed to follow the ore horizon defined by adjacent 2D composites often passed into waste or migrated to the wrong elevations when it was discovered that the composites were unrelated ().

These changes and several other issues relating to mining design led to the implementation of the following leading practices in resource and reserve estimating:

- A change to 3D wire-framing and grade estimation and an attendant shift to 3D mine design
- Changing from 2D compositing using economic criteria to 3D compositing using geological criteria correctly separated the two ore types leading to improved definition of the main mining horizon and much lower nugget effects
- Use of Vulcans "tetra-modeling" software to estimate ore grades "in the seam" of the orebody, accurately modeling thickness variability and elevation differences
- Better geographical domain selection led to improved variography and local estimates
- Inclusion of penalty elements after improved understanding of the geology of penalty element zones
- Comprehensive checking added confidence to the estimate
- External and internal auditing led to a high level of defensibility of the resource and reserve model and accelerated the learning process
- Inclusion of a high level of underground mapping data (>9km of mapped drifts to date) in the wireframe gives accuracy for 2nd pass mining
- Regular updates of the geological model (26 versions since 2000) led to streamlining of the process

## 5 MINING HEIGHT AND DILUTION

The original design called for a 3.6m minimum mining height, inclusive of dilution. Actual mining experience demonstrated that this was insufficient due to the small scale rolling of the orebody footwall between lighthouse boreholes. This "longitudinal dilution" was incorporated by designing mining drifts with flat floors, each of 12m length. The 3D designs incorporated this additional dilution leading to a grade drop in the published reserve.

Further changes came in 2004 when, based on measurement of the "effective" working heights of the fleet, the minimum mining height was increased to 4.5m. The following year, based on increasing confidence in dilution records from grade control, a factor for unplanned dilution of 1.5% was added to the reserve bottom line. This was later increased to 3.0% and currently rests at 3.75%.

## 6 EXPLORATION AND GROWTH

An aggressive campaign of near-mine exploration took place between 2003 and 2005. Although two satellite lenses were discovered they were too far from the current workings to cover their waste access costs and they did not make it into the mining reserve. A parallel, near-mine programme of Category IV drilling also took place, resulting in two "rediscoveries". The first of these, Bog Zone, is a very high grade group of satellites which has added approximately 2 years to Lisheen's life. The second is the Oolite Zone, which despite

having reasonable grades has proven too complex and contains excessively high penalty element (Ni + Cu) levels and has not added significant tonnes to the mining reserve.

## 7 MATURITY AND OUTLOOK

The main issue which affects the resource going forward is removal resulting from sterilization of areas of the orebody as final pillars, remnants too small to be economically removed and areas which cannot be safely extracted for geotechnical reasons.

A key issue affecting the reserve issues is the ability to carry out pillar recovery and at the same time maintaining a high production rate.

A further complexity is optimising the balance between the volume of paste fill which can effectively be placed underground and the capacity of the tailings dam to store sufficient tailings for the remainder of the mine life. Economic and production modelling is being carried out to help select the optimal balance between these issues.

## 8 LESSONS LEARNT

1. There are so many decisions resting on the quality of the mineral resource that it is critical to get it right first time. This requires:

a. Adequate density of drilling information
b. Assimilation of a wide range of data, including grades, geometry, hydrogeology, geotechnical as well as geometallurgical information in the model – often there is a disproportionate amount of effort assigned to understanding grade distribution
c. Experience in interpreting the information in the context of real mining scenarios. This points to a need for operational geologists to be involved in the resource estimate from an early stage
d. Methods of simulating the heterogeneity of the orebody should be used – these include not only statistical simulation techniques but could also include detailed scenario planning discussions with discipline experts aimed at painting a picture of how the orebody will change on a daily, monthly and yearly basis.
e. A related point is that drilling information is often required earlier than anticipated. At Lisheen the infill drilling was scheduled over the LOM but was eventually completed in the first 5-6 years.
f. New information from mining needs to be assimilated and added in rapidly.
g. This requires experienced staff and consideration should be given to staffing the mine with extra resources for the start-up period, and less for the maturity phase. At Lisheen maturity was reached after about 5 years.
h. The geological model needs to be supported by academic research as well as encouraging mine geologists to take an interest in the genesis of the orebody. This leads to the best possible interpretation of the geological data collected and consequently to the best possible model.

2. Constantly updating the resource model is critical to accelerate the learning process and to ensure that key information is passed to mining and processing as soon as it is available.

3. Dilution requires careful consideration by experienced staff using benchmarking from other operations. A careful balance is required between realistic and over-comfortable targets. Real mining data is always required to defend the inclusion of unplanned dilution.

4. A comprehensive grade control effort is required to optimize the extraction of the planned resources and reserves. It is critical that grade control is organised to supply information (mapping etc) which can be used to improve the model, as well as providing guidance to production. Often the latter takes precedence. At Lisheen a good mix of geologists and technicians has allowed implementation of a higher level of complexity into this critical process.

## 9 ACKNOWLEDGEMENTS

Special thanks are due to Murray Smith (Technical Services Engineer) for assistance with reserve issues; Noeleen Fox (Geo-data analyst) for assisting with diagrams and to John Elmes (Technical Services Manager, Lisheen) and Duncan Campbell (VP Mineral Resource Evaluation, AAplc) for their leadership and contributions to the activities summarised in this presentation.

# Gold particle clustering and implications for sampling

S.C. Dominy
*Snowden Mining Industry Consultants Ltd, Weybridge, England and University of Ballarat, Victoria, Australia*

I.M. Platten
*Snowden Mining Industry Consultants Ltd, Weybridge, England*

ABSTRACT: Current research indicates that an enhanced coarse gold problem may be present in some gold deposits. This can be due to the presence of gold particle clusters that give the effect of individual coarse-gold particles and leads to a high Constitution Heterogeneity. Once a sub-sample is pulverized, the effect of the clusters may be removed if the individual gold particles making up the clusters are liberated. Thus any resulting pulp will tend to have a low variability, unless true coarse-gold particles exist. Clusters are readily recognized in coarse gold deposits where they accentuate existing high nugget effect and Constitution Heterogeneity. Clusters may however also occur in fine gold deposits where they produce an apparent coarse gold style. If clustered particles exist, then proper protocol design at the field and early laboratory stage is paramount. The sample characterization stage should include an assessment of possible gold particle clustering, in addition to the standard descriptions of the gold particle size distribution.

KEYWORDS: gold particle sizing, particle clustering, heterogeneity, sampling optimization

## 1 INTRODUCTION

The issues of sampling gold deposits, and particularly those bearing so-called 'coarse gold', are well documented (Royle 1989; Dominy *et al.* 2000; Dominy, Johansen & Annels 2001; Dominy, 2004; Dominy & Petersen 2005; Johansen & Dominy 2005).

The nugget effect reflects the proportion of total nugget variance present in a data set. Nugget variance comprises 'geological' and 'sampling' nugget variance (Dominy 2004; Platten & Dominy 2003). The sampling nugget variance is related to errors induced by inadequate sample size, preparation methods and analytical procedures. The sampling nugget variance component is not fixed, being related to the physical and chemical processes in sampling and analysis (Dominy 2007).

Gold deposits can contain a range of gold particles sizes from very fine (<30 μm), to fine (30-100 μm), through coarse (>100 μm) and very coarse (>2,000 μm).

At each end of the spectrum, the 'samplability' of a deposit ranges from relatively simple for fine-grained 'disseminated' mineralization, through to extremely difficult for very coarse 'nuggetty' mineralization. In reality, any single deposit may contain a proportion of both particle size groups.

The relationship between the coarse and fine gold fractions can be complex. In some cases they are consistently proportional, and elsewhere uncorrelated and related to different stages of mineralization.

The proportion of coarse gold has a direct impact on the effectiveness of sampling, where more coarse gold will require bigger samples and more specialized protocols (Dominy & Petersen 2005; Johansen & Dominy 2005). Optimized sample protocols are required to minimize sampling error and lower resource risk.

## 2 GOLD PARTICLES AND HETEROGENEITY

### 2.1 *Definition of Heterogeneity*

Part of the total sampling error results from heterogeneities within the sample under study. Heterogeneity can be defined as the condition of a lot under which all the contained 'elements' are not identical. In essence, all particulate materials are effectively heterogeneous.

The Constitution Heterogeneity (CH) of a lot is the heterogeneity that is inherent to the composition of each fragment or particle making up the lot. The greater the difference in composition between each fragment, the higher will be the CH. The CH is the cause of the Fundamental Sampling Error (FSE: Gy 1982), which occurs when a sample is selected from a lot. Gold ores can show very high heterogeneity, where relatively few rock fragments contain gold particles.

### 2.2 *Determining Heterogeneity*

Heterogeneity ($IH_L$ – Heterogeneity Invariant) can be determined via the 'Sampling Tree' or '50 Piece' experiment (Gy 1982; Dominy, 2004). In the coarse gold environment, these tests can understate the true ore heterogeneity (Dominy & Petersen 2005).

$IH_L$ is a numerical measure of how heterogeneous a sample lot is (*e.g.* representing the CH), having the dimensions of mass in grammes, and is inversely proportional to grade (Gy 1982). The fact that FSE is proportional to $HI_L$ leads to two conclusions. Firstly, it is necessary to rely upon precise estimation of the $HI_L$, and secondly, when a factor can take values ranging from <0.001 g to >20,000 g, it is important to determine its order of magnitude (Gy 1982).

## 3 CLUSTERING AND SAMPLING

### 3.1 *Clustering Scenarios*

The clustering of gold particles has been noted in a number of deposits studied by the authors. This can occur for both fine and coarse particles and in some instances both.

The gold clustering can occur in a number of general scenarios:

1. clustered coarse-gold only;
2. dominant clustered coarse-gold with minor fine gold;
3. dominant clustered fine-gold with rare coarse gold; and
4. clustered fine-gold only.

For scenarios (1 & 2), the clustered coarse gold particles lead to a high heterogeneity, most particularly in a low-grade deposit. Small-scale grouping of coarse particles on the cm-scale will increase the heterogeneity in rock fragments. In scenario (2), the presence of fine-gold has limited impact on the overall coarse-gold dominated ore heterogeneity.

In scenario (3), the clustering of fine-gold particles is material to the overall heterogeneity of the ore. The presence of coarse gold particles is likely to be non-material as they are rare.

Scenario (4) is the interesting case of clustered fine-gold particles. Deposits with disseminated fine-gold generally show a low $IH_L$. However, where the gold clusters into discrete groups, then the effective $IH_L$ is greater in coarse rock fragments.

### 3.2 *Sampling induced clustering*

An apparent clustering may also be developed during the sampling process in fine-gold systems. Samples that contain very narrow veins with a large mass of barren wallrock produce two populations of rock chips in RC holes and during initial crushing of cores. There will be a gold-bearing population and a gold-free population, which need to be effectively represented in any sub-sample.

## 4 IDENTIFICATION

### 4.1 *Mineralogical Study*

Identification of gold particle clustering can only be gained through observation of drill core, rock samples, etc. Extensive mineralogical studies as part of wider paragenetic and geometallurgical work are required.

Studies involving metallurgical samples to determine gold particle sizing will give a false measure of heterogeneity as they do not allow for the spatial distribution (hence clustering) of gold particles. Highly localized 'niche' samples taken from specific geological domains may provide particle sizing for clustered zones, but again will not permit the nature of the clusters to be determined.

In coarse gold deposits, clustering can be more easily recognised and should be reported in face and core logs in addition to gold grain size data. This allows factoring of clustering into sampling protocols at an early stage. Recognition is intrinsically more difficult in fine-gold settings but evidence of clustering from thin and polished section studies should be reported if recognised.

A key issue in the identification of clustering is the determination of individual particle size and the number of particles in 3D space. At best this process is somewhat subjective, and based on the skilled assessment of the specialist. Further research on this matter is underway.

### 4.2 *Assay Variability Analysis*

Where fine-gold particles cluster, there will generally be high-assay variability in field samples. However, once a sub-sample is pulverized, the effect of the clusters is removed as the individual fine-gold particles making up the clusters are liberated. Any resulting pulp will tend to have a low variability. If coarse-gold particles exist in addition to fine-gold, then pulp variability will remain high. Screen fire assay of pulp provides an effective method for checking for coarse-gold.

## 5 EFFECTS ON HETEROGENEITY

### 5.1 *Introduction*

A commonly applied tool to optimize sampling protocols is Gy Sampling Theory (Gy 1982). This theoretical approach allows the FSE to be calculated for each stage of the sampling process.

The key input into the calculation is the value of $IH_L$ for each sampling stage. A theoretical example is presented on the effects of coarse- and fine-gold clustering on the value of $IH_L$ (Tables 1 & 2). The global grade is assumed to be 2.5 g/t Au and the nominal particle size is 1.2 cm (RC chippings).

Table 1. Coarse-gold scenario.

| Non-clustered | |
|---|---|
| Particle size | 1,000 µm |
| $IH_L$ | 32,000 g |
| **Clustered** | |
| Apparent clustered size | 2,200 µm |
| Particles making up cluster | 10 |
| $IH_L$ | 105,000 g |

Table 2. Fine-gold scenario.

| Non-clustered | |
|---|---|
| Particle size | 50 µm |
| $IH_L$ | 360 g |
| **Clustered** | |
| Apparent clustered size | 185 µm |
| Particles making up cluster | 50 |
| $IH_L$ | 2,500 g |

For the clustered data, the apparent particle size is based on 'merging' all particles as if they were one single particle. Tables 1 and 2, show the increased $IH_L$ value with particle clustering.

The coarse-gold scenario shows a high $IH_L$ with a single particle, and further heterogeneity with clustering. The fine-gold scenario is non-problematic with a low $IH_L$ value unclustered, but with clustering shows a much higher $IH_L$.

### 5.2 *Clustering and RC Sampling*

RC drilling produces potentially 40 kg to 50 kg of sample per metre drilled. Based on Gy Sampling Theory the mass of sample to be taken from a lot of 1.2 cm chippings can be calculated for a specific confidence interval. For the two scenarios given in Section 5.1, Table 3 shows the required sample mass that needs to be taken from the RC chipping to achieve a FSE of ±15% (68% confidence level).

Table 3. Masses of sample required to achieve a FSE of ±15% at a 68% confidence level from a 1 m composite of RC chippings. Same scenarios used as in Tables 1 & 2.

| Coarse-gold scenario | |
|---|---|
| Single particle | 1,400 kg |
| Clustered particles | 4,500 kg |
| **Fine-gold scenario** | |
| Single particle | 16 kg |
| Clustered particles | 113 kg |

In Table 3 the effect of particle clustering on sample size can be seen. In addition, it shows the general challenge of collecting field sub-samples from RC chippings in the presence of coarse-gold and at a low-grade. In many cases the theoretical sample size is much greater than the actual composite. Table 4 gives the FSE value for each gold particle scenario based upon a 40 kg RC interval and splitting off a 5 kg field sub-sample for submission to the laboratory.

Table 4. FSE values of splitting 5 kg field sub-sample from 40 kg primary RC field sample for a low-grade 2.5 g/t Au deposit. FSE reported at the 68% confidence level. Same scenarios used as in Tables 1 & 2.

| Coarse-gold scenario | |
|---|---|
| Single particle | ±237% |
| Clustered particle | ±428% |
| **Fine-gold scenario** | |
| Single particle | ±25% |
| Clustered particles | ±67% |

Table 4 shows clearly the extreme FSE values gained when extracting a sub-sample from the primary composite. All FSE values are unacceptably high. The precision required for a sample protocol should be better than ±15%, at the confidence level deemed appropriate.

The coarse-gold scenario gives a very high $IH_L$, the processing by gravity of the entire drill composite must be considered. Any splitting of the sample will yield a high FSE. If only clustered fine-gold is present, then once the gold is

liberated the $IH_L$ drops since the apparent clustered particle size no longer exists. Fine crushing of the entire sample to P90 -2 mm and then taking a 5 kg sample will reduce the FSE to an acceptable ±18%.

### 5.3 *Clustering and other Sample Types*

Similar effects of high FSE can be seen in core samples. Once the core has been crushed, then a sub-sample is required for pulverization and assay. Table 5 shows FSE values for sub-sampling crushed core, with high results for all samples except the single-particle fine-gold scenario.

Table 5. FSE values of splitting a 1 kg sub-sample from a crushed (P90 -2mm) full HQ core (8.5 kg) for a low-grade 2.5 g/t Au deposit. FSE reported at the 68% confidence level. Same scenarios used as in Tables 1 & 2.

| Coarse-gold scenario | |
|---|---|
| Single particle | ±140% |
| Clustered particle | ±250% |
| **Fine-gold scenario** | |
| Single particle | ±15% |
| Clustered particles | ±39% |

In many high-nugget systems an approach taken to estimate grade is via bulk sampling or trial mining (Dominy *et al*. 2001; Dominy & Petersen 2005). The splitting of broken development rock 'lots' into sub-samples for processing and assay can yield substantial FSE. As with other sample types, any clustering needs to be accounted for during protocol design.

A lot of broken development round containing coarse clustered-gold (Table 1) will need to be crushed to P90 -1 cm before taking a 3,000 kg sub-sample. Without crushing the entire lot, the sub-sample required is closer to 100 t.

## 6 CONCLUSIONS

The authors have shown that clustering can have a significant impact on sampling protocols, particularly during the early stages of sampling broken rock. Any new sampling programme must be accompanied by the full characterization of ore types to determine gold particle sizing, distribution and possible clustering. The authors stress the need for geological control of all sampling programmes to achieve reality.

## REFERENCES


Dominy SC (2004) Fundamental sampling error and its relationship to the nugget effect in gold deposits. In: *Proceedings of the Mining and Resource Geology Symposium 2004*. EGRU Contribution No 62: 30-45 (James Cook University, Townsville)

Dominy SC (2007) The importance of correct sampling and assaying practices: case studies from selected gold projects. In: Proceedings of the 9th Biennial SGA Meeting. *This volume* (Millpress, Rotterdam)

Dominy SC, Johansen GF, Annels AE, Cuffley BW (2000) General considerations of sampling and assaying in a coarse gold environment. *Trans Inst Min Metall* 109: B145-B167.

Dominy SC, Johansen GF, Annels AE (2001) Bulk sampling and its role in the grade evaluation of free gold-bearing quartz reefs. *Trans Inst Min Metall* 110: B176-B191.

Dominy SC, Petersen JS (2005) Sampling coarse gold-bearing mineralisation – developing effective protocols and a case study from Southern Greenland. In: *Proceedings of the Second World Conference on Sampling and Blending 2005,* 151-165 (AusIMM, Melbourne).

Gy PM (1982) *Sampling of Particulate Materials – Theory and Practice.* Elsevier Scientific, Amsterdam pp431.

Johansen GF, Dominy SC (2005) Development of sampling protocols at the New Bendigo Gold Project, Australia. In: *Proceedings of the Second World Conference on Sampling and Blending 2005*, 175-183 (AusIMM, Melbourne).

Platten IM, Dominy SC (2003) The occurrence of high-grade gold pockets in quartz reefs at the Gwynfynydd Mine, Wales, UK: A geological explanation of the nugget effect. *Explor Min Geol* 10: 249-272.

Royle AG (1989) Splitting gold assay pulps containing coarse gold particles. *Leeds Univ Mining Assoc Journ* 1989: 63-68.

# GOLD METALLOGENESIS:
# EUROPE & ASIA

EDITED BY:
GEORGES BEAUDOIN
GREGOR BORG

# Evidence for syngenetic gold in a world-class "orogenic" gold deposit: textures and LA-ICPMS trace element geochemistry of pyrite in Sukhoi Log, Siberia

Ross R. Large, Leonid V. Danyushevsky & Robert J. Scott
*CODES ARC Centre of Excellence in Ore Deposits, University of Tasmania, Private Bag 79, Hobart, Tasmania 7001*

Valery V. Maslennekov
*Institute of Mineralogy, Russian Academy of Sciences, Urals Branch, Miass, Russia*

ABSTRACT: LA-ICPMS trace element analyses on pyrite from the giant sediment-hosted Sukhoi Log deposit indicate that the early syngenetic and diagenetic pyrite 1 (py1) and pyrite 2 (py2) are enriched in lattice-bound gold and a suite of other trace elements (Mo, Sb, Ni, Co, Se, Te, Ag, Cu, Pb, Zn, Mn, Ba, Cr, U, V) which are similar to those metals concentrated by organic processes in euxinic sedimentary environments. Later generations of pyrite, from py3 to py5, including pyrite in bedding parallel quartz veins, contain progressively lower contents of lattice-bound gold and most other trace elements. However these syn-metamorphic and post-peak metamorphic pyrites contain micro inclusions of free gold, pyrrhotite, sphalerite and chalcopyrite. The paragenetic textural and chemical relationships at Sukhoi Log suggest that gold was initially introduced during sedimentation of the organic-rich shales and fixed during diagenesis within the structure of diagenetic arsenian pyrite. Subsequently, accompanying metamorphism, the gold was released from the diagenetic pyrite to become concentrated as free gold and gold tellurides within metamorphic pyrites and bedding-parallel pyrite-quartz veins.

KEYWORDS: sediment-hosted gold, orogenic gold, gold in pyrite, Sukhoi Log

## 1 INTRODUCTION

Sukhoi Log is a world-class sediment-hosted gold deposit, containing over 50 million ounces of gold at an average grade of about 2 g/t Au (Wood & Popov 2006; Goldfarb *et al.* 2005; Distler *et al.* 2004). The deposit is hosted by Neoproterozoic organic-rich sediments, located in the Lena Goldfield, a major alluvial gold district, on the eastern margin of the Siberian Craton, 850km north east of Irkutsk (Fig.1). The Sukhoi Log deposit is one of the world's largest undeveloped gold resources, however a small open cut mine, Zapadny, at the western end of the main deposit, commenced operations in 2005. The main gold resource at Sukhoi Log is hosted by pyritic black shales and siltstones in the core of an overturned anticline. Gold mineralization occurs both within the pyritic shales and in thin bedding-parallel pyrite-quartz veins which have been folded by the main deformation.

There has been considerable debate about the origin and timing of gold mineralization at Sukhoi Log (Yakubuchuk *et al.*, 2005). Genetic models vary from syngenetic to orogenic and/or granite- related (Buyak 1982; Buyak & Khemelevskaya 1997; Wood & Popov 2006; Goldfarb *et al.* 2001; Distler *et al*. 2004)

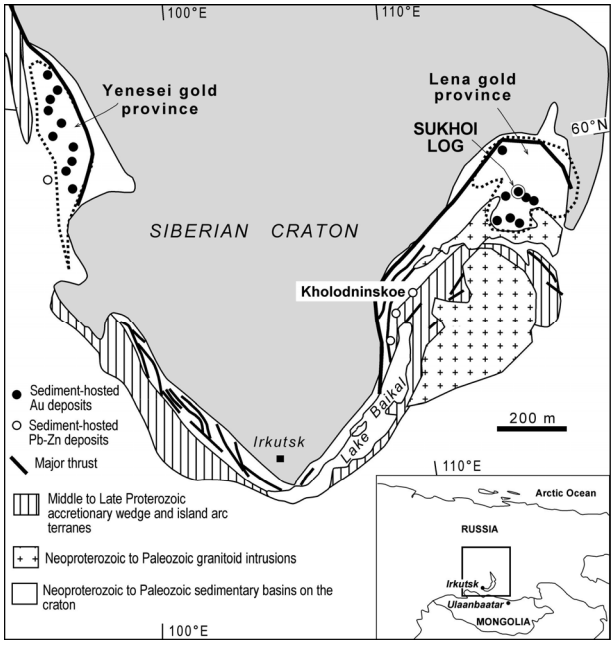


Figure1: Location of Sukhoi Log (after Yakubuchuk *et al.* 2005)

Petrographic study of over fifty polished mounts of ores and host rocks at the Sukhoi Log has revealed a multi-stage origin for both the pyrite and gold. This detailed study shows that the genesis of the gold ores involved at least five major stages of pyrite growth; denoted py1 to py5, in interpreted paragenetic order.

## 2 PYRITE PARAGENESIS

Py1 is very fine-grained pyrite concentrated in layers parallel to bedding, or as nodular concretions within the black shales. A zone of bedded semi-massive py1 in drill hole C1 is very similar to the pyritic facies found in SEDEX Zn-Pb deposits. Under the microscope, py1 commonly forms framboid-like clusters of pyrite euhedra from 30 to 100 microns across (Fig. 2a). Py1 is interpreted to be syn-sedimentary or early diagenetic in origin, similar to framboidal pyrite common to many black shale sequences.

Py2 is commonly associated with py1 and consists of clear euhedral pyrite from 20 to 300 microns across that appears to overgrow and surround py1 clusters. Py2 is interpreted to be early diagenetic and may form by the recrystallisation of py1 or by overgrowth on initial py1 clusters or framboids.

Py3 is coarser grained (0.2 to 5mm diameter) subhedral to euhedral pyrite developed commonly in sandstone bands within the black shale (Fig. 2b). Py3 contains abundant unoriented inclusions from 1 to 100 microns across of sediment matrix or minor sulphides; in particular pyrrhotite, chalcopyrite and sphalerite. Etching with nitric acid reveals the internal fabric of the pyrite, and indicates that py3 forms by replacement of the detrital and matrix sediment components. A weak fabric in the sandstone host is preserved in the internal pyrite structure in some samples, suggesting that py3 possibly developed during late diagenesis or early D1 deformation.

Py4 forms coarse isolated euhedra up to several cms across within the mudstone and shales. The py4 euhedra commonly show well developed quartz pressure shadows and a strong internal fabric of aligned inclusions parallel to the main D1 fabric developed in the shales. Etching reveals that py4 has replaced all detrital and matrix sedimentary components, and inherits the complete structural fabric of the sediments, including veining and folding (Fig. 2c). These features suggest that py4 developed late in the deformation history of the shales. Free gold is

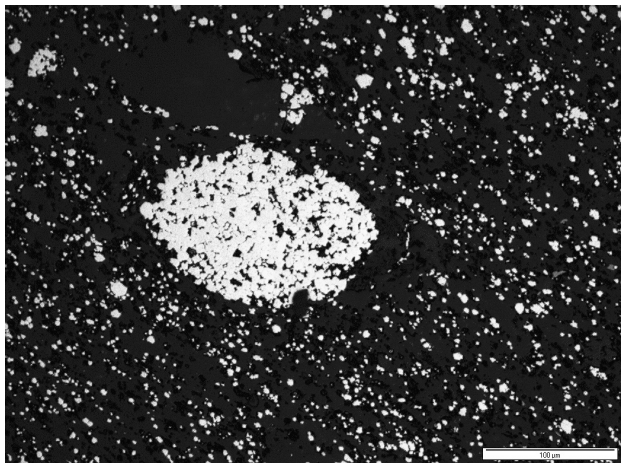


2a) Syngenetic or early diagenetic py1; mean Au = 3.3 ppm

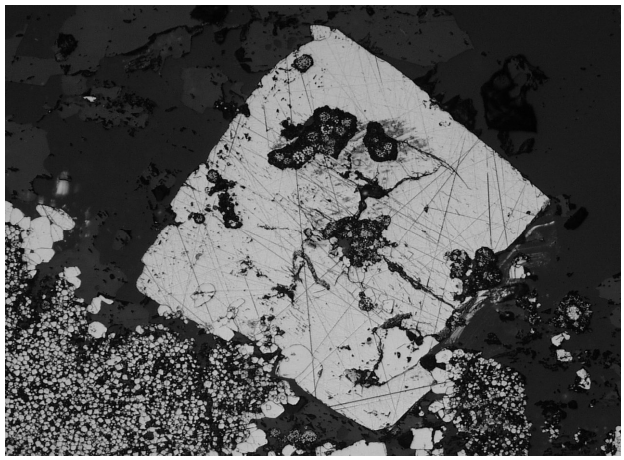

2b) Late diagenetic py3 euhedra (0.17 ppm Au) overgrowing framboidal early diagenetic py1 (6.6 ppm Au)

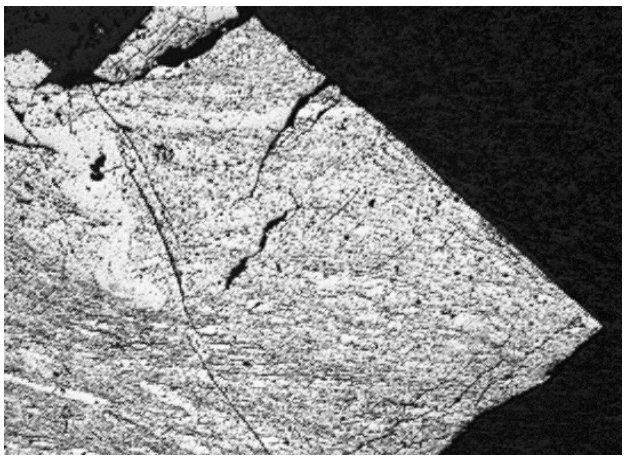

2c) Late metamorphic py4; etching by HNO3 has revealed that py4 has overgrown the metamorphic fabric in the black shale host (mean Au = 0.05 ppm Au)

Figure 2. Textures of Sukhoi Log pyrite

present within inclusions and cracks in py3 and py4.

Py5 is a clear featureless pyrite, which has very few inclusions, and commonly overgrows previous py3 and py4. Py5 is also present in veins cutting py4, where open space growth textures are evident. Py5 is the most common pyrite type within bedding-parallel quartz veins, where it commonly forms a thick rim surrounding cores of py3 and py4. Py5 is synchronous with bedding-parallel quartz vein development.

Pyrrhotite is commonly present in assemblages containing py4 and py5. It is interpreted as syn-metamorphic, concentrated within the reduced black shale facies, by replacement of earlier stages of pyrite. The paragenesis of arsenopyrite is yet to be determined, but initial work suggests two stages, one between py2 and py3 and a second post py4/5.

A preliminary sulphide and gold paragenesis is indicated by our textural studies. During sedimentation and diagenesis, py1 and py2 form in the black mudstones under anoxic conditions, by microbial reduction of sulphate from seawater. Py3 forms during late diagenesis and early metamorphism and deformation, due to preferential fluid flow in sandstone layers within the mudstone sequence. Later in the main deformation event, py4 forms within the black shales, overprinting the main deformation fabric. Pyrrhotite, plus minor chalcopyrite and sphalerite occur throughout the period of py3 and py4 development. Toward the end of the main deformation phase, py5 overgrows py3 and py4, and is synchronous with bedding parallel quartz vein growth.

## 3 LA-ICPMS ANALYSES OF PYRITE

Preliminary LA-ICPMS analysis of the five major stages of pyrite at Sukhoi Log was undertaken to determine gold and related trace element associations of each pyrite stage. This research aimed to answer the following key question: "was gold introduced during sedimentation and diagenesis; or later during deformation; or at both times?"

Over 210 spot analyses of pyrite were undertaken on selected samples from the ore bodies at Sukhoi Log and Zapadny and from their surrounding pyritic halos. The earliest formed diagenetic py1 is rich in a wide range of trace elements. Gold content varies from 0.44 to 12.1 ppm with a mean of 3.3 ppm (Fig. 3). Arsenic varies from 180 to 14,000 ppm with a mean of 1900 ppm . Pb content is high (mean 230 ppm) and Ni/Co >1. Late diagenetic py2 has a similar geochemistry to py1, but with generally higher As (mean 4260 ppm), higher Ni/Co ratio, and lower Pb (mean 80 ppm). Au content of py2 varies from 0.02 to 13 with a mean of 1.02 ppm (Fig. 3). Au and Tl show a strong positive correlation.

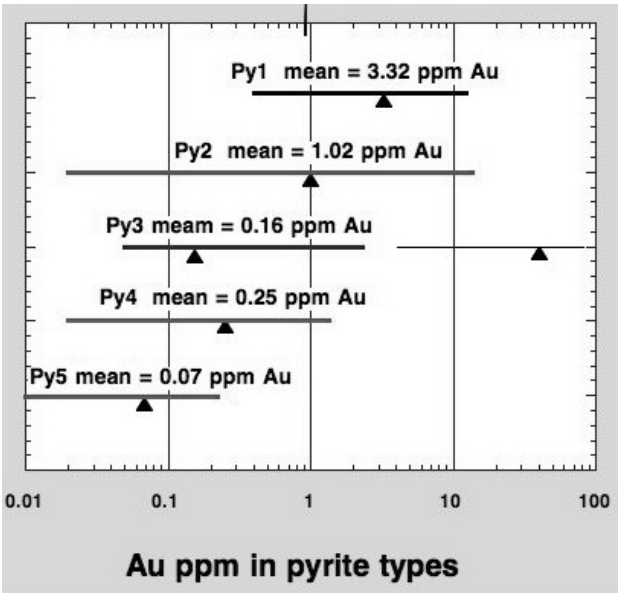


Figure 3. Range and mean content of lattice-bound gold in the five pyrite types at Sukhoi Log, determined by LA-ICPMS.

Although the syn-deformation py3 and py4 may contain microscopic grains of gold, the pyrite itself is depleted in gold compared to earlier py1 and py2. Py3 has a mean gold content of 0.16 ppm, compared with py4 with a mean of 0.25 ppm Au (Fig. 3). Py4 (hosted in shale beds) commonly display high Co/Ni ratios and higher contents of As, Au, Sb and Te compared to py3 (hosted in sandstone beds) which display higher contents of Cu, Zn, Mo and Ba. The most obvious chemical difference between the metamorphic pyrites (py3 and py4) and the diagenetic pyrites (py1 and py2) is that the former contain higher levels of titanium (means of 1200 ppm compared to 150 ppm). Also the metamorphic pyrites have lower Ni and Ba but higher Bi and Te than the diagenetic pyrites.

The post-peak metamorphic py5 is depleted in most trace elements compared to the earlier formed pyrites. Although As rich, py5 contains the lowest levels of gold with a mean of 0.07 ppm Au (Fig. 3). Pyrrhotite, which forms during metamorphism by replacement of py1 and py2 contains no gold, with a mean value of 0.002 ppm Au.

## 4 DISCUSSION AND CONCLUSIONS

The textures and LA-ICPMS geochemistry suggest a multi-stage genesis of pyrite and gold at Sukhoi Log. The early diagenetic pyrites have a Au-As association with high Pb and low Bi, whereas the late metamorphic pyrites have a Au-Te association with low Pb and high Bi and Ti. It is proposed here, that all the gold was introduced to the Sukhoi Log system during sedimentation and early diagenesis, now present within py1 and py2. During metamorphism and deformation the majority of the gold present in the earlier arsenian py1 and py2 was solubilized and concentrated in late diagenetic to metamorphic pyrites py3 and py4 as free gold and gold tellurides. Te and Bi, which we commonly regard as magmatic elements, may have been sourced from the organic-rich sediments.

This multi-stage process of gold concentration was probably critical to the formation of the Sukhoi Log deposit. An early stage of syn-sedimentary and diagenetic gold-pyrite deposition (py1 & py2) was following by syn-metamorphic up-grading, with location of the higher grade gold within py3 & py4 in the anticlinal core of the deposit. Other black shale-hosted "orogenic gold" deposits (*e.g*. Kumtor, Muruntau, Zarmitan, Amantaitau, Natalka, Nezhdaninskoye, Bakyrichik and Macreas Flat) may have a similar multi-stage origin that commenced with syngenetic gold accumulation in black shales.

## ACKNOWLEDGEMENTS

This research was supported by funding from the Australian Research Council by way of an ARC Centre of Excellence grant to RRL and RJS. Thanks to the Lena gold Mining Company in particular Chief Geologist Vladimir Martynyuk and deputy Valery Benedyk for providing valuable assistance and access to the drill core from Sukhoi Log, and to Ekaterina Evlapova, Chief Geologist of the Sukhoi Log Mining Company, for access to the Zapadny open cut mine. Thanks also to Eugene Sklyarov, Director of the Institute of Earth and Tectonics in Irkutsk, and to the late Adrianne Sntsov, Vladimir Simonov and Oktyabrin Sadyrov for providing assistant for the Sukhoi Log field visit, sampling and sample despatch. The LA-ICPMS analyses at UTAS would not have been possible without the excellent guidance and help of Sarah Gilbert. Bryce Wood first alerted RRL to the potential syngenetic origin at Sukhoi Log, for which the senior author is most grateful.

## REFERENCES

Buryak VA (1982) Metamorphism and ore formation: *Moscow*. *Nedra,* 256 pp(in Russian)

Buryak VA, Khmelevskaia NM (1997) Sukhoy Log, one of the greatest gold deposits in the world: genesis, distribution patterns, prospecting criteria. *Vladivostok: Dalnauka*, 156 (in Russian).

Distler VV, Yudovskaya MA, Mitrofanov GL, Prokof'ev VY, Lishnevskiy EN (2004) Geology, composition and genesis of the Sukhoi Log noble metals deposit, Russia. *Ore Geology Reviews* 24: pp 7-44

Goldfarb R, Groves DI, Gardoll S (2001) Orogenic gold and geologic time: A global synthesis. *Ore Geology Reviews* 18:1-75

Wood BL, Popov NP (2006) The giant Sukhoi Log gold deposit, Siberia. *Russian Geology and Geophysics* 47(3): pp 315-341

Yakubchuk AS, Shatov VV, Kirwin D, Edwards A, Tomurtogoo O, Badarch G, Buryak VA (2005) Gold and base metal metallogeny of the central Asian orogenic supercollage. *Econ Geol 100th Anniversary Volume*, pp 1035-1068

# Types of gold mineralization at Suzdal sediment-hosted gold deposit in East Kazakhstan

K.R. Kovalev, E.A. Naumov, Yu.A. Kalinin, I.G. Tretjakova, A.S. Borisenko & M. Kolesnikova
*Institute of Geology and Mineralogy of the RAS, Novosibirsk, 630090, Russia*

ABSTRACT: The Suzdal gold-sulphide deposit, characterized by fine gold hosted in Carboniferous-aged carbonaceous-terrigeneous-carbonate lithologies, is located in the Kalba gold-bearing belt in the eastern Kazakhstan. Three types of mineralized rocks are distinguished: 1) sedimentary and mélange calcareous breccias, 2) silicified tectonic breccias of sulphidized carbonaceous-terrigeneous rocks, and 3) sulphidized sandstones and carbonaceous siltstones. The first two types contain native gold. The third one contains invisible gold, which occurs preferentially in stellar-aggregated arsenopyrite and is chemically bonded.

KEYWORDS: disseminated gold, carbonaceous terrigeneous-carbonate rocks, poligenetic type ores, mineralogy of gold mineralization

## 1 INTRODUCTION

The Suzdal gold-sulphide deposit is located in the Semipalatinsk Irtysh area in eastern Kazakhstan, within the Kalba gold belt. It was discovered in 1983 and represents a classical object of gold-bearing weathering crust (Begaev & Stepanenko, 1995). The weathering crust of 40-80m thick of kaolin profile having gold content of 1.5-106 ppm has been already worked off. Currently, the primary low-sulphide fine-grained ores are mined by underground operations and open pits. Gold is extracted by bio-oxidation and heap leaching technologies. The gold content in ores varies from 18 to 55 ppm. The tentative gold reserves are estimated to be 80 to 100 t.

## 2 GEOLOGICAL SETTING

The deposit is located in the northwestern part of the gold-bearing western Kalba belt in the carbonaceous-terrigeneous-carbonate rocks area hosting tens of deposits and hundreds of gold occurrences of various formational types. The belt formed in the axial part of the Irtysh-Zaisan oceanic basin during convergence of the Kazakhstan and Gorny-Altay continental margins, and during collision in the Hercynian. Rhyolite-granodiorite magmatism occurred during the collision stage ($C_3$), while intra-continental (Semeitaus volcano-plutonic structure) formed in the Permian-Triassic. The Suzdal deposit is located at the southern margin of the Semeitauz structure within the conjunction zone of the Chara-Gornostaevsky deep fault of northwestern strike and the Suzdal fault of northeastern strike.

The ore-hosting section is represented bottom-up by: a) alternation of calcareous and coaly aleurolites and marls with limestone lenses and horizons of siliceous pelitolites, polymict gritstones, sandstones, tuffostones, tuffites, and lavas of intermediate composition at the bottom (160-180m); b) riftogenic limestones (3-100m); calc-coaly siltstones with limestone lenses (80-100m). Ore mineralization is confined to tectonic zone of northeastern strike and is about 4 km long and hosts 4 echelon-like ore zones with a dip angle of 40-90$^{o}$ to the southeast (Fig. 1). Ore bodies 1-40m thick are traced 200-800m along the strike and 500m in depth. Ores are of a gold-sulphide (Au-As) type with sulphide content ranging from 0.5 to 10-15 wt.%. They are represented by vein-disseminated ore and stratified mineralization. Ore bodies in ore zones 1-3 are located within the reef limestones and bioclasts. Ore zone 4 is confined to turbidite carbonaceus-sandy-siltstone rocks.

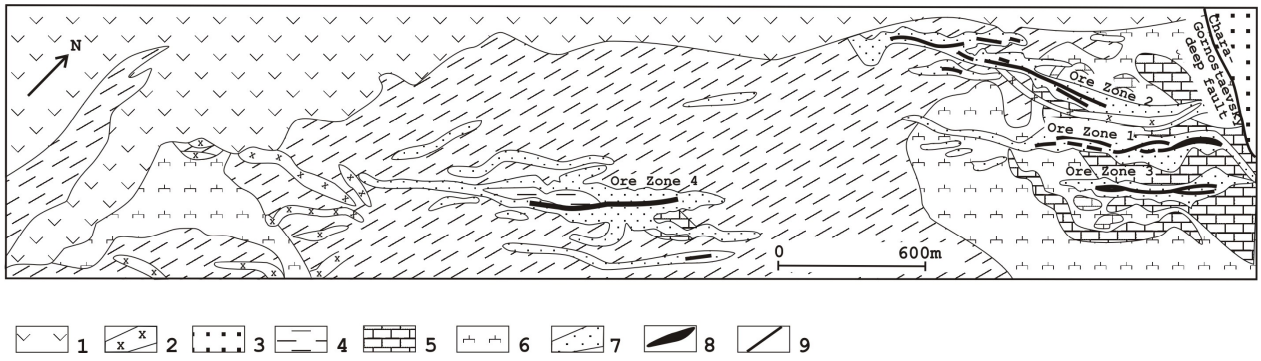


Fig. 1. Geological scheme of the Suzdal deposit (after I. P. Begaev, 1995). 1 - volcanites of the Semeitauz suite (T?), 2-granodiorites (T), 3 - Maitobinskaya suite molasse ($C_2$ ), 4-6 Lower Carboniferous sediments ($C_1$), 4-sandy-siltstone series, 5- organogenic limestones, bioclastic calcareous units, coal-bearing siltstones, siliceous mudstones, 6- sandstones, tuffs, lavas of intermediate composition, 7- mineralized zones, 8- ore bodies, 9- thrust zone.

## 3 LITHOLOGICAL AND GEOCHEMICAL CHARACTERISTICS OF THE ORES

Three main ore types are distinguished which differ in structural pattern, chemical composition and type of mineralization. The first ore type is represented by sulfidized, partly silicified and dolomitized, carbonaceous calcareous and polymictic sedimentogenic and melange-type breccias, bioclasts with abundant shelf fauna. They contain disseminated sulphide mineralization with visible gold and fragments of relic-bedded gold-bearing pyrite-arsenopyrite ores. The second type is represented by silicified rocks occurring in brecciation and schistosity zones within the sulphide-bearing sandstones and aleuropelites and calcareous rocks. They contain disseminated sulphide mineralization and visible gold. The third type is represented by sulphidized sandstones and carboniferous aleuropelites with the elements of soft deformation characterized by slump or "fuzzy-top" bedding. They have no exact evidence of hydrothermal alteration (Fig.2A). The main ore minerals of this ore type are fine-grained pyrite and arsenopyrite. Gold presents in an invisible form. Pyrite typically occurs as globular or fine-grained aggregates. Arsenopyrite occurs as an unusual stellar aggregate, evenly distributed over sandstone body (Figs. 2B, C). The first two ore types occur within ore zones in the eastern part of the deposits while the third one in the ore zone 4. The chemical composition of typical hand samples of these ore types is shown in Table 1.

The major minerals of the Suzdal deposit are

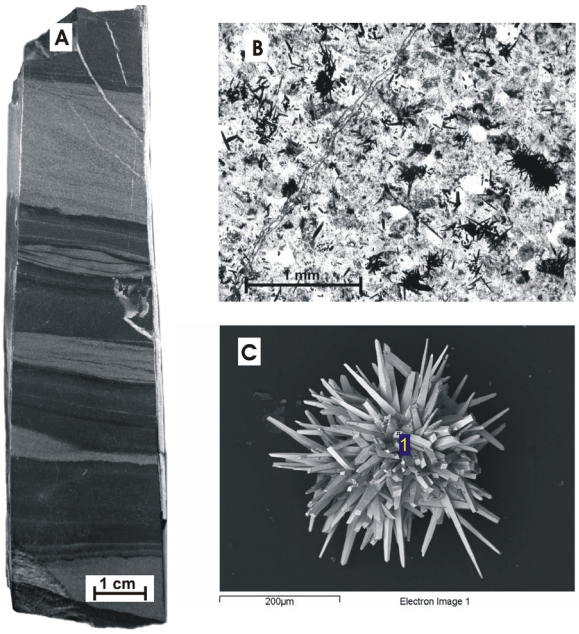


Fig.2. A. Photograph of turbidity carbonaceous terrigeneous rock with disseminated sulphide. B. Fine-grained and globular pyrite and stellar-aggregated arsenopyrite in sandstone. C. SEM back-scattering image of stellar-aggregated arsenopyrite.

pyrite and arsenopyrite. Pyrrhotite, marcasite, chalcopyrite, sphalerite (with high-iron content - up to 13 wt%), Sb-As-sulphosalts, ullmannite, willyamite, nickeline, aurostibite, westerveldite, rutile are less common. The typical nonmetallic minerals are dioctahedral mica, chlorites, quartz, siderite and dolomite. In addition, the relic minerals apatite, monazite, Cr-spinel, garnet and tremolite were found. Superimposed veined quartz-carbonate mineralization with antimonite, berthierite, native antimony, and rare cinnabar occur in the ore zones. The spec-

| Components/Ore types (samples) | Type 1 (S-29) | Type 2 (Su-13) | Type 3 | | |
|---|---|---|---|---|---|
| | | | (Su-24) | (Su-21) turbidity rock | |
| | | | sandstone | sandstone | siltstone |
| $SiO_2$ | 14.23 | 89.61 | 71.53 | 59.03 | 63.36 |
| $Al_2O_3$ | 3.62 | 2.45 | 14.32 | 16.72 | 17.89 |
| $Fe_2O_3$ | 4.33 | 3.90 | 4.66 | 9.33 | 6.29 |
| $TiO_2$ | 0.46 | 0.21 | 0.68 | 0.75 | 1.02 |
| MnO | 0.11 | 0.03 | 0.06 | 0.03 | 0.03 |
| CaO | 37.96 | 1.36 | 0.43 | 1.39 | 0.68 |
| MgO | 4.66 | 0.10 | 0.47 | 1.18 | 0.92 |
| $Na_2O$ | 1.89 | 0.72 | 0.30 | 0.74 | 0.73 |
| $K_2O$ | 0.30 | 0.44 | 2.63 | 3.42 | 4.14 |
| $P_2O_5$ | 0.10 | 0.03 | 0.11 | 0.08 | 0.10 |
| п.п.п. | 32.99 | 1.47 | 4.95 | 7.18 | 5.99 |
| Total | 100.65 | 100.32 | 100.14 | 99.85 | 101.16 |
| Au (ppm) | 15.0 | 54.01 | 32.2 | 3.6 | 1.8 |
| As (wt. %) | 0.15 | 0.3 | 2.34 | 1.42 | 1.5 |

Table 1. Chemical composition of ore-bearing ores from the Suzdal deposit (wt.%).

ific elements of the distinguished ore types are (ppm): Co (10-20), Ni (10-35), V (90-125), Ti (3000-5000), Ba (100-400), Sb (50-100), Mn (70-500), Ag (<1), Ce (20-60), Pt, Pd, Rh <0.5, Os <0.001. The arsenic content in hand samples is estimated to be a few tenths of percent, while in the third type it makes up 0.59-2.91 wt.%. The isotope composition of sulphur in pyrite is +0.5-0.0‰, in arsenopyrite it averages -1.8‰.

## 4 AU MINERALIZATION

92 % of gold in ores is recognized as fine metallic gold (Begaev & Stepanenko 1995). The normal size of gold particles is 3-25 μm while gold particles of 100-300 μm in size are of rare occurrence. It is irregularly distributed in ores. Gold content in hand samples varies from tens to hundreds ppm. By morphological features, crystalline, flaky and coral-like gold varieties are distinguished. The fineness of the first two varieties is 930-950‰. Silver is distributed quite irregularly in grains. Mercury is uncommon (about 0.2 wt.%). Coral-like gold surrounds crystalline gold and belong to pure variety (Fig. 3A). Gold is associated with pyrite, arsenopyrite, nickeline and williamite, and becomes overgrown with ullmannite, aurostibite and antimonite (Fig. 3B). Gold content in crystalline pentagon-dodecahedral pyrite amounts to 1000 ppm. Within zones of dynamometamorphism of carboniferous sulphide-bearing schists, gold is commonly associated with pyrrhotite, chalcopyrite and rutile. Submicroscopic gold impregnations can be observed in quartz and calcite. Invisible gold is recognized in sulphides of sandstones and carboniferous aleurolites. Gold content in hand samples varies from 200-300 ppb to 40-50 ppm. According to atomic-absorption analyses, gold content in monomineralic fractions of arsenopyrite stellar aggregates amounts to 800 ppm. Neither optical microscope nor electron scanning microscope found gold in arsenopyrite. In fine-grained crystalline and globular pyrite aggregates from the same ores, gold content is 10-340 ppm. According to X-ray spectroscopic analysis, stellar- aggregated arsenopyrite contain 0.53 wt.% of gold. Close correlation between Au and As is observed and gold in them is most likely present in a chemically bound form.

## 4 CONCLUSIONS

By its genetic features, the Suzdal deposit is considered to be a close analogue of Carlin-type deposit (Narseev, 2002). However, like some Carlin-type deposits, it has some distinctive features. At the same time, as all of the deposits of the Carlin trend there are some differences in the character of mineralization, conn-

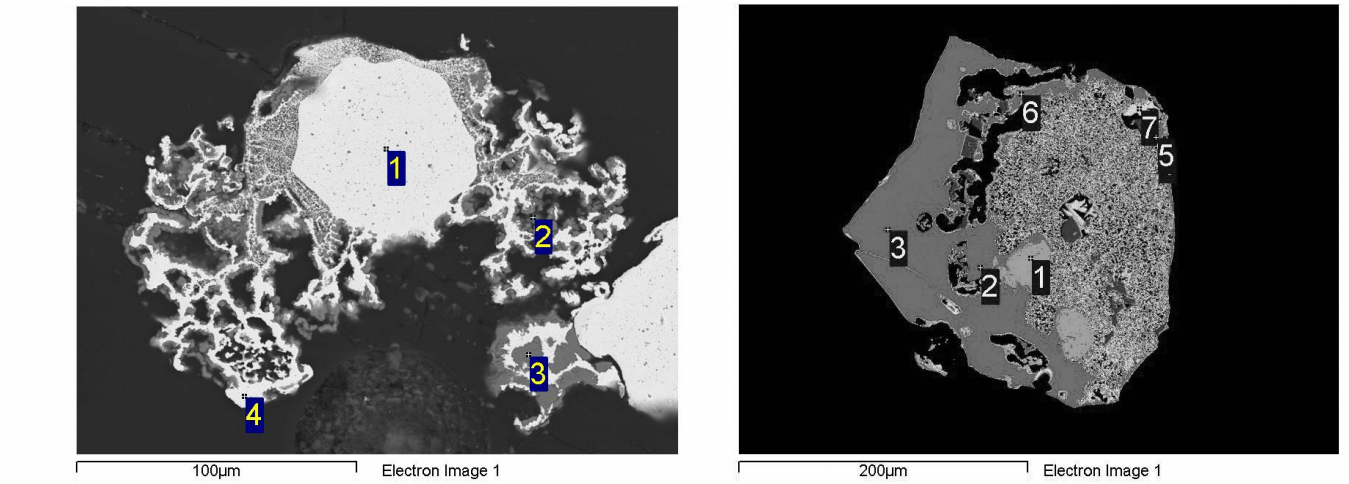


Fig. 3. A. SEM image of crystalline and coral-like gold. 1 – Ag-bearing gold, 2 – pyrite, 3- Ni-As-pyrite, 4 – pure gold. B. SEM backscatter image. 1 – Ag-gold, 2 – electrum, 3-6 –aurostibite, 7 – stibnite.

ection with magmatic rocks, and occurrences of stratiform mineralization. The main distinctive features of Suzdal deposit ores are the lack of gold-bearing zoned arsenian pyrite, thallium, and the poor occurrence of argillization processes which are typical of the Carlin deposit (Wells & Mullens, 1973; Arehart, 1996). The varieties of pyrite-arsenopyrite ores with invisible gold in carbonaceous terrigenous series are similar to ores of the Bakyrchik deposit in the Kyzyl folded zone within the Kalba gold-bearing belt. Such ores occur at large Siberian deposits hosted in black shale series, such as Olympiada, Sykhoi Log, Nezhdaninka, Natalka, and Maiskoe . The Suzdal deposit has distinct indications of stratiform mineralization, hydrothermal activity, and local processes of dynamothermal metamorphism, which allows us to attribute this deposit to polygenic formations.

## ACKNOWLEDGEMENTS

The work was supported by RFBR (grants 06-05-64697, 07-05-00889).

## REFERENCES

Begaev I. V., Stepanenko N.I. 1995. Gold-bearing weathering crust of Northern Kazakhstan and Semipalatisnk Irtysh area // *Geology and prospecting of Kazakhstan interior*, №5. C.29-33.

Narseev V.A. 2002. To the discussion on the genesis of Carlin-type. Suzdal-trend, Southwestern Altai //*Ores and metals*, №1.C.67-70.

Arehart G.B. 1996. Characteristics and origin of sediment-hosted gold deposits: a review //*Ore Geology Reviews,* Volume 11, Issue 6. P. 383-403.

Wells J.D. and Mullens T.E. 1973. Gold-bearing arsenian pyrite determined by microprobe analysis, Cortez and Carlin gold mines, Nevada //*Economic Geology*, Volume 68. P. 187-201.

# Model of multilevel structure of ore-columns and conditions of formation of large and superlarge Au-As-Sb disseminated deposits of invisible, refractory gold

A. V. Volkov
*Institute of Geology of Ore Deposits, Petrography, Mineralogy, and Geochemistry, Russian Academy of Sciences, Moscow, Russia*

ABSTRACT: The majority of large and super large deposits belong to the disseminated gold-sulphide ore type with refractory properties that hamper gold extraction by the commonly used method. The invisible gold prevails in many mesothermal stringer-disseminated gold-sulphide deposits with minor quartz veins. The data obtained support the concept of the metasomatic genesis of disseminated ores and indirectly testify to the possibility of their formation from gas-rich fluids. Hydrothermal fluids involved in ore formation may be produced by the mixing of ore-bearing gases and meteoric waters. Therefore, in order to reconstruct a multilevel vertical ore column, we used the data on different deposits located at different erosional and stripping levels within the same ore district or node. Models of the multilevel structure can be used for regional and deep mineralization prognosis.

KEYWORDS: disseminated, gold, deposit, fluid, gas, multilevel model

## 1 INTRODUCTION

Disseminated gold-sulphide deposits are known in metallogenic provinces of different ages. These deposits occur predominantly in terrigenous and terrigenous-carbonate carbonaceous members and are confined to zones of deep faults. They are characterized by a high Au/Ag ratio (up to 10 : 1 or higher) and a relatively homogeneous gold distribution. Gold is present mainly in finely dispersed inclusions in As-containing margins of pyrite grains (the As admixture is 1-5%) and arsenopyrite (the Sb admixture is 0.001-0.1%). Pyrite and arsenopyrite make up 5-10 vol % of ores (Fig.1). Gold-bearing sulphides form small and fine impregnations in zones of brecciation and shearing. The ore mineralization was continuously traced without changes in the composition and gold grades to a depth exceeding 1 km. Over this entire depth range, no mineral lateral or vertical zonality in orebodies was established. Gold and arsenic show a constant close correlation.

The deposits of gold-sulphide impregnated ores have nonproductive metamorphogenous substantially quartz and productive later gold-quartz, quartz-silver-polymetallic, and gold-bearing quartz-antimony veins. Thus, the ore bodies contain quartz veins and veinlets formed earlier or later than the main disseminated mineralization.

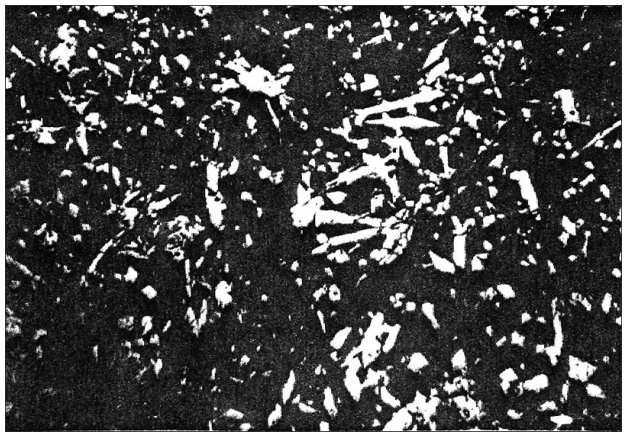

Fig.5. Gold-sulphide disseminated ores of Maisk deposits (needlelike arsenopyrite and pyrite with finely dispersed gold). Polished section magn. 50.

The gold-sulphide disseminated deposits are characterized by various conditions of ore localization and by various ratios of impregnated and vein mineralization. This allowed us to distinguish the following deposit subtypes: (1) proper disseminated gold-sulphide; (2) gold-

sulphide-quartz; (3) gold-antimony; and (4) gold-antimony-mercury.

The gold-sulphide disseminated deposits of the northeast of Russia were formed almost simultaneously in the late Cretaceous due to post-accretion processes of the tectono-magmatic activation that accompanied the formation of volcanic belts.

## 2 MODEL OF MULTILEVEL STRUCTURE OF ORE-COLUMNS

Ores from the Maisk and Carlin type's deposits are characterized by certain common features (Sidorov & Volkov, 1998). Recent facts and observations confirm this similarity and allow us to propose the multilevel model (Fig. 2). The uppermost level of Carlin-type mineralization is observed in the Alshar deposit (eastern Macedonia), where mineralization is distinctly related to volcanic activity (Volkov *et al.*, 2006). The ore zone formed beneath the screen of alkaline volcanics. Similarly to the Carlin trend (Nevada, United States), the near-surface level (above 500m) hosts jasperoid metasomatic ores with native mercury, arsenic, cinnabar, realgar, orpiment, and thallium minerals. Core from the interval of 700-1000m of the deep (over 1000m) structural borehole drilled within the Carlin trend shows the presence of acicular arsenopyrite in addition to the main gold-bearing minerals (As-pyrite and marcasite) (Theodore *et al*., 2003). Carlin-type disseminated ores from this level and deeper are virtually indistinguishable from ores of the Maisk deposit (Fig.1). Deep structural boreholes drilled at the Maisk and Nezhdaninsk deposits demonstrated that disseminated ores are continuously developed from the surface to depths of 1300 and 1500m, respectively. According to computer modeling, orebodies from deep levels (800-1000m and deeper) of the Maisk deposit are characterized by an almost two time decrease in the average As content (from 1.5 to 0.8-0.7%) as compared with higher levels and by similar Au concentrations (10-11 g/t). This fact can probably be explained by the decrease in the content of As in the disseminated As-pyrite in orebodies, which is accompanied by an elevated Au content in the acicular arsenopyrite. That will well be coordinated to temperatures of formation of As-pyrite (<200$^{o}$C; Tukova *et al*., 2005).

Consequently, the total mineralization interval can be as wide as 3000m or more (Fig. 2).

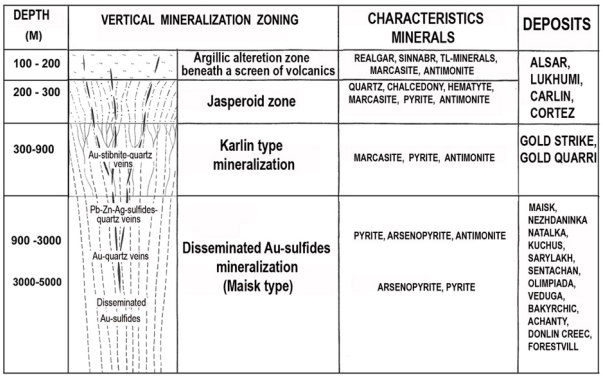


Fig. 2. Model of multilevel structure of ore-column.

Such a significant vertical interval of sulphide-disseminated mineralization is probably explained by the specific ore formation conditions in zones of tectono-magmatic activation. The proposed multilevel model explains the absence of large Carlin-type deposits in other gold ore provinces of the world in terms of the substantially high degree of erosion in these regions.

## 3 CONDITIONS OF THE FORMATION OF DISSEMINATED ORE

Figure 1 shows that the typical disseminated gold-sulphide ores of Maisk deposit have disseminated impregnations of gold-bearing needlelike arsenopyrite and pyrite that are not associated with quartz. The absence of quartz in disseminated ores (Fig.1) suggests that this mineralization is not related to typical hydrothermal processes.

In the 1990s, we attempted to obtain indirect data based on an examination of the pre-ore (metamorphogenic) quartz veins and veinlets that are abundant in ore bodies and host rocks of the Olimpiada giant gold deposit. The thin and short quartz veins of the Olimpiada ore field are conformable with the folding and bedding. Sometimes, the quartz veins are characterized by a ptygmatitic structure. Their mineral composition depends on the composition of country rocks. When the metamorphogenic quartz veins penetrate the ore deposition zone, they are enriched in pyrrhotite-pyrite, arsenopyrite, and berthierite-antimonite assemblages that correspond to the primary disseminated ore in terms of mineralogy. Quartz grains in the veins are characterized by larger dimensions. Quartz-antimonite-berthierite veins and veinlets formed after the productive stage distinctly crosscut the older metamorphosed veins and lodes of disseminated ores. Fluorite-

carbonate veinlets with local cinnabar are the youngest formations.

We assumed that, if pre-ore metamorphogenic veins are present, then disseminated mineralization should be reflected in its on ore formation zone. We took specimens of metamorphogenic quartz from all varieties of country rocks and ore bodies in all sectors of the Olimpiada ore field.

We examined 200 specimens, but only 120 specimens contained a significant number of fluid inclusions suitable for thermobarogeochemical investigation. Oval, drop-shaped, and less common angular gas inclusions prevailed in 22% of specimens. It should be mentioned that gas inclusions are absent in quartz from veins located beyond the ore bodies. The gaseous component includes different proportions of $CO_2$, $N_2$, and $CH_4$. Quartz from veins in ore bodies (hereafter, ore veins) also contains two- or three-phase inclusions. Primary inclusions are represented by the $CO_2$-bearing gas-liquid variety in the vein quartz from both ore bodies (group 1 inclusions) and country rocks (group 2 inclusions).

Table 1. Comparison of data on quartz-hosted fluid inclusions from metamorphogenic veins in and beyond ore bodies (groups 1 and 2, respectively)

| Parameters | Results of the study of fluid inclusions | |
|---|---|---|
| | Group 1 (68 specimens) | Group 2 (52 specimens) |
| Gas inclusions | Present (22% of total) | Absent |
| Boiling solution | Present | Absent |
| Three-phase inclusions | Present | Absent |
| Size of inclusions (μm) | 10–20 | 50–100 |
| Size of gas phase (vol %) | 20–30 | 15–20 |
| T hom (°C) | 270–200 | 200–190 |
| Temperature gradient, (°C/100 m) | 11/100 | 22/100 |

We compared fluid inclusion data on quartz grains of groups 1 and 2 in order to understand conditions of the formation of gold-sulphide dissemination (Table 1). The results indicate that the majority of gas-rich and gas-liquid inclusions in quartz of group 1 could have formed in the course of ore deposition. Specific features of the inclusions suggest that ore-forming fluids that were enriched in gas and hydrothermal solutions could have boiled up at the subsequent stage of ore formation.

The data obtained support the concept of the metasomatic genesis of disseminated ores and testify to the possibility of their formation from gas-rich fluids.

## THE NATURE AND OCCURRENCE MODE OF GOLD

The study of the nature and occurrence mode of gold makes it possible to elucidate ore formation conditions. Based on the Mossbauer spectroscopy data, arsenopyrites from the majority of disseminated gold-sulphide ore deposits contain gold in the chemically bonded or metallic form up to 2 nm in size (Genkin *et al.,* 1998).

In gold deposits of Russia, like in other deposits with the invisible gold, this element is mainly contained in the Au-bearing arsenopyrite. Based on the ICP-MS data, the Au content in arsenopyrites is 4700 g/t in the Olimpiada deposit, 1140 g/t in the Veduga deposit, 1400 g/t in the Nezhdanin deposit, 1900 g/t in the Maisk deposit, and 470 g/t in the Natalka deposit (Genkin *et al*., 1998; Volkov *et al*., 2006). Table 2 shows that arsenopyrites from ore veins and veinlets in gold-quartz and related to intrusive gold-rare-metallic deposits have a nearly stoichiometric composition (S/As = 0.9-1.14). In contrast, Au-rich arsenopyrites from disseminated ores of gold-sulphide deposits have a nonstoichiometric composition (S/As = 1.21-1.35). The maximum Au content is observed in arsenopyrites with the highest S/As values. S-rich arsenopyrites were recorded in the Maisk, Nezhdanin, Natalka, Olimpiada, and Veduga deposits (Table 2). Arsenopyrites from various ore types of the Natalka and Nezhdanin deposits are characterized by different compositions and S/As ratios (Table 2). These variations testify to different formation conditions of vein and disseminated ores in these deposits.

Many Russian researchers believe that the preferential Au concentration in early sulphides is related to the selective precipitation of this element in sulphides during the impact of late Au-bearing solutions. This mechanism was recorded at gold-quartz veins deposits. Our data support an alternative concept, according to which the major portion of gold in arsenopyrites is related to the joint crystallization of these minerals at the early stage of ore formation. These data also confirm the concept, according to which gold is transferred as complex S-As compounds.

Table 2. Average S/As ratios in arsenopyrite of different types of gold deposits (based on microprobe analyses)

| No | Deposit | Ore type | N | S/As |
|---|---|---|---|---|
| 1. | Natalka | veinlets | 50 | 1.04 |
| 2. | Natalka | disseminated | 37 | 1.31 |
| 3. | Maisk | disseminated | 19 | 1.28 |
| 4. | Nezhdaninka | disseminated | 161 | 1.35 |
| 5. | Nezhdaninka | veinlets | 43 | 1.09 |
| 6. | Olimpiada | disseminated | 43 | 1.23 |
| 7. | Veduga | disseminated | 13 | 1.21 |
| 8. | Chisty | veinlets | 3 | 0.86 |
| 9. | Teutedzhak | veinlets | 2 | 0.98 |
| 10. | Maltan | veinlets | 2 | 0.9 |
| 11. | Gaisk | veinlets | 6 | 1.02 |
| 12. | Svetloe | veins | 4 | 1.14 |
| 13. | Karalveem | veins | 3 | 1.0 |
| 14. | Igumenka | veins | 11 | 0.9 |
| 15. | Sovinoe | veins | 25 | 1.15 |

1-7 – disseminated gold-sulphide type, 8-11 – intrusion-related type, 12-15 – gold-quartz type.

Very small dimensions of the Au-bearing sulphides testify to high rates of their crystallization. Taking into consideration the facts mentioned above, we can assume that gold and S-As complexes were transported by high-temperature gaseous fluids. This mechanism is suggested by data on the modern ore-forming system of Kudryavyi Volcano (Judovskaja *et al.*, 2003).

## CONCLUSIONS

The initial composition of these disseminated ores governs the composition of veins and lodes at higher levels. The bulk mineralogical composition of orebodies from the upper level is close to that of ores from the lower level due to the differentiation of complex ores of the lower level. Models of the multilevel structure can be used for regional and deep mineralization prognosis.

The total pyrite-arsenopyrite disseminated mineralization interval of ore-column (3000m or more) and absence of ore zoning, also can be explained by precipitation of gold bearing sulphide from gas-rich fluids in larges shear and fault zones. Hydrothermal fluids involved in ore formation to quartz veins and veinlets in the upper levels (<3000m) of ore column may be produced by the mixing of ore-bearing gases and meteoric waters.

## ACKNOWLEDGEMENTS

This study was supported by the Russian Foundation for Basic Research (pr.no.06-05-64659).

## REFERENCES

Genkin AD, Bortnikov NS, Cabri L, et al. (1998) A Multilevel study of Invisible Gold in Arsenopyrite from Four Mesothermal Gold Deposits in Siberia, Russian Federation. *Econ. Geol.* 93 (24): 463-487.

Sidorov AA, Volkov AV, (1998) Same Analogy of Structure and Composition of Ore Lodes on Gold-Sulphide Deposits Carlin (USA, Nevada) and Maisk (Russia, Chukotka). *Dokl. Ross. Akad. Nauk*. 359 (2): 226-229.

Theodore TG, Kotlyar BB, Singer DA, Berger VI, Abbott EW, Foster AL (2003) Applied Geochemistry, Geology, and Mineralogy of the Northernmost Carlin Trend, Nevada. *Econ. Geol.* 98: 287-316.

Tukova EE (2005) The Structure and Paragenesis of Arsenopyrite in Reconstruction of a Geological History of Deposits (the Verkhne-Kolyma Region). Problems of Metallogeny of Ore Districts of Northeast of Russia. Magadan: *CVKNII DVO RAN*:125-156.

Volkov AV, Sidorov AA, Goncharov VI, Sidorov VA (2002) Gold-Sulphide Deposits of Impregnated Ores of the Northeast of Russia," *Geol. Rudn. Mestorozhd.*44 (3): 179-197.

Volkov AV, Genkin AD, Goncharov VI (2006) About forms of a Presence of Gold in Ores of Natalka and May Deposits (Northeast of Russia) *Tikhookeansk Geol.* (6): 21-39.

Judovskaja MA, Distler VV, Chaplygin IV (2003) Forms of a Presence of Gold in Products of Crystallization of Modern High-Temperature Gas Fluids of a Volcano Kudrjavi, Kuriles *Dokl. Ross. Akad. Nauk.* 391 (4): 535-539.

# Ore formation in the Charmitan gold-quartz vein deposit (Uzbekistan): Constraints from mineralogical and noble gas data

T. Graupner
*Federal Institute for Geosciences and Natural Resources (BGR), Stilleweg 2, 30655 Hannover, Germany*

S. Niedermann
*GeoForschungsZentrum Potsdam, Telegrafenberg, 14473 Potsdam, Germany*

R. Seltmann & C.T. Williams
*Centre for Russian and Central EurAsian Mineral Studies, Department of Mineralogy, Natural History Museum, Cromwell Road, London SW7 5BD, United Kingdom*

ABSTRACT: Mineral assemblages present within four mineralization stages have been studied within the Charmitan gold-quartz vein deposit. Native gold inclusions often associated with sulphide minerals and, during the early stages, also with scheelite, contain Ag (7.8–24.5 wt. %), Hg (≤ 1.0 wt. %), Fe (≤ 0.6 wt. %), Cu (< 0.15 wt. %) and Bi (≤ 0.2 wt. %). Noble gas isotope data for hydrothermal ore fluids trapped in gold-related sulphides suggest that diverse sources were involved in the formation of the Charmitan gold system. The noble gas data are indicative of a small, but significant input of fluids from external, deep-seated (mantle and possibly lower crust) sources.

KEYWORDS: Charmitan gold deposit; mineralization stages; gold chemistry; noble gas data

## 1 GEOLOGICAL BACKGROUND

The world class Charmitan gold deposit (>200 t Au) is located in the Nuratau Mountains gold district in Western Uzbekistan, which forms the eastern continuation of the Kyzylkum gold district within the South Tienshan gold province (*e.g.* Khamrabaev *et al.* 1971; Berger *et al*. 1994; Bortnikov *et al*. 1996). The deposit consists of two mines, the Guzhumsai mine to the west and the Charmitan mine to the east (Fig. 2), adjacent to the settlement Zarmitan.

Within the deposit, about 50 orebodies were defined, which are located both in the endocontact and the exocontact zones of the multiphase Koshrabad granitoid massif (*e.g.* Khramrabaev *et al.* 1973; Golovanov *et al.* 2001).

## 2 MINERALIZATION STAGES

The number of mineralization stages distinguished in the low-sulphide ore veins, veinlet zones and stockworks, as well as the characteristic mineral associations assigned to each stage differs between previous studies (four to six stages; *e.g.* Eshimov 1987; Bortnikov *et al.* 1996; Golovanov *et al*. 2001). The present study also indicates the presence of at least four mineralization stages: I – quartz-feldspar stage, II – quartz-pyrite-arsenopyrite-scheelite-gold(-telluride) stage (Fig. 2), III – quartz-sphalerite-galena-pyrite-sulphosalts-gold stage, IV – quartz-carbonate-fluorite(-pyrite) stage.

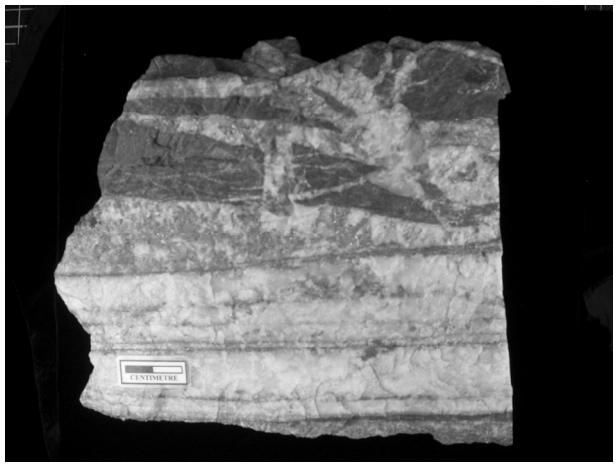


Figure 1. Quartz-arsenopyrite-scheelite-gold vein in meta-sedimentary rocks of the Dzhasbulaksk suite.

## 3 DISTRIBUTION AND CHEMISTRY OF GOLD

The distribution, paragenetic association and microchemistry of gold within the ore structures of Charmitan have been studied using detailed microscopic investigations (ore micros-

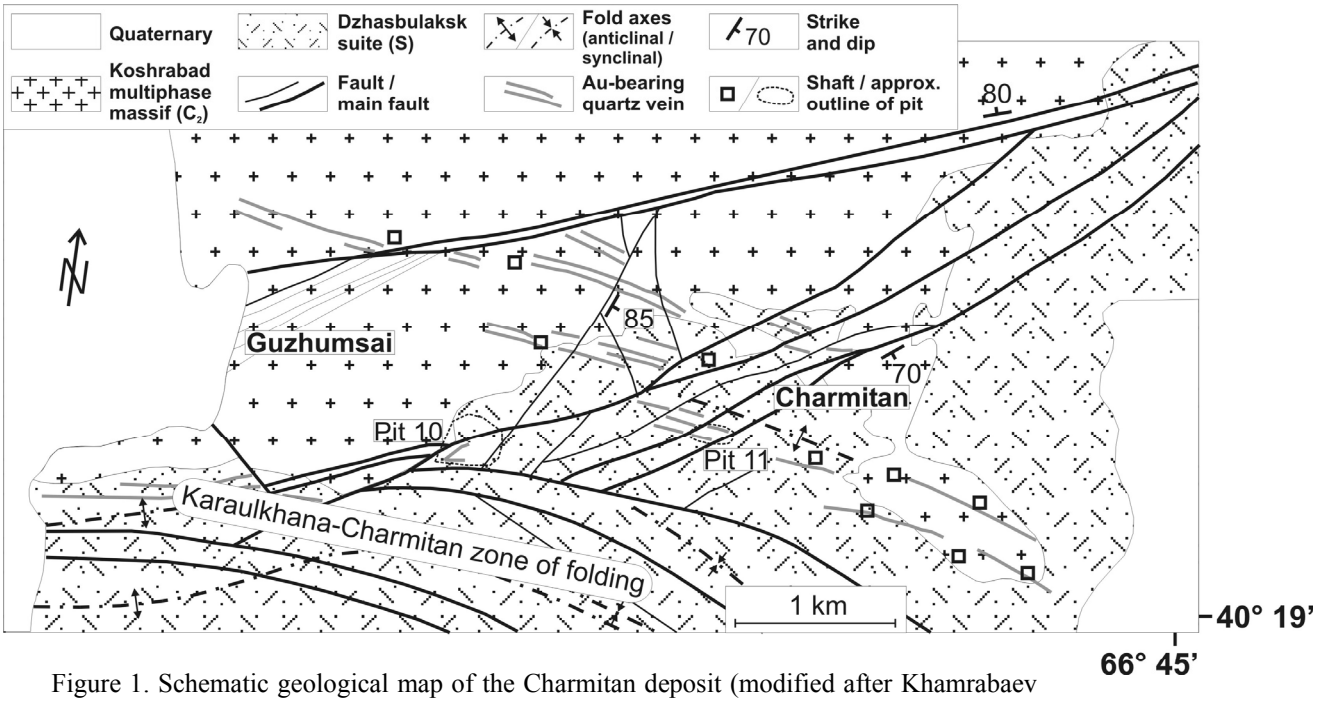


Figure 1. Schematic geological map of the Charmitan deposit (modified after Khamrabaev *et al.* 1973; Golovanov *et al.* 2001).

copy; hot-cathode cathodoluminescence microscopy), as well as scanning electron microscope (SEM) and electron microprobe analysis (EMPA).

Gold occurs irregularly distributed within sulphides (*e.g.* in narrow zones with increased gold concentrations in pyrite) and as micro-inclusions of native gold in vein minerals (*e.g.* Graupner *et al.* 2003).

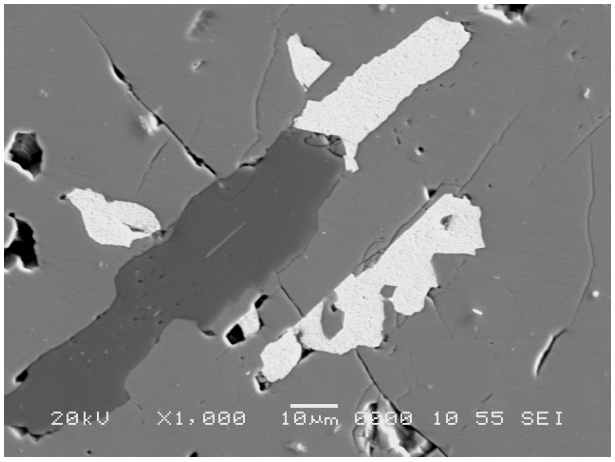


Figure 3. Intergrowth of native gold and pyrite in arsenopyrite. Arsenopyrite-quartz veinlet in meta-sedimentary rocks from the exocontact zone of the Koshrabad massif.

In the ore veins, scarce native gold was observed (i) as isolated, anhedral grains at grain boundaries between partly recrystallized grains of vein quartz. Rather frequent gold inclusions (ii) in quartz close to nests of arsenopyrite, (iii) in quartz-pyrite-scheelite(-arsenopyrite-rutile) or (iv) in arsenopyrite-quartz(-carbonate-scheelite) veinlets were all assigned to the important second ore stage.

In the arsenopyrite-dominated veinlets (iv), which cross-cut older, partly recrystallized quartz, the gold occurs as isometric (euhedral, deformed) crystals in newly formed quartz close to arsenopyrite aggregates, as anhedral aggregates cementing deformed arsenopyrite, or inside arsenopyrite crystals. Inclusions of euhedral arsenopyrite were observed in anhedral gold enclosed in arsenopyrite. Anhedral gold within arsenopyrite was also intergrown with pyrite (Fig. 3) and with Bi-tellurides – possibly joseite-b ($Bi_4S_{2.25}Te_{0.75}$).

Within the third (polysulphide) ore stage native gold occurs (v) in association with sphalerite and (vi) with sulphosalts.

All native gold particles from the sulphide-poor Charmitan deposit (Ag-rich gold grains from the third mineralization stage were not analysed) contain Ag (7.8–24.5 wt.%); Hg (up to 1.0 wt.%) is also usually present. Fe (<0.1–0.6 wt. %), Cu (<0.15 wt.%) and Bi (<0.1–0.2 wt.%) were detected in some of the gold grains. Compositional zoning and intra-particle variations in the Ag content are rather atypical of the gold grains from Charmitan, although a few anhedral grains with variations in their Ag concentrations were found. Anhedral gold, intergrown with pyrite and scheelite, occasionally shows narrow marginal zones with significantly lower Ag contents than the core of the grains.

The composition of the native gold inclusions at Charmitan (stages I and II) is similar to the data obtained for the anhedral gold II in the low-sulphide gold-quartz veins from the giant Au(-W) deposit Muruntau (Kyzylkum, Western Uzbekistan; Graupner *et al.* 2005) and also for native gold from early stages at the gold deposit Jilau (Tadjikistan; *e.g.* Graupner *et al*. 2003). Compositional zoning of native gold grains or aggregates is scarce in all three aforementioned deposits.

## 4 ORIGIN OF ORE FLUIDS

Five sulphide samples from the second and third auriferous ore stages at Charmitan (pyrite, arsenopyrite, sphalerite, galenite) were studied for the noble gas isotopic compositions of the trapped hydrothermal ore-related fluids. Noble gas concentrations and isotopic compositions were determined in a VG 5400 mass spectrometer. Preliminary $^{3}He/^{4}He$ ratios are ~0.2 to <0.4 Ra ($^{3}He/^{4}He$ ratios of samples are given in units of the sedimentary rocks of the Dzhasbulaksk suite, resulting from the Hercynian magmatic activity (Koshrabad massif), which produced hornfelses that were amenable for widespread fracturing and the localization of quartz-veinlike gold mineralization in fault structures, is a key factor in the localization of the deposit (*cf.* Wall *et al*. 2004 for a similar conclusion for the Muruntau gold deposit).

## ACKNOWLEDGEMENTS

The authors thank the Navoi mining company for allowing access to their property at Charmitan. We are very grateful to J. Spratt (NHM London) and Je. Lodziak (BGR Hannover) for their support during the microprobe work. J. Goetze (TU Bergakademie Freiberg) is thanked for his support in analyzing the quartz using CL microscopy and E. Schnabel (GFZ Potsdam) for performing the noble gas analysis. C. Stanley (NHM London) is acknowledged for providing sample material and for fruitful discussions. Special thanks to I.M. Golovanov and V.J. Wall for inspiring discussions during field work. The project was partly financed by a SYS-RESOURCE grant of the European Commission's Improving Human Potential (IHP) Programme. The paper is a contribution to the IGCP-473 project.

## REFERENCES

Ballentine CJ, Burnard PG (2002) Production, release and transport of noble gases in the continental crust. In: Porcelli et al. (eds), *Noble gases in geochemistry and cosmochemistry*. *Reviews in Mineral. and Geochem.* 47. The Mineralogical Society of America, Washington, pp 481-538

Berger BR, Drew LJ, Goldfarb RJ, Snee LW (1994) An epoch of gold riches: The late Paleozoic in Uzbekistan, Central Asia. *SEG Newsletter* 16 pp: 1-11

Bortnikov NS, Prokof'yev VYu, Razdolina NV (1996) Genesis of *Charmitan* quartz gold ores, Uzbekistan. *Geologiya Rudnykh Mestorozh-deniy* 38 pp: 238-257

Craig H, Lupton JE, Horibe Y (1978) A mantle helium component in circum Pacific volcanic gases: Hakone, the Marianas, and Mt Lassen. In: Alexander EC, Ozima M (eds), Terrestrial rare gases. *Sci. Societies Press,* Tokyo, pp 3-16

Eshimov TE (1987) Typomorphic character-istics of pyrite from Zarmitan as mineral-geochemical criteria for predicting gold mineralization. *Uzbekskiy Geologicheskiy Zhurnal* pp: 70-76

Golovanov IM, Akhmedov NA, Zav'yalov GE, Zemlyanov AA, Isakhodjaev BA, Paramonov YuI, Pirnazarov MM, Savchuk YuS (2001) The Charmitan ore deposit. In: Golovanov IM et al. (eds) *Ore deposits of Uzbekistan. GIDROINGEO, Tashkent*, pp 202-211

Graupner T, Seltmann R, Williams CT, Wilkinson JJ, Kim M (2003) Morphology, distribution and chemistry of Au and associated minerals in sulphide-poor and sulphide-rich orogenic Au deposits of the Southern Tien-Shan: a microscopic, cathodoluminescence and microprobe study. In: Akhmedov NA et al. (eds), Proceedings Int. *Scien.-Techn. Conf. 'Problems of ore deposits and maximizing the prospecting efficiency', Tashkent,* pp 339-342

Graupner T, Kempe U, Klemd R, Schüssler U, Spooner ETC, Götze J, Wolf D (2005) Two stage model for the Muruntau (Uzbekistan) high grade ore structures based on characteristics of gold, host quartz and related fluids. *N. Jb. Min. Abh.* 181/1 pp: 67-80

Graupner T, Niedermann S, Kempe U, Klemd R, Bechtel A (2006) Origin of ore fluids in the Muruntau gold system: Constraints from noble gas, carbon isotope and halogen data. *Geochim. Cosmochim. Acta* 70 pp: 5356-5370

Khamrabayev IKh, Chebotarev GM, Mansurov M, Tillyayev KhS, Dautov AI, Khrenov VA (1971) Some geologic and mineralogic characteristics of the gold ore deposit of Charmitan, western Uzbekistan. *Uzbekskiy Geologicheskiy Zhurnal* pp: 3-7

Khamrabayev IKh, Chebotarev GM, Mansurov M, Khorvat VA, Bertman EB, Tillyayev KhS (1973) Characteristics of tungsten minerali-zation of the Charmitan gold deposits in western Uzbekistan. *Uzbekskiy Geologicheskiy Zhurnal* pp: 3-11

Wall VJ, Graupner T, Yantsen V, Seltmann R, Hall GC (2004) Muruntau, Uzbekistan: a giant thermal aureole gold (TAG) system: In: *Proceedings of the SEG 2004 Meeting, Perth, Western Australi*a, pp: 199-203

# The Sirkka Au-Cu-Ni-Co occurrence, northern Finland: an orogenic gold deposit with multimetallic, atypical metal association

M.J. Holma
*Department of Geosciences, P.O. Box 3000, FI-90014 University of Oulu, Finland*

P. Eilu
*Geological Survey of Finland, P.O. Box 96, FI-02151 Espoo, Finland*

V.J. Keinänen & V.J. Ojala
*Geological Survey of Finland, P.O. Box 77, FI-96101 Rovaniemi, Finland*

ABSTRACT: The Palaeoproterozoic Sirkka gold occurrence in northern Finland has characteristics of an orogenic gold deposit ─ except for an atypical metal association (Cu, Fe, Ni, Au ± Ag, Co) for this ore type. The occurrence is but one of the many rather similar occurrences hosted by the WNW-ESE trending Sirkka Shear Zone (SSZ), a major structural break that has roots at the approximate depth of 20 km. Like other similar occurrences in the SSZ, the Sirkka occurrence consists of quartz-carbonate-sulphide vein networks and shear zone-hosted breccias. By volume, the main gold-related ore minerals are pyrrhotite, chalcopyrite and pyrite, and in lesser extent, arsenopyrite, gersdorffite and minor cobaltite and glaucodot. Native gold is primarily associated with the sulpharsenides and it occurs as inclusions and fracture fillings. The host sequence comprises mafic and ultramafic volcanic rocks, phyllite and graphitic phyllite, and a thin, massive sulphide-facies iron formation. The multimetallic character of the occurrence is the outcome of orogenic, auriferous, saline fluids reacting with this heterogeneous, sulphur-rich, predominantly reducing lithological sequence.

KEYWORDS: greenstone belt, Proterozoic, orogenic gold, Lapland, Finland

## 1 INTRODUCTION

The patterns of different gold mineralization types in Central Lapland, northern Finland (Fig. 1), are now better understood than ever before. The genetic types of epigenetic gold mineralizations recognized in the area are: 1) orogenic gold; 2) iron-oxide copper-gold (IOCG); and 3) paleoplacer (Eilu *et al.* 2003). The orogenic and IOCG deposits are clustered in different parts of the belt (Fig. 1). Regardless of genetic type, all gold deposits and occurrences are Palaeoproterozoic.

Orogenic gold mineralization in Central Lapland falls into two subtypes, which are, in the order of present economic importance, gold-only and multimetallic. The majority of deposits and occurrences are of the former type (*e.g.* the world-class Suurikuusikko deposit with the resources of >22 Mt at 4.9 ppm Au). In contrast, the multimetallic occurrences are enriched in Cu and Au (*e.g.* Saattopora mine), or in Au, Cu and Ni ± Co (*e.g.* Sirkka & Levijärvi-

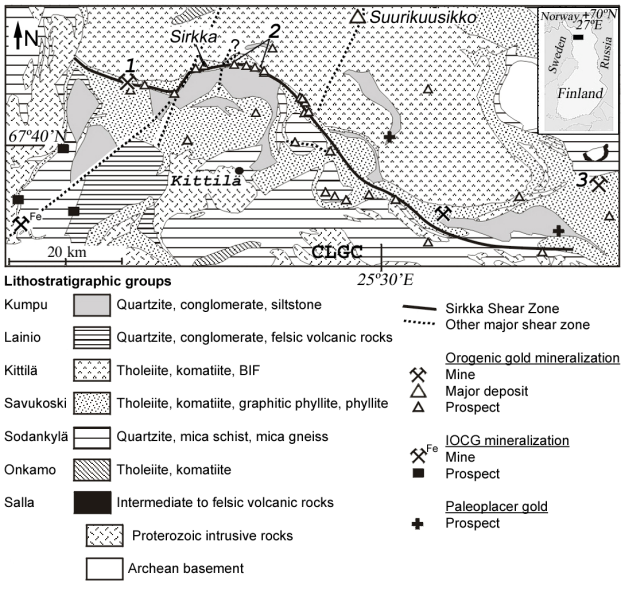


Figure 1. Epigenetic gold mineralization in the central parts of the Central Lapland greenstone belt. From shear zones, only a selected few are shown. 1 = Saattopora, 2 = Levijärvi-Loukinen, 3 = Pahtavaara, CLGC = Central Lapland granitoid complex. Geology from Lehtonen *et al.* (1998). Modified from Holma *et al.* (2003).

Loukinen) (Fig. 1). Although the latter have an atypical metal association for orogenic gold mineralization, they too are understood to be representative of this globally important genetic family of deposits (Groves *et al*. 2003). This stems from the observation that they nevertheless have practically all the other key features of orogenic gold mineralization (Holma & Keinänen 2007).

## 2 GEOLOGICAL SETTING

The Sirkka Au-Cu-Ni-Co occurrence is located ~145 km N of the Arctic Circle and ~18 km NNW of the local administrative center, the town of Kittilä (Fig. 1). Geologically, it is hosted by one of the major deformation zones in Central Lapland, the extensively gold-mineralized Sirkka Shear Zone (SSZ). SSZ separates a terrain dominated by volcanic rocks in the N from a volcanosedimentary belt in the S (Fig. 1). The S-dipping SSZ has roots at the depth of about 20 km (Patison *et al.* 2006).

## 3 MINERALIZATION AT SIRKKA

The occurrence is hosted by a sequence of Savukoski Group rocks, metamorphosed to mid- to upper-greenschist facies. They comprise tuffite, phyllite and graphitic phyllite intercalating with thicker units of mafic and ultramafic volcanic rocks. Importantly, the lithologic assemblage includes a minor *syngenetic* base metal mineralization, as demonstrated by a) the local beds of graphitic phyllite, variably rich in stratabound pyrrhotite and minor chalcopyrite, and b) some meters thick sulphidic banded iron formation located a few tens of meters N of the E-W trending gold-related vein stockwork and breccia zone (Holma *et al.* 2006). Since there are volcanic rocks in close spatial association with banded iron-rich formation(s), the host sequence is – at least in some extent – analogous to Algoma-type sulphide-facies iron formation.

Host rocks for the gold occurrence have been hydrothermally altered in several stages, including an event of albitization well before gold mineralization. The gold-related proximal alteration is characterized by the mineral assemblage quartz-carbonate-sericite/fuchsite. Albite, chlorite, pyrrhotite, pyrite, arsenopyrite and rutile are common accessory phases. As a rule, the exact alteration mineral assemblage strongly depends on the earlier composition and alteration intensity of each rock type.

Two partly overlapping *epigenetic* mineralization styles are recognized:

1) Cu±Ag mineralization (locally auriferous): base-metal rich zones characterized by veins composed of carbonate with minor quartz, pyrrhotite, chalcopyrite and, in places, pyrite.
2) Au-Cu-Ni±Co mineralization: gold-rich zones characterized by veins composed of carbonate with minor quartz, pyrrhotite, chalcopyrite, pyrite, gersdorffite, arsenopyrite and/or cobaltite/glaucodot. In a rare case, a vein is solely composed of a sulpharsenide(s).

Figure 2 represents a sample of the later mineralization style, although in this case the gold ore is exceptionally rich in sulpharsenides in excess of pyrrhotite and chalcopyrite; besides, pyrite is totally absent. This sample, splitted into two for chemical analysis and inspection of its internal structure, demonstrates a complex tectonic mixture of fragments of graphite-rich host rock and a distinctive gold-related vein. Sulpharsenide minerals are commonly concentrated on vein margins, in particularly wherever the host rock contains graphite. The veins tend to have a somewhat banded appearance, although generally the banding is much weaker than what is shown in the Figure 2 (it is assumed here that the topmost part of the boulder has broken off next to the graphite-rich wall rock, leaving behind only a mass of sulpharsenides that once were against it). Typically, such a banded texture is only poorly developed due to the erratic occurrence of sulpharsenides.

Sulpharsenides are paragenetically early and they are typically brecciated by, or enclosed within, a matrix of ankerite, Fe-dolomite and/or siderite, and, in lesser extent, quartz. These minerals, which form the bulk of most veins, are thus concentrated in the central parts of the veins. Also the vein gangue is commonly brecciated, mainly by pyrrhotite, chalcopyrite and/or pyrite. Other minerals detected in the veins include tourmaline and pentlandite. Gold occurs as inclusions and fracture fillings within the sulpharsenides. Silver, instead, occurs in two forms: it occurs not only in native gold (Au-Ag alloy), but also in veins where native gold and the sulpharsenides are entirely absent, but chalcopyrite is a major mineral. In the latter setting, the Ag is in argentopentlandite within chalcopyrite (according to the unpublished

M.Sc. thesis of Vesanto, 1978) (see the analysis from sample 4-MJH-03 in Table 1). Basically all these mineralogic features are identical with the Levijärvi-Loukinen gold occurrence ~4.5 km east of Sirkka (Holma *et al*. 2003; Holma & Keinänen 2007).

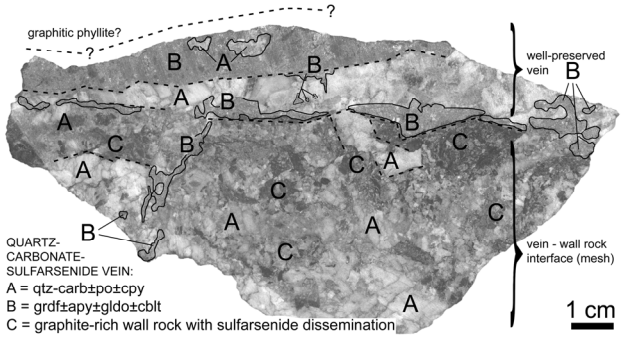


Figure 2. Polished slab of gold ore from Sirkka, sample 15-MJH-04. Abbreviations: apy, arsenopyrite; carb, ankerite/Fe-dolomite±siderite; cblt, cobaltite; cpy, chalcopyrite; gldo, glaucodot; grdf, gersdorffite; po, pyrrhotite; qtz, quartz. For chemical composition, see Table 1.

## 4 DISCUSSION

The Cu±Ag and Au-Cu-Ni±Co mineralizations described above are interpreted to be a product of the same mineralizing system, based on that a) they have spatial correlation; b) their vein textures and alteration assemblages are similar; c) there is no obvious crosscutting relationship between them; and d) in many cases, they grade into each other over a very short distance. Therefore they collectively form the Sirkka gold occurrence.

The Sirkka occurrence has much in common with the Levijärvi-Loukinen gold occurrence, the two of which are located only ~4.5km apart (Fig. 1). The area between them further supports the common genetic background, as this part of the shear zone hosts plenty of Cu-mineralized quartz-carbonate veins. However, the host sequence at Sirkka is markedly richer in sulphides than the rocks to the east of it. The apparently stronger sulphidation at Sirkka cannot simply be explained by variations in gold-related mineralization styles across the shear zone, because both Cu and Au-Cu-Ni-Co mineralization styles are recognized in the Levijärvi-Loukinen area as well. However, it can be explained by other means (see below).

Comparing Sirkka and Levijärvi-Loukinen, sulphidation is stronger in the former area because: 1) at Sirkka, there is a far more widespread pre-gold base-metal mineralization than at Levijärvi-Loukinen; 2) gold mineralization is superimposed on this earlier mineralization. This model gets support from that sulphidation appears to be strongest where the gold mineralization has been deformed in an active shear zone. As shearing is concentrated into areas rich in graphite and syngenetic stratabound pyrrhotite±chalcopyrite, the latter ore minerals have been remobilized to form an apparently stronger sulphidation zone.

Table 1. ICP-AES and GFAAS analyses (aqua regia leach) from hand-specimens from Sirkka. All values expressed in ppm.

| Sample | 13-MJH-04[1] | 11-MJH-04[2] | 10-MJH-03[3] | 4-MJH-03[4] | 4-MJH-04[5] | 1-MJH-04[6] | 2-MJH-04[6] | 15-MJH-04[7] |
|---|---|---|---|---|---|---|---|---|
| Ag | <1 | <1 | <1 | **14** | <1 | <1 | <1 | <1 |
| Al | 19400 | 23900 | 1090 | 188 | 3070 | 713 | 513 | 7980 |
| As | 135 | 1650 | 76 | <10 | 11 | 84 | 418 | 66600 |
| B | 7 | 15 | 25 | 38 | 16 | 31 | 35 | 30 |
| Ba | 17 | 64 | 18 | 6 | 14 | 16 | 13 | 23 |
| Be | <0.5 | 0.5 | <0.5 | <0.5 | <0.5 | <0.5 | <0.5 | <0.5 |
| Ca | 47900 | 1740 | 2090 | 5960 | 58800 | 6570 | 3200 | 164000 |
| Cd | <1 | <1 | <1 | 7 | <1 | <1 | <1 | 128 |
| Co | 55 | 109 | 57 | <1 | 12 | 68 | 71 | 4790 |
| Cr | 93 | 88 | <1 | 6 | 14 | 2 | <1 | 20 |
| Cu | 138 | 259 | 3430 | 102000 | 116 | 2150 | 2240 | 317 |
| Fe | 89700 | 45900 | 379000 | 102000 | 239000 | 523000 | 587000 | 108000 |
| K | 569 | 18000 | <200 | 276 | <200 | <200 | <200 | 3300 |
| Mg | 29300 | 15600 | 1650 | 2350 | 94300 | 3310 | 800 | 74700 |
| Mn | 2040 | 109 | 208 | 310 | 13200 | 360 | 94 | 3440 |
| Mo | <2 | 21 | 26 | 3 | 3 | 34 | 29 | 16 |
| Na | 649 | 318 | 207 | 580 | 336 | 213 | 193 | 497 |
| Ni | 126 | 490 | 427 | 21 | 469 | 535 | 580 | 31000 |
| P | 796 | 1030 | 100 | <50 | <50 | 283 | 1170 | 133 |
| Pb | <10 | <10 | 34 | <10 | <10 | 59 | 75 | <10 |
| S | 2400 | 8970 | 188000 | 103000 | 5700 | 228000 | 255000 | 40500 |
| Sc | 25.8 | 8.0 | 3.3 | 2.7 | 20.6 | 3.9 | 3.9 | 25.9 |
| Sr | 18 | 3 | 2 | 9 | 55 | 4 | 4 | 74 |
| Ti | 1640 | 1670 | 16 | 13 | 73 | 14 | 13 | 418 |
| V | 302 | 128 | 39 | 2 | 36 | 59 | 57 | 99 |
| Y | 3.4 | 6.1 | 2.6 | 2.2 | 6.0 | 5.0 | 5.1 | 19.5 |
| Zn | 15 | 5 | 29 | 801 | 6 | <1 | <1 | 79 |
| Bi | 0.12 | 0.37 | 9.58 | <0.01 | 0.11 | 6.18 | <0.01 | 0.02 |
| Sb | 0.69 | 0.17 | 3.91 | 0.03 | 0.16 | 9.26 | <0.03 | <0.03 |
| Se | 0.41 | 1.48 | 15.50 | 2.20 | 0.64 | 20.80 | <0.02 | 2.93 |
| Te | <0.01 | **0.08** | **1.41** | **0.11** | <0.01 | **0.68** | <0.01 | **0.56** |
| Pd | <0.01 | <0.01 | <0.02 | <0.01 | <0.01 | <0.01 | <0.01 | <0.01 |
| Pt | <0.01 | <0.01 | <0.02 | <0.01 | <0.01 | <0.01 | <0.01 | <0.01 |
| Au | <0.01 | **0.03** | **0.08** | **0.88** | **0.11** | **0.08** | **0.16** | **1.05** |

[1]Phyllite or tuffite. Only narrow barren carbonate veins
[2]Dark and fine-grained tectonic microbreccia containing clasts of former veins (sample is from the shear zone)
[3]A contact between altered phyllite or tuffite with a graphite-bearing phyllite. This sample contains pyrite and chalcopyrite
[4]A vein sample of coarse and quartz-rich quartz-carbonate vein with chalcopyrite and pyrite
[5]A vein sample of a very broad vein composed almost entirely of carbonate
[6]A massive sulphide-facies iron formation composed of microcrystalline pyrrhotite and minor quartz and graphite. Brecciated by Phase II pyrrhotite veinlets comprising minor amounts of quartz, carbonate and sulpharsenides (at least arsenopyrite)
[7]Gold ore (see Fig. 2). This vein sample in graphitic phyllite was exceptionally rich in sulpharsenides, as demonstrated by the high As, Ni and Co contents (arsenopyrite, gersdorffite ± cobaltite, glaucodot)

Further complexity is added by the existence of a banded sulphide-facies iron formation immediately N of the gold-mineralized zone (Holma *et al*. 2006). Veins consisting of secondary pyrrhotite and minor amounts of chalcopyrite and arsenopyrite brecciate this small syngenetic iron formation. Interestingly, we can connect these three ore minerals to the gold mineralization. No such iron formations have been found from the ~5 km long Levijärvi-Loukinen area, east of Sirkka (Fig. 1).

## 5 CONCLUSIONS

Quartz-carbonate-sulphide vein stockworks and breccia zones form the Sirkka occurrence. In one end of the spectrum, there are carbonate and quartz-carbonate veins variably rich in pyrrhotite and chalcopyrite ± pyrite, and in the other, quartz-carbonate veins containing variable amounts of pyrrhotite, chalcopyrite and sulfarsenides ± pyrite. Gold occurs in native form associated with the latter vein type, but also the other paragenesis, which is locally argentiferous, shows enrichment in gold. The occurrence is enriched in Cu, Fe, Ni, Au ± Ag and Co, from which the most valuable commodities are Cu and Au. Nickel±Co were gained from metakomatiites, and Fe±Cu from syngenetic mineralization.

Although the multimetallic association described above is an uncommon feature for orogenic gold deposit, we consider the Sirkka occurrence to belong to the orogenic category of gold mineralization. This conclusion is based on that the local enrichment of base metals can be traced back to their source rocks. Also, key features of other known gold deposit classes are missing. Therefore, there is no reason to classify the occurrence otherwise, and we conclude that: 1) the Sirkka occurrence is an example of the atypical metal association subtype of orogenic gold mineralization (*sensu* Goldfarb *et al*. 2001; Groves *et al*. 2003); 2) mineralization took place when a saline fluid reacted with reducing, sulphide-rich pre-gold mineralized host rocks.

## ACKNOWLEDGEMENTS

This work represents results of a larger PhD study of the first author. He acknowledges the financial support of the Finnish Graduate School in Geology.

## REFERENCES

Eilu P, Sorjonen-Ward P, Nurmi P, Niiranen T (2003) A review of gold mineralization styles in Finland. *Economic Geology* 98, 1329-1353.

Goldfarb RJ, Groves DI, Gardoll S (2001) Orogenic gold and geologic time: a global synthesis. *Ore Geology Reviews* 18, 1-75.

Groves DI, Goldfarb RJ, Robert F, Hart CJR (2003) Gold deposits in metamorphic belts: overview of current understanding, outstanding problems, future research, and exploration significance. *Economic Geology* 98: 1-29.

Holma MJ, Keinänen VJ, Ojala VJ, Eilu P (2003) The Levijärvi-Loukinen Au-Ni-Cu occurrence: A Palaeoproterozoic polymetallic orogenic gold mineralisation in the Sirkka Line tectonic structure, northern Finland. In: Eliopoulos D.G. et al. (eds) *Mineral Exploration and Sustainable Development*. Millpress, Rotterdam Netherlands, pp 1073-1076.

Holma MJ, Törmänen T, Gehör S (2006) Characteristics of the sulphide-facies iron formation near the Sirkka kaivos gold occurrence, northern Finland. In: Peltonen P, Pasanen A (eds) *Bulletin of the Geological Society of Finland, Special Issue* 1, p. 51.

Holma MJ, Keinänen VJ (2007) The Levijärvi-Loukinen gold occurrence: An example of orogenic gold mineralisation with atypical metal association. In: Ojala VJ (ed) Gold in the Central Lapland Greenstone Belt, Finland. *Geological Survey of Finland, Special Paper* 44 (in press)

Patison NL, Korja A, Lahtinen R, Ojala VJ, the FIRE Working Group (2006) FIRE seismic reflection profiles 4, 4A and 4B: insights into the crustal structure of northern Finland from Ranua to Näätämö. In: Kukkonen IT, Lahtinen R (eds) Finnish Reflection Experiment FIRE 2001-2005. *Geological Survey of Finland, Special Paper* 43, 161-222.

# Alteration vectors to ore, modelled by VSWIR reflectance at the Mataralampi orogenic gold occurrence, eastern Finland

Eilu, P., Kuosmanen, V. & Laitinen, J.
*Geological Survey of Finland, Espoo, Finland*

Ojala, V.J.
*Geological Survey of Finland, Rovaniemi, Finland*

ABSTRACT: The orogenic Mataralampi gold occurrence, in the Archaean Kuhmo greenstone belt in eastern Finland, is hosted by a sequence of felsic and intermediate rocks. Mineralization-related alteration is characterised by formation of muscovite, calcite and pyrite. Relative abundances of alteration minerals can be reliably and quickly defined by filtered SWIR spectra. In addition, a spectral parameter related to the distance of a sample from the gold mineralization was recognised at Mataralampi.

KEYWORDS: Archaean, Kuhmo, Finland, greenstone belt, gold, alteration, VSWIR

## 1 INTRODUCTION

The intensity of alteration typically shows extensive oscillation in profiles across orogenic gold deposits and their alteration haloes (*eg*. Skwarnecki 1988, Eilu *et al*. 2001). Although mineralogical changes are usually quite obvious, it can be visually hard to define any consistent mineralogical or geochemical trends that could be used as reliable vectors to potential ore in such profiles.

In hydrothermal ore deposits, there is always alteration with mineralogical and chemical zoning (McCuaig & Kerrich 1998, Eilu *et al*. 1999) but the complex structural setting tends to obscure the view of the explorationist, especially in the early stages of exploration when limited data are available. Hence, a quick standardized measurement of alteration mineral abundances, which could be used and give results *during* the logging of core, can be of great benefit for any exploration and research project.

In this context, we have tested the potential of the VSWIR measurements on samples from a profile across the Mataralampi Archaean orogenic gold deposit and its alteration halo in eastern Finland (Fig. 1).

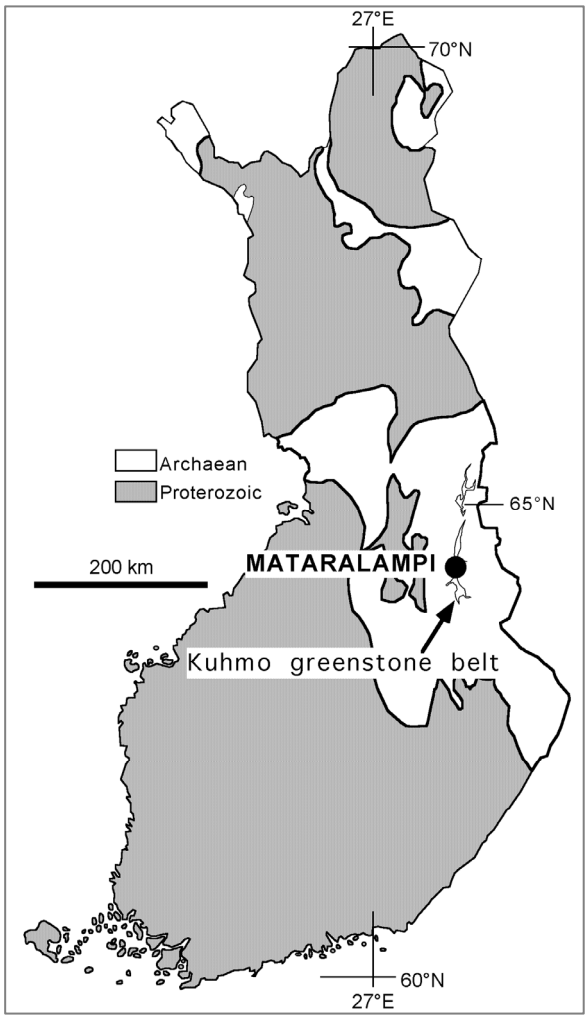


Fig. 1. Location of the Mataralampi gold occurrence in Kuhmo greenstone belt, eastern Finland.

## 2 MATARALAMPI GEOLOGY, MINERALIZATION

The Mataralampi gold occurrence is in the central part of the 100 km long, 10 km wide, N-

S trending Archaean Kuhmo greenstone belt in eastern Finland (Fig 1). Mataralampi is close to the western margin of the greenstone belt. From west to east, there is a steeply west-dipping sequence from granodiorite through quartz and feldspar porphyry to mafic lava (Fig. 2). The granodiorite can be regarded as a part of the TTG granitoids bounding the greenstone belt. The granodiorite and the porphyries are calc-alkaline and the mafic lava is Mg-tholeiitic in their primary composition. The quartz porphyry has an U-Pb zircon age of 2743±2 Ma (Hyppönen 1983). The sequence is cut by NW-trending Proterozoic dolerites and a N-trending alkalibasaltic dyke.

Four stages of Neoarchaean deformation (D1-D4) have been recorded in the Kuhmo belt (Luukkonen 2001). The Mataralampi gold occurrence is related to subvertical, N- to NNW-trending, 0.5-5m wide, shear zones containing quartz veins and intense alteration. The mineralized shear zones probably are local late-D3 or D4 structures whose age is somewhere between 2.70 Ga and 2.65 Ga (Luukkonen 1992, 2001), and the mineralization hence took place under peak or slightly post-peak metamorphic conditions, close to the greenschist-amphibolite facies boundary.

The main host rock to gold is the quartz porphyry unit, but the quartz-feldspar porphyry is also weakly mineralised.

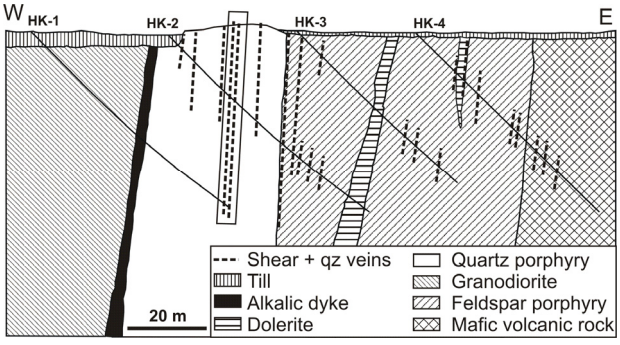


Fig. 2. Schematic geological section across the Mataralampi gold occurrence, Kuhmo greenstone belt, eastern Finland. The main mineralised zone is indicated by the shear zones within the subvertical rectangle. HK-1 to HK-4 indicate diamond-drill holes sampled by us.

## 3 ALTERATION PETROGRAPHY

All rock types in the investigated sequence have been metamorphosed to upper greenschist facies. The mineral assemblage in unaltered felsic to intermediate rocks is quartz - albite - K feldspar - biotite - epidote - titanite, and in mafic rocks hornblende - albite - epidote - titanite - ilmenite. All significant gold mineralization at Mataralampi is in the felsic to intermediate rocks, and these rock types also form most of the investigated section. Hence, we here consider alteration in these rock types.

When approaching the gold-mineralized zones, the following changes can be detected: 1) increase in the intensity of shearing and disintegration of feldspar phenocrysts, 2) increase in the volume of quartz-calcite±sulphide veins, and 3) replacement of the regional metamorphic mineral assemblage by muscovite-quartz-albite-calcite-rutile-pyrite. All these changes are gradual. Hence, definition of distinct zones in the alteration halo is difficult. Consequently, during core logging, the degree of alteration was classified according to the intensity of sericitisation (formation of muscovite) by using hand lens only. Thin section investigations confirmed macroscopic visual classification.

## 4 VSWIR REFLECTANCE METHODOLOGY

Alteration was here estimated using visible to short wave infrared (VSWIR, 350-2500nm) electromagnetic radiation reflectance spectra of the drill core samples. These wavelengths are widely used for mineral mapping by remote sensing of outcropped areas (*e.g.* Cudahy *et al.* 2000). In the current work, alteration intensity was revealed by the entire VSWIR spectra, but the individual alteration minerals muscovite, biotite and calcite were best mapped using high-pass filtered spectra of SWIR wavelengths (1500-2500nm). The samples studied in the current work are a set of small slabs originally sawn from diamond-drill core for thin section preparation. Each spectrum is recorded using 1 nm wavelength step and 3-10nm resolution.

The sample surfaces were grinded with a small hand-held tool in order to avoid total reflections from shiny crystal or cleavage surfaces. The reflectance was measured using the FieldSpecFR spectroradiometer which can measure over the VSWIR wavelength range.

To maximize Signal-to-Noise Ratio, each measurement was repeated 10 times. Reflectance of 'pure' mineral samples of sericite, biotite and calcite were also measured and the results were used as pure mineral models to estimate respective alteration. The 'pure minerals' are mainly single crystals of calcite, mus-

covite (sericite) and biotite from the Parainen marble mine in SW Finland.

The sample reflectance is exemplified by Figure 3, where the curves are ordered (shifted along y-coordinate) according to their relative depth. Their relative mutual amplitudes are unchanged. Similarity between the VSWIR or SWIR spectra were measured by cosα-similarity defined as

$$\cos\alpha = \frac{(\overline{\mathbf{m}} - \overline{\mathbf{m}}_\mathbf{a}) \cdot (\overline{\mathbf{n}} - \overline{\mathbf{n}}_\mathbf{a})}{|\overline{\mathbf{m}} - \overline{\mathbf{m}}_\mathbf{a}||\overline{\mathbf{n}} - \overline{\mathbf{n}}_\mathbf{a}|}$$

where

$\overline{\mathbf{m}}$ = model spectrum
$\overline{\mathbf{m}}_\mathbf{a}$ = mean albedo spectrum of the model
$\overline{\mathbf{n}}$ = sample spectrum
$\overline{\mathbf{n}}_\mathbf{a}$ = mean albedo spectrum of the sample

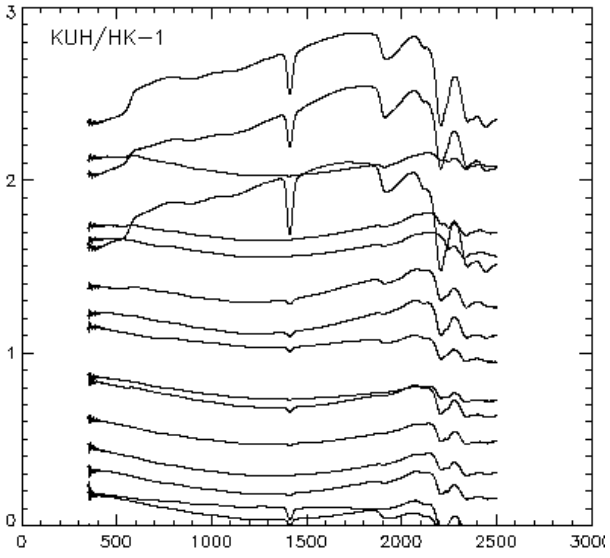


Fig. 3. The VSWIR reflectances from all samples measured from the drill hole no. 1 at Mataralampi. The curves are shifted according to the depth order of the samples. Wavelength on x-axis and 3*theoretical maximum reflectance on y-axis.

## 5 VSWIR RESULTS ON ALTERATION

The samples representing the most intense hydrothermal alteration (*e.g.* nos. 16 and 17 in Fig. 4) exhibit spectral similarity with their vicinities. The similarity can be approximated by a 3-degree polynomial trend function ('Polyn' in Fig. 4) of distance from the major shear zone. This function seems to extend through all the felsic and intermediate rock units of the sequence with moderate to high fit, R ≥ 0.5. For an average sample, which is not intensely altered, the respective fit is lower. In the Mataralampi area but outside the mafic volcanic rock, this trend function may serve as an estimate to the distance of a sample from the gold mineralization.

Alteration of the Härmänkylä rocks is indicated by an increase in the amount of sericite and calcite in felsic rocks and increase in biotite and calcite in mafic rocks. These minerals have special spectral reflectance characteristics, i.e. detailed forms of the curve, within the SWIR wavelength range, at 1500–2500nm. Therefore, the original reflectance curves were processed to enhance details of the curve and detectability of these individual minerals (*cf.* Martinz-Alonso *et al.* 1997). The curves were high-pass filtered over 301nm and thereafter only the SWIR wavelengths were used. As quartz, feldspars and hornblende (the major minerals in addition to micas at Mataralampi) are not too active within the SWIR wavelengths, their contribution to the spectra is very small. Therefore, the effect of the minerals produced by alteration becomes more pronounced in the SWIR spectra.

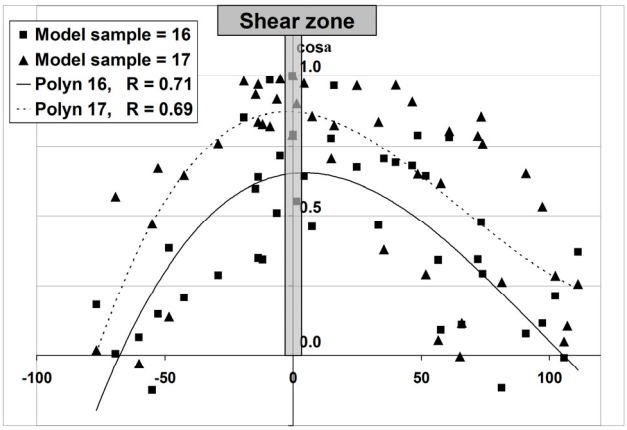


Fig. 4. Cosα similarities (y-axis) of the VSWIR spectra around (x-axis, meters) the shear zone between the samples 16 and 17 and all other samples. The respective correlation coefficients R for the fitted functions Polyn 16 and 17 are also shown.

The cosα-similarities between the high-pass filtered spectra of the pure minerals and all samples were computed and the results for the drill hole no. 1 are shown in Figure 5. The results show relative abundances of sericite, biotite and calcite, provided that other SWIR-active minerals are not present.

Thin sections from the same samples were also analysed using automatic Mineral Liberation Analysis (MLA), and the results were compared to the relative abundance estimation from the SWIR-spectra (Fig. 5). The sample surfaces studied in the spectral work are not ex-

actly the same as those in thin sections. The spectral estimator cosα for each alteration mineral was calibrated to the same average and standard deviation level with the MLA-result for Figure 5: despite the somewhat different target surface, the correlation between the SWIR and MLA data is clearly positive, and indicates the usability of the SWIR in quick mapping of alteration in drill core.

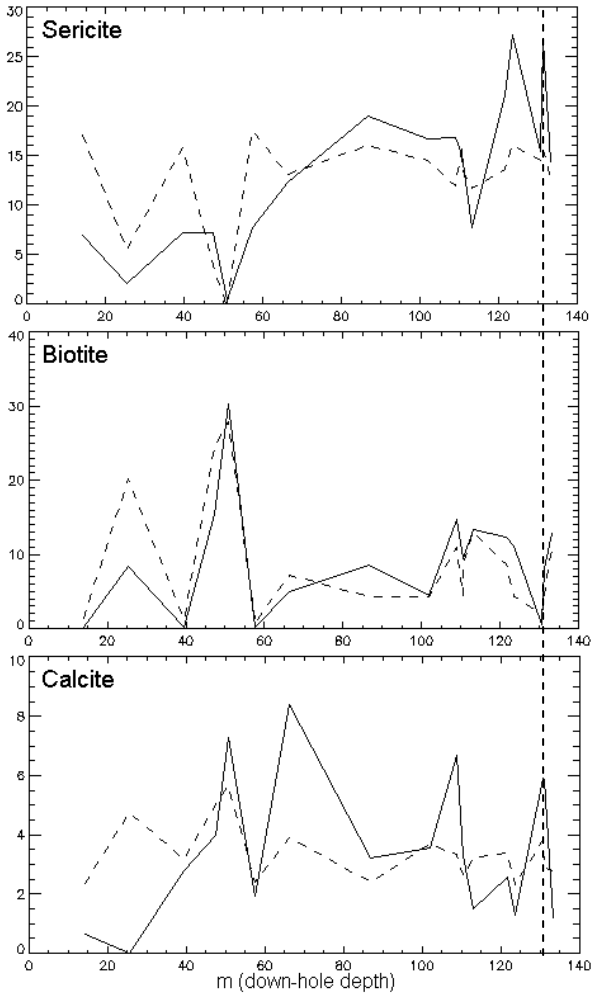


Fig. 5. The SWIR-estimated (dashed line) and MLA-determined (solid line) abundances (%, y-axis) of alteration minerals sericite, biotite and calcite for the drill hole no. 1 at Mataralampi. The main mineralized zone is at 130-132 m depth and marked with a dotted line.

## 6 CONCLUSIONS

At the Mataralampi gold occurrence, in Archaean rocks of eastern Finland, the following features characterise the alteration related to orogenic gold mineralization:

1. Regional metamorphic mineral assemblages are gradually,replaced towards the potential ore by the assemblage quartz-muscovite-calcite-albite-pyrite-rutile.
2. The extent of the hydrothermal alteration related to orogenic gold mineralization can be defined using VSWIR spectra.
3. Relative abundances of alteration minerals can be reliably and quickly defined by filtered SWIR spectra.
4. A spectral parameter, related to the distance of a sample from the gold mineralization, was recognised at Mataralampi

## ACKNOWLEDGEMENTS

Thanks to Polar Mining Oy for funding field work, thin section preparation and whole-rock geochemical analyses, and for the permission to publish the results.

## REFERENCES

Cudahy TC, Brauhart C, Okada K (2000) Targeting VMS-style Zn mineralization at Panorama, Australia, using airborne hyperspectral VNIR-SWIR Hymap data. In *Procs Fourteenth International Conference on Applied Geologic Remote Sensing, Las Vegas, Nevada*, 6-8 Nov 2000. 395-402.

Eilu P, Mathison CI, Groves DI, Allardyce W (1999) Atlas of Alteration Assemblages, Styles and Zoning in Orogenic Lode-Gold Deposits in a Variety of Host Rock and Metamorphic Settings. *Geology and Geophysics Department (Centre for Strategic Mineral Deposits) & UWA Extension, University of Western Australia, Publication* 30. pp64.

Eilu P, Mikucki EJ, Dugdale AL (2001) Primary geochemical dispersion related to the Bronzewing lode-gold deposit, Western Australia. *Mineralium Deposita* 36: 13-31.

Hyppönen V (1983) Explanation to the maps of Pre-Quaternary rocks, sheets 4411, 4412, 4413. *Geological Survey of Finland.* pp60.

Luukkonen E (1992) Late Archaean and Early Proterozoic structural evolution in the Kuhmo-Suomussalmi Terrain, eastern Finland. *Annales Universitatis Turkuensis.* Ser. A. II 78. pp37.

Luukkonen E (2001) Pre-Quaternary rocks of the Lentiira map-sheet area. Explanation to the bedrock maps 4414+4432 Lentiira. Geological map of Finland 1:100000. *Geol Survey of Finland*. pp68.

Martinz-Alonso SE, Atkinson WW, Goez AFH, Kruse FA (1997) Short Wave infrared (SWIR) spectrometry of illite ("sericite") to estimate temperature of formation of hydrothermal mineral deposits. *Proceedings of the 12th International Conference and Workshops on Applied Geologic Remote Sensing, Denver, Colorado.* II: 426-429.

McCuaig TC, Kerrich R (1998) P-T-t-deformation-fluid characteristics of lode gold deposits: evidence from alteration systematics. *Ore Geology Reviews* 12: 381-453.

Skwarnecki MS (1988) Alteration and deformation in shear zone hosting gold mineralization at Harbour Lights, Leonora, Western Australia. *Geology Department & University Extension, The University of Western Australia, Publication* 12: 111-130.

# Remobilization processes in the metamorphosed Boliden massive sulphide deposit: Insights from LA-ICP-MS analysis of invisible gold in arsenopyrite and pyrite

T. Wagner & T. Wenzel
*Institut für Geowissenschaften, Universität Tübingen, Germany*

R. Klemd
*Mineralogisches Institut, Universität Würzburg, Germany*

B. Mattsson
*Boliden Mineral AB, Boliden, Sweden*

ABSTRACT: The metamorphosed Boliden massive sulphide ore deposit, northern Sweden, is characterized by arsenopyrite-rich orebodies and unusually high gold enrichments (up to 300-600 g/t) in crosscutting veins. We performed a LA-ICP-MS study on the gold distribution in fine-grained massive arsenopyrite and pyrite ore, partially recrystallized arsenopyrite ore, and both arsenopyrite and pyrite porphyroblasts found in gold-rich veins. The gold concentrations in massive arsenopyrite are highest (30-50 ppm on average) and systematically decrease to 0-2.7 ppm with increasing degree of recrystallization. Gold concentrations in pyrite ore are much lower and do not exceed 0.2 ppm. The LA-ICP-MS data, coupled with textural constraints demonstrate that gold is progressively remobilized from massive sulphide ores during metamorphism and reprecipitated in veins and other low-strain sites.

KEYWORDS: remobilization, metamorphism, massive sulphide deposit, LA-ICP-MS, gold

## 1 INTRODUCTION

Gold-rich volcanic hosted massive sulphide deposits metamorphosed at upper-greenschist to amphibolite grade are often characterized by a significant redistribution and upgrading of the gold, resulting in economically valuable ore bodies (Huston *et al*., 1989). Based mainly on the geological observations, it was proposed that gold is liberated during fluid-facilitated metamorphic recrystallization of the massive sulphide ore bodies and redeposited within veins and fractures (Marshall & Gilligan, 1987; Larocque *et al*., 1995; Marshall *et al*., 2000). In order to test the metamorphic gold remobilization model, we performed a systematic LA-ICP-MS study of gold distribution in different textural types of arsenopyrite and pyrite ore from the gold-rich Boliden massive sulphide deposit, northern Sweden.

## 2 THE BOLIDEN DEPOSIT

The Boliden Au-Cu-As deposit is located in the Paleoproterozoic Skellefte district (Fig. 1), which hosts a large number of mainly submarine VHMS deposits (Weihed *et al.*, 1992; Allen *et al*., 1996). These deposits are hosed by a sequence of submarine volcanic and subvolcanic rocks with intercalations of clastic sedimentary units, which were formed in a volcanic arc setting at 1.89-1.85 Ga (Billström & Weihed, 1996). The Skellefte district was affected by regional Svecokarelian metamorphism at greenschist to amphibolite grade around 1.83-1.81 Ga (Billström & Weihed, 1996); peak metamorphic conditions in the Boliden area were estimated at 430 °C and 5-7 kbar (Berglund & Ekström, 1978).

Boliden is an unusually gold-rich (average grade of 15 g/t) VHMS deposit, which is hosted by a rhyolitic metavolcanic unit likely representing a cryptodome-tuff volcano (Allen *et al*., 1996; Bergman *et al*., 1996). The wall rocks show a distinctly zoned hydrothermal alteration, with an inner muscovite-andalusite and an outer chlorite zone (Bergman *et al.*, 1996). The massive sulphide ores, mainly composed of pyrite, arsenopyrite, and minor pyrrhotite, occur as elongate lenses along an approximately E-W oriented structure. Deformation and metamor-

phism resulted in widespread recrystallization of the massive ore bodies and the formation of crosscutting gold-rich quartz-sulphide-sulphosalt veins. These vein ores contain significant gold enrichments, as high as 300-600 g/t (Bergman *et al*, 1996, Weihed *et al*., 1996). Based on the vein mineralogy, fluid inclusion data and phase equilibria constraints, it was concluded that the gold-rich veins formed close to peak metamorphic conditions at about 400-450 °C and 5 kbar (*e.g*., Wagner & Jonsson, 2001).

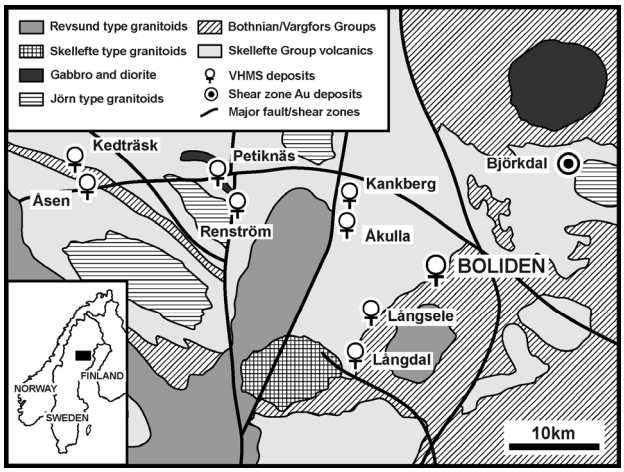


Figure 1. Geological sketch map of the eastern part of the Skellefte district, Sweden, showing the location of the Boliden deposit.

## 3 TEXTURAL RELATIONSHIPS

The massive sulphide orebodies are mainly composed of pyrite, which contains abundant lenses of arsenopyrite and minor irregular bodies of pyrrhotite. Massive arsenopyrite ore is very fine-grained with a spongy fabric. The degree of recrystallization is generally very low, but varies from ores that appear to be almost unaffected to ores with a clearly visible fine-grained recrystallization texture. In contrast, massive pyrite ore displays a penetrative recrystallization. Portions of the massive arsenopyrite ore lenses that are located adjacent to zones with enhanced fluid access such as veins and fractures are more coarse-grained and show a pronounced recrystallization.

The textural characteristics of arsenopyrite hosted by crosscutting gold-rich quartz-sulphide-sulphosalt veins are very different to those of the massive arsenopyrite ore. Arsenopyrite is present as large porphyroblasts, commonly associated with pyrite porphyroblasts of similar grain size and textural appearance. Both arsenopyrite and pyrite porphyroblasts are enclosed in a matrix of quartz, chalcopyrite, pyrrhotite, galena and a variety of complex Cu-Pb-Bi-Sb sulphosalts. Coarse-grained gold is generally concentrated in low-strain zones within these veins, *e.g.* along grain boundaries and in microfractures, and is associated with weaker sulphide minerals such as pyrrhotite, chalcopyrite and sulphosalt phases.

## 4 DISTRIBUTION OF INVISIBLE GOLD

The major element composition of arsenopyrite, pyrite, and vein-hosted gold was established by wavelength-dispersive electron-probe microanalysis. Gold concentrations in sulphide minerals were determined by laser ablation inductively coupled plasma mass spectrometry (LA-ICP-MS).

We performed 254 spot analyses of the gold concentration in arsenopyrite and pyrite. Gold distribution in arsenopyrite is plotted in Figure 2. The three texturally distinguishable arsenopyrite types show very different gold distributions. Gold concentrations in fine-grained massive arsenopyrite ore is highest and lies in the range of 3.8-108 ppm, with the majority of data being around 30-50 ppm. In contrast, partially recrystallized massive arsenopyrite ore and arsenopyrite porphyroblasts in gold-rich veins show much lower gold concentrations, in the range of 0.05-71.5 ppm and 0-2.7 ppm, respectively. The majority of data from the partially recrystallized massive arsenopyrite range from 0.05-19.0 ppm (Fig. 2, with only 6 out of 41 analyses having higher values. The gold concentrations in both massive pyrite ore and pyrite porphyroblasts are also very low, ranging from 0 to 0.22 and from 0 to 0.19 ppm, respectively.

## 5 GOLD COMPOSITION

The chemical composition of vein hosted gold shows pronounced variability, even within individual samples. The Au/(Au+Ag) ratios range from 0.39 to 0.93 and in most samples Hg is an essential constituent that can reach concentrations up to 8.6 wt.% (Fig. 3. The compositions found correspond well with analytical data reported from quartz veinlets in arsenopyrite ore and quartz-tourmaline veins (Bergman Weihed *et al.*, 1996; Wagner & Jonsson, 2001).

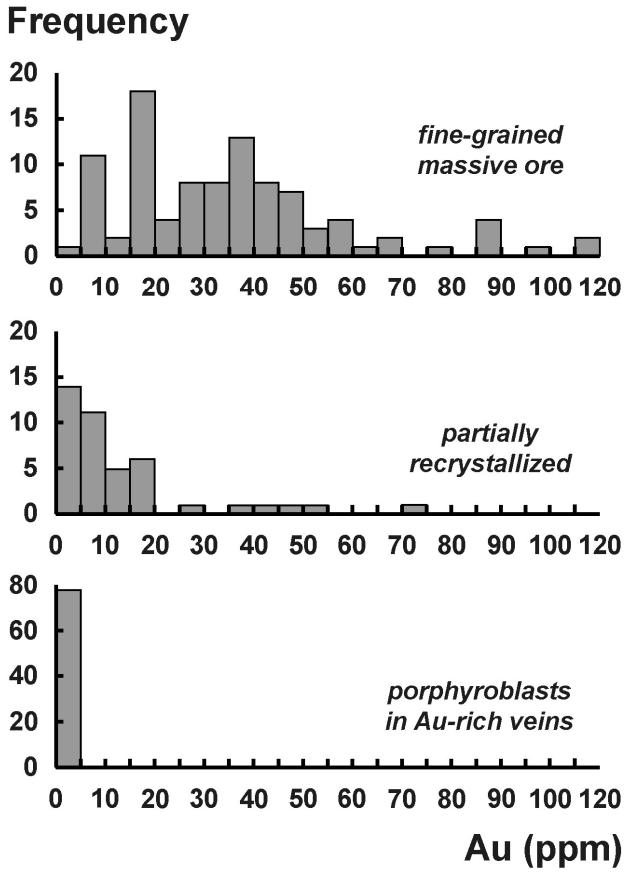


Figure 2. Gold concentrations (in ppm) in fine-grained massive arsenopyrite ore, partially recrystallized arsenopyrite ore, and arsenopyrite porphyroblasts in gold-rich veins.

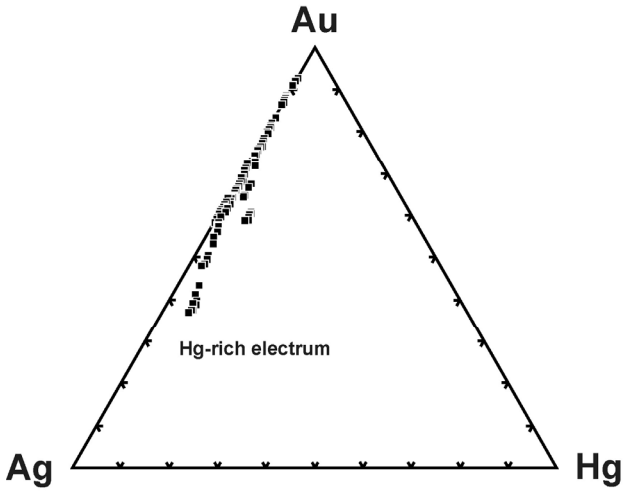


Figure 3. Composition of vein-hosted gold plotted in the system Au-Ag-Hg.

## 6 DISCUSSION AND CONCLUSIONS

Our LA-ICP-MS data for arsenopyrite clearly show that the degree of recrystallization is reflected by the gold distribution. The fine-grained massive arsenopyrite ore that experienced very little recrystallization has retained high gold concentrations, reaching up to 108 ppm. With increasing metamorphic recrystallization, gold was progressively remobilized. The arsenopyrite porphyroblasts found in the gold-rich veins are the final product of this process. Despite the extremely high gold grades in these veins, arsenopyrite contains very little gold, with maximum values on the order of a few ppm.

In contrast, both massive pyrite ore and pyrite porphyroblasts in gold-rich veins are very poor in gold. The penetrative recrystallization experienced by the pyrite-rich massive ore likely resulted in a complete loss of the original gold content. The observed gold distribution in pyrite and arsenopyrite likely reflects the different response of both minerals to deformation and metamorphism (McClay & Ellis, 1983; Craig & Vokes, 1993). Moreover, we clearly observed that the fluid access and fluid-facilitated mass transfer played a major role in the mobilization of gold. Strongly veined and brecciated parts of the arsenopyrite ore bodies experienced a substantial loss of gold, whereas massive ores with very little fluid access retained high gold concentrations.

The LA-ICP-MS data, coupled with our textural observations provide a conclusive evidence for the metamorphic upgrading model that has been proposed for metamorphosed VHMS deposits (Marshall & Gilligan, 1987; Marshall *et al*., 2000). Additional support to this model comes from the chemical composition of the vein-hosted gold. The gold alloys display highly variable Au/Ag ratios and pronounced Hg concentrations (Fig. 3). These compositional characteristics are different from that of gold found in shear zone hosted orogenic gold deposits, both in the Skellefte district and elsewhere (Morrison *et al*., 1991). We conclude that metamorphic upgrading is indeed the principal mechanism responsible for the significant gold enrichment observed at Boliden and many other metamorphosed VHMS deposits worldwide.

## ACKNOWLEDGEMENTS

This project was made possible by funding from the German Research Council (DFG) to TW. Boliden Mineral AB is thanked for granting access to sample material from the Boliden mine and for their support during the field

campaign. The assistance of H. Brätz during LA-ICP-MS analysis is very much appreciated.

## REFERENCES

Allen RL, Weihed P, Svenson SÅ (1996) Setting of Zn-Cu-Au-Ag massive sulphide deposits in the evolution and facies architecture of a 1.9 Ga marine volcanic arc, Skellefte District, Sweden. *Econ. Geol.* 91: 1022-1053.

Berglund S, Ekström TK (1978) Arsenopyrite and sphalerite as T-P indicators in sulphide ores from northern Sweden. *Mineral. Deposita* 15: 175-187.

Bergman Weihed JB, Bergström U, Billström K, Weihed P (1996) Geology, tectonic setting, and origin of the Paleoproterozoic Boliden Au-Cu-As deposit, Skellefte District, northern Sweden. *Econ. Geol*. 91: 1073-1097.

Billström K, Weihed P (1996) Age and provenance of host rocks and ores in the Palaeoproterozoic Skellefte District, northern Sweden. *Econ. Geol.* 91: 1054-1072.

Craig JR, Vokes FM (1993) The metamorphism of pyrite and pyritic ores: an overview. *Mineral. Mag.* 57: 3-18.

Huston DL, Large RR (1989) A chemical model for the concentration of gold in volcanogenic massive sulphide deposits. *Ore Geol. Rev*. 4: 171-200.

Larocque AC, Hodgson CJ, Carbri LJ, Jackman JA (1995) Ion-microprobe analysis of pyrite, chalcopyrite and pyrrhotite from the Mobrun VMS deposit in northwestern Quebec: evidence for metamorphic remobilization of gold. *Can. Mineral.* 33: 373-388.

Marshall B, Gilligan LB (1987) An introduction to remobilization: Information from ore-body geometry and experimental considerations. *Ore Geol. Rev*. 2: 87-131.

Marshall B, Vokes FM, Larocque, ACL (2000) Regional metamorphic remobilization: Upgrading and formation of ore deposits. *Rev. Econ. Geol.* 11: 19-38.

McClay KR, Ellis PG (1983) Deformation and recrystallization of pyrite. *Mineral. Mag.* 47: 527-538.

Morrison GW, RoseWJ, Jaireth S (1991) Geological and geochemical controls on the silver content (fineness) of gold in gold-silver deposits. *Ore Geol. Rev*. 6: 333-364.

Wagner T, Jonsson E (2001) Mineralogy of sulfosalt-rich vein-type ores, Boliden massive sulphide deposit, Skellefte district, northern Sweden. *Can. Mineral*. 39: 855-872.

Weihed P, Bergman J, Bergström U (1992) Metallogeny and tectonic evolution of the Early Proterozoic Skellefte district, northern Sweden. *Prec. Res*. 58: 143-167.

# Orogenic gold in southwestern Finland

K. Saalmann
*Geological Survey of Finland, P.O. Box 96, 02151 Espoo, Finland*

ABSTRACT: Many gold occurrences in southwestern Finland are hosted by quartz veins and shear zones truncating volcano-sedimentary successions with magmatic arc affinity. Because of a clear structural control on mineralization, as well as the relative timing late in the overall orogenic structural history, they are good examples for orogenic gold in this region. The orogenic evolution comprises an early 1.88-1.86 Ga collisional stage comprising folding and thrusting (D1+D2) followed by a 1.84-1.81 Ga post-collisional stage with a change from compression to dextral transpression (D3). While high-grade metamorphism and partial melting is widespread, especially in the southern regions, deformation in other areas took place at retrograde conditions. In many occurrences, gold mineralization is spatially and temporally associated with quartz veins and shear zones formed during D3. At regional scale, many prospects appear to be aligned along and controlled by SW-NE to W-E and NW-SE striking zones. Identification of orogenic gold occurrences and their possible genetic links, including dating of mineralization, are critical for future exploration in southwestern Finland.

KEYWORDS: orogenic gold, Svecofennian orogeny, structural evolution

## 1 INTRODUCTION

The host rocks of most gold prospects in southwestern Finland are deformed and metamorphosed mafic to felsic volcanic and pyroclastic rocks intercalated with metasedimentary rocks (mica schists and mica gneisses). Metavolcanic rocks ranging from basalt to rhyolite, with andesitic rocks being the most common, clearly dominate the lithology in this area. Geochemically, the calc-alkaline metavolcanic rocks show a subduction zone component and arc-affinity (Hakkarainen 1994, Lahtinen 1996) and thus, the succession represents a volcanic arc setting. The deposition of the volcano-sedimentary succession occurred at about 1.89-1.88 Ga, possibly starting already at about 1.91 Ga. Syn-tectonic plutonic rocks of gabbroic, (quartz-)dioritic, granodioritic and tonalitic composition intruded the succession. The rocks were metamorphosed at amphibolite conditions with the metamorphic grade increasing to the south and leading to local migmatisation and partial melting. Late-tectonic K-granites and pegmatitic veins are the youngest magmatic rocks.

Two sets of respectively SW-NE to WSW-ENE and NW-SE trending shear zones and faults control the overall geometry of the region (Fig 1) and are also developed on prospect- and outcrop-scale.

## 2 STRUCTURAL EVOLUTION

Early polyphase deformation (D1+D2) is characterized by compression leading to intense folding and stacking, and formation of subhorizontal structures. The compositional layering either represents the original sedimentary layering or an early foliation. On outcrop-scale, isoclinal folds are preserved in a cm- to dm-scale deforming the compositional layering and thin quartz veins. The dominant penetrative foliation and schistosity, which is represented by axial planar to isoclinal folds, formed during these events. In some localities, a SSE-plunging stretching and mineral lineation is well preserved, which is parallel to the fold axes. A lo-

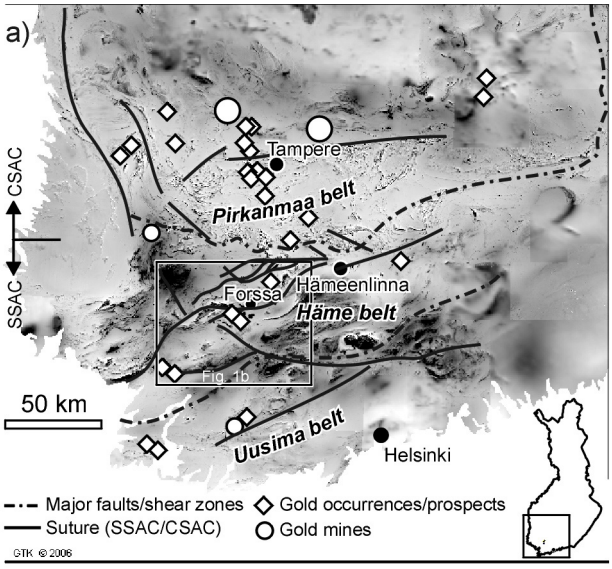


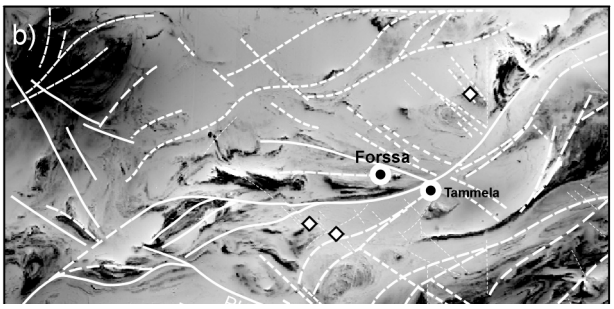


Fig. 1: Aeromagnetic maps and main faults in southwestern Finland (a) and in the Forssa-Somero area (b); FINGOLD database GTK. The SW-NE alignment of gold occurrences follows the approximate strike of major shear zones; NW-SE alignment corresponds with the orientation of NW-SE faults supporting the importance of these structures on gold deposition. In addition to major SW-NE to WSW-ENE trending lineaments, NW-SE faults are widespread in the whole area; they are parallel to the major Painio-Hirsjärvi shear zone (PHSZ). SSAC = Southern Svecofennian Arc Complex, CSAC = Central Svecofennian Arc Complex.

cally developed weak mylonitic fabric suggests that folding was associated with ductile shearing, possibly in relation to early thrusting, which, considering the steeply SE- to SSE-plunging lineation, was directed to the NW to NNW. The present-day steep dip and plunge of the structures result from later stages of folding. The early compressional stages are interpreted to result from the collision of the Southern Svecofennian Arc Complex (SSAC) with the Central Svecofennian Arc Complex (CSAC) in the north (Fig. 1a). Deformation was accompanied by metamorphism and synorogenic plutonism. This plutonism is dated at 1.88-1.86 Ga (Väisänen & Hölttä, 1999, Väisänen *et al*., 2002) providing constraints on the age of the 1.88-1.86 Ga collisional stage.

Following the collisional stage, a change from compressional to transpressional tectonics took place giving rise to the so-called post-collisional stage (D3) (*e.g*. Ehlers *et al*., 1993). While in some areas (*e.g*. northern parts of the Häme belt) this change post-dates the peak metamorphism (although it may follow shortly after it), crustal anatexis and formation of migmatites and granites is widespread in the Uusima belt and southern Häme belt. During this deformation phase, regional upright folds refolding earlier folds, with steep axial planes and SW-NE to W-E strike, have formed, which, in addition to subsequently developed shear zones and faults, represent the dominant map-scale structures and define the dominant trend in southwestern Finland.

Folding was accompanied by shearing and with time, shear deformation and localization of deformation became more important. Two sets of respectively SW-NE to WSW-ENE and NW-SE striking shear zones and faults are developed and the pattern suggests dextral transpression (Fig. 1b) in a regional stress field with $\sigma 1$ being oriented approximately WNW-ESE to NW-SE. In addition to a dextral strike-slip sense of shear, the fault displacement comprises a dip-slip component. The pattern can be observed from outcrop-scale to regional-scale. Magmas dated at 1840–1810 Ma (Huhma, 1986; Väisänen *et al.*, 2000) were emplaced along the transcurrent shear zones. Widespread crustal anatexis and granulite facies peak metamorphism started at 1.84–1.83 Ga, inferred from zircon growth in granulites and leucosomes, and is suggested to have continued to *ca.* 1.81 Ga (Väisänen *et al.*, 2002). In regions not affected by high-grade metamorphism during this stage (*e.g*. northern Häme belt), deformation took place during retrograde metamorphic conditions. Simultaneous occurrence of a variety of structures ranging from (semi-) ductile shearing to brittle fracturing is typical for the brittle-ductile transition, suggesting a temporal change to generally more brittle conditions during progressive deformation. In these areas, WSW-ENE to SW-NE striking quartz veins have formed (Fig. 2). They commonly show sheared margins, and the wall rocks of many quartz veins show a strong foliation parallel to the quartz vein margins.

Various faults and shear planes comprising NE-SW to W-E trending sinistral faults associated with NE-SW striking quartz veins that occur partly in tension gashes correspond to a

stress field of *ca*. NE-SW oriented compression related to a subsequent brittle deformation phase (D4). It involves reactivation of pre-existing faults and shear zones that have formed during earlier phases. In this new stress field, SW-NE to WSW-ENE striking D3 dextral or oblique contractional faults have been reactivated inversely as extensional or sinistral faults. Brittle overprinting of earlier fabrics probably also occurred along NW-SE oriented faults, which already formed during earlier stages (D2 or D3; *e.g*. as tear faults connecting variously displaced segments of a thrust).

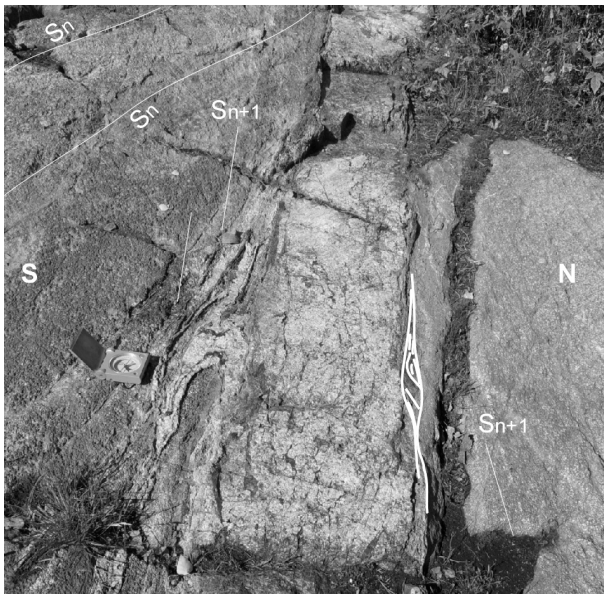


Fig. 2: W-E trending D3 quartz tourmaline vein in the southern parts of the Riukka prospect cutting the dominant foliation at acute angle. The sheared margin indicates a dextral component of shear during emplacement. Scale (compass) = 7.5 cm

## 3 STRUCTUAL CONTROL ON MINERALIZATION

Mineralization is closely related to quartz veins and WSW-ENE to SW-NE oriented shear zones formed during D3 (Fig. 2). Higher gold concentrations are in most cases, in addition to quartz veins, spatially associated with shear zones and faults, typically in brittle reactivated shear zones. Likewise, drill core data display a clear SW-NE trend of elevated gold contents. Quartz veins are in many places accompanied by sulphidization of the wall rock. On a map scale it is obvious that the gold occurrences are located at second and third order shear zones and faults parallel to the major SW-NE to W-E and NW-SE striking lineaments (Fig. 1b). In single prospects, elevated gold contents occur especially at intersection points of the two fault sets. Formation of various quartz veins is not restricted to D3 but also occurred during early and late phases of the structural evolution. Auriferous quartz veins, however, formed mainly during D3 and gold is clearly related to D3 structures. A stress field during D3 with $\sigma 1$ oriented NW-SE to WNW-ESE would cause (re)activation of NW-SE directed faults as extensional faults or fractures, especially during the later, more brittle stages of progressive D3 deformation. These steep faults would act as conduits for fluids during upward flow from deeper crustal levels while the fluid flow along WSW-ENE to SW-NE striking structures would occur along dilatant zones like dilatant jogs or fault oversteps.

## 4 OROGENIC GOLD IN SOUTHWESTERN FINLAND AND IMPLICATIONS FOR FUTURE EXPLORATION

A number of gold prospects have been investigated in southern Finland, which represent various genetic types, like metamorphosed epithermal, orogenic mesothermal, massive sulphide and submarine hydrothermal, whereas for some prospects, the origin is not resolved (Eilu *et al.* 2003). It is not yet studied if individual gold deposits, which have different origins and structural settings in the Häme belt, and possibly also in other areas in southern Finland, are temporarily linked or whether they belong to the same tectonic regime and event.

The occurrence of many gold occurrences in metamorphic terrains, their association with compressional/transpressional deformation, a strong structural control of mineralization, coexistence of ductile and brittle structures, mineralization occurring during the later, retrograde stages of orogenic evolution as well as the importance of auriferous quartz veins are all typical of orogenic gold deposits (*e.g.* Groves *et al.* 1998), and a number of prospects in southwestern Finland would correspond well to mesothermal orogenic gold *sensu* Groves *et al*. (1998).

Considering the regional structural evolution in this area and the ages of related tectonomagmatic events, mineralization of the orogenic gold is likely to have taken place during 1.84–1.81 Ga.

At regional scale, at least a number of gold occurrences in southern Finland seem to be controlled by shear zones or faults, mostly

striking SW-NE to W-E. This is also reflected in the SW-NE alignment of gold prospects in the southern regions (Häme and Uusimaa belts) (Fig. 1a). Within single prospect areas, a NW-SE alignment of neighbouring prospects is recognizable. Gold mineralization occurred late orogenic in many of these occurrences, implying that different tectonic blocks or terranes, for instance the Southern and Central Svecofennian Arc complexes, have already been juxtaposed. A dominance of (W)SW-(E)NE and NW-SE oriented structures in regions north of the Häme belt is also obvious, as is the NW-SE alignment of a number of gold occurrences further north between Tampere and Hämeenlinna (Fig. 1a). This alignment might be due to NW-SE oriented semi-brittle to brittle faults acting as fluid pathways, which could suggest a possible temporal and spatial relationship to the orogenic gold mineralization in the Southern Svecofennian Arc Complex (Häme/Uusimaa belts) and Central Svecofennian Arc Complex, and thus genetic links between distant deposits of previously attached but originally different tectono-stratigraphic terranes. On the other hand, however, many gold prospects cannot be correlated but record a different setting and/or timing in the relative structural evolution. Hence, it is unlikely that gold mineralization in southern Finland was connected to a single event but occurred during several episodes either pre-, syn- or post-peak metamorphic. Despite these differences, prospects of orogenic gold linked to late-orogenic mineralization might show similarities in style, timing and structural control implying a link to regional-scale and local-scale structures like shear zones and faults. Future prospecting should focus on second- and third-order structures branching from major WSW-ENE and NW-SE shear and fault zones. Aerogeophysical data and maps turned out to be especially useful for identification and evaluation of major folds and faults in the Häme and Uusimaa belts, and GIS-based exploration methods and stress mapping seem to be promising techniques for new findings in the future.

## ACKNOWLEDGEMENTS

The presented study is a contribution to the project "Geological and metallogenic bedrock modelling", Geological Survey of Finland. The author would like to thank M. Tiainen for fruitful discussions in the field.

## REFERENCES

Ehlers, C., Lindroos, A., Selonen, O. (1993) The late Svecofennian granite–migmatite zone of southern Finland — a belt of transpressive deformation and granite emplacement. *Precambr. Res.* 64: 295–309.

Eilu, P., Sorjonen-Ward, P., Nurmi, P. & Niiranen, T. (2003) A review of gold mineralization styles in Finland. *Economic Geology* 98: 1329-1354.

FINGOLD public database, Geological Survey of Finland (GTK). ed. by P. Eilu.; *Internet-link:*

*http://en.gtk.fi/ExplorationFinland/Commodities/Gold/gtk_gold_map.html*

Groves, D.I., Goldfarb, R.J., Gebre-Mariam, M., Hagemann, S.G. & Robert, F. (1998) Orogenic gold deposits: A proposed classification in the context of their crustal distribution and relationship to other gold deposit types. *Ore Geology Reviews* 13: 7-27.

Huhma, H. (1986) Sm–Nd, U-Pb and Pb–Pb isotopic evidence for the origin of the early Proterozoic Svecokarelian crust in Finland. *Geol. Surv. Finland Bull.* 337: 48p.

Väisänen, M., Hölttä, P. (1999) Structural and metamorphic evolution of the Turku migmatite complex, southwestern Finland. *Bull. Geol. Soc. Finland* 71: 177–218.

Väisänen, M., Mänttäri, I., Kriegsman, L.M., Hölttä, P. (2000) Tectonic setting of post-collisional magmatism in the Palaeoproterozoic Svecofennian Orogen, SW Finland. *Lithos* 54: 63–81.

Väisänen, M., Mänttäri, I. & Hölttä, P. (2002): Svecofennian magmatic and metamorphic evolution in southwestern Finland as revealed by U-Pb zircon SIMS geochronology. *Precambrian Research* 116: 111-127.

# Gold mineralization in the Greywacke Zone, Eastern Alps: T-X conditions constrained by IR microthermometry on tetrahedrite

J. G. Raith
*Department of Applied Geosciences and Geophysics, University of Leoben, Leoben, Austria*

H. Kucha
*University of Mining and Metallurgy, Krakow, Poland*

ABSTRACT: Infrared (IR) microthermometry allows the study of microtextures and fluid inclusions in As-poor (< 2.5 wt% As) tetrahedrite, which is opaque in the visible spectral range. The data allow constraining T-X conditions of tetrahedrite-hosted gold mineralization in the Greywacke Zone, Eastern Alps. Fluid inclusions in tetrahedrite are coeval with small solid inclusions of chalcopyrite, Au-oxysulphides, minor arsenopyrite and gold. They are of low salinity ($T_m$ –3 to –14°C) and homogenization temperatures range between ~85 and ~200 °C. Gold was transported by these low salinity aqueous fluids and not by synorogenic higher saline fluids found in gangue quartz. Gold-oxysulphides occur in the hydrothermal as well as in the supergene assemblages together with native gold of different chemical composition and microtexture. They indicate that sulphoxyanion species such as thiosulphate complexes played a major role in the mobilisation and transport of gold and its (re-) precipitation in low temperature geological environments.

KEYWORDS: gold, oxysulphides, fluid inclusions, infrared microthermometry, tetrahedrite

## 1 INTRODUCTION

The study of fluid inclusions by means of microthermometry has become a routine method for constraining the conditions (PVTX) of formation of hydrothermal ore deposits. Because most ore minerals are non-transparent in visible light fluid, inclusions normally cannot be studied in these opaque minerals. Alternatively, fluid inclusions in associated gangue minerals such as quartz or carbonates are measured. However, these studies are based on the (often) oversimplified assumption that the gangue minerals formed coevally with the ore minerals.

This assumption is not valid without restrictions, especially in complex poly-stage ore para-geneses. In the near infrared spectral range ($\lambda \leq 2.5\mu m$) some oxides and sulphides become transparent (Lueders, 1996) allowing microthermometric measurements of fluid inclusions hosted within the ore mineral of interest.

In this contribution we present fluid inclusion data for tetrahedrite, which has rarely been studied by IR microthermometry. The samples studied are from gold occurrences in the Greywacke Zone (GWZ), Eastern Alps, Austria. We constrain the T-X conditions of gold mineralization from microthermometric data and we discuss the possibility of gold transport by sulphoxyanion species during metamorphic hydrothermal and supergene processes.

## 2 GEOLOGICAL SETTING AND GOLD MINERALIZATION

The gold occurrences investigated are located in the Western Greywacke Zone (WGWZ), which is part of the Upper Austroalpine very low- to low-grade basement units of the Eastern Alps. The WGWZ includes Late Ordovician metaignimbrites and Silurian to Devonian carbonate platform sediments, as well as siliciclastic rocks deposited at a passive continental margin (Heinisch, 1988). Eoalpine metamorphism reached sub-greenschist to greenschist facies conditions and is of Cretaceous age.

Gold has been confirmed from several locations in the GWZ including Veitsch, Erzberg/Eisenerz, Rottenmann, Larzenbach/ Hüttau, Igelsbach, Giellach, St. Veit im Pongau, Mühlbach am Hochkönig (Mitterberg Südrevier, Hauptgang). The samples studied are from

historic Cu mines at Larzenbach and St. Veit im Pongau.

These two occurrences are part of the Cu district Mitterberg - Mühlbach - Larzenbach where the largest Cu mine of the Eastern Alps, located at Mitterberg (total ~250000 t Cu), was mined until the seventies of the last century. Details about gold mineralization and oxysulphides from Mitterberg and Veitsch have been published by Kucha (1995; 1997).

The comparable ores at Larzenbach are hosted by low-grade metasedimentary rocks, metabasites, metatuffs and metacarbonates. Strata-bound as well as discordant vein-type ores are distinguished. A gold content of 4 g/t in tetrahedrite-rich ore was reported from Larzenbach (Günther, 1978).

An uraninite U-Pb age of 90 ± 5 Ma Paar & Köppel, 1978) from Mitterberg confirmed formation of the discordant ores in this ore district during the Eoalpine orogeny.

## 3 GOLD OXYSULPHIDES

Several types of gold have been distinguished in the Greywacke Zone (Kucha *et al*., 1997). Most of the visible gold (a few to 250 µm in size) is found within and close to microfractures in tetrahedrite. The remaining visible gold is intergrown with or encapsulated by sulphoarsenides (mainly arsenopyrite). Some types of gold are associated with large amounts of low reflecting Au-oxysulphides (Fig. 1 A, B).

Two types of oxysulphides are distinguished: Type 1 oxysulphides are associated with primary gold and occur as inclusions in gold and within microfractures in tetrahedrite. These oxy-sulphides are intergrown with native gold of high fineness. It is to be noted that oxysulphides of Type 1 are not interconnected along microfratures but form isolated solid inclusions in primary gold (Fig. 1A). This observation indicates that Type 1 oxysulphides precipitated coevally with hydrothermal primary gold. Type 1 oxysulphides from Larzenbach have (in wt.%): Au 31.87 – 44.09, Cu 7.73 – 14.40, Ag 4.03-7.25, Fe 1.67-3.01, Sb 2.41 – 7.51 and S 6.07 – 13.11; they are quite variable in Hg.

Type 2 oxysulphides formed during weathering and are associated with cuprite, limonite and, less often, malachite. They are associated with Cu-rich secondary gold. In this supergene assemblage, oxysulphide grains are interconnected and the textures indicate local dissolution and re-precipitation of gold (Fig. 1 B). Oxysulphides of Type 2 are lower in Au and Ag and higher in Cu and Sb; (in wt.%) Au 6.95 - 10.22, Cu 22.02 - 24.77, Ag 1.83 – 2.74, Sb 12.40 - 12.79, and S 18.02 – 19.17.

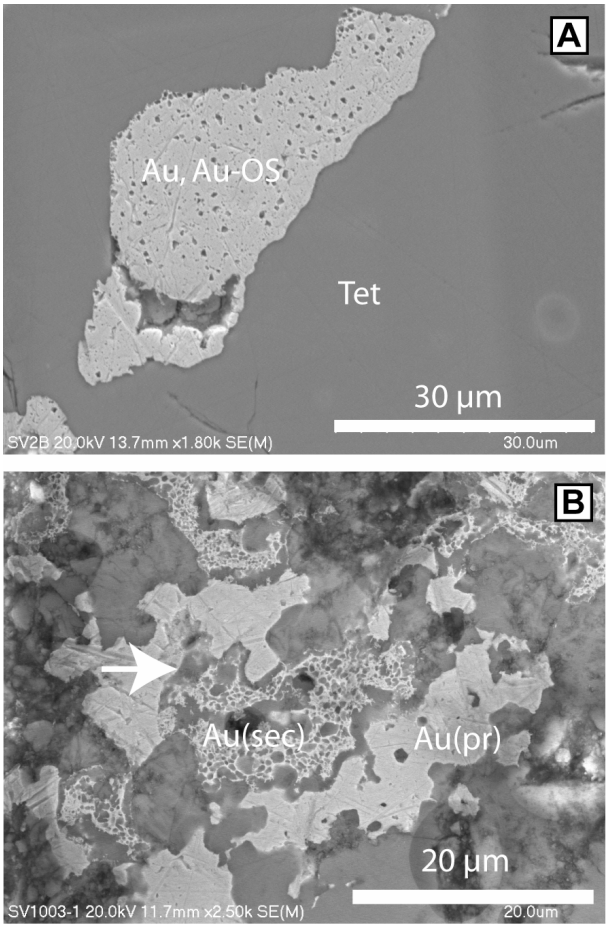


Fig. 1 SEM images. A. Primary hydrothermal gold (Au) with tiny isolated inclusions of Type 1 oxysulphides (Au-OS) in tetrahedrite (Tet). Sample SV4, St. Veit. B. Inclusion-free primary gold (Au (pr)) and spongy, Cu-rich secondary gold (Au (sec)); the latter is intergrown with darker Type 2 oxysulphides; arrow points out replacement of primary gold by secondary gold plus gold oxysulphides. Sample SV1003, St. Veit.

## FLUID INCLUSION STUDIES

### 3.1 *Transparency of tetrahedrite in IR- light*

IR microscopy has not been widely applied to fahlore-group minerals because their IR-transparency is limited by chemical composition. Our combined IR and mineral chemical study confirmed that IR transparency is restricted to As-poor tetrahedrite. The approximate As content where tetrahedrite becomes IR-opaque is about 2.0 - 2.5 wt.% As. Higher As contents cause rapid increase in opacity. In addition, it was observed that temperature has a

significant effect on the opacity of tetrahedrite.

Due to the opacity of arseniferous tetrahedrite, the system of microfractures developed in As-poor tetrahedrite and filled with arseniferous tetrahedrite can be made visible in IR light.

### 3.2 *Fluid inclusions in tetrahedrite*

Fluid inclusions in tetrahedrite are usually accompanied by myriads of small, solid, opaque inclusions of chalcopyrite and minor arsenopyrite, oxysulphides and gold (Fig. 2).

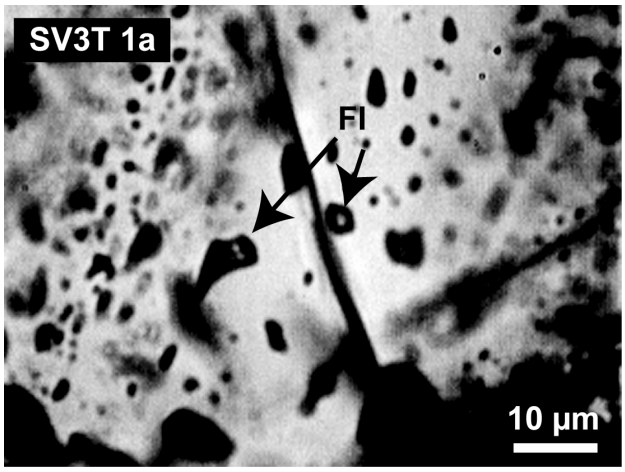


Fig. 2. Infrared (IR) microphotograph showing opaque solid and aqueous two-phase (L+V) fluid inclusions (arrows, FI) within IR-transparent tetrahedrite. Sample from St. Veit im Pongau.

Fluid inclusions in tetrahedrite are irregular and small (< 10 µm). They occur as individual inclusions along trails (Fig. 2). The inclusions are two-phase (L+V) aqueous inclusions and homogenize into the liquid phase (V ⌈ L). Within a single trail they show consistent L:V ratios (~ 70:30). Fluid inclusions of sample SV3 yielded temperatures of homogenization ($T_h$) between 140 and 185°C (Fig. 3). $T_m$ varies between –3 to –14°C and indicates fluids of low to moderate salinity. Fluid inclusion data for tetrahedrite sample LA1 from Larzenbach are less consistent. $T_h$ (V ⌈ L) ranges between 85 and 190°C, $T_m$ between –3 to –8.5°C (Fig. 3).

### 3.3 *Fluid inclusions in quartz*

Two types of fluid inclusions are distinguished in quartz:

*Quartz Type 1*. Fluid inclusions are intimately intergrown with As-poor tetrahedrite. They occur in clusters rather than in trails, are of irregular to rounded shape and small (<5 µm). They are aqueous two-phases (L+V) to one-phase (L) and have variable L:V ratios. $T_h$ (V ⌈ L) of individual two-phase inclusions within this cluster varies considerably (72-195°C).; $T_m$ for Type 1 inclusions ranges from –3 to –12°C, indicating low to moderate saline fluids.

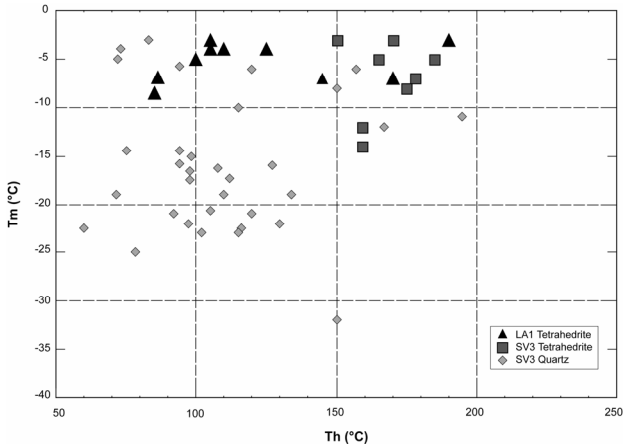


Fig. 3. $T_h$ vs. $T_m$ plot for fluid inclusions in tetrahedrite and quartz. Gold transporting fluids of low salinity were found in tetrahedrite and quartz. Higher saline aqueous fluids, unrelated to Au mineralization, are restricted to quartz.

*Quartz Type 2*. Most fluid inclusions in quartz are of higher salinity ($T_m$ down to –32 °C) and have lower $T_h$ (up to 150°C; Fig. 3). These aqueous inclusions are not directly related to tetrahedrite. They are small (<5 to 10 µm), show consistent L:V (90:10) ratios and preferentially occur along secondary inclusion trails. Low eutectic temperatures (quite consistently below –56°C) and the observation of final ice melting between –36.5 and –32°C suggest that, in addition to NaCl, there are other salts present in this fluid.

## 4 FLUID COMPOSITION AND ORIGIN

The gold mineralizing/mobilizing fluids entrapped in tetrahedrite are characterized as low to moderately saline aqueous solutions. From textural relationships it is concluded that formation of primary gold with Type 1 inclusions of Au-oxysulphides is related to these low salinity fluids and not to the high salinity fluids entrapped in quartz. The latter highly saline $CO_2$-free fluids (>240°C, ≥2 kbar) at Mitterberg were interpreted as fluids characteristic for "synorogenic" Cretaceous ore deposits in the Eastern Alps (Pohl & Belocky, 1994).

The gold transporting fluids in the polymetallic Cu deposits of the Greywacke Zone also differ significantly from those observed in Neoalpine mesothermal gold veins in the Alps; in the latter, low-salinity mixed aqueous-carbonic fluids predominate.

The minimum formation temperatures of gold mineralization in the WGWZ can be deduced from homogenization temperatures (Larzenbach: 122 ± 36 °C, St Veit: 165 ±13 °C) of fluid inclusions in tetrahedrite. Temperatures during the gold forming stage likely did not exceed ~250°C, because this is known as the upper stability limit of oxysulphides (Giggenbach, 1974). We hypothesize that Au mineralization in the WGWZ is related to late to post-orogenic processes in the Eastern Alps. The deduced T-X conditions differ from those in mesothermal gold veins of metamorphic origin.

## 5 TRANSPORT OF GOLD

The low salinity and the deduced temperature range of the fluids make the transport of gold by chloro-, hydroxychloro complexes unlikely; these are important at higher temperatures (~400°C) in fluids of high salinity and low activity of reduced sulphur (Seward, 1991). At temperatures below 350 °C with oxidation states buffered by sulphate-sulphide or $H_2$, thiosulphide species (*e.g.* $Au(HS)_2^-$) become significant (Schenberger *et al.*, 1989). At temperatures below 250°C, oxysulphide and polysulphide anions such as thiosulphates ($S_2O_3^{2-}$) may play a significant role in gold transport and deposition of gold (Seward, 1991).

The observation that both primary gold of hydrothermal origin as well as remobilized secondary gold formed during weathering processes are intimately intergrown with gold-oxysulphides can be regarded as direct evidence that in the Greywacke Zone sulphoxyanion complexes could have played a major role for gold mobilization and transport.

## ACKNOWLEDGEMENTS

R. Bakker is thanked for his help with fluid inclusion measurements. This study was funded by the Austrian Academy of Sciences (ÖAW), Kommission für Grundlagen der Mineralrohstoffforschung.

## REFERENCES

Giggenbach, W. F., 1974, Kinetics of the polysulfide-thiosulfate disproportionation up to 240 °C: *Inorganic Chemistry,* v. 13, p. 1730-1733.

Günther, W., 1978, Die Kupferkiesbaue der Kupfergewerkschaft Larzenbach bei Hüttau (Fritztal)/Salzburg: *Der Aufschluss, Sonderheft,* v. 29, p. 365-372.

Heinisch, H., 1988, Hinweise auf die Existenz eines passiven Kontinentalrandes im Altpaläozoikum der Noerdlichen Grauwackenzone Ostalpen. *Schweizerische Mineralogische und Petrographische Mitteilungen,* v. 68, p. 407-418.

Kucha, H., Prohaska, W., and Stumpfl, E. F., 1995, Deposition and transport of gold by thiosulphates, Veitsch, Austria: *Mineralogical Magazine*, v. 59, p. 253-258.

Kucha, H., Stumpfl, E. F., and Prochaska, W., 1997, Au-oxysulphide inclusions in gold and their meaning for gold transport and deposition, Mitterberg, Austria, *in* Papunen, H., ed., *Mineral Deposits: Research and Exploration. Where do They Meet?:* Rotterdam/Brookfield, Balkema, p. 225-228.

Lueders, V., 1996, Contribution of infrared microscopy to fluid inclusion studies in some opaque minerals (wolframite, stibnite, bournonite); metallogenic implications: *Economic Geology*, v. 91, p. 1462-1468.

Paar, W., and Köppel, V., 1978, Die Uranknollen-Paragenese von Mitterberg (Salzburg, Österreich): *Neues Jahrbuch für Mineralogie Abhandlungen*, v. 131, p. 254-271.

Pohl, W., and Belocky, R., 1994, Alpidic metamorphic fluids and metallogenesis in the Eastern Alps: *Mitteilungen der Österreichischen Geologischen Gesellschaft,* v. 86 (1993), p. 141-152.

Schenberger, D. M., Barnes, H. L., and Wood, S. A., 1989, Solubility of gold in aqueous sulfide solutions from 150 to 350 °C: *Geochimica et Cosmochimica Acta,* v. 53, p. 269-278.

Seward, T. M., 1991, The hydrothermal geochemistry of gold, *in* Foster, R. P., ed., *Gold Metallogeny and Exploration:* London, Blackie, p. 37-62.

# Comparison of geotectonic settings and age of gold formations in the Kaczawa Mountains (SW Poland) with those from European Variscan belt during Carboniferous-Permian

S.Z. Mikulski
*Polish Geological Institute, 4 Rakowiecka Street, 00-975 Warsaw, Poland,*

ABSTRACT: Gold mineralization inform the Kaczawa Mountains is comparable with that from the European Variscan belt. Four main stages from ($Au_1$ to $Au_4$) of gold formation during Carboniferous-Permian have been recognized. However, in the Kaczawa Mountains $Au_1$ stage connected with the emplacement of syn-collisional granite (Tournaisian) has not been recognized yet. $Au_2$ and $Au_3$ stages were connected with geotectonic transition from the post-collisional into the within plate settings. These gold stages implies a change from mesothermal to epithermal conditions of Au precipitation during post-magmatic and volcanic processes connected with orogenic uplift, and deep fracturing (Upper Namurian-Stephanian-Autunian). $Au_4$ stage was the result of oxidative low temperature hydrothermal processes connected with basins formation in Upper Permian and/or Triassic.

KEYWORDS: gold; geotectonic setting, Variscan belt, Kaczawa Mountains, Sudetes, Poland, Bohemian massif

## 1 INTRODUCTION

The terrane collision in front of the closing Rheic Ocean between Euamerica and Gondwana, during the period of 350-280 Ma, led to the formation of a series of European Variscan gold provinces in Bohemian and Iberian massifs (Goldfarb *et al.* 2000). The Kaczawa Mountains are located in the Western Sudetes, which constitute the north-eastern part of the Bohemian Massif. The basement of the Western Sudetes unit is considered as a continuation of the Saxothuringian Zone of the European Variscides. In the Kaczawa Mountains historical gold production since medieval times, came from several small and medium size vein/lode quartz-sulphide type deposits. Among them two are most important, namely: Radzimowice deposit and Klecza-Radomice deposit.

## 2 GEOTECTONIC SETTING OF VARISCAN MAGMATIC ROCKS FROM AURIFEROUS REGIONS

The Kaczawa Mountains during Early Carboniferous is characterised by tectonic regime of compression/transpression characters on the convergent margin within orogen first of an accretionary character followed by collisional setting (Franke & Zelazniewicz, 2000). After the first stage of Variscan granite emplacement in Namurian the late collisional setting changed into post-collisional.


Fig. 1. The schematic structural zone divisions of the European Variscan belt with area location in the Western Sudetes in SW Poland

The Kaczawa metamorphic complex was rapidly uplifted during Namurian/Westphalian. In that time faulting and formation of intramountain-basins took place. These processes

were accompanied by intensive volcanism and flysch-like sedimentation.

The granitoid and other igneous rocks of Zelezniak intrusions from the area of the Radzimowice Au-As-Cu deposit plot in the volcanic arc granites field on the Y + Nb versus Rb diagram close to a triple boundary point that is characteristic of post-collisional granites. On diagrams of $Zr/Al_2O_3$ versus $TiO_2/Al_2O_3$ samples from Radzimowice fall into the continental and post-collisional fields. Lamprophyre dykes predates auriferous sulphide mineralization there. The lamprophyres from Radzimowice plot in the post-collisional arc field. Most probably in Late Namurian - Early Westphalian formed deep-seated fractures that opened channel ways for the migration of post-magmatic mineralizing fluids related to heat and acidic magmas (granites of the post-collisional characteristic: the ridge granite of the Karkonosze massif, Zelezniak granite and two-mica granite of the Strzegom-Sobótka massif). They were most probably responsible for auriferous sulphide mineralization widespread in the considering part of Variscan belt. On the diagram of Rb/30-Hf-Tax3 the Karkonosze and Zelezniak granite fall within the late- and post-collisional granite fields and most of the Strzegom-Sobótka granite in the within plate granite field. Such transition to within plate-setting is consistent with tectonic interpretations of the area presented by Awdankiewicz (1999) for the volcanic suite of Upper Carboniferous-Permian age from the Sudetic basins. The fast continental break-up, uplift and deep fracturing switch the geotectonic settings. The transition from the post-collisional to within plate settings was favorable for the formation of gold mineralization of epithermal type in upraised areas of the Kaczawa Mountains.

## 3 CLASSIFICATION AND TECTONIC MODELS OF GOLD MINERALIZATION IN THE KACZAWA MOUTAINS

Two main genetic models of gold deposit mineralization in the Kaczawa Mountains are proposed (Mikulski 2007). The geological setting and ore structures, type of alteration, physical-chemical characteristics of mineralized fluids, high contents of silver and base metals in Radzimowice indicates gold mineralization in the magmatic systems. Furthermore, geotectonic setting of igneous rocks of the Zelezniak intrusion on the discrimination diagrams, ore textures, low Au/Ag ratios, and significant Cu content point to a formation within magmatic environment of a post-collisional continental arc setting. Strong alteration processes at first of acidic and than of alkalic nature produced mineral assemblages that are characteristic of alkaline-related gold deposits. It was possible to regard the early mineralization at the Radzimowice deposit as transitional between porphyry and epithermal, and the late mineralization as epithermal type (Mikulski 2005).

The geological setting in accreted metamorphic terranes and the strong structural control of the ore bodies is characteristic for the Klecza-Radomice Au-As deposit. Besides, a low Au/Ag ratios, insignificant base-metal contents, and low salinity of mineralizing fluids allowed Mikulski (2003) to regard the ore mineralization from the KROD as an orogenic gold type mineralization according to the classification proposed by Groves *et al*. (1998). Most of Au mineralization occurs within schists with no direct relation with any magmatic body.

The shift from mesothermal to epithermal conditions of the gold mineralization in quartz-lode type deposits in the European Variscan belt is recognized as a common feature driven by changes in the uplift rates, tectonic regimes and heat production (Cathelineau *et al*. 2003). The latter authors recognized that the series of late Carboniferous orogenic gold deposits shows identical patterns of P-T-X-t fluid evolution that strongly differ from the commonly accepted models for orogenic Au deposits, allowing the definition of a Variscan-type.

## 4 THE AGE COMPARISON OF GOLD EVENTS IN THE KACZAWA MOUTAINS WITH OTHER AREAS OF THE EUROPEAN VARISCIDES

The European Variscan orogenic gold deposits formed *ca*. 350-280 Ma in uplifting massifs along the active western edge of the Paleo-Thetys Ocean (Goldfarb *et al.* 2000; Groves *et al.* 2005; Kerrich *et al*. 2000). Those deposits are now exposed in the southern and central Europe. Processes of gold mineralization recognized in the Kaczawa Mountains are quite similar to gold-mineralization processes described from the other areas of the European Variscan belt. However, the age of the gold ore formation is variable. The similar features are mostly caused by geotectonic evolution, two- or

three-stage evolution of fluid compositions and mineral precipitation, characteristic mineral paragenesis and texture (*e.g*. Cathelineau *et al*. 2003; Moravek *et al.* 1996; Noronha *et al*. 2000). Gold formation, exhumation of host rocks, extensional tectonic setting and lamprophyre dyke appear coeval in the Massif Central, Central Bohemian Province (Bouchot *et al.* 2000, 2003) and in the Kaczawa Mountains as well (Mikulski 2007).

In the Kaczawa Mountains auriferous mineralization post-dated regional metamorphism of host rocks, orogenic deformation, and the oldest stage of late-Variscan magmatism (*ca.* 330 Ma). The upper limit of the Variscan tectonometamorphic and magmatic activity was dated at 314-312 Ma by $^{40}Ar/^{39}Ar$ method (Marheine *et al*. 2002). According to the Re-Os data the age of *ca.* 317 Ma for auriferous Co-arsenopyrite from the Radzimowice deposit is coeval with SHRIMP ages of igneous rocks from ZI (Mikulski *et al*. 2005). This age of arsenopyrite despite its close correlation with magmatic evolution in the Zelezniak intrusion is also close to Re-Os age of auriferous arsenopyrite from Klecza (316.6 ± 0.4 Ma). This auriferous mineralization is not simultaneous with gold events described from the Central Bohemian province *ca*. 338 Ma (Bouchot et al. 2003) or at 344 ± 2.8 Ma by Re-Os method on molybdenite (Zachariáš & Stein, 2001).

In the Massif Central auriferous lodes were deposited between 330 and 285 Ma) with a distinct peak at 310-305 Ma (Bouchot *et al.* 2000; Marcoux *et al.* 2004). Age of the first stage of gold mineralization in the Kaczawa Mountains is closer to age of gold formation described from the Massif Central and Iberian massif. According to Cuney *et al.* (2002) two stages of gold mineralization in the French Massif Central took place. The first stage of gold formed in the early extensional syn-convergence setting during high temperature condition in the period of 330-315 Ma and the second stage of low temperature gold deposits formed at 315-300 Ma. Also, a cross-cutting relationship from the lodes in northern Portugal indicates gold formation first subsequent to emplacement of *ca.* 320-305 Ma granitoid and later mineralization being coeval with post-tectonic 290-280 Ma granitoid (Noronha *et al.* 2000).

In the Autunian sandstone in the Massif Central auriferous epithermal sinter that formed *ca*. 295 Ma was recognized (Marcoux *et al.* 2004). The Re-Os pyrite ages *ca.* 294 and 280 Ma from the Radzimowice and Klecza gold deposits in the Kaczawa Mountains respectively are younger and strongly correlated with volcanic activities during rifting in a late Autunian (Mikulski *et al*. 2005).

The formation of gold associated with hematite in Lower Silesia (*e.g*. Piestrzynski & Wodzicki 2000) is connected with oxidized fluid migration during the basin formation in a wide range of time from Upper Permian to Triassic.

## 5 CONCLUSION

In general, within the European Variscan belt it is possible to distinguished four main stages of gold formation:

1) Stage $Au_1$ connected with emplacements of syn-collisional granite,
2) Stage $Au_2$ (mostly auriferous sulphide) directly followed the emplacement of post-collisional granite and development of regional deep fractures,
3) Stage $Au_3$ (mostly base-metal sulphides with visible gold) formed during orogenic uplift and development of subvolcanic and volcanic processes in transition from continental arc to within plate setting,
4) Stage $Au_4$ (gold-haematite association) originated during the basin formation.

The gap of age between the considered above gold formation stages is *ca*. 30-40 Ma. The comparison of gold formations within European Variscan belt with those from the Kaczawa Mountains indicates the lack of the oldest Variscan gold-stage (Au1 *ca*. 350-330 Ma) in the Kaczawa Mountains, which was connected with syn-collisional granite emplacement.

## ACKNOWLEDGEMENTS

The analytical work was supported by the National Committee Scientific Research, Grant 4 T12B 029 30.

## REFERENCES

Awdankiewicz M (1999) Volcanism in a late Variscan intramountain trough: the petrology and geochemistry of the Carboniferous and Permian volcanic rocks of the Intra-Sudetic Basin, SW Poland. *Geol. Sudetica,* 32: 83–111.

Bouchot V, Milesi JP, Ledru P (2000) Crustal scale hydrothermal Paleofield and related Au, Sb, W orogenic deposits at 310-305 Ma (Massif Central). *SGA Newsletter*, 10: 6–10.

Bouchot V, Faure M, Feybesse JL, Correira P, Zacharias J (2003) Variscan orogenic gold district related to a regional scale Viséan detachment in the Central Bohemian metallogenic province (Czech Republick): a geodynamic reassessment: 747–750. *Proc. of the 7th biennial SGA meeting.* Millpress. Netherlands.

Cathelineau M, Boiron MC, Fourcade S, Marignac C (2003) The shift from "mesothermal" to "epithermal" conditions in orogenic gold: definition of a Variscan-type of quartz lode gold deposits: 751–753. *Proc. of the 7th biennial SGA meeting*. Millpress. Netherlands.

Cuney M, Alexandrov P, Le Carlier De Veslud C, Cheilletz A, Raimbault L, Ruffet G, Scaillet S (2002) The timing of W-Sn-rare metals mineral deposit formation in the W Variscan chain in their orogenic setting: the case of the Limousin area (Massif Central, France). *Geological Society Special Publication* 204: 213–228.

Franke W, Zelazniewicz A (2000) The eastern termination of the Variscides: terranes correlation and kinematics evolution. *Geol. Soc. London Spec. Publ.,* 179: 63–89.

Goldfarb RJ, Groves DI, Gardoll S (2000) Orogenic gold and geologic time: a global synthesis. *Ore Geol. Rev.* 18: 1–75.

Groves DI, Goldfarb RJ, Gebre-Mariam M, Hagemann SG, Robert F (1998) Orogenic gold deposits: A proposed classification in the context of their crustal distribution on relationship to other gold deposit types. *Ore Geol. Rev.* 13: 7–27.

Kerrich R, Goldfarb R, Groves D, Garwin S, (2000) The geodynamics of World-class gold deposits: characteristics, space-time distribution and origins. *SEG Rev. in Econ. Geol.* 13: 501–551.

Marcoux E, Le Berre P, Cocherie A (2004) The Meillers Autunian hydrothermal chalcedony: first evidence of a ~295 Ma auriferous epithermal sinter in the French Massif Central. *Ore Geol. Rev.* 25: 69–87.

Marheine D, Kachlik V, Maluski H, Patocka F, Zelazniewicz A (2002) The Ar-Ar ages from the West Sudetes (NE Bohemian Massif): constrains on the Variscan polyphase tectonothermal development. *Geol. Soc. Spec. Pub.,* 201: 133–155.

Mikulski SZ (2003) Orogenic quartz-sulphide-gold veins from the Klecza-Radomice ore district in the Kaczawa Mountains (W Sudetes): 787–790. *Proceedings of the 7th Biennial SGA meeting*. Millpress. Netherlands.

Mikulski SZ (2005) Geological, mineralogical and geochemical characteristics of the Radzimowice Au-As-Cu deposit from the Kaczawa Mountains (Western Sudetes, Poland) - an example of the transition of porphyry and epithermal style. *Mineral. Deposita,* 39, 8: 904–920.

Mikulski SZ, Markey RJ, Stein HJ (2005) Re-Os ages for auriferous sulphides from the gold deposits in the Kaczawa Mountains (SW Poland): 793–796. *Proc. of the 8th biennial SGA meeting.*

Mikulski SZ (2007) The late-Variscan gold mineralization in the Kaczawa Mountains, Western Sudetes. *Special Papers of PGI* v. 2: 1-113.

Moravek P (eds.), Pertold Z, Puncochar M, Studnicna B, Zacharias J (1996) *Gold deposits in Bohemia:* 96 pp. CGS. Prague.

Noronha F, Cathelineau M, Boiron M, Banks MC, Doira A, Ribeiro MA, Norgueira P, Guedes A (2000) A three stage fluid flow model for Variscan gold metallogenesis in N Portugal. *J. of Geoch. Expl.,* 71: 209–224.

Piestrzynski A, Wodzicki A (2000) Origin of the gold deposit in the Polkowice-West Mine, Lubin-Sieroszowice Mining District, Poland. *Mineral. Deposita* 35: 37–47.

Zachariáš J, Stein H (2001) Re-Os ages of Variscan hydrothermal gold mineralizations, Central Bohemian Metallogenic Zone, Czech Republic: 851–854. *Proc. of the Joint 6th biennial SGA-SEG meeting*. A.A. Balkema.

# Lithogeochemistry of the El Valle disseminated gold deposits, Asturias, NW-Spain.

A. Cepedal, M. Fuertes-Fuente & A. Martin-Izard
*Department of Geology, University of Oviedo, Spain*

S. González-Nistal & M. Barrero
*Río Narcea Gold Mines, Cayés-Llanera, Asturias, Spain*

ABSTRACT: The aim of this paper is to present the geochemical characterization of a suite of subvolcanic dykes and associated alterations of their host-rock in the disseminated gold deposit of the El Valle. From the lithogeochemical study, two different types of felsic subvolcanic rocks are distinguished and are probably the result of compositional gradients in the magma chamber due to crystal-melt fractionation and liquid-fractionation processes. Moreover, the elemental fluxes during the associated alterations indicate a decarbonation process accompanied by silicification and argillization of K-Al-bearing phases. This may be accompanied by iron released from reactive Fe-bearing minerals and the precipitation of disseminated arsenian pyrite and arsenopyrite with "invisible gold" during a sulphidation proccess.

KEYWORDS: gold, subvolcanic dykes, host-rock alteration, El Valle deposit, Spain

## 1 INTRODUCTION

The El Valle deposit is a disseminated gold deposit in altered rocks, which had undergone a previous mineralizing event that formed Cu-Au skarns, related to the intrusion of a calc-alkaline granitoid complex (Cepedal *et al*. 2000). The granitoids, marble, skarns and hornfels were subsequently intruded by a suite of felsic subvolcanic dykes, which appear to be related to the gold-bearing alteration mentioned above (Cepedal *et al*. 2006). The present work focuses on the geochemical characterization of the subvolcanic dykes and the host-rock alteration in the El Valle Deposit.

## 2 THE EL VALLE DEPOSIT

The El Valle deposit is included within the El Valle-Boinás Au-Cu deposit located in the Río Narcea Gold Belt (Asturias, NW Spain) (Spiering *et al.* 2000), which was an important gold-producer in Europe until the end of 2006. The origin of the gold mineralization at the El Valle-Boinás deposit is related to at least two magmatic stages: the intrusion of type-I calc-alkaline granitoids at 303±6 Ma (Martin-Izard *et al.* 2000) that developed a Cu-Au skarn and the intrusion of felsic subvolcanic dykes that crosscut all pre-existing rocks and produced different types of alterations. This last process was more intense in the mineralized area of the El Valle deposit, where these dykes are mainly located. The alteration includes significant hypogene and supergene oxidation. The mining of El Valle was from an open pit, mainly of free-gold and native copper bearing oxidized ore.

The sub-volcanic dykes are divided into two types according to petrographic characteristics:

Dykes-1. Porphyritic rhyolites, with bipyramid quartz phenocrysts, scarce sericitized feldspar phenocrysts, and anecdotic biotite completely altered; the groundmass is made up of fine-grained quartz, sericite, and rutile. Accessory minerals are apatite, tourmaline, and sulphides (pyrite, chalcopyrite and tetrahedrite). These dykes are commonly adularitized. The age obtained by Ar/Ar in adularia is 289.9±1 Ma (Cepedal *et al.* 2006).

Dykes-2. Porphyritic dacites with phenocrysts of globular quartz, sericitized feldspar, biotite and probably hornblende replaced by muscovite, sericite, and rutile-leucoxene; crypto to microcrystalline groundmass of quartz and sericite. Accessory minerals are pyrite, marcasite, bravoite, ankerite, titanite and fluorapatite. The ages are from 284±8 to 272±5

Ma by K/Ar in sericite (Martin-Izard *et al.* 2000).

The different alterations associated with the intrusion of these dykes are adularization, sericitization, silicification, argillization and sulphidation. Sericitization and adularization mainly affected the subvolcanic rocks and granitoids. Silicification is developed in the host rock of the dykes and at brecciated contacts between the dykes and their host-rock. The silicified rocks show different generations of quartz and

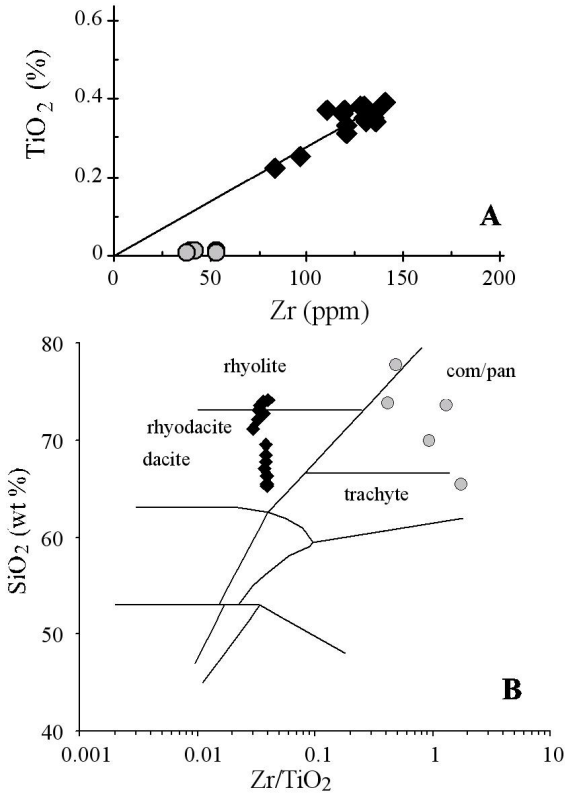


Figure 1. A. Bivariate plot of potentially immobile elements of the altered subvolcanic rocks from the El Valle deposit. B. El Valle subvolcanic rock distribution in the $Zr/TiO_2$ vs $SiO_2$ diagram of Winchester & Floyd (1977); circles and diamonds represent dykes 1 and 2, respectively

disseminated pyrite and arsenopyrite. Adjacent to the silicified zones, some areas are argillized, giving rise to masses of rock, consisting of fine-grained quartz, kaolinite±illite and disseminated pyrite and arsenopyrite. In altered zones with Au-grades, gold mainly occurs as "invisible gold" in the fine-grained arsenian pyrite and arsenopyrite, the former sulphide often occurring as pseudomorphic replacements of previous Fe-silicates, which indicates sulphidation.

## 3 LITHOGEOCHEMICAL STUDY

For the geochemical characterization of the subvolcanic rocks and the host-rock alteration at El Valle, samples of both were taken from drill-cores in Au-grade and barren zones. Major and minor elements were analyzed by ICP-ES and ICP-MS. Total carbon and sulphur were analyzed by Leco.

### 3.1 *Subvolcanic dykes*

All the subvolcanic rocks are altered. Thus, to facilitate the identification of different rock types and according to McLean & Kranidiotis (1987), plots of immobile element pairs were used (*e.g.* Fig. 1A). In these diagrams, dykes 1 and 2 plot separately, confirming that they are different rock types. These immobile elements were used to identify the protolith in the diagram $SiO_2$ vs. $Zr/TiO_2$ of Winchester and Floyd (1977) (Fig. 1B). Dykes-2 plot in the dacite/rhyodacite field and close to the limit with the rhyolite field, with consistent $Zr/TiO_2$. The dispersion in $SiO_2$ is due to the alteration rather than the degree of differentiation, since the immobile pairs indicate only one protolith. On the other hand, dykes-1 are in the comendite/pantellerite field, though we consider that their petrography does not support this classification.

Further differences are observed in the chondrite-normalized REE and N-MORB normalized trace-element patterns (Figs. 2A and B). In the REE diagram, dykes-2 show a steep pattern, whereas dykes-1 show a stronger Eu anomaly and a flat distribution of LREE, with a slightly deeper discontinuity at Nd. In the trace-element diagram, both dike types exhibit similar enrichment in LILE relative to HFSE, but dykes-2 have negative Sc, Ti, P and Ba anomalies, a Cs peak, and a trough at Nb and Ta, whereas dykes-1 have depletion in Zr-Hf and more significant negative Sc, Ti and P anomalies and neither the Cs peak nor the Nb-Ta trough. Both diagrams suggest that these igneous rocks were formed from subduction-related magmas, but it is not so clear in dykes-1. In the tectonic discrimination diagram after Pearce *et al*. (1984), dykes-1 plot in the syn-COLG field whereas dykes-2 plot in VAG and syn-COLG fields. The Rb-enrichment in these rocks may be a consequence of K-silicate and sericitic alteration or crustal contamination (Pearce *et al*. 1984).

Thus, the geochemistry of dykes-1 and 2 show differences. Similar chemical differences in acid volcanic sequences have been observed by other authors (Hildreth 1981; Lipman 1987).

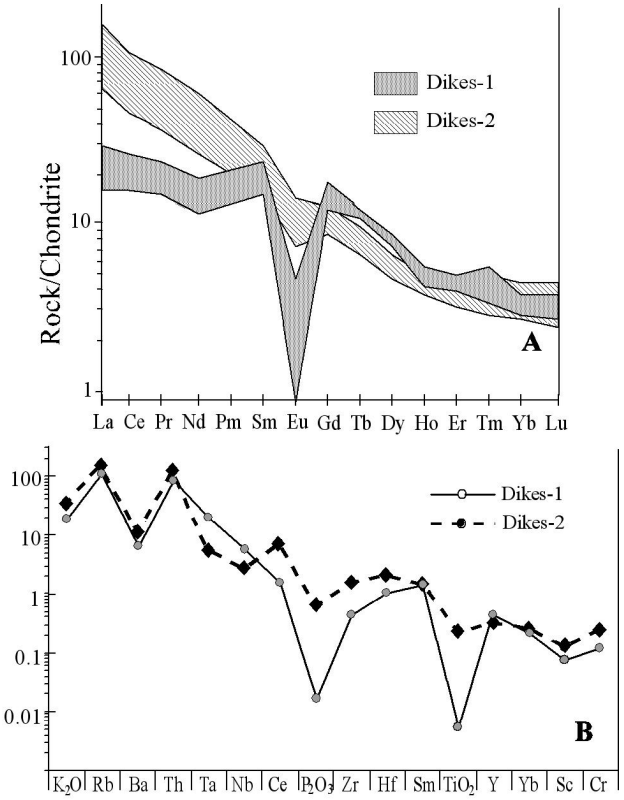


Figure 2. REE and trace-element diagrams of the El Valle subvolcanic rocks. A) Chondrite-normalized REE patterns, B) N-MORB normalized trace-element patterns

They suggest that these chemical peculiarities are difficult to explain by crystal-fractionation models and can be interpreted as due to liquid-state fractionation.

### 3.2 *Altered host-rocks*

Major and trace-elements of whole-rock samples from Au-grade altered zones and non-altered probable protolites from the El Valle deposit were used to obtain information on the chemical gains and losses resulting from the alteration. The change in concentration of mobile elements was determined using isocon diagrams (Grant 1986). Fig. 3 shows a selection of these diagrams in which element concentrations of altered samples are plotted against those of the corresponding precursor samples (granitoid, skarn or marble).They show that S, Au, As, Sb, Ag, Se and Hg have been consistently added to the original rock. Moreover, Cu and Bi are significantly added in altered samples, though not always.

Na, Mg and C and variable Ca and Mn were removed from the rocks during alteration. Ti, Al and $Fe_2O_3$ are relatively immobile whereas $P_2O_5$ shows a variable behaviour. Potassium is removed in strong argillized zones whereas it is

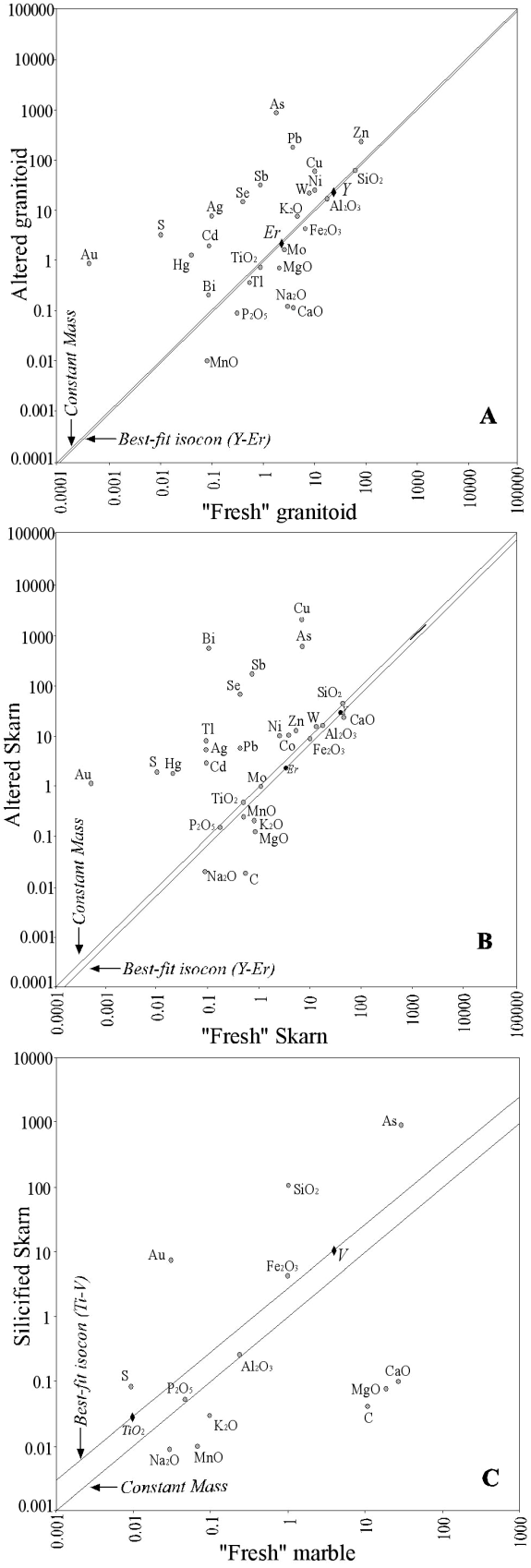


Figure 3. Representative isocon diagrams showing elemental fluxes associated with alteration of host-rocks at the El Valle deposit

added in some altered samples where sericitization is predominant. In these cases, the petro-

graphic study showed a feldspatization previous to the sericitization, which could explain the K addition. Minor $SiO_2$ was commonly added and, in silicified marble, it was significantly added, whereas Ca, Mg and C were removed.

## 4 CONCLUSIONS AND DISCUSSION

The El Valle deposit is a disseminated-Au deposit in altered rocks related to the intrusion of a suite of subvolcanic dykes. These rocks are felsic in character and their geochemistry enable to us to separate them into two different types. The chemical differences between both types may be the result of compositional gradients in the magma chamber due to a crystal-melt fractionation and a liquid-fractionation process. These high-level intrusions are interpreted as being situated in a post-collision environment and a product of a magma derived from an upper mantle of "arc" composition due to the adiabatic decompression that accompanies post-collision uplift and erosion during the Variscan Orogeny. The host-rocks of the dykes were altered, and the elemental fluxes during this alteration indicate a loss of Ca, Na, Mg, C and an addition of silica, which is more notable in silicified marble. The loss of these elements is consistent with a decarbonation process accompanied by silicification. Moreover, there was an alteration of Al±K silicates, which was more notable where the protoliths were igneous rocks. K-Al-bearing minerals were converted to kaolinite in areas of intense alteration with loss of potassium. In ore zones, the alterations may have been accompanied by Fe released from reactive Fe-bearing minerals and the precipitation of disseminated fine-grained arsenian pyrite and arsenopyrite together with "invisible gold". This could explain that Fe behaved as an immobile element, while sulphur has been added during alteration.

## ACKNOWLEDGEMENTS

The authors thank RNGM for data provided and financial support. This work has also bee financed by the CICYT project BTE2001-3469 (Educational Science Ministry of Spain).

## REFERENCES

Cepedal A, Martin-Izard A, Reguilón R, Rodríguez-Pevida L, Spiering E, González-Nistal S (2000) Origin and evolution of the calcic and magnesian skarns hosting the El Valle-Boinás copper-gold deposit, Asturias (Spain). *J Geochem Explor* 71: 119-151

Cepedal A, Fuertes-Fuente M, Martin-Izard A, González-Nistal S, Barrero M (2006) Gold –bearing arsenian pyrite and arsenopyrite from the El Valle gold deposit, NW of Spain. *In: Extended abstracts of 12th IAGOD Symposium* (CD-ROM), Moscow

Grant JA (1986) The isocon diagram-a simple solution to Gresen´s equation for metasomatic alteration. *Econ Geol* 81: 1976-1982

Hildreth W (1981) Gradients in silicic magma chambers: implications for lithospheric magmatism. *J Geophys Res* 86 (10): 153-192

Lipman PW (1987) Rare-earth-element compositions of Cenozoic volcanic rocks in the southern Rocky Mountains and adjacent areas. *U.S. Geol Surv Bull* 1668

Martin-Izard A, Fuertes-Fuente M, Cepedal A, Moreiras D, García-Nieto J, Maldonado C, Pevida LR (2000) The Río Narcea Gold Belt intrusions: geology, petrology, geochemistry and timing. *J Geochem Explor* 71: 103-117

MacLean WH, Kranidiotis P (1987) Immobile elements as monitors of mass transfer in hydrothermal alteration -Phelps Dodge massive sulfide deposit, Matagami, Quebec. *Econ Geol* 82: 951-962

Pearce JA, Harris NBW, Tindle AG (1984) Trace element discrimination diagrams for the tectonic interpretation of granitic rocks. *Jour Petrol* 25 (4): 956– 983

Spiering ED, Pevida LR, Maldonado C, González S, García J, Varela A, Arias D, Martin-Izard A (2000) The gold belts of western Asturias and Galicia (NW Spain). *J Geochem Explor* 71: 89-101

Winchester JA, Floyd PA (1977) Geochemical discrimination of different magma series and their differentiation products using immobile elements. *Chem Geol* 20: 325-343

# Late Palaeozoic orogenic gold-antimony deposits from the Dúrico-Beirã area (North Portugal) and their relation with hidden granitic apexes

H. Couto & F.S. Borges
*Dep. de Geologia da Faculdade de Ciências da Universidade do Porto/Centro de Geologia da Universidade do Porto, Portugal*
G. Roger
*Fontainebleau, France*

ABSTRACT: The Dúrico-Beirão gold-antimony mining district (North Portugal) hosts gold-antimony-tin-tungsten mineralizations. Most of the ore deposits were emplaced in the epimetamorphic Precambrian and/or Cambrian to Devonian sequences of the Valongo Anticline, and in the basal layers of Carboniferous basins immediately west of this structure. A direct spatial relationship between the mineralization and the outcropping granites could not be established. However, some data indicate that a genetic relationship with the non-outcropping granites may exist. The occurrence of minor Sn or W minerals in the first Fe-As stage of deposition in some Sb-Au deposits, the presence of acid, igneous rocks affected by intense albitization and by cataclase. In addition the cathodoluminescence (CL) properties, the chemical signatures of apatite from the hydrothermal veins and from granites, and the comparison with similar Hercynian metallogenic districts suggest an indirect genetic relationship between the Sb-Au veins and hidden granites.

KEYWORDS: orogenic gold, antimony-tin-tungsten, hidden granitic apexes, Iberian Variscan Orogeny

## 1 INTRODUCTION

The Dúrico-Beirão gold-antimony mining district is situated near the southwestern boundary of the axial part of the Iberian Variscan Orogeny, in the "Central-Iberian Zone" (CIZ). Country rocks of the area consist of a NW striking band of folded meta-sedimentary rocks, surrounded by pre- to post-orogenic Hercynian granites (Fig.1).

There is no close relationship between mineralized veins and outcropping granites. Most of the ore deposits are emplaced in the epimetamorphic Precambrian and/or Cambrian to Devonian sequences of the Valongo Anticline and in the basal layers of Carboniferous basins, immediately west of this structure (Fig. 1). The paragenetic study (Couto *et al.,* 1990; Couto, 1993) allowed to distinguish four paragenetic types: Sb-Au, Au-As, Pb-Zn-(Ag) and W-Sn, documenting different mineralization stages. Ore deposits are mostly veins, but the mineralization is partly stratiform (*e.g.* Banjas, Couto & Borges 2005, 2006).

The Hercynian deposits of the Dúrico-Beirão district draw in the broad outline NW-

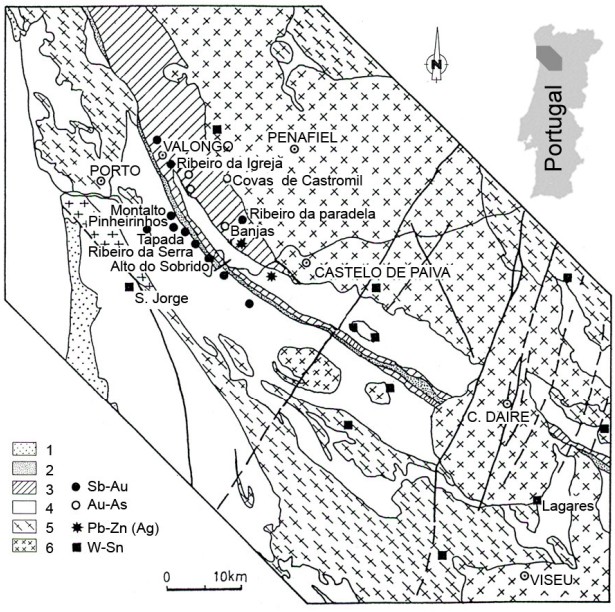


Fig 1 Location of the Sb-Au, Au-As, Sn-W and Pb-Zn-Ag deposits on a geological sketch map (modified after Couto et al. 1990). The name of the main deposits is underlined. 1-Quartenary; 2- Carboniferous; 3- Ordovician to Devonian; 4- Precambrian and/or Cambrian; 5- syn- to late- F3 granitoïds; 6- late- to post- F3 synorogenic biotite granitoïds.

SE striking bands, parallel to the major regional structures and also to the limit of the Castelo de Païva batholith. The W-Sn deposits are close to outcropping granites. Most of the Au-As deposits occur at about 4-6km and the Sb-Au deposits at about 8-10km from this granite (Fig. 1).

At first sight, it could be interpreted as a peribatholitic metallic zoning, by comparison with other districts, e.g. Vale de Ribas (Spanish Pyrenees), where the succession of deposits with decreasing temperature starts with Bi-W-Mo, followed by prevailing arsenopyrite, and finally by predominant stibnite (Robert, 1980). But a more careful examination of the data does not support this hypothesis. First, some deposits are not correctly emplaced in this zonation pattern: Covas de Castromil (Au-As) and Ribeiro de Paradela (Sb-Au) are close to the Castelo de Païva granite; Ribeiro da Igreja and Vale de Inferno Sb-Au deposits are in the North-Western prolongation of the Au-As deposits alignment. Moreover (Couto 1993) the emplacement of Sb-Au and Au-As deposits depends on different controls: mainly structural (for Sb-Au), and lithostratigraphic (for Au-As). Therefore, it can not be interpreted as a peribatholitic zoning related to an outcropping granite.

## 2 RELATION WITH HIDDEN GRANITIC APEXES

In spite of the absence of any close relationship between the mineralizations and outcropping granitic batholiths, the hypothesis of a relation with hidden granitic apexes has to be considered (Couto 1993). Ferreira *at al.* (1971) suggested a peribatholitic metallic zoning (Pb-Zn-Ag; Sb-Pb; Sb-Au) related to the post-tectonic granites outcropping near the NE border of the Dúrico-Beirão district. After the study of the relationship between the different ore parageneses and the study of mineralization controls (Couto 1993), it became evident that the location of the deposits depends mainly on lithostratigraphic and structural controls, and it cannot be interpreted as a simple peribatholitic zoning. Nevertheless, the following data suggest an indirect genetic relationship between the Sb-Au veins and hidden granites (Fig. 2):

1) The occurrence of minor Sn or W minerals (cassiterite, wolframite, scheelite) in the first Fe-As stage of deposition of some Sb-Au deposits (Ribeiro da Igreja, Vale do Inferno, Montalto, Pinheirinhos, Tapada) suggests a link between the Sb-Au and the W-Sn mineralizations, the later showing clear genetic relationships with post-Carboniferous granitic intrusions, *e.g*. the Lagares Sn-deposit, a few tens of kilometers SE from the Dúrico-Beirão district (Fig. 1), where the mineralization is hosted by an aplite-pegmatite vein (Derré *et al.*, 1987), or the Pedra Luz W-Au-Sb bearing quartz veins, in close proximity with a small leucogranitic apex (Maurel-Palacin *et al*., 1987). It is noticeable that, in most of the Sn and W deposits, Sb, Pb, Cu, Zn sulphides or sulfosalts are present in the late stages of deposition. Therefore, the parageneses of the W-Sn and As-Sb-Au mineralizations are globally similar, and the main difference consists in the relative importance of the different stages of deposition. Both may be related to the same metallogenic event, with a very different importance of the first W-Sn stage depending on the depth of emplacement, like in the French Massif Central (Touray *et al*. 1989).

2) Veins of acid igneous granitoid rocks affected both by intense albitization and by brecciation were discovered in the Ribeira da Serra Sb-Au mine (Couto *et al.*1999). They are emplaced in the Cambrian wall-rocks of the mineralised quartz vein, and controlled by the same fault structure. Their emplacement is later than the major folding phases and probably not a long time earlier than the mineralized veins. The occurrence of these igneous veins tends to show the existence of an acidic magmatic activity immediately preceding the metallogenic event, and to support the hypothesis of a relationship between the Sb-Au veins and a hidden granitic apex.

3) Apatite is a common mineral in two Sb-Au deposits: Tapada (in quartz veins) and Ribeiro da Igreja (in quartz stockwork). Apatite is deposited during the (Fe-As) stage 1, and commonly in close relation with pyrite crystals. The cathodoluminescence (CL) properties and the chemical signatures of apatite from these hydrothermal veins and from granites close to the Dúrico-Beirão district (Porto and Castelo de Paiva batholiths, Fig. 1) have been compared (Blanc *et al.*, 1994). The apatite from granites is charactized by a bright yellow CL colour due to $Mn^{2+}$, and to high grades in Mn ($\leq$7.3 wt.% MnO) and Fe. The apatite from Tapada quartz vein shows quite different characters: pale pink to violet CL colours due to REE, high contents in Si and very low contents in Mn and Fe. The apatite from Ribeiro da Igreja quartz stockwerk shows CL properties and chemical signature in-

termediate between these two types. Their similarity with apatite of magmatic origin attenuated but still clearly evidenced, supports the hypothesis of a genetic relation between the Sb-Au hydrothermal veins and a hidden granitic apex.

## 3 CONCLUSIONS

Vallance *et al.* 2003, in their studies about the Castromil gold deposit, corroborated our opinion of the inferred presence of a granite in the core of the Valongo Anticline. According to these authors, the P– T reconstruction also supports the presence of a granite at depth, the relatively low pressure and high temperature (up to 400 ºC for 80 MPa) implying a geothermal gradient of around 60 ºC/km, which is quite common at the exocontact zone of magmatic intrusions. They did not find magmatic fluids, considering also that the granite acted as a heat engine, enhancing hydrothermal circulation but not contributing directly to the metals or fluid fluxes. This supposed genetic relation does not necessarily mean a magmatic source for metals and sulphur.

According to Goldfarb *et al*. 2001, the consistent spatial and temporal association of orogenic gold with granitoids of different compositions indicates that melts and fluids were inherent products of thermal events during orogenesis. The role of the magmatism may be just a trigger of the hydrothermal activity, as suggested for example by Ortega *et al.* (1996) for the relationships between the Albuquerque batholith and the late-Hercynian Sb-Au deposit of Mari Rosa (Western Spain). Nevertheless, the "magmatic" signature, still present in the apatite from Ribeiro da Igreja Sb-Au deposit, may indicate the participation of a magmatic fluid in the hydrothermal mineralizing process, and a probable mixing with fluids of other origins (either hydrothermal or meteoric). It may well be that the granite emplacement generated fluids, which ascended along shear zones remobilizing the metals.

Our study establishes a similar metallogenic sketch, in the broad lines, for Sb-Au deposits in the Dúrico-Beirão district and in other Hercynian districts (Iberian Peninsula, France, Morocco), suggesting a genetic relationship between the mineralization and granitic intrusions. This can be either considered as a trigger for hydrothermal activity or as a magmatic source for fluids, metals, and sulphur. A priori, it seems likely that ore deposits showing similar observed paragenetic and gitologic characters result from a similar genetic history. In North Portugal, the hypothesis of a genetic relationship between gold concentrations and granitic intrusions was proposed for the Jales deposit (Neiva & Neiva, 1989), for deposits in the Mirandela region (Almeida & Noronha, 1988), and for concentrations in the Minho region (Noronha & Ramos, 1991), and in the Viseu region (Sousa & Ramos, 1991). Taking into account peribatholitic metallic zonations, the same hypothesis is proposed for other regions, *e.g.* in the Pyrenees for the Sb-Au Vale de Ribas deposits (Robert, 1980), the French

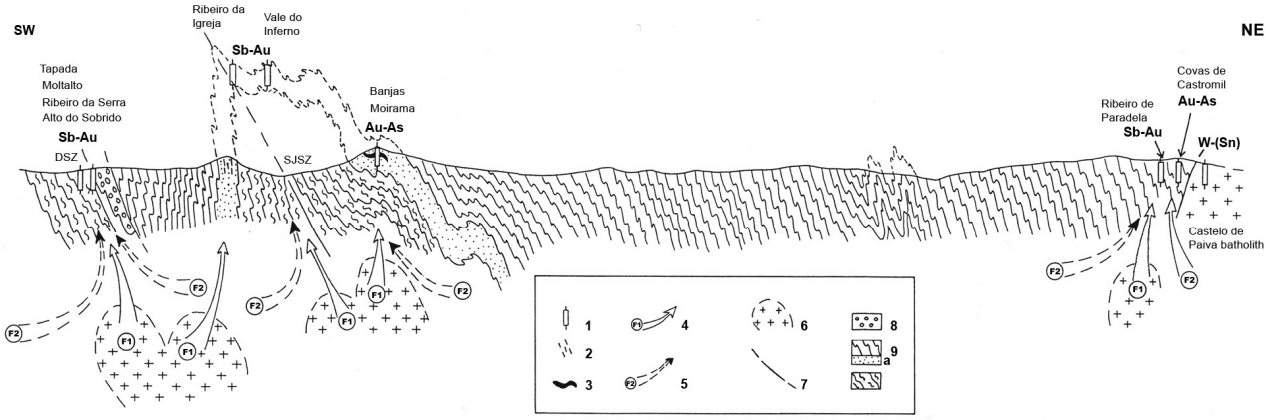


Figure. 2. Schematic cross-section of the Valongo Anticline and supposed genetic relation of the Sb-Au, Au-As and Sn-W deposits with hidden granitic apexes (modified after Couto 1993; cross-section based on the Geological map 9D). 1-Vein deposit (Sb-Au, Au-As or W-Sn); 2 - stratiform deposits; 3 - Arenigian black layers (Combes *et al* 1992, Couto & Borges 2005, 2006); 4 – magmatic fluids; 5 – metamorphic or meteoric fluids; 6 - supposed hidden granitic apex; 7- shear zone (DSZ – Douro Shear zone, SJSZ – Santa Justa Shear Zone); 8-Precambrian and/or Cambrian; 9 – Ordovician-Devonian: 9a- Arenig ; 10- Carboniferous. Note: Arrows suggest that mineralization is deposited by fluid mixing in different proportions, the magmatic source being more important for the early stages (Fe-Au-As), and the dilution by metamorphic or meteoric waters prevailing for late stages (Zn, Pb, Sb, Au) of deposition.

Massif Armoricain (Picot *et al.*, 1981), the French Massif Central (Touray *et al*., 1989), and the Central Morocco for polymetallic veins (Huvelin *et al*., 1978). The hypothesis of the enrichment of hydrothermal fluids by leaching metallic concentrations in surrounding rocks is suggested in most of the cited papers.

## ACKNOWLEDGEMENTS

This paper is part of the project TRANS-MASS of the Centro de Geologia UP, financed by the "Programa Operacional Ciência e Inovação 2010 (POCI 2010)". It was also supported by the "Accord de Coopération Université Pierre Curie de Paris (France) et l'Université de Porto (Portugal)", and by the JNICT-CNRS Cooperation.

## REFERENCES

Almeida A, Noronha F (1988) Fluids associated with W and Ag-Au deposits of the Mirandela area, NE Portugal: an example of peri-granitic zoning: *Bulletin de Mineralogie*, Paris 111: 331-341.

Blanc Ph, Roger G, Couto H (1994) Recherche de signatures magmatique et hydrothermale dans les apatites du nord du Portugal: étude par cathodoluminescence, microscopie électronique à balayage et microsonde électronique: *Bulletin Societe Geologique de France* 165 (4): 329-339

Combes A, Cassard D, Couto H, Damiao J, Ferraz P, Urien P (1992) Caractérisation structurale des minéralisations aurifères de l'Arénigien dans la région de Valongo (Baixo Douro, Portugal): *Chronique de la Recherche minière* 509: 3-15.

Couto, H & Borges, FS (2005) Stratiform Sb and Au mineralizations in the Hercynian Dúrico-Beirã area (North Portugal). Jingwen Mao & Frank P. Bierlein (Eds.) *Mineral Deposit Research: Meeting the Global Challenge*. Vols 1 and 2: 97-99.

Couto, H. & Borges, F, (2006) Lower Ordovician black-shales hosted gold deposits in North Portugal. *Proceedings of the 12th Quadrennial IAGOD symposium. Understanding the genesis of ore deposits. Moscow,* 4 pp.

Couto H, Roger G, Fonteilles M (1999) Occurrence of felsic igneous sills in the Ribeiro da Serra Sb-Au mine, Dúrico-Beirão district, north Portugal. Metallogenic implications. *Comptes Rendus de l'Academie de Sciences - Serie IIa: Sciences de la Terre et des Planetes* 329 (10): 713-719. DOI: 10.1016/S1251-8050(00)88490-6

Couto H, Roger G, Moëlo Y, Bril H (1990) Le district à antimoine-or Dúrico-Beirão (Portugal): évolution paragénétique et géochimique; implications métallogéniques: *Mineralium Deposita* 25: 69-81

Derré C., Lécolle M., Maurel-Palacin D., Noronha F., Roger G. (1987) Evolution granitique et minéralisations filoniennes à Sn-W dans le Nord du Portugal. *Chronique de la Recherche minière* 487: 63-74.

Ferreira M P., Oliveira J S, Andrade, R S (1971) Ocorrências de antimónio no Norte de Portugal: *1° Congresso Hispano Luso-Americano de Geologia Económica, Madrid-Lisboa,1971, Secç. 4 - Investigação Mineira* 1: 597-617.

Goldfarb R J., Groves D I, Gardol, S (2001) Orogenic gold and geologic time: a global synthesis. *Ore Geology Review.* 18, 1-75 DOI:10.1016/S0169-1368(01)00016-6

Huvelin P, Moëlo Y, Permingeat, Picot P (1978) Sur la minéralisation du champ filonien polymétallifère du Roc Blanc (Jebilet centrales, Maroc): *Notes Serv. géol. Maroc, Rabat,* 40: 239-248.

Maurel-Palacin, D., Noronha, F., and G. Roger, G., 1987, Les massifs granitiques de Santa Comba da Vilariça et de Pedra Luz (Trás-os-Montes, Portugal) et les minéralisations associées. *Universidade do Porto, Faculdade de Ciências, Museu e Laboratório Mineralógico e Geológico, Memória* n 1: 303-336.

Neiva J C, Neiva A R (1989) The gold area of Jales (Northern Portugal): *Terra Nova,* 2:143-254.

Ortega L, Oyarzun R, Gallego M (1996) The Mari Rosa late Hercynian Sb-Au deposit, western Spain. Geology and geochemistry of the mineralizing processes: *Mineralium Deposita,* v. 31: 172-187.

Touray, JC, Marcoux E, Hubert P, Proust D (1989) Hydrothermal processes and ore-forming fluid in the Le Bourneix gold deposit, Central France: *Economic Geology* 84: 1328-1339.

Vallance J, Cathelineau M, Boiron MC, Fourcade S, Shepherd TJ, Naden J. (2003) Fluid-rock interactions and the role of late Hercynian aplite intrusion in the genesis of the Castromil gold deposit, northern Portugal. *Chemical Geology* 194: 201-224.

# Gold mineralization associated with low temperature basinal brines in Connemara, western Ireland

P.A.J. Lusty, J. Naden, J.E. Bouch, J.A. McKervey
*British Geological Survey, Kinglsey Dunham Centre, Nicker Hill, Keyworth, Nottingham, UK*

J.A.S. McFarlane
*Omagh Minerals Limited, 56 Botera Upper Road, Omagh, County Tyrone, UK*

ABSTRACT: Fluids inclusion studies suggest that the gold mineralization occurring in a silica-rich fault zone in Silurian rocks at Bohaun in Connemara, western Ireland is associated with low temperature, moderate–high salinity fluids more consistent with a basinal brine than an orogenic gold lineage. This contrasts with other gold deposits in western Ireland that are typically orogenic in mineralization style. Remobilisation of pre-existing gold mineralization by low-temperature, high-salinity brines is recognised in a number of gold deposits worldwide. However, at Bohaun there is no evidence for earlier mineralization suggesting that low-temperature fluids can transport gold and potentially form gold deposits independent of other fluids.

KEYWORDS: gold, Connemara, Ireland, fluid inclusions

## 1 INTRODUCTION

Significant shear-hosted vein gold deposits are known from western Ireland including the occurrences at Lecanvey and Cregganbaun in Co. Mayo (Figure 1). The principal controls on mineralization are major crustal structures and the style of mineralization is typical of orogenic gold deposits (Aherne *et al.* 1992; Wilkinson & Johnston 1996). Additional gold occurrences are recorded from the Silurian and Dalradian rocks of eastern Connemara. This paper describes the Bohaun gold mineralization in eastern Connemara and discusses the nature and origin of possible fluid sources.

The Bohaun mineralization was discovered in the late 1980s during a commercial regional geochemical sampling programme. The mineralization is located on Bohaun mountain, south of the western end of Lough Kilbride, in Co. Galway (Figure 1). Elevated gold values were identified in rocks associated with a north–south trending brecciated and silicified zone hosted within Silurian rocks. Limited exploration was carried out, including the drilling of three shallow boreholes. Drilling intersected quartz-silica breccia containing limonite, chlorite, calcite, pyrite, chalcopyrite and visible gold to a minimum depth of 45m (*Ovoca Gold Exploration plc, unpublished data 1990*).

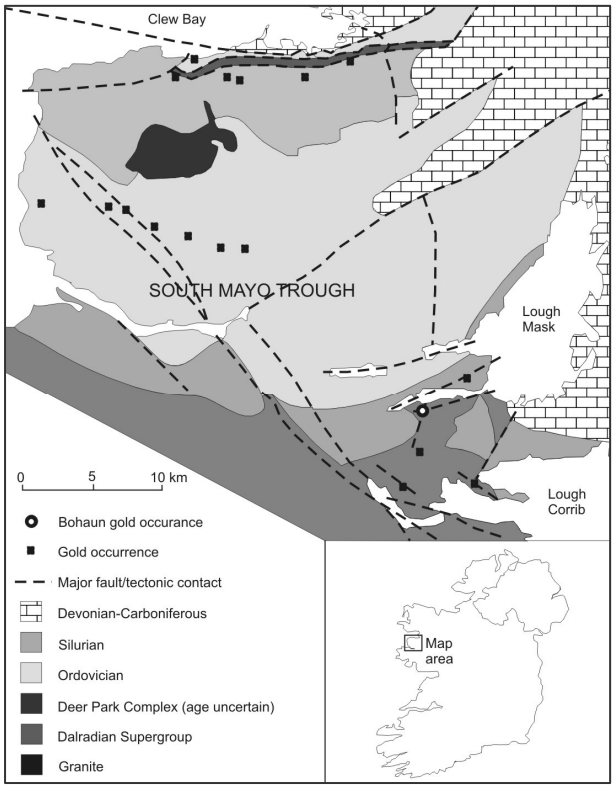


Figure 1. Location of Bohaun and other gold occurrences in relation to the regional geology of South Mayo and Connemara (adapted from Aherne *et al.* 1992)

## 2 GEOLOGICAL SETTING

The South Mayo Trough represents an arc-continent collision zone (Draut *et al*. 2002) consisting of a thick succession of Ordovician volcanic and sedimentary rocks (Clift & Ryan 1994) (Figure 1). Silurian sediments of the Croagh Patrick Succession unconformably overlie the Ordovician sequence to the north (Aherne *et al.* 1992). To the south Silurian strata extend inland east-south-east from south of Killary Harbour to the area around Lough Kilbride, before disappearing under the Carboniferous rocks of Lough Mask (Graham *et al*. 1989). The Killary Harbour-Joyces Country Succession rests unconformably on the Dalradian to the south and Ordovician rocks of the South Mayo Trough to the north (Morris *et al*. 1995). The main deformation in the South Mayo Trough occurred during the late Silurian to early Devonian. Folding was accompanied by large-scale thrusting in the area immediately south of Clew Bay, with other thrusts developed within the Silurian succession to the south (Aherne *et al.* 1992).

## 3 LOCAL GEOLOGY

The Bohaun mineralization is hosted by Silurian sediments of the Killary Harbour-Joyces Country Succession of Llandovery to Wenlock age. These unconformably overlie the Ben Levy Formation of possible Dalradian age. The mineralised area consists of a 1.5km long north-south trending silicified fault zone. The Silurian succession, comprising sandstones and shales, is folded into a synform which has been subsequently faulted.

## 4 MINERALIZATION AND ALTERATION

The mineralization consists of a series of anastomosing quartz veins cementing a major fault zone. A central area of intense silicification, in which discrete veins are hard to define, passes outwards into a stockwork of varying intensity. Mineralization has exploited the fault zone but is not confined to the main fracture. The veins display little deformation and there is no brecciation of pre-existing quartz suggesting mineralization post-dates fault development.

Quartz dominates all the veins and commonly displays multiple growth stages as resolved by cathodoluminescene and a variety of textures. Saccharoidal quartz is most common and gold enrichment is preferentially associated with this textural variant. Crustiform and comb textures, weakly developed colloform banding, vuggy quartz and euhedral, acicular crystals within open fractures are locally common. Fresh sulphides are extremely rare in outcrop, although significant remnant sulphide occurs in the quartz. Visible gold is observed in white to grey saccharoidal quartz which shows an intimate association with haematitic staining and/or a green-grey chloritic clay material. Rare occurrences of late-stage, well-developed dolomite and barite are found within vugs and cavities in the quartz. On an outcrop scale, visible gold shows a close association with bleached wall-rock suggesting this may be significant.

### 4.1 *Ore petrography*

A strong association is observed between gold and relatively late sericite veinlets both cutting the banded quartz and orientated subparallel to the quartz banding. Gold grains within these veinlets are relatively large, up to 890μm. These late-stage veinlets are not the only gold repository; smaller gold grains up to 15μm occur independently of discreet sericite veinlets surrounded by fine-grained, anhedral quartz with interstitial sericite. Specular haematite and/or haematitic quartz is closely associated with the gold, either occurring in zones roughly parallel to the edge of sericite veinlets or forming halos around isolated gold grains. Fine-grained chalcopyrite is associated with the specular haematite.

### 4.2 *Gold grain chemistry*

Electron microprobe analysis indicates that both Ag-rich and Ag-poor gold occur adjacent to one another in grains of similar morphology. Ag values vary from 16 to 21 wt.% and 39 to 42 wt.% defining a bimodal distribution. No systematic pattern in Ag variations is evident within the gold grains. However, some grains show a zonation from a relatively Ag-rich rim to Ag-poor core suggesting some form of Ag enrichment has variably affected the gold.

### 4.3 *Geochemistry*

Recent geochemical sampling by Alba Mineral Resources returned gold values up to 587 ppm in mineralized float samples (*Alba Mineral Resources, Regulatory News Service 14th Feb. 2006*). Reconnaissance sampling undertaken along the silicified zone at intervals iden-

tified elevated gold values throughout the strike length of the structure. Assays from the area returned a number of high-grade gold values including 51.1 ppm and 19.9 ppm Au, with associated silver values of 10.9 ppm and 1.4 ppm Ag respectively (*Alba Mineral Resources, Regulatory News Service 14th Feb. 2006*). Ag is the only element that correlates with Au, consistent with the presence of electrum.

## 5 FLUID INCLUSION STUDY

Preliminary fluid inclusion data (Figure 2) from gold-bearing samples indicate two distinct fluids. Fluid I is sodic with mass % NaCl equiv. ranging from 0.8 to 4.9. Fluid II is calcic (first melting temperatures in the region of –50ºC) and has distinctly higher salinities (10.0–20.3 mass % NaCl equiv.) with NaCl/(NaCl + $CaCl_2$) mass ratios between 0.74 and 0.90. Homogenization temperatures of both fluids are in the range of 141 to 180ºC. No evidence for the presence of carbon dioxide was recorded in any sample.

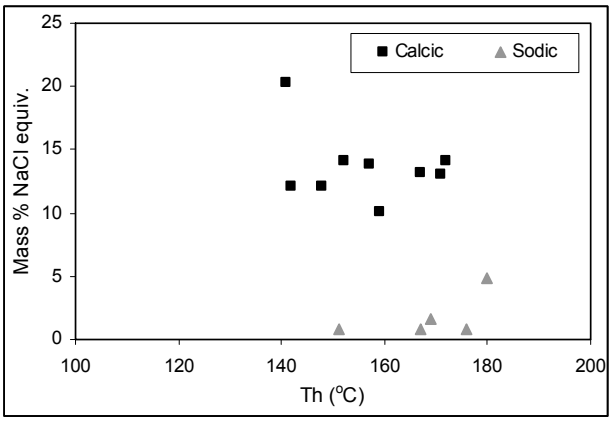


Figure 2. Homogenization temperature against salinity, illustrating the two separate fluids.

## 6 DISCUSSION

The fluids at Bohaun are atypical for orogenic gold (*e.g.* Groves *et al.* 2003) and volcanogenic epithermal-style mineralization (Cooke & Simmons, 2000). The lack of deformation and quartz textures suggestive of open space growth are more characteristic of epithermal environments. In the British Isles, calcic brines are a widely recognised fluid type associated with Carboniferous and later Pb–Zn mineralization (Wilkinson *et al.* 1995; Gleeson *et al.* 1999; O'Reilly *et al.* 1997). Late-stage, low-temperature, high-salinity fluids are reported from orogenic gold deposits worldwide (Guha & Kanwar 1987). Indeed, it is recognised that late-stage NaCl-$CaCl_2$ fluids are responsible for remobilising orogenic-style gold mineralization at Curraghinalt in Northern Ireland (Wilkinson *et al*. 1999). These late-stage fluids show some similarities to those identified at Bohaun. It has not been possible at Curraghinalt to determine whether the late-stage fluid introduced additional gold or just remobilised pre-existing mineralization (Wilkinson *et al.* 1999). There is no evidence at Bohaun for pre-existing mineralization from which gold could have been remobilised.

However, it is interesting to note that the fluids identified at Bohaun are similar in terms of their microthermometric data, to those found in red-bed style Au-Pd mineralization at a number of localities throughout Europe (Shepherd *et al*. 2005). Although there is an association of gold with haematite at Bohaun, the corresponding Pd and Se mineral assemblages noted by Shepherd *et al.* (2005) are absent.

A number of fluid sources can be envisaged. The underlying Dalradian is a possible source of basement brines. The Carboniferous Midlands Basin to the east could potentially yield low-$T_h$, high salinity fluids containing sulphate, consistent with the mineralogy at Bohaun.

## 7 CONCLUSIONS

The origin of the gold at Bohaun remains enigmatic. However, links to low-temperature basinal brines similar to those seen in red-bed Au-Pd mineralization or base metal deposits seem stronger than an orogenic gold lineage. Bohaun also provides further evidence that low-temperature brines can transport gold and potentially form gold deposits independent of other fluids.

## ACKNOWLEDGEMENTS

We acknowledge the support of Alba Mineral Resource plc for logistical support during fieldwork at the Bohaun deposit and providing historical data and assay results. PL, JN, JB and JM publish with the permission of the Executive Director, British Geological Survey (NERC).

## REFERENCES

Aherne S, Reynolds NA, Burke DJ (1992) Gold mineralization in the Silurian and Ordovician of south Mayo. In: Bowden AA, Earls PG O'Connor, Pyne

JF (eds) *The Irish Minerals Industry 1980-1990.* Irish Association for Economic Geology, pp 39-49.

Clift PD, Ryan PD (1994) Geochemical evolution of an Ordovician island arc, South Mayo, Ireland. *Journal of the Geological Society, London* pp 151: 95-329-342.

Cooke DR, Simmons SF (2000) Characteristics and genesis of epithermal gold deposits. *Reviews in Economic Geology* pp 13: 221-244.

Draut AE, Clift, PD (2002) The origin and significance of the Delaney Dome Formation, Connemara, Ireland. *Journal of the Geological Society, London* pp 159: 95-103.

Gleeson SA, Wilkinson JJ, Boyce AJ, Fallick AE, Stuart, FM (1999) On the occurrence and wider implications of anomalously low delta D fluids in quartz veins, South Cornwall, England. *Chemical Geology* pp 160: 161-173.

Graham JR, Leake, BE, Ryan PD (1989) *The Geology of South Mayo, western Ireland.* University of Glasgow, Scottish Academic Press.

Groves DI, Goldfarb RJ, Robert F, Hart CJR (2003) Gold deposit in Metamorphic Belts: Overview of Current Understanding, Outstanding Problems, Future Research, and Exploration Significance. *Economic Geology* pp 98: 1-29.

Guha J, Kanwar, R (1987) Vug brines-fluid inclusions: A key to the understanding of secondary gold enrichment processes and the evolution of deep brines in the Canadian Shield. *Geological Association of Canada Special Paper* pp 33: 95-101.

Morris JH, Long CB, McConnell B, Archer JB (1995) Geology of Connemara. *Geological Survey of Ireland.*

O'Reilly C, Jenkin GRT, Feely M, Alderton DHM, Fallick AE (1997) A fluid inclusion and stable isotope study of 200 Ma of fluid evolution in the Galway Granite, Connemara, Ireland. *Contrib. Mineral. Petrol* pp 129: 120-142.

Shepherd TJ, Bouch JE, Gunn, AG, McKervey JA, Naden, J, Scrivener RC, Styles MT, Large DE (2005) Permo-Triassic unconformity-related Au-Pd mineralization, South Devon, UK: new insights and the European Perspective. *Mineralium Deposita* pp 40: 24-44.

Wilkinson JJ, Jenkin GRT, Fallick, AE, Foster, RP (1995) Oxygen and hydrogen isotopic evolution of Variscan crustal fluids, south Cornwall, U.K. *Chemical Geology* pp 123: 239-254.

Wilkinson JJ, Johnston JD (1996) Pressure fluctuations, phase separation, and gold precipitation during seismic fracture propagation. *Geology* pp 24: 395-398

Wilkinson JJ, Boyce AJ, Earls G, Fallick AE (1999). Gold remobilization by low-temperature brines: evidence from the Curraghinalt gold deposit, Northern Ireland. *Economic Geology* pp 94: 289-296.

# Hybrid Carlin gold and core complex exhumation sulphide mineralization: the Asimotrypes deposit of submicroscopic gold, Rhodope Massif, N. Greece

D.G. Eliopoulos
*Institute of Geology and Mineral Exploration*

S.P. Kilias
*Athens University, Department. of Economic Geology and Geoenvironment*

ABSTRACT: The Asimotrypes deposit of submicroscopic Au, NE Greece, is hosted by marbles of the Rhodope Metamorphic Core Complex in the vicinity of the regional Neogene SW dipping low-angle Strymon Valley Detachment system. Based on geological and geochemical characteristics, the Asimotrypes Au deposit may be interpreted as an orogenic collapse-related hybrid system, bearing similarities to both Carlin-type Au deposits and base–metal sulphide deposits associated with metamorphic core complex exhumation and detachment faults. Extensional structures like the Strymon Valley Detachment fault system may have played a critical role for Au mineralization by providing feeder structures that concentrated ore fluids, driven by uplift, high heat flow and increased fracture permeability resulting from crustal extension, at the intersections with permeable and chemically favourable carbonate strata (*i.e*. marbles).

KEYWORDS: hybrid, Rhodope metamorphic core-complex, Carlin Au, carbonate-hosted Au

## 1 INTRODUCTION

A genetic link between hydrothermal base- and precious-metal mineralization and fluid circulation driven by high heat flow associated with metamorphic core complex exhumation and uplift along extensional low–angle detachment fault systems (mainly of Oligocene age), has been recently recognized in the Rhodope Massif (Blundell *et al.* 2005; Marchev *et al*. 2005). This relationship is well known from precious and base metal ore districts in Canada and the western USA (Spencer & Welty 1985; Beaudoin *et al.* 1991; 1992), and it has been recently suggested in the Ada Tepe syndetachment sediment-hosted epithermal Au deposit (Marchev *et al.* 2004), and the Madan core-complex Pb-Zn sulphide replacement and vein-type deposit (Kaiser-Rohrmeier *et al*. 2004). The carbonate-hosted Asimotrypes Au deposit occurs in the footwall of a large Neogene low-angle extensional fault system, the Strymon valley detachment (SVD) System (Dinter & Royden 1993; Dinter 1998). The SVD has been associated with the unroofing of the Rhodope Metamorphic Core Complex (RMCC) (Dinter & Royden 1993; Sokoutis *et al*. 1993; Dinter 1998) that represents core complex exhumation of basement rocks, during late Oligocene (30 Ma) (Lips *et al.* 2000) or early-Middle Miocene [26 Ma (Krohe & Mposkos 2001) or 21 Ma (Dinter 1998)]–early Pliocene (Dinter 1998) NE-SW extension of the Alpine collisional orogen in NE Greece. Therefore, it offers a very good opportunity to study the origin of Au mineralization in relation to extension and core complex formation, in the framework of the recent genetic hypotheses on hydrothermal mineralization and late-orogenic evolution of the Rhodope Massif (Blundell *et al.* 2005; Marchev *et al*. 2005).

## 2 GEOLOGICAL SETTING AND MINERALIZATION

The Asimotrypes submicroscopic Au deposit is hosted by marbles of the "Transitional Unit" of the Pangeon Mountain, Rhodope Massif, NE Greece that belongs to the Rhodope Metamorphic Core Complex (RMCC). The Pangeon Mountain forms a domed structure consisting from top to bottom of: (1) a "carbonate unit" of ~500m thickness comprising sheared white coarse-grained calcitic marble with intercalations of dolomite lenses and ribboned-crystalline siliceous marble at its lower part. (2)

a "transitional unit" ~600m thick: an early Miocene regional ductile shear zone consisting of alternating layers of albite-gneiss (20-25m thick) and mica-schists (5-15m thick) and lenses or blocks of mylonitized ribonned and foliated siliceous marble (a few to 100m thick) and actinolite-plagioclase amphibolite; (3) the "Pangeon gneiss", ~1500m thick, and consists of plagioclase-rich paragneiss and mica schist. Calc-alkaline late kinematic granitoids were emplaced into the crustal sequence and underlie the entire Pangeon Mountain. These rocks are medium-grained to locally porphyritic granodiorite and are known as the Pangeon granodiorites. (Mesolakia, Mesoropi, and Nikisiani plutons). These bodies have been dated at 13-15 Ma (Harre *et al*. 1968), and have been reinterpreted by Dinter & Royden (1993) as cooling ages related to the unroofing of the Symvolon pluton in the footwall of the Strymon Valley Detachment.

The mineralization has been developed in the vicinity of the regional SW dipping low-angle Strymon Valley Detachment system. Mineralization is clearly post-metamorphic and related to syndeformational fluid flow in a complex and dynamic environment linked to extension, decompressive uplift through the ductile-brittle transition, and concurrent exhumation of the RMCC.

The main Asimotrypes mineralization occurs in the form of parallel to the shear planes elongate discontinuous replacive sulphide-bearing orebodies that consist mainly of quartz, and sericite-clay minerals, as well as rare calcite- and dolomite-relics; sulphides may constitute up to 35 % by volume. These orebodies are 1-2m wide, ~1 m thick and ~5m long; they contain, or are separated by, complex mixtures of phyllonitic, variably silicified, sulphidized, argillized and locally dedolomitized wall rock. They occur at the intersections of steep NW-trending feeder quartz-veins with several marble/micaschist horizons within shear planes parallel to the Strymon Valley Detachment system. Sulphide ore is dominated by arsenopyrite and As-pyrite with subordinate sphalerite, galena, chalcopyrite, pyrrhotite, Bi-Pb± Sb sulphosalts, and marcasite. Gold is invisible in arsenopyrite and As-pyrite.

## 3 FLUID INCLUSIONS

Quartz that hosts the auriferous sulphides is characterized by ductile strain textures overprinted by brittle fractures; it contains Type I carbonic $CO_2$ ($\pm H_2O$) and Type II aqueous-carbonic $H_2O$-$CO_2$-NaCl inclusions with low to moderate salinity (0.6-7.3 mass% NaCl equiv.) randomly coexisting with Type III naturally decrepitated/leaked type IV, and rare Type III aqueous $H_2O$-NaCl ($\pm CO_2$) inclusions· most type III inclusions occur in crosscutting brittle fractures. Natural decrepitation, and leakage, textures of type IV inclusions are attributed to internal overpressures due to decompression. A wide range in types I and II fluid inclusion $CO_2$:$H_2O$ phase ratios, calculated bulk densities and apparent P-T trapping conditions indicate heterogeneous fluid state due to a combination of $CO_2$-$H_2O$ immiscibility, fluid mixing, and post-entrapment modifications accompanying decompression.

The Au-bearing fluids were probably trapped at 250-300$^o$C at pressures between 1 and 3 kbar under transitional conditions from near-lithostatic (*i.e.* 12 to 4 km) to hydrostatic conditions (*i.e*. 5 to <1 km) where deep hot (> 300$^o$C) $CO_2$-rich near-lithostatic (over pressured) fluids come to contact with shallow aqueous low salinity and cooler hydrostatic fluids. Decompression probably occurred at rather constant temperatures between 250 and 300$^o$C implying sustained heat flow due to rapid uplift, and may have caused $CO_2$-$H_2O$ fluid unmixing of the deep fluid, as well as mixing of the two fluids.

## 4 STABLE ISOTOPES

$\delta^{13}C$ values in marble calcite range between 1. 9 to 2.9 ‰ and are indicative of a marine environment of deposition.$\delta^{18}O$ values of the gold-bearing quartz range between 20.8 and 22.6 ‰. The estimated $\delta^{18}O_{fluid}$ values at the inferred temperatures of mineralization range from 11.8 to 16 ‰ and overlap with the measured $\delta^{18}O$ values of fluid inclusion water extracted from mineralized quartz (15.8 -16.5 ‰) suggesting a highly exchanged crust-equilibrated meteoric fluid (Goldfarb *et al.* 2004; Kuehn & Rose 1995). Measured δD values for inclusion fluids from auriferous quartz, range between -125 and -105 ‰, indicate variably exchanged meteoric water (*e.g*. Cline *et al*. 2005). Gold-associated hydrothermal sulphides are characterized by $\delta^{34}S$ values between +2.2 to +3.1 ‰, with the sulphur derived through leaching of metamorphic rocks (*e.g.* (Ohmoto & Goldhaber 1997).

## 5 DISCUSSION

The Asimotrypes Au deposit shows affinities to three deposit types: (i) Base metal sulphide deposits associated with metamorphic core complex exhumation, (ii) Carlin-type Au and (iii) orogenic Au deposits. Asimotrypes shares a broadly similar extensional tectonic setting, metamorphic core complex host rocks, structural control, and possible mineralization timing with the Pb-Zn(-Ag)-dominated core complex vein and replacement deposits (CCVR) in the Bulgarian Rhodope (Marchev *et al* 2005), and as well as extensional core complex-related Ag-Pb-Zn vein and replacement deposits in Canada (Beaudoin *et al.* 1991; 1992). Moreover, ore and fluid geochemisty, and hydrothermal alteration show many features in common with Carlin-type Au deposits in Nevada (Hofstra & Cline 2000; Kuehn & Rose 1995) and China (Rui-Zong *et al.* 2002), although the host rocks are different. These are: (1) association with shear zones at the ductile-brittle transition; (2) localization of Au ore at intersections of extensional structures with permeable and reactive carbonate strata (i.e. marbles); (3) complete silicification and sulphidation of impure carbonate strata, and spatially coincident dedolomitization and argillization; (4) refractory gold in As-pyrite and arsenopyrite; (5) fluids that are $CO_2$-rich with evidence of $CO_2$-$H_2O$ immiscibility and $^{18}O$-enriched at the inferred temperatures of mineralization between 250 and 300°C (*i.e.* 12-13.5 $^{o}/_{oo}$ at 250°C); (6) $\delta^{18}O_{fluid}$ and $\delta D_{fluid}$ composition showing the involvement of meteoric waters; and, (7) fluid inclusion and isotope evidence for interaction of deep- and shallow-level fluids. Some of the above features are also shared by CCVR ores in Canada that were formed during late stages of orogenic collapse (Beaudoin *et al.* 1991; 1992). Furthermore, the fluids of Asimotrypes have all the features that are typical of orogenic gold deposits in metamorphic belts (Goldfarb *et al.* 2005). However, Asimotrypes differs substantially from orogenic gold deposits because most of the latter are the products of fluids associated with major mantle–crustal devolatilization, magmatism and deformation associated with evolving collisional to transpretional orogeny (Goldfarb *et al* 2005); whereas Asimotrypes has been associated with mixing of deep-and shallow- level fluids during post-orogenic extension.

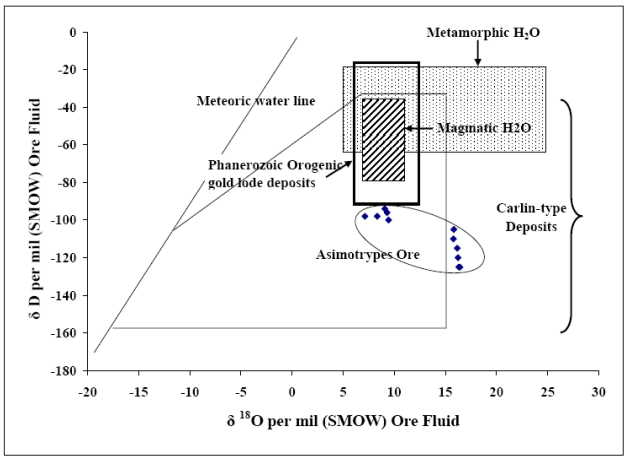


Figure 1. Plot of $\delta D_{inclusion\ fluids}$ versus $\delta^{18}O_{fluids}$ of the Asimotrypes gold deposit. The isotopic composition of the Asimotrypes fluids clearly lies outside of the metamorphic and magmatic water fields. Isotopic composition of the Asimotrypes hydrothermal fluids plots clearly within the range of values that characterize ore fluids associated with Carlin-type gold deposits in Nevada and SW China (Rui-Zhong *et al.* 2002; Hofstra & Cline 2000).

## 6 CONCLUSIONS

The classification of the Asimotrypes mineralization into conventional Au metallogenetic models is not clear-cut, and based on geological and geochemical characteristics it may be interpreted as an orogenic collapse-related hybrid system bearing similarities to both Carlin-type Au deposits and Pb+Zn+Ag deposits associated with metamorphic core complex exhumation and detachment faults. The Strymon Valley Detachment fault system may have played a critical role for Au mineralization by providing feeder structures that concentrated ore fluids, driven by uplift, high heat flow and increased fracture permeability resulting from crustal extension, at the intersections with permeable and chemically favorable strata (*i.e.* marbles).

## ACKNOWLEDGEMENTS

Funding has been provided by the EU (Brite-Euram MA2M-CT90-0015). Thanks are due to T.J. Shepherd, J. Naden, J. Baker, R. Hellingwerf, N. Arvanitides, J. Chatzipanagis, and M. Vartis-Mataranga who have been involved with this project. Special thanks go to Dr. S. Chryssoulis for SIMS analyses.

## REFERENCES


Beaudoin G, Taylor BE, Sangster DF (1991) Silver–lead–zinc veins, metamorphic corecomplexes, and hydrologic regimes during crustal extension. *Geology* 19:1217–1220.

Beaudoin G, Taylor BE, Sangster DF (1992) Silver-lead-zinc veins and crustal hydrology during Eocene extension, southeastern British Columbia, Canada. *Geochim Cosmochim Acta* 56: 3513-3529

Blundell D, Arndt N, Cobbold PR, Heinrich CA (2005) Geodynamics and ore deposit evolution in Europe: Introduction. *Ore Geol Rev* 27:5 – 11.

Cline JS, Hofstra AH, Muntean JL, Tosdal RM, Hickey KA (2005) Carlin-Type gold deposits in Nevada: critical geologic characteristics and viable models. *Econ Geol, 100th Anniversary Volume* pp 451-485

Dinter DA (1998) Late Cenozoic extension of the Alpine collisional orogen, northeastern Greece: Origin of the north Aegean basin. *Geol Soc Am Bull* 110(9): 1208-1230

Dinter DA., Royden, L (1993) Late Cenozoic extension in northeastern Greece: Strymon Valley detachment system and Rhodope metamorphic core complex. *Geology* 21: 45-48

Goldfarb RJ, Baker T, Dubé B, Groves DI, Hart CJR, Gosselin P (2005) Distribution, character, and cenesis of gold Deposits in metamorphic terranes. *Econ Geol 100th Anniv Vol* pp. 407-450.

Goldfarb RJ, Ayuso R, Miller ML, Ebert SW, Marsh EE, Petsel SA, Miller LD, Bradley D, Johnson C, McClelland W (2004) The late Cretaceous Donlin Creek gold deposit, southwestern Alaska: controls on epizonal ore formation. *Econ Geol* 99:643-671

Harre W, Kockel F, Kreuzer H, Lenz H, Muller P, Walther HW (1968) Uber Rejuvenationen im Serbo-Madzedonischen Massiv (Deutung radiometrischer Altersbestimmungen). *Proc of the 23rd Intern Geol Congress, Prague* 6:223-236

Hofstra AH, Cline JS (2000) Characteristics and models for Carlin-type gold deposits. *Econ Geol Rev* 13:163-220

Kaiser-Rohrmeier M, Handler R, von Quadt A, Heinrich CA (2004) Hydrothermal Pb–Zn ore formation in the central Rhodopian dome, south Bulgaria: review and new time constraints from Ar–Ar geochronology. *Schweiz Mineral Petrog Mitt* 84:37–58

Krohe A, Mposkos E (2001) Kinematics of Successive Eocene to Miocene Low-Angle Detachment Systems (Rhodope Zone, N Greece). *Proccedings of EUG XI Meeting, Strasbourg, Franc*e, pp. 264

Kuehn CA, Rose AW (1995) Carlin gold deposits, Nevada: Origin in a deep zone of mixing between normally pressured and over pressured fluids. *Econ Geol* 90:17-36

Lips ALW, White SH, Wijbrans JR (2000) Middle-Late Alpine thermotectonic evolution of the Rhodope massif, Greece. *Geodyinamica Acta* 13: 1-12

Marchev P, Kaiser-Rohrmeier M, Heinrich CA, Ovtcharova M, von Quadt A, Raicheva R (2005) Hydrothermal ore deposits related to post-orogenic extensional magmatism and core complex formation: The Rhodope Massif of Bulgaria and Greece. *Ore Geol Rev* 27:53–89

Ohmoto H, Goldhaber MB (1997) Sulphur and carbon isotopes. In: Barnes HL (ed), *Geochemistry of hydrothermal deposits,* 3rd ed, New York, John Wiley and Sons pp 517-612

Rui-Zong H, Wen-Chao S, Xian-Wu B, Guang-Zhi T, Hofstra AH (2002) Geology and geochemistry of Carlin-type gold deposits in China. *Miner Deposita* 37:378-392

Sokoutis D, Brun J, Van Den Driessche, Pavlidis S (1993) A major Oligocene-Miocene detachment in southern Rhodope controlling north Aegean extension: *J Geol Soc London* 150: 243-246

Spencer J, Welty J (1985) Possible controls of base- and precious metal mineralization associated with Tertiary detachment faults in the Lower Colorado River Trough, Arizona and California. *Geology* 14:195-198

# Structural control of epithermal gold mineralization in the Rosario-Bunawan district, Mindanao Island, Philippines

Jochen Kolb
*Centre for Exploration Targeting (CET), School of Earth and Geographical Sciences, University of Western Australia*
*Institute of Mineralogy and Economic Geology, RWTH Aachen University, Germany*

Steffen Hagemann
*Centre for Exploration Targeting (CET), School of Earth and Geographical Sciences, University of Western Australia*

Ernie Apostol
*Medusa Mining Ltd., Como 6152, Western Australia*

ABSTRACT: The "Co-O" mine and various gold prospects are located in the Rosario-Bunawan district. This district is situated east of the NNW-SSE trending, sinistral strike-slip Philippine fault between two splays, which acted as a lateral ramp system during the oblique convergence of the Philippine Sea and the Eurasian plates in the Late Miocene. The gold mineralization is confined to 0.2 – 4m wide veins in volcanic and volcanoclastic wall rocks. Two stages of auriferous hydrothermal overprint are distinguished: (1) Quartz-chalcedony ± calcite at vein selvages formed at about 180°C by isothermal mixing of a low salinity with a high salinity fluid. (2) The central part of the veins is filled by bladed or blocky calcite, quartz ± barite and hydrothermal breccia. The second stage probably formed from boiling aqueous fluids between 200-250°C in the Co-O mine and surrounding prospects and at about 180°C further east. The veins have distinct alteration halos: (1) A proximal illite-calcite, (2) an intermediate sericite-chlorite, and (3) a distal chlorite ± epidote alteration zone. Three major vein orientations are distinguished: (1) the NNW-SSE trending, sinistral strike-slip Philippine fault trend, (2) the ENE-WSW trending, dextral strike-slip Palawan trend, and (3) the WNW-ESE trending conjugate Co-O trend. During $D_1$ all three major vein systems formed by near vertical opening and thrusting of the wall rocks to the northwest. During $D_2$ and eastward thrusting, the veins were reactivated by horizontal close to N-S opening. A syn-late $D_2$ diorite intrusion may have formed a heat source for the second auriferous stage. The formation of the veins may, therefore, be strongly related to the change from compressive to transcurrent tectonics and a concomitant increase of the geothermal gradient.

KEYWORDS: Epithermal gold, auriferous veins, Mindanao, Philippines

## 1 INTRODUCTION

The Philippines are known as one of the largest provinces for gold deposits. Exceptionally large are the epithermal Lepanto (about 100 t Au) and Baguio (< 700 t) deposits, and the copper porphyry Far Southeast (441 t) and Santo Tomas II (230 t) deposits (Sillitoe 1997, Hedenquist *et al.* 2000). All these large deposits are structurally controlled by faults (Sillitoe 1997). The strong gold endowment appears, however, to be restricted to the northern island of Luzon in the Philippine archipelago.

In this paper, we present detailed structural data, the alteration petrography, and fluid inclusion data of the epithermal gold veins in the Rosario-Bunawan district of the southern island of Mindanao. The data is used to develop a structural mineralization model, which can aid in the regional exploration for the gold-rich veins in Mindanao.

## 2 REGIONAL GEOLOGY

The Rosario-Bunawan district, including the Co-O gold mine, is located in the East Mindanao ridge on the Mindanao island, Philippines. The central part of the Mindanao island is separated from the East Mindanao ridge by the NNW-SSE trending sinistral Philippine fault, which behaved as a zone of decoupling, where a component of oblique collision at about 15 Ma between the Philippine Sea and the Eurasian plates was accommodated (Rangin 1991). The volcano-sedimentary rocks, which

cover the > 65 Ma basement of Mindanao, are related to subduction processes along trenches to the west (Pubellier *et al.* 1991). The massive andesites and dacites hosting most of the epithermal gold mineralizations are dated at 20 – 17 Ma (Bellon & Rangin 1991). Magmatism and subduction ceased at about 15 Ma during oblique collision. Sinistral strike-slip deformation along the Philippine fault started at that time in the late Miocene, reactivating earlier extensional structures.

## 3 DISTRICT GEOLOGY

The Rosario-Bunawan district is situated in the central part of the East Mindanao Ridge between the towns of Rosario in the north and Bunawan in the south. In this district, gold is produced from the Co-O gold mine and several small-scale operations. Total gold resources for the Co-O mine are estimated at 252,000 t with 29.7 g/t Au (*Medusa Mining Ltd. 2006*). Mining is concentrated on up to 4 m wide auriferous veins of variable orientations. The wall rocks are dominated by andesitic to basaltic volcanic and volcanoclastic rocks (Fig. 1). Limestones are thrusted over these lithologies in the northeastern part of the district. The lithologies are intruded by a diorite body to the west of the Gamuton prospect. This intrusion has a several meter wide hornfels halo in the volcanic rocks and the limestones. All the lithological units are unconformably overlain by sandstones and conglomerates, which contain alluvial gold.

Two deformation events are distinguished in the district: $D_1$ is characterized by NW-SE compression in the Late Miocene. The volcanic and volcanoclastic rocks were thrust to the NW onto basement rocks. Auriferous veins formed in three different orientations (Fig. 1): (1) the NNW-SSE Philippine fault trend with a sinistral strike-slip sense of deformation, (2) the ENE-WSW Palawan trend with a dextral strike-slip sense of deformation, and (3) the conjugate, reverse WNW-ESE Co-O trend. The $D_2$ deformation is characterized by E-W compression. The limestones were thrust eastward onto the volcanic and volcanoclastic rocks. Auriferous veins of the Co-O, the Philippine fault and the Palawan trends were reactivated. Late $D_2$ N-S trending faults crosscut all the auriferous veins and thrust zones, but host locally gold mineralization. The diorite intruded late to post $D_2$ thrusting of the limestone.

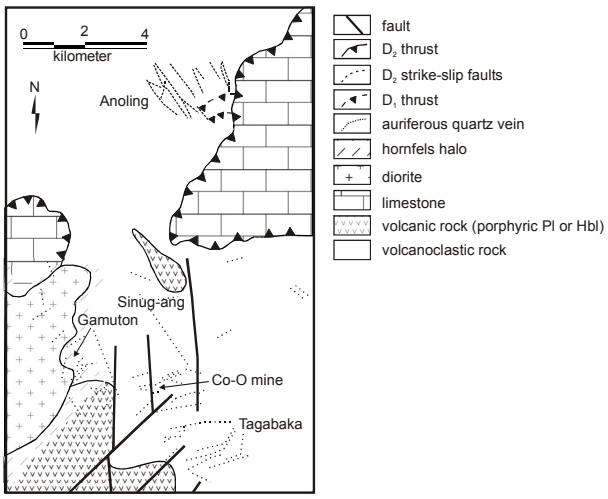


Figure 1: Schematic geological map of the Rosario-Bunawan district showing the mineralized structures of the Co-O mine and the various prospects (modified after Medusa Mining Ltd. 2006).

## 4 GOLD MINERALIZATION IN THE CO-O MINE

The Co-O underground mine is characterized by a series of 0.2 – 4 m wide auriferous veins, which strike over a length of at least 600 m and were drilled to a maximum depth of 200 m (Fig. 2).

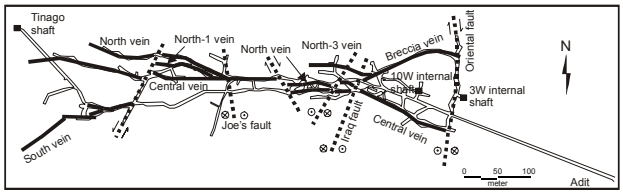


Figure 2: Schematic map of the Co-O mine (projection from the 3150 level, modified after Medusa Mining Ltd. 2006).

The most common vein type is laminated or crustiform at the selvages, with locally developed breccia, and massive with gray to milky quartz, calcite, and barite in the center. The ore mineralogy consists of pyrite, chalcopyrite, gold, and locally sphalerite and galena. The vein selvages have a fibrous texture with syntaxial idiomorphic growth of chalcedony grains into open cavities. The breccia contains up to 10cm wall rock and black chalcedony fragments cemented by hydrothermal precipitates, which points to reactivation of the vein. The central part of the veins is locally an open cavity or is filled by blocky to bladed calcite. Fluid inclusion data indicates that the first mineralization stage occurred at about 180°C by fluid mixing probably of a low-salinity (< 2 wt.% NaCl eq.), heated meteoric fluid with a high-

salinity (> 12 wt.% NaCl eq) magmatic fluid. The second stage formed at 200-250°C probably from a boiling aqueous solution.

Three alteration zones are distinguished: (1) A distal green alteration; (2) an intermediate, several 10's of meters wide gray-white alteration; and (3) a proximal, 10 – 20cm wide white, local yellow-brown alteration.

Hydrothermal chlorite, sericite, calcite, quartz, and pyrite characterize the distal alteration. Supergene halloysite and opaline are locally documented.

The intermediate alteration comprises muscovite, chlorite, calcite, quartz, pyrite and locally chalcopyrite.

The proximal alteration consists of sericite, calcite, chalcedony, pyrite and locally anhydrite. Characteristic for this alteration is the white color, the very fine-grained nature and the proximity to veins and veinlets.

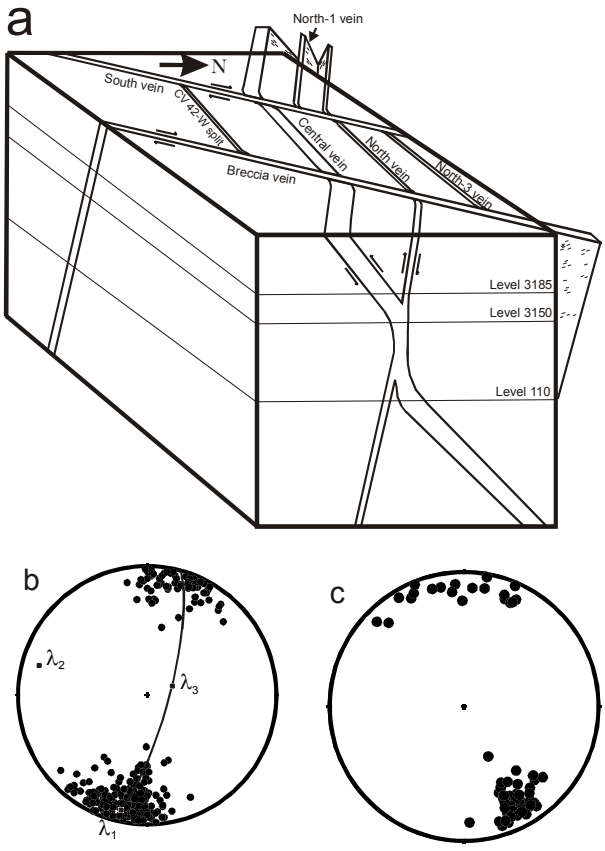


Figure 3: (a) 3D sketch of the vein geometry in the Co-O mine. (b) Poles to the Central and the North veins with estimated orientation of the principal strain axes (lower hemisphere, equal area). (c) Poles to the Breccia and the South vein

## 5 AURIFEROUS VEIN STRUCTURE

Two major vein systems are distinguished based on their orientation (Figs. 2, 3): (1) North and Central vein (the Co-O trend), and (2) South and Breccia vein (the Palawan trend). In the central part of the mine, the North and the Central vein strike E-W to 280-310°. The Central vein dips 70-85° north, whereas the North vein dips 80-89° south. The veins intersect at the 3185 level and form an almost vertical section over 50m. These conjugate veins have a down-dip lineation and a reverse sense of movement, the North vein displaced and transposed the Central vein slightly into a vertical direction. The intersection of the Central and the North veins is currently mined and marks the high-grade ore shoot within the mine.

The central part of the mine, where Central and North veins trend E-W, is set between South vein in the west and Breccia vein in the east, which trend at about 50-70° and dip between 60-85° to the NNW. The vein surfaces display a near horizontal lineation and a dextral strike-slip movement is recorded, which resulted in a sinistral rotation of the Central and North veins to the E-W direction (Fig. 3).

## 6 GEOLOGY OF THE GOLD PROSPECTS

Four gold occurrences are explored in the Rosario-Bunawan district (Fig. 1): the Gamuton, Tagabaka, Sinug-ang, and Anoling prospects. The auriferous veins have a similar mineralogy, fluid inclusion systematic and alteration halo than described for the Co-O mine. Only the Tagabaka and the Anoling prospects record lower mineralization temperatures of around 180°C for the second gold-stage.

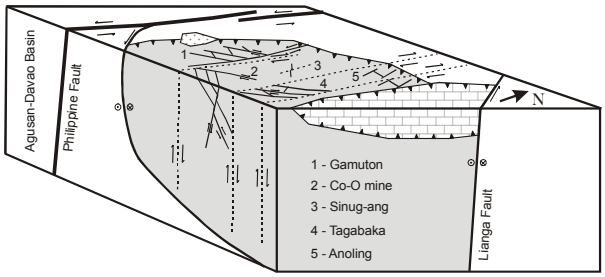


Figure 4: 3D sketch of the vein geometry in the Rosario-Bunawan district and the regional structures related to the oblique compressional tectonics and sinistral strike-slip deformation along the Philippine fault.

Structurally veins with a 50-70° strike and dips at 60-80° are the most prominent (Palawan trend, Fig. 4). They have a near horizontal lineation, record a dextral strike-slip deformation and show higher-order splays with a Riedel geometry ($R_1$, $R_2$) linking the main veins. Veins

parallel to the Co-O and the Philippine fault-trend are not well developed. Locally, breccia zones formed at the vein intersections increasing the volume of mineralized rock.

## 7 A MODEL FOR EPITHERMAL GOLD MINERALIZATION

The auriferous veins in the Rosario-Bunawan district show a characteristic structural pattern with three major mineralized orientations (Figs 1, 4). Most of the veins have a first gold mineralization stage at their selvages. The central part of the Palawan trend and the conjugate veins of the Co-O trend is filled by minerals related to the second gold-stage. Some of the conjugate veins of the Co-O trend and all of the N-S trending veins lack this mineral paragenesis.

During $D_1$, the conjugate veins of the Co-O trend were formed, which requires a near vertical, very steep N to NNE plunging opening vector (Fig. 3). All veins (Philippine fault, Palawan, N-S trend) dipping to westerly directions are also oriented in an ideal geometry to facilitate vein opening. However, the near horizontal stretching lineation on the Palawan trend veins is inconsistent with such a steep opening vector. This suggests that the veins were reactivated during $D_2$ by dextral strike-slip deformation. The opening vector is near horizontal, trending approximately N-S during the E-W compression. Vein opening, therefore, is possible for veins in the Palawan, the Philippine fault, and the Co-O trend, which is correlated with the second gold-stage paragenesis. The N-S trending structures are perpendicular to the shortening direction and, therefore unfavorably oriented for vein opening.

The $D_1$ veins formed during regional NW-SE compression in the Late Miocene during collision between the Philippine Sea and the Eurasian plates. Saline fluids migrated upwards and mixed with low salinity fluids isothermally at about 180°C in the auriferous veins.

During $D_2$, the auriferous veins were reactivated with a near-horizontal, N-S trending opening vector. This suggests that the regional tectonics changed from a $D_1$ compressional regime to a $D_2$ transcurrent regime after collision of the two plates. The auriferous $D_2$ veins and the late $D_2$ diorite intrusion to the west of the Gamuton prospect suggest that magmatism and hydrothermal mineralization possibly was coeval. The intrusion may have represented the heat source for the 200-250°C hydrothermal fluids, which formed the auriferous veins in the Co-O mine, the Gamuton, and the Sinug-ang prospects most probably by boiling processes. Lower temperatures of around 180°C are recorded for the formation of auriferous $D_2$ veins in the Tagabaka and Anoling prospects further away from the diorite intrusion (Figs. 1,4). The auriferous Rosario-Bunawan district is bounded to the north and to the south by splays from the Philippine fault, which acted, together with the thrusts, as lateral and frontal ramp systems. The locally higher temperature for the second gold-stage is explained by an increase of the geothermal gradient during the change from collisional tectonics to a transcurrent system and coeval magmatism. The formation of the auriferous veins is, therefore, strongly related to the oblique convergence and related oblique tectonics in the district.

## ACKNOWLEDGEMENTS

Medusa Mining Ltd. is thanked for the financial support of JK and the permission to publish the results of this work. We would like to thank S. Afdal, J. Baguio, J.C. Estoque, and R. Almanza for help during field work and fruitful discussions.

## REFERENCES

Bellon H, Rangin C (1991) Geochemistry and isotopic dating of Cenozoic volcanic arc sequences around the Celebes and Sulu Seas. In: Silver EA, Rangin C and von Breymann MT (eds.) *Proceedings of the Ocean Drilling Program, Scientific Results. College Station,* pp 321-338

Hedenquist JW, Arribas A, Jr., Gonzales-Urien E (2000) Exploration for epithermal gold deposits. Reviews in *Economic Geology* 13: 245-277

Pubellier M, Quebral R, Rangin C, Deffontaines B, Müller C, Butterlin J, Manzano J (1991) The Mindanao Collision Zone: a soft collision event within a continuous Neogene strike-slip setting. *Journal of Southeast Asian Earth Sciences* 6: 239-248

Rangin C (1991) The Philippine Mobile Belt: a complex plate boundary. *Journal of Southeast Asian Earth Sciences* 6: 209-220

Sillitoe RH (1997) Characteristics and controls of the largest porphyry copper-gold and epithermal gold deposits in the circum-Pacific region. *Australian Journal of Earth Sciences* 44: 373-388

# Bi-tellurides and sulphosalts in relation with different types of golds from Permian mineralized quartz-veins, El Cabaco area, Spain

M.C. Moro, F.J. López-Moro, A. Fernández & M.L. Cembranos
*Geology Department, Salamanca University, Spain*

ABSTRACT: Characteristic mineral assemblages in relation to different textural and chemical gold types have been described from W-Au quartz vein swarms in the West of Spain. This is the first chemically-documented report of Bi-ramdohrite and Sb-lillianite-gustavite in Permian gold deposits from the Iberian massif. The high temperature differences between arsenopyrite thermometry (<400 ºC) and some of its micro-inclusions (*e.g*. native gold and hedleyite; hedleyite eutectic to 266 ºC) is difficult to reconcile, from current knowledge, with their coeval deposition, suggesting that Bi-Te phases have not had much to do as scavengers of gold in this event, or, more probably, heyleyte is associated with a late fluid input. Regarding the second gold deposition (electrum), available thermometric data of related fluids (<300 ºC) are not very dissimilar from the eutectic of Bi-Te phases, suggesting, in this case, that the latter could be Au scavengers, however the scarcity of Bi-Te makes this relationship unclear.

KEYWORDS: gold, Bi-Te phases, El Cabaco area

## 1 INTRODUCTION

The El Cabaco district is conventionally known for secondary gold works from Roman times. However, from the Second World War it has been known that significant quantities of wolframite, cassiterite and primary gold existed in the area. This fact gave place to some prospective research in the eighties and research works later (Antona, 1991; Moro, 2000). However, they aren't currently under exploitation. With respect to gold, the later research indicated the close relationship between certain elements (*e.g.* Au vs. Bi from a very good correlation between the two of them), as well as the occurrence of two textural gold types suggesting at least two different kinds of fluids within the gold deposition, and the presence of a characteristic group of minerals associated with the two types of gold, although they weren't characterized at all. It was suspected that this group of minerals belonged to different sulphosalt types and tellurides, the latter especially interesting because they have recently been thought to be Au pathfinders (Ciobanu *et al.*, 2005). The aims of this work were as follows: to verify whether the different textural gold types show chemical variations, to characterize the set of minerals associated with golds types and, finally, to constrain the deposition conditions of gold.

## 2. THE EL CABACO W-AU-QUARTZ VEIN

The most intensively studied area of the El Cabaco district displays four q-vein swarms, with quite a similar strike (N140-165ºE, Fig. 1) and, in all cases, a strong dipping to the NE. The thickness of the q-veins changes from 2 mm up to 40cm, the most common between 2 and 10cm. These mineralized q-veins are hosted in Variscan granitoids and in Upper Proterozoic metasediments. There are some marked mineralogical differences between the quartz veins hosted by metasediments or granitoids, with abundant tourmaline in the selvage and in the vein itself when metasediments are metasomatized. On the other hand, veins hosted by granitoids frequently show abundant muscovite that make up a selvage-style greisen, which can frequently be enveloped by a reddish rim due to the alteration of alkali feldspar and the chloritization of biotite.

In granitoids it is also not uncommon to find

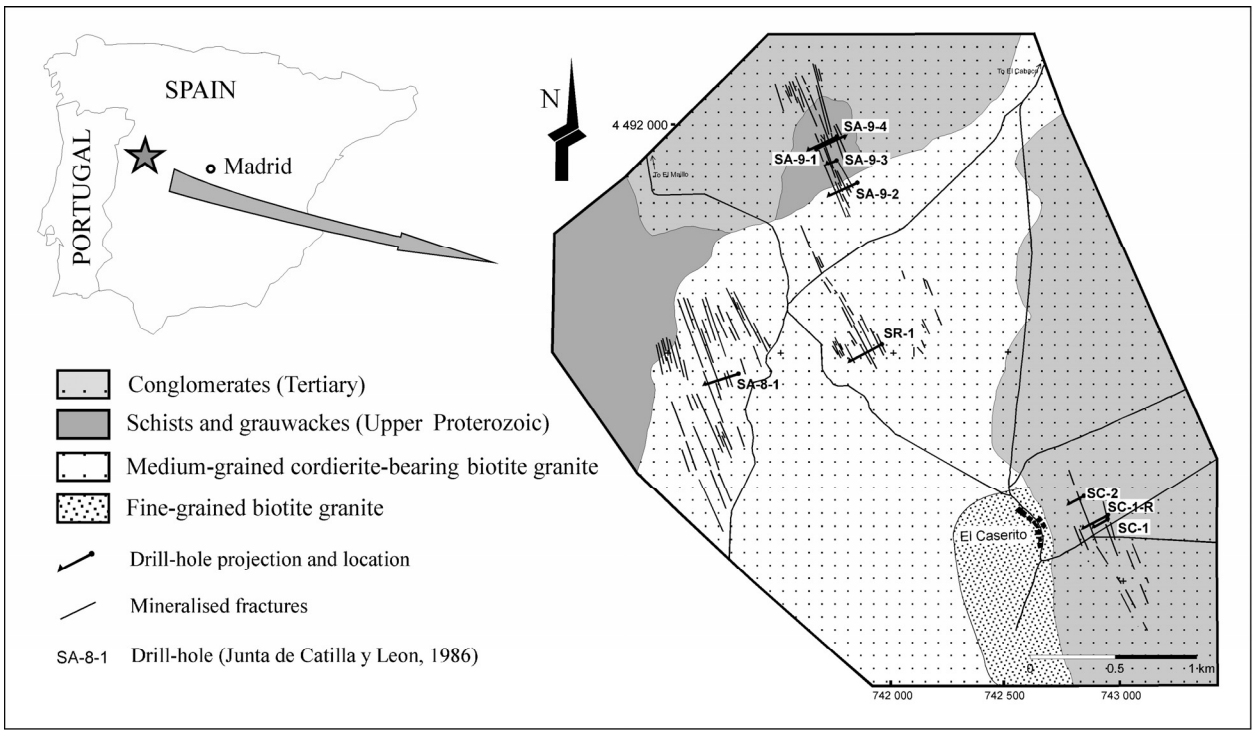


Figure 1. Geological sketch map of the El Cabaco area with the location of W-Au quartz vein swarms.

alkali feldpsar (adularia) veins, which develop a very scarce or null alteration on the host rock. Also, although more rarely, quartz veins develop a centimetric-wide metasomatic rim of albite. Nevertheless, no significant mineralogical differences have been found between any of the types of veins in relation to the granitoid-facies type in which they were enclosed.

In most cases, quartz veins show clear evidence of a complex geological history, involving successive openings and closings, mainly healed by quartz and carbonates.

The greissen-type alteration event has been dated as Permian age (255-256 ± 5 Ma; Antona, 1991) by K-Ar method.

## 3 ORE SEQUENCE

Basically, four ore stages can be distinguished in these vein swarms:

- wolframite ± molibdenite ± cassiterite ± uraninite deposition (oxide stage) joined to a feldspatization/albitization process or, though rare, to an early silicification without sulphides.
- As-Fe-S deposition (sulphide stage) and scheelite linked to the main silicification (milky quartz). This is by far the most abundant deposition in terms of volume. Some traces of native gold, tellurosulphides, native Bi and bismuthinite, and very small drops in arsenopyrite, could be associated with this deposition event.
- electrum, base-metal sulphides, Bi-tellurides, tellurides and sulphosalts (main gold stage). All of them may occur filling arsenopyrite cracks or in droplets. This stage relates to significant carbonatation, choritization and a new silicification (clear quartz).
- supergene stage, involving an Ag-enriched electrum, bismite, Sb-Uytenbogaardite and marcasite.

## 4 COMPOSITIONAL DATA OF GOLD TYPES AND RELATED ORE MINERALS

### 4.1 *Microinclusions enclosed in arsenopyrite*

This section includes a set of microinclusion minerals enclosed in arsenopyrite and without evidence of small cracks or conducts where any kind of fluid/melt has penetrated through (Fig. 2 a ). The mineral associations are as follows:

- Native gold ($Ag_{12}$) + native Bi + Joseite
- Native gold ($Ag_6$) + native Bi + Hedleyite
- Native gold ($Ag_{11}$) + native Bi

### 4.2 *Irregular vug- or crack-filling mineral associations*

The mineral associations in this section are

more abundant and diversified than previous ones. Vugs can be either located outside ore minerals or enclosed within them. In the latter case, a connection with the gangue is always evident. The associations with gold, differentiated according to whether they occur in vugs (V) or microcracks, (C) are as follows (see Figs. 2b and 3):

- Electrum ($Ag_{32-38}$) + native Bi + hessite (V)
- Electrum ($Ag_{33-38}$) + chalcopyrite + tetraedrita + sphalerite (V)
- Electrum ($Ag_{25}$) + bismuthinite (C)

Other associations that fill vugs and cracks but without gold are as follows (also see Fig. 2):

- Vikingite + (Bi,Ag) galenas
- Native Bi + hessite + galena
- Native Bi + galena + argenthite + pyrargyrite
- Chalcopyrite + gustavite + Sb-lillianite-gustavite + (Bi, Ag) galenas
- Boulangerite + Galena + Pirrothite
- Bi-ramdohrite
- Hedleyite + Galena
- Cosalite + native Bi

### 4.3 *Rim-like gold and associated minerals*

This kind of gold is very scarce and can probably be associated with a supergene stage as has been inferred by Greffié *et al*. (2002).

The association is as follows (Fig. 2c):

Electrum ($Ag_{81}$) + Sb-uytenbogaardite ± bismite ± marcasite.

## 5 DISCUSSION AND CONCLUSIONS

Based on textural and chemical data, three different gold types have been distinguished in the El Cabaco district (native gold, electrum I ($Ag_{25-38}$) and electrum II ($Ag_{81}$)). Considering the two types of hydrothermal gold, their deposition was joined to characteristic mineral associations. Thus, the first gold deposition, in microinclusions and very scarce in volume, was accompanied mainly by Bi and bismuthinite, while Bi-tellurides and tellurosulphides were scarce. The second hydrothermal gold deposition is the most significant in volume, and occurs with base-metal sulphides, Ag-tellurides, lillianite homologous series and bismuth-lead sulphosalts, with Bi minerals scarce, in contrast to the previous case.

Another interesting feature of the El Cabaco district is the occurrence of minerals that are otherwise very rare in nature, such as the Bi-ramdohrite or the Sb-lillianite-gustavite, which have seldom been previously reported. The presence of gold microinclusions in arsenopyrite is a controversial subject, because it implies a deposition in relatively high P-T conditions (>400 ºC and 300-200 MPa) joined to carbonic or aqueous carbonic fluids (Antona, 1991). On

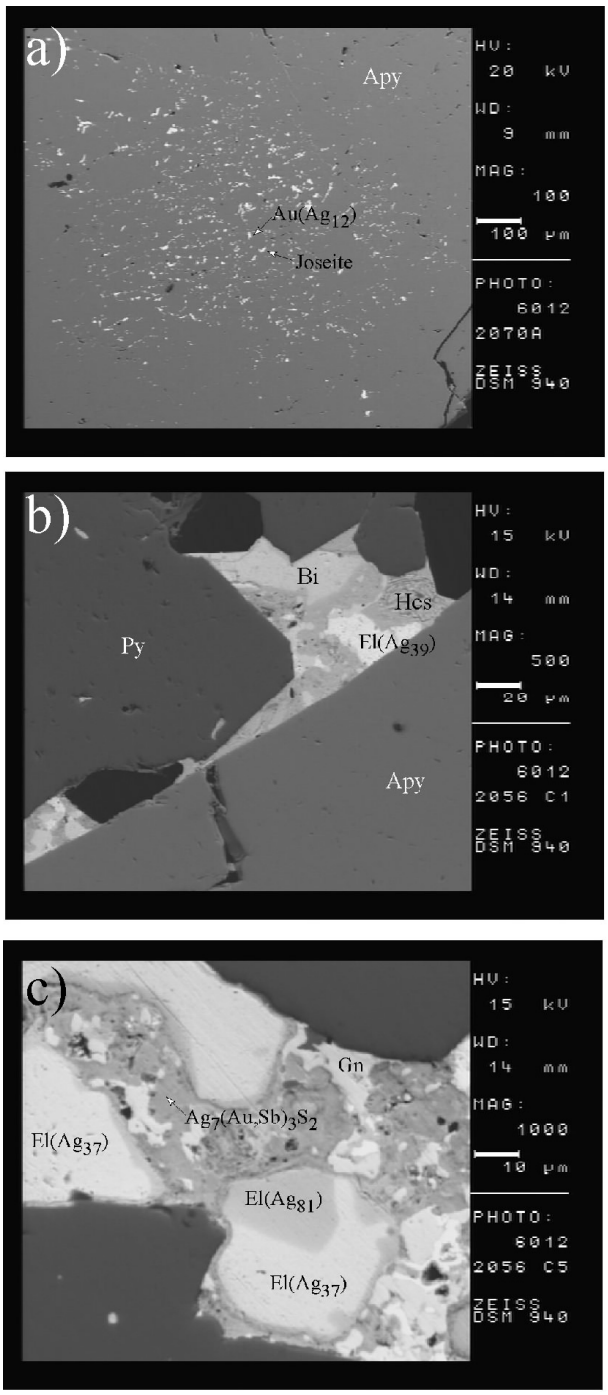


Figure 2. Different gold types and associated ore minerals. a) Microinclusions of native gold ($Ag_{12}$) and joseite in arsenopyrite. b) Electrum ($Ag_{39}$), native Bi and hessite filling vugs. c) Supergene stage: Ring-like gold ($Ag_{81}$) and Sb-uytenbogaardite

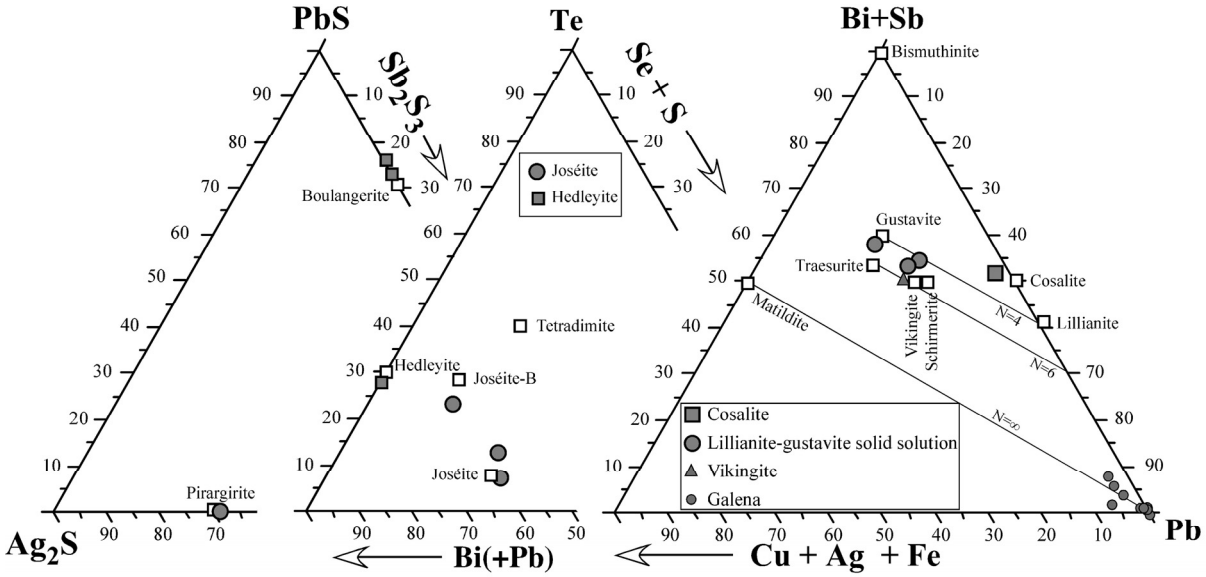


Figure 3. Ternary diagrams showing the chemical composition of analyzed sulphosalts.

the other hand, the potential of Bi-Te melts as Au scavengers has been inferred, although some of Bi-Te phases in apparent equilibrium with native gold in El Cabaco (hedleyite) presents a eutectic at 266 ºC (*see* Ciobanu *et al*., 2005) and it would be difficult to reconcile with the temperature obtained from fluid inclusions and arsenopyrite thermometry. It would suggest that hedleyite microinclusions could be either later than arsenopyrite, probaly filling the arsnopyrite microporous (Michel *et al.,* 1994), or less probably, an unmixing product of a more tellurium parental melt.

Thermometric results obtained from minerals in equilibrium with hydrothermal electrum, such as chlorite, carbonates, are similar to Bi-Te phases eutectic (<300 ºC), suggesting a probable relationship between electrum and Bi-Te phases as scavengers of Au. However, the scarcity of Bi-Te phases in relation to electrum suggests that another kind of process could have been involved in gold genesis. A large number of factors, not necessarily mutually exclusive, may explain the greater second gold deposition: the higher specific surface of microcracked arsenopyrite, higher contents of gold in solution owing to a higher reworking time or the presence of new gold-bearing sources (*e.g*. arsenopyrite layers previously deposited).

ACKNOWLEDGEMENTS

This work was supported by the Comunidad Autónoma de Castilla y León (Research Project Ref. SA015A06). The authors are in debt to Regional Government of Castilla y León for the facilities to study the whole of drill holes from the El Cabaco area.

REFERENCES

Antona F (1991) Fluidos mineralizadores en los yacimientos de oro de Saucelle y El Cabaco (Salamanca) *PhD Thesis Univ Salamanca*.

Ciobanu CL, Cook NJ, Pring A (2005) Bismuth tellurides as gold scavengers. *8th SGA Biennial Meeting, Beijing,* Chapter 13-2, 1383-1386.

Greffié C, Bailly L, Milési JP (2002) Supergene alteration of primary ore assemblages from low-sulfidation Au-Ag epithermal deposits at Pongkor, Indonesia, and Nazareño, Perú. *Economic Geology* 97: 561-571.

Michel D, Giuliani G, Pulz GM, Jost H (1994) Multistage gold deposition in the Archean Maria Lázara gold deposit (Goiás, Brazil). *Min Deposita* 29: 94-97.

Moro MC (2000) Estudio de las mineralizaciones hidrotermales de oro y metales asociados de la Comunidad Autónoma de Castilla y León (España). *FEDER project* (1FD97-0235).

# Native tin in supergene Au-Ag ores from Pukanec, Central Slovakia – a source of inherited Sn in gold artefacts?

A. Schmiderer, S. Stelter, S. Klatt & G. Borg
*Petrology & Economic Geology Research Group, Institute for Geosciences, Martin-Luther-University Halle-Wittenberg, Germany*

E. Pernicka
*Institute for Prehistoric Archaeology, University of Tübingen, and Curt-Engelhorn-Center for Archaeometry, Mannheim, Germany*

ABSTRACT: The Au-Ag mineralization at Pukanec is part of an epithermal vein system, on the foothill of the Tertiary stratovolcano of Banská Štiavnica. Hypogene auriferous base metal sulphide ore grades upward into Au-enriched supergene oxidised "clay ore", containing Fe-Mn-hydroxide (pseudomorph after sulphide minerals) and gold, electrum, and tin particles. Precious metal placers, associated with the deposit, contain gold and electrum nuggets, but here, no native tin particles have been found in the placers to date. The supergene paragenetic association of native Au and Sn could explain elevated Sn contents of gold artefacts as a feature inherited from the original ore. Such an explanation is more likely than the metallurgically difficult contamination of Au with Sn from cassiterite.

KEYWORDS: native tin, electrum, supergene enrichment, hydrothermal, metallurgy

## 1 GEOLOGICAL SETTING

The former mining area of Pukanec is situated in the Central Slovakian Neogene Volcanic Field. A number of small Au-Ag deposits are situated on the southern foothills of Banská Štiavnica, the biggest stratovolcano in this area (Fig. 1).

The deposits have been mined intermittently, at least since medieval times. Early-stage andesitic to rhyolitic lava flows and epiclastic/pyroclastics deposits have been intruded by a late-stage rhyolitic porphyry (Koděra *et al*. 2005). This magmatic event was accompanied by hydrothermal fluids, which generated a large quartz-calcite-sulphide-vein system. The latest stage of this vein system was the formation of gold and silver-bearing lodes (Bahna & Chovan 2001). The latter have been affected by secondary alteration and oxidation in the near-surface environment.

The formation of an enrichment zone with Au-Ag nuggets has been interpreted as a result of mixing of magmatic and meteoric fluids (Koděra *et al.* 2005) although a hypogene magmatic origin with subsequent supergene, meteoric modification might be more likely.

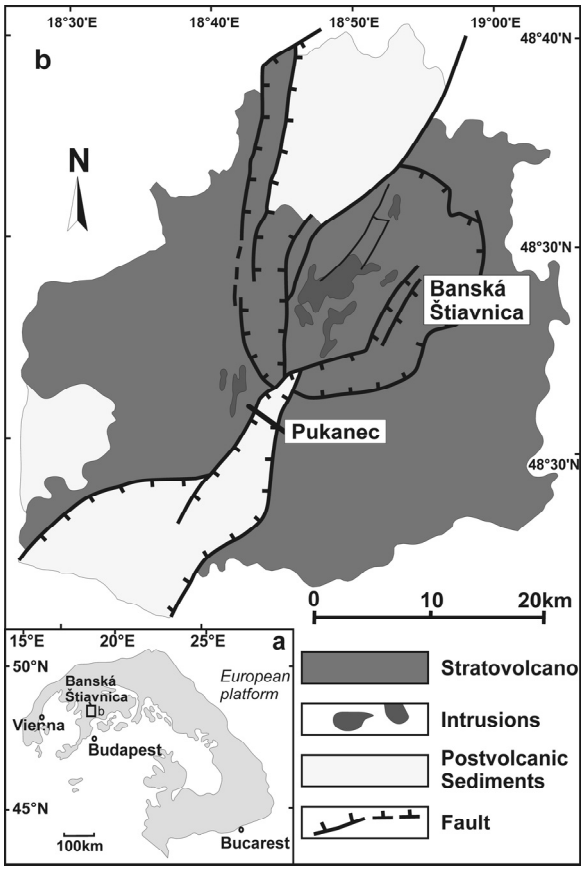


Fig. 1: The Banská Štiavnica region (insert map) with the Pukanec mining area (after Koděra *et al*. 2005).

## 2 MAIN CHARACTERISTICS OF THE SUPERGENE ORE ZONE

The hydrothermal vein system of the Banská Štiavnica stratovolcano, including Pukanec, has been affected by secondary near-surface oxidation processes. This alteration zone reaches down to at least 50m depth (Bahna *et al*. 2003). The deposit has been mined from a huge system of galleries (Fig. 2) during medieval times, some of these still accessible to date. The vein system strikes N-S with a steep dip of 60 to 90° to the East. The veins are up to 1.5m wide and filled with hypogene quartz and calcite and supergene "clay ore", composed of secondary clay minerals (illite, montmorillonite, kaolinite) and Fe-/Mn-hydroxides. The supergene "clay ore" contains electrum and native tin particles, which developed close to surface in the secondary enrichment zone. Samples from five accessible old gallery systems contained electrum particles (with up to 58 % Ag), whereas native tin was present in two samples. The size of the electrum and tin particles is less than 1mm.

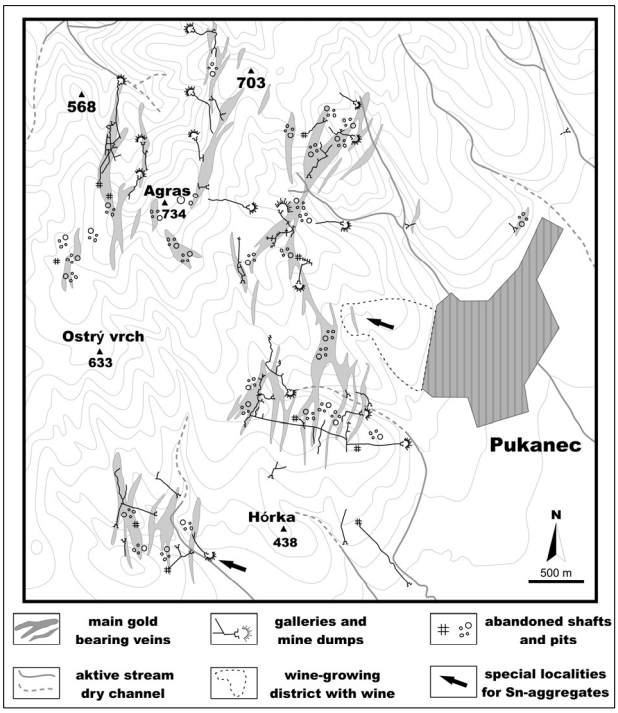


Fig. 2: Map of the vein system (after Bakos, 2004)

## 3 ELECTRUM & NATIVE TIN

In this study, we refer to the native precious metals in the supergene, vein-hosted ores as "particles" and in placers as "nuggets", to avoid terminological confusion. The Au-Ag mineralization in the supergene ores as well as in soils and river sediments (placers) occurs as electrum.

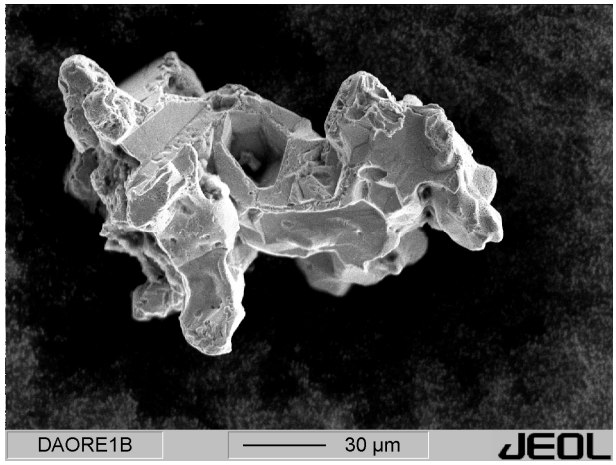


Fig. 3a: SEM image of an electrum particle from supergene ore (Ag 56.4%, Au 43.6%)

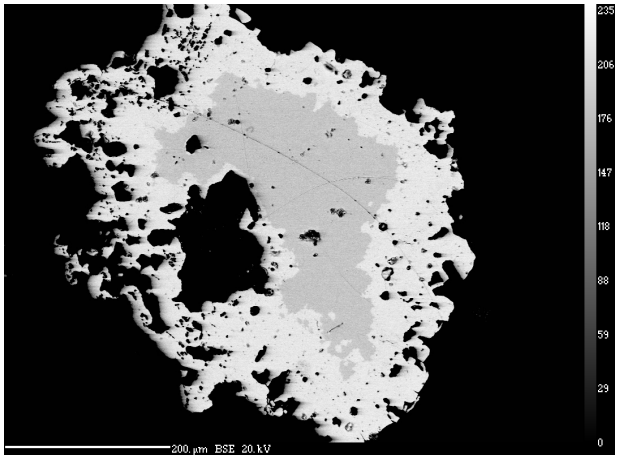


Fig. 3b: Highly porous placer nugget with electrum core (medium grey, Au 46.7% Ag 53.3%) and gold-rich rim (light grey, Au 68.03% Ag 31.97%) (BSE image)

The native metal particles from the supergene ore as well as from the soil are very small, *i.e.* less than 100µm. Their shapes are highly irregular and delicate (Fig. 3a) and sometimes flake-shaped. The electrum particles display a much brighter (silvery) colour when compared with typical gold nuggets.

In contrast to the small supergene electrum and tin particles, the nuggets found in placer samples are commonly much larger in size (up to 3mm).

Some nuggets show rims enriched in gold but with silver contents still above 30% (Fig. 3b). These rims are either the result of supergene growth or of the dissolution of silver during fluviatile transport.

The native tin particles found in the supergene ores range from 0.7 to 1mm and have a

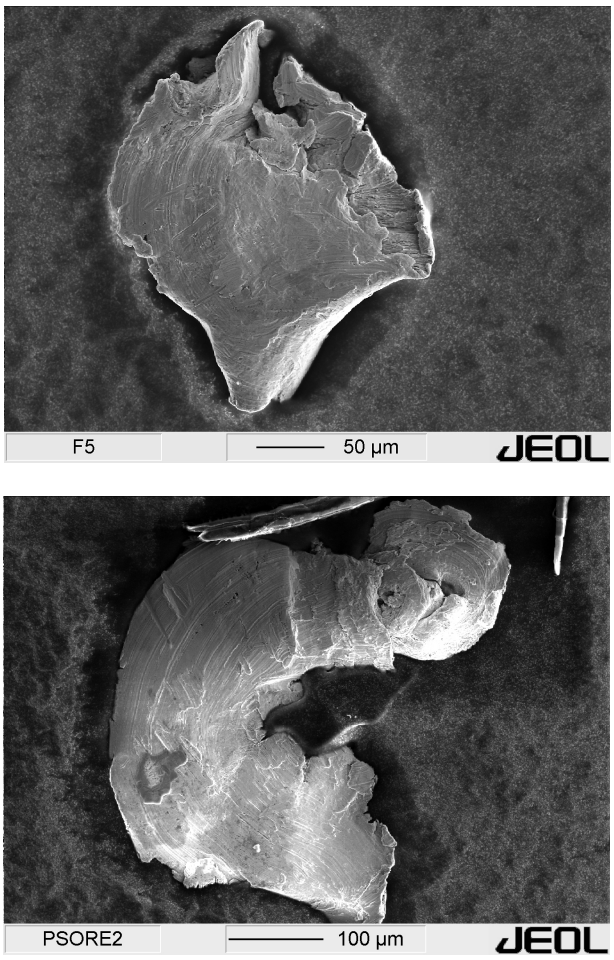


Fig. 4: SEM-images of native tin particles from supergene ore from Pukanec.

"fibrous" to lamellar morphology, possibly representing growth textures (Fig 4).

## 4 ANALYTICAL METHODS AND RESULTS

Analyses of all types of metallic particles and nuggets were carried out by electron-microprobe (EMPA), scanning electron microscope (SEM) with an energy dispersive spectrometer (EDS). Several electrum and native tin grains were additionally examined by laser-ablation ICP-MS on polished sections or directly on nuggets and particles. For laser ablation ICP-MS, a New Wave 213nm laser connected with a Thermo XseriesII CCT Quadrupole Mass Spectrometer was used. The ablation gas was helium, mixed with argon from an external MCN-6000 desolvation unit. Quantification was achieved by liquid calibration as described by Halicz & Guenther (2004), combined with external calibration.

Whole rock samples of ores and wall rocks were analyzed by XRF, and trace and precious element concentrations by ICP-MS. XRD spectra were obtained with a Bruker AXS.

## 5 ORIGIN OF NATIVE TIN

Few occurrences of native tin have been documented and these have been associated with ultrabasic, basic and even sedimentary rocks (Dekov *et al*., 1996). Within our study area, we have been able to identify tin particles in the supergene enrichment zone only. No native tin has been discovered in hypogene ore or placer deposits around Pukanec yet, but whole rock analyses show elevated tin contents in the ppm-range. We interpret the peculiar morphological textures of one of the native tin particles as the result of growth in the supergene environment. LA-ICP-MS analyses of electrum particles associated with the native tin revealed significantly elevated Sn-contents. We thus interprete the native tin as being the product of exsolution from sulphide ores or Sn-rich electrum particles during supergene metallogenesis. Tin forms both Au- and Cu-alloys and solid solutions of copper and tin alloys are well documented (Dekov *et al.*, 1996). Therefore a natural Au-Ag-(Cu)-Sn alloy could explain the tin contents in the electrum particles. However, no micro-inclusions of native tin or other minerals in gold or electrum particles have been identified by EMPA or by laser ablation during our study.

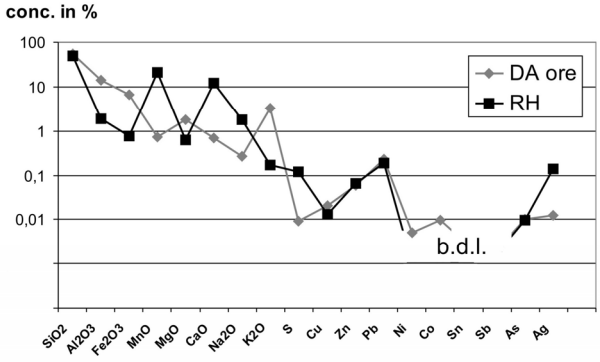


Fig 5: XRF data of typical ore samples, comparing hypogene ore (RH) and supergene ore (DA).

## 6 GEOARCHAEOLOGICAL IMPLICATION

The origin of tin in archeological gold artefacts is (archaeo-)metallurgically still not fully understood. The source of the tin is usually unknown and commonly explained by uninten-

tional contamination, addition of small amounts of tin bronze, or mixing of gold nuggets and cassiterite as a highly stable heavy mineral in placer deposits. Experimental melting tests of gold and cassiterite ($SnO_2$) grains have revealed that under reducing conditions up to 1% Sn can be taken up by the gold (Gumprich 2004).

Our investigation suggests a new and alternative possibility for tin to occur in gold. Particles of native tin from supergene ores, formed above hypogene Au-Ag- Sn(-Cu) sulphide ores and possibly in associated placer deposits. (Prehistoric) miners would have mixed native tin and gold unintentionally and the contemporary metallurgists would have produced - as unintentionally - Sn-bearing gold.

## 7 CONCLUSIONS

The supergene gold-silver ores of Pukanec have formed from hypogene vein-type Cu-Au-Ag-Sn sulphide ores. The mineralization is associated with eluvial and fluviatile gold placers, which contain electrum and gold nuggets with silver-depleted rims. Supergene ore minerals comprise not only electrum but also discrete particles of native tin. Tin is also detectable in bulk analyses of hypogene and supergene ores and as traces in supergene electrum particles and gold nuggets from placers. To date, discrete native tin particles been identified during our laboratory study within supergene samples only and no follow-up sampling programme for native tin in other ore types has been initiated yet. Descriptions of native tin particles are rare and are mainly known from metalliferous sediments of the East Pacific Rise (Dekov *et al.*, 1996). Here the tin particles show a similar shape and morphology compared with our examples. At the East Pacific Rise, the native tin occurs at the top of a (submarine) hydrothermal mineralized system compared to the high-level within in the epithermal (hypogene) system at Pukanec.

The newly found paragenetic association of native tin and gold or electrum has far-reaching implications for the interpretation of tin-bearing archaeological gold artefacts. Such natural mixtures of native metals would alloy easily, in contrast to the metallurgically unfeasible process of melting gold and cassiterite.

## ACKNOWLEDGEMENTS

The study is part of a geoarcheological research project of "The Skydisc of Nebra", funded by "Deutsche Forschungsgemeinschaft" (DFG FOR 550). The authors are grateful to K. Bente and H.-J. Höbler, University of Leipzig, for microprobe analyses. XRF and LA-ICP-MS analyses were carried out at the CEZ-Mannheim with the help of J. Lutz. P. Koděra and F. Bakos are acknowledged for support during field-work.

## REFERENCES

Bahna B, Chovan M (2001) Low-Sulphidation Type of Epithermal Au-Ag Mineralization near Pukanec (Central Slovakia Neogene Volcanic Fields) *Praha: GeoLines* 13: 11-13.

Bahna B, Smirnov A, Chovan M, Bakos F (2002) River transport – induced changes in chemical composition of alluvial gold: *XVII Congr. Carpathian-Balkan Geol.Assoc.* 53: p 5.

Bakos F, Chovan M a kolektív (2004) *Zlato na Slovensku – Gold in Slovakia.* Bratislava: Slovenský skauting. 298 p.

Dekov VM, Damyanov ZK, Mendova ED (1996) Native tin and tin alloys from axial metalliferous sediments of an ultra-fast spreading centre: East Pacific Rise, 21° S survey area. *N. J. Miner.; Mh.* 9: 385-409.

Gumprich A (2004) Archäometrische Untersuchungen an den Goldteilen aus dem Hortfund von Nebra. Unpublished diploma thesis, TU Bergakademie Freiberg, 80 p.

Halicz, L. & Günther, D. (2004) Quantitative analysis of silicates using LA-ICP-MS with liquid calibration, *Journal of Analytical Atomic Spectrometry*, vol. 19: 1539-1549

Koděra P, Lexa J, Rankin AH, Fallic AE (2005) Epithermal goldveins in a caldera setting: Banská Hodruša: *Min. Dep*. 39: 921-943.

Pernicka, E, Wunderlich, H (in print) Experimentelle Schmelzversuche im System Gold-Zinn – *Implikationen für das Gold der Himmelsscheibe von Nebra*. In: Meller, H. (Ed.) Der Griff nach den Sternen. Halle.

# Major Gold and Silver deposits of North-Eastern Russia: Descriptive Models

Gamyanin, G.N., Bortnikov, N.S., Prokofiev, V.Yu., Anikina, E. Yu., Vikentieva, O.V.
*Institute of Geology of Ore Deposits, Petrography, Mineralogy and Geochemistry of Russian Academy of Sciences*

Goryachev, N.A., Golub, V.V.
*North-East Interdisciplinary Reseach Institute Far East Branch RAS (NEISRI FEB RAS)*

Alpatov, V.V.
*Institute of Geology of Diamond and Precious Metals, Siberian Branch, Russian Academy of Sciences, Yakutsk, Russia*

ABSTRACT: Geodynamic, geological and mineralogico-geochemical characteristics of major gold and silver deposits of North-Eastern Russia have been considered. A descriptive model for their formation are suggested.

Keywords*:* gold and silver deposits, NE Russia,

## 1 INTRODUCTION

Numerous major gold deposits (Nezhdaninskoye, Natalka, Kyuchus, Mayskoye), gold-antimony deposits (Sarylakh and Sentachan), and silver-base metal deposits (Prognoz) Have been discovered within accretionary-fold belts in the North-Eastern territory of Russia (Fig. 1). These accretionary-fold belts formed during the Cenozoic to Mesozoic eras as a result of an interaction of the Siberian palaeocontinent with Pacific oceanic plates (Parfenov *et al*., 1993; 1995; Shpikerman, 1998; Shpikerman & Goryachev, 1997).

The accretionary structure of north-eastern Asia consists of terranes of different origins amalgamated to the craton over an extended period of time (Parfenov *et al*., 1993). The tectonomagmatic activization related to the formation of the Chukotsk–Okhotsk volcano-plutonic belt has played a very important role in the creation and metallogeny of the development of these accretionary-fold belts. As a result, a spatial superimposition of mineralizations of different styles is suggested in many ore districts and fields within this belt. In this paper, particular attention is given to the tectonic, geodynamic, structural and mineralogical-geochemical characterization of these deposits to find certain common features typical of these major deposits within the northeastern territory of Russia.

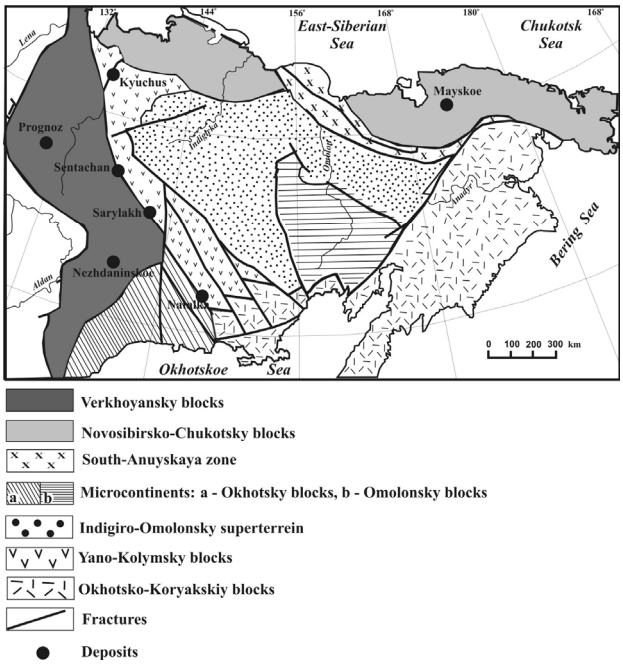


Figure 1. The position of the major gold and silver deposits within the Mesozoic tectonic structure of the North-East Asia.

## 1 DESCRIPTIVE MODEL

### 1.1 *General characterization*

Almost all the major gold deposits in north-eastern Russia are hosted by terriginous rocks formed on passive continental margins. These deposits are confined to zones of large, long-lived, thrust faults and strike-slip faults deeply

penetrating into the crust (Nezhdaninskoye, Natalka, and Mayskoye). These faults generally form boundaries to large tectonic blocks. The gold deposits are localized in supra-intrusion zones of elongated, weakly eroded, granitoid belts or above deep granitoid batholiths giving rise to dyke swarms at the present surface. The deposits were formed during several episodes ("superstages"). Their pre-history superstage occurred under conditions of extension, either within passive continental margin or within back basins of active continental margins. The terrigenous sequences which often contain lithologies rich in organics, disseminated pyrite, are the principal host rocks to gold, silver, arsenic, antimony, lead, and zinc mineralization. This mineralization has been redistributed and concentrated in mobile zones of intense folding and during metamorphism at the early stage of collision and subduction. The consequential history of metal accumulation is believed to have been related to orogenic magmatic activity. The early gold mineralization of economic importance was deposited in the compressional regime whilst silver was dominant in the extensional regime. The late productive superstage and associated metasomatism in different deposits originated in different environments. Finally, they were formed in palaeo-geodynamic environments of compression of active continental or transform margins with long-living magma centers displayed the crust-mantle interaction. The time gap between superstages might account for a few tenths of million years in collision-type fold belts (Sarylakh, Prognoz, Kyuchus, Nezhdaninskoye) or a few million years in continental-margin magmatic belts (Mayskoye).

### 1.2 *Characterization of gold deposits*

The first stage of the deposit formation is associated with granitoid magmatism of I- and S-types which generated ore-bearing fluid flows and gave rise to thermostatic control of transformational environment of ore-enclosing rocks and ore emplacement. An interaction of magmatic fluid with host rocks under conditions of collision compression caused the formation of thick linear halos of ore-bearing "beresites" with auriferous disseminated veinlet sulphide mineralization. The volume of these halos depends on the duration of compression regime, composition and physical-mechanical properties of host rocks. Several paragenetic mineral assemblages have been recognized in these deposits: (1) auriferous pyrite-arsenopyrite with invisible gold; (2) chalcopyrite-sphalerite-galena and "fahlore"-sulphoantimonite with free native gold; (3) quartz-ankerite and (4) quartz-stibnite. A spatial superimposition of gold-bearing associations led to a formation of ore shoots. Vertical mineralogical and cryptic wave zoning of the deposits were revealed. Its amplitude varies from 200 to 300m and more.

A study of stable isotopes of sulphur, oxygen, and carbon inferred the common sources of these components in gold-quartz deposits. They suggested the predominant role of a magmatic fluid and the involvement of metamorphic fluids and components leached from host rocks. Fluid regime of mineral formation is characterized by a change of oxidizing environment during metasomatite formation into reducing one when veins were formed (Bortnikov *et. al.*, 1993, 2004). Ores were deposited due to immiscibility of $H_2O$–$CO_2$–$NaCl \pm CH_4 \pm N_2$ fluids at a wide temperature range (370-250$^oC$), salinity of 9.6 to 1.2 wt%. NaCl eq, and variable fluid pressure (1950-720 bar).

The second superstage of the deposit formation occurred under condition of the extension of back-arc environments or strike-slip faults of the transform margin. The mineralization of this superstage bears specific features due to superimposition of the of late metallogenic belts onto the early ones. Mineralization of this stage was controlled by large strike-slip faults. Metasomatic alteration (dickite, pyrophyllite), sulphide parageneses with inter-metallide and oxide minerals, structural-textural fabrics (rhythmic-festoon, cryptogranular, spherulitic ores) infer low-depth ore deposition. Widespread corrosion and dissolution of the early-superstage minerals, occurrences of regenerated quartz, compositionally complex newly-formed inter-metallides of gold-antimony, gold-mercury and metastable compounds indicate an intensive interaction between late fluids with early deposited minerals aggregates. Ores were deposited from aqueos fluid with salinity of 26.3-2.4wt%. .NaCl eq. at a temperature range of 290 to 130$^oC$ under conditions of unstable pressure. Superimposed stibnite ores are richer in isotopically heavy sulphur as compared to sulphur of the early-stage sulphides.

### 1.3 *Characterization of silver deposits*

Silver deposits form under conditions of back-arc extension. At the early superstage,

noncommercial cassiterite-sulphide mineralization surrounded quartz-sericite halos replaced host rocks were deposited in silver-base metal deposits which are considered to be derivatives of tin-bearing hydrothermal-magmatic systems related to granitoid magmatism (Gamyanin *et al*., 2005). The injection of subvolcanic granite-porphyry dikes preceded frequently the second (major) silver-base metal superstage. The alteration halos accompanied these ores consists of predominant carbonates (dolomite – ankerite), rare argentiferous pyrite, arsenopyrite, galena, and sphalerite. Orebodies are composed of a successive series of mineral assemblages: (1) rhythmic-zonal siderite-sphalerite-galena; (2) quartz-polysulphide-sulphosalt; (3) quartz-pyrite-sphalerite-ankerite-dolomite, and (4) quartz-calcite. Ores were formed at a temperature range of 280 to 100$^{o}$C from fluids with salinity varied from 3 to 30 wt% NaCl. eq.. Gas phase contains $CO_2$, $CH_4$ and high $N_2$ contents. Widespread festoon, cockade and crustified structures, heterogeneity of mineral composition, mineral decomposition textures are interpreted to have been resulted from effervescence (boiling up) of fluids in low-depth conditions. Variations of isotopic mineral composition ($\delta^{34}S$, $\delta^{13}C$ and $\delta^{18}O$) alongside with $Sr^{87}/Sr^{86}$ crust ratio in carbonates infer to a significant mixing of magmatic and meteoric fluids in depositional sites.

## 2 SUMMARY

The above consideration allows to conclude that the major gold and silver deposits of the North-East of Russia share several common intrinsic features that are as follows:

(1) the deposits are usually located: (a) in terrigenic sediments contained the strata rich in both organic matter and precious metals deposited on active continental margins with; (b) within zones of large long living deep-seated crustal faults which are marginal for some large tectonic blocks; (c) in supra-intrusion zones of extended and weakly eroded granitoid magmatic belts.

(2) the deposits contain a combination of disseminated mineralization remobilized with the influx of ore-forming fluid exsolved from granitoid magmas.

(3) the deposits are polygenic-polychronous in the formation due to the overprinting of late productive stage shallow level ores upon the earlier productive stage moderate formation depth ores, with the development of intensive corrosion, re-deposition of minerals and redistribution of valuable ore components.

(4) the deposits are composed of superimposed mineralization of different genetic types (gold-quartz, silver-base metal, quartz-stibnite, quartz-cinnabar) found in world-class polygenic gold deposits, and mineralization deposited at different depth of a single hydrothermal-magmatic systems responsible for the formation of world-class silver deposits.

(5) the deposits display a difference in fluid regime of formation of various superstages and an involvement of compositionally and isotopically different fluid influx into the systems from different sources and mixed rapidly in the depositional sites.

## ACKNOWLEDGMENTS

This study was supported by the Russian Foundation for Basic Research, project nos. 05-05-64803, 06-05-64369, Siberian Branch of Russian Academy of Sciences (project nos. 11), and Department of Earth Sciences (Program “Large and super-large ore deposits and their origin”.

## REFERENCES

Bortnikov N.S., Gamyanin G.N., Naumov V.B., Nosik L.P. The Nezhdaninskoye mesothermal gold deposit, Russia: ore-forming fluid and deposition environment *Current research in geology applied to ore deposits. Granada: Univ. Granada*, 1993. P. 419−422.

Bortnikov N.S., Bryzgalov I.A.,Kryvytskaya, N.N. Mayskoe polydivision veinlet-impregnated gold-sulphide deposit (Chukotka, Russia):mineralogy, fluid inclusions, stable isotopes (O and S), history and formation conditions *Geology of ore deposits.* 2004. V. 46. N6. pp. 475−509.

Gamyanin G.N., Anikina E.Yu., Bortnikov N.S., Alpatov V.V. Sillver-polymetalic deposit Prognos: mineralogy-geochemical features and genesis. *Geology of ore deposits*.1998, V.40. N5. pp.440-458

Gamyanin G.N., Bortnikov N.S., Anikina E.Yu., Borisenko A.S., Borovikov A.A.. Generalized model of development of ore-magmatic systems of Verkhoyan-Kolyma mesozoids *Proceedings of Meeting «Noble and rare metals of Siberia and Far East:ore-formation systems of complex and nontradition ore types deposits. Irkutsk.* 2005. pp. 111-114.

Parfenov L.M., Natapov L.M., Sokolov S.D., Tsukanov N.V. Terrein and accretion tectonics of Nord-East Asia *Geotectonics*. 1993. N 1. pp.68-78.

Parfenov L.M., Prokopiev A.V., Gaiduk V.V. Cretaceous frontal thrusts of the Verkhoyansk fold belt, East-

ern Siberia *Tectonics*.1995.V. 14. N 2. pp. 342-358.

Shpykerman V.I., Goryachev N.A. Metallogenetic history of Nord-East Asia on the base of accretion tectonics. New data for geology and metallogeny of Nord-East Russia. `. 1997, pp. 146-161.

Shpykerman V.I. Pre-Cretaceous mineralogenia of North-East Asia. Magadan *SVKNII DVO RAN*. 1998. 333 c.

# Trace element and rare-earth systematics, fluid inclusion and stable isotope studies of the Nezhdaninsk gold-quartz deposit, Sakha-Yakutia, Russia

N.S. Bortnikov, G.N. Gamyanin, O.V. Vikentieva & V.Yu. Prokof'ev
*Institute of Geology of Ore Deposits, Petrography, Mineralogy, and Geochemistry, Russian Academy of Sciences, Moscow, Russia*

ABSTRACT: REE distribution in rock and mineral and stable isotopes indicate multiple sources of fluids. Three fluids were involved in the Nezhdaninsk hydrothermal system: (1) $H_2O+CO_2+NaCl+MgCl_2\pm N_2\pm CH_4$ (7.1-0.8 wt % NaCl equiv), (2) $CO_2$ vapor-rich and (3) $H_2O+NaCl+MgCl_2$ (31.1-1.9 wt % NaCl equiv). Gold-quartz ores formed at 368-267°C and 1870-490 bars. A magmatic fluid is proposed to have deposited the commercial gold ores.

KEYWORDS: Nezhdaninsk deposit, REE, trace elements, fluid inclusion, stable isotope

## 1 INTRODUCTION

The Nezhdaninsk deposit is a major mesothermal low-grade disseminated and lode gold deposit, located within a terrigenous sequence (Gamyanin *et al*. 2001). The deposit is situated on the western slope of the Suntar-Khayata Mountain Range about 440km east of Yakutsk.

Hypotheses for the origin of mesothermal gold deposits span a broad range including metamorphic, magmatic and meteoric models. This study contains the original results of a trace and rare-earth element geochemistry study of minerals and rocks, compositions and PT-parameters of fluid inclusions, and stable isotopes. These data allow to propose a model for the formation of the Nezhdaninsk gold deposit.

## 2 GEOLOGICAL SETTING

The Nezhdaninsk deposit (Fig. 1) is hosted by a thick sequence of interlayered siltstones and sandstones, metamorphosed to low greenschist facies. These rocks contain up to 2 wt.% of organic matter. The ore bodies are controlled by a tectonic zone which includes foliation, brecciation, and shear zones. The sedimentary sequence was intruded by small stocks of diorite and numerous dykes of aplite, spessartite, kersantite and diorite porphyries.

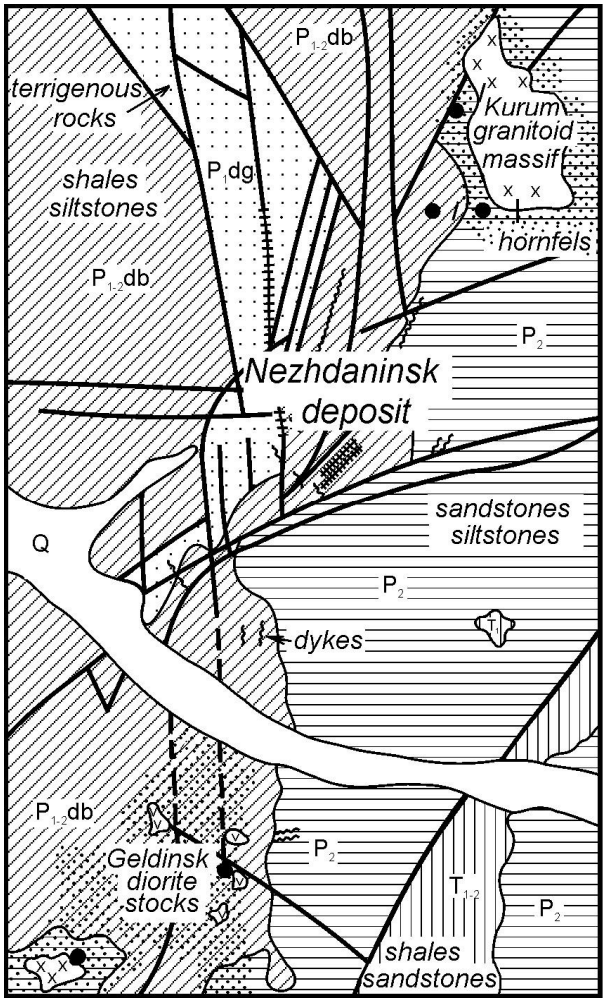


Figure 1. Sketch map of Nezhdaninsk deposit. Solid circles = gold-rare metal occurrences.

## 3 MINERALIZATION

Three episodes of mineralization have been assumed. Numerous barren quartz veins and veinlets originated during the earliest event. Auriferous quartz veins and disseminated zones were formed during the second episode. Several paragenetic mineral assemblages have been recognized. These are: (1) scheelite + pyrite + arsenopyrite + quartz with native gold; (2) chalcopyrite + galena + sphalerite; (3) tetrahedrite + lead sulphantimonites with native gold; (4) stibnite. Numerous quartz veinlets containing owyheeite, pyrargyrite, freibergite were formed during the third episode.

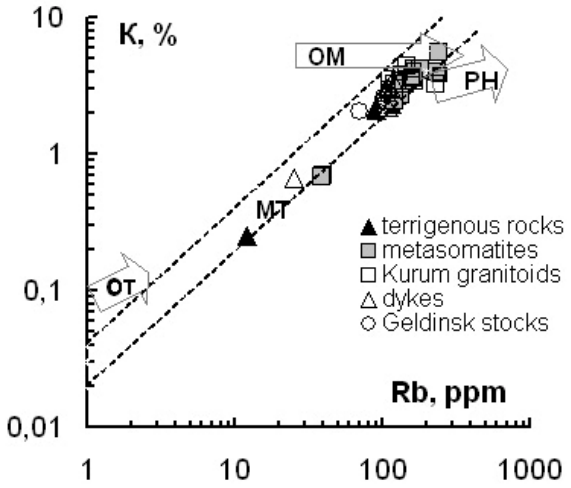


Figure 2. K-Rb ratios in rocks. MT = main trend of igneous rocks, OT = ocean tholeites, PH = pegmatite-hydrothermal trend, OM = orthomagmatic Mo-W greisen (Kerrich 1989, Shaw 1968)

## 4 TRACE AND RARE-EARTH ELEMENT SYSTEMATICS

REE distribution in minerals and rocks was studied. In *terrigenous rocks,* K/Rb, K/Ba and K/Cs ratios range from 313 to 411, from 23 to 60 and from 5410 to 250000, respectively. They are richer in LREE (La/Yb=7.6-11.3). Siltstones display small Eu (Eu/Eu*=0.8-0.9) and Ce (Ce/Ce*=1.2-1.3) anomalies.

In *magmatic rocks of Kurumsk massif* K/Rb and K/Ba ratios range from 298 to 338 and from 50 to 95 for granite, and from 314 to 396 and from 38 to 39 for granodiorite (Fig. 2). The Kurumsk granodiorite and adamellite yielded the highest whole-rock REE concentrations (∑REE=120.3-170.5 ppm), and also the highest La/Yb ratios (11-15). The aplitic granite has about half as much total REE (76.3 ppm) and a very flat condrite-normalized pattern (La/Yb=1.6) broken only by the extreme negative Eu anomaly (Eu/Eu*=0.06).

The *Geldinsk diorite stock* has total REE concentrations of 151.3-156.3 ppm and an inclined chondrite-normalized pattern of distribution (La/Yb=7.3-8.8). In diorites K/Rb and K/Ba ratios range from 258 to 294 and from 21 to 25, respectively.

Even distribution of trace and rare-earth elements *in dykes* occur. The K/Rb and K/Ba ratios range from 197 to 296 and from 9 to 21, respectively. The rocks have high total REE concentration (270.3-354.3 ppm) and also the high La/Yb ratio (30.9-39.2).

In pre-ore *berezites,* K/Rb, K/Ba and K/Cs ratios range from 359 to 378, from 55 to 75 and from 3950 to 6897, respectively. In syn-ore metasomatites K/Rb, K/Ba and K/Cs ratios range from 275 to 380, from 35 to 83 and from 3649to 99000, respectively. The $REE_N$ patterns for altered rocks are characterized by the LREE prevalence over HREE (La/Yb up to 50.7 in pre-ore berezites). The ratio of Eu/Eu*=1 suggests the high $Eu^{3+}/Eu^{2+}$ ratios in metasomatising fluids.

The preore *ankerite* has the highest total REE concentration (104.2 ppm). It is richer in LREE (La/Yb=3.8) and has Eu anomaly (Fig. 3). In carbonates of gold-quartz stage, a total REE concentration varies from 6.0 to 36.2 ppm. The regenerated carbonates exhibit hump-shaped type of $REE_n$ pattern which are light REE depleted (La/Yb=0.3-1.6). They contain 10.8-28.9 ppm REE.

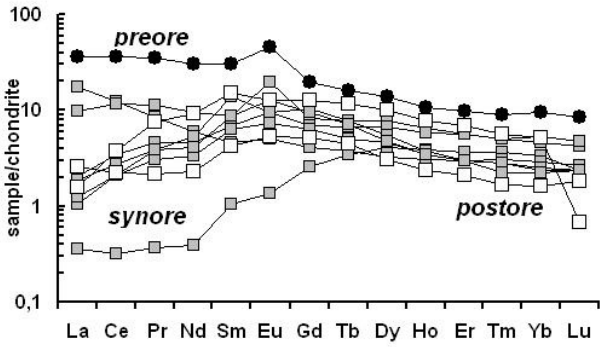


Figure 3. Chondrite-normalized REE pattern for carbonates.

*Scheelite* I of gold-quartz stage and regenerated scheelite II were studied. Scheelite I has highest total REE concentration (1101-1642 ppm) compare scheelite II (30.8-61.2 ppm). Both scheelites are richer in LREE (La/Yb=7.5-

11.8 for early and La/Yb=2.4-9.2 for later) and have positive Eu anomaly (Eu/Eu*=4.0-10.4 for early and Eu/Eu*=6.2-38.8 for later) (Fig. 4). Scheelite I display a weak positive Ce anomaly but scheelite II has the negative Ce anomaly.

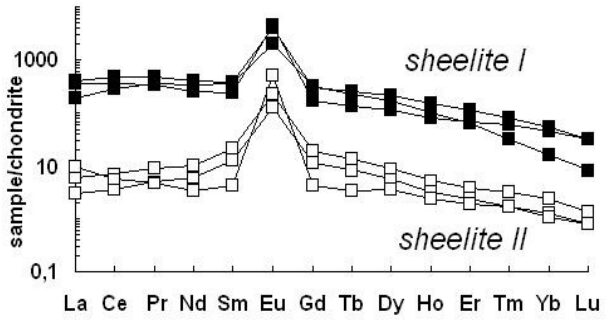


Figure 4. Chondrite-normalized REE pattern for scheelites.

## 5 FLUID INCLUSIONS

### *5.1. General descriptions*

Fluid inclusions in quartz range from 5 to 30 μm in size and are generally ellipsoidal, irregular or negative crystals in shape. The primary and secondary inclusions are identified following the criteria outlined by Roedder (1984).

Inclusions are classified on the basis of phase compositions at room (+21°C) temperature. Type I are two-phase fluid inclusions consisting of $H_2O$ liquid and $CO_2$ vapor and three-phase fluid inclusions with $H_2O$ liquid, $CO_2$ vapor and $CO_2$ liquid. Type II is vapor-rich $CO_2$ one- or two-phase fluid inclusions with minor $CH_4$ and $N_2$. Type III fluid inclusions are two-phase liquid-vapor aqueous inclusions. Type IV is three-phase fluid inclusions consisting of $H_2O$ liquid, gas bubble and solid halite.

### *5.2. Microthermometry*

Gold-quartz ores of the Nezhdaninsk deposit precipitated from a $CO_2$-$H_2O$ fluid with salinity 7.1-0.8 wt % NaCl equiv, 7.2-3.0 mol/kg solution $CO_2$, and 1.0-0.5 mol/kg solution $CH_4$ at 368-267°C and 1870-490 bar and from vapor-rich fluids consisting of dense (0.97-0.47 g/cm$^3$) $CO_2$ with trace (7-4 mol %) $CH_4$ and $N_2$ (Fig. 5). Crystal-like quartz in silver-base metal ore mineralization precipitated from $CO_2$-$H_2O$ fluids within wide ranges of temperature (387-129°C) and pressure (1890-790 bar) at 8.6-2.4 wt % NaCl equiv, 3.9-0.1 mol/kg solution $CO_2$, and 1.6-0.5 mol/kg solution $CH_4$. Gold-rare metal ores in the outer contact of the Kurum massif formed from aqueous-salt fluids with 31.1-1.9 wt % NaCl equiv, 1.8-0 mol/kg solution $CO_2$, and 2.5-1.5 mol/kg solution $CH_4$ at 374-199°C and 630-570 bar.

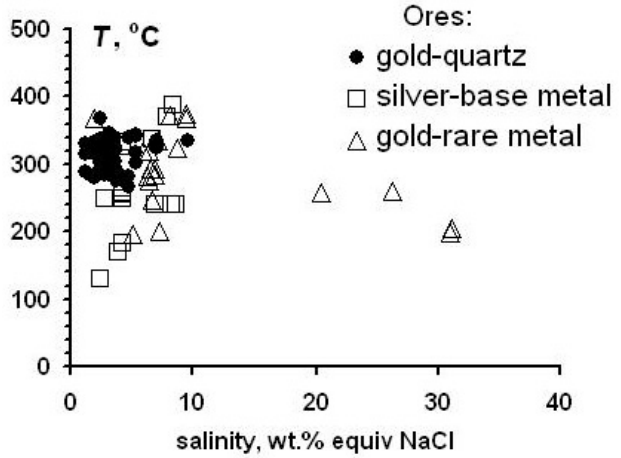


Figure 5. Homogenization temperatures versus salinity plot.

## 6 STABLE ISOTOPES OF OXYGEN

The quartz from altered rocks has the $\delta^{18}O$ values of +15.9 to +16.4‰. The $\delta^{18}O$ values of quartz from the veins formed during the gold-quartz megastage lie within +14.8 to +16.6‰. The $\delta^{18}O$ values of quartz from the veins formed during the silver-polymetallic megastage are from +13.5 to +16.9‰. The calculated $\delta^{18}O_{H2O}$ in equilibrium with quartz from altered rocks at 360°C is +10.9 to +11.4‰, with quartz from gold-quartz megastage at 320°C is +8.1 to +10.2‰, and with quartz from silver-polymetallic megastage at 260°C is +5.2‰ to + 8.6‰ (Fig. 6). The enrichment of $^{16}O$ isotope in late megastage is evident as well. The $\delta^{18}O$ values of fluid deposited gold-bearing quartz lie within the range of primary magmatic waters.

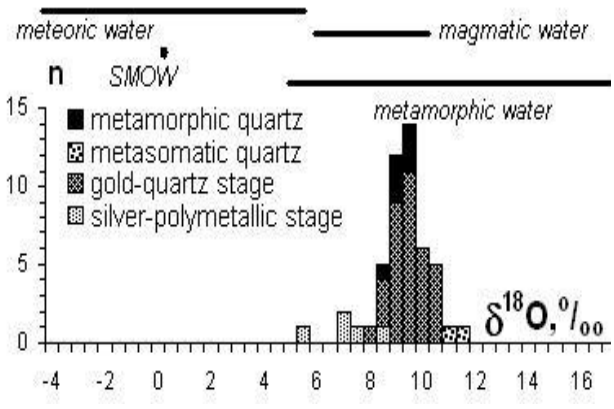


Figure 6. Oxygen isotope composition of hydrothermal fluid equilibrium with quartz.

## 7 CONCLUSIONS

The distribution of trace elements in the Kurum granitoids are likely the result of crystal fractionation. Hydrothermal processes involving formation of metasomatites tend to diminished K/Cs and enhanced K/Ba ratios magmatically. Thus, a magmatic fluid may have been responsible for the formation of the deposits. The compliance of K/Rb and K/Ba ratios in metasomatites with values characteristic of main-trend igneous rocks or "average" crust implies that K, Rb, and Ba were partitioned into the hydrothermal ore-forming fluids in approximately the same ratios as in the source rocks. The K/Rb, K/Ba, Ba/Rb, and K/Cs ratios for metasomatites and spatially associated granitoids are similar that suggest a co-genetic relation between these.

All studied rocks and minerals are enrichhed in LREE. Depleting of the total concentration and enhancing of part of the HREE occurred in hydrothermal processes from preore to synore metasomatites, from preore to regenerate carbonate and from early to later scheelite.

Variations of REE distribution in carbonate depend on composition of coexisting assemblage and/or from carbonate composition.

High Eu/Eu* ratios indicate scheelite crystallization from reduced fluids and/or from fluids with positive Eu anomalies.

The fluid inclusion study showed that three compositionally contrasting fluids circulated within the Nezhdaninsk ore-forming system: a $H_2O$+$CO_2$-dominated fluid with $N_2$, $CH_4$ and dissolved NaCl+$MgCl_2$ (7.1-0.8 wt.% NaCl equiv.), a vapor-rich $CO_2$ fluid and an aqueous fluid with salinity of 31.1-1.9 wt.% NaCl equiv.. Temperature and pressure of the water-bicarbonate fluids were 368-267$^{o}$C and 1870-490 bars, respectively. The temperature of the aqueous fluid ranges within 374-199$^{o}$C.

It is interesting to note that the fluids of the late stage were enriched in isotopically light oxygen. These data suggest that productive (auriferous) quartz precipitated from magmatic water (from +5.5 to +9.0‰, Ohmoto 1986).

Our investigations do not support hypotheses purely of a metamorphogenic, meteoric, or magmatic nature of the fluids responsible for the formation of mesothermal gold deposits. The fluid, which formed the deposit was of multiple origin and consisted of magmatic, metamorphic, and meteoric components. Variations of the chemical and isotopic composition of the mineral-forming fluid indicate the mixing of these components close to or at the site of ore deposition. The magmatic fluid has apparently dominated the ore formation. Our model suggests that the mesothermal deposit formed closely related to magmatic activity. This model includes a variety of mechanisms of fluid generation, such as direct input of fluids from the magma chamber, and mobilization of components during the dehydration and decarbonatization of host rocks due to the contact or contact-regional metamorphism.

## ACKNOWLEDGEMENTS

This study was supported by the Russian Foundation for Basic Research (Projects 05-05-64803, 05-05-64369, 05-05-96070r), the Earth Science Branch of RAS (Project Superlarge deposits) and the grant of the President of the Russian Federation (MK-510.2006.5).

## REFERENCES

Gamyanin GN, Bortnikov NS, Alpatov VV (2001) The Nezhdaninskoye gold ore deposit – a unique deposit of the Northeastern Russia. Moscow: *GEOS*. pp230 [in Russian].

Kerrich R (1989) Source processes for Archean Au-Ag vein deposits: evidence from lithophile-element systematics of the Hollinger-McInture and Buffalo Ankerite deposits, Timmins. Canad. *J. Earth Sci.* 26: 755-781.

Ohmoto H (1986) Stable isotope geochemistry of ore deposits. *Review Mineralogy* 16: 491-560.

Roedder E (1984) Fluid inclusions. *Reviews in Mineralogy* 12. pp644.

Shaw DM (1968) A review of K-Rb fractionation trends by covariance analysis. *Geochim. et Cosmochim. Acta*. 32: 573-601.

# The evolution of a W, Au-Ag-Te and Au-Ag hydrothermal system, Tinos Island, Cyclades, Greece

S.F. Tombros, K. St. Seymour, D. Zouzias, & N. Mastrakas
*Department of Geology, Laboratory of Ore Deposits and Volcanology, University of Patras, 265.00, Patras, Hellas, Department of Geography, Concordia University, Montreal, Canada.*

P.G. Spry
*Department of Geological and Atmospheric Sciences, 253 Science I, Iowa State University, Ames, Iowa 50011-3212, U.S.A..*

A.E. Williams-Jones
*Department of Earth and Planetary Sciences, McGill University, 3450 University Street, Montreal, Quebec H3A 2A7, Canada.*

ABSTRACT: At Tinos Island, Greece, the physicochemical evolution of the hydrothermal system and the associated stages of metallic mineralization that are developed in the vicinity of the Tinos granodiorite-leucogranite has been studied, based on fluid inclusion studies and chemical reactions modeling. Early tungsten mineralization was related to the metasomatic stage of contact metamorphism and precipitated at ~ 350$^{o}$C, from moderate saline (10.4 to 14.8 wt% NaCl eq.), $CO_2$-effervescing fluids, that contained variable amounts of $CaCl_2$ and $MgCl_2$. Panormos Bay Au-Ag-Te mineralization, located 16 km away from the intrusive site, was deposited from cooler 200$^{o}$ to 300$^{o}$C, and low to moderate saline (0.2 to 13.2 wt% NaCl eq.) mineralizing fluids. Au-Ag mineralization at Apigania Bay, which represents a late evolutionary phase, was deposited from even cooler (125$^{o}$ to 235$^{o}$C) and dilute (0.2 to 6.8 wt % NaCl eq.) fluids. In all, the mineralization stage precipitation was controlled by two principal factors: the exsolution of gaseous phase and an increase in pH from 3.3 to 7.6

KEYWORDS: Tungsten, Gold-silver-tellurium, Gold-silver-bearing mineralization, Skarn, Panormos Bay, Apigania Bay, Tinos, Greece

## 1 INTRODUCTION

Unexploited tungsten-molybdenum mineralization occurs within the contact aureole of the syntectonic calc-alkaline Tinos intrusion, and may be genetically related to gold-silver telluride mineralization at Panormos Bay, and gold-silver mineralization at Apigania Bay, Tinos Island, Greece. In this study, detailed investigations of paragenetic and fluid inclusions characteristics have been conducted to constrain the evolution and provenance of the mineralizing fluids at the three localities.

## 2 GEOLOGICAL SETTING

The tectonic stratigraphy at Tinos consists of a series of stacked nappes cut by a Miocene pluton (Melidonis, 1980). The lowest of these nappes, the Basal Unit, consists of a platform of late Triassic to late Cretaceous neritic carbonate rocks. This unit is overlain by the Intermediate nappe or Blueschist Unit, a package of tholeiitic mafic to felsic volcanic rocks and associated metasediments metamorphosed to blueschist facies (40-50 Ma), and subsequently retrograded to greenschist facies (*ca*. ~ 25 Ma) (Andriessen *et al.*, 1987). Overlying this are the klippen of the Upper Unit, which represent ancient oceanic crust metamorphosed to greenschist facies that was emplaced at ~ 18 Ma (Andriessen *et al.*, 1987). The Tinos pluton was intruded syntectonically, and displays thermal-tectonic contacts with the Blueschist and Upper Units (Mastrakas, 2007).

## 3 TINOS PLUTONIC ROCKS, CONTACT AUREOLE AND SKARNS

The Miocene Tinos pluton consists of a central body of I-type biotite-hornblende granodiorite that was emplaced at *ca*. 17 Ma (Altherr *et al.*, 1982) under compression (Mastrakas and St. Seymour, 2000). An S-type leucogranite with the assemblage biotite-muscovite-garnet-

tourmaline was emplaced peripherally to the granodiorite, and also as sills at shallow levels in an extensional regime (Mastrakas & St. Seymour, 2000). The age of emplacement of the leucogranite has been determined as *ca.* 14 Ma (K-Ar ages, Altherr *et al.*, 1982). The genesis of the granodiorite magma is attributed to partial melting of mafic lower crustal rocks, whereas the leucogranite melt with melt contribution from the granodiorite represents a hybrid partial melt consisting mainly of metasedimentary country rock. Geobarothermometric studies indicate that the granodiorite was emplaced at a temperature range of 750° to 800°C and at pressures of ~ 4.7 kbars, whereas the leucogranite was emplaced *ca.* 680°C and at ~ 2 kbars (Mastrakas, 2007). The latter experienced intense retrograde boiling as evidenced by numerous miarolitic cavities. The Tinos pluton caused contact metamorphism at *ca*. 14 Ma (Bröcker *et al*., 1993). A discontinuous scapolite zone is surrounded successively by pyroxene-, hornblende-, albite- and epidote-hornfels zones (Mastrakas, 2007).

Skarn rocks are developed within amphibolite schists and marbles of the Blueschist Unit, and outcrop as podiform, lensoid and vein-like bodies and mainly as an exoskarn near marble-amphibolite schist contacts. In general, skarns are spatially related to leucogranite apophyses and aplitic stockworks. Skarns consist predominantly of garnet and clinopyroxene. Hornblende replaced clinopyroxene and grew in open spaces with calcite, quartz, feldspar, titanite and epidote. Accessory minerals include apatite, tourmaline, allanite and wollastonite, locally, in the marbles. Application of the pyroxene-garnet geothermometer of Pattison & Newton (1989) to pyroxene-garnet skarn rocks gave non-equilibrium results, with frequency peaks occurring at 680°, 550°C (attributed to an early contact metamorphic thermal-isochemical stage); and a number of values between 375° and 320° C (related to a late infiltration metasomatism event, which occurred at pressures of < 500bars; Mastrakas, 2007).

## 4 ORES ASSOCIATED WITH THE TINOS PLUTON

### *4.1. Scheelite Mineralization*

Tungsten mineralization is hosted in skarns and hornfelses. Scheelite occurs as disseminations and mainly as massive aggregates in discontinuous zones, up to 30 cm wide, subparallel to the schistosity, particularly in silicified-carbonatized zones or as residual crusts on fractures. Scheelite mineralization, which makes up to 20 vol. % of the skarn, occurs in garnet-pyroxene skarns (grossular-rich grandite coexisting with hedenbergite during the contact metamorphic episode evolved to andratite-rich oscillatory zoned garnet coexisting with salite-diopside) containing magnetite, chalcopyrite, pyrrhotite, pyrite and lesser sphalerite. Open spaces in the skarn are locally filled with calcite, apatite, hornblende, chlorite, titanite, quartz, feldspar, molybdenite and scheelite. Scheelite deposition was likely controlled by the reaction:

$$CaCO_{3(s)} + H_2WO_4^{0}{}_{(aq)} = CaWO_{4(s)} + H_2O_{(l)} + CO_{2(g)} \quad (1)$$

### *4.2. Panormos Bay mineralized vein system*

The Panormos Bay mineralized vein system is hosted in marbles of the Basal and Blueschist Units and consists of 30 subparallel steeply dipping banded, syntaxial stockworks of quartz veins. Marble units are intruded by two generations of veins, an older, northeasterly-trending set of milky quartz veins and a younger group of northwesterly trending clear quartz veins.

Alteration haloes formed as concentric shells and planar bodies that envelope milky and clear quartz veins. Blueschist Unit marbles develop assemblages composed of muscovite, albite and tourmaline, whereas alteration haloes in dolomitic marbles of the Basal unit consist of two successive zones: an inner *talc zone* and an outer *chlorite zone*. Talc zones are characterized by an assemblage of milky quartz, talc, calcite, brucite, muscovite, and albite. Chlorite zones consist of major clear and minor milky quartz, chlorite, epidote, muscovite, albite and barite. Formation of talc-brucite-calcite is interpreted to have been controlled by the reaction:

$$CaMg(CO_3)_{2(s)} + 4SiO_{2(aq)} + 2Mg^{+2} + 3H_2O_{(l)} = Mg_3Si_4O_{10}(OH)_{2(s)} + CaCO_{3(s)} + CO_{2(g)} + 4H^{+} \quad (2)$$

Seventy metallic and gangue minerals, including Cu-cervelleite and an unnamed Ag-Au-Cu sulphotelluride were identified. Eight paragenetic stages of hypogene mineralization

with the assemblages: pyrite, arsenopyrite, pyrrhotite (Stage I); tetrahedrite, tennantite, goldfieldite (Stage II); bornite, chalcopyrite (Stage III); Sn sulphides, sulphosalts of As and Sb and arsenides of Ni or Co (Stage IV); tellurides (Stage V); galena, betekhtinite, argentite (Stage VI); wurtzite, greenockite, smithsonite (Stage VII); native gold, silver, copper, arsenic, stromeyerite, pyrargyrite (Stage VIII) were followed by supergene mineralization (stage IX) (Tombros *et al.*, 2004, 2005). Precipitation of Ag-, and Au- tellurides was likely associated with reactions (3) and (4), whereas native precious metals were deposited by reactions (5) and (6):

$$2Ag(HS)^-_2 + HTe^-_{(aq)} = 4HS^-_{(aq)} + Ag_2Te_{(s)} + H^+_{(aq)} \quad (3)$$

$$Au(HS)^-_{2(aq)} + 2HTe^-_{(aq)} + 0.75O_{2(g)} + H^+_{(aq)} = 2HS^-_{(aq)} + AuTe_{2(s)} + 1.5H_2O_{(l)} \quad (4)$$

$$0.5H_2O_{(l)} + Au(HS)^-_{2(aq)} = Au_{(s)} + 2HS^-_{(aq)} + H^+_{(aq)} + 0.25O_{2(g)} \quad (5)$$

$$Ag(HS)^-_{2(aq)} + 0.5H_2O_{(l)} = Ag_{(s)} + H^+_{(aq)} + 2HS^-_{(aq)} + 0.25O_{2(g)} \quad (6)$$

*4.3. Apigania Bay mineralized vein system*

The Apigania Bay vein system is hosted in marbles, blueschists, greenschists, amphibolites and ultramafics of the Blueschist Unit (Tombros, 2001); and consists of five high-angle quartz veins, which bear considerable resemblance to veins at Panormos Bay. Alteration haloes comprise an inner *epidote zone* and an outer *chlorite zone*. The epidote zone is associated with milky quartz, albite, muscovite and ankerite, whereas the chlorite zone contains clear and minor milky quartz, chlorite, calcite, albite and muscovite.

There are three paragenetic stages of hypogene mineralization: pyrite, sphalerite, pyrrhotite, arsenopyrite, magnetite, argentite, electrum, stephanite, xanthoconite, proustite, canfieldite (Stage I); tetrahedrite, famatinite, chalcopyrite, rammelsbergite, laggisite, cassiterite (Stage II); and galena, argentite-acanthite, polybasite, electrum, argentopyrite (Stage III). A supergene stage (Stage IV) follows the hypogene stages (Tombros & St. Seymour, 1998). Electrum precipitation in Stages I and III was controlled by reaction (7):

$$0.5H_2O_{(l)} + 0.7Au(HS)^-_{2(aq)} + 0.3Ag(HS)^-_{2(aq)} = Au_{0.7}Ag_{0.3(s)} + 2HS^-_{(aq)} + H^+_{(aq)} + 0.25O_{2(g)} \quad (7)$$

## 5 FLUID INCLUSION STUDIES

Microthermometric measurements were made in the Laboratory of High Temperature Processes at the Department of Earth and Planetary Sciences of McGill University. Temperatures were measured with an alumel-chromel thermocouple, and the readings were calibrated with synthetic inclusions. Measurements are accurate to within ± 1°C. Microthermometric data were reduced using the FLINCOR software (Brown, 1989).

At room temperature, fluid inclusions were classified into three types based on the number and proportion of phases: (i) L-V inclusions predominate, and consist of aqueous liquid + vapor (< 25 vol. %). They contain no solids, whereas formation of gas hydrates was observed during freezing and these homogenize to liquid upon heating, (ii) V-L inclusions with irregular shapes and consisting of aqueous liquid + vapour (up to 80 vol. %). The V-L inclusions are primary, infrequently observed and homogenize to the vapor phase upon heating, and (iii) L-L-V inclusions consist of aqueous liquid + carbon dioxide liquid + vapor. Formation of gas hydrates was observed in some of the L-L-V inclusions during freezing.

L-L-V primary fluid inclusions (~5 % of inclusion population) occur in milky quartz veinlets cross cutting garnet cores from the skarn, and in milky quartz and calcite from Panormos Bay. V-L primary inclusions occur in scheelite and milky quartz veinlets, smoky and milky quartz and calcite from Panormos Bay mineralization. L-V primary, pseudosecondary and secondary inclusions are located in all three mineralizations.

The temperatures of last melting of ice ($T_{m\text{-}ice}$) and clathrates ($T_{m\text{-}clathrate}$) of the L-V, V-L and L-L-V inclusions, in scheelite and associated milky quartz vary from -10.4° to -10.2°C and 0.7° to 5.7°C, respectively. These values correspond to salinities of 10.4 to 14.8 wt% NaCl equivalent, using the equations of Brown & Lamb (1989) and Darling (1991). The homogenization temperatures ($T_h$) of these inclusions vary from 315° to 400 °C. The $T_{m\text{-}ice}$ and $T_{m\text{-}clathrate}$ values for fluid inclusions in smoky quartz range from -6.6° to -5.7°C and 6.7° to 7.7°C, respectively, corresponding to salinities

of 4.5 to 6.8 wt% NaCl equivalent, whereas the $T_h$ values range from 281° to 320°C.

At Panormos Bay, the $T_{m\text{-}ice}$ and $T_{m\text{-}clathrate}$ values of fluid inclusions in milky vein and clear quartz range from -4.4° to -2.3°C, 7.7° to 8.5°C, and -4.1° to -2.0°C, 8.8° to 9.6°C corresponding to salinities of 1.1 to 7.9 and 0.8 to 5.6 wt% NaCl equivalent. The $T_h$ values of inclusions range from 245° to 292°C and 198° to 253°C, respectively. At Apigania Bay the $T_{m\text{-}ice}$ values of fluid inclusions in milky vein and clear quartz range from -4.3° to -0.4°C, and -3.6° to -0.1°C, respectively, corresponding to salinities of 3.0 to 6.8 and 0.2 to 5.5 wt% NaCl equivalent. The $T_h$ values range from 173° to 235°C and 125° to 168°C, respectively.

## 6 DISCUSSION

Based on results derived from reactions 1 to 7, it is likely that precipitated the mineralizations ore deposition on Tinos Island were controlled by pH, $CO_2$-effervescence, depletion of $H_2S$, and changes in the oxidation state of the ore fluid. Effervescence of $CO_2$ causes a sharp increase in pH, which in turn destabilizes the tungsten and precious metal-bearing complexes. This suggests that the deposition of scheelite, Au-Ag tellurides and native precious metals and electrum was due to phase separation related to $CO_2$-effervescence. The escape of volatiles neutralized the pH of the mineralizing fluid from 3.3 at 400°C to 4.6 at 300°C, 5.7 at 250°C and 6.5 at 200°C for the Panormos Bay ores and from 6.9 at 200°C to 7.6 at 150°C at Apigania Bay (Tombros, 2001). In conclusion, W, Au-Ag-Te and Au-Ag ore deposition was predominantly controlled by gaseous phase separation, which resulted in pH neutralization.

## ACKNOWLEDGMENTS

We thank the European Social Fund (ESF), Operational Program for Educational and Vocational Training II (EPEAEK II), and particularly the Program Pythagoras II, for funding the above work as a grant to KStS and postdoctoral fellowship to S. Tombros.

## REFERENCES

Altherr R, Kreuzer H, Wendt I, Lenz H, Wagner G, Keller J, Harre W, Hohndorf A (1982) A late Oligocene/Early Miocene high temperature belt in the Attico-Cycladic crystalline complex (Greece). *Geol Jah* 23: 971-164

Andriessen, P, Banga G, Helbeda (1987) Isotopic age study of Pre-Alpine rocks in the basal units on Naxos, Sikinos and Ios, Greek Cyclades. *Geol Mijn* 66: 3-14

Bröcker M, Kreuzer H, Matthews A, Okrusch, M (1993) $^{40}Ar/^{39}Ar$ and oxygen isotope studies of polymetamorphism from Tinos island, Cycladic Blueschist Belt, Greece. *J Metam Geol* 11: 223-240

Brown E (1989) FLINCOR: A microcomputer program for the reduction and investigation of fluid inclusion data. *Amer Miner* 74: 1390-1393

Brown E, Lamb E (1989) P-V-T properties of fluids in the system NaCl ± $H_2O$ ± $CO_2$: New graphical presentations and implications for fluid inclusions studies. *Geoch Cosmoch Acta* 53: 1209-1221

Darling S (1991) An extended equation to calculate NaCl contents from final clathrate melting temperatures in $H_2O$-$CO_2$-NaCl fluid inclusions: Implications for P-T isochore location. *Geoch Cosmoch Acta* 55: 3869-3871

Mastrakas N (2007) Tinos granite and the associated skarn deposits. *PhD thesis (unpublished), University of Patras*

Mastrakas N, St. Seymour K (2000), Geochemistry of Tinos granite: A window to the Miocene microplate tectonics of the Aegean region. *N Jarh Min Abh* 175: 295-315

Melidonis N, (1980) The geological structure and mineral deposits of Tinos Island (Cyclades, Greece): A preliminary study. *I.G.M.E.* 13: 1-80

Pattison D, Newton R (1989) Reversed experimental calibration of the garnet-clinopyroxene Fe-Mg exchange thermometer. C*ontr Miner Petrol* 101: 87-103

Tombros S, St. Seymour K (1998) Applied geothermometry of the hydrothermal Au-Ag vein mineralization, Apigania. *Bull Geol Soc Greece* 32: 165-172

Tombros S (2001) The Au-Ag-Te polymetallic mineralization of Tinos island, Cyclades, Aegean sea, Hellas. *PhD thesis (unpublished), University of Patras*

Tombros S, St. Seymour K, Spry P (2004) Description and conditions of formation of new unnamed Ag-Cu and Ag-Cu-Au sulfotellurides in epithermal polymetallic Ag-Au-Te mineralization, Tinos Island, Hellas. *N Jhb Min Abh* 179: 295-310

Tombros S, St. Seymour K, Spry P, Williams-Jones A (2005) Description and conditions of formation of new unnamed Zn-rich greenockite in epithermal polymetallic Ag-Au-Te mineralization, Tinos island, Hellas. *N Jhb Min Mon* 182: p. 1-9

# Micromineralogy of gold-telluride ores at deposit Samarchuk of Kyzylalmasai ore field

A.Z. Umarov
*National University of Uzbekistan. Tashkent, Uzbekistan*

ABSTRACT: Kyzylalmasai ore field is located on the right bank of the Angren river, in the eastern part of Shavas-Duken graben. Samarchuk deposit is one of the sections of the ore field. It is confined to the southern flank of Karabau fault.Seven mineral assemblages associated with gold mineralization are developed in Samarchuk deposit. The main productive assemblage of Samarchuk deposit is quartz-carbonate-gold-telluride-polymetallic assemblage. The recognized microparageneses of gold, tellurides, selenides appear to be clear indications of gold ores with gold-telluride mineralization of Kochbulak type.

KEYWORDS: Samarchuk, Karabau fault, gold vein, Kyzylalmasai, Chumauk, explosive breccias, grey ores, assemblages, quartz, pyrite.

## 1. INTRODUCTION

The Kyzylalmasai ore field is located on the right bank of the river Angren, in the eastern part of Shavas-Dukent graben (Beloplotova *et al* 1969)

The Samarchuk gold deposit is one of the sections of the ore field. It is confined to the southern flank of the Karabau fault, which forms the boundary of the basement formations and the volcanic cover (dacite-andesite formation "$C_{2-3}$"). Mineralization takes the form of quartz replacements at this contact.

The Zolotaya Vein is spatially controlled by the Karabau fault system. It dips in the range of 40-70$^{o}$, and its true thickness varies from 20-25m.

The mineralized contact zone is accompanied by several zones of felsite dykes which can form both the footwall and hangingwall to the mineralization and occasionally cut the orebody. At these contacts infiltration breccia are developed.

## 2. METHODOLOGY

Over recent times additional research materials have become available from deep core drilling testing the deepest horizons in the Samarchuk deposit. This study has been based upon the use of a JEOL Superprobe JXA-8800R microanalyser which uses X-ray fluorescence analysis of bulk samples and on separated heavy fractions of crushed drill core samples.

The results of this study are given below Table 1 and are shown in comparison with data from the Kysylalmasai deposit.

## 3 MINERAL ASSEMBLAGES

The following mineral associations with gold mineralization are developed in the Samarchuk gold deposit (Koneev & Umarov, 1995).

1. An assemblage of pre-ore metasomatites Comprised of quartz, sericite, carbonate, pyrite and other gangue minerals.

2. Quartz-gold-pyrite assemblage which makes up the main part of the "Zolotaya" vein. Generally this is low-sulphide bearing and with low overall gold tenor and its overall volume is not so high. Gold is finely disseminated and associated with arsenious pyrite, ankerite and rarely, marcasite.

3. A quartz (carbonate) polymetallic gold-telluride assemblage. This phase has a higher sulphide content whilst its peculiarity is its widely developed assemblage of gold, silver, bismuth and antimony telluride minerals as well as the presence of tin-bearing and selenide

mineralization. This assemblage is generally low to moderately – sulphide rich with marked amounts of galena sphalerite, chalcopyrite, tennantite-tetrahedrite ("grey coppers") and minor cassiterite and scheelite.

Table 1: Comparative Characteristic of Au-Te and Au-Ag mineralization of Kysylalmasai ore field.

| Formation / Indications | Gold-telluride, | Gold-silver |
|---|---|---|
| Regional position | Cross-section zone of Shavas-Dukent graben by meridional Dukent-Gushai fault | |
| Geological position | Intraformational zone with breccias in contact with granitoids and volcanites. | Positive structural-horst, composed of syenito-diorites, sericite-chlorite slates etc. |
| Economic assemblage | Gold-selenide-telluride polymetallic | Electrum-selenide-polysulphide |
| Compounds Au-As | $Au_2Ag$, $Au_3Ag$ (700-900) | AuAg, $Au_2Ag_3$, $Au_2Ag_3$ (<700) |
| Matrix | Annivite, tennantite, galena, Co-pyrite | Freibergite, As-Ni-pyrite, chalcopyrite |
| Microparagenesis | Hessite, sylvanite, algaite, tetradymite, volynskite telluro-antimonide? | Silver, allargentum, acanthite, polybasite, naumannite, bogdanovichite jordisite |
| Elements – indicators | Te, Se, Bi, Pb, Cd, Hg | Ag, Se, Sb, As, Ni, Mo |
| Au:Ag | 5:1-1:10 | 1:10-150 |
| Se:Te | 1:5-1:20 | 5:1-1:5 |
| As:Sb:Te | 2:2:1 | 60:40.1 |
| Co:Ni | 1:1-1:2 | 1:1-1:3 |
| $T^0C$ | $<350\text{-}400^0$ | $<200\text{-}250^0$ |

The peculiarity of this assemblage lies in the textures of the ore minerals as colloform banded aggregates within hydraulic fracture breccias, as it seems to be specific to gold – telluride deposition.

4. Quartz – carbonate assemblage with chalcopyrite and bismuth mineral assemblage. Siderite is the dominant carbonate within which wittichenite and native bismuth occur. There also occurs cobaltiferous pyrite, pale coloured sphalerite, galena and free gold. Generally it is seen in the form of small veinlets dominated by siderite – chalcopyrite.

5. A quartz – barite and quartz – calcite assemblages in the form of barite-quartz-calcite veins with galena and chalcopyrite. Post-ore mineralization calcite veinlets are ubiquitous throughout the mineralized body.

The main economic association in the Samarchuk deposit is the quartz-carbonate-gold-telluride-polymetallic assemblage (Stages 2, 3 and 4).

Quartz-carbonate mineralization with electrum-selenide-sulphide mineralization is also occasionally recognized in the near-surface parts of the Zolotaya Vein.

The study of the gold-telluride-ores of the deposit showed that gold and the tellurides-selenide phases accompanying it occur exclusively in micromineral forms (Koneev *et al*, 1994).

The composition of tellurides and other microminerals is highly variable and a number of hitherto unrecognized mineral phases have been identified (see Table 2).

The observed paragenesis of gold, tellurides, and selenides are clear indicators of mineralization of "Kuchbulak type" (Koneev & Umarov, 1995).

## ACKNOWLEDGEMENTS

I express my sincere gratitude to my scientific adviser Prof. R.I. Koneev for assistance and advice in my work. Moreover, thanks are due to Asst. Prof. Y..N Ignaticov for providing analysis to support my paper.

Table 2: Micromineral composition of gold – silver tellurides in the Samarchuk deposit.

| Sample No. | Au | Ag | Cu | Fe | Bi |
|---|---|---|---|---|---|
| HESSITE | | | | | |
| 8267 | 0.04 | 65.89 | 0.20 | 0.15 | 0.02 |
| STÜTZITE | | | | | |
| 754/190 | - | 58.23 | - | - | - |
| PETZITE | | | | | |
| 8267 | 22.69 | 42.00 | | 0.04 | 0.05 |
| SYLVANITE | | | | | |
| 8267 | 22.28 | 14.99 | - | 0.03 | 0.06 |
| NATIVE - Te | | | | | |
| 746/325-8 | | 7.69 | - | 2.24 | - |
| TELLURIC BISMUTHINITE | | | | | |
| 748/307-1 | - | 0.56 | 0.02 | 0.13 | 48.98 |
| Se - VOLYNSKITE | | | | | |
| 748/307-3 | - | 15.58 | - | 1.36 | 41.21 |
| Bi – HESSITE | | | | | |
| 749/314-1 | - | 50.99 | - | - | 7.92 |
| PHASE 1 | | | | | |
| 746/325-3 | - | 26.51 | - | 2.65 | 48.98 |
| PHASE 2 | | | | | |
| 746/325-1 | - | 14.27 | - | 7.35 | 28.06 |

| Sample No. | As | Sb | Te | Se | S |
|---|---|---|---|---|---|
| HESSITE | | | | | |
| 8267 | 0.03 | 0.26 | 35.28 | - | 0.08 |
| STÜTZITE | | | | | |
| 754/190 | - | - | 41.23 | - | - |
| PETZITE | | | | | |
| 8267 | 0.01 | 0.13 | 34.57 | - | 0.05 |
| SYLVANITE | | | | | |
| 8267 | - | 0.43 | 61.64 | - | 0.10 |
| NATIVE – Te | | | | | |
| 746/325-8 | - | - | 86.94 | 0.26 | 1.02 |
| TELLURIC BISMUTHINITE | | | | | |
| 748/307-1 | - | 0.76 | 50.75 | - | 0.03 |
| Se - VOLYNSKITE | | | | | |
| 748/307-3 | | | 34.59 | 5.76 | 1.48 |
| Bi - HESSITE | | | | | |
| 749/314-1 | | 1.84 | 38.17 | 0.56 | 1.28 |
| PHASE 1 | | | | | |
| 746/325-3 | - | - | 0.21 | 7.30 | 10.46 |
| PHASE 2 | | | | | |
| 746/325-1 | - | - | 0.07 | 5.36 | 18.10 |

## REFERENCES


Beloplotova O.O., Kurbanov P.F., Martynov V.V. Suleimanov M.O. 1969 Geology of Kyzylalmasai ore field. Ore formations and main features of metallogeny of gold in Uzbekistan. *Tashkent, Fan.*

Koneev R.I., Umarov A.Z. 1995 On gold – argental and gold – telluric mineralization of Kyzylalmasai ore field. *Uz.geo.* №6, pp.24-27.

Koneev R.I., Kushmuradov O.K., Turesebekov A.Kh. 1994 Micromineralogy – subject, techniques, application. *Tashkent University press,* p.89.

# The Amantaytau gold-sulphide deposit, Uzbekistan: mineralogy and geochemistry of primary and oxidized ores

A.V. Jukov
*National University of Uzbekistan, Tashkent, Uzbekistan*

ABSTRACT: The Amantaytau deposit, along with the Muruntau, Kokpatas, Daugyztau deposits and others, form the Kyzylkum gold "ore field" of the Beltau-Kurama volcano plutonic belt. According to mineralogical composition and technological properties, the deposit is distinguished by two types of ore: 1) primary (sulphide) and 2) secondary (oxidized). As, Te, Sb, Ag are accumulated in primary ores of the deposit along with gold, whereas As, Te, Bi occur in the oxidized ores. The primary ores of the Amantaytau deposit are complex and are amenable for the simultaneous extraction of gold, silver, W, Mo, Sb, Bi, Te and other metals.

KEYWORDS: Amantaytau deposit, gold-sulphide ores, Uzbekistan, primary, sulphide, oxidized, minerals, Kyzylkum, Besapan Suite, pyrite, arsenopyrite, gold.

## 1 INTRODUCTION

The deposit of Amantaytau, along with the deposits of Muruntau, Kokpatas, Daugyztau and others from the Kyzylkum gold "ore knot" of the Beltau-Kurama volcanoplutonic belt (Fig. 1). The belt originated as a result of subduction of the crust of the Turkestan paleooceanic basin under the Kazakhstan-Kyrgyz microcontinent and subsequent processes (Dalimov *et al*., 2002).

## 2 GEOLOGY OF THE DEPOSITS

The rocks enclosing the mineralization are the equivalent of the upper part of the Auminzabesapan complex of the Kyzylkums, which are of Upper Ordovician to Lower

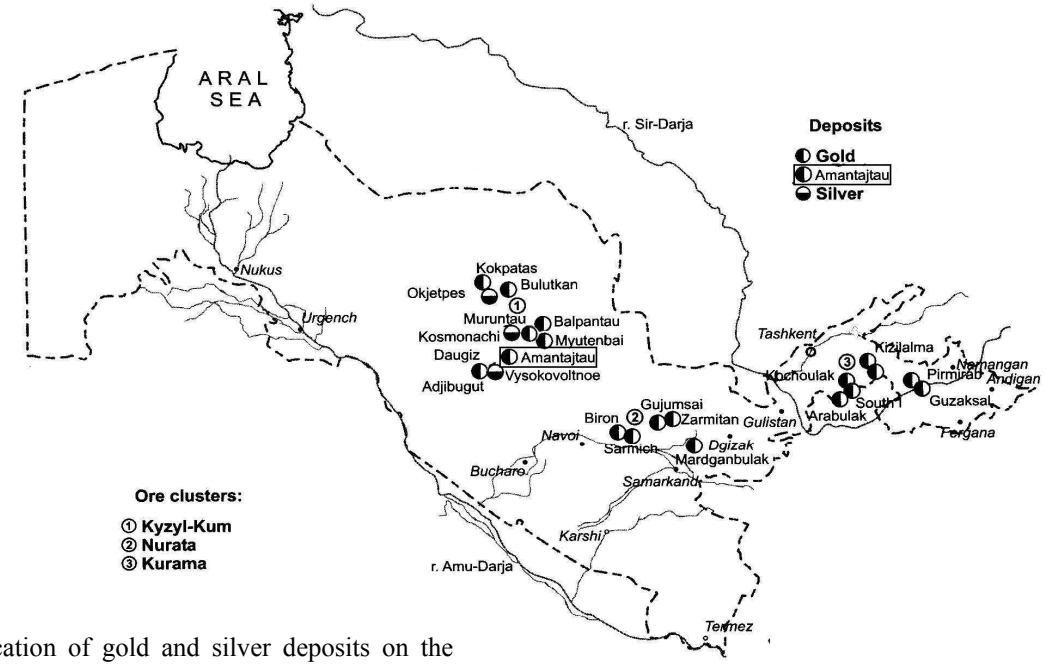


Fig. 1. Location of gold and silver deposits on the territory of Uzbekistan (Akhmedov, 2002).

Silurian age (Fig. 2). These comprise interbedded sandstones, siltstones and metapelites and they can be distinguished by their degree of cleavage and metasomatic overprint.

The ratio of sandstones to siltstones to metapelites in bulk is about 2:2:1. The location of the ore zones within the deposit area is controlled by faults. One of the largest faults is well-traced in the area towards Muruntau and divides the Amantaytau deposit into approximately equal parts – a south-eastern and a north-western part. Within the area of the Amantaytau gold ore zone, the host rocks are albitized, silicified, sericitized, chloritized and carbonatized. Silicification is pervasivelt developed across the ore zone as a whole (Paramonov, 2001).

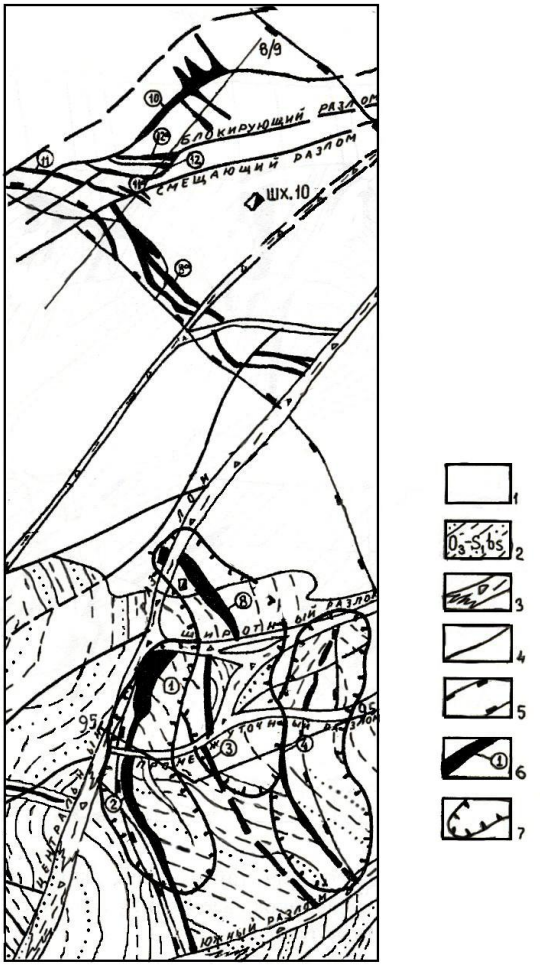


Fig. 2. Geological structure of the Amantaytau deposit (Paramonov, 2001).

1 – Mezozoic deposits; 2 – Besapan Suite [fourth suite ($O_3$-$S_1$)] sandstones, siltsotones, metapelites; 3 – crumpling zone / crush zone; 4 – faults; 5 – outline of Amantaytau ore zone; 6 – ore bodies and their numbers; 7 – contours of projected open-pits.

## 3 MINERALOGICAL COMPOSITION AND GEOCHEMISTRY OF THE GOLD ORES

As a result of mineralogical studies, more than 120 minerals, representing 16 classes of compounds (Paramonov, 2001; Chebotaryov, 1994) have been found at the Amantaytau deposit. The most important are listed in Table 1. The most common mineral at the deposit is pyrite, its overall content varies up to 85% in pyrite veins. By composition, the pyrite is arsenious, and the concentration of arsenic reaches 3.4% (Table 2). Arsenopyrite is present in the form of tiny inclusions in pyrite, rarely in quartz, as well as occurring in the carbon-bearing slates of the wallrocks.

According to microanalysis (Table 2), the admixture of antimony is present in arsenopyrite, but the sulphur concentration is higher than the theoretical one. Native gold is of high finenesss (958-978) and occurs finely disseminated and dust-like. It is seen in pyrite, quartz, carbonates, chalcopyrite, sphalerite and other minerals. Iron (Table 2) is found in gold in the oxidized zone. Other sulphides such as galena, chalcopyrite, sphalerite, cupriferous "grey ores", pyrrhotite, marcasite, pentlandite and others are common in the form of microminerals containing 1-2% of the ore mass.

Table 1. Ore minerals of the Amantaytau deposit.

| **Primary sulphide ores** | | **Secondary oxidized ores** | |
|---|---|---|---|
| Gold | Marcasite | Gold | Mimetite |
| Silver | Antimonite | Chalcocite | Turquoise |
| Lead | Molybdenite | Covellite | Chrysocolla |
| Antimony | Chalcopyrite | Bornite | |
| Graphite | Tetrahedrite | Chlorargyrite | |
| Silver | Arsenopyrite | Iodyrite | |
| Amalgam | Miargyrite | Cuprite | |
| Stistaite | Jamesonite | Minium | |
| Acanthite | Famatinite | Pyrolusite | |
| Pentlandite | Boulangerite | Limonite | |
| Galena | Altaite | Jarosite | |
| Sphalerite | Naumannite | Cerrusite | |
| Pyrrhotite | Polybasite | Malachite | |
| Freibergite | Wolframite | Anglesite | |
| Cinnabar | Scheelite | Chalcanthite | |
| Pyrite | | Scorodite | |

The highest gold content is attributed to quartz-sulphide veins and heavy impregnations of sulphides. On the whole, the content of gold is defined by the amount of gold-(arseno-pyrite)-pyrite and gold-pyrite-arsenopyrite mineral assemblages. By compositional and technological properties there are two types of

ores at the Amantaytau deposit: 1) primary (sulphide) and 2) secondary (oxidized).

1) Primary, sulphide ores are contained within silicified siltstones and sandstones of dark grey and black colour with diseminations, veinlets and veins of sulphides. The basic ore minerals are pyrite, arsenopyrite, chalcopyrite, galena, and sphalerite. Gangue minerals are quartz, feldspar, mica, carbonates, rutile, sphene, graphite and carbonaceous matter (Table 1).

2) Secondary, oxidized ores are limonitized, kaolinitized sandstones and siltstones of mottled colour. Ore minerals include – native gold, goethite, hydrogoethite, scorodite, jarosite, semi-oxidized pyrite, and arsenopyrite. Gangue minerals are quartz, mica, dickite, gypsum, kaolinite, and carbonates (Table 1).

Table 2. Chemical composition of key minerals of the ores at the Amantaytau deposit (mass. %)

| Mineral | S | Fe | Cu | Zn | As | Ag |
|---|---|---|---|---|---|---|
| Gold | - | 2.45 | - | - | - | 0.10 |
| | - | - | - | - | - | 4.80 |
| | - | - | - | - | - | 7.40 |
| Pyrite | 52.70 | 45.90 | - | - | 0.90 | - |
| | 52.00 | 45.10 | - | - | 1.60 | - |
| | 52.50 | 45.10 | - | - | 1.80 | - |
| | 49.00 | 44.00 | - | - | 3.40 | - |
| Arsenopyrite | 23.14 | 35.62 | - | - | 43.56 | - |
| | 21.99 | 33.46 | - | - | 43.66 | - |
| Antimonite | 30.72 | 3.74 | - | - | - | - |
| Chalcopyrite | 36.52 | 30.10 | 33.30 | - | - | - |
| Tetrahedrite | 22.57 | 2.52 | 35.59 | 6.91 | 0.62 | 0.82 |
| Galena | 14.15 | 4.38 | 14.17 | - | - | 0.31 |
| | 13.07 | 2.22 | - | - | - | 0.18 |

Second part of Table 2.

| Mineral | Au | Sb | Bi | Te | Se | Pb |
|---|---|---|---|---|---|---|
| Gold | 97.34 | - | - | - | - | - |
| | 97.80 | - | - | - | - | - |
| | 95.80 | - | - | - | - | - |
| Pyrite | - | - | - | - | - | - |
| | - | - | - | - | - | - |
| | - | - | - | - | - | - |
| | - | - | - | - | - | - |
| Arsenopyrite | - | 006 | - | - | - | - |
| | - | 0.04 | - | - | - | - |
| Antimonite | - | 66.43 | - | - | - | - |
| Chalcopyrite | - | - | - | - | - | - |
| Tetrahedrite | - | 27.57 | 0.56 | - | - | - |
| Galena | - | - | - | 0.36 | 1.35 | 75.02 |
| | - | - | - | 0.12 | 1.00 | 83.21 |

Note: according to results of electron-probe analysis. Data compiled by the author and M.G.Chebotaryov (1994).

Presently, the oxidized ores are mined commercially from an open pit at the Amantaytau deposit and gold is extracted by a gravity-cyanidation process.

To investigate the geochemical bonds of gold and define the ore complexity, the ICP-MS technique was used to study ore concentrates of primary ores. Calculations were made for coefficients of elements concentration with respect to Clark values in the earth's crust after A.P.Vinogradov (1962). The primary ores of the Amantaytau deposit contain gold, As, Te, Sb, Pt, Pd and the oxidized ores elements such as As, Te, and Bi.

## 4 CONCLUSIONS

The deposit of Amantaytau is a gold-sulphide deposit of Au-As orogenic type (Koneev, 2001).

The primary ores of the Amantaytau deposit are complex and are amenable for the simultaneous extraction of gold, silver, W, Mo, Sb, Bi, Te and other metals.

## ACKNOWLEDGEMENTS

I express my profound gratitude to Rustam I. Koneev for his valuable advice in processing the factual material and Moses T. Khon for the opportunity in selecting sample material from the deposit of Amantaytau.

## REFERENCES

Akhmedov N.A. (2002) Strategy for base development of basic types of mineral products in the republic of Uzbekistan *Geology of Mineral Resources,* 3. pp. 11-15.

Chebotaryov M.G. (1994) Mineralogy and geochemical peculiarities of goldore deposit Amantaytau (central Kyzylkums), *Abstract for a candidates degree in geology and mineralogy. Tashkent.* pp. 18.

Dalimov T.N., Koneev R.I., Ganiev I.N., Ishbaev Kh.D. (2002) Geodynamics of northern margin of Turkestan paleooceanic basin and some peculiarities of formation of gold ore deposits of Uzbekistan *Geology, genesis and issues of developing complex deposits of precious metals. Moscow*. pp. 142-144.

Koneev R.I. (2003) Sistematization of gold ore deposits of Uzbekistan on the basis of micromineral parageneses *Ores and metals, №3.* pp. 20-28.

Paramonov Yu.I. (2001) Amantaytau deposit *Ore deposits of Uzbekistan. Tashkent.* HYDROINGEO, editor-in-chief Akhmedov N.A. pp. 303-312.

Vinogradov A.P. (1962) Mean content of chemical elements in the main types of igneous rock of the earth's crust *Geochemistry,* №7. pp. 551-571.

# Vertical zoning of nanominerals within the epithermal gold-silver deposit of Kysylalmasai, Uzbekistan.

R.A. Khalmatov
*National University of Uzbekistan, Tashkent, Uzbekistan*

ABSTRACT: The ores of the epithermal Au-Ag Kysylalmasai deposit have been studied by electron-microprobe research. A vertical zoning in the distribution of Au-Ag compounds, selenides and tellurides was revealed. Selenides Ag (naumannite, aguilarite) are mostly developed at the upper levels; lenaite, dyscrasite, seleno-tellurides of silver at the middle level and tellurides of silver, selenides of bismuth, and acanthite at the deeper level of the deposit.

KEYWORDS: Uzbekistan, Kysylalmasai, vertical zoning, gold-silver deposit, nanomineralogy, tellurides, selenides.

## 1 INTRODUCTION

The gold-silver deposit at Kyzylalmasay is located within the territory of the Republic of Uzbekistan, in the south-western spurs of the Chatkal range. Geologically the area lies within the Kurama zone of the Beltau-Kurama volcano-plutonic belt of the Western Tian-Shan (Fig.1) (Dalimov *et al*., 2002). The depoits forms part of the eponymous ore field (Fig.2)

## 2 GEOLOGY OF THE DEPOSITS

The ore field is confined to the structural zone formed at the intersection of the polygenic Shavaz-Dukent graben and the meridional Dukent-Gushsai deep fault. The Kyzylalmasay deposit (Tsentralny Section) is located on an isolated horst block of uplifted Caledonion granitoids saturated by a large amount of xenolithic slates (Ordovician-Silurian) and dy-

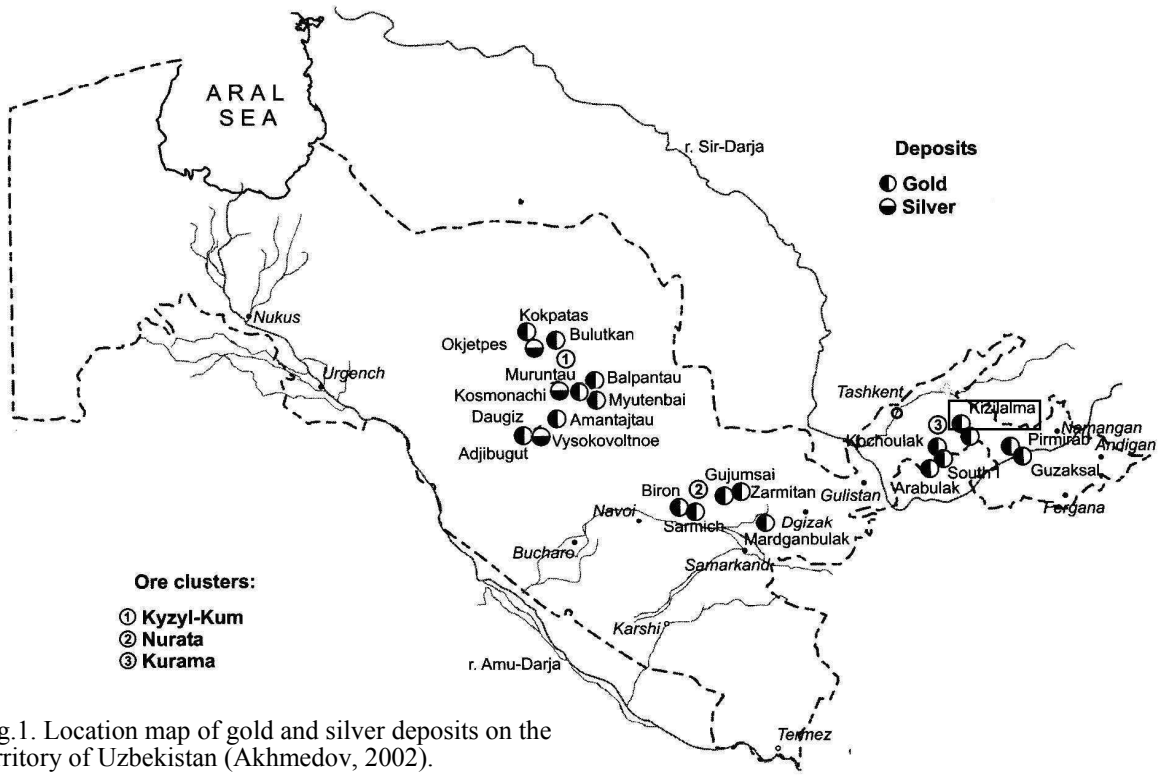


Fig.1. Location map of gold and silver deposits on the territory of Uzbekistan (Akhmedov, 2002).

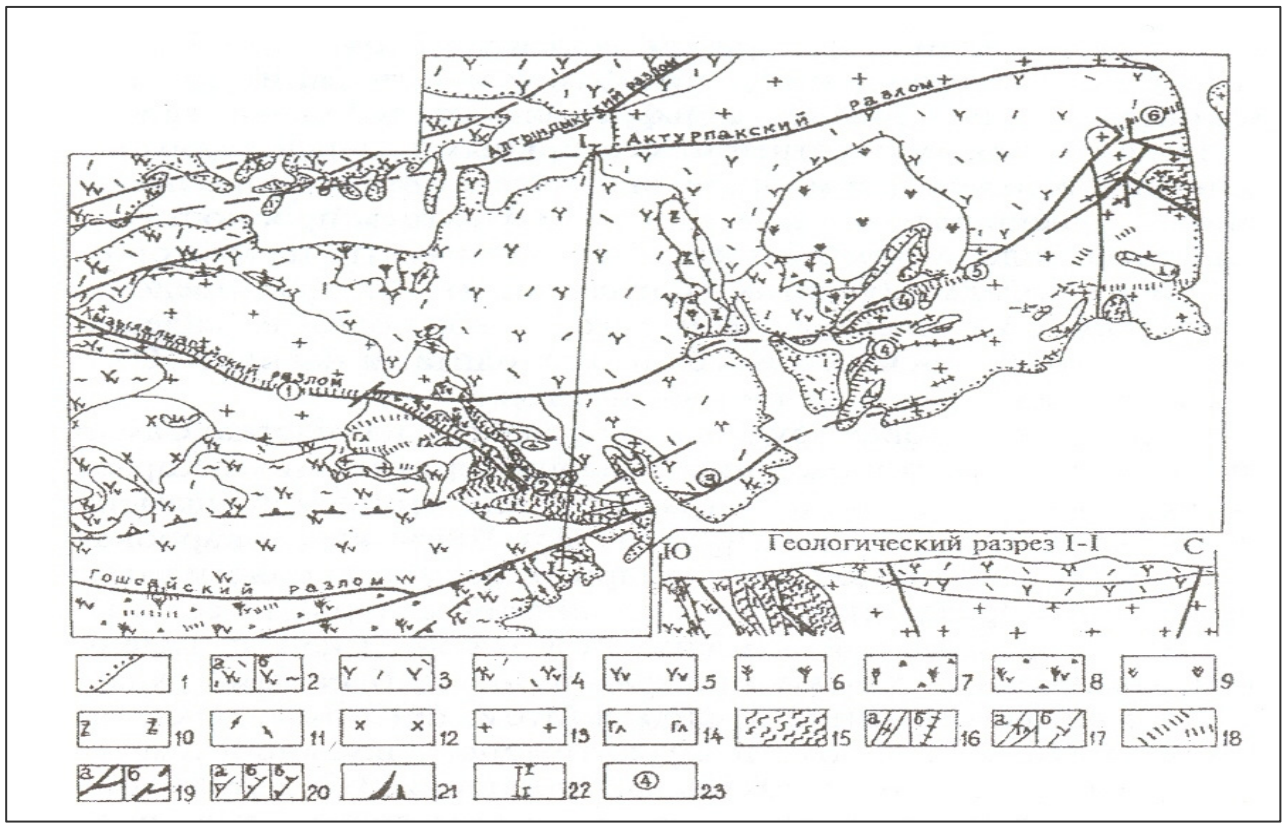


.Fig.2 Geological map of the Kyzylalmasay ore field. (Zavyalov, 2001).

1-outcrops of Palaeozoic rocks; 2-tuffs (a) and their ignimbrites (b) andesites / dacites; 3-andesite tuffs; 4-trachyandesite tuffs; 5-andesites / dacites; 6-andesites; 7-andesitic autobreccias; 8- andesitic / dacitic autobreccias; 9-dacites; 10-trachybasalts; 11-rhyolites; 12-two-mica granites; 13-granite-porphyry; 14-gabbro-diorites; 15-slates: Dykes; 16-felsites; 17-syenito-diorites (a- in scale; b-not to scale); 18-quartz veins; 19-faults traced, ($a_1$)-assumed (b); 20-vent ($a_1$), extrusive (b), subvolcanic (c) facies of volcanites; 21-ore bodies; 22-line of section; 23-districts of Kyzylalmasay deposit: 1-Severo-Zapadny; 2-Tsentranly, 3-Mezhdurechie, 4-Samarchuk, 5-Chumauk II, 6- Chumauk II.

kes of syenito-diorites and felsites (Zavyalov, 2001).

The ore bodies of the deposit are formed by two ecomomically important gold assemblages:

1. A subordinate Gold-pyrite-arsenopyrite; with arsenious pyrite, crystalline arsenopyrite, gersdorffite, löllingite, and disseminated native gold.

2. The major economic stage of Electrum-selenide-polysulphides; with intermetallides, sulphides, sulphosalts, selenides, and seleno-tellurides of silver which are only seen in micro and nanomineral form. The size these nanominerals are not more than 50-100 mμ (Table 1)..

## 3 NANOMINERALOGY OF GOLD-ARGENTAL ORES

Nanomineralogical studies (Koneev, 2006) Have enabled the recognition of vertical zoning within the deposit by means of nanomineral distribution within the two main ore bodies, 1 and 10 (Fig.3).

The uppermost part of the ore zone is typified by an assemblage of native silver, allargentum, küstelite ($AuAg_3$), naumannite, aguilarite, Se-stephanite, polybasite (horizons of Adits –II, -IV and X).

Dyscrasite, Te-polybasite, pyrargillite lenaite, electrum ($Au_2Ag_3$) occur in the itermediate ore horizons (Horizon 1, Adits -II and -V).

Acanthite, sternbergite and compounds of the general composition Ag-Se-Te are common in the deeper horizons of the Kyzylalmasay deposit, associated with bogdanovichite, tellurides of silver (servelite, hessite, znigriite) and a large range of transitional compounds of the systems Ag-Te-Se-S (Table 1). Gold grade increases due to the increasing presence of native AuAg compound. (Adit -VII)

Vertical zoning within the Kyzylalmasay deposit is seen in the regular change of nanoensembles. Selenides are common in the upper horizons, whilst the characteristics of the deeper horizons are seleno-tellurium compounds with a gradual transition to tellurides of

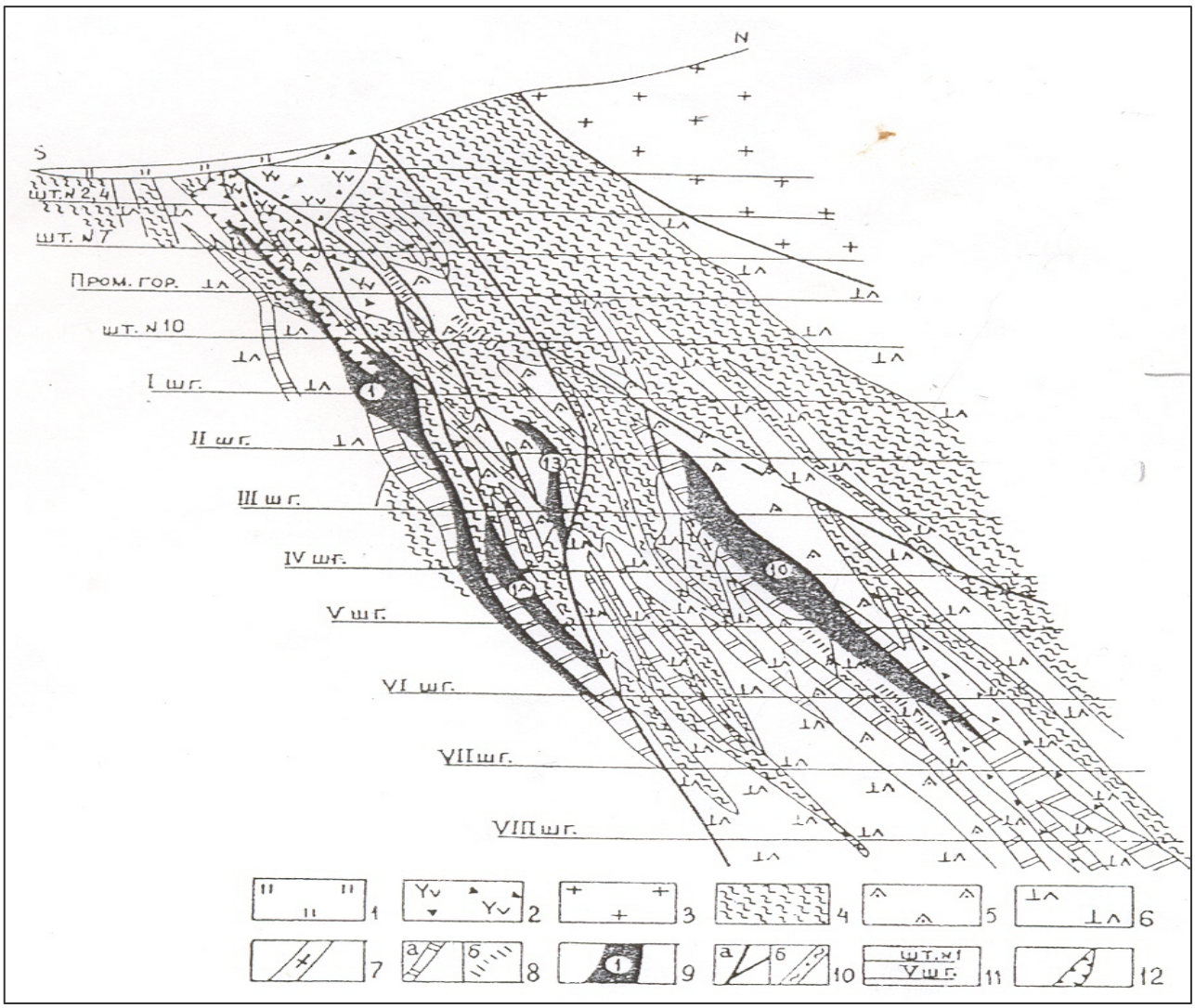


Fig.3 Vertical geological section through the Kyzylalmasay deposit

1-loesses; 2-automagmatic breccias; 3-granites; 4-slates; Dykes; 5-quartz diorites; 6-syenito-diorites; 7-felsites; 8-quartz veins (a) and veinlets (b); 9-ore bodies and their numbers; 10-faults (a), zones of crushing and mylonitization (b); 11-horizons of adits; 12-old stopes.

silver, selenides of bismuth. In addition the overall gold grade rises with depth. These peculiarities revealed by this study have established nanomineralogical analysis as an efficient method for defining zoning, evaluation of the erosional level of mineral deposits and, typification of the Au-Ag mineralization

## ACKNOWLEDGEMENTS

I express my sincere gratitude to Prof. Rustam I. Koneev for his advice during the research and in writing the article.

## REFERENCES

Akhmedov N.A. 2003 Strategy for base development of basic types of mineral products in the republic of Uzbekistan *Geology of Mineral resources*, 2002.3. pp. 11-15.

Dalimov T.N., Koneev R.I., Ganiev I.N., Ishbaev Kh.D. 2002 Geodynamics of northern margin of Turkestan paleooceanic basin and some peculiarities of formation of gold ore deposits of Uzbekistan *Geology, genesis and issues of developing complex deposits of precious metals*. Moscow: pp. 142-144.

Koneev R.I. 2006 Nanomineralogy of gold. *St-Petersburg: Delta*. pp. 220

Zavyalov G.E. 2001 Kyzylalmasay deposit *Ore deposits. Tashkent: Hydroingeo*. pp. 227-240

Table 1. Composition of nanominerals at Kyzylalmasay deposit (mass. %)

| No | Mineral | Au | Ag | Cu | Zn | Fe | As |
|---|---|---|---|---|---|---|---|
| 1 | Gold | 62.66 | 37.06 | 0.15 | - | - | - |
| 2 | | 59.72 | 39.90 | 0.01 | - | 0.12 | - |
| 3 | | 48.26 | 53.14 | 0.02 | - | 0.28 | - |
| 4 | | 24.01 | 74.06 | 0.07 | - | 0.17 | - |
| 5 | | 12.62 | 84.56 | 0.11 | - | 0.07 | - |
| 6 | Siver | 0.30 | 98.90 | 0.03 | - | - | - |
| 7 | | - | 97.40 | 0.10 | - | - | - |
| 8 | Allargentum | 0.50 | 82.30 | 0.21 | - | - | - |
| 9 | | - | 82.37 | 0.18 | - | - | - |
| 10 | Dyscrasite | - | 77.84 | 0.11 | - | - | - |
| 11 | Acanthite | 0.30 | 81.33 | 0.72 | - | - | - |
| 12 | Polybasite | - | 76.27 | 3.31 | - | - | - |
| 13 | | - | 71.80 | 4.03 | - | 0.82 | 0.42 |
| 14 | | - | 67.37 | 8.65 | - | 0.02 | 0.68 |
| 15 | | - | 65.32 | 7.93 | - | 0.36 | 1.68 |
| 16 | Te-polybasite | - | 69.55 | 2.42 | - | 0.43 | - |
| 17 | | - | 74.48 | 2.89 | - | 0.11 | - |
| 18 | Pyrarguirite | 7.88 | 54.76 | 0.66 | - | 0.21 | - |
| 19 | Lenaite | - | 47.24 | 2.65 | 0.56 | 19.00 | - |
| 20 | Sternbergite | - | 32.93 | - | - | 31.80 | - |
| 21 | Naumannite | - | 73.63 | 0.03 | - | 0.05 | 0.20 |
| 22 | | - | 70.38 | 0.01 | - | 0.21 | - |
| 23 | | 0.03 | 69.55 | 0.02 | - | 0.05 | - |
| 24 | | 0.03 | 67.99 | 0.83 | - | 0.23 | 0.07 |
| 25 | Aguilarite | 1.02 | 74.19 | 1.18 | - | 1.12 | - |
| 26 | | - | 77.94 | 0.63 | - | 0.68 | - |
| 27 | | - | 80.43 | 0.38 | - | 0.15 | - |
| 28 | Bogdanovechite | - | 20.62 | 0.39 | - | 0.41 | - |
| 29 | | - | 30.92 | - | - | 0.15 | - |
| 30 | | - | 43.36 | 0.31 | - | 2.30 | 0.35 |
| 31 | Sezvelite | 0.31 | 73.44 | 0.24 | - | - | - |
| 32 | | 0.09 | 72.78 | 0.42 | - | - | - |
| 33 | Znigriite | - | 60.63 | 2.61 | - | 0.79 | 0.43 |
| 34 | | - | 59.18 | 2.29 | - | 2.23 | - |
| 35 | Hessite | 0.06 | 63.51 | 0.04 | - | 0.01 | - |
| 36 | | 0.11 | 63.61 | 0.16 | - | 0.40 | - |
| 37 | Ag-Se-Te | 0.32 | 73.71 | 1.36 | - | 0.97 | 0.30 |
| 38 | | 0.16 | 72.26 | 1.49 | - | 0.92 | 0.23 |
| 39 | | 0.09 | 69.41 | - | - | - | - |
| 40 | | - | 63.75 | 1.77 | - | 1.01 | - |
| 41 | Ag-Se-Te-S | 0.03 | 71.57 | 1.15 | - | 1.02 | - |
| 42 | Ag-Sb-Te-S | 5.15 | 30.72 | 0.48 | - | 0.47 | - |
| 43 | | 3.23 | 22.31 | 0.53 | - | 0.46 | - |

Second part of Table 2.

| No. | Mineral | Sb | Bi | Hg | Se | Te | S |
|---|---|---|---|---|---|---|---|
| 1 | Gold | 0.01 | - | - | 0.02 | 0.02 | - |
| 2 | | 0.02 | - | - | 0.04 | - | - |
| 3 | | 0.11 | - | 0.04 | - | 0.06 | - |
| 4 | | - | - | 0.43 | 0.03 | 0.05 | - |
| 5 | | 2.03 | - | 0.45 | 0.05 | 0.03 | - |
| 6 | Siver | 0.80 | - | - | 0.05 | 0.02 | - |
| 7 | | 2.50 | - | - | - | - | - |
| 8 | Allargentum | 17.00 | - | - | - | - | - |
| 9 | | 17.64 | - | - | - | - | - |
| 10 | Dyscrasite | 20.45 | - | - | - | 0.03 | - |
| 11 | Acanthite | 3.10 | - | - | - | - | 12.50 |
| 12 | Polybasite | 8.81 | - | - | - | - | 12.60 |
| 13 | | 11.33 | - | - | - | - | 13.72 |
| 14 | | 9.54 | - | - | - | 0.22 | 14.98 |
| 15 | | 6.30 | - | - | 1.84 | 1.06 | 14.52 |
| 16 | Te-polybasite | 8.57 | - | - | - | 9.05 | 10.23 |
| 17 | | 4.79 | - | - | - | 7.58 | 9.65 |
| 18 | Pyrarguirite | 21.55 | - | - | 0.06 | 1.87 | 13.17 |
| 19 | Lenaite | - | - | - | 0.33 | 1.55 | 28.51 |
| 20 | Sternbergite | - | - | - | - | - | 35.74 |
| 21 | Naumannite | - | - | - | 24.90 | 0.02 | 0.07 |
| 22 | | - | 0.07 | - | 30.24 | 0.48 | 0.08 |
| 23 | | - | 0.10 | - | 29.61 | 0.36 | 0.21 |
| 24 | | - | - | - | 28.63 | 1.20 | 0.22 |
| 25 | Aguilarite | - | - | - | 18.82 | 0.07 | 4.88 |
| 26 | | - | - | - | 14.11 | 0.11 | 7.38 |
| 27 | | - | - | - | 12.45 | 0.08 | 6.52 |
| 28 | Bogdanove- | 0.46 | 44.24 | - | 32.04 | 0.02 | 1.80 |
| 29 | chite | - | 37.78 | - | 30.07 | 0.07 | 1.08 |
| 30 | | 0.16 | 25.22 | - | 24.23 | 0.87 | 2.22 |
| 31 | Sezvelite | - | - | - | - | 19.78 | 6.09 |
| 32 | | - | - | - | 0.25 | 20.70 | 5.69 |
| 33 | Znigriite | 7.43 | - | - | 0.01 | 19.86 | 8.05 |
| 34 | | 6.13 | 1.08 | - | 0.31 | 18.10 | 9.55 |
| 35 | Hessite | 0.10 | - | - | 0.07 | 36.56 | 0.05 |
| 36 | | - | - | - | 0.08 | 37.34 | 0.46 |
| 37 | Ag-Se-Te | - | - | - | 20.59 | 2.47 | 0.24 |
| 38 | | - | - | - | 21.15 | 4.16 | 0.30 |
| 39 | | - | - | - | 20.13 | 8.87 | 0.60 |
| 40 | | - | - | - | 10.39 | 21.74 | 0.90 |
| 41 | Ag-Se-Te-S | - | - | - | 15.36 | 7.08 | 3.17 |
| 42 | Ag-Sb-Te-S | 55.55 | - | 1.23 | - | 2.23 | 3.96 |
| 43 | | 64.25 | - | 0.66 | - | 4.59 | 3.48 |

# GOLD METALLOGENESIS:
# AMERICAS & AUSTRALIA

EDITED BY:
AL HOFSTRA
DAVE LENTZ

# The ~ 1864 Ma Stubbins Formation and the prospectivity of orogenic gold in the early Tanami basin, Western Australia

Leon Bagas[1, 2], Frank P. Bierlein[1]
[1]*Centre for Exploration Targeting, School of Earth and Geographical Sciences, The University of Western Australia, 35 Stirling Highway, Crawley, WA 6009, Australia, and*
[2]*Geological Survey of Western Australia, 100 Plain Street, East Perth, WA 6004, Australia*

Jim Anderson, Luc English
*Tanami Gold NL, P.O. Box 1892 West Perth, WA 6872, Australia*

David L. Huston, David Maidment
*Geoscience Australia, GPO Box 378, Canberra, ACT 2601, Australia*

ABSTRACT: The Palaeoproterozoic Stubbins Formation is a succession of turbiditic and pelagic sedimentary rocks interbedded with basalt and abundant dolerite sills. A study of the geochemistry of basalt and dolerite from the top 200m of the formation suggests that these rocks 1) have tholeiitic affinities; 2) are related to the same magmatic events; and 3) based on comparisons with modern analogues were deposited in a back-arc basin between the Halls Creek and Arunta orogens. Deposition in the back-arc basin ceased during compressional (collisional) deformation ~1850 Ma. In general, orogenic lode-Au deposits throughout the world are associated in space and time with collisional and accretionary tectonics similar to those inferred for the western Granites–Tanami Orogen, confirming that this region is significantly prospective for gold mineralization.

KEYWORDS: orogenic gold, geochemistry, Palaeoproterozoic, Stubbins Formation, Granites–Tanami Orogen

## 1 INTRODUCTION

Orogenic and intrusion-related ore systems (Goldfarb *et al*. 2001) have been identified in several Palaeoproterozoic (2500-1600 Ma) regions of Australia. Examples include the Pine Creek, Granites-Tanami (GTO), and Arunta orogens (Fig. 1).

Gold deposits in the GTO are hosted by various rock types, including carbonaceous siltstone, ferruginous siltstone and shale, chert, basalt, dolerite, and turbiditic sedimentary rocks. The majority of the host rocks have been metamorphosed to sub- to greenschist grade, and locally to amphibolite grade) at The Granites (Tunks & Cooke 2007).

Most Au deposits in the GTO are associated with relatively late, oblique strike and reverse faults, and many deposits are localized where these late faults intersect anticlines. Huston *et al.* (2007) suggested that Au deposition in the GTO was controlled by varied mechanisms that include competency contrasts, decarbonation and sulphidation of host rocks, fluid mixing and fluid pressure fluctuation. Another factor could include local perturbations in the temperature gradients that influence the movement of mineralized fluids in structurally prepared sites. The larger deposits appear to be located where

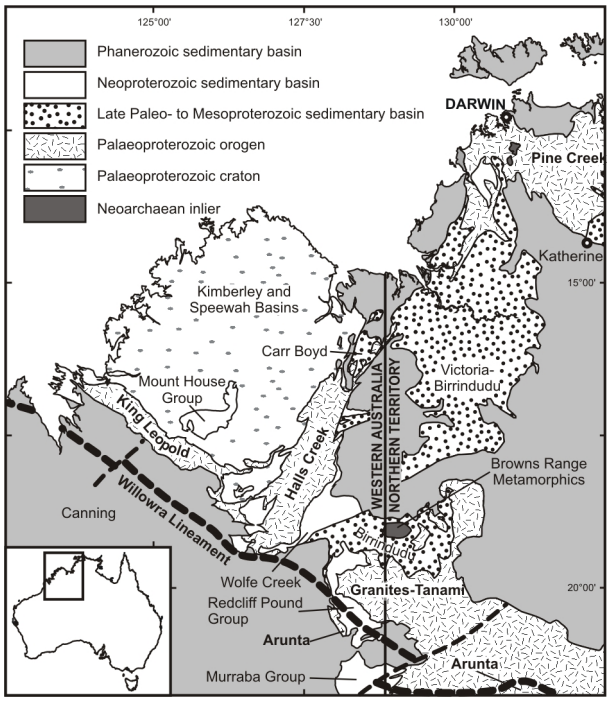


Figure 1. Location of the Granites–Tanami Orogen

many factors coincide that control Au mineralization (Huston *et al.* 2007).

In Western Australia no detailed study of the GTO was undertaken until recently. This paper documents a geochemical study of four oriented diamond-drill cores from the Bald Hill area. The study was aimed at improving our understanding of the early tectonic evolution of the Tanami basin during the early Palaeoproterozoic, and better understanding the potential for economic gold in the western part of the GTO and other Palaeoproterozoic terrains in the region.

## 2 REGIONAL GEOLOGY

The GTO is situated between the Halls Creek and Arunta orogens (Huston *et al.* 2007; Fig. 1). The oldest Palaeoproterozoic units in the GTO were previously thought to be included in the Tanami Group, which is subdivided by Crispe *et al.* (2007) into the ~1840 Ma Dead Bullock Formation and the overlying ~1835 Ma Killi Killi Formation. However, current thinking is that the ~1864 Ma Stubbins Formation (described later), located in the western part of the GTO, is the oldest unit.

The Dead Bullock Formation is a 1km-thick, upward-fining succession of sandstone, turbiditic sandstone, siltstone, and rare volcanic rocks that are overlain by deeper water chert and ferruginous siltstone and shale (Crispe *et al.* 2007). The Dead Bullock Formation hosts two of the three major goldfields in the Northern Territory, the Dead Bullock Soak, and The Granites goldfields.

The Stubbins and Dead Bullock formations lithologically resemble each other, and both are overlain by an up to 4km thick succession of turbiditic siliciclastic rocks assigned to the Killi Killi Formation. These three units are intruded by dolerite sills and ~1820-1790 Ma granites.

Previous workers have suggested links between Au mineralization and granite intrusion in the GTO (*e.g.* Tunks & Cooke 2007). Preliminary analyses of hydrothermal xenotime from the Coyote deposit (*Tanami Gold NL, unpublished data*) suggest that Au deposition occurred at 1810-1790 Ma, which overlaps the ages of granites in the region.

## 3 LOCAL GEOLOGY

The Bald Hill area includes several gold prospects hosted by the ~1864 Ma Stubbins Formation over a 15km strike length. The ~1864 ± 3 Ma SHRIMP U–Pb zircon age of the formation places some uncertainty on the generally accepted age and stratigraphic succession for the Tanami Group in that there are various turbiditic successions in the Tanami basin that have significantly different ages. These successions are the lower part of the ~1864 Ma Stubbins Formation, the ~1835 Ma Killi Killi Formation, and ~1825–1815 Ma Ware Group (*cf.* Huston *et al.* 2007).

The Stubbins Formation comprises a lower, 2-3 km thick succession of interlayered turbiditic sandstone, siltstone, shale, and common dolerite sills. These rocks are transitionally overlain by an upper, approximately 200m thick section of iron-rich shale, graphitic and carbonaceous shale, banded and nodular chert, siltstone, interstratified pillow basalt, minor dolerite sills, and rare turbiditic sandstone and rhyolite. The association of pillow basalt, chert, carbonaceous siltstone, shale and turbiditic sandstone is indicative of deep-water conditions during deposition.

The Stubbins Formation differs from the overlying Killi Killi Formation by the presence of a layer parallel ($S_1$) foliation. The contact of the Stubbins Formation with the Killi Killi Formation is a layer-parallel fault (early $D_2$), which may represent a faulted unconformity. Folds formed during $D_2$ ($D_1$ of Crispe *et al.* 2007) are tight to isoclinal with an $S_2$ cleavage present in both the Stubbins and Killi Killi formations, and are $F_3$ ($F_2$ of Crispe *et al.* 2007) refolded.

$F_2$ folds are typically asymmetrical, angular, tight, and have a wavelength of < 1km (Crispe *et al.* 2007). The folds are locally overturned, inclined, verge south, plunge moderately to the east, and trend SE, consistent with NNE-SSW compression. The folds also have an $S_2$ axial-planar spaced cleavage that dips steeply to NNE, and $D_2$ faults are developed locally on overturned $F_2$ fold limbs. Mineral occurrences in the area are hosted by $D_2$ faults, in axial-planar zones of $F_2$ folds where they intersect SE-trending faults or fractures, and along lithological boundaries.

## 3 GEOCHEMISTRY

Basalt samples from the Stubbins Formation have undergone hypogene alteration (presumably due to either greenschist facies metamorphism or associated with mineralizing events), which has affected the more mobile elements

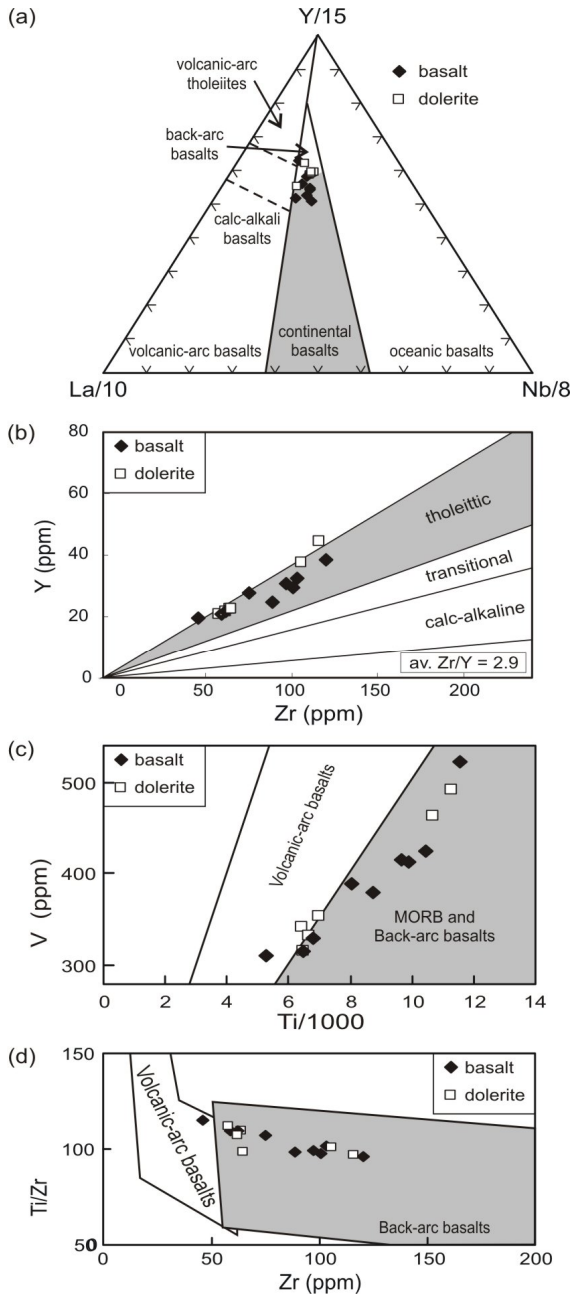


Figure 2. Petrogenetic discrimination diagrams: (a) Y/15–La/10–Nb/8 (from Cabanis & Lecolle 1989) indicating back-arc basin or continential basalt affinities; (b) Y verses Zr (from Barrett and MacLean 1999) illustrating the tholeiitic nature of the mafic rocks; (c), V verses Ti/1000 (from Shervais 1982) indicating MORB or back-arc basin affinities; and (d) Ti/Zr versus Zr (from Woodhead *et al.* 1993) indicating a back-arc basin affinity for basalts and dolerite in the Stubbins Formation.

that might be used as tectonic discriminators. In order to ascertain the geotectonic setting for basalts in the Stubbins Formation, their geochemistry is compared against modern analogues of basaltic volcanic rocks using relatively immobile elements, assuming that hydrothermal alteration processes in the area did not involve very high fluid/rock ratios, where relatively immobile elements may be mobilised.

### *3.1 Discrimination plots*

The Y/15–La/10–Nb/8 plot for both the mafic volcanic rocks and doleritic sills from the Stubbins Formation indicates that they have basaltic compositions (Fig. 2a). The Zr/Y ratios indicate that these rocks have a tholeiitic affinity (Fig. 2b), while the Ti/1000-V plot indicates that they have MORB or back-arc basalt affinities (Fig. 2c), while Fig. 2d indicates back-arc affinities.

Comparison of N–MORB-normalised patterns for REE illustrates the chemical resemblance that exists between basalt units and dolerite sills investigated herein from the Stubbins Formation (Fig. 3). These rocks are also characterised by relatively flat profiles close to unity when normalised to N–MORB.

In summary, the geochemistry of a range of ~1864 Ma mafic rocks (tholeiities and dolerite sills) from the Stubbins Formation indicates they are genetically related, and at least some of were deposited in a back-arc basin tectonic environment.

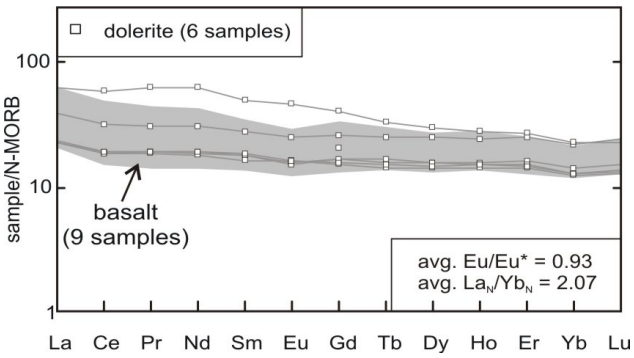


Figure 3. N-MORB normalized REE plots (Sun & McDonough 1989) for ~1864 Ma mafic units from the Stubbins Formation.

## 4 DISCUSSION AND CONCLUSIONS

The geochemistry of volcanic rocks and dolerite sills in the Stubbins Formation have similar REE characteristics (Fig. 3), suggesting they have a common or similar source, and are metamorphosed equivalents of back-arc basin basalts (Fig. 2). In addition, the presence of interstratified pillowed basalts affirms the subaqueous depositional environment. The feldspathic and quartz-rich composition of the turbiditic rocks also suggests that they were sourced from a continental crust containing

granitic rocks or represent recycled metasedimentary rocks. The lack of mature sandstone and conglomerate units in the study area, and wave-induced sedimentary structures suggests volcanism in >200m deep water. The location of such a continental crust is difficult to pinpoint, because of the rarity of exposure of rocks older than the Stubbins Formation in northern Australia.

From this study, early Palaeoproterozoic marine turbiditic sediments forming the lower part of the Stubbins Formation probably accumulated unconformably upon older (?Archaean) rocks. Volcanic-arc activity was likely due to a subduction zone that also triggered or controlled the opening of the Tanami basin due to the ocean-ward migration of the active arc. The turbiditic sedimentary rocks fine upward into a pelagic siltstone-shale-chert association at the top of the Stubbins Formation during a time of basin stability. Pelagic sedimentation was synchronous with mafic and rare felsic volcanism and associated dolerite sills in a back-arc basin setting (Fig. 2). The volcanism ceased before continued deposition of turbiditic sediments now included in the Killi Killi Formation.

Plate convergence by and shortly after ~1850 Ma (as suggested by Griffin *et al.* 2000 for the Kimberley region) lead to the cessation in deposition of the Stubbins Formation and the eventual resumption of deposition of turbiditic successions in an active tectonic environment (now included in the Killi Killi Formation). The convergence would have been protracted and included the $D_1$ and $D_2$ events in western GTO.

Orogenic lode-gold deposits are defined as a distinctive class of gold deposits, associated in space and time with collisional and accretionary tectonics (Goldfarb *et al.* 2001). A worldwide episode of orogenic gold deposition took place during ~2100-1800 Ma (Goldfarb *et al.* 2001). Orogenic gold systems formed in the western part of northern Australia during this period are related to collision and accretion of the Kimberley Basin along the Halls Creek Orogen. Therefore, gold introduction in these two regions may be related to coeval tectonic events making both regions highly prospective for Au mineralization.

## ACKNOWLEDGEMENTS

This contribution is published with permisssion of the Director of the Geological Survey of Western Australia, the Directors of Tanami Gold NL., and the Chief Executive Officer of Geoscience Australia.

## REFERENCES

Barrett TJ, MacLean WH (1999) Volcanic sequences, litho-geochemistry and hydrothermal alteration in some bimodal VMS systems. *Reviews in Economic Geology* 8: 101–131

Cabanis B, Lecolle M (1989) Le diagramme La/10-Y/15-Nb/8: an outil pour la discrimination des series volcaniques et la mise en evidence des processus de melange et/ou de contamination crustale. *Comptes Rendus de l'Academie des Sciences* Series II 309: pp 2023–2029

Crispe AJ, Vandenberg LC, Scrimgeour IR (2007) Geological framework of the Archean and Paleoproterozoic Tanami Region, Northern Territory. *Mineralium Deposita* 42: 3–26

Goldfarb RJ, Groves DI, Gardoll S (2001) Orogenic gold and geologic time: a global synthesis. *Ore Geology Reviews* 18: 1–75

Griffin TJ, Page RW, Sheppard S., Tyler IM (2000) Tectonic implications of Palaeoproterozoic post-collisional, high-K felsic igneous rocks from the Kimberley region of northwestern Australia. *Precambrian Research* 101: 1–23

Huston DL, Vandenberg LC, Wygralak A, Mernagh T, Bagas L, Crispe A, Lambeck L, Cross A, Fraser G, Williams N, Worden K, Meixner A, Goleby B, Jones L, Lyons P, Maidment D (2007). Lode gold mineralization in the Tanami region, northern Australia. *Mineralium Deposita* 42: 175–204

Sun SS, McDonough WF (1989) Chemical and isotope systematics of oceanic basalts; implications for mantle composition and processes. *Geological Society of London Special Publication* 42: 313–345

Tunks AJ, Cooke DR (2007) Geological and structural controls on gold mineralization in the Tanami District, Northern Territory. *Mineralium Deposita* 42: 107–126

Woodhead J, Eggins S, Gamble J (1993) High-field strength and transition element systematics in island arc and back-arc basin basalts: evidence for multi-phase melt extraction and a depleted mantle wedge. *Earth Planetary Science Letters* 114: 491–504

# Alkaline fluids in a volcanic-hydrothermal system – Savo, Solomon Islands

D.J. Smith & G.R.T. Jenkin
*Department of Geology, University of Leicester, United Kingdom*

J. Naden, M.G. Petterson, H. Taylor & W.G. Darling
*British Geological Survey, United Kingdom*

A.J. Boyce
*Scottish Universities Environmental Research Centre, East Kilbride, United Kingdom*

T. Toba
*Department of Mines & Energy, Ministry of Natural Resources, Honiara, Solomon Islands*

ABSTRACT: Savo volcano, Solomon Islands, is host to an active hydrothermal system that is potentially analogous to high sulphidation epithermal Au deposits. Chemical and stable isotope data from fluids discharged at the surface indicate a relatively shallow condensate layer fed by magmatic volatiles including $SO_2$. Acidic condensates are buffered to high pH by wall rock reaction, leading to the precipitation of unusual carbonate-silica sinters at the surface, in an environment where low pH fluids and associated products would be expected.

KEYWORDS: High sulphidation; epithermal; volcanic-hydrothermal; Savo; Solomon Islands;

## 1 INTRODUCTION

Volcanic-hydrothermal systems are believed to be the environment of formation of high sulphidation epithermal Au deposits (Hedenquist *et al.* 1993). Current models for the genesis of high sulphidation deposits suggest a two-stage genesis, with a pre-ore alteration stage, when low pH magmatic vapor condensates attack the host rocks and generate the characteristic advanced argillic and "vuggy silica" alteration assemblages, followed by a later mineralization stage (*see* Cooke & Simmons 2000, *and references therein*).

Studies of active volcanic-hydrothermal systems typically identify acidic fluids and associated alteration at the surface (*e.g.* Delmelle *et al*. 2000), yet a significant number of high sulphidation deposits show evidence of higher pH fluids and alteration, and clear evidence of fluid neutralization by water-rock interaction (*e.g.* Hedenquist *et al*. 1994).

Hot springs at Savo volcano, Solomon Islands, are neutral to high pH, and produce unusual carbonate-silica-sulphate sinters at the surface, features not typically associated with active volcanic-hydrothermal systems.

## 2 GEOLOGICAL SETTING

Savo is an andesite to dacite stratovolcano related to the north-eastwards subduction of the Woodlark Basin at the South Solomon Trench System, which initiated in the Upper Miocene. Savo has been subaerial for less than 100,000 years and last erupted in the 1840's (Petterson *et al.* 2003). Partial melting of the young oceanic crust of the Woodlark slab exerts an important control on magma chemistry across the Solomon arc (*e.g.* Konig *et al*. 2007), and may be responsible for high sodium contents in the more evolved portions of the igneous suite at Savo (up 8 wt% $Na_2O$ in dacites). Much of the island is covered by heavily vegetated pyroclastic deposits and dacite domes.

Savo's active hydrothermal system is expressed at the surface in the central crater by fumaroles and steaming ground, and by hot springs and steaming ground on the flanks. There are no springs in the crater.

## 3 METHODS

Water samples were collected from a number of different hot springs and cold wells. Samples were filtered to <0.45 μm, with fractions taken for cation determination by ICP-

AES and anion determination by ion chromatography.

## 3 METHODS

Sulphur isotope analysis on native sulfur from fumaroles and aqueous sulphate from hot springs (precipitated as $BaSO_4$) was performed using standard techniques.

Water was collected from hot springs and condensed from crater fumaroles for $\delta^{18}O$ and $\delta D$ determination.

A range of altered samples and hot spring precipitates were taken from active thermal areas. Mineralogy was determined by XRD and SEM.

Table 1: Typical compositions of fluids discharged at Savo volcano. Units mg/l unless noted otherwise.

| | Alkaline Sulphate | Acid Sulphate |
|---|---|---|
| pH | 8.23 | 2.54 |
| Al (µg/l) | BDL | 15790 |
| Ca | 119.6 | 57.6 |
| Fe | BDL | 24.1 |
| Mg | 9.96 | 15.5 |
| Na | 205.8 | 45.4 |
| Si | 176.3 | 62.8 |
| Cl | 41.5 | 4.4 |
| $SO_4^{2-}$ | 692 | 549 |
| $HCO_3^-$ | 87 | 70 |

## 4 RESULTS

Steaming ground and fumaroles in the crater were just above 100°C, *i.e.* slightly superheated steam. Areas of steaming ground are accompanied by advanced argillic assemblages (residual silica + kaolinite ± alunite ± native sulphur).

Fumarole native sulphur $\delta^{34}S$ ranges from -3.9 to -6.2 ‰ (Fig. 1). Stable isotopes of condensed steam plot on a trend showing relative depletion in the heavy isotopes compared to hot springs and local meteoric and ground water (Fig. 2).

Hot springs classified as acid sulphate have pH <7 and temperature 95-100°C. Acid sulphate springs are found in a number of locations on the flank, closely associated with areas of steaming ground. Springs are no more than 30cm in diameter, and the water is rich in suspended solids. $\delta^{34}S_{SO4}$ ranges from 0.6 to -3.5 ‰ (Fig. 1). The springs have higher $\delta^{18}O$ and $\delta D$ than cold groundwater (Fig. 2).

Alkaline sulphate springs are found in a number of locations on the upper flanks of the volcano (less than 1km from the crater wall). In some locations they occur within a few meters of acid sulphate springs and steaming ground. The water in the springs is clear, and may be discharged under pressure forming "spouters". The temperature of these springs is 100°C, and many can be observed to boil at the surface. pH is near-neutral to alkaline (6.5 to 8.5). $\delta^{34}S_{SO4}$ ranges from 4.0 to 6.5 ‰ (Fig. 1). Alkaline sulphate waters have higher $\delta^{18}O$ and $\delta D$ than the non-thermal groundwater samples from Savo (Fig. 2).

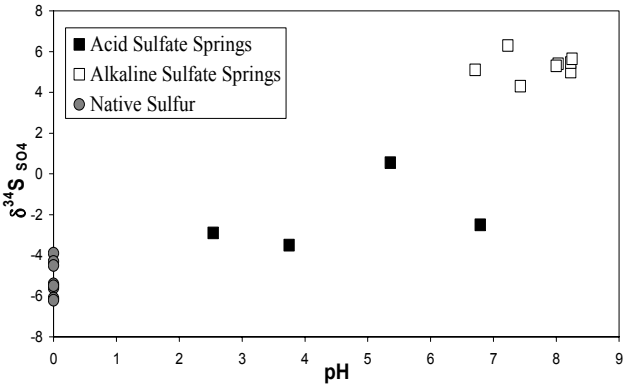


Fig. 1: $\delta^{34}S$ of $SO4^{2-}$ vs. pH for hot springs. $\delta^{34}S$ of native sulphur from fumaroles also shown.

Alkaline sulphate hot springs are commonly surrounded by precipitates consisting of amorphous silica + calcite ± anhydrite. Textures are similar to those seen in silica sinters and geyserites from low sulphidation style geothermal systems.

In both spring types, sulphate is the dominant anion, and $Cl^-$ is negligible (Table 1).

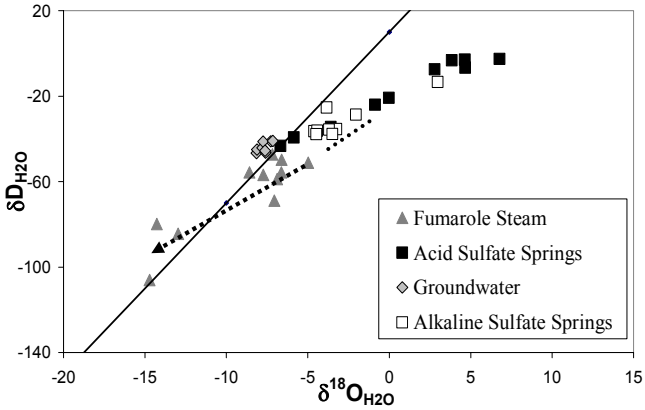


Fig. 2: Stable isotopes of water. Shows condensation trend from Equation 2 (dashed arrow), liquids produced by condensation (dotted line) and global meteoric water (solid line).

## 5 DISCUSSION

### 5.1 *Sulphur Isotopes*

The isotopically heavy $\delta^{34}S$ of the alkaline sulphate springs can be related to the low $\delta^{34}S$ values of the acid sulphate fluids and fumarole sulfur by the process of condensation of magmatic volatiles in the upper levels of the volcanic edifice and disproportionation of $SO_2$. At temperatures below 350°C this will produce isotopically heavy $SO_4^{2-}$ and lighter $H_2S$:

$$4SO_2 + 4H_2O = 3H_2SO_4 + H_2S \qquad (1)$$

The isotopically heavy sulphate is carried in the alkaline sulphate waters. The $H_2S$ produced is largely non-condensable until oxidation to sulphate and native sulfur with negative $\delta^{34}S$ values in the near-surface. Sulphate formed by $H_2S$ oxidation is found in acid sulphate springs (Rye 2005).

### 5.2 *Water isotopes*

The trend in $\delta^{18}O$ and $\delta D$ values of fumarole steam samples is consistent with a Rayleigh condensation process acting in the subsurface at ~150°C. The dashed arrow on Fig. 2 represents the equation:

$$(1000 + \delta_r) / (1000 + \delta_i) = f^{\alpha-1} \qquad (2)$$

where $\delta_r$ = the isotopic composition of steam after condensation, $\delta_i$ = composition before condensation (the isotopically heaviest steam sampled), $f$ = fraction of steam condensed, and $\alpha$ = fractionation factor at 150°C.

The liquid produced by condensation of the steam in Equation 2 correlates closely to the alkaline sulphate waters (dotted line, Fig. 2), allowing for a small degree of mixing with meteoric water. Along with the sulphur isotopes, this suggests that alkaline sulphate waters are derived by condensation of magmatic volatiles in the upper edifice of the volcano.

Acid sulphate springs show strong enrichment in the heavier isotopes of water. This phenomenon has been reported for a number of steam-heated hot springs, and is due to kinetic fractionation by evaporation (Giggenbach & Stewart 1982). Alkaline sulphate springs are less prone to evaporative enrichment as they have a much higher recharge rate.

Boiling of the alkaline sulphate water will produce the steam that heats and supplies $H_2S$ to the acid sulphate waters, and accounts for their close spatial association.

### 5.3 *Chemistry and Alteration*

The condensed magmatic volatiles would be initially low pH due to sulphuric and carbonic

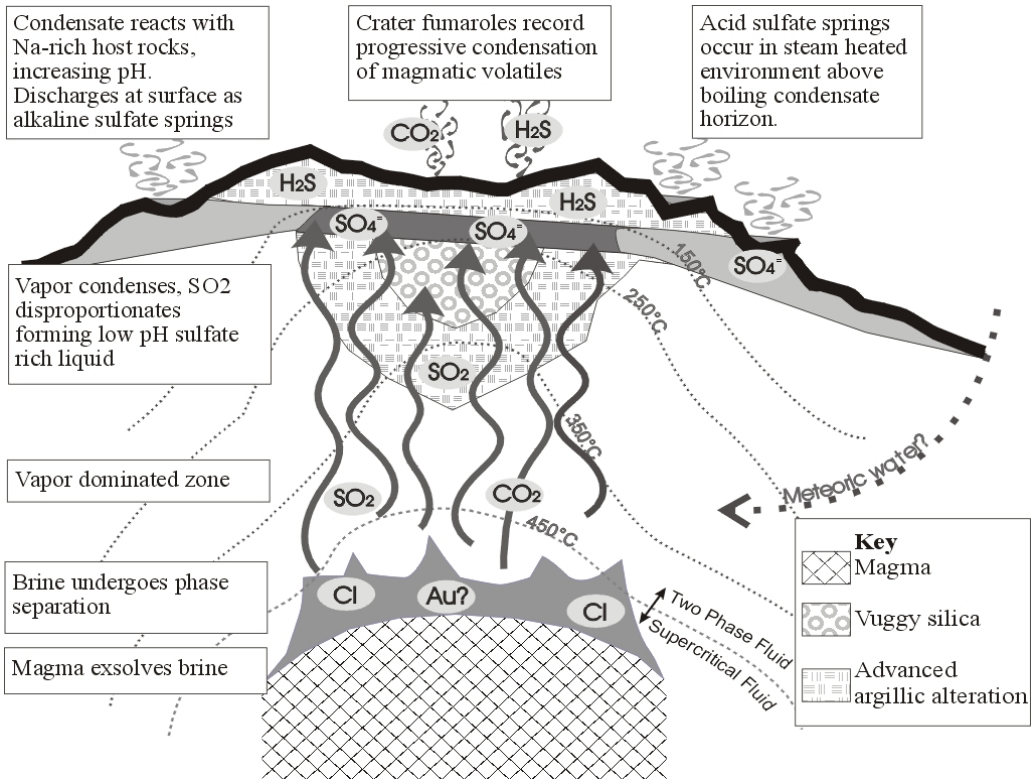


Fig. 3: Schematic model of hydrothermal system at Savo. Not to scale.

acid. The high sodium (as albite) content of the host rocks provides an effective neutralizing agent for the acidity. The core of the system would be dominated by low pH fluids, grading out to progressively higher pH as the fluids continue to react with the host rocks. Subsurface boiling provides a final increase in pH before surface discharge as alkaline sulphate springs. The chemistry of the acid sulphate springs is consistent with a steam-heated derivation, with $H_2S$ oxidation producing low pH fluids. Cation chemistry is a result of non-equilibrium acid leaching, which produces advanced argillic alteration. $H_2S$ oxidation around crater fumaroles produces alteration similar to that near acid sulphate springs.

### 5.4 *Model for the Hydrothermal System of Savo*

The positive $\delta^{34}S$ in the alkaline sulphate waters suggests an origin from a magmatic-derived, $SO_2$ bearing vapor. The absence of significant amounts of chloride in the thermal waters discharged at the surface suggests that it is being retained in an aqueous phase at depth (Fig. 3). An aqueous phase at temperatures above 350°C would be capable of retaining Cl and allowing $SO_2$ to remain in the vapor phase. Thus the model involves aqueous brine separating from magma at depth and then boiling. A vapor dominated zone separates the brine from the shallow condensate layer. Such a brine is capable of introducing Au into the epithermal environment (Cooke & Simmons 2000).

The condensate is initially low pH, producing advanced argillic alteration. Wall rock reaction increases the pH, producing alkaline sulphate waters. Where these waters boil beneath the surface, steaming ground is formed above. Perched aquifers and surface waters may be heated by the steam, and $H_2S$ carried with the steam is oxidized to produce acid sulphate springs.

## 6 CONCLUSIONS

Based on chemical and isotopic characteristics, we suggest the fluids discharged at Savo volcano are the surface expression of a volcanic-hydrothermal system that is potentially analogous to high sulphidation deposits.

Unusual carbonate-silica-sulphate sinters and alkaline sulphate fluids record neutralization of acidic condensates by wall rock interaction. Alkaline fluids and their products may be present in the lithocap of high sulphidation deposits and as such may represent important exploration pathfinders.

## ACKNOWLEDGEMENTS

Thanks to A MacDonald and J Dougans of SUERC; NC White, JB Gemmell and RO Fournier for helpful discussions; G Albert, W Satokana and A Ramo of the Solomon Islands Department of Mines and Energy; and the people of Savo Island. JN, MGP, HT & WGD publish with the permission of the Executive Director, British Geological Survey (NERC). DJS acknowledges funding and support for PhD research from NERC, BGS University Collaboration Scheme and the Society of Economic Geologists.

## REFERENCES

Cooke DR, Simmons SF (2000) Characteristics and genesis of epithermal gold deposits In: Hagemann SG, Brown PE (eds) *Gold in 2000. Society of Economic Geologists,* Boulder, CO, pp 221-244.

Delmelle P, Bernard A, Kusakabe M, Fischer TP, Takano B (2000) Geochemistry of the magmatic-hydrothermal system of Kawah Ijen Volcano, East Java, Indonesia. J*ournal of Volcanology and Geothermal Research* 97: 31-53.

Giggenbach WF, Stewart MK (1982) Processes controlling the isotopic composition of steam and water discharges from steam vents and steam-heated pools in geothermal areas. Geothermics 11: 71-80.

Hedenquist JW, Matsuhisa Y, Izawa E, White NC, Giggenbach WF, Aoki M (1994) Geology, Geochemistry, and Origin of High Sulphidation Cu-Au Mineralization in the Nansatsu District, Japan. *Economic Geology* 89: 1-30.

Hedenquist JW, Simmons SF, Giggenbach WF, Eldridge CS (1993) White Island, New Zealand, volcanic-hydrothermal system represents the geochemical environment of high-sulphidation Cu and Au ore deposition. *Geology* 21: 731-734.

Konig S, Schuth S, Munker C, Qopoto C (2007) The role of slab melting in the petrogenesis of high-Mg andesites: evidence from Simbo Volcano, Solomon Islands. *Contributions to Mineralogy and Petrology* 153: 85-103.

Petterson MG, Cronin SJ, Taylor PW, Tolia D, Papabatu A, Toba T, Qopoto C (2003) The eruptive history and volcanic hazards of Savo, Solomon Islands. *Bulletin of Volcanology* 65: 165-181.

Rye RO (2005) A review of the stable-isotope geochemistry of sulphate minerals in selected igneous environments and related hydrothermal systems. *Chemical Geology* 215: 5-36.

# Orogenic gold without intrusions: comparison between Klondike (Canada) and Otago (New Zealand)

Dave Craw
*Geology Department, University of Otago, PO Box 56, Dunedin, New Zealand*

Jim Mortensen
*Earth and Ocean Sciences, University of British Columbia, Vancouver, BC, Canada*

Doug MacKenzie
*Geology Department, University of Otago, PO Box 56, Dunedin, New Zealand*

ABSTRACT: Orogenic gold deposits of the Otago Schist and the Klondike Schist are unusual in that they formed in complex collisional metamorphic terranes with no coeval igneous activity in the immediate vicinity of the deposits. Most preserved gold deposits are hosted in extensional sites associated with late-stage compressional structures formed during uplift through the brittle-ductile transition. Both belts have evidence for widely-dispersed or disseminated gold, in shear zones and numerous small auriferous veins, rather than in well-defined large quartz vein systems. This dispersed gold has been concentrated into giant placer deposits by subsequent erosion in both terranes.

KEYWORDS: mesothermal gold, structure, collisional tectonics, Circum-Pacific

## 1 INTRODUCTION

Collisional orogens around the world and throughout geological time have hosted hydrothermal gold deposits, and these deposits have been one of the principal sources of mined gold, either directly (hard rock mines) or indirectly (eroded to form placer deposits) (Goldfarb *et al.* 2005). Igneous intrusions commonly accompany collisional orogenesis and associated formation of complex metamorphic belts that host the gold. Determination of the relative contributions of metamorphic processes and igneous intrusions to metallogenesis is controversial (Goldfarb *et al*. 2005). The best places to study the metallogenetic effects of metamorphism alone are in metamorphic belts that do not have coeval magmatism and gold mineralization. Such belts are rare, and include the two terranes described in this study: the Otago Schist of New Zealand, and the Klondike Schist of Yukon Territory, Canada. Both these metamorphic terranes are predominantly Mesozoic in origin, and occur in the circum-Pacific convergence zone.

## 2 GEOLOGY AND GOLD DEPOSITS

### 2.1 *Otago Schist*

The Mesozoic Otago Schist is a pile of predominantly metasedimentary schists with minor metabasic schists. The rocks were deformed and metamorphosed, mainly to greenschist grade, during collisional Jurassic orogenesis. The metamorphic pile was deformed and stacked by late metamorphic recumbent folding and thrusting. During this late metamorphic deformation, strain was progressively localized into narrower zones as the rocks were uplifted through the brittle-ductile transition.

Economic concentrations of gold are preserved in structures formed in the latter stages of compressional deformation, and in extensional structures formed during post-collisional uplift and erosion. The largest gold deposit, the active Macraes mine, is a *ca* 6 Moz deposit that is dominated by low grade disseminated gold with subordinate small (typically metre scale) auriferous quartz veins (Mitchell *et al.* 2006). This deposit occurs in a greenschist facies graphitic shear zone (30km long and locally >100m thick) that developed as the host schists passed through the brittle-ductile transition in the early Cretaceous (Fig. 1). A similar auriferous shear zone is currently being prospected 80km away.

Other Otago Schist auriferous veins are small and widely dispersed through *ca* 100 000km$^2$ of schist. These small veins generally fill extensional sites in normal faults, and most were formed during post-orogenic regional extension in the middle Cretaceous.

Erosion of these Mesozoic gold-bearing

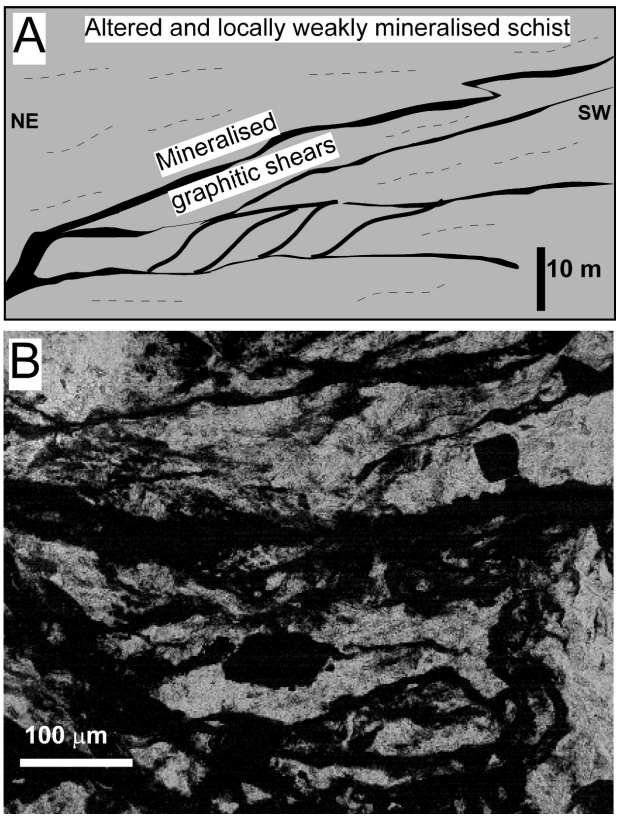


Figure 1. Mineralized rocks from the Macraes mine, Otago. A. Outcrop geometry of the shear zone. B. Mineralized schist, with graphitic microshear seams and sulfides replacing metamorphic minerals

veins has resulted in formation of placer gold concentrations of economic interest, from the Cretaceous through to modern rivers. Constant recycling of placer gold since the Cretaceous has caused progressive concentration of gold, although some dilution is currently occurring in regions of rapid uplift and erosion. Placer gold dominated (*ca* 95%) historical production of ca 8 Moz, but production of low grade disseminated gold from the Macraes hard rock mine (>2 Moz) is progressively changing this balance.

## 2.2 *Klondike Schist*

The Klondike Schist consists of interlayered metasedimentary and meta-igneous rocks that were originally metamorphosed to mainly greenschist facies in the Permian (Mortensen 1996). The Klondike Schist was juxtaposed via thrust stacking with other schists, metabasites, and serpentinite, in the Jurassic. This stacking involved recumbent folding, shearing, faulting, and kink folding as the rocks were uplifted through the brittle-ductile transition (MacKenzie *et al.* 2007). The rock sequence underwent regional Cretaceous extension.

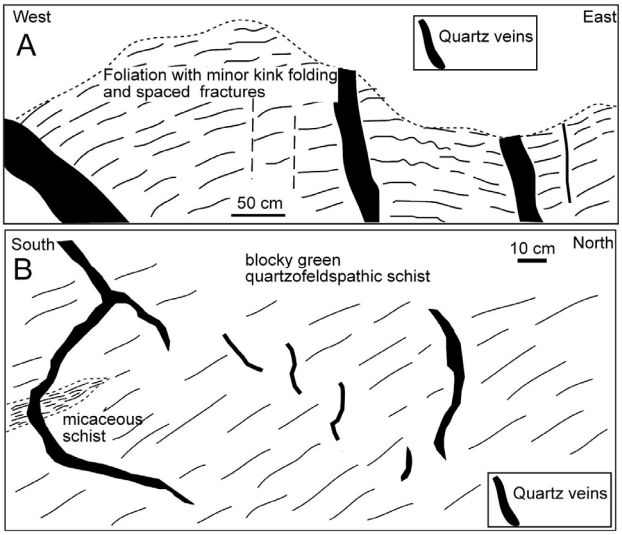


Figure 2. Mesothermal gold-bearing veins, Klondike Schist. A. Veins hosted in fold-related fractures. B. Veins hosted in irregular fractures at the hinge of a regional fold.

Mesothermal gold mineralization occurred towards the end of the Jurassic compressional deformation. Numerous small (cm-m scale) gold-bearing veins are dispersed throughout a relatively small area (*ca* 400 km$^2$) of Klondike Schist, with little evidence of mineralization outside this area. The auriferous veins are hosted in a wide variety of small extensional sites throughout the schist, especially fold axial surface fractures developed in and near late stage kink folds (MacKenzie *et al.* 2007). Disseminated gold, without quartz veins, occurs in some rock types, typically near to major vein swarms. Mineralization occurred under subgreenschist facies conditions within a few kilometres of the surface, with some meteoric water component to the fluid (Rushton *et al.* 1993). Some additional hydrothermal activity accompanied Cretaceous and Cenozoic normal faulting, but the later activity appears to have had little effect on the distribution of gold.

Erosion of the dispersed gold veins yielded abundant alluvial gold that has been progressively concentrated in the late Cenozoic to form the famous Klondike placer deposits (>13 Moz; Lowey 2005). These placer deposits are extremely localized in and near the small area of Klondike Schist that has dispersed auriferous quartz veins.

# 3 SIMILARITIES AND DIFFERENCES

Both terranes have evidence for dispersed gold mineralization in the latter stages of major

regional rock stacking processes that occurred during (and caused?) uplift of the mineralized rocks through the brittle-ductile transition. The gold mineralization occurred in the latter stages of this event in both terranes: under greenschist facies conditions in Otago, and at shallower levels in the Klondike. The nature and geometry of the dispersed gold in the two terranes at least partially reflects the different depths at which mineralization occurred.

There was a relatively close temporal relationship between host rock metamorphism (Jurassic) and gold mineralization (early Cretaceous) in Otago. The Macraes gold deposit was formed by auriferous metamorphic fluids generated by prograde reactions still occurring at depth as collision persisted in the early Cretaceous. In contrast, Klondike Schist was pervasively metamorphosed in the Permian, *ca* 100 million years before mineralization. The Jurassic stacking was clearly a major regional deformation event, and crustal thickening during this stacking may have generated auriferous fluids that formed the Klondike gold veins. However, the apparent restriction of gold mineralization to a small area of Klondike Schist is not yet understood. The general similarity of structural and metamorphic histories in Otago and Klondike, and the similar history of giant placer mining in the two terranes, makes the Klondike area appear highly prospective for low grade mesothermal gold mineralization, as Otago has turned out to be.

## 4 CONCLUSIONS

Dispersed gold mineralization occurred without associated igneous activity in greenschist grade rocks in the Otago Schist (New Zealand) and Klondike Schist (Canada). These terranes have broadly similar geological, structural, and metamorphic histories in the circum-Pacific collisional belt. The main stage of gold mineralization occurred in the late Mesozoic in both terranes, following major regional compressional deformation and structural stacking. Gold mineralization occurred in the latter stages of this regional event in both terranes, during uplift through the brittle-ductile transition in Otago and at the end of brittle compression in the Klondike. Mineralization resulted from structural control of auriferous metamorphic fluids in both terranes. Both terranes are highly prospective for large-volume, low-grade gold deposits, and the Otago Schist already has one such deposit (Macraes) with 6 Moz Au.

## ACKNOWLEDGEMENTS

This research was funded by NZ Foundation for Research, Science and Technology, Klondike Star Mineral Corporation, and University of British Columbia. Discussions with Tim Liverton, Richard Norris, and Brigitte Petrie were valuable in developing our ideas.

## REFERENCES

Goldfarb RJ, Baker T, Dube B, Groves DI, Hart CJ, Gosselin P (2005) Distribution, character and genesis of gold deposits in metamorphic terranes. *Econ Geol. 100th Anniv. Vol:* 407-450

Lowey GW (2005) The origin and evolution of the Klondike goldfields, Yukon, Canada. *Ore Geol Rev* 28: 431-450

MacKenzie DJ, Craw D, Mortensen JK, Liverton T (2007) Structure of the schist in the vicinity of the Klondike goldfield, Yukon. In: Yukon Exploration and Geology 2006, *Yukon Geological Survey*, pp 197-212

Mitchell M, Maw L, Angus PV, Craw D (2006) The Macraes gold deposit in east Otago. *Australasian Inst Min Metall Monog* 25: 313-318

Mortensen JK (1996) Geological compilation maps of the northern Stewart River map area, Klondike and Sixtymile Districts. *Indian and Northern Affairs Canada, Open File* 1996-1 (G), 43 pp

Rushton RW, Nesbitt BE, Muehlenbachs K, Mortensen JK (1993) A fluid inclusion and stable isotope study of Au quartz veins in the Klondike district, Yukon Territory, Canada: a section through a mesothermal vein system. *Econ Geol* 38: 647-678

# Nature of gold mineralization in the Walhalla Goldfield, eastern Victoria, Australia

Megan A. Hough, Laurent Ailleres
*School of Geosciences, Monash University VIC 380, Australia*

Frank P. Bierlein
*Centre for Exploration Targeting, University of Western Australia WA 600, Australia*

Adele Seymon
*Geoscience Victoria, GPO Box 4440, Melbourne VIC 3001, Australia*

Stuart Hutchin
*Goldstar Resources, Rawson VIC 3825, Australia*

ABSTRACT: Comparisons are made between three gold deposits (Cohen's Reef, Eureka, Tubal Cain) to predict favourable sites of mineralization throughout the historically important (>80 t Au produced) Walhalla-Woods Point Goldfield in southeastern Australia. The goldfield hosts anomously large deposits, in comparison to similar-aged goldfields in the region. In this regard, the ten highest yielding deposits within the Walhalla-Woods Point Goldfield are either hosted within, or spatially associated with, intrusions of the Devonian Woods Point Dyke Swarm. By comparing the three deposits, we hope to establish the principal structural, rheological and chemical controls on gold mineralization in this region.

KEYWORDS: gold mineralization, Walhalla, Devonian, dykes

## 1 INTRODUCTION

The state of Victoria in southeastern Australia is host to one of the world's major orogenic gold provinces, having produced approximately 2,500 tonnes of gold since the 1850's (Ramsay *et al*. 1998; Bierlein & Maher 2001).

The sixth largest gold-producing region in Victoria with over 400 known reef and alluvial gold deposits is the Walhalla-Woods Point Goldfield, situated 150 kilometres east of Melbourne.

The focus of this project has been on three gold deposits (Cohen's Reef, Eureka and Tubal Cain), near the historical township of Walhalla, in conjunction with recent mapping by Geoscience Victoria and current exploration by Goldstar Resources.

Cohen's Reef, historically the most productive gold deposit in the Walhalla-Woods Point Goldfield, is a predominantly sediment-hosted, shear zone-associated, laminated to massive auriferous quartz vein system, in close proximity to a thin (< 1.7 metres) hornblende-diorite dyke. The reef was mined to a depth of over one kilometre, and produced 46 tonnes of gold (Ramsay & Willman 1988).

In contrast, the Tubal Cain and Eureka gold deposits are predominantly dyke-hosted. Visible and disseminated gold in these deposits is associated with parallel ladder veins. Eureka was mined from 1867 to 1915, to a depth of approximately 130m, and produced 70 kg gold (Vandenberg *et al*. 2006). Tubal Cain was worked from 1866 to 1911, to a depth of 100m, and produced 120 kg (Vandenberg *et al*. 2006).

The aim of our research is to understand, and eventually predict, favourable sites of gold mineralization in the three different gold depos-

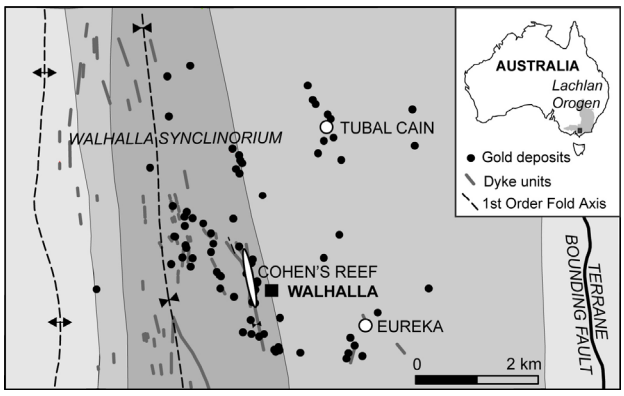


Figure 1. Geological map of the three gold deposits within the Walhalla Goldfield (modified from Morand *et al.* 2006)

its, and throughout the goldfield, from drill hole data, structural mapping and historical adit map plans.

Thirty-eight samples from Cohen's Reef, eleven samples from Eureka, and seventeen samples from Tubal Cain were collected from recent exploration drilling by Goldstar Resources NL, allowing detailed petrological analysis of the lithologies, the extent of alteration and mineralization, and specific siting of gold.

Preliminary results from petrological and geochemical analyses, including whole-rock and quantitative XRD, of the altered/ unaltered dyke and host metasediments from Cohen's Reef, have reinforced results from hand sample and thin section studies. 3D mapping of the gold system from drillhole data and adit maps allowed the structural and lithological context of the alteration and mineralization to be constrained.

## 2 TECTONIC SETTING AND REGIONAL GEOLOGY

The Walhalla-Woods Point Goldfield lies within the Late Devonian Walhalla Synclinorium, near the eastern margin of the Western Lachlan Orogen.

The Western Lachlan Orogen is one of three major thrust systems that formed due to plate convergence during the tectonic evolution of the Lachlan Orogen (450-340 Ma; Gray & Foster 2004). In regards to orogenic gold deposits, the Lachlan Orogen is comparable to other Phanerozoic orogens that formed by accretion of continental crust along the complex subduction zone of Gondwana (Gray & Foster 2004).

The Woods Point Dyke Swarm intruded the Walhalla Synclinorium along reverse faults and shear zones, commonly parallel to the strike of the fold axis, at 378-376 Ma (Bierlein *et al*. 2001) shortly before hydrothermal activity and gold mineralization at 374-372 Ma (Bierlein *et al.* 2001). The dyke swarm forms a 150-kilometre long belt of N to NW-trending dykes, and is associated with over 30% of the known quartz-gold ("reef") deposits in the field. Throughout the region, the dyke compositions vary from basic gabbros to hornblende diorites. The higher yielding dyke-hosted gold deposits within the Walhalla-Woods Point Goldfield, are hosted within west-dipping faults structures and/ or conjugate faults sets, such as Morning Star, A1 and Loch Fyne further to the north.

Three phases of orogenic gold mineralization are recognised in the Western Lachlan Orogen. The first phase was closely associated with peak metamorphism at 440-455 Ma (Bierlein *et al.* 2001) and produced most of the mesothermal, structurally controlled and economically important gold deposits in the Western Lachlan, such as Ballarat and Bendigo (Ramsay *et al*. 1998). The second phase occurred due to fault reactivation at 420-400 Ma (Gray & Foster 1998) and a thermal event at ~400 Ma (Gray & Foster 1998). The third phase, at 390-360 Ma produced mostly smaller deposits, with the notable exception of the Walhalla-Woods Point Goldfield (Bierlein *et al.* 2001; Gray & Foster 2004).

## 3 CHARACTERISTICS OF GOLD DEPOSITS ON THE WALHALLA GOLDFIELDS

The three deposits were chosen due to the availability of drill core and safe mine access. The deposits differ in regards to host lithology – Cohen's Reef is sediment-hosted but dyke-associated, whereas Eureka and Tubal Cain are both dyke-hosted. The dykes at Tubal Cain and Eureka are uniquely different to most dykes in the goldfield, as they are fine-grained and have an uncharacteristic porphyritic texture.

### 3.1 *Cohen's Reef*

The known extent of Cohen's Reef (Fig. 1) is approximately 1500m long and 1134m deep, along the valley of the township of Walhalla. The extensive and continuous reef is predominantly a laminated quartz-carbonate vein with some associated stockwork veins, and in places incorporates sheared dyke and meta-sedimentary rocks.

Cohen's Reef is hosted within a steeply west-dipping reverse fault (Tomlinson *et al*. 1988). The reverse fault lies along the margin of an extensive but narrow dyke, within a complex fifty metre wide shear zone.

The shear zone is associated with tight steeply plunging asymmetric folds, suggesting strike-slip movement, prior to the emplacement of the dyke.

### 3.2 *Eureka*

The Eureka dyke (Fig. 1) is elongate, almost arcuate with a central bulge. The approximate north-south strike length of the dyke is 340m, with a known depth of 512m. At the bulge, the

width of the dyke is 106m, although the average width is 56m.

Three reefs were historically worked with Goldstar Resources recently discovering four more auriferous reefs at depth. The parallel ladder reefs are hosted within high-angle reverse faults, which dip uncharacteristically to the east.

### 3.3 *Tubal Cain*

Tubal Cain (Fig. 1) is the largest known intrusion of the Woods Point Dyke Swarm.

Recent drilling has defined the shape of Tubal Cain of a length of 200m, a width of 180m and depth of 600m (*Goldstar Resources, unpublished data*). Eight reefs were historically worked with Goldstar Resources recently discovering seven more auriferous reefs at depth. The parallel ladder reefs dip to the southwest.

## 4 PRELIMINARY RESULTS

Based on geochemical drillhole traverses, petrological analyses, and 3D mapping of the gold deposit systems, a number of comparisons can be made.

Historical production along Cohen's Reef concentrated on visible gold within the laminated reef system. Recent assay results have highlighted the increased levels of visible gold, and also the presence of disseminated gold, especially along dyke margins.

The ten highest gold assay results (5 – 12 ppm) from recent drilling in proximity to Cohen's Reef are found in laminated veins within or on the margins of dyke; or in laminated or brecciated veins within metasedimentary rock, predominantly shale.

At Tubal Cain, elevated gold assay results are associated with laminated quartz veins, mineralized dyke with minor veins, and quartz breccia. Gold values greater than 10 ppm (15 – 211 ppm) are most commonly associated with the quartz breccia zones.

Highest gold assay results at Eureka (5603 ppm) are also associated with quartz breccia. Elevated gold values (10 – 285 ppm) are found in laminated quartz reefs, whereas gold grades of 1 – 10ppm are commonly found in mineralized dolerite with quartz veins, laminated veins and quartz breccia.

Based on observations from recent drillhole intersections, laminated veins are more common in the sediment-hosted Cohen's Reef, whereas brecciated quartz veins are more common in the dyke-hosted deposits such as Eureka and Tubal Cain, especially at depth.

Hydrothermal alteration, in particular the extent of the sulphide mineralization, also varies between deposit and vein type. At Cohen's Reef hydrothermal alteration is more extensive within the dyke. Visible carbonate bleaching varies from 4cm to over 1m, depending on the width and concentration of the quartz veins. Visible sulphide alteration is localized to within a few centimetres of the mineralized vein, although elevated arsenic values can be detected up to 15 metres from the mineralized zone. Altered and bleached metasedimentary rocks exhibit an increase in $SiO_2$ and $CO_2$, and decrease in $Al_2O_3$, $Fe_2O_3$ and $K_2O$. The highest gold and sulphur values are found within the dyke.

Arsenopyrite is commonly a good indicator for gold mineralization, although at Cohen's Reef elevated gold values do not correspond with presence of arsenopyrite. Instead, the elevated gold values (7 ppm) correspond with increased pyrite and arsenic (< 6000 ppb), therefore refractory gold may be found in the arsenic-rich pyrite rims.

Within the Eureka and Tubal Cain, the extent of hydrothermal alteration surrounding the mineralized quartz veins is also very limited, from 10cm to 2m, depending on the width of the quartz veins. Commonly, the extent of the sulphides does not correspond with high gold values. Elevated values of arsenic are confined to quartz breccia zones, or mineralized dolerite, although the highest arsenic values are not associated with the highest gold values.

Geochemical traverses along drill core from Eureka and Tubal Cain revealed local variation of a number of elements. Within quartz breccia with gold contents greater than 50ppm, elevated As, Bi, Mo, Cu, Sb, Pb and Zn were observed, and in conjunction with depletion of Co and Ni. With gold values less than 50 ppm, elevated As, Bi, Mo, Pb, Sb were observed, but decreased values of Co, Cu, Ni, Sn, and Zn. Anomously elevated contents of As (> 10000ppm), Pb (> 60 ppm), Mo (3ppm) and Sb (~200 ppm), related to elevated gold values within the dyke-hosted breccia zones, may be a signature of magma-related mineralization (Ramsay *et al.* 1998), although further analysis is required.

## 5 CONCLUSIONS

Based on current research, favourable sites for gold mineralization in the Walhalla-Wood's Point Goldfield are dyke-hosted quartz breccia zones.

The ten highest-yielding gold deposits within the Walhalla-Wood's Point Goldfield are either dyke-hosted or dyke-associated/ sediment hosted.

A number of hydrothermal phases are evident in all three deposits, from initial barren quartz or carbonate veins, to quartz-carbonate veins associated with sulphides, to later gold-rich quartz veins. The initial phases of hydrothermal activity formed the crack-seal laminated quartz-carbonate veins with minor sulphide and host rock selvages. The later hydrothermal events occurred at shallower levels under more brittle conditions, and are characterized by open space vein fill with vugs, brecciated quartz zones, and the highest gold values.

The extent of hydrothermal alteration in wallrock is an exploration tool best suited to gold associated with laminated veins. Sulphide mineralization associated with breccia zones is more localised, and not necessarily indicative of gold values.

## ACKNOWLEDGEMENTS

ARC Linkage funding, along with direct and in-kind support from collaborative partners Geoscience Victoria and Goldstar Resources supported this research. Stafford McKnight is thanked for assistance in SEM and XRF analyses.

## REFERENCES

Bierlein FP, Hughes M, Dunphy J, McKnight S, Reynold P, Waldron H (2001) Tectonic and economic implications of trace element, 40Ar/39Ar and Sm-Nd data from mafic dykes associated with orogenic gold mineralization in central Victoria, Australia. *Lithos* 58: 1-31

Bierlein FP, Maher S (2001) Orogenic disseminated gold in Phanerozoic fold belts — examples from Victoria, Australia and elsewhere. *Ore Geology Reviews* 18: 113-148

Gray DR, Foster DA (1998) Character and kinematics of faults within the turbidite-dominated Lachlan orogen: implications for tectonic evolution of Eastern Australia. *Journal of Structural Geology* 20: 1691-1720

Gray DR, Foster DA (2004) Tectonic evolution of the Lachlan Orogen, southeast Australia: historical review, data synthesis and modern perspectives. *Australian Journal of Earth Sciences* 51: 773-817

Morand VJ, Wilman CE, Taylor DH, Quinn C, Vandenberg AHM, Seymon AR, Hough M (2006) Walhalla and parts of Seaton and Moe 1:50 000 geological map. *GeoScience Victoria. Department of Primary Industries*.

Ramsay WRH, Bierlein FP, Arne DC, VandenBerg AHM (1998) Turbidite-hosted gold deposits of central Victoria, Australia; their regional setting, mineralising styles, and some genetic constraints. *Ore Geology Reviews* 13: 131-151

Ramsey WRH, Willman CE (1988) Economic Geology. In: Douglas JG, Fergusson JA (eds) Geology of Victoria. *Geological Society of Australia (Victorian Division) Publication,* pp 454-481

Tomlinson KM, Wilson CJL, Hazeldene R, Lohe EM (1988) Structural control on gold mineralization at Walhalla, Victoria. *Australian Journal of Earth Sciences* 35: 421-444

VandenBerg AHM, Cayley RA, Willman CE *et al.* (2006) Walhalla – Woods Point – Tallangallook special map area geological report. *Geological Survey of Victoria Report* 127: pp455

# Multiple hydrothermal fluid pulses through time at the Kambalda gold deposits, Yilgarn Craton, Western Australia

K. J. Petersen, S. G. Hagemann, P. Neumayr
*Centre for Exploration Targeting, School of Earth and Geographical Sciences, M006, The University of Western Australia, 35 Stirling Highway CRAWLEY Western Australia 6009, Australia*

J. L. Walshe
*CSIRO Exploration and Mining, ARRC, 26 Dick Perry Av, Kensington, Western Australia 6151*

ABSTRACT: The Kambalda gold deposits are characterized by a distinct hydrothermal alteration and fluid evolution with an overall increase in $CO_2$, salinity and decrease of temperature over time. At the time of gold precipitation, significant increases of $CO_2$ and variations in the $CO_2/CH_4$ ratio of the hydrothermal fluids are recorded that are compatible with large redox gradients during precipitation of gold at the Kambalda gold deposits. The rapid change in physico-chemical conditions points towards pulsating hydrothermal fluid fluxes during multiple seismic events.

KEYWORDS: Kambalda, gold, hydrothermal fluids, PIXIE analyses, LA-ICPMS analysis

## 1 INTRODUCTION

The Yilgarn craton hosts several of the most studied orogenic gold deposits in the world, but still presents challenges for the understanding of the complex geometry of hydrothermal fluid flow and the chemical evolution of hydrothermal fluids that played a role in the formation of these deposits. Most of the previous studies focused strongly on the composition of hydrothermal fluids immediately in the gold environment and exactly at the time of gold mineralization. The future challenge will be to better understand the composition and physico-chemical processes of hydrothermal fluids spatially within a gold camp and throughout the evolution of a gold mineral system.

This paper presents preliminary data on the different hydrothermal fluids in the Kambalda gold camp (8.55 Moz of gold produced from 1981 to today) with the aim to: 1) establish a relationship between the hydrothermal fluids, 2) characterize the different pulses of the fluid systems, and 3) develop a fluid evolution model.

## 2 REGIONAL GEOLOGY

The Kambalda gold camp is located in the southern part of the Norseman-Wiluna greenstone belt within the Eastern Goldfields Province of the Yilgarn craton of Western Australia. The camp is hosted in predominantly mafic-ultramafic lavas and intrusions that have been metamorphosed to upper greenschist and lower amphibolite facies. The greenstone sequence has been intruded by felsic to intermediate porphyry stocks that predate, are synchronous with and post-date gold mineralization (Nguyen 1997).

The Kambalda gold camp is bounded by two major NNW-trending regional structures: the Boulder-Lefroy fault to the east and the Merougil fault to the west, and has undergone four major Archaean deformation events. The first (D1) produced regional south-over-north thrusts. The second (D2) produced upright, NNW-trending, gently plunging folds, such as the Kambalda anticline. The third event (D3) generated brittle-ductile, NNW-trending, oblique-sinistral wrench fault systems that show locally major N-trending, reverse, gold-bearing shear zones. During the fourth event (D4), NE-trending, dextral faults offset stratigraphy and earlier fault systems, and caused dextral±reverse reactivation of these earlier faults. Gold mineralization is mainly controlled by the D3 and D4 deformation events (Nguyen 1997).

## 3 TEMPORAL CONSTRAINTS OF HYDROTHERMAL ALTERATION

Three types of alteration assemblages are recognized as stages of hydrothermal alteration

(Neumayr *et al*., 2003; 2005) and formed mainly through the D2 and D3 events. The relative timing of the alteration minerals is based on textural observations, especially cross-cutting textures, and is indicated by numbers after the mineral name: Stage 1 (reduced and oxidized): epidote - calcite - magnetite1 - pyrite1 ± pyrrhotite - chalcopyrite - quartz alteration. Stage 2A (reduced assemblage): pyrrhotite - carbonate - amphibole - biotite ± quartz ± arsenopyrite ± pyrite. Stage 2B (oxidized assemblage): distal (to Au) chlorite- carbonate; intermediate: biotite - magnetite 2 - carbonate alteration; proximal (to Au) plagioclase (mainly albite), carbonate (Fe-rich dolomite to ankerite), pyrite 1 (with mineral inclusions) ± Au ± magnetite 2 ± haematite. Stage 3: quartz vein system (+Au?) with pyrite 2 (without mineral inclusions) + chlorite (host rock alteration), which overprinted Stages 1, 2A and 2B alteration assemblages.

## 4 FLUID INCLUSION OCCURRENCE AND SHAPE

Hydrothermal alteration Stage 1 contains primary fluid inclusions (FI) in epidote, carbonate and quartz. These irregular to negative crystal shaped FI (<15µm in length) occur as individual, isolated inclusions or as clusters that show random three-dimensional distribution throughout a single grain. Hydrothermal alteration Stage 2A occurs as primary FI in albite with sizes between 2 and 10µm and irregular to regular forms in carbonate with 5 to 10µm in size with negative crystals to irregular forms, and in isolated quartz inclusions in pyrite 1, 10 to 20µm in size and irregular to regular forms. Hydrothermal alteration Stage 3 contains primary FI in carbonate with sizes between 3 and 10µm showing negative crystals, regular to irregular shapes, and primary to pseudosecondary FI in quartz, 5 - 25µm in size, and irregular to regular shapes. Daughter crystals of halite and carbonate (dolomite) are observed.

## 5 FLUID INCLUSION CHARACTERISTICS OF STAGES 1 TO 3

The FI of the Stage 1 are predominantly aqueous and show a small gas bubble at room temperature. The eutectic temperatures for epidote-hosted FI varies from -38 to -49°C suggesting the presence of Ca and/or Mg cations; The total homogenization temperatures into liquid are between 219 and 276°C, the salinity varies from 0.8 to 7.3 wt% NaCl eq., and density is in the range of 0.8 to 0.9 g/cm. FI of alteration Stage 2A are preserved in shielded quartz inclusions in pyrrhotite. Optically they show a relatively large gas bubble with some liquid at the margins. These FI did not show any phase transitions during normal microthermometric freezing experiments (down to -180°C). Laser-Raman analysis revealed a mixture of $CH_4$-$N_2$-$CO_2$, locally with an equal ratio of $CH_4$ and $N_2$. FI of Stage 2B are trapped in plagioclase, are <5 µm in length and are predominantly carbonic, and locally aqueous-carbonic (aq-carb). The carbonic FI in plagioclase do not contain any other gases than $CO_2$ and show a eutectic temperature range of -37 to -44°C. Salinity varies from 1.0 to 4.1 wt% NaCl eq., and density is about 0.3 to 0.6 g/cm$^3$. A Stage 2B growth-zoned carbonate grain reveals a complex fluid evolution from lower temperature saline aqueous to low salinity, higher temperature aq-carb: a) FI in the carbonate core homogenize to liquid between 138 and 154°C and contain between 22 and 23 wt% NaCl eq. at a density of 1.0 g/cm$^3$, b) FI in the intermediate/rim zone homogenize to liquid between 268 to 277°C, and contain between 0.4 and 1.6 wt% NaCl eq. at a density of 0.8 g/cm$^3$. Overall, FI in carbonate show eutectic temperatures between -38 and -45°C and homogenization temperatures to liquid from 268 to 310°C. The salinity is highly variable showing values between 0.0 to 15.2 wt% NaCl eq. and a density of 0.3 g/cm$^3$. Alteration Stage 3 FI in quartz are aqueous, carbonic and aq-carb in nature with variable $H_2O/CO_2$ ratios. The eutectic and homogenization temperatures varies from -32 to -58°C and from 53 to 337°C (to liquid), respectively. Salinity ranges from 0 to 37 wt% NaCl eq. and density from 0.4 to 1.2 g/cm$^3$. Stage 3 FI in carbonate are aqueous, carbonic and aqueous-carbonic (variable $CO_2/H_2O$ ratios). Eutectic and homogenization temperatures range from -0 to -59°C and from 80 to 300°C (to liquid), respectively. Salinity varies between 0 and 22.8 wt% NaCl eq. and density 0.7 to 1.1 g/cm$^3$.

## 6 FLUID VARIATION AT THE STAGE 3 (QUARTZ)

The third hydrothermal alteration stage shows several sub-stages in a relative time sequence:

| | Stage 3 A | | Stage 3 B | | Stage 3 B (CARB) | | Stage 3 B (CAB) | | Stage 3 B (FSP) | | Stage 3 C | |
|---|---|---|---|---|---|---|---|---|---|---|---|---|
| | LD7113A/067.50 (F) | | LD7113A/042.80 (A) | | LD7113A/067.50 (A) | | LD7113A/133.50 (E) | | LD7114/173.50 (B) | | LD7113A/133.50 (B) | |
| | PIXIE | LA-ICPMS | PIXIE | LA-ICPMS | PIXIE | LA-ICPMS | PIXIE | LA-ICPMS | PIXIE | LA-ICPMS | PIXIE | LA-ICPMS |
| | n=4 | n=5 | n=0 | n=3 | n=1 | n=6 | n=4 | n=3 | n=4 | n=3 | n=1 | n=4 |
| **Cl** | 19454 | - | - | - | 39768 | - | 230164 | - | 106792 | - | - | - |
| **K** | 5746 | 8334 | - | 5380 | 6875 | 6242 | 166754 | 1203 | 8914 | 15420 | 2851 | 115022 |
| **Ca** | 6761 | 33781 | - | 153368 | 32747 | 14421 | 22977 | 5663 | 20414 | 14002 | 8001 | 15946 |
| **Mn** | 349 | 254 | - | 2971 | 753 | 340 | - | 150 | - | 60 | - | 320 |
| **Fe** | 7425 | 41794 | - | 4310 | 10376 | 16032 | 63241 | 18601 | 32025 | 11210 | 234 | 43531 |
| **Fe57** | - | 468 | - | 2645 | - | 3755 | - | 6216 | - | 7343 | - | 28437 |
| **Cu** | 404 | 310 | - | 86 | - | 414 | 693 | 67 | 1569 | 2722 | - | 229 |
| **Zn** | 335 | 164 | - | 185 | 880 | 341 | 2917 | 163 | 699 | 273 | - | 688 |
| **Zn67** | - | 166 | - | 293 | - | 682 | - | 188 | - | 832 | - | 747 |
| **As** | 611 | 4494 | - | 733 | - | 1690 | 802 | 13 | 541 | 198 | - | 291 |
| **Rb** | - | 23 | - | 9 | - | 19 | - | 4 | - | 30 | - | 161 |
| **Sr** | 266 | 291 | - | 58 | - | 214 | 9842 | 252 | 4730 | 178 | 2267 | 556 |
| **Cs L** | 2158 | 11 | - | 3 | 3942 | 5 | 7677 | 1 | 9093 | 3 | 1382 | 9 |
| **Ba L** | 1303 | 44 | - | 1147 | 3145 | 75 | 14396 | 94 | 8215 | 1231 | 1834 | 12239 |
| **Pb L** | 543 | 691 | - | 122 | 1138 | 489 | 6707 | 8 | 3511 | 185 | 411 | 1016 |
| **Na** | - | 33440 | - | 19670 | - | 43147 | - | 42330 | - | 15066 | - | 26790 |
| **Mg** | - | 617 | - | 1215 | - | 2971 | - | 1798 | - | 6728 | - | 13398 |
| **Cr** | - | 153 | - | | - | 715 | - | 118 | - | 280 | - | 251 |
| **Ni** | - | 400 | - | 62 | - | 4326 | - | 1172 | - | 213 | - | 461 |
| **Bi** | - | 39 | - | - | - | 4 | - | 9 | - | 350 | - | - |

Table 1. PIXE and LA-ICPMS results in ppm for fluid inclusions trapped during Stage 3 alteration. LD = drill holes at Revenge/St. Ives followed by the depth in meters; n = number of FI analysed, - = below detection and/or host contamination.

Stage 3A: Association of FI shielded by the progressive crystal growth of pyrite with relatively large FI, with aq-carb inclusion that contain about vol. 30% $CO_2$ and halite daughter crystals;

Stage 3B: Association of fluid inclusions in quartz, which replaced carbonate and crosscut the early Stage 1 epidote-magnetite alteration with aq-carb fluid inclusions showing halite daughter crystals. Association of FI in quartz pseudomorph of feldspar (3B (FSP)) and carbonate (3B (CARB)) with relatively smaller aq-carb FI with a daughter crystal (halite?); and Stage 3C represented by aq-carb FI with daughter crystals (halite) are the latest fluids of this stage. Table 1 displays PIXIE and LA-ICPMS results (in ppm) for the different FI associations.

## 7 PALAEOHYDROTHERMAL EVOLUTION

The plot of total homogenization versus salinity (Fig. 1) shows the difference in the NaCl content as well as the decreasing temperature through Stages 1 to 3. The proportions of $CH_4$ relative to $CO_2$ reveal the redox differences between the fluids, especially the large variation in alteration Stage 2B. Alteration Stage 1 (epidote - calcite - magnetite 1 - pyrite 1 - chalcopyrite - quartz) contains a predominantly aqueous fluid with low salinity. The FI from amphibole bearing veins are interpreted to be related to alteration Stage 2A (pyrrhotite - carbonate - amphibole - biotite ± quartz ± arsenopyrite ± pyrite), and were found as quartz crystals in pyrrhotite, therefore shielded from subsequent deformation and recrystallization FI shows no visible water and extreme $CH_4$-$N_2$)/$CO_2$ ratios. The main gold mineralization event is related to the plagioclase - carbonate - pyrite 1 ± Au ± magnetite 2 ± hematite. Crosscutting macro textures revealed a later timing for this alteration in relation to the epidote dominant alteration Stage 1. Fluids of Stage 2A have higher and variable volatile contents, indicated by the occurrence of $CO_2$ - rich inclusion and variable $CO_2$/$CH_4$ ratios. Alteration Stage 3 (late quartz) is characterized by fluids that are out of chemical equilibrium with the Stage 2A plagioclase as indicated by dissolution textures of the plagioclase and carbonate. The predominantly brecciated pathways for this alteration indicate brittle conditions. Large variations in the $H_2O$/$CO_2$ ratios, salinities (0 to up to 37 wt% NaCl eq.) and presence or absence of daughter crystals (halite and/or carbonate) may be partially caused by dissolution of pre-existing carbonate and plagioclase from the alteration wallrocks. During Stage 3B fluids transport significant amount of metals, but are more depleted in metals during Stage 3C. This may be explained by the dissolution process of feldspar and carbonate which can release several of the metals that are enriched in the fluid inclusions. The fluids are enriched in Pb, Cu, Zn, As, Sr, Ba, Mg, Cr, and Ni (Table 1). Fluid inclusions in zoned carbonate crystals show a

rapid change in size and $CO_2/H_2O$ ratio across growth zones. This may have been caused by the entering of deep fluid fluids during aftershock seismic events (Cox & Rumming, 2004).

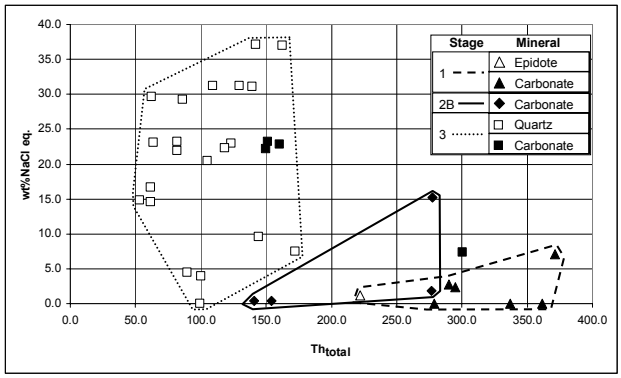


Figure 1. Total homogenization versus salinity for the three main fluid evolution stages.

## 8 CONCLUSIONS

The general fluid evolution displays an overall increase in $CO_2$ and salinity and a decrease in temperature with time. Furthermore significant increases of $CO_2$ and fluctuations in the $CO_2/CH_4$ ratio characterized the fluids at the time of gold precipitation. The large range in salinity and/or total homogenization temperatures of Stage 3 fluid inclusions may be explained by one, or a combination of the following phenomena: post-entrapment modification of FI (*e.g.,* temperature of total homogenization and density), and variable release of chemical components into the fluid during dissolution of plagioclase and carbonates *(e.g.*, salinity), subsequent influx of low temperature brines, chemical reactions between the anhydrous fluids of the gold stage and low-salinity aqueous fluids.

## ACKNOWLEDGEMENTS

The study is financially supported by the Predictive Mineral Discovery Cooperative Research Centre (pmd*CRC) Y3 project, MERI-WA and St. Ives Gold Mining Company (Pty) Ltd. (SIGMC) The authors acknowledge the permission to publish. Geologists at SIGMC are thanked for their support.

## REFERENCES

Cox SF, Ruming K, Nguyen PT, Stone WE (2001) The behaviour of faults, fluids and gold in a crustal scale shear system, St. Ives Goldfield, WA; a case of golden aftershocks? *Specialist Group in Tectonics and Structural Geology conference, Ulverstone, Tasmania, Australia,* Feb. 20:12-16.

Neumayr P, Hagemann SG, Walshe J, Morrison RS (2003) Camp- to deposit-scale zonation of hydrothermal alteration in the St. Ives gold camp, Yilgarn Craton, Western Australia: evidence for two fluid systems? In *Min. Exploration and Sustainable Development, Seventh Biennial SGA Meeting, Athens*, pp. 799-802.

Neumay, P., Petersen, K.J., Gauthier, L., Hodge, J., Hagemann, S.G., Walshe, J.L., Prendergast, K., Connors, K., Horn, L., Frikken, P., Roache, A., and Blewett, R., 2005, Mapping of hydrothermal alteration and geochemical gradients as a tool for conceptual targeting: St Ives Gold Camp, Western Australia: *8th Biennial SGA meeting, Beijing, China, Mineral Deposit Research: Meeting the Global Challenge,* Vol. 2, Mao and Bierlein (eds.) 2005, p. 1479-1482.

Nguyen TP (1997) Structural controls on gold mineralization at the Revenge Mine and its tectonic setting in the Lake Lefroy area, Kambalda, Western Australia. *Unpub. Ph.D. thesis, The University of Western Australia*, 195 pp.

# Variations in fluid inclusions from Au-bearing and barren quartz veins, Fairbanks district, Alaska

Jodie L. Gibson & John R. Ridley
*Department of Geosciences, Colorado State University, Ft. Collins, Colorado 80523*

ABSTRACT: A comparison between fluid inclusions from auriferous and barren quartz veins from both intrusive and metamorphic rocks within the Fairbanks district of east-central Alaska has been conducted. Auriferous veins from intrusions (IRGD) are typically dominated by low-salinity, $CO_2$-rich inclusions, whereas barren intrusion-related veins are typically $CO_2$ deficient, containing only low salinity, aqueous inclusions. There was no observable distinction, based on microthermometry, between IRGD and Au-quartz veins in metamorphic rocks. The only observable difference between auriferous and barren metamorphic veins was presence of detectable $CH_4$ within some of the auriferous veins.

KEYWORDS: orogenic gold, intrusion-related gold deposits, fluid inclusions, Tintina gold belt, Alaska

## 1 INTRODUCTION

The Tintina gold belt (TGB) of east-central Alaska and Yukon contains several high tonnage - world class gold deposits that were emplaced during the mid-Cretaceous. Two gold deposit types are recognized in the province and include gold-quartz±K-feldspar veins within mildly alkalic and moderately reduced, I type intrusions (intrusion-related gold deposits or IRGD), and fault- to shear-hosted gold-quartz veins within dominantly upper greenschist – lower amphibolite facies metamorphic rocks of the Yukon-Tanana terrain (McCoy *et al.* 1997; Goldfarb *et al.* 2005).

Studies have proposed that all shear-hosted gold quartz veins in the province are intimately related to IRGD emplacement, that the ore fluid was derived from the intrusions, and that variations of ore style, setting, and chemistry can be understood in terms of distance of fluid travel and depth of formation (Newberry *et al*. 1995; McCoy *et al*. 1997; Thompson *et al*. 1999). This classification, however, does not allow a distinction between IRGD's and ores of the well-established orogenic or "mesothermal" gold deposit class that are common in many metamorphic belts, including orogenic belts of the style represented by the TGB. Furthermore, no studies to date have compared the hydrothermal fluid chemistry of barren and auriferous quartz veins in mid-Cretaceous intrusions and metamorphic-shear zones in the TGB. This distinction is important in determining the hydrothermal fluid history of the region and may have important implications for ore genesis and future exploration practices.

For this study, the chemistry of barren and auriferous quartz veins was investigated in both intrusion and metamorphic host rocks in the Fairbanks district of east-central Alaska. The Fairbanks district was selected because it is generally considered to host the most economically important gold deposits within the TGB, including the Fort Knox, Ryan Lode, and True North deposits, as well as numerous smaller lodes with historic production (Tolovana, Cleary Hill, Christina, Hiyu, Scrafford, Fox Creek, *etc.*; Mueller *et al.* 2004).

## 2 GOLD DEPOSITS IN THE FAIRBANKS DISTRICT

Gold deposits within the Fairbanks district share overlapping characteristics. IRGD deposits generally comprise pegmatitic and steeply dipping, sheeted stockwork veins within calc-alkaline granodiorite and biotite granite plutons. The largest of the deposits, Fort Knox, has an anomalous metal suite that includes some

combination of Bi, W, As, Sn, Mo, Te, and Sb. Gold-bearing stockwork quartz veinlets typically have a low sulphide content (<3%) and Au is commonly associated with Bi and other base metals. Quartz, K-feldspar, albite, sericite, and carbonate are typical alteration minerals. Fluid inclusions interpreted as representative of the ore fluids are typically low salinity, $CO_2$-rich (7-22 mol%), and have homogenization temperatures of 300° – 350°C. (McCoy *et al*. 1997; Mueller *et al*. 2004; Goldfarb *et al*. 2006)

Gold-bearing quartz veins in metamorphic rocks typically occur along high-angle, NE- to E-trending faults, with dip slip and left-lateral movement (Newberry *et al*. 1995). Ore bearing veins are commonly clustered in vein fields with strike lengths of a few kilometres. Gangue minerals may include carbonates, chlorite, and sericite, with silicification, carbonatization, and sericitization of the host rocks. Gold typically occurs with arsenopyrite and pyrite, but also occurs with masses of stibnite ± galena in historically mined (Scrafford) deposits throughout the district (Robinson & Bundtzen 1982). Fluid inclusions are very similar to those observed in IRGD deposits. They are typically $H_2O$ dominant with approximately 5 -15 mol % $CO_2$, salinities <8 wt% NaCl, homogenization temperatures between 225° – 375°C, and variable amounts of $CH_4$, $N_2$, and $H_2S$ (Goldfarb *et al.* 1997).

$^{40}Ar/^{39}Ar$ conducted is the district indicates that peak regional metamorphism ended at approximately 100-105 Ma, with Au-mineralization and intrusion emplacement occurring coevally between 87 – 93 Ma (Table 1). Several of the historic deposits remain undated (Hiyu, Scrafford) or have anomalously young dates (Christina ~ 77 Ma, Cleary Hill ~ 70.1 – 90.5 Ma; McCoy 2000). The hiatus in mineralization relative to metamorphism has led to the conclusion that Au mineralization is strictly related to intrusion emplacement. However, several major orogenic gold deposits worldwide postdate associated regional metamorphism (Goldfarb *et al.* 2005). Stuwe (1998) suggested that metamorphism, and associated devolatilization, could occur later at deeper depths in the crust. This "deep-later" metamorphism may produce hydrothermal fluids that migrate upward to deposit "post-metamorphic" quartz-gold veins at shallower levels. Recent dating on mid-Cretaceous plutons of the this suite within the Big Delta quadrangle, Alaska indicates significantly earlier intrusion in this part of the region, and suggests the need for additional age dating on mid-Cretaceous plutons within the Fairbanks district (Warren Day, *personal communication*).

## 3 FLUID INCLUSION CHARACTERISTICS

Preliminary fluid inclusion petrography and microthermometry have revealed enigmatic results. Only planar assemblages and trails of pseudo-secondary and rare primary inclusions were investigated in this study. However, it was observed that there are typically secondary trails of low homogenization temperature (<150°C), low salinity (1 – 3 wt% NaCl), aqueous inclusions in all vein types.

Gold-bearing quartz veins from undisputed IRGD deposits (Fort Knox) are dominated by low-salinity, aqueous–carbonic fluids. However, only low salinity aqueous inclusions, within primary and pseudo-secondary assemblages, have been observed in quartz from miarolitic cavities, pegmatitic veins, and shear veins from mid-Cretaceous plutons with no known significant gold mineralization (Gilmore Dome and Pedro Dome). Metamorphic shear-hosted quartz veins have yet to show a clear pattern regarding fluid chemistry. Both barren and auriferous veins may contain aqueous inclusions, carbonic inclusions, or a mixture of both. For example, a metamorphic rock hosted quartz vein rich in Au-As-Sb-Pb (up to 24 ppm Au; Forbes *et al*. 1968) from Cleary Summit contains only low salinity aqueous inclusions (Tm -1.1 to – 4.5°C, Th 265° – 270°C). Based on initial microthermometry results, it is apparent that the aqueous-carbonic inclusions in auriferous veins may also contain $CH_4$ or $N_2$ up to about 5 mol %.

## 4 DISCUSSION AND FUTURE RESEARCH

The preliminary fluid inclusion observations indicate that the presence or absence of $CO_2$ in hydrothermal fluids may be a significant difference between intrusions that host IRGD deposits and barren plutons of the same magmatic suite. However, there is no micro-thermometric distinction between aqueous-carbonic fluid inclusions in IRGD and those in shear zone-hosted, Au-bearing quartz veins in metamorphic rocks. It is also noted that there is no clear differentiation between the fluids of barren and mineralized quartz veins in metamorphic

Table 1. Compilation of Dates from mid-Cretaceous intrusions and Au deposits of the Fairbanks District, Alaska

| Deposit/Location | Date (Intrusion) | Date (Au) | References |
|---|---|---|---|
| *Intrusions* | | | |
| Fort Knox | 92.5 ± 0.5 Ma | 92.6 ± 0.9 Ma | Bakke 1995; Selby *et al.* 2002 |
| Ryan Lode | 89.2 - 90.6 Ma | 87.7 - 89.2 Ma | McCoy *et al.* 1997 |
| Pedro Dome* | 93.0 - 95.3 Ma | ----- | Forbes 1982 |
| Gilmore Dome* | 90.4 - 93.0 Ma | ----- | Blum 1983, |
| *Metamorphic hosted* | | | |
| Tolovana | ------ | 90.7 ± 2.3 Ma | Newberry *et al*. 1995 |
| Christina | ------ | 77 Ma (?) | Goldfarb *et al.* 1997 |
| Cleary Hill | ------ | 70.1 - 90.5 Ma (?) | McCoy 2000 |

*Mid-Cretaceous intrusions with no known Au-mineralization

rocks, although there may be a correlation between gold mineralization and the presence of detectable $CH_4$ and/or $N_2$. Other factors to be considered as possible controls on fluid composition include immediate host rocks and fluid temperature in the veins.

Future research in the region will focus on the geochemistry of the hydrothermal fluids responsible for Au deposition and what properties distinguish those fluids from barren counterparts. This research plan will include detailed petrographic investigations of vein mineralogy and alteration assemblages, fluid inclusion microthermometry, and multi-element analyses.

## ACKNOWLEDGEMENTS

This work was supported by the U.S. Geological Survey. Thanks to Rich Goldfarb, Erin Marsh, Lang Farmer, and David Adams for assistance and guidance in the field, Curt Freeman of Avalon Development Corp. for access to samples and drill core, Bob Bodnar for laboratory access, direction, and assistance with fluid inclusion petrography and microthermometry, and David Lentz and Albert Hofstra for their helpful review of this manuscript.

## REFERENCES

Goldfarb RJ, Miller LD, Leach DL, Snee, LW (1997) Gold deposits in metamorphic rocks of Alaska. *Economic Geology Monograph* 9, pp 151-190.

Goldfarb RJ, Baker T, Dube B, Groves D, Hart CJR, Gosselin P (2005) Distribution, character, and genesis of gold deposits in metamorphic terranes, in, Hedenquist J, Thompson JFH, Goldfarb RJ, Richards JP, (eds) *Economic Geology: One Hundredth Anniversary Volume*, 1905-2005, pp 407-450.

McCoy D, Newberry RJ, Layer P, DiMarchi JJ, Bakke A, Masterman JS, Minehane DL (1997) Plutonic-related gold deposits of interior Alaska. *Economic Geology Monograph* 9, pp 191-241.

McCoy D (2000) Mid-Cretaceous gold deposits of interior Alaska: Metallogenesis, characteristics, gold associative mineralogy and geochronology. *Doctoral Dissertation, University of Alaska, Fairbanks.*

Mueller SH, Goldfarb RJ, Hart CJR, Mair JL, Marsh EE, Rombach CS (2004) The Tintina Gold Province, Alaska and Yukon New world-class gold resources and their sustainable development. *PACRIM 2004*, pp 189-198.

Newberry RJ, McCoy DT, and Brew DA (1995) Plutonic-hosted gold ores in Alaska igneous vs. metamorphic origin. *Resource Geology Special Issue* 15: 57-100.

Robinson MS and Bundtzen TK (1982) Geology of the Scrafford antimony-gold lode deposit, Fairbanks mining district, Alaska. *Alaska Open File Report* 173.

Stuwe K (1998) Tectonic constraints on the timing relationships of metamorphism, fluid production, and gold-bearing quartz vein emplacement. *Ore Geology Reviews* 13: 219-228.

Thompson JFH, Sillitoe RH, Baker T, Lang, JR, and Mortensen JK (1999) Intrusion- related gold deposits associated with tungsten-tin provinces. *Min Dep* 34: 323-334.

# Tectonic setting of Late Cretaceous gold and mercury metallogenesis, Kuskokwim Mineral Belt, southwestern Alaska, USA

M.L. Miller, D.C. Bradley, & R.J. Goldfarb
*U.S. Geological Survey*

T.K. Bundtzen
*Pacific Rim Geological Consulting, Fairbanks, AK, USA*

ABSTRACT: A significant and widespread metallogenic episode in southwestern Alaska occurred over a short time period at ~70 Ma. Gold and mercury mineralization took place in a continental-margin back-arc that was the site of strike-slip faulting. Possible regional tectonic controls of ore formation during that time include low-angle subduction, slab breakoff, opening of a slab window related to ridge subduction, and tectonic extrusion, the last being our preferred model.

KEYWORDS: southwestern Alaska, strike-slip tectonics, gold, mercury, late Cretaceous

## 1 INTRODUCTION

A major episode of epigenetic ore deposit formation took place in late Cretaceous time in what is now southwestern Alaska. Several large-scale tectonic factors came together during a relatively short time frame, leading to a widespread pulse of magmatism, gold mineralization, and mercury mineralization—all at ~70 Ma. The gold and mercury deposits help delineate the ~190,000 km$^2$ Kuskokwim Mineral Belt. Total production includes approximately 100,000 kg of gold, 16,000 kg of silver, and 1.3 million kg of mercury.

The Kuskokwim Mineral Belt lies within a broad zone of dextral strike-slip faults that have been active since at least late Cretaceous time (Miller *et al*. 2002). The belt occurs in a back-arc position along the northern Pacific continental margin, about 350-450 km inboard of the present-day Aleutian subduction zone (Fig. 1). The southwestern Alaska dextral faults lie at the western end of a continental-scale, strike-slip system that curves around the Canadian-Alaskan continental margin.

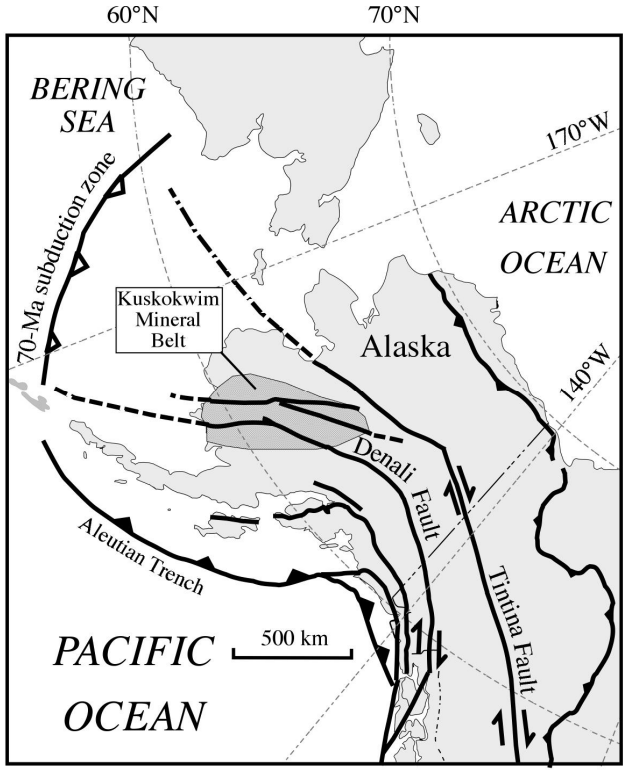


Figure 1. Map of Alaska showing major strike-slip faults and the Kuskokwim Mineral Belt.

## 2 REGIONAL GEOLOGIC SETTING

Southwestern Alaska is underlain by a variety of Jurassic and older terranes that were assembled by mid-Cretaceous time and then overlapped by Upper Cretaceous flysch (Decker *et al.* 1994). The older terranes include Palaeoproterozoic metamorphic rocks, a Neoproterozoic to Jurassic microcontinental fragment, and Palaeozoic to Mesozoic oceanic and arc assemblages. The overlapping Kuskokwim Group flysch was deposited into a basin that subsided

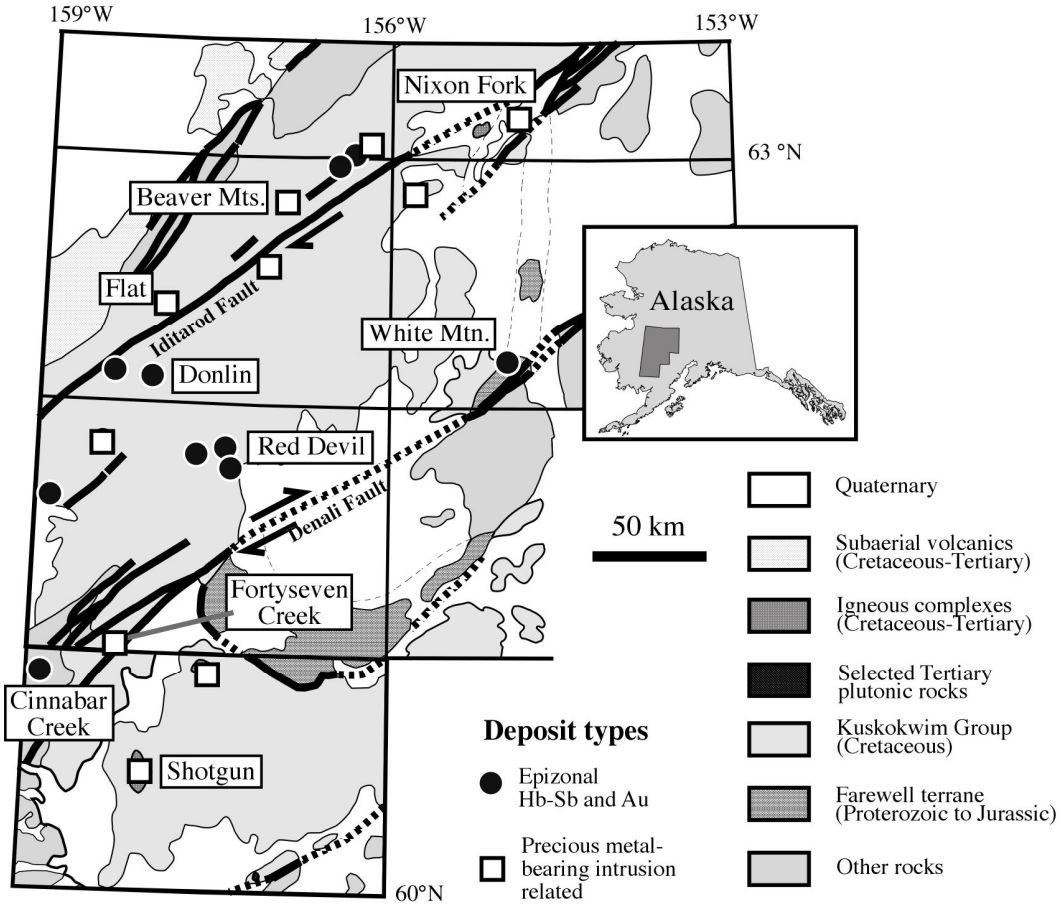


Figure 2: Geologic map of the central Kuskokwim Mineral Belt showing location of major Au and Hg deposits.

between some of the terranes; this unit forms the dominant bedrock of the Kuskokwim Mineral Belt.

The Kuskokwim Group is mainly composed of sandstone and shale turbidites. These rocks were deposited from ~95 Ma to ~76 Ma. The waning stages of deposition were accompanied by minor volcanism, marking the beginning of a period of magmatism during which numerous intrusive igneous complexes and subaerial volcanic rocks were emplaced (Fig. 2). Although the magmatism was widespread and relatively continuous between 76 and 63 Ma, it dramatically peaked ~70 Ma.

The intrusive rocks produced in the late Cretaceous are of two types, both of which are spatially associated with mineralization: volcanic-plutonic complexes and structurally controlled dykes, sills, and stocks. The volcanic-plutonic complexes consist of quartz monzonitic plutons and subaerial volcanic rocks; chemistry indicates a mantle component. The volcanic section and underlying sedimentary rock are intruded and baked by the comagmatic plutons. The structurally controlled, hypabyssal dykes, sills, and stocks (too small to show on Fig. 2) are felsic to intermediate and commonly peraluminous in composition. These are the same age as the volcanic-plutonic complexes, but have a melted crust signature.

## 3 GOLD AND MERCURY DEPOSITS

Two important mineral deposit types formed ~70 Ma: (1) precious metal-bearing, boron-rich, high-temperature deposits genetically related to the volcanic-plutonic complexes, and (2) epizonal deposits, many of which are structurally associated with relatively competent sill/dyke systems that make a favorable host (Fig. 2).

The Shotgun prospect, which typifies the precious metal-bearing intrusion-related deposit type, is hosted by quartz-feldspar porphyry—a phase thought to be related to a main granodiorite stock. The porphyry is cut by ~70 Ma gold-bearing quartz veins, breccias, and stockworks, which contain arsenopyrite, pyrite, pyrrhotite and chalcopyrite (Rombach & Newberry 2001). Gold-rich samples contain 0.1-0.5 % arsenic, as well as anomalous copper, molybdenum, and

tellurium. Tourmaline veinlets are ubiquitous and indicate a boron-rich magmatic fluid phase; albite alteration is widespread.

The epizonal deposits are primarily mercury-antimony systems such as Red Devil and Cinnabar Creek, but also include gold deposits, such as the giant Donlin Creek system. Red Devil, Alaska's largest mercury mine, closed in the 1970s after producing over 1.2 million kg of mercury. The ore consists of cinnabar in quartz-carbonate veinlets, but abundant stibnite was found deeper in the system. Smaller deposits of this type are found throughout the region and many are notably anomalous in gold. They are mainly hosted in Kuskokwim Group sedimentary rocks at or near high-angle structures, and are locally spatially associated with intermediate to mafic dykes. At Cinnabar Creek, the mercury ore is notable in that it contains native mercury in addition to cinnabar.

Some of the epizonal deposits contain economic amounts of gold, the best example being the Donlin deposit, which is estimated to contain 780,000 kg of gold. Donlin consists of about 16 prospects within and adjacent to an 8-km-long dyke/sill complex. The dykes are hypabyssal porphyritic intrusions of mainly granitic composition. Metalliferous quartz veinlets fill brittle, extensional fractures in the dykes and were formed within a few million years of crystallization of the dykes. The ore-forming fluids were derived by either devolatilization of flysch above rising mantle melts deep in the Kusko-kwim basin or by exsolution from a flysch melt magma (Goldfarb *et al*. 2004).

## 4 STRUCTURAL SETTING OF THE GOLD AND MERCURY DEPOSITS

The Kuskokwim Mineral Belt lies in a broad zone of dextral strike-slip faults (Fig. 2) that have been active intermittently since about 95 million years ago. The Iditarod-Nixon Fork fault shows at least 90 km dextral offset since the Late Cretaceous and the Denali fault, in this part of Alaska, shows dextral offset of at least 134 km (Miller *et al.* 2002). Most significantly, that study indicated that strike-slip motion on these faults was taking place *at the same time as* the ~70 Ma igneous activity and coeval hydrothermal mineral deposition. Some of the deposits are spatially associated with strike-slip faults; others lie between the master faults.

Intrusion-related gold deposits that lie along the main faults exhibit structural features suggesting they were formed synkinematically during dextral strike-slip. For example at the Fortyseven Creek gold-tungsten deposit, vein orientations are consistent with dextral strike-slip on the Denali Fault. At the Nixon Fork gold skarn deposit, which lies along the Iditarod-Nixon Fork fault, ~70 Ma intrusive bodies were emplaced parallel to the master fault and the mineralization occurs in strain shadows that are consistent with dextral shear.

In contrast, structural data for two ~70 Ma deposits that lie between the first-order faults (Donlin Creek and Red Devil) suggest a roughly north-south principal compression direction, which is perpendicular to what would be expected in a dextral regime near the main strike-slip faults. For example at Donlin Creek, the earliest deformation was reported by Ebert *et al.* (2000) to be approximately north-south compression. At Red Devil, northwest-striking mineralized dextral faults are consistent with a roughly north-south principal compression direction, again perpendicular to what would be expected in a dextral regime on the main northeast-striking master faults.

## 5 TECTONIC FRAMEWORK

To understand the regional tectonic framework during the critical latest Cretaceous time, it is useful to work back through the history of interactions between southwestern Alaska and the plates of the Pacific. Such interactions are not straightforward, even for the current situation. At present, the North America-Pacific plate boundary is a *dextral* transform along most of its length (*e.g.* San Andreas and Queen Charlotte faults), but in southwestern Alaska, the plate boundary is a subduction zone with a minor *sinistral* component of obliquity. Inboard of the plate boundary, the Denali fault has Neogene dextral offsets along its entire length, even above the sinistrally oblique subduction zone. Dextral strike-slip in this region thus requires another explanation besides oblique subduction, but can be explained by a push from the rear (Miller *et al.* 2002), tectonic extrusion toward a free face in the Bering Sea (Redfield *et al*. 2006), or a combination of the two.

Uncertainties mount further back in time. At ~55 Ma, dextral motion in southwestern Alaska may have been accentuated by "megakinking" during oroclinal bending. At ~60 Ma, the identity of the subducting plate comes into question, as discussed in depth by Miller *et al.* (2002).

The three alternatives, each of which has specific plate kinematic implications, are the Kula, the Farallon, and the newly proposed Resurrection Plate (our preferred model).

Some of the tectonic factors operating during the critical ~70 Ma episode of widespread Au and Hg metallogenesis in southwestern Alaska are known, but questions remain. Subduction was most certainly occurring along the Gulf of Alaska margin at this time, based on the presence of the Chugach accretionary complex and arc rocks in the Alaska Range. Dextral strike-slip was likely driven by oblique plate convergence, perhaps in concert with escape tectonics. Late Cretaceous dextral displacement enhanced crustal dilation and fluid migration. It is still not clear why (1) the 70 Ma magmatism occurred over such a wide area, (2) both mantle and crustal melts were present, and (3) the region of elevated geotherms was so extensive.

Geometric complexities involving a curved margin, the consumption of the Kula and then Resurrection Plates, and possible escape on the free western face led to a complicated set of forces that likely played a role in ore genesis of the region. What scenario would allow a broad region to experience a flare up of magmatism and widespread elevated thermal gradient? Four possibilities are listed below; we currently favor the last one.

1) *Low-angle subduction*—this would seem to be a reasonable mechanism for a wide belt of magmatism, but it's not obvious how this would explain the voluminous pulse just at 70 Ma. It is interesting to note, in the Andes, areas above zones of flat slab subduction lack volcanoes, so it is not a given that low-angle subduction causes widespread arc magmatism.

2) *Slab breakoff* (or a variant, delamination)—this would generate a slab window, but without subducting a ridge. It would seem to account for the regional mercury belt and for the magmatic flare-up; however, there is no independent evidence that it happened.

3) *Ridge subduction beneath the Bering Sea margin*—ridge subduction is the normal mechanism for forming a slab window and thus generating a broad area of high heat flow (*e.g.* northern California Hg belt). On Alaska's Pacific margin, ridge subduction didn't start until 61 Ma, too young to explain 70 Ma events. The Bering margin *was* a subduction zone at 70 Ma, but ridge subduction there has not been documented; regardless, the Kuskokwim region seems too far inland to have been affected.

4) *Escape tectonics*—has southwestern Alaska moved toward the free face in the Bering Sea and was this process operating at 70 Ma? In the Neogene of Turkey, escape along active strike-slip faults produced a broad magmatic province not related to subduction (Pearce *et al*. 1990). This process may have operated in the late Cretaceous in southwestern Alaska.

## ACKNOWLEDGEMENTS

We thank reviewers B. Gamble and J. Kurtak.

## REFERENCES

Decker J, Bergman S, Blodgett R, Box S, Bundtzen T, Clough J, Coonrad W, Gilbert W, Miller M, Murphy J, Robinson M, Wallace W (1994) The geology of southwestern Alaska. In: Plafker G, and Berg H (eds) The geology of Alaska. *Geological Society of America DNAG* Series G-1, pp285-310

Ebert S, Miller L, Petsel S, Dodd S, Kowalczyk P (2000) Geology, mineralization, and exploration at the Donlin Creek project, southwestern Alaska. *British Columbia and Yukon Chamber of Mines Special Volume* 2: 99-114

Goldfarb RJ, Ayuso R, Miller ML, Ebert SW, Marsh EE, Petsel SA, Miller LD, Bradley D, Johnson C, McClelland W (2004) The Late Cretaceous Donlin Creek gold deposit, southwestern Alaska: Controls on epizonal ore formation. *Econ. Geol* 99: 643-671

Miller ML, Bradley DC, Bundtzen TK, McClelland W (2002) Late Cretaceous through Cenozoic strike-slip tectonics of southwestern Alaska. *Journal of Geology* 110: 247-270

Pearce JA, Bender JF, DeLong SE, Kidd WSF, Low PJ, Guner Y, Saroglu F, Yilmaz Y, Moorbath S, Mitchell JG (1990) Genesis of collision volcanism in Eastern Anatolia, Turkey. *J Volcanology and Geothermal Research* 44: 189-229

Rombach CS, Newberry RJ (2001) Shotgun deposit: Granite porphyry-hosted gold-arsenic mineralization in southwestern Alaska, USA. *Mineralium Deposita* 36: 607-621

Redfield TF, Scholl DW, Beck ME, Fitzgerald PG (2006) The extrusion of Alaska: past, present, and future. *Eos Transactions AGU 87, Fall Meeting Suppl.*, Abst T43D-1682

# Controls on endowment and prospectivity of the Sierra Foothills gold province, central California

F.P. Bierlein, H.J. Northover, D.I. Groves
*Centre for Exploration Targeting, University of Western Australia, Crawley WA 6009, Australia*

R.J. Goldfarb, E.E. Marsh
*United States Geological Survey, Box 25046, MS 964, Denver CO 80225, USA*

ABSTRACT: Assessment of spatial relationships between the location, abundance and size of orogenic gold deposits in the highly-endowed Sierra Foothills gold province via a GIS-based analysis illustrates the power of such an approach to the genetic characterization of mineral systems and the prediction of areas likely to host economic mineralization. Results from regional stress mapping confirm empirical findings, highlight the close spatial relationship between gold deposits and first-order faults, and indicate the importance of structural permeability contrasts, rheological gradients, and variations in fault orientation (giving rise to dilational/compressional jogs) along first- and higher-order faults in localising mineralization. Although this approach has produced promising results at the province-scale, significantly enhanced geological, structural, geophysical and geochronological data density is required to enable the generation of regionally consistent, high-quality input layers that improve predictive goldfield-scale targeting.

KEYWORDS: Sierra Foothills, California, orogenic gold, GIS, endowment, prospectivity analysis

## 1 INTRODUCTION

The Sierra Foothills gold province is host to 13,000 mines and prospects which are distributed for approximately 300km throughout the northern and central Sierra Nevada Foothills Metamorphic Belt (SNFMB) in California (Fig. 1). The region has yielded >120 million ounces (Moz) Au from lode and placer deposits, making it one of the world's premier gold provinces (Böhlke 1999). Yet, when compared with analogous gold provinces elsewhere, the distribution of gold ores along the length of the Sierra Foothills remains relatively poorly documented.

The structurally-controlled deposits are characteristic of orogenic lode gold deposits world-wide, and are centred on a series of transcrustal curvilinear faults that played a pivotal role in the late Palaeozoic-early Mesozoic accretionary evolution of the SNFMB. About 60% of the total production was from lode deposits, mainly concentrated within the Mother Lode belt, Grass Valley district, and Alleghany district. The largest gold lodes were the adjacent Empire and Idaho-Maryland deposits in Grass Valley, with a combined production of almost 10 Moz Au; these were followed by about 20 deposits throughout the SNFMB each with 0.3-1.8 Moz Au production.

At a fundamental level, the Sierra Foothills gold province fulfils all criteria required for the generation of an exceptionally well-endowed orogenic gold province. This includes a short pre-mineralization history of the hosting terranes, thin syn-mineralization lithosphere (as indicated by contemporaneous magmatism), and the presence of primitive mafic (source) rocks and deep-seated fluid conduits (Bierlein *et al.* 2006). On the other hand, disparities in size and location of deposits within the gold province are likely to represent significant variations in the degree of conjunction of endowment parameters (Groves *et al.* 2000) that operate at the belt-scale.

In this study, geological and geophysical characteristics that aid in the assessment of primary controls on gold mineralization in the belt are identified. These are then interpreted within a GIS framework to statistically define relevant empirical and conceptual relationships. The power of such an approach lies in its ability to genetically characterize minerals systems and the prediction of well-endowed areas.

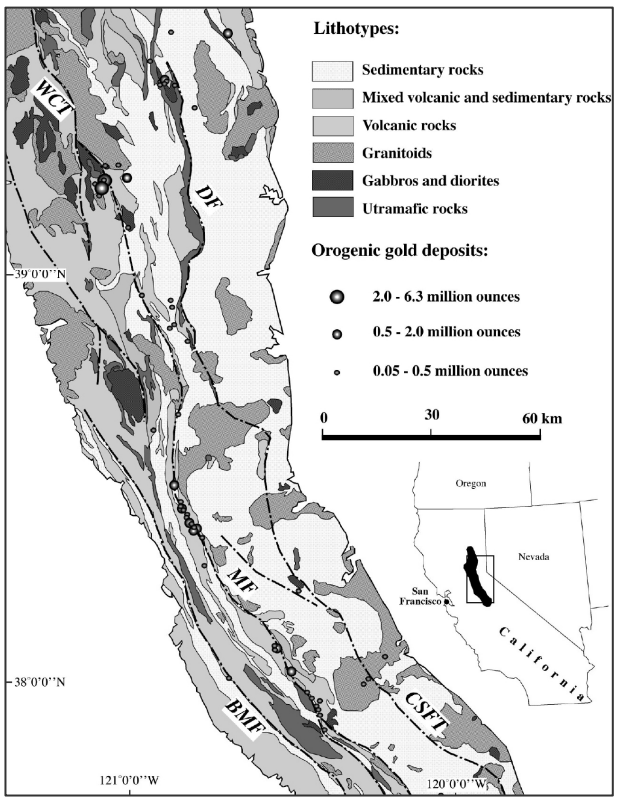


Figure 1. Map of the Sierra Foothills gold province showing major lithotypes, selected first-order faults (WCT = Wolf Creek Thrust; MF = Melones Fault; DF = Downieville Fault; BMF = Bear Mountains fault; CSFT = Calaveras-Shoo Fly Thrust) and location and size of major orogenic gold deposits (after Clark 1992; Saucedo *et al*. 2000; Snow & Scherer 2006).

## 2 TECTONIC SETTING AND REGIONAL GEOLOGY

The SNFMB is part of the North American Cordilleran orogen that extends from Alaska to California. It is comprised of turbiditic terranes, island-arc complexes, and back-arc basins accreted to the North American craton (Dilek & Harris 2004). During the early Palaeozoic, the southern part of this orogen was primarily a passive margin setting. In the late Palaeozoic, oceanic Antler and Sonoma allochthons were thrust over the continental margin**.** Transition to an accretionary margin commenced in the Mesozoic, with the Nevadan orogeny (163-152 Ma) marking the final, regionally pervasive deformation within the SNFMB (Böhlke 1999). Plutonism within the accreted terranes took place from early Jurassic through early Cretaceous, with emplacement of the massive Sierra Nevada batholith late in this period and about 20-30km to the east of the lode deposits.

The SNFMB comprises a diverse collage of Palaeozoic and Mesozoic metasedimentary and metavolcanic rocks. Five terranes were progressively accreted from east to west (*i.e*. Northern Sierra and Feather River terranes, Calaveras Complex, Jurassic-Triassic Arc Belt, Middle-Late Jurassic Arc Sequence; Snow & Scherer 2006). These terranes are bounded by a series of transcrustal, curvilinear faults (*e.g*. Melones Fault, Bear Mountains Fault, Downieville Fault, Calaveras-Shoo Fly Thrust, Wolf Creek Thrust; Fig. 1) which themselves comprise tectonic mélanges of medium to high metamorphic-grade wall rock fragments.

## 3 CHARACTERISTICS OF DEPOSITS IN THE MOTHER LODE GOLD BELT

Geological, structural and petrographic evidence confirms that quartz-gold veins throughout the belt formed late during the *ca*. 151-123 Ma deformation of the SNFMB (Böhlke 1999). The lode deposits developed in amphibolite- to greenschist-facies volcanic and sedimentary rocks, and less commonly granitoid intrusions, proximal to the first-order Melones Fault system. At the deposit-scale, there is a close spatial relationship with altered ultramafic bodies (serpentinites). Structural analysis indicates multiphase formation of the lode structures in a subhorizontally-oriented, E-W far-field stress regime, with compression resulting in reverse reactivation of pre-existing structures in the form of minor east-over-west thrusting. Mineralization is concentrated in zones of minimum principal stress and dilational structures, including conjugate shears (*e.g.* Empire); granitoid pressure shadows; dilational jogs linked to flattening of the footwall contact (*e.g*. Sixteen-to-One); fault jogs (*e.g.* Harvard); and along lithological contacts with pronounced competency gradients (*e.g*. Idaho-Maryland, Sierra Butte and Sutter Creek). Vein formation in most deposits is temporally related to a switch from normal-sinistral to dextral transpression, giving rise to the commonly steeply north-plunging ore shoots. The vein-hosted gold in these deposits typically is coarse-grained, with a low abundance of pyrite and arsenopyrite, and pervasive sericitization, carbonatization and chloritization.

Ar-Ar, K-Ar and Rb-Sr age constraints indicate that the majority of deposits formed between *ca.* 125 and 115 Ma, corresponding with significant gold-mineralizing events elsewhere in the Circum-Pacific region (Böhlke & Kistler 1986; Goldfarb *et al*. 1998).

The above field observations and spatial relationships, when placed in the context of the tectonic evolution of the SNFMB, allow for the construction of a genetic model for the Sierra Foothills gold province in a GIS framework, which can then be interrogated in terms of a prospectivity assessment.

## 4 GIS DATA COMPILATION

Due to the regional scale of this investigation, a variety of disparate data sources (*e.g.* Clark 1992; Saucedo *et al*. 2000; Snow & Scherer 2006) of varying density were compiled into broadly consistent empirical and derived layers of solid geology, structural elements, deposit locations, magnetics, and gravity (Bouguer anomaly and isostatic residual gravity). Uncertainties and discrepancies in production figures, deposit names and spatial distribution were considerably reduced via the compilation of a gold production data base that contained 1,252 'significant' deposits (>5,000 oz Au), re-calculation of production values, cross-referencing of deposits, and ground-proofing. Lithologically disparate units within each terrane were grouped into six general lithotypes (after Saucedo *et al*. 2000): sedimentary rocks, mixed volcanic and sedimentary rocks, volcanic rocks, granitoids, gabbros and diorites, and ultramafic rocks (Fig. 1). The structural layer incorporates all terrane-bounding (first-order) and major intra-terrane faults. Higher-order structures are poorly represented, in part due to the scale of the study, but also because many are not recorded in existing data sets, particularly where they coincide with lithological boundaries. The solid geology and structural layers were cross-validated with a high-resolution, total magnetic-intensity layer.

## 5 PROSPECTIVITY ANALYSIS

Empirical and derived layers were examined to highlight geological and spatial controls on the distribution and size of gold deposits throughout the Sierra Foothills gold province. These controls also represent quantifiable proxies for fluid source(s), transport pathways and efficient traps within a conceptual mineral systems framework. Whereas ore sources remain undefined, abundant primitive mafic rocks throughout the SNFMB are the most likely sources of significant volumes of ore constituents (*e.g*. Bierlein *et al*. 2006). The close spatial relationship between first-order structures and gold deposits is illustrated by the occurrence of approx. 75% of the deposits within 4.5km of such faults in the Mother Lode gold belt (90% within 8.6km). This relationship is based on the ability of trans-crustal faults to enhance the efficient channeling of ore-bearing fluids from their source to shallower crustal levels (*e.g*. Groves *et al.* 2000). With the exception of deposits in the Grass Valley district, almost all gold deposits display a spatial affinity with the Melones Fault. Seismic profiling correlates this structure with a prominent regional reflector that persists to at least mid-crustal levels (Nelson *et al*. 1986).

Sites of gold deposition correlate well with the occurrence of both dilational and compressive jogs along first-order structures. This relationship is illustrated by the coincidence of major gold deposits and fault segments with an orientation significantly different (*i.e.* $\geq 15^{\circ}$) from that of the overall regional trend ($\sim 154^{\circ}$).

Only 35% of the deposits in the belt, however, correlate with second- and third-order faults as the most proximal structure. The most probable cause for this low correlation is the inadequacy of the structural layer in terms of higher-order faults. By contrast, many of the gold deposits display a strong spatial affinity to regions of magnetic gradients, and approx. 90% occur within 2km of a lithological contrast. These correlations strongly support the notion that many (mapped) lithological contacts are faults, and also emphasise the importance of rheological and permeability contrast in focusing fluid flow and controlling ore deposition. Although the epigenetic nature of the deposits implies that host lithology is secondary, there is a strong preference towards volcanic rocks in terms of gold production ($kg/km^2$) versus host rock type (normalized by area), with production from deposits in volcanic rocks outstripping the combined production from deposits hosted in granitoids, gabbros and ultramafic rocks. There is no consistent spatial relationship between gold deposits and granitoids in the province. A test of the correlation between geophysical gradients and the location of known gold occurrences reveals that Bouguer gravity is a more efficient parameter than magnetic intensity, at least in part due to the higher resolution of the former data set.

## 6 CONCLUSIONS

The effectiveness of spatial parameters in identifying province-scale prospective areas is undoubtedly dependent on input data density. Lack of complete data sets, limited geochronological constraints, unreliable records (*e.g.* production) and insufficient spatial resolution all introduce uncertainties that severely limit the capability of any GIS-based analysis to determine and rank potentially prospective areas. Nevertheless, this study confirms conceptual and empirically established findings regarding the importance of certain geological and structural parameters in controlling the spatial distribution, abundance and size of orogenic gold deposits. These parameters include proximity to first-order, terrane-bounding structures, spatial affinity with 'misaligned' fault segments that generate dilational or compressional jogs, lithological contacts with strong rheological contrasts, and regions characterised by geophysical, such as magnetic-intensity and/or gravity, gradients. In the Mother Lode belt, deposits are centered on N-NW-trending gravity highs associated with the first-order Melones Fault. The majority of deposits are sited within higher-order fault segments that parallel lithological contacts and trend ≥15˚ from the regional average of ~154˚. On the basis of these findings and the successful identification of known gold deposits, basic GIS analysis has the potential to predict more highly prospective regions in this province. This approach, when combined with enhanced data density and high-quality input parameters, should prove equally successful when applied to exploration in analogous regions elsewhere.

## ACKNOWLEDGEMENTS

We are grateful for generous in-kind support from Idaho-Maryland Mining and Sutter Creek Mine staff, as well as input by R. Wittkopp, R. Cortney, M. Payne, R. Grunewald, K. Testerman, R. Pease and PS Peggy. The USGS, CET TSRC, and ARC (DP0342488 to FPB) are acknowledged for financial support.

## REFERENCES

Bierlein FP, Groves DI, Goldfarb RJ, Dubé B (2006) Lithospheric controls in the formation of provinces hosting giant orogenic gold deposits: *Mineralium Deposita* 40: pp 874-886

Böhlke JK (1999) Mother Lode Gold. *Geological Society of America Special Paper* 338, 67pp

Böhlke JK, Kistler RW (1986) Rb-Sr, K-Ar, and stable isotope evidence for the ages and sources of fluid components of gold-bearing quartz veins in the northern Sierra Nevada foothills metamorphic belt, California. *Economic Geology* 81: pp 296-322

Clark WB (1992) Gold Districts of California: *California Division of Mines and Geology, Bulletin* 193, 186 pp.

Dilek YD, Harris R (2004) Continental margins of the Pacific Rim: introduction. *Tectonophysics* 392: pp 1-7

Goldfarb RJ, Phillips GN, Nokleberg WJ (1998) Tectonic setting of synorogenic gold deposits of the Pacific Rim. *Ore Geology Reviews* 13: pp 185-218

Groves DI, Goldfarb RJ, Knox-Robinson CM, Ojala J, Gardoll S, Yun GY, Holyland P (2000) Late-kinematic timing of orogenic gold deposits and significance for computer-based exploration techniques with emphasis on the Yilgarn Block, Western Australia. *Ore Geology Reviews* 17: pp 1-38

Nelson KD, Zhu TF, Gibbs A, Harris R, Oliver, JE, Kaufman S, Brown L, Schweickert RA (1986) COCORP deep seismic reflection profiling in the northern Sierra Nevada, California: *Tectonics* 5: pp 321-333

Saucedo GD, Bedford DR, Raines GL, Miller RJ, Wentworth CM (2000) GIS data for the geologic map of California, CD-ROM 2000-007, *California Department of Conservation, Division of Mines and Geology*

Snow CA, Scherer H (2006) Terranes of the Western Sierra Nevada Foothills Metamorphic Belt, California: A critical review: *International Geology Review* 18: pp 46-62

# Role of Reduced Sedimentary Rocks in Formation of the Great Basin Gold Province: Implications for Exploration in Analogous Settings

Albert H. Hofstra & Poul Emsbo
*United States Geological Survey, MS-973, Box 25046, Denver, CO 80225, USA*

ABSTRACT: The array of gold deposit types (sedex, orogenic, reduced intrusion-related, porphyry-distal disseminated, Carlin-type, epithermal) and amount of gold (~9800 t) in the Great Basin is remarkable. It constitutes a "sulphide-gold suite" that reflects the ability of reduced sedimentary rocks to shift the redox and sulphidation state of diverse fluids to conditions that facilitate gold transport by sulphide complexes (convergent evolution). The key lithologies implicated in these systems are carbonate and/or siliciclastic sedimentary rocks that typically contain pyrite and carbon and little or no reactive Fe, from which S was frequently derived. Recognition of the potential impact of such reduced rocks on various hydrothermal systems provides a practical geochemical process indicator for exploration that compliments the requisite geologic frameworks. In other passive margin settings with long and complex histories, the presence of reduced sedimentary rocks increases the probability that gold deposits of different types and ages will be present, particularly along reactivated structures in mineral belts.

KEYWORDS: Great Basin, reduced sedimentary rocks, sulphide complexes, gold, Nevada

## 1 INTRODUCTION

Discussions of gold metallogeny in the Great Basin have emphasized the tectonic setting, geologic architecture, sources, driving mechanisms, and structural and stratigraphic controls on fluid flow and ore deposition (*e.g.*; Cline *et al*. 2005; Emsbo *et al*. 2006). The lithologic controls on the redox and sulphidation state of ore fluids, in source regions and/or along fluid pathways, has received less attention. Chemical modeling suggests fluids that move through reduced marine sedimentary rocks (pyrite, carbon, ±barite) with low concentrations of reactive Fe-bearing minerals and low $Fe^{+3}/Fe^{+2}$ will maintain low redox and evolve to high sulphidation states as they cool. When $H_2S$ is generated by dissolution (or desulphidation) of pyrite, breakdown of organic S compounds, or reduction of sulphate, the sedimentary S source is reflected in the $\delta^{34}S$ of sulphides. The high $m_{H_2S}$ enhances the solubility of Au at the 450°-150°C formation temperatures of most gold deposits (*e.g.* Heinrich 2005 *and references therein*).

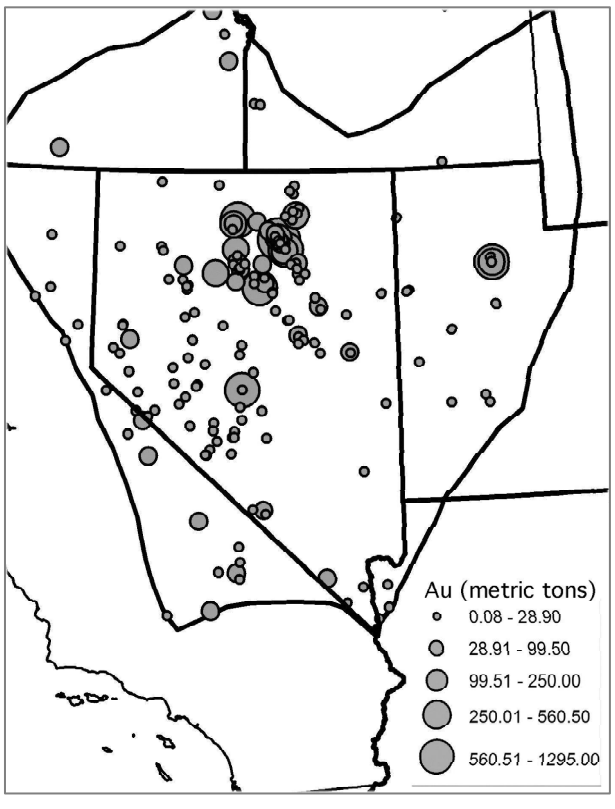


Figure 1. Gold deposits in the Great Basin, western USA.

The Great Basin gold province encompass-

ing the state of Nevada in the western United States is remarkable because it contains numerous significant and several giant gold districts of different types and ages that together contain ~9800 t Au (Fig. 1). The purpose of this communication is to highlight deposits in this province that demonstrate a common theme, namely, that fluid / reduced sedimentary rock reactions stabilized sulphide complexes, facilitating Au transport to the sites of ore formation in diverse hydrothermal systems again and again.

## 2 GREAT BASIN TECTONICS AND REDUCED SEDIMENTARY ROCKS

The miogeocline on the western margin of North America was initiated by the Neoproterozoic breakup of the Mesoproterozoic supercontinent Rodinia. The ensuing Phanerozoic tectonic evolution of the Cordilleran orogen in the Great Basin included a series of contractional orogenies that thrust terranes comprised of basin facies onto slope and shelf facies and thickened the crust (Fig. 2; Dickinson 2006).

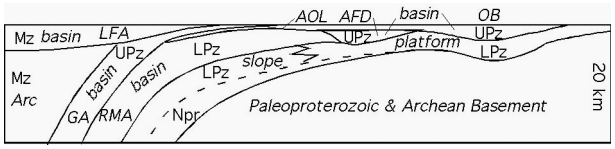


Figure 2. W-E section showing sedimentary rocks below the Great Basin gold province. LFA=Luning-Fencemaker allochthon, AOL=Antler overlap, AFD= Antler foredeep, OB=Oquirrh basin, GA=Golconda allochthon, RMA= Roberts Mountains allochthon. L=lower, U=upper, Pz=Palaeozoic, Mz=Mesozoic, Npr=Neoproterozoic.

Strata in basin, slope, and restricted shelf environments were frequently deposited under dysoxic, anoxic, or euxinic conditions as evidenced by their gray to black colour, preservation of carbon, high degree of pyritization of Fe, and low $Fe^{+3}/Fe^{+2}$. During global oceanic anoxic events in the Neoproterozoic, Cambrian, Ordovician, Devonian, Permian, and Late Triassic, carbonaceous rocks were deposited that have anomalous Au contents (Titley 1991).

## 3 GREAT BASIN GOLD SYSTEMS

The Great Basin physiographic province is the worlds 2nd leading gold producer and contains a succession of diverse gold-rich mineral deposits that constitute a "sulphide-gold suite".

Reduced sedimentary rocks are frequently observed at the deposit level or are portrayed on cross sections to underlie the deposits. While the source of water in the systems varies, the $\delta^{34}S$ of sulphides is often indicative of sedimentary S sources (Table 1).

| Name | Type+ | Ma | Au t | Fluid^ | $\delta^{34}S$ (ä) | Rock* |
|---|---|---|---|---|---|---|
| U Rodeo | Sedex | ~365 | 60 | Brine | **14**±4fw | LPz-Npr |
| BaldMtn | RIR-**DD** | 159 | 47-**19** | Mag | **18**±8 | LPz-Npr |
| Robinson | Por-**DD** | 112 | 145-**15** | MagMw | **0**±8 | Upz, Lpz |
| NW-NV | Oro | ~100 | 30 | Meta | **2**±2 | Mz, Pz |
| JerrittCyn | CT | 39 | 350 | Mw | **8**±4 | LPz-Npr |
| Meikle | CT | 39 | 220 | Mw | **10**±2 | LPz-Npr |
| BatMtn | Por-**DD** | 39 | 550-**250** | Mag-Mw | **3**+3-40 | UPz,LPz |
| BingCyn | Por-**DD** | 38 | 1570-**36** | Mag-Mw | **0**±3 | Upz, Lpz |
| RndMtn | LS | 26.5 | 358 | Mw | **12**±2 | LPz-Npr |
| BskNat | LS | 16.2 | 6 | Mw | **-7**±2 | Mz, UPz |
| MuleCyn | LS | 15.6 | 40 | Mw | **4**±5 | LPz-Npr |
| CroLew | LS | 4-2 | 28 | Mw | **-13**±2 | Mz, Upz |
| FlorCyn | LS | 2 | 52 | Mw | **4**+3-10 | Mz, UPz |
| DixCom | LS | <1 | 3 | Mw | **-5**±2 | Mz |

Table 1. Deposits of the "Sulphide Gold Suite".

+ Sedex= sedimentary exhalative, RIR= reduced intrusion related, Oro= orogenic, CT= Carlin-type, Por-**DD**=porphyry-distal disseminated, LS=low sulphidation epithermal. ^ Mag= magmatic water, Meta=metamorphic water, Mw=meteoric water. * Npr= Neoproterozoic miogeocline; LPz=Lower Paleozoic miogeocline, RMA; Upz= Upper Palaeozoic GA, AFD, and OB; Mz=FMA. See text for references on the deposits listed.

The upper zone of the Rodeo deposit, in the Carlin trend, is an end-member sedex gold deposit (Emsbo 2000). It formed during an episode of extension, near the shelf/slope break, where hot $H_2S$-bearing brine and petroleum vented into a restricted basin. The $\delta^{34}S$ of gold bearing-sulphides (14±4‰) in hydrothermal dolomite along footwall faults is consistent with thermal decomposition of S-bearing organic matter and petroleum, or TSR, which probably occurred at depth in the miogeocline where Au was likely scavenged.

Proximal stockwork through distal disseminated deposits around Mesozoic to Cenozoic porphyry intrusions contain ~ 2300 t Au. About 2000 t of this Au is in Eocene deposits. Depending on the degree of assimilation or interaction with reduced sedimentary rocks, normal oxidized arc magmas, and the hydrothermal fluids exsolved from porphyries, evolve to more reducing conditions and contain a greater proportion of sedimentary S. Reduced fluids preclude precipitation of significant anhydrite (*e.g.* Bald Mountain and Bingham Canyon, Table 1). At one extreme is the Jurassic Bald Mountain

reduced intrusion-related gold district on the southern extension of the Carlin trend (Nutt & Hofstra *in press*). Petrographic studies of the quartz monzonite porphyry indicate it evolved from an initial oxidized magnetite stable state to a reduced ilmenite stable state as it crystallized. Sulphides in all of the proximal to distal deposits are comprised of sedimentary S (18±8‰) derived from subjacent Cambrian and Neoproterozoic siliciclastics. At the other extreme, the enormous Eocene Bingham Canyon porphyry Cu-Mo-Au system has sulphide-saturated porphyries and reduced fluids, but magmatic S (0±3‰; Bowman *et al*. 1987). While there is no S isotopic evidence for significant assimilation of reduced sedimentary country rocks, they may have contributed to the reduced state of the system. There is clear evidence that magmatic fluids migrating upward through siliciclastic rocks evolved to higher sulphidation states (Inan & Einaudi 2002).

Distal disseminated (DD) deposits form from magmatic fluids discharged from cupolas into reduced sedimentary rocks and convecting meteoric waters. They occur in positions analogous to the pyritic halo of porphyry systems outward through locations where intermediate to low sulphidation veins typically occur in igneous host rocks. Although the $\delta^{34}S$ of sulphide minerals can be near 0‰ (*e.g*. DD at Bingham Canyon) or similar to those of sulphides in proximal deposits (*e.g*. DD at Bald Mountain), values often diverge to higher or lower values due to influx of sedimentary S (DD at Robinson) or low T oxidation and BSR as the systems wane *(e.g*. DD at Battle Mountain).

On the east side of the Sierra Nevada batholith in northwestern Nevada, Cretaceous plutonism and prograde metamophism of a thick stack of reduced basinal facies rocks (Table 1) resulted in the formation of a small belt of orogenic gold deposits along fissures that opened in a transpressional regime (Cheong *et al*. 2000). The volume of hydrothermal fluid generated from metamorphism may have been too small and the discharge points too widely distributed to form large deposits.

The unusual Palaeogene patterns of arc magmatism during slab rollback were accompanied by a pulse of Eocene extensional faulting and formation of enormous Carlin-type deposits with ~6000 t Au. The relative importance of magmatic vs. other fluids in these systems is controversial. While some ore bodies have $\delta^{34}S$ ( -1 to 7‰) that permit magmatic inputs, some of the larger and better studied deposits have high $\delta^{34}S$ values indicative of sedimentary S sources (Cline *et la*., 2005). In the Carlin trend, the most compelling evidence for sedimentary S comes from Meikle, the largest, high-grade deposit yet discovered, with ore comprised of up to 15% pyrite with % As, 1000's ppm Au, and $\delta^{34}S$ values of 10±2‰ (Emsbo *et al*. 2003). In the Jerritt Canyon district, similar pyrite in lower grade ore also has similar $\delta^{34}S$ values of 8±4‰. Regardless of whether gold was derived from magmas or leached from sedimentary rocks ± older gold deposits in mineral belts, the importance of reduced S in these systems derived from the Neoproterozoic-Devonian miogeocline is undeniable.

The ensuing Oligocene-Miocene ignimbrite flare-up produced a large number of calderas, but only a few volcanic-hosted epithermal deposits, such as Round Mountain, which is the country's largest low sulphidation deposit. It formed from dilute meteoric water and has S (12±2‰) derived from underlying Palaeozoic sedimentary rocks (Fifarek & Gerike 1991).

Neogene extensional tectonics and magmatism produced a plethora of epithermal deposits with ~1500 t Au. The high to low sulphidation deposits associated with the ancestral Cascades arc (*e.g*. Goldfield, Comstock) are centered on hydrous, oxidized, calc-alkalic volcano-plutonic complexes, exhibit clear evidence of magmatic inputs (water and S), and generally have Au/Ag < 0.1. Reduced sedimentary rocks were generally not involved. In contrast, the low sulphidation deposits coeval with Yellowstone hot spot magmatism generally have Au/Ag > 0.1 and occur near anhydrous, reduced, tholeiitic, bimodal, rhyolitic (*e.g*. Buckskin-National) and basaltic (*e.g.* Mule Canyon) volcanic centers. Such magmas discharge little water when they crystallize. Consequently, related low sulphidation deposits formed from convecting meteoric water that obtained S from underlying reduced sedimentary rocks (Table 1). The abundant Se in these systems also was likely derived from underlying carbonaceous rocks. Ivanhoe, in the Carlin trend, may have derived gold from older deposits. At Mule Canyon the $\delta^{34}S$ of hydrothermal pyrite in the ores (mean of 4‰, up to 11‰) is much higher than magmatic pyrrhotite in glassy basalts (mean of -1.8‰) suggesting S was derived primarily from sedimentary rocks (John *et al*., 2003). Buckskin-National is underlain by Mesozoic metasedimentary rocks and has $\delta^{34}S$

values of -7‰ indicative of a different sedimentary source of S (Vikre *in press*). While Au might have been introduced by $CO_2$-rich magmatic vapours or scavenged from sedimentary rocks, the reduced sedimentary S in convecting meteoric waters facilitated Au transport to the shallow sites of ore formation in overlying volcanic rocks.

The Great Basin also has a young group (<7 Ma) of low sulphidation gold deposits (Table 1) and active geothermal systems that are associated with north- to northeast-striking range front faults that accommodated differential translation along the Walker Lane. While isolated exposures of bimodal volcanic rocks can be present in neighboring areas (Florida Canyon, Crofoot Lewis), in others they are absent (Dixie-Comstock). Convection of meteoric water through reduced Mesozoic sedimentary rocks is evident in these systems by their setting, $\delta^{34}S$ values (Table 1), and high Se contents (Vikre 1994, *in press*; Ebert & Rye 1997; Fifarek & Hofstra unpublished data).

## 4 CONCLUSIONS & IMPLICATIONS

Together with the sedimentary source of S, the abundance of gold deposits of different types and ages in areas underlain by reduced marine sedimentary rocks suggests that convergent chemical evolution of basinal, metamorphic, magmatic, and meteoric fluids to $H_2S$-rich compositions via fluid rock reactions was critical to Au transport and formation of the Great Basin gold province. The succession of gold deposit types in mineral belts, such as the Carlin trend, underlain by reactivated crustal structures demonstrates the interplay between convergent evolution and structural inheritance, creating a situation where gold in older deposits may be cycled into younger ones (Emsbo *et al*. 2003, 2006).

The Yangtze craton in Southern China has a similar Phanerozoic tectonic history, thick sequences of reduced sedimentary rocks, and a similar suite of sulphide gold deposits (Hofstra *et al*. 2005). In analogous settings around the world (*e.g*. Tien Shan, Lachlan, Northern Appalachian orogens), such convergent evolution may be the unidentified crustal process that Titley (1991) proposed must exist to explain the empirical correlation between varied gold deposits and reduced Phanerozoic passive margin sequences with complex histories.

## REFERENCES


Bowman JR, Parry WT, Kropp WP, Kruer SA (1987) Chemical & isotopic evolution of hydrothermal solutions at Bingham, Utah. *Economic Geology* 82: 395-428

Cheong S, Peters SG, Iriondo A (2000) Summary of structural setting and fluid characteristics of low-sulfide Au-quartz veins in northwestern Nevada. *Geological Society of Nevada Symposium Proceedings:* 473-506

Cline JS, Hofstra AH, Muntean JL, Tosdal RM and Hickey KA (2005) Carlin-type gold deposits in Nevada. *Economic Geology 100th Anniversary Vol*: 451-484

Dickinson WR (2006) Geotectonic evolution of the Great Basin. *Geosphere* 2: 353–368

Ebert SW, Rye RO (1997) Secondary precious metal enrichment by steam-heated fluids in the Crofoot-Lewis hot spring deposit. *Economic Geology* 92:: 578-600

Emsbo P (2000) Gold in sedex deposits. Reviews in *Economic Geology* 13: 427-437

Emsbo P, Hofstra AH, Lauha EA, Griffin GL, and Hutchinson RW (2003) Origin of high grade gold ore and genesis of Meikle and neighboring Carlin-type deposits, Nevada. *Economic Geology* 98: 1069-1106

Emsbo P, Groves DI, Hofstra AH, Bierlein, FP (2006) The giant Carlin gold province: A protracted interplay of orogenic, basinal, and hydrothermal processes above a lithospheric boundary. *Mineralium Deposita* 41: 517–525

Fifarek RH, Gerike GN (1991) Oxidation of hydrothermal sulfides at Round Mtn., Nevada. *Geology and Ore Deposits of the Great Basin Sym Proc*: pp 1111-1121

Heinrich CA (2004) The physical and chemical evolution of low salinity magmatic fluids at the porphyry-epithermal transition. *Mineralium Deposita* 39: 864-889

Hofstra AH, Emsbo P, Hu R, Zhang X, Su W, Nutt CJ, and Fifarek RH (2005) Diverse origins of disseminated gold deposits in the Great Basin and China. *Geological Society of Nevada Symposium*: 1315–1316

Inan EE, Einaudi, MT (2002) Nukundamite-bearing Cu ore in the Bingham porphyry deposit, Utah; result of upflow through quartzite. *Economic Geology* 97: 499-515

John DA, Hofstra AH, Fleck RJ, Saderholm EC, Brummer JE (2003) Geologic Setting and Genesis of the Mule Canyon Low-Sulfidation Epithermal Gold-Silver Deposits, Nevada. *Economic Geology* 98: 425-464

Nutt CJ, Hofstra AH (in press), Bald Mtn., Nevada: A reduced intrusion-related Au district. *Economic Geology*

Titley SR (1991) Phanerozoic ocean cycles and sedimentary-rock hosted gold ores. *Geology* 19: 645-648

Vikre PG (1994) Gold mineralization and fault evolution at the Dixie Comstock Mine, Nevada. *Economic Geology* 89: 707-719

Vikre G (in press) Sinter-vein correlations at Buckskin Mountain National district, Nevada. *Econ Geol.*

# Transport of Au in petroleum: Evidence from the northern Carlin trend, Nevada

P. Emsbo & A.E. Koenig
*United States Geological Survey, Denver, Colorado USA*

ABSTRACT: Laser ablation ICP-MS analyses reveal that bitumen in the Upper Zone of the Rodeo deposit contains up to 100 ppm Au, 0.7%V, and *ca.* 0.1% (Ni, As, Hg, Cu). This represents a previously unrecognized type of Au mineralization in the world's third largest Au producing district. Recent studies of the Rodeo deposit have shown that the deposit contains both Devonian sedimentary exhalative (Sedex) Au and Eocene Carlin type mineralization. Sedex Au ore with up to 68 g/t Au is stratabound in the Devonian Upper Mud Member (UM) of the Popovich Fm. The UM is a carbonaceous mudstone that regionally contains 5-15% TOC. Burial diagenesis with emplacement of the Roberts Mountain Allochthon in early Mississippian time caused these carbonaceous ores to generate petroleum. Petroleum, now bitumen, occurs as veins that cut the Sedex mineralization. Laser ablation ICP-MS line scans across bitumen grains reveal two distributions of gold. A homogeneous signal suggests that gold and related elements are chemically bound in the bitumen. Some samples display a heterogeneous Au signal with discreet Au spikes indicating, as observed petrographically, micro-inclusions of native Au. Bitumen occasionally contains grains of cinnabar, pyrite, base metal sulphides, and native Au (<1 um). Gold and related trace elements show no enrichment on outer margins of bitumen grains. This along with (1) the distinct chemical signature, (2) paragenetic relationships that constrain Au-rich bitumen to a Mississippian age, (3) the absence of hydrothermal alteration, and (4) the lack of Au in bitumen from high-grade Carlin ore outside the Sedex Au horizon all suggests that metal enrichments are not the result of Carlin hydrothermal fluids. Together these relationships suggest that Au and associated metals were remobilized and transported from Sedex mineralization in petroleum as organo-metallic compounds during oil generation and migration. The Au concentration in bitumen in rocks containing up to 15 % TOC suggest that substantial amounts of Sedex Au were remobilized during petroleum formation/migration and that a proportion of the Au mined from the Rodeo resides in bitumen. These observations demonstrate a new environment and mechanism of Au transport with significant implications for Au metallogeny.

KEYWORDS: bitumen, gold, petroleum, Sedex Au, Nevada

## 1 INTRODUCTION

Carlin-type deposits in north-central Nevada have become the third largest Au-producing district in the world. The Rodeo deposit is located on the northern Carlin trend. The deposit contains two mineralized stratigraphic horizons. Extensive geologic, petrographic, geochemical, isotopic, and geochronologic study of the Upper Zone has identified two types mineralization. Locally the deposit contains mineralization with all the alteration and geochemical, and isotopic characteristics of "classic" Carlin-type mineralization. The second, and dominant, ore-type is stratabound in the Devonian Upper Mud Member (UM) of the Popovich Formation (Figure 1) and exhibits none of the geologic or geochemical characteristics of Carlin-type ore. This newly recognized ore-type has been established to be sedimentary exhalative (Sedex) in origin (Emsbo *et al.* 1999; Emsbo 2000).

The goal of this paper is to present evidence that bitumen in Rodeo contains highly anomalous Au along with V, Ni, Mo, Zn, and As and that these elements were remobilized from sedex mineralization by organo-metallic compounds during petroleum generation and migration with emplacement of the Lower Mississippian Roberts Mountains Allocthon.

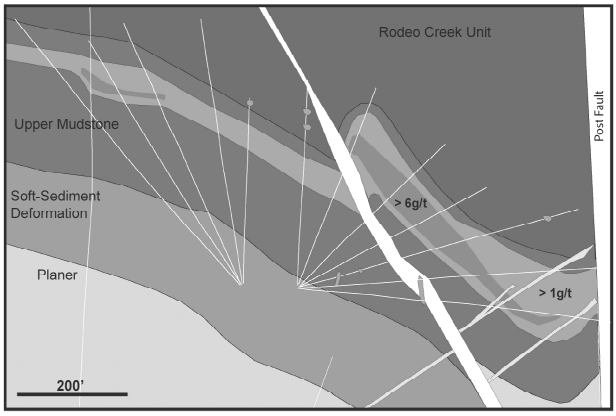


Figure 1. Cross section showing the distribution of gold grades in stratiform Sedex ore horizon of Rodeo

## 2 DEVONIAN SEDEX GOLD MINERALIZATION

The Upper Zone of the Rodeo deposit contains *ca.* 2 million oz Au most of which is sedimentary exhalative (Sedex) gold mineralization with grades as high as 68 g/t Au in the UM. Detailed chemostratigraphic and isotopic study of drill core from an area > 30 km$^2$ of the northern Carlin trend shows that the ore horizon in the Upper Mud Member contains 0.2 - 3.0 ppm Au (and highly elevated abundances of other ore related elements) and is systematically zoned around the Rodeo deposit. The UM is a carbonaceous mudstone (15% total organic C) with pyrite laminations that contain sphalerite, barite, tetrahedrite, chalcopyrite, and gold and isolated lenses of bedded barite and massive sulphide. Grains of native gold (<1 mm) are disseminated in mudstone and occur as inclusions in barite and base metal sulphides. Base metal sulphides and syn- to diagenetic pyrite also contain high concentrations of Au (10's to 1000's ppm). Gold has a strong positively correlation ($r^2 > 0.6$) with Zn, V, Cd, Cu, Se, Ni, Hg, and Mo. This ore type is interpreted to be Sedex because; 1) it predates compaction and lithification of its host rocks; 2) the ore horizon is stratiform, highly anomalous in ore metals and systematically zoned around the deposit over 30 km$^2$, and metal anomalous > 70 km from Rodeo; 3) barite exhibits $\delta^{34}S$ and $\delta^{18}O$ values identical to other Sedex barite deposits in NV; 4) ore sulphides contain biogenic $\delta^{34}S$ (-20 to –10‰); 5) synsedimentary debris flows terminate mineralized beds; 6) synsedimentary faulting during mineralization, as is characteristic of Sedex basins; and 7) the absence of alteration and $\delta^{13}C$ and $\delta^{18}O$ isotopic shifts of primary carbonate minerals and the presence Au inclusions in base metal sulphides in ore-grade rocks is strong evidence that Au was not introduced by the younger Carlin-type system.

## 3 AGE CONSTRAINTS ON PETROLEUM MIGRATION

A complex diagenetic history is apparent in the carbonaceous and calcareous mudstones of the UM that includes early diagenetic pyrite and barite, several ages of cross-cutting quartz veins, migration of petroleum, dolomite veins, and stylolites, all of which are cut by Late Jurassic dykes. Of the different quartz veinlets, the most distinctive are those that contain grains of bitumen intergrown with quartz and/or calcite. These veinlets, typically less than 5 mm thick, cut at least three older sets of thin, quartz-filled fractures. Bitumen grains up to >100 mm in diameter, form a good clear polished surface, are slightly anisotropic, and contain syneresis cracks and occasionally contain micron inclusions of vanadium-rich mica. Bitumen grains also occasionally contain fine, randomly oriented inclusions that are up to 2 mm long and <0.3 mm wide in bitumen that contains no fractures, disruptions, or alteration. Bitumen veinlets are commonly perpendicular, but sometimes oblique to bedding. They are best developed in argillites and cherts, and commonly pinch out in more calcareous beds. Quartz textures are variable, ranging from intergrown granular to fibrous grains exhibiting syntaxial and composite growth structures that indicate growth during formation of dilatent fractures. Fibrous textures are typically parallel to bedding and exhibit little curvature, indicating relatively constant stress during growth. Bitumen veins are commonly cut by quartz veins with a distinctive high content of gas-rich fluid inclusions which in turn, are cut by very thin quartz-filled fractures. Bitumen also fills intergranular porosity and surrounds grains of pre-diagenetic dolomite, pyrite, Au, and base metal sulphides. Pores lined by bitumen are commonly been compressed parallel to bedding planes.

Minerals of the above paragenetic sequence are cut by bedding parallel, anastomosing stylolites that contain abundant insoluble residues derived from surrounding rock, including tattered and disrupted grains of bitumen, pyrite and subordinate amounts of sphalerite, tetra-

hedrite, chalcopyrite, and grains of native gold. Where cut by the stylolites, the margins of quartz veins are clearly offset and bitumen grains are clearly disrupted and concentrated in the stylolites. These latter are, in turn, cut by thin veinlets of dolomite containing a distinct, whitish yellow, pyrite-free sphalerite.

Late Jurassic intrusive rocks are important because of their well-constrained ages (Emsbo *et al.* 1999; Ressel *et al.* 2000) and because they clearly cut the entire above paragenetic sequence. Moreover, laser raman analysis has demonstrated increasing bitumen crystallinity toward the Jurassic Goldstrike stock. Considering these age constraints and that petroleum migration occurred prior to maximum burial, the most likely time of petroleum generation was during emplacement of the Roberts Mountains Allocthon in Lower Mississippian time. Importantly, the Jurassic dykes are significantly older than Eocene Carlin-type mineralization so that hydrothermal mineralization cut by these dykes clearly cannot be part of the latter.

## 4 BITUMEN CHEMISTRY

Trace element concentrations of bitumen were determined using laser ablation ICP-MS (LA-ICP-MS). A CETAC LSX-500 LA system (266 nm) coupled to a PerkinElmer ELAN6000 ICP-MS. Signals were calibrated using a prototype USGS microanalytical organic reference material (Wilson *et al.*, in prep.). The reference material is a synthetic organic matrix doped with trace elements of interest. The reference material was analyzed 5 times at the beginning of the analytical session and monitored throughout the session for drift. Concentrations were determined using off-line calculations following the protocol of Longerich *et al*. (1996). Signals were screened for heterogeneities such as micro-inclusions or zoning.

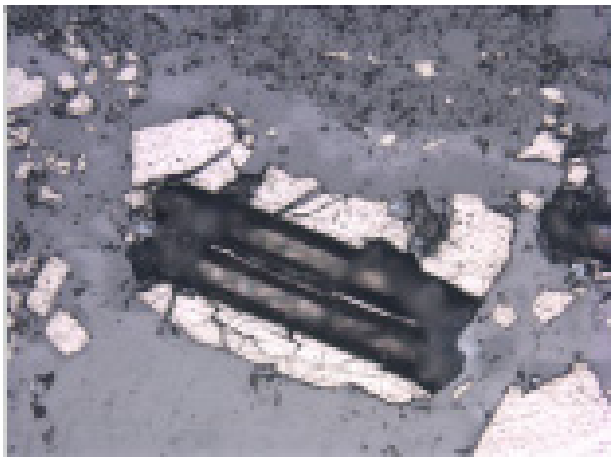

Figure 2. Laser ablation trace (25 um-wide) across a bitumen grain in a bitumen-quartz vein cutting Rodeo Sedex ore.

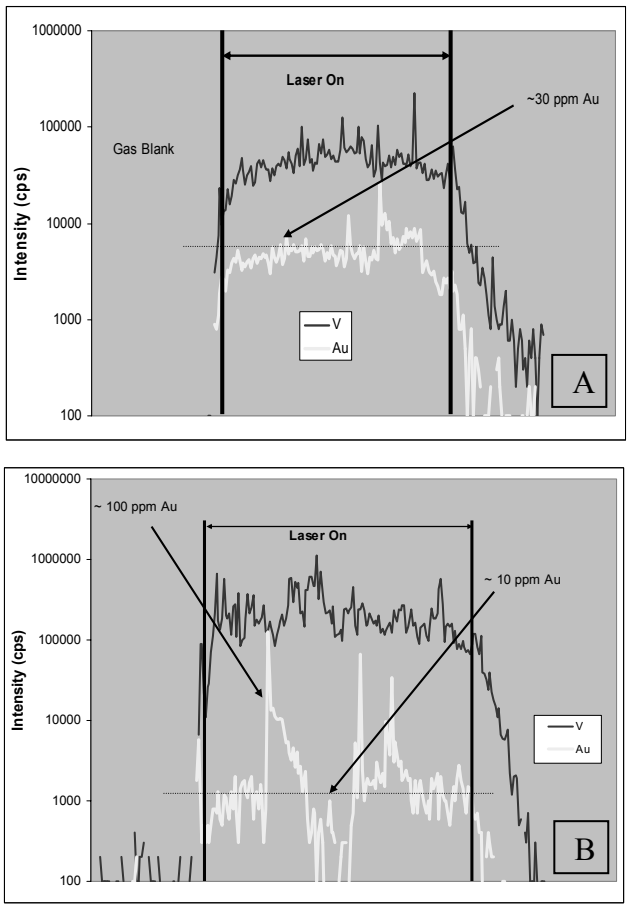


Figure 3. Laser ablation data for Au and V from two bitumen in high-grade Rodeo ore samples with calculated Au gold concentrations on the graph. A) shows a fairly homogenous profile. B). discreet spikes suggest micro-inclusions of native gold.

Laser line analyses across most grains (Figure 2) reveal relatively homogenous distributions of trace elements in most grains (Fig. 3 a) with concentration up to 100 ppm Au, 1% V, 0.5% Zn and As, and ~ 0.1 to 0.2 % Ni and Mo, and Hg and Se between 100 and 1000 ppm. The lack of core to rim zoning within grains and homogeneous line traces in these samples suggest that these metals are chemically bound in the bitumen. However, several samples revealed heterogeneous values for Au (Fig. 3b) and Hg suggesting these metals occasionally occur as included mineral phases which could be verified by submicron inclusions of native Au and cinnabar in the bitumen.

It is noteworthy that analyses of bitumen from high-grade, Carlin-type ore stratigraphically below the Upper Mud Member in the Meikle mine, despite being surrounded by pyrite with ~3000 ppm Au, contains below detec-

tion Au. This is consistent with a thorough evaluation of Carlin deposits that revealed no correlation between ore grade and carbon in the host rock (Hofstra & Cline 2000) and chemical modeling that shows that Au in a reduced, $H_2S$-rich, Carlin-type fluid is not likely to precipitate from its interaction with organic carbon (Hofstra & Cline 2000).

## 5 CONCLUSION

(1) Petroleum generation and migration on the northern Carlin-trend (including carbonaceous Sedex ores in Rodeo) occurred in lower-Mississippian time with emplacement of the Roberts Mountains Allocthon.

(2) Bitumen contains homogenous enrichments (as high as 100 ppm) that correlate with V (~1%), Ni, Hg, As, and Se. Some bitumen also contains evenly distributed micron-inclusions of native Au.

(3) The homogenous distribution Au and related trace elements in bitumen grains without enrichment on outer margins imply that Au and other elements were not introduced after bitumen formation.

(4) The distinct chemical signature and absence of hydrothermal alteration of the rock and bitumen show that metal enrichments are not the result of Carlin-related hydrothermal fluids. This is further supported by the absence of Au in bitumen from high-grade Carlin ore outside the Upper Mudstone.

(5) Together these relationships suggest that Au and associated metals were remobilized and transported from Sedex mineralization in petroleum as organo-metallic compounds during oil generation and migration.

(6) The Au concentration in bitumen in rocks containing up to 15 % TOC demonstrates that substantial amounts of Sedex Au was remobilized during petroleum formation and that a significant proportion of the Au mined from the Rodeo resides in bitumen.

(7) These observations demonstrate a new environment and mechanism of Au transport with significant implications for Au metallogeny.

## REFERENCES


Emsbo P (2000) Gold in sedex deposits. Gold in 2000, *Reviews in Economic Geology* 13, pp 427-437

Emsbo P, Hutchinson RW, Hofstra AH, Volk JA, Bettles, KH, Baschuk GJ, Johnson, CA (1999) Syngenetic Au on the Carlin Trend; implications for Carlin-type deposits. *Geology* 27: pp 59-62

Hofstra AH, Cline JS (2000) Characteristics and models for Carlin-type gold deposits, Chapter 5. In: Hagemann SG, Brown PE (eds) Gold In 2000, *Reviews in Economic Geology* 13, pp163-220

Longerich HP, Jackson, SE, Günther D (1996) Laser ablation-inductively coupled plasma-mass spectrometric transient signal data acquisition and analyte concentration calculation. *J. Analytical Atomic Spectrometry* 11: 899-904

Ressel MW, Noble DC, Henry CD (2000) Dike-hosted ores of the Beast deposit and the importance of Eocene magmatism in gold mineralization of the Carlin trend. *Economic Geology* 95: 1417-1444

# Gold Deposits in the Avalonian Tectonic zone of the Southeastern United States

N.K. Foley, R.A. Ayuso & R.R. Seal, II,
*Mailstop 954 National Center U.S. Geological Survey, Reston, Virginia 20192*

ABSTRACT: Gold- and iron sulphide-bearing deposits of the southeastern United States have distinctive mineralogical and geochemical features that provide a basis to construct models of ore genesis that may be used in the assessment of gold resources. The largest known gold deposits of the region, including subvolcanic quartz porphyry, volcanic-sedimentary rock-hosted, and shear-zone-hosted styles of gold mineralization, are primarily hosted by rocks that share a geologic affinity to the classic Avalonian tectonic zone.

KEYWORDS: gold, pyrite, volcanogenic, genesis, Avalonia

## 1. INTRODUCTION

Gold deposits of the Avalonian tectonic zone, which extends from southeastern United States northward to Maritime Canada, emphasize the im portance of this zone as highly prospective for Au ore of many types (Huard & O'Driscoll 1986; Dubé *et al*. 1998; O'Brien *et al*. 1998, 2001; Ayuso *et al*. 2005). The Carolina slate belt, a part of the Carolina zone (Secor *et al*. 1983; Butler & Secor 1991; Hibbard & Samson 1995), which shares a geologic affinity to the Avalonian tectonic zone (Williams & Hatcher, 1982), extends from Georgia into Virginia and consists of a sequence of late Proterozoic to early Palaeozoic metaigneous and metasedimentary rocks (Fig. 1).

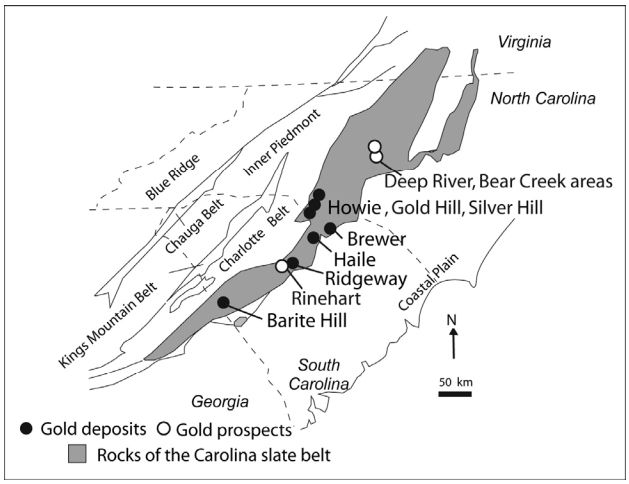


Figure 1. Location map showing rocks of the Carolina slate belt and gold deposits and prospects cited in text.

Gold deposits occur stratigraphically between sequences of late Precambrian to Cambrian orogenic metavolcanic rocks and an overlying sequence of volcaniclastic and epiclastic rocks (Worthington & Kiff 1970). The change in rock type may be a result of the transition from an arc-related subaerial constructional phase to a rift-dominated, ring-fracture collapse of the arc below sea level (Feiss & Vance 1995). In North Carolina, gold deposits occur in the Albemarle basin sequence of late Proterozoic-early Palaeozoic age, a thick stack of mudstone and siltstone with felsic to intermediate volcanic layers. They cluster along the base of the Albemarle sequence, just above a rhyolite unit, and in shear zones. Rocks in shear zones are mostly mudstone or siltstone, with lenses of rhyolitic or andesitic rocks. In South Carolina, gold deposits also occur near the top of a rhyolite that is beneath rocks equivalent to parts of the Albemarle basin sequence.

In the southeast United States, the Carolina slate belt hosts over 400 gold prospects and several large-tonnage low-grade pyrite-rich Au deposits (Feiss & Slack 1989), including the

Neoproterozoic (Ayuso *et al.* 2005) Barite Hill, Brewer, Haile, and Ridgeway deposits (Fig. 1). The Howie mine, another historic producer, is located along strike with the Gold Hill shear zone. Recent exploration efforts have identified new areas having potential for significant tonnages from shallowly emplaced porphyry style (Deep River) and related volcanic-sedimentary style (Rinehart, Bear Creek) deposits (*Erin Ventures 2007, Gold Summit Corporation 2006*). We present here new data for Howie, Barite Hill, Ridgeway, and Brewer and provide a brief analysis of mineralization styles and models.

## 2 MINERALOGY

Howie, Gold Hill, and Silver Hill mines comprise a group of historic gold producers that occur within the Gold Hill shear zone. Gold Hill and Silver Hill are interpreted as sheared and deformed volcanogenic massive sulphide deposits (Feiss & Slack 1989), like Barite Hill. All three were significantly affected by regional deformation. Howie is hosted by a mixture of laminated mudstone and felsic volcanic to volcaniclastic layers. Pyrrhotite constitutes 95% of the total sulphide content of ore lenses. Pyrite, sphalerite, chalcopyrite, galena, arsenopyrite, and Pb-telluride minerals are admixed with quartz, K-feldspar, calcite, and chlorite. Ore minerals include electrum, Ag-sulphide, and Ag-telluride minerals. Ion microprobe data show that pyrite contains a trace element suite similar that of Haile pyrite: Au, Hg, As, Se, Te, Pb, and Zn. Fluid inclusion thermometry data indicate minor $CO_2$ and temperatures of 200-300°C consistent with greenschist facies overprint.

Mineralized zones of the Brewer deposit occur within metamorphosed crystal tuffs, volcaniclastic rocks, and siltstones. The high-sulphidation epithermal-style Au occurs in breccias associated with subvolcanic quartz porphyry that intruded rhyodacite to rhyolitic flows and tuffs (Zwaschka & Scheetz 1995). Leaching produced advanced argillic, sericitic, and propylitic hydrothermal alteration zones. Pyrophyllite, andalusite, and kyanite, together with kaolinite and sericite are commonly found in association with the plutonic rocks. Gold is related to the quartz porphyry breccia, particularly with heterolithic crystal tuff breccias in the argillic alteration zone (quartz, andalusite, pyrite, alunite, dickite, topaz, rutile). The main host is andalusite-quartz breccia, although significant Au occurs in a massive sulphide gossan. Fluid inclusion data indicate two coeval high-temperature assemblages: chalcopyrite-pyrite and pyrite-enargite-covellite-electrum. A later lower temperature assemblage consists of electrum-Fe oxides-alunite ±jarosite.

The Ridgeway deposits occur in a basinal setting within metamorphosed crystal tuffs, volcaniclastic rocks, and siltstones near a faulted contact with overlying epiclastic rocks (Gillon *et al*. 1998). Gold contents are highest in the central potassic and silicic alteration zones that developed in thinly bedded turbidites. The main gold-bearing layers are chert that contains disseminated pyrite, electrum, Au-telluride, and molybdenite. Early pyrite-bearing, silicified layers are deformed. Pyrite also occurs as metacrysts enclosing inclusions of sphalerite, arsenopyrite, chalcopyrite, galena, rutile, REE-bearing phosphate, Ag-telluride minerals, and as sediment grains in graded beds. Detailed microprobe analysis of replaced pumice, rimmed volcaniclasts, and colloform structures point to coeval deposition of Au, As-pyrite, and related sulphide minerals with felsic tuffs and volcaniclastic rocks.

## 3 DEPOSIT MODELS

Current models for the Barite Hill, Brewer, Haile, and Ridgeway deposits are syngenetic, relating mineralization to volcanic and volcaniclastic processes active when the host rocks formed, and present long before deformation events. These deposits, like Howie, are all metamorphosed, with some alteration products and mobilization of gold clearly associated with deformation.

Howie and other deposits of the Gold Hill fault zone bear the imprint of deformation and recrystallization typically associated with shear zone-hosted Au deposits. The sequence of mobilization events, however, does not require that mineralization originated coeval with deformation. The presence of inclusions of altered rock in pre-deformation dykes indicates alteration took place well before the shear event. Silicification is widespread, but cleavage of early bedding persists suggesting that the rock was already silicified. Deformation simply redistributed silica on a local scale. Deformation likely was focused and intensified at deposits because of a ductility contrast offered by pre-existing altered, mineralized ground. The

deformation concentrated fluids and remobilized sulphides, Au, Si, and K derived, perhaps, from a basinal setting, such as at Ridgeway.

Gold ores at Ridgeway represent the disseminated shallow water, submerged tuffaceous equivalents of intrusion-related high-sulfidation ores such as those deposited at Brewer. Haile also has petrographic and mineralogical features that support a stockwork disseminated model of pyrite Au-sericite mineralization where a significant portion of the ore was also deposited in sediments at or very near the surface (Foley *et al.* 2001). Individually these deposits represent distinct components of large intrusion-centered hydrothermal systems consisting of clusters of base-metal-Au deposits (*e.g.* Barite Hill, Clark *et al*. 2000; Seal *et al.* 2001) and more extensive, disseminated gold-bearing pyrite bodies (*e.g*. Ridgeway) localized in basins distributed around the subvolcanic quartz porphyry-related gold deposits (*e.g*., Brewer).

## 4 GEOCHEMISTRY

Regional contrasts in Pb isotope compositions also distinguish the deposits. Sulphides from Barite Hill ($^{206}Pb/^{204}Pb<18.077$) are less radiogenic than from Ridgeway ($^{206}Pb/^{204}Pb>18.169$), Haile ($^{206}Pb/^{204}Pb>18.233$), and Brewer ($^{206}Pb/^{204}Pb>18.311$). Diversity in values of $^{206}Pb/^{204}Pb$ and the relatively high values of $^{207}Pb/^{204}Pb$ suggest that the deposits evolved adjacent to or closely related to continental blocks, likely linked to a back-arc tectonic setting. Mantle-derived isotopic contributions were more important at Barite Hill, the least radiogenic of the deposits, than at Brewer, Haile, and Ridgeway, which developed in thinned continental crust. Neodymium isotope compositions also show differences that help to explain the metallogenic contrasts among the deposits. Barite Hill ($\varepsilon_{Nd554} \sim +7$ to -1; crustal residence ~0.7-1.2 Ga), the closest analogue to a classical volcanogenic massive sulphide, has the highest mantle-derived contribution. Ridgeway, representing the largest Neoproterozoic gold deposit in the region, has the highest crustal contribution ($\varepsilon_{Nd554} \sim +5$ to -5, crustal residence ~0.7-1.9 Ga). Brewer ($\varepsilon_{Nd554} \sim +3$ to +0.5, crustal residence ~0.8-1.5 Ga) and Haile ($\varepsilon_{Nd554} \sim +3$ to -0.5, crustal residence ~0.8-1.5 Ga) are relatively homogeneous, nearly identical, and consistent with a common origin closely related to a magmatic system. Howie includes juvenile to crustal material ($\varepsilon_{Nd554} \sim +1$ to -3, crustal residence ~1.0-1.6 Ga).

## 5 PALAEOGRAPHIC CORRELATIONS

The Avalonian and various other terranes (*e.g.* Cadomia, West Avalonia, East Avalonia) were peripheral to Gondwana during the late Proterozoic to early Ordovician. Correlations among peri-Gondwanan terranes and adjacent cratonal blocks (Baltica, Amazonian, and West African) remain controversial, but many studies suggest that they were located along the northern flank of present-day South America and northwestern Africa (Nance & Murphy 1996; Murphy *et al.* 1999). Exact metallogenic or isotopic analogues to these gold deposits have not yet been recognized in South America or in other peri-Gondwanan cratonal blocks. Pb isotope compositions of Avalonian rocks in the northern Appalachians and new data for the gold deposits and Persimmon Fork Formation in the Carolina terrane do support a broad correlation with South American basements (Ayuso *et al*. 2005).

## 6 SUMMARY

Exploration strategies applied to eastern North America benefit from using subvolcanic and basinal models for syngenetic gold mineralization in the Avalonian tectonic zone. In the southeast United States, areas of Avalonian basement covered by coastal plain sediments may also contain significant gold resources.

## ACKNOWLEDGEMENTS

We thank J. Scheetz and M. Zwaschka (Brewer Gold), T. Kilbey and J. Maddry (AMAX Gold, Piedmont Mining), L. Mitchell and K. Gillon (Kennecott Ridgeway Mining Co.), and D. LaPoint for providing support and access at the mines. We thank Jeff Doebrich and Suzanne Nicholson for thoughtful reviews.

## REFERENCES

Ayuso RA, Wooden, JL, Foley NK, Seal RR, II, Sinha AK (2005) U-Pb zircon ages and Pb isotopic geochemistry of gold deposits in the Carolina Slate Belt of South Carolina. *Econ Geol* 100: 225-252.

Butler JR, Secor DT (1991) The Central Piedmont: *Carolina Geological Society Fiftieth Anniversary Volume*, pp 59–78.

Clark SHB, Gray KJ, Back JM (2000) Geology of the Barite Hill gold-silver deposit in the southern

Carolina slate belt. *Econ Geol* 94: 1329–1346.

Dubè B, Dunning G, Lauziere K (1998) Geology of the Hope Brook mine, Newfoundland, Canada: A preserved Late Proterozoic high-sulfidation epithermal gold deposit and its implications for exploration. *Econ Geol* 93: 405–436.

Erin Ventures (2007) On-line press release dated January 22, 2007.

Feiss G, Slack JF (1989) Mineral deposits of the U.S. Appalachians. Geological Society of America, *Geology of North America,* F-2, pp 471–494.

Feiss PG, Vance RK (1995) The Carolina terrane gold district: Rift-related volcanogenic gold deposits of the southern Appalachian Piedmont [abs]. *Geol*

O'Brien SJ, Dube, B; O'Driscoll CF (2001) Epithermal-style hydrothermal systems in Late Neoproterozoic Avalonian rocks on the Avalon peninsula, Newfoundland: Implications for gold exploration. *GAC-MAC, Field trip guidebook* A6, pp 1-29.

Seal RR II, Ayuso RA, Foley NK, Clark SHB (2001) Sulfur and lead isotope geochemistry of hypogene mineralization at the Barite Hill gold deposit, Carolina slate belt, southeastern United States: A window into and through regional metamorphism. *Min Dep* 36: 137–148.

Secor DT, Samson S, Snoke A, Palmer, P (1983) Confirmation of the Carolina slate belt as an exotic terrane. *Science* 221: 649–651.

Williams H, Hatcher, RD (1982) Suspect terranes and accretionary history of the Appalachian orogen. *Geology* 10: 530–536.

Worthington JE, Kiff IT (1970) A suggested volcanogenic origin for certain gold deposits in the slate belt of the Carolina piedmont. *Econ Geol* 65: 529–537.

Zwaschka M, Scheetz, JW (1995) Detailed mine geology of the Brewer gold mine, Jefferson County, South Carolina. *Society of Economic Geologists Guidebook Series* 24, pp 95–146.

*Soc Am Abst Prog* 27, p 27 Gold Summit Corporation (2006) On-line press releases dated July 19, 2006, December 12, 2007.

Hibbard JP, Samson SD (1995) Orogenesis exotic to the Iapetan cycle in the southern Appalachians. *Geol Assoc Can Spec Paper* 41, pp 191–205.

Huard A, O'Driscoll CF (1986) Epithermal mineralization in Late Precambrian volcanic rocks of the Burin peninsula. *Current Research, Newfoundland Department of Mines, Energy, Mineral Development Division Report* 86-1, pp 65–78.

# Devonian polymetallic orogenic quartz vein deposits of the Sierras Pampeanas, Argentina: microstructures and isotopes

D. Mutti, C. Méndez & A. Di Marco
*Departament of Geology, University of Buenos Aires, Argentina*

ABSTRACT: New field work in selected districts led to recognition of the spatial and temporal relationship between deformation and recrystallization of blue gray quartz, gold, sulphide minerals (pyrite, galena, chalcopyrite, sphalerite) and sulphosalts. Isotope data suggest metals and sulphide were derived from homogenized crust with an igneous input.

KEYWORDS: Sierras Pampeanas, collisional belt, sulphide-gold assemblage, quartz vein system

## 1 INTRODUCTION

Three types of Devonian polymetallic quartz-vein mineralization are distinguished in the Neoproterozoic-Palaeozoic Sierras Pampeanas metamorphic fold belt: 1) Au ± Cu, 2) W ± Bi, Mo, Cu, Au, and 3) Ag, Pb, Zn ± Au (Fig. 1). They have been attributed to a hybrid style of mineralization with characteristics of both orogenic and intrusion-related systems (Skirrow *et al.* 2000). The mineralization was worked intermittently. Ore zones with resources ranging up to 60,000 oz of gold are estimated.

Our studies indicate that gold particles are usually associated with a late base metal-sulphide stage. Most particles are "invisible" in < 40 μm thick overgrowths on pyrite; visible inclusions are uncommon (Fig. 2a). In zones of weathering, the primary sulphides were replaced by supergene minerals that contain "visible" gold flakes (< 500μm) (Fig. 2b).

As quartz is typically the dominant phase deposited throughout vein growth, its form reflects changing conditions during vein growth, including those extant during precipitation of the late sulphide-gold assemblage.

This paper shows that microstructures in late quartz sulphide-gold veins of the Sierras Pampeanas formed in a tensional regime. Possible metal and sulphide sources during one stage of gold deposition are also identified.

## 2 GEOLOGICAL SETTING

The Sierras Pampeanas in central-west Argentina display the main events of the pre-Carboniferous geological evolution of the SW margin of Gondwana. The evolution of the eastern region, from the Neoproterozoic to the Early Carboniferous, is the result of three main orogenic cycles; Pampean, Famatinian, and Achalian.

The Pampean cycle began with passive margin (660-560Ma ago) sedimentation with interbedded E-MORB basalt, which evolved into an active margin with development of penetrative deformation, regional metamorphism of upper amphibolite-lower granulite facies and generation of an Andean-type magmatic arc 533-528 Ma ago. It concluded about 523 Ma ago with orthogonal-style collision, resulting in significant crustal thickening, anatexis and generation of S-type granites as the Pampean terrane or microcontinent was incorporated into the Río de la Plata Craton.

The Famatinian cycle began 499 Ma ago and is characterized by metamorphism of amphibolite facies and compositionally zoned magmatism, with I-type granodiorites and large S-type granite batholiths. This cycle is ascribed to oblique collision of the preCordillera terrane with the Gondwana margin. During the late Ordovician, the Cambrian basement and continental margin magmatic arc underwent E-W, non-coaxial compressive deformation at regional greenschist facies metamorphic conditions. In

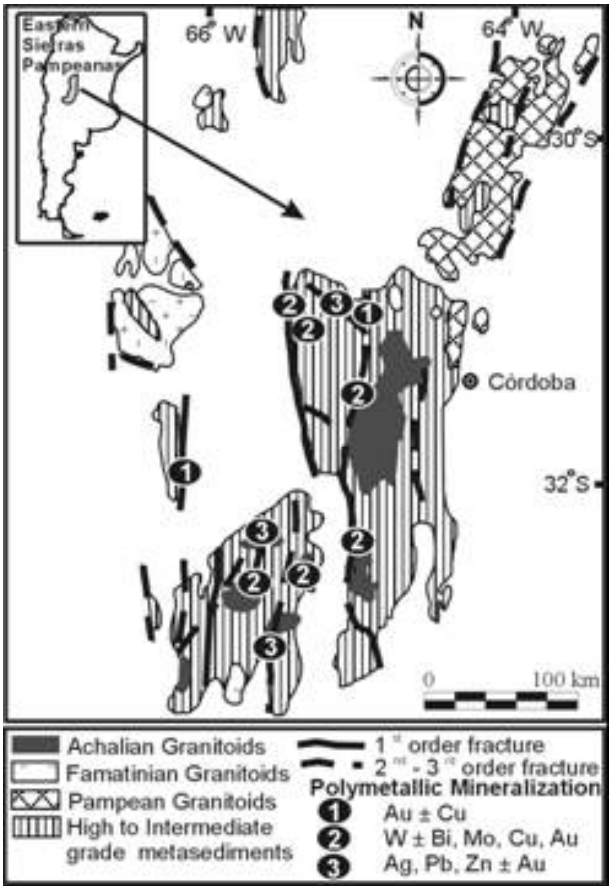


Figure 1. Simplified geological map of the eastern Sierras Pampeanas showing the location of the studied districts.

zones of high strain, up to 15km wide, major N-S mylonitic shear zones were formed (Fig. 1). These ductile shear zones are mostly east-dipping and show orthogonal, westerly directed thrust movement.

Subduction appears to have been reestablished from Devonian to Early Carboniferous time during the Achalian cycle. This cycle is characterized by reactivation of shear zones and emplacement of felsic metaluminous to peraluminous magmatism, which constitutes batholiths that crop out along major reverse and strike-slip shear and fault zones (Fig. 1).

The Achalian cycle has been related with the accretion of Chilenia terrane to the protomargin of Gondwana.

## 3 ORE DEPOSITS

The polymetallic mineral deposits of Au ± Cu, W ± Bi, Mo, Cu, Au and Ag, Pb, Zn ± Au formed during, and up to 20 – 30 Ma after, a period of widespread Devonian granitic magmatism. Most are high angle vein-type deposits associated with Riedel conjugate sets of second and third order NW- and NE-trending shear zones. These subsidiary lineaments are connected with N-trending regional mylonitic zones.

Most deposits occur in a 1 to 5km wide corridor of brittle - ductile deformation in the vicinity of transpressional structures in mylonitized siliciclastic gneisses, amphibolites and granites. Quartz veins, 0.1 to 200cm in width, show sigmoidal and en-échelon morphology, and subsidiary stockwork structure in siliceous zones. Buck, ribbon, laminated, breccia and comb textures are common. In this paper, the term “buck” is used in the sense of Dowling and Morrison (1989).

The mineralogy of studied veins is simple and uniform, although the proportions of vein-forming minerals varies from one location to another. Veins are mostly composed of quartz (commonly 80-90 vol.%) and subordinate sulphide minerals (commonly 10-20 vol.%). Pyrite, sphalerite, galena, and chalcopyrite comprise more than 90% of the sulphide volume. Polymetallic sulphosalts are frequently present. Arsenopyrite and pyrrhotite are uncommon. Wolframite and molybdenite are common in tungsten districts. Hydrothermal alteration of the wallrock progresses outward from proximal silicification and sericitization to distal chloritization, argillitization, and propylitization.

### 3.1. *Quartz-vein microstructures*:

Two major quartz microstructure groups are recognized in hand specimens and thin sections: 1) primary growth microstructures, which represent the initial vein fill; and 2) secondary or superimposed microstructures, which are restricted to preexisting quartz and reflect multiple overprinting events of deformation, dissolution, and recrystallization (Fig. 2c).

Primary microstructures are characterized by milky subhedral buck and comb quartz types, which have been cemented everywhere by finer grained blue gray quartz and sulphide minerals. Up to 60 % of the vein volume is composed of secondary microstructures, which give rise to a blue gray quartz domain derived from progressive fracturing, resorption, and recrystallization of the buck and comb quartz substrate, rather than by precipitation of new quartz.

The deformed quartz aggregate include: 1) grains with sweeping undulatory and patchy extinction, 2) grain boundary serration, 3) deformation lamellae and subgrain formation, 4) subgrain rotation, 5) curved dislocation (Fig.

2d), 6) stylolitized boundaries between paragenetically early buck and later quartz, 7) localized microfractures in quartz that may have formed as a result of sulphide crystallization, 8) fibrous bands in crack-seal cycles, 9) pyrite selectively replaced dusty buck quartz along discontinuous microfractures or microfissures (Fig. 2e), and 10) sulphide mineral aggregates along microfractures, parallel to and/or at < 45º angle to the strike of the vein (Fig. 2e).

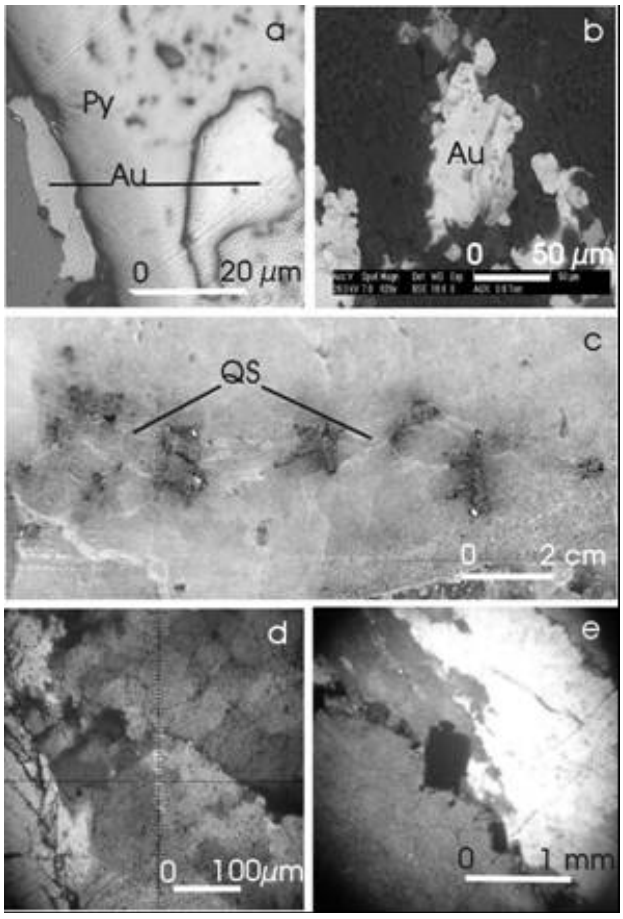


Figure 2. a, b, d, e: Photomicrographs of a) Gold (Au) inclusion and overgrown on pyrite (Py) surface. b) Gold in limonite, SEM, back scattered image. c) Photograph of typical sample with buck quartz and blue gray quartz-sulphide bearing minerals (QS) across microfissures. d) Curved dislocation, patchy extinction and formation of subgrains. e) Late minute sulphide minerals in microvein cutting deformed and recrystallized early quartz, note euhedral pyrite grain replaced early quartz.

In ore zones, veins with gold are typically characterized by: 1) high blue gray quartz: buck quartz ratio, 2) high sulphide minerals: buck quartz ratio and 3) well-developed overprinting secondary microstructures and structurally controlled sulphide microfissuring.

## 4 ISOTOPE STUDIES

Sulphur isotope compositions were determined for 13 representative samples from selected districts. Pyrite, galena, and chalcopyrite grains were picked and analysed at the Actlabs laboratory. The results are summarized in Figure 3, together with 15 $\delta^{34}S$ values reported by Skirrow *et al.* (2000).

The $\delta^{34}S$ values of sulphide minerals lie in the range 3.6-10 ‰$_{(CDT)}$ with the highest values from Au ± Cu deposits (range 5.5-10 ‰$_{(CDT)}$, n = 8). W ± (Bi, Mo, Cu, Au) and Ag-Pb-Zn ± Au mineralization have similar values of 4.5-7.4 ‰$_{(CDT)}$ (n = 10) and 3.6-7.2 ‰$_{(CDT)}$ (n = 10), respectively.

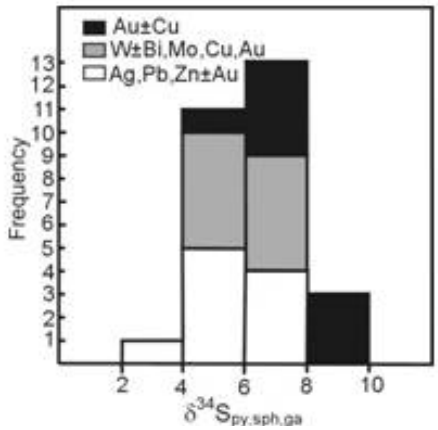


Figure 3. Histogram of sulphur isotopic values from late sulphide minerals.

The calculated $\delta^{34}S_{(fluid)}$ range, of 3.5 to 9.7 ‰, is slightly higher than the -3-+3 ‰$_{(CDT)}$ range established for sulphur derived from a typical magmatic source (Field & Fifarek 1985) and also from the range 0-5 ‰$_{(CDT)}$ recognized in gold deposits related with intrusions (Lang & Baker 2001). The $\delta^{34}S$ values may indicate sulphur was derived from a mixture of magmatic and metasedimentary sources.

Lead isotope ratios were determined on 5 galenas, 3 pyrites, and 2 chalcopyrites in representative samples from each deposit type. The analyses were performed at the Actlabs laboratory using HRICP-MS techniques. These data plot in the diagram of Zartman & Doe (1981) close to the orogene evolution curve (Fig. 4). The population shows a radiogenic lead source characteristic of homogenized continental crust. However, inputs of igneous or mantle lead are evident in one W ± (Bi, Mo, Cu, Au) sample and two Ag-Pb-Zn ± Au samples.

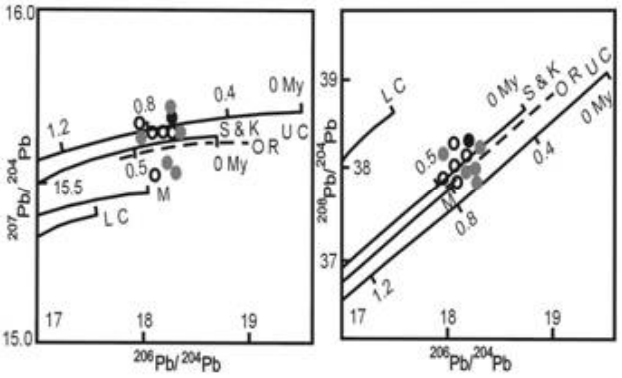


Figure 4. Diagrams showing the lead isotope values of sulphide minerals from the late sulphide-gold assemblage discussed in the text. Evolutionary curves from Zartman & Doe (1981). Deposit abbreviations as in Figure 3.

## 5 DISCUSSION AND CONCLUSIONS

Ore deposits in the Sierras Pampeanas collisional belt reflect the complex interplay between tectonic and hydrothermal activity during the Achalian cycle. Successive stages of evolution may be identified before and during the late stage of sulphide-gold ore deposition: 1) tectonic shortening and block uplifting along reactivated crustal-scale fractures under greenschist facies conditions, 2) melt production in thickened crust, with melt emplacement at depths < 7 km in transpressional sites controlled by regional shear zones, near the transition from lithostatic to hydrostatic conditions, 3) recurrence of brittle-ductile to brittle deformation along major shear zones and widespread conjugate fracture systems with en-echelón and rectilinear geometries, 4) crustal-scale hydrothermal activity, 5) structurally controlled early buck and comb milky quartz deposition within 2nd and 3rd order fracture zones up to 5 km wide, 6) fracturing an cementation of preexisting quartz veins in an extensional regime, 7) Achalian magmatism may be invoked as the source of heat energy necessary to drive fluids, 8) persistence and/or recurrence of a tensional regime during multiepisodic microfissuring events of the quartz substrate, 9) fluid production with metals and sulphide mobilized from the homogenized crust (by evolved meteoric waters?) and from a subordinate igneous reservoir, 10) dissolution-reprecipitation and chemisorption *(e.g*. Widler & Seward 2002) may explain the overgrown gold-sulphide link in veins.

Our results are consistent with the proposed metallogenic model of Skirrow *et al*. (2000) and the deposit types are similar to the Variscan-type of orogenic gold deposits (Cathelineau *et al.* 2003).

## REFERENCES

Cathelineau M, Boiron M, Fourcade S, Marignac C (2003) The shift from "mesothermal" to "epithermal" conditions in orogenic gold: definition of a Variscan-type of quartz lode gold deposits. Proceedings of the seventh biennial SGA meeting, Athens, Demetrios G. Eliopoulos et al. (eds), *Mineral Exploration and Sustainable Development,* pp 751-754.

Dowling K, Morrison G (1989) Application of quartz textures to the classification of gold deposits using north Queensland examples. In: Keays R, Ramsay W, Groves D (eds) The geology of gold deposits-the perspective in 1988. *Econ Geol Monograph* 6, Soc Econ Geol, Littleton, pp 342-355.

Field C, Fifarek R (1985) Light stable-isotope systematics in the epithermal environment. In: Berger, B. and Bentheke, P (eds): *Geology and geochemistry of epithermal systems*. Reviews in Econ Geol 2: 99-128.

Lang J, Baker T (2001) Intrusion-related gold systems: The present level of understanding. *Min Dep* 36: 477-489.

Skirrow R, Camacho A, Lyons P, Pieters P, Sims J, Stuart-Smith P, Miró R (2000) Metallogeny of the southern Sierras Pampeanas, Argentina: geological $^{40}Ar$-$^{39}Ar$ dating and stable isotope evidence from Devonian Au, Ag-Pb-Zn-W ore formation. *Ore Geo Rev* 17: 39-81.

Widler A, Seward T (2002) The adsorption of gold (I) hydrosulphide complexes by iron sulphide surfaces. *Geochim Cosmochim Acta* 66: 383-402.

Zartman R, Doe B (1981) Plumbotectonics-the model. *Tectonophysics* 75:135-162.

# The geology of the Manantial Espejo district and its vein-hosted epithermal Ag(-Au) deposit, Deseado Massif, Argentina

S. Wallier & R.M. Tosdal
*Mineral Deposit Research Unit, Earth & Ocean Sciences, The University of British Columbia, Vancouver, Canada*

E.O. Escalante
*Pan American Silver Corporation*

ABSTRACT: The 47 Moz Manantial Espejo Ag deposit is one of several low-sulphidation epithermal vein districts hosted by the Middle to late Jurassic Chon Aike Formation in the Deseado Massif, southern Argentina. These rocks are part of the Chon Aike Province, a large bimodal igneous province active during the initial breakup of Gondwana that formed the South Atlantic Ocean. On the Manantial Espejo property, economically important hydrothermal veins show characteristic features of a low-sulphidation epithermal deposit with crustiform and colloform banding, bladed calcite replaced by quartz and abundant adularia, and a well developed alteration halo of adularia, illite, illite-smectite, pyrite, chlorite, and kaolinite. The veins formed during initial development of normal faults cutting through a more than 400m thick sequence of volcanic rocks mainly consisting of silicic ignimbrites which were deposited in only 1 Ma.

KEYWORDS: Manantial Espejo, Chon Aike Province, epithermal, alteration

## 1 INTRODUCTION

The Manantial Espejo low-sulphidation epithermal deposit is a major Ag deposit with by-product Au in the Deseado Massif, south Argentina. Exploration prior to the onset of mining revealed 47 Moz Ag and 0.7 Moz Au (measured and indicated, end of 2005), and therefore has a similar Ag content as Cerro Vanguardia, the largest epithermal deposit in the Deseado Massif. Located about 140km west-northwest of Puerto de San Julián, and about 100km southwest of Cerro Vanguardia, the Manantial Espejo deposit spreads out over an area of about 200km$^2$, consisting of hundreds of major and minor veins, stockworks and disseminations formed in a low-sulphidation epithermal system. The project is owned by Pan American Silver Corporation.

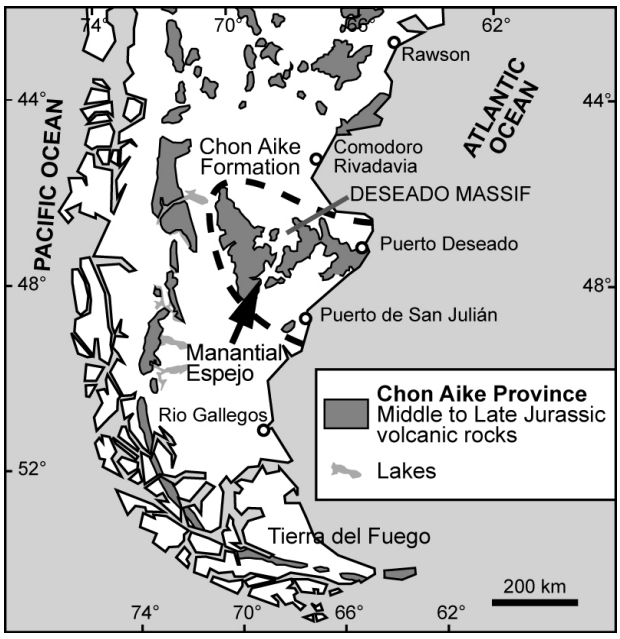


Figure 1. Map of south Southamerica showing outcrops of the Chon Aike Province and the Chon Aike Formation (modified after Pankhurst *et al*., 1998).

## 2 GEOLOGICAL SETTING OF THE DESEADO MASSIF

Middle to late Jurassic andesites to rhyolites of the Chon Aike Province, a large bimodal igneous province dominated by silicic volcanic rocks, form the Deseado Massif (Fig. 1). Jurassic magmatism accompanied extensional tectonics, manifested by normal faults, horst and graben, and block rotation during the opening of the south Atlantic Ocean, which was likely initiated by back arc extension and the impact of a mantle plume (Pankhurst *et al.*, 1998). The up to several 100 m thick dacitic to rhyolitic

Chon Aike Formation is the most voluminous formation of the Chon Aike Province in the Deseado Massif. Ignimbrites, intercalated air-fall and reworked ash units cut by rhyolitic dikes and domes compose the formation. The rocks overlie the mainly andesitic Bajo Pobre Formation. The Chon Aike Formation is in turn overlain by the La Matilde Formation, composed of reworked volcaniclastic rocks derived from the Chon Aike Formation. The two silicic-rich formations, together included in the Bahia Laura Group, are locally overlain or intruded by andesitic to dacitic units. Tertiary volcanic and sedimentary rocks unconformably overlie the Jurassic volcanic sequence (Pankhurst *et al.,* 1998; Panza, 1998).

## 3 STRATIGRAPHY AND GEOCHRONOLOGY OF THE DISTRICT

The stratigraphically lowest outcropping unit is a more than 200 m thick variably welded and crystal-rich rhyodacitic ignimbrite of the Chon Aike Formation (Fig. 2). It is overlain by a sequence of fine ash units and densely welded rhyolitic ignimbrites of variable crystal and pumice content. The youngest mapped unit of the Chon Aike Formation consists of rhyolitic

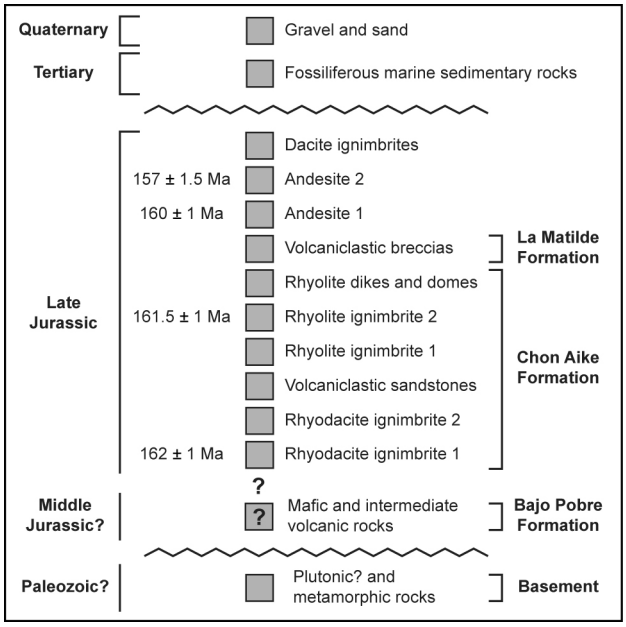


Figure 2. Simplified stratigraphy of the Manantial Espejo district. Ages are interpreted on zircons by U-Pb SHRIMP-RG method.

dikes and domes. U-Pb SHRIMP-RG ages on zircons from basal and top ignimbrite units of the Chon Aike Formation are 162 ± 1 Ma, indicating that the deposition of the at least 400m thick sequence happened in only 1 Ma. The formation is covered by thin reworked ash and lithic tuff units of the La Matilde Formation. In the eastern-part of the Manantial Espejo district, the silicic volcanic rocks are overlain and intruded by small volume, intermediate volcanic rocks with U-Pb ages of 160 to 157 Ma. U-Pb geochronology on zircons from a granite xenolith within an andesite unit indicates that coeval silicic plutonic rocks were emplaced at depth. The Jurassic volcanic sequence is overlain by Tertiary marine and continental sedimentary rocks.

## 4 THE MANANTIAL ESPEJO SILVER (GOLD) DEPOSIT

As with the other vein deposits in the Deseado Massif, the epithermal veins at Manantial Espejo fill normal faults cutting silicic and intermediate rocks of the Chon Aike Province (*e.g.* Schalamuk *et al.*, 1997). The major normal faults strike west-northwest, whereas minor faults strike east-northeast to east. Two different styles of epithermal mineralization are present. The dominant and economically most important style has a characteristic low-sulphidation epithermal paragenesis with textures such as crustiform and colloform banding, bladed calcite replaced by quartz and abundant adularia. These veins are Ag-rich and have relatively low base-metal concentrations. They are known as the Maria Vein-style, based on the Maria Vein, the major ore body of the deposit. The second and less common style, known as the Mesa Vein-style, includes low-grade Ag but base-metal-rich veins. These show characteristics of an intermediate sulphidation deposit with coarse-grained Fe-poor sphalerite, galena, and chalcopyrite. The Maria Vein-style occurs only within silicic rocks of the Chon Aike Formation, whereas veins of the Mesa Vein-style occur in felsic rocks of the Chon Aike Formation and in the younger intermediate volcanic units.

Extensive, massive silicified bodies are broadly distributed in the Manantial Espejo district. They are interpreted as steam-heated paleo-water tables, where permeable rocks hosting an aquifer were partially or completely replaced by opaline silica and chalcedony. Clear indicators for sinter deposits such as fossil plant fragments, highly irregular lamination and columnar structures perpendicular to lamination are missing.

### 4.1 *The Maria Vein*

Four economic vein systems are known in the Manantial Espejo deposit. All of them are Maria Vein-style. The largest is the Maria Vein, a classic example of a low-sulphidation vein that filled a complex structure of linked listric normal faults. The curviplanar vein dips 60-70° SSW and continuously outcrops over 920m strike length with a variable thickness of up to 17m. The upper part of the vein marks the contact between a thick rhyodacite ignimbrite in the footwall and younger rhyolitic volcaniclastic rocks in the hanging wall. The vein shows characteristic textures of crustiform and colloform banding, replacement of bladed calcite by quartz, and abundant adularia. Hydrothermal and tectonic breccias are common.

Six hydrothermal stages are identified in the Maria Vein. These are: 1) Metal-bearing, crustiform banded, fine-grained (recrystallized) quartz; 2) Low-grade, massive to vuggy white quartz with replaced bladed calcite; 3) Low-grade, colloform banded quartz ± amethyst, adularia, platy replaced calcite/barite, and increasing abundance of adularia with depth; 4) Mainly low-grade tectonic and hydrothermal breccias with fine-grained quartz-pyrite cement, and less common but important high-grade Ag and base metal-rich breccias, thin veins, open space infill, and replacements; 5) Thin veins and open space infill of base-metal sulphides; and 6) Post-mineral chalcedony. Stages 1 and 4 are economically important. Vughs and replacements in stages 2 and 3 served as host for younger minerals. Stage 1 is Ag- and Au-rich and carries minor base-metals, Stage 4 is particularly Ag-rich with abundant base-metals but low Au-grade with a common Ag/Au ratio of >1000. The major ore minerals in the deposit are acanthite and Ag-sulphosalts; electrum carries the minor gold.

The distribution of hydrothermal stages along the vein controls grade and reflects the history of fault and vein formation. Mapping of hydrothermal stages along the outcrop of the

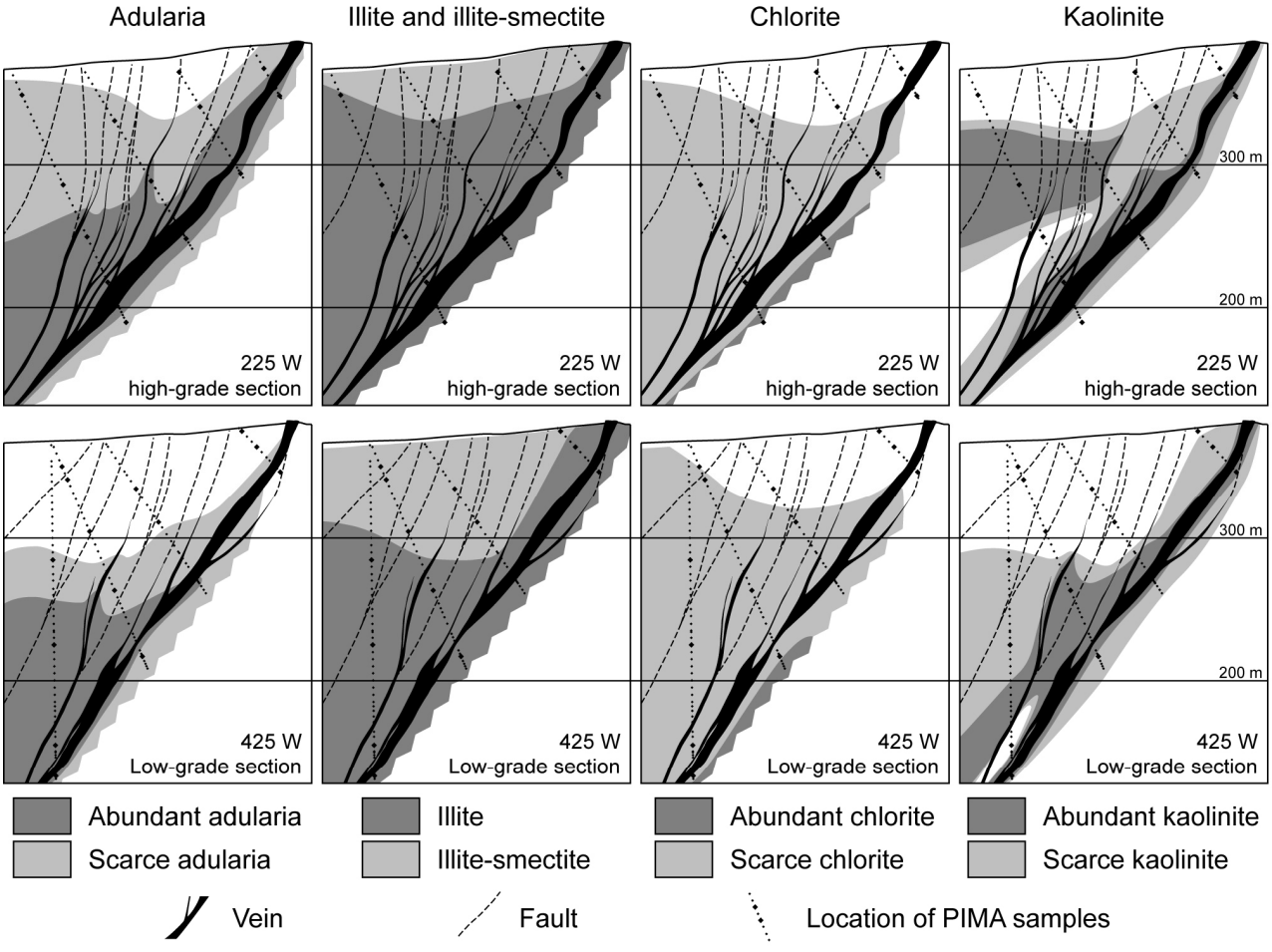


Figure 3. Sections through a high-grade segment (225 W) and a low-grade segment (425 W) of the Maria Vein. In the high-grade segment, adularia extends over a broader halo and the transition from illite to illite-smectite occurs at shallower level.

Maria Vein showed that high-grade stage 1 only occurs in two vein segments, which are interpreted as two unconnected faults/veins. The two vein segments remained separate until stage 3, when they linked across to form a single curviplanar vein.

Petrography and PIMA analysis demonstrate intense but varying thickness of alteration in the hanging wall of the vein. An alteration zonation typical of an epithermal low-sulphidation system is present (Fig. 3). Quartz, pyrite, ± illite and abundant adularia are proximal to the vein and in the deeper part of the system indicating higher temperatures. Lower-temperature interlayered illite-smectite lies distal to the vein and at shallow levels. The transition is marked by quartz, pyrite, illite and scarce adularia. Chlorite is most intense along the footwall of the vein. Kaolinite appears mainly to be supergene, and overprints the hypogene assemblages along the fault-fracture mash. The high-temperature assemblage is wider and better developed in the high-grade section of the Maria Vein.

## 5 CONCLUSIONS

The Manantial Espejo Ag-Au deposit formed during Middle to Late Jurassic extensional tectonics and volcanic activity which deposited the bimodal large igneous Chon Aike Province. The economically important low-sulphidation veins show characteristic features such as colloform banding and bladed calcite replaced by quartz. In Maria Vein, six hydrothermal stages formed the vein, but only stages 1 and 4 contributed metal. Alteration zoning about the vein shows higher temperature mineral assemblages extending over a broader halo and to shallower levels along a high-grade segment of the Maria Vein where compared to a low-grade segment.

## ACKNOWLEDGEMENTS

Thanks to Pan American Silver Corporation for financial and logistic support, as well as for many constructive discussions in the field. Teck Cominco Limited is thanked for use of the PIMA.

## REFERENCES

Pankhurst RJ, Leat PT, Sruoga P, Rapela CW, Marquez M, Storey BC, Riley TR (1998) The Chon Aike province of Patagonia and related rocks in West Antarctica: A silicic large igneous province. *Journal of Volcanology and Geothermal Research* 81: 113-136

Panza JL, Marin G, Zubia M (1998) Hoja Geológica 4969-I, Gobernador Gregores, escala 1:250.000, provincia de Santa Cruz. 239: 104

Schalamuk IB, Zubia M, Genini A, Fernandez RR (1997) Jurassic epithermal Au-Ag deposits of Patagonia, Argentina. *Ore Geology Reviews* 12: 173-186

# Epithermal vein system of the Josefina prospect, Deseado Massif, Patagonia Argentina.

P. Moreira, R.R. Fernández & I.A. Schalamuk
*Instituto de Recursos Minerales (INREMI), Universidad Nacional de La Plata, CICBA, Argentina*

ABSTRACT: The central sector of the La Josefina Au-Ag Prospect contains eight structurally controlled quartz veins hosted in middle to upper Jurassic volcaniclastic rocks. The alteration and vein minerals, Au/Ag ratios, fluid inclusion temperatures and salinity results indicate that La Josefina is an epithermal occurrence. The stable isotopic compositions of the quartz point to an important meteoric water component. The $\delta^{34}S$ value of barite indicates sulphate was derived from a magmatic source. The bimodal volcanism and extensional tectonic setting of the Deseado Massif and the attributes of the veins (structural control, hydrothermal alteration, banded quartz textures and late carbonate-replacement texture) are consistent with the low sulphidation model. Alternatively, the barite, specular haematite, and abundance of thick comb texture quartz are characteristic of the intermediate sulphidation model.

KEYWORDS: precious metal, epithermal vein system, Deseado Massif, Patagonia Argentina

## 1 INTRODUTION

The Deseado Massif (DM) is located in the southern Argentinean Patagonia (Fig. 1). In this region, the most important unit is a volcanic complex of middle to upper Jurassic age with bimodal features marked by andesitic and rhyolitic rocks of the Bajo Pobre and Chon Aike formations. These units crop out over about 30, 000 sq. km.

The DM has several epithermal precious-metal deposits that comprise the Deseado Auroargentiferous Province (DAP) of Schalamuk *et al.* (1999). These epithermal deposits are upper Jurassic in age and are spatially and genetically related to the volcanic rocks (Arribas *et al.*, 1996; Schalamuk *et al.*, 1997). At present, the DM has two projects under exploitation for epithermal ore; they are Cerro Vanguardia and Mina Martha.

Cerro Vanguardia is a world-class quartz vein deposit with mineable reserves of 9 Mt at an average grade of 10 g/t Au and 113 g/t Ag (*Cerro Vanguardia S.A. annual report, 1999*). Mina Martha is a small, high-grade bonanza Ag deposit hosted in the Martha vein. It has a resource of 100,000 t containing 232 t Ag eq. at a grade of 2,320 g/t Ag (*Yamana Resources Inc. Annual report, 2000*). San José, Manantial Espejo and Cerro Negro are prospects under feasibility studies. Other intensely explored areas are the Josefina, Cerro Moro and Cerro León prospects.

This paper focuses on an epithermal vein system located in the central sector of the Josefina prospect (JP). This prospect is currently under exploration and is situated in the central part of the DM (Fig. 1). This study is based on detailed surface mapping, drill core and petrographic observations , vein geochemistry, fluid inclusion and stable isotope data.

In the central sector of the JP (Fig. 1), the Jurassic rocks are comprised of the Chon Aike Formation that includes a crystal-rich ignimbrite, reworked pyroclastic facies (tuffites and conglomerate breccias), rhyolitic lavas and a talus breccia. Palaeogene-Neogene basaltic flows and modern detritus cover the Jurassic volcanic rocks.

All of the veins are hosted in the crystal-rich ignimbrite, which is a quartz-feldspar-biotite welded rock with some flattened pumice rich layers that are dated at 153.2 ± 3.6 My (Arribas *et al.* 1996).

## 2 MINERALIZATION

The central sector consists of a series of-northwest-trending sigmoidal veins that outcrop over a distance of nearly 1.5km (Fig. 1). There are eight quartz veins (María Belén (MB), Las Latitas (LL), Ailín (Ai), Adularia (Ad), Frida (F), Lola (L), Simona (S) and Upi (U)). Lengths of vein exposures are between 220 to 600m with variable thicknesses of up to 2m. Veins are vertical to subvertical, with a tendency to dip to the northeast.

Hydrothermal alteration associated with the veins is represented by silicification, argillization (illite, adularia, illite-smectite interlayers, and some kaolinite), chloritization and pyritization

| VFT | Mineralogy | Texture | Veins |
|---|---|---|---|
| 1 | Native gold + hm + py + ga + sl + white qtz | Banded | Ai MB |
| 2 | Native gold + hm + py ± ga ± sl | Massive to breccia | Ai |
| 3 | Py ± cp ± bn ± ga ± sph + white and green qtz | Colloform banded to comb qtz | Ad LL MB |
| 4 | White and translucent qtz + ad + red opal | Colloform banded to weak banded | Ad MB |
| 5 | Native gold + electrum + fahlore + py + asp + cp + bn + hm + ga + sph + td + transparent qtz + amethyst + cal + ad | Massive, breccia and comb qtz | U-F Ad Ai MB-LL |
| 6 | Electrum + py + grey qtz ± cp ± bn | massive | S-L-F-Ad |
| 7 | Bar + qtz | massive | S |
| 8 | Qtz | Comb qtz | U-S-L |
| 9 | White, grey and translucent qtz | banded | L-F |
| 10 | Translucent qtz | Comb qtz | U-F |
| 11 | Transparent and green qtz | Comb qtz | L-Ad Ai-MB |
| 12 | Red and green opal + Fe-Mn oxides | mosaic | U-MB |
| 13 | Light brown opal | banded to mosaic | U-S L |

Table 1. Vein fill types (VFT) from the central sector veins of the JP. Abbreviations: qtz - quartz, hm - specular haematite, py - pyrite, asp - arsenopyrite, cp - chalcopyrite, bn - bornite, gn - galena, sl - sphalerite, cal - platty calcite, ad - adularia, td - tetrahedrita, bar - barite

Table 1 summarizes the vein fill types (VFT). Quartz and other silica minerals constitute more than 90% of the vein fill. VFT 1, 2, 5 and 6 are important by the Au-Ag mineralization

## 3 GEOCHEMICAL CHARACTERISTICS

The geochemical signature of the central sector veins of the JP is presented in Table 2. Most of the veins have a geochemical signature that is typical of epithermal deposits with anomalous values in precious metals and Cu, Pb and Zn. The maximum Au and Ag values are in the Ailín Vein with 78 ppm and 163 ppm, respectively, in surface samples and 253 ppm and 200 ppm, respectively, in drill core samples. The Au/Ag ratios range from 1/1.5 to 1/9, although the Simona vein constitutes an exception, because it has high Ag contents

| Vein | N | Au | Ag | Cu | Pb | Zn | Au/Ag |
|---|---|---|---|---|---|---|---|
| U | 5 | 0.33 | 1.42 | 149 | 673 | 261 | 1/4.3 |
| S | 6 | 0.32 | 85 | 239 | 866 | 343 | >1/200 |
| L | 4 | 0.46 | 3.25 | 42 | 278 | 143 | 1/7.1 |
| Ad | 12 | 0.28 | 2.03 | 74 | 739 | 330 | 1/7 |
| Ai | 8 | 11.8 | 32.0 | 350 | 1958 | 441 | 1/3 |
| LL | 29 | 0.83 | 7.4 | 215 | 1342 | 234 | 1/9 |
| MB | 82 | 11.0 | 17.0 | 226 | 1444 | 334 | 1/1.5 |

Table 2. Average geochemical values (ppm) from JP central sector veins. N: number of samples analyzed

## 4 FLUID INCLUSIONS

Fluid inclusions (FI) were studied in pseudorhombic adularia crystals from the Adularia vein (VFT5). FI are scarce and small (up to 50 μm). Primary FI are isolated or have negative crystal form and mostly two phase, composed of liquid and vapour, with the bubble occupying 20% of the inclusion. The salinity values are near 4.6 wt % NaCl eq. and the homogenization temperatures range between 250° and 270°C. These data are in accord with those of Ríos *et al.* (2000) for quartz-FI from the Ailin vein (VFT1)

## 5 STABLE ISOTOPES

### *5.1. Oxygen*

Five samples of quartz from central sector veins and veinlets of the JP were analyzed for

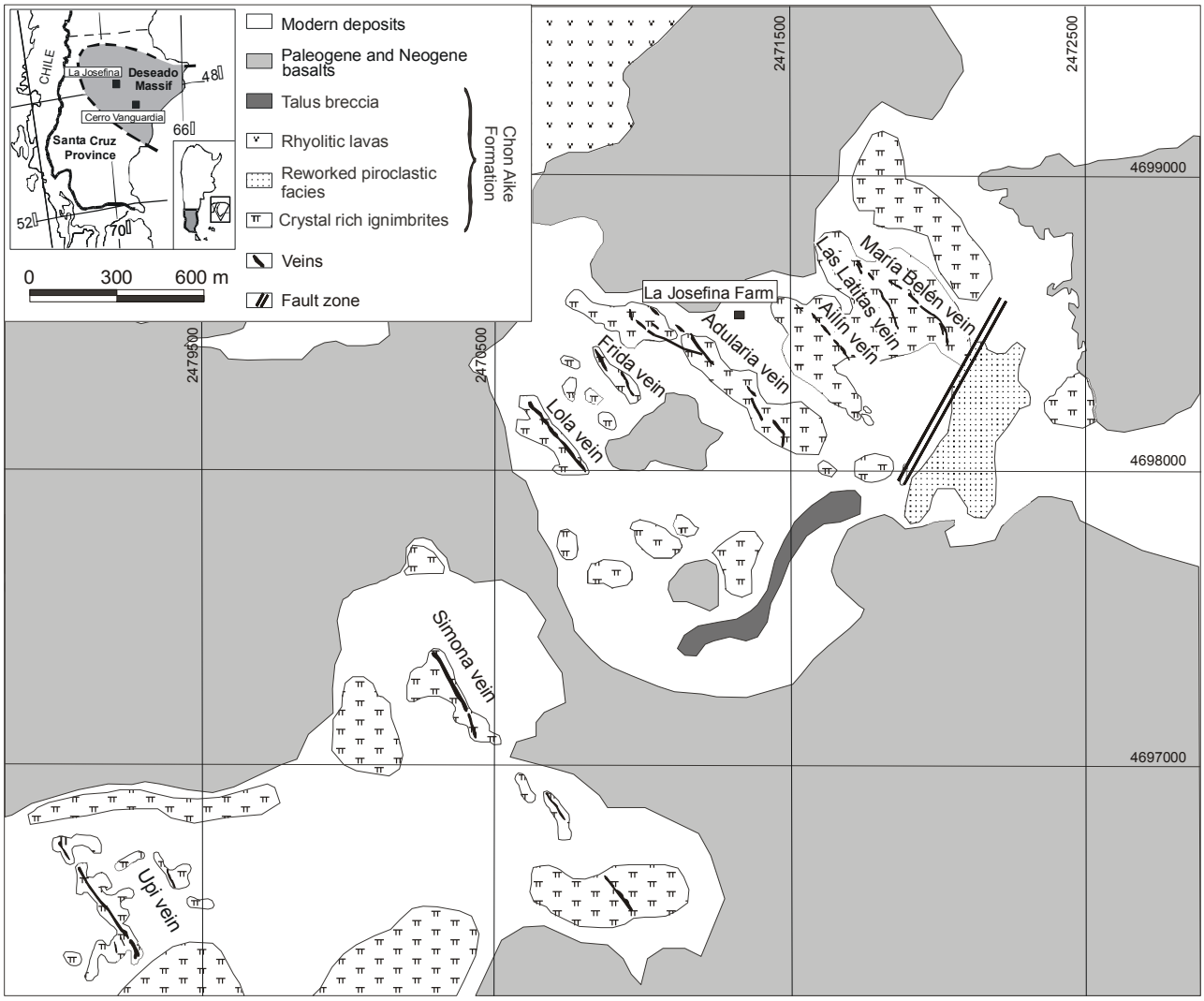


Figure 1. Location and geology of the central sector of the JP.

oxygen isotopes. The measured $\delta^{18}O$ are in Table 3. The $\delta^{18}O$ of the fluid was calculated using a temperature of 250°C (Adularia FI studies) and the fractionation equations by Zheng (1993). The $\delta^{18}O$ of the fluid in equilibrium with quartz was calculated to range from -3.47 and -4.97 ‰ (Table 3)

### *5.2. Sulphur*

Sulphur isotopic analysis (relative to CDT) of barite from the Simona vein (VFT7) yielded a $\delta^{34}S$ value of 14.5 ‰

| sample | Vein/veinlets | $^{18}O_{min}$ ‰ | $^{18}O_{fluid}$ ‰ |
|---|---|---|---|
| 1 | veinlets | 3.0 | -4.97 |
| 2 | Ailín (VFT1) | 3.3 | -4.67 |
| 3 | Ailín (VFT1) | 3.5 | -4.47 |
| 4 | Upi (VFT5) | 4.5 | -3.47 |
| 5 | Upi (VFT5) | 4.5 | -3.47 |

Table 3. Oxygen isotopic composition (relative to SMOW) of quartz from central sector veins of the JP

## 6 CONCLUSIONS

The structural control, banded quartz texture, hydrothermal alteration and minor late carbonate-replacement texture are attributes characteristic of Low Sulphidation (LS) epithermal systems described by Hedenquist *et al.* (2000).

Nevertheless, the barite, specular haematite and abundance of thick comb texture quartz, permits that the JP could be assigned to the Intermediate Sulphidation (IS) type of Sillitoe and Hedenquist (2003).

The range of Au/Ag ratios (1/1.5 to 1/9), temperatures (250 and 270°C), and the salinity (~4.6% wt% NaCl equiv.) are characteristic of epithermal deposits, but do not allow us to define a specific model. The stable isotopic compositions of the fluids (-3.47 to -4.97) point to an important meteoric water component and in agreement with the LS epithermal fluid compo-

sition of Cooke & Simmons (2000). The $\delta^{34}S$ value of barite indicate sulphate was derived from a magmatic sulphur source. This value is within the epithermal range proposed by Bethke *et al.* (1973). The bimodal volcanism and extensional tectonic setting of the DM (Schalamuk *et al.* 1999; Echavarría *et al.* 2005), is similar to the model proposed for the LS deposits (Sillitoe & Hedenquist 2003).

ACKNOWLEDGEMENTS

The authors are grateful to the Agencia Nacional de Promoción Científica y Tecnológica (FONCyT) and the Santa Cruz state mining company (FOMICRUZ S.E.) for the support and close cooperation during this research.

REFERENCES

Arribas Jr A, Schalamuk I, de Barrio R, Fernández R, Itaya T (1996) Edades Radimétricas de Mineralizaciones Epitermales Auríferas del Macizo del Deseado, Provincia de Santa Cruz, Argentina. In: *XXXIX Congresso Brasileiro de Geología*: 254-257

Bethke, PM, Barton PB, Rye RO (1973) Hydrogen, oxygen and sulphur isotopic compositions of ore fluids in the Creede District, Mineral County, Colorado. *Econ Geol* 68: 1205

Cooke D, Simmons, S (2000) Characteristics and genesis of Epithermal Gold Deposits. *SEG Reviews* 13: 221-244

Echavarría LE., Schalamuk IB, Etcheverry, RO (2005) Geologic and tectonica setting of Deseado Massif epithermal deposits, Argentina, basedon El Dorado-Monserrat. *Journal of South American Earth Sciences* 19: 415-432.

Hedenquist J, Arribas A, González-Urien E (2000). Exploration for epithermal gold deposits, *Reviews in Economic Geology* 13: 245-278

Rios FJ, Alves JV, Fuzikawa K, Schalamuk I A, De Barrio R, Del Blanco M (2000) Fluid Evolution in the La Josefina Au-epithermal system, Macizo del Deseado, Southern Patagonia, Santa Cruz, Argentina. *Revista Brasileña de Geociencias* 30 (4): 769-774

Schalamuk I, Zubia M, Genini A, Fernández R (1997) Jurassic epithermal Au-Ag deposits of Patagonia, Argentina. *Ore Geology Reviews* 12-3: 173-186

Schalamuk I, de Barrio R, Zubia M, Genini A, Echeveste H (1999) Provincia Auroargentífera del Deseado, Santa Cruz. In: Zappettini, E. (ed) *Recursos Minerales de la República Argentina, Instituto de Geología y Recursos Minerales SEGEMAR, Anales* 35: 1177-1188

Sillitoe R, Hedenquist J (2003) Linkages between volcanotectonic settings, ore-fluid compositions, and epithermal precious metal deposits. In: *Volcanic, Geothermal, and Ore-Forming Fluids,* Simmons, S.F., Graham, I. (eds). SEG Special Publication 10: 315-343

Zheng YF (1993) Calculation of oxygen isotope fractionation in anhydrous silicate minerals. *Geochimica et Cosmochimica Acta* 57: 1079-1091

# The low sulphidation Au-Ag deposit of Rio Blanco (Ecuador): Geology, Mineralogy, Geochronology (U-Pb and Ar-Ar) and Isotope (S, Pb, Sr) Geochemistry

T. Binelli Betsi, M. Chiaradia & R. Spikings
*Department of Mineralogy, University of Geneva, 13 Rue des Maraîchers, 1205 Geneva, Switzerland*

ABSTRACT: The Au-Ag mineralization at Rio Blanco (Western Cordillera of southwestern Ecuador) displays textures, mineral associations, and sphalerite Fe contents indicative of an epithermal low sulphidation deposit. Gold (electrum) occurs either within pyrite and pyrrhotite or as free electrum grains. The Ag mineralization consists mainly of pyrargyrite and tetrahedrite. Sericite associated with the mineralization yields an Ar-Ar plateau age of 18.9 ± 0.5 Ma. Zircons of two nearby dioritic intrusive bodies yield $^{206}Pb/^{238}U$ weighted ages of 35.77 ± 0.06 Ma and 15.70 ± 0.08 Ma, respectively. The Ar-Ar age is likely a maximum age for mineralization because of Ar loss due to recoil and the presence of alteration in the younger diorite. Isotopic data suggest Pb and S in the ore was derived primarily from igneous sources. Electrum precipitated after boiling as Fe-bearing breccia fragments were sulphidized.

KEYWORDS: Rio Blanco, Ecuador, low sulphidation, epithermal deposit, Au-Ag mineralization

## 1 INTRODUCTION

The Rio Blanco Au-Ag prospect, located in the Western Cordillera of southwestern Ecuador (Fig. 1), is one of the most important precious metal deposits of Ecuador. Ore reserves of the Alejandra Vein (the principal vein of the prospect) exceed 2 Mt at average grades of 8.9 g/t Au and 68 g/t Ag, respectively, with bonanza grades up to 800 g/t Au (Appleyard 2003). The Au-Ag mineralization of Rio Blanco is hosted by the Oligo-Miocene Rio Blanco Formation (Fig. 1) consisting of volcaniclastic rocks, andesitic lavas, felsic ignimbrites and dacitic tuffs, intruded by diorite intrusions and porphyry andesitic dykes (Appleyard 2003).

## 2 WALL ROCK CHARACTERISTICS

Volcanic rocks of the Rio Blanco Formation and associated intrusions range from andesitic to rhyolitic in composition and mainly have calc-alkaline to transitional affinity. On tectonomagmatic discrimination diagrams, they plot in the field of volcanic arc rocks (Fig. 2).

U-Pb single grain zircon ID-TIMS dating of two dioritic intrusions cutting the Rio Blanco Formation yielded $^{206}Pb/^{238}U$ weighted ages of 35.77 ± 0.06 Ma and 15.70 ± 0.08Ma, respectively, suggesting multiphase magmatism in the area.

Volcanic rocks have undergone pervasive biotite-quartz and propylitic alteration (carbonate, chlorite, epidote, actinolite-tremolite, pyrite, pyrrhotite, chalcopyrite and tetrahedrite), followed by phyllic alteration (fine-grained muscovite and quartz) and local silicification as well as argillic alteration. Intrusive rocks are crosscut by Ca-silicates and hematite-pyrite bearing veins.

Lead isotope compositions of the volcanic rocks of the Rio Blanco Formation and of the intrusions show variably elevated $^{207}Pb/^{204}Pb$ values (15.62-15.70) indicating mixing between crustal and mantle sources, with a dominant crustal contribution.

Initial $^{87}Sr/^{86}Sr$ values range from 0.704 to 0.707, also indicating a crustal origin for the host volcanic and intrusive rocks.

Correlations of Sr and Pb isotopes with various fractionation indices suggest $^{87}Sr/^{86}Sr$ values of intrusive rocks increase with the evolution of magma, and $^{207}Pb/^{204}Pb$ and $^{206}Pb/^{204}Pb$ values of volcanic rocks also increase with the magma evolution; therefore, this indicates that

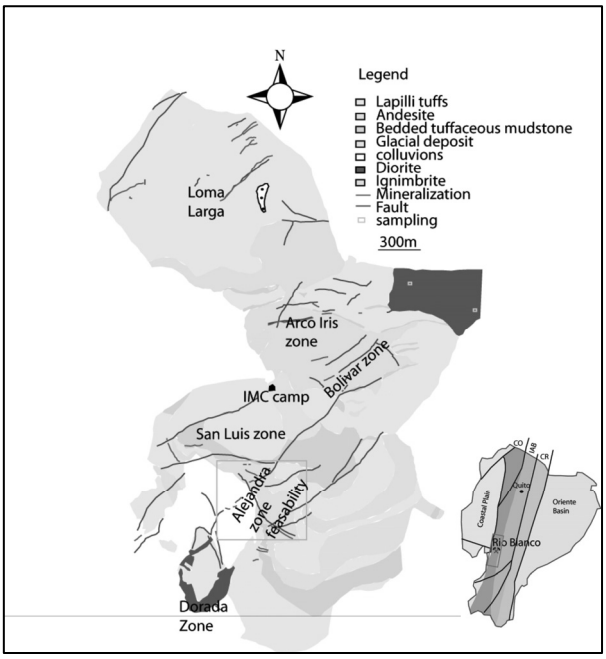


Figure 1. Location of Rio Blanco within the Western Cordillera of southwestern Ecuador and simplified geologic map of the prospect.

magmatic rocks in the Rio Blanco area have acquired their radiogenic Pb and Sr isotope compositions, while fractionating and assimilating crustal rocks. Black shales of the crystalline basement may have been assimilated because they have suitable Pb and Sr isotopic compositions (Chiaradia *et al.*, 2004).

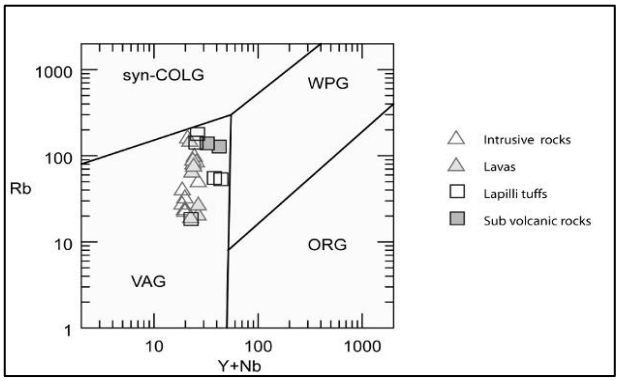


Figure 2. Geochemical discrimination (Y+Nb vs. Rb) diagram for Rio Blanco rocks (Pearce *et al.*, 1984) displaying a volcanic arc setting.

## 3 MINERALIZATION

Mineralization occurs as veins - hosted hydrothermal breccias and silicified zones, single or stockwork veins crosscutting wall rocks, open space filling and dissemination. The Au-Ag mineralization mainly occurs for several

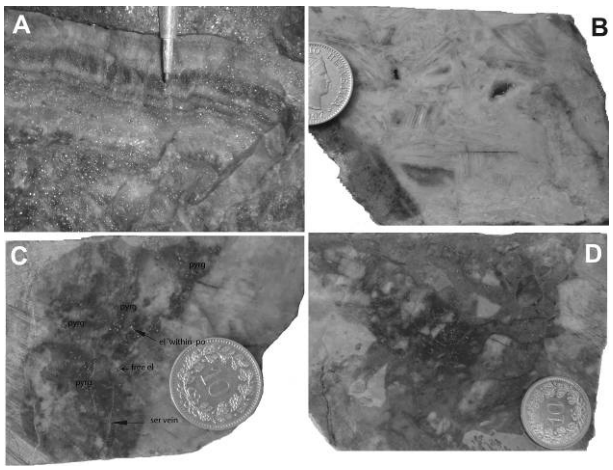


Figure 3: Photographs of mineralized vein showing crustiform (A, Alejandra vein, adit BP01) and replacement textures (B, drill core BC 122-197.78m). Mineralization is found both in silicified zones (C, drill core BC95-251.9m) and within breccias (D, drill core BC 116, 44.45m).

hundred metres within ENE-trending brecciated and silicified veins dipping at angles >45° towards the SE. The extensional veins were formed during dextral strike-slip movements along NNE-trending faults, likely induced by oblique subduction of the Nazca plate under the continental crust of Ecuador during the Tertiary. The veins show different textures including crustiform quartz (Fig. 3A), quartz after bladed carbonate (Fig. 3B), as well as a variety of breccia types (monomictic, polymictic, matrix-supported, clast-supported and jig-saw).

Breccias are mainly comprised of clasts of hydrothermal milky quartz, crustiform white and black quartz bands, quartz pseudomorphs after bladed carbonates, adularia, and lithic fragments. The matrix consists of fine-grained black quartz, sericite, carbonates, and accessory chlorite and actinolite-tremolite. Mineralization in the breccia matrix is comprised of pyrite, pyrrhotite, pyrargyrite (65-58 wt.% Ag), tetrahedrite (34-22% Ag), As-bearing (up to 2 wt. %) tetrahedrite (20-6 wt.% Ag), arsenopyrite, and accessory amounts of Fe-rich (10 mole % FeS) sphalerite, galena, chalcopyrite, dyscrasite, and electrum (60-44% Au). The total amount of sulfides is <2 vol.%. Electrum is concentrated in volumes of a few $cm^3$ within breccias (Fig. 3C) and silicified zones (Fig. 3D) where it mainly is associated with pyrrhotite (Figs.4A & 3C), but also with pyrite (Figs. 4A & 4B) and pyrargyrite (Fig. 3B), locally with sphalerite (Fig. 4A), and in places as free grains (Fig. 4D). Gold-rich electrum occurs at greater

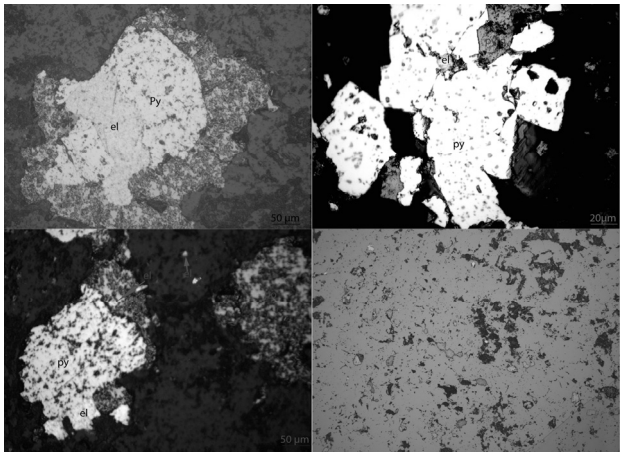


Figure 4: Photomicrographs of electrum (el) inclusions within pyrite (A&B), pyrrhotite (A & C) and free grains (D).

depths, whereas the highest Ag grades are encountered at shallower levels of the deposit.

Sericite associated with the mineralization yielded an Ar-Ar plateau age of 18.9±0.5 Ma. This has to be considered as a maximum age, because sericite is usually affected by Ar loss by recoil due to its small size. Whereas this maximum age might indicate that the Au-Ag deposit of Rio Blanco is unrelated to the older Eocene intrusion (~35.7 Ma), it does not exclude the possibility of a genetic association of the mineralization with the younger, Miocene intrusion (~15.7 Ma). In fact, the younger intrusion is overprinted in places by hydrothermal alteration such as silicification and silication, thus may have been emplaced before mineralization.

Lead isotope compositions of four pyrite samples (three sampled from silicified wall rock and one from a stockwork vein hosted by altered lava), two galena samples from mineralized veins, and a pyrrhotite sample from disseminated ore hosted by altered lava are identical within error. They are characterized by high $^{206}Pb/^{204}Pb$ (19.040-19.139) and $^{207}Pb/^{204}Pb$ (15.664-15.689) values. The ore Pb isotope compositions are more radiogenic than those of the Miocene intrusion in terms of $^{207}Pb/^{204}Pb$, but overlap the most radiogenic end of the host Rio Blanco volcanic rock fields (Fig.5), possibly suggesting lead derivation from the latter.

The $\delta^{34}S$ values of pyrite and galena (of the same samples used for Pb isotope analyses) range from -3 to +4 ‰, consistent with a magmatic source of S. Pyrrhotite occurring within disseminated ore in altered lava yielded a $\delta^{34}S$ value of -23.2 ‰ indicating a contribution of sedimentary S, probably related to black shales of the underlying basement, which are also found as clasts in the breccias.

## DISCUSSION AND CONCLUSIONS

Textures, gangue and sulphide mineralogy of Rio Blanco, as well as Fe contents of sphalerite are typical of an epithermal low sulfidation-type deposit. In low-T, low sulphidation systems Au is transported as a bisulphide complex and its precipitation usually occurs by boiling (Hedenquist 1991). Evidence of boiling is provided by bladed carbonate in mineralized

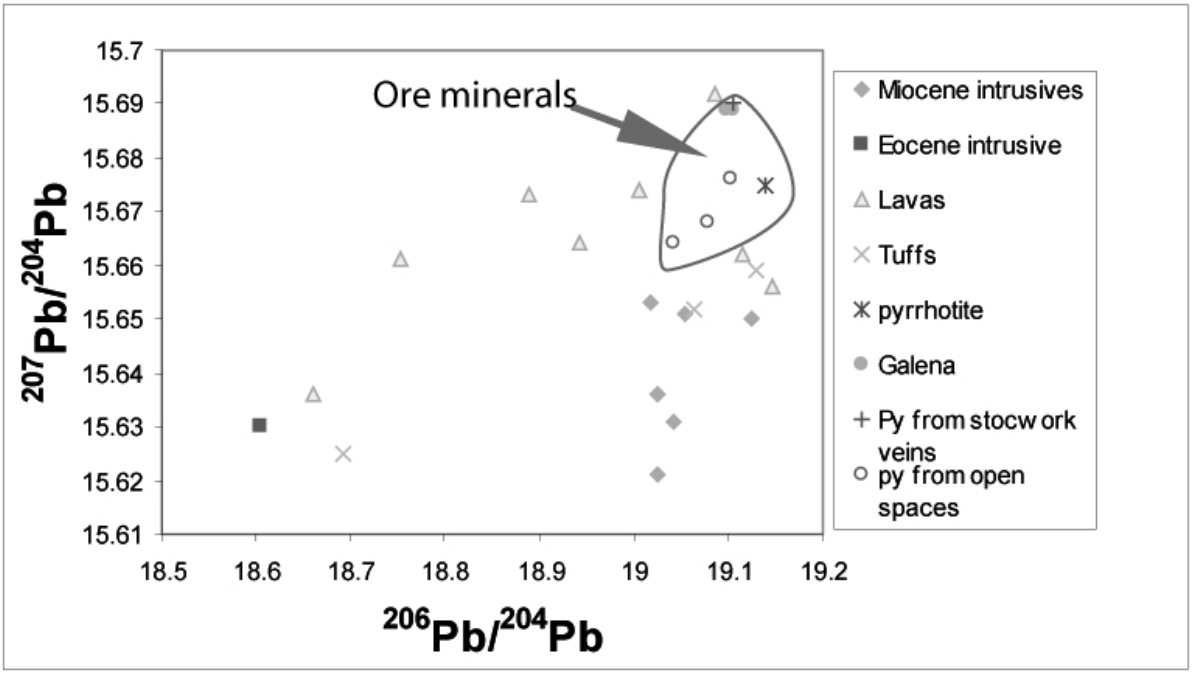


Figure 5: Uranogenic Pb isotope plot for Rio Blanco ore and associated volcanic and intrusive rocks.

veins at Rio Blanco. However, the Au-Ag mineralization always postdates the formation of bladed carbonate, which occurs as clasts within the Au-bearing breccia matrix. Therefore, Au precipitation may have resulted from sulphidation of Fe-bearing clasts within the breccia. Evidence of this process is provided by the frequent occurrence of pyrite around clasts, and of pyrite, pyrrhotite and Au within relict, now completely silicified clasts of the breccias. Sulphur and Pb isotope data for vein sulphides are consistent with a magmatic origin of these elements in the main ore. While our dating results at first glance rule out a genetic relationship between the diorite bodies and the mineralization, the hydrothermal alteration in the diorites is at odds with this scenario. The discussed uncertainty of the Ar-Ar (maximum) age of the mineralization-related sericite might account for these differences.

Further dating of mineralization-related phases, such as adularia or biotite, could help in clarifying this issue.

## ACKNOWLEDGEMENTS

We thank the Augustin Lombard foundation for financial support to TBB, IMC (International Mineral Corporation), the Rio Blanco prospect staff, and Dr. Bernado Beate (Escuela Politecnica Nacional, Quito, Ecuador) for logistic support.

## REFERENCES

Appleyard N (2003) Rio Blanco, Ecuador. *Technical Report for International Minerals Corporation*, 90 p

Chiaradia M, Fontboté L, Paladines A (2004) Metal sources in mineral deposits and crustal rocks of Ecuador (1°N-4°S): a lead isotope synthesis. *Econ. Geol.* 99: 1085-1106

Hedenquist JW (1991) Boiling and dilution in the shallow portion of the Waiotapu geothermal system, New Zealand. *Geoch. Cosmoch. Acta* 55: 2753-2765

Hedenquist JW, Arribas AJ & Gonzales-Urien E (2000) Exploration for epithermal gold deposits. *Reviews in Econ. Geol*. 13: 245-277

Pearce JA, Harris NBW & Tindle AG (1984) Trace elements discrimination diagrams for the tectonic interpretation of granitic rocks. *Journal of Petrology* 25: 956-983

# The Fruta del Norte epithermal Au-Ag deposit, SE Ecuador

Peter W. Stewart
*The Valley Geological Services Inc., Dundas, Ontario, Canada.*

Stephen Leary
*Aurelian Resources Inc., Quito, Ecuador*

ABSTRACT: The Fruta del Norte Au-Ag deposit represents an important discovery of large and locally high- grade epithermal mineralization under over 130m of barren to weakly altered, but in part syn-mineralization, epiclastic cover. Intermediate sulphidation-style mineralization with high manganese and base metal zones upward and northward into As+Sb enrichments and ultimately to weakly sulphidic, metal-poor, but gold-enriched quartz veins. The discovery has revealed a third important style of Jurassic arc-related gold metallogeny in the Cordillera del Condor.

KEYWORDS: gold-silver, epithermal, intermediate-sulphidation, Ecuador, Jurassic

## 1 INTRODUCTION

The Cordillera del Condor region of SE Ecuador has produced gold from alluvial and bedrock sources by small-scale artisanal mining intermittently since Spanish colonization (Gemuts *et al.* 1992). Historic bedrock sources include skarn-related deposits in the Nambija district, and andesite-dacite hosted intermediate-sulphidation epithermal veins and breccias in the Chinapintza district (Prodeminca 2000). Modern exploration has been limited for political (no mining law before 1985, uneven enforcement of the Mining Act, exploration bans near Peruvian border) and logistical reasons (challenging topography, dense tropical forest, low population and few roads). Aurelian Resources Inc. began field investigations and land acquisition in 2001 and commenced systematic exploration in 2003 of the Cordillera del Condor property which consists of over 95,000ha under concession. The La Zarza concession is roughly central to this block and hosts former informal bedrock mining sites. Alluvial mining continues to be widespread on rivers flowing through the property.

Detailed exploration (trenching, diamond drilling, mapping, geophysics) of the La Zarza concession was complemented by regional stream sediment surveying. Exploration in 2003-2005 focused on near-surface gold-silver prospects and included the delineation of inferred mineral resources in the Bonza-Las Peñas epithermal deposit (778700E, 9582000N, PSAD 1956) of about 15 million tonnes grading 1.07 g/t Au and 11.6 g/t Ag (Hennessey & Puritch 2005). Bonza-Las Peñas and other prospects are hosted in Jurassic andesites within the regional north-striking Las Peñas fault zone, which forms the eastern margin of the overlying epiclastic cover.

The exploration strategy changed in late 2005 when it became clear that basin sedimentation post-dated mineralising events in the fault zone, except for a weak late pulse of alteration. The new exploration model predicted that dilational basin margin faults may host epithermal mineralization beneath the fault-bounded basin. Diamond drilling at Fruta del Norte initially targeted a north-striking band of chalcedonic silicification in the epiclastic cover about 1.5 km north of Bonza-Las Peñas. Surface samples in the silicified area were generally low in Au+Ag, but anomalous in As+Sb±Hg.

Epithermal veining, stockworks and breccias have been intersected beneath 130-250m of generally weakly altered cover. Impressively long and rich intercepts are exemplified by CP-06-57 with 189.2m @ 24 g/t Au and CP-06-58 with 255.0m @ 12.55 g/t Au (0.5 g/t lower cutoff, no upper cutoff, up to 5m of internal dilution) (*Aurelian press releases, 06/06/2007 and 21/06/2006 respectively*) (Fig. 1). Drilling to

the end of 2006 reveals an apparently continuous, sub-vertical body grading several grams per tonne gold (Table 1) that is at least 1 km in strike length, over 200m in vertical extent and locally up to 125m in width (Fig. 2).

Table 1. Average metal contents of mineral zones (ppm, except as noted; 1 g/t and 200 g/t Au cutoffs, 0-7m of internal dilution).

| Zone | FDN1 | FDN2 | FDN4 | FDN3 | FDN5 |
|---|---|---|---|---|---|
| Au | **6.91** | **7.55** | **6.95** | **14.53** | **22.68** |
| Ag | **12.8** | **11.6** | **8.3** | **10.1** | **44.3** |
| Mn | 11756 | 255 | 353 | 134 | 7655 |
| As | 682.5 | 811.6 | 105.9 | 61.9 | 317.8 |
| Sb | 37.9 | 49.4 | 8.8 | 20.8 | 40.6 |
| Fe-% | 3.96 | 2.84 | 1.27 | 0.40 | 1.73 |
| S-% | 3.58 | 2.88 | 1.03 | 0.16 | 1.93 |
| Cu | 461 | 136 | 25 | 51 | 121 |
| Pb | 578 | 221 | 44 | 734 | 1442 |
| Zn | 1261 | 542 | 119 | 35 | 2142 |
| Hg | 0.9 | 1.5 | 1.1 | 4.9 | 1.8 |
| Mo | 7.7 | 10.7 | 2.2 | 1.7 | 3.2 |
| assays (length) | 844 (804.3) | 845 (838.2) | 461 (459.8) | 52 (48.9) | 94 (92.6) |

## 2 GEOLOGY

The Cordillera del Condor region lies immediately east of the Andes mountains, and is underlain primarily by Jurassic arc-related plutonic and volcanic rocks and pre- and syn-Andean orogeny cover. The La Zarza concession is dominated by the approximately 8km by 2km Suarez Formation epiclastic basin which overlies Misahualli andesite, the main arc-related volcanic sequence in the region. The basin fines upward from +100m of basal heterolithic conglomerate into a mixed sequence of interbedded siltstone, sandstone and conglomerate, which is overlain locally by younger (Fruta) andesite (Fig. 1). Post-arc early to mid-Cretaceous sequences blanketed the peneplained region prior to commencement of the Andean orogeny.

The Las Peñas fault zone bounds the Suarez basin to the east. The Jurassic Zamora batholith and poorly defined northwest-striking structures bound the basin to the west and northwest. The Fruta del Norte mineralization lies between two parallel strands of the Las Peñas fault zone near the eastern and northern basin margins and the intersection of the Las Peñas fault zone with northwest-, and possibly east- and northeast-striking structures. The age and sense of movement on the structures is poorly constrained at this time, and some, such as the Las Peñas fault zone, are inferred to have protracted histories with multiple senses of motion.

Epithermal vein and altered andesite clasts in basal conglomerate demonstrate hydrothermal activity that predates initial deposition of the Suarez Formation and basin formation. Rapid burial of an active hydrothermal system is indicated by siliceous sinter that is locally preserved at the volcanic/basal conglomerate contact. Silicified conglomerate at the contact is widespread and occurs locally in the overlying sequence. These relationships require continued hydrothermal activity after epiclastic deposition commenced. The two fault strands that bracket the deposit may be related to a step-over of the north-trending fault zone near the basin termination thereby creating an extensional setting conducive to hydrothermal activity continuing after burial by conglomerate.

## 3 MINERALIZATION

Fruta del Norte mineralization is characterized by multi-phase quartz-carbonate-sulphide-adularia stockwork veining and brecciation.

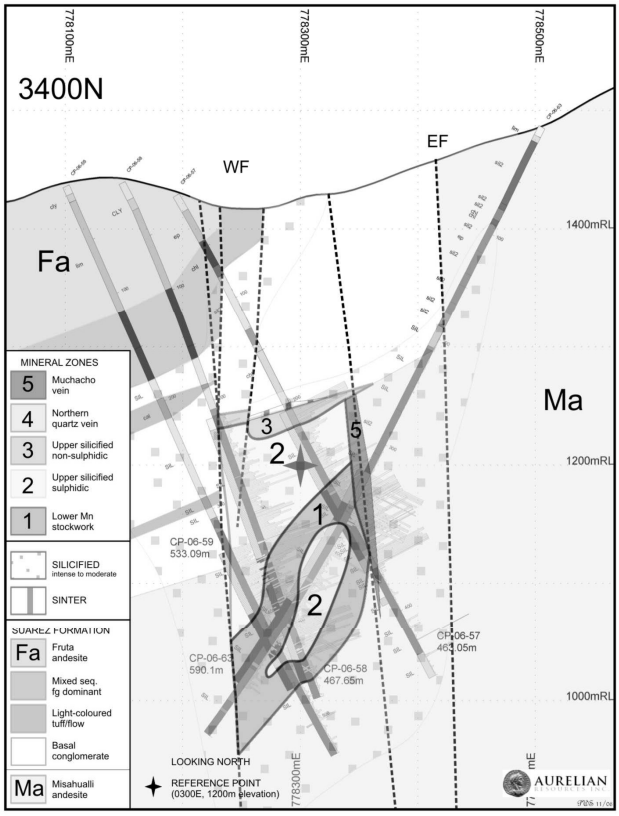


Fig. 1. Interpretative cross section (line 3400N) through the Fruta del Norte deposit. WF = west fault; EF = east fault

The veins exhibit classic epithermal textures with crustiform-colloform banding, bladed calcite (usually pseudomorphed by quartz) and crackle (hydrothermal) brecciation textures present throughout the system. Vein and breccia fill mineralogy consists of mm- to cm-wide laminations of chalcedonic to crystalline quartz, manganese carbonates, calcite, adularia and sulphides (one or both of marcasite and pyrite with subordinate sphalerite, galena, chalcopyrite and trace tetrahedrite and silver sulphosalts). Alteration of andesite and sedimentary rocks consists of proximal silicification within a broad illite halo that grades outward into widespread propylitic alteration.

Mineralization is zoned geochemically with the southern and deeper regions characterised by veins and stockworks, base metals and Mn (FDN1) (Fig. 2; Table 1). This intermediate-sulphidation style domain is flanked to the west, and succeeded upward to the Suarez contact by micro-veined and silicified rocks, elevated As and Sb and low Mn (FDN2). Intense white siliceous veining floods the northern domain (FDN4) which lacks elevated sulphides and metals. Gold averages about 7 g/t in each zone. High grade non-sulphidic silicified rocks (FDN4) underlie and flank sinter at the Suarez basal contact in the centre of the system. Quartz+carbonate±sulphide bonanza veins (FDN5) occur locally to the east (Fig. 1).Two mechanisms of mineral precipitation are proposed to produce the FDN hydrothermal system with geochemically and texturally distinctive mineral zonation. In the lower zone, boiling is identified by bladed calcite textures within finely banded crustiform-colloform quartz-manganese-carbonate-adularia-sulphide stockwork veins and breccias. In the upper zones where the mineralization penetrates into the epiclastic sequence, mixing and quenching of the rising mineralizing fluid with surficial waters formed a zone of pervasive silicification and repeated hydrothermal brecciation, largely devoid of manganese-carbonates.

The bulk of the gold is relatively fine and occurs in veins and silicified rocks. Coarse visible gold is common and visible gold occurs in all five zones.

## 4 CONCLUSIONS

The extent of gold-silver mineralization at Fruta del Norte is not defined and mineral resources are not yet estimated as drilling is limited to 100m-spaced sections. Infill drilling is in progress. With discovery less than one year ago, the following interpretations are consid-

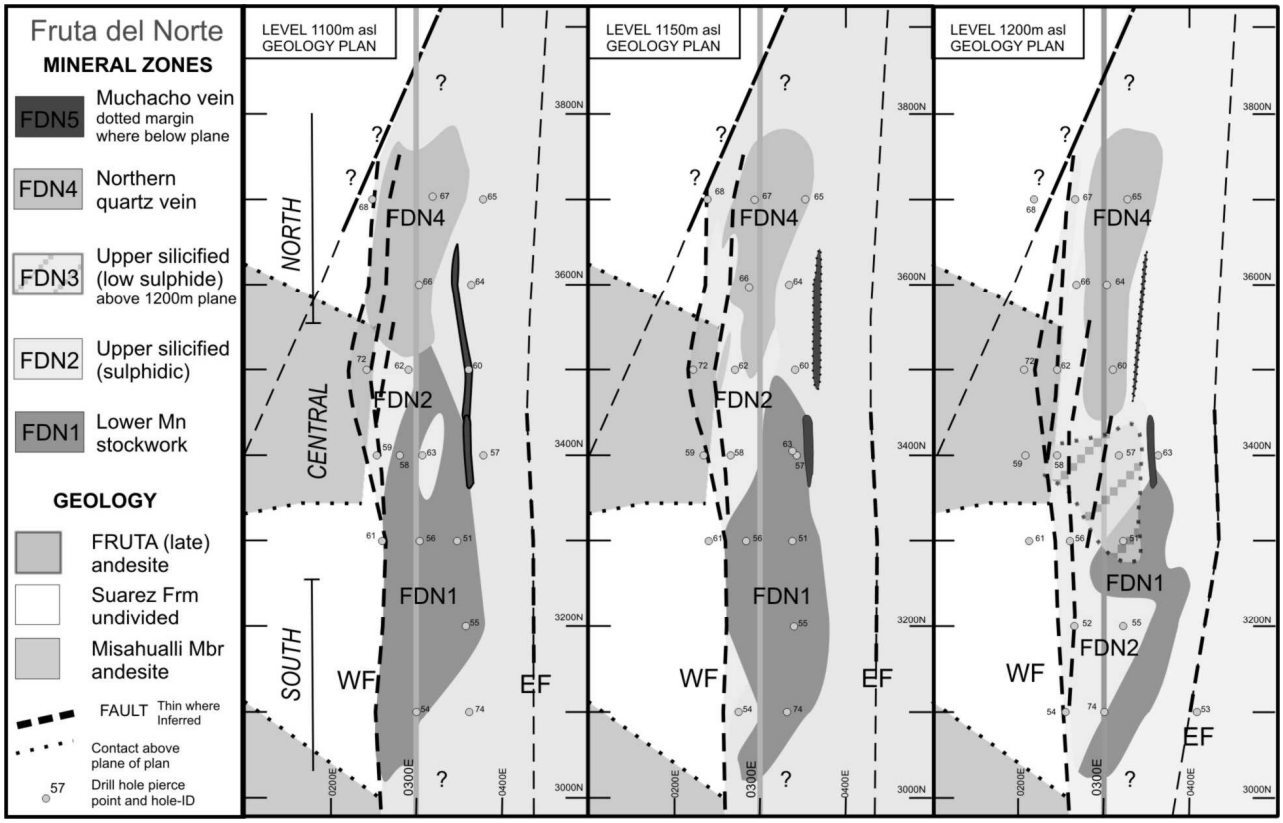


Fig. 2 Plan maps showing vertical and lateral mineral (geochemical) zonation at Fruta del Norte.

ered preliminary and modifications are likely as the Fruta del Norte system is explored and becomes better understood.

The hydrothermal system developed during initial stages of extensional faulting and formation of the Suarez pull-apart basin. Alteration and mineralization appears concentrated at and below the base of the Suarez Formation and with sub-basin faults. Widespread textural evidence for boiling and hydrothermal brecciation suggests that the system remained active and robust for some period after deposition of the cover. The continuation of the hydrothermal system under shallow cover is interpreted to have contributed to the exceptional size of the system, and the bonanza grades locally present.

It is clear even at this early stage of exploration that Fruta del Norte represents the discovery of a large and locally high-grade Au-Ag deposit. This discovery validates the prospective metallogeny of the under-explored Cordillera del Condor region perceived by Aurelian management in 2001.

## ACKNOWLEDGEMENTS

Management of Aurelian, especially Patrick Anderson, is thanked for supporting our attempts to understand the Fruta del Norte hydrothermal system. Aurelian geologists (J. Lema, C. Santa Cruz, V. Pazmay and C. Soto) contributed significantly to the original discovery and subsequent exploration. Discussions with ex-pat Aurelian geologists (K. Roa, B. Alloway, B. Nicolson) and R. Sillitoe have contributed to the ideas presented here.

## REFERENCES

Gemuts I, Lopez G, Jimenez F (1992) Gold deposits of Southern Ecuador. *Society of Economic Geologists Newsletter*: No 11, pp 1, 13-16

Hennessey BT, Puritch G (2005) A mineral resource estimate for the Bonza-Las Penas deposit, Cordillera del Condor project, Zamora-Chinchipe province, southeastern Ecuador. *Report for Aurelian Resources Inc, January 2005,* 88 p. (available at www.sedar.com)

Prodeminca (2000) Porphyry and epithermal-mesothermal deposits associated with Cordillera del Condor intrusions. *Evaluacíon de Distritos Mineros del Ecuador* 5: June 2000, Quito, Ecuador, 223 p

# The role of deformation partitioning and foliation reactivation in localizing gold mineralization in the Choco 10 complex, Venezuelan Guyana Shield

A. Ham[1], R.J. Gradim[2], M.E. Dusci[2], J.M.Gressier[2] & P. Hodkiewicz[3]
1 *SRK Consulting (Canada) Inc., Suite 800, 1066 West Hastings Street, Vancouver, B.C. V6E 3X2*
2 *Promotora Minera de Guayana, Gold Fields Venezuela, Vía El Limón, Sector La Ramona, El Callao 8050, Est. Bolívar, Venezuela*
*3 SRK Australasia, 1064 Hay St, West Perth, WA 6005, Australia*

ABSTRACT: The Gold Fields Choco 10 mineralized complex in Venezuela exhibits strong structural controls on mineralization. Gold is hosted primarily in lower strain domains, which are characterized by spaced crenulation cleavage and parasitic folds. Adjacent high-strain domains are less well mineralized, characterized by planar and penetrative foliations. Mineralization occurs with pyrite, ankerite-dolomite, and quartz veins, with variable degrees of silica and sericite alteration. Structural textures and spatial relationships indicate that mineralization was at least partially synchronous with $D_3$ deformation, although the gross geometry of mineralized domains occurs within $D_2$ high- and low-strain zones. Higher grade mineralization developed in $D_2$ lower strain domains because of strain heterogeneity during $D_3$. $D_2$ high-strain domains are poorly mineralized and are characterized by very planar foliations ($S_1$ and $S_2$), which were favourably oriented to reactivate during $D_3$.

KEYWORDS: Gold, Choco 10, Venezuela, Deformation Partitioning, Reactivation

## 1 INTRODUCTION

The development of a robust structural model has been a key element in realizing the potential of the Choco 10 gold complex. The structural understanding has been applied to the development of new drill targets, delineation of high-grade ore shoots and in geological modeling for resource estimation.

The Choco 10 mineralized complex is located in the southeastern part of Venezuela in the Bolivar state, approximately 15 kilometres west of the town of El Callao. The El Callao District is an historic gold mining region and was regarded as an important producer in the late 19th Century. Open pit production commenced on Choco 10 in August 2005. There are currently four primary ore deposits; Rosika, Coacia, Pisolita (RCP), and Villa Balazo-Karolina (VBK) (Fig. 1). During November 2005 Gold Fields Limited and Bolivar Gold Corp entered into an agreement providing for Gold Fields to acquire all outstanding securities of Bolivar Gold. The purchase, finalized in March 2006, has given Gold Fields 95% ownership of the Choco 10 Mine. The current resource is 63.6Mt @ 1.7g/t Au for 3.47 Moz of gold (December 2005).

## 2 GEOLOGICAL SETTING

The Choco 10 gold deposits are located in the central portion of the Guasipati Greenstone Belt, part of a large Palaeoproterozoic terrane in the Venezuelan Guyana Shield, including metavolcano-sedimentary rocks of the Pastora-Botanamo Province and granitoids of the Supamo Complex. These rocks were metamorphosed, deformed and mineralized in the 2.1-1.9 Ga Trans-Amazonian Orogeny, which caused the accretion of various volcanic centres (precursors of the greenstone belts) around the Archaean Imataca palaeocontinent (Vanderhaeghe *et al.* 1998). The boundary between these two terranes is the Guri Structure, a major ENE-trending ductile shear zone (Fig. 1).

The Guasipati Belt contains the type sections of the Pastora Supergroup, which at the base includes tholeiitic basalts and volcaniclastic rocks of the Carichapo Group (Menéndez 1994). The Choco 10 complex is hosted in this basal portion, metamorphosed in the lower greenschist facies.

From stratigraphic base to top (west to east),

the four main rock units in the camp are: 1) tholeiitic basalts, flow-top breccias and mafic volcaniclastic rocks dominant on the VBK and Pisolita deposits, 2) calc-alkaline intermediate volcaniclastic sediments dominant on the Rosika-Coacia deposits, 3) gabbro sill intruding unit 2, and 4) trondhjemite pluton and associated dykes intruding the whole sequence (Fig. 1).

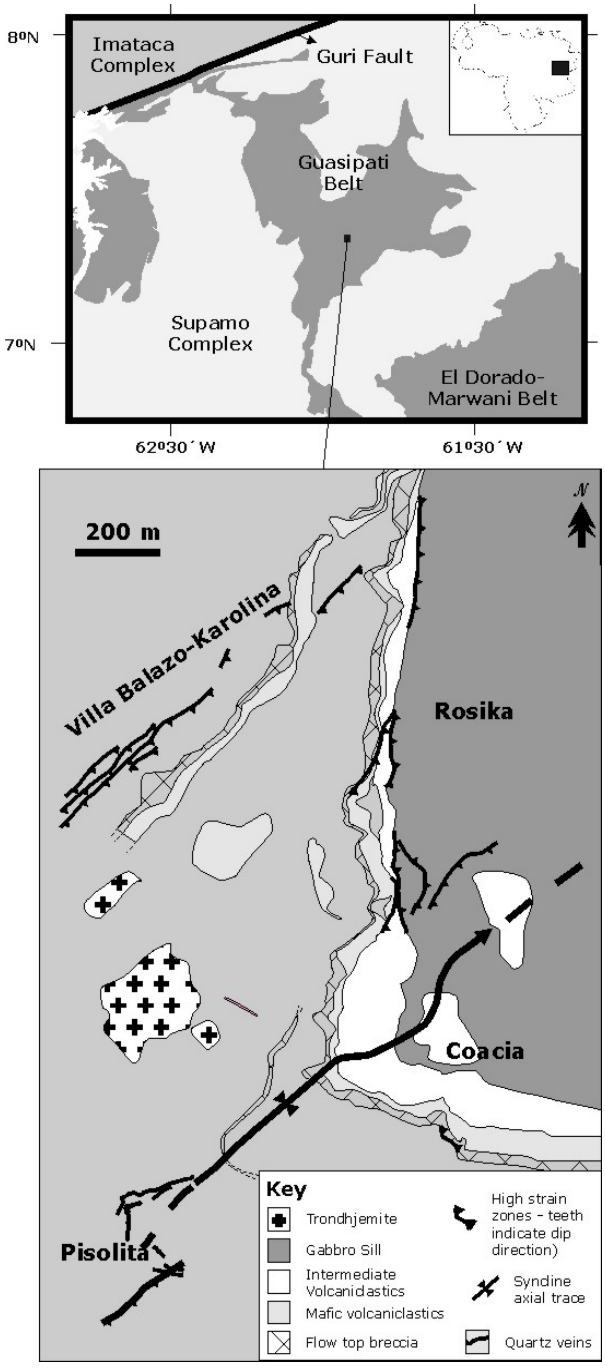


Figure 1. Location of El Callao District and simplified geological map of RCP-VBK complex.

## 3 DEFORMATION FRAMEWORK

The Choco 10 gold complex is located in a regional NE-plunging synclinal hinge zone (Fig.1). The structural architecture is dominated by folds and ductile fabrics indicating a long history of compressional deformation. Deformation partitioning is highly developed, and as a result there are large volumes of rock that preserve primary features (low-strain zones), while deformation is concentrated in zones of intense development of ductile fabrics (high-strain zones). At least four generations of foliations representing different stages of crenulation cleavages have been identified (A. Ham unpublished data): 1) a penetrative slaty cleavage $S_1$ sub-parallel to $S_0$ and axial planar to rare $D_1$ folds, 2) a NE-striking, SE-dipping weak to fully differentiated crenulation cleavage $S_2$ characteristic of mineralized zones, 3) a NNE- to N-striking, steeply dipping crenulation cleavage of variable intensity occurring within discrete shear zones where it rotates $S_2$, and 4) a rare NW-striking, kink-like crenulation usually found overprinting $S_2$ and locally $S_3$.

The geometry of mineralization is strongly controlled by $S_2$. $D_2$ high-strain zones can be further divided into higher-strain – cleavage/limb domains where $S_0$ and $S_1$ have been rotated into parallelism with $S_2$, and lower-strain – microlithons/hinge domains where $D_1$ folds are preserved. Ductile or brittle shear zones that accommodate large displacements are absent; strain has been accommodated instead by foliation development and large volume loss throughout the rock package, leading to a model of bulk shortening (P. Hodkiewicz *unpublished data*). The deformation history of the Choco 10 mineralized complex is summarised as follows:

a) Early Trans-Amazonian NE-SW to E-W directed bulk shortening that forms a steep $S_1$ fabric and rotates $S_0$ to a moderate dip.
b) $D_2$ NW-SE bulk shortening forming NE- to ENE-trending folds of $S_0$ and $S_1$.
c) WNW to ESE shortening during $D_3$ partitions deformation into discrete zones of high-strain. During development of $D_3$ shear zones in VBK the $S_2$ fabric is reactivated.
d) Late NE-SW shortening during $D_4$ producing weak kink-like crenulation.

## 4 GOLD MINERALIZATION

The characteristics of gold mineralization are varied as a result of a complex interplay between host rock rheology, permeability and geochemistry, proximity to structures and hydrothermal fluid composition.

Gold mineralization is frequently accompanied by carbonate alteration, dominantly ankerite and dolomite, and varying degrees of silica and sericite. Pyrite is the most abundant sulphide phase and occurs in relatively low concentrations (2-10%) and has a good correlation with gold tenor. Replacement-style hydrothermal alteration is common in more permeable host rocks, such as coarse-grained volcaniclastics and flow-top breccias of basalts. In less permeable massive basalts and gabbros vein-hosted mineralization is common and often contains visible gold. Mineralization is principally hosted in lower strain zones, which comprise spaced crenulation and less commonly brecciation and cataclasites, coupled by well developed continuous foliations typical of high-strain domains.

Alteration assemblages of low-grade halos to mineralization typically consist of chlorite± carbonate±sericite±magnetite and contain on the order of 100-500 ppb Au. The intense alteration in the halos associated with high-strain domains tends to obliterate any primary igneous or sedimentary textures.

## 5 STRUCTURAL CONTROLS ON GOLD MINERALIZATION

Rheological heterogeneities resulting from the distinct stratigraphic sequence form the dominant geometrical control on mineralization at Rosika, which dips to the east along the contact between volcaniclastic and basaltic units parallel to $S_1$ (Fig. 1). SE-dipping $S_2$ domains host economic mineralization at Rosika and Coacia. High-grade ore shoots occur in lower strain zones at the intersection of these two foliations at Rosika, and are controlled by a NE-plunging syncline axis at Coacia. Mineralization at Pisolita is dominantly controlled by a stack of sub-horizontal quartz veins, which formed as extensional veins in the hinge zone of the syncline to the SW of Coacia.

There are two different structural controls on the geometry and genesis of mineralization of the VBK ore zone. Mineralized veins are primarily located within $D_2$ lower-strain zones, where veins have formed sub-parallel to the folded $S_1$. A less common but second style of mineralized vein includes those that have formed parallel to the $S_2$ foliation. In some instances, veins that have formed parallel to the $S_2$ fabric represent quartz replacement of the folded $S_1$ cleavage within the Q domain of a crenulation cleavage. However, there are examples where the mineralized vein cuts both the $S_1$ (at a high angle) and $S_2$ (at a low angle). This suggests that at least one phase of mineralization has occurred post $D_2$. In fact, subtle deflections and displacement of the pervasive $S_2$ fabric were identified within or adjacent to certain zones of mineralization. This overprinting of $D_2$ fabrics is attributed to $D_3$, although $D_3$ shear zones show minor displacement and are relatively difficult to recognize in drill core.

The structural framework created during $D_2$ is the main geometrical control on mineralization at the Choco 10 system. The timing of mineralization is not well constrained. It is plausible that the majority of gold formed in $D_2$ lower strain domains with subsequent modification during $D_3$ causing gently doubly plunging folds to high-grade shoots. Although a large volume of mineralization can be explained in the timeframe of $D_2$, at least part of the mineralization appears to be coeval with $D_3$. This is emphasized below as an example of the role of deformation partitioning and foliation reactivation in localizing gold.

Crenulated and folded zones of lower $D_2$ strain provide areas where the foliation geometry promotes dilation and vein formation during $D_3$. These areas have become sinks for fluids and allowed the mineralizing reactions to proceed to completion. In the $D_2$ higher-strain zones, the $S_2$ fabric is more penetrative and planar. The geometry of the $S_3$ fabrics is at a low angle to $S_2$, and the shear sense of $S_3$ relative to $S_2$ suggests that a great deal of strain during $D_3$ has been accommodated by reactivation of $S_2$ in the $D_2$ high-strain domains. In $D_2$ lower strain domains, the variable geometry of $S_1$ and the coarsely spaced and less penetrative $S_2$ are zones where reactivation during $D_3$ could not take place. Therefore, $D_3$ strain accumulates by dilation and vein formation and the open folding of $S_2$. In summary, there are two structural controls of mineralization within VBK. The first is the geometry of $D_2$ lower strain zones (zones of $D_2$ folding and spaced crenulation development), which are areas with very irregular foliation geometry that cannot ac-

commodate $D_3$ strain by reactivation. The second is the presence of $D_3$ as this deformation event is at least partially synchronous with mineralization. Consequently, the internal geometry and continuity of the mineralization within VBK is controlled by the geometry and continuity of $D_2$ lower strain zones. The gross scale geometry and controls of the deposit may be controlled by $D_3$; this is presently being tested by drilling programs and detailed mapping as the open pit mines develop.

## 6 SIGNIFICANCE OF DEFORMATION PARTITIONING AND REACT-IVATION ON GOLD MINERALIZATION

During orogenesis, deformation partitions into zones of progressive shortening and shearing. Zones of progressive shearing can be crenulation cleavage seams or discrete shear/high-strain zones and the zones of progressive shortening become crenulation hinges or folds (Ham & Bell 2004). Deformation partitioning is influenced by a number of parameters that include rheology, pre-existing anisotropies, grain size, relative position in the crust and the metamorphic grade. An important aspect is the development of anisotropies through the rock, as this allows processes such as reactivation to accommodate strain.

Reactivation (Bell 1986) is an important process as it is a sympathetic process to accommodate displacement of rock units during bulk shortening. Foliation reactivation during bulk shortening is a fundamental process in accommodating strain. However, in areas where reactivation cannot proceed, strain will accumulate. Higher strain is either accommodated by ductile processes (such as folding, foliation or shear zone development), or by brittle processes if the elastic strain of the rock is exceeded (*e.g.* cataclasis, fault development). Where strain accumulates in this way, there are more potential sites available for hydrothermal or metasomatic fluids. That is, in areas where there is increased folding, there are more sites available for dilation (such as hinges, short limbs of folds, zones of brecciation). Therefore, understanding which limb of a fold can reactivate can be a powerful tool in predicting sites of mineral/metal deposition.

The concentration of mineralization in $D_2$ lower strain domains could be explained by a dominant mineralizing event coeval with $D_2$, which extended into $D_3$. The role of $D_3$ may have involved shortening, which partitioned strain into discrete zones of shear, with the majority of the strain accommodated by reactivation of the $S_2$ and $S_1$ foliation on the long limbs of $D_2$ folds. However, on the short limbs of $D_2$ folds, $S_1$ was in a geometry where it could not reactivate and therefore, further shortening and dilation developed on these limbs. In areas where $D_3$ shear zones developed and on the reactivated long limbs of $D_2$ folds, strain was accommodated primarily by shearing (*i.e.* dissolution). In contrast, $D_3$ shortening in the short limbs of $D_2$ folds increased fold amplitude, allowing dilation of hinge zones, preferentially channelling mineralizing fluids into these zones.

## ACKNOWLEDGEMENTS

Acknowledgment and thanks go to the numerous people involved in the collection of geological data over the years, who have contributed to development of the geological understanding of the Choco 10 mineralized system. The authors are also grateful to Gold Fields for permission to publish this paper.

## REFERENCES

Bell Th (1986) Foliation development and refraction in Metamorphic Rocks: Reaction of earlier foliations and decrenulation due to shifting patterns of deformation partitioning. *J Met Geol* 4: 421-444.

Ham AP, Bell TH (2004) Recycling Of Foliations During Folding. *J Struct Geol* 26:1989-2009.

Menéndez A (1994) Cinturones de Rocas Verdes del Escudo de Guayana en Venezuela, Revisión Estratigráfica. III *Simposio Internacional de Oro en Venezuela.* Libro de Memorias. Asoc. Venez. Del Oro, Caracas, pp 123-139.

Vanderhaeghe O, Ledru P, Thieblemont D, Égal E, Cocherie A, Tegyey M, Milési JP (1998) Contrasting mechanisms of crustal growth. Geodynamic evolution of the Paleoproterozoic granite-greenstone belts in French Guiana. *Precamb Res* 92:165-194.

# Miocene El Indio epithermal gold belt (Northern Chile): an evolving tectonomagmatic scenario

R. Oyarzun[1], J. Lillo[2], J. Oyarzún[3], P. Higueras[4]
[1] *Departamento de Cristalografía y Mineralogía, Facultad de Ciencias Geológicas, Universidad Complutense, 28040 Madrid, Spain*
[2] *Escuela Superior de Ciencias Experimentales y Tecnología, Universidad Rey Juan Carlos, Tulipán s/n, 28933 Móstoles (Madrid), Spain*
[3] *Departamento de Minas, Facultad de Ingeniería and CEAZA, Universidad de La Serena, Casilla 554, La Serena, Chile*
[4] *Departamento de Ingeniería Geológica y Minera, Escuela Universitaria Politécnica de Almadén, Universidad de Castilla-La Mancha, Plaza M. Meca 1, 13400 Almadén, Spain*

ABSTRACT: El Indio gold belt is a metallogenic province of Miocene age, located in the Coquimbo region (northern Chile). The belt formed during Late Miocene, and comprises barren advanced argillic alteration zones, and world class Au-Cu-As epithermal deposits, such as El Indio. We relate the origin of the belt to a major shift in magmatism, during subduction of an oceanic ridge, associated crustal uplift, and reactivation of older NNE R2 type regional fractures.

KEYWORDS: Gold mineralization, tectonomagmatism.

## 1 INTRODUCTION

Ore deposits are anomalous features in the Earth's crust that typically form by a very unusual combination of geologic processes. The Coquimbo Region, in the northern part of Chile, contains numerous mineral deposits (Fig. 1). The Andean realm of this region is host to a spectacular belt of hydrothermal alteration that encompasses economic gold deposits of the epithermal type. Notable among these is the world class El Indio Au-Cu-As deposit (Fig. 1). The belt formed during late Miocene time (Bissig *et al*. 2002) and most of the alteration zones and deposits in the Coquimbo Region occur along a relatively narrow NNE-trending corridor (Figs. 1, 2). This communication discusses the regional structural lineaments present in the Andes of the Coquimbo Region and interprets them in the context of an evolving structural scenario, characterized by the presence of a large SE-trending fault zone and associated $R_1$ and $R_2$ type structures of probable Oligocene age (Oyarzun *et al*. 2006). We suggest that the epithermal belt may have formed along reactivated $R_2$ shears (structural corridors), during a major shift in the locus of late Miocene magmatism.

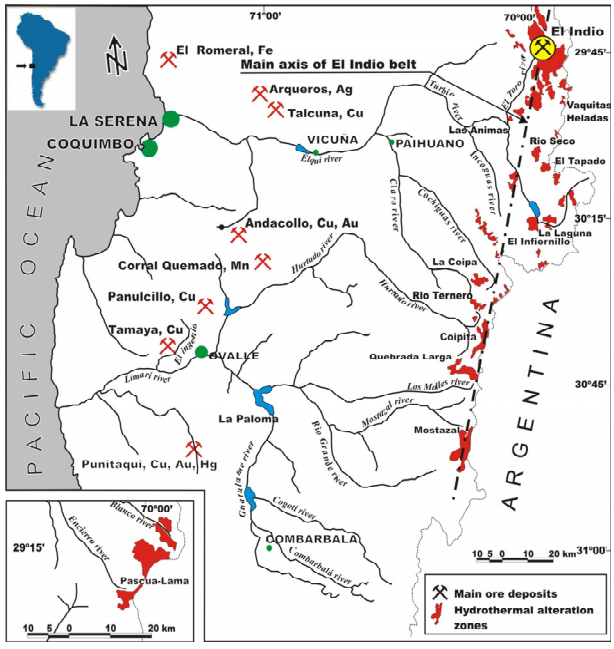


Figure 1. The Coquimbo Region of Chile and location of major mineral deposits and alteration zones. Location of ore deposits and hydrothermal alteration zones (modified after Maksaev *et al*. 1984; Higueras *et al*. 2004).

## 2 ADVANCED ARGILLIC ALTERATION

More than thirty large alteration zones of Miocene age can be defined along the high Andes within a *ca*. 200 x 20 km belt in the Ata-

cama and Coquimbo regions (Maksaev *et al*. 1984). Volcaniclastic facies of the Doña Ana Formation are the most commonly altered rocks along the belt, although older units also have been affected. The Coquimbo segment of the belt strikes NNE and includes alteration zones, such as those at El Indio, Vaquitas Heladas, Las Animas, Rio Seco, El Tapado, La Laguna, El Infiernillo, La Coipa, Rio Ternero, Coipita, Quebrada Larga, and Mostazal (Figs. 1, 2; Maksaev *et al.* 1984). Many of the El Indio belt alteration zones are comprised of advanced argillic alteration mineral assemblages, with kaolinite, alunite, and silica jaspers. The Miocene history of hydrothermal processes in this realm is complex, even though mineralization processes took place over a short 9.4-6.2 Ma interval of time (Bissig *et al.* 2002).

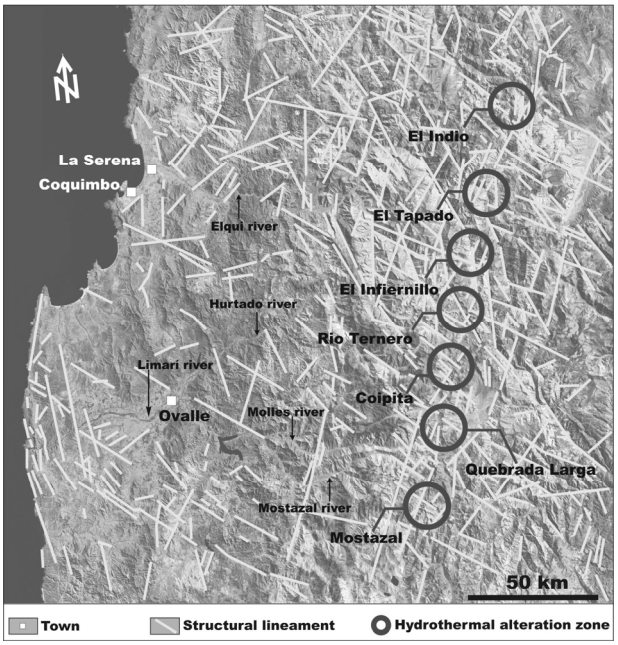


Figure 2. LANDSAT 7 image including approximate location of some of the main alteration zones, prospects, and epithermal ore deposits (black circles), and major structural lineaments (white lines). See figure 3 for an interpretation of the structural lineaments.

## 3 EPITHERMAL DEPOSITS

The most conspicuous deposit along the belt is the world class El Indio. This deposit (Araneda 1985) is a vein-type deposit (tensional fractures) bound by NNE-SSW faults thus defining a 500m long, 100-150m wide mineralized corridor. The deposit is hosted by volcaniclastic rocks of the Tilito Member of the Doña Ana Formation (rhyolitic to dacitic welded tuffs). The deposit (before mining) hosted two types of veins: 1. Gold-quartz (up to 6m thick), with native gold and calaverite, enargite, and tetrahedrite-tennantite, with some chalcopyrite, sphalerite and galena at depth. Cu grades were in the range of 1-5% and mean gold grades were of 240 g/t, although localized sectors exceeded these concentrations up to contained more than 1,000 g/t (and 86 g/t Ag). 2. Massive sulphide veins (up to 12m thick) with enargite, pyrite, and minor chalcopyrite and tetrahedrite-tennantite. Cu grades were in the range of 8-14%, whereas those of gold and silver ranged from 8-10 g/t and 140-160 g/t respectively. Advanced argillic alteration (quartz-phyrophillite, alunite) occurs together with phyllic and propylitic mineral assemblages, and silicification. The nearby El Tambo deposit constitutes a different case, characterized by the presence of hydrothermal breccias with clasts of dacitic tuffs cemented by silica, barite, and alunite. Au and silver grades range from 7 to 22 and 1 to 54 g/t, respectively. Although the Pascua – Lama epithermal deposit is located farther north, in the Atacama Region (Figs. 1, 4), and is displaced slightly westward from the main NNE trend, it also deserve merits attention, because of its size and present economic importance. Despite some initial environmental concerns, the mining project will become fully operational in the next few years. Reserves are estimated at 225 Mt grading 1.98 g/t Au, 66 g/t Ag, and 0.05% Cu (Chouinard *et al.* 2005). The ore is hosted by Triassic granites and Miocene breccia pipes.

## 4 TECTONOMAGMATIC EVOLUTION

Although mineral deposition is ruled by relatively well known physical chemical processes, the framework in which the appropriate conditions are met to form large ore deposits comes from a rather fortuitous combination of geological events, in both time and space. This assertion is particularly valid in the case of formation of precious metal deposits.

We cannot explain ore deposit formation in restricted terms, for example, magmatism or structure alone. On the contrary, in order to answer major questions such as "why here and not there" or "why in this particular time-span and not before or after" we have to analyze very carefully the many geological events that were occurring during ore deposit formation. After all, ore deposits are geological anomalies, and as such, their study requires a broader

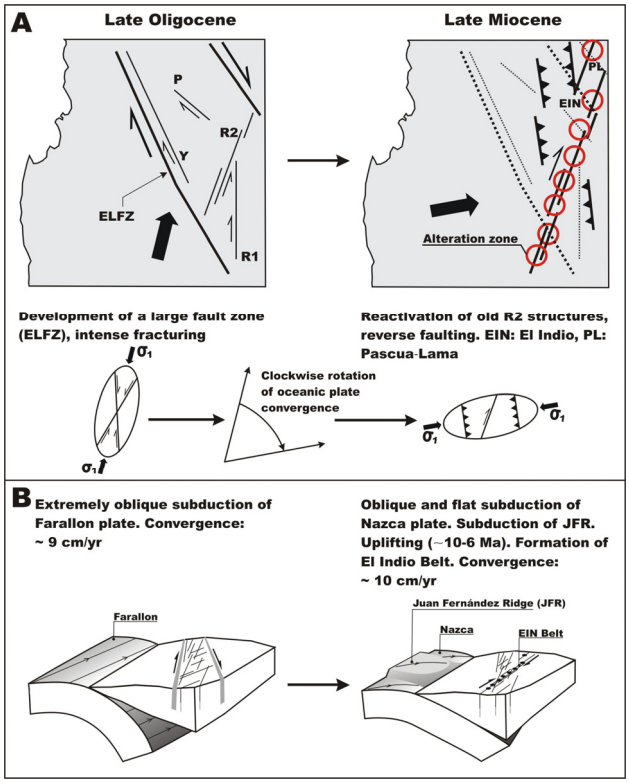


Figure 3. A) Structural interpretation of lineaments in terms of a NW-SE fault zone (ELFZ) and tectonic evolution from Late Oligocene to late Miocene. EIN: El Indio; PL: Pascua-Lama. B) Plate tectonic evolution during the same time span, from Farallon to Nazca and structural emplacement of the El Indio belt. EIN: El Indio.

view. The late Miocene in central northern Chile can be regarded as a crucial period when a number of favourable conditions coincided to generate a metallogenic belt such as that of El Indio. These conditions included ridge subduction, increased plate coupling, and a change in magmatism. Increased plate coupling reactivated older NNE structures, along which the El Indio belt formed. Fault reactivation during ridge subduction may have been enhanced by coeval massive erosion – peneplain formation and uplift of structural blocks. In addition, the composition and style of magmatism changed from mainly andesitic edifices to dacitic dome or dyke complexes. This change restricted discharge of volatiles, which in turn led to enhanced retention of $SO_2$ and metals, and therefore, to formation of sulphur- and metal-rich hydrothermal solutions. This scenario would explain why some deposits (*e.g.* El Indio) of the belt were so rich in sulphur and gave rise to Cu-Au-As-S mineral parageneses of major economic importance.


Figure 4. The NW and NNE trends, and location of El Indio and Pascua-Lama deposits. Both deposits are separated by a distance of ~58 km. Google Earth oblique image.

## ACKNOWLEDGEMENTS

This study has been funded by Spanish Agency of International Cooperation (AECI), and by Spanish Ministry of Science and Education (grant PPQ2003-01902).

## REFERENCES

Araneda R (1985) Nuevos aportes al conocimiento de la geología de El Indio, yacimiento de oro, plata y cobre. Coquimbo, *Chile. Rev Minerales* 168: 27-39.

Bissig T, Clark AH, Lee JKW, Hodgson CJ (2002) Miocene landscape evolution and geomorphologic controls on epithermal processes in the El Indio-Pascua Au-Ag-Cu belt, Chile and Argentina. *Econ Geol* 97: 971-996.

Chouinard A, Williams-Jones AE, Leonardson RW, Hodgson CJ, Silva P, Téllez C, Vega J, Rojas F (2005) Geology and genesis of the multistage high-sulfidation epithermal Pascua Au-Ag-Cu deposit, Chile and Argentina. *Econ Geol* 100: 463-490.

Higueras P, Oyarzun R, Oyarzún J, Maturana H, Lillo J, Morata D (2004) Environmental assessment of copper–gold–mercury mining in the Andacollo and Punitaqui districts, northern Chile. *Appl Geochem* 19: 1855-1864.

Maksaev V, Moscoso R, Mpodozis C, Nasi C (1984) Las unidades volcánicas y plutónicas del Cenozoico Superior en la alta cordillera del Norte Chico

(29º-31ºS): geología, alteración hidrotermal y mineralización. *Rev Geol Chile* 21: 11-51.

Oyarzun R, Lillo J, Oyarzún J, Higueras P, Maturana H (2006) Strong metal anomalies in stream sediments from semiarid watersheds in northern Chile: when geological and structural analyses contribute to the understanding of environmental disturbances. *Intern Geol Rev* 48: 1133-1144.

# Granitic Magmatism as a Fluid Source for Lode Gold Deposits in the Atlantic City-South Pass City Area, Wyoming

E.S. Vaughn & J.R. Ridley
*Dept. of Geosciences, Colorado State University, CO, USA*

ABSTRACT: The Louis Lake Batholith is intruded into the South Pass Greenstone Belt, which hosts the lode gold deposits near Atlantic City and South Pass City, Wyoming. Because of its proximity to the deposits, the Louis Lake Batholith is a potential ore fluid source. Fluid inclusion work has provided evidence of Archaean age aqueous-carbonic and hypersaline fluids derived from a crystallizing granite at depth. These fluids provide the potential for carrying metals in solution, because they are similar to fluids found in lode gold deposits and porphyry deposits.

KEYWORDS: fluid inclusion, lode gold, Wind River Range

## 1 INTRODUCTION

The origin of the ore fluid of lode gold deposits has long been in debate. There are three major models for the origin of the fluids. These include fluids exsolved from a felsic magma, metamorphic devolatilization, and circulating meteoric waters. The model of exsolving fluids from a crystallizing granitic magma is examined in this paper. The Archean Louis Lake Batholith, located adjacent to the South Pass Greenstone Belt in the southern end of the Wind River Mountains, Wyoming, was chosen for this study because of its proximity to lode gold deposits of a similar age. This granite contains numerous pegmatites and aplitic dykes as evidence of late stage fluid movement.

Samples of the granite and late phases, such as aplites, pegmatites, and quartz segregations, were sampled. Fluid inclusion work was completed to determine the chemistry of the fluids in these late phases. Petrology and fluid inclusion data is used to determine the conditions within the pluton during the late phases of crystallization.

## 2 GEOLOGIC HISTORY OF THE SOUTHERN WIND RIVER RANGE

### 2.1 *General Geology*

The Louis Lake Batholith is an Archaean age batholith that intruded into a sequence of metasedimentary and metavolcanic rocks, and earlier granitic gneisses. It is believed that the batholith was intruded during the accretion of a volcanic arc. The batholith was emplaced about 2.63 Ga (Frost *et al*. 1998). Gold in the South Pass Greenstone Belt is present in gold-quartz veins found in late tectonic shear zones. Frost *et al* (2006) dated a shear zone within the greenstone belt, and found an age of about 2.61 to 2.63 Ga. Total gold production is estimated to be approximately 348,600 ozs (Hausel 1991). The Wind River Mountains were uplifted during the early Tertiary Laramide Orogeny along the Wind River Thrust (Hausel 1991). Figure 1 gives a location map of the field area.

### 2.2 *Geology of the Louis Lake Batholith*

The Louis Lake Batholith is the largest of several Archaean batholiths at the southernmost tip of the Wind River Mountains. The batholith varies in composition from granite to granodiorite and varies in texture from equigranular to porphyritic (Frost *et al.* 1998). Oxygen isotope data and geochemical data by Cheang *et al.* (1986) define the Louis Lake Batholith as being a metaluminous, I-type granite. The dominant mineral assemblage is quartz-plagioclase-potassium feldspar-biotite, but in some areas, hornblende is also present. Minor minerals include magnetite, ilmenite, and titanite. Metamict crystals of allanite are

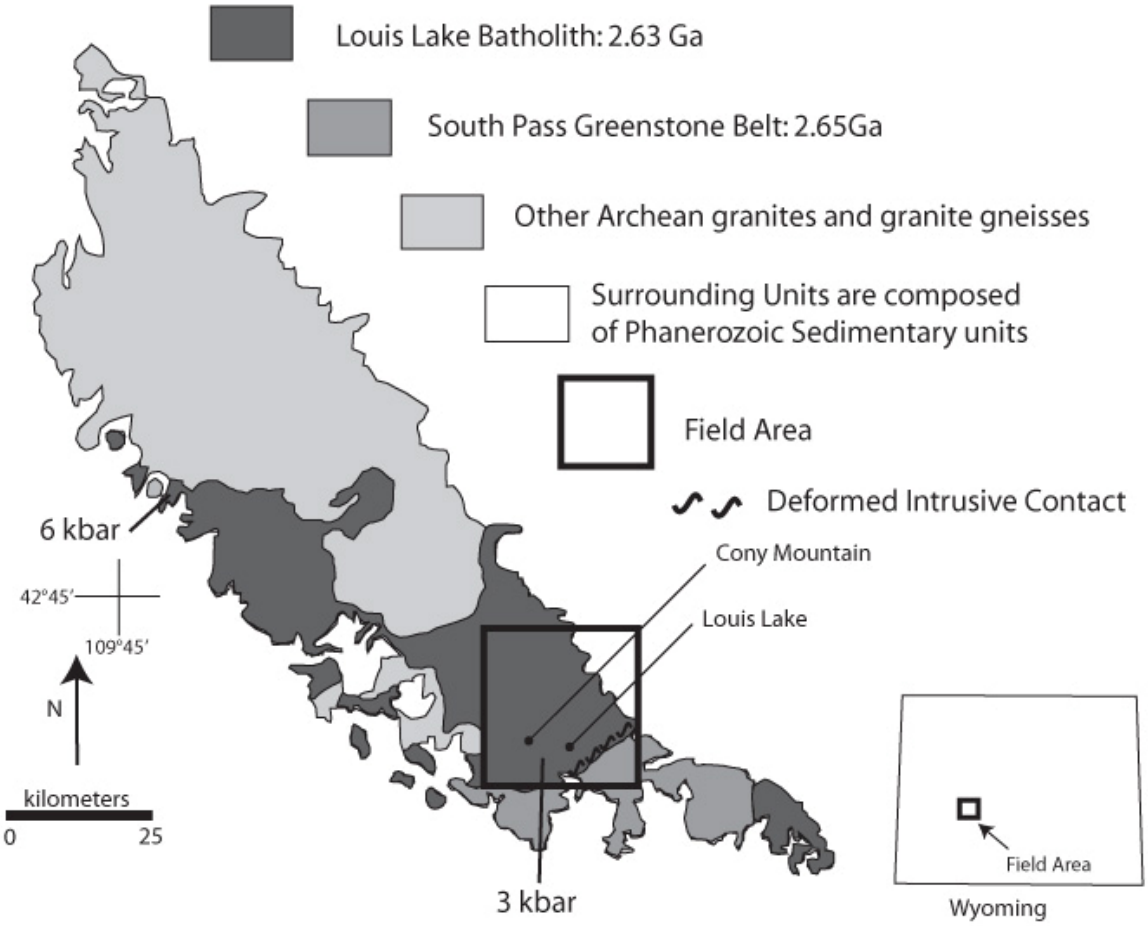


Figure 1: Location Map of the Wind River Range, Wyoming, showing the study area. Pressure measurements are those by Frost *et al*. (2000) and represent pressures during contact metamorphism.

also present. The mineralogy points toward an intermediate oxidation state. The Louis Lake Batholith contains numerous aplites and pegmatites. These vary in size and are found primarily along the southern and western margins. Some areas, such as Cony Mountain (Fig. 1), contain up to 20% aplitic dykes. Other areas contain rare aplite and pegmatite dykes. Although pegmatites and aplites are not as common in some areas, quartz segregations can be found throughout the batholith. Quartz segregations range in size from 1 to 10 cm in diameter.

There is evidence for multiple injections of magma into the magma chamber. This is evidenced by the presence of magma mingling and mafic enclaves. These enclaves are elongated and flattened. Concentrations of magnetite along the rim of the enclaves are interpreted as evidence of assimilation of a mafic magma.

The southern end of the batholith is of special interest because this portion of the batholith represents a structurally higher level than that of the northern end. Frost *et al* (2000) determined the conditions of contact metamorphism from the Louis Lake Batholith to be about 3 kb and temperatures greater than 700°C in the south and 6 kb and 800°C in the north. This means that the southern end of the batholith is likely at a level at which late fluids accumulated and released.

The majority of the batholith has experienced little internal deformation after crystallization. As noted by Schmitz (2005), most of the deformation experienced by the batholith is syn-intrusion and not related to later metamorphism. Thin epidote veins that cut throughout the batholith are attributed to retrograde metamorphism. These veins show little interaction with the wallrock. Serrated grain boundaries provide evidence of dynamic recrystallization in the quartz grains of some samples. This recrystallization is minor and has left the cores of the grains unaffected.

There is also evidence of mineralization within the batholith. Sulphide mineralization is present as veins and within a shear zone near

Louis Lake (Fig. 1). Pearson *et al.* (1973) noted minor amounts of copper mineralization south of Louis Lake. Placer gold in the northern part of the range is believed to be reworked from a palaeoplacer possibly derived from ore zones in the batholith (Pearson *et al.* 1971).

## 3 FLUID INCLUSIONS OF THE LOUIS LAKE BATHOLITH

### 3.1 *Primary Fluids*

Quartz from quartz veins, quartz segregations, aplites, and pegmatites was used for the fluid inclusion work. The samples were taken from different parts of the batholith, including the aplite dykes of Cony Mountain. Because many of the samples have experienced dynamic recrystallization, the inner parts of quartz crystals were studied to find primary inclusions. By using criteria, for instance, that primary inclusions predate the syn-intrusion dynamic recrystallization, multiple primary fluids in the samples have been distinguished and named Type 1 and Type 2. Observations and measurements were taken using a Linkam Stage.

### 3.2 *Type 1 Inclusions*

Type 1 inclusions are the most abundant and have been found in all samples. These inclusions are mainly small (7 to 10 μm) and have shapes that are irregular or negative crystals. Type 1 inclusions are found only in trails. They are a low to medium salinity aqueous-carbonic fluid, with the volume percentages ranging from 10 to 20% to 70% $CO_2$. The $T_{eutectic}$ was found to be fairly consistent at -57ºC. Clathrate melting temperatures range from 5 to 9ºC. $T_{homogenization}$ to $CO_2$ ranged from 18 to 30ºC. Total homogenization temperatures ranged from 260 to 290ºC.

### 3.3 *Type 2 Inclusions*

Type 2 inclusions appear to be localized around the Cony Mountain area, which lies within an area of abundant aplite dykes. They are larger than Type 1 inclusions and are aqueous with up to four daughter solids. They also are found in trails, but occasionally, they are found as isolated inclusions. Three of the solids were determined to be halite, sylvite, and possibly a Ca salt. A low temperature of liquid-vapour homogenization of about 105ºC gives a high density for the fluid, which means that the fluids were likely trapped at high pressures. Temperatures of total homogenization were found to range greatly from 180ºC for inclusions with one solid to above 350ºC for inclusions with more than one solid. This evidence points toward a hypersaline fluid with minimum salinities of 58%.

## 4 CONCLUSIONS

This study has determined that there were two late stage fluids moving through the batholith at the end of crystallization. The first of the fluids was an aqueous-carbonic fluid and the second was a halite-sylvite-Ca salt- water fluid. The first fluid is important because of compositional similarities with the fluids of lode gold deposits. The second fluid provides evidence of hypersaline fluids derived from granites that have crystallized at deeper levels. It is compositionally similar to the highly saline fluids of porphyry deposits.

## ACKNOWLEDGEMENTS

Funding for this project was provided by Colorado State University, Newmont Mining Corporation, Society of Economic Geologists, and the Wyoming Geological Society.

## REFERENCES

Cheang K K Wenner D B Stuckless J S (1986) Oxygen Isotopic Constraints on the Origin of the Precambrian Granites from the Southern Wind River Range and the Granite Mountains, Central Wyoming, *U.S. Geological Survey Bulletin* 1622, pp 109-129

Frost BR Chamberlain KR Swapp S Frost CD Hulsebosch TP (2000) Late Archean Structural and Metamorphic History of the Wind River Range: Evidence for a Long-lived Active Margin on the Archean Wyoming Craton, *GSA Bulletin* 112: 564-578

Frost CD Frushey BL Chamberlain KR Frost BR (2006) Archean crustal growth by lateral accretion of juvenile supracrustal belts in the south-central Wyoming Province, *Canadian Journal of Earth Sciences* 43: 1533-1555

Frost CD Frost BR Chamberlain KR Hulsebosch TP (1998) The Late Archean history of the Wyoming province as recorded by granitic magmatism in the Wind River Range, Wyoming. *Precambrian Research* 89: 145-173

Hausel WD (1991) Economic Geology of the South Pass Granite-Greenstone Belt, Southern Wind River range, Western Wyoming, *Geological Survey of Wyoming,* Report of Investigations No. 44, pp129

Pearson RC Kiilsgaard TH Patten LL (1971) Mineral Resources of the Popo Agie Primitive Area, Fremont and Sublette Counties, Wyoming, *United States Geological Survey Bulletin* 1353-B pp 54

Pearson RC Patten LL Gaskill DL (1973) Mineral Resources of an Area Near the Popo Agie Primitive Area, Fremont County, Wyoming, *United State Geological Survey Bulletin* 1391-A pp 16

Schmitz PJ (2005) Emplacement of the Late Archean Louis Lake Batholith and Accretion of the Miner's Delight Formation Allochthon, Southern Wind River Range, Wyoming, *Master's Thesis, University of Wyoming,* pp128

# Asymmetrical filling of inclined crustified hydrothermal gold veins: An example from Hadleigh Castle Mine, North Queensland

I.M. Platten
*Snowden Mining Industry Consultants Ltd, Weybridge, England*

S.C. Dominy
*Snowden Mining Industry Consultants Ltd, Weybridge, England and University of Ballarat, Victoria, Australia*

ABSTRACT: Crustified mineral vein fills are commonly composed of two zones with similar internal structure that meet in a central axial suture. This paper reports strongly asymmetrical structures in inclined veins with three zones and an axial suture above the central plane. The zone at the footwall is not represented in the hanging wall sequence. The asymmetry indicates the operation of a gravity-controlled process during or shortly after nucleation that controls subsequent *in situ* mineral growth. The nature of such processes is uncertain at present.

KEYWORDS: narrow gold veins, vein textures, crustified vein fill, vein asymmetry

## 1 INTRODUCTION

This work forms part of a programme of study of fine structure within narrow veins. We have recently described vein fill asymmetry resulting from the sedimentation of a fine silica phase on the footwall of inclined Pb-Zn veins (Platten & Dominy 2007). This paper records asymmetric layers where the asymmetric distribution of nuclei controls later extensive in-situ growth from solution.

Hadleigh Castle mine lies near Charters Towers, south of Townsville. It extracted 180,000 tpa at a grade of 7 g/t Au between 1997 and 2005 (Dominy *et al*. 1999). The gold-bearing veins of the Charters Towers district (Peters & Golding 1989; Hodkinson 1998; Kreuzer 2003) cut post-tectonic Ordovician and early Devonian granitoid plutons of the Ravenswood Batholith. The veins are emplaced by brittle fracture associated with reverse faults/shear zones. Pre-vein dykes remain vertical, so observed vein dips are considered to remain close to the original values. Fluid inclusion studies indicate vein emplacement temperatures between 240°C and 300°C. Phyllic and propylitic alteration occurs in the wall rocks.

Hadleigh veins form a gently to moderately dipping (40°) array in granitoid rocks (Hodkinson 1998). Lodes are composed of a narrow vein (<1.0m) or array of several veins. This paper is based on samples from the 1100-1130 B Lode stopes. The samples are not fully oriented, but the hangingwall and footwall are known. The sampled vein has a dip of 30°. Samples show vein thicknesses of 4-13cm. Internal vein structures are complex (Kreuzer *et al*. 2002). Most veins are crustified. Some show symmetrical wall parallel crustification with a central axial suture, but the samples described here show asymmetrical fills with the axial suture above the vein centre (Fig. 1).

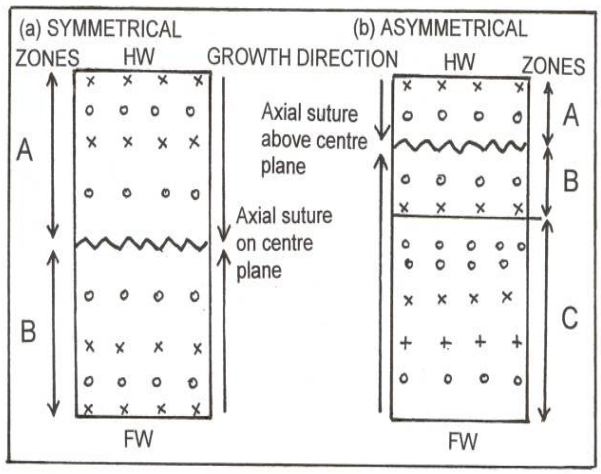


Figure 1. Schematic drawing showing (a) symmetric wall parallel crustification marking two zones (A, B) and (b) asymmetrical axial suture and wall parallel crustification zones (A-C).

## 2 PRIMARY MINERAL ASSEMBLAGE AND TEXTURE

The mineral assemblage is predominantly quartz and pyrite with subsidiary galena, sphalerite, and feldspar. Most primary gold is fine (40μm) and associated with the pyrite, but rare visible grains are found. Most of the minerals show primary space filling textures (Figs 2 & 3). Quartz forms conspicuous elongate (4-40 mm) prisms with hexagonal cross section that grow perpendicular to the walls and other surfaces. Other coarse quartz forms anhedra moulded against euhedral sulphide. Finer grained quartz (0.2-1mm) is relatively equigranular, but can show inwards coarsening. Sulphides are coarse (2-10mm) equant grains. Some are anhedral, but many show euhedral terminations facing into the vein. Some galena is deposited syntaxially on euhedral pyrite terminations. Some of the finer grained quartz domains carry abundant disseminated small (<1 mm) grains of sulphides. Euhedral terminations, facets and overgrowths indicate the direction of growth.

## 3 DESCRIPTION OF ZONES AND LAYERING

The axial suture is recognized from growth directions and zones B and C from local mineral assemblage and texture. Fig. 1 shows a model pattern and Figs 2 & 3 illustrate details from actual examples. Zone A forms on the hanging wall and grows down towards the axial suture. Zones B and C form on the footwall and grow up towards the axial suture. Zone B contains a mineral sequence that generally matches Zone A. Zone C contains a sequence that is not represented in the hanging wall infill, Zone A. Zone C can form up to 75% of the total vein thickness and formed before either zones A or B.

Internal layering is present in all three zones. It is marked by grain size variation, variation in mineral proportions (sulphide rich to sulphide poor) and variation in dominant sulphide (galena relative to pyrite). Mineral proportions can change markedly along a layer or zone (Fig. 3). Layers in the C zone can have very limited lateral extent and can be oblique to the wall.

The finer grained quartz and quartz with disseminated pyrite is most common in Zone C (Fig. 3). It is locally present in Zone B but is absent from Zone A, *i.e.*, absent above the axial suture. This material locally forms convex drapes over the tops of large sulphide crystals and concave drapes between sulphide crystals. Layers also abut against large sulphide grains. Fine quartz layers can be traced through large pyrite crystals as trails of small quartz grains in some specimens.

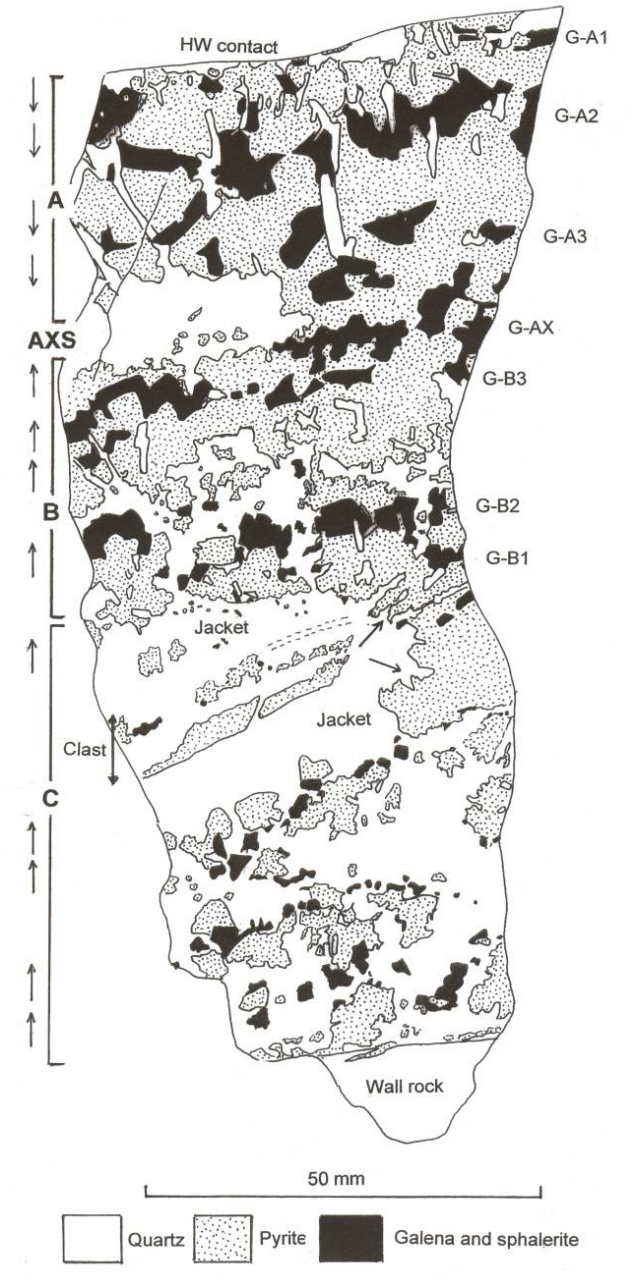


Figure 2. Drawing showing position of the axial suture (AXS), zones A-C and presence of clast of earlier vein material with a quartz jacket. Arrows mark growth direction proved from whole block. Illustrates layering, quartz texture and sulphide overgrowths. Matching layers of discontinuous galena G-A1, G-B1 etc are shown. G-AX marks galena at the axial suture. Note the less continuous and locally oblique layering and smaller grain size in C and smooth, nearly planar hanging wall and footwall contacts.

Rare fragments of wall rock and vein material occur in some veins. They lie below the axial suture in zones B and C (Figs. 2 & 3). The fragment in Figure 2 is jacketed by elongate quartz prisms, which grew immediately after the fragment was deposited.

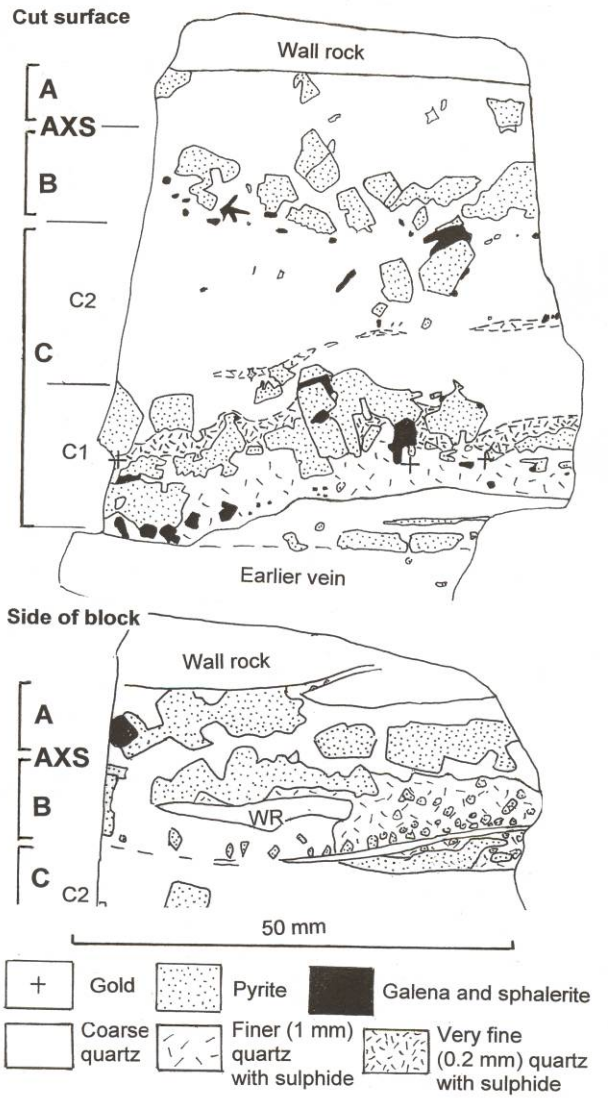


Figure 3. Drawing of 2 sides of a block showing axial suture (AXS) and zones A- C. Zone C forms a very large proportion of vein infill. The lower part (C1) is sulphide rich and shows a very fine quartz layer near the base forming convex and concave drapes over and between pyrite crystals. Visible gold is present in the quartz just below the very fine layer. Zone A shows a rapid change in quartz/pyrite proportion between front and side surface. Zone B shows a flake-like wall rock fragment marking the position of a lateral change in texture.

## 4 DISCUSSION

The broadly symmetrical A and B zones show the texture and form associated with normal crustified vein fills and represent the final stages of vein filling. Fragments, local fine quartz layers and generally slightly smaller grain size in the B zone can mar the symmetry between the A and B Zones. The C Zone is different as it has accumulated by upward growth from the footwall yet there is no record of synchronous deposition on the hanging wall. This asymmetry suggests that deposition was, in part, influenced by a gravity-controlled process. The residual void becomes restricted progressively to the upper part of the vein opening and the hanging wall remains in direct contact with hydrothermal fluids during formation of the C zone. It would therefore be interesting to look for any differences of wall rock alteration that may be related to the different exposure times of the upper and lower contacts.

The fine quartz and fine quartz and sulphide layers seen in Zone C, and locally in Zone B, show draped forms over and between large sulphide crystals and also abut against euhedral sulphide surfaces cf. sedimented fine quartz described by Platten & Dominy (2007). These show that the coarse sulphide grains were present at the local top surface of C zone material at the time the fine material accumulated.

The gross texture of the C Zone is space filling so, although some sulphide occurs as a coarse assemblage of equant grains, there is no indication that the observed grains were transported and settled onto the footwall in their present form. The bulk of the grains in Zone C have been grown *in situ* directly from solution. The hanging wall contact is planar and smooth at the scale of the vein grain size and host rock grain size in some samples (Fig. 2), showing little evidence of spalling. Elsewhere small steps in the hanging wall contact and rare flakes in the vein fill indicate the continued availability of wall rock detritus from the hanging wall, but there is no evidence that hanging wall detritus forms more than a few percent by volume of the fill below the axial suture.

The asymmetry reflects either the sedimentation of small particles that act as nuclei for growth of the bulk of the crystal mass or the effective restriction of nucleation to the footwall during accumulation of the C Zone. These processes have to be repeated to produce the internal layering in the zone, but are effectively switched off during later growth of the synchronous A and B zones.

Possible mechanisms for generating these effects include: 1) the failure of nucleation on the hanging wall due to presence of migrating

vapour sheets or swarms of vapour bubbles; 2) failure of nucleation in the hanging wall due to circulating convection flows in the fissure giving up-flow on the hanging wall and down flow on footwall; 3) nuclei may have formed on the hanging wall, but crystals detached and settled before significant crystal growth; and 4) there may be no nucleation *in situ,* but the particles forming nuclei for growth of the C Zone may be introduced and then settle. We do not have information to evaluate these mechanisms at Hadleigh Castle. By drawing attention to the vein asymmetry, we hope that other examples will be described and understanding of the processes advanced.

## 5 COMPARISON WITH TYNDRUM

Asymmetrical infills with axial sutures above the centre plane occur in gently inclined segments of sphalerite- and galena-bearing veins at Tyndrum, UK (Platten & Dominy 2007). Lack of internal markers commonly prevents the recognition of separate B and C zones, but a few clear examples were found in tip material. Some gently dipping segments also show asymmetrical sulphide growth, with sulphide crystals restricted to the footwall sequence. Normal symmetrical distribution of sulphide is observed in steep veins.

Some downward closing steep veins contain axial fills of fine silica sediment. Other axial fills show gently dipping, crude layering of wall rock clasts, fine silica and coarse sulphides. Symmetrical crustified wall lining is seen in upwards tapering veins. These patterns show that gravity controlled features are present in some steep veins.

## 6 POTENTIAL APPLICATIONS

The observed asymmetry indicates that fill sequences may also be complex in other parts of the Hadleigh Castle system.

Vein fill constituents in low to moderately inclined vein segments may record different proportions of early and late deposited materials than occur in associated steep vein segments. Up and down closing fissure terminations may show analogous differences with down closing fissures filled with predominantly C zone material and up closing fissures filled with predominantly A and B zone material. In gold-bearing systems this could lead to grade variation if gold deposition from fluids was not uniform during fluid flow in the fissure.

## 7 CONCLUSIONS

Asymmetrical C zone fill shows that some gravity controlled process is operating. The bulk of C zone material is however deposited by *in situ* growth from solution. No effective deposition occurs on the hanging wall and residual void space, becomes restricted to the hanging wall side of the original fissure. Hydrothermal fluids remain in free contact with the hanging wall until the onset of growth of zone A. This contact only becomes sealed during final stages of deposition marked by onset of growth of zones A and B. The C zone therefore provides an important part of paragenetic sequence that cannot be obtained from the hanging wall. This effect may also affect mineral (gold at Hadleigh Castle) distribution in up and down closing fissure segments.

## ACKNOWLEDGEMENTS

The authors wish to thank SMC Gold Ltd and former Chief Geologist, Ian Hodkinson, for his support.

## REFERENCES

Dominy SC, Hodkinson IP, Kidd RG (1999) Meeting the challenges of narrow-vein gold mining: Hadleigh Castle Mine, North Queensland, Australia. *Trans Inst Min Metall* 108: A192-A205.

Hodkinson IP (1998) Geology of the Hadleigh Castle Mine, Charters Towers. In: *Economic Geology of Northeast Queensland - the 1998 Perspective.* Geological Society of Australia, pp 230-241.

Kreuzer OP, Dominy SC, Platten IM, Raine MD (2002) Ore controls and grade distribution in the Charters Towers Goldfield. In: *Applied Structural Geology for Mineral Exploration and Mining*. Australian Institute of Geoscientists, Perth, 96-99.

Kreuzer (2004) *Unpublished PhD Thesis, James Cook University, Townsville, Queensland*.

Peters SG, Golding SD (1989) Geologic, fluid inclusion and stable isotope studies of granitoid hosted gold-bearing quartz veins, Charters Towers, Norteastern Australia. In: *The Geology of Gold Deposits – the perspective in 1988.* Economic Geology Monograph, Society of Economic Geologists, 260-273

Platten IM, Dominy SC (2007) Fine quartz formed by the sedimentation of hydrothermal precipitates in mineral veins: an example from Tyndrum, Scotland, UK. *Explor Min Geol* 16: in press.

# ADVANCES IN HYDROTHERMAL GEOCHEMISTRY

EDITED BY:

ADRIAN BOYCE

JAMES CLEVERLEY

# The origin of hydrothermal fluids in the mid-crust: Evidence from the noble gases and halogens

M.A. Kendrick & D. Phillips
*pmd*CRC, The School of Earth Sciences, The University of Melbourne, Victoria 3010, Australia*

G. Mark,
*pmd*CRC, The School of Geosciences, Monash University, Victoria, Australia*

N.H.S. Oliver, T. Baker, D. Gillen & L. Fisher
*pmd*CRC, The School of Earth Sciences, James Cook University, Northern Queensland, Australia*

ABSTRACT: The Eastern Fold Belt of the Proterozoic Mt Isa Inlier of NE Australia is widely affected by Na-Ca metasomatism (albitisation) and hosts several economically important Fe-oxide-Cu-Au (IOCG) deposits that formed at mid-crustal levels of 6-10km. The intense albitisation and mineralization are usually related to aqueous and carbonic fluids preserved as fluid inclusions in coeval quartz veins. Similar fluid inclusions are seen in other IOCG provinces including prospects from the Wernecke Mountains, Canada. In most cases, the fluid inclusions are dominated by fluids that are geochemically similar to typical sedimentary formation waters with $^{40}Ar/^{36}Ar$ of ~300-2,500, favouring an upper-crustal origin. Furthermore, Br/Cl values as low as $0.3\times10^{-3}$ and maximum salinities of ~30-70 wt % NaCl eq. favour the widespread dissolution of halite. However, some samples from both the Isan and Wernecke IOCG provinces contain fluid inclusions with maximum $^{40}Ar/^{36}Ar$ values of greater than ~25,000 that are most likely to represent deeply-derived magmatic fluids. Magmatic fluids may have been sourced from regionally extensive A-type granites in the Mt Isa Inlier but have an uncertain source in the Wernecke mountains. Liquid $CO_2$ fluid inclusions have variable $^{40}Ar/^{36}Ar$ values, but are dominated by $^{20}Ne/^{22}Ne$ values of <9.8 indicating a dominantly crustal, metamorphic-origin. However, the highest value of ~10, accompanied by a $^{40}Ar/^{36}Ar$ value of ~14,000 is arguably compatible with a minor magmatic component derived from a juvenile source. Finally, the Br/Cl and I/Cl values of these samples, and those from elsewhere in the Proterozoic Mt Isa Inlier, encompass a similar range as Phanerozoic fluid inclusions, suggesting similar processes have controlled halogen geochemistry since at least ~1.5 Ga.

KEYWORDS: fluid inclusion, halogen, neon, argon, isotopes, Mt Isa, Wernecke, IOCG.

## 1 INTRODUCTION

The efficient transport of metals in hydrothermal solution is enabled by high concentrations of complexing ligands such as Cl. Therefore, to understand the origin of many giant ore deposits, it is necessary to understand the origin of both the hydrothermal fluids and their aquisition of salinity.

The isotopic and elemental composition of noble gases varies by orders of magnitude (Table 1) and together with the halogens (Cl, Br, I) can be used to provide unambiguous evidence on the origin of a hydrothermal fluid. The noble gases have some additional advantages over traditional stable isotope techniques. For example, isotopic signatures are added to during fluid-rock interaction, but not lost, and the concentration of $^{36}Ar$ can be used to monitor the extent of fluid-rock interaction (Kendrick *et al*., 2006). However, despite this, most hydrothermal fluids in the upper crust have $^{40}Ar/^{36}Ar$ values of between 296 and ~3000; and Kr/Ar values of between air and Air Saturated Water (ASW = meteoric or seawater; *e.g*. Kendrick *et al.,* 2001, 2002). These data indicate that in the

Table 1: Noble gas reference values

| | $^{4}He/^{3}He$ | $^{20}Ne/^{22}Ne$ | $^{40}Ar/^{36}Ar$ | $^{84}Kr/^{36}Ar$ |
|---|---|---|---|---|
| Air | 1 Ra | 9.8 | ~296 | 0.02 |
| ASW | 1Ra | 9.8 | ~296 | ~0.04 |
| Cr | 0.05 Ra | <9.8 | >>296 | 0.02-0.04 |
| Man | 8 Ra | 12.2 | 44,000 | |

ASW - Air saturated water; Cr – crust; Man - mantle

upper crust, surface-derived fluid components are substantial and can overprint the noble gas signature of deeper (magmatic) fluids inferred by traditional techniques.

In this study we highlight that hydrothermal fluids in the mid-crust (6-10 km) better preserve their primary noble gas signature. Mid-crustal fluids preserve $^{40}Ar/^{36}Ar$ values of ~30,000-40,000, when deeply-derived magmatic or metamorphic fluids are present (Kendrick et al., 2006; 2007). The variable preservation of noble gas signatures in the mid versus upper crust provides insight on fluid processes as well as fluid origins: noble gases were not quantitatively lost during $CO_2$-$H_2O$ unmixing in the mid-crustal samples (Kendrick *et al*., 2007).

The Br/Cl and I/Cl composition of deeply-derived metamorphic fluids are variable, reflecting the variability of crustal rocks. Evaporite dissolution in the upper crust leads to low Br/Cl and I/Cl values (*e.g*. Br/Cl $\sim 0.1\times10^{3}$), because Br and I are preferentially excluded from the halite lattice. Greater than seawater values (Br/Cl > $1.5\times10^{-3}$) can be produced at low water-rock ratios by preferential substitution of Cl over Br in silicate minerals. In exceptional cases, Br/Cl values of >$12\times10^{-3}$ may result (higher than achieved on the modern day seawater evaporation trajectory; Kendrick *et al*., 2006). Magmatic fluids derived from crustal melts are also variable. However, those evolved from 'I-type' intrusions with mantle input, or by melting of mantle-derived igneous rocks, are mostly ~$0.8\text{-}2\times10^{-3}$ (Kendrick *et al*., 2001). Sedimentary formation waters most commonly preserve greater than seawater Br/Cl and I/Cl values indicative of seawater evaporation (bittern brine origin).

## 2 STUDY AREAS AND SAMPLES

The Eastern Fold Belt of the Proterozoic Mt Isa Inlier hosts several economically important iron-oxide-copper-gold (IOCG) deposits (Mark *et al.*, 2006). Most of these deposits formed during the later half of the Isan Orogeny, concurrently with intrusion of regionally extensive 1550-1490 Ma A-type granites and albitic alteration. Mineralization usually overprints the greenschist-amphibolite facies fabric of metasedimentary/ igneous host rocks.

The Wernecke IOCG prospects in Canada, are hosted by greenschist facies metasediments in the ~1595 Ma Wernecke breccia. Unlike the Eastern Fold Belt contemporaneous granite does not outcrop in the area (Hunt *et al.*, 2005).

Quartz samples related to regional scale Na-Ca alteration, and IOCG mineralization were selected for analysis. Both the IOCG and albitisation related samples comprise mixed assemblages of variably saline aqueous fluid inclusions (5-65 wt % salts), pure carbon dioxide fluid inclusions and mixed aqueous carbonic fluid inclusions (Fig 1). Carbon dioxide fluid inclusions are more common in the Mt Isa IOCG than in the Wernecke IOCG prospects.

The different types of fluid inclusion have different decrepitation temperatures which means they are partially deconvolved by stepped heating analysis. Mixed aqueous-carbonic ($LL_c$ and $LL_cD$) fluid inclusions decrepitate at the lowest temperatures of 200-250°C; and the highest salinity aqueous fluid inclusions are preferentially decrepitated at higher temperatures of >400-450°C (Kendrick *et al*., 2007).

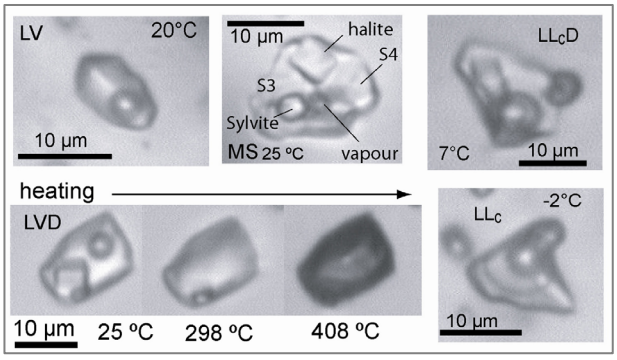


Figure 1. Common IOCG related fluid inclusions: LV – liquid-vapour; MS – multi solid; LVD – liquid-vapour-daughter; LLc – liquid $CO_2$ and water; $LL_cD$ – liquid $CO_2$, water and daughter. Pure $CO_2$ not shown.

## 3 METHODS

Fluid inclusion wafers or chips (10-80 mg) are irradiated in a nuclear reactor (as for Ar-Ar dating). Fluid inclusions are then decrepitated in an ultra high vacuum by either crushing or stepped heating (200-1560°C). The variable fluid inclusion decrepitation temperatures enable partial resolution of different types of fluid inclusion (Fig 1; refs in Kendrick *et al*., 2007).

The noble gases are isotopically analysed for Ar, Kr and Xe, using a magnetic sector noble gas mass spectrometer at the University of Melbourne. Cl, Br, I, K, Ca and U are determined simultaneously from the neutron-produced nucleogenic isotopes (*e.g*. $^{38}Ar_{Cl,}$ $^{39}Ar_{K}$). The high sensitivity of this technique enables multiple

determinations of Br/Cl and I/Cl in milligram sized samples. Furthermore, noble gas fluid concentrations are calculated from the Ar/Cl ratios and the mean salinity determined by microthermometry (refs in Kendrick *et al*., 2007).

Non-irradiated samples are isotopically analysed for Ne in addition to Ar, Kr and Xe. The isotopes of He are not quantitatively retained by quartz. Therefore, complementary He isotope analyses are undertaken on co-existing dense sulphide minerals.

## 4 HALOGENS AND Ar ISOTOPES

Fluid inclusions in samples selected from IOCG deposits (Ernest Henry, Eloise, Osborne) and regional Na-Ca alteration in the Mt Isa Inlier and Werencke IOCG prospects (Hoover, Olympic, Igor, Slab, Slats), have extremely heterogenous Br/Cl, I/Cl and $^{40}Ar/^{36}Ar$ values (Figs 2 and 3).

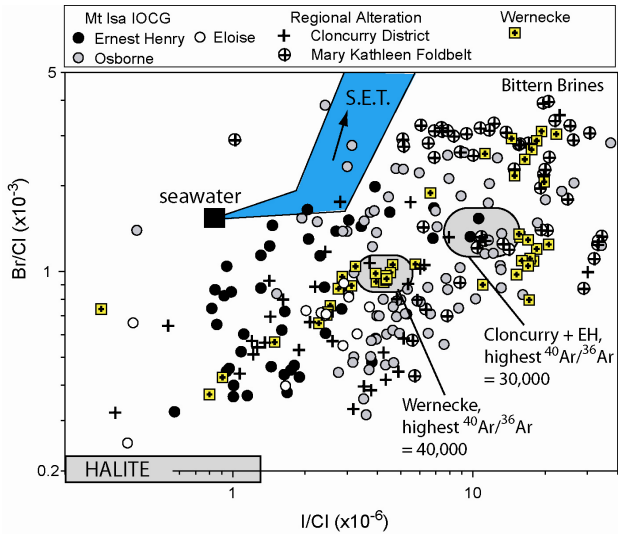


Figure 2. log-log I/Cl versus Br/Cl plot. The seawater evaporation trajectory (S.E.T.), bittern brine field and halite are shown for reference. The fluids with the highest $^{40}Ar/^{36}Ar$ values of 30,000-40,000 are most likely to represent a magmatic fluid, see Fig 3.

The heterogenous data indicate that multiple fluid sources and/or processes account for the ore fluids in each IOCG prospect/deposit. However, the compositional range is similar for both the Mt Isa Inlier and the Wernecke Mountains suggesting that the variable fluid sources and/or processes were analogous in both IOCG terrane.

Measured Br/Cl values of up to ~$4\times10^{-3}$ together with elevated I/Cl values (Fig 2) are typical of bittern brine sedimentary formation waters. The lowest Br/Cl value of $0.3\times10^{-3}$ and

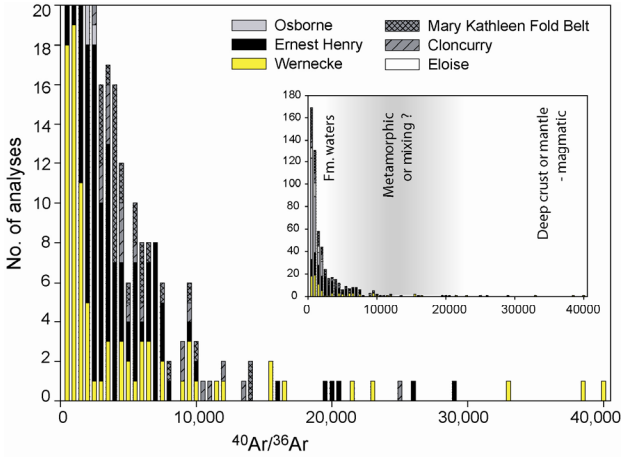


Figure 3. $^{40}Ar/^{36}Ar$ versus frequency for IOCG deposits and regional Na-Ca alteration.

the ultra-high salinities of 30-70 wt % are indicative of halite dissolution. Sedimentary formation waters typically have $^{40}Ar/^{36}Ar$ of <2500, as observed (Fig 3).

The highest $^{40}Ar/^{36}Ar$ values of >25,000 obtained for fluid inclusions from both the Ernest Henry IOCG, the Wernecke prospects and regional Na-Ca alteration in the Mt Isa Inlier, have a much narrower range of Br/Cl and I/Cl (highlighted by grey circles in Fig 2):

In the Mt Isa Inlier, the Br/Cl values of high $^{40}Ar/^{36}Ar$ fluids cluster in a range fairly similar to Phanerozoic Porphyry Copper Deposits and the mantle (Fig 2). This fluid probably represents a magmatic fluid sourced from regionally abundant A-type granites with a crustal (not mantle) source (Kendrick *et al*., 2007).

The source of magmatic fluids in the Wernecke Mountains is unknown. However, as sedimentary rocks are depleted in Br relative to the silicate earth, the lower Br/Cl (and I/Cl) values obtained for high $^{40}Ar/^{36}Ar$ fluids in the Wernecke prospects (Fig 2) may be explained if sediments were involved in melt generation, or if the magmatic fluid dissolved halite.

## 5 Ne ISOTOPES

Liquid carbon dioxide associated with both regional alteration and IOCG mineralization in the Mt Isa Inlier has an equivocal origin. $CO_2$ fluid inclusions have an abundance of 80 % in samples from the Knobby Quarry (Mt Isa Inlier) and potential sources include the mantle or the calc-silicate rocks that host alteration. Ne isotopes help constrain these alternatives (Fig 4). Lower than atmospheric $^{20}Ne/^{22}Ne$ val-

ues (<9.8) indicate nucleogenic $^{22}Ne$ produced from F in the crust (Fig 4). $^{20}Ne/^{22}Ne$ values significantly greater than the atmospheric value of 9.8 provide definitive evidence for the involvement of mantle volatiles (Ozima & Podosek, 2002).

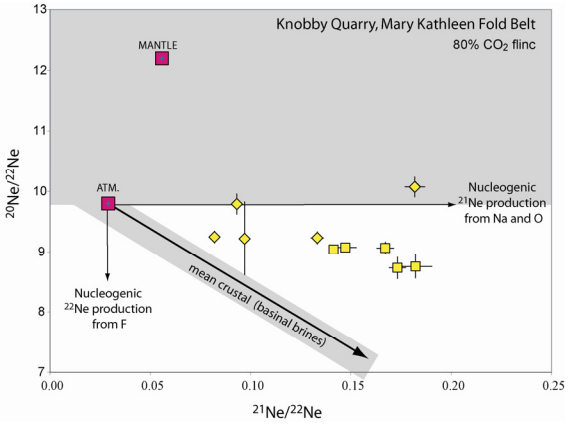


Fig 4. Ne isotope plot for the Knobby Quarry samples of the Mary Kathleen Fold Belt.

The majority of data points obtained by multiple crushes of two samples from the Knobby Quarry have $^{20}Ne/^{22}Ne$ values of less than 9.5 and define a mixing array that is slightly enriched in $^{20}Ne$ relative to the average crust (Fig 4). These data could be interpreted to represent a mixture of atmospheric, crustal and minor mantle Ne. However, as only one data point lies just inside the range of compositions that require a mantle component (shaded grey - Fig 4) the array could also reflect an origin from non-average crust only.

Further work including He isotope analysis on coexisting sulphide samples will further delimit the possible contribution of mantle volatiles. However, the data presented thus far demonstrate that crustal fluid sources dominate. Furthermore, similar processes involving the convective circulation of upper crustal fluids, driven by intrusion of granites and the occasional entrainment of magmatic fluids are favoured for both the Isan and Wernecke IOCG.

## ACKNOWLEDGEMENTS

This work was funded by the pmd*CRC Fluid History, Fluids and Mt Isa Terrane projects and is presented with permission.

## REFERENCES

Hanor J. S. (1994) Origin of saline fluids in sedimentary basins. In Geofluids: Origin, migration and Evolution of Fluids in Sedimentary Basins. In *Geological Society Special Publication*, Vol. 78 (ed. J. Parnell), pp. 151-174.

Hunt J., Baker T., Thorkelson D. (2005) Regional-scale Proterozoic IOCG-mineralised breccia systems: examples from the Wernecke Mountains, Yukon, Canada. Min. Dep. 40, 492-514.

Kendrick, M. A., Burgess, R., Pattrick, R. A. D., and Turner, G. (2001) Fluid inclusion noble gas and halogen evidence on the origin of Cu-Porphyry mineralising fluids.: *Geochim Cosmochim Acta* **65**, p. 2651-2668.

Kendrick, M. A., Burgess, R., Pattrick, R. A. D., and Turner, G., 2002, Hydrothermal fluid origins in a fluorite-rich Mississippi Valley-type deposit: Combined noble gas (He,Ar,Kr) and halogen (Cl,Br,I) analysis of fluid inclusions from the South Pennine Orefield, United Kingdom.: *Economic Geology* **97**, p. 435-451.

Kendrick M. A., Duncan R. J., and Phillips D. (2006) Noble gas and halogen constraints on mineralizing fluids of metamorphic versus surficial origin: Mt Isa, Australia. *Chemical Geology* **235**, 325-351.

Kendrick M. A., Mark G., and Phillips D. (2007) Mid-crustal Fluid Mixing in a Proterozoic Fe oxide-Cu-Au deposit: Evidence from Ar, Kr, Xe, Cl, Br, I, Ernest Henry, Australia. *Earth and Planetary Science Letters* **256,** 328-343.

Mark G., Oliver N. H. S., and Carew M. J. (2006) Insights into the genesis and diversity of epigenetic Cu-Au mineralisation in the Cloncurry district, Mt Isa Inlier, northwest Queensland. *Australian Journal of Earth Science* **53**, 109-124

Ozima M. and Podosek F. A. (2002) *Noble Gas Geochemistry*. Cambridge University Press.

# Multiple micro-analytical analyses of ore forming fluids from the Osborne IOCG deposit, northwest Queensland, Australia

L.A. Fisher, P.J. Williams , T. Baker & R. Mustard
*pmd*CRC, Economic Geology Research Unit, James Cook University, Townsville, Australia*

M.A. Kendrick
*pmd*CRC, School of Earth Sciences, University of Melbourne, Australia*

C.G. Ryan
*CSIRO Exploration and Mining, Clayton, Australia*

T. Ulrich
*Department of Earth and Marine Sciences, Australian National University, Canberra, Australia*

ABSTRACT: A fluid inclusion study of the Osborne IOCG deposit, in the Proterozoic Mt Isa Inlier of Australia, was conducted utilizing multiple geochemical techniques to generate a unique data set incorporating LA-ICP-MS and PIXE analyses. A two order magnitude range of Br/Cl values (0.2-18 × $10^{-3}$) indicate multiple sources of salinity. Mn/Fe ratios (0.04 – 0.32) of high salinity fluid inclusions reflect the redox state of the ore lens mineral assemblages, indicating they are the primary ore fluids. Cu concentrations are low in all fluids suggesting high fluid flux was required to form the 15.2 Mt deposit. Examination of the data obtained on the same fluid inclusion using the different micro-analytical methods provides a direct comparison of these increasingly widely used techniques and permits greater understanding of the chemistry of the ore forming fluids and of fluid processes.

KEYWORDS: fluid inclusion, halogen, IOCG, LA-ICP-MS, PIXE

## 1 INTRODUCTION

Studies of fluid inclusions trapped within hydrothermal ore minerals provide information on the nature of the mineralizing fluids and into fluid processes, and offer insight into PVTX conditions during ore formation. Laser ablation inductively coupled plasma mass spectrometry (LA-ICP-MS) and proton induced X-ray emission (PIXE) are two micro-analytical techniques that are becoming widely used in the study of fluid inclusion chemistry (*e.g.* Ulrich *et al.*, 1999; Ryan *et al.*, 2001).

Some of the samples analyzed by these micro-analytical methods have also been studied using a combined noble gas and halogen technique in which a semi-selective bulk analysis of fluid inclusion halogen (Cl, Br, I) ratios can be achieved. In an extension of Ar-Ar methodology both neutron-produced nucleogenic and naturally occurring noble gas isotopes are measured simultaneously. $^{38}$Ar, $^{80}$Kr and $^{128}$Xe are proxies for Cl, Br and I and data from studies of this kind can be used to identify fluid reservoirs (Böhkle & Irwin, 1992; Kendrick *et al*. 2001).

The iron oxide-copper-gold (IOCG) class of ore deposits encompasses a relatively diverse group of ore bodies and there is considerable debate over their genesis (Hitzman *et al,* 1992; Barton & Johnson, 1996; Pollard, 2006). The Eastern Fold Belt of the Mt Isa Inlier is one of the world's premier IOCG provinces and IOCG deposits within it exhibit a wide range of alteration styles and mineral associations (Mark *et al*, 2006). Thus it can be considered an good natural laboratory in which to study the formation of these deposits and the chemistry of their ore fluids.

In a study of the chemistry of the ore forming fluids at the Osborne IOCG deposit (15.2Mt @ 1% Cu and 1.05 g/t Au), situated off the southeastern tip of the Mt Isa Inlier, data were collected using PIXE, LA-ICP-MS and combined noble gas and halogen analysis.

These multiple data-sets enable thorough elucidation of the chemistry of the ore forming fluids and permit direct comparison of the different analytical techniques.

## 2 METHODS AND RESULTS

The paragenetic sequence for the Osborne fluid inclusions was determined using the criteria of (Roedder, 1984). The Osborne ore deposit is comprised of several ore lenses in two domains, defined by host rock type. Ore lenses in the western domain (1S and 2M) are sited along the contact of laterally extensive banded ironstones with feldspathic psammites while ore lenses in the eastern domain are hosted by schists and pegmatites (Adshead *et al,* 1998). Samples in the study were taken from three ore lenses (1S, 2M and 3E) and associated pegmatites. Inclusion types were initially classified based on phases present at room temperature and then further by microthermometric characteristics. The Osborne deposit is characterized by extensive coarse-grained hydrothermal quartz, termed 'silica flooding', which hosts the Cu-Au mineralization. This extensive quartz is an unusual feature, not found in other IOCG deposits in the region. Cathodoluminescence imaging reveals most Osborne silica flooding samples comprise two generations of quartz and both primary and secondary fluid inclusions are therefore related to the ore fluids.

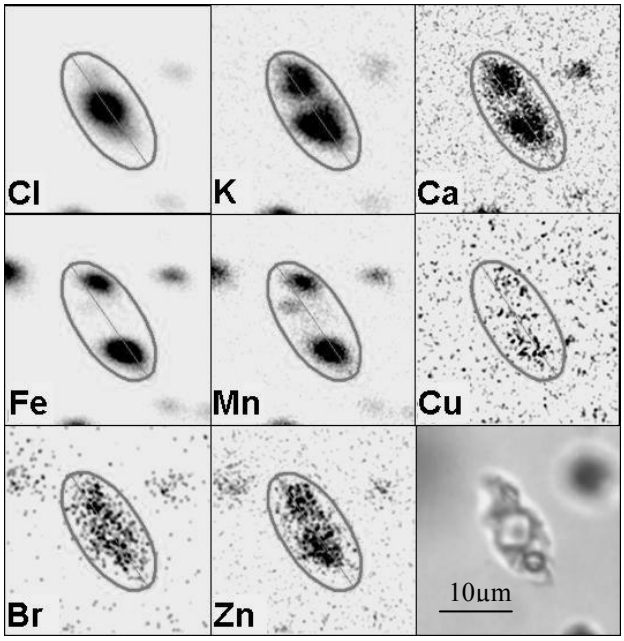


Figure 1. PIXE element maps for an MS inclusion. Highest concentrations are denoted by darkest colouration.

On petrographic criteria the fluid inclusions comprise ultra-high-salinity multi-solid (MS), high salinity liquid-vapour-daughter (LVD), moderate salinity two phase liquid-vapour (LV), liquid carbon dioxide ($CO_2$) and carbon dioxide bearing brines (CB). LVD inclusions are observed on trails that radiate from sulphide grains and are considered to have entrapped ore fluids. MS and CB inclusions were trapped at high temperatures with Th > 400$^{o}$C (homogenisation by dissolution of daughter minerals).

Selected MS and CB inclusions were studied by PIXE analysis. The inclusions were imaged as X-ray maps providing information on distribution of elements within phases (Fig.1).

Individual MS and LVD fluid inclusions were also analyzed by LA-ICP-MS. The equivalent wt.% NaCl value from microthermometric experiments, on inclusions of the same type, in each sample was used as an internal standard.

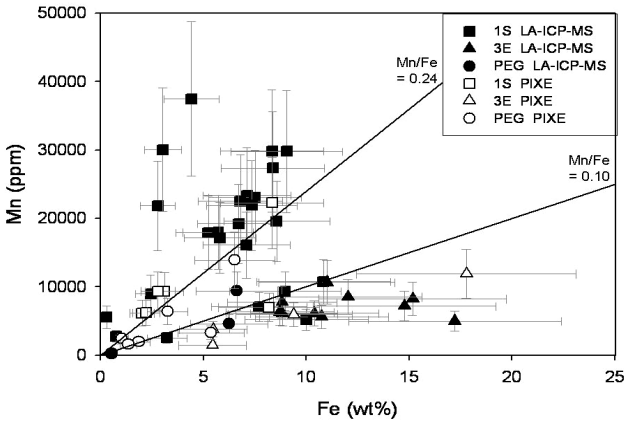


Figure 2. Mn/Fe plot for samples from 1S and 3E ore lens and pegmatites. Bottrell & Yardley (1991) defined fluids with Mn/Fe below 0.24 as reduced.

PIXE images show considerable variation in element phase association; most notably with Ca, Ba and Zn which are observed associated with solid phases in some inclusions and dissolved in the liquid phase in others. The inclusions contain high Fe (<20 wt %) Many of the inclusions also have high concentrations of Mn (<4 wt %). Both PIXE and LA-ICP-MS show Mn/Fe to be variable, from 0.04 to 0.32, with variation appearing to reflect the oxidation state of the ore lens mineralogy (Fig. 2).

PIXE element maps of MS fluid inclusions suggest Cu is associated with Fe-bearing minerals (Fig 1.). However, once an iron-silica X-ray pile-up artifact is removed in many cases the measured Cu is below the detection limit for the method (typically <100ppm). The low Cu content of the ore fluids is confirmed by the LA-ICP-MS with the majority of analyses measuring Cu concentrations below 100ppm.

K/Ca values measured by both PIXE and LA-ICP-MS show nearly two orders of magni-

tude variation (0.2-10) in inclusions from all samples (Fig 3.). Br/Cl ratios from PIXE analyses also show several orders of magnitude variation with values ranging from 0.2 – 18 × $10^{-3}$.

## 3 ORE FLUID CHEMISTRY AND PROCESSES

Br/Cl ratios of LVD and MS fluid inclusions analyzed by PIXE show considerable variation, indicative of multiple sources of salinity. Very few values fall in the field of halogen compositions associated with magmatic fluids. Osborne ore fluids have $^{40}Ar/^{36}Ar$ values below 2000 consistent with values measured in sedimentary formation waters (Kendrick *et al,* 2002). Thus the combined noble gas and halogen data, as well as Br/Cl values obtained from individual fluid inclusions by PIXE are consistent with a sedimentary formation water origin for the Osborne IOCG fluids and any magmatic component is minor. Highest Br/Cl values exceed the range of values found in bittern brines and may indicate a metamorphic fluid component.

The broad variation observed in K/Ca values shows no correlation with ore lens, salinity, Mn/Fe values or Br/Cl values but does vary systematically with Fe concentrations in the LA-ICP-MS data set. The extent of the variation suggests that K/Ca values may be controlled by local fluid-wall rock reactions.

Mn/Fe values can be considered a proxy for redox (Bottrell & Yardley, 1991), with fluids with a Mn/Fe value below 0.24 being considered reduced. The 3E ore lens at Osborne has a pyrrhotite rich mineral assemblage while the 1S ore lens is dominated by chalcopyrite and pyrite. The redox state of the fluid entrapped in the MS inclusions reflects the redox state of the ore assemblages. While petrographic studies show a clear link between LVD inclusions and sulphide deposition the MS inclusions are not clearly linked to the sulphide deposition. The evidence from Mn/Fe values strongly supports an association with the MS inclusions also. Thus the MS inclusions can be considered to have entrapped pre-deposition ore fluids while the LVD inclusions contain the 'spent' ore fluids.

## 4 TECHNIQUE COMPARISON

Both PIXE and LA-ICP-MS techniques were used to study the MS inclusions. Many of the same trends in data are observed using both methods. However, for almost all samples, higher concentrations of most elements were measured by LA-ICP-MS (e.g. Fe and Mn in Fig 2.). This may indicate underestimation of concentrations by PIXE due to errors in calculating the geometry and mean salinities of the fluid inclusions. The difference in concentrations measured by each method is variable between elements but consistent across the data set indicating that element ratios remain useful sources of information. In particular K/Ca values measured by both LA-ICP-MS and PIXE show order of magnitude ranges, but values measured by LA-ICP-MS are lower, between 0-4 whereas PIXE values extend from 2-10 (Fig.3).

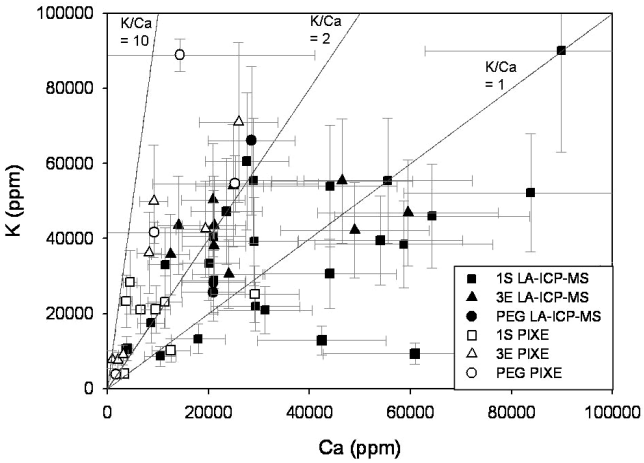


Figure 3. K/Ca values vary widely. Values measured by PIXE are higher than those measured by LA-ICP-MS

Examination of data sets where both methods have been applied to the analysis of a single inclusion suggest that greatest disparity between the methods is observed in Ca analysis. In contrast Mn/Fe ratios measured by both methods are consistent (Fig 2.).

Br/Cl values measured by stepped heating analyses together with noble gas ratios (Kendrick *et al,* 2006) are variable between 0.3 and 2.4 × $10^{-3}$ (Fisher *et al.*, 2006). The Br/Cl values obtained for individual fluid inclusions by PIXE (Fig. 4) exhibit even greater variation (0.2 – 18.3 × $10^{-3}$) but are subject to much higher uncertainty (>30%). This variation is interpreted as evidence for at least two sources of salinity: halite dissolution and bittern brines. They also show that the degree of inter- and intra-sample variation measured in the bulk analysis of the noble gas study, is also observed

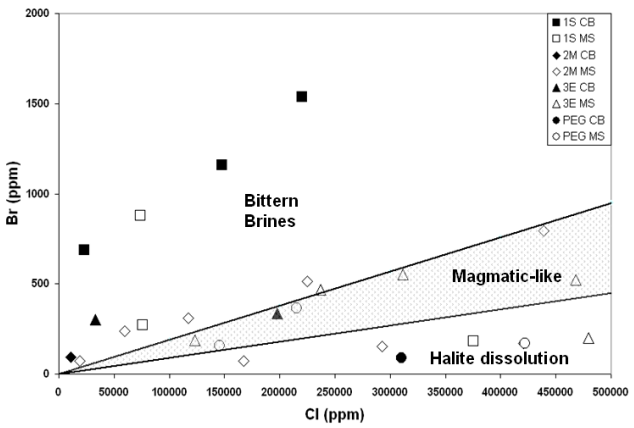


Figure 4. Br/Cl ratios vary over nearly two orders of magnitude

to varying extent, between individual inclusions.

## ACKNOWLEDGEMENTS

This work was funded by the pmd*CRC and forms part of LF's PhD work funded by an IPR scholarship. Barrick Gold and Osborne Mine provided access to samples and mine data and mine geologist Britt Kuhneman gave advice on the project.

## REFERENCES

Adshead, N. D., Voulgaris, P., and Muscio, V. N., 1998, Osborne copper-gold deposit, *in* Berkman, D. A., and Mackenzie, D. H., eds., *Geology of Australian and Papua New Guinean Mineral Deposits:* Melbourne, The Australasian Institute of Mining and Metallurgy, p. 793-800.

Barton, M. D., and Johnson, D. A. (1996) Evaporitic-source model for igneous-related Fe oxide-(REE-Cu-Au-U) mineralization: *Geology*, v. 24, p. 259-262.

Böhlke, J. K., and Irwin, J. J. (1992) Brine history indicated by argon, krypton, chlorine, bromine and iodine analyses of fluid inclusions from the Mississippi Valley type lead-fluorite-barite deposits at Hansonburg, New Mexico: *Earth Plan Sci Lett,* v. 110, p. 51-66.

Bottrell, S. H., and Yardley, B. W. D. (1991) The distribution of Fe and Mn between chlorite and fluid: Evidence from fluid inclusions: *Geochim Cosmochim Acta,* v. 55, p. 241-244.

Fisher, L. A., Kendrick, M. A., Mustard, R., Ulrich, T., Ryan, C. G., and Van Achterberg, E. (2006) Tracing the source and evolution of the Osborne IOCG ore fluids: *Geochim Cosmochim Acta*, v. 70, p. A176.

Hitzman, M. W., Oreskes, N., and Einaudi, M. T. (1992) Geological characteristics and tectonic setting of Proterozoic iron oxide (Cu-U-Au-REE) deposits: *Precamb Res,* v. 58, p. 241-287

Kendrick, M. A., Burgess, R., Pattrick, R. A. D., and Turner, G. (2001) Fluid inclusion noble gas and halogen evidence on the origin of Cu-Porphyry mineralising fluids.: *Geochim Cosmochim Acta,* v. 65, p. 2651-2668.

Kendrick, M. A., Burgess, R., Pattrick, R. A. D., and Turner, G., 2002, Hydrothermal fluid origins in a fluorite-rich Mississippi Valley-type deposit: Combined noble gas (He,Ar,Kr) and halogen (Cl,Br,I) analysis of fluid inclusions from the South Pennine Orefield, United Kingdom.*: Economic Geology*, v. 97, p. 435-451.

Mark, G., Oliver, N. H. S., and Carew, M. (2006) Insights into the genesis and diversity of epigenetic Cu-Au mineralisation in the Cloncurry district, Mt Isa Inlier, northwest Queensland.: *Aus J. Earth Sci,* v. 53, p. 109-124.

Pollard, P.J. (2006) An intrusion-related origin for Cu-Au mineralisation in iron-oxide-copper-gold (IOCG) provinces: *Min Dep*, v.41, p.179-187.

Roedder, E. (1984) Fluid Inclusions: Washington, *Mineralogical Society of America,* 644 p.

Ryan, C.G., McInnes, B.M., Williams, P.J., Dong, G., Tin Tin Win., and Yeats, C.J. (2001) Imaging fluid inclusion content using the new CSIRO-GEMOC nuclear microprobe: *Instrum. Methods. Phys. Res. B*. v.181, p.570-577.

Ulrich, T., Günther, D., and Heinrich, C.A. (1999) Gold concentrations of magmatic brines and the metal budget of porphyry copper deposits: *Nature,* v.399, p. 676-679.

# Source and evolution of IOCG-related hydrothermal fluids in the Wernecke Mountains, Canada

David Gillen & T. Baker
*Predictive mineral discovery Cooperative Research Centre (pmd*CRC), School of Earth and Environmental Sciences, James Cook University, Townsville, Queensland, Australia.*

Julie Hunt
*CODES, University of Tasmania, Australia*

Chris Ryan
*pmd*CRC, CSIRO Exploration and Mining, Australia*

Thomas Ulrich
*Earth and Marine Science Department, ANU, Canberra, Australia*

ABSTRACT: Evaporitic processes, temperature changes during hydrothermal circulation, and fluid-wall rock interaction were the major controls on the character of IOCG-related fluids in the Wernecke Mountains. The importance of these factors is revealed using compositional information obtained by multi-technique analysis of fluid inclusions coupled with the examination of whole-rock geochemical data.

KEYWORDS: Hydrothermal fluids, fluid inclusions, IOCG, PIXE, LAICPMS

## 1 INTRODUCTION

The goals of this study include resolving the character, source and evolution of hydrothermal fluids in the Wernecke Mountains by application of modern microanalytical techniques to fluid inclusions. This is the first significant fluid study in the Wernecke Mountains, and provides an opportunity to contribute substantially to the genetic model for this IOCG district. The lack of an obvious major magmatic influence on the district also provides a rare chance to study the importance of potentially end-member basinal brines that are distinct from the magmatic fluids that commonly form IOCGs deposits. Thus the results of this study could have further implications for the genetic model of IOCG deposits in general.

## 2 GEOLOGY OF THE WERNECKE MOUNTAINS

IOCG prospects in the Wernecke Mountains, Canada are hosted by numerous breccia zones occurring within the Proterozoic Wernecke Supergroup (WSG). The sequence is divided into three main components, the basal unit being the Fairchild Lake Group (FLG), which is comprised of mainly siltstone. Bedding parallel layers of scapolite within a zone of albite alteration are observed in the upper FLG (Hunt *et al.*, 2005) and may be an indication of pre-existing evaporite beds. Overlying this is the Quartet Group (QG) made up of predominantly black carbonaceous shale, with minor siltstone and fine grained sandstone, while uppermost is the Gillespie Lake Group (GLG) dominated by dolostone. Extensive metasomatic alteration accompanies the brecciation and associated IOCG mineralization. Potassic (K-feldspar) alteration dominates prospects located within the upper levels of the WSG (*i.e.* the GLG and QG) with prospects hosted at deeper stratigraphic levels (FLG) characterised by albite alteration.

## 3 GEOCHEMISTRY

Isocon analysis (Grant, 1986; 2005) was performed using whole-rock geochemical data from Thorkelson (2000), for samples from the three major units of the Wernecke Supergroup. Compositions of unaltered WSG rocks were plotted against rocks with varying intensities of alteration in order to quantify which elements were gained and lost during alteration (Fig. 1). Isocon analysis reveals that altered samples were enriched in Fe at all stratigraphic levels, consistent with the widespread occurrence of haematite and/or magnetite at all of the studied prospects. Sodium and Ca were found to be lost in significant amounts from altered rocks in the uppermost GLG, while there were large gains

in K. Altered QG samples show large losses in Na, but large gains in Ca and K, while the altered FLG samples were enriched greatly in Na and Ca, but lost K. The strong decrease in K/Na ratio with depth is consistent with the observed change in alteration mineralogy from potassic at shallow stratigraphic levels to sodic at deeper levels. This may be strongly controlled by the effect of depth/temperature on K-Na equilibrium, as discussed by Hitzman *et al.* (1992).

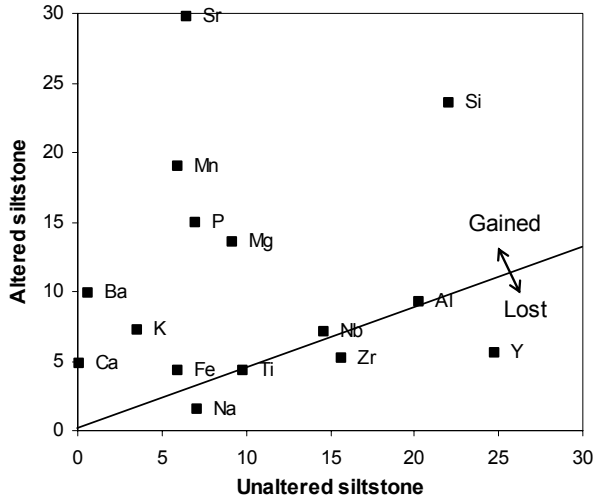


Figure 1: Isocon plot of an unaltered QG siltstone sample against a sample representing its altered equivalent, to illustrate the changes in chemistry that occurred during alteration. Al & Ti are used as immobile elements. Isochore slopes of <1 for QG and FLG suggest an overall mass increase during alteration of these units, however GLG isocons have greater slopes (>1) indicating overall mass loss.

Other notable variations include a strong depletion in Mn in altered GLG rocks with a strong enrichment in lower units. Alteration increased Ba levels dramatically in QG samples, in keeping with significant barite observed at the QG-hosted Igor prospect. Barium was also enriched in GLG rocks and depleted from the lower level FLG rocks.

## 4 FLUID INCLUSIONS

A suite of microanalytical techniques were employed to analyse fluid inclusions from several IOCG prospects in the Wernecke Mountains, in order to determine the character of the hydrothermal fluids responsible for brecciation and associated IOCG mineralization. The study included prospects from each stratigraphic unit of the WSG: Olympic (GLG), Igor (QG), Slats-Frosty (QG-FLG), Hoover (FLG) and Slab (FLG).

Fluid inclusions observed were predominantly 2 or 3 phase aqueous inclusions (L+V±H) with average salinities ranging from 20 to 45 wt% NaCl equiv. Homogenization temperatures were used along with pressure estimates to calculate trapping temperatures of between 150 and 330°C. LAICPMS (laser-ablation inductively coupled plasma mass spectrometry) and PIXE (proton induced X-ray emission) were used to perform multi-element analyses of individual fluid inclusions. Ca/K ratios vary considerably between the different prospects (Fig. 2), however the majority of inclusions contained Ca/K>1, and Slab inclusions had the highest values with a mean of 6. Notably Olympic Ca/K mean values are lowest with Ca/K=0.6. Mn/Fe ratios also vary between prospects. Slab fluid inclusions returned by far the highest Mn/Fe ratios with a mean of 3.3, while all other prospects had values of close to or below 1. Copper is low in inclusions from all prospects and was commonly below detection limits.

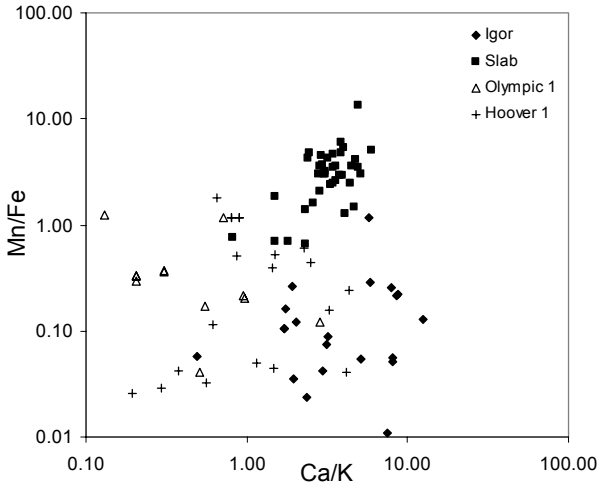


Figure 2: Fluid data showing significant compositional differences between prospects. The PIXE and LAICPMS datasets display a high level of agreement, and are therefore combined into a single dataset for analysis. Agreement is strongest when element ratios are used, avoiding the extra uncertainties in calculating absolute concentrations.

Halogens (Br, Cl) were analysed by PIXE and are important conservative tracer elements that can be used to identify the source of salinity (Fig. 3; *e.g.*, Yardley & Graham, 2002). Slab and Igor values fall in the region of the plot defined by bittern brines (high Br/Cl), while Olympic and Hoover values fall in a region that can indicate an influence of halite dissolution (low Br/Cl).

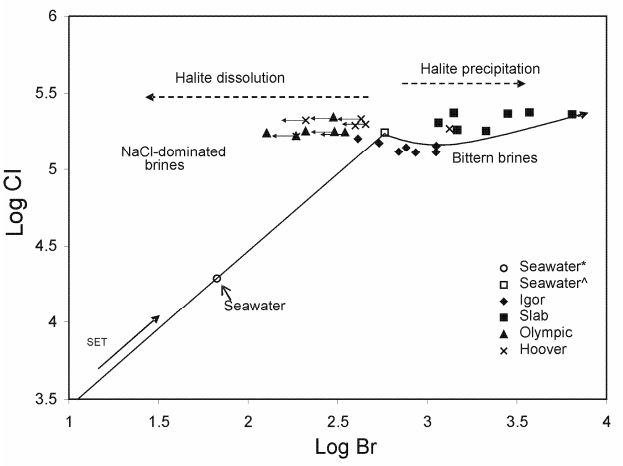


Figure 3: PIXE halogen data showing fluids plotting in the bittern brine and halite dissolution regions. The halogen composition of seawater (circle) is plotted, and SET represents the seawater evaporation trend, ie. the path seawater follows on the plot if it is evaporated to and past the point of halite precipitation (hollow square). Arrows indicate data points with Br below detection, in such cases detection limits were used as upper estimates.

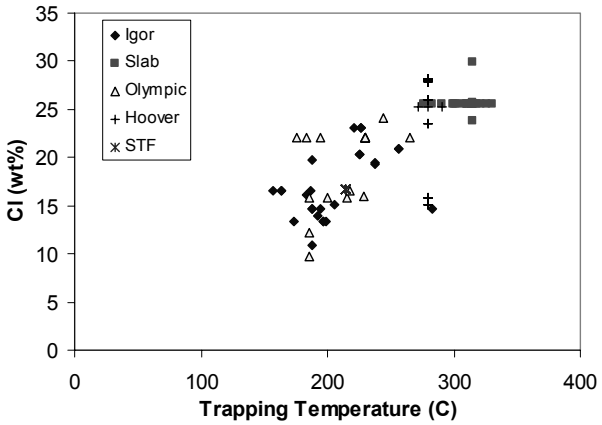


Figure 4: Correlation between salinity and trapping temperatures

## 5 DISCUSSION

The absence of significant magmatic intrusions in the Wernecke Mountains, in particular of similar timing to major brecciation events (1595 Ma), led Thorkelson (2000), Hunt (2004) and others to suggest a potentially non-magmatic source for the hydrothermal fluids, and fluid compositions obtained in this study support this (although Kendrick *et al*., *this volume* suggest there may be potential for some magmatic contribution). Halogen evidence from PIXE analysis suggests that the preserved hydrothermal fluids represent evolved seawater-derived brines, a finding also supported by Kendrick *et al* (*this volume*). The calcic nature of the Wernecke fluids (mostly Ca>K), along with moderate trapping temperatures and salinities are additional features of the fluids that are consistent with basinally-derived brines, and the dataset lacks the high temperature, high salinity multisolid inclusions and high K/Ca fluids that are commonly associated with magmatically-derived fluids.

Despite a probable shared origin, the fluid inclusions from each of the prospects differ considerably in some aspects, due to either having followed different pathways through the crust and/or being trapped at different stages of their evolution. PIXE Cl and Br data show evidence of evaporation past the point of halite precipitation (forming bittern brines), and also of local dissolution of residual halite horizons (Fig.3), which had previously been thought possible given the meta-evaporite horizons observed by Hunt (2004)

Temperature represents another influence on fluid composition (Yardley, 2005). The genetic model proposed by Hunt (2004) involved temperatures in the WSG increasing with depth. This is supported by the fluid inclusion trapping temperatures and also implied by alteration patterns, with transition from shallow potassic alteration to deeper sodic alteration. Figure 4 also shows a positive correlation between fluid inclusion trapping temperatures and salinities, suggesting that depth and temperature represent a major control on fluid salinities and therefore on the solute carrying capacity of the fluids. Positive correlations are observed between higher temperature fluid inclusions and higher element concentrations (particularly Cl, Br, K, Ca, Mn, Zn, Rb, Sr and Ba) in the combined LAICPMS and PIXE datasets. In addition the abovementioned interaction of fluids with existing halite horizons could also have the effect of increasing salinity and hence metal-carrying capacity, particularly in those fluids for which halite dissolution is implied by halogen values.

Fluid-rock interaction represents another control on fluid compositions. The importance of this interaction is evident from the large-scale, intense metasomatic alteration in the region, indicating significant mass exchange between fluid and wallrock. Comparison of wallrock gains and losses for altered samples, and compositions of related fluids reveal strong relationships between the two. Calcium and K gains and losses via alteration in each unit strongly reflect the Ca and K levels of the fluids samples from those units. In the Olympic prospect hosted in GLG the fluids exhibit the lowest

Ca/K ratios and are associated with strong K enrichment and Ca depletion, while prospects in the lower parts of the stratigraphy (*e.g.*, Slab in the FLG) contain fluid inclusions with Ca>K and are associated with strong sodic-calcic Ca-rich alteration and K depletion. Similarly, low Mn/Fe in fluid inclusions hosted in the GLG (*e.g.*, Olympic prospect) have depleted the Mn/Fe ratio in the wall-rock, while high Mn/Fe fluids caused the opposite to occur in the FLG (*e.g.* Slab prospect) with highly altered rocks displaying a 500% increase in Mn/Fe. In the QG (*e.g.*, Igor prospect) high Ba fluids are associated with large Ba gains in altered rocks. A strong interrelationship between fluid and wall-rock chemistry can therefore be demonstrated.

## 6 CONCLUSIONS

The evolution of the Wernecke fluids likely began with strong evaporation of seawater, resulting in a bittern brine and formation of residual halite horizons. As the brine began circulating in the crust, two major mechanisms influenced its chemistry. Firstly changes in salinity occurred, either due to interaction with halite horizons, and/or as a result of increasing or decreasing temperatures. Secondly the interaction (mass exchange) with different host rocks impacted the fluid chemistry particularly with respect to major element such as K, Ca, Mn and Fe. The changes in temperature, salinity and wall rock composition also influenced the capacity of the fluid to transport or deposit Cu, Pb and Zn.

A more complete understanding of fluid evolution will benefit from a planned closer evaluation of redox conditions at the time of trapping, assessment of fluids that may represent spent or post-alteration fluids, and consideration of precipitation mechanisms for IOCG mineralization.

## ACKNOWLEDGEMENTS

Funding for this study was provided by the Yukon Geology Survey and the pmd*CRC.

## REFERENCES

Grant, J.A. (1986) The isocon diagram—a simple solution to Gresens equation for metasomatic alteration. Economic Geology 81, 1976–1982.

Grant, J.A. (2005) Isocon analysis: A brief review of the method and applications *Physics and Chemistry of the Earth* 30 (2005) 997–1004.

Hitzman, M.W., Oreskes, N., and Einaudi, M. T. (1992) Geological characteristics and tectonic setting of Proterozoic iron oxide (Cu-U-Au-REE) deposits: *Precambrian Research,* v. 58, p. 241-287.

Hunt, J. (2004) The Geology and Genesis of Iron Oxide-Copper-Gold Mineralization Associated with Wernecke Breccia, Yukon, Canada. *James Cook University, PhD Thesis.*

Hunt, J., Baker, T., and Thorkelson, D. (2005) Regional-scale Proterozoic IOCG-mineralized breccia systems: examples from the Wernecke Mountains, Yukon, Canada. *Mineralium Deposita*, v. 40, no. 5, p. 492-514.

Kendrick, M.A., Mark, G., Oliver, N., Baker, T., Gillen, D., and Fisher, L. (2007) The origin of hydrothermal fluids in the mid-crust: Evidence from the noble gases and halogens. *This volume.*

Thorkelson, D.J. (2000) Geology and mineral occurrences of the Slats Creek, Fairchild Lake and "Dolores Creek" areas, Wernecke Mountains (106D/16, 106C/13, 106C/14), *Yukon Territory.*, 73 p.

Yardley, B.W.D., and Graham, J. T. (2002) The origins of salinity in metamorphic fluids: *Geofluids*, v. 2, p. 249-256.

Yardley, B.W.D. (2005) 100th Anniversary Special Paper: Metal Concentrations in Crustal Fluids and Their Relationship to Ore Formation. *Economic Geology,* v. 100, no. 4, p. 613-632.

# The Kipushi Cu-Zn mineralization in the Katangan Copperbelt (DRC): Quantitative fluid inclusion analysis using bulk crush-leach and laser ablation inductively coupled plasma-mass spectrometry

W.Heijlen & D.A.Banks
*School of Earth and Environment, University of Leeds, Leeds LS2 9JT, United Kingdom*

Ph. Muchez
*Geodynamics and Geofluids Research Group, K.U.Leuven, Celestijnenlaan 200E, B-3001 Leuven, Belgium*

ABSTRACT: We report quantitative analysis of the mineralizing fluid from the carbonate-hosted epigenetic Cu-Zn mineralization at Kipushi (Katanga, Democratic Republic of Congo). Fluid inclusions in dolomite and quartz associated with the main stage of sulphide mineralization were analysed by microthermometry, bulk crush-leach analysis and LA-ICP-MS. The fluids are highly saline Na-K-Ca-Cl brines (~35 eq. wt% NaCl) which show homogenisation temperatures around 275°C. The anion composition of the mineralizing and younger fluids has Cl/Br around or higher than the seawater ratio, indicating mainly dissolution of evaporites as a source of salinity. With respect to their temperature and salinity, the fluids have high concentrations of ore metals (Cu, Zn, Pb) and are highly evolved in terms of water-rock interaction. It is proposed that they represent late hydrothermal fluids, expelled in a post-orogenic extensional tectonic setting.

KEYWORDS: Copperbelt, Sediment-hosted Cu-Zn deposits, Fluid inclusion analysis, Lufilian orogen

## 1 INTRODUCTION

The Copperbelt of Central Africa (Zambia and the Democratic Republic of Congo) is mainly known as one of the major Cu-Co ore provinces in the world. However, very high-grade vein-type base metal deposits are known as well, both in the Lufilian thrust-and-fold belt ("Copperbelt" sensu strictu) and in its foreland. These deposits played an important role in the mining history of the region. Known occurrences in the Katangan part of the Copperbelt include Zn-Pb deposits of Lombe and Kengere, the recently exploited Cu-Ag deposit of Dikulushi and the giant Cu-Zn-Pb-Ge-Ag mineralization at Kipushi. The latter, located about 20 km west of the city of Lubumbashi has been mined continuously from 1922 to 1993 and produced about 60Mt of ore at a grade of 11% Zn, 6.8% Cu, 1% Pb, 0.3% Ge and ~160g/t Ag. It has been one of Africa's biggest producers of Cu and Zn during the last century. Recent studies on potential redevelopment of the underground mine by Adastra Minerals indicate reserves of 8.9 Mt at 16.7% Zn and 2.32% Cu.

We represent data on the nature and physico-chemical properties of the mineralizing fluids, obtained by microthermometry, bulk crush-leach analysis and laser ablation inductively coupled plasma-mass spectrometry.

## 2 GEOLOGIC SETTING AND NATURE OF MINERALIZATION

Unlike stratiform Cu-Co and vein-type U mineralization, which are mainly hosted in siliciclastic rocks of the lowermost part (Roan Group) of the Katangan Supergroup of Central Africa, the vein-type Zn-Cu-Pb deposits are hosted by younger carbonate rocks. In the case of Kipushi these are mainly dolomites of the Kakontwe formation (Muombe Subgroup; Lower Nguba Group). Base metal mineralization is located in the northern flank of a longitudinally broken-up ENE-trending anticline. This structure is made up of Lower Nguba lithologies, but its core contains a discordant megabreccia consisting of fragments of mainly Roan rocks. The breaking up of the core of anticlinal structures is a common deformation fea-

ture in the fold-and-thrust belt and this style of deformation has been attributed to the influence of salt tectonics (Cailteux & Kampunzu, 1995). De Magnée & François (1988) interpreted this axial breccia at Kipushi as a diapiric solution collapse breccia, with halokinesis piercing and breaking the anticlinal core along extrusion faults. The Kipushi mineralization is located along such fault. However, it was realised long since that the major control on the specific location of mineralization was the occurrence of a huge slab of silty dolomitic shale in between the carbonate host rocks and the breccia. This slab forms the impermeable roof of the vein deposit and is considered to be of younger, Kundulungu age.

Economic mineralization occurs along the fault zone (Kipushi fault) and spreads out in lodes at the contact between the massive dolomites and overlying alternating dolomites and silty dolomitic shale. In addition, some Zn-rich pipes shoot of the orebody into the dolomite host rocks. The paragenesis of gangue and ore minerals can be complex and varies spatially within the deposit (Ottenburghs, 1964). However, a generalised paragenesis for the vein mineralization involves a first Fe-poor dolomite generation (D1) and an overgrowing second generation of coarse-grained Fe-rich, rhomboedral dolomites (D2). The main sulphide mineralization can be associated with both D1 and D2 and consists of pyrite, chalcopyrite, sphalerite, tennantite, arsenopyrite and galena. Renierite and briartite are frequently associated with this phase. In some places, primary chalcopyrite has been replaced by bornite, chalcosite and other secondary Cu-minerals. Intimately associated, yet slightly later than sulphide deposition is a generation of quartz (Q). This quartz shows a bright, zoned blue luminescence under cold cathodoluminescence. Rhomboedral Fe-poor dolomites (D3) overgrow quartz and earlier sulphides, but are followed by a new sequence of sulphide deposition, involving mainly sphalerite, pyrite, chalcopyrite and galena.

## 3 FLUID INCLUSION ANALYSIS

Fluid inclusions interpreted as primary in the first (D1) and second generation (D2) of dolomites and in the quartz (Q) associated with the main stage of sulphide deposition are found isolated in the crystals, in clusters or in growth zones. They are often large (10-50µm) and generally contain an aqueous liquid, a halite crystal and a 10-20 vol% vapour bubble (L+H+V inclusions). Especially in the dolomites, they frequently have one or more other unidentified rounded, transparant daughter crystals (5-10 vol%). This is much less the case for the inclusions in quartz. Liquid-vapour homogenisation temperatures ($Th_{bub}$) are between 221 and 339°C (mode of 275°C; n = 31) and $Th_{bub}$ generally occurs at temperatures higher then those of halite dissolution (Tsh). The latter takes place between 140 and 360°C (mode of 251; n = 69), indicating salinities between 30 and 43 eq. wt. % NaCl (average of 35 eq. wt% NaCl). The unidentified solids in the inclusions mostly did not show any change upon heating and possibly represent trapped crystals.

Later fluid flow events are recorded in several generations of secondary, intergranular trails in the dolomite and quartz crystals and in primary inclusions in late stage sphalerite. They show a drop in homogenisation temperature and a trend towards lower salinities. While some of the secondary trails also have L+H+V inclusions, others only have an aqueous liquid and a vapour phase (L+V; Th as low as 117°C) or are monophase liquid, indicating formation temperatures lower then ~80°C. Salinity can vary widely in the latter inclusions ($Tm_{ice}$ of artifically stretched inclusions indicates salinities between 2 and 26 eq. wt% NaCl). The latest sphalerite generation has primary L+V inclusions with Th between 80 and 150°C and a salinity between 23 and 26 eq. wt% NaCl (n = 18).

In order to reconstruct the anion and cation composition of the mineralizing fluids, fluid inclusions were analysed by bulk crush-leach analysis and by laser ablation ICP-MS at the University of Leeds. Na, K and Li were analysed with both methods. Fig. 1 shows that there is a large offset in K/Na ratio (a similar offset exists for Li/Na), yet both methods yield a similar trend between the samples. Since the discrepancy is least for those samples having a low amount of secondary fluid inclusions compared to primary ones (*i.e.* HC15D1 and HC07D2 in Fig. 1), the discrepancy is interpreted as due to mixing with Na-rich, K- and Li-poor secondary fluid inclusions. This conclusion is substantiated by LA-ICP-MS analyses of secondary inclusions.

Molar Cl/Br ratios obtained by crush-leach analysis range between 744 and > 4500, *i.e.* higher then that of contemporary seawater

(~640). However, there is a clear positive relation between the Cl/Br ratio obtained and the difference in K/Na between crush-leach and LA-ICP-MS. This indicates that secondary inclusions have higher Cl/Br and the primary inclusions are characterized by a ratio close to that of seawater.

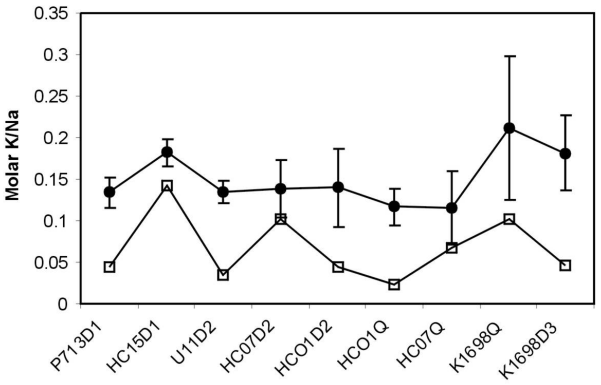


Fig. 1. Molar K/Na ratio of fluid inclusions obtained by bulk crush-leach analysis (open squares) and LA-ICP-MS of primary inclusions (solid circles). Error bars represent 1 σ.

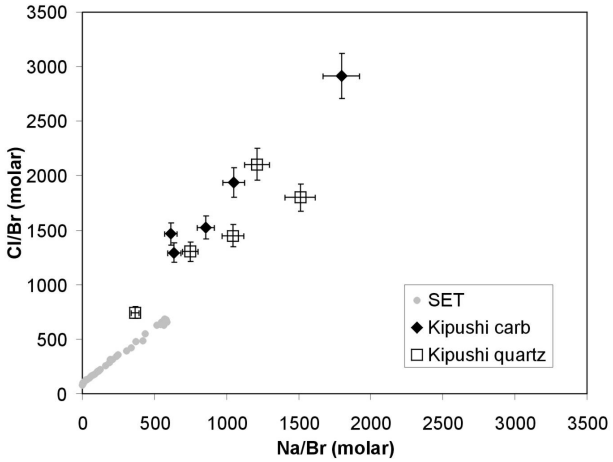


Fig. 2. Molar Na/Br vs. Cl/Br for mineralizing fluids from Kipushi. See text for discussion.

LA-ICP-MS analysis show that the mineralizing fluids have high amounts of alkali metals (Li, K, Na, Rb, Cs), alkaline earths (Mg, Ca, Sr, Ba) and ore metals (Cu, Zn, Pb). Table 1 gives the average molar ratios to Na for some analysed elements for inclusions in dolomite (D1, D2) and quartz, as well as the reconstructed concentration of the fluid in quartz. The latter was calculated using the salinity of inclusions for the respective quartz samples obtained from microthermometry and recalculation of the Na concentration using the charge-balance approach.

Table 1. Molar ratios to Na in dolomite and quartz and reconstructed concentration of selected cations in quartz.

| | D1+2 | Q | reconstructed concentration in Q (ppm) |
|---|---|---|---|
| Na | | | 73200 |
| Li | 0.0580 | 0.0092 | 230 |
| Mg | n.a. | 0.0382 | 2900 |
| K | 0.1459 | 0.1478 | 18900 |
| Ca | n.a. | 0.1867 | 22700 |
| Mn | n.a. | 0.0120 | 1900 |
| Fe | n.a. | 0.0408 | 6700 |
| Cu | 0.0007 | 0.0005 | 105 |
| Zn | 0.0426 | 0.0306 | 6340 |
| Pb | 0.0143 | 0.0050 | 3500 |

## 4 INTERPRETATION AND CONCLUSIONS

Structural field relationships clearly show that the epigenetic vein-type mineralization of Kipushi postdated the main tectonic deformation, occurring between 580 and 510 Ma (Muchez *et al*., 2007). Late- to post-orogenic hydrothermal high salinity fluids have been recognised at a number of places throughout the Lufilian orogen. Richards *et al*. (1988) reported on highly saline (~55wt% NaCl+KCl), high temperature (minimum trapping temperature of ~397°C) fluids in crosscutting quartz-haematite veins at Musoshi. These veins were dated at 514 ± 2 Ma (U-Pb on rutile) and are considered to have formed during peak metamorphism. Greyling *et al*. (2005) identified highly saline (18-23 eq.wt% NaCl) though lower temperature (130-160°C) fluids as late secondary fluids at the Chambisi deposit in Zambia. In both cases, carbonic inclusions are found associated with the highly saline ones. Recently, El Desouky *et al* (2007) identified highly saline (38 and 47 eq.wt% NaCl), high temperature (324-439°C) fluids in breccia cementing quartz at Luiswishi in the DRC. The mineralizing fluids at Kipushi have similar high salinity and elevated homogenisation temperatures. The micrometric data indicate an average minimum temperature of formation of the main mineralization at Kipushi of ~275°C. Ottenburgs (1964) used sphalerite geothermometry to estimate the formation temperature of the Zn-rich ore pipes between 305 and 380°C. Electron microprobe data of chlorite associated with quartz, dolomite and sulphides from Kipushi were reported by Chabu (1995). Chlorite geothermometry using these

data yield formation temperatures of ~370°C. At this temperature, the primary fluid inclusions indicate a relatively low confining pressure of ~1.4 kbar.

The Cl and Br relationships of the mineralizing fluids are markedly different from those of similar mineralization in the Damaran orogen (Namibia). Chetty & Frimmel (2000) showed that the fluids that caused mineralization at Tsumeb essentially were bittern brines with Cl/Br values lower than that of seawater. Our results demonstrate the importance of leaching of evaporates as a contribution to the high salinity of the mineralizing fluids. Moreover, the Cl/Br signature of low-temperature, secondary fluid inclusions suggest that such leaching continued long after the main phase of deformation and metamorphism.

The cation composition of the mineralizing fluids evidences extensive water-rock interaction. When compared with fluids in other sedimentary basins and metamorphic terranes worldwide, they have very high K/Na and Li/Na ratios. In addition, for their temperature and salinity, they contain an exceptionally high concentration of dissolved ore metals. We propose that late hydrothermal fluids, highly evolved in terms of water-rock interaction were expelled in a post orogenic extensional tectonic setting.

## ACKNOWLEDGEMENTS

This research was supported by a Marie Curie Intra-European Fellowship to WH within the 6th European Community Framework Programme

## REFERENCES

Cailteux J, Kampunzu AB (1995) The Katangan tectonic breccias in the Shaba province (Zaire) and their genetic significance. In: Wendorff M, Tack L (eds) Late Proterozoic Belts in Central Africa. MRAC, *Annales des Sciences Géologiques* 101, 63-76.

Chabu M (1995) The geochemistry of phlogopite and chlorite from the Kipushi Zn-Pb-Cu deposit, Shaba, Zaire. C*anadian Mineralogist* 33: 547-558.

Chetty D, Frimmel HE (2000) The role of evaporites in base metal sulphide in the Northern Platform of the Pan-African Damara Belt, Namibia: Geochemical and fluid inclusion evidence from carbonate wall rock alteration. *Mineralium Deposita* 35: 364-376.

De Magnée I, Francois A (1988) The origin of the Kipushi (Cu, Zn, Pb) deposit in direct relation with a Proterozoic salt diapir. Copperbelt of Central Africa, Shaba, Republic of Zaire. In: Friedrich GH, Herzig PM (eds) *Base Metal Sulphide Deposits,* Springer-Verlag, Berlin, pp. 74-93.

El Desouky H, Dewaele S, Haest M, Muchez Ph, Cailteux J, Heijlen W (2007) Fluid flow evolution in the Katangan Copperbelt, DRC. *this volume*

Greyling LN, Robb LJ, Master S, Boiron MC, Yao Y (2005) The nature of early basinal fluids in the Zambian Copperbelt: A case study from the Chambisi deposit. *Journal of African Earth Sciences* 42: 159-172.

Muchez Ph, Brems D, El Desouky H, Dewaele S, Haest M, Vanderhaegen P, Heijlen W, Mukumba W (2007). Base metal ore deposit evolution and geodynamics in the Central African Copperbelt. *This volume*.

Ottenburgs R (1964) Metallogenetische en geochemische Studie van het blende-erts te Kipushi, Katanga. U*npublished PhD thesis, K.U.Leuven, Belgium,* 115 p

Richards JP, Kroch TE, Spooner ETC (1988) Fluid inclusion characteristics and U-Pb rutile age of late hydrothermal alteration and veining at the Musoshi stratiform copper deposit, Central African Copperbelt, Zaire. *Economic Geology* 83: 118-139.

# NIR/SWIR microscopy and microthermometry of fluid inclusions from Fe-rich sphalerites, Cerro León (Zn-Pb-Ag-In-Au) polymetallic vein deposit, Deseado Massif, Patagonia, Argentina.

S.M. Jovic, D.M. Guido & I.B Schalamuk
*CONICET-Instituto de Recursos Minerales, Universidad de Nacional de La Plata, Argentina.*

F.J. Rios, K. Fuzikawa & J.V. Alves
*Laboratory of Fluid Inclusion and Metallogenesis (LIFM) CDTN/CNEN, Cx. Ps. 941, 30123-970, Belo Horizonte, Brazil.*

ABSTRACT: An alternative IR microscopy system in the NIR (near infrared, up to 10 μm) and SWIR (short wavelength infrared, up to 1.4 μm) has been used for the study (microscopy and micro thermometry) of fluid inclusions in opaque Fe-rich sphalerites from the Cerro León (Zn-Pb-Ag-In-Au) polymetallic vein deposit, Deseado Massif, Patagonia, Argentina. Under transmitted light, the fluid inclusions are invisible but under IR it is possible to observe large primary (L + G) aqueous fluid inclusions (up to 100μm) with homogenization temperatures that vary between 255 and 265.2 ºC and salinities between 4.34 to 8.81 wt% NaCl, located the mineralization in the epithermal systems range and define as a polymetallic epithermal deposit. This alternative IR system represents an important tool for the study of opaque minerals fluids from polymetallic mineralization ores.

KEYWORDS: IR, fluid inclusions, Fe-rich sphalerites, polymetallic mineralization, Argentina

## 1 INTRODUCTION

Most ore minerals (sulphides and oxides) behave as opaque mineral when are observed in thin sections under a visible light spectrum (0.35-0.75 μm). But when are observed under IR radiation, some of these minerals became transparent and it is possible to discriminate several features like zoning, growth lines, and solid and fluid inclusions that otherwise would be unseen under normal light.

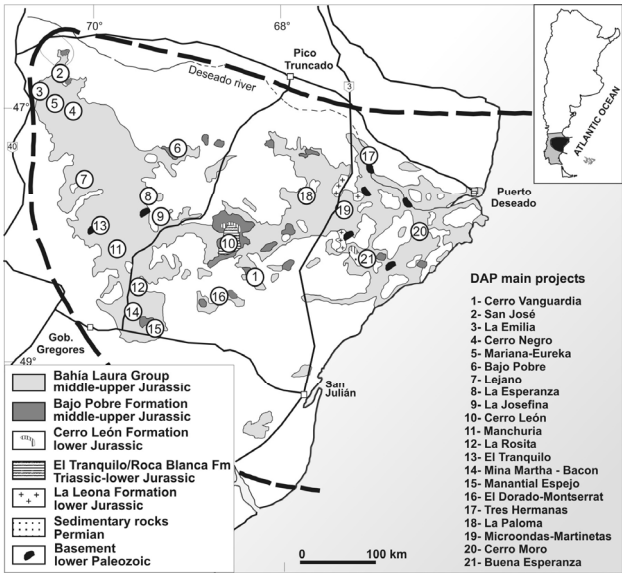


Figure 1. Geology and location of Cerro León deposit and mining projects in the DM.

An alternative methodology have been developed at the Laboratory of Fluid Inclusion and Metallogenesis (LIFM) of the Centro da Desenvolvimiento da Tecnologia Nuclear (CDTN) at Belo Horizonte, Brazil, and are based on infrared (IR) microscopy and microthermometry for NIR, near infrared, up to 1 μm and SWIR, short wavelength infrared, between 1.0 and 1.4 μm (Rios *et al,* 2006). This paper presents the application of this alternative system in the studies of Fe-rich sphalerites from the Cerro León (Zn-Pb-Ag-In-Au) polymetallic mineralization, Deseado Massif, southern Patagonia, Argentina.

## 2 METALLOGENESIS

### 2.1 *Deseado Massif Gold Deposits*

The Deseado Massif (DM) geological province is located in southern Argentinean Patagonia (Fig. 1). The region is an important Au-Ag producer, with two active mines (Cerro Van-

guardia and Mina Martha). This region is characterized by the presence of low sulphidation (LS) epithermal deposits that are spatially, temporally and genetically related to a complex, middle to late Jurassic bimodal volcanic event. Mineralization in the DM is typically controlled by structures with a NW strike, plus minor NE and E-W trends. Deposits characteristically consist of quartz veins and veinlets, stockworks and hydrothermal breccias. The gangue is dominated by quartz with minor chalcedony and some opal accompanied by calcite, adularia, barite, fluorite, and zeolites. The quartz veins are commonly massive, brecciated, crustiform and colloform bands with comb, cockade, and lattice-blade textures. Metalliferous minerals are scarce, representing commonly less than 1 percent by volume, including pyrite, native-gold, electrum, argentite, native silver, Ag-sulphosalts, haematite, sphalerite, galena and chalcopyrite. The geochemical signature from quartz veins is typical of LS epithermal deposits, with anomalies in precious metals (Au-Ag). Hydrothermal fluids were characterized as neutral to alkaline $H_2O$-NaCl solutions, with salinities of 0.18 to 8 wt% eq. NaCl. The homogenization temperatures for quartz and adularia range between <100º to 320º C.

### 2.2 *Cerro León Polymetallic Deposit*

Cerro León deposit is located in the central part of the Deseado Massif, 40km northwest from Cerro Vanguardia mine. This deposit is composed of 58.7km NW-WNW strike structural controlled vein system hosted in Triassic continental sedimentary rocks and lower Jurassic epi-volcaniclastic rocks that are intruded by lower Jurassic subvolcanic intermediate to basic rocks that presents as sills and andesitic porphyries. These veins are associated to a major fault located in the center of a 15km dome structure.

#### 2.2.1 Polymetallic Mineralization

The polymetallic mineralization is characterized by the presence of massive sulphide veins and sulphide breccias up to 12m thick, with very anomalous contents of Zn, Pb, Ag, In, Au, Cu, Cd and Sn.

The mineralization is developed in three stages. The first stage is characterized by the presence of pyrite, arsenopyrite, chalcopyrite, cassiterite, wolframite (hübnerite-ferberite) and quartz. During the second stage of mineralization the first stage is replaced by a complex sulphur-rich mineralogy composed of Fe-rich sphalerite, galena, ferrokesterite - kesterite, bournonite, tetrahedrite, freibergite, Ag-Pb-Bi sulphosalts (possibly new minerals) and enargite.

Finally the third mineralization stage represented by botroydal Fe-poor sphalerite, euhedral greenockite, spherulitic stolzite and crandallite are filling geodic porosity (Crespi *et al*, 2006).

## 3 INFRARED MICROSCOPY AND MICROTHERMOMETRY OF FLUID INCLUSIONS

### 3.1 *Methodology*

The alternative IR microscopy system developed by LIFM-CDTN consists of an IR emitter (fitted up in a Leica DRMX microscope), filters, high resolution objectives, IR chambers and a Sony Trinitron monitor with video printer. The high sensitivity emitter runs at variable current and with IR LEDs and IR lamp bulbs sources.

To capture images a high resolution camera Sony ExwaveHad black and white, very near-IR camera with excellent sensitivity in NIR, max. 1.2 μm (Rios *et al.*, 2006).

In the microthermometric studies carried out with these types of sources, a USGS Fluid Inclusion heating/freezing system stage to a Leica DMR-XP microscope was used. No sample temperature variation was recorded during IR analysis under room temperature (25ºC).

### 3.2. *Results*

IR microscopy and microthermometry analysis of sphalerites were carried out on double polished, 200-300 um thick. The freezing temperature ($T_f$) was measured first, then the eutectic temperature (Te), the temperature of final ice melting ($Tm_{ice}$) and finally the homogenization temperature (Th).

Under transmitted light, Fe-rich sphalerites have a pale grey color and the fluid inclusions and other features are opaque or indistinguishable. (Fig. 2 A and C). IR microscopy permitted the observation of several remarkable features usually not seen in the Fe-rich sphalerites under normal light, such as growth lines, solid and fluid inclusions.

Under IR it is possible to observe large primary (L + G) aqueous fluid inclusions (up to 100μm) with different shapes (tube like, spher-

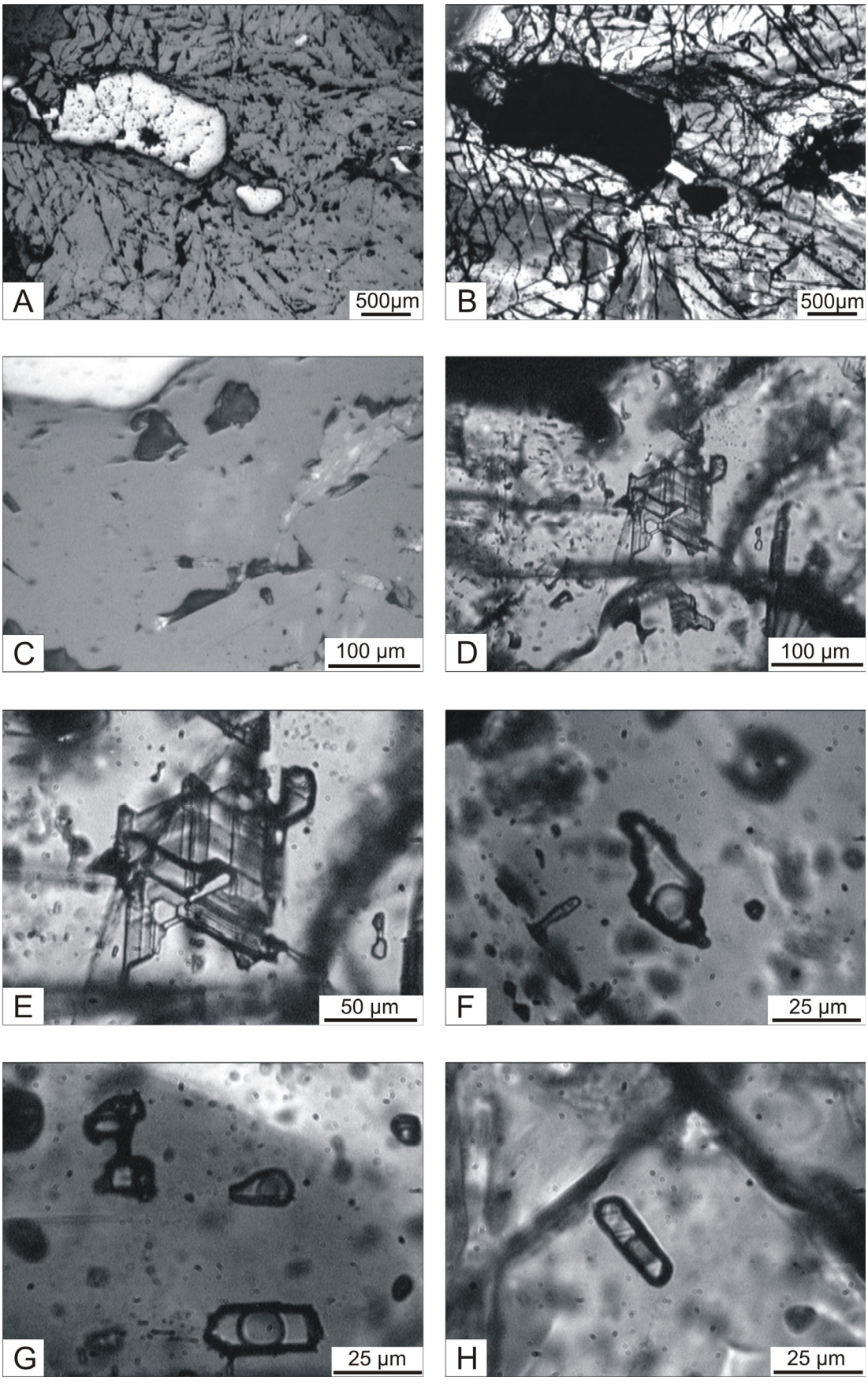


Figure 2. Microscopic features of the sphalerites analyzed under normal light and infrared radiation; Sphalerite and pyrite crystals under normal light, (A) and under infrared radiation, (B). Sphalerite under normal light, (C) and under infrared radiation with a "cleavage morphology" fluid inclusion, (D) and (E). Primary fluid inclusions in sphalerites, (F), (G) and (H).

Table 1. Microthermometric data of the studied sphalerites.

| Mineral | Fe-rich sphalerite |
|---|---|
| n | 13 |
| Eutectic temperature (º C) | -15.3 to -7.1 |
| Ice meeting temperature (º C) | -2.6 to -5.7 |
| Salinity (wt% NaCl) | 4.34 – 8.81 |
| Homogenization temperature (º C) | 255 – 265.2 |

rical and cleavage morphology) See Figure 2 B, D, E, F, G and H.

The fluid inclusion microthermometric results are given in Table 1.

During microthermometry, the eutectic temperatures range between -15.3 and -7.1 ºC indicating an H2O-NaCl composition.

Ice melting was measured between -2.6 and -5.7 ºC, which indicates low to moderate salinity (between 4.34 and 8.81 wt% NaCl, Bodnar & Vityk, 1994) and homogenization temperatures between 255 and 265.2 ºC.

In freezing and heating runs, no development of clathrates or melting or homogenization of $CO_2$ was observed, thus document the $CO_2$-free nature of this inclusions

## 4 DISCUSION

Cerro León polymetallic mineralization is represented by a high percentage of sulphides (up to 100% in volume), complex sulphide mineralogy and a geochemical signature (Zn, Pb, Ag, In, Cd, Au, Cu, Sn) that clearly differ from the typical DM LS epithermal mineralization.

With the infrared (NIR/SWIR) microscopy and microthermometry studies in the Fe-rich sphalerities, was possible to measure the homogenization temperatures that vary between 255 and 265.2 ºC and the salinity of the fluids that vary from 4.34 to 8.81 wt% NaCl.

These values of Th and salinity located the polymetallic mineralization in the range of the epithermal systems and could be defined as polymetallic epithermal deposit.

Cerro León polymetallic mineralization could be compared with the polymetallic (Au-Ag-Pb-Zn) veins deposits from the Somuncura Massif, central Argentinean Patagonia, that presents Th values between 129º and 343ºC and salinity values between 2.0 and 10.4 wt% NaCl (Dejonghe, 2002).

## 5 CONCLUSIONS

Fe-rich sphalerite is one of the principal's mineral in the Cerro León polymetallic mineralization ore. Under normal light the fluid inclusions and other features are opaque or indistinguishable. The alternative infrared system used here, allows studied the opaque Fe-rich sphalerite in the NIR and SWIR range and made microscopy and microthermometry studies from the fluid inclusions with the measured of the homogenization temperature and salinity of the fluids.

The results of this study allow us to locate Cerro León polymetallic mineralization in the epithermal systems range and define as a polymetallic epithermal deposit.

This infrared alternative system represents an important tool for the study of the opaque minerals fluids from polymetallic mineralization ores.

## REFERENCES


Crespi, A., Jovic, S., Guido, D., Proenza, J., Melgarejo, J.C., Schalammuk, I.B. 2006. El prospecto Cerro León, Macizo del Deseado, Patagonia, Argentina: Un depósito de Ag-Sn. /*Macla*/, *6*, 143-145.

Rios, J., Alves, J., Perez, C., Costa, E., Rosiere, C., Fuzikawa, K., Correia Neves, J., Chaves, A., Prates, S., de Barrio, R. 2006. Combined investigations of fluid inclusions in opaque ore minerals by NIR/SWIR microscopy and microthermometry and synchrotron radiation X-ray fluorescence. *Applied Geochemistry*. 21, 813-819

Dejonghe, L., Darras, B., Hughes, G., Muchez, P., Scoates, J., Weis, D. 2002. Isotopic and fluid-inclusion constraints on the formation of polymetallic vein deposits in the central Argentinian Patagonia. *Mineralium Deposita*. 37: 158-172.

# Present-day geothermal fluids from northern Tunisia: a key for understanding the dynamic of the fossil mineralizing fluids?

A. Charef
*Centre de Recherche et de la Technologie dês Eaux, Soliman, Tunisia*

F. Noronha & A. Guedes
*Departamento de Geologia e Centro de Geologia da Universidade do Porto, Faculdade de Ciências, Porto, Portugal*

ABSTRACT: More than 95% of metals extracted in Tunisia are derived from three important structural zones located in the north of the country. Geological studies of the actual thermal sources in North Tunisia show that hot fluids emerge from two main conjugated fault system. To investigate the relationship between the fossil fluids trapped in different calcite generations (fluid inclusions) and the present-day deep groundwater (geothermal fluids), their physical and chemical characteristics were studied. Significant similarities exist between fossil hydrothermal and present-day geothermal fluids in that both show important fluctuations in temperature, salinity and fluid composition. This may contribute to develop a different strategy in mineral exploration of the Pb-Zn deposits in northern Tunisia.

KEYWORDS: Fossil hydrothermal fluids, Present-day geothermal fluids, Pb-Zn deposits, Tunisia

## 1 INTRODUCTION

Northern Tunisia is composed of a "nappe" zone, a diapir zone, and an oriental zone. More than 95% of the metals extracted in the country are distributes within these zones. Several authors proposed that the Pb-Zn-Ba-F ore deposits are of Mississipi Valley type (MVT) (*e.g.*, Rouvier *et al*. 1985, Charef & Sheppard 1987). The tectonic history of northern Tunisia is very complex and the sedimentary basins have a limited extension.

In this work the characteristics of the hydrothermal fluids and their changes with time and space (dynamic systems) are studied according to the method of Cathles & Smith (1983) who showed that polyphased and dynamic fluid evolution can be responsible for the generation of ore deposit in a limited basin area. The hydrothermal fluids can leach large quantities of metal from sedimentary columns in a relatively limited area when important variations of temperature and chemical composition of fluids do occur. Variation of physical and chemical fluid parameters will contribute to the dissolution and the leaching of metals in the sediments.

The present-day E-W, NE-SW and N-S active fault systems correspond to pathways for fluid circulation and calcite deposition. It is also most likely that these systems correspond also to mineralized palaeosystems.

The geological studies of fifteen actual thermal water emergences in northern Tunisia show that hot fluids emerge from the main fault systems. Tebib Hlali (1992) shows that thermal water sources are randomly scattered in the area and the distance between them can reach several kilometres. Therefore, the actual position of thermal sources should be different from their original position; the calcite in the fractures may correspond to ancient emergencies and the calcites we observe today in the different fracture systems may result from the precipitation of the oldest thermal fluids.

Trapped fluid studies of the different calcite generations can provide valuable information on the evolution of the thermal fluid physical and chemical compositions in time and space. First, petrographical observations were carried out to classify calcite generations, then geochemical and fluid inclusion studies are used to define the chemical evolution of the fluids.

The results may contribute to develop a new strategy in mineral exploration of the Pb-Zn deposits in northern Tunisia.

## 2 GEOLOGIC SETTING

Northern Tunisia is subdivided in three structural zones. (1) The "nappe" zone is composed mainly of Cretaceous and Oligo-Miocene fysch-type sedimentation and form the Tell Atlas thrust belt. (2) The "Diapir zone" is characterized by several outcrops of the Triassic evaporitic formation over a 300km along the NE-SW trending belt. The Triassic formation is brought to the surface under the Atlasic tectonic events. It is composed of highly deformed evaporitic lithologies that consist of chaotic mass of gypsum, anhydrite, halite, marls, sandstones and carbonates. The post Triassic formations comprise limestones, sandstones and marls. (3) the Oriental zone is a horst-graben where the sediments are dominantly composed by limestones, marls and some volcanic rocks.

The actual structures in North Tunisia are the results of three major dynamic episodes: (1) during the middle Triassic to early Cretaceous, rifting affected the northern part of the Tunisian Atlas (Perthuisot 1972, Bédir *et al.* 2001); this Thetyan rifting is controlled by Hercynian E-W, N-S, NW-SE and NE-SW faults; (2) during the Cretaceous and Cenozoic, the dominantly compressive and transpressive Pyrenean and Alpine collision affected all north Africa and involved the northern Tunisian Atlas.

The main NE-SW structural trends are similar to those of Mediterranean Hercynian. During this period, explosive magmatism and/or major vertical faults involved both basement and sedimentary basins (Bouaziz *et al*. 2002); (3) the Quaternary tectonic evolution in most part of Tunisia is controlled by the NE-SW to E-W trending faults; and (4) a post-Lower to Middle Pleistocene, compressional phase and an extensional strike-slip faulting of Tyrrhenian time reactivate the E-W trending faults (Amari & Bedir1989; Zaouaari 1995). These structures are well observed in all Tunisia except the N-S fractures which are not clearly observed in the extreme North. Therefore, the E-W, NE-SW, NW-SE and N-S fault systems are active during the different tectonic events since the Triassic period, however it is not possible to attribute and age to this fault systems This study was carried out on several sites distributed over the three structural zones and characterised by the occurrence of thermal springs: 1) Dhaoui, H. Bourguiba and Kef-Ettout from «nappe" zone; 2) Mellègue, Biadha from diapir zone; and 3) Jdidi, Oust, Korbouss from the oriental zone.

## 3 ANALYTICAL TECHNIQUES

Fluid inclusion studies (FI) were carried out on calcites collected from the E-W, NE-SW and N-S fractures. The salinities of FI are presented in wt% equivalent NaCl and the salinities of geothermal emergences in mNaCl. Gases ($CH_4$, $CO_2$ and $N_2$) were analysed using Raman Spectroscopy (a Labram Dilor-Jobin spectrometer with a He–Ne laser excitation source of 632.8nm). 100ml of present-day thermal water samples were collected in polyethylene bottles then filtered using 0.45µm millipore membranes, and finally acidified to 1% with nitric acid. The samples were stored at 4°C and subsequently analysed by Atomic Absorption Vario type with graphite furnaces. Their free gases are analysed following the Morette method by Gas Chromatography.

## 4 RESULTS

### *4.1 Calcite petrography*

Field observations show that coloured cal-

| Zone | Emergences | Faults E - W | | | | NE Š SW | | N - S | |
|---|---|---|---|---|---|---|---|---|---|
| | | Ct1 | Ct2 | Ct3 | Ct 4 | Ct 1 | Ct 2 | Ct 1 | Ct 2 |
| "Nappe" | Dhaoui | 68.5, $CH_4$ | 76.0 ($CH_4$)-($CO_2$) | | | 55 (CO2)-($CH_4$) | | | |
| | H.Bourguiba | 73.5 | 81.0 ($CO_2$) | | | 48.5, ($CO_2$)-($CH_4$) | | | |
| | Kef-Ettouf | 73.0 $CO_2$ | 82.5 $CO_2$-$N_2$ | | | 53.5 ($CO_2$) | | | |
| Diapir | Mell¸gue | 76.5, ($CH_4$) | 97.0, ($CH_4$)-($CO_2$) | | | 55.5 | 67.5 | | |
| | Biadha | 101 | 118.5 $CH_4$-$CO_2$ | 80.5($N_2$)-$CO_2$ | 75.5 $CH_4$ | 52.0 ($CO_2$) | 69.0 $CH_4$-$CO_2$ | | |
| Oriental | Jdidi | 142 | 128 $CH_4$-$CO_2$ | 115 $CO_2$ | | 53.5 $CH_4$ | 65.5 $CH_4$-$CO_2$ | 179 | 145 CH4-$CO_2$-($N_2$) |
| | Oust | 129 $CO_2$ | 117 $CO_2$-$CH_4$ | | | 65.5 $CO_2$-$CH_4$ | | 140 | 101 |
| | Korbous | 140 | 118 $CH_4$-$CO_2$ | | | 56.0, ($CH_4$) | 65.0 $CH_4$-($N_2$) | 142 $CO_2$-$CH_4$ | 103 ($CH_4$)- ($N_2$) |

Table 1: Th mode (°C) and relative abundance of $CO_2$, $CH_4$ and $N_2$ in different calcite generations of the three-fault system ( ): trace

cite precipitate symmetrically at the edges of the distensive E-W fractures, then precipitate up to four duplicated generations of calcite (Ct1, Ct2, Ct3, Ct4 and Ct'1, Ct'2, Ct'3, Ct'4, respectively). In the NE-SW faults, any symmetrical distribution of different calcite generations is observed in or near the fractures. The different calcite minerals comprise centimetre to decimetre white- beige to red crystals. The colour of the mineral is controlled by the amount of iron oxides present in the crystal. Petrographical observations show that Ct1, Ct2, Ct3 and Ct4 are equivalent to Ct'1, Ct'2, Ct'3 and Ct'4 respectively.

### *4.2 Calcite geochemistry*

Trace element (Fe, Cu, Sr, Ni, Co, Al) data show that Ct1 and Ct'1 from Jdidi have high Al (4600 ppm) and Fe (~5%) contents and Sr (680 ppm) concentration. On the other hand, Ct2 and Ct'2 samples have low Al (507 ppm) and Fe (1.25%) content but high of Sr (1021 ppm) contents. Within the E-W faults, Ct1, Ct2 and Ct3 calcites show similar composition to their symmetrical Ct1', Ct2', Ct3' but differences exist between each layer. These results suggest that there are three generations of calcite.

### *4.3 Fluid inclusion data fluids*

Fluid inclusion (FI) studies were carried out on calcites that were precipitated from fossil fluids. The microthermometric data show that:

- All fluid inclusions homogenise into the liquid phase;
- The Th of primary fluid inclusions range from 44 to 190°C and the salinities vary between 4.2 and 21 wt % eq. NaCl.
- The Th of secondary fluid inclusions varies between 70 and 122°C.
- The Th of the different FI generations does not show systematic decrease or increase. For example, in NE-SW fault calcites of Biadha and Jdidi, the Th increases from the first to the second generation of FI (53°C to 67°C, respectively). However, in the E-W fault calcites of Biadha, the Th increases from 100 to 118°C then decreases to 80°C. At Jdidi, the Th decreases from the first to the third generation (142°C to 115°C, respectively).
- The salinity of the different FI generations varies between 4.2 and 21.2 wt % eq. NaCl). In Ct1 the observed Te of -53°C is close to the eutectic temperature of $H_2O$-NaCl-$CaCl_2$-$MgCl_2$ system. In Ct2, the Te range from -36.5 to -24.8°C which correspond to intermediate eutectic temperature between the $H_2O$-NaCl–(KCl) and the $H_2O$–NaCl–$MgCl_2$ systems. Fluids of Ct3 have a Te of -21.9°C which corresponds to $H_2O$-NaCl system. The calcites from Biadha E-W fault system, Te data indicate that the fluid trapped in Ct1, Ct2, Ct3 and Ct4 represent respectively the $H_2O$-NaCl-$CaCl_2$-$MgCl_2$, $H_2O$-Nacl or $H_2O$-NaCl-KCl, $H_2O$-NaCl-$MgCl_2$ and $H_2O$-NaCl-$CaCl_2$-$MgCl_2$ systems. Therefore, the Th variations are also followed by fluctuation of fluid composition.

All fluid inclusion generations were investigated for their gas contents. The results are listed on Table 1 and show that the nature and the relative abundances of these gases in the different calcites are variables within the fault systems and the FI generations in each system.

### *4.4 Present-day geothermal fluids*

Water temperature in the present-day geothermal emergences, varies between 37 and 58°C. Geochemical data indicates that these waters are controlled by at least five dynamic systems which are distinguished essentially by their major elements contents (Sadki 1998).

Dissolved $CH_4$, $CO_2$ and $N_2$ contents show variable abundances. For example, in Dhaoui, Biadha, Jdidi and Oust waters emergences, the fluids are $CH_4$-rich and $CO_2$ and $N_2$ contents show high fluctuations.

## 5 CONCLUSIONS

The fossil fluids are in a dynamic system because they show important fluctuations in Th, salinity and fluid composition, namely the nature of cations ($Na^+$, $K^+$, $Ca^{2+}$, $Mg^{2+}$) and the volatile compound abundances.

The salinity, composition and temperature vary from one calcite generation to another, and the wide salinity variation occurs within only restricted homogenisation temperatures. Therefore, each hydrothermal fluid generation was derived from approximately the same geologic level and the variation of geochemical compositions of the leached geological series during each period is probably the origin of the salinity fluctuations.

There are similarities between the present-day and the fossil fluid types, but the salinities of present-day deep ground waters are lower.

In each tectonic event, the new faults and the reactivation of the pre-existing fractures provoked changes in both the extension of the crack and the local regional rocks permeability.

Therefore, waters can infiltrate into different geological levels and though different rock compositions acquiring different fluid temperatures and compositions.

In conclusion, the present-day geothermal and fossil hydrothermal fluids show poly-phase activity with change of physical and chemical fluid characteristics. The nature of these hot fluids that were derived from different geological levels was controlled by both the nature and composition of the geological series, and tectonic events because the fluid circulation systems have a dynamic evolution.

This study may contribute to develop a different strategy in mineral exploration of the Pb-Zn deposits in North Tunisia, since until now the exploration is based only on sedimentary criteria.

## ACKNOWLEDGEMENTS

The authors wish to thank the Grices (Portugal) -INRST (Tunisia) cooperation and POCI 2010.

## REFERENCES

Amari A & Bedir M (1989) Dynamique des bassins sédimentaires quaternaires du Sahel

Central de Tunisie : Genèse et évolution des Sebkhas en contexte dépression compressif et distensif. *Revue Géodynamique* 4: 49-65.

Bedir M, Boukadi N, Tlig S, Ben Timzel F, Zitouni L, Alouani R, Slimane F, Bobier C & Zargouni F (2001) Subsurface mesozoic basins in the central Atlas of Tunisia : tectonic, sequence deposit distribution and hydrocarbon potentiel. *AAPG Bull.* 85: 885-907.

Bouaziz S, Barrier E, Soussi M, Turki M M & Zouari H. (2002) Tectonic evolution of the North Africa margin in Tunisia from paleostress data and sedimentary record. *Tectonophysics* 357: 327-353.

Cathles LM & Smith A T (1983) Thermal constraints on the formation of Mississippi Valley Type lead-Zinc deposits and their implications for episodic basin dewatering and deposit genesis. *Economic Geology* 78: 983-1002.

Charef A & Sheppard S M F (1987) Pb-Zn mineralization associated with diapirism: fluid inclusion and stable isotope (H, C, O) evidence for the origin and evolution of the fluids at Fedj-el-Adoum, Tunisia. *Chem. Geol*. 61: 113-134.

Perthuisot V (1972) L'évolution d'un diapir tunisien: le djebel echeid. *Rev. Géogr. Phys. Et Géol. Dyn, 2ème série* 14: 145-152.

Rouvier H, Perthuisot V & Mansouri A (1985) Pb-Zn deposits and salt bearing diapirs in southern Europe and North Africa. *Economic Geology* 80: 666-687.

Sadki O (1998) Etude des systèmes hydrothermaux du Nord de la Tunisie : Géochimie des intérractions Eaux-roches et circulation hydrothermale. *Thèse de 3ème cycle. Université de Tunis.* pp246.

Tebib Hlali H (1992) Etude des émergences de la Tunisie Nord-oriental de la Tunisie; *Thèse de 3ème cycle. Tunis.* pp182.

Zouari H (1995) Evolution géodynamique de l'Atlas Centro-méridional de la Tunisie: stratigraphie, analyse géométrique, cinématique et tectono-sédimentaire. *Thèse.Tunis*. pp277.

# The solubility of gold in crude oil: implications for ore genesis

A.E. Williams-Jones & A.A. Migdisov
*Department of Earth and Planetary Sciences, McGill University, Montreal, Q.C., Canada*

ABSTRACT: The two principal resources of gold on the planet, the Carlin-type deposits and the deposits of the Witwatersrand Basin, South Africa, are notable for the common association of gold with pyrobitumen (or in some Carlin deposits liquid oil) interpreted to represent residues of oil migration. Where this association is considered to have genetic significance, it is that the hydrocarbons promoted hydrothermal deposition of the gold. However, another possibility is that hydrocarbons served as a medium of gold transport. In order to test this possibility, we have conducted preliminary experiments designed to determine the solubility of gold in crude oil. The results of these experiments show that the solubility ranges from ~ 2 to 3 ppb Au at 100 °C to 18 ppb Au at 200 °C. The actual speciation of the gold is unknown. However, by analogy with what is known about the behaviour of V and Ni, an Au-bearing porphyrin is a distinct possibility as are species involving asphaltene molecules. Irrespective of how gold dissolves in liquid petroleum, the essential conclusion of this study is that Au solubility is in the range required for liquid petroleum to act as an ore fluid for gold.

KEYWORDS: Hydrocarbons, gold, solubility, experiments

## 1 INTRODUCTION

Accepted models for the formation of Carlin-type gold deposits (second only to the Witwatersrand deposits in gold production) and for the re-mobilization of gold in the Witwatersrand basin attribute transport of the metal to hydrothermal fluids (*e.g.*, Robb and Meyer, 1995; Frimmel *et al,* 1999; Hofstra & Cline, 2000). However, hydrocarbons are commonly seen in close association with gold in both environments.

In the Carlin deposits of Northern Nevada, hydrocarbons and gold frequently occupy the same structures. Typically, the hydrocarbons are in the form of pyrobitumen, and are interpreted to have predated gold mineralization, which has led to the suggestion that the orebodies formed in fossil oil reservoirs. It also led to ideas that the hydrocarbons provided a reducing environment conducive to hydrothermal deposition of gold, or that they facilitated hydrothermal gold transport by converting sulphate to the $H_2S$ needed for its aqueous complexation (Hofstra & Cline, 2000). However, in some cases, *.e.g.*, the Yankee Basin deposits, the hydrocarbons are in the form of liquid petroleum, and appear to have been introduced not only prior to but also contemporaneously with gold mineralization (Hulen & Collister, 1999). It is thus possible that they may have played a role in gold transport, as was recently proposed by Emsbo & Koenig (2005) to explain concentrations of Au of up to 100 ppm in bitumen from the Rodeo deposit of the Northern Carlin Trend, Nevada.

The genesis of the Witwatersrand gold deposits has been a matter of considerable recent debate, with some authors arguing that they are palaeoplacer deposits, which were partly remobilized by hydrothermal processes (modified placer model), *e.g.*, Robb & Meyer (1995), and others arguing that they are entirely hydrothermal *e.g.*, Phillips & Law (1997). However, a feature of the Witwatersrand deposits, which has received much less attention than perhaps it deserves, is the close association of the gold with hydrocarbons. According to Nagy (1993), as much as 40% of Witwatersrand gold production has come from thin carbon seams, which in

the Carbon Leader, Basal Reef and Vaal Reef have been shown to contain in excess of 1,000 ppm Au and in some cases up to 30,000 ppm Au (Halbauer, 1986). During the 1970's and 1980's, these seams were widely interpreted to be Agal mats which trapped and biochemically remobilized detrital gold (Halbauer, 1975). Recently, however, their origin has been reinterpreted on the basis of their organic geochemistry and stable isotopic composition (*e.g.*, Spangenberg & Frimmel, 2001) and on the occurrence of liquid hydrocarbons preserved as fluid inclusions in overgrowths on detrital quartz grains (England *et al.*, 2002). As a result of these studies, the carbon seams are now generally considered to represent residues from the migration of liquid hydrocarbons. In light of this interpretation, proponents of the hydrothermal model for the genesis of the Witwatersrand gold deposits have suggested that the hydrocarbons may have acted as a reducing agent for the destabilization of $Au(HS)_2^-$ and the deposition of the gold (Phillips & Law, 1997). However, the possibility that the hydrocarbons may have been the medium of primary gold transport or gold remobilization (modified placer model) has been virtually ignored.

In order to test the hypothesis that liquid hydrocarbons may play a role in the transport of gold, an essential first step is to demonstrate that they can dissolve ore-forming concentrations of this metal. We report here the results of preliminary experiments designed to evaluate this possibility by investigating the solubility of gold in crude oil at elevated temperature

## 2 METHODOLOGY

Experiments were conducted in titanium autoclaves at temperatures between 100 and 200°C and saturated vapour pressure, and involved measuring the solubility of gold wire in two samples of light crude oil supplied by Shell Canada (Fig. 1). The autoclaves were heated in a Fisher Isotemp forced draft oven modified to reduce thermal gradients to < 1°C by adding an aluminium box with 1.5-cm-thick walls. Each autoclave was pre-conditioned with nitric acid to produce a protective layer of $TiO_2$ on the internal surface. Before an experiment, a current of nitrogen was pumped through the autoclave for 40 minutes to remove atmospheric gases. A known mass of crude oil was placed in the bottom of the autoclave. The autoclave was then loaded with an open silica glass ampoule containing a known mass of gold wire. In order to isolate the gold wire from the oil at the beginning and end of an experiment, the ampoule was inserted in a silica glass holder designed to hold the top of the ampoule above the upper surface of the liquid. At the end of an experiment, the autoclave was quenched to room temperature in cold water and a sample of crude oil was collected for analysis.

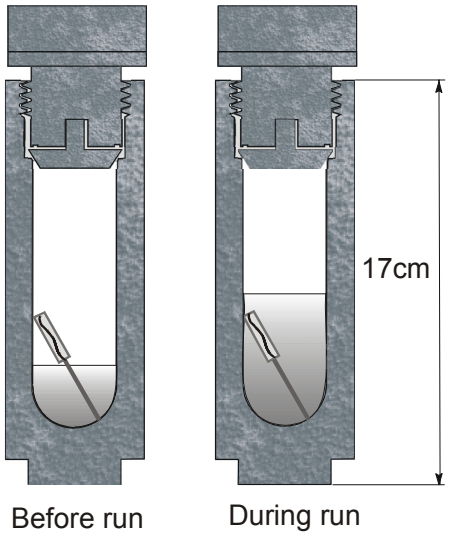


Figure 1. Autoclaves containing crude oil and an ampoule loaded with gold wire in a silica glass holder.

Gold precipitated on the walls of the autoclaves during quenching was dissolved by aqua regia after removal of the crude oil. Concentrations of gold in the oil and the washing solutions were determined using neutron activation analysis. Blank experiments to establish background gold concentrations were conducted in the manner described above, but without the introduction of gold wire. The duration of all experiments was equal to or greater than 7 days.

## 3 RESULTS

A total of 15 solubility experiments were conducted on the two samples of light crude oil, seven on Sample A, which is light-coloured and eight on Sample B, which is darker-coloured. These included one and two repeat experiments with sample A at 100 and 125 °C, respectively, and two repeat experiments at these temperatures with Sample B. In addition, two blank experiments were conducted on each oil sample, one at 100 and one at 125 °C. After the experiments at 150 and 200 °C, both samples were noticeably darker, although the change in Sample B was greater, and after the 200 °C experi-

ments this sample also contained a small amount of dark precipitate. This suggests that there was significant hydrocarbon cracking, particularly in Sample B.

The solubility of gold increased systematically from average concentrations in Sample A and Sample B of 2.4 ppb and 2.5 ppb at 100 °C, respectively, to concentrations in the two samples of 18 ppb and 11 ppb at 200 °C, respectively (Fig. 2). Based on the experiments conducted at 100 and 125 °C, the reproducibility of the solubility determinations, as indicated by the standard deviation, was 0.6 and 0.9 ppb, respectively, for Sample A and 0.5 and 0.7 ppb, respectively, for Sample B. The concentration of gold determined in the blank experiments was below the detection limit of 0.5 ppb.

A significant finding of the experiments, which will be discussed below, was that an appreciable proportion of the gold remained dissolved in both oils after quenching. At 100 and 125 °C, this amount was ~ 1 ppb, *i.e.*, roughly half the total dissolved gold, and reached 6 ppb at the highest temperature investigated (200 °C).

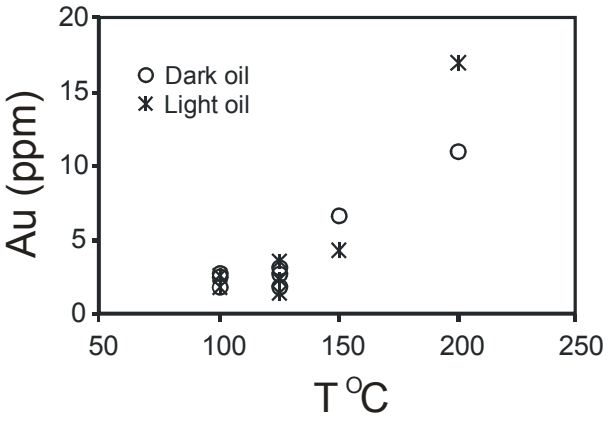


Figure 2. The solubility of gold in Sample A (light oil) and Sample B (dark oil) as a function of temperature.

## 4 DISCUSSION

The results of this study suggest that liquid petroleum dissolves relatively low concentrations of gold at 100 °C but that these concentrations increase significantly with increasing temperature. However, the results are very preliminary and ignore the role of crude oil composition in gold solubility, *e.g.*, the concentration of sulphur, to which gold is known to have a strong affinity. This will be the focus of future experiments.

### *4.1 Gold Speciation*

Unfortunately, our understanding of how metals dissolve in liquid petroleum is relatively poor and most of the information that is available is for Ni and V. These metals have been shown to occur as metal-tetrapyrrole complexes or metalloporphyrins, in which the metal is bonded to four nitrogen atoms (Fig. 3). However, appreciable Ni and V concentrations are also present in non-porphyrin form, particularly

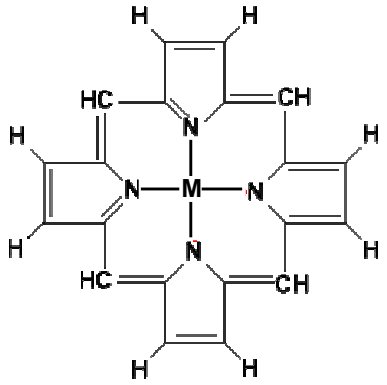


Figure 3. Porphyrin molecule in which the metal (M) is bonded to four nitrogen atoms.

in asphaltene-rich fractions, where they are thought to occur mainly as metalloporphyrin-like species bound by π-π bonds to asphaltene sheets, or to occupy sites in the sheets where they are bonded with N, S or O (Filby, 1994). Based on our current understanding of metal dissolution in liquid petroleum, it is thus reasonable to speculate that the gold in our experiments dissolved as a metalloporphyrin and/or was bonded directly or indirectly to asphaltene molecules. As the latter exist in the oil in colloidal form, this might also help to explain the fact that appreciable gold remained in the crude oil after quenching of the autoclaves.

### 4.2 *Applications to nature*

In order to understand the significance of our results, a first step is to relate them to what is known about the gold content of ore-forming hydrothermal fluids. The most reliable estimates of these concentrations come from analyses of geothermal fluids and these suggest low ppb levels. For example, Brown (1986) showed that the gold concentration of the Broadlands-Ohaaki deep fluid is about 1.5 ppb. At current flux rates these fluids would produce an economic gold deposit containing 1 million oz. Au

in only 4,700 years. Whether the somewhat higher concentrations measured for gold in our study would be sufficient for liquid petroleum to be an ore fluid is less clear as this will depend on the flux of hydrocarbons through appropriate structures and the duration of this flux.

An important issue not considered so far is the temperature of oil migration. Our experiments were designed assuming temperatures of hydrocarbon migration governed by the oil window (85 to 165 °C). However, if the heating were rapid, such as might be the case in the presence of an intrusion and/or hydrothermal system, liquid petroleum migration might be possible at temperatures as high as 350 °C (Price, 1993). At such temperatures, the solubility of gold in liquid petroleum is likely to be much higher than we have measured and hydrocarbon transport of gold correspondingly more feasible.

## 5 CONCLUSIONS

The results of this study show that crude oil can dissolve ppb levels of gold at temperatures between 100 and 200 °C and that Au solubility increases with increasing temperature. These concentrations are in the range that may be required for an ore fluid, and suggest that liquid petroleum could have played a role in metal transport in some Carlin-type deposits and may have been involved in gold remobilization in the Witwatersrand.

## ACKNOWLEDGEMENTS

Shell Canada is thanked for providing the crude oil samples required for this research.

## REFERENCES

Brown KL (1986) Gold deposition from geothermal discharges in New Zealand. *Economic Geology* 81: 979-983.

Emsbo P (2005) Discovery and significance of gold-bearing bitumen in the Rodeo Deposit, northern Carlin Trend, Nevada. *Geochimica et Cosmochimica Acta* 69: A123.

England GL, Rasmussen B, Krapež, Groves DI (2002) Archaen oil migration in the Wiwatersrand Basin of South Africa. *Journal of the Geological Society* 159: 189-201.

Frimmel HE, Halbauer DK Gartz VH (1999) Golod mobilizing fluids in the Witwatersrand Basin; composition and possible sources. *Mineralogy and Petrology* 66: 55-81.

Filby RH (1975) The nature of metals in petroleum. In Yen TF (ed). *Role of trace metals in petroleum* . Ann Arbour Scientific Publications: 31-58.

Hofstra, AH, Cline, JS (2000) Characteristics and models for Carlin-type deposits. *Reviews in Economic Geology* 13: 163-220.

Hulen JB, Collister JW (1999) The oil-bearing, Carlin-type gold deposits of Yankee Basin, Alligator Ridge District, Nevada. *Economic Geology* 94: 1029-1050.

Phillips GN, Law JD (1997) Hydrothermal origin for Witwatersrand gold. *Society of Economic Geologists Newsletter* 31: 26-33.

Price LC (1993) Thermal stability of hydrocarbonbs in nature. *Geochimica et Cosmochimica Acta* 57: 3261-3280.

Robb LJ, Meyer, FM (1995) The Witwatersrand Basin, South Africa: Geological framework and mineralization processes. *Ore Geology Reviews* 10: 67-94.

Spangenberg JE, Frimmel HE (2001) Basin-internal derivation of hydrocarbons in the Witwatersrand Basin, South Africa: evidence from bulk and molecular $\delta^{13}C$ data. *Chemical Geology* 173: 339-355.

# Thermodynamic modeling of Au-Bi-Te melt precipitation from high-temperature hydrothermal fluids: Preliminary results

T. Wagner
*Institut für Geowissenschaften, Universität Tübingen, Germany*

ABSTRACT: Textural observations from several hydrothermal ore deposits indicate that Au-Bi-Te melts could play an important role in the precipitation of gold from high-temperature fluids. This hypothesis has been tested through thermodynamic modeling of complex fluid-melt equilibria. Because the properties of Au-Bi-Te melts show substantial deviation from ideal solution behaviour, a new activity model for such melts was developed. This was combined with appropriate standard state and activity models for hydrothermal fluids at elevated temperatures and pressures. The results of the calculations show that Au-Bi-Te melts will precipitate even from hydrothermal fluids that are moderately undersaturated with the pure solid (Au) and liquid (Bi, Te) metals. Calculated melt compositions tend to be either Bi-Te-rich with about 3-5 percent gold, or Au-Te-rich. Upon cooling, these melts transform to Bi-telluride+gold and Au-telluride+gold assemblages, consistent with mineral associations that are commonly observed in gold ores.

KEYWORDS: fluid-melt equilibria, Au-Bi-Te system, thermodynamic modeling, gold deposits

## 1 INTRODUCTION

Textural observations from a number of hydrothermal ore deposits, combined with implications from experimental phase relationships (Gather & Blachnik, 1974), indicate that metal-rich melts may play a major role in gold deposition and enrichment.

Metal-rich melts containing substantial amounts of metals with low melting points such as bismuth or antimony may be involved (1) via partial melting of sulfide ores during medium- to high-grade metamorphism (Frost *et al.*, 2002; Tomkins & Mavrogenes, 2002), and (2) through direct precipitation from hydrothermal fluids. The abundant textural association of gold with Bi telluride and selenide phases in several orogenic and other hydrothermal gold deposits (*e.g.*, Ciobanu & Cook, 2006) points to the likely formation of Au-Bi-Te-(Se) melts in these hydrothermal systems. In order to test the hypothesis of gold precipitation via scavenging by Au-Bi-Te melts, thermodynamic modeling of non-ideal fluid-solid-melt equilibria has been performed.

## 2 THERMODYNAMIC MODEL

Calculation of fluid-melt equilibria was performed on the system Au-Bi-Te-S-C-Cl-Na-K-Ca-O-H using the GEM-Selektor code (*e.g.*, Karpov *et al.*, 1997; Kulik, 2002). The properties of aqueous species are described by the HKF equation of state and the calculation of activity coefficients applied an extended Debye-Hückel equation (Oelkers & Helgeson, 1990). Most of the thermodynamic data for aqueous species were taken from the updated SUPCRT92 database (*e.g.*, Johnson *et al.*, 1992). Data for aqueous Au species came from the compilation by Akinfiev & Zotov (2001) and those for aqueous Te complexes from McPhail (1995). The SUPCRT92 database contains only data for the $Bi^{3+}$ ion and for aqueous Bi hydroxides, but no data for Bi chloride complexes. Therefore, a set of HKF parameters for those species was derived from the experimental Bi solubility data of Kolonin & Laptev (1982). Thermodynamic data for solid and liquid metals were taken from the SGTE database (Dinsdale *et al.* 1991), which are in close agreement with the data contained in the SUPCRT92 dataset. The properties of melts in

the system Au-Bi-Te are highly non-ideal and required the development of an appropriate activity model that is described below.

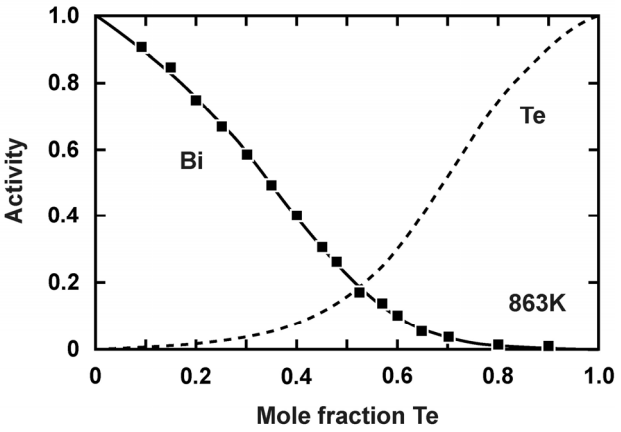


Figure 1. Comparison of calculated (thick line) and experimentally determined (black dots) bismuth activities in Bi-Te melts at 863 K. Experimental activity data are from Feutelais *et al.* (1991).

## 3 PROPERTIES OF AU-BI-TE MELTS

The first step in developing an activity model for Au-Bi-Te melts involved an assessment of the limiting binary subsystems *(i.e.*, Au-Bi, Au-Te and Bi-Te) from data available in the literature. Excellent thermodynamic descriptions of the two binaries Au-Bi and Au-Te were published recently (Servant *et al.*, 2006; Wang *et al*., 2006), and were used in the present study. These thermodynamic descriptions are also based on the SGTE unary data for the elements (Dinsdale, 1991), resulting in excellent data consistency. No complete thermodynamic description of the system Bi-Te has yet been published, which required an assessment of the Bi-Te melt properties from experimental data in the literature. A considerable body of experimental information on Bi-Te liquids is available, including calorimetrically measured excess enthalpies (Blachnik & Enninga, 1974; Morgant *et al.*, 1990) and, most importantly, activity data (Feutelais *et al.*, 1991).

Because direct splitting of the activity data into enthalpy and entropy contributions is associated with a large error, a different approach was chosen. First, an appropriate excess function was fitted to the calorimetric excess enthalpy data, which was assumed to be independent of temperature. Then the experimental activity data were converted into excess Gibbs energies and the excess entropy contribution was calculated by difference. Finally, the resulting excess entropies were described by a third order Redlich-Kister function and the actvities recalculated accordingly. Comparison of calculated and measured activity data shows that the new thermodynamic model essentially duplicates the experimental data (Fig. 1). The assessed thermodynamic data for the three binaries were combined into a ternary model using the Muggianu formalism coupled with a multicomponent extension of the Redlich-Kister function (Hillert, 1998).

It is noted that the liquid phase in all three binary subsystems of the system Au-Bi-Te shows negative deviation from ideality. This effect is most pronounced in the Bi-Te binary and amounts to a maximum excess Gibbs energy of –7.8 kJ/mol at 400 °C. This implies that the melt phase in the Au-Bi-Te system will be considerably more stable (*i.e*., less soluble in fluids) than predicted by an ideal solution model.

## 4 MODELING RESULTS

Because Au-Bi-Te-rich assemblages have been described from orogenic gold-type deposits, among others, bulk fluid characteristics reported for typical greenschist- (300°C, 2.0 kbar) and amphibolite-facies (550°C, 3.5 kbar) fluids (Mikucki & Ridley, 1993; Mikucki, 1998) were used for the modeling. With these starting fluids, two different types of simulations were performed. In the first series, the concentrations of Au, Bi and Te were systematically varied. Because absolute concentrations of these elements in natural fluids are largely unknown, the fluid compositions were expressed relative to saturation with the pure solid (Au) or liquid (Bi, Te) metals. The second series involved several runs where the fluids were increasingly cooled, in order to evaluate the temperature range over which Au-Bi-Te melts most likely precipitate.

The results of the calculations at 550°C and 3.5 kbar show that Au-Bi-Te melts will precipitate even if the hydrothermal fluid is moderately undersaturated with the pure solid (Au) and liquid (Bi, Te) phases (Fig. 2). Calculated melt compositions tend to be either Bi-Te-rich ($Au_{0.04}Bi_{0.41}Te_{0.55}$ to $Au_{0.03}Bi_{0.47}Te_{0.50}$) or Au-Te-rich ($Au_{0.33}Te_{0.67}$ to $Au_{0.50}Te_{0.50}$).

Upon cooling, such melts would transform to Bi-telluride+gold and Au-telluride+gold assemblages, both mineral associations being well known from orogenic gold deposits. The cooling simulations show that the precipitation

sequence strongly depends on the initial composition of the fluid. If the starting fluid precipitates Bi-Te-rich melts, these melts will become increasingly more Te-rich with decreasing temperature. Below approximately 420-470°C, tellurobismuthite+tellurium or tellurobismuthinite+bismuthinite assemblages will be most stable. Only a fluid that is strongly oversaturated with Bi (at least 10-100 times) will continue to precipitate very Bi-rich melts upon cooling.

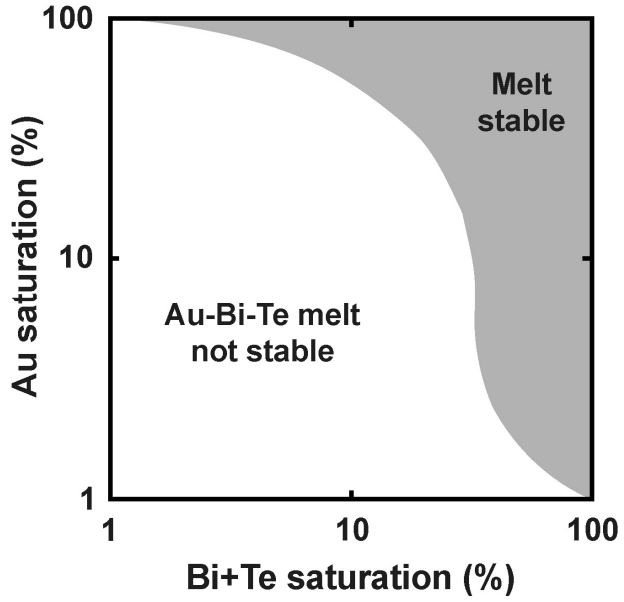


Figure 2. The calculated melt stability field at 550 °C and 3.5 kbar plotted as a function of Au, and (Bi+Te) saturation. The saturation (given in percent) is calculated as the ratio of the element concentrations in the fluid and the concentration where precipitation of pure solid (Au) and liquid (Bi, Te) phases occurs.

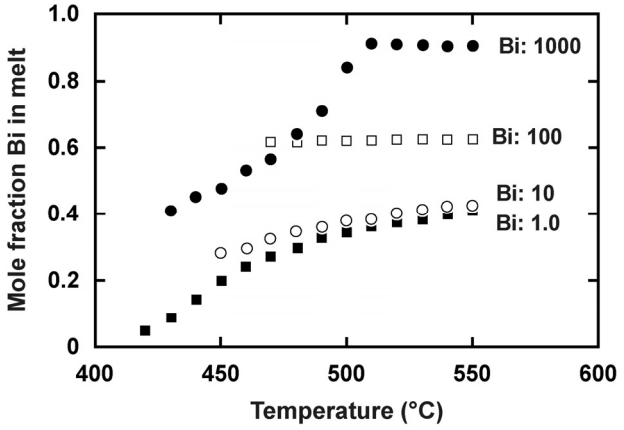


Figure 3. Results of cooling simulations using starting fluids with different degrees of Bi saturation (ranging from 1.0 to 1000).

## 5 DISCUSSION AND PERSPECTIVE

The calculated equilibria shed light on the likely conditions that favor the precipitation of Au-Bi-Te melts from high-temperature hydrothermal fluids. Melts very rich in gold will precipitate if the fluids are relatively close to saturation with metallic gold. By contrast, precipitation of Bi-Te-rich melts with a few weight percent gold requires a lower degree in saturation with metallic gold, but much higher levels of bismuth saturation. Taken together, the thermodynamic model is able to reproduce the essential features of Au-Bi-Te assemblages observed in hydrothermal gold ore deposits.

Unfortunately, the relative importance of additional aqueous complexes of Bi and Te could not be evaluated, due to the lack of sufficient experimental data on their stability. If Bi sulfide complexes such as $Bi_2S_4^{2-}$ and $HBi_2S_4^-$ are important in the transport of bismuth, sulphidation reactions during fluid-rock interaction might destabilize both Au and Bi sulfide complexes and result in precipitation of Au-Bi-Te melts. Similarly, mixed Au-Te complexes, *e.g.* $Au(HTe)^0$ and $Au(HTe)_2^-$, could be important for co-transport of gold and tellurium and would add to the factors that control precipitation of Au-Bi-Te melts from fluids.

From these considerations, it appears that the current thermodynamic model for fluid-melt equilibria involving Au-Bi-Te melts needs further refinement to become fully predictive. In addition to the uncertainties associated with the relative role of additional aqueous Bi and Te complexes, it appears that accurate treatment of the phase relationships in the Bi-Te binary requires some efforts in improving the available thermodynamic datasets. As a first step towards such an improved model, a complete thermodynamic optimization of the Bi-Te phase diagram is currently under way. This optimization will result in refined properties for the most important solid Bi-Te phases, including $Bi_2Te_3$ (tellurobismuthite), BiTe (tsumoite), $Bi_2Te$, and $Bi_{14}Te_6$ (hedleyite). Combined with an improved aqueous speciation scheme, the conditions favorable for the precipitation of Au-Bi-Te melts will be better understood.

## REFERENCES

Akinfiev, N.N., Zotov, A.V. (2001) Thermodynamic description of chloride, hydrosulfide, and hydroxo complexes of Ag(I), Cu(I), and Au(I) at tempera-

tures of 25-500°C and pressures of 1-2000 bar. *Geochem. Intern.* 39: 990-1006.

Blachnik, R., Enninga, E. (1974) Solution enthalpy in the liquid bismuth-tellurium system. *Thermochim. Acta* 9: 83-86.

Ciobanu, C.L., Cook, N.J. (2006) Gold scavenged by bismuth melts: An example from Alpine shear-remobilizates in the Highis Massif, Romania. *Mineral. Petrol*. 87: 351-384.

Dinsdale, A.T. (1991) SGTE data for pure elements. *Calphad* 15: 317-425.

Feutelais, Y., Morgant, G., Legendre, B. (1991) Liquid-state electrochemical study of bismuth-tellurium liquid alloys. *J. Less Comm. Met.* 169: 197-207.

Frost, B.R., Mavrogenes, J.A., Tomkins, A.G. (2002) Partial melting of sulfide ore during medium- and high-grade metamorphism. *Can. Mineral.* 40: 1-18.

Gather, B., Blachnik, R. (1974) The gold-bismuth-tellurium system. *Z. Metallk*. 65: 653-656.

Hillert, M. (1998) *Phase equilibria, phase diagrams and phase transitions. Their thermodynamic basis.* Cambridge University Press, Cambridge, 538 pp.

Johnson, J.W., Oelkers, E.H., Helgeson, H.C. (1992) SUPCRT92: A software package for calculating the standard molal thermodynamic properties of minerals, gases, aqueous species, and reactions from 1 to 5000 bar and 0 to 1000 °C. *Comp. Geosci.* 18: 899-947.

Karpov, I.K., Chudnenko, K.V., Kulik, D.A. (1997) Modeling chemical mass transfer in geochemical processes: Thermodynamic relations, conditions of equilibria, and numerical algorithms. *Amer. J. Sci.* 297: 767-806.

Kolonin, G.R., Laptev, Y.V. (1982) Study of dissolution of α-$Bi_2O_3$ (bismite) in and complex formation in hydrothermal solutions. *Geokhimiya* 1982: 1621-1631.

Kulik, D.A. (2002) Gibbs energy minimization approach to modelling sorption equilibria at the mineral-water interface: thermodynamic relations for multi-site surface complexation. *Amer. J. Sci*. 302: 227-279.

McPhail, D.C. (1995) Thermodynamic properties of aqueous tellurium species between 25 and 350°C. *Geochim. Cosmochim. Acta*: 59, 851-866.

Mikucki, E.J. (1998) Hydrothermal transport and depositional processes in Archean lod-gold systems: A review. *Ore Geol. Rev*., 13, 307-321.

Mikucki, E.J., Ridley, J.R. (1993) The hydrothermal fluid of Archaean lode-gold deposits at different metamorphic grades: compositional constraints from ore and wallrock alteration assemblages. *Mineral. Deposita* 28: 469-481.

Morgant, G., Feutelais, Y., Legendre, B., Castanet, R., Coulet, A. (1990) Thermodynamic behaviour of Bi-Te alloys. *Z. Metallk*. 81: 44-48.

Oelkers, E.H., Helgeson, H.C. (1990) Triple-ion anions and polynuclear compexing in supercritical electrolyte solutions. *Geochim. Cosmochim. Acta* 54: 727-738.

Servant, C., Zoro, E., Legendre, B. (2006) Thermodynamic reassessment of the Au-Bi system. *Calphad* 30: 443-448.

Tomkins, A.G., Mavrogenes, J.A. (2002) Mobilization of gold as a polymetallic melt during pelite anatexis at the Challenger gold deposit, South Australia: A metamorphosed Archean deposit. *Econ. Geol*. 97: 1249-1271.

Wang, J.H., Lu, X.G., Sundman, B., Su, X.P. (2006) Thermodynamic reassessment of the Au-Te system. *J. Alloys Comp.* 407: 106-111.

# Characteristics of Sub-Microscopic Gold and Trace Element Geochemistry of Enargite in the Martabe High-Sulphidation Epithermal Deposits, North Sumatra, Indonesia

Bronto Sutopo & J. Bruce Gemmell
*CODES ARC Centre of Excellence in Ore Deposits University of Tasmania, Private Bag 79, Hobart, Tasmania 7001*

Brian K. Levet
*Newmont Australia Pty Ltd, 10 Richardson Street, West Perth, WA 6005, Australia*

ABSTRACT: The Martabe high-sulphidation epithermal district is located on the NW coast of western Sumatra in the western Sunda-Banda magmatic arc. In this paper we report laser ablation ICP-MS results of trace element concentrations in enargite from the Au-stage of the paragenesis from the Purnama, Baskara and Gerhana deposits. The spatial distribution indicates that Au, Te, Se, Bi and Sn are enriched in enargite from the Purnama deposit, while Bi and Au are depleted in enargite from Baskara deposit. Zn-Pb (± Cd) is enriched in enargite in both Gerhana and Baskara deposits, but these elements are depleted in enargite from the Purnama deposit. These results indicate significant variability in the composition of enargite among the three deposits. In summary, the presence of sub-micron Au and the variable Ag content in the enargite explains why Au and Ag content varies between the various high-sulphidation deposits of Martabe district.

KEYWORDS: Martabe, high-sulphidation, epithermal, enargite

## 1 INTRODUCTION

The Martabe high-sulphidation epithermal district is situated on the north-west coast of North Sumatra, Indonesia (Figure 1). Gold anomalies in Martabe were first identified by stream BLEG during a regional reconnaissance program in late 1996.

Follow-up of a 14 ppb gold BLEG anomaly identified mineralized silica float assaying up to 20 g/t Au and 76 g/t Ag, which was traced to a series of prominent silica cliffs and ledges. Subsequent geological mapping, soil sampling, geophysical methods and drilling identified numerous prospects over a seven-kilometer strike length, including Purnama, Baskara, Pelangi, Kejora and Gerhana. This mineralization is directly associated with silica alteration forming a distinctive steep topography (Sutopo *et al*., 2003). In 2006 the Martabe mineral resources estimate was 91.28 million tonnes @1.5 g/t Au and 18.7 g/t Ag for Purnama and 27.50 million tonnes @1.1 g/t Au for Baskara (www.agincourtresources.com).

Previous studies have documented the district discovery (Levet *et al*., 2003; Sutopo *et al*., 2003) and the regional geology of the area (Harlan *et al*., 2005). No detailed geochemical trace element studies have been published on Martabe.

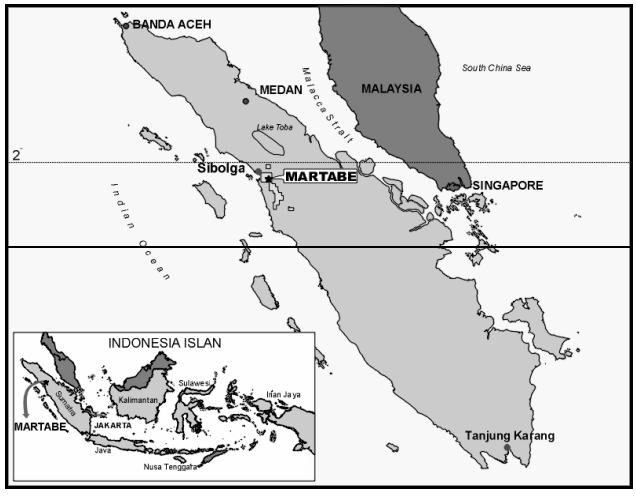


Figure 1. Map showing the location of the Martabe district, North Sumatra Province, Indonesia

.

The development of laser ablation (LA)-ICP-MS offers an inexpensive and reliable method for in-situ microanalysis of a diverse suite of elements at low detection limits. Several studies (*e.g.* Baker *et al.*, 2006) have applied this technology to the examination of trace elements in sulphides, but the trace element chemistry of enargite has been rarely investigated.

At Martabe, gold is rarely observed in hand samples but is identified by optical microscopy to be associated with the sulphide and sulphosalt minerals, leading to the hypothesis that the sulphide and sulphosalt minerals may contain significant sub-microscopic gold. In general, enargite occurs as the primary sulphide with lesser amounts of tetrahedrite-tennantite, galena and tellurides. In many similar high-sulphidation deposits, enargite is intimately involved with Au-stage mineralization in the systems (*e.g.* Arribas *et al*., 1995; Hedenquist *et al.*, 1998). Therefore, Martabe provides a good test case for examining the trace element composition using LA-ICP-MS of enargite from the Au-stage from the Martabe gold district, including the Purnama, Gerhana and Baskara deposits.

## 2 GEOLOGY AND ORE DEPOSITS IN THE MARTABE DISTRICT

The Martabe district is located in the western Sunda-Banda magmatic arc, within and adjacent to a Late Tertiary porphyritic dacite-andesite dome and diatreme complex that was emplaced into a volcano-sedimentary sequence comprising interlayered sandstone, siltstone, carbonaceous mudstone and andesite lava flows. The Martabe district is located near a series of fault splays that form part of the Sumatra Fault System (Levet *et al.*, 2003; Sutopo *et al.*, 2003). This structural framework has played an important role for the multi-phase magmatic, phreatomagmatic-phreatic and hydrothermal events at Martabe (Figure 2).

Economic gold mineralization is hosted within the vuggy quartz and advanced argillic alteration zones. Gold is only present as submicron-sized native gold grains associated with quartz, Fe-oxides, enargite, tetrahedrite-tennantite and covellite-digenite. Alteration and mineralization occurred at 2.0 to 3.3 Ma based on Ar-Ar dating of hypogene vein alunite.

Petrographic studies on polished sections and core samples suggests the following sequence of mineralization events: (1) hydrothermal alteration, (2) pre-Au-stage sulphide, (3) Au-stage mineralization (mainly late pyrite and Cu-sulphides,) (4) post-Au-stage minerals (*i.e*. barite), (5) supergene Cu-sulphides, and (6) native sulphur deposition.

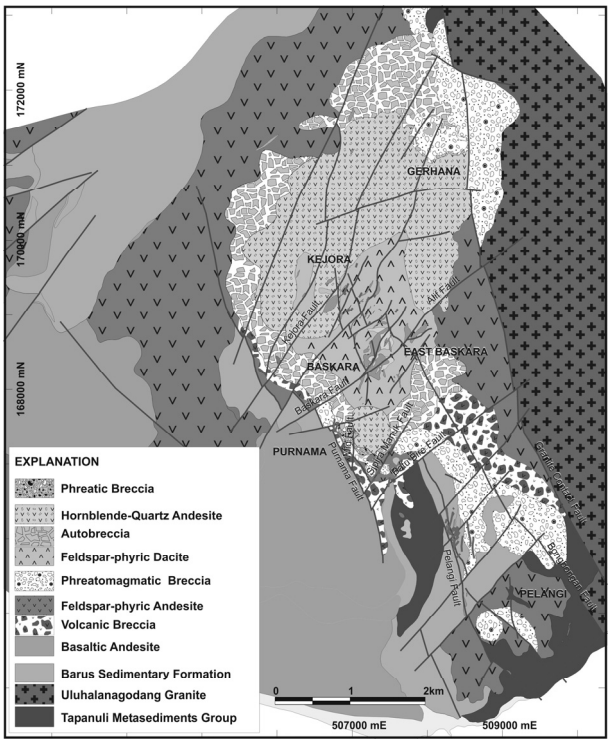


Figure 2. Regional geology map of the Martabe district and the location of epithermal deposits within the district.

Enargite samples were collected from drill core samples collected from deposits throughout the Martabe epithermal district, including the Purnama, Baskara and Gerhana deposits. The main criterion used for sample selection was to obtain samples from ore zones associated with massive sulphide or vuggy quartz alteration

## 3 METHODS OF ANALYSIS

Enargite samples (n = 10) were initially analyzed by electron probe microanalysis (EPMA) at University of Tasmania to determine their major and selected trace elements compositions (Fe, As, S Au, Cu, Zn, P, Bi, Ag, Sb, Te, Se) and for internal standardization. These enargite samples were then analyzed by LA-ICPMS also at the University of Tasmania to determine their trace element compositions. Details of the LA-ICP-MS methodology, including descriptions of instrumentation, sample preparation, laser analysis, data reduction and interpretation are given by Danushevsky (2005).

We report the analyses of 98 enargite grains. These samples were analyzed for 26 elements: Ti, Cr, Mn, Fe, Cu, Co, Ni, Zn, As, Se, Zr, Mo, Ag, Cd, Sn, Sb, Te, Ba, La, W, Au, Tl, Pb, Bi, Th and U. Beam size varied between 30 and 40 µm with mostly 40 µm, depending on enargite grain size. Multiple grains were analyzed from each sample, and the number of analysis spots per grain was dependent on the crystal size. Results are illustrated in Figure 3.

Data reduction and quantification used stoichiometric Cu as the internal standard, based on the near-stoichiometric Cu/S ratios returned by EPMA analyses. The analyses indicate near-stoichiometric enargite compositions for the majority of sample analyzed.

## 4 ANALYTICAL RESULTS

LA-ICP-MS analyses indicate substantial incorporation of Fe and Sb in enargite. Other elements such as Bi, Se, Te, Ag and Sn occur at values exceeding 1 wt%. The spatial distribution of enargite between the various deposits indicates that high concentrations of Au, Te, Se, Bi and Sn are in enargite from Purnama, while there are low concentrations of Au, Bi, Se and Te in enargite from Baskara. Enargite from Gerhana and Baskara has high concentrations in Zn+Pb (± Cd), but these elements are lower in concentration in enargite from the Purnama deposit (Figure 3).

The micro-scale compositional variability observed in enargite is commonly the result of either inclusions and/or growth zoning (Figure 4). However, most samples show relatively simple compositional patterns. The most common inclusion types are minor Au (± Bi-Sn-Ag-Te-Se) bearing phases, as well as inclusions containing variable combinations of Bi-Te-Pb-Sn-Fe. There are only a few samples with Zr-Ti-bearing inclusions in enargite.

Complex growth zoning was also observed locally in enargite. This compositional zoning is primarily due to different combinations of Sb-Bi-Te-Se-Pb-Sn-Fe that do not appear to be in inclusions, but overall there are very few consistent elemental correlations in the enargite. Rare Bi-selenides and Sn-bearing phases are also present.

## 5 CONCLUSIONS

In general, three distinct patterns of gold distribution are revealed by LA-ICP-MS analytical traverses across enargite. In most cases, the Au exhibits smooth time-resolved LA-ICP-MS patterns (Figure 4a) and therefore it is thought to be structurally bound within the crystal lattice.

A different LA-ICP-MS Au pattern is found in samples with complicated growth zoning and/or multi-element inclusions within the crystal (Figure 4b). In these cases, it is suggested that Au is associated with zones containing higher concentrations of Bi-Ag-Pb-Te-Se-Sn±Fe. In rare cases, Au occurs as distinct inclusions associated with Bi, Ag, Te, Sn, and Pb. Overall there are moderate correlations between Ag-Sb, Pb-Te, Ag-Bi, Ag-Te, Te-Se, and Te-Sb. In addition, Bi is strongly correlated with Pb and Se, and moderately with Te.

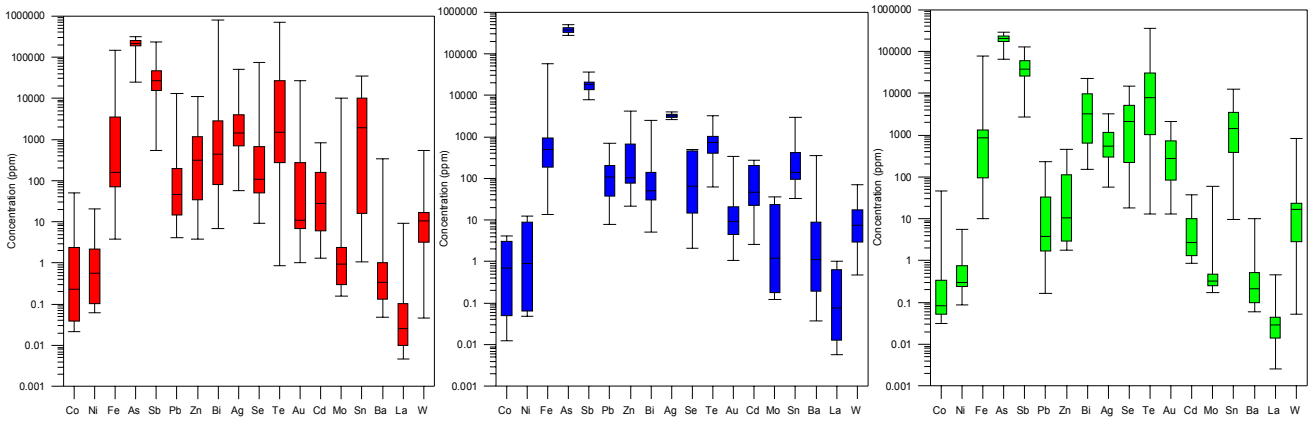


a. Gerhana prospect b. Baskara prospect c. Purnama prospect

Figure 3. Box and whisker plots of range of enargite LA-ICPMS trace element data (ppm) for selected analyses in this study include a. Gerhana prospect (4 samples, 44 analyses); b. Baskara prospect (2 samples, 26 analyses); c. Purnama prospect (4 samples, 42 analyses).

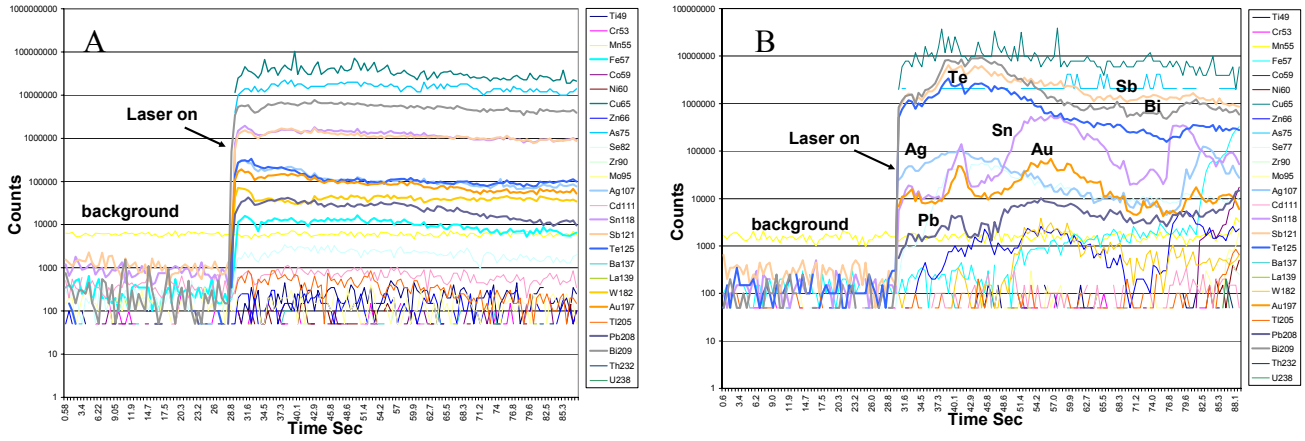


Figure 4. Time-resolved laser ablation ICP-MS analysis for selected trace elements in enargite from the Martabe district, a) flat to smooth varying trace elements indicated the elements are occurred within enargite bound structure, and b) complex variation of Au-Sn-Pb+Ag, and Sb-Bi-Te within the grain.

In summary, the presence of sub-micron Au and the variable Ag content in the enargite explains why Au and Ag varies between the various high sulphidation epithermal deposits in the Martabe district. These results also indicate significant variability in the composition of enargite samples from one high sulphidation deposit to another.

## ACKNOWLEDGEMENTS

We thank to L. Danyushevsky and S. Gilbert for assistance with LA-ICP-MS analyses and interpretation. Reviews of this abstract by the SGA committee were appreciated. We also thank Newmont Mining Corporation for support and permission to publish this paper.

## REFERENCES

Arribas AJr (1995) Characteristic of high-sulphidation epithermal deposits, and their relation to magmatic fluid: *Mineralogical Association of Canada Short Course Series,* v.23 pp 419-454.

Baker T, Mustard R, Brown V, Pearson N, Stanley CR, Radford NW, Butler I (2006) Textural and chemical zonation of pyrite at Pajingo: a potential vector to epithermal gold veins, *Geochemistry: Exploration, Environment, Analysis*, v.6 pp 283-293.

Danyushevsky L, Gilbert S (2005) Laser Ablation ICPMS methodology, *CODES University of Tasmania, unpublished report,* 9 p.

Harlan JB, Jones MJ, Sutopo B, Hoschke T (2005) Discovery and characterization of the Martabe epithermal gold deposits, North Sumatra, Indonesia, *Geological Society of Nevada Symposium* 2005.

Hedenquist JW, Arribas AJr, Reynolds TJ (1998) Evolution of an intrusion-centered hydrothermal system: Far Southeast-Lepanto porphyry and epithermal Cu-Au deposits, Philippines. *Economic Geology*, 93 (4) pp 373-404.

Levet BK, Jones ML, Sutopo B (2003) The Purnama gold deposit in the Martabe district of North Sumatra, Indonesia; *SMEDG – AIG Symposium 2003, Sydney,* 8 p.

Sutopo B, Jones ML, Levet BK (2003) The Martabe gold discovery: A high sulphidation epithermal gold-silver deposit, North Sumatra, Indonesia in NewGen Gold 2003 *Conference Proceedings, Perth WA*, pp 147-158.

# Application of the "ppm – mineralogy" technique for isotope dating and mineralogical study of ore deposits in mafic-ultramafic complexes based on minute accessory minerals

V.V. Knauf, N.S. Guseva, O.V. Knauf
*NATI Research jsc, Saint-Petersburg, Russia*

ABSTRACT: Dating of geological processes and stages of ore formation based on individual grains of accessory minerals by isotope geochemistry methods yields more detailed information which can not be obtained by bulk rock or ore sample analysis. Extraction of minute accessory minerals-carriers of chemical elements suitable for isotope analysis, at their concentration in rocks less than ~0.01 - ~0.1 ppm represents a special problem, that predetermines the success of subsequent isotope analysis

KEYWORDS: Accessory minerals, ultramafic rocks, isotopic research, ppm-mineralogy technique

## 1 INTRODUCTION

The contents of chemical elements used for studies based on U-Pb and Re-Os isotope systems, in rocks of various mafic-ultramafic complexes are usually quite low: less then ~0.01ppm in barren ultramafic rocks and less than ~0.1ppm in pyroxenites, norites and gabbros. This note relates to the low contents of minerals-carriers of these elements (*e.g.* zircon, baddeleyite, uraninite, minerals of Os, U, Th-monazite and apatite (REE)). Usually these minerals are rare accessories whose grain size does not exceed 70-80μm. Meanwhile, extraction of these minerals from mafic and ultramafic rocks allows isotope measurement in individual grains *in situ* (SIMS, SHRIMP) or high-sensitivity measurements of isotope ratios and element contents (REE, for example) in the solutions obtained by chemical decomposition of single grains.

## 2 SAMPLE PROCESSING

The "ppm-mineralogy" technique is an approach to high sensitive mineralogical works, based on appropriate metrological maintenance (V. Knauf, 1996) allowing to extract and study the heavy minerals and especially the minerals-carriers of gold and platinum group elements (PGE) at theirs content in rock less than 1 ppm (*see* details in www.natires.com).

This technique was applied to gold grains extraction during the study of till samples (<50μm) from Finland (V. Knauf *et al*., 2000) and Kola region of Russia with mineralogical sensitivity less than 0.2 ppb of Au. Detection of the complete mineral associations for all six PGE in Kraubath ultramafic massif is an another application of the "ppm-mineralogy" technique (K. Malitch *et al*., 2003). Mineralogical research of the PGE mineralization in various dunite-clinopyroxenite zonal complexes revealed the primary and secondary PGM associations (O. Knauf, 2005). Investigation of the sulphide concentrates obtained by "ppm-mineralogy" technique led to discovery of the new rhenium mineral - tarkianite (K. Kojonen *et al*., 2004).

The "ppm-mineralogy" technique has been adapted to extraction of fine grains of rare accessory minerals for subsequent isotope analysis. As an example of one sample processing there are from 30 to 50 units of intermediate products, including mineral concentrates of various granulometric fractions (Fig. 1a). For coarse fractions of concentrates (>50μm) it is possible to apply optical diagnostics of minerals, manual extraction of grains (Fig. 1b) and mounting of grains on a carbon stage (Fig. 1c) for subsequent checking under scanning electron microscope with ED spectrometer (SEM+EDS).

For grains less than 50μm and for larger

Fig. 1. Single grains and mineral concentrates

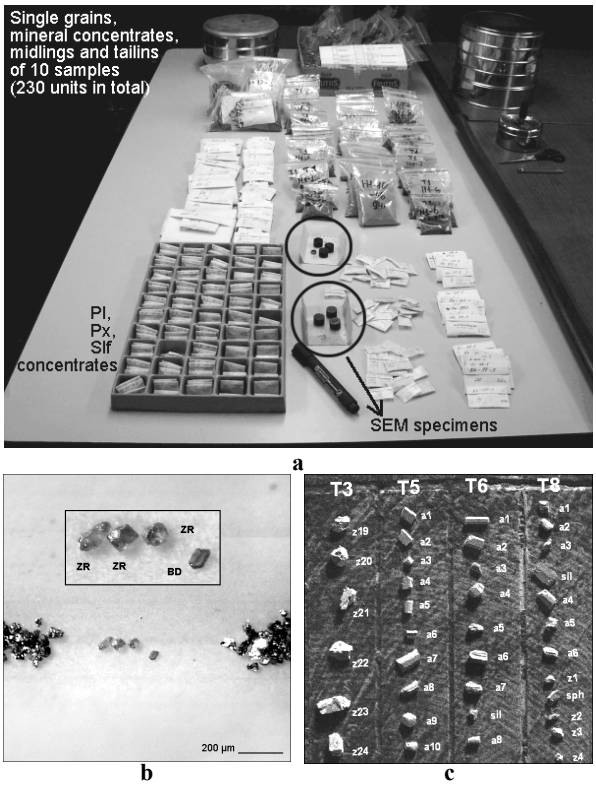


Pl – plagioclase, Px-pyroxene, Slf-sulphides, ZR-zircon, BD-baddeleyite.

Fig. 2. An example of mineral localization

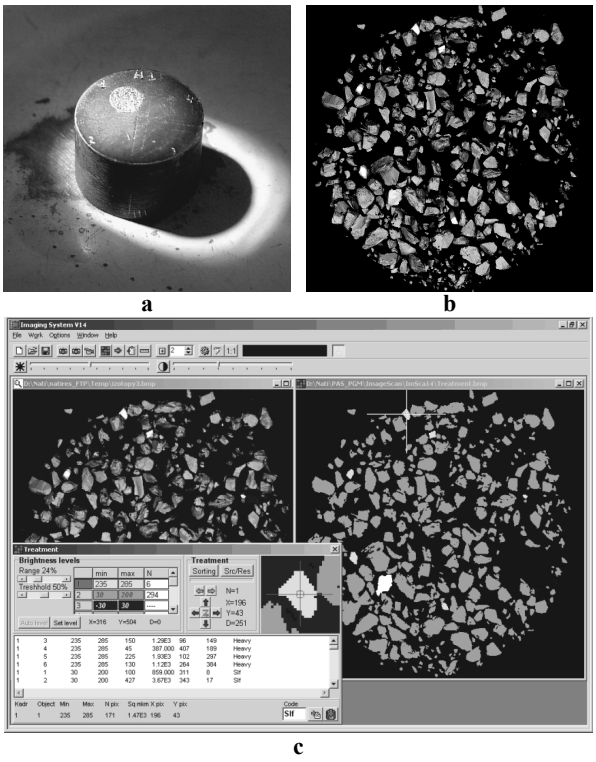


mineral grains whose optical diagnostics are not reliable all the material of the concentrate (1-20mg) is mounted on a carbon stage for SEM+EDS examination (Fig. 2a, b).

In this case, the diagnostics of minerals runs under the control of a specially developed electronic device connected to an SEM and computer program for image processing (Fig. 2c).

All the mineral grains mapped on a BSE-image of the scanned area are grouped according to brightness, which is proportional to average atomic number of minerals, and each group is given a certain brightness range. The program operates the electron beam and positions it on grains of each brightness range, carries out diagnostics of the mineral by chemical composition (by X-ray spectrum), codes the mineral and adds its coordinates to the table (Fig. 2c).

The BSE images and coordinates of grains allow identification of grains on the SEM specimen, facilitating isotope analysis (Fig. 3a-g).

In addition to extraction of single grains of accessory minerals it is possible to separate rock-forming minerals from intermediate products for Sm-Nd, Rb-Sr isotopic studies, sulphide concentrates (isotopy of S), Cr-spinel concentrates (isotopy of noble gases) and heavy concentrates for study of platinum group minerals (Fig. 3h).

For single grains of zircon, - there are many reasons to provide more detailed optical and cathodoluminescence study before isotope research starts (Fig. 3i, j, transmitted light).

Many zircon grains are not homogenous and consist of an inner core and one or more zonal rims.

Dating of core and rims separately inside one zircon grain may provide very different ages.

## 3 CONCLUDING REMARKS

The main advantage of the approach described above is the possibility of obtaining complete isotope data for mafic-ultramafic rocks and connected ore deposits.

High sensitivity of the mineral processing technique allows the use of relatively small volumes of initial samples (parts of drill core, for example) to get geochemical, isotopic and mineralogical data.

Fig. 3. Minerals for isotopic study

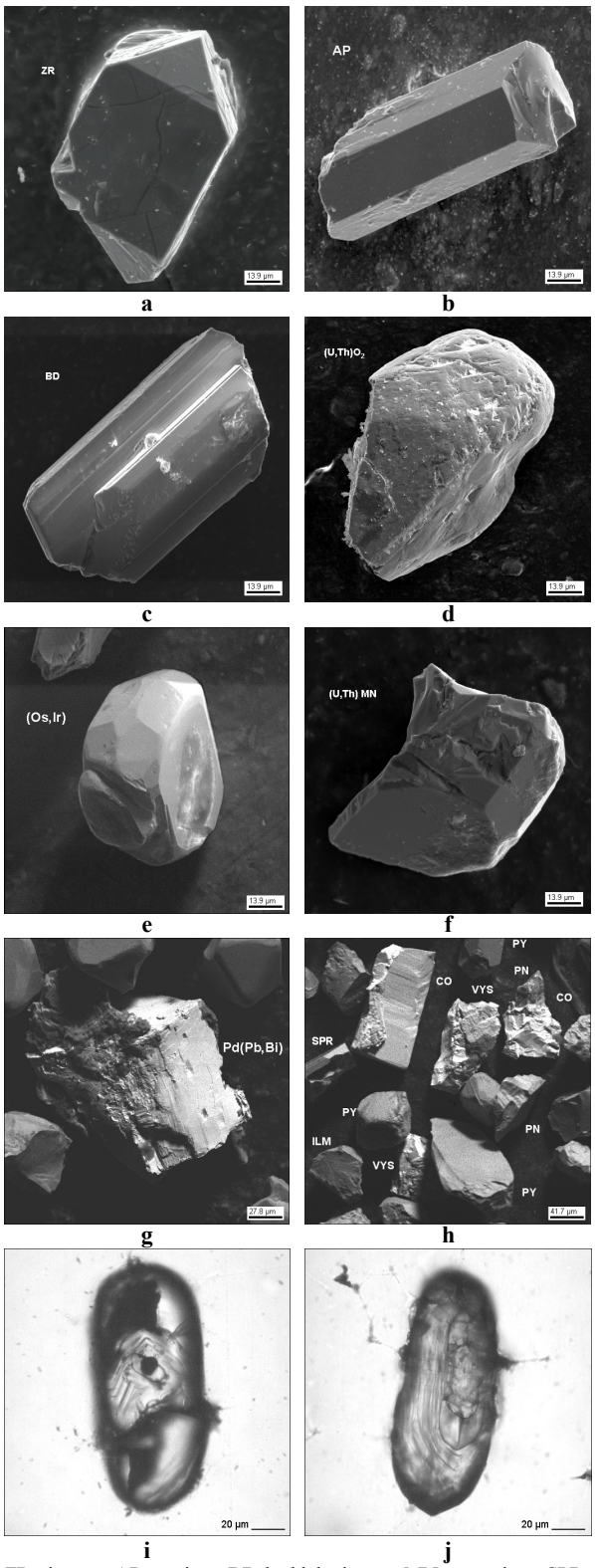


ZR-zircon, AP-apatite, BD-baddeleyite, MN-monazite, SPR-sperrylite, CO-cooperite, VYS-vysotskite, PN-pentlandite, PY-pyrite.

## ACKNOWLEDGEMENTS

The authors gratefully appreciated to our reviewer Dr. Julian F. Menuge for significant efforts to correction of our English.

## REFERENCES

Knauf O.V. (2005) The sparse platinum group minerals (PGM) in dunite and clinopyroxenite rocks of zonal complexes Ural type (Kytlym and Galmoenan massifs, Russia). Platinum-Group Elements – from Genesis to Beneficiation and Environmental Impact. *Extended abstracts of 10th international platinum symposium. Oulu, Finland,* pp 400-403.

Knauf V.V. (1996) The metrological maintenance of mineralogical investigations. *Proceedings of the Russian Mineralogical Society* Pt CXXV, N6, pp109-113 (in Russian).

Knauf V., Sandberg E., Sokolov P., Tabuns E. (2000) Gold geochemistry and mineralogy of till fines: a new approach for data integration. *Bulletin of the Geological Society of Finland,* 72, Parts 1-2, pp57-69.

Kojonen K.K., Roberts A.C., Isomäki O.P., Knauf V.V., Johanson B., Pakkanen L. (2004) Tarkianite, $(Cu,Fe)(Re,Mo)_4S_8$, a new mineral species from the Hitura mine, Nivala, Finland. *The Canadian Mineralogist,* V42, N2, pp539-544.

Malitch K.N., Thalhammer O.A., Knauf V.V., Melcher F. (2003) Diversity of platinum-group mineral assemblages in banded and podiform chromitite from the Kraubath ultramafic massif, Austria: evidence for an ophiolitic transition zone? *Mineralium Deposita*, V38, N3, pp282-297.

# Hydrothermal insights into the deposition of invisible and visible gold within arsenopyrite

A.A. Morey*, A.G. Tomkins & R.F. Weinberg
*School of Geosciences, Monash University, Australia. *predictive mineral discovery CRC*

F.P. Bierlein
*Centre for Exploration Targeting, School of Earth and Geographical Sciences, University of Western Australia*

S. McKnight
*School for Science and Engineering, University of Ballarat, Australia*

G.J. Davidson
*ARC Centre of Excellence in Ore Deposits, Department of Earth Sciences, University of Tasmania, Australia*

ABSTRACT: By studying backscatter electron (BSE) micrographs, and the major- and trace-element geochemistry of gold bearing arsenopyrite from the late-Archaean Bardoc Tectonic Zone, Western Australia, this study helps constrain the hydrothermal conditions of gold deposition associated with this common ore mineral. Invisible gold is located within initial growth stages of arsenopyrite, and visible gold is associated with later-stage alteration rims. Ore textures, BSE and electron microprobe analyses indicate that alteration rims dominantly form at grain boundaries and fracture margins, and are the result of arsenic enrichment (~1.5 atomic percent) of initial arsenopyrite. With the use of phase stability diagrams, these results imply the alteration of arsenopyrite and associated visible gold deposition was driven by an increase in both temperature (broadly between 310 and 415$^{o}$C) and sulphur fugacity (up to 6 orders of magnitude) of the hydrothermal fluid.

KEYWORDS: Gold, arsenopyrite, hydrothermal evolution

## 1 INTRODUCTION

Both visible and invisible gold is found within sulphide-bearing orogenic deposits. Invisible gold refers to gold in solid solution within the host sulphide lattice, or as <1 μm, sub-microscopic particles. Visible gold refers to gold inclusions within sulphides, or as isolated grains within microfractures and along grain boundaries (*e.g*. Boyle 1979; Mumin *et al.* 1994; Genkin *et al*. 1998).

For orogenic systems, both forms of gold are present, where invisible gold within arsenopyrite is overprinted by later-stage visible gold (Mumin *et al.* 1994; Oberthür *et al.* 1997; Genkin *et al*. 1998).

This study expands on this observation, and assesses the textures, overprinting relationships and major- and trace-element geochemistry of composite gold-bearing arsenopyrite grains from the Bardoc Tectonic Zone (BTZ), Eastern Goldfields Province (EGP), Western Australia, to further constrain hydrothermal processes associated with this style of mineralization.

## 2 ANALYTICAL METHODS

Backscattered electron (BSE) images were acquired using an Oxford Instruments four element quadrant detector linked with a Jeol™ JSM 6300 SEM at the University of Ballarat. Electron microprobe (EMP) data were acquired using a Cameca SX50 electron microprobe with four vertical wavelength dispersive spectrometers at the School of Earth Sciences, University of Melbourne. A New Wave OP213 laser probe and HP4500 quadrupole inductively coupled plasma mass spectrometer (ICP-MS) located at the ARC Centre of Excellence in Ore Deposits, University of Tasmania, Hobart was utilised for major and trace element analysis. Calibration techniques for the LA-ICP-MS follow Norman . (2003).

## 3 RESULTS

Mineralized samples from five localities within the BTZ (Paddington, Talbot South, Nerring Nerrin, New Boddington and Yunndaga; Fig. 1) were used in this study to understand gold distribution and the geochemistry of

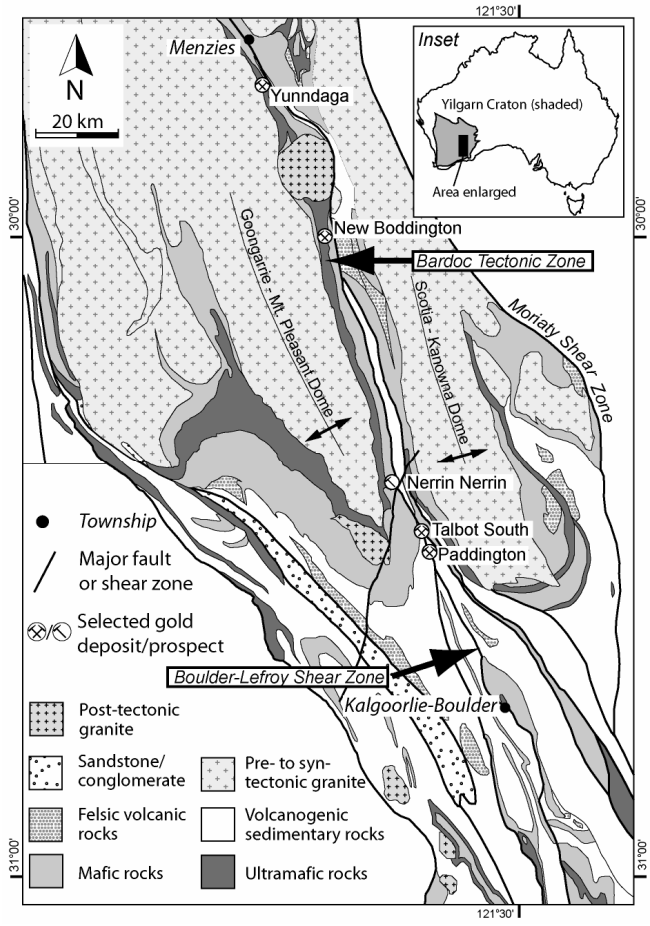


Figure 1. Map of the southern Eastern Goldfields Province showing the gold deposist referred to in this study (modified after Swager & Griffin 1990).

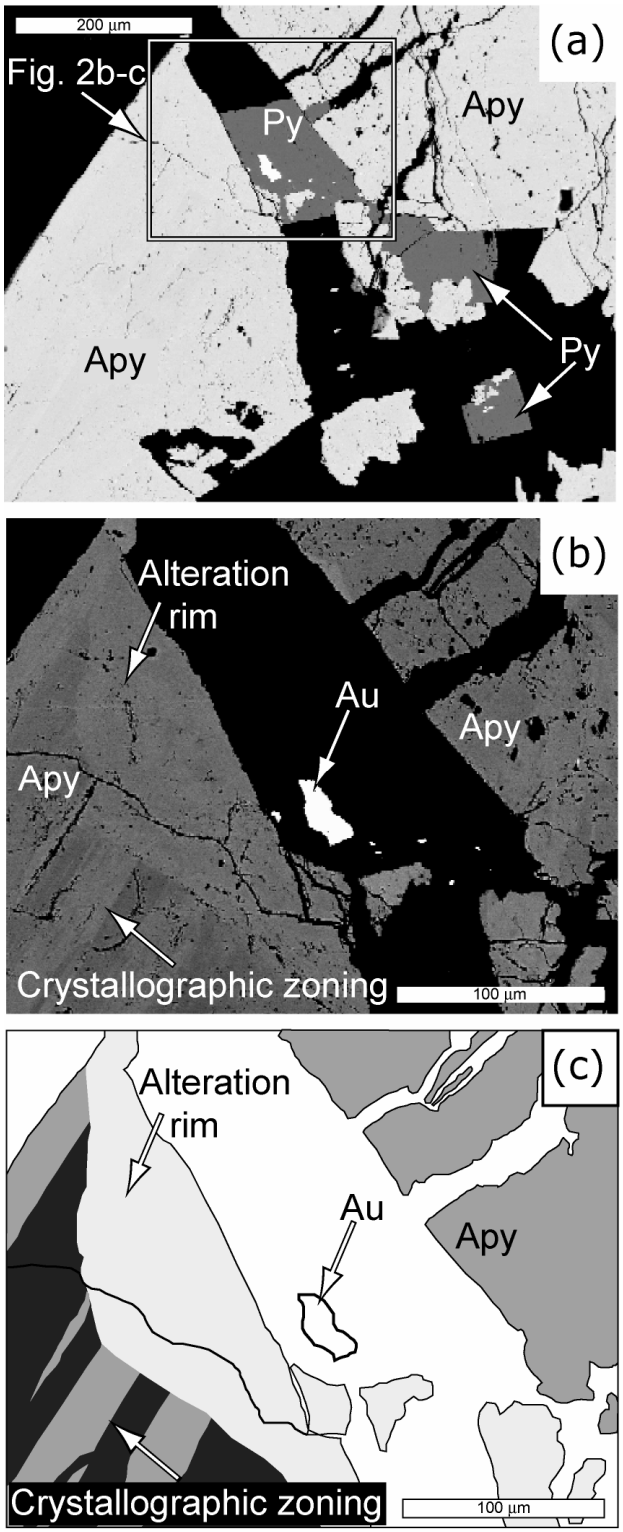


Figure 2. a – b. Representative BSE micrographs of a fractured arsenopyrite (Apy) grain from gthe Paddington deposits showing pyrite (py) + invisible gold filling a fracture within arsenopyrite. C. A trace of the micrograph shown in b. defining the alteration rim.

arsenopyrite. All mineralized rocks are hosted within mafic extrusive or intrusive units and were collected from arsenopyrite-rich wallrock alteration halos directly adjacent to quartz-carbonate veins.

In decreasing order of abundance, the alteration assemblages at leach location consist of calcite ± ankerite, silica, sericite, chlorite, arsenopyrite, sulphides, ± biotite ± epidote ± rutile and gold. The sulphides comprise pyrite, pyrrhotite, chalcopyrite and sphalerite ± galena (Fig. 2).

Even though the quartz-carbonate vein structures vary from brittle to ductile styles, the overprinting relationships between the sulphide, sulpharsenide and oxide phases define a uniform 3-stage alteration paragenesis; Stage 1 pyrrhotite, followed by Stage 2 arsenopyrite + invisible gold, and Stage 3 pyrite + visible gold + base metal sulphides ± rutile ± ilmenite.

Evidence for invisible gold associated with Stage 2 arsenopyrite is supported by LA-ICP-MS analyses, where ablation spots away from visible gold particles within Stage 2 arsenopyrite have above detection limit Au concentrations, varying between 1 and 28 ppm (Table 1). Common to all deposits investigated, BSE images reveal that the Stage 2 arsenopyrite grains are fractured, and grain boundaries and fracture margins define <250 µm-wide, secondary al-

teration rims that are characterised by a higher than average atomic mass. Representative images of alteration rims within arsenopyrite are shown in Figure 2. Textural evidence suggests that the alteration rims formed by post-crystallisation alteration of pre-existing arsenopyrite grains. Alteration was most likely synchronous with the formation of Stage 3 pyrite and visible gold (Fig. 2).

Electron microprobe analyses suggest the higher than average atomic mass of the alteration rims is likely due to As enrichment. The major element concentrations of Stage 2 (unaltered) and Stage 3 (altered) arsenopyrite indicate that alteration rims are enriched in As on average by 1.5At% (Tables 2 and 3).

## 4 DISCUSSION AND INTERPRETATION

This study indicates that invisible gold within arsenopyrite from the BTZ (Fig. 1) is only detectible within unaltered Stage 2 arsenopyrite. On the other hand, later-stage arsenopyrite and associated fractures and alteration rims control the distribution of visible gold. This is in agreement with many other studies on orogenic systems, where visible gold is found in fractures within arsenopyrite (*e.g.* Mumin *et al*. 1994; Oberthür *et al.* 1997; Genkin *et al*. 1998). As there is no detectible invisible gold associated with Stage 3 arsenopyrite or pyrite, it is possible that the invisible gold was remobilised to form at least part of the visible gold (*cf.* Mumin *et al*. 1994). The observed widespread occurrence of invisible gold within arsenopyrite (Cabri *et al*. 1989; Cathelineau *et al*. 1989), suggests that the hydrothermal alteration of arsenopyrite to produce visible gold may be a potentially important factor for understanding the formation of orogenic deposits.

With the use of the averaged arsenopyrite compositions in Tables 2 and 3, and the arsenopyrite phase stability diagram in Figure 3, the transition from Stage 2 arsenopyrite to Stage 3 arsenopyrite + pyrrhotite ± pyrrhotite + visible Au likely involves an increase in temperature (310 to 415$^{o}$C) and sulphur fugacity (up to 6 orders of magnitude) of the evolving hydrothermal fluid. The textural similarities between Au-bearing arsenopyrite from the BTZ and other orogenic Au systems (*e.g*. Mumin *et al*. 1994; Oberthür *et al*. 1997) suggest that the hydrothermal constraints indicated by this study may be applicable to orogenic gold deposits elsewhere.

Table 1. Invisible Au and Ag concentrations within Stage 2 arsenopyrite from LA-ICP-MS analyses

| Location | Au (ppm) | Ag (ppm) | Det. limit (ppm) | Precision |
|---|---|---|---|---|
| Paddington | 23 | 1.42 | 1 | ± 8% |
| Paddington | 11 | < 1 | 1 | ± 6% |
| Talbot South | 9.8 | < 1 | 1 | ± 9% |
| Nerrin Nerrin | 8.2 | < 1 | 1 | ± 5% |
| New Boddington | 28 | < 1 | 1 | ± 5% |
| Yunndaga | 1.6 | < 1 | 1 | ± 14% |

Table 2. Electron microprobe data (At%) of Stage 2 unaltered arsenopyrite

| Location | Fe | S | As |
|---|---|---|---|
| Talbot South | 33.8 | 35.9 | 30.3 |
| Talbot South | 33.8 | 36.5 | 29.7 |
| Paddington | 34.0 | 35.2 | 30.8 |
| Paddington | 33.9 | 34.6 | 31.4 |
| Paddington | 33.8 | 35.8 | 30.4 |
| Paddington | 33.7 | 36.3 | 30.0 |
| Paddington | 33.8 | 36.5 | 29.7 |
| Paddington | 33.9 | 36.8 | 29.2 |
| Paddington | 33.6 | 34.8 | 31.6 |
| Paddington | 33.7 | 35.4 | 30.9 |
| Paddington | 33.7 | 35.1 | 31.2 |
| Nerrin Nerrin | 33.5 | 36.2 | 30.2 |
| New Boddington | 33.7 | 37.4 | 28.9 |
| New Boddington | 33.9 | 35.8 | 30.3 |
| Yunndaga | 33.7 | 35.6 | 30.7 |
| **Average** | **35.9** | **33.7** | **30.4** |
| **±2σ** | **0.232** | **1.55** | **1.55** |

Table 3. Electron microprobe data (At%) of alteration rims within Stage 3 altered arsenopyrite

| Location | Fe | S | As |
|---|---|---|---|
| Talbot South | 33.7 | 35.3 | 30.9 |
| Talbot South | 33.6 | 35.2 | 31.2 |
| Talbot South | 33.9 | 35.2 | 30.8 |
| Talbot South | 33.9 | 34.9 | 31.2 |
| Paddington | 33.8 | 34.9 | 31.2 |
| Paddington | 33.6 | 33.6 | 32.8 |
| Paddington | 33.9 | 33.6 | 32.4 |
| Paddington | 33.8 | 34.4 | 31.8 |
| Paddington | 33.7 | 34.5 | 31.8 |
| Paddington | 33.6 | 34.7 | 31.7 |
| Nerrin Nerrin | 33.5 | 33.5 | 33.0 |
| Nerrin Nerrin | 33.7 | 33.8 | 32.4 |
| New Boddington | 33.8 | 34.2 | 31.9 |
| New Boddington | 33.8 | 34.2 | 32.0 |
| Yunndaga | 33.6 | 33.6 | 32.7 |
| Yunndaga | 33.5 | 33.3 | 33.2 |
| **Average** | **33.7** | **34.3** | **31.9** |
| **± 2σ** | **0.311** | **1.34** | **1.51** |

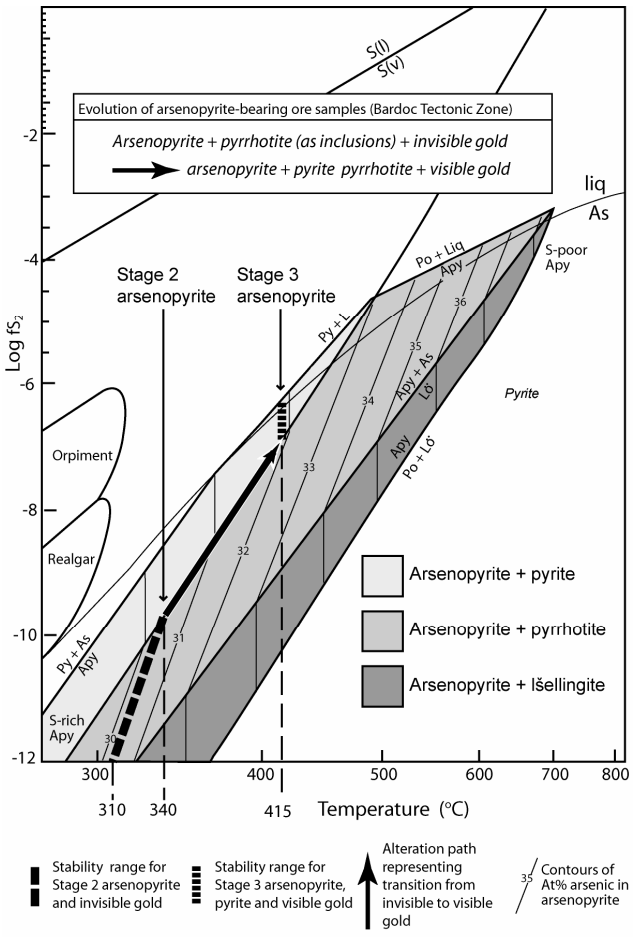


Figure 3. Phase stability diagram for arsenopyrite showing the alteration path for Stage 2 arsenopyrite to Stage 3 arsenopyrite + visible gold + pyrite ± pyrrhotites. Modified after Sharp *et al* (1985)

## ACKNOWLEDGEMENTS

This abstract has been released with permission from the CEO, *pmd**CRC. The authors thank Sarah Gilbert (LA-ICP-MS) and Graham Hutchinson (EMP) and review comments from Julie Hunt, James Cleverley, Peter Neumayr and Geordie Mark were highly appreciated.

## REFERENCES

Boyle RW (1979) The geochemistry of gold and its deposits (together with a chapter on geochemical prospecting for the element). *Geological Survey of Canada Bulletin* 280.

Cabri LJ, Chryssoulis SL, de Villiers JPR, Laflamme JHG, Buseck PR (1989) The nature of "invisible" gold in arsenopyrite. *The Canadian Mineralogis*t 27:353-362

Cathelineau M, Boiron M-C, Holliger P, Marion P, Denis M (1989) Gold in arsenopyrites; crystal chemistry, location and state, physical and chemical conditions of deposition. In: Keays RR, Ramsay WRH, Groves DI (eds) The geology of gold deposits; the perspective in 1988. *Economic Geology Mono-graph* v. 6, pp 328-341

Norman M, Robinson P, Clark D (2003) Major- and trace-element analysis of sulphide ores by laser-ablation ICP-MS, solution ICP-MS, and XRF: New data on international reference materials. *The Canadian Mineralogist* 41: 293-305.

Genkin AD, Bortnikov NS, Cabri LJ, Wagner FE, Stanley CJ, Safonov YG, McMahon G, Friedl J, Kerzin AL, Gamyanin GN (1998) A multidisciplinary study of invisible gold in arsenopyrite from four mesothermal gold deposits in Siberia, Russian Federation. *Economic Geology* 93:463-487

Mumin AH, Fleet ME, Chryssoulis SL (1994) Gold mineralization in As-rich mesothermal gold ores of the Bogosu-Prestea mining district of the Ashanti gold belt, Ghana; remobilization of "invisible" gold. *Mineralium Deposita* 29:445-460

Oberthür T, Weiser T, Amanor JA, Chryssoulis SL (1997) Mineralogical siting and distribution of gold in quartz veins and sulphide ores of the Ashanti mine and other deposits in the Ashanti belt of Ghana: genetic implications. *Mineralium Deposita* 32:2-15

Sharp ZD, Essene EJ, Kelly WC (1985) A re-examination of the arsenopyrite geothermometer: Pressure considerations and applications to natural assemblages. *The Canadian Mineralogist* 23:517-534

Swager CP, Griffin TJ (1990) Geology of the Archaean Kalgoorlie terrane, northern and southern sheets, 1: 250 000. *Geological Survery of Western Australia, Perth*

# What is a common ground for mineral deposition: theory and implications

Nina G. Stenina
*Novosibirsk State University of Architecture and Civil Engineering, Novosibirsk 630008, Russia*

ABSTRACT: Formation of metalliferous, hydrocarbon and diamond deposits is considered integral part of the evolution of rock matter providing by the [2(T, Si)$O_3$□ – $OH_2$ – $M^{n+}2M^{m+}O`_4$] aqua-complex. Aqua-complexes found first as water-impurity defects in quartz proved to be universal crystallochemical units of mineral matter responsible for its alteration and conversion of energy in the process. Mineralization results from disintegration of aqua-complexes under fluctuations of pressure, temperature and especially Ox/Red. Prognostic power of the theory is exemplified by localizing of hidden mineralizations.

KEYWORDS: aqua-complex, mineral deposits, prospecting

## 1 INTRODUCTION

Mineral deposits exhibit a variety of geologic settings and differ strongly in conditions of their formation. This is most pronounced in the case of ore, hydrogen and diamond deposits. At the same time, every mineralization is a geochemical anomaly and, as such, it is integral with the evolution of the Earth's matter. This implies that there must be a common ground for mineral deposition. If so, the question of wondering is what specific mechanism guides the alteration of mineral matter, and does a universal mechanism for various rocks exist? Our earlier developments (Stenina 1995) declared that the universal law of evolution of mineral matter is aqua-complex:

$$[2(T,Si)O_3□ – OH_2 – M^{n+}2M^{m+}O`_4]$$

Where: (T is four-valent cation: C, Ti, *etc.*, □ is atomic vacancy, $M^{n+}$ is uni and bivalent cation: Na, Au, $Fe^{2+}$, *etc.*, $M^{m+}$ is multivalent cation: $Al^{3+}$, $Fe^{3+}$, P, etc., O` is O and F, Cl, S).

## 2 CONCEPT OF AQUA-COMPLEX

### *2.1 Origin and Properties*

Aqua-complexes were originally found as water-impurity defects in natural quartz (Stenina *et al*. 1984). Crystallochemical model for aqua-complex (Fig.1a) was proposed on the basis of studies of natural quartz by TEM combined with other methods, data of special experiments and analysis of literature data on water and trace elements in silica minerals. Aqua-complex is composed of three parts: the left part ($SiO_2$) is acidic, the right ($MO_2$) is basic, and a tetrahedrally-charged water molecule builds up in the centre as a Redox bridge between both parts. The principal point here is that the oxygen of water molecule is simultaneously the bridge oxygen in Si—O—Si.

The case of magmatic replacement in the Kaakhem pluton rocks (Tuva, South-East Siberia) allowed us to understand the intermediating role of aqua-complex in alteration of mineral matter within gabbro-granite series (Stenina & Distanova 1991). Henceforward, as a result of analysis of a great bulk of geological data, the aqua-complex was proposed as a geochemical entity responsible for:

i) the diversity of mineral matter, ii) its structural-chemical transformation and redeposition iii) element associations, iv) formation of granite melt, v) conversion of energy within the Earth's crust.

The last property of the aqua-complex unravels the nature of interplay between tectonics, metamorphism, magmatic and hydrothermal activities in the course of formation of mineral deposits.

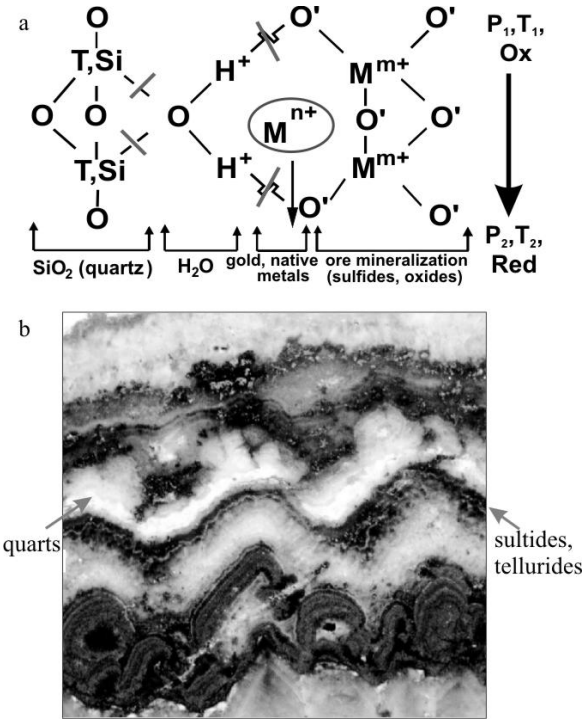


Figure 1. *a* - aqua-complex; *b* - a texture of self-organization (Kochbulak gold-ore deposit, Uzbekistan)

### *2.2 Aqua-complex as interplay between geologic processes*

Continuum of rock matter is composed of silicate minerals which have complex structures with $[SiO_4]$ and $[AlO_4]$ tetrahedra as major building units. Within the aqua-complex they are combined into a single entity through a water molecule. As a result, aqua-complex becomes a smallest species from which all minerals can be derived. In effect, the left part of aqua-complex corresponds to quartz and other simple oxides; the right part – to complex oxides, sulfides and other salts. Integration of both parts and whole aqua-complexes yields a great diversity of silicate minerals. This property allows the aqua-complex to perform structural-chemical rearrangements of mineral matter which proceed by exchange of chemical bonds. Water facilitates these processes due to weak donor-acceptor and hydrogen bonds it forms with the left and right parts of aqua-complex. So, it is a constant participant of mineral reactions resulting in mineral replacement (metamorphism). The aqua-complex concept also explains the driving forces for metamorphic replacement. The latter is stimulated by eliminating the excess energy in mineral system caused by strain in rock deformation and/or sediment burial compaction. The aqua-complex possesses a wide range of energies due to varying bond strengths of T and M cations within oxygen polyhedra (Table 1). Energy imbalances in a mineral system are reduced by extraction from mineral matter of cations with appropriate M(T)—O bond energies, incorporating them into aqua-complexes and, finally, into new mineral phases. This induces mineral matter to rearrange and such a process parallels metamorphic replacement. If metamorphism itself is insufficient to reduce energy excess in the mineral system, the aqua-complexes randomly arranged in solid minerals begin to form a regular 3D network. This process refers to anatexis and formation of a granite melt. The aqua-complex becomes a unit cell of its structure. If granitization does not annihilate an energy imbalance in a mineral system, the high energy cations and F (O`) begin to replace positions $M^{m+}(M^{n+})$. Crystallization of this portion of the melt results in the formation of pegmatites and ongonites. This process is extremely energy-consuming as inferred from a huge enthalpy of $LiAlF_4$ formation (Table1). Further ways of reducing energy imbalance in the mineral system are connected with evolution of acidic magma to basic one. In these processes metals are extracted from the host rocks, are mobilized into intermediating aqua-complexes and migrate. When a mineral system is subjected to P, T, especially, Ox/Red drops, aqua-complexes are disintegrated into the constituents $SiO_2$, $H_2O$, $M^{n+}$, $MO_2$ which are often sulphides as $S^0$ appears at the point of Ox/Red inversion (Fig.1a). As it takes place, water and metals invisible during metamorphic replacement become visible. This results in ore mineralization, the liberated water making metasomatic alteration of enclosing rocks.

Table 1. Energies of chemical bonds with oxygen (Gurvich *et al.* 1974)

| Elements | E (kcal/mol) |
|---|---|
| C (T) | 256.16 ± 0.08 |
| Si | 190 ± 2 |
| U | 180 ± 4 |
| Al ($M^{m+}$) | 120 ± 3 |
| Fe | 97 ± 3 |
| W | 160 ± 10 |
| Y | 170 ± 3 |
| Nb | 180 ± 3 |
| La (REE) | 190 ± 10 |
| Cu ($M^{n+}$) | 63 ± 10 |
| $LiAlF_4$ (enthalpy of the formation) | -441.3 |

### 2.3 Aqua Complex and synergetic paradigm in geology

Synergetic character of evolution of rock matter is evident from the fractal geometry of many rock ensembles. It was exemplified by gold-ore fields (Stenina *et al.* 1999). Self-organization of mineral matter implies long-term interactions between units of mineral continuum. Intermediate aqua-complexes facilitate these interactions due to weak bonds within these species. Figure 1b illustrates how a rhythmically-zoned pattern of self-organization is produced by aqua-complex. Light (quartz) and dark (Sb-Te minerals, sulphides; silicates) layers correspond to the left and right parts of aqua-complex and non-disintegrated species respectively (Fig.1a).

## 3 FORMATION OF MINERAL DEPOSITS

A property of aqua-complex to convert energy in the mineral system offers a unified basis for understanding mineralizations of various styles.

### 3.1 Ore deposits

Differentiation of metals by the energies of their bonding within the aqua-complexes (Table 1) explains in outline association of specific metals with the rocks. Low-energy base metals are concentrated during metamorphism and self-organization of sedimentary rocks, forming strata-bound deposits. High-energy rare metals overcome as a rule a granulite stage of metamorphism and are mineralized in granites, pegmatites and ongonites. The aqua-complex $[2SiO_3 - OH_2 - (Au, M^{n+}) (Fe, M^{m+})O_4]$ is responsible for co-migration of gold with iron (Stenina *et al.* 1993). Fe is the fourth abundant element of the Earth's lithosphere and has a low energy of bonding with oxygen. This explains ultrahigh ability of gold for concentrating and association of gold deposits with faults.

### 3.2 Petroleum and Diamonds

Energy aspect of evolution of mineral matter is universally applied to formation of petroleum-gas and diamond deposits. C → Si replacement effectively reduces excessive energy in a mineral system as it consumes 66 kcal per mol (Table1). Such a replacement proceeds easily because C ($2p^2$) and Si ($3p^2$) have the same outer electron-shell structure. A mechanism proposed for generation of petroleum in nature (Stenina *et al*. 2005) implies that kaolinite matrix, in which carbon substitutes for silicon, acts as nucleus for mineral transformations. Kaolinite corresponds stoichiometrically to the (Si, Al) aqua-complex. C → Si replacement reduces excess energy in the argillaceous-carbonate-organic rocks caused by their burial compaction. Organic matter provides reducing potential in the aluminosilicate matter, that is, in the network formed by kaolinite aqua-complexes. This stimulates their disintegration and reduction of the constituent radicals. $C^0$ generated during reduction participates in both oxidizing and reducing reactions to yield $MCO_3$ and $C_nH_m$ products. In a metamorphic reaction:

$Al_2(OH)_4[Si_2O]_5$ + carbonates + sulphates +organics + (ΔP) → $SiO_2 + Al_2O_3 + H_2O + MCO_3$ + MS + new silicates + $C_nH_m$,

Hydrocarbon end products incorporate modified biogenic compounds of sediments that determine the complex characters of mature petroleum.

In the case of diamonds, C → Si replacement proceeds in a basic magma developed from the acid (granite) magma under increasing temperature and pressure. In a basic magma hydrogen escapes into interstitial positions and water looses its chemical "face". Crystallization of diamonds occurs as a result of reduction of (Si, C) $M^{m+}$-oxygen network (Stenina 2003), occurring as a response of the system to the remaining energy imbalance. In this process, oxygen binds with interstitial hydrogen and yields water, which provides additional pressure in magmatic chamber. Under these conditions carbon liberated as a result of reduction of the oxygen network can be crystallized only in the most closely packed diamond modification.

## 4 IMPLICATIONS

A prognostic power of the theory was shown at the example of prediction of rare metal deposit among the gold deposits of the Yenisei Ridge (Stenina & Petrov 2003). By now, the most mineral deposits having been exposed to the day surface are found. So, prospecting of mineral deposits increasingly more has to do with hidden mineralizations overlain by sediment series. In this connection, the satellite means of prospecting are intensely mastered. The views of the mineral-forming process based on the energy concept of the aqua-complex guides us in prospecting of hidden deposits. As an example, we present here the case

of finding two gold mineralizations (Fig. 2). Geological map shows that the known deposit as well as the assumed occurrences are localized in a close vicinity of the boundary between the basic and acid rocks and are associated with the faults.

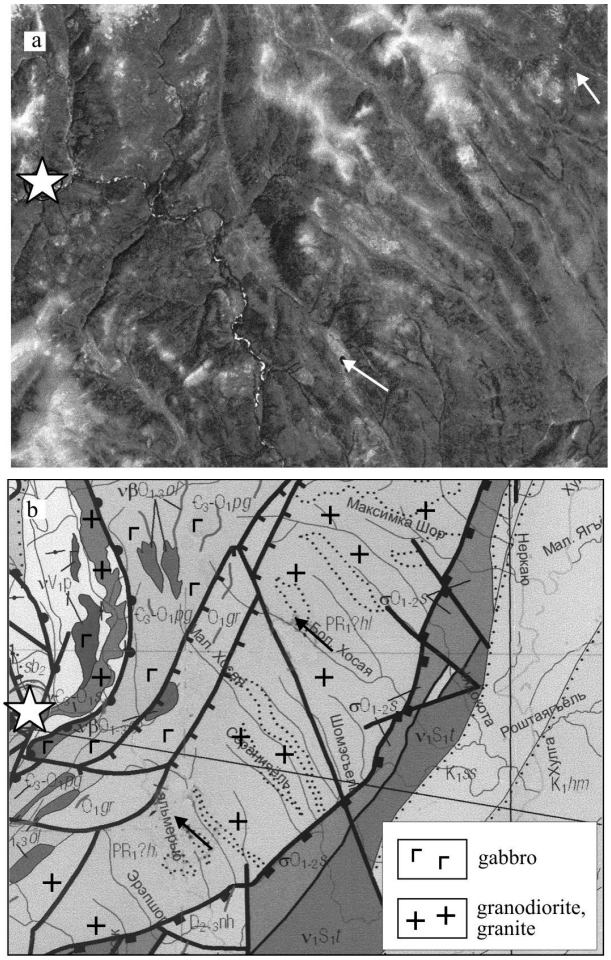


Figure 2. Remote prospecting gold deposits: (a) satellite image, (b) geological map (star is known deposit; arrows show hidden mineralizations)

## CONCLUSIONS

Thus, formation of ore, hydrocarbon and diamond deposits has a common ground in terms of aqua-complex concept as a law of development of mineral matter. The theory considers mineralization of various styles from the viewpoint of moving energy rather than moving substance. In the process, the data evidence a crucial role of Redox inversion and the Redox energy in accumulation of useful elements in deposits. The new approach proves itself promising in the prospecting of hidden deposits.

## ACKNOWLEDGEMENTS

The author thanks SGA for attention to the idea of aqua-complex and for financial support of participating in the I-VIII SGA Meetings.

## REFERENCES

Gurvich LV, Karachevtsev GV, Kondrat'ev VN, Lebedev YA, Medvedev VA, Potapov VK, Khodeev YS (1974) Energies of breaking of chemical bonds. Potentials of ionization and electron affinity. Moscow: *Nauka*. pp351 (in Russian)

Stenina NG (1995) Energy aspect in the formation of granitic magma and ore deposits. Mineral deposits: from their origin to their environmental impacts; *Proceedings SGA Meeting:* 539-541.

Stenina NG (2003) Formation of diamonds in nature: the key role of the energy of Redox. Carbon: Mineralogy, Geochemistry and Cosmochemistry. *Proceedings International Conference:* 76-78. (in Russian)

Stenina NG, Alabin LV, Gutakovskii AK (1999) Fractal properties of the gold-ore fields. Mineral deposits: Processes to processing. *Proceedings SGA Meeting:* 1037-1040.

Stenina NG, Bazarov LS, Scherbakova MY, Mashkovtsev RI (1984) Structural state and diffusion of impurities in natural quartz of different genesis. *Phys Chem Miner* 10: 180-186

Stenina NG, Distanova AN (1991) Structural-chemical transformations of silicate minerals as indicator of their genesis (Kaakhem pluton). *Novosibirsk: OIGG&M*. pp.76. (in Russian)

Stenina NG, Distanova AN, Berezin YA (1993) Au-Fe associations in silicate phases as an evidence of gold transportation via aqua-complexes. Current research in geology applied to ore deposits; *Proceedings SGA Meeting:* 567-570.

Stenina NG, Gutakovskii AK, Plyasova LM (2005) Generation of hydrocarbons: Mechanism of reaction, geologic and experimental evidence. Mineral deposit research: meeting the global challenge; *Proceedings SGA Meeting*, v 1: 179 – 182

Stenina NG, Petrov VG(2003) Gold deposits of the Yenisei Ridge (Russia), with special reference to mechanism of tectonogenesis. Mineral exploration and sustainable development; *Proceedings SGA Meeting*,v 2: 721-724

# A Primary Study on Fluid Inclusions at the Saidu Gold Deposit, Southern Altai, Xinjiang, China

Jh. Xu, Yl. Xie, Gr. Zhang & Lh. Shan
*Department of Resource Engineering, University of Science and Technology Beijing, Beijing 100083, China*

S.J. Zhang & Ch. Zous
*Altai Zhengyuan International Mining Company, Habahe, Xinjiang 836700, China*

ABSTRACT: The Saidu gold deposit, located 18km northeast of Habahe County in southern Altai, Xinjiang, occurs in metamorphic sedimentary and volcanic rocks of Devonian age. The main tectonic belt is the Marcakuli shear zone which strikes NW to SE, extending 100km with 1~3km of width. The gold-bearing veins are controlled by secondary shear zones. Hydrothermal mineralization can be divided into 4 stages: early silicification stage (I), disseminated pyrite-white quartz stage (II), polymetallic sulphide-smoky gray quartz stage (III), and late quartz-carbonate stage (IV). Fluid inclusions in vein quartz at the Sarekoubu are abundant. Three types can be identified: 1) Aqueous inclusions ($L_{H2O}$-V); 2) $CO_2$-$H_2O$ inclusions ($L_{CO2}$-$L_{H2O}$); and 3) $N_2$-rich or $CO_2$- rich inclusions. Investigations, including microthermometry and Laser Raman microprobe analysis, have been carried out on these inclusions. The results show that from the early to late stage of gold mineralization, the fluid inclusion type changed from $CO_2$-$H_2O$ inclusions and pure $N_2$/$CO_2$ inclusions to aqueous inclusions, with homogenization temperatures from 252~408$^{o}$C to 101~296$^{o}$C.The salinities of aqueous inclusions are 0.35~5.7 wt% NaCl equiv., based on melting temperatures of ice. They are similar to those from other orogenic gold deposits in the south margin of Altai area.

KEYWORDS: Fluid inclusions, Saidu, Altai, Orogenic Gold

## 1 INTRODUCTION

The Saidu gold deposit, located 18km northeast of Habahe County in the southern margin of the Altai Mountains, is a typical shear zone type found deposit in Xinjiang province. The deposit has been of interest to many economic geologists since 1990s. Cheng & Rui (1995) made an initial study on the geological and geochemical characteristics of the Sarekoubu deposit. An initial study on fluid inclusions at the Saidu was also made by Cheng & Rui (1997). No significant advance has been made to interpret PVTX properties of ore-forming fluids during orogeny since then. In this study we present new data on fluid inclusions related to the mineralizatiion in this deposit.

## 2 GEOLOGICAL SETTING

### 2.1 *Regional Geology*

The Altaids are an orogenic collage of Neoproterozoic-Pleozoic rocks in the central Asia, which hosts numerous gold, silver, copper-molybdenum, lead-zinc, and nickel deposits of late Proterozoic to early Mesozoic age (Yakubchuk, 2004). The orogenic architecture of the Altaids has long been recognized as different from that of classical collisional orogens such as the Alps and the Himalayas (Sengör *et al.*, 1993). Xiao *et al*., (2004) presented a new model for the tectonic evolution of the southern Altaids, which was generated by a sequence of north to south tectonic processes. The southern margin of the Altai Mountains in Xinjiang is one of the most important metallogenic provinces in China. Continental margin rift and orogenic ore-forming systems were formed during an extension of the continental margin in the early-Middle Devonian and convergence-collision occurred in the late Devonian-Permian (Wang, *et al*., 1998). The Kazakhstan-Junggar Plate and the Siberia Plate were sutured by subduction during the Middle Devonian and the basin disappeared in the early Carboniferous. Gold deposits were formed during or at the end

of Palaeozoic tectonism, (isotopic ages of 265-320Ma, Rui *et al*., 2002), which is confirmed by regional metamorphic ages (Zheng *et a*l., 2005). This is also in agreement with late Palaeozoic tectonic events in the Altai (Hu *et al*., 2006; Xiao *et al.*, 2004, 2006).

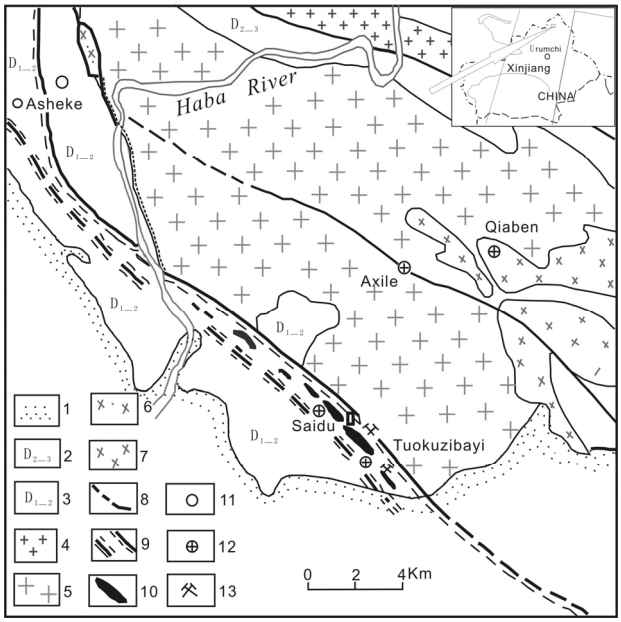


Fig. 1 Sketch map of the Saidu gold deposit, southern Altai, Xinjiang, China (Modified after Chen, 1995)

1-Quartary; 2-Middle-Upper Devonian; 4-Granite; 5-Plagioclase granite; 6-Diabase and diorite; 7-Pyroxene diorite; 8-Faults; 9-Ductile shear zone; 10-Gold-bearing veins; 11-Copper mine; 12-Gold mine; 13-Mining pit

### 2.2 *Gold-bearing vein systems*

The great Markakuli ductile fault controls the gold-bearing vein systems of the Saidu gold deposit, while the secondary shear zones control the ore shoots. There are four en-echelon-like gold-bearing vein systems in the ore field, named No.1, No.2, No.3 and No.4 from southeast to northwest respectively, striking $300^{o}$~$340^{o}$ and dipping $60^{o}$~$85^{o}$ to southwest. The ore shoots, occur in mylonites and fractures zones, are 100 to 400m in length, 65 to 500m in depth, 3 to 50m in thickness and 3.71 to 8.18g/t Au in average grade (Cheng & Rui, 1995).

### 2.3 *Ore minerals*

Ore minerals in vein systems are mainly native gold, electrum, pyrite, pyrrhotite, chalcopyrite, sphalerite, galena and magnetite. Gangue minerals are dominated by quartz, calcite, sericite, chlorite and clay minerals. Hydrothermal mineralization can be divided into 4 stages: early silicification stage (I), disseminated pyrite -white quartz stage (II), polymetallic sulphide-smoky gray quartz stage (III), and late quartz-carbonate stage (IV).

Pyrite occurs as various forms in the vein systems. Three generations of pyrite can be distinguished. The first generation (Py1), occurs as an integrated crystal form, and is disseminated in silicified wallrocks. The second generation of pyrite (Py2) occurs as monominerallic veinlets, coarse grains and disseminated aggregates within vein quartz. This generation of pyrite is usually cut or replaced by aggregates of-chalcopyrite and sphalerite. The third generation of pyrite (Py3) is associated with chalcopyrite, pyrrhotite and sphalerite, and generally occurs as xenomorphic grains.

Chalcopyrite, commonly occurs next to pyrite, generally as veinlets or disseminated xenomorphic grains. It is associated with sphalerite, galena, and pyrrhotite, and fills the tiny fissures in vein quartz and Py2. Occasionally veinlets composed of chalcopyrite, magnetite, and pyrite occur in the schistose cleavage of metamorphic tuffs near the vein quartz.

## 3 FLUID INCLUSION STUDY

The samples studied here were mostly collected from the open pit of No.1 vein system (Tuokuzibayi in Fig.1), and drill cores ZK78-3, ZK82-2 and ZK86-3 ( located in the south of No.1 vein system). Some samples were collected from No.2 vein system. Three kinds of quartz can be distinguished: milk white quartz (Q1) occurring in stage II, smoky gray quartz (Q2)occurring in stage III, and white quartz having good transparence (Q3)associated with smoky gray quartz of stge III.

### 3.1 *Fluid inclusion petrography and microthermometry*

Fluid inclusion observations were made from quartz of all the different generations. Based on the phases present at room temperature and the microthermometry study, the fluid inclusions can be divided into three types: (1) Aqueous inclusions ($L_{H2O}$-V); (2) $CO_2$-$H_2O$ inclusions ($L_{CO2}$-$L_{H2O}$) ; and (3) $N_2$-rich or $CO_2$- rich inclusions

#### 3.1.1 Aqueous inclusions

Aqueous inclusions (Type A), are usually found in Q2 and Q3 (cores ZK82-2 and ZK86-3) at the Saidu deposit, generally with size of 2-

10 μm, consist of two phases (Type A1, a liquid $H_2O$ phase and a vapour phase, with 10%~30% of V/L volume ratios) or only one liquid phase (Type A2). They are restricted within the host quartz grains, so they have primary origin (Roedder, 1984). Type A1 homogenized between 101~296°C (506 fluid inclusions, homogenized to liquid water phases, Fig.2), and have ice melting temperatures from -3.8 to -2.1°C . Type A2 inclusions are abundant, and associated with type A1 in Q2 and Q3 of stage III, which have the same $T_{m,ice}$ (-0.2~-2.9) as A1. No bubble appears when cooled from liquid phase to solid phase (ice), so these inclusions were trapped at low temperatures.

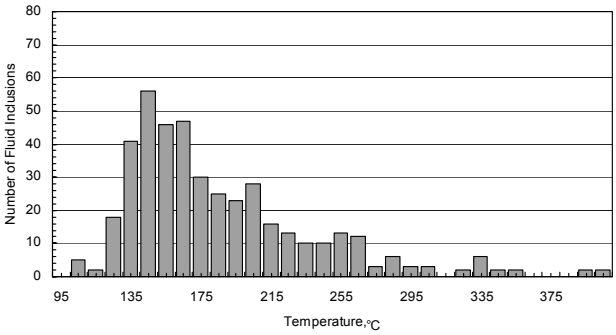


Fig.2 Homogenization temperature ranges of fluid inclusions from the Saidu

### 3.1.2 $CO_2$-$H_2O$ inclusions ($L_{CO2}$-$L_{H2O}$)

$CO_2$-$H_2O$ inclusions consist of a liquid $CO_2$ phase and a liquid $H_2O$ phase ( with 25%~40% of $CO_2/H_2O$ volume ratios), occurring usually in Q1 of stage II, and are associated with primary aqueous inclusion. The final homogenization of these inclusions occurs at 252~408°C (28 inclusions, homogenized to liquid of water phases). Clathrate melting between 7.5~9.1°C is observed in some samples.

### 3.1.3 $N_2$-rich or $CO_2$- rich inclusions

$N_2$-rich inclusions, appear as dark monophase bubble, and are commenly observed in Q1 of stage II and associated with $CO_2$-$H_2O$ inclusion. No change is observed when cooling occurred down to -190°C indicating the inclusions contain a low density vapour. Laser Raman Microprobe analyses shows $N_2$ spectra show weak peaks at a Raman shift of 2327~2329 $cm^{-1}$. *$CO_2$- rich inclusions* can be also seen in Q1 of stage (II) and Q2 of stage (III). These inclusions consist of a single phase at room temperature (higher than 20°C). The melting temperatures of frozen phases ($T_{m,CO2}$) are less than -57°C, even lower to -63.1~-64.5°C, indicating some other volatiles mixed in fluid, such as $CH_4$ (Roedder, 1984). These inclusions are commonly found in orogenic gold deposits (Graupner *et al*., 2001; Schmidt & Oberthür, 1997; Xu *et al*., 2005).

### 3.2 *Laser Raman Microprobe Analysis*

Typical fluid inclusions were analysed by Laser Raman Microprobe. The measurement was conducted at Fluid Inclusion Laboratory of Institute of Geology and Geophysics, Chinese Academy of Sciences (IGG-CAS) with a Renishaw RM-2000 Laser Raman Microspectrometer with a 514nm $Ar^+$ laser as excitation. The count time for each spectrum is 10 seconds, and the laser bean is 1μm.

$CO_2$ spectra peaks can be seen at Raman shifts of 1384 $cm^{-1}$ and 1278 $cm^{-1}$, with no $CH_4$ or other spectra peak observed (SD2-16 in Fig.3). $N_2$ spectra peaks are also observed at Raman shifts of 2327~2329 $cm^{-1}$ (SD2-3, SD2-7 in Fig.3). However, water spectra peaks are not very clear about 3500 $cm^{-1}$ for A2 type inclusions. More detailed research should be done in the future.

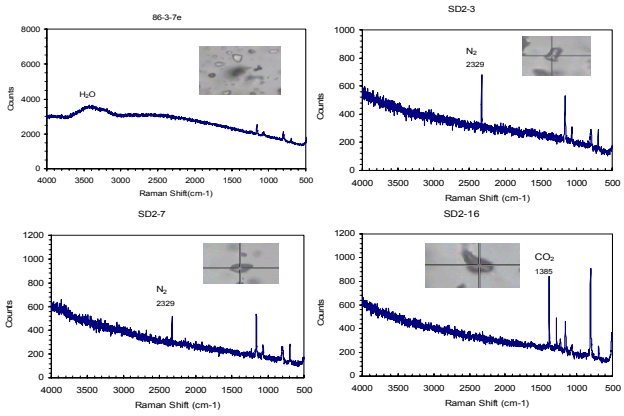


Fig.3 Laser Raman spectrograms of fluid inclusions from the Saidu (Sample number is shown on the top of each spectrogram)

## 4 DISCUSSION AND CONCLUSIONS

The main mineralizing epoch (290~300Ma, Yan *et al*., 2004) for the Saidu deposit was related to ductile-brittle shearing of the regional Ertix belt, which was identical with the intrusion of plagioclase granite in the erea. Hydrothermal mineralizing stages I, II and III might related to this epoch.

Fluid inclusion study shows that from early

to late stage of gold mineralization, the fluid inclusion types change from $CO_2$-$H_2O$ inclusions and pure $N_2/CO_2$ inclusions to aqueous inclusions, with homogenization temperatures being from 252~408°C to 101~296°C. The salinities of the aqueous inclusions are 0.35~5.7wt% NaCl equiv., based on melting temperatures of ice. They are similar to those from other orogenic gold deposits in the south margin of Altai district.

## ACKNOWLEDGEMENTS

This study was supported by NSFC (Natural Science Foundation of China, 40572066 and 40672060).

## REFERENCES

Cheng ZF, Rui XJ (1995) Minerogenetic characteristics of Saidu gold deposit in Habahe County. Xinjiang *Geology,* 14(3): 247-254

Cheng ZF, Rui XJ (1997) Ore-forming geochemical environments of Saidu gold deposit in Habahe, Xinjiang. *Volcanology and Mineral Resources,* 18(1):27-36

Graupner T, Kempe U, Edward TC (2001) Microthermometric, Laser Raman spectroscopic and volatile-Ion Chromatographic analysis of hydrothermal fluids in the Paleozoic Muruntau Au-bearing quartz vein ore field, Uzbekistan. *Economic Geology* 96, 1-23

Hu AQ, Wei GJ, Deng WF, Chen LL (2006) SHRIMP zircon U-Pb dating and its significance for gneisses from the southeast area to Qinghe County in the Altai, China. *Acta Petrologica Sinica* 22, 1-10

Li HQ, Xie CF, Chang HL(1998) Study on metallogenetic chronology of nonferrous and precious metallic ore deposits in north Xinjiang, China. Beijing: *Geological Publishing House,* 26 ~ 133 ( in Chinese with English abstract)

Şengör AMC, Natal'in BA, Burtman VS (1993) Evolution of the Altaid tectonic collage and Paleozoic crustal growth in Eurasia. *Nature* 364, 299-307

Schmidt MA, Oberthür T, Vetter U, Blenkinsop TG (1997) High $CO_2$ content of fluid inclusions in gold mineralisations in the Ashanti Belt, Ghana: a new category of ore forming fluids? *Mineral. Deposita* 32, 107-118

Roedder E (1984) Fluid inclusions. *American Mineralogy Society*, 12. pp644

Rui ZY, Goldfarb RJ, Qiu YM, Zhou TH, Chen RY, Pirajno F, Yun G (2002) Paleozoic–early Mesozoic gold deposits of the Xinjiang Autonomous Region, northwestern China. *Mineralium Deposita,* 37, 393–418

Wang JB, Qin KZ, Wu ZL, Hu JH, Deng JN (1998) Volcanic-exhalative-sedimentary lead-zinc deposits in the southern margin of the Altai, Xinjiang (in Chinese with English abstract). Beijing: *Geological Publishing House,* pp18-95

Xiao WJ, Windley BF, Badarch G, Sun S, Li J, Qin KZ, Wang ZH (2004) Palaeozoic accretionary and convergent tectonics of the southern Altaids: implications for the lateral growth of Central Asia. *Journal of the Geological Society, London,* 161, 339-342

Xiao WJ, Han CM, Yuan C, Chen HL, Sun M, Lin SF, Li ZL, Mao QG, Zhang JE, Sun S, Li JL (2006) The unique Carboniferous-Permian tectonic-metallogenic framework of Northern Xinjiang (NW China): Constraints for the tectonics of the southern Paleoasian Domain. *Acta Petrologica Sinica,* 22, 1362-1376

Xu JH, Ding RF, Xie YL, Zhong CH, Yuan X (2005) Pure $CO_2$ fluids in the Sarekoubu gold deposit at southern margin of Altai Mountains in Xinjiang, West China. *Chinese Science Bulletin,* 50 (4), 333-340

Yakubchuk, A (2004) Architecture and mineral deposit settings of the Altaid orogenic collage: a revised model. *Journal of Asian Earth Sciences*, 23, 761–779

Yan SH, Chen W, Wang YT, Zhang ZC, Chen BL ( 2004 ) , $^{40}Ar/^{39}Ar$ dating and its significance of the ertix gold metallogenic belt in the Altay orogeny, Xinjiang, *Acta Geologica Sinica* , ( 8 ) , 500-506

Zheng CQ, Xu XC, Enami M, Kato T (2005) Features and PT condition study of the adnalusite-sillimanite type progressive metamorphic belt in Altai (in Chinese with English abstract). Xinjiang, *Journal of Mineralogy and Petrology* 25(4), 45-51

# Major Mesothermal Gold Ore Deposit of Russia: Composition and Origin of Ore-Forming Fluids

N.S. Bortnikov & V.Y. Prokofyev
*Institute of Geology of Ore Deposits, Petrography, Mineralogy, and Geochemistry, Russian Academy of Sciences, Staromonetnyi per. 35, Moscow, 119017 Russia*

ABSTRACT: A chemical and oxygen isotope composition of ore-forming fluids responsible for the formation of major mesothermal gold deposits in Russia have been studied. The Au mineralized ore bodies formed from the $H_2O$-$CO_2$-NaCl±$CH_4$±$N_2$ fluids that had low to moderate salinity ranging from 1.2 to 16.8 wt % NaCl equiv. at temperatures from 190° to 430°C, and pressures of 0.8 to 3.7 kb. The calculated $\delta^{18}O_{H2O}$ values fall in the range of +5.5 to 9.0‰, that overlap with magmatic and metamorphic water compositions.

KEYWORDS: Fluid inclusions, oxygen isotopes, gold deposits,

## 1 INTRODUCTION

The source and chemistry of fluids responsible for the formation of mesothermal gold deposits remain controversial (Ridley & Diamond, 2000). Proposed hypothesis on fluid sources include (1) granitoid-related orthomagmatic solutions, (2) convecting meteoric water, (3) mantle-derived fluids, and (4) fluids generated by deep devolatilization and dehydration at metamorphism of ocean crust and sediments (Kerrich, 1990).

Fluid inclusion and oxygen isotope studies have been carried out on major world-class gold deposits in Russia to determine the compositions and nature of the associated fluids responsible for gold mineralization.

## 2 GENERAL DESCRIPTION OF DEPOSITS

Major gold deposits with proven and estimated reserves ranged from 78 to 650 tonnes of gold (*after* Lashkov *et al.*, 2000) are situated in the different regions in Russia (Table). There are differences in general characteristics of these deposits: some of them are located within intrusive rocks, while others are within terrigenous sequence. All deposits are spatially related to magmatic rocks.

## 3 FLUID INCLUSIONS

Four main types of fluid inclusions are recognized in quartz at room temperature (Fig. 1): (1) two-phase aqueous inclusions, containing liquid and vapour (Fig. 1a); (2) type II, two- or

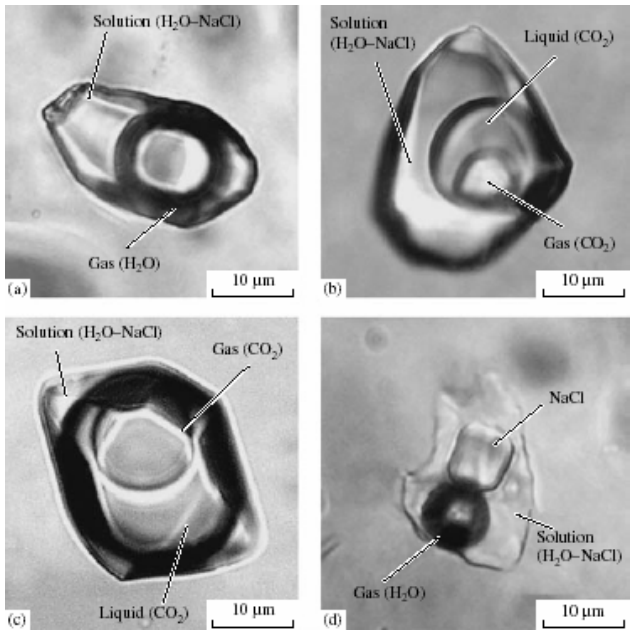


Fig. 1. Types of fluid inclusions in the minerals of studied mesothermal gold deposits. (a) Two-phase inclusion of diluted solution; (b) $CO_2$ –aqueous inclusion of vapour-rich fluid; (c) vapour-rich inclusion; (d) multiphase inclusion of chloride brine.

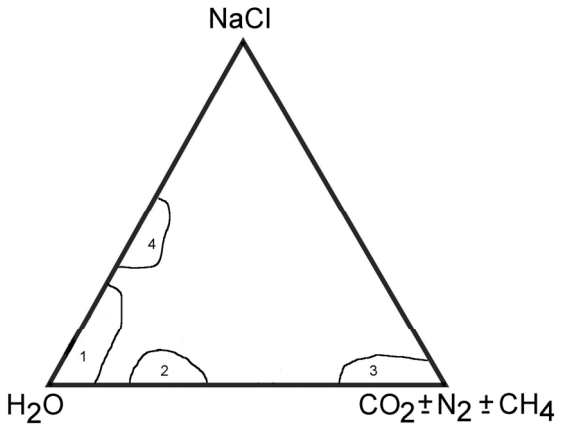


Fig. 2. Types of ore-forming fluids of investigated mesothermal deposits: 1 - the diluted solution, 2 – the gas-saturated fluid, 3 – the gas, 4 – the chloride brine.

three-phase, $(H_2O)L + (CO_2)V$ or $L + (CH_4)V$ or L fluid inclusions, including IIa, $H_2O$-$CO_2$-$CH_4$, and IIb, $(H_2O)L$-$(CO_2)V \pm (CO_2)L$ fluid inclusions (Fig. 1b); (3) type III, vapour-rich inclusions (Fig. 1c), rarely with small liquid rims or meniscus, including IIIa, $(CO_2)V + (CO_2)L$, and IIIb $(CO_2)V + N_2 + NH_4$; and (4) type III, salt-rich inclusions containing $(H_2O)L$-$(H_2O)V$, and solid-daughter mineral identifying as halite on the basis of habit and optical characteristics (Fig. 1d). Types of fluid recognized were rarely found in a single deposit: type II and type III were occurred in auriferous quartz in deposits under considerations, type I is typical of late post-ore quartz associated with native gold and stibnite or sulphosalt minerals, type III were mainly observed in quartz bearing cassiterite, molybdenite and wolframite. Data from fluid inclusions (Fig. 2) suggest (1) a diversity of fluids involved in the formation of deposits studied, and (2) variations in the fluid compositions and regime of their formation. However, it seems to be evident, that hydrothermal ore-forming fluids responsible for gold mineralization are in the $H_2O$–$CO_2$–$NaCl \pm CH_4 \pm N_2$ system, whereas those of early quartz-gold-rare metal veins in the Nezdaninsk deposit and post-ore cassiterite-quartz veinlets in the Maisk deposit are salt-rich and later gold-sulphide-quartz are dilute $H_2O$-NaCl in the composition.

Fluid inclusions of types II and III form irregular clusters which occur in the same growth zones of quartz grains. This suggests that they have been simultaneously trapped. This is evidence for immiscibility of $H_2O$–$CO_2$–$NaCl \pm CH_4 \pm N_2$ protofluid into liquid-rich and vapour-rich phases due a temperature and pressure drop. Freezing runs showed that (1) fluids associated with auriferous veins have low- to moderate salinity ranging from 1.2 to 16.8 wt % NaCl equiv, in general; (2) the fluid salinity varies from a deposit to a deposit (Fig. 2, 3): fluids with salinity <9±1 wt % NaCl equiv responsible for the formation of gold ore bodies at Nezhdaninsk, and Maisk deposits, while fluids with salinity > 7 wt % NaCl equiv formed ores of Kochrar' and Svetlinsk deposits, salinities fluids responsible for the depositions of Au mineralization in Olimpiada and Beresovsk de-

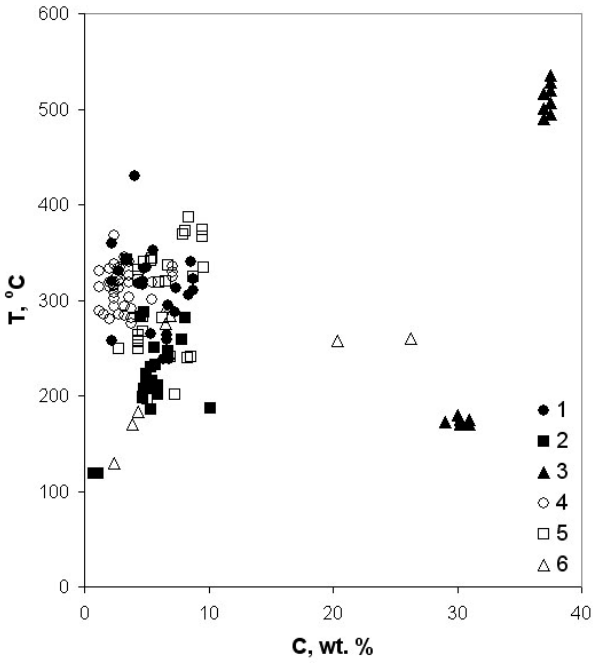


Fig. 3. Variations of homogenization temperature versus salinity of the fluid inclusions in quartz from the mesothermal Maisk (1-3), and Nezhdaninsk (4-6) gold deposits.

posits ranged from 2 to 15-17 wt % NaCl equiv. Homogenization temperature of fluid inclusions in auriferous quartz range from 190 to 430°C. The fluid pressure are estimated to vary from 0.8 to 3.7 kb.

Compositionally diverse fluids were involved in the formation of most of deposits studied. Fluids associated with unprofitable quartz veins (late stages) have dilute to moderate salinity ranging from 0.7 to 20 wt NaCl equiv. Salt-rich fluids with salinity >30 wt NaCl equiv. were participated in the formation of unprofitable rare mineralization at Nezhdaninsk and Maisk deposits.

It should be emphasized that $H_2O$-$CO_2$ fluids have not detected in the Au mineralized sulphide-quartz veins in the Darasun deposit that has been considered as a typical example of

mesothermal gold deposits. The aqueous fluids with salinity ranged from 4.8 to 22.2 wt % NaCl equiv. and 12.8 to 2.2 wt % NaCl equiv are responsible for the formation of auriferous and late sulphosalts-bearing quartz veins. Pre-ore mineralization was formed from brines with salinity of 30.5 to 44.8–wt % NaCl equiv.

## 3 OXYGEN STABLE ISOTOPES

Aureferous quartz from the deposits studied exhibits a narrow range of $\delta^{18}O$ values from +11.9 to +18.3‰ (Fig. 5). These data are similar to the range of +12 to +17 ‰ reported for the most of Phanerozoic mesothermal deposits (Kerrich, 1990). The range of $\delta^{18}O$ values vary from a deposit to a deposit: these figures lie within +14.8 to +16.8‰ in the Nezhdaninsk quartz, +11.8 to +14.5‰ in the Maisk deposit, +10.4 to +11.0‰ in the Berezovsk gold-bearing quartz, and +12 to +14‰ in most quartz samples from the Kochkar' deposit. The calculated $\delta^{18}O_{H2O}$ values fall in the range of +5.5 to 9.0‰, that overlap with magmatic and metamorphic water compositions, and indicate that there is no meteoric water in the fluids. Calculated fluid $\delta^{18}O_{H2O}$ values of Darasun ore-stage quartz are less 0‰, that could be explained an an incursion evolved meteoric fluid, while the early stage pre-ore salt-rich fluids exibit signatures of magmatic origin ($\delta^{18}O_{H2O}$ values are +5 to +8‰

The δD and $\delta^{18}O$ values in minerals from metasomatic rocks surrounded auriferous veins at Berezovsk deposit, vary from –48 to –63‰ and from +6.1 to +10.8‰. The values of δD in equilibrium with metasomatic minerals at 275°C, from –39 to –63‰ and from +5.2 to +8.1‰, respectively, that corresponds well to the primary magmatic fluid.

An incursion of highly evolved meteoric water or basinal brine could account for the shift to lower calculated $\delta^{18}O$ fluid values (<+3.5‰) that formed late-stage mineralization at the Maisk and Svetlinsk deposits and early-stage rare-gold-quartz mineralization in the Nezhdaninsk deposit.

## 4 DISCUSSION

The data obtained indicate that fluids responsible for the formation of the commercial ore bodies in mesothermal deposits studied consisted of the low- to moderate salinity to mixture of $H_2O$+CO+NaCl±$CH_4$±$N_2$. Fluids deposited auriferous quartz in some deposits exibit the higher salinity that has been previously reported for orogenic gold deposits (Ridley & Diamond, 2000). A feature of the ore-bearing fluids at some deposits is their high $CH_4$ and/or $N_2$ contents. Similar $CH_4$-bearing fluids have also been reported from some Australian lode gold deposits (Mernagh, Wygralak 2007). These methane-rich fluids were interpreted to have been resulted from reduction of $CO_2$. Commonly, fluids formed due to devolatilization and dehydration of rocks during their metamorphism have salinity less 6.0 wt. % NaCl-equiv. Thus, higher salinity of fluids formed the deposits studied can be considered as evidence for their exsolution from silica magma at its solidification. The $CH_4$ and $N_2$-bearing fluids could result from the fluid reaction with micaceous host rocks due to release of the $NH^{4+}$-ions from mica followed its oxidation to $N_2$ (Bottrell & Miller, 1990):

$$K^+ + NH_{4(\text{in mica})} = NH_3 + H^+ + K_{\text{mica}},$$

that was accompanied by a reduction of $CO_2$ to methane

$$8NH_3 + 3CO_2 = 4N_2 + 3CH_4 + 6H_2O.$$

An oxygen isotope data for the auriferous fluids do not allow us to discriminate between magmatic and metamorphic waters due to their overlap with figures ascribed to these both sources. The Au-bearing fluids reported from some Achaean and Phanerozoic lode gold deposits exibited enrichment in heavy oxygen isotope. We believe, that good correspondence of $\delta^{18}O_{H2O}$ values with the magmatic water range rather suggests their magmatic origin.

Dilute aqueous fluids the post-ore mineralization could be derived during evolution of a protofluid $H_2O$–$CO_2$–NaCl±$CH_4$±$N_2$ (Bortnikov *et al*., 1996). However, oxygen isotope data presume rather an incursion evolved meteoric water.

Therefore, the genetic model for the formation of the gold ore bodies that infer their relation to the magmatic activity seems to be most preferable.

## ACKNOWLEDGEMENTS

This study was supported by the Russian Academy of Sciences and the Russian Foundation for Basic Research (Projects 05-05-64803-a and 07-05-00479-a).

## REFERENCES


Bortnikov NS, Prokof'ev VY, and Razdolina NV. (1996) Origin of the Charmitan gold–quartz deposit (Uzbekistan). *Geol. Ore Dep*. 3: 208-226

Bortnikov NS, Sazonov VN, Vikent'ev IV et al. (1998) Role of the magmatogenic fluid in the formation of the mesothermal Berezov gold–quartz deposit. *Dokl. Earth Sci*. 363: 1078-1081

Bottrell SH, Miller MF (1990) The geochemical behaviour of nitrogen compounds during the formation of black shale hosted quartz - vein gold deposits, north Wales. *Appl. Geochem.* 5: 289 - 296.

Hageman SG and Cassidy KF (2000). Archean orogenic lode deposits. Gold in 2000. Rev. *Econ. Geol*. 13: 9-68

Kerrich R (1990) Mesothermal gold deposits: a critique of genetic hypotheses. Greenstone gold and crustal evolution. *Geol. Assoc. Can*.: 13-31

Mernagh AT, Wygralak PS (2007) Gold ore-forming fluids of the Tanami region, Northern Australia. *Miner Deposita* 42:145–173

Ridley JR and Diamond LW (2000) Fluid Chemistry of Orogenic Lode Gold Deposits and Implication for Genetic Models. Gold in 2000. *Rev. Econ. Geol*. 13: 141-162


Table. Characterization of major mesothermal gold deposits

| Deposit name, province | Reserves, t Au | Host rocks | Morphology of ore bodies | Age, Ma |
|---|---|---|---|---|
| Beresovsk, Urals | 350 | Volcanogenic-terrigenous sequence, granite-porphyry dikes | Ladder veins | 364 |
| Kochrar', Urals | 280 | Granodiorite-adamellites | Veins and stockwork | 260 |
| Svetlinsk, Urals | 78 | Volcanogenic-terrigenous sequence and magmatic rocks | Veins, stringers | 350 |
| Nezhdaninsk, Sakha | 560 | Terrigenous sequence: sandstones and siltstones with carbonaceous matter | Veins, stringers, disseminated ores | 154-94 |
| Maisk, Chukotka | 277 | Terrigenous sequence: sandstones and silstones with carbonaceous matter | Veins, stringers, disseminated ores | 118-64 |
| Darasun, Transbaikalian | 137 | Gabbroids, and granitoids | Veins and mineralized zones | 118-82 |
| Olimpiada, Enisei Range | 650 | Micaceous-quartz, carbonaceous muscovite-quartz, and sericite-quartz-carbonate schists | stratabound lenses of disseminated ores | 856-792 |

# Sorption of heavy metal cations by low-temperature deposits of Pacific hydrothermal fields

I.V. Vikentyev
*Institute of Geology of Ore Deposits, Petrography, Mineralogy, and Geochemistry, Russian Academy of Sciences, Moscow, Russia*

G.V. Novikov & O.Yu. Bogdanova
*Shirshov Institute of Oceanology, Russian Academy of Sciences, Moscow, Russia*

ABSTRACT: Cation exchange reactions with participation of heavy metals were studied in oceanic low-temperature hydrothermal deposits of various mineral compositions and in hydrogenic Fe-Mn crusts. Individual minerals and their assemblages differ significantly in absorptive capacity, which increases in the following order: haematite << Si-protoferrihydrite < protoferrihydrite < goethite < nontronite << Fe-vernadite + Mn-feroxyhyte < Fe-free vernadite < bernessite + Fe-free vernadite < bernessite; *i.e.*, it successively increases from the mineral with a coordination type of lattice to minerals with a layer-type structure. The exchange complex of all minerals includes $Na^{+}$, $K^{+}$, $Ca^{2+}$, and $Mg^{2+}$, *i.e.*, the main cations of seawater. In Mn-minerals, $Mn^{2+}$ is the main exchange component. Hydrothermal Mn minerals display the highest absorptive capacity among the examined low-temperature oceanic deposits (hydrothermal oxides, hydroxides, Fe-aluminosilicates, and hydrogenic Fe-Mn minerals). The absorptive capacity of all examined Mn minerals relatively to heavy metals increases in the same order: Ni < Zn < Cd < Mn < Co < Pb < Cu.

KEYWORDS: Sorption, heavy metals, Fe-Mn minerals

## 1 INTRODUCTION

Low-temperature sorption may be considered a mechanism responsible for the formation of anomalous metal concentrations in the process of lithogenesis because many ore-forming elements are efficiently extracted from natural waters and accumulate in sediments (Chelishchev *et al*. 1992, Lead *et al.* 1999). During epigenetic hydrothermal processes associated with pulses of magmatic or tectonic activity, metallogenically specialized sedimentary sequences could serve as a source of mobilized metals, in addition to their supply from deep-seated chambers. The concept of regeneration of primary metal concentrations by subsequent processes (Schneiderhöhn 1952) remains popular and is used in models of polygenetic deposits (U-Bi-Co-Ni-Ag, Au, Cu, Pb-Zn, *etc*.). Therefore, the forms of primary syngenetic accumulation of dispersed metals during sedimentation remain an important subject of investigations.

The diversity of viewpoints on mechanisms of syngenetic concentration of metal ions by different minerals can be reduced, in fact, to the following two models: either microcomponents co-precipitate along with macrocomponents from seawater during the formation of mineral phases or the microcomponents are adsorbed on the surface of earlier phases. It is assumed that precisely sorption controls the microcomponent chemical composition of aluminosilicates, phosphates, and Mn and Fe minerals in almost all oceanic sediments, although experimental data that would confirm this statement are scarce.

Indeed, sorption is one of the main physicochemical processes responsible for differentiation of metal ions during mineral formation in the ocean. The ion exchange properties of many natural compounds such as aluminosilicates, phosphates, carbonates, Mn oxides-hydroxides, and Fe hydroxides provide differentiation of elements owing to interaction between suspended particles of these minerals and seawater and to filtration of the latter through the sedimentary sequence and underlying rocks. In the

ocean, sorption proceeds relatively intensely, particularly at the active water-sediment geochemical barrier. The modern metalliferous sediments associated with hydrothermal vents at the oceanic bottom also may be enriched in heavy metals owing to their sorption by particles of Fe and Mn hydroxides, although the mechanisms of this phenomenon remain ambiguous as yet.

Of the total diversity of oceanic sediments, only pelagic Fe-Mn nodules and sedimentary crusts from seamounts have been subjected to systematic experimental studies to determine their sorption properties (Chelishchev *et al*. 1992, Novikov & Cherkashev 2000). It was established that they are highly selective natural sorbents of metal ions, primarily, cations of heavy and rare metals, and are characterized by high exchange capacity, selectivity coefficients, and kinetic parameters. Fe-Mn nodules and crusts can efficiently absorb cations of heavy and rare alkali metals from natural waters, which provide high metal concentrations therein.

With respect to their spatial distribution and genesis, low-temperature hydrothermal deposits occupy an intermediate position between sulphides deposited near hot hydrothermal vents, on the one hand, and metalliferous sediments that form dispersion halos at flanks of hydrothermal fields distant from discharge zones of relatively high-temperature sulphide-forming fluids, on the other hand. Using a complex of mineralogical and geochemical methods, we studied low-temperature hydrothermal sediments and hydrogenic Fe-Mn crusts sampled by Pisces manned submersibles in the peripheral zone of the *Axial Seamount* hydrothermal field (Juan de Fuca) during cruise of the R/V Akademik Mstislav Keldysh (Bogdanova *et al.* 1990) and by a Mir deepwater manned submersible in the active low-temperature field of *Franklin Seamount* during cruise of the same research vessel (Binns *et al.* 1993, Bogdanov *et al.* 1997).

## 2 RESEARCH METHODS

Analytical transmission electron microscopy was used in this study. Microdiffraction of electrons was the main method used for identification of mineral phases. Their composition was controlled by a KEVEX-5100 spectrometer. Exchange reactions between water solutions of metal salts with concentrations $C_0$ = 1.0-0.001 g-equiv/l and low-temperature hydrothermal and hydrogenic deposits were used for the study of their sorption properties under similar conditions irrespective of the mineral compositions of samples. Experiments were conducted in the static regime at a temperature of 20 ±1°C and intense stirring of phases with a constant liquid/solid proportion equal to 100. For all samples, the sorption of metal cations was studied in three parallel runs with solution concentrations $C_0$ = 1.0 and 0.001 g-equiv/l and in two parallel runs with concentrations $C_0$ = 0.1 and 0.01 g-equiv/l. The reproducibility of measurements was 98.1-99.3%. Nitrate (Ni, Co, Cu, Cd, Pb), chloride (Mn), and sulphate (Zn) solutions were used in experiments. The period to attain equilibrium cation species of mineral assemblages was 7-10 days. The metal cation concentrations in the respective solutions (after decomposition of samples) were measured with flame atomic absorption spectroscopy (AAS) on a Perkin-Elmer 503 device.

## 3 RESULTS

Low-temperature hydrothermal deposits are largely composed of Fe minerals (mostly protoferrihydrite and ferrihydrite as a product of protoferrihydrite recrystallization, nontronite), Fe-Mn and Mn minerals (Table 1).

Table 1. Mineral compositions of Fe and Mn deposits

| Deposits | Minerals | Franklin Seamount | Axial Seamount |
|---|---|---|---|
| Hydrothermal Fe | Protoferrihydrite | ++ | ++ |
| | ferrihydrite | ++ | ++ |
| | nontronite | ++ | |
| | haematite | + | + |
| Hydrothermal Mn | Fe-free vernadite | ++ | ++ |
| | bernessite | ++ | + |
| Hydrogenic Fe-Mn | Mn-feroxyhyte | ++ | ++ |
| | Fe-vernadite | ++ | ++ |
| | Fe-free vernadite | + | + |
| | bernessite | + | + |
| | goethite | | + |

The absorptive capacity of *Fe minerals* varies from 0.03 to 0.98 mg-equiv/g, with maximal (0.44-0.98 mg-equiv/g) and minimal (0.03-0.28 mg-equiv/g) values characteristic of goethite and haematite, respectively. In general, the sorption activity of Fe minerals increases in the following order: haematite < Si-bearing protoferrihydrite < protoferrihydrite < goethite. At the same time, all examined samples demonstrate the prevalence of the sum of removed

metal cations over the quantity of absorbed metal cations, with an increase in the pH of equilibrium solutions by 0.20-0.35 units relative to the pH of initial solutions. This implies that Fe minerals also absorb protons $H^+$ in addition to heavy metal cations.

The absorptivity of *nontronite* (0.34-1.30 mg-equiv/g) is substantially higher than that of Fe minerals. The exchange complex of nontronite as well as that of Fe minerals consists of $Na^+$, $K^+$, $Ca^{2+}$, and $Mg^{2+}$, their reactivity decreases in the following order: Na > Ca > Mg > K. The contribution of each exchange cation to the total capacity of the mineral decreases in the same direction. Like Fe minerals, nontronite also absorbs protons $H^+$ in addition to heavy metal cations: the pH of equilibrium solutions increases by 0.15-0.25 units relative to the pH of initial solutions.

In exchange capacity, hydrothermal *Mn minerals* (1.92-3.58 mg-equiv/g) substantially exceed not only the studied Fe minerals and aluminosilicates of the same genesis but also hydrogenic Mn minerals (1.42-2.70 mg-equiv/g). The following order of Mn minerals is established in accordance with increasing exchange capacity with respect to all metals: Fe-vernadite, Mn-feroxyhyte < vernadite < bernessite + vernadite < bernessite. The series of decreasing reactivity of metal cations and their contribution to the exchange capacity of Mn minerals coincide: Ca > Na > Mg > $Mn^{2+}$ > K > (Ba, Ni, Zn, Cu, Co). The sum of cations from the exchange complex of Mn minerals passing into solution is higher by 0.14-0.37 mg-equiv/g than the amount of absorbed $Ni^{2+}$, $Zn^{2+}$, $Cd^{2+}$, and $Mn^{2+}$ (the first group of cations). At the same time, the exchange capacity of these minerals with respect to $Co^{2+}$, $Pb^{2+}$, and $Cu^{2+}$ (the second group) exceeds by 0.15-0.30 mg-equiv/g the quantity of removed cations of the exchange complex, $Mn^{2+}$ included. The exchange equivalency is retained in the first case owing to sorption of protons $H^+$ by Mn minerals, and in the second case, by passage of protons that occupy certain positions in Mn minerals into solution. Correspondingly, sorption is accompanied by an increase in the pH of equilibrium solutions by 0.20 units (on average) relative to the pH of initial solutions in the case of metal cations belonging to the first group and by a decrease in the pH by 0.40-0.55 units in the case of metal cations of the second group. This means that protons $H^+$ enter into the exchange complex of Mn minerals during sorption of $Co^{2+}$, $Cu^{2+}$, and $Pb^{2+}$. The second specific feature of exchange reactions is related to sorption of $Co^{2+}$, which is accompanied by the complete removal of $Mn^{2+}$ from hydrothermal Mn minerals, whereas, during sorption of $Cu^{2+}$ and $Pb^{2+}$, only 88.8-94.5% of divalent Mn is removed. Sorption of other cations of heavy metals is accompanied by much lesser removal of $Mn^{2+}$, which does not exceed 35.8-43.7% of its initial content in samples.

Taking into account the concentrations of solutions of heavy metal salts, the exchange capacity of Mn minerals, the quantity of exchange cations passing into solutions, and the pH of equilibrium solutions, one may state that the mechanism responsible for sorption of $Ni^{2+}$, $Zn^{2+}$, and $Cd^{2+}$ is equivalent irrespective of the concentrations of these solutions, while the mechanism of $Co^{2+}$, $Cu^{2+}$, and $Pb^{2+}$ sorption is superequivalent relative to the exchange cations of metals, $Mn^{2+}$ included, in the case of their sorption from 1.0-0.01 N solutions and is equivalent in sorption from 0.001 N solutions. The equivalent exchange in sorption of $Co^{2+}$ $Cu^{2+}$, and $Pb^{2+}$ from diluted (0.001 N) solutions with the pH approaching the neutral value indicates the decreased role of protons $H^+$ in exchange reactions.

## 4 CONCLUSIONS

The sorption activity of low-temperature minerals from Pacific hydrothermal fields increases in the following succession: haematite << Si-bearing protoferrihydrite < protoferrihydrite < goethite < nontronite << Fe-vernadite + Mn-feroxyhyte < Fe-free vernadite < bernessite + Fe-free vernadite < bernessite, i.e., increases from the mineral with a coordination type of lattice toward minerals with a layer structure. By exchange capacity, the minerals are divided into four groups. The first group includes haematite, characterized by a very low capacity (up to 0.1 mg-equiv/g), in which the cation exchange is realized by surface isomorphic replacements (Novikov & Cherkashev 2000). The second group consists of protoferrihydrite and goethite, whose exchange capacity varies from 0.23 to 0.98 mg-equiv/g. The third group is represented by nontronite, whose capacity ranges from 1.04 to 1.30 mg-equiv/g with respect to most of the examined cations and from 0.34 to 0.43 mg-equiv/g with respect to $Mn^{2+}$ and $Zn^{2+}$. The mechanism of absorption of heavy metal cations by minerals of the second and third

groups is equivalent. The fourth group is composed of Mn minerals, which reveal striking sorption properties irrespective of their genesis and are characterized by a high capacity relative to heavy metal cations (1.42-3.58 mg-equiv/g). The exchange capacity within this group increases distinctly from hydrogenic Fe-vernadite toward hydrothermal bernessite and Fe-free vernadite. The sorption of $Ni^{2+}$, $Cd^{2+}$, $Zn^{2+}$, and $Mn^{2+}$ proceeds in line with the equivalent ion exchange mechanism (as in the case of minerals belonging to the second and third groups) at any concentration of metal salt solutions. The sorption of $Co^{2+}$, $Pb^{2+}$, and $Cu^{2+}$ is superequivalent even taking into account $Mn^{2+}$ in the exchange complex of minerals when these cations are absorbed from concentrated solutions and equivalent when they are absorbed from diluted solutions. Two series of the absorbed metal cations are distinguished. As concerns Fe-Mn minerals, these series are identical. The difference consists only in the combination of $Co^{2+}$ with $Pb^{2+}$ and $Cu^{2+}$ into a common series in Mn minerals. The series for nontronite reveals a difference accounted for by its lower selectivity with respect to $Mn^{2+}$ and $Zn^{2+}$ relative to other heavy metal cations. The study of products of ion-exchanging reactions carried out by electron microdiffraction did not establish new phases despite high contents of heavy metal cations, particularly $Pb^{2+}$, $Cd^{2+}$, and $Cu^{2+}$, in examined minerals, primarily, in Mn varieties.

The exchange complex of minerals distinct in chemical composition, lattice structure, and genesis consists of $Na^{+}$, $K^{+}$, $Ca^{2+}$, and $Mg^{2+}$, *i.e.*, of the main cations of seawater. Mn minerals, irrespective of their genesis, include also $Mn^{2+}$ as a main exchange component, which makes a substantial contribution to the exchange capacity of these minerals (up to 0.5 mg-equiv/g) and thus redistributes the shares of the other cations in the total capacity. The contribution of all the above cations to the exchange capacity of minerals amounts to 90-98%. $Ni^{2+}$, $Cu^{2+}$, and $Zn^{2+}$ are involved in exchange reactions with participation of Mn minerals, although their contribution to the capacity of minerals is insignificant: 0.05-0.07 mg-equiv/g, or 2.0-3.5 wt% of their content in samples.

The differences in ion-exchanging properties of samples similar in genesis but different in chemical and mineral compositions are substantially greater than in the case of samples composed of minerals of the same class but belonging to different genetic groups.

## ACKNOWLEDGEMENTS

The authors thank A.Lisitsyn, N.Bortnikov and Ju.Bogdanov for cooperation, N.Zavadskaya, L.Fedorova and N.Tolmacheva for AAS analyses. This study was supported by the Russian Foundation for Basic Research (06-05-64614) and Russian Science Support Foundation.

## REFERENCES

Binns RA, Scott SD, Bogdanov YuA et al. (1993) Hydrothermal Oxide and Gold-Rich Sulphate Deposits of the Franklin Seamount, Western Woodlark Basin, Papua New Guinea. *Econ. Geol.* 88: 2122-2153.

Bogdanov YuA, Lisitzyn AP, Binns RA et al. (1997) Low-Temperature Hydrothermal Deposits of the Franklin Seamount, Woodlark Basin, Papua New Guinea. *Mar. Geol.* 142: 99-117.

Bogdanova OYu, Gorshkov AI, Dubinina GA (1990) Origin of Ferric-Ferrous and Manganese Oxides. *Geological Structure and Hydrothermal Deposits in the Juan de Fuca Ridge*. Moscow: Nauka: 77-80 [in Russian].

Chelishchev NF, Gribanova NK, Novikov GV (1992) *Sorption Properties of Oceanic Ferromanganese Nodules and Crusts.* Moscow: Nedra. pp317 [in Russian].

Lead JR, Hamilton-Taylor J, Davison W, Harper M (1999) Trace Metal Sorption by Natural Particles and Coarse Colloids. *Geochim. Cosmochim. Acta* 63 (11/12): 1661-1670.

Schneiderhöhn H (1952) Genetische Lagerstattengliederung auf geotektonischer Grundlage. *Neues Jahrb. Monatsh.* 2: 47-63, 3: 65-89.

# Molecular and Compound-specific Isotopic Composition of Hydrocarbons in Lower Cambrian Black Shales from the Yangtze Platform, South China

Hartwig E. Frimmel,
*Institute of Mineralogy, University of Würzburg, Am Hubland, D-97074 Würzburg, Germany*

Jorge E. Spangenberg
*Institute of Mineralogy and Geochemistry, University of Lausanne, Humense, CH 1015 Lausanne, Switzerland*

ABSTRACT: First molecular and compound specific isotope data for carbonaceous matter in mineralized Lower Cambrian black shale from the margin of the Yangtze Platform in South China indicate the presence of marine, biogenic, very mature bitumen that was derived from algae and various bacteria (including cyanobacteria) in a marine, in places saline, restricted basin. No systematic differences were noted between finely dispersed bitumen (bulk of carbonaceous shale) and discrete, black bitumen nodules, but differences in the molecular and isotopic composition between samples point to variation in the source.

KEYWORDS: Organic geochemistry, hydrocarbons, Lower Cambrian, Yangtze platform

## 1 INTRODUCTION

The lower Cambrian black shales of the Niutitang Formation (and equivalents) in southern China are famous for hosting extraordinary syn-sedimentary deposits. These include the world's largest accumulation of barite, China's largest phosphate deposits, and a very thin (cm-scale), laterally discontinuous sulphide-rich layer that is, in places, strongly enriched in Ni, Mo, V, Co, Cr, Au, U, As, Pb, Zn, Cu, Re, and PGE. While metal enrichment in carbonaceous marine shales relative to seawater (and also other sedimentary rocks) is predicted due to the removal of trace metals from seawater at the interface with anoxic bottom environments – an effect that is particularly pronounced in the case of low sedimentation rates (Holland 1979) - metal enrichment by one to two orders of magnitude greater than in average black shale has been recorded from several areas, notably from southern China (Mao *et al*. 2002). Several models have been put forward to explain such extreme metal enrichment. These include enrichment by diagenetic fluids (Coveney *et al*. 1987), syn-sedimentary hydrothermal exhalation (Pasava *et al*. 1996; Steiner *et al*. 2001), extraterrestrial impact, syn-sedimentary enrichment from seawater (Mao *et al*. 2002), and discharge of petroleum into the basin (Emsbo *et al*. 2005). The marked spatial association of metal enrichment and carbonaceous matter makes a genetic relationship most likely. Although most workers would agree that the carbonaceous matter is biogenic, it remains unclear whether that organic matter is derived from a uniform source (*e.g*. Murowchick *et al*. 1994) or from several sources as implied by the hypothesis presented by Emsbo *et al*. (2005) according to which extraneous sourced petroleum was deposited with carbonaceous sediment as “tar balls”, now occurring in the form of C-rich, and in places sulphidic and/or phosphoritic nodules. To contribute to the debate on this unusual type of deposit, we analyzed the molecular and compound-specific isotopic composition of representative, mineralized black shale samples, including C-rich nodules, from two sites in the Guizhou Province of South China.

One sample locality is the Dahebian barite deposit in the easternmost Guizhou Province (27°02'53"N, 109°07'37"E). There barite occurs stratiform, as nodules, or as laminated to massive, layered to lenticular bodies within lowest Cambrian carbonaceous shale that is notably enriched also in V, Ni, Mo, and Se, and rests above a siliceous phosphorite-rich bed all of

which constitute the Liuchapo Formation. The second locality is the Ni-Mo-PGE occurrence in black shale of the Lower Cambrian Niutitang Formation near Songlin in the Zunyi county (27°48'28"N, 106°45'54"E). The host shale is rich in well-rounded pyrite disks, reaching several centimeters in diameter. The cm-thick, stratiform sulphidic ore bed is underlain by carbonaceous dolomite, which is locally replaced by domains of coarse-grained sparitic calcite. Mud cracks in the black shale testify of a very shallow, low-energy depositional environment.

Sample preparation and analytical protocol followed modified procedures as described in Spangenberg & Frimmel (2001).

## 2 RESULTS

The total organic carbon (TOC) content of the analyzed samples is between 5.5 and 8.2 wt. %. The hydrogen and oxygen indices were calculated from the RockEval parameters S1, S2 and S3. As both the S1 (free hydrocarbons) and S2 (pyrolytic hydrocarbons) parameters are less than 0.2, the derived parameters $T_{max}$, oxygen and hydrogen indices, and oil production index, are not significant. This may be attributed to high thermal maturation or extensive oxidative or bacterial degradation of the organic matter. Based on the obtained values, the kerogen would correspond to the Type IV (gas prone) with effectively no remaining hydrocarbon potential.

Low- to medium-molecular weight normal alkanes, acyclic isoprenoids, branched alkanes, and alkylcycloalkanes are the main extractable compounds. Pronounced unresolved naphthenic humps in the *n*-alkanes in the $C_{18} - C_{26}$ range are present in all samples. The *n*-alkanes in the $C_{11} - C_{31}$ range (maximum at $C_{16}$, bimodal distribution with further maxima at $C_{22}$ or $C_{26}$ in some samples, slight even-over-odd dominance), pristine (Pr) and phytane (Ph), and alkyl-cyclohexanes in the range $C_{11} - C_{28}$ (with unimodal distribution maximizing at $C_{17}$ and further dominance at $C_{22}$ in some samples, slight odd-over-even dominance) are the main resolvable compounds, with trace amounts of cyclopentanes, in the gas chromatograms of the saturated hydrocarbons from all samples (Fig. 1). Some samples contain also hopanes and steranes, with the latter dominating over the former. The range in Pr/*n*-$C_{17}$ (1.07 - 1.31) and Ph/*n*-$C_{18}$ ratios (0.99 - 1.35) is limited, whereas the Pr/Ph ratio varies between 0.60 and 1.35. The Carbon Preference Index (CPI) for *n*-alkanes ranges from 0.65 to 1.04. No systematic differences in the molecular composition could be observed between carbonaceous matter dispersed in black shale and C-rich nodules. The aromatic hydrocarbon fractions of all samples mainly contain oxidized organic compounds. Pure aromatic hydrocarbons, such as alkylbenzenes, naphthalene, and alkylnaphthalenes, were detected only in very minor concentrations.

The $\delta^{13}C$ and $\delta^{15}N$ ratios of the kerogen range respectively from -31.5 to -35.4 ‰ (relative to V-PDB) and from –1.4 to 0.6 ‰ (relative to air). Sulphur isotopic data of molecular sulphur could only be obtained from two black shale samples from the Dahebian deposit ($\delta^{34}S$ = 13.9 and 15.8 ‰ relative to CDT). The compound-specific C isotope analyses gave $\delta^{13}C$ values for most of the *n*-alkanes and isoprenoids across the C-number range between –33 and –25 ‰, irrespective whether they are black shale or C-rich nodules. However, a few black shale samples differ by showing significant depletion in $^{13}C$ at $C_{15}$, $C_{16}$ ($\delta^{13}C$ = -38 ‰), pristane (by up to 6 ‰ compared to $C_{17}$ and $C_{18}$ *n*-alkanes), and $C_{19}$. The most prominent deviation from the general pattern was noted for the clearly secondary sparitic calcite from Songlin, which shows the strongest depletion in $^{13}C$ at $C_{16}$ (by 16 ‰), pristine and $C_{20}$.

## 3 HYDROCARBON SOURCE

The hydrocarbon distribution and the very low $\delta^{13}C$ ratios are consistent with organic sources, such as algae and bacteria. An abiotic origin can be ruled out, because such hydrocarbons have $\delta^{13}C$ ratios that are typically about 10 to 20 ‰ higher. Furthermore, abiotic hydrocarbons are dominated by molecules with less than six C atoms ($C_{<6}$), though longer chains ($C_{16} - C_{29}$) have been reported from a hydrothermal field on the seafloor (Holm & Charlou 2001). The $C_{<6}$-hydrocarbons are highly volatile compounds, and were, therefore, not detected in our samples. More diagnostic of a biogenic derivation is the presence of steranes and hopanes.

The *n*-alkanes with $C_{\leq 22}$ are generally interpreted as marine algal and/or bacterial derivatives. A significant contribution from marine higher plants and higher organisms, which did not exist at the time of deposition and thus could point to possible contamination during sample preparation and analysis, would be re-

flected by *n*-alkanes of medium molecular weight, with no odd-over-even carbon predominance and a maximum at $C_{19}$ (*e.g.* Hunt 1996). Such a pattern was not found in the analyzed samples. The molecular compositions are, therefore, interpreted as reflecting marine algal and bacterial sources but with significant variations in the respective contribution from algae and bacteria. Differences in the depositional environment of the source are indicated by some samples that display a predominance of even-chain-length *n*-alkanes in the $C_{20}$ to $C_{30}$ range – a feature that is known to occur in sediments deposited in a highly saline anoxic environment.

The wide range in $\delta^{13}C$ of the kerogen (~4 ‰) is most likely due to variations in the primary composition of the organic matter and/or the extent of hydrothermal chemical and bacterial degradation. The $\delta^{15}N$ ratios of the kerogen around 0 ‰ point to a major contribution from molecular nitrogen fixers, such as photosynthetic cyanobacteria.

The slight odd-over-even carbon number preference obtained for the alkycyclohexanes indicates derivation from cyclization and decarboxylation of algal straight-chain fatty acids and reduction of bacterial cyclic fatty acids. The enrichment of the *n*-alkanes in $^{13}C$, relative to the isoprenoids, points to phytol contribution from other sources than algal or cyanobacterial lipids, e. g. various groups of bacteria. Similarly, the small amounts of steranes and hopanes can be explained by derivation from algae and bacteria, respectively (Peters *et al*. 2005). However, the overall low concentrations of these biomarkers indicate a highly mature, variably recycled organic source.

## 4 CONCLUSIONS

The molecular and compound-specific isotopic composition of carbonaceous matter in the Lower Cambrian black shale on the Yangtze platform clearly supports a biologic source that comprised marine algae and various bacteria (including photosynthetic cyanobacteria). The lack of systematic differences between hydrocarbons that are finely dispersed in black shale and C-rich nodules speaks against a model of in-situ derivation of the organic material dispersed in the black shale and an extraneous source for the petroleum that led to the formation of the nodules. However, differences between black shale samples point to variable sources and to differences in the sources' depositional environments, which included that of a saline, anoxic, restricted basin. Consequently, the bitumen nodules are likely to represent hydrocarbons that have migrated and were deposited with the sediment and evolved only subsequently to bitumen in the course of diagenetic maturation.

## ACKNOWLEDGEMENTS

P. Emsbo is thanked for a highly constructive, critical discussion of our results. Funding from the South African National Research Foundation (grant No. FA2004033100023 to HEF), the Deutsche Forschungsgemeinschaft (travel grant to HEF) and the Swiss National Science Foundation (grant No. 200021-109421/1 to JES) is gratefully acknowledged.

## REFERENCES

Coveney RM, Jr., Leventhal JS, Glascock MD, Hatch JR (1987) Origins of metals and organic matter in the Mecca Quarry Shale Member and stratigraphically equivalent beds across the Midwest. *Economic Geology* **82**, 915-933.

Emsbo P, Hofstra A, Johnson CA, Koenig A, Grauch R (2005) Lower cambrian metallogenesis of south China: Interplay between diverse basinal hydrothermal fluids and marine chemistry. In: J Mao and FP Bierlein (eds.) *8th Biennial SGA Meeting, Mineral Deposit Research: Meeting the Global Challenge*. Beijing., **1**, 115-118, Heidelberg, Springer.

Holland HD (1979) Metals in black shales - a reassessment. *Economic Geology* **74**, 1676-1680.

Holm NG, Charlou JL (2001) Initial indications of abiotic formation of hydrocarbons in the Rainbow ultramafic hydrothermal system, Mid-Atlantic Ridge. *Earth and Planetary Science Letters* **191**, 1-8.

Hunt JM (1996) Petroleum geochemistry and geology. New York, Freeman, 753 p.

Mao J, Lehmann B, Du A, Zhang G, Ma D, Wang Y, Zeng M, Kerrich R (2002) Re-Os dating of polymetallic Ni-Mo-PGE-Au mineralization in Lower Cambrian black shales of South China and its geological significance. *Economic Geology* **97**, 1051-1061.

Murowchick JB, Coveney RM, Jr., Grauch R, Eldrigde CS, Shelton KL (1994) Cyclic variations of sulfur isotopes in Cambrian stratabound Ni-Mo-(PGE-Au) ores of southern China. Geochim. Cosmochim. Acta 58: 1813-1823.

Pasava J, Hladikova J, Dobes P (1996) Origin of Proterozoic metal-rich black shales from the Bohemian Massif, Czech Republic. *Economic Geology* **91**, 63-79.

Peters KE, Walters CC, Moldowan JM (2005) Biomarkers and Isotopes in Petroleum Exploration and Earth History, The Biomarker Guide, The

University Press, Cambridge.

Spangenberg JE, Frimmel, HE (2001) Basin-internal derivation of hydrocarbons in the Witwatersrand Basin, South Africa: evidence from bulk and molecular d13C data. *Chemical Geology* **172**, 339-355.

Steiner M, Wallis E, Erdtmann, B.-D., Zhao Y, Yang R (2001) Submarine-hydrothermal exhalative ore layers in black shales from South China and associated fossils - insights into a Lower Cambrian facies and bio-evolution. *Palaeogeography Palaeoclimate Palaeoecology* **169**, 165-191.

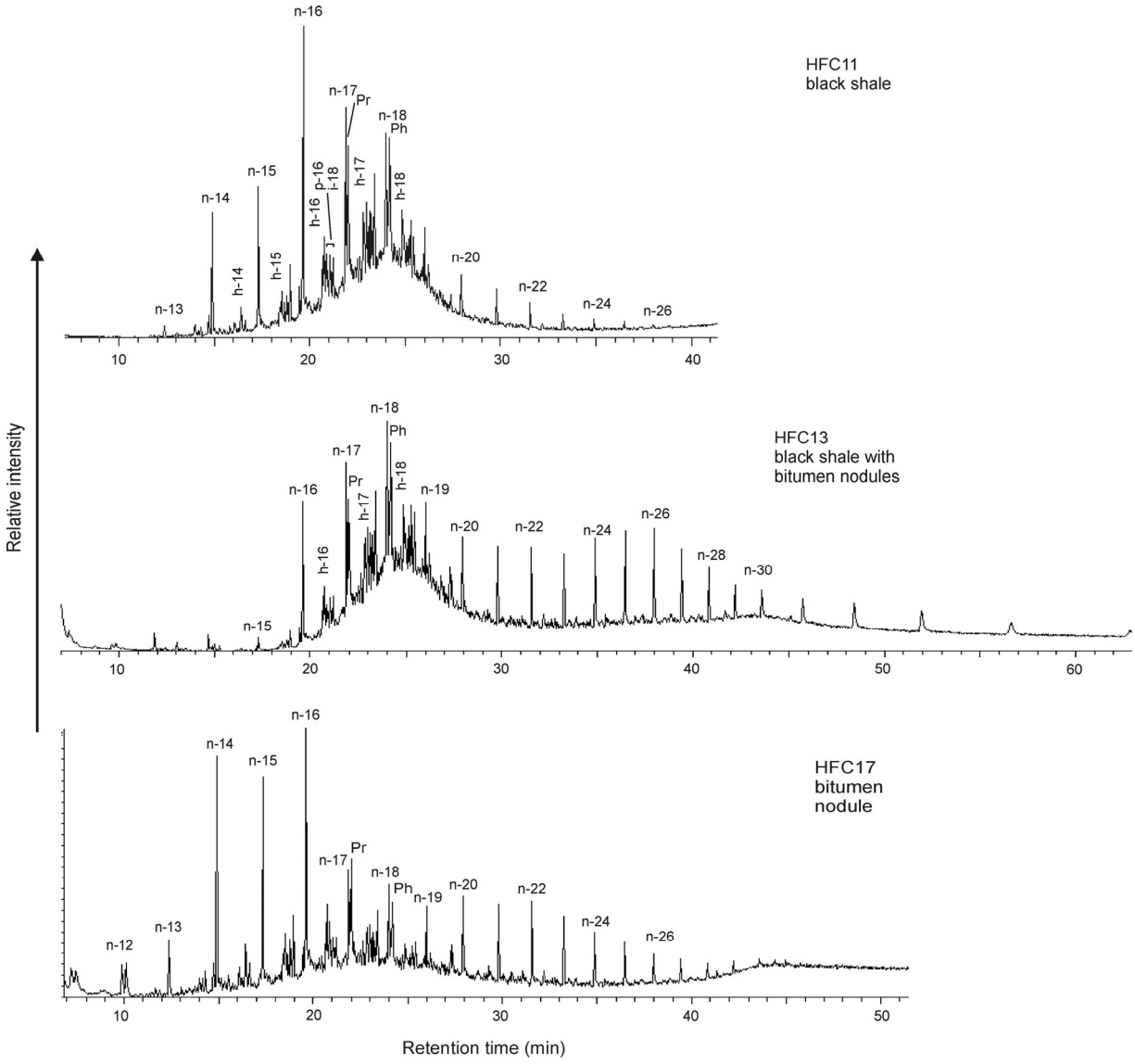


Figure 1. Examples of gas chromatographs of the saturated hydrocarbons in Lower Cambrian black shale and bitumen nodules (Dahebian barite deposit), Yangtze platform

# Fluid inclusion study of gold-bearing quartz-sulphide veins and cassiterite from the Czarnow As deposit ore (SW Poland)

S.Z. Mikulski[1], A. Kozlowski[2] & S. Speczik[1]
[1]*Polish Geological Institute, 4 Rakowiecka Street, 00-975 Warsaw, Poland,*
[2]*Institute of Geochemistry, Mineralogy and Petrology of the Warsaw University, Al. Zwirki i Wigury 93, 02-089 Warszawa, Poland,*

ABSTRACT: Primary fluid inclusions in three generations of auriferous quartz from the Czarnow As deposit were examined. Two first generations of investigated quartz contain refractory and non-refractory gold. The major auriferous period of mineralization occurred in temperatures from 400 to 200°C, while lowest temperature quartz-late carbonate mineralization is devoid of gold. In the ore assemblage cassiterite was an early mineral, which formed at 440-384 and 340-315°C, under pressure 1.2-1.1 kbar from liquid solutions of the total salinity 24-16 wt. % of NaCl equivalent.

KEYWORDS: gold, cassiterite, fluid inclusion, Czarnow, Rudawy Janowickie Mountains, Western Sudetes, SW Poland, Bohemian massif, European Variscides

## 1 INTRODUCTION

The Czarnow As-polymetallic deposit is located in the Western Sudetes and more precisely in the eastern metamorphic cover of the Variscan Karkonosze granitoid massif. This area belongs to eastern elongation of Saxothuringian zone of central European Variscides.

At the Czarnow deposit mining operations were carried out, with numerous stops, from the beginning of 18$^{th}$ Century until 1925. During prosperous years the annual production was *ca.* 3 000 t of As ore with an average content of arsenic 10%. Cu, Zn, Pb, Sn, Fe, and limited quantities of Ag, and Au were also produced as a by-product.

## 2 GEOLOGICAL SETTING OF CZARNOW DEPOSIT ORES

The Czarnow deposit is situated within the rocks of Kowary-Czarnow Unit (Kozdrój 2003). On the West it is bordered by the Karkonosze granitoids, on East – along dislocation – with Leszczyniec Unit. The rocks that compose Kowary-Czarnow Unit trending NNE-SSW have about 1 km thickness, dip 65-80° to SE and S (Teisseyre 1973). From 50 to 200m belt of Kowary gneisses intimately associate with Karkonosze granitoids, the gneisses reveled age of 511 – 492 Ma (U-Pb on zircon; Oliver *et al.* 1993). Westward gneisses are gradually replaced by mica schists, with minor intercalations of other rock, from several up to some ten meter thick. The central part of mica schist's belt contains predominantly intercalations of biotite amphibolites and leptynites, while in eastern part of belt diopside-hornblende amphibolite schists dominate. In the lowermost part of eastern belt the gneisses show symptoms of contact metamorphism. Minor crystalline dolomites and erlanes also occur.

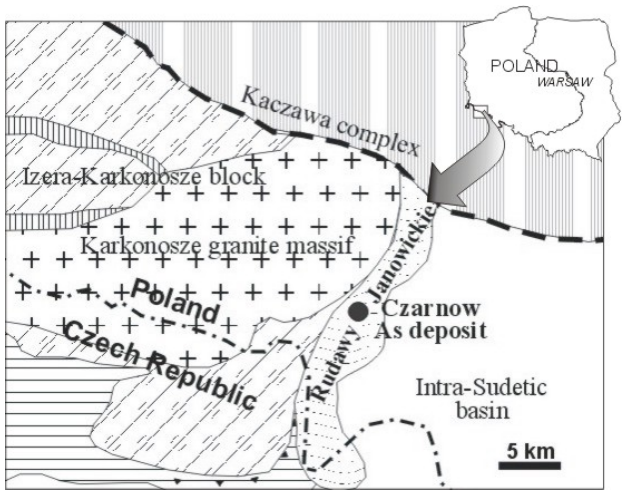


Fig. 1. Location of Czarnow As deposit in Sudetes Mts.

## 3 ORE MINERALIZATION

Steeply dipping quartz-ore vein (*ca.* 80° to the SE) associate with Lower Paleozoic mica schists, calc-silicate rocks, amphibolites, and gneisses. The vein is several meters thick and about 500m long and has SW-NE direction of strike. The ore mineralization composed mostly of arsenopyrite and pyrrhotite forms lens-like bodies within the vein up to 4m thick (average 0.4m). Those minerals in disseminated form occur also in adjacent erlans and mica schists. They are associated with base metal sulphides, bornite, stibnite, pyrite, marcasite and weathered minerals (Zimnoch 1985; Mikulski & Speczik, 1997). Native gold was found together with electrum, native bismuth, bismuthinite and scheelite as fine inclusions up to 20μm in size within arsenopyrite and chalcopyrite and as micro-veinlets infilling fractured arsenopyrite (Mikulski 1997).

The genesis of the deposit is considered to be the result of multiply hydrothermal activity around Upper Carboniferous post-kinematics granitoids intrusion of the Karkonosze massif (Petrascheck 1934; Mochnacka 1982; Zimnoch 1985) and later remobilization in the regional shear zones (Mikulski 1997). The possibility also exist that Czarnow deposit originated from poly-metamorphic processes before the emplacement of Karkonosze massif (Banas 1967). The main quartz-ore vein is extensively fractured and faulted with NW-SE transform type faults. The circulation of hydrothermal fluids facilitated by intensive fracturing lasted relatively long. The age measurement on galena from Czarnow vein give age of 250 to 210 Ma (Legierski 1973).

## 4 FLUID INCLUSION STUDIES IN QUARTZ

### 4.1 *Methods*

The investigations were performed on double-side polished preparations *ca*. 0,3 mm thick in the *Fluid Co.* microscope heating stage, calibrated on the commercial and self-prepared standards. The accuracy of the measurements in the temperature range 80–500°C was ±1°C, and from –70 to +50°C achieved ±0.05°C. The heating stage was assembled with the Leitz Laborlux S microscope.

### 4.2. *Fluid inclusions in quartz veins from Czarnow*

Mineralized samples collected from quartz veins of As Czarnow deposit were subject to fluid inclusion studies. All samples used for fluid inclusion studies contain gold from traces up to a few ppm. Three generations of vein quartz are distinguished:

1) White –gray quartz;
2) White-milky quartz;
3) Transparent quartz.

White-gray quartz and white-milky quartz often occur together in clear succession while white-milky quartz is later. The results of vein quartz primary fluid inclusion measurement (°C) together with salinity (in weight % equivalents NaCl) are presented on Fig 2. Primary fluid inclusions from white-gray quartz that associate with Au-rich arsenopyrite crystallized at temperatures from 330 to 420°C of medium salinity fluids (10-16 wt% NaCl equivalent) that had pressure of 0.8 to 1.1 kbar. White-milky quartz that associate with sulphides (chalcopyrite, galena, sphalerite), native bismuth and carbonate reveled temperatures from 250 to 320°C and crystallized from medium-low salinity fluids (5 to 8 wt% NaCl equivalent) with pressure from 0.8 to 0.9 kbar. Microscopic inclusions and intergrowths of Au in fractures and veins that contain chalcopyrite,

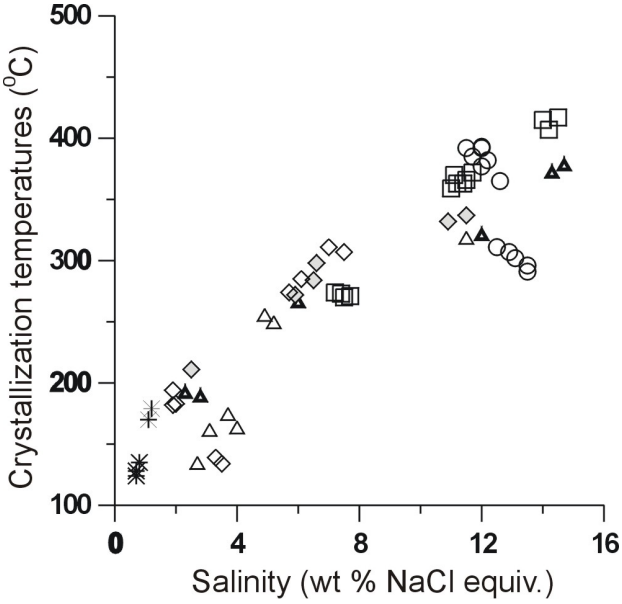


Fig. 2. Crystallization temperatures vs. salinity diagram of fluid inclusions hosted by quartz of various generations at the Czarnow As deposit. Notice: graphic symbols indicate different quartz samples.

galena Ag-Bi sulphosalts and Pb-Cu and Bi-tellurides are also members of white-milky quartz association.

Third quartz generation intimately associate with late carbonates. Temperature of crystallization of this association based on fluid inclusion studies is 130 to 210°C, low salinity (0.5 to 4 wt% NaCl equivalent) with pressure from 0.5 to 0.7 kbar.

## 5 FLUID INCLUSION STUDIES IN CASSITERITE

Cassiterite forms euhedral or anhedral grains with quartz in sulphide ore sample (Fig 3). Its colour is gray-brownish of various tints. Cassiterite contains moderate amounts of only few admixture elements: FeO up to 2 wt. %, $TiO_2$ up to 0.7 wt. %, $Nb_2O_5$ and $Ta_2O_5$ up to 0.5 wt % each (Cameca SX-100 electron microprobe analyses made in the Inter-Institution Laboratory of Microanalysis, Faculty of Geology, the analyst Dr. P. Dzierzanowski). Contents of trace elements (Ta and Nb) in cassiterite is low and similar to light color cassiterite reported by Mochnacka et al., (2001) from Redziny quarry, which is located only 2km northward from Czarnow deposit.

Fluid inclusions in cassiterite occurred rarely: in 20 grains of this mineral 26 water-solution-filled inclusions and 7 carbon-dioxide-filled ones were found, which were suitable to make measurements on them. Measurements made possible the estimation of the crystallization temperature and pressure by the method of the crossed isochores. Seventeen aqueous inclusions and five $CO_2$ inclusions yielded temperatures 440-384°C and pressure 1.2-1.1 kbar. Nine inclusions in younger cassiterite indicated temperatures 340-315°C and pressure 1.1 kbar. The older cassiterite crystallized from more concentrated solutions, with the total salt contents 24-19 wt. % of the NaCl equivalent. Three of the studied inclusions contained at room temperature minute daughter NaCl crystals. The younger cassiterite, which either forms small grains up to 0.05 mm in length or outer rims on the older one, formed from more dilute solutions of the total salt concentration *ca*. 16 wt. % of the NaCl equivalent.

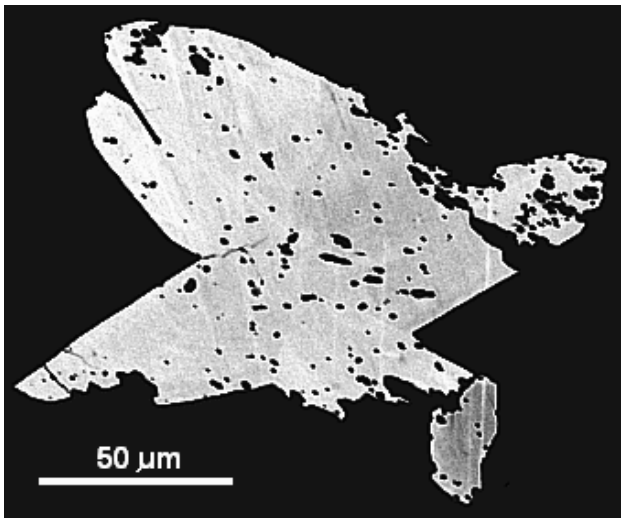


Fig. 3. Backscattered electron image of cassiterite crystals aggregate in quartz of ore-bearing sample from Czarnow.

The cassiterite formation in part preceded thus the Au accumulation episode in the studied veins and belongs to the high-temperature stage of the ore mineralization in the veins at Czarnow. After a certain interruption, the middle temperature event of tin inflow (or re-deposition?) occurred together with the gold including into sulphide ore mineralization.

## 6 CONCLUSION

The mineral formation in the veins was a poly-stage process, even if considering one mineral or one element. It was distinctly marked by two episodes of the cassiterite precipitation. Although here not presented in details, other ore and barren minerals formed in two or more stages, yielding several generations. Also gold accumulation at Czarnow occurred in two stages: the first includes precipitation of submicroscopic gold inclusions in arsenopyrite and pyrrhotite that associate with first white-gray quartz generation in temperatures around 400°C; and the second connected with microscopic size gold in paragenesis with Cu-Pb-Zn sulphides, Pb-Sb-Ag sulphosalts, carbonates and crystallization temperatures not exceeding 320°C.

The multistage origin of Czarnow deposit mineralization support an idea with long lasting hydrothermal activity related to acidic (granitoids) magmatism. In the near vicinities of Czarnow deposit beside the Upper Carboniferous Karkonosze granitoids, occurs Middle Cambrian granites (Kowary gneisses). Therefore, it is still debatable, whether the individual stages of mineralization were caused by a series of independent inflows of solutions from one or more sources, though all probably connected with the Karkonosze intrusion. We believe that these activities were rather facilitated by post-

kinematics Variscan tectonic. Another possibility is, that the ore-forming solutions were mixtures of at least two fluids, one concentrated and possibly carrying metals, another one dilute and barren. When the latter appeared in increasing volume, it might have slowed down or stopped ore precipitation. The third possibility to investigate is the re-deposition of the metals, precipitated at the earlier stages of the mineral assemblage formation.

ACKNOWLEDGEMENTS

The analytical work was supported by the National Committee Scientific Research, Grant 4 T12B 029 30. The contribution of A. K. was financed in part by the Faculty of Geology grant No. BW 1726/15.

REFERENCES

Banas M (1967) Arsenic ore deposit in Czarnow. *Przeg. Geol*. 5: 239 (in Polish).

Legierski J (1975) Model age and isotopic composition of ore leads of the Bohemian Massif. *Cas. Miner. Geol*. 18/1: 1–23.

Kozdrój W (2003) Geotectonic evolution of the metamorphicum of the Eastern Karkonosze *In*: Ciezkowski W, Wojewoda J, Zelazniewicz A (eds.): *Western Sudetes: from Vendian to Quaternary:* 67-80. PTG, Wroclaw (in Polish).

Mikulski SZ (1997) Native gold and electrum from the Czarnow arsenic deposit (Western Sudetes). *In:* Muszer A (ed.): Noble metals in NE part of Bohemian Massif and its surroundings, genesis, occurrence, perspectives. *Jarnoltowek* 19-21.06.1997: 29-34 (in Polish).

Mikulski SZ & Speczik SW (1997) Gold-polymetallic deposits within metamorphic covers of Palaeozoic granitoids in Sudetes (SW Poland). *In:* Bekzhanov GR et al. (eds.): Paleozoic granite-related Au, Cu, Mo, W, REE deposits and epithermal gold deposits. *Programme, Abstracts and Excursion Guidebook. IUGS / UNESCO Deposit Modeling Program. Workshop, August 31- September 14, 1997. Kazakhstan and Kyrgyzstan. Budape*st.

Mochnacka K (1982) Polymetallic mineralization of the Eastern metamorphic cover of the Karkonosze granite and its connection with geologic evolution of the area. *Biul. IG* 341: 273–289 (in Polish with English summary).

Mochnacka K, Pieczka A, Golebiowska B, & Kozlowski A (2001) Cassiterite from Redziny and its relationship to the tin-bearing schist of Izera area (SW Poland). *In:* Piestrzynski et al. (eds.): *Minerals Deposits at the beginning of the 21st Century:* 457-460. Swets & Zeitinger Publishers Lisse. The Nederlands.

Oliver GJH, Corfu F, Krogh TE (1993) U-Pb ages from SW Poland: evidence for a Caledonian suture zone between Baltica and Gondwana. *Jour. of Geol. Soc., London.* 150: 355-369.

Petrascheck WE (1934) Die Vererzung der Sudetten. *Mitteilungen der geologischen Gesellschaft*. Bd 26. Wien.

Teisseyre JH (1973) Metamorphic rocks of the Rudawy Janowickie and Lasocki Ridge. *Geologia Sudetica* 8: 7-111 (in Polish with English summary).

Zimnoch E (1985) *Ore mineralization from Czarnow. Rocznik* PTG 53:289-306 (in Polish with English summary).